Hongjun Li
Shuang Xia
Yubo Lyu
Editors

Radiology of Infectious and Inflammatory Diseases - Volume 2

Head and Neck

Science Press
Beijing

Springer

Radiology of Infectious and Inflammatory Diseases - Volume 2

Hongjun Li • Shuang Xia • Yubo Lyu
Editors

Radiology of Infectious and Inflammatory Diseases - Volume 2

Head and Neck

Science Press
Beijing

Springer

Editors
Hongjun Li
Capital Medical University
Beijing YouAn Hospital
Beijing, China

Yubo Lyu
Department of Medical Imaging
Jiahui International Hospital
Shanghai, China

Shuang Xia
Department of Radiology
Tianjin First Center Hospital
Tianjin, China

ISBN 978-981-16-8840-9 ISBN 978-981-16-8841-6 (eBook)
https://doi.org/10.1007/978-981-16-8841-6

Jointly published with Science Press
The print edition is not for sale in China (Mainland). Customers from China (Mainland) please order the print book from: Science Press.

This Springer imprint is published by the registered company Springer Nature Singapore Pte Ltd.
The registered company address is: 152 Beach Road, #21-01/04 Gateway East, Singapore 189721, Singapore

Preface

Social and economic boom in modern times have changed people's lifestyle and population mobility. As a result, human subsistence and socio-economic development are increasingly affected by infectious and inflammatory diseases. The document issued by the National Health Commission stresses that all the hospitals at level II and above need to set up an infectious diseases department and an infection control office, to attach the greatest importance to the hazards of infectious diseases on human health. During the past 30 years, the development of medical imaging diagnosis and treatment technologies has greatly boosted the improvement on diagnosis and treatment modes in modern times. Since the modern medicine is highly dependent on medical imaging technologies, the medical imaging is granted an important mission in diagnosis and differential diagnosis of infection and inflammatory diseases.

During long-term clinical practices and scientific researches, my team and I realized that due to the neglect and lack of construction for key discipline system of infection and inflammatory diseases as well as researches on related theory system and specification guidance, the quality and effectiveness of the diagnosis and treatment provided for patients have been seriously affected, resulting in the abuse of clinical antibiotics, thus compromising patients' health and quality of life and increasing the economic burden on family and society. Based on the above considerations, the Book gathers a number of experts and scholars from the Infectious Diseases Group of the Chinese Society of Radiology, Infection Imaging Professional Committee of the Chinese Medical Doctor Association Radiological Branch, Professional Committee on Radiology of Infection and Inflammation of the Chinese Research Hospital Association, Working Committee on Infection (Infectious Disease) Imaging of Chinese Association of STD & AIDS Prevention and Control; Infectious Disease Imaging Group of Avocation of Infections Disease Hospital and Beijing Imaging Diagnosis and Treatment Technology Innovation Alliance. Clinical resources associated with infection and inflammatory diseases across the nation are integrated and the imaging characteristics and evolution rules of infection and inflammatory disease are summarized herein. Meanwhile, this book has revealed the pathological basis of infections and inflammatory diseases and put forward the essential points of imaging diagnosis and differential diagnosis of infectious and inflammatory diseases. I believe that the series of books will boost the academic development on prevention and control, rational drug use, and radiological diagnosis for infections and inflammatory diseases, thereby helping deliver accurate diagnosis and treatment in clinic.

This series of books systematically introduces the theory of the radiology of infection and inflammation for the first time. The books are divided into six volumes (Brain and Spinal cord, Head and Neck, Heart and Chest, Abdomen and Pelvis, Skeletal Muscle, and Children). It covers four types of pathogens related to infectious diseases (bacteria, fungi, viruses, parasites) and inflammatory diseases such as autoimmune diseases.

The set of books is characterized in that: (1) it provides clinically-relevant data for a wide array of diseases ranging from clinically common and frequently occurring diseases to rare infectious and inflammatory diseases; (2) it provides complete data and objective basis of diagnosis, with a focus on the integrity, representativeness, consistency, and authenticity of cases, images and graphics therein; (3) the editors, by virtue of their accumulated clinical experience and practice, contribute most of the data, and some materials adopted herein have

been authorized by international peers. By absorbing and quoting the latest research results at home and abroad, this series of books bring readers a refreshing feel both in compilation form and contents.

To ensure the smooth publication of the books, we established an advisory committee and an expert committee, spending over 1 year to accomplish the compilation from outline designing to draft finalizing, while seeking for scientific design and systematic demonstration. The English version will be published simultaneously with the Chinese version by the publisher Springer. The editorial board put a high premium on the compilation of this series and trained members of the editorial board on standardized writing, professional review, and finalization of drafts for several times. In the meantime, the editorial board also assigned specific personnel to engage in the review, revision, and supplement. As the editor-in-chief, I would like to express my cordial thanks for their unremitting efforts. Unfeigned gratitude is also extended to the members of the National Infectious Disease Imaging Group who devoted themselves to the compilation of this book.

Facing the severe situation of prevention and treatment of infections and inflammatory diseases, this series of monographs will serve as another powerful tool fighting against infections and inflammatory diseases and play an essential role in raising the physicians' level of diagnosis and treatment, improving patients' quality of life and prolonging their lives.

Amidst scientific development, we have gained deeper insight gradually. For this reason, errors are also inevitable, so we sincerely welcome your criticisms and suggestions that can refine the book step by step.

Beijing, China
November 2019

Hongjun Li

Preface

Over the past several decades, the challenge posed by infectious and inflammatory diseases has been alleviated, the incidence and mortality thereof, however, cannot be overstated. Head and neck, where the anatomical structures are complicated with essential physiological functions, must be diagnosed and treated as early as possible in case of any disease involved, otherwise grave consequence ensues. As medical imaging techniques flourish, they have become increasingly crucial to the early diagnosis of many infectious and inflammatory diseases. In line with requirements of Healthy China 2030 Strategy, we compiled the *Radiology of Infection and Inflammation: Head and Neck*, which provides references on disease diagnosis and treatment for clinicians and radiologists as well as theoretical supports for teaching activities, with a view to helping medical workers meet their development goals in the new era.

The book was co-edited by experts who have long engaged in clinical forefront and excel in diagnosis and treatment of head and neck infectious and inflammatory diseases with contributions to scientific research and rich teaching experience. Besides, some outstanding young physicians also participated in the compilation, infusing new blood into the book. The editors seek to provide a valuable reference book on head and neck infectious and inflammatory diseases for our readers by reviewing a large number of the latest domestic and foreign literature and aligning theory with experience.

The book consists of a basic theory and monographs. The basic theory makes an outline of the book, systematically introducing the overview, classification, and laboratory diagnostic techniques and methods of head and neck infectious and inflammatory diseases. It enables readers to gain a preliminary insight into the status quo of these diseases and latest laboratory test techniques thereof, so that they can combine imaging findings with clinical practices. The monographs introduce the imaging techniques and imaging anatomy for various sites of the head and neck, making readers fully understand normal findings of imaging examination. Following the monographs, the book introduces relevant diseases corresponding to each site. To make readers thoroughly understand the cause of abnormal imaging findings, each chapter covers clinical, pathological, and imaging findings, key points of diagnosis and differential diagnosis, thus enabling readers to gain systemic and overall understanding of the diseases, with proper diagnostic thought and sufficient capability to differential diagnosis. On top of that, status quo and research progress of each disease are included, providing guidance on scientific research, treatment, and prognosis evaluation. The book illustrates head and neck inflammatory diseases with abundant pictures, and it is characterized by being clearly structured with a combination of textual and graphical data in a concise, easy-to-understand language for convenient reference. We are committed to building the book into a novel and practical guideline on infection and inflammation for readers based on prudent attitude, strict requirements, and rigorous methods.

Finally, we would like to express our heartfelt thanks to the editors and sincere respect to predecessors in the field. Restricted by the time and editors' expertise, there may be improprieties and errors in the book. We sincerely welcome any suggestion or correction that can refine the book.

Tianjin, China
February 2020

Shuang Xia

Introduction

The book consists of a basic theory and monographs. The basic theory provides overview, classification and laboratory diagnostic techniques and methods for infectious and inflammatory diseases of neck and head, while monographs detail imaging techniques, imaging anatomy and relevant diseases of various parts of neck and head. Clinical, pathological, and imaging findings, key points of diagnosis, differential diagnosis, and status quo and research progress of each disease are included, thus enabling readers to gain systemic and overall insight into the diseases, with proper diagnostic thought and sufficient capability to differential diagnosis. The book stands out among other similar books for being clearly structured with a mix of textual and graphical data in a concise, easy-to-understand language for convenient reference.

It aims to provide guidance and reference for imaging physicians, medical students, otolaryngology and head and neck surgeons, and related professionals.

Contents

Editors and Contributors

About the Editors

Hongjun Li doctor of medicine, chief physician, professor, doctoral and postdoctoral supervisor, returnee expert, national outstanding contribution experts, and State Department special allowance expert. He is listed in the first batch of Beijing "Ten Hundred Thousand Excellent Health Professionals." He is included in the first batch of academic leader (backbone) of senior health talents in Beijing 215 talent training program (namely, selection of 20 leading talents, 100 academic leaders, and 500 academic backbones). He is the distinguished professor, chief medical imaging expert, and expert in infectious disease medical imaging of the National Clinical Research Center for Infectious Diseases, and the founder of the international standard system for infectious disease imaging innovation discipline.

He is an expert in modern medical imaging and has been engaged in the clinical and scientific research of infectious disease radiology for more than 30 years. He mainly focuses on the imaging diagnosis for infectious diseases, inflammatory diseases, and inflammation-related oncology. He is dedicated to noninvasive and accurate grading diagnosis based on the fusion of imaging and multi-source heterogeneous data. His work breaks through the gaps in the academic and application of modern imaging technology at home and abroad in the field of infectious diseases, and promoted the development of infectious disease prevention and treatment technology in China and even internationally.

He serves as a Director of the Medical Imaging Center of Beijing YouAn Hospital, Capital Medical University and a Deputy Director of the Medical Imaging Department of Capital Medical University. He is a chief editor of *Journal Radiology of Infectious Diseases* and an associate editor of *BMC Neurology*, the guest editor of Frontiers Neuroscience, and the sub-editor of Wily BMC Neurology. Now he acts as a Chairman of the National Health and Health Technology Promotion and Application Project Radiology Professional Committee, a Chairman of the Infectious Diseases Radiology Professional Committee of the Chinese Society of Radiology, a Chairman of the Infection Imaging Professional Committee of the Chinese Medical Doctor Association Radiological Branch, a Chairman of the Professional Committee on Radiology of Infection and

Inflammation of the Chinese Research Hospital Association, a Chairman of the Working Committee on Infection (Infectious Disease) Imaging of Chinese Association of STD & AIDS Prevention and Control, a President of the Beijing Imaging Diagnosis and Treatment Technology Innovation Alliance. He is included in the National Science and Technology Progress Award evaluation experts, China Medical Science and Technology Progress Award evaluation experts, the Ministry of Science and Technology major research and development special evaluation experts, the National Natural Science Foundation of China project evaluation experts, and the National Study Abroad Fund Committee evaluation experts.

In recent years, he has undertaken 3 the Ministry of Science and Technology major research and development projects chief and international cooperation focus on research and development chief scientist projects, and 6 projects funded by the National Natural Science Foundation of China. Among them, he presided 1 key project and 4 general projects funded by the National Natural Science Foundation of China, 2 projects funded by the Natural Science Foundation of Beijing, and more than 20 other projects. Li Hongjun has published more than 200 papers. He has won 2 national invention patents and 23 IP registrations. He has won 9 prizes at provincial and ministerial level, including the Chinese Medical Science and Technology Award. He was awarded the title "Accomplished Teacher for Training an Apprentice" by Beijing Federation of Trade Unions. The scientific research team led by him was given the title "Science & Technology Innovation Cultivation Team" by the Beijing Municipal Administration of Hospitals, and the title "Staff Innovation Studio at Municipal Level" jointly by the Beijing Federation of Trade Unions and the Beijing Municipal Science & Technology Commission. In 2020, Li Hongjun Innovation Studio was named Beijing Demonstration Innovation Studio.

He is the managing editor of 48 monographs, 5 textbooks, 2 guidelines, 8 standards, and 16 English-language professional originals (including in press) published by the internationally renowned Springer Nature-PMPH series. *Radiology of HIV/AIDS* and *Radiology of Infectious Diseases 1-2* under his general editorship were, respectively, granted 2014 and 2015 Excellent Exported Book Award. Besides, the two books won the 2017 General Award issued by the State Administration of Press, Publication, Radio, Film and Television of the People's Republic of China. He and his team created four medical integration and multidisciplinary cross-integration transformation products (tuberculosis integrated management system, multilingual user information management system, and 5G-Internet digital medical new model system).

He follows the discipline construction concept—"international vision, patient needs, systematic thinking, overall promotion" and international discipline construction idea—"medical technology standardization, technology and equipment modernization, medico-engineering cooperation informatization, technical team specialization." He pioneered

the global systematic innovation theory system of AIDS radiology, infectious disease radiology, infection and inflammatory radiology, infection inflammation-related tumor radiology. He also created the modern medical imaging information subject model centered on teaching materials, norms, guidelines, standards, and subject systems. He pioneered the discipline of modern infectious disease imaging informatics in the world, and international, modern innovative integration discipline with diagnosis, treatment, and testing into a uniform.

Shuang Xia chief physician, doctoral and graduate student supervisor of Tianjin Medical University and Nankai University. She was rated as an excellent first-level candidate of Tianjin "131" Innovative Talent Cultivation Project in 2014. She was listed in the first batch of Tianjin "Jinmen Medical Talent" by Tianjin Municipal Health Committee, and granted Award for Tianjin Medical University Teacher Excellence in 2018 and the title of Excellent Teacher by Chinese Medical Doctor Association in the following year. Besides, she has been awarded the title of "Excellent Teacher of National Standardized Training for Resident Physicians" for several times. She completed 3-month study in Wayne State University in 2012, and 1-month training for teaching of resident physician in the American College of Radiology from March to April 2019. She takes the lead in a National Key R&D Program of China organized by Ministry of Science and Technology; three programs of National Natural Science Foundation of China (two general and youth programs); three programs of National Social Science Foundation; a China Postdoctoral Science Foundation Funding Program; a Tianjin Science & Technology Major Plan and Special Program; a Tianjin Science & Technology Major Special and Engineering Program; a Tianjin Healthcare Industry Key Program as well as a key funding project of Tianjin Municipal Health Office Science & Technology Foundation. She was granted a total of 18 Tianjin Scientific and Technological Achievements. She published 44 SCI papers with a total of 77 factors of influence, and over 40 papers on Chinese core periodicals. She edited 6 books, wherein she served as a chief editor and an associate editor for, respectively, 2 and 3 of the books. As a graduate student supervisor, she has enrolled 12 doctoral candidates, instructed 38 master degree candidates, and assisted in instructing more than 20 master degree candidates. She has taught a total of 50 graduates of diagnostic imaging center. Now she is teaching 26 students of the center. She has participated in several top-level academic conferences at home and abroad and been invited to give special reports.

She is currently a member of youth committee of the Chinese Society of Radiology, Chinese Stroke Association Medical Imaging Branch, Head and Neck Imaging Professional Committee on Chinese Medical Doctor Association Radiological Branch, China International Exchange and Promotion Association for Medical and Healthcare Radiology Branch, China Medical Imaging Integration Association

Council, Tianjin Medical Association Radiology Branch. She serves as an editorial board member of *Radiology of Infectious Diseases*, *International Journal of Medical Radiology, and Chinese Journal of Clinical Medicine,* and reviewer of *Chinese Journal of Radiology*, *Journal of Magnetic Resonance Imaging* and *Medicine*.

Yubo Lyu doctor of medicine, associate chief physician. He was graduated from the Imaging Medicine and Nuclear Medicine Department of Shandong University Cheeloo College of Medicine, and granted fully-funded program by China Scholarship Council to complete 2-year postdoctoral research in Johns Hopkins University. Besides, he visited the Department of Radiology and Cancer Center of Harvard University Affiliated Massachusetts General Hospital for in-depth clinical learning. He is currently a member of the Radiological Society of North America (RSNA), professional committee on Chinese Medical Doctor Association Radiological Branch, professional committee on neuroradiology of Chinese Medical Doctor Association Neurological Branch, non-public medical group of Shanghai Medical Association Radiology Branch, imaging professional committee on Shanghai Association for Non-government Medical Institution, professional committee on Radiology of Infection and Inflammation of Chinese Research Hospital Association, and Beijing Imaging Diagnosis and Treatment Technology Innovation Alliance council. He published, as the first author, original papers on *Invest Radiol, Eur Radiol,* and the like. He is the managing editor of *Magnetic Resonance-Guided Minimally Invasive Treatment & Diagnosis*, and is a co-editor of *Imaging of CNS Infections and Neuroimmunology* (English version). He participated, as a translator, in the compilation of the world-class Gastrointestinal Diagnostic Imaging (original 3rd edition). In addition, he has delivered speeches in conferences organized by the Radiological Society of North America (RSNA) and the International Society for Magnetic Resonance in Medicine (ISMRM). He had been worked on imaging diagnosis and intervention in Shandong Medical Imaging Research Institute affiliated to Shandong University for over a decade. In 2017, he joined Shanghai Jiahui International Hospital as a member of Shanghai Talents Introduction initiative to carry out imaging diagnosis and treatment. He specializes in and excels at diagnosis based on magnetic resonance, CT and X-ray imaging finds, and imaging-guided tumor aspiration biopsy and minimally invasive diagnosis and treatment.

Contributors

Xuedong Bai Affiliated Hospital of Chengde Medical University, Chengde, China

Chen Cao Tianjin Huanhu Hospital, Tianjin, China

Yang Cao Shiyan Renmin Hospital, Affiliated People's Hospital of Hubei University of Medicine, Shiyan, China

Wen Chen Shiyan TAIHE Hospital (Affiliated Hospital of Hubei University of Medicine), Shiyan, China

Hui Dai Affiliated Hospital of Zunyi Medical University, Zunyi, China

Huazheng Dong Tianjin Academy of Traditional Chinese Medicine Affiliated Hospital, Tianjin, China

Yan Gong Tianjin Hospital of ITCWM Nankai Hospital, Tianjin, China

Jie Hu Affiliated Hospital of Zunyi Medical University, Zunyi, China

Wenxiao Jia Xinjiang Medical University, Xinjiang, China

Ting Liang First Affiliated Hospital of Xi'an Jiao Tong University, Xi'an, China

Bangguo Li Affiliated Hospital of Zunyi Medical University, Zunyi, China

Fuxing Li Tianjin Baodi District People's Hospital (Baodi Clinical College of Tianjin Medical University), Tianjin, China

Guoquan Li Chongqing Three Gorges Central Hospital, Chongqing, China

Hongjun Li Beijing YouAn Hospital, Capital Medical University, Beijing, China

Li Li Beijing YouAn Hospital, Capital Medical University, Beijing, China

Mingyu Li Affiliated Hospital of Chengde Medical University, Shanghai, China

Heng Liu Affiliated Hospital of Zunyi Medical University, Zunyi, China

Jingzhe Liu First Hospital of Tsinghua University, Beijing, China

Wenya Liu The First Affiliated Hospital of Xinjiang Medical University, Ürümqi, China

Xinjiang Liu Shanghai Pudong Hospital, Fudan University Affiliated Pudong Medical Center, Shanghai, China

Zhao Lu Shengjing Hospital of China Medical University, Shenyang, China

Ya'nan Lyu Dalian Municipal Central Hospital, Dalian, China

Yubo Lyu Jiahui International Hospital, Shanghai, China

Haibing Mei Ningbo Woman and Children's Hospital, Zhejiang, China

Shinong Pan Shengjing Hospital of China Medical University, Shenyang, China

Zhongwei Qiao Fudan University Affiliated Children Hospital, Shanghai, China

Meiji Ren Beijing YouAn Hospital, Capital Medical University, Beijing, China

Wen Shen Tianjin First Central Hospital, Tianjin, China

Shuangyan Sun Jilin Cancer Hospital, Changchun, China

Min Tang Shanxi Provincial People's Hospital, Taiyuan, China

Wenwei Tang Womans Hospital of Nanjing Medical University, Nanjing, China

Zuohua Tang Eye and ENT Hospital of Fudan University, Shanghai, China

Xiaoping Tong Chengdu Aerospace Hospital, Chengde, China

Jingshi Wang Dalian Women and Children Medical Center, Dalian, China

Lijun Wang The First Hospital of Dalian Medical University, Dalian, China

Tao Wang The First Affiliated Hospital of USTC (Anhui Provincial Cancer Hospital), Hefei, China

Yu Wang The Affiliated Hospital of Shandong University of TCM, Jinan, China

Shuang Xia Tianjin First Central Hospital, Tianjin, China

Zujiang Xiong Chongqing Fifth People's Hospital, Chongqing, China

Jianrong Xu Renji Hospital of Shanghai Jiao Tong University School of Medicine, Shanghai, China

Li Yao Affiliated Stomatology Hospital of Zunyi Medical University, Zunyi, China

Xianjun Ye Anhui Provincial Hospital, Hefei, China

Mengmeng Yu Binzhou Medical University Hospital, Binzhou, China

Haorong Zhang Children's Hospital of Shanghai, Shanghai, China

Huanlei Zhang Yidu Central Hospital of Weifang, Qingzhou, China

Jing Zhang The First Affiliated Hospital of USTC (Anhui Provincial Cancer Hospital), Hefei, China

Xuening Zhang Second Hospital of Tianjin Medical University, Tianjin, China

Meizhu Zheng Tianjin Third Central Hospital, Tianjin, China

Shaowei Zheng The First Hospital of Dalian Medical University, Dalian, China

Jun Zhou Shenyang Fourth People's Hospital, Shenyang, China

Ying Zou The First Affiliated Hospital of Tianjin University of TCM, Tianjin, China

Part I

General Introduction to Infectious and Inflammatory Diseases of Head and Neck

Conventional Imaging Techniques

1

Yu Wang, Huanlei Zhang, and Shuang Xia

Imaging techniques for infectious and inflammatory diseases of neck and head mainly involve X-ray, computed tomography (CT), magnetic resonance imaging (MRI) and digital subtraction angiography (DSA).

1.1 X-Ray Imaging Techniques

Orbit: To understand the changes in orbital morphology and orbital bone, as well as calcification and radiopaque foreign bodies.

Temporal bone: To observe implanted artificial cochlea.

Paranasal sinus: To understand paranasal sinus morphology and changes in nasal bone and maxilla.

Oral and maxillofacial region: To observe dental and periodontal lesions, and lesions in jaw bone and temporal-mandibular joint.

Throat: X-ray examination relies only on changes in the contour of air in throat cavity and morphology of the cavity surface to observe abnormity in nasopharynx roof wall, posterior pharyngeal wall, soft palate, epiglottic cartilage, laryngeal vestibule, vocal area, subglottic portion, and lower posterior pharyngeal wall.

Neck: Rarely use X-ray examination.

Y. Wang
The Affiliated Hospital of Shandong University of TCM, Jinan, China

H. Zhang
Yidu Central Hospital of Weifang, Weifang, China

S. Xia (✉)
Tianjin First Central Hospital, Tianjin, China

1.2 CT Scan Techniques

1.2.1 Orbit

The size, location and structure of eyeball and intraorbital lesions, especially subtle bone changes, can accurately reflect direct or indirect signs of orbital fracture. Besides, relationship between mass and adjacent blood vessels and the extent of inflammation can be evaluated by location of foreign body.

1.2.1.1 Basic Acquisition Technique

Scanning baseline: Reid's base line (RBL) is taken as the baseline of transverse plane, spanning from supraorbital border to infraorbital border, covering the entire orbit. Coronal plane can better show the orbital roof, orbital floor, orbital apex and superior and inferior rectus muscles than transverse plane and clearly indicates the relations between optic nerve and extraocular muscle.

Field of view (FOV) is between 14 cm × 14 cm and 16 cm × 16 cm. Matrix is not smaller than 512 × 512. Reconstruction of bone algorithm and soft tissue algorithm. Bone window: window width: 3000–4000 HU, window level: 500–700 HU; Soft tissue window: Window width: 300–400 HU, window level: 40–50 HU. Voltage ≥ 120 kV, current ≥ 200 mA (adjust according to body weight, age, and other factors). Acquisition slice thickness ≤ 1.25 mm, and pitch ≤ 1.

1.2.1.2 Image Reconstruction and Post-Processing

Non-enhanced CT scan is a conventional method for eye CT examination. When the lesions need to be observed from different angles, post-processing techniques such as multiple planar reformation (MPR) and 3D reconstruction are needed [1, 2].

H. Li et al. (eds.), *Radiology of Infectious and Inflammatory Diseases - Volume 2*,
https://doi.org/10.1007/978-981-16-8841-6_1

When performing reconstruction of conventional bone algorithm and soft tissue algorithm, the reconstruction slice thickness of the source image is equal to the acquisition slice thickness, and the slice increment is less than 50% of the acquisition slice thickness. Reconstruction parameters are selected as required (images with a smaller slice thickness can be reconstructed in case of any suspicion). MPR imaging is recommended in most cases. Coronal plane and sagittal plane are commonly used for reconstruction. Besides, oblique sagittal plane is also an option as required. Bone changes are mainly observed by bone algorithm images, while other lesions by soft tissue algorithm images. Post-processing methods, including maximal intensity projection (MIP) and shaded surface display (SSD) imaging, can be selected as demanded.

1.2.1.3 Enhanced Scan

It is mainly used for soft tissue lesions through soft tissue algorithm reconstruction, and can raise the density difference between normal tissue and lesion tissue, thus providing better qualitative diagnosis for the lesion and showing extraocular involvement. Refer to *Guidelines for the Use of Iodine Contrast Agents (Edition 2)* [3] for the application of contrast agents. The injection rate of contrast agent is 2.0–3.0 ml/s, and the dose for adults is 60.0–100.0 ml (the dose for children is 1.0–1.5 ml/kg). The injection dose must not exceed what is allowed in the product manual, with delay time depending on the lesion and the equipment.

1.2.1.4 Privileged Sites: Optic Canal

For optic canal fracture or optic nerve tumor.

1. Transverse Plane: Connecting line between apex of nasal bone and superior border of posterior clinoid process is taken as the baseline, spanning from superior wall and inferior wall of optic canal. Bone window is used.
2. Coronal Plane: The baseline is taken as perpendicular to the RBL, spanning from orbital apex to anterior clinoid process.
3. Double Oblique Sagittal Plane: The baseline is taken as being parallel to the long axis of optic canal, including medial and lateral wall of optic canal. Bone window is used.

1.2.2 Temporal Bone

Show the changes in bony structures, such as external auditory canal, middle ear and inner ear, as well as the extent of lesions and involved bony structures.

The temporal bone is mainly composed of complex, subtle bony structures and gases, which is suitable for high-resolution CT imaging [4, 5].

1.2.2.1 Basic Acquisition Technique

Supraorbitomeatal line (SML) is taken as the baseline for transverse plane scanning.

FOV is between 14 cm × 14 cm and 18 cm × 18 cm. Matrix is not smaller than 512 × 512. Reconstruction of bone algorithm and soft tissue algorithm. Bone window: window width: 3000–4000 HU, window level: 500–700 HU; As for soft tissues such as ligament, tendon, and tympanic membrane and stapes, window width is 3000–4000 HU, and window level is not greater than 200 HU. Soft tissue window: Window width: 300–400 HU, window level: 40–50 HU. Voltage ≥ 140 kV, current ≥ 300 mA. The minimum slice thickness of multi-row CT is selected as the slice thickness, which is not greater than 0.75 mm, with pitch less than 1 (The smaller the pitch, the higher the image quality. Pitch of 0.5 is recommended). The scanning baseline should keep away from crystalline lens.

1.2.2.2 Image Reconstruction and Post-Processing

1. MPR: the most common technique for clinical image post-processing. It can be used to obtain coronal plane and sagittal plane images in the imaging diagnosis of the aural region. If a transverse plane image is bilaterally asymmetric, it can be adjusted to bilaterally symmetric via MPR (Fig. 1.1a).
2. Curved Planar Reformation (CPR): The curved surface of curves drawn through the region of interest can be expanded into a plane. In the aural region, it can show labyrinthine segment, tympanic cavity segment and mastoid process segment of facial nerve canal in one plane. It is worthy of mention that CPR may occasionally fail to truly reflect the spatial relationships of anatomical structures.
3. MIP: It can display the morphology of the ossicle. When compared with MPR, thin slice MIP delivers a higher definition in the display of incudomalleolar joint level (Fig. 1.1b).
4. Volume Rendering (VR): To show the general shape of temporal bone. VR is similar to SSD in the display of ossicular chain, which can clearly show the morphology of malleus and incus. It is, however, not as good as MPR in terms of displaying the stapes. As for labyrinth of inner ear, the voxel displayed by VR includes endolymph and perilymph. For this reason, VR shows the morphology of bony labyrinth rather than membranous labyrinth (Fig. 1.2).

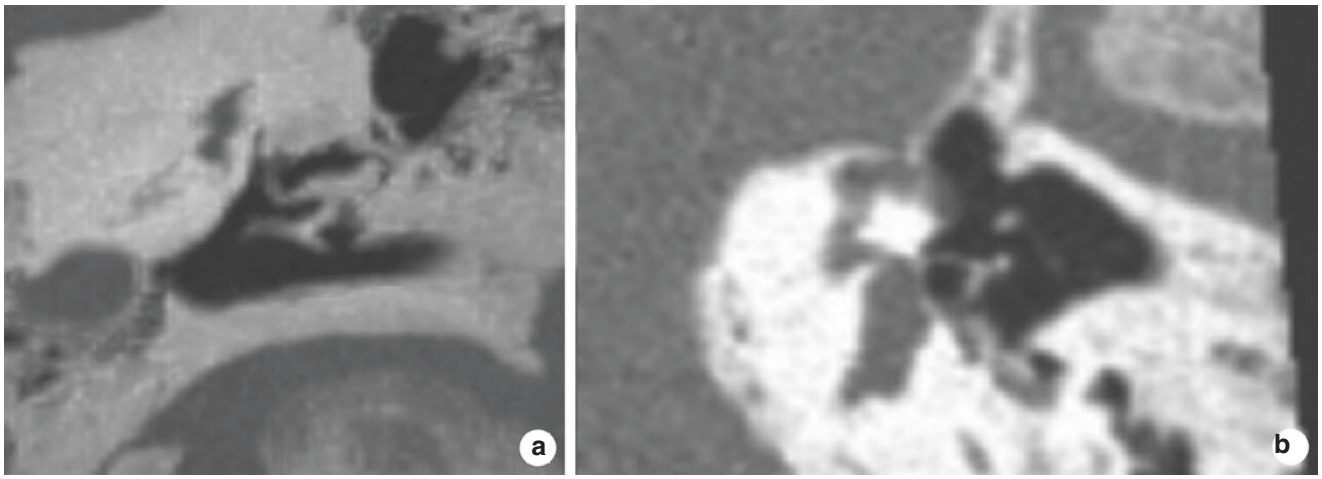

Fig. 1.1 Temporal bone image reconstruction and post-processing. (**a**) MPR showing stapes; (**b**) MIP showing ossicle

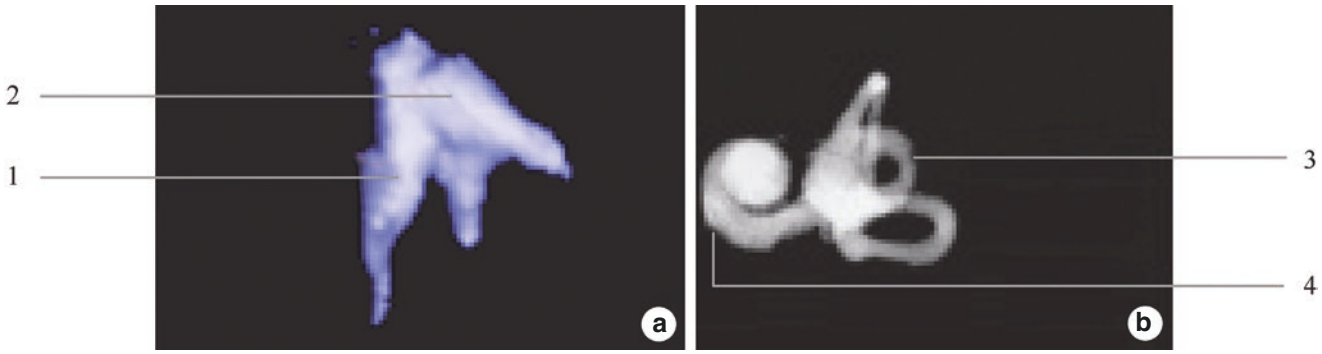

Fig. 1.2 Temporal bone VR technique. (**a**) VR showing ossicle; (**b**) VR showing labyrinth of the inner ear; 1. Incus; 2. Malleus; 3. Semicircular canal; 4. Cochlea

5. CT Virtual Endoscopy (CTVE): It can be used to observe from the external auditory canal, middle ear cavity, ossicle, and fundus meatus acustici interni (Fig. 1.3).

1.2.3 Paranasal Sinus

CT is commonly used to show the subtle bony structures of paranasal sinus, manifestations of various diseases and relationships with adjacent anatomical structures.

1.2.3.1 Basic Acquisition Technique

RBL is taken as the baseline for transverse plane scanning, spanning from hard palate to frontal sinus superior border (Fig. 1.4a); Coronal plane reconstruction: Perpendicular to RBL, spanning from frontal sinus anterior border to cervical vertebra anterior border or sphenoid sinus posterior border (Fig. 1.4b). Scanning can be properly expanded in range based on specific situation [6].

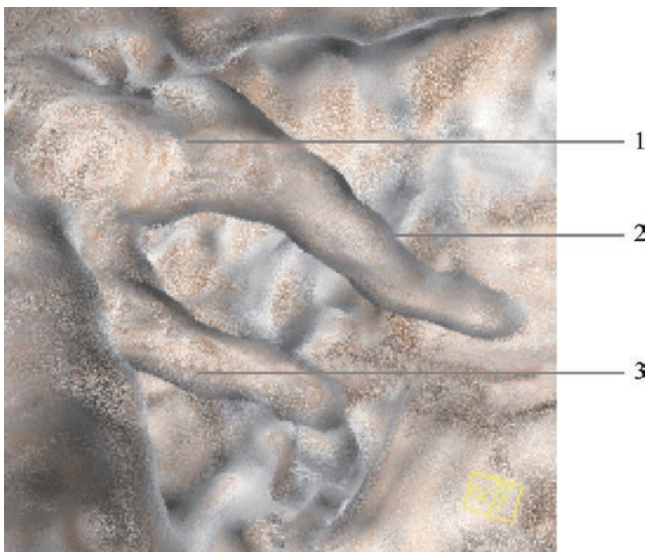

Fig. 1.3 CTVE showing ossicle. 1. Manubrium mallei; 2. Collum mallei; 3. Long crus of incus

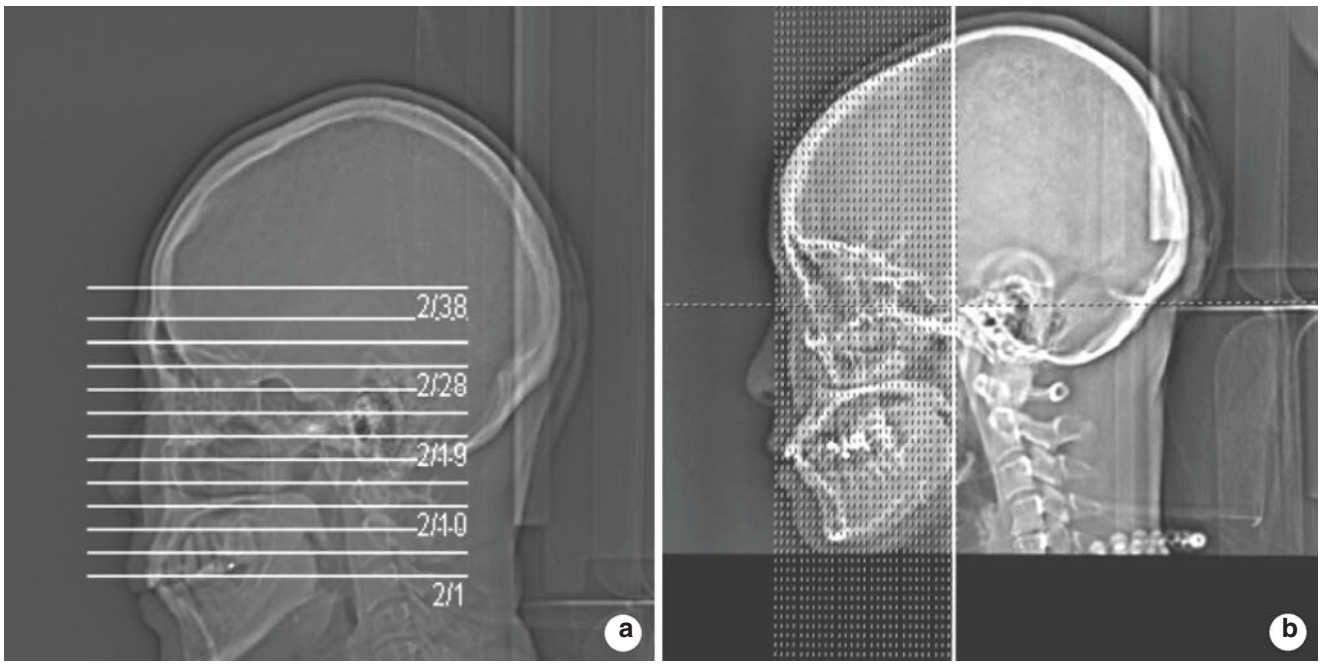

Fig. 1.4 Paranasal sinus scanning image. (**a**) Scanning for paranasal sinus at transverse plane; (**b**) Reconstruction of paranasal sinus at coronal plane

FOV is between 14 cm × 14 cm and 16 cm × 16 cm. Matrix is not smaller than 512 × 512. Reconstruction of bone algorithm and/or soft tissue algorithm-bone window: window width: 2000–4000 HU, window level: 500–700 HU; Soft tissue window: Window width: 300–400 HU, window level: 40–50 HU. Voltage ≥ 120 kV, current ≥ 200 mA. Slice thickness ≤ 1.25 mm, and pitch ≤ 1.5 (such as 0.7–1.0) [2].

1.2.3.2 Image Reconstruction and Post-Processing

Standard algorithm or bone algorithm reconstruction. Reconstruction of bone algorithm and soft tissue algorithm can be employed while observing soft tissue, so as to observe whether the paranasal sinus bone is damaged. CT imaging for paranasal sinus mainly uses bone algorithm and may need sagittal plane reconstruction occasionally. 3D image reconstruction and post-processing are carried out based on clinical demands, including maximal intensity projection, shaded surface display reconstruction and virtual reality [7].

1.2.3.3 Enhanced Scan

Generally, enhanced scan is necessary for differential diagnosis of soft tissue lesions. Besides, enhanced scan can be used to figure out the extent of intracranial tumor involvement or blood supply of lesion in case of any bone destruction at skull base. Automatic syringe and nonionic iodinated contrast agent, with a total volume of 50.0–70.0 ml at an injection speed of 2.0–3.0 ml/s, are recommended. The delayed scanning time is a function of the lesion condition. As for regular vascular lesions, scanning starts 20 s later since the injection of contrast agent; as for infectious and inflammatory lesions, scanning starts 40 s later since the injection of contrast agent [8].

1.2.4 Pharynx

Pharynx CT examination is essential for determining the position and extent of the lesion, its relationship with important peripheral anatomical structures, and any lymph node metastasis that occurred [4, 9–11].

1.2.4.1 Basic Acquisition Technique

RBL is taken as the baseline for transverse plane scanning, during which the patient needs to perform eupnea or breath-holding without swallowing.

FOV is between 14 cm × 14 cm and 16 cm × 16 cm. Matrix is not smaller than 512 × 512. Soft tissue window: Window width: 300–400 HU, window level: 40–50 HU. Bone window: Window width:2000–4000 HU, Window level: 200–700 HU. Voltage ≥ 120 kV, current ≥ 200 mA; Acquisition slice thickness and pitch are not greater than 0.75 mm and 1.0 mm respectively.

1.2.4.2 Image Reconstruction and Post-Processing

Reconstruction slice thickness of source image is equal to acquisition slice thickness. Slice increment is less than 50%

of acquisition slice thickness. 3D image reconstruction and post-processing, including MIP, SSD, and virtual endoscopy, are employed based on clinical needs.

1.2.4.3 Enhanced Scan

The contrast agent is injected at a flow rate of 2.0 ~ 3.0 ml/s, with a total volume of 80.0 ~ 100.0 ml. The delayed scanning time depends on actual conditions of the disease and equipment; Soft tissue algorithm reconstruction.

1.2.5 Larynx

1.2.5.1 Basic Acquisition Technique

RBL is taken as the baseline for transverse plane scanning, during which swallowing and coughing should be avoided. The scanning ranges from superior portion of hyoid bone to inferior portion of cricoid cartilage. The scanning direction should be parallel to the true vocal cord or false vocal cord. Continuous phonation of "Yi" can better display larynx structures such as posterior pharyngeal wall, aryepiglottic fold, piriform recess, and vocal cord.

FOV is between 14 cm × 14 cm and 16 cm × 16 cm. Matrix is not smaller than 512 × 512. Soft tissue window: Window width: 300–400 HU, window level: 40–50 HU. Bone window: Window width:2000–4000 HU, Window level: 200–700 HU. Voltage ≥ 120 kV, current ≥ 200 mA; Acquisition slice thickness and pitch are not greater than 0.75 mm and 1.0 mm, respectively. Soft tissue algorithm is employed with the minimum slice thickness without reconstruction increment [9].

1.2.5.2 Image Reconstruction and Post-Processing

Coronal plane reconstruction baseline is parallel to the longitudinal diameter of cervical vertebra at sagittal plane, while sagittal plane reconstruction is parallel to larynx cavity airway at coronal plane.

1.2.5.3 Enhanced Scan

In regular enhanced scan, iodinated contrast agent (dosage for adult: 60.0–80.0 ml; dosage for children: 2.0 ml/kg) is injected intravenously via a high-pressure injector. Injection rate is 2.5–3.0 ml/s [10], and the delayed scanning time is 35–40 s.

Spiral computed tomography (SCT) can obtain 2D and 3D reconstructed images with volume data without increasing the patient's exposure. Currently, MPR (Fig. 1.5), CTVE and virtual reality (Fig. 1.6) are commonly used in the clinic for image post-processing, which can obtain high-quality, high-resolution, multi-directional, and multi-angle stereo images. This facilitates the display and diagnosis of lesions.

1.2.6 Oral and Maxillofacial Region

Oral and maxillofacial region, characterized by diverse anatomical structures and complicated positional relationship, mainly employs CT to detect the lesions therein at transverse plane, sagittal plane and coronal plane. The diseases of infratemporal fossa, pterygopalatine fossa, parotid gland, submandibular gland, nasopharynx, oropharynx, floor of mouth, and temporal-mandibular joint can be evaluated with CT in different directions. Position and extent of the lesion and the relationship with peripheral structures are evaluated.

1.2.6.1 Basic Acquisition Technique

RBL is taken as the baseline for transverse plane scanning.

FOV is between 14 cm × 14 cm and 16 cm × 16 cm. Matrix is not smaller than 512 × 512. Reconstruction of bone algorithm and/or soft tissue algorithm-bone window: window width: 2000–4000 HU, window level: 500–700 HU;

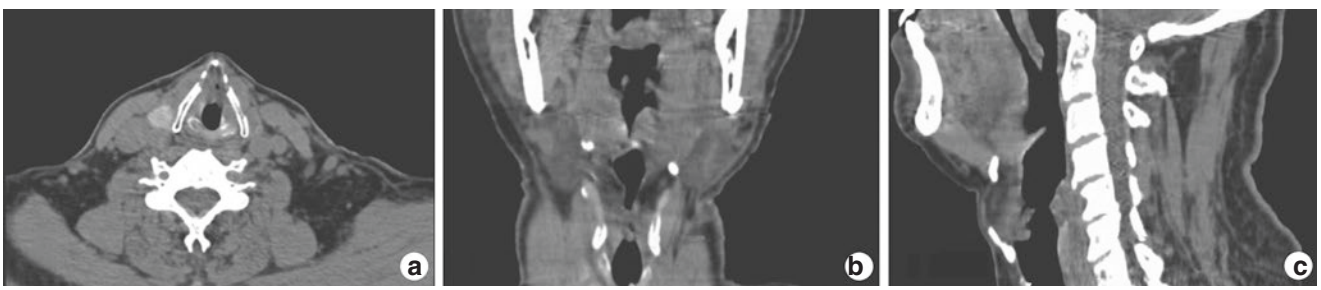

Fig. 1.5 CT and reconstruction image of larynx at transverse plane. A 58-year-old male patient, who was admitted to hospital due to larynx discomfort. Volume data larynx non-enhanced scan image (**a**) is acquired through larynx helical scan, and is subject to reconstruction and post-processing to obtain images at coronal plane (**b**) and sagittal plane (**c**), displaying accurately, clearly the position, morphology, and density of the vocal cord polyp, as well as its relationship with peripheral tissues in all directions. This delivers more effective images to clinical treatment

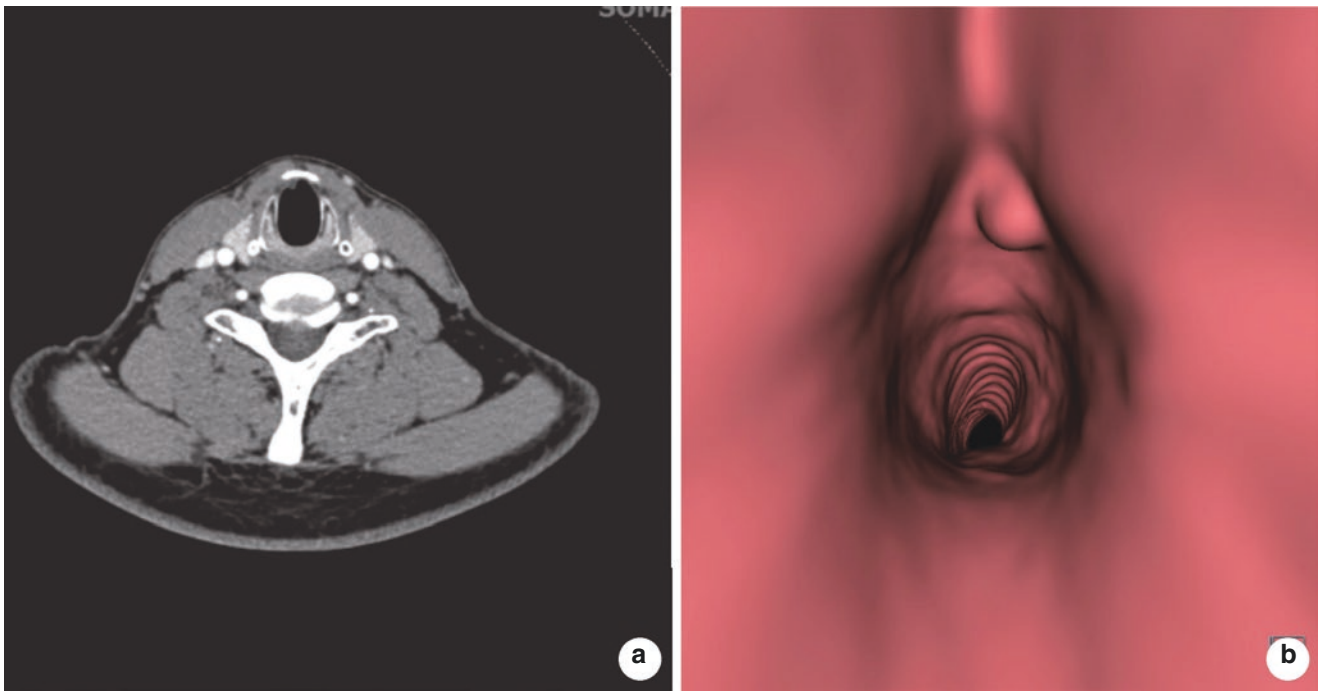

Fig. 1.6 Enhanced CT and CT virtual endoscopy (CTVE) images of larynx at transverse plane. A 46-year-old male patient, who suffered with chronic onset and had previous history of malignant laryngeal neoplasm resection, was admitted to hospital 4 month later since relapse. (**a**) Enhanced CT scan of larynx arterial phase shows a nodule-like mass located to the right of cricothyroid membrane midline, with smooth margin; (**b**) CTVE indicates that the nodule is located to the right of cricothyroid membrane at infraglottic portion, with smooth surface. The display of the lesion is extremely clear. The postoperative pathology shows inflammatory granuloma

Soft tissue window: Window width: 300–400 HU, window level: 40–50 HU. Voltage ≥ 120 kV, current ≥ 200 mA. Acquisition slice thickness ≤ 1.25 mm, and pitch ≤ 1.0 (The smaller the pitch, the higher the image quality. Pitch of 0.5 is recommended).

1.2.6.2 Image Peconstruction and Post-Processing

Frankfort plane is taken as the baseline for transverse plane reconstruction. The reconstructed slice thickness is equal to the scan slice thickness, with slice increment less than 50% of the scan slice thickness. Bone algorithm reconstruction is used (If the patient needs to be observed for soft tissues in case of any tumor or tumor-like lesion, both bone algorithm and soft tissue algorithm should be used for reconstruction.). Let us take the temporal-mandibular joint as an example.

Image of required sections is acquired with MPR technique, or other section or curved planar reformation can be acquired as needed. The temporal-mandibular joint disc (window width: 1000 HU/200 HU) can be displayed by a reconstructed sagittal plane that passes through the middle point of medial-lateral diameter of condyloid process and is perpendicular to the long axis of the medial-lateral diameter.

1. SSD: It can be used to obtain the 3D anatomical image of the entire temporal-mandibular joint, and the image can be rotated freely to obtain the overall impression of temporal-mandibular joint (Fig. 1.7).
2. MPR: The method is to draw a line on a transverse plane CT image as required, and then reconstruct a series of transverse planes along the line to obtain a 2D reconstructed image of the line plane, including coronal plane, sagittal plane and oblique plane images at any angle (Fig. 1.8).
3. MIP: In the post-processing for images of certain structure with MIP, thin maximal intensity projection (MIP) is often employed to avoid excessive overlap of the structure (Fig. 1.9).

1.2.6.3 Enhanced Scan

It is recommended to perform MR enhanced scan, rather than CT enhanced scan, for lesions in soft tissue and articular disc. If MRI is not available or an enhanced CT scan is preferred, an automatic syringe and nonionic iodinated contrast agents, with a total volume of 80.0–100.0 ml at an injection rate of 2.0–3.0 ml/s, are recommended. The delayed scanning time depends on actual conditions of the disease and equipment. Soft tissue algorithm is employed for reconstruction.

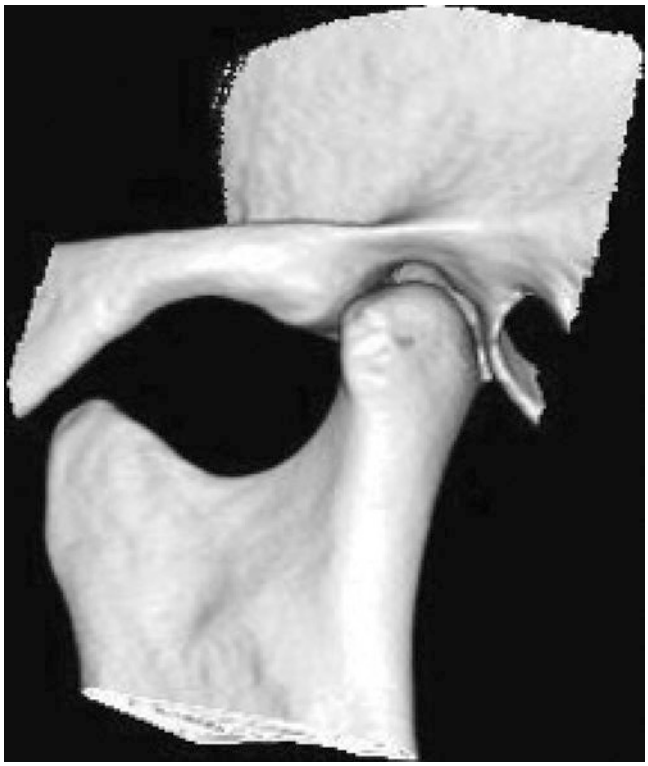

Fig. 1.7 SSD imaging of temporal-mandibular joint

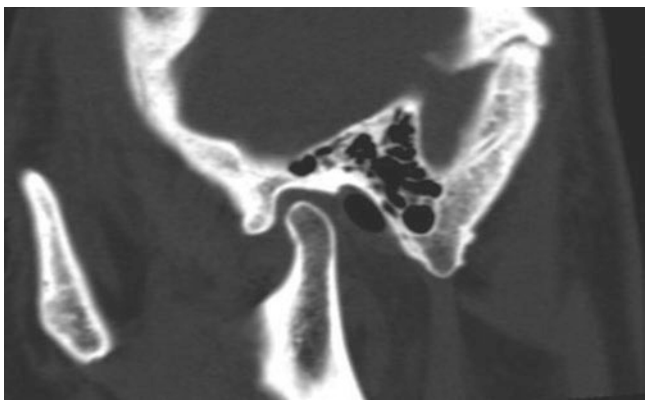

Fig. 1.8 MPR image of temporal-mandibular joint (at sagittal plane)

1.2.7 Neck

CT evaluates anatomical structures of the neck, as well as location and extent of cervical lesions, whereas CTA observes the vasculopathy or lesion-blood vessel relationship.

1.2.7.1 Basic Acquisition Technique

Scan spanning from thoracic inlet to angle of mandible [11].

FOV is between 10 cm × 10 cm and 14 cm × 14 cm. Matrix is not smaller than 512 × 512. Reconstructed slice thickness

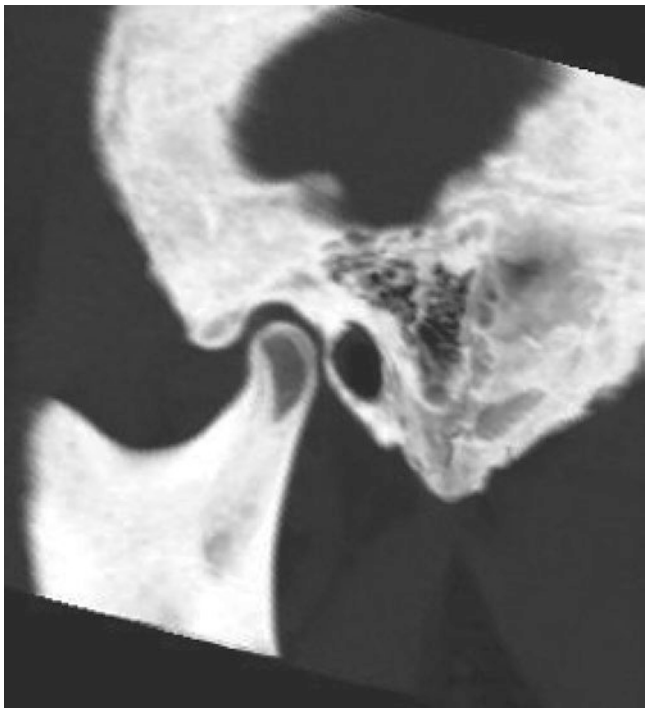

Fig. 1.9 MIR image of temporal-mandibular joint (at sagittal plane)

and increment are not greater than 5 mm. Regular soft tissue algorithm is employed. Window width: 250–350 HU, window level: 30–50 HU. If the lesion invades bone tissues, the bone algorithm needs to be added, with a window width of 1000–1500 HU and a window level of 500–700 HU.

1.2.7.2 Image Reconstruction and Post-Processing

MPR, MIP, SSD, and VR are used for post-processing and multi-directional observation. As for lesions in cervical space, it is necessary to observe the tumor–blood vessel relationship and the extent to which inflammatory lesions involve peripheral structures. The reconstructed line of coronal plane is parallel to the longitudinal diameter of carotid artery at sagittal plane, and the reconstructed line of sagittal plane is parallel to the longitudinal diameter of carotid artery at coronal plane. Maximal intensity projection can be used as necessary to show the carotid artery images more directly. As for paravertebral tumors, despite tumor—carotid artery relationship, it is also necessary to observe the tumor—cervical vertebra relationship, in particular the relationships between the tumor and intervertebral foramen or vertebral canal. To show the relationships between the tumor and the above-mentioned structures, angle of the recombination line should be changed repeatedly. Besides, soft tissue and bone window should be selected under normal circumstances to achieve the optimum efficiency.

1.2.7.3 Enhanced Scan

Enhanced scan is often needed for neck, to understand the extent of involvement, distinguish blood vessels from lymph nodes and identify location and nature of the mass. Dosage of contrast agent for adult is 60.0–80.0 ml; dosage for children is 2.0 ml/kg. Injection rate is 2.5–3.0 ml/s, and the delayed scanning time is 30 s. If it is necessary to observe the tumor-artery relationship, the delayed scanning time is between 15 and 17 s.

1.2.8 Salivary Gland

CT has a high spatial resolution, thus can accurately display the relationship between salivary gland and peripheral tissues. For this reason, it is the first choice for salivary gland diseases, especially calculus or inflammatory lesions.

1.2.8.1 Basic Acquisition Technique

RBL is taken as the baseline for transverse plane scanning, with scan range based on clinic demands. Three pairs of major salivary glands can be scanned from infraorbital border to hyoid bone. Slice thickness is 2.0 mm.

FOV is between 14 cm × 14 cm and 16 cm × 16 cm. Matrix is not smaller than 512 × 512. Soft tissue algorithm, soft tissue window: Window width: 200–450 HU, window level: 300–600 HU. If it is necessary to observe bone conditions, the bone algorithm needs to be added. Bone window–window width: 1500–2000 HU, window level: 300–600 HU. Voltage ≥ 120 kV, current ≥ 200 mA. Acquisition slice thickness ≤ 1.25 mm, and pitch ≤ 1.0.

1.2.8.2 Image Reconstruction and Post-Processing

Line perpendicular to RBL is taken as the reconstructed baseline for coronal plane. Reconstructed baseline at sagittal plane is parallel to median sagittal plane, or other section or curved surfaces are reconstructed as necessary. Slice thickness is not greater than 2 mm or adjusted according to clinical conditions, and slice increment is not greater than the slice thickness.

1.2.8.3 Enhanced Scan

Enhanced CT examination can be used for most salivary gland lesions, such as calculus, inflammation, or infection. Dosage for adult is 80.0–100.0 ml (dosage for children is 2.0 ml/kg). Injection rate is 2.0–3.0 ml/s. The delayed scanning time may depend on the lesion and equipment conditions. Having said that, 60 s delayed time is sufficient for the optimal tissue and vascular enhancement in most cases. Some institutes use separate bolus injection to further refine the scanning parameters, with a delayed time of 120 s. In venous phase, the image acquisition should span from Circle of Willis to aortic arch, while the residual parameters and image reconstruction are consistent with non-enhanced scan [12].

1.2.9 Skull Base

Different from conventional brain scan, scan of skull base requires two kinds of window images: soft tissue window that observes the normal structures of soft tissue and blood vessel and pathologic change therein, and bone window that observes anatomical structure and pathological changes of bones [13].

1.2.9.1 Basic Technique

Supraorbitomeatal line (SML) is taken as the baseline for transverse plane scanning. FOV is between 14 cm × 14 cm and 18 cm × 18 cm. Matrix is not smaller than 512 × 512. Reconstruction of bone algorithm and soft tissue algorithm. Bone window: window width: 3000–4000 HU, window level: 500–700 HU; Soft tissue window: Window width: 300–400 HU, window level: 40–50 HU. Voltage ≥ 140 kV, current ≥ 300 mA. The minimum slice thickness of multi-row CT is selected as the slice thickness, which is not greater than 0.75 mm, with pitch less than 1 mm (The smaller the pitch, the higher the image quality. Pitch of 0.5 is recommended). The scanning baseline should keep away from crystalline lens.

Reconstruction of images with different slice thicknesses. Soft tissue window prefers the slice thickness of 1.5 mm, which enhances, rather than reduces, the quality of post-processed images (such as coronal MPR), thus better helping identify soft tissue structures and analyze soft tissue lesions. Bone window prefers the slice thickness of 1 mm or submillimeter (such as 0.5 mm or 0.6 mm). This is because the thinner slice thickness enables spatial resolution to better help analyze the osseous tissue structures and identify pathologic changes.

1.2.9.2 Image Reconstruction and Post-Processing

1. MPR: the most common technique for clinical image post-processing. It can be used to obtain coronal plane and sagittal plane images in the imaging diagnosis of aural region. If a transverse plane image is bilaterally asymmetric, it can be adjusted to bilaterally symmetric via MPR.
2. As for 3D display of skull base bone with VR, it is necessary to use soft tissue algorithm to reconstruct a group of images, of which the VR images are smooth with a higher quality. This mainly aims to observe changes in overall morphology rather than changes in internal structures of bones.

1.2.9.3 Enhanced Scan

CT scan for skull base diseases (except trauma) often require enhanced scan. This is crucial to confirm the size and location of lesions and the extent of involvement. To observe whether the lesion is enhanced or not, and whether the enhancement is homogeneous or heterogeneous, as well as the enhancement degree is vital to determine the disease nature. Proper injection rate & total dosage of contrast agent and delayed time hold the key to observe vascular changes. Low-dosage test and threshold activation are recommended to ensure sufficient plasma concentration in blood vessels.

1.3 MRI Scanning Technique

MRI, which is free of radiation and provides high resolution for soft tissue, scans from axial, coronal, sagittal and oblique views to deliver multi-directional, multi-sequencing images. Magnetic resonance angiography (MRA) can also be performed to understand lesion–blood vessel relationship, and MR perfusion weighted imaging (PWI) to understand blood supply of tumor. Diffusion-weighted imaging (DWI) can also be used.

Qualitative diagnosis, including changes in morphology, size, density/signal, border, bone and peripheral structures, is determined according to image findings. Infectious diseases can be accurately diagnosed by combination of various imaging examination techniques.

1.3.1 Orbit

1.3.1.1 MRI Scanning Method

Coil

Head coil is commonly used, and surface coil can be used for scanning eyeball or preseptal structures.

Range and Position

RBL is taken as the baseline for transverse plane scanning. Line perpendicular to RBL is taken as the baseline for coronal plane scanning. The baseline for oblique sagittal plane scanning should be parallel to the optic nerve [14].

Scanning Parameters

Slice thickness: 3.0–5.0 mm. slice increment: 0–1.0 mm.

Scanning Sequence

1. Regular non-enhanced scan: Transverse plane T_1 weighted image (T_1WI) and T_2 weighted image (T_2WI) on conventional sequence, and coronal plane fat suppression T_2WI. If mass sees hyperintense in T_1WI, transverse plane fat suppression T_1WI should be increased. Oblique sagittal plane sequence and DWI sequence can be added properly.
2. Enhanced Scan: When tumor nature needed to be further identified, dynamic enhanced scan at transverse plane can be performed to draw dynamic enhancement curves. Enhanced sequence is T_1WI at transverse plane. T_1WI at coronal plane or oblique sagittal plane is optional, among which the better plane is subject to fat suppression.
3. If a patient with suspected varicosity has proptosis when lowering head, pressurized scanning should be performed. It is necessary to perform transverse plane T_2WI sequence scanning first, then strap cuff at patient's neck for pressurization, and re-scan according to regular sequence after neck pressurization [1]. If the patent cannot control eye movement, propeller sequence (Blade and Windmill techniques) can be used for scanning.

1.3.1.2 Effect and Limit

MRI, with a desirable resolution for soft tissue, is the first choice for evaluating complex orbit diseases. It can clearly show extent of complex lesions, including extraocular tumors, vascular malformation, and complicated inflammation. Besides, MRI is also excellent for displaying the extent of malignant orbital diseases, including peripheral nerve tumor invasion, optic nerve invasion, hematogenous or cerebrospinal fluid spreading and metastasis, and intracranial invasion. Although ultrasound is the first choice for eye imaging, MRI can display retrobulbar conditions more precisely. Besides, MRI examination can clearly display eyeball. Having said that, it displays bone cortex and calcification poorly, with in-vivo metal as a contraindication.

New MRI techniques are widely used for optic nerve, mainly including MRI high-resolution imaging and diffusion-weighted imaging (DWI).

In theory, the signal-to-noise ratio (SNR) of 3 T MRI is twice that of 1.5 T MRI, but problems emerge because T_2 relaxation time is shortened, thus reducing the T_2WI image contrast and presenting more chemical artifacts and magnetic susceptibility artifacts. Image quality can be improved with radial gradient-echo volume interpolated breath-hold examination (VIBE) and half-Fourier acquisition single-shot turbo spin-echo imaging [15].

Both acute optic nerve ischemia and acute optic neuritis show limited diffusion. DWI helps to differentiate acute optic neuritis relevant to multiple sclerosis and neuromyelitis optica [15]. Diffusion tensor imaging (DTI) and fiber tractography imaging can further observe integrity of axonal optic nerve and nerve sheath. DTI parameters is closely related to optic neuritis in patients with multiple sclerosis, but the scan time is longer. Future development of new coils and faster high-resolution techniques are promising to remarkably improve the orbital and optic nerve images.

1.3.2 Temporal Bone

1.3.2.1 MRI Scanning Method

Coil

Head quadrature coil or multi-channel coil can be used. When only scanning the outer, middle and inner ear structures, surface coil can be used.

Scanning Position

SML is taken as the baseline for transverse plane scanning. Line perpendicular to RBL is taken as the baseline for coronal plane scanning. Oblique sagittal position should be added for facial nerve scanning (The scanning baseline is parallel to the horizontal facial nerve).

Scanning Parameters

Unless otherwise marked in the specific sequence, slice thickness is generally 2.0 ~ 3.0 mm, slice increment is 0 ~ 0.3 mm, FOV is between 16 cm × 16 cm and 20 cm × 20 cm, and matrix is not smaller than 256 × 256. As for high-resolution T2WI imaging, slice thickness can be 2.0 mm without increment, and matrix is not smaller than 320 × 256.

Scanning Sequence

1. Regular Non-enhanced Scan: Two-dimensional spin-echo is the basic sequence most commonly used in MRI for detecting internal auditory canal small acoustic tumors and whenever enhanced T1WI is needed [4].

   When using three-dimensional gradient recalled echo (3D GRE) and three dimensional-spoiled gradient recalled (3D-SPGR), flip angle is 20°–30° and slice thickness is 1.0–1.3 mm. Head coils can be used for simultaneously scanning both sides.

   When using three-dimensional constructive interference in steady-state (3D-CISS), TR is 12.5 ms, TE is 5.9 ms, flip angle is 30°, with heavily T2 weighted image obtained, to display membranous labyrinth, facial nerve in internal auditory canal and vestibulocochlear nerve (Fig. 1.10a).

   Three-dimensional fast spin-echo (3D FSE) T_2 weighted image: TR is 3000–4000 ms, TE is 102–250 ms, and slice thickness is 1.0–1.5 mm, without increment. Maximal intensity projection post-processing can clearly display images of inner eardrum labyrinth (Fig. 1.10b).
2. Enhanced Scan: Gd-DTPA, which is used as a contrast agent, with a concentration of 469 mg/ml and a dosage of 0.1 ml/kg, can be injected intravenously via a high-pressure injector at an injection rate of 2.5 ml/s. Enhanced scan aims to show facial nerves and lesion in temporal bone lateral to internal auditory canal.

1.3.3 Nose and Paranasal Sinus

1.3.3.1 MRI Scanning Method

Coil

Head quadrature coil, head phase array coil or head and neck joint coil.

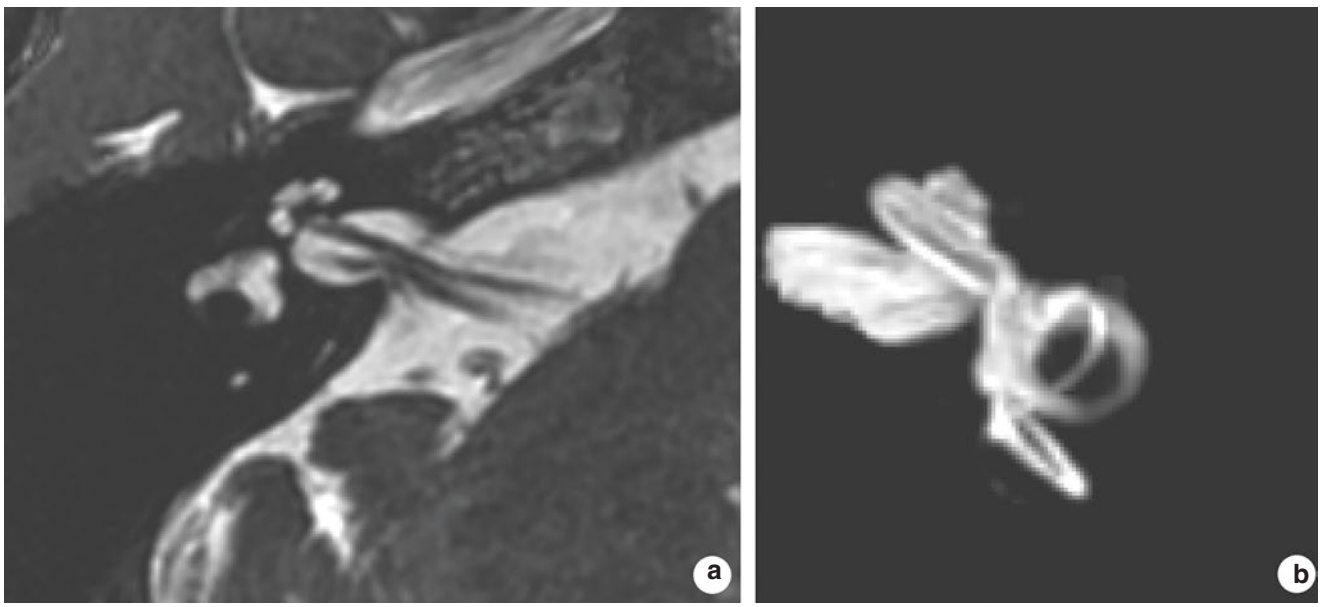

Fig. 1.10 Temporal bone MRI examination technique. (**a**) MRI showing course of nerves in internal auditory canal; (**b**) MRI showing 3D image of membranous labyrinth

Scan Range and Position

RBL is taken as the baseline for transverse plane. Line perpendicular to RBL is taken as the baseline for coronal plane. Baseline for sagittal plane is parallel to median sagittal plane. In principle, the whole lesion is included [6].

1. Transverse Plane: Parallel to hard palate, ranging from superior border of anterior cranial fossa base, at diaphragma sellae level, to inferior border of soft palate (around inferior border of the second cervical vertebra) (Fig. 1.11a).
2. Coronal Plane: Parallel to coronal line of maxillofacial region, or parallel to coronal line of connecting line between nasal tip and nasal root, ranging from anterior border of frontal sinus to posterior border of sphenoid sinus (Fig. 1.11b).
3. Sagittal Plane: Parallel to the median sagittal line of maxillofacial region, including lateral wall of the maxillary sinus on both sides (Fig. 1.11c).

Scanning Parameters

2D sequence typically uses a slice thickness of 3.0–5.0 mm, a slice increment of 0.5 mm, a FOV between 18 cm × 18 cm and 24 cm × 24 cm and a matrix not smaller than 288 × 224; See Tables 1.1 and 1.2 for specific parameters.

Scanning Sequence

1. Regular Non-enhanced Scan: Spin-echo (SE) pulse sequence is commonly used in MRI examination for nose and paranasal sinus.

   Thanks to echo train, fast spin-echo (FSE) sequence has a much shorter acquisition time, thus can acquire T_1WI and T_2WI images quickly.

   The three-dimensional fast spoiled gradient recalled (3D-FSPGR) has a much higher imaging speed, which can be used in dynamic enhanced scan.
2. Enhanced Scan: Gd-DTPA is injected intravenously. Combination of enhanced scan and fat suppression can help the differential diagnosis of lesion and improve the contrast between tumor and peripheral tissues, thereby clearly displaying the extent of the lesion and its involvement of peripheral structures. Dynamic enhancement can display intensity-time variation of tumor blood supply dynamically, which is conducive to the qualitative and differential diagnosis of tumor.
3. MR Hydrography: Hydrography greatly helps diagnose cerebrospinal fluid rhinorrhea and display fistulas. In particular, 3D acquisition can deliver original images with thin slice thickness without increment, thus reducing missed diagnosis. What is more, the images can be subject to various post-processing [8, 16, 17].

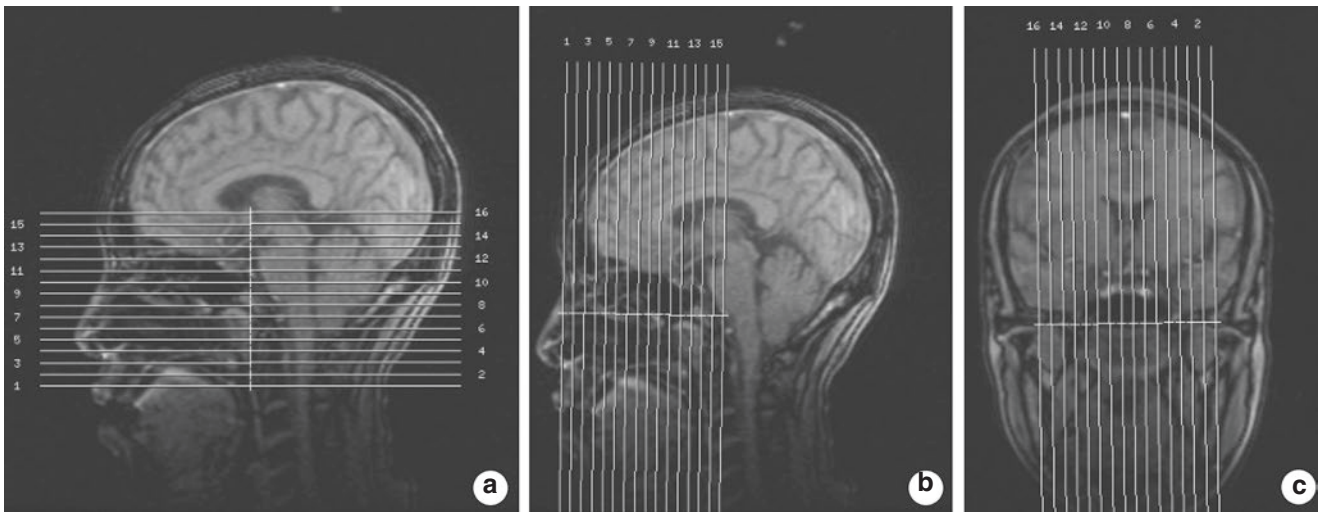

Fig. 1.11 Paranasal sinus scanning image. (**a**) Scanning for paranasal sinus at transverse plane; (**b**) Scanning for paranasal sinus at coronal plane; (**c**) Scanning for paranasal sinus from sagittal plane

Table 1.1 Non-enhanced MRI scan sequences and parameters of paranasal sinus

Sequence description	Position	Repetition time (ms)	Echo time (ms)	Slice thickness/ increment (mm)	Scanning FOV	Matrix	Fat suppression or not	Average time
T1WI	Transverse view	400 ~ 450	12 ~ 15	4/0.5	180 ~ 240	288 × 224	No	2
T2WI	Transverse view	4000 ~ 4500	85 ~ 120	4/0.5	180 ~ 240	288 × 224	No	2
T2WI	Transverse view	4000 ~ 4500	85 ~ 120	4/0.5	180 ~ 240	288 × 224	Yes	2
T2WI	Coronal	4000 ~ 4500	42 ~ 105	4/0.5	180 ~ 240	288 × 224	Yes	3 ~ 4

Table 1.2 Enhanced sequence and parameters of paranasal sinus MRI

Sequence description	Position	Repetition time (ms)	Echo time (ms)	Slice thickness/ increment (mm)	Scanning FOV	Matrix	Fat suppression or not	Average time
T1WI	Transverse view	600	15	5/1	180 ~ 240	288 × 224	Yes	2
T1WI	Coronal	600	15	5/1	180 ~ 240	288 × 224	Yes	2
T1WI	Sagittal	600	15	5/1	180 ~ 240	288 × 224	Yes	2

1.3.4 Pharynx

When displaying pharynx and peripheral tissues and structures, MRI has a higher resolution than CT, thus it can clearly display the lesion's nature and peripheral tissues involvement. MRI is mainly used for evaluating the lesions in nasopharynx, oropharynx, and cervical lymph node [4, 9].

1.3.4.1 MRI Scanning Method

Coil

Head quadrature coil (or multi-channel coil).

Scan Range and Position

RBL is taken as the baseline for transverse plane. Line perpendicular to RBL is taken as the baseline for coronal plane. Sagittal plane reconstructed baseline is parallel to median sagittal plane.

Scanning Parameters

2D sequence typically uses a slice thickness of 3.0–5.0 mm, a slice increment of 0.5 mm, a FOV between 18 cm × 18 cm and 24 cm × 24 cm and a matrix not smaller than 288 × 224.

Scanning Sequence

1. Regular Non-enhanced Scan: Transverse plane T1WI and T_2WI and coronal plane (sagittal plane if necessary) T_1WI are applied. T2WI should be performed on the optimal section showing the lesion. In case of T_1WI showing hyperintense, fat suppression T_1WI should be performed on the optimal section showing the lesion. Equipment with low field intensity or poor chemical shift fat suppression can perform short-time inversion recovery (STIR) sequence.
2. Enhanced Scan: Dynamic enhancement and transverse plane, coronal plane and/or sagittal plane T_1WI are applied. While fat suppression is added at one of these sections.

1.3.5 Larynx

MRI coronal plane imaging can clearly display vocal cord, ventricular fold and laryngeal ventricle, thus helping observe paraglottic space, deep layer of neck and presence of lymphadenectasis. Sagittal plane can display preepiglottic space, epiglottis, and arytenoid cartilage. Transverse plane can clearly show cricoid cartilage, thyroid cartilage and peripheral tissues. Coronal plane and sagittal plane can reflect the relationship between larynx and peripheral structures, while transverse plane is good for left-right contrast.

When compared with CT examination, MRI can show larynx lesions in an earlier and more accurately way. Besides, fat suppression T_1WI and enhanced scan can better display the extent of lesion involvement. CT can directly show bone destruction, whereas MRI is more sensitive to bone marrow infiltration of the lesion in early stage, thus can identify the involvement and metastasis of bone lesion earlier.

1.3.5.1 MRI Scanning Method

Coil

Neck surface coil, head & neck joint coil, and spine phase array coil [10].

Scan Range and Position

RBL is taken as the baseline for transverse plane scanning. Transverse plane is perpendicular to the long axis of larynx cavity, ranging from superior border of epiglottis to inferior border of the six cervical vertebral body; Sagittal plane is parallel to median sagittal line of larynx cavity, covering the lateral soft tissue on both sides of the larynx [15]; Coronal plane is parallel to the long axis of hypopharynx cavity, ranging from thyroid cartilage to posterior mastoid process. Bilateral display is symmetric, showing fine structure of larynx and lymph nodes in neck, without artifacts such as swallowing movement and vascular pulsation [10].

Scanning Parameters

Slice thickness is smaller than 3 mm and greater than slice increment. FOV is between 20 cm × 20 cm and 24 cm × 24 cm or less. Acquisition matrix is 256 × 512.

Scanning Sequence

1. Regular Non-enhanced Scan: T_1WI, T_2WI, and fat suppression (FS) T_2WI sequence or STIR sequence are scanned mainly at transverse plane, and sagittal

plane T_2WI, T_1WI, and coronal plane FS-T_2WI sequences are added.
2. Enhanced Scan: Gadolinium-based contrast agent is injected at regular dosage and rate [10], and transverse plane, sagittal plane and coronal plane FS-T_1WI shall be scanned.

1.3.5.2 Status Quo and Progress of Research

As CT hardware and software techniques continue to develop, CT has become a preferred method for imaging examination of larynx. Among them, CT spectral imaging is a research hotspot in imaging research [18], which can differentiate absorption of different x-ray energy spectra by tissues and lesions, thus displaying anatomical structures in a more precise way. It is of revolutionary significance to realize substance separation and quantitative analysis. As one of the four tools of energy spectrum CT, single energy CT can better detect lesions in subtle larynx anatomical structures with small density difference, thus clearly showing normal structures and contour and extent of lesions [18].

MRI, which is time-consuming and expensive with high imaging requirements, is not the first choice for larynx imaging examination. However, thanks to its high resolution for soft tissue, MRI can assist CT in examination to achieve a higher accuracy rate of diagnosis. It is mainly used for evaluating invasion of cartilage by laryngeal cancer and its postoperative relapse. Dynamic contrast-enhanced MRI (DCE-MRI) uses intravenously injected gadolinium-based contrast agents to evaluate perfusion and permeability of local micro-circulation in lesions. Rapid accumulation of contrast agents in the local vascular system of lesion provides some quantitative information. These techniques are not widely applied in clinic due to lack of quantitative criteria and long post-processing time. Besides, the application experience of MRI perfusion, diffusion, spectrum, and other functional imaging techniques in larynx is yet to be further evaluated [19]. There are few reports on MRI virtual endoscopy, and its clinical value requires further research.

1.3.6 Oral and Maxillofacial Region

It is mainly used for detecting tumors in oral and maxillofacial region and temporomandibular disorders [20, 21], wherein T_1WI and T_2WI are normally applied.

In the routine examination for oral and maxillofacial region, examination for head and face can be performed at transverse plane, coronal plane and sagittal plane, and oblique position can also be employed to observe the lesion extent from different angles.

In temporal-mandibular joint examination, the patient's oral cavity should be scanned at median jaw position and wide-open mouth position from each level. Coronal plane shall be scanned at median jaw position, with a slice thickness of 3.0 mm. Oblique sagittal FSE sequence T_1WI, GRE sequence T_2WI, fat suppression proton density-weighted imaging (PDWI) and oblique coronal PDWI and GRE sequence T_2WI are employed at closed-mouth position. Oblique sagittal fat suppression PDWI and oblique coronal GRE sequence T_2WI are employed at open mouth position. PDWI sequence helps show articular disc. Oblique sagittal FSE T_2WI scanning is performed in case of any exudative lesion suspected.

Enhanced scan is needed for patients with mass, suspected tumors, or suspected articular disc inflammation. Gd-DTPA, which is used as a contrast agent, with a concentration of 469 mg/ml and a dosage of 0.1 mmol/kg, can be injected intravenously via a high-pressure injector at an injection rate of 2.5 ml/s.

1.3.7 Neck

1.3.7.1 MRI Scanning Method

Coil

Neck coil, head and neck joint coil or spine coil can be employed for neck and cervical vertebra scanning.

Scan Range and Position

RBL is taken as the baseline for transverse plane. At coronal plane and sagittal plane, supine position is determined based on organs, parts or structures to be scanned or displayed.

Scanning Parameters

Slice thickness is 3.0–5.0 mm, slice increment is 0.5 mm, FOV is between 18 cm × 18 cm and 24 cm × 24 cm, and matrix is not smaller than 288 × 224;

Scanning Sequence

1. Regular non-enhanced scan: Cervical vertebra MRI mainly involves sagittal plane and transverse plane. Generally, T_1WI employs fast spin echo and T_2WI employs fast spin echo or fast recovery fast spin-echo sequences. To show nerve roots, a dual excitation balanced steady-state free precession sequence can be used.
2. Enhanced Scan: Dynamic enhancement and transverse plane, coronal plane and/or sagittal plane T_1WI are applied, while fat suppression is added at one of these sections.

1.3.7.2 Status Quo and Progress of Research

With a high contrast for soft tissue, MRI can be used to examine pharynx, larynx, thyroid gland, parathyroid gland, neck muscles, soft tissues and lymph nodes. MRI has a

higher resolution for tissues and structures of neck than CT, thus can clearly display lesion's site, extent, nature, and its relationship with peripheral structures. Due to its sensitive to calcification, CT is often used for diagnosing lymph node tuberculosis [22]. What is more, MRI can identify the cystic features of cystic lesions. CT is most commonly used for detecting neck infection and differentiating reactive hyperplasia and suppurative lymph node. Having said that, given the ionization radiation of CT, it is recommended to use MRI in initial examination for children. In the differentiation of infectious and metastasizing lesions of lymph nodes, DWI, and dynamic contrast-enhanced MRI can be used as supplementary to improve the sensitivity and specificity of diagnosis. CT and MRI have their own comparative strength in diagnosing inflammatory and infectious diseases of spinal peripheral soft tissues. For example, when diagnosing calcific tendinitis of longus colli, CT is more sensitive than MRI because of hydroxyapatite and other calcium salts deposited in tendon. In the examination for soft tissue infection peripheral to spine, both CT and MRI can determine the extent of infection, wherein CT is more sensitive to bone destruction of the spine arising from infection, while MRI can better observe the extent of spinal dura mater and spinal cord compression caused by infection [23]. In addition, although CT is the most commonly used technique for evaluating necrotizing fasciitis, it is not effective in differentiating necrotizing fasciitis from non-necrotizing fasciitis due to its poor specificity. By contrast, MRI is a golden standard for diagnosing necrotizing fasciitis, with a whopping 93% of sensitivity [24]. Both CT and MRI are employed, and complement each other, in the observation of neck tissue injury caused by radiotherapy. CT excels in observing soft tissue injury caused by radiotherapy and osteoradionecrosis, while MRI can better observe injury of central nervous system and spinal cord injury caused by radiotherapy. Ultrasound is the preferred in examination of thyroid gland diseases, such as thyroiditis and nodules, but CT and MRI can better observe the extent of the lesion and its relationship with important peripheral tissue structures.

1.3.8 Salivary Gland

MRI examination, boasting good soft tissue contrast and multi-plane data acquisition, has great advantage in salivary gland imaging, thus making it a commonly used method for evaluating salivary gland tumor lesions.

1.3.8.1 MRI Scanning Method

Coil

Head and neck joint coil or head coil is employed.

Scan Range and Position

The scan range is adjusted according to the lesion. As for parotid gland, scanning ranges from OML to mental region of mandible. Patients should be instructed to close their mouth during scanning.

Scanning Parameters

As for regular acquisition, FOV $\leq$ 25.0 cm × 25.0 cm, slice thickness $\leq$ 5.0 mm, and slice increment $\leq$ 1.0 mm. The FOV, slice thickness and increment are adjusted according to the region of interest.

Scanning Sequence

1. Regular Non-enhanced Scan: Axial position plus coronal position are applied, with sequences including SE or FSE sequence T_1WI, STIR T_1WI, STIR T_2WI.
2. Enhanced Scan: Anterior axial position, sagittal, and coronal T_1WI, as well as posterior axial position and coronal fat suppression T_1WI are enhanced. Enhanced scan uses Gd-DTPA as a contrast agent with a concentration of 469 mg/ml and a dosage of 0.2 mmol/kg. The contrast agent is given from elbow veins by bolus injection with a high-pressure injector at an injection rate of 2.0 ml/s.

Magnetic Resonance Sialography (MRS)

Heavily T2 weighted techniques are used to evaluate sialodochium lesions via spittle development.

The patient wearing head coil enters in supine position, head first. FOV should cover the whole region of interest, and scanning ranges from mastoid process tip to vocal cord. Acquisition sequence should include axial non-enhanced T_1WI SE sequence, axial non-enhanced T_2 half-Fourier acquisition single-shot turbo spin-echo (HASTE) sequence and coronal STIR sequence. The patient should hold sialagogue (citric acid or vitamin C) in oral cavity for 30s and then swallow it. After that, the patient should be instructed to avoid swallowing during acquisition.

After applying the sialagogue, high-resolution image acquisition can be performed for gland of interest. Parotid gland uses oblique sagittal thick-layer positioning, with axial surface parallel to zygomatic arch, and coronal plane parallel to zygomatic arch/mental protuberance. The optimum imaging position for submandibular gland: axial plane is parallel to mandible body and coronal plane is parallel to zygomatic arch/mental protuberance. T2 HASTE sequence and inversion recovery turbo spin-echo sequence are acquired at axial and oblique coronal positions, with a slice thickness of 20 mm. At last, FOV is acquired, positioned, and determined with the above-mentioned T_2WI. 3D-CISS sequence or sampling perfection with application optimized contrasts using different flip angle evolution (SPACE) sequence acquisition is performed at oblique axial position.

MR Imaging Sequence of Facial Nerve Parotid Segment

Facial nerve extracranial segments leave skull from stylomastoid foramen and pass through parotid gland in a curved shape. In conventional MRI images, facial nerves show slightly hypointense T_1WI, wherein parotid segment does not present a striking contrast with peripheral tissues, thus making it difficult to differentiate. For this reason, other new imaging techniques are normally applied.

The patient, wearing head coil or small coil, enters in supine position, head first. 3D double-echo steady-state with water excitation (3D-DESSwe) is performed [25], with FOV of 14 cm × 14 cm and slice thickness of 0.5 mm, without increment. After scanning, MPR, CPR, or MIP is performed according to course of facial nerve. 3D-DESSwe sequence is commonly used. On top of that, 3D reversed fast imaging with steady-state precession and diffusion-weighted imaging (3D-PSIF-DWI) [26] sequence can also clearly display facial nerves course in parotid gland.

1.3.9 Skull Base

The anatomical structure of the skull base is extremely complex. Thanks to the new progress in imaging, MRI is capable of delivering multi-directional, multi-parameter imaging with special sequence design, thus can display detailed anatomy of the skull base and help better detect the lesion and determine its nature.

Conventional transverse SE sequences (T_1WI and T_2WI) are the most basic scanning procedures. It is also necessary to scan the target region at coronal plane. Coronal scanning, which can observe skull base from a perspective different from the transverse plane, serves as a necessary supplement for transverse plane when observing cavernous sinus, oval foramen and internal auditory canal (acoustic-facial nerves). Sagittal plane scanning can also supplement the above examination.

Fast SE sequence T_2WI cannot effectively suppress fat signals, making it difficult to distinguish hyperintense of fat from that of lesions in many cases, thus badly hindering the detection of lesions and determination of lesion's range and extent. At this point, T_2WI with fat suppression becomes necessary.

As for lesions in bone marrow cavity of skull base, SE sequence T_1WI, in which the destruction of bone marrow shows hypointense, is much more sensitive than fast T_2WI, where lesion signals are often mixed with signals of peripheral normal bone marrow and are difficult to identify. Therefore, T_2WI with fat suppression should be used for suspected intra-osseous lesions.

TOF vascular imaging sequence is vital to the identification of blood vessels. It is applied for observing not only vascular abnormalities, but also the presence of neurovascular compression in cistern.

3D acquisition techniques with heavily T2 weighted sequence capable of suppressing cerebrospinal fluid pulsation, such as 3D-CISS and FIESTA, are crucial to the observation of intracisternal cranial nerves. In such cases, pulsation artifact of hyperintense cerebrospinal fluid is removed, and the section is submillimeter thin layer, thereby can well display cistemal segment of cranial nerve, cochlea, vestibule, semicircular canal, and cochlear nerve, facial nerve, superior & inferior vestibular nerve in internal auditory canal and their sequences.

In addition, diffusion-weighted imaging (DWI) has made progress in differential diagnosis for skull base lesions. It has been reported in literature that measuring apparent diffusion coefficient (ADC) helps distinguish infection necrosis from tumor necrosis, and people remain divided over the differentiation of tumor classifications, which needs to be further confirmed in future studies [13].

1.4 DSA Technique

Currently, digital subtraction angiography (DSA) is deemed as the golden standard for vascular disease diagnosis. It can precisely locate the vasculopathy and identify its nature and blood supply, providing a good tool for interventional therapy. DSA is limited in the diagnosis of head & neck inflammation, so it is not commonly used for such diseases. It can serve as an auxiliary diagnosis in case of any suspected cervical vasculitis.

1.5 Radionuclide Imaging and PET/CT

The sensitivity of imaging techniques is ever-growing amidst technical development, such as positron emission tomography (PET). PET/CT is essential for the diagnosis and evaluation of solid tumor, lymphoma and other malignant diseases. Furthermore, as for inflammatory reactions arising from various causes, their metabolic activities against neutrophil, monocyte/macrophage, activated lymphocytes and other inflammatory cells are as high as that of tumor cells, with elevated uptake of 18F-fluorodeoxyglucose (18F-FDG). For this reason, lesions of infectious or non-infectious inflammatory diseases show remarkably high uptake on PET/CT [27]. In cases where it is difficult to differentiate inflammatory lesions from neoplastic lesions, PET/CT can serve as an auxiliary examination for differential diagnosis. Besides, PET/CT can evaluate the therapeutic effect of some vasculitis lesions [28].

References

1. Head and Neck Group of Chinese Society of Radiology. Expert consensus on eye CT and MRI examination & diagnosis. Chin J Radiol. 2017;51(9):648–53.
2. Wen J, Ji Y. Imaging examination techniques for head and neck. Zhenjiang: Jiangsu University Press; 2017.
3. Working Group on Contrast Agent Safety of Chinese Society of Radiology. Guideline on use of iodinated contrast agent (edition 2). Chin J Radiol. 2013;47(10):869–72.
4. Editorial Board of Chinese Journal of Radiology. Guideline on CT and MR specification for head and neck (revised draft). Chin J Radiol. 2007;41(9):996–9.
5. Xian J, Ma L, Wang Q. Progress, challenge and future for imaging of ear. Chin J Otol. 2018;16(5):589–92.
6. Shi M, Wang M, Yu J. Guidance for clinical practice of radiologists. Beijing: People's Medical Publishing House; 2013.
7. Head and Neck Group of Chinese Society of Radiology. Expert consensus on nasal CT and MRI examination & diagnosis. Chin J Radiol. 2017;51(9):660–4.
8. Yang Z, Feng F, Wang X. A guide to technique of magnetic resonance imaging. Beijing: People's Military Medical Press; 2013.
9. Chinese Society of Imaging Technology, Chinese Society of Radiology. Expert consensus on CT examination technique. Chin J Radiol. 2016;50(12):916–28.
10. Chinese Society of Imaging Technology, Chinese Society of Radiology. Expert consensus on MRI examination technique. Chin J Radiol. 2016;50(10):724–39.
11. Yu J, Shi M, Fu H. Advanced courses for radiation medicine technique. Beijing: Chinese Medical Multimedia Press; 2016.
12. Atkinson C, Fuller J, Huang B. Cross-sectional imaging techniques and normal anatomy of the salivary glands. Neuroimaging Clin N Am. 2018;28(2):137–58.
13. Liu Y, Ai L, Yang B. Head and neck imaging·skull base. Beijing: People's Medical Publishing House; 2016.
14. Hoch MJ, Bruno MT, Shepherd TM. Advanced MRI of the optic nerve. J Neuroophthalmol. 2017;37(2):187–96.
15. Wan H, He H, Zhang F, et al. Diffusion-weighted imaging helps differentiatemultiplesclerosisandneuromyelitisoptica-relatedacuteoptic neuritis. J Magn Reson Imaging. 2017;45(6):1780–5.
16. Whyte A, Boeddinghaus R. The maxillary sinus: physiology, development and imaging anatomy. Dentomaxillofac Radiol. 2019;48(8):20190205.
17. Wang X, Liu Y, Chen Q, et al. Evaluation of multiparametric MRI differentiating sinonasal angiomatous polyp from malignant tumors. Neuroradiology. 2019;61(8):891–6.
18. Jia Y, He T. Clinical application and research progress of gemstone spectral CT. J Pract Radiol. 2016;32(5):799–801.
19. Sairah RK, Mubarik A, Kathryn W, et al. What's new in imaging for gynecologic cancer? Curr Oncol Rep. 2017;19(12):85.
20. Wurm MC, Behrends TK, Wüst W, et al. Correlation between pain and MRI findings in TMD patients. J Craniomaxillofac Surg. 2018;46(8):1167–71.
21. Kaimal S, Ahmad M, Kang W, et al. Diagnostic accuracy of panoramic radiography and MRI for detecting signs of TMJ degenerative joint disease. Gen Dent. 2018;66(4):34–40.
22. Koch BL, Hamilton BE, Hudgins PA, et al. Diagnostic imaging head and neck. Amsterdam: Elsevier; 2016. p. 193–220.
23. Tso DK, Singh AK. Necrotizing fasciitis of the lower extremity: imaging pearls and pitfalls. Br J Radiol. 2018;91(1088):20180093.
24. Lancerotto L, Tocco I, Salmaso R, et al. Necrotizing fasciitis: classification, diagnosis, and management. J Trauma Acute Care Surg. 2012;72(3):560.
25. Qin Y, Zhang J, Li P, et al. 3D double-echo steady-state with water excitation MR imaging of the intraparotid facial nerve at 1.5T: a pilot study. AJNR Am J Neuroradiol. 2011;32(7):1167–72.
26. Jiang Y, Sun C, Li C. Progress in imaging of intraparotid facial nerve. J Med Imaging. 2018;28(10):1749–52.
27. Liu S, Zhu Q, Li N. Progress in imaging of systemic vasculitis. J Med Imaging. 2018;28(03):492–5.
28. Smiyan S, Holovach I, Komorovsky R, et al. Role of PET/CT in the diagnosis of large vessel vasculitis in a patient with systemic inflammatory response syndrome. Eur J Rheumatol. 2014;1(4):174–5.

Functional and Molecular Imaging Techniques

2

Chen Cao, Shuang Xia, and Wen Chen

Regular imaging can display anatomical structures of the human body in an omnidirectional way. That said, it is unable to show the physiological and pathological processes thereof. As imaging techniques flourish, functional and molecular imaging has moved from experimental research to clinical application, capable of reflecting conditions of human body and analyzing pathogenesis at cellular and molecular level.

2.1 Functional Imaging

Functional imaging has been upgrading amidst the development of modern imaging technology, becoming a powerful tool for diagnosis and differential diagnosis. Moreover, emerging new techniques help display the functional status of organs and tissues in a more accurate way. Mature functional imaging techniques in clinical include CT perfusion imaging (CTP), MR perfusion weighted image (PWI), diffusion weighted imaging (DWI), diffusion tensor imaging (DTI), blood oxygenation level-dependent MRI (BOLD), susceptibility weighted imaging (SWI), and dynamic contrast-enhanced MRI (DCE-MRI).

DWI can reflect the voluntary motion of water molecules in tissues through quantitative measurement, wherein the molecular diffusion extent can be quantified by ADC. The higher the ADC value, the greater the diffusion rate, while the decreased ADC value represents limited diffusion. Diffusion that is direction-dependent is called anisotropy. DTI can reflect anisotropy in multiple directions. In case of ocular abscess or rhinogenic brain abscess, viscous fluid formed by bacteria, inflammatory cells, mucin, and cell fragments in vomica will limit the diffusion of water molecules. In such a case, DWI shows a characteristic hyperintense, and ADC value decreases [1]. Acute optic nerve ischemia and acute optic neuritis can also be manifested as limited diffusion, wherein DWI shows hyperintense, and ADC value decreases. DWI helps identify acute optic neuritis relevant to multiple sclerosis and neuromyelitis optica. DTI fiber tractogrpahy can further show the integrity of optic nerve axon and nerve sheath, and its related parameters have a close correlation with optic neuritis [2]. Alongside that, in case of small lesion of middle ear cholesteatoma and postoperative residual or recurrence, MR enhanced scan can hardly differentiate the lesion from peripheral inflammatory tissue and inflammatory swelling of the middle ear mucosa. At this point, the specific hyperintense on DWI is of value for determining the presence of cholesteatoma.

Magnetic resonance spectroscopy (MRS) performs in vivo biochemical analysis for human lesions, and it can realize quantitative analysis for metabolites in the human body at the molecular level in a non-invasive way. The most commonly used is ^{1}H-MRS, whose resonant peaks mainly include N-aceytl aspartate (NAA), creatine (Cr), choline (Cho), lactate (Lac), lipid (Lip), and myo-inositol (MI). When inflammations in the head and neck result in abscesses, NAA, Cho, and Cr peaks are reduced, and the surrounding anaerobic glycolysis increases, with visible Lac peak [3]. Detecting malignant tumors of masticatory intermuscular space and choline levels in chronic infection with single voxel^{1}H-MRS is of great significance for differentiating the above two diseases.

Perfusion imaging can reflect tissue's micro hemodynamics, which is built on the capacity of blood flow to transfuse nutrient to peripheral tissues via the capillary network. With this technique, blood vessel perfusion can be measured by exogenous intravenous injection of contrast agent, and tissue hemodynamics can be measured by endogenous blood flow labeling, such as arterial spin labeling (ASL). Perfusion imaging can quantitatively analyze cervical lymphadenopathy

C. Cao
Tianjin Huanhu Hospital, Tianjin, China

S. Xia (✉)
Tianjin First Central Hospital, Tianjin, China

W. Chen
Shiyan TAIHE Hospital (Affiliated Hospital of Hubei University of Medicine), Shiyan, China

H. Li et al. (eds.), *Radiology of Infectious and Inflammatory Diseases - Volume 2*,
https://doi.org/10.1007/978-981-16-8841-6_2

of different pathological types and is of certain clinical value in distinguishing benign and malignant cervical lymph nodes. The increased disordered, immature new vessels, incomplete basement membrane of blood vessels, raised pressure in new vessels, faster blood flow, and shortened blood circulation in malignant lymph node lesions result in hyperperfusion of hemodynamics, shortened mean transit time (MTT), and increased permeability surface (PS). By contrast, inflammatory enlarged lymph nodes are, on the contrary, showing desirable specificity [4, 5].

2.2 Molecular Imaging

When compared with regular imaging, molecular imaging focuses more on changes in an early stage caused by abnormal genes, molecules, and proteins, than on morphological changes as regular imaging does. By using molecular probes and multiple imaging techniques, it delivers images for specific target sites in the human body, capable of showing pathophysiological process at cellular and molecular levels in a highly efficient way. Currently, molecular imaging methods that are commonly used include single-photon emission computed tomography (SPECT), positron emission tomography (PET), MR molecular imaging, optical imaging, ultrasound imaging, and CT molecular imaging, with gene expression and protein molecular imaging as the main contributions.

When studying molecular imaging of infection and inflammation, the first task is to identify pathophysiological response after inflammation, based on which the specific targeted contrast agent is selected. Secondly, it is necessary to figure out whether the contrast agent has specificity. When inflammation occurs, local blood flow increases significantly, raising the vascular permeability. Under the action of chemokines and adhesion molecules, leukocytes pass through the blood vessel wall to reach inflammatory lesion area. According to the above changes, which are essential for localization diagnosis of molecular imaging in an early stage of inflammation, a specific contrast agent can be selected. The agent is characterized in that it can deposit on and be rapidly removed from the inflammatory lesion, with high specificity and accuracy, easy labeling, and free of toxic and side effects. Despite high accuracy and specificity for acute and chronic inflammations, radionuclide labeled leukocyte imaging is complicated to operate, thus may induce cross-infection. Technetium-99 bone scan is a good choice when CT fails to fully display the bone destruction and extent caused by inflammation in the external auditory canal. CT is not good at displaying bone changes capable of evaluating the effect of antibiotic treatment, whereas the gallium-67 bone scan can do better [6]. Technetium-99 methylene diphosphonate (^{99}mTc-MDT) three-phase bone scan is highly sensitive and specific to diagnosis for maxillary sinus osteomyelitis.

PET/CT and PET/MRI provide molecular-level imaging targeted at inflammation characteristics with new development direction. Levofloxacin, which can inhibit bacterial DNA racemase, is the third generation of broad-spectrum quinolone antibiotic that is widely used in clinical. The radionuclide marker ^{18}F-levofloxacin of the antibiotic can also be used for targeted imaging of inflammation, with high sensitivity, accuracy, and ease of operation. As ^{18}F-levofloxacin only concentrates in bacterial infection, infectious inflammation can be differentiated from non-infectious ones, and efficacy of inflammatory drugs can be evaluated dynamically, thus providing guidance for clinic treatment. ^{18}F-FDG is a commonly used positron radiopharmaceutical. Inflammatory reaction makes inflammatory cells in lesion area active in glucose metabolism, thus quickly depositing at infected site. In addition, combined with the high resolution of PET, ^{18}F-FDG-PET has its unique advantage. ^{18}F-FDG PET/CT can deliver complete morphological and functional images of sarcoidosis inflammatory activity location, and follow up the evaluation of treatment effect of patients with sarcoidosis. It is of great clinical value, especially for atypical, complicated and multi-system involved cases, which is manifested as increased local metabolism of the lesion. Besides, its sensitivity to sarcoidosis at throat can reach 80%. Many studies on interstitial magnetic resonance lymphography have been carried out in recent years. By using magnetic resonance contrast agents combined with macromolecules, which has a large molecular weight and molecular volume, the technique can make target lymph node maintain at a higher enhanced level within an extended period, thus effectively developing the morphology of lymph vessels and lymph nodes in drainage area for reactive hyperplasia of lymph node and lymph node tumor metastasis. In this sense, it is of value for differentiating cervical lymph node metastasis and reactive hyperplasia [7]. Based on the difference in FDG uptake, PET/CT can also distinguish vertebral body tuberculosis of various pathological types. Caseous necrosis tuberculosis has a low intake of FDG, while proliferative vertebral body tuberculosis and mixed vertebral body tuberculosis have a high FDG uptake, owing to langerhans cells, epithelioid cells and lymphocytes contained therein and the high level of glucose metabolism. Metabolism of FDG indicates the shape, range, and activity of lesions in vertebral body tuberculosis, thus can provide guidance for early diagnosis and differential diagnosis of the disease, while helping observe response of the lesion to drugs for further treatment [8].

References

1. Ferreira TA, Saraiva P, Genders SW, et al. CT and MR imaging of orbital inflammation. Neuroradiology. 2018;60(12):1253–66.
2. Wan H, He H, Zhang F, et al. Diffusion-weighted imaging helps differentiate multiple sclerosis and neuromyelitis optica-related acute optic neuritis. J Magn Reson Imaging. 2017;45(6):1780–5.
3. Liu B, Guo J, Dong G, et al. Comparative analysis of proton magnetic resonance spectroscopy for tuberculosis and malignant tumor of vertebral body. J North Sichuan Med Coll. 2019;3:359–62.
4. Wang B, Tan H, Wang P, et al. One-stop CT gemstone spectral and perfusion imaging for prediction in rabbit axillary lymph nodes. Chin J Med Imaging Technol. 2019;2:175–80.
5. Abdel Razek AAK, Nada N. Arterial spin labeling perfusion-weighted MR imaging: correlation of tumor blood flow with pathological degree of tumor differentiation, clinical stage and nodal metastasis of head and neck squamous cell carcinoma. Eur Arch Otorhinolaryngol. 2018;275(5):1301–7.
6. Balakrishnan R, Dalakoti P, Nayak DR, et al. Efficacy of HRCT imaging vs SPECT/CT scans in the staging of malignant external otitis. Otolaryngol Head Neck Surg. 2019;161(2):336–42.
7. Tzankov A, Dirnhofer S. A pattern-based approach to reactive lymphadenopathies. Semin Diagn Pathol. 2018;35(1):4–19.
8. Tan B, Guo J. Study on ^{18}F-FDG PET/CT imaging features of thoracolumbar tuberculosis. Chongqing Med. 2017;26:74–6.

3 Application of Imaging Techniques in Head and Neck Infectious and Inflammatory Diseases

Yan Gong, Shuang Xia, and Wen Chen

Overview

Head and neck are composed of head and face and neck. The former mainly includes orbit, aural region, nasal cavity and paranasal sinus, salivary gland, oral, and maxillofacial region, while the latter mainly includes pharynx, larynx, trachea, thyroid gland, submandibular gland and other structures. Head and neck infection and inflammatory diseases usually refer to inflammatory diseases caused by various pathogenic microorganisms (including viruses, bacteria, parasites, fungi, rickettsia, spirochetes, etc.) invading various organs and tissues of the head and neck and their spaces. Common diseases include pharyngitis, tonsillitis, laryngitis, epiglottitis, otitis media and rhinosinusitis, among which acute otitis media, acute pharyngitis, acute rhinosinusitis and acute tonsillitis are the most common infectious diseases in the head and neck. The causes of the disease are usually decreased resistance, fatigue, or other reasons, which are caused by the spread of adjacent infection focus. Descending mediastinitis, intracranial infection, orbital infection and respiratory tract obstruction are all severe complications that threaten patients' lives, and the incidence rate accounts for about 12.02% of patients with head and neck multi-space infection.

According to the types of pathogen, it can be divided into bacterial infection (such as *Staphylococcus aureus*, *Pseudomonas aeruginosa*, *Streptococcus haemolyticus*), fungal infection (such as *Candida albicans*, *Candida tropicalis*, *Candida glabrata*), parasitic infection and special pathogen infection (rickettsia, spirochete, etc.). Compared with bacteria, fungi generally do not produce endotoxin and exotoxin, and the pathogenicity of fungi may be associated with the mechanical damage caused by its reproduction in vivo and the enzymes and acidic metabolites produced [1].

Imaging Examination

1. *X-ray Examination*. It can only rely on the change of air show contour and cavity surface morphology in the larynx cavity to observe the abnormalities of the nasopharyngeal roof, the posterior wall of pharynx, the soft palate and epiglottic cartilage, the laryngeal vestibule, glottic region, subglottic region and the posterior wall of pharynx, while X-ray examination is hardly needed for the neck lesions due to the lack of natural density contrast.
2. *CT Examination* It has become a routine examination technique for head and neck diseases, which can show the location and scope of head and neck inflammation, whether it is complicated with abscess formation and the etiology of some inflammatory diseases. If neck inflammation with abscess formation is suspected, enhanced CT examination can determine whether abscess formation exists and whether incision and drainage are needed clinically.
3. *MRI Examination*. It has the advantages of high resolution of soft tissue and no radiation. It can be multi-directional and multi-sequence imaging and can be scanned by different methods such as axial, coronal, sagittal, and oblique. In addition to conventional T_1WI and T_2WI imaging, DWI can also show the scope of inflammatory lesions, the existence of abscess, and so on.

3.1 Bacterial Infection

Overview

Bacterial infections of head and neck are mostly caused by trauma, postoperative, and radiotherapy. Common pathogens are Staphylococcus aureus, Pseudomonas aeruginosa, Streptococcus haemolyticus, etc.

Y. Gong
Tianjin Hospital of ITCWM Nankai Hospital, Tianjin, China

S. Xia (✉)
Tianjin First Central Hospital, Tianjin, China

W. Chen
Shiyan TAIHE Hospital (Affiliated Hospital of Hubei University of Medicine), Shiyan, China

H. Li et al. (eds.), *Radiology of Infectious and Inflammatory Diseases - Volume 2*,
https://doi.org/10.1007/978-981-16-8841-6_3

Imaging Findings

1. X-ray Examination. It cannot reflect the direct signs of bacterial infection, but barium swallow X-ray (BSX) can clearly show the piriform recess of larynx and the duct in the course area of neck esophagus. if there is local filling defect, it can indicate local soft tissue swelling caused by inflammatory reaction.
2. *CT Examination*. CT multiplanar and curved planar reformation and virtual endoscopy can better show the fine bone structure and sinus of head and neck. Bacterial infection often leads to simple inflammation and abscess formation. The value of CT mainly lies in evaluating the location, scope, and etiology of inflammation. Enhanced CT can also evaluate whether abscess formation exists in the lesions. When there is abscess in the lesion, incision, and drainage are needed clinically. In early stage of inflammation, it shows low-density lesions with blurred local margins, which suggestes that active anti-inflammatory treatment could be taken clinically and then reexamined. In case of abscess formation in the later stage of the lesion, it can manifest as central low-density liquefactive necrosis area, with pneumatosis and air–fluid level shadow in some lesions and adjacent soft tissues. By enhanced scan, the enhancement of low-density area in abscess is unremarkable, and the abscess wall shows ring or septa enhancement, with smooth and complete medial wall and fuzzy edge of lateral wall. At this time, it is suggested that the clinical treatment measures such as incision and drainage should be taken to intervene, and the patients should be followed up.
3. *MRI Examination*. It has high resolution in soft tissue examination. MRI can provide direct and indirect signs of inflammatory lesions in soft tissue of head and neck. Imaging characteristics of inflammatory changes caused by infection include swelling of soft tissue, the disappearance of fat layer and skin discontinuity caused by deep ulcer. Blood vessels and soft tissues can be differentiated by conventional sequences. Because fat shows hyperintense on T_1WI and hyperintense on T_2WI, and all tissue spaces in the head and neck are filled with adipose tissue, the anatomical changes of tissues can be clearly differentiated. T_2WI supports the localization and qualitative diagnosis of pathological tissues by reflecting the difference in signal intensity among tissues. MRI scan will show the imaging signs of infection, determine the swelling degree of soft tissue, whether fascia and space are involved, and even judge whether it is bloody exudation by the difference of liquid exudation signal in space; If abscess is formed, the abscess wall may show isointense or slightly hyperintense on T_1WI and slightly hypointense on T_2WI. The pus in the vomica shows hypointense on T_1WI and hyperintense on T_2WI. Inflammatory exudation around abscess shows slightly hypointense on T_1WI and slightly hyperintense on T_2WI. By enhanced scan, the abscess wall is markedly enhanced. DWI sequence shows significantly hyperintense, which is characteristic. MRI can show the evolution process of inflammation exudation, absorption, encapsulation and organization in and around abscess focus, which provides an important basis for the therapeutic effect [2].

3.2 Virus Infection

Overview

Viral infection can cause human nonspecific immunity and specific immunity, and the performance of human nonspecific immunity is basically consistent with bacterial infection, and local inflammatory reaction can occur; Imaging can also show the relative characteristic changes of organs or local soft tissues for clinical reference.

Imaging Findings

1. *X-ray Examination*. It cannot reflect the direct signs of viral infection, so it is not used as routine examination when viral infection occurs.
2. *CT Examination*. In case of immune complex deposition in head and neck lesions, CT can show the density of soft tissue, the margin is not clear, and the inflammatory reaction caused by peripheral exudation is less than that caused by common bacterial infection, and the inflammatory involvement of adjacent organs and structures is also lighter. Because CT is sensitive to the change of tissue density, the aggregation and dissipation of immune complexes can be quickly judged by measuring CT values.
3. *MRI Examination*. T_2WI sequence shows local heterogeneous signal of lesion, mild swelling of soft tissue, less inflammatory exudation, and limited scope. By enhanced scan, it shows mild homogeneous or heterogeneous enhancement. If the abscess is caused by bacterial infection locally, the manifestation is consistent with the formation of bacterial infection abscess, but the inflammatory involvement of adjacent organs and structures is less than that of common bacterial infection. Therefore, through the observation of suspected lesions by MRI, we can find out whether secondary bacterial infection occurs in time, which provides an important reference for clinical combination medication scheme [3].

3.3 Fungal Infection

Overview

Common Fungal Infections include Candida albicans, Candida tropicalis and Candida glabrata. Compared with bacteria, fungi generally do not produce endotoxin and exotoxin, and the pathogenicity of fungi may be associated with the mechanical damage caused by its reproduction in vivo and the enzymes and acidic metabolites produced. If the Fungal Infection of the head and neck is adjacent to the bony structure, such as fungal rhinosinusitis, the bone is easily eroded and destroyed, complicated with mild hyperostosis and osteosclerosis; Viral infection invading blood vessels can lead to fungal aneurysm and internal carotid artery ectasia; Painless mass is found in neck and parapharyngeal space.

Imaging Findings

1. *X-ray Examination*. If calcification is found in enlarged lymph nodes of head and neck, punctate high-density foci are found in the shadow of soft tissue anterior to neck. However, X-ray plain film shows poor soft tissue and fine structure of head and neck, so it is seldom used.
2. *CT Examination*. Fungal infection invading bone structure shows bone erosion and destruction, complicated with slight hyperostosis and increased density. If fungi are suspected to invade blood vessels, CTA examination is needed, and local aneurysmal dilatation can be found. Soft tissue density masses in neck and larynx are indistinct and can have infiltration growth with low central density. Adjacent soft tissues, including muscles, may be invaded. Multiple cervical spaces can be involved across fascia, and the enhancement is mild and relatively homogeneous. If there is central purulent necrosis, granulation tissue and strong fibrosis around it, a marked ring enhancement can be found. Some cases may have mild regional reactive lymph node proliferation.
3. *MRI Examination*. Heterogeneous signal in the affected area, mainly manifesting as slightly hypointense on T_1WI and hypointense on T_2WI, with irregular shape, and the lesion could extend along the intermuscular space and bony space. The involved bony structures and bones show heterogeneous signal intensity, with patchy slightly hypointense on T_1WI and patchy slightly hyperintense on T_2WI with unclear margin. In case of fungal brain abscess, irregular edema belts are found around the lesion, and MRI enhancement shows ring enhancement of the capsule wall, homogeneous thickness of the enhancement ring, thickening, and enhancement of the adjacent meninges [4].

3.4 Parasitic Infection

Overview

Parasitic diseases of head and neck are rare. Usually, the inflammation of lymph nodes in the head and neck increases after infection of blood, digestive tract, skin, and muscular tissue. Patients have significant systemic symptoms, which can be diagnosed by exposure history, clinical manifestations and laboratory test. Imaging can dynamically observe the number, shape, border, density, and signal of enlarged lymph nodes in head and neck, so as to monitor and re-examine the course of disease development and treatment effect.

Imaging Findings

1. *X-ray Examination*. If calcification is found in enlarged lymph nodes of head and neck, punctate high-density foci are found in the shadow of soft tissue anterior to neck. However, X-ray plain film shows poor soft tissue and fine structure of head and neck, so it is seldom used.
2. *CT Examination*. It shows solitary or multiple enlarged lymph nodes in the neck, with different sizes, homogeneous density and clear margin, which may be complicated with gravel calcification, usually without low-density necrotic area, with mild to moderate enhancement and less exudation around.
3. *MRI Examination*. A series of enlarged lymph nodes and fused nodules (rarely complicated with liquefactive necrosis) were found in the head and neck. They show isointense on T_1WI and heterogeneous hyperintense on T_2WI, heterogeneous enhancement by enhanced examination, with less inflammatory exudation around the lesions and less swelling of adjacent soft tissues. MRI has high soft tissue resolution, so it can more sensitively show the characteristic manifestations of parasitic infections such as scolex and cyst [5].

References

1. Huang L, Jiang B, Cai X, et al. Multi-space infections in the head and neck: do underlying systemic diseases have a predictive role in life-threatening complications. J Oral Maxillofac Surg. 2015;73(7):1–10.
2. Kosko J, Casey J. Retropharyngeal and parapharyngeal abscesses: factors in medical management failure. Ear Nose Throat J. 2017;96(1):12–5.
3. Tzankov A, Dirnhofer S. A pattern-based approach to reactive lymphadenopathies. Semin Diagn Pathol. 2018;35(1):4–19.
4. Zhong H, Dong C, Du J. Etiological characteristics of fungal infection in patients with head and neck neoplasm. J Pathog Biol. 2018;139(07):88–91.
5. Huang L, Chen J, Yan J, et al. Review and analysis of risk factors of severe complications of multi-space infection in head and neck. Chin J Oral Maxillofac Surg. 2019;17(01):48–51.

4 Application of Imaging Techniques in Autoimmune Diseases of Head and Neck

Shuangyan Sun, Shuang Xia, and Wen Chen

Overview

Autoimmune disease (AD) is a kind of chronic and heterogeneous disease caused by the production of a large number of autoimmune antibodies and immune complexes due to the absence of immune tolerance to autoantigen [1]. It can be divided into organ-specific and systemic autoimmune diseases. Organ-specific autoimmune diseases mainly include chronic ulcerative colitis, myasthenia gravis, pulmonary hemorrhage-nephritis syndrome, and so on. Systemic autoimmune diseases include systemic lupus erythematosus (SLE), rheumatoid arthritis (RA), scleroderma, and so on. Its specific pathogenesis is unknown. Some scholars believe that it is a complicated process affected by environmental and other factors on the basis of genetic susceptibility [2]. Each disease has specific target cells and target organs, often involving multiple organs and multiple parts. Autoimmune diseases are diagnosed mainly based on laboratory tests and clinical manifestations. Tissue biopsy and pathological diagnosis are the gold standards, and imaging examination is used to assist in judging the extent, depth, and other aspects of the lesion. When the autoimmune disease involves head and neck organs, corresponding clinical and imaging findings will appear. Take the IgG4-related disease for example. It can affect many parts and organs such as orbital soft tissue, salivary gland, head and neck skin, nervous system, and thyroid gland. Imaging shows specific manifestations such as symmetrical enlargement of the lacrimal gland, submandibular gland or parotid gland, thickening of pituitary stalk or pituitary goiter, and thyroid change. For lesions of the atlantoaxial joint synovium of rheumatoid arthritis (RA), imaging can be used to determine the atlantoaxial involvement, whether it is combined with atlantoaxial joint dislocation, synovial lesions, spinal cord compression, and so on. The common imaging techniques clinically used at present include conventional X-ray, CT, MRI, and molecular imaging. Different imaging techniques have their own advantages and limitations. As new imaging technologies develop rapidly, imaging examination techniques are more and more widely used in the diagnosis of autoimmune diseases. This chapter mainly summarizes various imaging examination techniques applicable to autoimmune diseases of the head and neck, including their characteristics and differences, as well as the advances of new imaging techniques. In this way, imaging examination techniques can be chosen for the parts to be examined in a targeted way so that they can play the best role in diagnosing different diseases.

Imaging Examination

1. *X-ray examination*. Due to lacking natural contrast in the neck, the forms of nasopharynx, oropharynx and hypopharynx can only be approximately observed depending on the air display contour in the hypopharynx cavity. In addition, soft tissues cannot be clearly displayed. Therefore, an X-ray examination is seldom used.
2. *CT examination*. As a routine examination technique for the lesions in head and neck, it can show the bony changes and soft tissue changes of head and neck. When an autoimmune disease is clinically suspected, CT examination is the first choice because the wide range involved by the lesions requires the CT examination to cover all head and neck organs. High-resolution CT (HRCT) can better show the fine structure of bone, such as joint bone changes and joint space changes caused by rheumatoid arthritis. 3D images of the head and neck can be constructed by the CT volume reconstruction technology to visually reflect for example the appearance of skin lesions caused by dermatomyositis (DM) digitally, while enhanced CT examination can help better show soft tissue lesions such as subcutaneous nodules caused by immune complex

S. Sun
Jilin Cancer Hospital, Changchun, China

S. Xia (✉)
Tianjin First Central Hospital, Tianjin, China

W. Chen
Shiyan TAIHE Hospital (Affiliated Hospital of Hubei University of Medicine), Shiyan, China

H. Li et al. (eds.), *Radiology of Infectious and Inflammatory Diseases - Volume 2*,
https://doi.org/10.1007/978-981-16-8841-6_4

deposits. CT spectral imaging can express the differential absorption of different X-ray energy spectra by tissues and lesions to display the anatomical structure more finely. Of the revolutionary significance of realizing material separation and quantitative analysis, it can improve the qualitative diagnosis accuracy of lesions. CT examination is non-invasive. It can be applied to the parts that are not suitable for biopsy and is repeatable, having certain advantages.

3. *MRI examination*. Safe, nonradiative, and having a high soft-tissue resolution, MRI examination can be used for imaging of multiple positions such as axial, coronal, sagittal, and oblique positions, and can clearly show the glands, joints, and endolymph nodes in interstitial spaces. In addition, it is also capable of functional magnetic resonance imaging including PWI, DWI, and MRS based on the conventional sequence. PWI can comprehensively reflect the microvessel distribution and blood perfusion in tissues by quantitative analysis to provide hemodynamic information. DWI is the only way to non-invasively detect the diffusion of water molecules in in vivo tissues, while MRS, as the only method that can be used to non-invasively detect the chemical substances in in vivo tissues, can provide the metabolism information of such tissues. The functional magnetic resonance imaging examination methods mentioned above can be used to diagnose autoimmune diseases of the head and neck and determine the involvement of organs etc.

References

1. Shen HH, Yang YX, Meng X, et al. NLRP3: a promising therapeutic target for autoimmune diseases. Autoimmun Rev. 2018;17(7):694–702.
2. Pan H, Leng R, Wu G, et al. Progress in epidemiologic study on major autoimmune diseases. Chin J Dis Control Prev. 2018;22(11):11–13, 23.

Part II

Imaging Anatomy of Head and Neck

Imaging Anatomy of Eye

5

Zhao Lu, Shaowei Zheng, and Lijun Wang

5.1 Foundation of Imaging Anatomy

The visual organ of eye is located at a position most of which are in the orbit. It consists of the eyeball and the accessory organs of eye. The eyeball is mainly composed of the eyeball wall and contents. It is stimulated by the light wave, converts the light stimulation into nerve impulses and then transmits them to the brain's visual center through the visual pathway to generate vision. The accessory organs of eye support, protect, and move the eyeball [1, 2].

5.1.1 Orbit

The orbit, as a square vertebral body-shaped deep bony cavity, accommodates the eyeball and the accessory organs of eye. It consists of frontal bone, zygomatic bone, maxilla, palate bone, ethmoid bone and sphenoid bone, and has an orbital apex, an orbital aperture facing the front, and four orbital walls,

5.1.1.1 Orbital Apex

Facing the posteromedial direction, it is a part via which the optic canal is connected to the inside of skull.

5.1.1.2 Orbital Aperture

An opening in the front of orbit.

5.1.1.3 Orbital Wall

It include superior wall, inferior wall, medial wall, and lateral wall.

1. Superior Wall: the orbital roof, which is slightly triangular in shape and uneven in thickness. Its front is composed of the horizontal plate of frontal bone (orbital plate of frontal bone), and its back is composed of the lesser wing of sphenoid bone. It separates the anterior cranial fossa from the orbit. Main anatomical structures of the superior wall include the following items from front to back: (1) supraorbital notch, which is at 1/3 of the junction of the anterior border of superior wall and by which supraorbital nerve and blood vessel pass; (2) fossa for lacrimal gland, which, behind the zygomatic process of frontal bone, is an external even depression in front of the orbit, and accommodates the lacrimal gland; (3) trochlear fossa, which, located in the upper corner of the orbit, is adjacent to the protruding trochlea spine, with trochlear cartilage or ligament as its common signs of ossification.
2. Inferior Wall: the orbital floor, which mainly consists of orbital surface of maxilla, orbital surface of zygomatic bone, and orbital process of palate bone. The bone of the inferior wall is relatively thin, with the part at the infraorbital groove or infraorbital canal the thinnest. In the middle of the inferior wall, there is an infraorbital groove starting from the inferior orbital fissure and extending forward to the infraorbital canal, with an opening made in the infraorbital foramen for infraorbital vessels and infraorbital nerves to pass through.
3. Medial Wall: Rectangular, wide in the front and narrow in the back, it consists of frontal process of maxilla, lacrimal bone, ethmoid bont and corpus sphenoidale (a small part) from front to back. The front part is the fossa for lacrimal sac formed by the frontal process of maxilla and the lacrimal bone. It is connected to the nasal cavity through the nasolacrimal duct downward, which can be clearly shown by CT. Most of the medial wall consists of the orbital plate of ethmoid bone (ethmoid bont). It is the thinnest part of the orbital wall. In the front section at the junction between the ethmoid bont and the orbital part of frontal bone, there is an anterior ethmoidal foramen for the anterior ethmoid artery and the nasal nerves to pass through, and in the rear section, there is a posterior

Z. Lu
Shengjing Hospital of China Medical University, Shenyang, China

S. Zheng · L. Wang (✉)
The First Hospital of Dalian Medical University, Dalian, China

H. Li et al. (eds.), *Radiology of Infectious and Inflammatory Diseases - Volume 2*,
https://doi.org/10.1007/978-981-16-8841-6_5

ethmoidal foramen for the posterior ethmoidal artery to pass through.

4. Lateral Wall: Slightly triangular, and with the front 1/3 consisting of the orbital surface of zygomatic bone and the rear 2/3 consisting the orbital surface of greater wing of sphenoid bone, it is the strongest orbital wall and not adjacent to any paranasal sinus. Following anatomical structures can be observed in the lateral wall: (1) Merkel spina recti lateralis, which, as a small blunt round bony protrusion of the greater wing of sphenoid bone and located at the inferior border of the junction between wide and narrow parts of the superior orbital fissure, is the starting point of a part of the lateral rectus; (2) Jugal groove, which extends from the front of the inferior orbital fissure to the large jugal foramen and then the jugal canals which includes the zygomaticofacial canal and the zygomaticotemporal canal for the zygomatic artery and zygomatic nerve of the same name to pass through [2], supplying and innerving the surrounding areas of orbit as well as the face.

5.1.1.4 Fissure and Canal between Orbital Walls

1. Superior Orbital Fissure: Located between the lateral wall and the top wall of the orbit, it is a fissure between greater and lesser wings of sphenoid bone. The superior border is the lesser wing of sphenoid bone, and the inferior border is the greater wing of sphenoid bone. With the ophthalmic branch (ophthalmic nerve) of trigeminal nerve, the oculomotor nerve, the trochlear nerve, the abducent nerve and the superior ophthalmic vein passing through, it is the largest passage between the orbit and the middle cranial fossa.
2. Inferior Orbital Fissure: It is a narrow fissure between the inferior wall and the lateral wall, with the maxilla and the orbital process of palate bone at the anterior boundary, and the inferior border of orbital surface of greater wing of sphenoid bone at the posterior boundary. The inferior orbital fissure constitutes a passage between the orbit and the pterygopalatine fossa and between the orbit and the infratemporal fossa for the maxillary branch of trigeminal nerve (maxillary nerve) and the inferior ophthalmic vein branch to pass through.
3. Optic Canal: Located at the apex of superior wall and consisting of two roots of the lesser wing of sphenoid bone as well as the superolateral part of corpus sphenoidale, it connects the orbital apex and the middle cranial fossa. The optic nerve, the ophthalmic artery and the sympathetic nerve pass through it. The optic canal is adjacent to the sphenoid sinus and the posterior ethmoidal sinus, and its canal wall is thin. If the bone is partially absorbed, the optic nerve will be placed in the sinus cavity. Therefore, patients with rhinosinusitis often have optic neuritis.
4. Anterior Orbital Canal and Posterior Orbital Canal: Located in the frontoethmoidal suture between superior wall and medial wall or adjacent frontal bone, they consist of frontal bone and ethmoid bone. Since openings for anterior ethmoidal foramen and posterior ethmoidal foramen are made in the orbital wall, openings for anterior orbital canal and posterior orbital canal are made in the foramina ethmoidale anterius of anterior cranial fossa medially along the foramens. The anterior ethmoid artery and the posterior ethmoidal artery (ophthalmic artery branch) pass through them respectively to supply the lateral part of nasal cavity, the superior part of nasal septum, and the ethmoidal sinus. They also form a plexus together with the sphenopalatine artery [2].

5.1.1.5 Orbital Space

There are four spaces in the orbit, including episcleral space, central space, peripheral space, and subperiosteal space.

1. Episcleral Space: It refers to the potential space between fascia and sclera of the eyeball. Effusion in the space as well as inflammatory infiltration usually can be observed in case of ocular tendonitis.
2. Central Space: It is located in the muscle cone surrounded by four recti and intermuscular ligaments. There is orbital fat, nerves, and blood vessels in the central space, and Its front part is closely connected to the fascia of eyeball and the orbital septum. Therefore, the inflammation occurring in the space usually does not affect the eyelid or conjunctiva.
3. Peripheral Space: It is located between the muscle cone surrounded by four recti and intermuscular ligaments and the orbital periosteum, and its front part is the orbital septum.
4. Subperiosteal Space: It refers to the potential space between the orbital periosteum and the orbital bone. Except being tightly connected to parts such as the fossa for the lacrimal sac, the orbital margin and each porous dehiscence, it is loosely connected to most other parts. Therefore, it is easy for the orbital periosteum to peel in case of inflammation.

5.1.2 Eyeball

The eyeball is mainly composed of eyeball wall and contents. Located in the orbit and approximately spherical, it is connected to the orbital wall by the fascia. The eyeball is protected by the eyelid in front, and connected to the optic chiasma of diencephalon through the optic nerve at the back. It is surrounded by lacrimal glands, ocular muscles and so on [1, 2].

5.1.2.1 Wall of Eyeball

The wall of eyeball can be divided into three layers from the outside to the inside, i.e., fibrous tunic, vascular tunic and retina.

1. Fibrous Tunic: The front 1/6 of it, as the cornea as well as convex outside and concave inside, is used for refraction. The rear 5/6 of it, as sclera, is opaque and porcelain white. The corneal limbal is at their junction [1, 2].
2. Vascular Tunic: Located on the deep surface of the fibrous tunic of eyeball and rich in blood vessels, chromocytes and connective tissues, it is composed of iris, ciliary body and choroid from front to back. Located in the most front part of the vascular tunic, the iris is a disc-shaped thin tunic in the most front part of the vascular tunic, with a round pupil in the center. There are two directions of smooth muscle in the iris. One direction of smooth muscle, which surrounds the pupil, is called as the sphincter pupillae. It is subject to parasympathetic innervation and can shrink the pupil. Another direction of smooth muscle, which is radially arranged, is called as dilator pupillae muscle. It is subject to sympathetic innervation and can expand the pupil. The iris controls the amount of light reaching the retina by controlling the pupil's size. Located between the iris and choroid, the ciliary body is the thickest part of the vascular tunic. It contains the ciliary muscle, which is subject to sympathetic innervation. The ciliary body controls the power and shape of the lens and is where aqueous humor is produced. The choroid occupies posterior 2/3 of the vascular tunic. Its outer surface is loosely connected to the sclera, its inner surface closely clings to the pigment layer of the retina, and the optic nerve passes through at its back. The choroid supplies oxygen and nutrients to the outer layer of the retina [1–4].
3. Retina: Located on the inner surface of the vascular tunic of eyeball, it is divided into iridial part of retina, ciliary body part and choroid part from front to back. Attached to inner surfaces of the iris and the ciliary body, thin and without photosensitization, the iridial part and the ciliary body part are collectively called the blind part of retina. Attached to the inner surface of choroid, wide in the range, and with photosensitization, the choroid part is also called as pars optica retinae [1–3].

5.1.2.2 Contents of Eyeball

The contents of eyeball include lens, vitreous body and aqueous humor, all of which are colorless, transparent, and without vascular structures. They are capable of refraction.

1. Lens: Located between the iris and the vitreous body, it is hung by a ligament attached to the anterior part of the ciliary body. Biconvex lens-shaped, elastic, and connected to the ciliary body by the ciliary zonules, it is a main part for the eyeball to adjust the refraction. Containing a lot of protein, it has the highest CT value in human soft tissues.
2. Vitreous Body: Located between the lens and the retina, it occupies about the posterior 4/5 of space in the eyeball cavity. The vitreous body contains 98.5% of water so its density is low on the CT image, and the MRI shows hypointense on T_1WI and hyperintense on T_2WI.
3. Aqueous Humor: It is filled in the aqueous chamber, which is the space between the lens and its suspensorium and cornea. The aqueous chamber is divided into the anterior chamber and the posterior chamber by the iris. The anterior chamber includes the space between iris and cornea, and the posterior chamber refers to the space between iris and vitreous body. Because the main component of aqueous humor is water which takes up about 98.1%, the CT examination shows low density, and the MRI image shows hypointense on T_1WI and hyperintense on T_2WI [1–6].

5.1.3 Accessory Organs of Eye

The accessory organs of eye include structures such as eyelid, conjunctiva, lacrimal organs, ocular muscles, adipose body of orbit, and orbital fasciae.

5.1.3.1 Eyelid

Located in the front of eyeball, it is a protective barrier for the eyeball. The eyelid is classified into the upper eyelid and the lower eyelid, the fissure between which is called as palpebral fissure. The eyelid includes five layers from front to back: skin layer, subcutaneous layer, muscular layer, fibrous layer and palpebral conjunctiva layer. The skin layer of eyelid is thin. The subcutaneous tissue layer is loose and mainly composed of connective tissue and a small amount of fat. The muscular layer mainly includes pars palpebralis muscles, levator palpebrae superioris and Müller's muscle. The fibrous layer is mainly composed of the tarsus and orbital septum.

The tarsus is a half-moon-shaped dense connective tissue plate, with one on the top and one on the bottom. Composed of dense connective tissues, it supports the eyelid.

The orbital septum is an elastic connective tissue membrane that connects the tarsus and the orbital margin. With surrounding areas extending to the periosteum of the orbital margin, it is a barrier between the eyelid and the internal structure of the orbit, able to prevent the spread of inflammation.

5.1.3.2 Lacrimal Organs

1. Lacrimal Gland: It is an exocrine gland located in the fossa for lacrimal gland in the outer upper front part of the orbit. It is divided into the larger orbital lobe (lacrimal gland of orbital part) in the upper part and the smaller eyelid lobe (lacrimal gland of eyelid) by the Whitnall ligament of the levator palpebrae superioris. The orbital lobe is located in the fossa for lacrimal gland, and eyelid lobe in the front lower part of the upper eyelid.
2. Tear Drainage System: Mainly composed of dacryon, lacrimal ductule, lacrimal sac, nasolacrimal duct and so on, it mainly drains tears.

   The dacryon (lacrimal punctum) is located in the center of the medial lacrimal papilla of the free margin of the upper and lower eyelids. It is the opening of the lacrimal ductule. The lacrimal ductule, as a membranous duct, connects the dacryon and the lacrimal sac. The lacrimal sac is located in the fossa for lacrimal sac formed by the lacrimal bone and the frontal process of the maxilla. It is a membranous sac, with the upper a blind end and the lower opening continuous with nasolacrimal duct. The anterior wall of the lacrimal sac at the lower edge of the medial canthus ligament is weak so it is easy to perforate here from a fistula in case of lacrimal abscess. The nasolacrimal duct, as a membranous duct, is embedded into the bony nasolacrimal duct composed of the lacrimal groove of maxilla, the lacrimal groove of lacrimal bone and the lacrimal process of Inferior turbinate. It can connect the orbit and the inferior meatus.
3. Tear drainage pathway: superior and inferior lacrimal punctums → upper and lower lacrimal ductules → confluence into the common lacrimal duct → lacrimal sac → nasolacrimal duct → inferior meatus.

5.1.3.3 Extraocular Muscle

As movement devices of optic organs, they are essential for the movement of eyeball. There are 6 extraocular muscles (including 4 recti and 2 oblique muscles for eyeball movement) on each side as well as the levator palpebrae superioris eyelid movement. All such muscles are skeletal muscles (Table 5.1). They work together to make the eyes move in all directions.

1. Superior rectus, inferior rectus, medial rectus, and lateral rectus: As four recti for eyeball movement, they are located at superior, inferior, medial, and lateral parts of the eyeball. They originate from the vicinity of the optic canal and the medial common tendinous ring of the superior orbital fissure, anterior to the equator, and insert into the superior, inferior, medial, and lateral parts of the sclera respectively. When they contract, the pupil turns upwards and inwards, downwards and inwards, inwards, and outwards.
2. Superior Oblique and Inferior Oblique: The superior oblique originates from the corpus sphenoidale, which is located between the superior rectus and the medial rectus, courses forward along the orbital roof and the medial wall to the trochlear (the trochlear of an over 25-year-old person can be calcified), turns to the rear lateral after passing through the trochlear, and inserts on the sclera posterior to the equator of eyeball. When it contracts, the pupil turns downwards and outwards.

   Originating from the anteromedial side of the inferior wall (the lateral side of the lacrimal groove on the orbital surface of maxilla), the inferior oblique lies between the infraorbital wall and the inferior rectus. It inclines posterolaterally and inserts at the sclera posterior to the equator under the eyeball. It contracts to turn the pupil to the superolateral side.
3. Levator Palpebrae Superioris: It originates from the orbital wall in the anterosuperior part of the optic canal, courses forward above the superior rectus, and terminates at the skin and superior tarsus of the upper eyelid. It lifts the upper eyelid and opens the palpebral fissure [1, 2, 6].

Table 5.1 Origins and insertions, actions, and innervations of ocular muscles

Name	Origin	Insertion	Action	Innervation
Levator palpebrae superioris	Orbital wall anterosuperior to optic canal	Upper eyelid skin and superior tarsus	Lift the upper eyelid	Oculomotor nerve
Superior oblique	Corpus sphenoidale	Posterior sclera of the equator posterolateral to the eyeball	Turn the pupils downwards and outwards	Trochlear nerve
Inferior oblique	Medial part of the inferior wall	Posterior sclera of the equator inferior to the eyeball	Turn the pupils upwards and outwards	Oculomotor nerve
Superior rectus	Common tendinous ring	Sclera anterior to the equator of eyeball	Turn the pupils upwards and inwards	Oculomotor nerve
Inferior rectus	Common tendinous ring	Sclera anterior to the equator of eyeball	Turn the pupils downwards and inwards	Oculomotor nerve
Medial rectus	Common tendinous ring	Sclera anterior to the equator of eyeball	Turn the pupils inwards	Oculomotor nerve
Lateral rectus	Common tendinous ring	Sclera anterior to the equator of eyeball	Turn the pupils outwards	Abducent nerve

5.1.3.4 Adipose Body of Orbit and Orbital Fascia

1. Adipose Body of Orbit: It is the adipose tissue that fills the eyeball, ocular muscles and orbital periosteum, which protects and supports various structures in the orbit. There are many adipose tissues between the optic nerve and various muscles of the eyeball behind the eyeball, and the optic nerve forms a relationship similar to that between articular head and acetabulum with the eyeball. Therefore, the eyeball may do multi-axis movement and reduce the impacts of external vibration.
2. Orbital Fascia: It includes ocular fascial sheathe of eyeball, fasciae musculares bulbi, periorbita, and orbital septum from inside to outside.
   (a) Fascial Sheathe of Eyeball: Also known as Tenon's capsule, it is the thin and dense fibrous tunic between the adipose body of orbit and the eyeball. The sheathe wraps most of the eyeball, starts from the corneal limbus in the front, ends around the optic nerve in the back, fuses with the bulbar conjunctiva. Bounded by the part where the four recti pass, the fascial sheathe of eyeball is divided into two parts, with the front part thinner than the back part.
   (b) Fasciae Musculares Bulbi: It is sheathe-shaped and wraps the ocular muscles.
   (c) Periorbita: It is a dense connective tissue covering the surface of the orbital bone. Except being adhered to bones at the orbital margin, orbital fissure, orbital foramen, orbital suture, fossa for lacrimal sac, trochlear fovea and other positions, it is generally loosely attached to the orbital wall and connected to the cerebral dura mater by the superior orbital fissure, optic canal, anterior orbital canal and posterior orbital canal.

      The annulus of Zinn is a connective tissue ring formed by periorbita at the orbital apex. It is closely connected with the tendons at the origins of 4 recti. It fuses with the cerebral dura mater at the optic foramen. Therefore, the patient will feel painful when the eyeball rolls.
   (d) Orbital Septum: As a thin layer of connective tissue located between the superior border of upper tarsus and the inferior border of lower tarsus, it is connected to superior border and inferior border of the orbit, respectively, and extends to the orbital periosteum [1, 2].

5.1.4 Nerves and Blood Vessels of Orbit

5.1.4.1 Nerves of Eyes

There are many sources of nerves that innervate the eyes. The optic nerve originates from the medial of the posterior pole of eyeball, courses backward, passes through the optic canal into the middle cranial fossa and is connected to the optic chiasma. The oculomotor nerve innervates ocular muscles (superior rectus, inferior rectus, medial rectus, inferior oblique), sphincter pupillae and ciliary muscles. The trochlea and abducent nerve innervate the ocular muscles. The facial nerve innervates the orbicularis oculi muscle of the eyelid, its parasympathetic nerve the lacrimal gland, and its sympathetic nerve the dilator pupillae muscle. The sensory nerve of visual organs mainly comes from the ophthalmic nerve branch of the trigeminal nerve.

5.1.4.2 Blood Vessels of Eyes

The ophthalmic artery originates from the internal carotid artery, courses in the medial inferior direction of the optic nerve in the optic nerve sheath, and enters the orbit through the optic canal. It is divided into branches such as central retinal artery, short posterior ciliary artery, long posterior ciliary artery, anterior ciliary artery, anterior ethmoid artery and posterior ethmoidal artery along the way to supply the eyeball, ocular muscles, lacrimal gland and eyelid.

Veins of the eye include intraocular veins and extraocular veins. Intraocular veins mainly include the central retinal vein, vortex vein and anterior ciliary vein. They collect venous blood in the orbit and join the superior ophthalmic vein and inferior ophthalmic vein with other veins. Extraocular veins include superior ophthalmic vein and inferior ophthalmic vein. The former originates from the superior orbital angle and then enters the cavernous sinus through the superior orbital fissure. The latter comes from the diffuse vascular plexus at the bottom of the eyelid, is anastomosed with the superior ophthalmic vein before entering the cavernous sinus or enters the cavernous sinus alone, and is also anastomoses with the pterygoid plexus through the inferior orbital fissure [1, 2].

5.2 CT Imaging Anatomy

According to the CT image, the orbital bone shows a high density; the eyeball wall, lacrimal gland, extraocular muscle and optic nerve show an equidensity; and the lens shows a homogeneous high density, exactly like calcification and with a CT value of up to 120 ~ 140HU; the vitreous body shows a slight low density; the capsula adiposa bulbi shows a low density; and the muscle belly of extraocular muscle is thicker than the tendon and the Zinn common tendinous ring.

The eyeball is approximately spherical, and the average anteroposterior diameter of the eyeball of a normal adult is about 24 mm. The eyeball is located in the front of the orbit. The eyeball wall, also known as eye ring, shows a uniform ring shadow of the soft tissue density. Therefore, CT cannot distinguish the layers of the eyeball wall. The lens is biconvex disc-shaped, with the iris in the front and the vitreous

body at the back. Containing a lot of protein, the lens has the highest CT value in human soft tissues. The vitreous body is water-like and of low density. It is located between the lens and the retina, of which water takes up about 99% [7].

5.2.1 Transverse Plane of Orbit

Most of the intraorbital and middle cranial fossa structures can be shown on the transverse plane. On the same level, the medial wall and the lateral wall can be shown in the bone window. The medial rectus, lateral rectus, optic nerve and so on can be shown in the standard window in addition to the superior ocular vein, which can be clearly shown. However, it is difficult to completely show the superior rectus, the inferior rectus the superior oblique and the inferior oblique on the same level. The orbital roof wall and the inferior wall shall also be continuously observed on multiple levels. The superior orbital fissure, inferior orbital fissure and optic canal can also be observed in the orbital apex region (Fig. 5.1).

5.2.2 Coronal Plane of Orbit

The image of coronal plane can clearly show the planes of four orbital walls, extraocular muscle, optic nerve and others at the same level. In addition, it can also show various foramens and fissures in the orbital apex region better than the transverse plane. The superior orbital fissure and the inferior orbital fissure have an "8"-shaped structure. The superior orbital fissure separates the greater wing and lesser wing of sphenoid bone. The inferior orbital fissure is located between the orbital plate of the greater wing of sphenoid bone and that of the maxilla. The optic canal is enclosed by the two roots of the lesser wing of sphenoid bone and the superolateral part of corpus sphenoidale. The levator palpebrae superioris is close to the superior rectus and located above it. it is difficult to completely distinguish the posterior part of muscle belly, which is thus collectively called as the supraocular muscle group. The inferior small round shadow is the superior ophthalmic vein. The superior oblique can be seen above the medial rectus. Unilateral or bilateral symmetrical punctate calcification can be seen at the point near the medial wall on the anterior layer of the upper quadrant of the orbit. It is the ossified trochlear fibrous cartilage at which the superior oblique muscle turns backward to the lateral side. At the equatorial level of the eyeball, the inferior oblique coursing from the superolateral side to the medial inferior side can be observed between the eyeball and the inferior wall, above which the plane of the inferior rectus tendon can be seen. At the posterior level of the eyeball, the central space surrounded by four recti and the superior oblique can be seen, where the optic nerve passes through with the ophthalmic artery coursing along with it. The fine punctate shadow on the lateral side of the inferior rectus is the inferior ophthalmic vein (Fig. 5.2).

5.2.3 Optic Canal

The optic foramen is located at the apex of the superior wall. Formed by two roots of the lesser wing of sphenoid bone, it extends backward to the medial side to form the optic canal and then reaches the middle cranial fossa. The optic nerve, ophthalmic artery and the sympathetic nerve pass through the 4 ~ 9 mm long and 4 ~ 6 mm wide optic canal (Fig. 5.3).

5.3 MR Imaging Anatomy

On MR images, the bone cortex of orbital wall shows no signal, both the bone marrow cavity and the capsula adiposa bulbi show hyperintense, and blood vessels in the orbit show flow void. T_1WI: The eyeball wall, extraocular muscle, optic nerve and so on show isointense; the lens shows isointense and hypointense, and the vitreous body shows hypointense. The eyelid contains fat and shows hyperintense. The fibrous orbital septum shows hypointense. T_2WI: The eyeball wall and the extraocular muscle show hypointense; the optic nerve shows slightly hypointense or isointense; the lens extremely hypointense; the vitreous body hyperintense, and the subarachnoid space hyperintense. The iris has a sub-millimeter-level thickness, making it unclear on MRI images. The 0.2 ~ 0.3 mm thick retina is indistinguishable from the choroid. The supraocular vein originates under the trochlear and is anastomosed with the angular vein as an extension of the nasofrontal vein. Continuing at the posterior side of the eye, it is initially at the anteromedial side to the optic nerve and then enters the superior orbital fissure at the posterolateral side of ophthalmic artery. The lacrimal gland, located in the superolateral part of the eyeball, shows isointense on T_1WI and hypointense on T_2WI (Figs. 5.4, 5.5, and 5.6).

On the enhanced T_1WI image of fat suppression, the iris, ciliary body and choroid show marked enhancement, the retina is unclear, and the sclera containing fibrous structure shows hypointense. Both the extraocular muscle and the lacrimal gland show homogeneous marked enhancement. The optic nerve is not enhanced, and the capsula adiposa bulbi shows no signal due to adopting the fat pressure technique.

The T2WI fat-suppressed sequence of coronal plane can be used to show the optic nerve and its surrounding subarachnoid space better. The intraorbital segment of the optic nerve shows hypointense, and its surrounding subarachnoid space shows hyperintense. It is difficult to observe the intravascular segment and the intracranial segment.

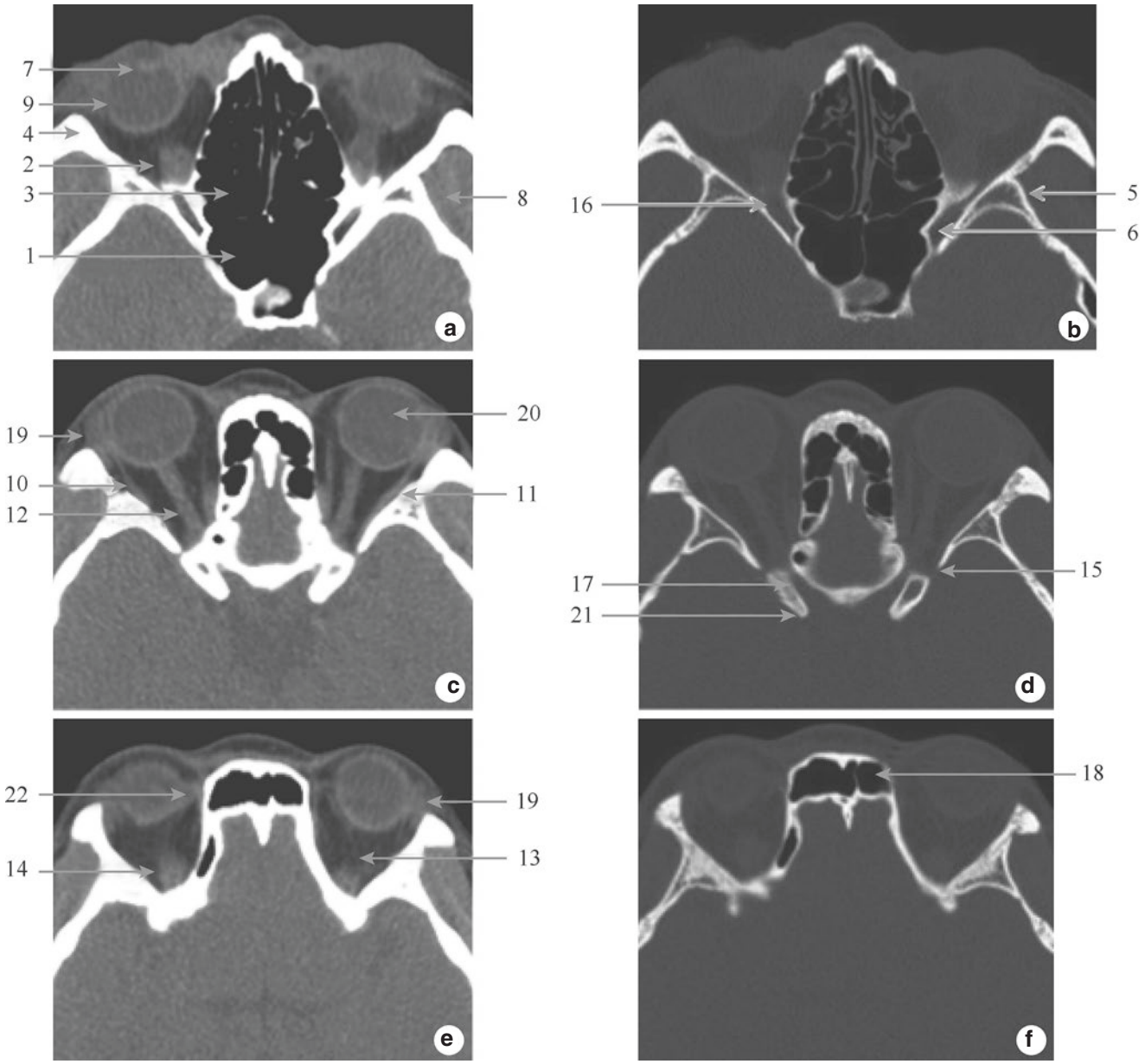

Fig. 5.1 CT images of the transverse plane of orbit. (**a**, **c**, **e**) Images of the soft tissue window of orbit; (**b**, **d**, **f**) Images of bone window. 1. Sphenoid sinus 2. Inferior rectus; 3. Ethmoidal sinus; 4. Zygomatic bone; 5. Temporal bone; 6. Pterygopalatine fossa; 7. Lens; 8. Temporal fossa; 9. Sclera; 10. Medial rectus; 11. Lateral rectus; 12. Optic nerve; 13. Superior ophthalmic vein; 14. Superior rectus; 15. Superior orbital fissure; 16. Inferior orbital fissure; 17. Optic canal; 18. Frontal sinus; 19. Lacrimal gland; 20. Vitreous body; 21. Anterior clinoid process; 22. Trochlea

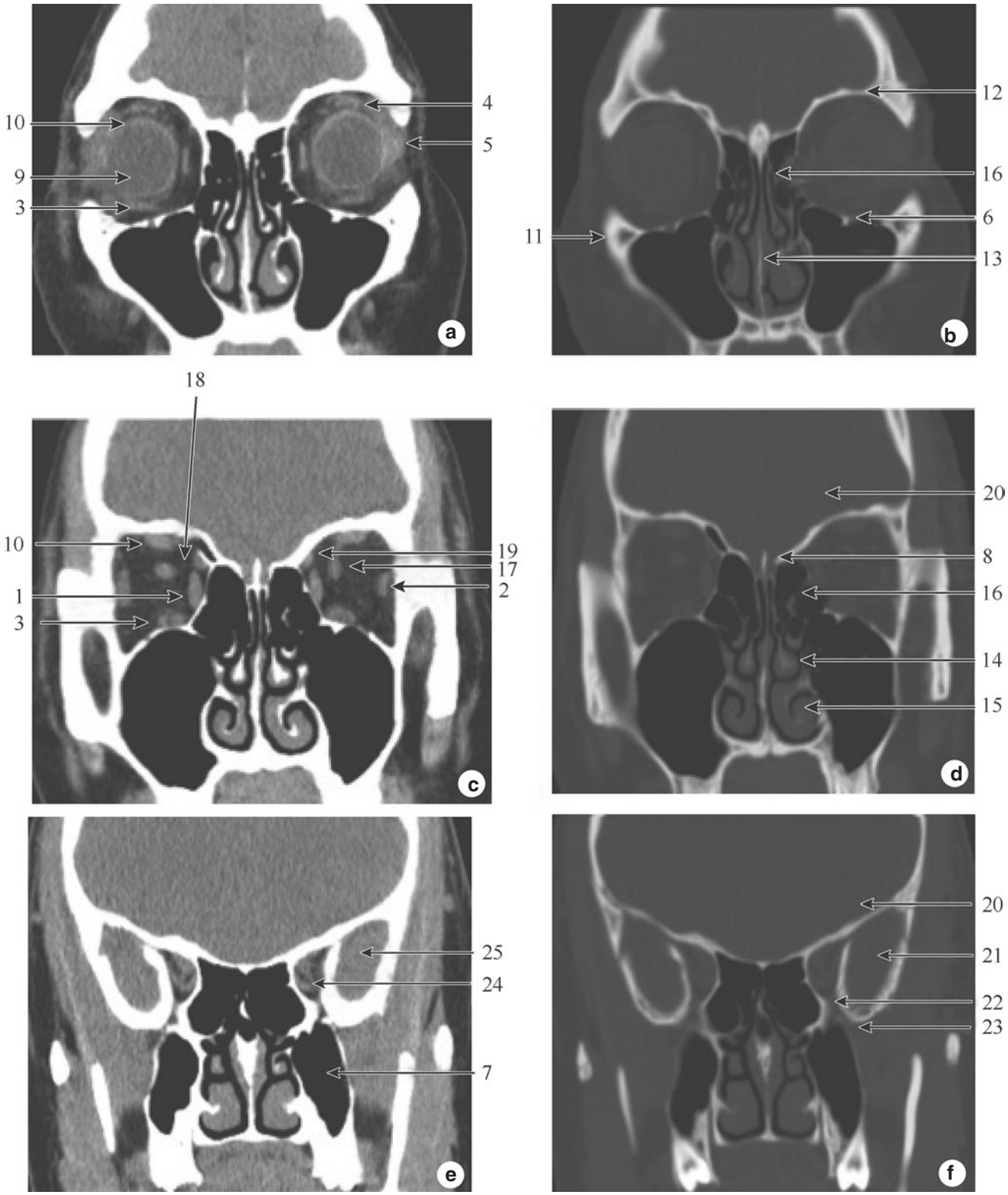

Fig. 5.2 CT images of the coronal plane of orbit. (**a**, **c**, **e**) Images of the soft tissue window of orbit; (**b**, **d**, **f**) Images of the coronal plane of bone window. 1. Medial rectus; 2. Lateral rectus; 3. Inferior rectus; 4. Superior rectus and levator palpebrae superioris; 5. Lacrimal gland; 6. Infraorbital foramen; 7. Maxillary sinus; 8. Olfactory sulcus; 9. Vitreous body; 10. Sclera; 11. Zygomatic bone; 12. Roof wall; 13. Nasal septum; 14. Middle turbinate; 15. Inferior turbinate; 16. Ethmoidal sinus; 17. Optic nerve; 18. Superior ophthalmic artery; 19. Superior oblique; 20. Anterior cranial fossa; 21. Middle cranial fossa; 22. Inferior orbital fissure; 23. Pterygomaxillary fissure; 24. Orbital apex; 25. Temporal lobe

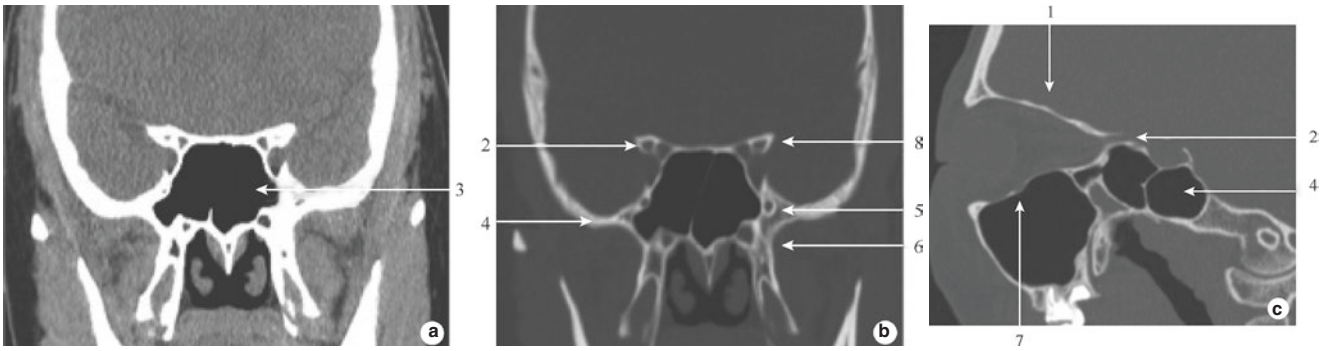

Fig. 5.3 CT images of optic canal. (**a**) Coronal image of soft tissue window; (**b**) Coronal image of bone window; (**c**) Image of bone window of long-axis reconstruction. 1. Orbital process of frontal bone; 2. Optic canal; 3. Sphenoid sinus; 4. Sphenoid bone; 5. Foramen rotundum; 6. Pterygoid process; 7. Inferior wall; 8. Anterior clinoid process

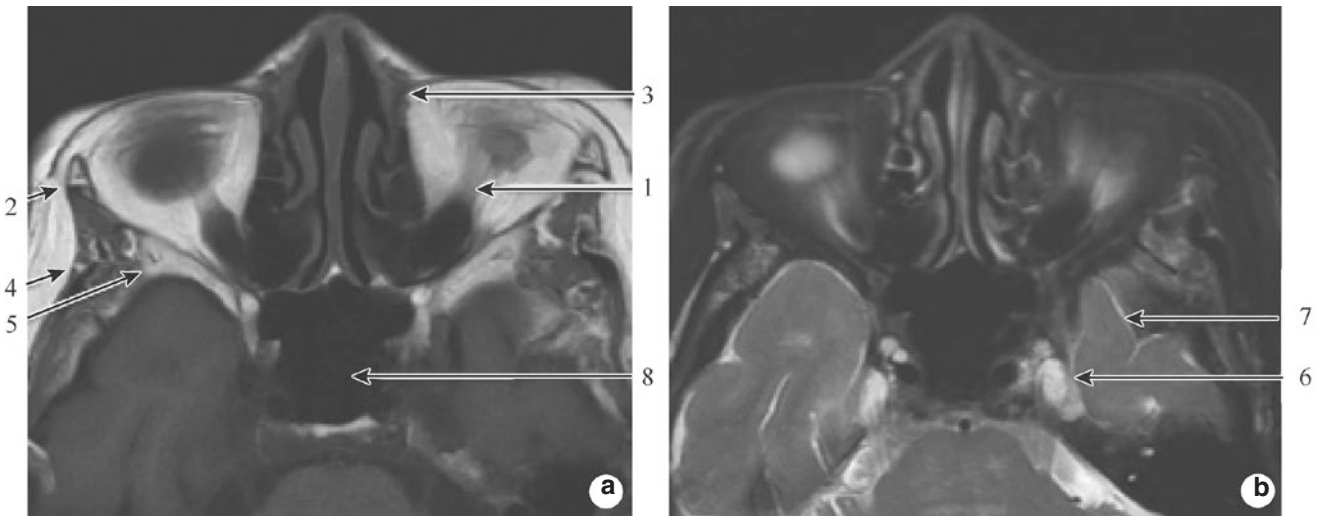

Fig. 5.4 MRI images of the transverse plane of orbit. (**a**, **c**, **e**) images of transverse plane of orbit on T_2WI; (**b**, **d**, **f**) Images of fat suppression on T_2WI. 1. Inferior rectus; 2. Zygomatic bone; 3. Lacrimal sac; 4. Temporalis; 5. Temporal bone; 6. Trigeminal ganglion; 7. Temporal lobe; 8. Sphenoid sinus; 9. Ethmoidal sinus; 10. Internal carotid artery; 11. Optic nerve; 12. Medial rectus; 13. Lateral rectus; 14. Vitreous body; 15. Lens; 16. Ciliary body; 17. Lacrimal gland; 18. Posterior orbital fat; 19. Hypophysial fossa; 20. Pituitary stalk; 21. Ophthalmic artery; 22. Superior ophthalmic vein; 23. Superior rectus; 24. Optic chiasma; 25. Frontal lobe; 26. Middle cerebral artery

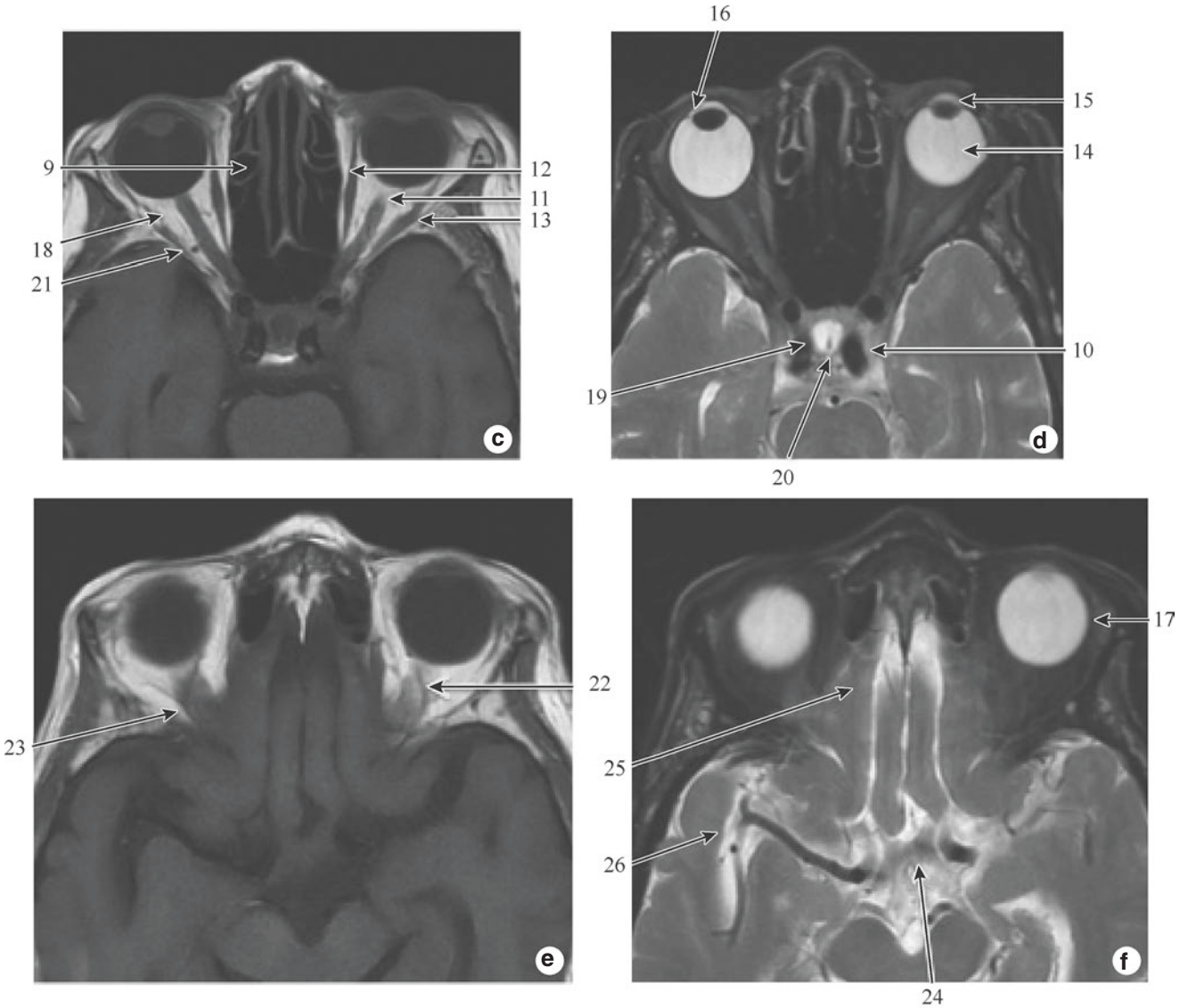

Fig. 5.4 (continued)

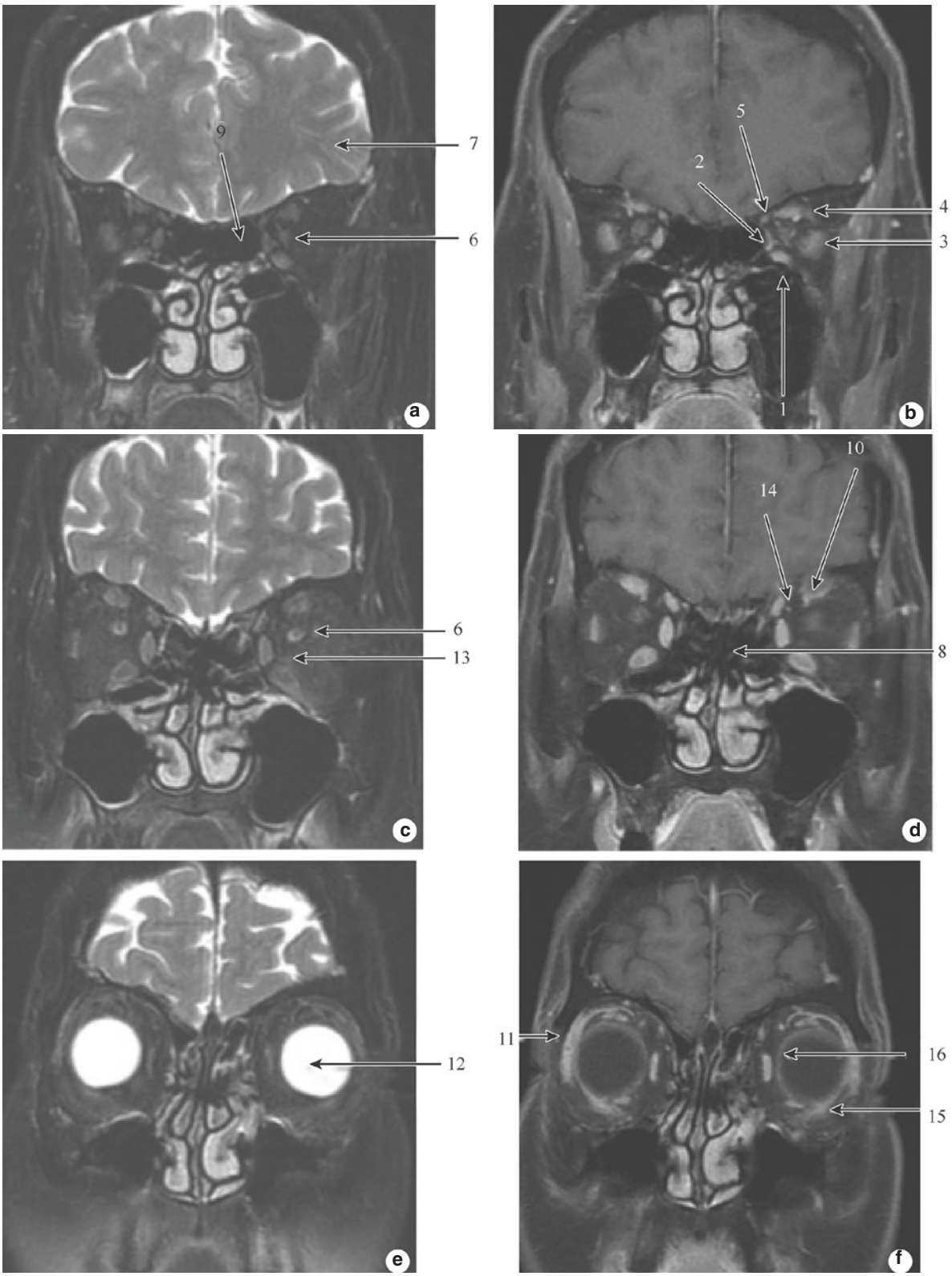

Fig. 5.5 MRI images of the coronal plane of orbit. (**a**, **c**, **e**) Images of fat suppression on T_2WI; (**b**, **d**, **f**) Images of fat suppression on T_1WI. 1. Inferior rectus; 2. Medial rectus; 3. Lateral rectus; 4. Superior rectus and levator palpebrae superioris; 5. Superior oblique; 6. Optic nerve; 7. Frontal lobe; 8. Ethmoidal sinus; 9. Sphenoid sinus 10. Superior ophthalmic vein; 11. Lacrimal gland; 12. Vitreous body; 13. Posterior orbital fat; 14. Ophthalmic artery; 15. Inferior oblique; 16. Sclera

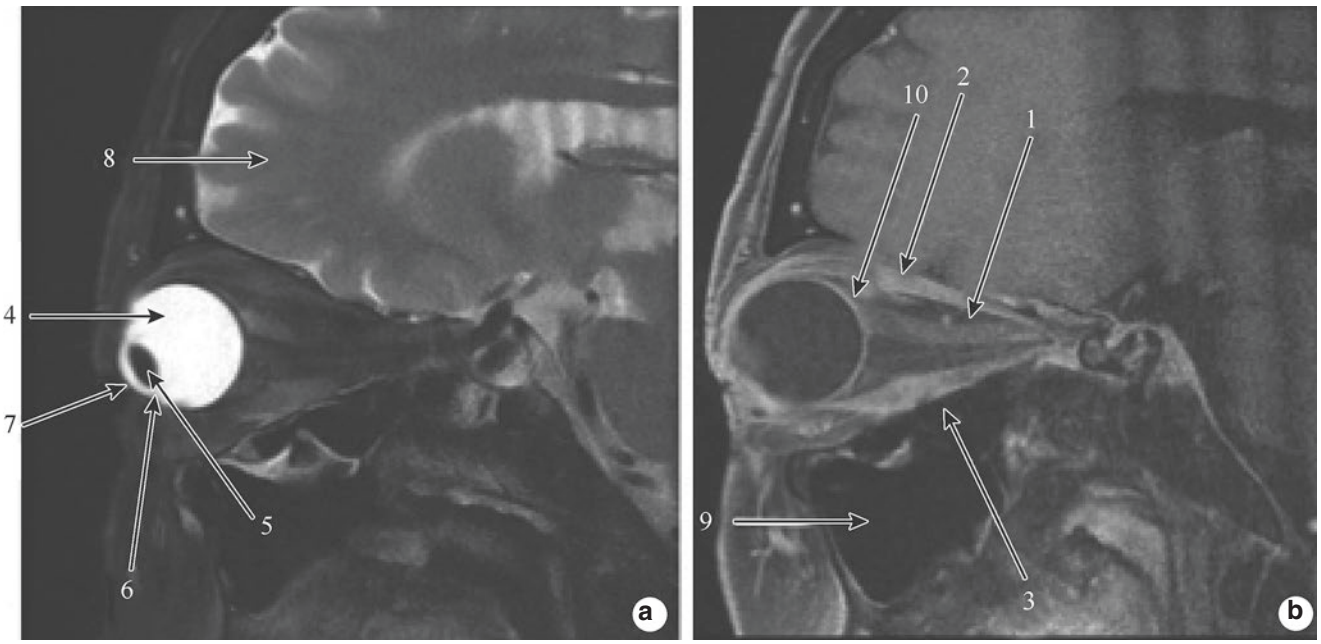

Fig. 5.6 Oblique sagittal MRI images of orbit. (**a**) Image of fat suppression on T_2WI; (**b**) Image of fat suppression on T_1WI. 1. Optic nerve; 2. Superior rectus; 3. Inferior rectus; 4. Vitreous body; 5. Lens; 6. Ciliary body; 7. Anterior chamber; 8. Frontal lobe; 9. Maxillary sinus; 10. Sclera

References

1. Bai S, Ying D. Systematic anatomy. 8th ed. Beijing: People's Medical Publishing House; 2013.
2. Lan B. Chinese imaging-head and neck volume. Beijing: People's Medical Publishing House; 2002.
3. Wen J, Ji Y. Imaging examination techniques for head and neck. Zhenjiang: Jiangsu University Press; 2017.
4. Willoughby CE, Ponzin D, Ferrari S, et al. Anatomy and physiology of the human eye: effects of mucopolysaccharidoses disease on structure and function-a review. Clin Exp Ophthalmol. 2010;38:2–11.
5. Kolb H, Fernandez E, Nelson R. Visual acuity-webvision: the organization of the retina and visual system. Clin Radiol. 1995;38(1):657.
6. Fu S, Xu G. Sectional anatomy. 3rd ed. Beijing: Higher Education Press; 2019.
7. Xian J, Shi D, Tao X. Imaging of the head and neck·ophthalmology. Beijing: People's Medical Publishing House; 2014.

Imaging Anatomy of Ear

6

Yubo Lyu and Xinjiang Liu

6.1 Foundation of Imaging Anatomy

6.1.1 Overview

The aural region includes outer ear, middle ear and inner ear. The outer ear is composed of the auricle as well as the cartilaginous part and bony part of external auditory canal. The middle ear is composed of tympanic cavity, auditory tube, tympanic antrum and mastoid process. The inner ear is composed of cochlea, vestibule, and semicircular canal. The middle ear and the inner ear lie within the temporal bone.

6.1.2 Main Anatomic Parts of Aural Region

6.1.2.1 Gross Anatomy of Temporal Bone

Important anatomical structures of the aural region lie within the temporal bone between the parietal bone, the sphenoid bone and the occipital bone. It participates in the formation of the skull base and the lateral wall of the cranial cavity and is connected to the mandible through the temporal-mandibular joint. The temporal bone is irregularly shaped, with internal structures overlapping each other and having different directions and positions are different. This makes the anatomic relationship extremely complicated. Taking the external auditory canal as center, it can be divided into five parts: squamous part, petrous part, tympanic part, mastoid portion, and styloid process.

1. **Squamous Part.** It mainly constitutes the lateral wall of the middle cranial fossa but also a small part of the superior wall and posterior wall of the bony part of the external auditory canal. Located in the anterosuperior direction, it resembles fish scales. Its lateral surface, also known as the temporal surface, is involved in forming the medial wall of the temporal fossa and attached by the temporalis muscle. The parietal border is connected with the parietal bone, and the joint is called as the squamous suture. The sphenoidal margin forms the pterion together with the parietal bone, frontal bone and greater wing of sphenoid bone. The posterior border of the squamous part of temporal bone connects the parietal bone and the occipital bone, with the joints called as the parietomastoid suture and the occipitomastoid suture, respectively. There is a zygomatic process below the anterior part, and the posterosuperior curved line of the process is the temporal line. The temporal line is the posterior boundary of the point which the temporalis is attached to, and is attached with the temporal fascia. The squamous part and the mastoid portion meet at the point about 1 cm below the temporal line. The zygomatic process extends forward horizontally and is connected with the temporal process of zygomatic bone to form the zygomatic arch. The posterior root of zygomatic arch, the extension line of the anterior border of mastoid process and the posterior wall of external auditory canal form the superior triangle of external auditory canal, which is the lateral wall of mastoid antrum. The deep surface of zygomatic arch is the temporal fossa which is filled with temporalis. The inner surface of the squamous part of temporal bone, also known as the cerebral surface, is uneven, and the coursing of anterior and posterior branches of the sulcus for the middle meningeal artery is visible.
2. **Petrous Part**. Located at the skull base and of the cone shape, the petrous part, also known as petrous pyramid, includes the inner ear, internal auditory canal and petrous apex. The bone of the petrous part has a density between

Y. Lyu (✉)
Department of Medical Imaging, Jiahui International Hospital, Shanghai, China

X. Liu
Shanghai Pudong Hospital (Fudan University Affiliated Pudong Medical Center), Shanghai, China

H. Li et al. (eds.), *Radiology of Infectious and Inflammatory Diseases - Volume 2*,
https://doi.org/10.1007/978-981-16-8841-6_6

those of occipital bone and sphenoid bone and inclines from the posterolateral side to the anteromedial side. It is the attachment point of the lateral border of tentorium of cerebellum, and also the mark of the boundary between middle cranial fossa and posterior cranial fossa. The petrous part contains vestibulocochlear organ, facial never canal, facial nerve, carotid canal and so on. It consists of anterior surface, posterior surface, inferior surface, an apex and a base. The base of petrous part of temporal bone is continued by the squamous part and the mastoid portion. Facing the anteromedial side, the apex of the petrous part of temporal bone constitutes the posterior wall of foramen lacerum. It is located between the occipital bone and the greater wing of sphenoid bone and has the internal opening of carotid canal. The anterior surface of the petrous part of temporal bone is the posterior part of middle cranial fossa. It is connected to the inner surface of squamous part by the petrosquamosal suture. The posterior surface of petrous part faces the posterior fossa, and is connected to the medial surface of mastoid portion, with the internal acoustic pore near the central part. It is connected to the about 1 cm long internal auditory canal where the facial nerve, vestibulocochlear nerve and labyrinthine artery pass. The inferior surface of petrous part is uneven. It forms a part of the external surface of skull base, with the external aperture of carotid canal near the central part.

3. **Tympanic Part**. The tympanic part is also called as tympanic bone. The tympanic part of temporal bone of an adult is a "U"-shaped structure which constitutes most of the anterior, inferior, and posterior walls of the bony part of external auditory canal. The tympanic ring is on the medial side of tympanic bone, the inferior side of squamous part and the anterior side of mastoid portion. As a curved osteocomma, it constitutes the bony parts of external acoustic pore and external auditory canal The narrow groove on its medial side is called as tympanic sulcus. It is attached by the tympanic membrane. The lateral side of superior border is continued by the posterior wall of mandibular fossa, and its medial side by that of petrotympanic fissure. With thin medial part and thick lateral part, the inferior border houses the styloid process. The lateral border is attached by auricular cartilage. The medial border is combined with the petrous part, squamous part, and mastoid portion to form the anterior wall of tympanomastoid fissure. The external auditory canal, about 2 cm long, inclines from the posterolateral to the anteromedial side, with the middle part slightly convex. The inferior part of its anterior, inferior, and posterior walls is the tympanic part, and the superior part of its superior and posterior walls is the squamous part. The fundus of the external auditory canal is closed by the tympanic membrane, the upper boundary of external acoustic pore is the posterior root of the zygomatic process, and the suprameatal spine is under the root.
4. **Mastoid Portion**. The mastoid portion is located on the posteroinferior side of squamous part of temporal bone. It begins to develop after birth. The mastoid portion gradually extends downward and becomes round and pointed to form a mastoid. Its lateral surface is rough and attached with occipitalis and posterior auricular muscle attached. There are many small foramens on the lateral surface. The mastoid foramen is the largest one, where the emissary vein runs to the transverse sinus or a branch of the occipital artery runs. The mastoid process varies in size, with that of a male generally larger than that of a female. It is the insertion of sternocleidomastoid. There are varying numbers and various sizes of mastoid cells in the mastoid process. Generally, mastoid cells in the superior part are larger and contain air, and then become smaller and smaller towards inferior part until becoming the smallest and containing marrow near the apex. Some persons have no mastoid cell, and their mastoid processes are solid. There are mastoid sinuses in the superior part of mastoid process. Their sinus cavities are large and irregular, and connected to mastoid cells on the inferior side and the epitympanum on the anterior side. The superior boundary of mastoid antrum is the tegmen tympani which is adjacent to the middle cranial fossa; the inferior boundary the mastoid process; the lateral boundary the superior triangle of external auditory canal; and the medial boundary the horizontal semicircular canal. There is a groove for sigmoid sinus on the medial surface of mastoid process, which is separated from the adjacent mastoid cell only by a thin bone plate.
5. **Styloid Process**. Located on the inferior side of tympanic part, it is a slender bony structure anteroinferiorly extending from the tympanic part. With a variable length, the styloid process extends from the inferior side of temporal bone to the anteroinferior side. It is attached by stylohyoid ligament, stylomandibular ligament, styloglossus, stylopharygeal muscle and stylohyoid muscle. The stylohyoid ligament is connected to the lesser horn of hyoid bone. Sometimes the ligament can be partially or completely ossified.

6.1.2.2 Regional Anatomy of Temporal Bone

1. **Tympanic Cavity.** It consists of attic, mesotympanum, and hypotympanum. The attic, also known as epitympanum, is the part above the level of the superior border of partes tensa of tympanic membrane, with the tegmen tympani as its top and the line connecting tympanic scutum to tympanic segment of facial nerve as its bottom. The mesotympanum, also known as inherent tympanic cavity, refers to the tympanic cavity between the planes on superior and inferior borders of the partes tensa of

tympanic membrane, which is the area between the line connecting superior tympanic scutum and the tympanic segment of facial nerve and that connecting the inferior tympanic ring to the promontory of cochlea. The hypotympanum refers to the part below the level of the inferior border of partes tensa of tympanic membrane, which is the area between the line connecting the tympanic ring to the promontory of cochlea and the bottom wall of tympanic cavity.

The tympanic cavity has anterior, posterior, superior, inferior, lateral, and medial walls. The lateral wall is the tympanic membrane, with its upper 1/4 part as the pars flaccida, its lower 3/4 part as the partes tensa, and its center as the umbo of tympanic membrane. The superior wall is also known as the tegmen tympani, which is a thin bone plate. The inferior wall is the jugular wall, which is isolated from the inferior jugular vein by a thin bone plate. The anterior wall is the carotid wall, i.e., the posterior wall of carotid canal. The superior part is the junction between the petrous part of temporal bone and the squamous part. The semicanal of tensor muscle of tympanic membrane is located in the superior part, and that of the auditory tube on the inferior side. The posterior wall is the mastoid wall, with the entrance to mastoid antrum in the superior part. The medial wall is the labyrinthine wall and also the lateral wall of the vestibular portion of the inner ear. There is a round bulge in the middle of the wall, which is called as promontory. The posterosuperior part of the promontory is the vestibular window (oval window). The posteroinferior part of the promontory is the cochlear window (round window). The posterosuperior arcuate protuberance of the vestibular window is called eminentia fallopii, which contains the facial nerve.

There are three ossicles in the tympanic cavity, namely malleus, incus, and stapes.

The malleus is the largest of the three ossicles. It is divided into three parts: the head, the neck and the handle. The head of malleus, as an enlarged part of the superior extremity, is located in the attic. There is a long saddle-shaped articular surface on the posteromedial surface, which forms the incudomalleolar joint together with the saddle-shaped joint on the lateral side of the body of incus. The interior part of the head of malleus is slightly thinner, which is the neck of malleus. There is a long process on the lateral side of the neck as well as a protruding short process (lateral process) at the junction of neck and handle. The thin flat part below the neck of malleus is the manubrium mallei. The bicuspid incus is between the incus and the stapes. It consists of body of incus, long crus and short crus. The body of incus is located in the attic. Its anterior surface forms the incudomalleolar joint with the head of malleus. The short crus of incus is about 5 mm long. The end of the long crus of incus is slightly enlarged, which is called as the lenticular process. It forms the incudostapedial joint with the head of stapes. The stirrup-shaped stapes are the smallest of the ossicles and located at the innermost end of the ossicles. It is divided into head, neck, anterior crus, posterior crus and base (or foot plate). The head of stapes has great size and shape variations. Its top is a concave articular surface, which forms the incudostapedial joint with the lenticular process of incus. The neck of stapes is short, making it difficult to identify it sometimes. The anterior crus is thinner, shorter, and straighter than the posterior crus, which is relatively longer and more curved. The size and shape of the base of stapes are equivalent to those of the vestibular window.

The auditory tube is the passage between the tympanic cavity and the nasopharynx. It can be divided into the anteromedial cartilaginous part and posterolateral bony part. Generally, the cartilaginous part accounts for about 2/3 of the length of the auditory tube, while the bony part about 1/3 of the full length of the auditory tube. The isthmus of auditory tube is at their junction. The auditory tube of an adult is long and inclined, while that of a child is short, thick, and horizontal.

2. **Inner Ear**. The inner ear, also known as the labyrinth, is located in the petrous part of the temporal bone. It consists of the bony tube and the membranous tube on its deep surface, namely, bony labyrinth and membranous labyrinth.
   (a) Bony Labyrinth: Consisting of dense bones, It is composed of the vestibule, cochlea, and semicircular canal from the lateral side to the posterior side. The lateral wall of the vestibule is the medial wall of the tympanic cavity. The medial wall is aligned with the internal acoustic canal to form the base of the latter. The vestibule communicates anteriorly with the cochlea and posterosuperiorly with the semicircular canals by five foramens. The vestibular aqueduct is a curved duct in the temporal bone, which is located on the posterolateral side of the internal acoustic pore. It houses a part of ductus endolymphaticus and endolymphatic sac. Bony semicircular canal is three semicircular canals, namely lateral (horizontal), superior (anterior) and posterior semicircular canals. The three semicircular canals are perpendicular to each other. Each semicircular canal has two ends, with the enlarged one called as the ampulla and another end called as single crus. The single crus of the lateral semicircular canal and that of the posterior semicircular canal form a crus commune. Therefore, the three semicircular canals communicate with the vestibule by five foramens. The cochlea is formed by the cochlear spiral canal wrapping the modiolus by 2.5 to 2.75 turns (or circles), with its bottom as the basal

turn (circle), the middle as the middle turn (circle) and the top as the apical turn (circle). The osseous spiral lamina originating from the modiolus extends into the cochlear spiral canal without reaching its lateral wall. The basement membrane continuing the osseous spiral lamina reaches the lateral wall to divide the cochlear spiral canal into superior and inferior parts. The superior part is divided into two cavities by the vestibular membrane. Therefore, there are three lumens in the cochlear spiral canal, namely, the vestibular scale in the superior part; the cochlear duct in middle, which is also known as the scala media (a membranous labyrinth); and the scala tympani in the inferior part. There is a cochlear window at the origin of the scala tympani, which is closed by the cochlear window membrane (also called the second tympanic membrane). The cochlear aqueduct has an opening (internal opening) near the point to which the cochlear window membrane is attached to and an external opening in the triangular fovea on the medial side of jugular foramen crest under the petrous part. The perilymph of scala tympani communicates with the subarachnoid space via the cochlear aqueduct.

(b) Membranous Labyrinth: The membranous labyrinth is a membranous duct and capsule located in the bony labyrinth. Its diameter is smaller than that of the bony labyrinth. It consists of the utricle and saccule in the vestibule; the membranous semicircular duct of bony semicircular canal, which communicates with the utricle via five foramens; and the cochlear duct in the cochlear spiral canal. The utricle and the saccule extend out a small duct, respectively, which then merge into the endolymphatic duct, with the end expanding into the endolymphatic sac. The endolymphatic duct lies in the vestibular aqueduct. A small part of the endolymphatic sac lies in the distal segment of the vestibular aqueduct, which is called as the internal part of bone. Its wall has abundant folds, which is also called as the rough part of the endolymphatic sac. At the external aperture of the vestibular aqueduct, the endolymphatic sac migrates into the cerebral dura mater part posterior to the petrous part of temporal bone, which is also called as the lateral part of the bone. Because its wall is smooth and the cystic cavity is flat, it is also called as the smooth part.

3. **Facial Nerve.** It consists of five segments, including intracranial segment, internal auditory canal segment, labyrinthine segment, tympanic segment and mastoid segment.

The intracranial segment originates from the pontopeduncular area, courses through the cerebellopontine angle pool, and inserts at the internal acoustic pore. It contains motor fiber and sensory fiber. The 10–14 mm long motor fiber takes up 70%.

The internal auditory canal segment is a facial nerve area from the internal acoustic pore to the fundus of the internal auditory canal. It is 7–8 mm long. The first and second segments of the facial nerve are accompanied by the vestibulocochlear nerve and the labyrinthine artery branch (internal auditory artery) of the basilar artery. It is extremely easy for the cochlear nerve tumor here to compress the facial nerve to produce infranuclear facial paralysis.

The labyrinth segment is the shortest segment, only 2.5–3 mm long. It courses laterally to slightly incline anteriorly and then reaches the geniculate ganglion between vestibule and the cochlea.

The facial nerve in the tympanic segment is also called as the horizontal segment. It turns posteriorly from the geniculate ganglion and slightly inferiorly, and finally reaches the posterior wall of tympanic cavity via the posterosuperior part of the vestibular window of the medial wall of tympanic cavity. It is the most vulnerable site for otitis media lesions and surgery. The segment of facial nerve is 8–12 mm long. The facial nerve of tympanic segment turns from the horizontal plane to the vertical plane and then enters the mastoid process. It bends into an angle of 110°–127° opening forward, and the turning knee is 2–3 mm long.

The facial nerve of the mastoid segment originates from the point 1–2 mm inferior to the cone bulge, or its superior extremity lies inferiorly to the posterior extremity of the lateral semicircular canal, which is equivalent to below the short crus of incus and the plane of cone bulge, and then extends inferiorly to the stylomastoid foramen. The facial nerve of the mastoid segment is fully 15–20 mm long.

4. **Mastoid Antrum and Mastoid Cell.** The mastoid antrum lies posterior to the epitympanum and communicates with the mastoid cells posteroinferiorly. Mastoid cells are formed by gasification of the spongy bone in the mastoid portion. The mucosa of this part is continuous with the mucosa of mastoid antrum and tympanic cavity. Therefore, the inflammation of middle ear can invade this part through the mastoid antrum and cause mastoiditis.

6.1.2.3 Common Developmental Variations

1. **Mastoid Process.** The imaging findings are related to the type of mastoid process. The mastoid process can be classified into pneumatic type, diploetic type, sclerotic type and mixed type according to the gasification degree of the mastoid [1]. (1) The mastoid process of pneumatic type is characterized by transparent and clear mastoid cells,

complete and sharp septa, and varying sizes of mastoid cells, with those close to the border and especially apex of the mastoid process larger. (2) The mastoid process of diploetic type is characterized by small and numerous air cells, thick air cell septum, thick lateral bone, and diploe structure resembling the skull. (3) The mastoid process of sclerotic type is characterized by undeveloped air cells and dense bone. (4) The mastoid process of mix type is between the diploetic type and the pneumatic type.

2. **Anteriorly Placed Sigmoid Sinus.** Axial CT shows that the sigmoid sinus plate is less than 1 cm away from the posterior wall of external auditory canal. It is the anteposition of sigmoid sinus. The anteriorly placed sigmoid sinus usually occurs in the mastoid process of sclerotic type, which can easily cause massive hemorrhage if being touched during surgery.
3. **Low Tegmen Tympani**. The coronal CT image shows that the superior tegmen tympani is less than 5 mm away from the superior border of the porus acusticus externus, prompting the inferior position of tegmen tympani. In case of failure to realize the development characteristics of tegmen tympani during operation, it is easy to destroy the tegmen tympani at the bottom of middle cranial fossa and then cause intracranial complications [2].
4. **High Jugular Bulb.** The axial CT image shows that the highest level of the jugular bulb exceeding the basal turn of the cochlea, the upwardly protruding part having the same density as and connected to the jugular vein, as well as Smooth and undestroyed surrounding bone structure. The MRI image shows eddy current signals of blood.

6.2 CT Imaging Anatomy

6.2.1 CT Imaging Anatomy of Transverse Plane

1. **Semicircular Canal Level of Anterior Bone**. Cross-sectional images of anterior crus and posterior crus of the anterior semicircular canal can be seen in the bone of petrous part of temporal bone, showing two small punctate low-density shadows. A fine tubular fossae subarcuata can be seen between anterior crus and posterior crus, in which the subarcuate lies. The posterior crus of the anterior semicircular canal and the superior crus of the posterior semicircular canal are a common crus, i.e., common bony crus. The superior crus and inferior crus of the posterior semicircular canal are shown as linear tube shadows (Fig. 6.1a) on the adjacent level. Three punctate tube sections are shown on lower levels, which are the anterior crus of the anterior semicircular canal, the common bony crus, and the arc part of the posterior semicircular canal [3, 4].
2. **Semicircular Canal Level of Lateral Bone**. The lateral semicircular canal is shown as a ring structure. Its medial side is connected with the vestibule, the anterior part on the lateral side is the superior attic which is connected to the mastoid antrum via the entrance to mastoid antrum, and the posterior round punctate shadow is the posterior semicircular canal. The tubular structure inclining anterolateral between the medial superior part of vestibule and the basal turn of cochlea is the labyrinthine segment of facial nerve canal. It is anteriorly connected to the geniculate nerve fossa, and the thicker inner tubular structure is the internal auditory canal (Fig. 6.1b).
3. **Vestibular Window Level**. Two bony structures can be seen in the tympanic cavity. The anterior round bone structure is the head of malleus, and the posterior triangular structure is the body of incus and the short incus of incus. The head of malleus and the body of incus form the incudomalleolar joint. The anterolateral linear low-density shadow is the tensor of tympanic membrane, and the linear structure on the superior level is the tympanic segment of facial nerve canal. The medial elliptical low-density shadow is the vestibule, and its lateral side communicates with the bone absence area of tympanic cavity, i.e., the vestibular window, which is closed by the stapes footplate. The internal auditory canal is on the medial side of vestibule, and the basal and middle turns of cochlea on the anterior side. The common bony crus entering the vestibule can be seen in the posterior part of the vestibule, the punctate cross-section shadow of posterior semicircular canal can be seen in the posterolateral part, and the posteromedial linear low-density shadow is the vestibular aqueduct (Fig. 6.1c).
4. **Cochlea Level**. This level of cochlea is spiral. The anterolateral isodensity line shadow of cochlea is the tensor of tympanic membrane, and the lateral part of tensor tendon of periosteum being connected to the manubrium mallei by the tensor tendon of tympanic membrane can be seen at the superior level. The bony structure of the basal turn of cochlea, which protrudes from the basal turn of cochlea into the tympanic cavity, is called as the promontory. After the basal turn of cochlea is connected with, the posterior bone absence area is the cochlear window. Two bony structures can be seen in the medial part of tympanic cavity, including the anterior punctate structure as the section of the neck of malleus and the linear structure as the long crus of incus. The medial bony bulge of the posterior wall of tympanic cavity is called as the pyramidal eminence, the medial recess of which is called as the sinus tympani or pyramidal recess. The posteromedial linear low-density shadow of pyramidal recess is the inferior crus of posterior semicircular canal, and the vestibular aqueduct and its opening can be seen in its posterior part (Fig. 6.1d)

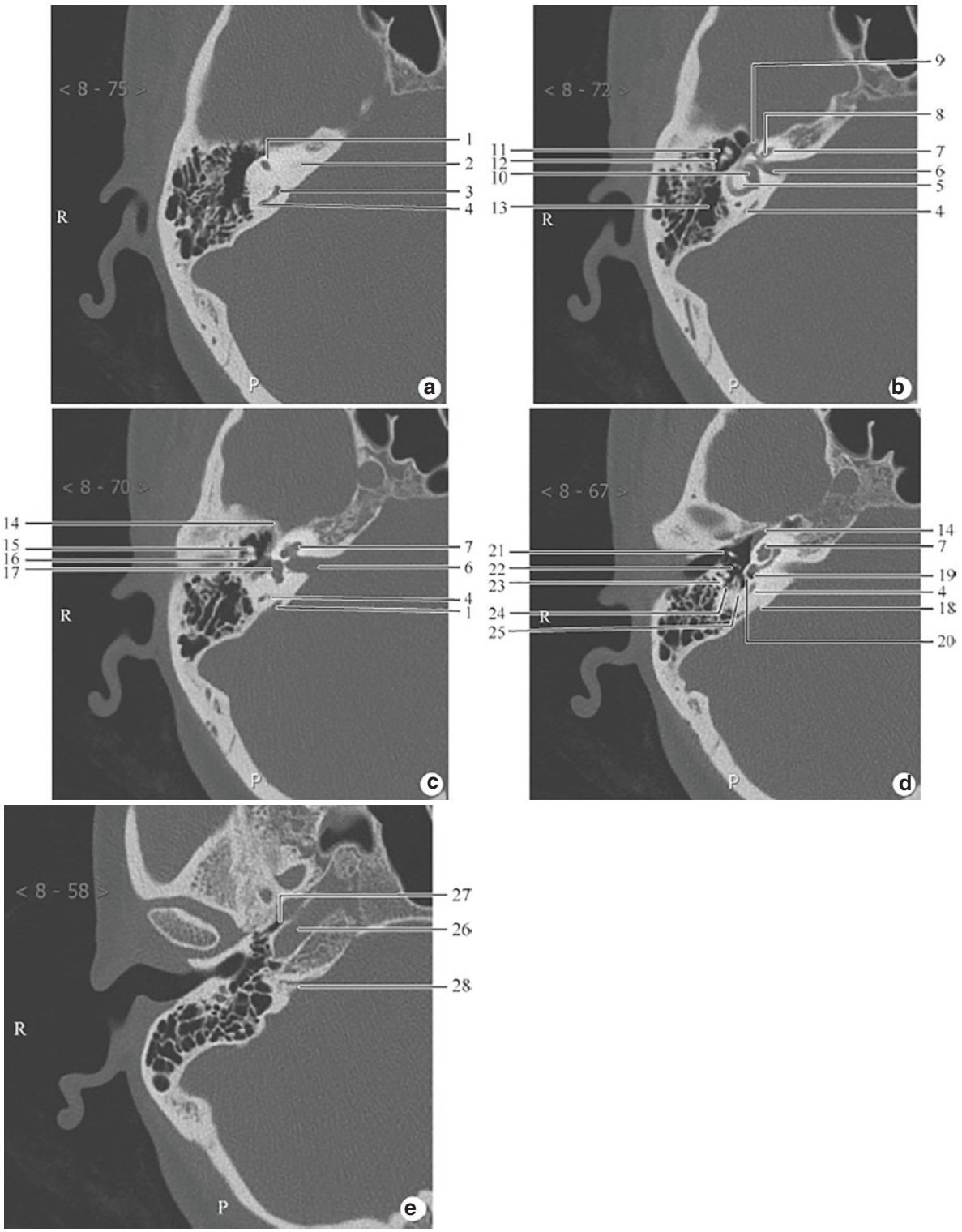

Fig. 6.1 Imaging anatomy of CT transverse plane of ear. (**a**) CT anatomic image of anterior semicircular canal level; (**b**) CT anatomic image of lateral semicircular canal level; (**c**) CT anatomical image of vestibular window level; (**d**) CT anatomic image of cochlea level; (**e**) CT anatomic image of carotid canal level; 1. Anterior semicircular canal; 2. Fossae subarcuata; 3. Common bony crus; 4. Posterior semicircular canal; 5. Lateral semicircular canal; 6. Internal auditory canal; 7. Cochlea; 8. Labyrinthine segment of facial nerve canal; 9. Geniculate ganglion; 10. Vestibule; 11. Attic; 12. Entrance to mastoid antrum; 13. Mastoid antrum; 14. Tensor tympani; 15. Head of malleus; 16. Body of incus; 17. Vestibular window; 18. Vestibular aqueduct; 19. Round window; 20. Promontorium tympani; 21. Neck of malleus; 22. Long crus of incus; 23. Facial nerve recess; 24. Pyramidal eminence; 25. Sinus tympani; 26. Internal carotid artery; 27. Auditory tube; 28. Cochlear aqueduct

5. **Carotid Canal Level**. The lateral oblique air-filled canal structure of carotid canal is the auditory tube, the opening of which is the tympanic cavity; the lateral tubular air-filled structure is the external auditory canal, and the posterior air-filled cell-like structure is the mastoid air cell. The petrous part of temporal bone inclines from the posterolateral side to the anteromedial thick tubular structure, which is the carotid canal, and the posterior round low-density shadow is the jugular bulb. The flared structure between them is the opening of cochlear aqueduct (Fig. 6.1e).

6.2.2 CT Imaging Anatomy of Coronal Plane

1. **Petrous Apex Level.** The section of the elliptical tubular structure of the petrous apex part is the carotid canal. The lateral punctate low-density shadow is the tensor tympani, the more lateral air-filled tube is the auditory tube, and the most lateral part is the temporal-mandibular joint (Fig. 6.2a).
2. **Cochlea Level.** The head and neck of malleus as well as the manubrium mallei can be seen in the tympanic cavity. The spiral structure of the petrous part of temporal bone is the cochlea [5], and two punctate low-density shadows can be seen in the anterolateral part of the cochlea, which are the labyrinthine segment of facial nerve canal and the tympanic segment, respectively. The tensor tympani is visible inferiorly to the tympanic segment of facial nerve, and the connection between tensor tympani and neck of malleus is visible. The lateral wall of the attic extends in the medial inferior direction as a scutum, and the space formed by it with the head and neck of malleus is called the Prussak space (Fig. 6.2b).
3. **Vestibular Window Level.** The vestibule is connected to the anterior crus of anterior semicircular canal superiorly, the horizontal semicircular canal laterally, and the basal turn of cochlea inferiorly. The medial low-density shadow in the dense bone of the petrous part of temporal bone is the vestibule, and the lateral bone structure absence part is the vestibular window. The inferior punctate low-density shadow of the horizontal semicircular canal is the tympanic segment of the facial nerve canal, and the medial tubular structure of the vestibule is the internal auditory canal (Fig. 6.2c).
4. **Cochlear Window Level**. The inferior bone absence area of the vestibule is the cochlear window, the punctate high-density structure in the superior dense bone of the vestibule is the arch of the anterior semicircular canal, the lateral size is connected to the horizontal semicircular canal, the superolateral air-filled structure is the entrance to mastoid antrum, and the medial part of the vestibule is the internal auditory canal (Fig. 6.2d).
5. **Common Bony Crus Level.** The vertical tubular structure in the middle of the dense bone is the shared crus (common bony crus) of the anterior semicircular canal and the posterior semicircular canal. The inferior medial tubular structure is the cochlear aqueduct, and the larger lateral bony depression area is called as the jugular bulb. The lateral horizontal tubular structure is the horizontal semicircular canal, and the superior linear structure is the fossae subarcuata. Two small punctate low-density shadows can be seen in the petrous part of temporal bone. There are cross-sectional images of anterior crus and posterior crus of the anterior semicircular canal, respectively. A tubule shadow coursing wards and forwards can be seen between anterior crus and posterior crus, which is called as the fossae subarcuata where the subarcuate courses (Fig. 6.2e).
6. **Level of Mastoid Segment of Facial Nerve Canal.** The tubular structure coursing vertically in the middle is the vertical segment of the facial nerve canal, that is, the mastoid segment. Its two medial superior high-density punctate structures are cross-sections of the posterior semicircular canal which is in the arc-shaped line pattern as observed and where the medial sigmoid sinus can be seen.

6.3 MR Imaging Anatomy

In the structure of aural region, the middle ear is composed of air and bone structures, which shows no signal shown on the MRI image. The lymphatic fluid of membranous labyrinth of inner ear and the cerebrospinal fluid of internal auditory canal show hyperintense on T_2WI, and the nerve shows isointense. In the T_2WI transverse plane, the cerebrospinal fluid of internal auditory canal shows hyperintense; the facial nerve, the cochlear nerve and the vestibular nerve show isointense running through them; and both the cochlea and the semicircular canal show hyperintense (Fig. 6.3a). Four punctate isointenses between the hyperintenses of cerebrospinal fluid can be seen in the plane of the internal auditory canal, with the facial nerve in the anterosuperior direction, the cochlear nerve in the anterior inferior direction, the superior vestibular nerve in the posterosuperior direction, and the inferior vestibular nerve in the posteroinferior direction (Fig. 6.3b). After being processed by VR, the membranous labyrinth of inner ear can also be shown on a three-dimensional image to be observed at any rotation angle (Fig. 6.3b) [6].

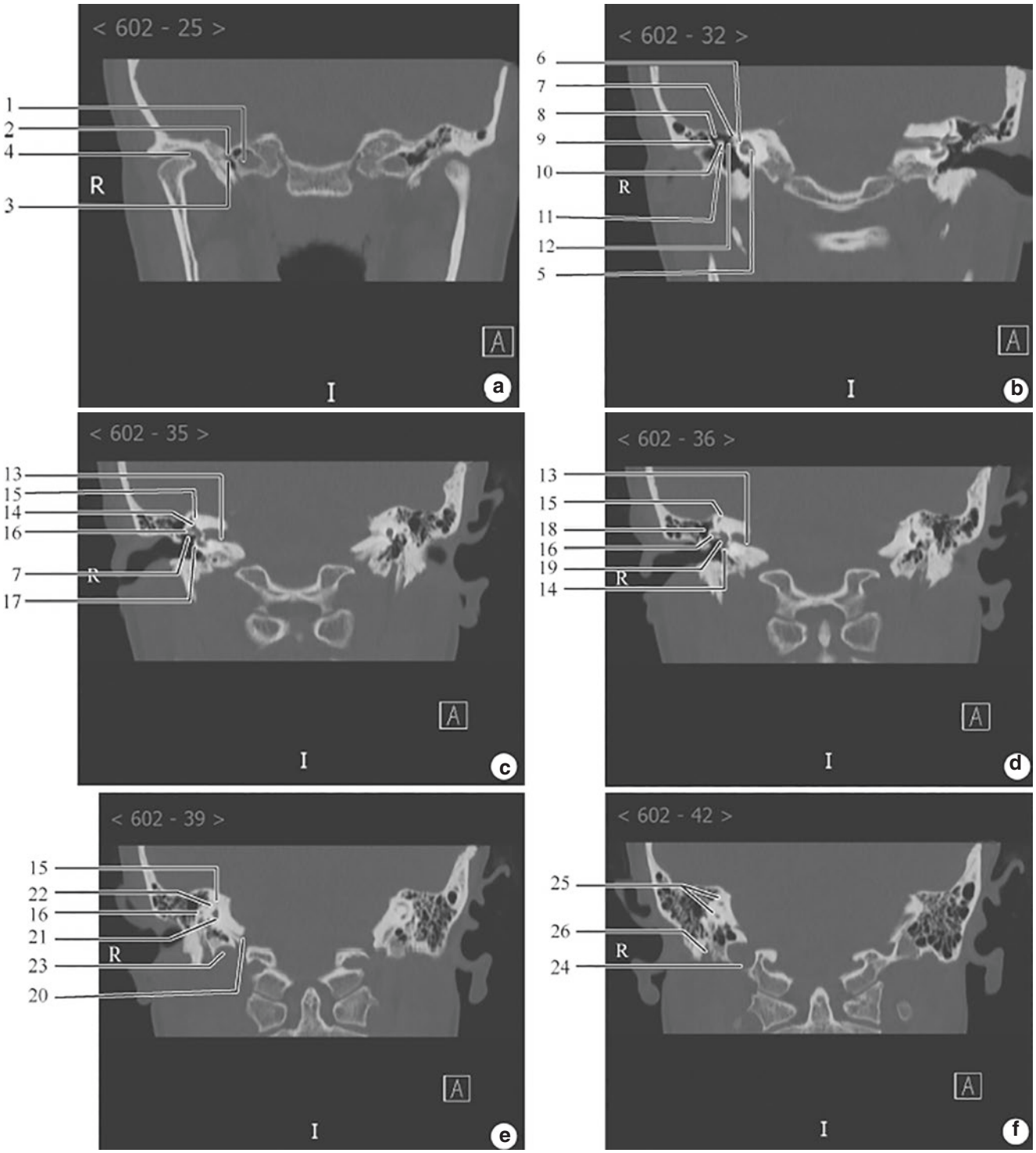

Fig. 6.2 Imaging anatomy of CT coronal plane of ear. (**a**) CT anatomic image of petrous apex level; (**b**) CT anatomic image of cochlea level; (**c**). CT anatomic image of vestibular window level; (**d**) CT anatomic image of cochlear window level; (**e**) CT anatomic image of common bony crus level; (**f**) CT anatomic image of mastoid segment of facial nerve level. 1. Internal carotid artery; 2. Tensor tympani; 3. Auditory tube; 4. Temporal-mandibular joint; 5. Cochlea; 6. Labyrinthine segment of facial nerve canal; 7. Tympanic segment of facial nerve canal; 8. Head of malleus; 9. Scutum; 10. Neck of malleus; 11. Manubrium mallei; 12. Tensor tympani; 13. Internal auditory canal; 14. Vestibule; 15. Anterior semicircular canal; 16. Lateral semicircular canal; 17. Vestibular window; 18. Entrance to mastoid antrum; 19. Round window; 20. Cochlear aqueduct; 21. Common bony crus; 22. Fossae subarcuata; 23. Jugular bulb; 24. Sigmoid sinus; 25. Posterior semicircular canal; 26. Mastoid segment of facial nerve canal

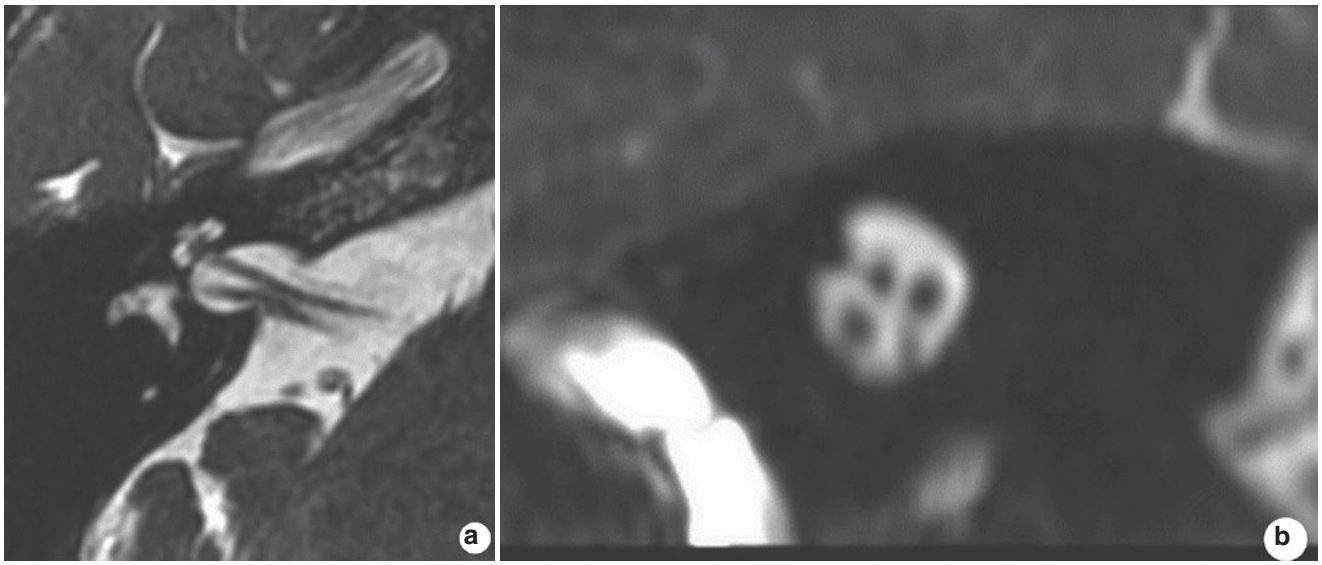

Fig. 6.3 Images of internal auditory canal. (**a**) Axial image of the inner ear of internal auditory canal, which shows the cochlear nerve, cochlea, and semicircular canal of the internal auditory canal; (**b**) Cross-sectional image of the internal auditory canal, which shows the cochlear nerve, facial nerve, superior vestibular nerve and inferior vestibular nerve

References

1. Demin H. Otorhinolaryngology head and neck surgery. Beijing: Peking University Medical Press; 2013.
2. Qihua W. Practical anatomy of otorhinolaryngology - head and neck surgery. Beijing: People's Medical Publishing House; 2010.
3. Editorial Board of Chinese Journal of Radiology. Guideline on CT and MR specification for head and neck (revised draft). Chin J Radiol. 2007;41(9):996–9.
4. Junfang X, Lin M, Qian W. Progress, challenge and future for imaging of ear. Chin J Otol. 2018;16(5):589–92.
5. Ling S, Zhixiang W. The application of CT in the diagnosis and treatment of children with inner ear malformations before surgery. Chin J CT MRI. 2018;16(6):62–4.
6. Quan W, Lijie B, Chenyi S, et al. Application value of the magnetic resonance hydrography (MRH) of middle and inner ears in the diagnosis of BPPV. China Med Dev. 2017;32(3):69–72.

Imaging Anatomy of Nose and Paranasal Sinus

7

Yu Wang, Jie Hu, and Heng Liu

7.1 Foundation of Imaging Anatomy

The nasal part is composed of the external nose, the nasal cavity and the paranasal sinus. The external nose and the nasal cavity are often collectively referred to as the nose. Therefore, the nasal part can also be divided into the nose and the paranasal sinuses. The paranasal sinus lies in the superior and posterosuperior directions of and on both sides of the nasal cavity. The nasal cavity and each paranasal sinus are separated from the orbit, the anterior cranial fossa and the middle cranial fossa only by a thin bone plate. Therefore, the nasal cavity or paranasal sinus disease can involve the orbit or the intracranial part [1].

Feeding arteries and innervations of the nose and paranasal sinus are as shown in Table 7.1.

7.2 CT and MR Imaging Anatomy

The imaging examination of paranasal sinus is conducted mainly by CT. When tumors and other diseases are suspected, if the natures of such diseases cannot be identified by CT, MRI can be used to identify different diseases based on their different pathological characteristics.

7.2.1 External Nose

The external nose features the superior part narrower than the inferior part, having the pyramid shape. The external nasal stent is mostly cartilage, with a small proportion of bone components. The cartilage stent is mainly composed of paired superior nasal cartilage and greater alar cartilage on the left and right sides. The bony stent of the external nose is composed of the frontal nasal process, the nasal bone, and the frontal process of maxilla (Figs. 7.1, 7.2, and 7.3). The septum nasi osseum is mainly composed of the perpendicular plate of ethmoid and the vomer, and the cartilaginous nasal septum is mainly composed of the nasal septal cartilage. Turbinate is the osseous anatomy of the lateral wall of

Table 7.1 Feeding arteries and innervations of the nose and paranasal sinus

Position	Composition	Main feeding artery	Main innervation
External nose	Bony part and cartilaginous part	Facial artery and ophthalmic artery branch	Buccal branch of facial nerve, ophthalmic nerve, maxillary nerve, etc.
Nasal cavity	Nasal vestibule and nasal fossa proper	Ophthalmic artery and maxillary artery	Olfactory nerve, sensory nerve and autonomic nerve
Paranasal sinus	Maxillary sinus	Sphenopalatine artery and infraorbital artery	Infraorbital nerve and superior alveolar nerves
	Frontal sinus	Supraorbital artery and anterior ethmoid artery	Medial branch of frontal nerve
	Ethmoidal sinus	Sphenopalatine artery and infraorbital artery	Anterior ethmoidal nerve, posterior ethmoidal nerve and sphenopalatine nerve
	Sphenoid sinus	Posterior ethmoidal artery and maxillary artery	Posterior ethmoidal nerve, and orbital branch of sphenopalatine nerve

Y. Wang
The Affiliated Hospital of Shandong University of TCM, Jinan, China

J. Hu · H. Liu (✉)
Affiliated Hospital of Zunyi Medical University, Zunyi, China

H. Li et al. (eds.), *Radiology of Infectious and Inflammatory Diseases - Volume 2*,
https://doi.org/10.1007/978-981-16-8841-6_7

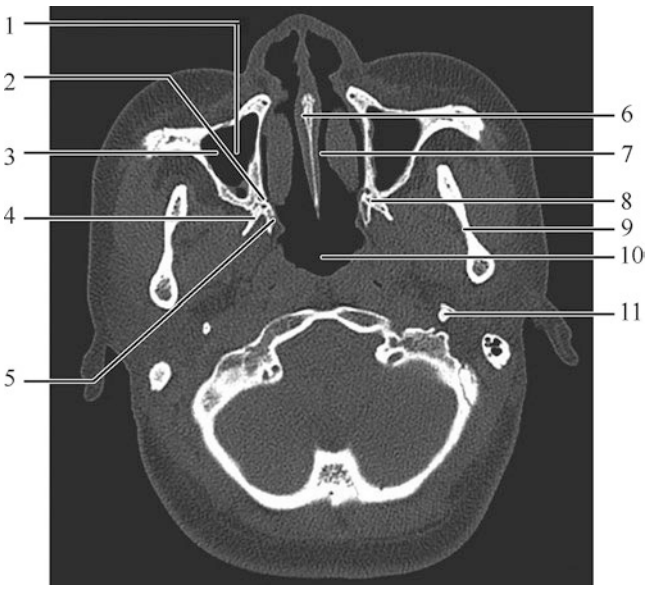

Fig. 7.1 CT image of the transverse plane of paranasal sinus (1). 1. Inferior turbinate; 2. Foramen palatinum majus; 3. Maxillary sinus; 4. Lateral pterygoid plate; 5. Medial pterygoid plate; 6. Septum nasi osseum; 7. Nasal cavity; 8. Lesser palatine foramen; 9. Mandible; 10. Nasopharyngeal cavity; 11. Styloid process

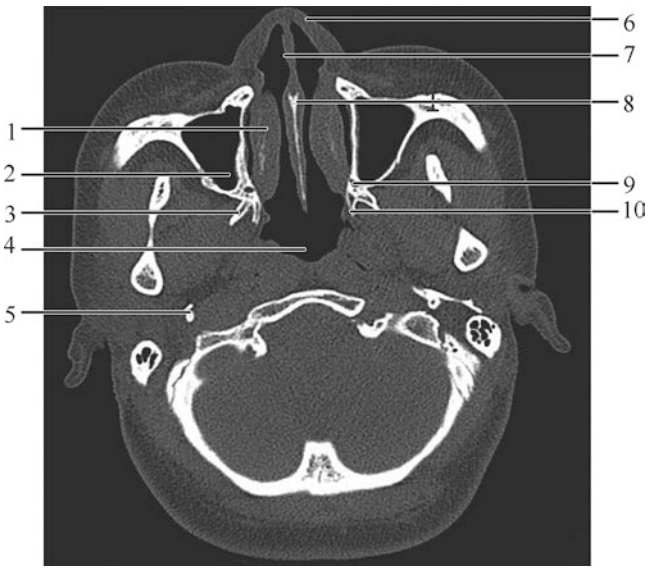

Fig. 7.2 CT image of the transverse plane of paranasal sinus (1). 1. Inferior turbinate; 2. Maxillary sinus; 3. Lateral pterygoid plate; 4. Nasopharyngeal cavity; 5. Styloid process; 6. Ala nasi; 7. Cartilaginous nasal septum; 8. Septum nasi osseum; 9. Foramen palatinum majus; 10. Medial pterygoid plate

nasal cavity. There are superior, middle, and inferior turbinates, below which are superior, middle, and inferior nasal meatus. Superior and middle turbinates compose the medial wall of the ethmoid bone, while the inferior turbinate is a

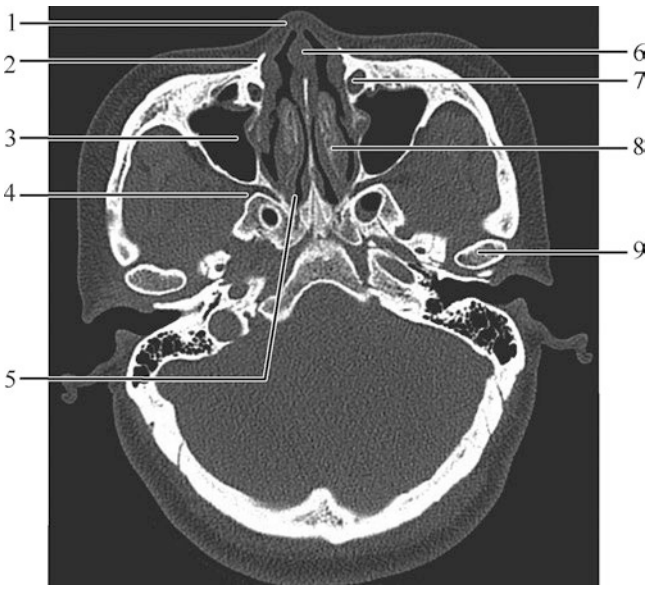

Fig. 7.3 CT image of the transverse plane of paranasal sinus (3). 1. Ala nasi; 2. Frontal process of maxilla; 3. Maxillary sinus; 4. Pterygopalatine fossa; 5. Choana; 6. Nasal septum 7. Nasolacrimal duct; 8. Middle turbinate; 9. Condyloid process

separate bony structure laterally connected to the maxilla (Figs. 7.1, 7.2, and 7.3).

7.2.2 Nasal Cavity

The nasal septum divides the nasal cavity into left and right cavities, both of which feature the superior part narrower than the inferior part. Originating from the anterior nares and inserting at the posterior nares, communicating with the nasopharynx. The top and bottom of the nasal cavity are roughly parallel. The nasal cavity is divided into the nasal vestibule and the nasal fossa proper by the nasal limen [1–3] (Figs. 7.4, 7.5, 7.6, and 7.7). The nasal vestibule is the relatively enlarged part of the anterior inferior part of the nasal cavity. It mainly lies on medial surface of ala nasi and apex nasi. As a main part of the nasal cavity, the nasal fossa proper lies in the posterior part of the nasal cavity. It is formed by covering the osseous nasal cavity and cartilaginous nasal cavity with mucosa.

7.2.3 Paranasal Sinus

Paranasal sinus includes frontal sinus, ethmoidal sinus, maxillary sinus and sphenoid sinus. Paranasal sinuses can be divided into anterior and posterior groups of nasal sinuses according to the location of the opening. The anterior group of nasal sinuses includes frontal sinus, anterior, and medial

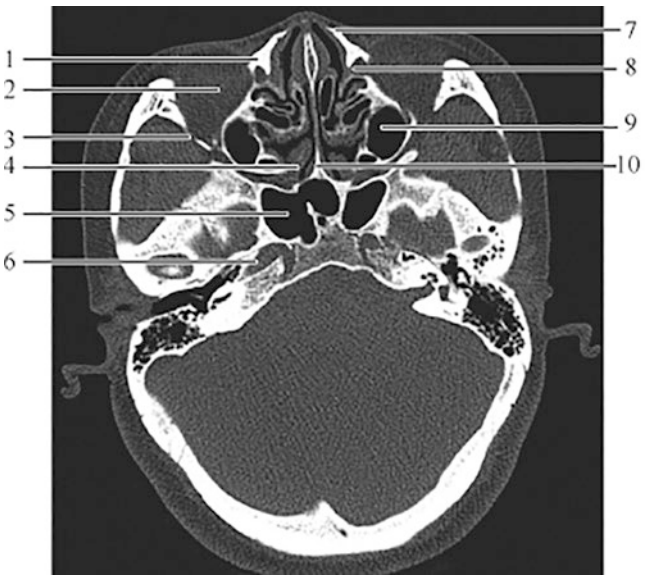

Fig. 7.4 CT image of the transverse plane of paranasal sinus (4). 1. Anterior lacrimal crest; 2. Eyeball; 3. Inferior orbital fissure; 4. Superior turbinate; 5. Sphenoid sinus 6. Internal carotid artery canal; 7. Frontal process of maxilla; 8. Fossa for lacrimal sac; 9. Maxillary sinus; 10. Sphenoid ridge

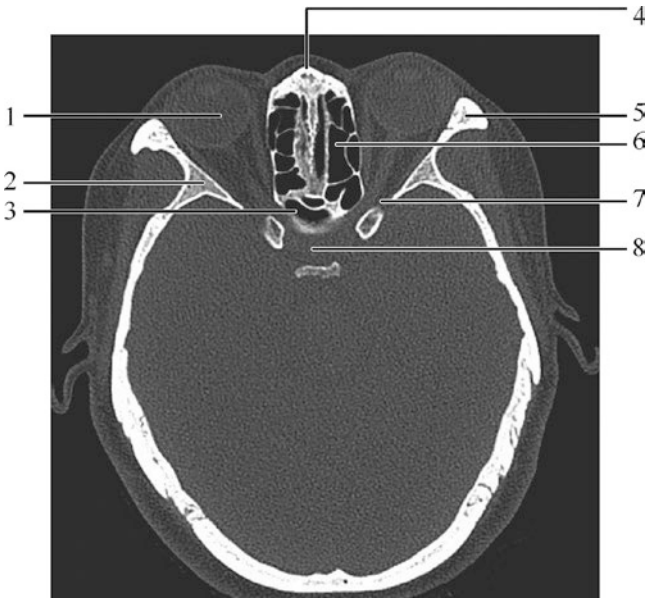

Fig. 7.6 CT image of the transverse plane of paranasal sinus (6). 1. Eyeball 2. Greater wing of sphenoid bone; 3. Sphenoid sinus; 4. Nasal bone; 5. Orbital process of the zygomatic bone of styloid process; 6. Ethmoidal sinus; 7. Superior orbital fissure; 8. Hypophysial fossa

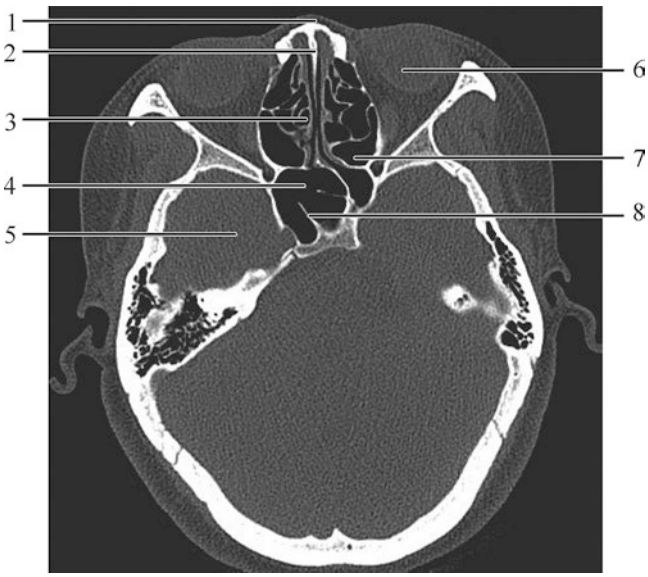

Fig. 7.5 CT image of the transverse plane of paranasal sinus (5). 1. Nasal bone; 2. Septum nasi osseum; 3. Ethmoidal sinus; 4. Sphenoid sinus; 5. Infratemporal fossa; 6. Eyeball; 7. Maxillary sinus; 8. Bony septum in sphenoid sinus

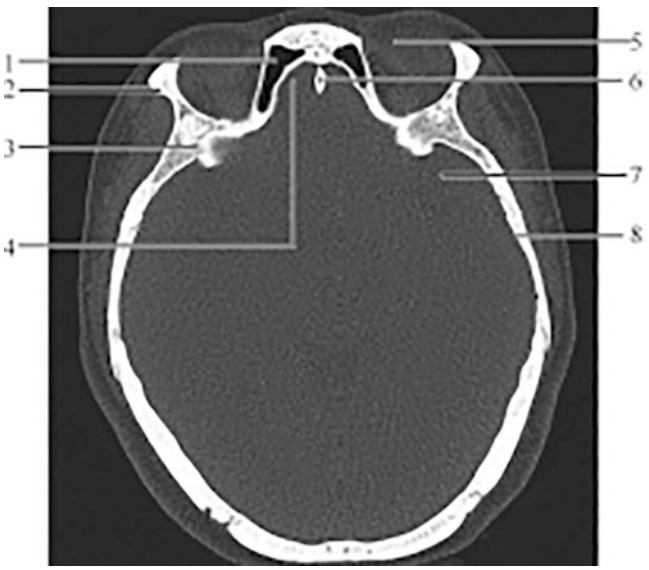

Fig. 7.7 CT image of the transverse plane of paranasal sinus (7). 1. Frontal sinus 2. Orbital process of frontal bone; 3. Greater wing of sphenoid bone; 4. Anterior cranial fossa; 5. Orbit; 6. Cockscomb; 7. Middle cranial fossa; 8. Temporal bone

ethmoidal sinus cells, and maxillary sinus, with their openings in the middle nasal meatus. The posterior group of nasal sinuses includes the posterior ethmoidal sinus cell and the sphenoid sinus, with the opening of the former in the superior meatus and that of the latter in the sphenoethmoidal recess. Paranasal sinuses can be divided into superior and inferior groups by their locations. The superior group of nasal sinuses includes frontal sinus, ethmoidal sinus and sphenoid sinus, which as a complete group of air cells. This group is separated from the intracranial tissues only by a thin bone plate. Therefore, it is easy for the lesions of these paranasal sinuses to involve the intracranial part. The inferior

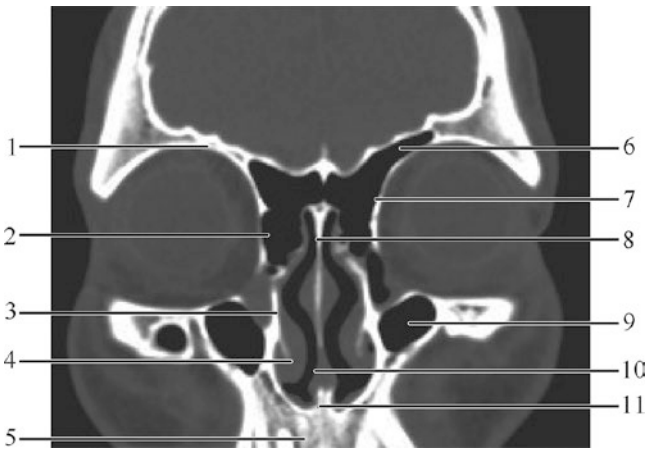

Fig. 7.8 CT image of the coronal plane of paranasal sinus (1). 1. Orbital part of frontal bone; 2. Anterior ethmoidal sinus; 3. Frontal process of maxilla; 4. Inferior turbinate; 5. Incisive bone; 6. Frontal sinus; 7. Ethmoid bont; 8. Perpendicular plate of ethmoid bone; 9. Maxillary sinus; 10. Cartilaginous part of nasal septum; 11. Vomer

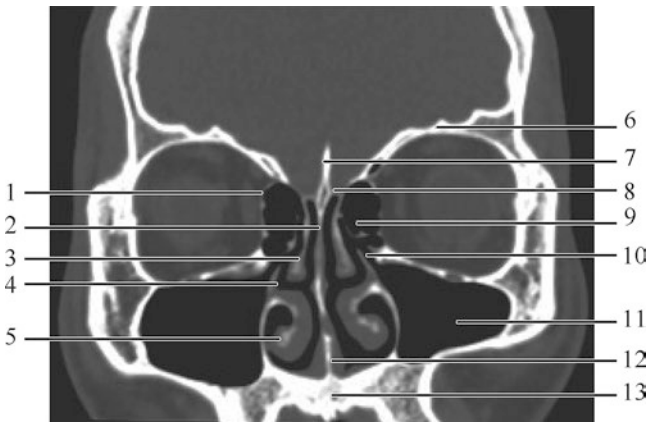

Fig. 7.10 CT image of the coronal plane of paranasal sinus (3). 1. Ethmoid bont; 2. Nasal septum; 3. Middle turbinate; 4. Uncinate process; 5. Inferior turbinate 6. Orbital part of frontal bone; 7. Cockscomb; 8. Cribriform plate; 9. Anterior ethmoidal sinus; 10. Opening of maxillary sinus; 11. Maxillary sinus; 12. Vomer; 13. Hard palate

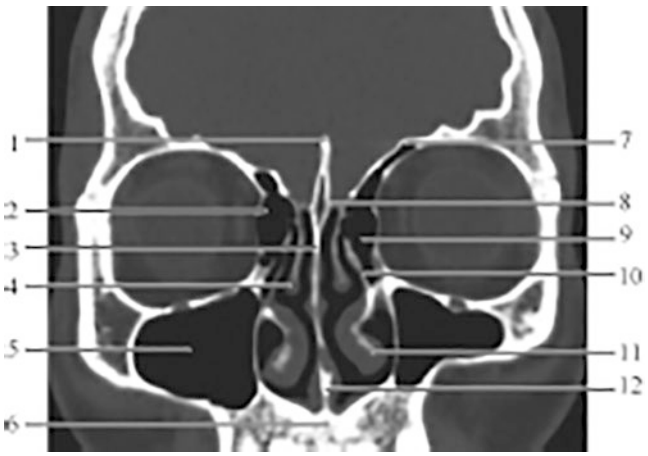

Fig. 7.9 CT image of the coronal plane of paranasal sinus (2). 1. Cockscomb 2. Ethmoid bont; 3. Nasal septum; 4. Middle turbinate; 5. Maxillary sinus; 6. Hard palate; 7. Frontal sinus; 8. Cribriform plate; 9. Anterior ethmoidal sinus; 10. Uncinate process; 11. Inferior turbinate; 12. Vomer

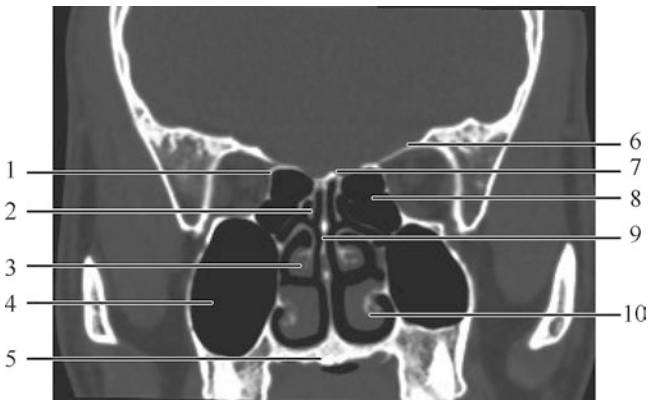

Fig. 7.11 CT image of the coronal plane of paranasal sinus (4). 1. Ethmoid bont; 2. Superior turbinate; 3. Middle turbinate; 4. Maxillary sinus 5. Hard palate; 6. Orbital part of frontal bone; 7. Cribriform plate; 8. Anterior ethmoidal sinus; 9. Nasal septum; 10. Inferior turbinate

group of nasal sinuses is the maxillary sinus, which is at an inferior location and far away from the brain. Therefore, it is not easy to cause intracranial complications [1–3] (Figs. 7.8, 7.9, 7.10, 7.11, 7.12, 7.13, 7.14, and 7.15).

7.2.4 Ostiomeatal Complex

The ostiomeatal complex (OMC) is a functional anatomical area proposed after the development of functional endoscopic sinus surgery. It is not an independent anatomical structure. As a surrounding area with the ethmoidal infundibulum as center, it includes uncinate process, ethmoidal bulla, semilunar hiatus, ethmoidal infundibulum, middle nasal meatus, middle turbinate, anterior ethmoidal sinus, aperture of frontal

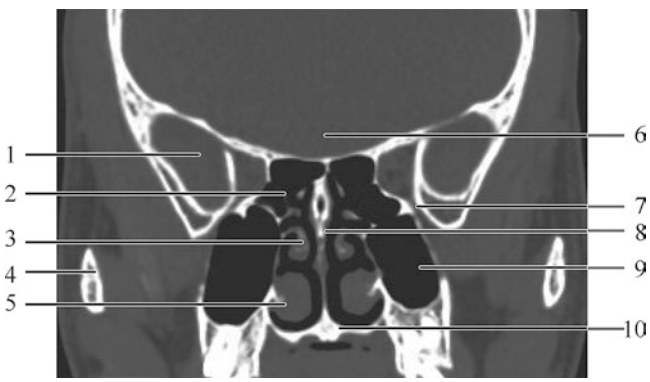

Fig. 7.12 CT image of the coronal plane of paranasal sinus (5). 1. Middle cranial fossa; 2. Anterior ethmoidal sinus; 3. Middle turbinate; 4. Zygomatic process of maxilla; 5. Inferior turbinate 6. Anterior cranial fossa; 7. Inferior orbital fissure; 8. Nasal septum; 9. Maxillary sinus; 10. Hard palate

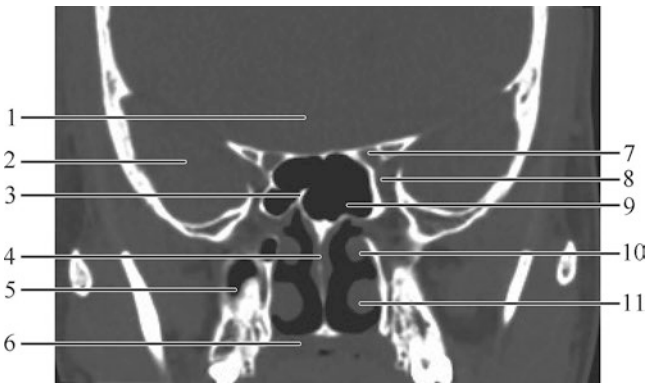

Fig. 7.13 CT image of the coronal plane of paranasal sinus (6). 1. Anterior cranial fossa; 2. Middle cranial fossa; 3. Sphenoid sinus septum; 4. Nasal septum; 5. Maxillary sinus; 6. Soft palate; 7. Optic canal; 8. Pterygopalatine fossa; 9. Sphenoid sinus 10. Middle turbinate; 11. Inferior turbinate

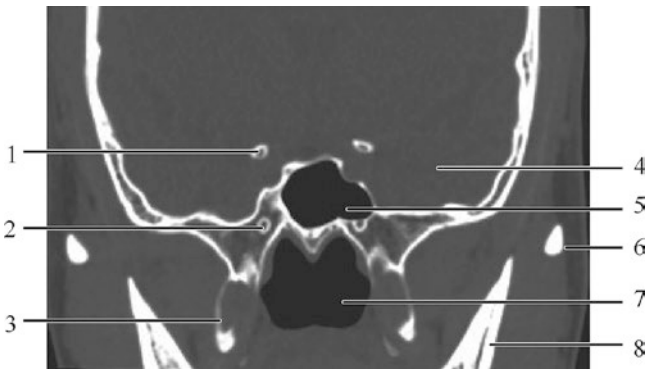

Fig. 7.15 CT image of the coronal plane of paranasal sinus (8). 1. Anterior clinoid process; 2. Foramen rotundum; 3. Lateral pterygoid plate; 4. Middle cranial fossa; 5. Sphenoid sinus 6. Zygomatic arch; 7. nasopharyngeal cavity; 8. Mandible

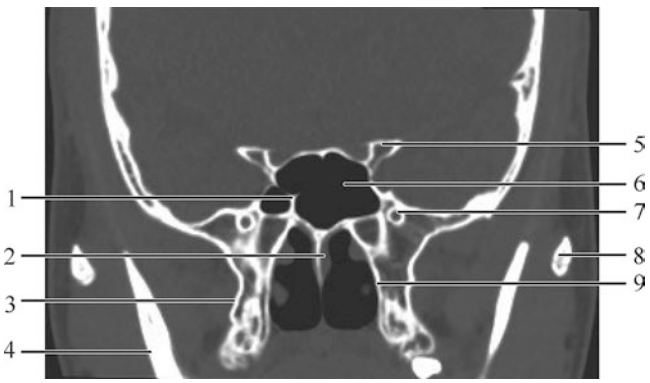

Fig. 7.14 CT image of the coronal plane of paranasal sinus (7). 1. Sphenoid sinus septum; 2. Nasal septum; 3. Lateral pterygoid plate; 4. Mandible 5. Anterior clinoid process; 6. Sphenoid sinus 7. Foramen rotundum; 8. Zygomatic arch; 9. Medial pterygoid plate

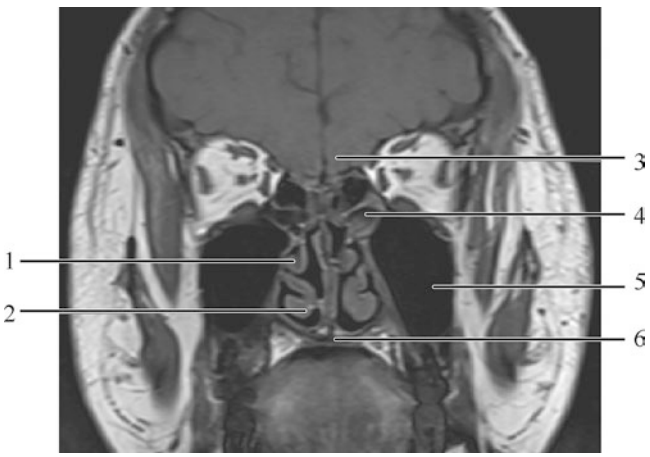

Fig. 7.16 MRI image of the coronal plane of paranasal sinus on T_1WI. 1. Middle turbinate; 2. Inferior turbinate; 3. Anterior cranial fossa; 4. Ethmoidal sinus; 5. Maxillary sinus; 6. Hard palate

sinus, and opening of maxillary sinus. It is the common ventilation and the drainage channel for frontal sinus, anterior ethmoidal sinus and maxillary sinus (Figs. 7.16 and 7.17).

7.2.5 Spaces Relevant with the Nose and the Paranasal Sinus

1. **Infratemporal Fossa.** The infratemporal fossa lies on the side of the viscerocranium, inferior to the temporal fossa and posterior to the maxilla. It is inverted cone-shaped. The infratemporal fossa is connected to the middle cranial fossa through the oval foramen and the foramen spinosum posteriorly, to the pterygopalatine fossa through the pterygomaxillary fissure medially, to the orbit through the inferior orbital fissure anterior, and to the temporal fossa superiorly [4].

2. **Pterygopalatine fossa**. Located on the medial side of the infratemporal fossa, it is an inverted triangular space surrounded by the pterygoid process of sphenoid bone, the

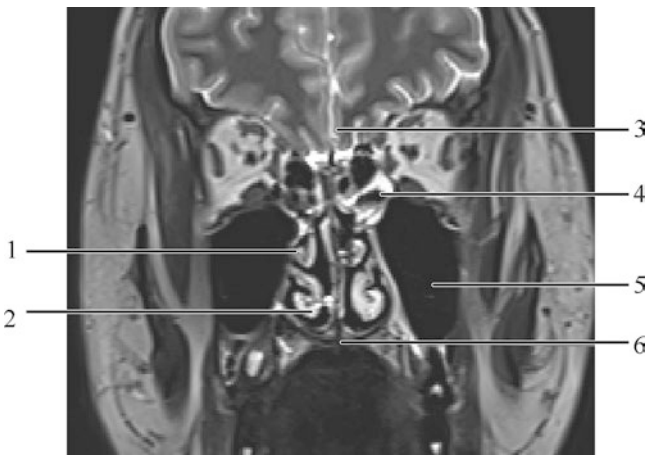

Fig. 7.17 MRI image of the coronal plane of paranasal sinus on T_2WI. 1. Middle turbinate; 2. Inferior turbinate; 3. Anterior cranial fossa; 4. Ethmoidal sinus; 5. Maxillary sinus; 6. Hard palate

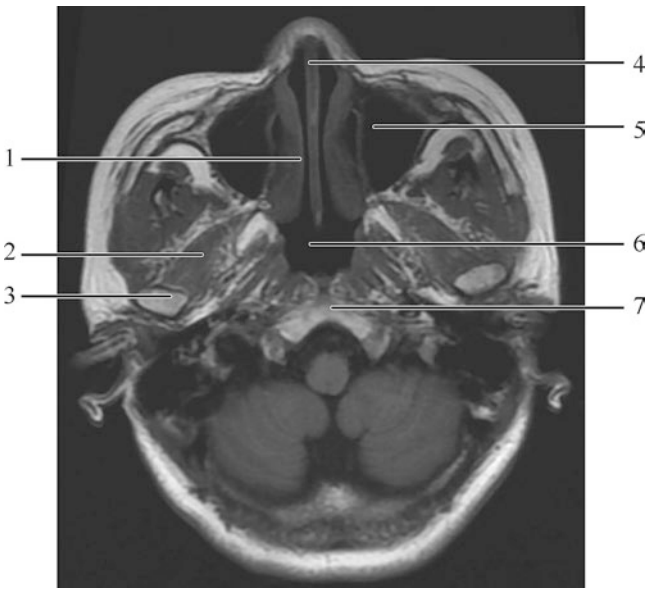

Fig. 7.18 MRI image of the transverse plane of paranasal sinus on T_1WI (1). 1. Middle turbinate; 2. Lateral pterygoid; 3. Mandibular condylar; 4. Nasal septum; 5. Maxillary sinus; 6. Nasopharyngeal cavity; 7. Basilar clivus

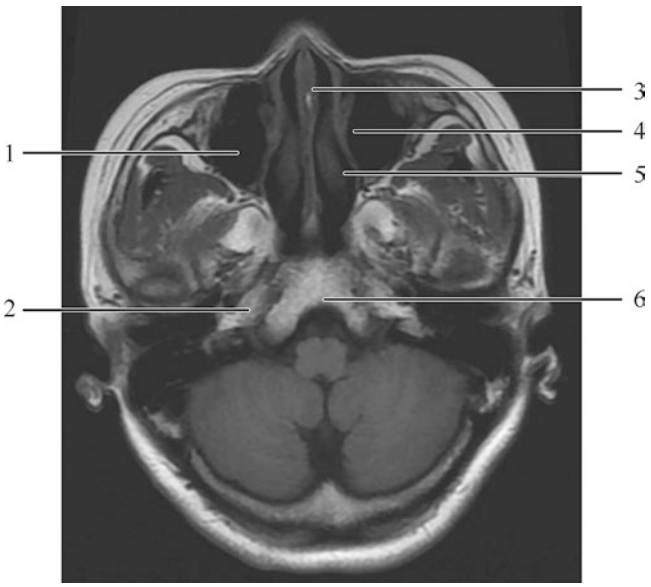

Fig. 7.19 MRI image of the transverse plane of paranasal sinus on T_1WI (2). 1. Maxillary sinus; 2. Petrous apex; 3. Nasal septum; 4. Medial wall of maxillary sinus; 5. Superior turbinate; 6. Basilar clivus

body of maxilla, the palatine bone and the infratemporal fossa. Also located in the superior part of the pterygomaxillary fissure, it houses the sphenopalatine ganglion (also known as the pterygopalatine ganglion) and the maxillary branch of trigeminal nerve (maxillary nerve). The pterygopalatine fossa directly communicates with many adjacent anatomical areas, and the inflammation or tumor can spread through it. The relationship between the pterygopalatine

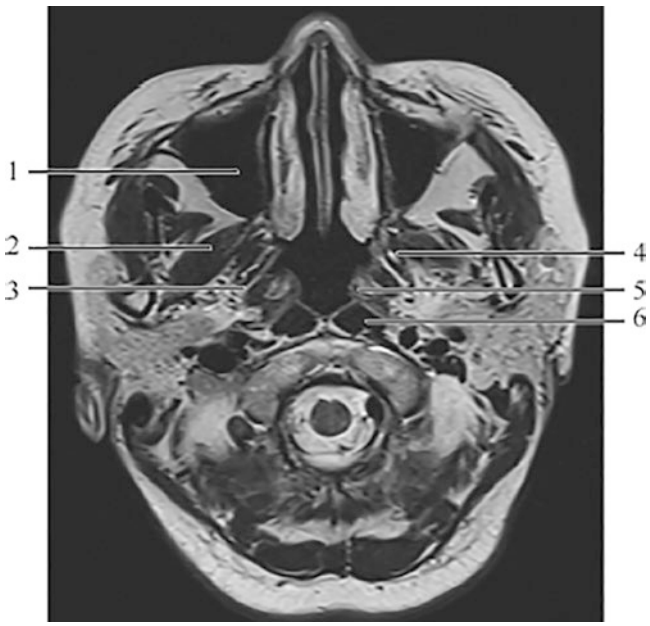

Fig. 7.20 MRI image of the transverse plane of paranasal sinus on T_2WI. 1. Maxillary sinus; 2. Lateral pterygoid; 3. Levator veli palatini; 4. Tensor veli palatini; 5. Tubal torus; 6. longus capitis

fossa and its surrounding areas can be summarized as follows: its posterosuperior foramen communicates with the middle cranial fossa (the maxillary nerve passes through the foramen rotundum). It communicates with the orbit through the inferior orbital fissure anterosuperiorly. It becomes thinner as inferiorly extending towards the pterygopalatine fossa to form the canalis pterygopalatinus where the palatine nerve and the descending palatine artery pass. The pterygopalatine fossa communicates with the oral cavity through the canalis pterygopalatinus, the greater palatine canal and the lesser palatine canal. It interiorly communicates with the sphenoethmoidal recess and the nasal cavity through the sphenopalatine foramen. It communicates with the infratemporal fossa laterally and forms the pterygomaxillary fissure [4] together with the medial pterygoid plate and lateral pterygoid plate on its lateral side (Figs. 7.18, 7.19, and 7.20).

References

1. Zhenchang W, Jun X, Baosen L. Chinese imaging medicine - head and neck. 2nd ed. Beijing: People's Medical Publishing House; 2011.
2. Odat H, Almardeeni D, Tanash M, et al. Anatomical variation of the sphenoid sinus in paediatric patients and its association with age and chronic rhinosinusitis. J Laryngol Otol. 2019;133(6):482–6.
3. Shuling B, Dajun Y. Systematic anatomy. Beijing: People's Medical Publishing House; 2008.
4. Yan S, Dehong L, Hengguo L. Imaging of the head and neck·- otolaryngology, head and neck surgery. Beijing: People's Medical Publishing House; 2014.

Imaging Anatomy of Pharynx

8

Meizhu Zheng, Shuang Xia, and Zuohua Tang

8.1 Foundation of Imaging Anatomy

8.1.1 Gross Anatomy

The pharynx is a funnel-shaped muscular flat duct. Located anterior to the C1 to C6 vertebral bodies, it is a common channel for digestion and breathing. The pharynx of an adult is about 12 cm long. It originates from the skull base, courses down to the inferior border of the cricoid cartilage and then is connected with the esophageal entrance. Adjacent to the nasal cavity, oral cavity and larynx cavity, it can be divided into nasopharynx, oropharynx, and hypopharynx (Fig. 8.1).

8.1.2 Main Structures and Peripharyngeal Space

Auditory tube: The auditory tube is provided with medial, anterior, and inferior openings in the pharyngeal ostium of auditory tube in the nasopharyngeal cavity from the ostium tympanicum. It inclines at an inclined angle of about 40° with the horizontal plane. The ostium tympanicum, funnel-shaped, is 2 to 2.5 cm higher than the pharyngeal ostium. About 4.5 mm wide, it is the widest part of the inner diameter of the bony part, which then becomes narrower as it goes medially. It is the narrowest at the junction of bony part and cartilaginous part, with an inner diameter of only 1 to 2 mm. Since then, it gradually becomes wider again when extending toward the duct at the pharyngeal ostium and finally becomes the widest at the pharyngeal ostium, with both superior and inferior diameters up to 9 mm. The pharyngeal ostium of auditory tube is an important structure of the nasopharyngeal cavity. Its posterolateral 1/3 part is the bony part. The remaining 2/3 part is the cartilaginous part.

Tubal torus: It is formed by the lip-like bulge of the cartilage of the medial wall of the auditory tube.

Pharyngeal recess: As the depression between the torus and the posterior pharyngeal wall, it is only about 1 cm away from the foramen lacerum of skull base. The disappearance of the pharyngeal recess indicates the lesion of nasopharynx.

Vallecula Epiglottica: It is the spaces on both sides of the median glossoepiglottic ligaments between the root of

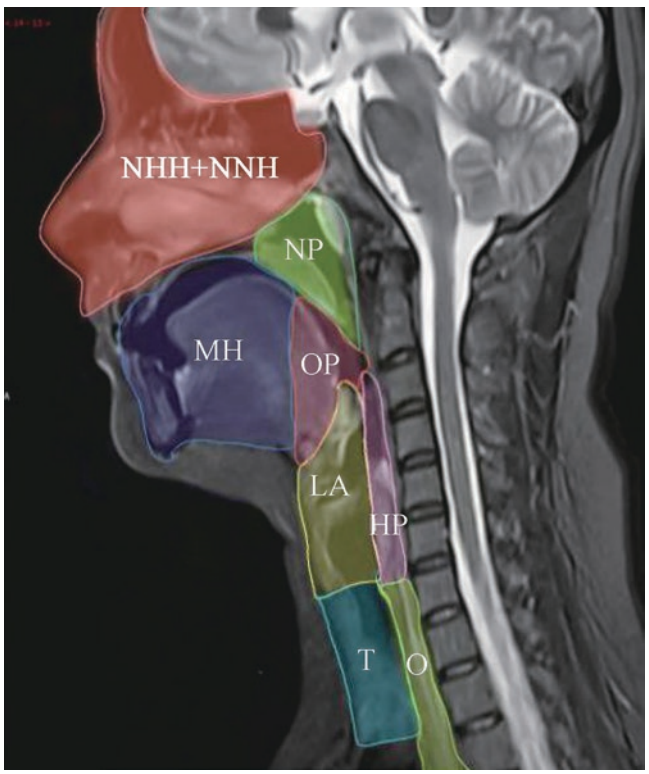

Fig. 8.1 Midian sagittal MRI image. NHH, nasal cavity; NNH, paranasal sinus; NP, nasopharynx; MH, oral cavity; OP, oropharynx; LA, larynx; HP, hypopharynx; T, trachea; O, esophagus

M. Zheng · S. Xia (✉)
Tianjin Third Central Hospital, Tianjin, China

Z. Tang
Eye & ENT Hospital of Fudan University, Shanghai, China

H. Li et al. (eds.), *Radiology of Infectious and Inflammatory Diseases - Volume 2*,
https://doi.org/10.1007/978-981-16-8841-6_8

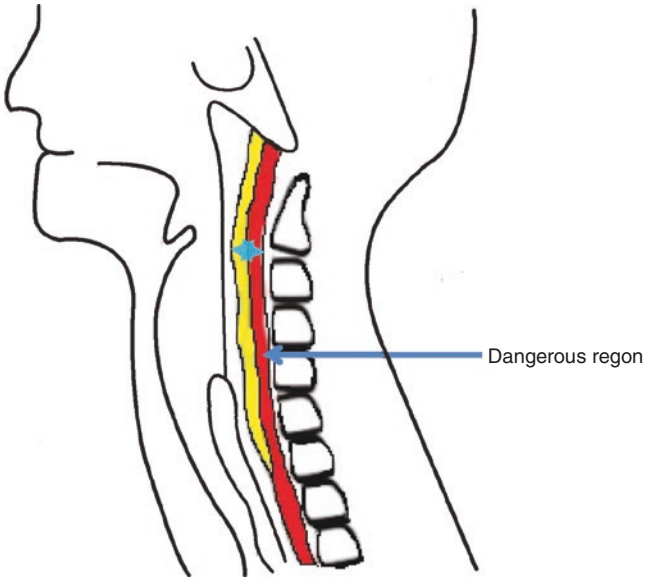

Fig. 8.2 Schematic diagram of the fascia of retropharyngeal space

tongue and the epiglottic cartilage, where foreign bodies often remain.

Pyriform Sinus: It is the lateral inferior deep fossa of the aryepiglottic folds on both sides.

Postcricoid Space: Located between two pyriform sinuses and posterior to the cricoid cartilage, it communicates with the esophageal entrance. When swallowing, the pyriform sinus opens in a funnel shape, and the food enters the esophagus through the postcricoid space.

Spaces of the pharynx include suprahyoid spaces and infrahyoid spaces. Suprahyoid spaces include parapharyngeal space (PPS), pharyngeal mucosal space, parotid space, submasseteric space, pterygopalatine fossa, submandibular space, and sublingual space. Infrahyoid spaces include the visceral space and the anterior cervical space. Suprahyoid spaces and infrahyoid spaces include carotid space, retropharyngeal space (RPS), paravertebral space and posterior cervical space.

The schematic diagram of the fascia of retropharyngeal space is as shown in Fig. 8.2. The real retropharyngeal space (yellow) lies between the wing fasciae and the wing facia of the deep layer fascia of the neck. The danger region (red) lies between posteroinferior and prevertebral layers of the deep fascia of the neck (Fig. 8.2). These two components are indistinguishable on the MRI and CT images of healthy people. The danger region of the retropharyngeal space extends from the clivus to the mediastinum. Therefore, the mediastinal infection must be excluded for the patients involved in postpharyngeal tissue infection.

8.1.3 Lymph, Blood Vessels, and Nerves

The pharyngeal lymphoid ring mainly includes endolymphatic ring and perilymphatic ring.

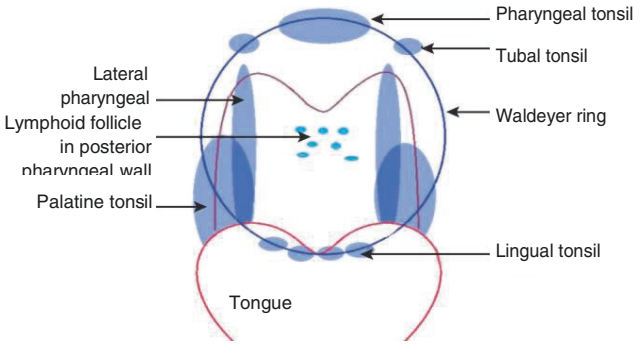

Fig. 8.3 Schematic diagram of the pharyngeal lymphoid ring

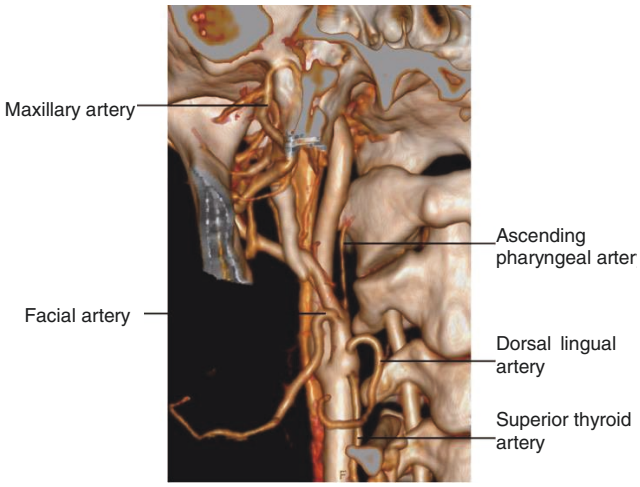

Fig. 8.4 CTA of the pharynx

The endolymphatic ring (Waldeyer ring) is mainly composed of "6 tonsils" (1 pharyngeal tonsil, 2 tubal tonsils, 1 lingual tonsil, and 2 palatine tonsils).

The perilymphatic ring formed by the endolymphatic ring and the lymphonodi cervicales communicating with each other. It mainly includes the retropharyngeal lymph node, the mandibular angle lymph node, the submandibular lymph node and the submental lymph node. In addition to the fact that the perilymphatic ring is connected to the endolymphatic ring, the latter flows to the former and the former also flows to the latter. When the infection of the pharynx cannot be controlled by the endolymphatic ring, it will spread from the endolymphatic ring to the perilymphatic ring (Fig. 8.3).

The pharynx is mainly supplied by branches of the external carotid artery, including ascending pharyngeal artery, superior thyroid artery, facial artery, dorsal lingual artery and maxillary artery (Fig. 8.4). The cervical venous return flows back into the common jugular vein through the superficial jugular vein and the deep jugular vein.

8.2 CT Imaging Anatomy

Anatomical structures such as nasopharynx, oropharynx, and hypopharynx can be observed successively on the transverse plane (Figs. 8.5, 8.6, 8.7, 8.8, 8.9, and 8.10). The pharyngeal ostium of auditory tube, the torus tubarius, the epiglottis, the aryepiglottic fold and other structures can be clearly shown. Glands such as submandibular gland and parotid gland can also be shown clearly. CT is very advantageous in showing bone structures, but the structure of the peripharyngeal space is an exception due to lack of natural contrast. In addition, the upper respiratory tract in the pharynx can also be three-dimensionally reconstructed with CT and its volume can be evaluated quantitatively [1].

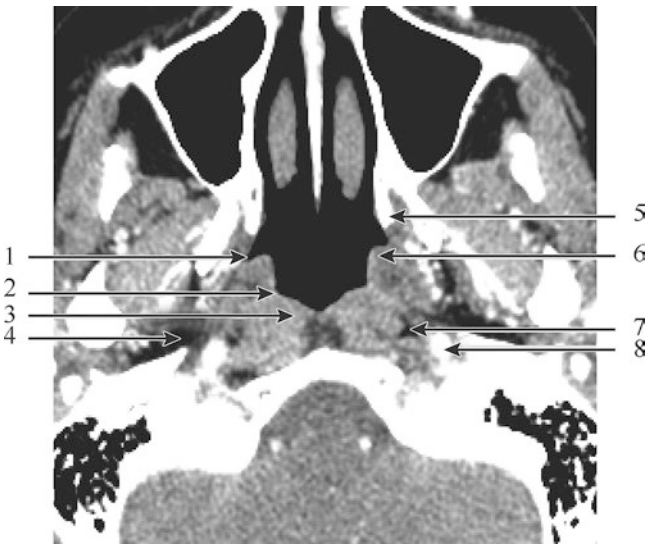

Fig. 8.5 Transverse plane of the nasopharyngeal cavity. 1. Pharyngeal ostium of auditory tube; 2. Tubotympanic recess; 3. longus capitis; 4. Parapharyngeal space; 5. Medial pterygoid plate; 6. Torus tubarius; 7. Retropharyngeal space; 8. Internal carotid artery

8.3 MR Imaging Anatomy

X-ray and CT are highly sensitive in detecting pharyngeal masses but have the structure superposition problem. Magnetic resonance imaging (MRI) of the laryngeal part provides a good anatomical description of surface and deep layer structures, including local muscles, major blood vessels, laryngeal cartilage, and esophagus. The mesenchyme surrounding these structures, especially fat, helps separate them. The mucosal layer, auditory tube, longus capitis, longus colli, tensor veli palatini and levator veli palatini can be clearly shown on T_2WI. With the fat as the background, the parapharyngeal space and the retropharyngeal space are also shown clearly on the transverse plane and the coronal plane [2]. Lymph nodes, blood vessels and nerves in the parapharyngeal space show slightly hypointense shadows on T_2WI. The thyroid cartilage structure can also be observed at the glottis level (Figs. 8.11, 8.12, and 8.13).

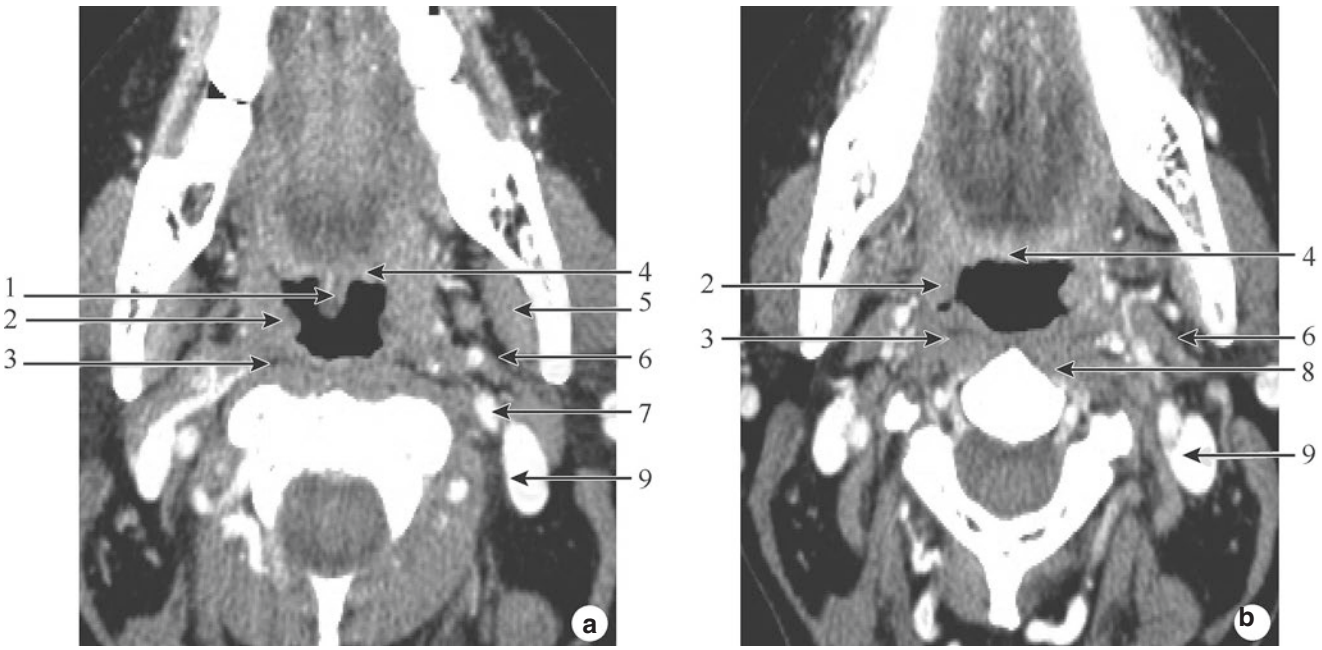

Fig. 8.6 Transverse plane of the oral-pharyngeal cavity. 1. Uvula; 2. Lateral oropharyngeal wall (palatine tonsil); 3. Retropharyngeal space; 4. Soft palate (lingual tonsil); 5. Medial pterygoid; 6. Parapharyngeal space; 7. Internal carotid artery; 8. Longus colli; 9. Internal jugular vein

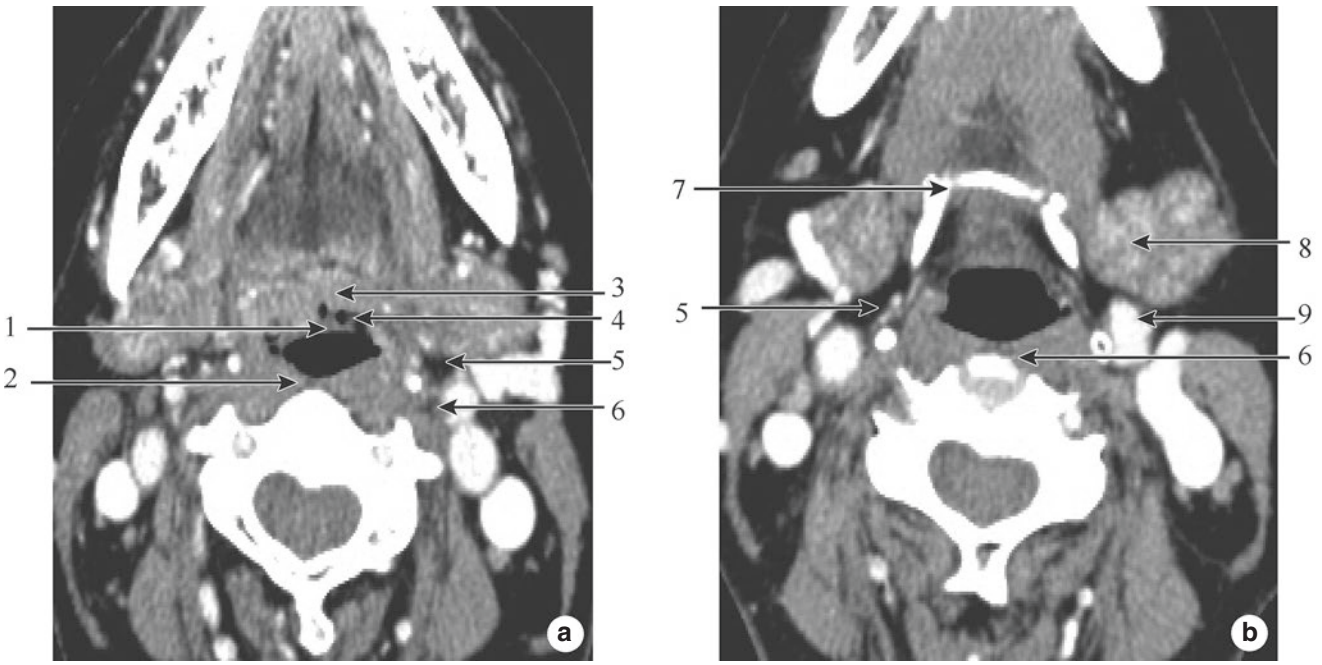

Fig. 8.7 Transverse plane of the hypopharynx cavity (1). 1. Epiglottis; 2. Posterior pharyngolaryngeal wall; 3. Root of tongue; 4. Vallecula epiglottica; 5. Parapharyngeal space; 6. Retropharyngeal space; 7. Hyoid bone; 8. Submandibular gland; 9. Bifureation of common carotid artery

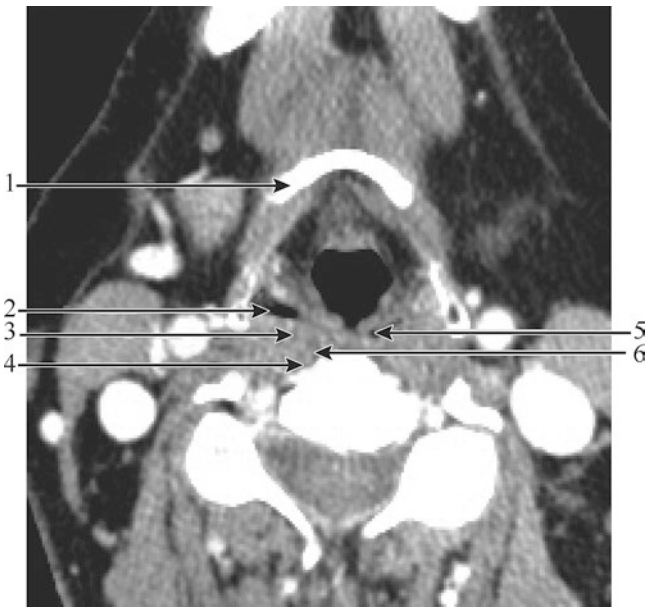

Fig. 8.8 Transverse plane of the hypopharynx cavity (2). 1. Thyroid cartilage; 2. Piriform recess; 3. Posterior pharyngeal wall; 4. Prevertebral soft tissue; 5. Aryepiglottic fold; 6. Retropharyngeal space

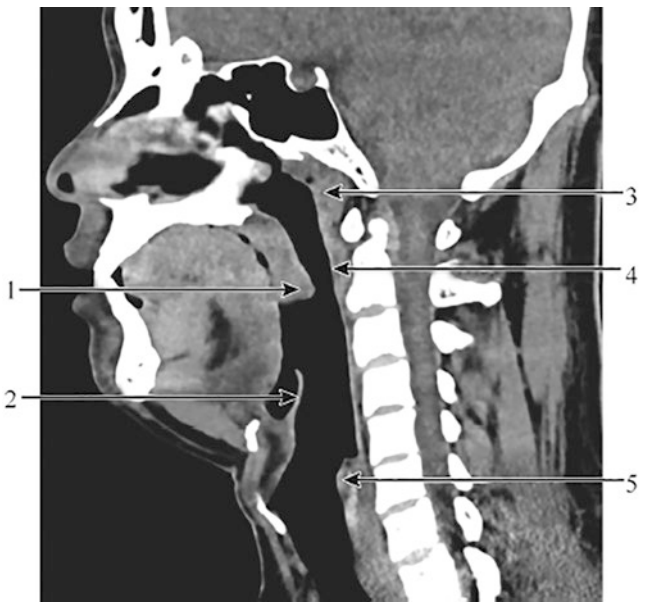

Fig. 8.9 Median sagittal plane of hypopharynx cavity. 1. Soft palate; 2. Epiglottis; 3. Roof wall of the nasopharynx; 4. Retropharyngeal space; 5. Hypopharyngeal cavity

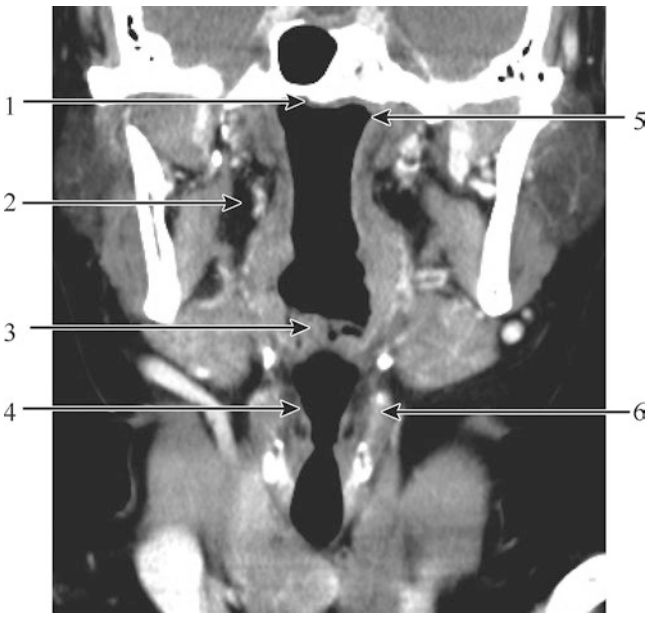

Fig. 8.10 Coronal plane of the hypopharynx cavity. 1. Soft tissue in the nasopharyngeal roof; 2. Parapharyngeal space; 3. Epiglottis 4. Vocal cord; 5. Pharyngeal ostium of auditory tube; 6. Thyroid cartilage

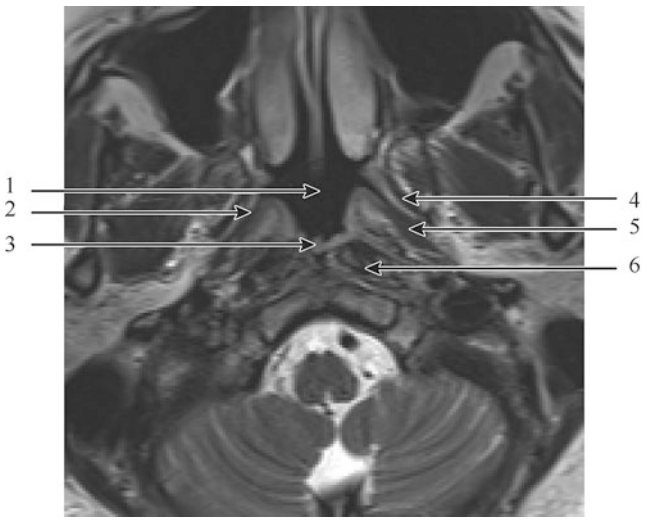

Fig. 8.11 Image of the nasopharynx level on T_2WI. 1. Nasopharyngeal cavity; 2. Auditory tube; 3. Nasopharyngeal roof mucosa; 4. Tensor veli palatini; 5. Levator veli palatini; 6. longus capitis

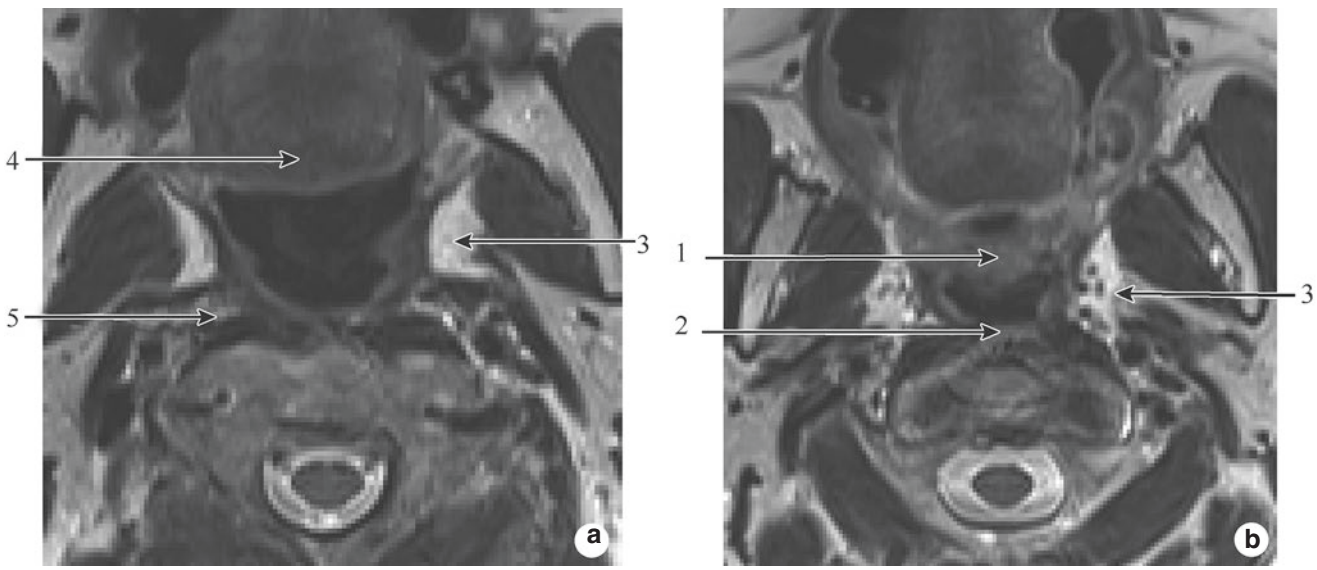

Fig. 8.12 Image of the transverse plane of oropharynx on T_2WI. 1. Soft palate; 2. Oropharyngeal mucosa; 3. Parapharyngeal space; 4. Tongue; 5. Retropharyngeal space

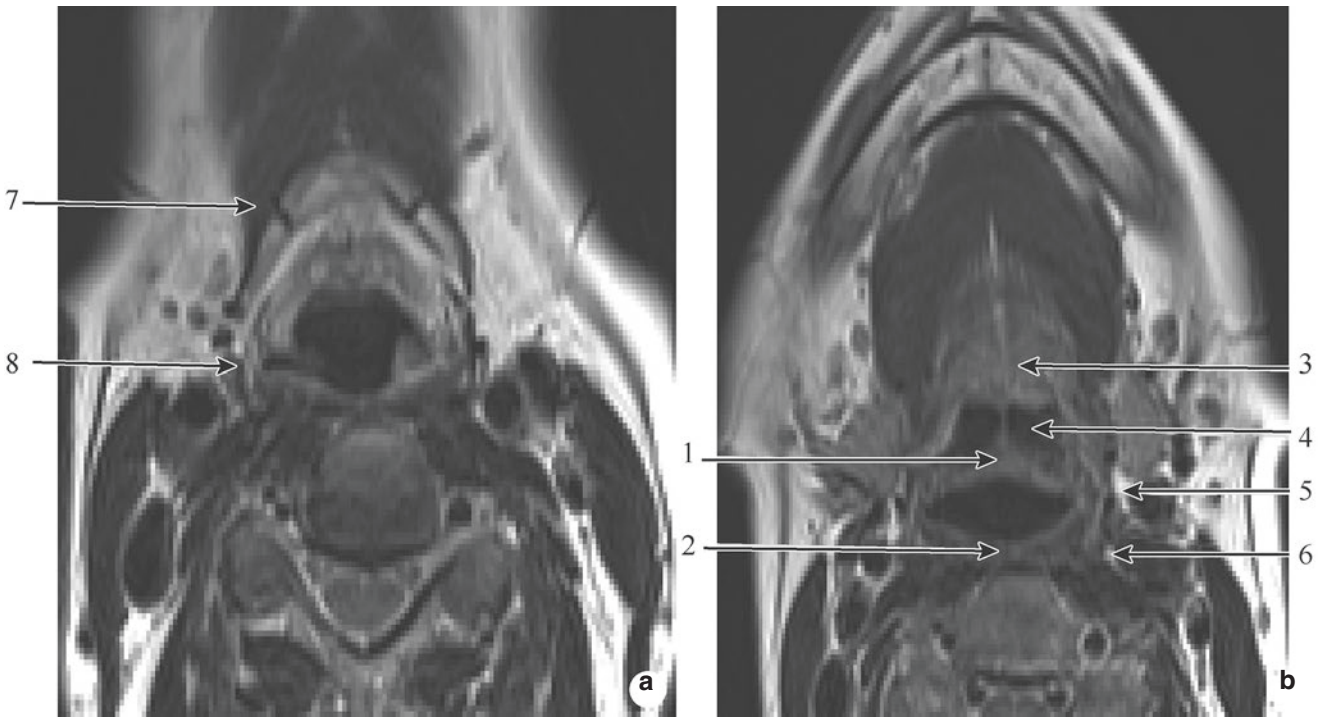

Fig. 8.13 Image of the transverse plane of hypopharynx cavity on T_2WI. 1. Epiglottis; 2. Posterior pharyngolaryngeal wall; 3. Root of tongue; 4. Vallecula epiglottica; 5. Parapharyngeal space; 6. Retropharyngeal space; 7. Hyoid bone; 8. Piriform recess

References

1. Wani TM, Rafiq M, Talpur S, et al. Pediatric upper airway dimensions using three-dimensional computed tomography imaging. Paediatr Anaesth. 2017;27(6):604–8.
2. Chen H, Aarab G, de Ruiter MH, et al. Three-dimensional imaging of the upper airway anatomy in obstructive sleep apnea: a systematic review. Sleep Med. 2016;21:19–27.

Imaging Anatomy of Larynx

9

Huazheng Dong and Yubo Lyu

9.1 Foundation of Imaging Anatomy

The larynx is the main organ for breathing and pronunciation. It lies in the middle of neck, is inferior to the hyoid bone and approximately between the third cervical vertebra and the inferior border of the sixth cervical vertebra, and communicates with the hypopharynx superiorly and the trachea inferiorly (Fig. 9.1). The larynx is supported by cartilage (Fig. 9.2), and the cartilage gap is composed of the joints, muscles, and ligaments that are connected together. The larynx is structurally complex and delicate. Therefore, its fine structures, divisions, and important tissue spaces shall be carefully observed on corresponding images.

9.2 CT Imaging Anatomy

The CT image of the transverse plane of larynx shows the epiglottis, the vallecula epiglottica, the preepiglottic space, the piriform recess, the aryepiglottic fold, the ventricular fold, the laryngeal ventricle, the vocal cord, and the laryngeal cartilage from top to bottom (Fig. 9.3a–g). The CT image of median coronal plane can better show the relationship among the true vocal cord, the laryngeal ventricle, and the false vocal cord (Fig. 9.3h). On non-enhanced CT, lateral and medial cortexes of the ossified cartilage show high density, the marrow cavity in the center shows low density due to the presence of adipose tissue, and the non-ossified hyaline cartilage and the elastic fibrocartilage show soft tissue density. In enhanced CT, the submucosal pharyngeal mucous membrane on the surface of larynx often shows mild enhancement. The bone cortex, fatty marrow, and non-ossified hyaline cartilage show no enhancement after the intravenous injection of iodine-containing contrast agent [1, 2].

9.3 MR Imaging Anatomy

The mucosa of the larynx cavity has a smooth surface. It shows hypointense to isointense on T_1WI, isointense or hyperintense on T_2WI, and mild enhancement after enhancement. The muscle shows isointense on T_1WI and slightly hyperintense on T_2WI. The uncalcified laryngeal cartilage shows isointense or slightly hypointense, and the external bone cortex of the calcified cartilage show no signal. The medulla part contains adipose tissues, showing hyperintense on T_1WI and isointense on T_2WI. The vocal cord shows muscular isointense. The ventricular fold (false vocal cord) contains abundant loose connective tissues, showing a higher hyperintense than the vocal cord. It is difficult to show the laryngeal ventricle and laryngeal saccules between the ventricular fold and the vocal cord on the transverse plane, but they can be shown the most clearly on the coronal plane. The subglottic portion is marked by cricoid cartilage, and its medial mucosa is only about 1mm thick. The anterior epiglottic space and the paraglottic space on the deep surface of the larynx cavity are filled with adipose tissues, showing hyperintense on T_1WI as well as isointense and hyperintense on T_2WI [1, 2]. Normal lymph nodes in the larynx are not shown in most cases, and their diameters are only about 5mm. Sometimes the larynx body or the endolaryngeal structure is asymmetrical and thus has an unequal thickness, easy to be misdiagnosed as pathological changes (Fig. 9.4).

H. Dong
Tianjin Academy of Traditional Chinese Medicine Affiliated Hospital, Tianjin, China

Y. Lyu (✉)
Jiahui International Hospital, Shanghai, China

H. Li et al. (eds.), *Radiology of Infectious and Inflammatory Diseases - Volume 2*,
https://doi.org/10.1007/978-981-16-8841-6_9

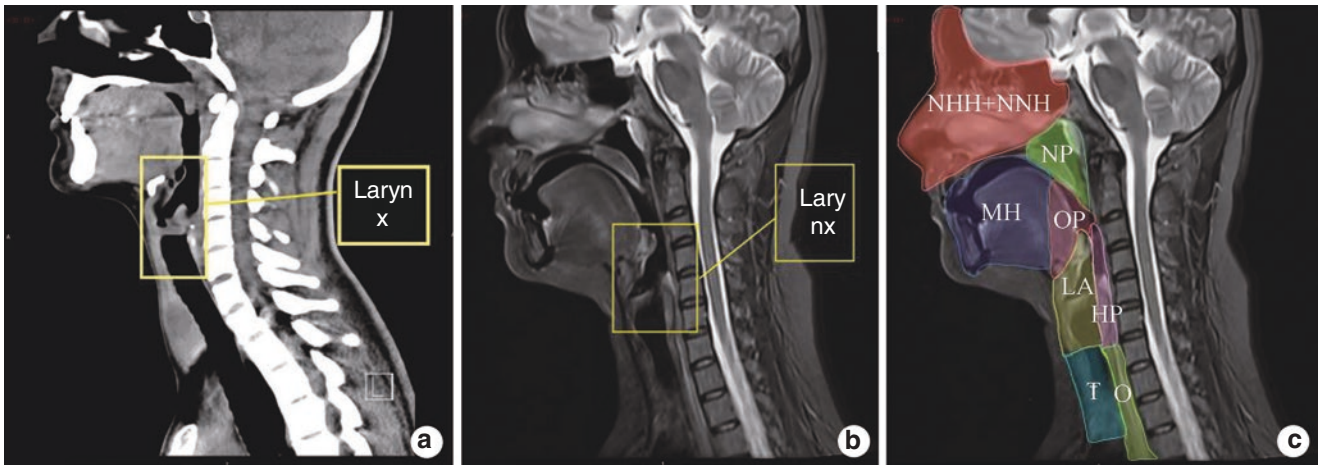

Fig. 9.1 CT and MRI images of the sagittal plane of larynx. (**a**) CT image of the soft tissue window on the sagittal plane of larynx; (**b**) MRI FS-T2WI image of the sagittal plane of larynx; (**c**) Schematic diagram of structure of the sagittal plane of larynx. *NHH* nasal cavity, *NNH* paranasal sinus, *NP* nasopharynx, *MH* oral cavity, *OP* oropharynx, *LA* larynx, *HP* hypopharynx, *T* trachea, *O* esophagus

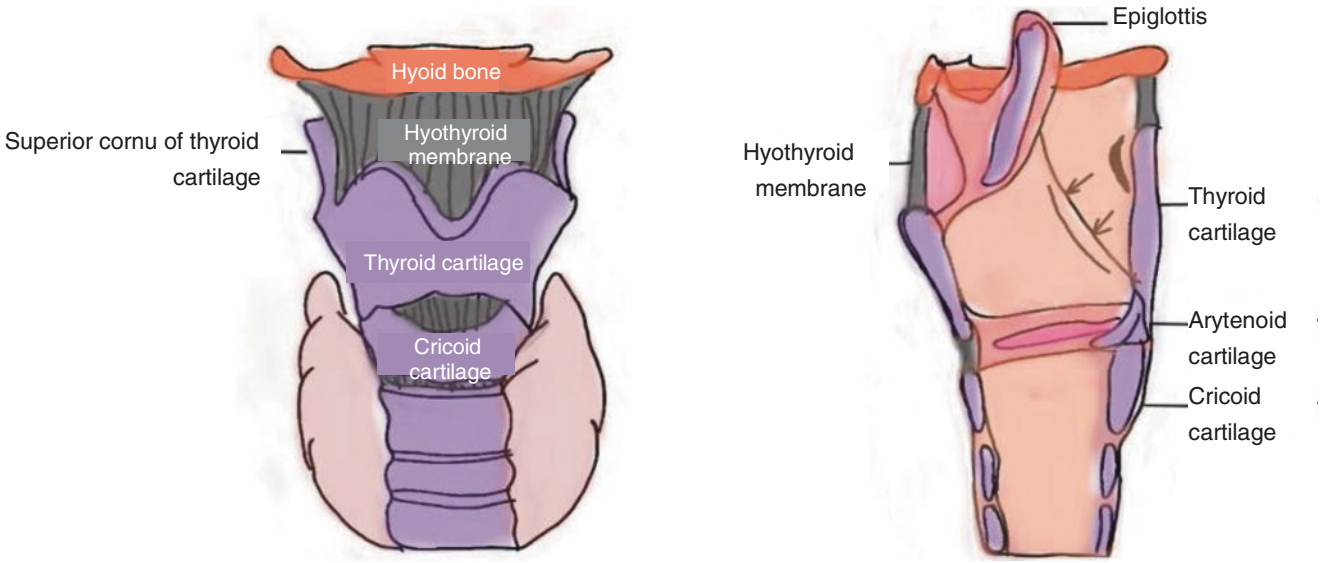

Fig. 9.2 Schematic diagram of laryngeal cartilage

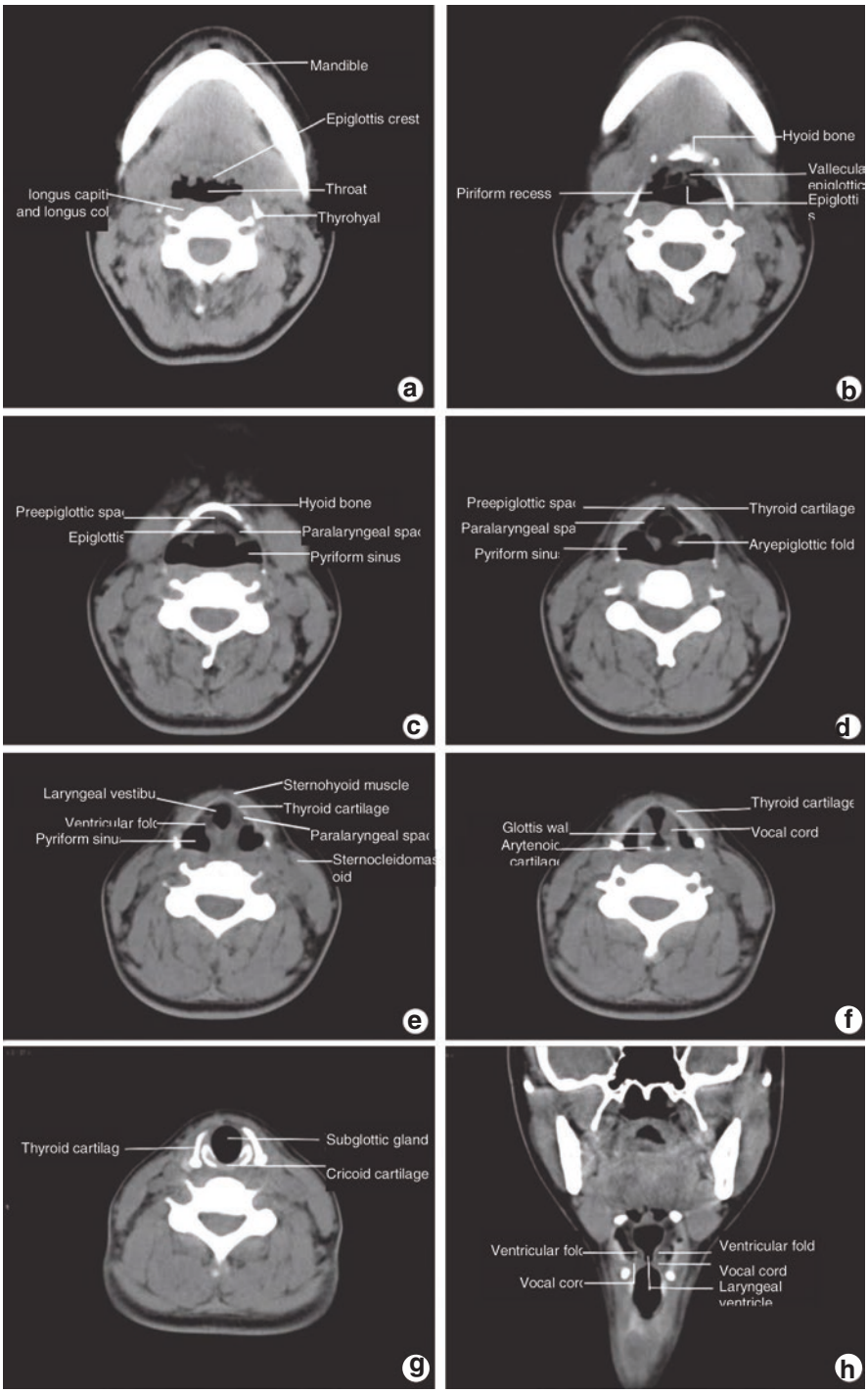

Fig. 9.3 CT anatomical images of the normal larynx. (**a**) Superior border level of epiglottis on the transverse plane; (**b**) Vallecula epiglottica level on the transverse plane; (**c**) Piriform recess level on the transverse plane; (**d**) Superior border level of thyroid cartilage on the transverse plane; (**e**) Ventricular fold level on the transverse plane; (**f**) Vocal cord level on the transverse plane; (**g**) Cricoid cartilage level on the transverse plane; (**h**) Bilateral vocal cords, bilateral ventricular folds and laryngeal ventricle visible on the coronal plane

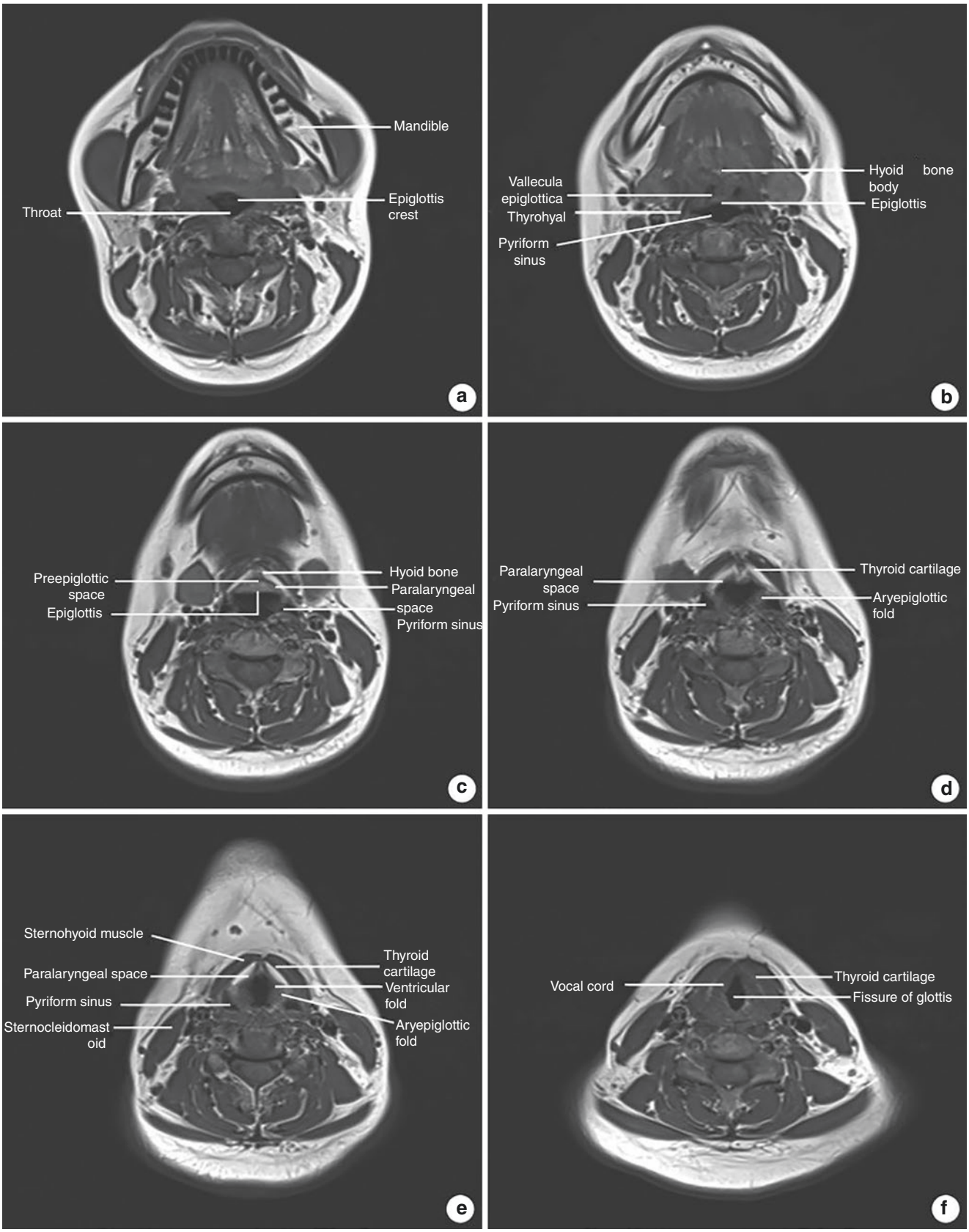

Fig. 9.4 MRI anatomical images of the normal larynx. (**a**) Superior border level of epiglottis on the transverse plane; (**b**) Vallecula epiglottica level on the transverse plane; (**c**) Piriform recess level on the transverse plane; (**d**) Superior border level of thyroid cartilage on the transverse plane; (**e**) Ventricular fold level on the transverse plane; (**f**) Vocal cord level on the transverse plane; (**g**) Cricoid cartilage level on the transverse plane

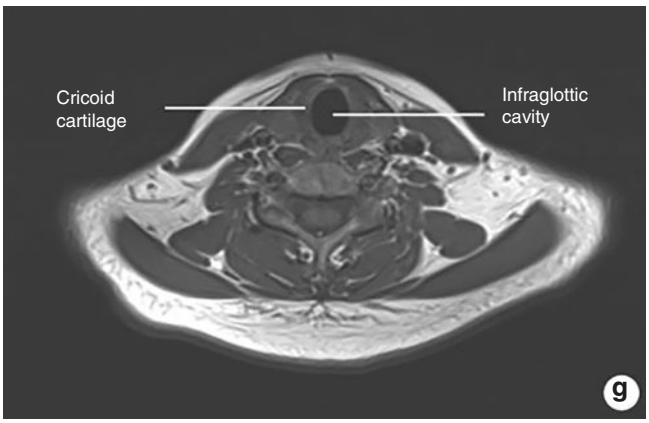

Fig. 9.4 (continued)

References

1. Mafee MF, Valvassori G, Becker M. Valvassori's imaging of the head and neck, Edition 2. Translation: Liu Huaijun, et al. Beijing: China Medical Science Press, 2011.
2. Nowinski WL. 3D atlas of the brain, head and neck in 2953 pieces. Neuroinformatics. 2017;15(4):395–400.

Imaging Anatomy of Maxillofacial Region

10

Li Yao and Heng Liu

10.1 Foundation of Imaging Anatomy

10.1.1 Overview

Maxillofacial region ranges from hairline to inferior border of the mandible, flanked by posterior border of ascending ramus of mandible. According to anatomy, maxillofacial region can be divided into parotideomasseteric region, deep part of lateral face, orbital region, infraorbital region, buccal region, frontal region, temporofacial region, zygomatic region, nasal region, lip region and mental region.

10.1.2 Main anatomic Parts of Maxillofacial Region

10.1.2.1 Parotideomasseteric Region

Parotideomasseteric region refers to the region where parotid gland, masseter and their superficial soft tissues are located. Anterior boundary is anterior border of masseter. Posterior boundary is anterior border of sternocleidomastoid, mastoid process and posterior belly of digastric. Superior border is zygomatic arch inferior border and external auditory canal. Inferior border is inferior border of mandible. The medial and lateral sides are respectively parapharyngeal space and skin. The main structures include parotid gland, masseter and relevant facial artery, retromandibular vein and facial nerve.

Parotid gland, located in parotid space, is tapered, with base facing outwards and tip projecting inward into parapharyngeal space. Parotid gland is covered with parotid masseter muscle fascia, which comes from superficial layer of cervical fascia. The fascia is divided into superficial and deep layers at posterior border of parotid gland, enveloped by parotid gland, forming parotid capsule, and integrates at anterior border of parotid gland, forming fascia masseterica, expanding forward and covering masseter to reach anterior border of masseter. Parotid capsule is fine and dense, and there is a fissure between styloid process and medial pterygoid. Deep lobe of parotid gland communicates with parapharyngeal space and pterygomandibular space via this fissure. When parotid gland suppurates, parapharyngeal abscess may be formed through this fissure. Parotid capsule emits many septa and extends into the gland, dividing the gland into many lobules. When the parotid gland suppurates, scattered, separate small abscesses may be formed. The upper part of parotid capsule is closely connected to the external auditory canal, and emits fiber bundles that extend into the fissure in the cartilage at the anteroinferior wall of the external auditory canal. Therefore, pyogenic infection of parotid gland can spread to the external auditory canal. The profound surface of parotid gland deep lobe is adjacent to styloid process muscles and deep internal carotid artery that is encompassed by cellular tissues and internal jugular vein and the ninth-twelfth cranial nerves. For this reason, it is also known as parotid bed [1].

10.1.2.2 Deep Part of Lateral Face

Deep part of lateral face is located at the profound surface of anterior parotideomasseteric region. Anterior boundary is posterior side of maxilla, posterior boundary is deep lobe of parotid gland, interior boundary is lateral pterygoid plate and exterior boundary is ramus of mandible. In the deep part of lateral face, there are pterygoid plexus, maxillary artery, and mandibular nerves, which are located between the ramus of mandible, medial & lateral pterygoid, and lateral pterygoid plate, encompassed by cellular tissues.

10.1.2.3 Maxillofacial Cellular Tissue Space

Maxillofacial cellular tissue space refers to the potential space between fascias, fascia and muscle, muscle and

L. Yao
Affiliated Stomatology Hospital of Zunyi Medical University, Zunyi, China

H. Liu (✉)
Affiliated Hospital of Zunyi Medical University, Zunyi, China

H. Li et al. (eds.), *Radiology of Infectious and Inflammatory Diseases - Volume 2*,
https://doi.org/10.1007/978-981-16-8841-6_10

periosteum, and between periostea. Each space is filled with loose connective tissues, wherein vessels and nerve pass through. Some spaces have salivary gland and lymph gland. Adjacent spaces communicate with each other, and cellular tissue, along with the neurovascular bundle, enters a space from another. Therefore, space infection may be limited in one space or spread to multiple spaces, and even spread upwards to intracranial region or downwards to cervical space. In this sense, diagnosis and treatment of space infection should be built on an understanding of location, content and intercommunication of cellular tissues in oral, maxillofacial and cervical regions [2].

1. Infraorbital space. Located anteroinferior to orbit. The superior boundary is infraorbital border, inferior boundary is maxilla alveolar process, medial boundary is nasal lateral border, lateral boundary is zygomatic major, and profound surface is maxilla anterior wall. There are cellular tissues, infraorbital nerves and blood vessels in the space. Purulent inflammation of maxillary anterior teeth and premolar may spread to infraorbital space. The space communicates backward with buccal space, with facial vein and facial artery passing through. Facial vein is connected to angular vein and communicates with cavernous sinus, so that inflammation can spread along the facial vein to cause intracranial infection.

2. Buccal space. It is inverted cone-shaped and located between buccinator and masseter. The anterior boundary is anterior border of masseter and posterior boundary is ramus of mandible and anterior border of temporalis. Space is filled with buccal nerve, buccal artery, deep facial vein and adipose tissue. Buccal space communicates with adipose tissue in masseteric space, pterygomandibular space, infraorbital space, infratemporal space and temporal space. For this reason, abscess in buccal space can communicate and spread to the above spaces.

3. Masseteric space. It is located between masseter and the ascending ramus of mandible. The anterior boundary is anterior border of masseter, posterior boundary is posterior border of ramus of mandible, superior boundary is inferior border of zygomatic arch, and inferior boundary is the site where masseter is attached to the inferior border of ramus of mandible. What is located to the lateral of the space is hard, thick masseter, and to the medial is ramus of mandibular ramus wall. What is located superior and inferior to the space are dense connective tissue and muscles attached to zygomatic arch and ramus of mandible. Thereby, inflammation therein is not easy to spread but may spread to the profound side, thus involving mandible, complicated by marginal osteomyelitis of ramus of mandible. Masseteric space communicates with pterygomandibular space, buccal space, temporal space and infratemporal space.

4. Pterygomandibular space. Pterygomandihular space is located between medial ramus of mandible and medial pterygoid. Anterior boundary is temporalis and buccinator, posterior boundary is parotid gland, superior boundary is inferior border of lateral pterygoid, and inferior boundary is the site where medial pterygoid is attached to the inferior border of ramus of mandible. Cellular tissue in the space communicates upwards with infratemporal space and temporal space, forward with buccal space, downwards with sublingual space and submandibular space, backward with parapharyngeal space, and outwards with masseteric space. Besides, along nerves and vessels of skull base, it can enter intracranial region via oval foramen.

5. Infratemporal space. It is located superior to pterygomandibular space. Anterior boundary is posterior maxilla, posterior boundary is profound part of parotid gland, medial boundary is lateral pterygoid plate of sphenoid bone, lateral boundary is upper part of ramus of mandible and zygomatic arch, superior boundary is infratemporal surface and infratemporal crest of the greater wing of sphenoid bone and inferior boundary is the plane wherein inferior border of lateral pterygoid is located. Pterygoid plexus, maxillary artery and its branches, and branches of maxillary and mandibular nerves pass through the space. Loose connective tissues in the space extend into adjacent spaces along with the above vessels and nerves, so that the infratemporal space is in communication with pterygomandibular space, buccal space, temporal space, pterygopalatine space, as well as parapharyngeal space. Besides, the infratemporal space is also connected to intraorbital area via inferior orbital fissure, to cranial cavity via oval foramen and foramen spinosum, and to cavernous sinus via plexus pterygoideus. What is more, the space is located at the center of spaces in deep maxillofacial region, so the infection of infratemporal space typically occurs along with adjacent spaces rather than exists alone.

6. Temporal space. It is located in temporal region, demarcated by surface of zygomatic arch and infratemporal crest and infratemporal space. The space can be divided into superficial temporal space and deep temporal space. The former is located between deep temporal fascia and temporalis, while the latter is located between temporalis and temporal fossa. The deep temporal fascia of the space is dense and temporalis is hard and thick. The squamous portion is the thinnest in temporal fossa, in which there are few diploes at medial and lateral lamella. Therefore, temporal abscess formed can hardly be punctured by itself, thus leaving pus at the surface of squamous portion, pressing bone and resulting in osteonecrosis and osteomyelitis. At the same time, the infection can directly spread into intracranial region or along blood vessels of adjacent meninges, causing meningitis, brain abscess and other complications. Temporal space communicates with buccal space, masseteric space, pterygomandibular space and Infratemporal space.

7. **Parotid space**. Located in parotid capsule, it is filled with parotid gland, and blood vessels, nerves and lymph nodes passing through the gland. The medial side of parotid space is not closed, directly connecting anterior parapharyngeal space with pterygomandibular space.

8. Parapharyngeal space. It is inverted cone-shaped and located between medial pterygoid, deep lobe of parotid gland and lateral wall of pharynx, ranging from skull base to hyoid bone surface. Anterior boundary is pterygomandihular ligament and posterior boundary is lateral side of prevertebral fascia. It is separated from submandibular gland by hyoglossus. Parapharyngeal space is split into anterior and posterior parts via styloid process and styloid process muscles. The anterior part is called anterior parapharyngeal space and the posterior part is called posterior parapharyngeal space or posterior styloid process space. Anterior parapharyngeal space is small, in which there are cellular tissues. It is adjacent to superior constrictor of pharynx and palatine tonsil. Abscess peripheral to palatine tonsil can outward puncture lateral wall of pharynx directly and enter into anterior parapharyngeal space. Posterior parapharyngeal space is large, in which there are internal carotid artery, vein, ninth-twelfth cranial nerve and superior deep cervical lymph node. Parapharyngeal space communicates with pterygomandibular space, infratemporal space, sublingual space, submandibular space, parotid space, and retropharyngeal space. Blood vessels and nerve tracts therein communicate upwards with intracranial region and pass through downwards perivisceral spaces and other connected mediastina, thus can result in the spread of inflammation.

9. Pterygopalatine space. Located inferior to orbital apex and medial to infratemporal fossa, it is an elongated triangular space, also known as pterygopalatine fossa. Anterior boundary is maxilla body, posterior boundary is pterygoid process of sphenoid bone, superior boundary is greater wing of sphenoid bone and inferior boundary is perpendicular plate of palatal bone. In pterygopalatine space, there are ramus of maxilla of trigeminal nerve (maxillary nerve), sphenopalatine ganglion (also known as pterygopalatine ganglion), the third section of maxillary artery and its braches. The pterygopalatine space communicates forward with orbit via inferior orbital fissure, inward with nasal cavity via sphenopalatine foramen, outwards with infratemporal space via pterygomaxillary fissure, downwards with oral cavity via pterygopalatine canal, backward and upward with cranial cavity via foramen rotundum.

10. Sublingual space. It is horseshoe-shaped. Anterior boundary is the mucosa at mouth floor, inferior boundary is the mylohyoid muscle and hyoglossus, the anterolateral side is medial bone wall of mandible body and posterior boundary is root of tongue. Via genioglossus and geniohyoid, sublingual space is bisected into symmetrical left and right parts, which are in communication with each other at deep surface of tongue frenulum. In sublingual space, there are sublingual gland, deep part of submandibular gland and its duct, lingual nerve, hypoglossal nerve, sublingual artery, and sublingual vein. Sublingual space communicates backward with the submandibular space, backward and upward with pterygomandibular space, and backward & inward with parapharyngeal space.

11. **Deep lingual space.** It refers to space located between external lingual muscles at lingual root, including intergenioglossus space and genioglossus-hyoglossus intermuscular space.

(1) Intergenioglossus space: It is located between bilateral genioglossus, and includes cellular tissues, with sectorial median sagittal plane and elongated frontal plane. Superior boundary is septum of tongue and inferior boundary is geniohyoid. The space communicates forward with sublingual space.
(2) Genioglossus-hyoglossus intermuscular space: It is located between genioglossus and hyoglossus, one on each side, wherein cellular tissue and lingual artery are located. The space communicates forward with sublingual space.

12. Masticator space. It is located between masticatory muscle and lateral lamella of ascending ramus of mandible. The superior boundary is divided into upper medial boundary and upper lateral boundary. The upper medial boundary is skull base, and the masticator space inferior to the skull base is also known as infratemporal fossa. The upper lateral boundary, namely, the entheses of temporalis along the skull, is also known as temporal fossa, which is divided into deep and superficial temporal spaces by temporalis. The inferior boundary is entheses of medial pterygoid and masseter at angle of mandible. The space between medial pterygoid and ramus of mandible is called pterygomandibular space, while the space between masseter and ramus of mandible is called masseteric space. Anterior boundary is anterior border of masseter adjacent to buccal fat pad and buccinator. Posterior boundary is posterior border of ascending ramus of mandible. Medial boundary is fascia stretching from medial medial pterygoid to medial border of oval foramen at skull base, separated from parapharyngeal space. Lateral boundary is parotid gland, parotid gland masseter fascia and masticatory muscle [3]. Contents therein include masticatory muscle, mandible ramus, body, nerve, blood vessel, fat and other tissues.

10.2 CT Imaging Anatomy

Conventional CT examination of maxillofacial region, including scanning at coronal plane, transverse plane and sagittal plane, mainly mains to observe the location and size of maxillofacial lesions and their relationship with peripheral anatomical structures [3].

Transverse non-enhanced scans can display different tissue structures at different levels (Fig. 10.1). Scanning at orbital plane can display images of eyeball, orbital wall, medial rectus, lateral rectus, inferior rectus muscle, optic nerve, ethmoidal sinus and sphenoid sinus. Scanning at skull

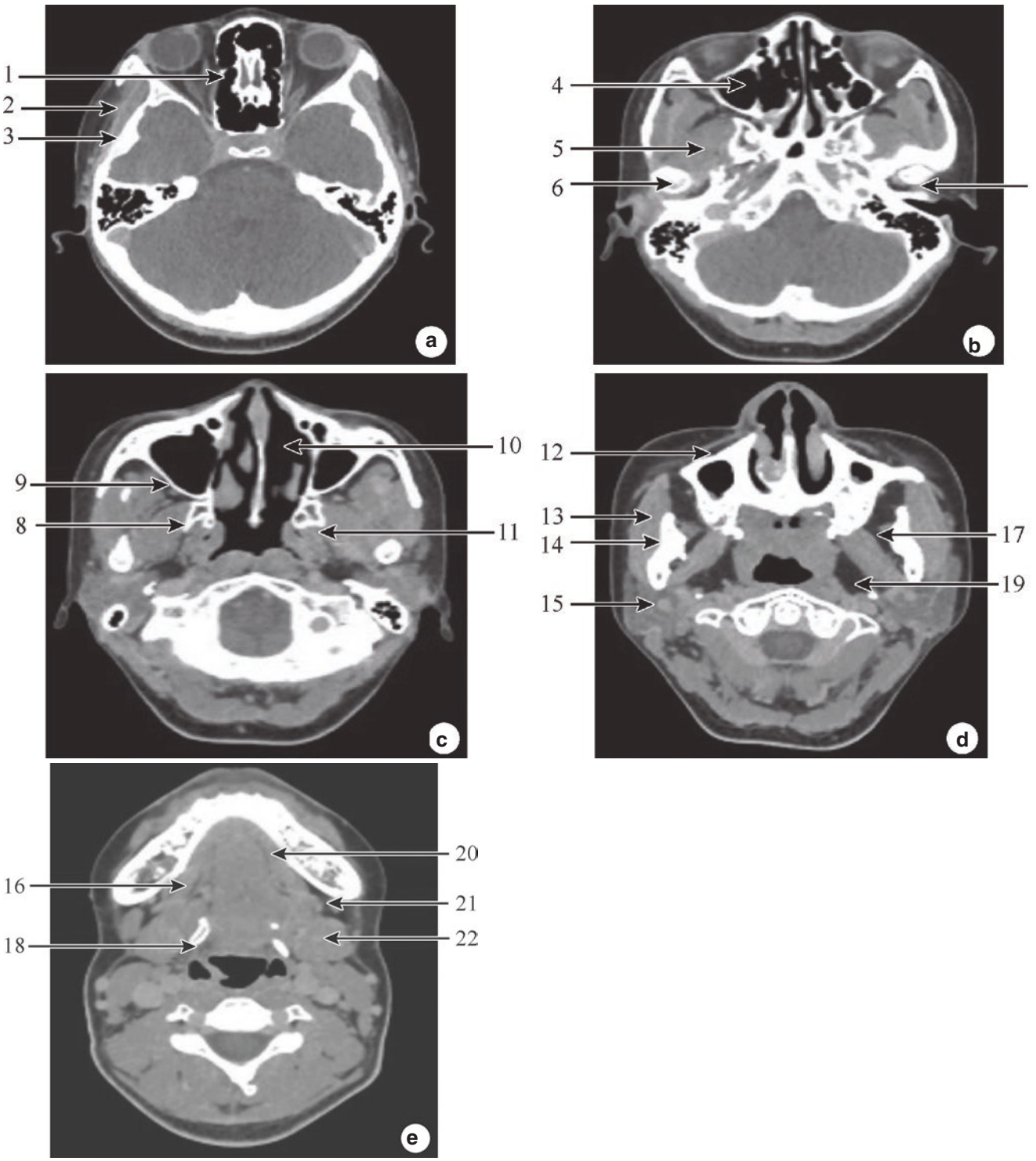

Fig. 10.1 Non-enhanced CT scan of maxillofacial region at transverse plane. (**a**) Orbital plane (**b**) Surface of upper maxillary sinus (**c**) Surface of middle maxillary sinus (**d**) Surface of bottom maxillary sinus (**e**) Mandible body plane. 1. Ethmoidal sinus 2. Temporal space 3. Temporalis 4. Maxillary sinus 5. Lateral pterygoid 6. Condyle process 7. Temporal-mandibular joint fossa 8. Lateral pterygoid plate 9. Infratemporal space 10. Nasal cavity 11. Pterygopalatine fossa 12. Infraorbital space 13. Masseter 14. Masseteric space 15. Parotid gland 16. Sublingual gland 17. Pterygomandibular space 18. Hyoid bone 19. Parapharyngeal space 20. Sublingual space 21. Submandibular space 22. Submandibular gland

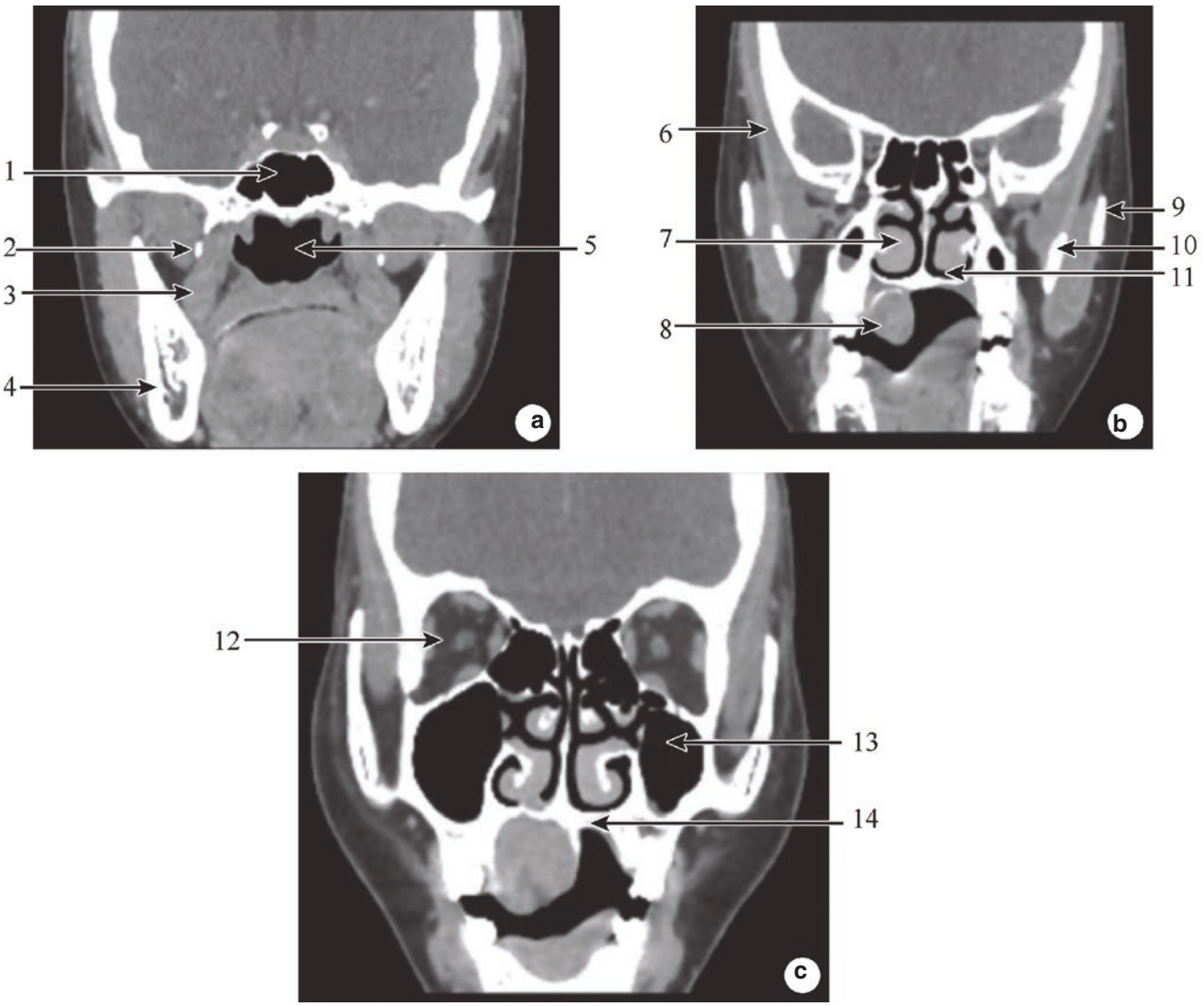

Fig. 10.2 Non-enhanced CT scan of maxillofacial region at coronal plane. (**a**) Coronal plane of nasopharyngeal cavity (**b**) Coronal plane of posterior maxillary sinus (**c**) Coronal plane of middle maxillary sinus. 1. Sphenoid sinus 2. Styloid process 3. Medial pterygoid 4. Angle of mandible 5. nasopharyngeal cavity 6. Temporalis 7. Inferior nasal concha 8. Tumor 9. Zygomatic arch 10. Coracoid 11. Nasal cavity 12. Orbit 13. Maxillary sinus 14. Palate plate

base can display ethmoidal sinus, sphenoid sinus, zygomatic arch and temporalis. Scanning at maxillary sinus upper plane can display maxillary sinus cavity, sinus wall, nasal cavity, medial pterygoid plate, lateral pterygoid plate, pterygopalatine fossa, lateral pterygoid, condyle process and infratemporal fossa. Scanning at maxillary sinus middle plane can display nasopharyngeal cavity, ascending ramus of mandible, masseter, styloid process, mastoid process and parotid gland. Scanning at maxillary sinus base plane can display maxillary sinus base, parotid gland, medial pterygoid, masseter, parapharyngeal space and pharyngeal cavity. Scanning at mandible body plane can display mandible, lingua, masseter, medial pterygoid, sublingual gland, submandibular gland, and mouth floor.

Coronal non-enhanced scans can display different tissue structures at different levels (Fig. 10.2). Scanning at coronal plane of nasopharyngeal cavity can display base of middle cranial fossa, sphenoid sinus, styloid process, angle of mandible, constrictor of pharynx, medial pterygoid, parotid gland and parapharyngeal space. Scanning at coronal plane of posterior maxillary sinus can display maxillary sinus, nasal cavity, turbinate, posterior ethmoidal sinus, postorbital space and temporalis. Scanning at coronal plane of middle maxillary sinus can clearly display maxillary sinus, palate plate, postorbital space, inferior orbital fissure, ethmoidal sinus, oropharynx part and superior & inferior alveolar process.

Normal image of non-enhanced sagittal scan: Scanning at nasal septum sagittal plane can display skull base, sphenoid

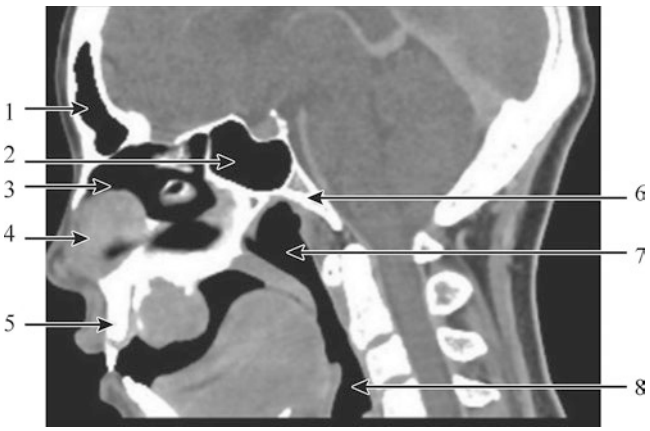

Fig. 10.3 Non-enhanced CT scan of maxillofacial region at sagittal plane (nasal septum plane). 1. Frontal sinus 2. Ethmoidal sinus 3. Nasal cavity 4. Nasal concha 5. Superior alveolar process 6. Skull base 7. Nasopharynx 8. Oropharynx

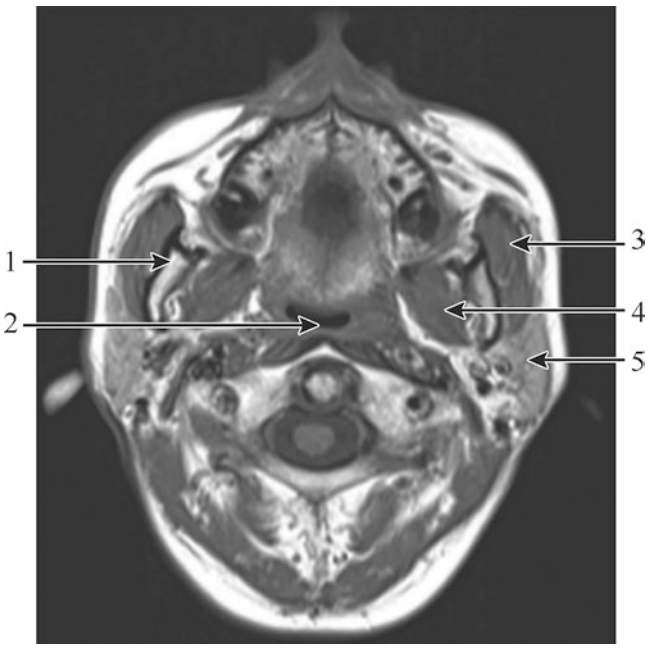

Fig. 10.4 Non-enhanced MRI scan of parotid gland at transverse plane. 1. Ascending ramus of mandible 2. Pharyngeal cavity 3. Masseter 4. Medial pterygoid 5. Parotid gland

sinus, nasopharynx, oropharynx, nasal cavity, turbinate, alveolar bone and frontal sinus (Fig. 10.3).

10.3 MR Imaging Anatomy

MRI shows the same anatomical structures of sections as CT but different image features (Figs. 10.4 and 10.5). On MRI images, a compact bone substance is black without signal

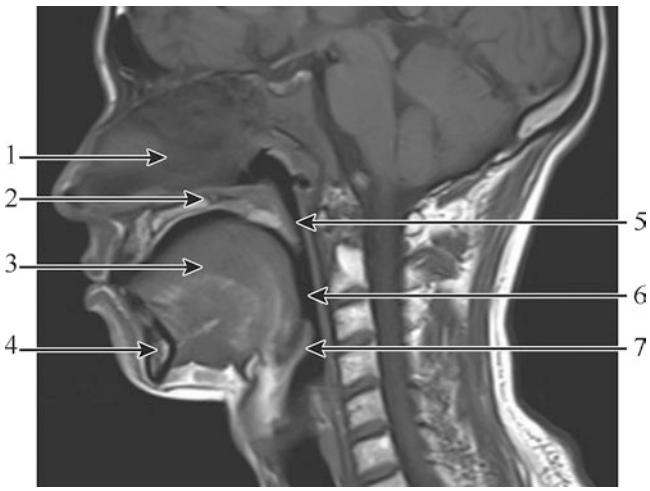

Fig. 10.5 MRI scanning at midline sagittal plane. 1. Nasal cavity 2. Palate plate 3. Lingua 4. Mandible 5. Nasopharynx 6. Oropharynx 7. Epiglottis

intensity, while adipose tissue shows hyperintense due to a large number of movable hydrogen ions. Bone marrow, which contains a lot of adipose tissues, also shows hyperintense. The signal intensity of other soft tissues varies by different compositions contained therein. As lipoid glandular tissues, parotid gland and submandibular gland show higher intensity than peripheral muscular tissues. MRI is better than CT in development of soft tissues, so it mainly applies to detect lesions in oral and maxillofacial region soft tissues and temporal-mandibular joint [4], and serves as the primary examination method for disturbance syndrome of temporomandibular joint [5, 6].

References

1. Meiqing W. Oral anatomy and physiology. Beijing: People's Medical Publishing House; 2012.
2. Demin H. Otorhinolaryngology head and neck surgery. Beijing: Peking University Medical Press; 2013.
3. Gohel A, Oda M, Katkar AS, et al. Multidetector row computed tomography in maxillofacial imaging. Dent Clin North Am. 2018;62(3):453–65.
4. Zadravec D, Badel T, Smoljan M, et al. Zygomatic air cell defect- magnetic resonance imaging of the temporomandibular joint compared with panoramic radiographs. Acta Clin Croat. 2018;57(2):227–34.
5. Abouzari M, Sajjadi A, Djalilian HR. Regarding clinical implications of magnetic resonance imaging in temporomandibular disorder patients presenting ear fullness. Laryngoscope. 2019;129(5):158.
6. Miller E, Inarejos CEJ, Tzaribachev N, et al. Imaging of temporoma- ndibular joint abnormalities in juvenile idiopathic arthritis with a focus on developing a magnetic resonance imaging protocol. Pediatr Radiol. 2018;48(6):792–800.

Imaging Anatomy of Cervical Space

11

Xiaoping Tong and Heng Liu

11.1 Foundation of Imaging Anatomy

Cervical region contains the common carotid artery and its branches, jugular vein and vagus nerve posterior to carotid sheath. Cervical region is divided into hyoid bone upper and lower parts by hyoid bone, with thyroid cartilage, sternocleidomastoid, manubrium, and clavicle as main body surface symbols, and mandible, hyoid bone, thyroid cartilage, cricoid cartilage, cervical vertebra, and sternocleidomastoid as main imaging anatomic landmarks. The cervical fascia is divided into superficial and deep cervical fascia. The superficial cervical fascia, which is composed of subcutaneous tissue and platysma muscle, surrounds the whole neck. Deep cervical fascia is divided into superficial layer (cover layer), middle layer (visceral layer), and deep layer (perivertebral layer), wherein twelve main cervical spaces are constituted, namely, sublingual space, submandibular space, buccal space, submasseteric space, carotid artery space, posterior cervical space, parotid gland space, pharyngeal mucosa space, parapharyngeal space, retropharyngeal space, viscera space and prevertebral (paravertebral space). Among them, some cervical spaces overlap with maxillofacial region. Cervical region is relevant to the development of branchial arch and branchial sac, so it is prone to occur congenital diseases, such as branchial cleft cyst and lymphatic vessel cyst. Besides, owing to rich lymphatic drainage in head and neck, wherein lymph nodes across the whole body are gathered, the region is more likely to occur inflammation, infection, and tumor metastasis, thus resulting in enlargement of cervical lymph nodes.

11.2 CT Imaging Anatomy

11.2.1 Transverse Plane of Neck

1. Oropharynx inferior level at transverse plane. Mandible is arch-shaped, posterior to which genioglossus, sublingual gland, submandibular space, and submandibular gland therein are located. Intermediate gas density is oropharynx cavity, and retropharyngeal space is located between prevertebral fascia and oropharynx posterior wall. Carotid sheath is located between lateral wall of pharynx and sternocleidomastoid. The position of common carotid artery bifureation varies from person to person with variation. The portion located most posterior to the level is high-density cervical vertebra and equidensity muscle, in which intramuscular space contains fat, showing hypointense (Fig. 11.1).

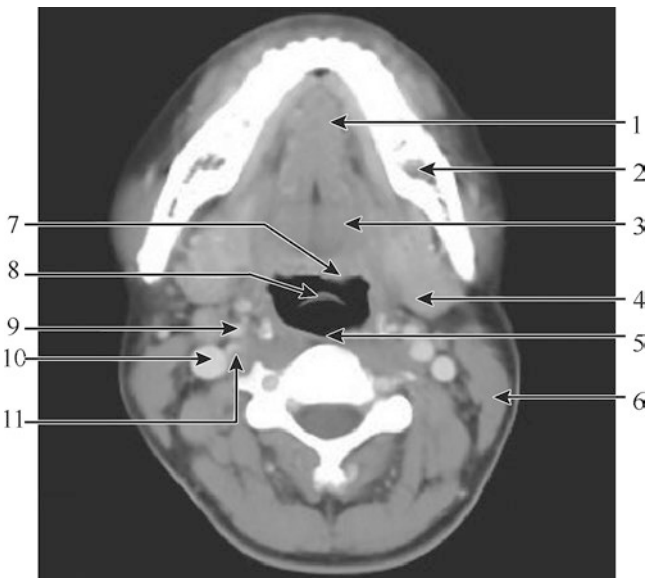

Fig. 11.1 Oropharynx inferior level. 1. Genioglossus 2. Mandible 3. Sublingual gland 4. Submandibular gland 5. Retropharyngeal space 6. Sternocleidomastoid 7. Oropharynx 8. Epiglottis 9. External carotid artery 10. Internal jugular vein 11. Internal carotid artery

X. Tong
Chengdu Aerospace Hospital, Chengde, China

H. Liu (✉)
Affiliated Hospital of Zunyi Medical University, Zunyi, China

H. Li et al. (eds.), *Radiology of Infectious and Inflammatory Diseases - Volume 2*,
https://doi.org/10.1007/978-981-16-8841-6_11

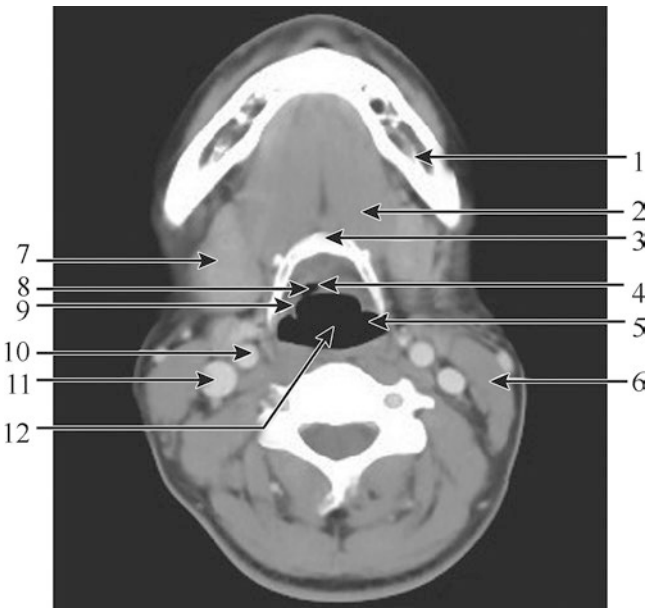

Fig. 11.2 Through hyoid bone body level. 1. Mandible 2. Mylohyoid muscle 3. Hyoid bone 4. Epiglottis 5. Piriform recess 6. Sternocleidomastoid 7. Submandibular gland 8. Vallecula epiglottica 9. Aryepiglottic fold 10. Common carotid artery 11. Internal jugular vein 12. Laryngeal vestibule

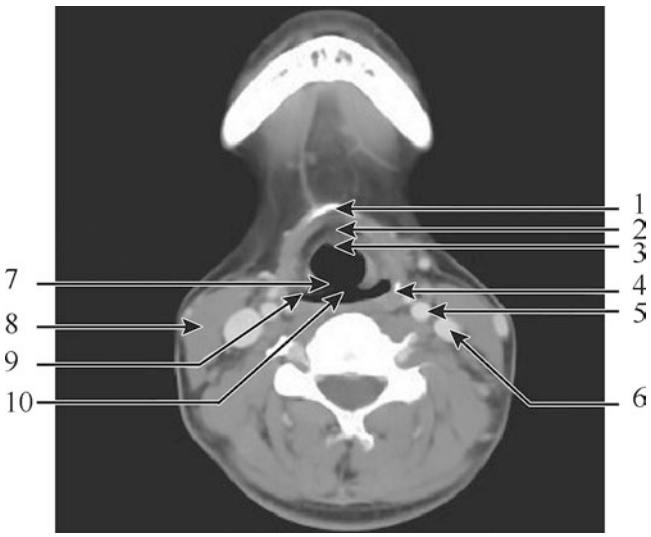

Fig. 11.3 Through superior level of thyroid cartilage. 1. Hyoid bone 2. Thyroepiglottic ligament 3. Epiglottis 4. Thyroid cartilage 5. Common carotid artery 6. Internal jugular vein 7. Epiglottis anterior fold 8. Sternocleidomastoid 9. Piriform recess 10. Laryngeal vestibule

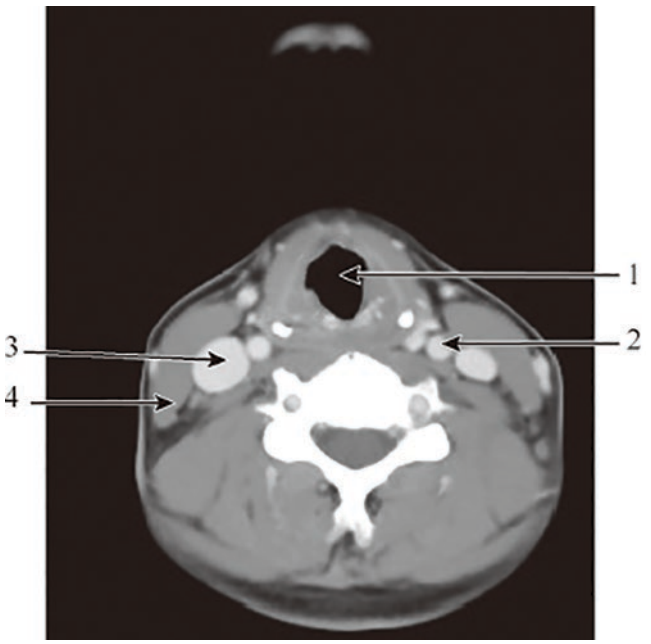

Fig. 11.4 Through intermediate cavity of larynx level. 1. Larynx cavity; 2. Common carotid artery; 3. Internal jugular vein; 4. Sternocleidomastoid.

2. Through hyoid bone body level. Mandible and its posterior hyoid bone form a big and a small arch portions with high density, between which geniohyoid and mylohyoid muscle are located. Epiglottis body, which is located posterior to hyoid bone, shows arc line shadows. Between epiglottis body and aryepiglottic fold on both sides and anterior hyoid bone body, there is vallecula epiglottica or preepiglottic space, which is filled with adipose tissues, thus showing hypointense. Posterior to it, there are laryngeal vestibule and bilateral piriform recesses, which are air-filled cavity. Carotid sheath and sternocleidomastoid are located posterolateral to lateral wall of pharynx (Fig. 11.2).

3. Through superior level of thyroid cartilage. This plane is approximately flush with the 5th cervical vertebra. Between the front end posterior border of thyroid cartilage and epiglottic cartilage is thyroepiglottic ligament. The bilateral low-density areas are preepiglottic space. At this level, the airway shows a characteristic "felt cap" shape, wherein the top of the hat is epiglottic cartilage and two cap peaks are aryepiglottic fold (Fig. 11.3).

4. Through intermediate cavity of larynx level. Intermediate cavity of larynx is the part of larynx cavity between rima vestibule plane and fissure of glottis. It is the narrowest part of larynx cavity, with oblate or slit-shaped section, which is dependent on the open/close status of glottis. Arytenoid cartilage is located posterolateral to intermediate cavity of larynx plane. The anterior end of vocal cord starts from medial side of thyroid cartilage anterior horn middle section, and the posterior end terminates at the vocal process of arytenoid cartilage. The narrow fissure that is approximately triangular-shaped between the vocal cords on both sides is called fissure of glottis (Fig. 11.4).

5. Through cricoid cartilage level. This plane is approximately flush with the 6th cervical vertebra. The circular lucency shadow surrounded by cricoid cartilage is inferior larynx cavity (infraglottic cavity) and inferior breathing tube.

Soft tissues anterior to and posterolateral to cricoid cartilage arch are respectively infrahyoid muscles and thyroid gland bilateral lobes. Posterior to lamina of cricoid cartilage, there is pharynx and esophagus junction (Fig. 11.5).

6. Isthmus of thyroid gland plane. This level is approximately flush with the 7th cervical vertebra. Thyroid gland is located on both sides of trachea, and isthmus of thyroid gland is anterior to trachea. Infrahyoid muscles and sternocleidomastoid are respectively located anterior and lateral to lateral lobe. Triangle of vertebral artery is the space between longus colli anterior to vertebral body and anterior scalene muscle lateral to vertebral body, with important structures including vertebral artery, vertebral venous plexus, inferior thyroid artery, cervical sympathetic trunk, and cervicothoracic ganglion (Fig. 11.6).

7. Neck root plane. This level is flush with the 1st thoracic vertebra body. At the center of anterior section is trachea with a circular section, and the anterolateral side is surrounded by thyroid gland. Esophagus is posterior to trachea. Section of ribs can be seen lateral and posterior to vertebral body (Fig. 11.7).

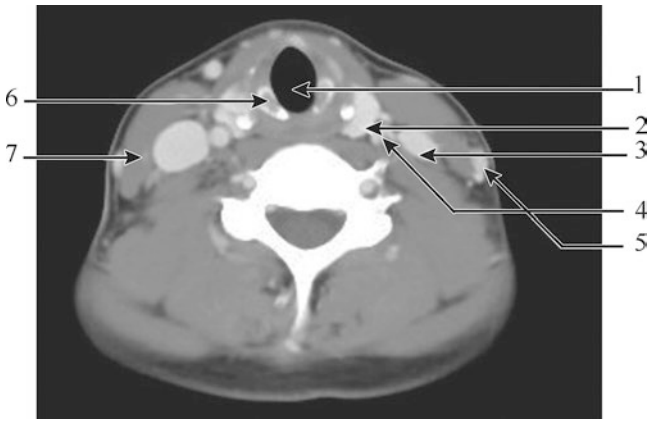

Fig. 11.5 Through cricoid cartilage level. 1. Infraglottic cavity; 2. Thyroid gland; 3. Internal jugular vein; 4. Common carotid artery; 5. External jugular vein; 6. Cricoid cartilage; 7. Sternocleidomastoid.

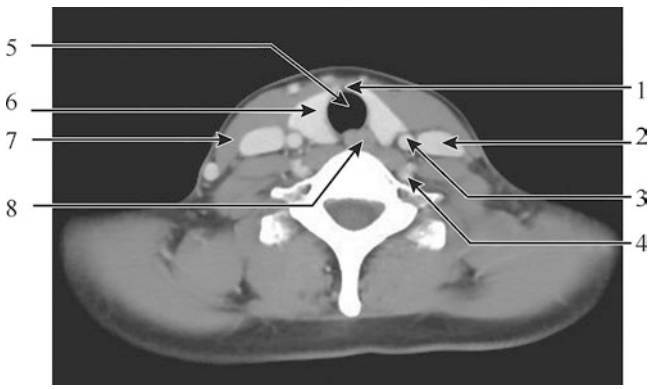

Fig. 11.6 Isthmus of thyroid gland level. 1. Isthmus of thyroid gland 2. Internal jugular vein 3. Common carotid artery 4. Vertebral artery 5. Trachea 6. Thyroid gland 7. Sternocleidomastoid 8. Esophagus

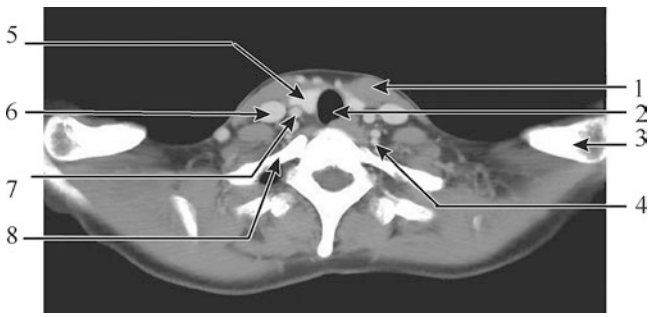

Fig. 11.7 Neck root level. 1. Sternocleidomastoid 2. Trachea 3. Clavicle 4. Vertebral artery 5. Thyroid gland 6. Internal jugular vein 7. Common carotid artery 8. The 1st rib

11.2.2 Sagittal Plane of Neck

Mid-sagittal of neck can display oropharynx, hypopharynx, and peripheral structures. oropharynx is between velum palatinum free edge and epiglottis superior border plane. The epiglottis is located posterior to root of tongue, extending into pharyngeal cavity in a leaf-shaped manner. Hypopharynx communicates upwards with oropharynx cavity, and downwards with trachea. It is continuous with esophagus between the section below epiglottis superior border and the inferior border of the 6th cervical vertebra body. Laryngeal ventricle is located between ventricular fold (false vocal cords) in hypopharynx and vocal cords. laryngeal vestibule is above the ventricular fold, and infraglottic cavity is below vocal cords (Fig. 11.8).

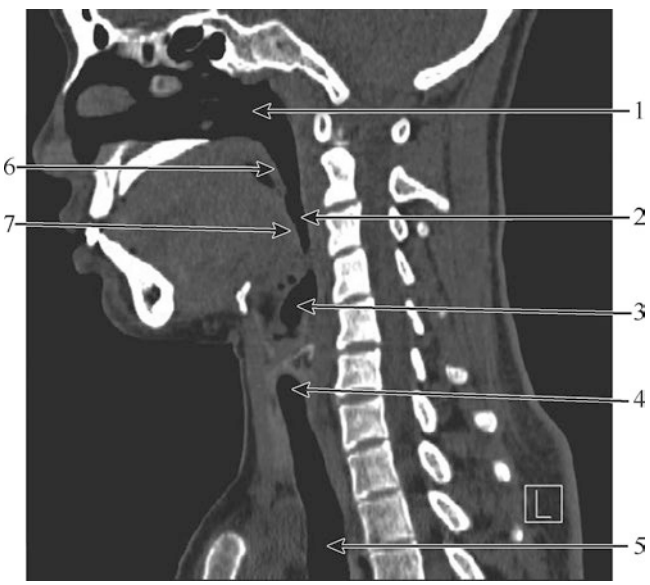

Fig. 11.8 Sagittal plane of neck. 1. Nasopharynx; 2. Oropharynx; 3. Hypopharynx; 4. Infraglottic cavity; 5. Trachea 6. Soft palate; 7. Root of tongue.

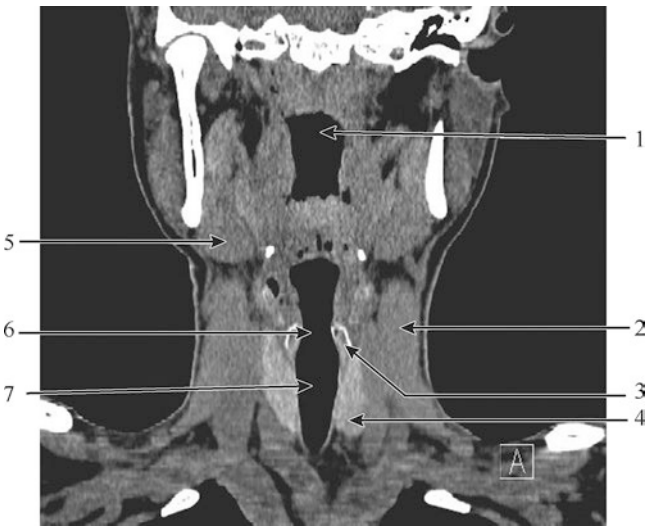

Fig. 11.9 Coronal plane of neck. 1. Oropharynx; 2. Sternocleidomastoid; 3. Thyroid cartilage; 4. Thyroid gland; 5. Submandibular gland; 6. Infraglottic cavity; 7. Trachea;

11.2.3 Coronal Plane of Neck

Scanning at mid-coronal plane of laryngeal ventricle shows that epiglottis is in a splayed shape, above which is oropharynx and below which is hypopharynx. The air-filled triangular cavity space between aryepiglottic fold and oropharynx wall is piriform recess. Below aryepiglottic fold, there are two processes protruding toward the middle of cavity, among which the upper one is vestibular fold formed by ventricular folds, and the lower one is vocal fold. The recess between the two processes is laryngeal ventricle, namely, the recess extending from the intermediate cavity of larynx to the two sides. Cricoid cartilage, thyroid gland, common carotid artery, internal jugular vein, and sternocleidomastoid can be seen lateral to infraglottic cavity and trachea (Fig. 11.9).

11.3 MR Imaging Anatomy

Subcutaneous fat of neck and fat space between tissues show hyperintense on both T_1WI and T_2WI. Muscle, nerve, and lymph node show moderate hypointense, air-filled canals show no signal, and larynx, trachea, esophagus and thyroid gland in the anterior cervical viscera region are clearly displayed.

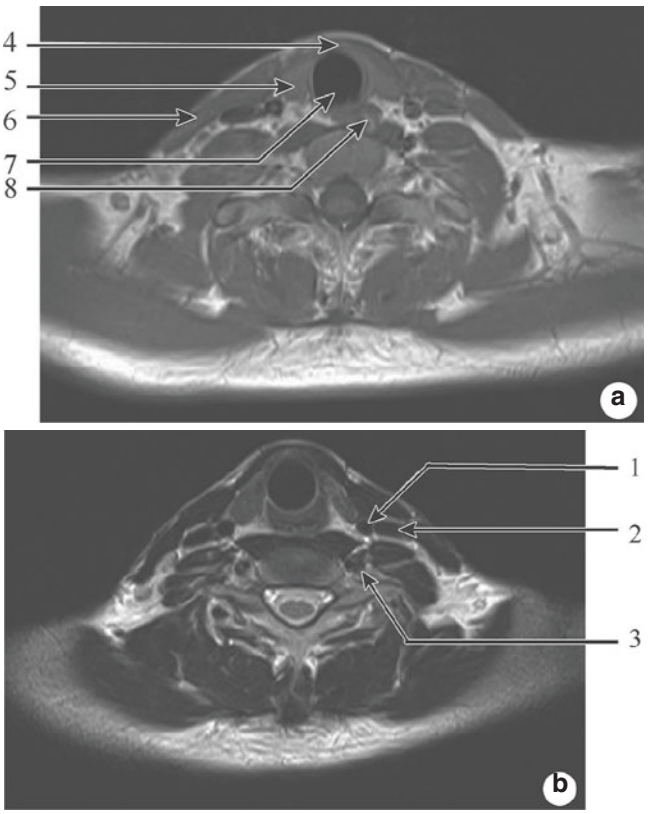

Fig. 11.10 Isthmus of thyroid gland level. 1. Common carotid artery 2. Internal jugular vein 3. Vertebral artery 4. Isthmus of thyroid gland 5. Thyroid gland 6. Sternocleidomastoid 7. Trachea 8. Esophagus

Laryngeal cartilage shows homogeneously isointense on T_1WI and T_2WI. Thyroid gland shows moderate hyperintense on T_1WI and T_2WI. Due to the flowing void effect, arteries and veins in carotid sheath show hypointense, while small or slow bloodstream may also show hyperintense. Transverse plane shows vessel section, and sagittal plane sometimes shows the entire artery. Posterior region of neck is composed of cervical vertebra and peripheral muscles, including scalene muscles anterior or lateral to cervical vertebra and extensor muscles posterior to cervical vertebra, which can be distinguished via the hyperintense signals of intermuscular fats [1] (Fig. 11.10).

Reference

1. Renju B, Ping H, Chunshui Y. Medical imaging diagnostics. Beijing: People's Medical Publishing House; 2018.

Imaging Anatomy of Thyroid Gland

12

Ying Zou, Shuang Xia, and Wen Chen

12.1 Foundation of Imaging Anatomy

12.1.1 Position and Composition of Thyroid Gland

Thyroid gland is below the thyroid cartilage that is located anterior and median to the neck. As the biggest endocrine gland of human body, thyroid gland is H or butterfly-patterned, reddish brown, composed of left and right lateral lobes and isthmus therein. Lateral lobes of thyroid gland are located anterolateral to hypolarynx and cervical part of trachea. The left and right lateral lobes are divided into anterior and posterior borders, superior and inferior extremities, anterolateral and anteromedial sides. Its highest point is flush with the midpoint of thyroid cartilage, and its lowest point reaches the 6th tracheal ring. The rear is flush with the height of C5-7. The isthmus of thyroid gland in the middle is located anterior to the 2-4th tracheal rings, connecting left and right lateral lobes. Sometimes, it can be seen that a pyramidal lobe protrudes upwards from isthmus of thyroid gland. The lobe is of varying lengths, and the longest can reach hyoid bone plane [1].

12.1.2 Thyroid Gland Envelope and Blood Supply

Thyroid gland has two layers of envelope, among which the outer one is called true envelope. Sheath of thyroid gland is also known as false envelope, which is cervical visceral layer fascia that envelops the true capsule. The true envelope is a fibrous capsule that extends into thyroid gland parenchyma and divides the gland into lobes of different sizes. Thyroid gland is enveloped by pretracheal fascia, which forms thyroid gland capsule called sheath of thyroid gland. The space between two layers of envelope is capsule sheath space, in which connective tissues, blood vessels, nerves, parathyroid gland and other important structures are located. The thickened medial sheath of thyroid gland forms suspensory ligaments of thyroid gland, thus connecting the thyroid gland with thyroid cartilage, cricoid cartilage and tracheal ring at its medial left and right lobes and isthmus. For this reason, thyroid gland can move up and down along with the larynx when swallowing [1, 2].

Thyroid gland has rich blood supply. Feeding artery is mainly superior and inferior thyroid arteries. About 13% of people have the lowest thyroid artery. Superior thyroid artery, as the first branch of the external carotid artery, typically originates from the initial part therein. At the upper pole of thyroid gland lateral lobe, it is divided into anterior and posterior branches entering into gland. Most of inferior thyroid arteries originate from subclavian artery branch thyrocervical trunk. It is divided into superior and inferior branches that enter thyroid gland from the posterior side of lateral lobe. The lowest thyroid artery originates from aortic arch, brachiocephalic trunk, right common carotid artery and subclavian artery, varying greatly, and extends upward along anterior trachea into isthmus of thyroid gland. The three main veins of thyroid gland are superior, middle, and inferior thyroid veins. Superior thyroid vein accompanies with superior thyroid artery, while middle thyroid vein often runs alone, and they converge into internal jugular vein. Inferior thyroid vein, which has a lot of branches, accompanies with inferior thyroid artery and converges into brachiocephalic vein [3].

12.1.3 Nervous and Lymphatic System of Thyroid Gland

Interstitial tissue of thyroid gland contains a small number of sympathetic nerves, vagus nerves, and peptidergic nerve

Y. Zou
The First Affiliated Hospital of Tianjin University of TCM, Tianjin, China

S. Xia (✉)
Tianjin First Central Hospital, Tianjin, China

W. Chen
Shiyan TAIHE Hospital (Affiliated Hospital of Hubei University of Medicine), Shiyan, China

H. Li et al. (eds.), *Radiology of Infectious and Inflammatory Diseases - Volume 2*,
https://doi.org/10.1007/978-981-16-8841-6_12

fibers. Thyroid gland is innervated by superior laryngeal nerve and recurrent laryngeal nerve, wherein the superior laryngeal nerve accompanies with superior thyroid artery and superior thyroid vein. It is located superior to thyroid gland. The recurrent laryngeal nerve intersects with inferior thyroid artery and inferior thyroid vein. It is located inferior to thyroid gland. Superior laryngeal nerve originates from the nodose ganglion of vagus nerve and mainly innervates cricothyroid muscle, with some branches innervating thyroid gland. Recurrent laryngeal nerve originates from thoracic segment of vagal nerve trunk and returns to cervical region, clinging closely to the posterior thyroid gland. There is close anatomical relationship between recurrent laryngeal nerve and thyroid gland [3, 4].

The lymphatic system of thyroid gland is extremely rich, and there are lymphatic capillaries around capillary plexus peripheral to follicle. The latter gradually converges into lymphatic vessels, coursing in the connective tissue between the lobules, converging into the deep lymph nodes arranged along the internal jugular vein, and then injecting into thoracic duct and right lymphatic duct [3].

12.1.4 Adjacent Relationship Around Thyroid Gland

Anterior to thyroid gland, there are skin, superficial fascia, superficial and middle layers of deep fascia, and infrahyoid muscles, in which there are four muscles that are divided into deep and superficial layers. Paratactic superficial longitudinal rows form the medial sternohyoid muscle and lateral omohyoid muscle. The deep layer is divided into upper thyrohyoid muscle and lower sternothyroid. Posterior to thyroid gland, there are cervical sympathetic trunk and 4 neck visceral canals, namely, larynx, trachea, pharynx and esophagus. The degree and extent to which left and right lobes of thyroid gland expand upwards, downwards and backwards, and carotid sheath, which is located lateral to thyroid gland, shifts outwards can be determined by the four canals [4].

12.2 CT Imaging Anatomy

The superior-inferior diameter of normal thyroid gland is 6–7 cm, the left-right diameter is 2–3 cm, and the anterior-posterior diameter is 2–3 cm. The above diameters are slightly smaller in female than in male. Due to the high iodine content of thyroid gland, X-ray is attenuated more through thyroid gland than through peripheral soft tissues. For This reason, thyroid gland shows slightly brighter on CT image, with a CT value of 70HU ± 10HU. On CT images, thyroid gland is manifested as soft tissues with high, homogeneous density and well-defined borders that are located on both sides of the lower cervical trachea. Its density is similar to that of bilateral internal jugular veins (Figs. 12.1, 12.2 and 12.3). When applying enhanced scan, thyroid gland is quickly and remarkably enhanced in a homogeneous way, and the enhancement lasts a long time [4–6].

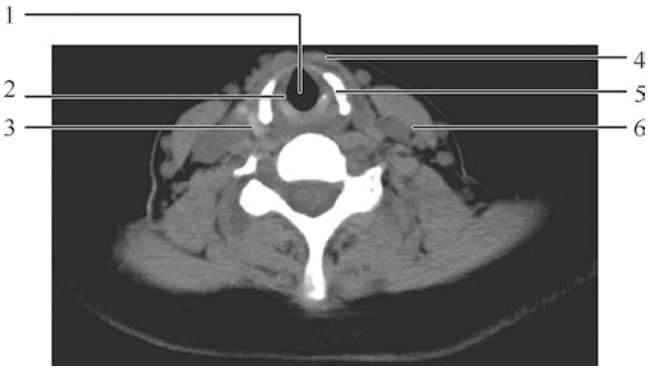

Fig. 12.1 Non-enhanced CT scan of cervical region at transverse plane (1). 1. Fissure of glottis 2. Cricoid cartilage 3. Thyroid gland lateral lobe 4. Infrahyoid muscle 5. Thyroid cartilage 6. Sternocleidomastoid

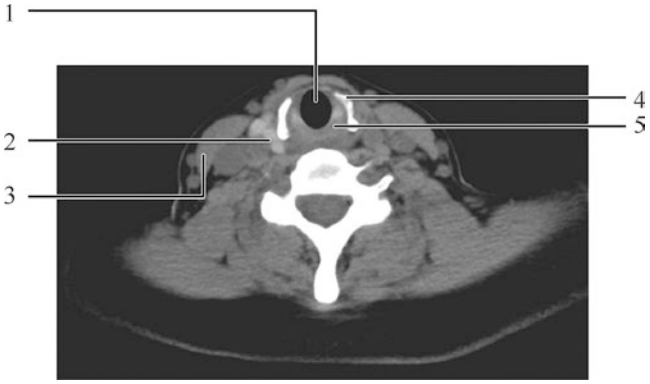

Fig. 12.2 Non-enhanced CT scan of cervical region at transverse plane (2). 1. Infraglottic cavity; 2. Thyroid gland lateral lobe; 3. Sternocleidomastoid 4. Thyroid cartilage 5. Cricoid cartilage

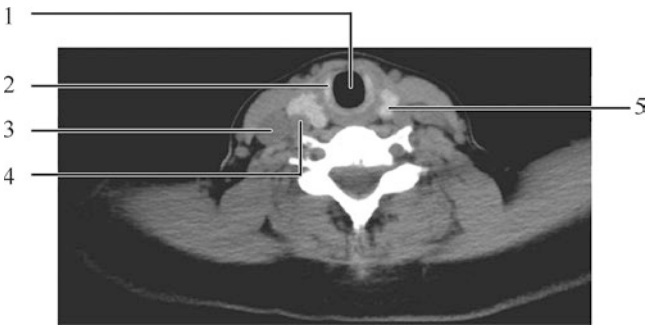

Fig. 12.3 Non-enhanced CT scan of cervical region at transverse plane (3). 1. Infraglottic cavity; 2. Cricoid cartilage 3. Internal jugular vein; 4. Common carotid artery; 5. Thyroid gland lateral lobe;

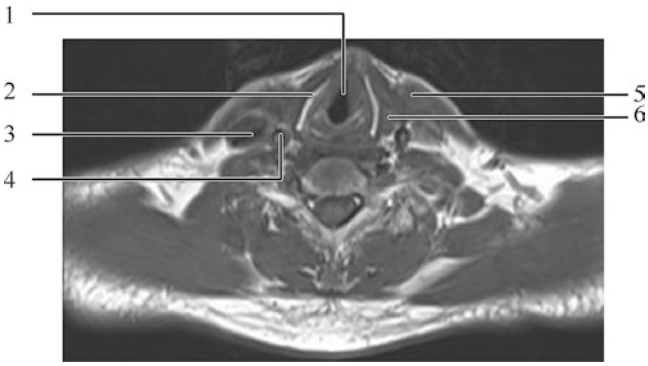

Fig. 12.4 Non-enhanced MRI scan of cervical region at transverse plane (1). 1. Fissure of glottis 2. Thyroid cartilage; 3. Internal jugular vein; 4. Common carotid artery; 5. Sternocleidomastoid; 6. Thyroid gland lateral lobe

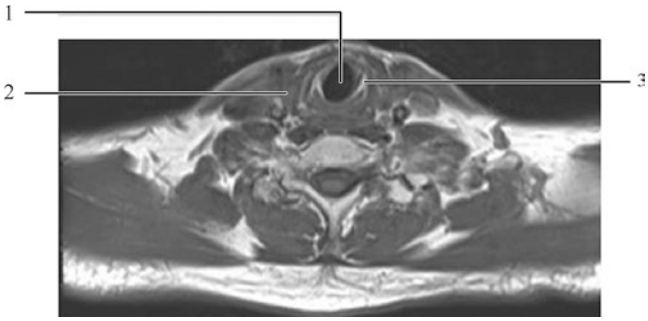

Fig. 12.5 Non-enhanced MRI scan of cervical region at transverse plane (2). 1. Infraglottic cavity; 2. Thyroid gland lateral lobe; 3. Cricoid cartilage

12.3 MR Imaging Anatomy

In MRI scanning for normal thyroid gland, thyroid gland lateral lobe is isointense relative to muscle on T_1WI sequence. Thyroid gland bilateral lobes show homogeneous signals on T2WI sequence and hyperintense relative to peripheral muscle tissues of neck (Figs. 12.4, 12.5 and 12.6). Fat suppression shows homogeneously isointense or slightly hyperintense on T_1WI and T_2WI. After enhanced scan, thyroid gland bilateral lobes are enhanced remarkably and homogeneously [3, 7].

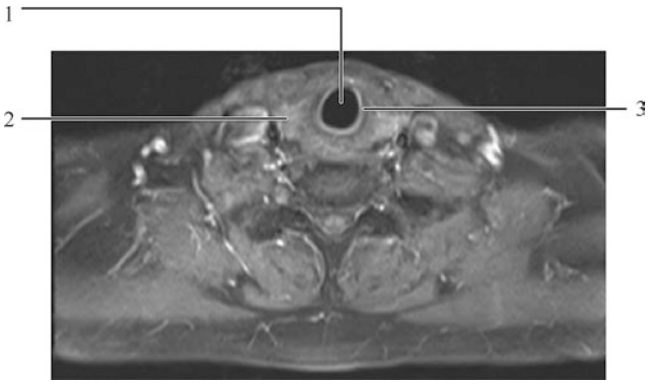

Fig. 12.6 Non-enhanced MRI scan of cervical region at transverse plane (3). 1. Infraglottic cavity; 2. Thyroid gland lateral lobe; 3. Cricoid cartilage

References

1. Wenlong D, Xuezheng L. Systematic anatomy. 8th ed. Beijing: People's Medical Publishing House; 2018.
2. Qiangxiu W, Haiyan C. Diagnosis and treatment of thyroid gland diseases. Shanghai: The Second Military Medical University; 2015.
3. Zhijiang H, Lingyun B, Wenhui C. Thyroid gland and parathyroid gland contrast imaging diagnosis. Beijing: People's Medical Publishing House; 2016.
4. Jinbo L, Dongyou Z, Guofang Y. Glandular diseases imaging diagnostics. Jinan: Shandong Science & Technology Press; 2007.
5. Vazquez BJ, Richards ML. Imaging of the thyroid and parathyroid glands. Surg Clin. 2011;91(1):15–32.
6. Guangda X. Clinical thyroid diseases. Beijing: People's Medical Publishing House; 2013.
7. Frunzac RW, Richards M. Computed tomography and magnetic resonance imaging of the thyroid and parathyroid glands. Front Horm Res. 2016;45:16–23.

Imaging Anatomy of Skull Base

13

Jie Hu and Heng Liu

Skull base is an interface between osseous tissue and soft tissue. Anatomically, it is divided into many segments, mainly composed of the orbital plate of temporal bone, cribriform plate of ethmoid bone, sphenoid bone, occipital bone and petrous part of temporal bone.

13.1 Anatomic Foundation of Inner Skull Base

The medial skull base consists of anterior skull base, middle skull base and posterior skull base. Skull base has a host of pore canals, through which major blood vessels and nerves pass. See Table 13.1 for details.

Table 13.1 Composition of medial skull base and major arteries and nerves coursing therein

Position	Composition	Major coursing arteries	Major coursing nerves
Anterior skull base	Frontal squamous part, ethmoidal sinus, cribriform plate and cockscomb	Anterior cerebral artery	Olfactory nerve
Middle skull base	Minor wing of sphenoid bone, corpus sphenoidale and greater wing of sphenoid bone	Cerebral arterial circle	Optic nerve, oculomotor nerve, trochlear nerve, trigeminal nerve and abducent nerve
Posterior skull base	Petrous part of temporal bone and occipital bone	Jugular venous bulb Sigmoid sinus Vertebrobasilar artery	Facial nerve, vestibulocochlear nerve, vagus nerve, glossopharyngeal nerve, accessory nerve and hypoglossal nerve.

13.1.1 Anterior Skull Base

The anterior boundary of anterior skull base is frontal squamous part composed of frontal bone orbital plate on both sides. The posterior boundary is minor wing of sphenoid bone. In the midline area of anterior skull base at superior aspect, there is a concave olfactory pit, in which olfactory bulb, olfactory tract and olfactory fila are located. Horizontal plate of ethmoid bone is located below, separating anterior cranial cavity from nasal cavity. Just above the horizontal plate of the ethmoid bone, there is a projection known as cockscomb. There are many sieve pores on both sides of cockscomb. A tubular structure, dubbed foramen cecum, is located in frontal-ethmoidal junction area anterior to cockscomb. It is an original pore canal connecting anterior cranial fossa and nasal cavity. In embryonic development period, foramen cecum contains a layer of dural diverticula that connect anterior cranial fossa and nasal cavity mucosal. Under normal conditions, all diverticula are closed, and there are only connective tissues and osseous tissues in foramen cecum. Foramen cecum is common in infants, while the incidence in adults is less than 1.5% (Figs. 13.1 and 13.2).

Cockscomb: Entheses of cerebral falx.

Cribriform plate and olfactory nerve: There are about 40 small holes distributed on cribriform plate around cockscomb. The olfactory nerve, which originates from olfactory mucosa at the top of nasal cavity, passes upwards through pores of cribriform plate to enter anterior skull base, thus forming olfactory bulb, olfactory tract and olfactory fila [1].

J. Hu · H. Liu (✉)
Affiliated Hospital of Zunyi Medical University, Zunyi, China

H. Li et al. (eds.), *Radiology of Infectious and Inflammatory Diseases - Volume 2*,
https://doi.org/10.1007/978-981-16-8841-6_13

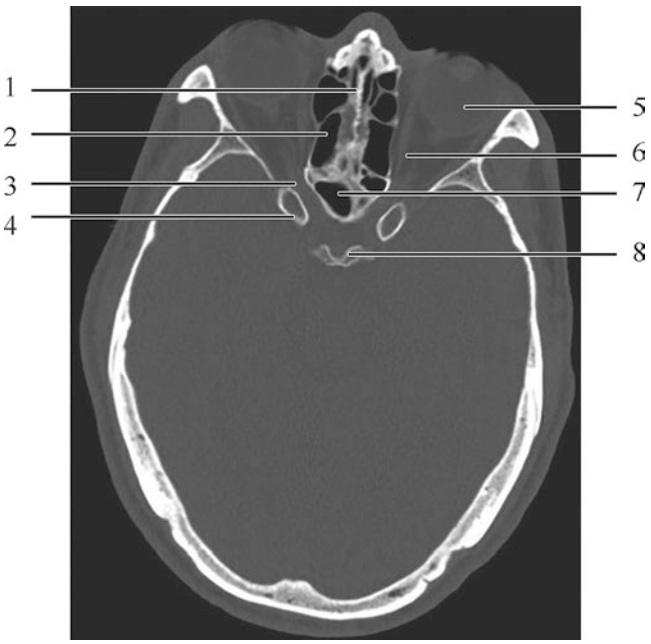

Fig. 13.1 Optic canal of anterior skull base at transverse plane. 1. Cockscomb 2. Ethmoidal sinus 3. Optic canal 4. Anterior clinoid process 5. Eyeball 6. Medial rectus 7. Sphenoid sinus 8. Dorsum sellae

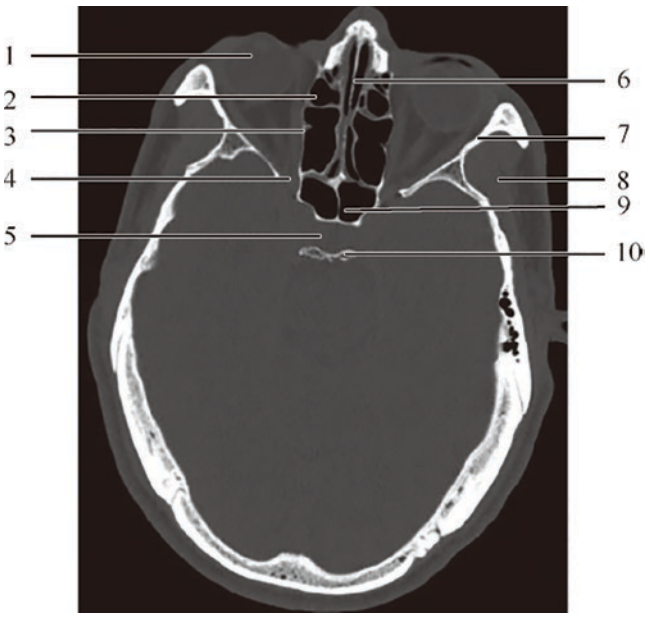

Fig. 13.2 Superior orbital fissure of anterior skull base at transverse plane. 1. Eyeball 2. Ethmoidal sinus 3. Medial wall 4. Superior orbital fissure 5. Hypophysial fossa 6. Nasal septum 7. Greater wing of sphenoid bone 8. Pterygoid fossa 9. Sphenoid sinus 10. Dorsum sellae

13.1.2 Middle Skull Base

The anterior boundary of middle skull base is minor wing of sphenoid bone and the tuberculum sellae. Its base wall is mainly composed of the corpus sphenoidale and greater wings of sphenoid bone on both sides. The posterior boundary is separated from posterior skull base by petrous part of temporal bone and dorsum sellae. Sella turcica in the center of the middle skull base and peripheral structures are called sellar region. Besides, there are many pores and lumina in the middle skull base (Table 13.1, Figs. 13.3, and 13.4).

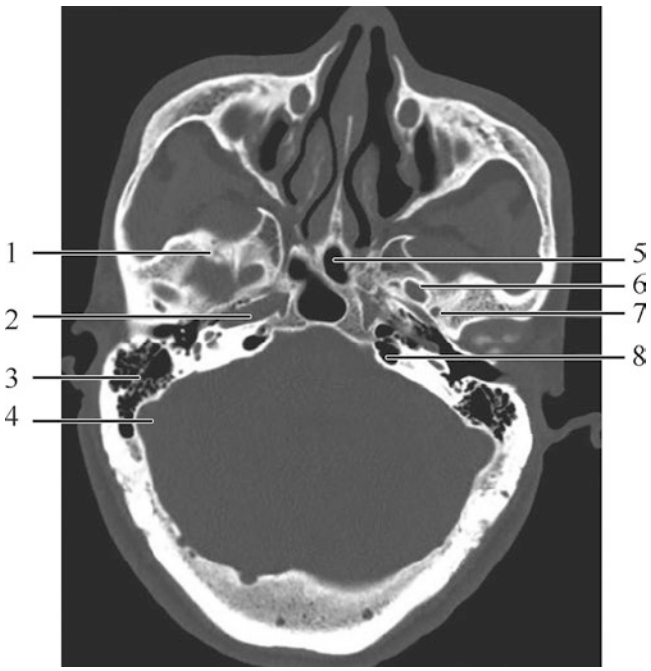

Fig. 13.3 Oval foramen of middle skull base at transverse plane. 1. Greater wing of sphenoid bone 2. Carotid canal 3. Mastoid air cell 4. Sigmoid sinus 5. Sphenoid sinus 6. Oval foramen 7. Foramen spinosum 8. Foramen lacerum

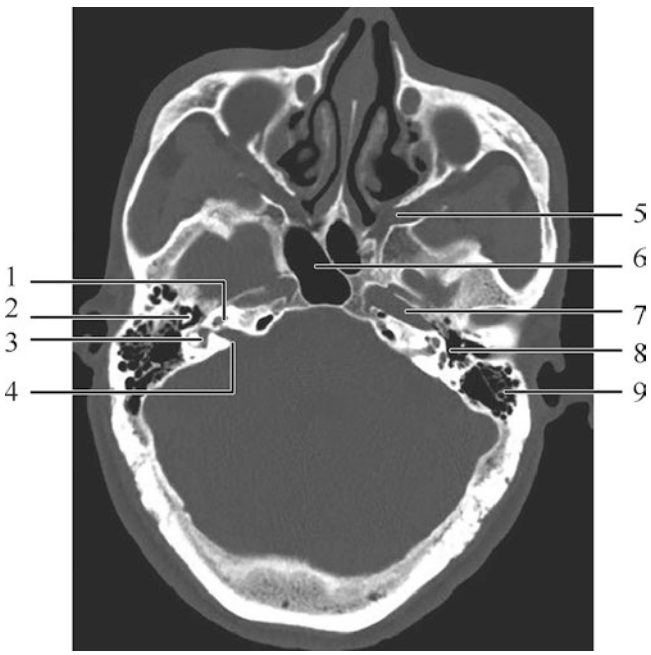

Fig. 13.4 Transverse plane scanning of cochlea at middle skull base. 1. Cochlea 2. Head of malleus 3. Vestibule 4. Internal auditory canal 5. Pterygopalatine fossa 6. Sphenoid sinus 7. Carotid canal 8. Tympanic cavity 9. Mastoid air cell

13.1.2.1 Sellar Region

1. Sella Turcica. It is saddle-shaped, located at the center of the middle skull base, including anterior clinoid process, tuberculum sellae, sulcus prechiasmaticus at the front, posterior clinoid process and dorsum sellae at the rear, and pituitary fossa in the middle, wherein pituitary is located.

2. Cavernous Sinus. It is an irregular space between two layers of cerebral dura mater on both side of sellar, one on each side. It extends forwards to superior orbital fissure and backwards to tip of petrous part of temporal bone. The lateral border is flat and straight or slightly convex, with a length of around 2 cm and an inner-outer width of 1 cm. There are internal carotid artery and abducent nerve in the cavity, and maxillary ramus and ophthalmic ramus of oculomotor nerve, trochlear nerve, and trigeminal nerve at lateral wall [2].

3. Sphenoid Sinus. Located inferior to saddle bottom.

4. Meckel's Cave. It is located at the trigeminal nerve impression at the tip of petrous part of temporal bone posterior to cavernous sinus. There are trigeminal ganglion and trigeminal cistern in the cave.

13.1.2.2 Pores and Lumina

1. Foramen Lacerum. Located most posterior to middle skull base, it is surrounded by tip of petrous part of temporal bone, corpus sphenoidale, and lateral border of occipital bone clivus. Internal carotid artery passes through lacerum to enter intracranial area.

2. Foramen Rotundum, Oval Foramen and Foramen Spinosum. Foramen rotundum (maxillary nerve), oval foramen (mandibular nerve) and foramen spinosum (middle meningeal artery) are distributed orderly at medial border of the greater wing of sphenoid bone from anteromedial to posterior side.

3. Optic Canal. It is surrounded by minor wing of sphenoid bone and lateral border of corpus sphenoidale, lined with cerebral dura mater, and communicates with orbit and middle skull base [3]. In addition, the optic nerve and ophthalmic artery pass through the optic canal.

4. Carotid Canal. Located in petrous part of temporal bone, it courses horizontally from posterior-lateral to anteromedial side. Its external aperture is located anterior to external aperture of jugular foramen, and its internal aperture connects foramen lacerum and communicates with cavernous sinus and carotid space, through which internal carotid artery and sympathetic plexus pass [1].

13.1.3 Posterior Skull Base

The anterior boundary of posterior skull base is boundary between dorsum sellae and middle skull base. Posterior border of petrous part of temporal bone in anterolateral boundary is opening of internal acoustic canal. Posterior skull base is surrounded by occipital bone on both sides and posterior boundary. At occipital base, there is a occipital foramen connecting cranial cavity and vertebral canal (Table 13.1 and Fig. 13.5).

1. Internal Acoustic Canal. It is a bony canal located in petrous part of temporal bone, coursing approximately horizontally from medial to lateral, wherein facial nerve, vestibulocochlear nerve and accompanying labyrinthine artery and vein pass through.

2. Occipital Foramen. It is located at the base of occipital bone, flanked by occipital condyle, forming atlanto-occipital joint with superior articular process of atlas [1].

3. Hypoglossal Canal. It is located posterior to occipital condyle, coursing forwards, downwards, and outwards, wherein the internal and external apertures are respectively located anterosuperior to occipital foramen and inferior to jugular tubercle. Hypoglossal nerve courses in hypoglossal canal.

4. Jugular Foramen. Located posterior to petrooccipital fissure, it is an irregular canal with internal aperture, cavity bore and external aperture, surrounded by jugular notch in petrous part of temporal bone and occipital bone notch in occipital bone. Internal aperture is connected with groove of sigmoid sinus; External aperture is separated from external aperture of hypoglossal nerve canal. Cavity bore is separated from hypotympanum. Jugular foramen is divided into nerve part at anteromedial side and blood vessel part at posterolateral side by intrajugular process [3]. Intrajugular process constitutes the posterior border of jugular foramen, extending outwards from the second half of occipital condyle. It is a crucial landmark for operative route of jugular foramen lesions.

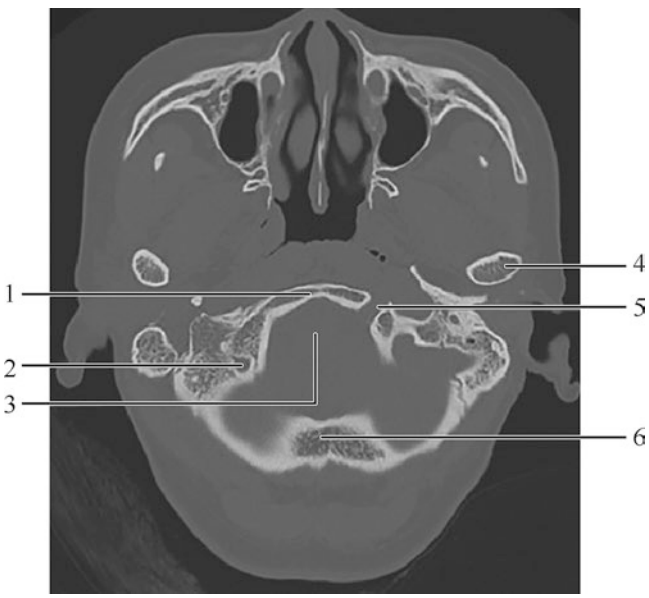

Fig. 13.5 Hypoglossal nerve canal of posterior skull base at transverse plane. 1. Base of occipital bone 2. Jugular foramen 3. Occipital foramen 4. Mandible 5. Hypoglossal canal 6. Internal occipital crest

13.2 Imaging Anatomy of Lateral Skull Base

Lateral skull base refers to the area posterior to skull base. According to the van Huijzer (1984) method commonly used for partitioning lateral skull base, when drawing extension lines along inferior orbital fissure and fissure petrooccipitalis posterior to skull base, the two lines intersect inwards at nasopharynx apex and outwards point to posterior border of zygomatic bone and posterior border of mastoid process respectively. At this point, the triangular area enclosed by the two lines is called the lateral skull base [1].

1. Partition. Lateral skull base is divided into infratemporal region, auditory tube region, nasopharynx region, articular region, auditory region, and neurovascular region. Wherein, oval foramen, foramen spinosum, foramen lacerum, vidian canal, auditory tube, and jugular foramen are located at the lateral side of lateral skull base, while foramen rotundum, superior orbital fissure and cavernous sinus are located at the medial side. In addition, there are also infratemporal fossa, pterygopalatine fossa, temporal-mandibular joint and cranial nerves and blood vessels coursing therein.

2. Infratemporal Region. It is located between auditory tube region and inferior orbital fissure, with inferior orbital fissure as anterior boundary, temporal-mandibular joint and infratemporal crest as lateral boundary, and styloid process as medial boundary. This region contains part of greater wing of sphenoid bone, lower part of temporal bone, foramen rotundum, oval foramen, foramen lacerum, foramen spinosum and medial and lateral pterygoid.

3. Auditory Tube Region. Lateral to nasopharynx region, it is the bony part of auditory tube. Anterior to the region is scaphoid fossa formed by base of pterygoid process, which provides attachment site for tensor veli palatini and levator veli palatini. Auditory tube is the passageway between tympanic cavity and nasopharynx part, with opening at the base of tympanic cavity anterior wall and ending at lateral wall of nasopharyngeal cavity. It can balance atmospheric pressure and tympanic cavity pressure.

4. Nasopharynx Region. It communicates forwards with nasal cavity and is connected downwards to oropharynx, with sphenoid bone base and clivus as superior boundary, and prevertebral muscle as posterior boundary. Lateral to the region is soft tissues and infratemporal fossa in parapharyngeal space. The bilateral nasopharynx regions jointly shape nasopharynx roof.

5. Articular Region. Located anterolateral to auditory area, the region contains mandible condyloid process, condyloid fossa, articular knuckle and articular disc, with attachment site of temporomandibular articular capsule as boundary.

6. **Auditory Area**. Anterior boundary is squamotympanic fissure and inferior boundary is styloid process. Located anterolateral to neurovascular area, it is composed of tympanic part of temporal bone, with main structures of petrous part of temporal bone, outer ear, middle ear and inner ear.

7. Neurovascular Area. Located posterior to auditory tube area, it is composed of external aperture of internal carotid artery canal, jugular foramen, hypoglossal foramen and styloid process foramen [1, 4, 5].

13.3 Imaging Anatomy of Craniocervical Junction Region

Craniocervical junction region contains osseous structures such as occipital bone, atlas and axis, and key supporting ligaments, such as apical ligament of dens, check ligament, and cruciate ligament. There are also internal carotid artery, internal jugular vein, vertebral artery and vein, glossopharyngeal and vagus accessory nerve, hypoglossal nerve and C_1 & C_2 nerves in the region.

13.3.1 Anatomical Foundation and Imaging Anatomy of Osseous Structure

Joints are formed by atlas date-cavity and odontoid process anterior border of axis, as well as by lateral mass articular fovea, occipital condyle and superior articular process of axis. Between atlas and axis, there are four joints that are collectively known as atlantoaxial joint. Atlanto-occipital joint is formed by occipital condyle matching with superior articular surface of atlas (Fig. 13.6).

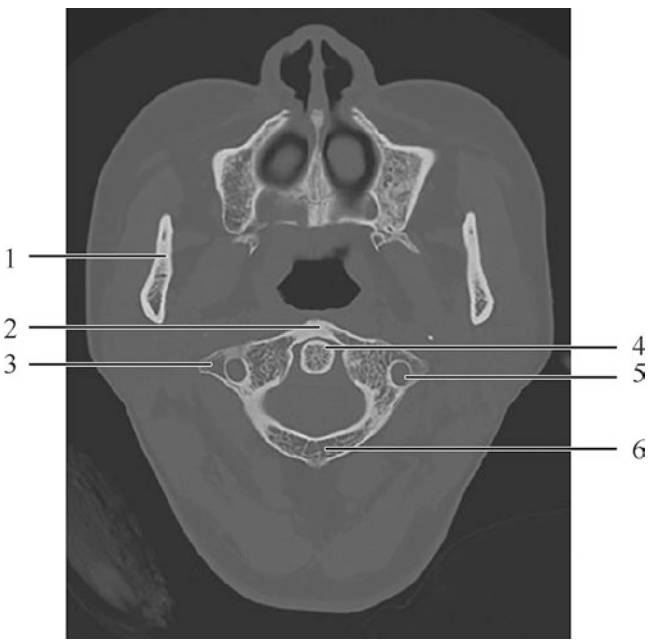

Fig. 13.6 Odontoid process joint of atlas at transverse plane. 1. Mandible 2. Anterior arch of atlas 3. Transverse process of atlas 4. Odontoid process of axis 5. Atlas transverse foramen 6. Posterior arch of atlas

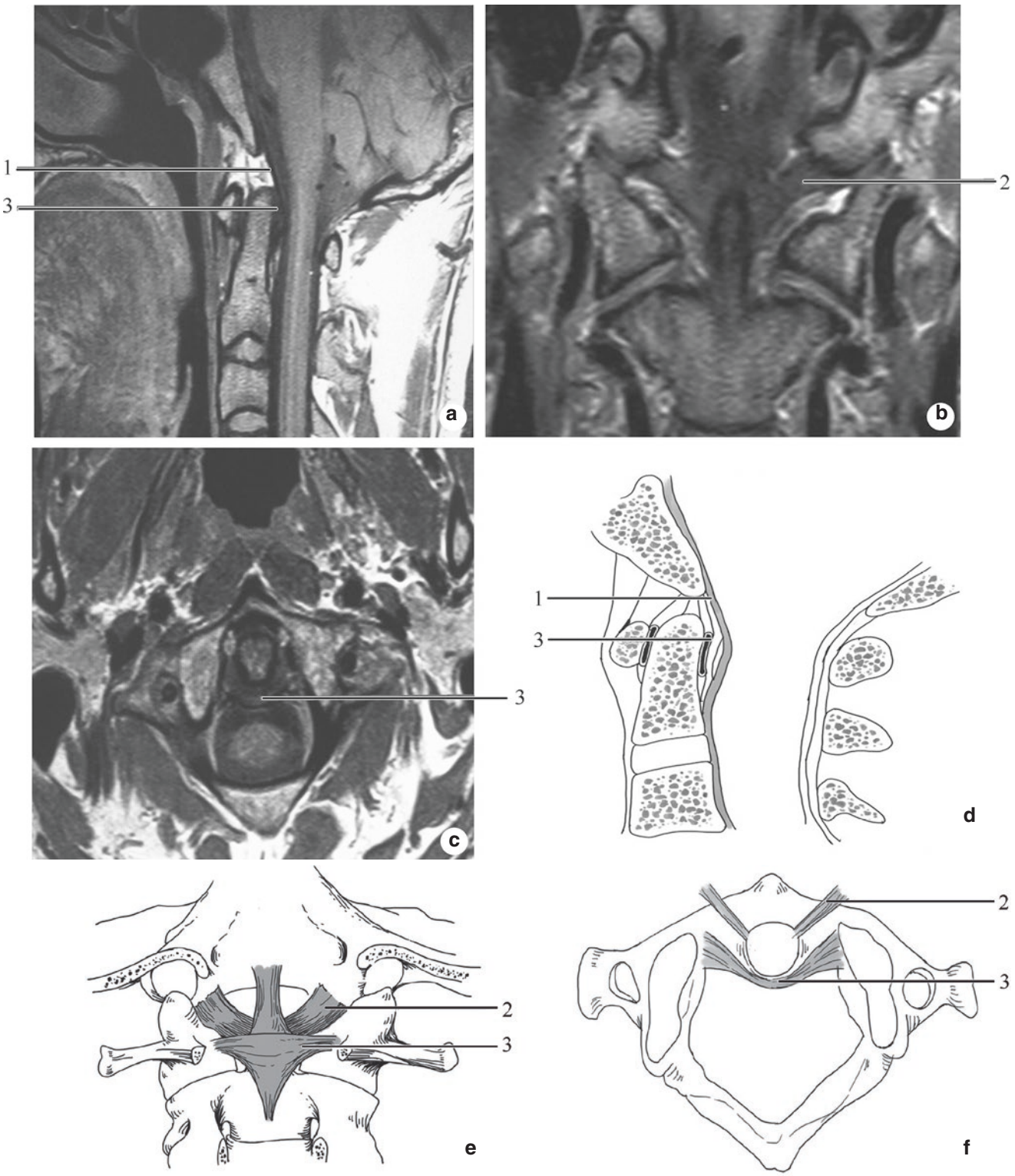

Fig. 13.7 MRI image and schematic diagram for odontoid process joint of atlas. 1. Prostheses 2. Alar ligament 3. Transverse ligament

X-ray plain film of cervical vertebra opening at frontal plane rarely shows overlap of occipital bones. The low-density fissure inferior to lateral mass is atlantoaxial joint, whose articular surface is inclined outwards and downwards, with bilateral symmetry in a splayed shape. Shadow of lateral cervical vertebra mastoid process overlaps with that of atlanto-occipital joint. CT thin scan multi-planar reconstruction (MPR) has outstanding advantages in the display of osseous structures [1].

13.3.2 Anatomical Foundation and Imaging Anatomy of Important Ligament

In craniocervical junction region, there are multiple ligaments (apical ligament of dens, check ligament, and cruciate ligament) and fibrous tunic (anterior and posterior atlanto-occipital membrane, and tectorial membrane) structures to maintain interosseous stability. Apical ligament of dens is longitudinal fiber bundles connecting tip of odontoid process and anterior border of occipital foramen. It is located between atlas anterior membrane and superior longitudinal fasciculus of cruciate ligament. There are a large amount of fibrous connective tissues and fats and a small amount of venous plexus between apical ligament of dens and superior longitudinal fasciculus of cruciate ligament. The check ligament, which originates from the dorsolateral side of odontoid process, is a fasciculus coursing in outward-inclined direction. It is attached at inferior-medial side of ipsilateral occipital condyle, with wing-shaped bilateral symmetry. Cruciate ligament is composed of horizontal part and vertical part, forming cruciform cross posterior to odontoid process. The vertical part is the thin longitudinal fasciculus (upper and lower longitudinal fasciculus), while the horizontal part is the transverse fasciculus of nodule at medial surface of atlas lateral masses. Tectorial membrane is longitudinal fiber bundles covering odontoid process and surface posterior to cruciate ligament. The membrane is thin, starting from posterior axis vertebral body, and reaching the upper part of occipital bone base anterior to occipital foramen. It laterally attaches to the medial side of atlanto-occipital joint and is upward extension of posterior longitudinal ligament. The anterior and posterior atlanto-occipital membranes respectively start from anterior and posterior arch of atlas, and communicate downwards with anterior longitudinal ligament and yellow ligament, respectively.

Ordinary X-rays cannot show ligament structure. It determines whether the transverse ligament is damaged based on width of anterior atlanto-odontoid space. CT is mainly used for displaying the morphology of bone and joint.

MRI: Generally, slice thickness is 2cm in image acquisition. Tectorial membrane is best shown at sagittal plane as thick, threadlike shadows. Transverse ligament is best shown at transverse plane as grey or black fasciculus. Check ligament are best shown at coronal plane as ash black, bilaterally symmetric signal shadows in strip pattern [3] (Fig. 13.7).

References

1. Zhenchang W, Junfang X. Imaging of the head and neck·skull base. Beijing: People's Medical Publishing House; 2016.
2. Shengqi F, Guocheng X. Sectional anatomy. Beijing: Higher Education Press; 2019.
3. Zhenchang W. Chinese clinical medical imaging·head and neck. Beijing: Peking University Medical Press; 2016.
4. Qixin Z, Minghua L. Imaging of lateral skull base. Shanghai: Shanghai Scientific & Technical Publisher; 2018.
5. Conley LM, Phillips CD. Imaging of the central skull base. Radiol Clin North Am. 2017;55(1):53–67.

Part III

Infectious and Inflammatory Diseases of Eye

Eyeball Lesions

14

Shaowei Zheng, Lijun Wang, and Zuohua Tang

14.1 Uveitis and Scleritis

14.1.1 [Overview]

Uveitis, a common disease leading to blindness, arises from inflammation of vascular tunic at middle layer of eyeball wall. It is prone to occur in young adults between 20 and 50 years old, among which male patients slightly outnumber female patients. Causes of the disease, which are very complicated, maybe infection, immunity, and trauma. According to anatomical position, uveitis can be classified as anterior uveitis, middle uveitis, posterior uveitis, and panuveitis [1–5]. Anterior uveitis, the most common uveitis, occurs in the iris or iris ciliary body, mainly manifested as eye pain radiating toward ipsilateral superciliary arch and cheek, accompanied by photophobia, tears, vision impairment. Physical examination shows ciliary congestion, aqueous humor flare, keratic precipitate, and iris nodule. Middle uveitis occurs in flat portion of ciliary body, vitreous base, and peripheral retina, accompanied by floater, blurred vision, and sore or swollen eyes. No positive sign can be observed by macrography. Posterior uveitis occurs in choroid, posterior vitreous body and retina, mainly manifested as flash sensation, visual distortion, dark spots, and vision impairment; Concurrence of anterior, middle, and posterior uveitis results in panuveitis, typically manifested as a visual disorder. Examination reveals vitreous body opacity and chorioretinal diseases.

Scleritis is a rare chronic inflammatory disease, mostly caused by adjacent tissues or systemic disease. Mainly characterized by edema in sclera and superficial layer of sclera, the disease is common in the middle-aged people ranging from 40 to 60 years old, especially occurring frequently among 50-year-old people and females. It can be classified as episcleritis, anterior scleritis, and posterior scleritis by lesion site. It can also be divided into simple, diffuse, nodular, and necrotizing perforating scleritis by lesion nature (Fig. 14.1). In clinical practices, diagnosis is often made by combining lesion site and nature, such as diffuse posterior scleritis.

Common symptoms include eye congestion, eye distension and pain, eyeball tenderness, and impaired vision. Severe cases may experience proptosis and/or diplopia. Patients may suffer from severe pain that is persistent, profound, and pulsatile. This may arise from direct stimulation by inflammation, thus resulting in traction of nerve terminals, lacrimation, and photophobia. No mucinous purulent secretion will be formed. Fundus changes accompanied by the disease include optic disc edema, cystoid macular edema, and optic neuritis. The disease may evolve from mild self-limited inflammation to necrosis, which may be related to visual-threatening complications including uveitis, glaucoma, cataract, keratitis, retinal edema, and optic neuropa-

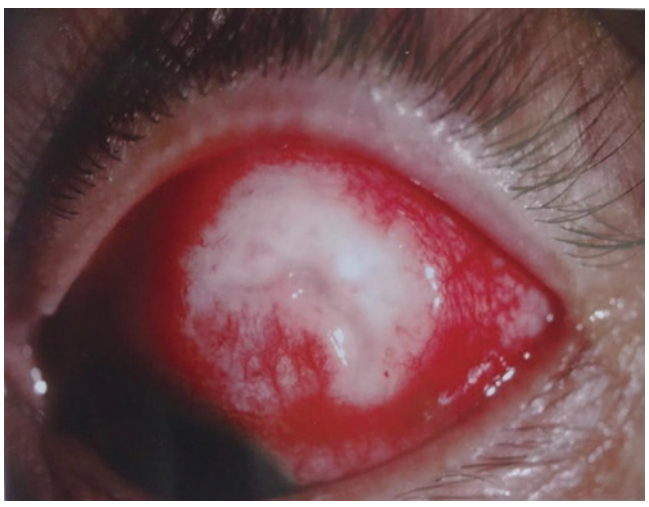

Fig. 14.1 Scleritis. A 37-year-old male patient. Image for anterior segment of eye with necrotizing scleritis shows that sclera is congestive with edema

S. Zheng · L. Wang (✉)
The First Hospital of Dalian Medical University, Dalian, China

Z. Tang
Eye and ENT Hospital of Fudan University, Shanghai, China

H. Li et al. (eds.), *Radiology of Infectious and Inflammatory Diseases - Volume 2*,
https://doi.org/10.1007/978-981-16-8841-6_14

thy. Around 50% of cases are related to systemic autoimmune abnormalities, such as rheumatoid arthritis, relapsing polychondritis, polyarteritis nodosa, systemic lupus erythematosus, spondylarthritis, Wegener granulomatosis, and giant cell arteritis. Laboratory tests may show accelerated erythrocyte sedimentation rate, positive rheumatoid factor, antinuclear antibody positive. 45% of necrotic scleritis and 30% of posterior scleritis are related to systemic diseases.

14.1.2 [Pathology Findings]

In an early stage, as inflammatory agents destroy blood-aqueous humor barrier or blood-retina barrier, some macromolecular proteins and cells in the blood infiltrate intraocular tissue space or intraocular cavity, so that uveitis is mainly manifested as exudative changes. In the advanced stage, proliferative changes are dominant. Recurrent exudation and proliferation result in atrophy of eyeball or bulbi phthisis.

Simple scleritis is mainly characterized by angiotelectasis and lymphocytes infiltration. Diffuse scleritis is mainly manifested as the bulk of sclera being surrounded by granuloma, forming diffuse, hypertrophic lesion.

Nodular scleritis is mainly manifested as nodule being enveloped by fibroblasts and multinucleated giant cells, causing thickening of tissues. As for necrotizing scleritis, tissue necrosis can occur in the central area of the lesion, followed by fatty degeneration and calcification. After the necrosis is absorbed, it can cause changes in sclera staphyloma. Besides, the disease can also be divided into three types by histological type of inflammation: 1. Autoimmune scleritis, featured with mixed palisading granulomas, necrosis, and vasculitis of all kinds; 2. Infectious scleritis, hallmarked by acute inflammation and necrosis; 3. Idiopathic scleritis, characterized in that chronic nonspecific inflammation is accompanied by follicle and fibrosis of varying degrees.

14.1.3 [Imaging Findings]

1. Ultrasonography. With high specificity, it works the best in the diagnosis of posterior scleritis [2]. Characteristic findings include flattened posterior eyeball, thickening of posterior eye (choroid and sclera), and retrobulbar edema. On top of that, posterior scleral thickening can occur with fluid accumulation in the Tenon's capsule space. A dark hypoechoic area caused by fascial capsule edema that is connected with optic nerve can form a typical T-shaped sign [3–5].

2. CT examination. As for anterior and middle uveitis, no remarkable abnormality can be seen on CT images. Posterior uveitis is mainly manifested as homogeneous or heterogeneous thickening of eye ring, wherein some local thickenings are nodular with mild enhancement; In case of lesion accompanied by choroidal or retinal detachment, CT shows the morphology of detached retinal, mostly in the shape of "V" or crescent.

Scleritis is characterized by uveoscleral thickening with homogeneous density. In the space of Tenon's capsule, the thickened soft tissue density is often seen with undefined borders. Marked enhancement is shown in the enhanced scan. Posterior scleritis often involves optic nerve and adjacent extraocular muscles, manifested by thickening of nerve front end and adjacent extraocular muscles [3–5].

3. MRI examination. According to MRI findings, posterior uveitis shows diffuse thickening of eyeball wall, wherein some local thickenings are nodular. The disease shows hypointense on T_1WI and hyperintense on T_2WI, with mild and moderate enhancement in enhanced scan. In case of choroidal or retinal detachment, inflammatory exudate typically shows hypointense on T_1WI and hyperintense on T_2WI. Those with a high protein content show hyperintense both on T_1WI and T_2WI [3–5].

Diffuse posterior scleritis is featured with diffuse thickening of sclera, which is typically located in posterior pole, and shows slightly hyperintense on T_1WI and hypointense on T_2WI when compared with vitreous body. Enhanced scan shows moderate to marked enhancement. MRI can better show some relevant eye symptoms, such as optic perineuritis and orbital inflammation.

Nodular posterior scleritis is manifested as a local raised mass, which shows slightly hyperintense on T_1WI and hypointense on T_2WI when compared with vitreous body. Nodular posterior scleritis shows mild enhancement in enhanced scan. Posterior scleritis may manifest as choroid folds and retinal banding.

14.1.4 [Key Points of Diagnosis]

1. Uveitis. It is common in young adults, clinically manifested as ocular pain, muscae volitantes, sore and swollen eye, and visual disturbance. Imaging findings include thickened eye ring and local nodular pattern, with mild to moderate enhancement.

2. Scleritis. Common in middle-aged women, clinically manifested as red, swollen orbit and pain in deep part of eye with visual impairment. Imaging findings show diffuse thickening of eyeball wall or nodular thickening of posterior wall, which may be accompanied by anterior optic nerve thickening and extraocular muscle thickening. Diagnosis can be made according to mild to moderate enhancement.

14.1.5 [Differential Diagnosis]

1. Retinal pigment degeneration. Similar to old posterior uveitis, it is characterized by night blindness, abnormal electroretinogram, or absence of wave.

2. Choroidal melanoma. Common in the middle-aged and elderly. Most of the patients suffer from unilateral onset and visual impairment, without ocular pain. Typically, the lesion protrudes toward vitreous body in a mushroom shape. When compared with vitreous body, the tumor shows hyperintense on T_1WI, and hypointense on T_2WI. In an enhanced scan, the tumor shows moderate to marked enhancement, yet the surrounding effusion shows no enhancement.

3. Choroidal metastatic tumor. It is manifested as thickening of choroid and sclera, but rarely causes pain or inflammation. Primary malignant lesion is quite common.

4. Retinal detachment. Exudative cases suffer from sudden vision loss and visual field defects, without eye pain or sclera thickening. Rhegmatogenous cases suffer from retinal detachment first and then uveitis.

5. Nodular scleral thickening. It causes severe pain, wherein the color of mass is similar to that of adjacent normal retina pigment epithelium, with chessboard pattern of choroid as normal.

14.1.6 [Status Quo and Progress of Research]

CT and MRI are rarely used for uveitis and scleritis, with main findings including thickening of eye ring. DWI shows remarkable hyperintense in case of any pyogenic infection abscess formed. CT and MRI stand out for the visual display of extraocular changes, such as changes in other orbital structures and optic nerve.

The diagnosis of uveitis and scleritis mainly relies on clinical manifestations, such as ocular pain and inflammation symptoms. In addition, ophthalmological examinations, including optical coherence tomography (OCT), have already become important tools for detecting posterior segment diseases. These tools cannot only diagnose infectious or noninfectious uveitis but also follow up the disease course and monitor therapeutic effect.

14.2 Vitreous Abscess

14.2.1 [Overview]

Vitreous abscess, an infectious disease that can cause grave damage in eyeball structure and vision, is often manifested as the involvement of eyeball in addition to sclera. It is often caused by trauma or pyogenic infection in other body parts. Aseptic or noninfectious vitreous abscess is often caused by residue of intraocular lens substance and toxic drugs. It is characterized by acute onset, rapid progress, poor curative effect, and serious consequences. The disease has no obvious gender difference and is common in children and elder population, with unilateral or bilateral onset. The common clinical manifestations include redness and swelling of eyeball, orbit pain, sharp loss of vision or blindness. Specialty examination indicates conjunctival congestion in affected eyeball, weakened or absent response of pupil to light, shallow or absent anterior chamber of eye.

14.2.2 [Pathology Findings]

In acute phase, a large number of neutrophils, lymphocytes, and monocytes/macrophages appear in vitreous body, wherein abscess is distributed throughout entire vitreous body in a diffuse or multilocular manner. In chronic phase, it can be seen that proliferated fibrous tissue grows into vitreous body, resulting in vitreous body contraction, retinal and choroidal detachment, and even atrophy of eyeball.

14.2.3 [Imaging Findings]

1. CT examination. It can detect any foreign object in eye and combined infection occurred. In acute phase of abscess, eyeball grows bigger slightly, and vitreous body shows a higher density in the non-enhanced scan, equivalent to that of eye ring. Single or multiple low-density areas can be observed in abscess with round or elliptical changes and unclear borders. After enhanced scan, circular or petaloid enhancement pattern and soft tissue structures peripheral to eyeball can be observed, with some lesions accompanied by eyelid swelling. In chronic phase, eyeball grows smaller, eye ring is thickened obviously, while the lesion is typically manifested as low density and subject to mild enhancement after enhanced scan.

2. MRI examination. It is rarely applied, yet can be used for cases with orbital infection and involved cavernous sinus as required. Compared with normal vitreous body, it shows isointense or hyperintenseon T_1WI in non-enhanced scan and hyperintense on T_2WI and DWI, with ring enhancement after enhanced scan. Fluid attenuated inversion recovery (FLAIR) sequence can better show the T_2WI hyperintense of vitreous body. When inflammation involves orbit, orbital fat may be manifested as a cord-like soft tissue signal shadow. Uvea involvement can be better shown on T_1WI.

14.2.4 [Key Points of Diagnosis]

1. CT shows increased density in vitreous body and low-density areas therein; MRI shows increased signal on T_1WI and T_2WI; After enhancement, the abscess wall is remarkably enhanced, showing ring or petaloid enhancement; Eye ring is often thickened.
2. It is common in children and the elderly who may have a history of trauma or infection at other sites.
3. Clinical manifestations include sudden swelling, redness and pain of eyeball, sharp loss of vision, and even blindness.

14.2.5 [Differential Diagnosis]

1. Persistent hyperplasia of vitreous body. It is more common in infants and children. CT or MRI shows a cord or strip of soft tissue shadow spanning from posterior border of lens to optic disc, accompanied by mild enhancement and microphthalmia deformity.

2. Retinoblastoma. Ninety percent (90%) cases occur in children below 3 years old, and CT or MRI shows intravitreal irregular soft tissue mass that originates from eye ring, mostly accompanied by patchy calcification, with marked enhancement after enhanced scan. The lesion can occur bilaterally, and result in trilateral retinoblastoma if intracranial region is involved at the same time.

3. Vitreous traumatic bleeding. As for explicit trauma history, CT or MTI displays irregular patchy lesion in vitreous body. The lesion shows high density on CT, heterogeneous signal on MRI T_1WI and hyperintense on T_2WI, with undefined border and site. Other traumatic changes in orbit can also be shown, such as hematoma and fracture.

14.2.6 [Status Quo and Progress of Research]

DWI can clearly display purulent abscess, showing obvious hyperintense, with lowered ADC. As vomica is filled with viscous liquid containing bacteria, inflammatory cells, mucin, and fragments of cell tissue, these components, as well as the combination of water and macromolecules, limit the diffusion of water molecules, so the ADC value is remarkably lowered [6].

14.3 Choroidal Granuloma

14.3.1 [Overview]

Choroidal granuloma inflammations with various causes are collectively called choroidal granuloma, including tuberculous ophthalmia, nodular ophthalmia, uveoencephalitis, sympathetic ophthalmia, and choroidal granuloma inflammations caused by fungus, virus, and parasite [6]. Tuberculous granulomas mostly occur in young adults. Sarcoid granuloma is more common in adults aged 30 to 60. Koyanagi-Harada syndrome mostly occurs in yellow race, most frequently among people aged 20 to 40. Sympathetic ophthalmia often involves ocular trauma and intraocular surgery.

Progressive vision loss and ocular pain are common symptoms. Choroidal nodular lesions often occur at the posterior pole unilaterally or bilaterally. Intraocular fluid microscopy of tuberculous granuloma shows mycobacterium tuberculosis, increased serum levels immunoglobulins of sarcoidosis granuloma and positive Kveim test result. According to fundus fluorescein angiography, nodule shows hypofluorescence in an early stage and hyperfluorescence in the advanced stage.

14.3.2 [Pathology Findings]

The pathological changes caused by choroidal granuloma vary greatly by etiology, which is common in tuberculosis and sarcoidosis. Nodules are usually less than 2 mm in diameter. Tuberculous choroidal granuloma is manifested as single or multiple miliary yellow-white nodules at the posterior pole of fundus, few of which can form large lumps; Microscope findings show granulomas composed of a large number of macrophages, epithelial cells, and lymphocytes, multinucleated giant cells can also be observed sometimes. The central area is dominated by caseous necrosis. Tubercle bacilli in the necrotic area can be seen by acid-fast staining. Sarcoid choroidal granulomas are characterized by yellow-white or gray-white exudation peripheral to blood vessels at the posterior pole. The exudation is shaped like wax drops or yellow nodular lumps; Microscopy findings are similar to tubercle, yet there is no caseous necrosis in the nodules.

14.3.3 [Imaging Findings]

The imaging findings of choroidal granuloma are single or multiple nodules in choroid, wherein large nodules are mass-shaped with clear border, or diffuse, miliary nodules, with blurred border.

1. CT examination. Eye ring is thickened and homogeneous in density, showing isodense as extraocular muscle. Large nodules protrude into the eyeball. Tuberculous nodules may show heterogeneous density, and a small number of lesions have calcification. Mild to moderate enhancement is shown in the enhanced scan.

2. MRI examination. It is recommended to use surface coils for collection. High-resolution surface coils can display lesions with a diameter above 2 mm. MRI findings show small or medium-sized elevated lesions. Compared with vitreous body, the lesion shows slightly hyperintense on T_1WI and hypointense or isointense to hyperintense heterogeneous signals on T_2WI. Tectorial membrane adjacent to eyeball is thickened and soft tissue shadows can be seen in Tenon capsules space. Mild to moderate homogeneous or heterogeneous enhancement is shown in the enhanced scan. A small number of cases show changes related to retinal detachment.

14.3.4 [Key Points of Diagnosis]

1. CT and MRI show thickening of eye ring and single or multiple nodules in choroid, which can also be fused into masses. The lesion shows mild to moderate enhancement after the enhanced scan.
2. Among young adults, the disease results in slow progressive vision loss and pain in eyes.
3. Systemic diseases such as tuberculosis and sarcoidosis can occur at the same time.

14.3.5 [Differential Diagnosis]

1. Choroidal hemangioma. Non-enhanced CT scan is of little significance in the diagnosis of choroidal hemangioma, which shows marked enhancement after the enhanced scan. MRI is better than CT in diagnosis, wherein the lesion shows hyperintense on T_1WI and hypointense on T_2WI when compared with vitreous body. Beyond that, the lesion shows marked enhancement in enhanced scan, typically complicated by retinal detachment.

2. Choroidal melanoma. Owing to the paramagnetism of melanin, the tumor shows hyperintense on T_1WI, hypointense or heterogeneous on T_2WI, and moderate to marked enhancement in enhanced scan.

3. Choroidal metastatic tumor. Eyeball wall has local thickening or nodular bump, which shows marked enhancement after enhanced scan. In addition, the patient has a history of primary tumors in other parts of the body.

14.3.6 [Status Quo and Progress of Research]

CT and MRI show thickening of eye ring and single or multiple nodules in choroid, which can also be fused into masses. The lesion shows mild to moderate enhancement after enhanced scan. MRI high-resolution coil and scanning method can show 2 mm small choroidal nodules.

14.4 Ocular Tendonitis

14.4.1 [Overview]

Ocular tendonitis refers to an acute inflammation of fascia peripheral to eyeball. It is relatively rare in clinical, with an unknown cause. It is generally believed that the disease arises from vasogenic edema caused by an allergy. Usually, the disease is divided into serous and suppurative ocular tendonitis. Serous ocular tendonitis typically involves bilaterally, with common symptoms of conjunctiva edema of eyeballs, characterized by a sudden onset and rapid progression. The disease is usually related to autoimmune disease, complicated by systemic immune diseases, and is easy to relapse. Suppurative ocular tendonitis typically is unilateral, whose symptoms are more severe than serous ocular tendonitis, characterized by sharp, severe pain or tenderness on unilateral eye, swelling of eyelid, chemosis as well as limitation of eye movement. It usually arising from the spread of suppurative inflammation in adjacent structures, trauma or iatrogenic infection. Visual acuity and fundus are generally not involved, yet patient may experience double vision. Therapeutic schedule includes hot compress, eyeball fixation, oral administration or local injection of steroid hormone and oral administration of sodium salicylate at a high dose. Suppurative cases require systemic antibiotics application for anti-inflammation. In case of any abscess formed, abscess incision drainage is required. Without timely and effective treatment, orbital abscess or ophthalmitis may appear, accompanied by serious complications, resulting in vision loss.

14.4.2 [Pathology Findings]

Basic pathological changes include bulbar conjunctiva hyperemia and subconjunctival yellow pus. Eyeball may attach to fascia after the inflammation fades away.

14.4.3 [Imaging Findings]

1. CT examination. Eye ring is locally thickened with coarse borders, and its density is similar to that of the adjacent eyeball wall. Some cases may be accompanied by thickening of extraocular muscle and enlargement of Tenon's capsule. Marked enhancement or ring enhancement is shown after enhanced scan.

2. MRI examination. Eye ring is locally thickened, with slightly hypointense on T_1WI, and slightly hyperintense on T_2WI, which is markedly enhanced after enhancement. It can be manifested as a "T"-shaped hyperintense shadow in retrobulbar fascial space, suggesting Tenon's capsule edema effusion.

14.4.4 [Key Points of Diagnosis]

1. Sudden onset, bulbar conjunctiva edema, proptosis, and movement limitation, with specific infection history.
2. Laboratory test shows increased leukocyte count and erythrocyte sedimentation rate.
3. Imaging findings show local thickening and marked enhancement of eye ring.

14.4.5 [Differential Diagnosis]

1. Intraorbital cellulitis. Monocular onset is common, with obvious local symptoms, typically accompanied by high fever, failure, and other systemic symptoms.

2. Eyeball lymphoma. It typically involves conjunctiva or preorbital area while forms conjunctiva edema and painless pink, fish meat-like lump in subconjunctival region. MRI findings are characteristic. The lesion shows isointense or slightly hypointense on T1WI and T2WI, and hyperintense on DWI. It can be moderately enhaced after enhancement.

3. Uveitis. Common in young adults, with imaging findings manifested as thickened eye ring and local nodular pattern, with mild to moderate enhancement. Scleritis is common in middle-aged females. Imaging findings show diffuse thickening of eyeball wall or nodular thickening of posterior wall, which may be accompanied by anterior optic nerve thickening and extraocular muscle thickening. Diagnosis can be made according to mild to moderate enhancement.

14.4.6 [Status Quo and Progress of Research]

The disease is rare, with unknown cause. CT only displays thickened eye ring, coarseness, and other inflammations, with enlarged tenon's capsule and annular enhancement in enhanced scan. MRI can better show inflammation and effusion than CT. Pyogenic infection shows marked hyperintense on DWI.

References

1. Li Z, Wang LL, Mei J, et al. Ophthalmic imaging features of posterior scleritis. Int Eye Sci. 2014;14(7):1331–3.
2. Junfang X, Dapeng S, Xiaofeng T. Imaging of the head and neck ophthalmology. Beijing: People's Medical Publishing House; 2014.
3. Ambika S, Veena N, Padmaja MS. Atlas of imaging in ophthalmology (first deition). New Delhi: Jaypee Brothers Medical Publishers; 2014.
4. Diogo MC, Jager MJ, Ferreira TA. CT and MR imaging in the diagnosis of scleritis. AJNR Am J Neuroradiol. 2016;37(12):2334–9.
5. Li CQ, Cho AA, Edward NJ, et al. Magnetic resonance imaging of uveitis. Neuroradiology. 2015;57(8):825–32.
6. Ishihara M, Shibuya E, Tanaka S, et al. Diagnostic and therapeutic evaluation of multiple choroidal granulomas in a patient with confirmed sarcoidosis using enhanced depth imaging optical coherence tomography. Int Ophthalmol. 2018;38(6):2603–8.

Orbital Lesions

15

Shaowei Zheng, Lijun Wang, and Zuohua Tang

15.1 Orbital Inflammation

15.1.1 Intraorbital Cellulitis and Periorbital Abscess

15.1.1.1 [Overview]

Intraorbital cellulitis is an acute inflammation of intraorbital soft tissue caused by bacterial infection. It is most common in children and is a chief culprit for proptosis among them. Two in three cases are secondary to rhinosinusitis, and around 25% of orbital infections occur in the wake of trauma. Besides, orbit is involved in 8%–10% of cases involve due to skin infection. Among adults, intraorbital cellulitis is mainly caused by acute and chronic dacryocystitis. The site of lesion is crucial. Preseptal infection rarely affects orbital function, whereas postseptal infection can undermine optic nerve and eye movement. Intraorbital cellulitis can be roughly divided into the following five types by its development phase: 1. Inflammatory edema; 2. Subperiosteal cellulitis and abscess; 3. Intraorbital cellulitis; 4. Orbital abscess; 5. Thrombosis in ocular vein and cavernous sinus. It is difficult to strictly differentiate each phase due to the overlapped symptoms. Both preseptal and postseptal cellulitis may be manifested as swelling of periorbital soft tissue and chemosis, but impaired vision and ophthalmoplegia are often a measure of postseptal cellulitis. Retarded or even absent light reflex may occur after irreversible injury of optic nerve. Therefore, as for children who cannot perform visual examination, light reflex of pupil can only serve as one of the criteria to judge visual acuity impairment. Without timely treatment, the infection can lead to superior ophthalmic vein thrombophlebitis and orbital abscess. The presence of somnolence and related neurological symptoms often prompts that the disease has already involved brain. Severe intracranial complications, such as cavernous sinus thrombophlebitis, meningitis, or brain abscess, occurred can be life-threatening, to which high attention must be paid.

Chief complaints include that periorbital tissues are remarkably red, swollen, hot, and painful, which may be accompanied by fever, anorexia, dysphoria, weakness, and other systemic symptoms. Eye examination can reveal extensive swelling of soft tissue, including redness, swelling, heat and pain of eyelid, congestion and edema in bulbar conjunctiva, proptosis, disorder of ocular movement or visual loss (Fig. 15.1).

15.1.1.2 [Pathology Findings]

The main pathological findings are inflammatory cell infiltration in the lesion area. When combined with abscess, cystic cavity is necrotic tissue, and cyst wall is new granulation tissue.

15.1.1.3 [Imaging Findings]

1. CT Examination. CT findings vary by different stages of intraorbital cellulitis. In an early stage of inflammation, eyelid soft tissue is thickened with a higher density. Preseptal soft tissue is swollen, with blurred boundary, and the intraorbital structure is normal. As the disease progresses, the lesion can involve area lateral to intraocular muscles, often accompanied by thickened extraocular muscle with blurred border. Besides, the retrobulbar fat density is slightly increased, with more spots and cord shadows therein. Afterwards, orbital structural interface becomes blurred, and density of intraorbital soft tissue increases diffusely, complicated by proptosis, thickening of optic nerve and coarse border. Lesions in periorbital structures can also be shown in scanning, which helps identify the source of infection (Fig. 15.2). CT can show changes in bone structures (Fig. 15.3). The absence of lamina papyracea portion at medial wall can be seen in some cases. Congenital absence or thinning of lamina papyracea at medial wall can result in intraorbital inflammation, while

S. Zheng · L. Wang (✉)
The First Hospital of Dalian Medical University, Dalian, China

Z. Tang
Eye and ENT Hospital of Fudan University, Shanghai, China

H. Li et al. (eds.), *Radiology of Infectious and Inflammatory Diseases - Volume 2*,
https://doi.org/10.1007/978-981-16-8841-6_15

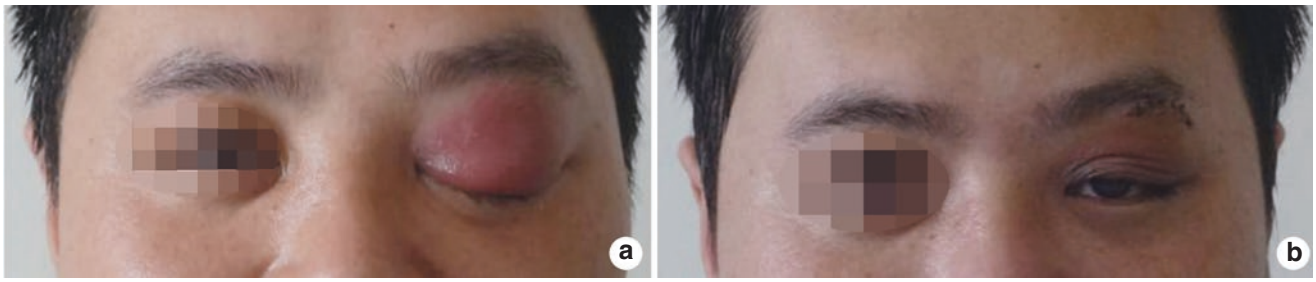

Fig. 15.1 Left intraorbital cellulitis and periorbital abscess. A 50-year-old male patient. (**a**) Left eyelid swelling (**b**) Eyelid swelling is significantly relieved after incision and drainage

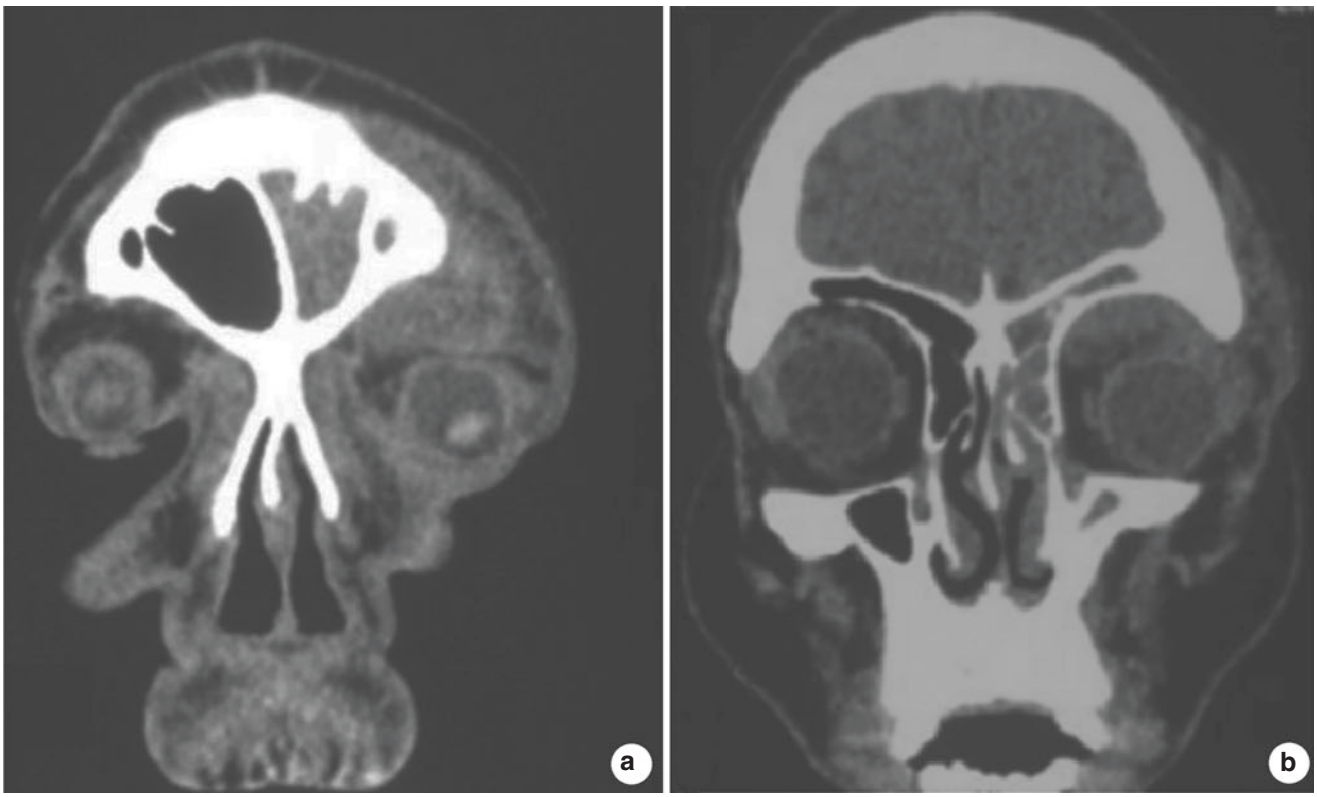

Fig. 15.2 Left intraorbital cellulitis and periorbital abscess. A 50-year-old male patient (the same patient as Fig. 15.1) (**a** and **b**). CT at coronal plane shows swollen subcutaneous soft tissue on the left side of face, with blurred boundary; Soft tissue in left supraorbital region is obviously swollen. A low-density shadow can be seen therein, suggesting abscess formation

inflammation of ethmoid sinus can also affect osseous erosion, giving rise to the absence of orbital wall lamina papyracea. When the lesion spreads into intracranial area, it may cause subdural abscess or meningitis. In such case, enhanced scan or MRI examination is required for diagnosis. Enhanced scan can reveal ring enhancement of abscess wall. Most cases are subperiosteal abscess of orbit, which may be complicated by preseptal or intraorbital abscess; Enhanced scan also shows thickening of meninges.

2. MRI Examination. MRI scan can clearly show structures and lesions medial and lateral to orbit. The common diffuse inflammation is mainly manifested as blurred subcutaneous fat or postorbital fat space, showing diffusely hyperintense on T_2WI with fat suppression sequences and is enhanced on MRI T_1WI with fat suppression sequences. In an early stage of inflammation, lesions are limited to orbital peripheral space, most of which are located at medial orbit, adjacent to paranasal sinus. When compared with extraocular muscle, the lesion shows isointense on T_1WI and hyperintense on T_2WI, with blurred, irregular borders, typically accompanied by rhinosinusitis at adjacent side. Diffuse cellulitis can result in blurred intraorbital structures and proptosis of varying degrees. According to T1WI fat suppression enhanced scan, intraorbital inflammatory tissue is enhanced diffusely. Abscess formed is manifested as a mass shadow of soft tissue with blurred borders in orbital fats. The abscess

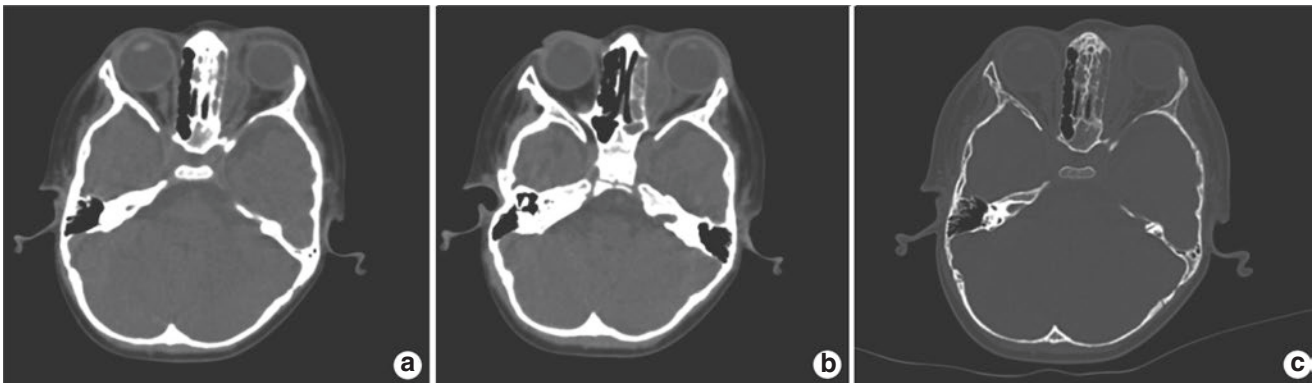

Fig. 15.3 Left intraorbital inflammation, subperiosteal abscess. A 24-year-old male patient. The left eye was red, swollen and painful for 1 week and worsened for 3 days. (**a** and **b**) CT soft tissue window shows peripheral space soft tissue shadow at left orbit. The lesion is closely related to the left ethmoid sinus, in which soft tissue can be also seen. Left medial rectus moves inward by compression, and left soft tissue in left dacryocyst area is swollen; (**c**) Bone window shows thinning of the left cribriform plate

shows hypointense on T_1WI and hyperintense on T_2WI because pus contains rich necrotic components. Owing to abundant fibrous tissues, abscess wall shows hypointense on T_1WI and isointense or slightly hypointense on T_2WI. According to enhanced scan, abscess wall shows marked enhancement, the central necrotic area is not enhanced, and the inner and outer abscess walls are relatively smooth. In case of optic nerve involved, the optic nerve can be thickened with coarse border. The lesion shows elevated signal on fat suppression T_1WI. After enhanced scan, optic nerve border is enhanced in a sheath-like manner on fat suppression T_1WI. MRI also reveals the thickened eyeball wall and elevated fat suppression T_2WI signal at intraocular area and eyeball wall. Cellulitis can also cause cavernous sinus thrombosis and supraorbital vein thrombophlebitis. Compared with the contralateral side, intraorbital fat of the affected side shows hypointense on T_1WI and hyperintense on T_2WI. Magnetic resonance shows dilated cavernous sinus, thickened supraorbital vein, and formation of subdural abscess or cerebral infarction. The abscess, with limited internal diffusion, shows hyperintense on DWI sequence.

15.1.1.4 [Key Points of Diagnosis]

1. The disease is common in children, with acute onset, characterized in that eyelid is swollen and painful with erythema in an early stage, and intraorbital area is involved, thus causing proptosis as well as ophthalmoplegia.
2. Lesions are mostly located at medial orbit and adjacent to paranasal sinus. CT and MRI show blurred, irregular border of lesion, which can make orbital structures blurred in severe cases; Through enhanced scan, intraorbital inflammatory tissues show diffuse enhancement, most of which are heterogeneous, with limited abscess diffusion, smooth wall and ring enhancement.

15.1.1.5 [Differential Diagnosis]

1. Orbital Tumor. Intraorbital cellulitis needs to be differentiated from tumors that develop rapidly in orbit. For example, rhabdomyosarcoma also features with acute onset, accompanied by redness, swelling, heat, pain, and other symptoms of inflammatory lesions. Based on image findings, rhabdomyosarcoma involves limited range, with homogeneous density and signal, mostly accompanied by bone destruction of orbital wall.

2. Subperiosteal Lesion. Subperiosteal abscess of orbit needs to be distinguished from other subperiosteal lesions, such as dermoid cyst, and subperiosteal hematoma. Epidermoid cyst or dermoid cyst are congenital lesions, mostly adjacent to sutura. CT shows homogeneous or heterogeneous fat density, with osseous changes in orbital wall caused by compression. The lesion is usually not difficult to distinguish. Subperiosteal hematoma is usually accompanied by orbital wall fracture, rupture of eyeball and other eye traumas.

3. Inflammatory Pseudotumor. Cellulitis needs to be distinguished from inflammatory pseudotumor. Inflammatory pseudotumor is a nonspecific inflammation of intraorbital soft tissue with unknown origin. In most cases, the lesion is similar to tumor, mainly located in inner & outer spaces of muscle cone. The lesion is typically accompanied by thickening of eye ring and ocular muscle. By contrast, cellulitis shows diffuse lesion, with more severe clinical symptoms.

4. Ocular Changes Caused by Cavernous Sinus and Fistula. Intraorbital cellulitis needs to be differentiated from ocular changes caused by cavernous sinus and fistula. The latter occurs in the wake of craniofacial trauma, which may also feature with proptosis, conjunctival edema and thickened extraocular muscle. As for cavernous sinus and fistula, however, proptosis is mostly pulsatile, accompanied by typical symptoms of intracranial murmur. Besides, intracranial hemorrhage and ischemia and subarachnoid space hemorrhage can be found in craniocerebral CT examination.

15.1.1.6 [Status Quo and Progress of Research]

Diagnosis for intraorbital cellulitis and orbital abscess relies mainly on clinical findings. Imaging findings aim to assess the extent of lesion and the presence of abscess formed. CT examination is essential for detecting small subperiosteal abscesses at the upper and lower orbital walls. Besides, it can also clearly show the relationship between the lesion and bone structure and whether it is accompanied by osteomyelitis. MRI examination can identify the extent of intraorbital cellulitis in an early stage, while assess whether optic nerve is involved or presence of thrombosis in cavernous sinus area. DWI can clearly show the presence of abscesses, and it has been a routine examination for orbital inflammatory diseases [1–3].

15.1.2 Idiopathic Orbital Inflammatory pseudotumor

15.1.2.1 [Overview]

Inflammatory pseudotumor, also known as idiopathic orbital inflammatory pseudotumor, is a nonspecific granuloma with unknown cause. It is called inflammatory pseudotumor as its clinical symptoms and signs are similar to tumors, manifested as chronic inflammatory cell infiltration under microscope. Currently, the disease is deemed as relevant to autoimmune response, rhinosinusitis and virus infection. The disease occurs regardless of age, but is more common in adults, with incidence significantly higher in males than females. Most patients suffer from the acute monocular onset with fast progression. The prognosis is poor in some cases. As for adults, the presence of bilateral lesions often suggests systemic vasculitis or systemic dysplasia of lymphoid tissue. Children account for 6% to 16% of patients with inflammatory pseudotumor. About one in three child patients suffer from bilateral involvement, which is rarely related to systemic diseases. The disease ranks the 3rd in orbital lesions, accounting for 7.1%, second only to thyroid-associated ophthalmopathy and lymphoproliferative diseases. The lesion can invade a variety of intraorbital structures, but typically focuses on certain tissues, including eyeball, extraocular muscle, optic nerve, and fat. It constitutes one of the most common causes of unilateral proptosis [4].

15.1.2.2 [Pathology Findings]

The most basic pathological changes of inflammatory pseudotumor are pleomorphic inflammatory cell infiltration, lymphocyte maturation and fibrovascular proliferation. It can be divided into lymphocytic infiltration, fibrous hyperplasia and mixed types based on components of cells.

1. Lymphocytic Infiltration Type. The most common type, typically occurring in orbital fiber adipose tissue and lacrimal gland, manifested as fragile off-white mass, without capsule. Microscopic findings show contiguous lymphocytes that may form follicles, accompanied by plasma cells, eosinophils, neutrophils, and histiocytes. A small number of blood vessels and the proliferation of fibrous tissue can be seen in the lesion.

2. Fibrous Hyperplasia Type. Clinically known as sclerotic inflammatory pseudotumor, which can invade a variety of orbital tissues (including fibrous fat, extraocular muscle, optic nerve sheath, periosteum and tenon's capsule), thus forming sclerotic scar tissue. Microscopic findings show a large number of fibrous connective tissue hyperplasia and collagenization, in which a few chronic inflammatory cells are scattered or a few lymphocytes are around contiguous collagen fibers.

3. Mixed Type. Mainly manifested as chronic inflammatory granuloma. There are abundant lymphocyte infiltrations in the hyperplastic microvascular tissues, while epithelioid cells, plasma cells and eosinophil can also be observed. The lesion can involve single structures in orbital cavity, such as eyelid, extraocular muscle, tenon's capsule and optic nerve sheath, or involve the entire orbit in a diffuse manner.

15.1.2.3 [Clinical Manifestation]

This disease may have acute, subacute or chronic onset and development. Common clinical manifestations are proptosis, ocular pain, disorder of ocular movement, orbital nodule or lump, visual impairment, optic disc edema or atrophy, and diplopia. Clinical manifestations vary by sites involved, type of affected tissue and disease course. When pathogen passes through blood vessels (especially main artery and arteriole), it causes thrombosis and ischemia, infarction and necrosis of adjacent tissues.

15.1.2.4 [Imaging Findings]

1. CT Examination. CT findings vary by different structures involved by the lesion. Generally, the lesion exhibits the same density as soft tissue and can be enhanced to varying degrees after enhancement. Lesion mainly manifested as hyperplastic mass may occur in any part of orbit, typically showing irregular soft tissue mass shadows, with clear border. The adjacent extraocular muscle is displaced due to compression, with indefinite border. Lesion involving the lacrimal gland is typically manifested as lacrimal gland enlargement, wherein both orbit and eyelid can be involved in most cases. There is no specific focal mass, lesion density is homogeneous, and adjacent fat space is blurred, which

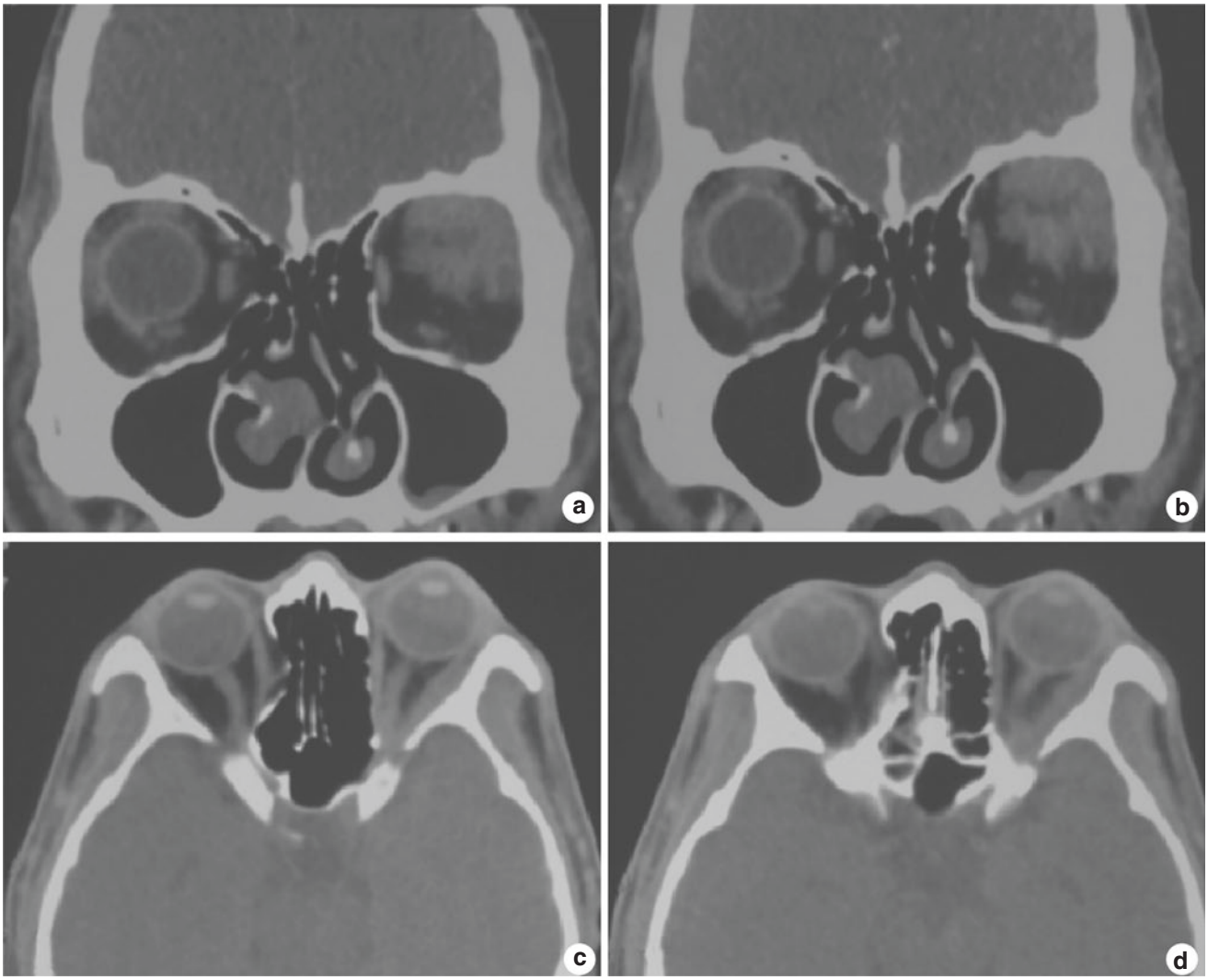

Fig. 15.4 Inflammatory pseudotumor at left lacrimal gland. A 48-year-old male patient. Inflammatory pseudotumor of left lacrimal gland, before and after treatment (**a**) Non-enhanced CT scan of orbit at coronal plane shows enlargement of left lacrimal gland and blurred boundary between lesion and lateral rectus or superior rectus; (**b**) The lesion is moderately enhanced after enhanced scan; (**c** and **d**) CT at transverse plane shows that left lacrimal gland is significantly reduced after steroid pulse therapy. It suggests that the disease is remarkably relived

may occur grid-shaped changes spreading to peripheral structures. A thickened eyelid can also be observed (Figs. 15.4 and 15.5). Lesion involving extraocular muscle is manifested as diffuse thickening of one or multiple extraocular muscles, with coarse borders and thickened involvement at entheses of tendon in most cases. Lesion involving tenon's capsule is manifested as thickened eyeball wall, coarse border, and blurred adjacent fat space, which can be enhanced after enhancement. Lesion involving optic nerve sheath is manifested as diffuse thickening of optic nerve, with coarse border. After enhancement, ring enhancement can be achieved at border of optic nerve. Diffuse inflammation is manifested as retrobulbar diffuse soft tissue density, with blurred boundary between the rest of the structures, absence of low density of adipose body of orbit, thickened optic nerve, and blurred borders. Lesions may involve extraocular structure through orbital pore and canal, while the orbital wall bone is typically not involved.

2. MRI Examination. It clearly shows the morphology and involvement scope of the lesion, while judges the pathological types according to the different signals. As for cases characterized by lymphocytes infiltration, the lesion shows hypointense on T_1WI and isointense on T_2WI; As for cases characterized by fibroplasia, the lesion shows hypointense

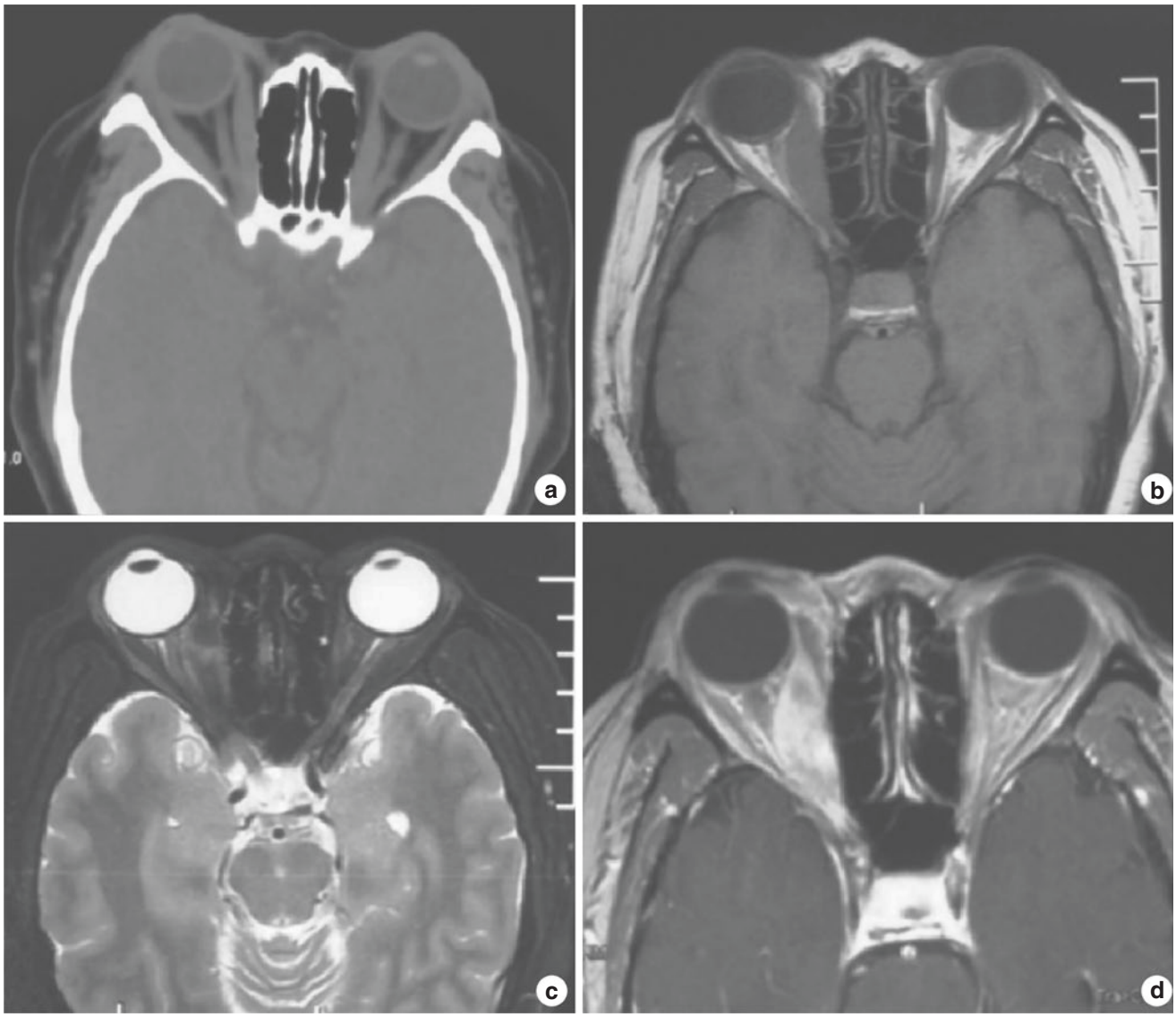

Fig. 15.5 Inflammatory pseudotumor at bilateral extraocular muscles, more severe on the right side. A 68-year-old female patient. The patient suffered from bilateral orbital pain for half a year, accompanied by lacrimation. Anti-inflammatory treatment was ineffective. (**a**) Orbital CT at transverse plane shows thickening of left medial rectus, right medial rectus and lateral rectus. The lesion involved both tendons and muscle belly. (**b**) Thickened right medial rectus shows isointense on T_1WI; (**c**) Lesion shows heterogeneously hypointense on T_2WI; (**d**) Enhanced MRI shows marked enhancement of right medial rectus

on both T1WI and T2WI; Enhancement of varying degree can be shown in enhanced scan (Figs. 15.6 and 15.7).

15.1.2.5 [Key Points of Diagnosis]

1. CT and MRI examination can show abnormal changes in single or multiple intraorbital structures, including enlargement of lacrimal gland and involvement of eyelid and orbit; Extraocular muscle and tendon entheses are thickened. Tenon's capsule is thickened, with coarse borders. Border is enhanced after enhanced scan.
2. Density and signal of intraorbital region are diffuse and abnormal, with blurred borders among structures. Bone of orbital wall is not involved notably.
3. Hormone therapy is effective.

15.1.2.6 [Differential Diagnosis]

1. Lymphoma. Inflammatory pseudotumor mainly characterized by lymphocyte infiltration can hardly be distinguished from lymphoma. As for lymphoma mainly characterized by fibroplasia, the lesion shows slightly hypointense on T_2WI, which is different from lymphoma signal. Lump formed by inflammatory pseudotumor may be located inside or outside muscle cone or involve both. Lymphoma is common in middle aged and elderly people, mostly in the lacrimal gland area and peribulbar tenon's capsule. Lymphoma, in particular, mostly arises from lymphoid tissue of preseptal space. There is no lymphoid tissue in postseptal area, so simple postseptal lymphoma is rare.

2. Graves Ophthalmopathy. Thickening of ocular muscles usually does not involve tendons, borders of extraocular muscle are smooth, and surrounding fat spaces exist.

3. Intraorbital Cellulitis. Common in children, the lesion is mostly located medial to orbit and adjacent to paranasal sinus; CT and MRI show blurred, irregular border of lesion, which can make orbital structures blurred in severe cases; Through enhanced scan, intraorbital inflammatory tissues show diffuse enhancement, most of which are heterogeneous, with limited abscess diffusion, smooth wall and ring enhancement.

4. IgG4 Related Disease. It is a chronic systemic disease closely related to IgG4, characterized by increased serum IgG4 levels and diffuse infiltration of IgG4-positive plasma cells in lacrimal glands, extraocular muscles, supraorbital nerves and other ocular appendages. CT shows diffuse thickening of the lacrimal gland and extraocular muscles, as well as thickening of supraorbital nerves. Glucocorticoid is effective.

5. Epithelial Tumors of Lacrimal Gland. Typical epithelial tumors of lacrimal gland often involve orbital part of lacrimal gland and appear as focal masses on images. Bone destruction and displacement of eyeball suggest high possibility of epithelial tumors.

6. Intraorbital Solid Tumor. Including cavernous hemangioma, optic nerve sheath meningioma, optic nerve sheath meningiomas, optic nerve glioma, orbital schwannoma and metastatic tumors. Solid tumors usually deliver a space-occupying effect, thus may result in changes in eyeball shape, bone destruction and extraocular involvement.

15.1.2.7 [Status Quo and Progress of Research]

MRI signal characteristics of lesion are crucial to judge pathological type of inflammatory pseudotumor and therapeutic effect. If the lesion shows hyperintense on T_2WI and marked enhancement after enhanced scan, it is mainly lymphocyte and granuloma. In such cases, hormonotherapy can deliver desirable curative effect. When the lesion shows hypointense on T2WI and mild to moderate enhancement after enhanced scan, the bulk of the lesion may be fiber composition. In such cases, hormonotherapy is not effective. When it comes to differentiation between orbital inflammatory pseudotumor and lymphoma, high ADC value indicates high possibility of idiopathic inflammatory pseudotumor [5].

15.1.3 Orbital Granuloma Caused by Mucor infection

15.1.3.1 [Overview]

Mucor is an opportunistic pathogen. Diabetic patients, especially those with compromised immune function, such as those with ketoacidosis, are especially vulnerable. Acute fungal infections caused by mucor are classified into rhino-orbito cerebral (also known as rhinocerebral) type, lung type, gastrointestinal type, skin type, and central type by the site of

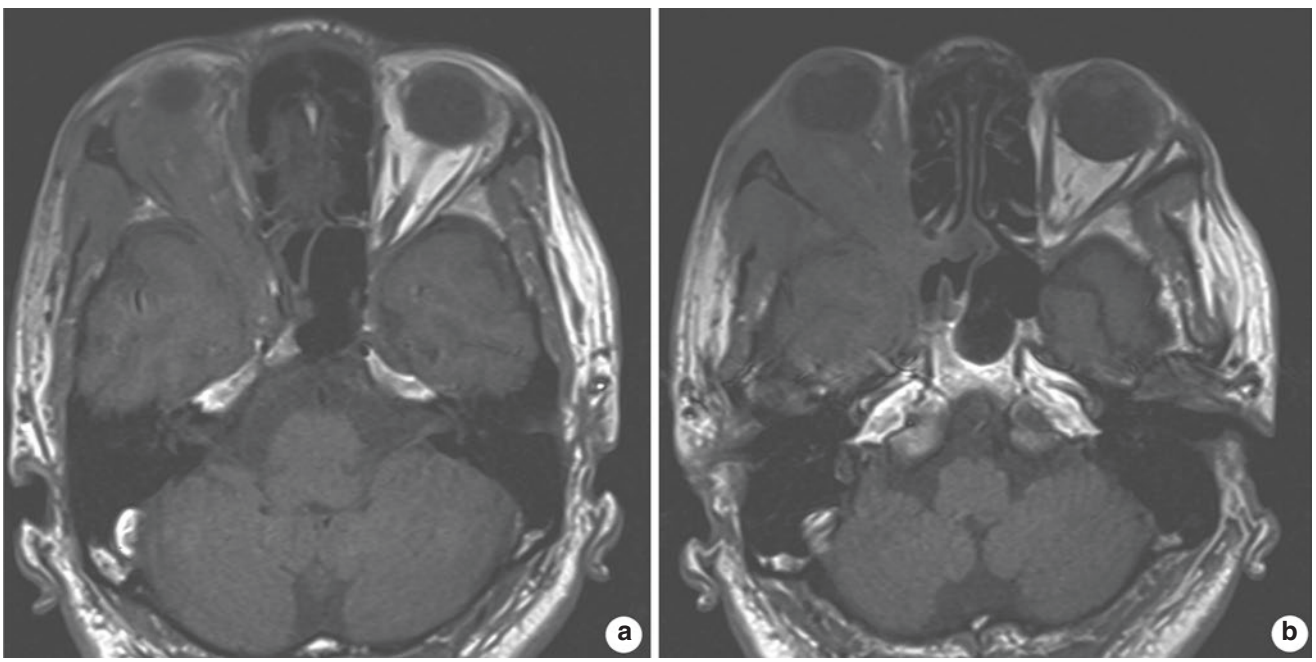

Fig. 15.6 Inflammatory pseudotumor at right orbit and lacrimal gland. A 44-year-old male patient. She suffered from right orbital pain and swelling with impaired vision. (**a** and **b**) MRI T_1WI shows that diffuse isointense T1 signal shadow is found at the right orbit, with blurred border of the lesion, the right eyeball is compressed and deformed, and the right lacrimal gland is involved. The lesion involved the right cavernous sinus along superior orbital fissure. (**c** and **d**) The lesion shows isointense on T_2WI (**e**). The lesion and subcutaneous soft tissues on the right side of the face show marked enhancement in enhanced scan

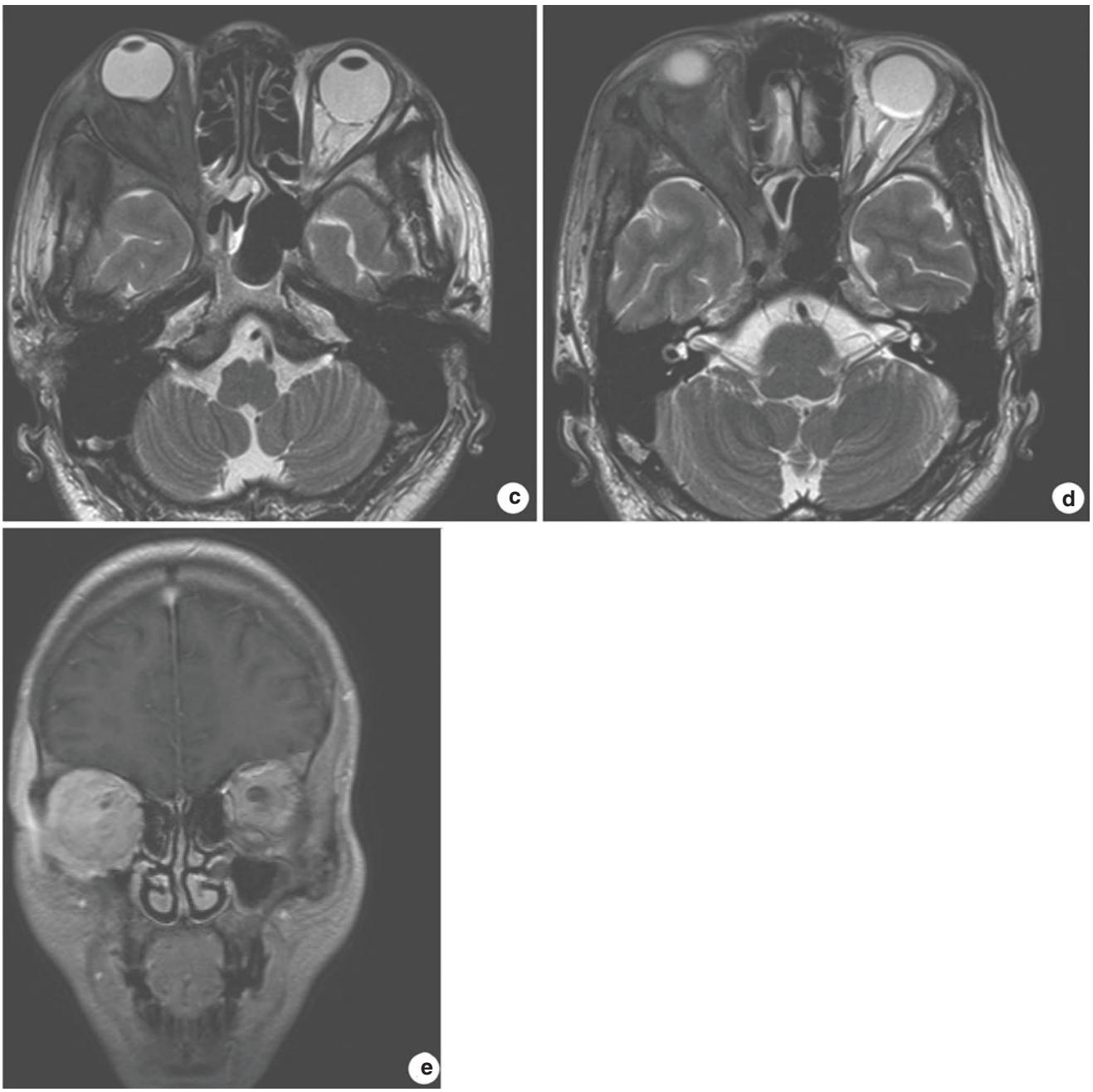

Fig. 15.6 (continued)

infection, among which rhino-orbito cerebral type is the most common one. Bacteria often invade from nostrils into paranasal sinus (most common in maxillary sinus and ethmoid sinus) and orbit along with nasal fluid. They can reach brain via blood vessels, thus causing severe meningitis, which is highly fatal.

15.1.3.2 [Clinical Manifestation]

Immunocompromised population are vulnerable to mucor infection. The disease, with acute onset, typically progresses rapidly. According to involved sites, symptoms include inflammatory reaction of nasal sinus, changes in eye, symptoms of central nervous system, and pain in orbit, head and

face, which may be accompanied by fever, and palpable, hard lump on head and face, with clear border and poor mobility. In the early stage, nonspecific nasal manifestations such as nasal obstruction and thick nasal mucus appear first. When bacteria infect orbit, symptoms including proptosis, ophthalmoplegia, corneal edema, swollen eyelid, ptosis, vision loss and even blindness occur. When ischemic necrosis caused by vascular thrombosis occurs at eyelid and periorbital skin, the skin shows black purple, accompanied by hemorrhagic effusion characterized by periorbital dark circles. The black pus at orbital vomica is of diagnostic significance. Laboratory test shows increased leukocyte and neutrophil counts.

15.1.3.3 [Pathology Findings]

The characteristic pathological changes caused by mucormycosis are infiltration, thrombosis and necrosis. After hematoxylin-eosin staining, nasal cavity, paranasal sinus mucosa biopsy or secretions from skin wounds show a large number of thick, right-angled branched and non-nodule fungal hyphae under microscope. Besides, fungal hyphae can also be found in granulomatous megakaryocyte, which is more obvious in specimen subject to special staining methods, such as periodic acid Schiff reaction (PAS), Warthin-Starry sliver staining and Grocott methenamine silver stain. MUC5B is negative. Histopathologic slice can show toxic hyphae in the blood vessel wall. When bacteria pass through blood vessels (especially main artery and arteriole), they cause thrombosis, ischemic infarction and necrosis at adjacent tissues. Patients who suffer from retinal artery occlusion caused by mucor thrombosis have segmental thrombus in their blood vessels, and this is different from other causes of intraorbital cellulitis.

15.1.3.4 [Imaging Findings]

Imaging findings in an early stage may deliver negative results, and CT examination is helpful in showing the extent of lesion involvement. Mucosa of paranasal sinus is thickened and soft tissue mass appears. Air-fluid level can be seen in paranasal sinus effusion cavity, and periorbital soft tissue is swollen. The disease progresses rapidly, wherein sinus wall and orbital bone destruction often occur in the wake of soft tissue necrosis (Fig. 15.8). Intraorbital granuloma is irregular in shape, with rough borders. Intraorbital mass,

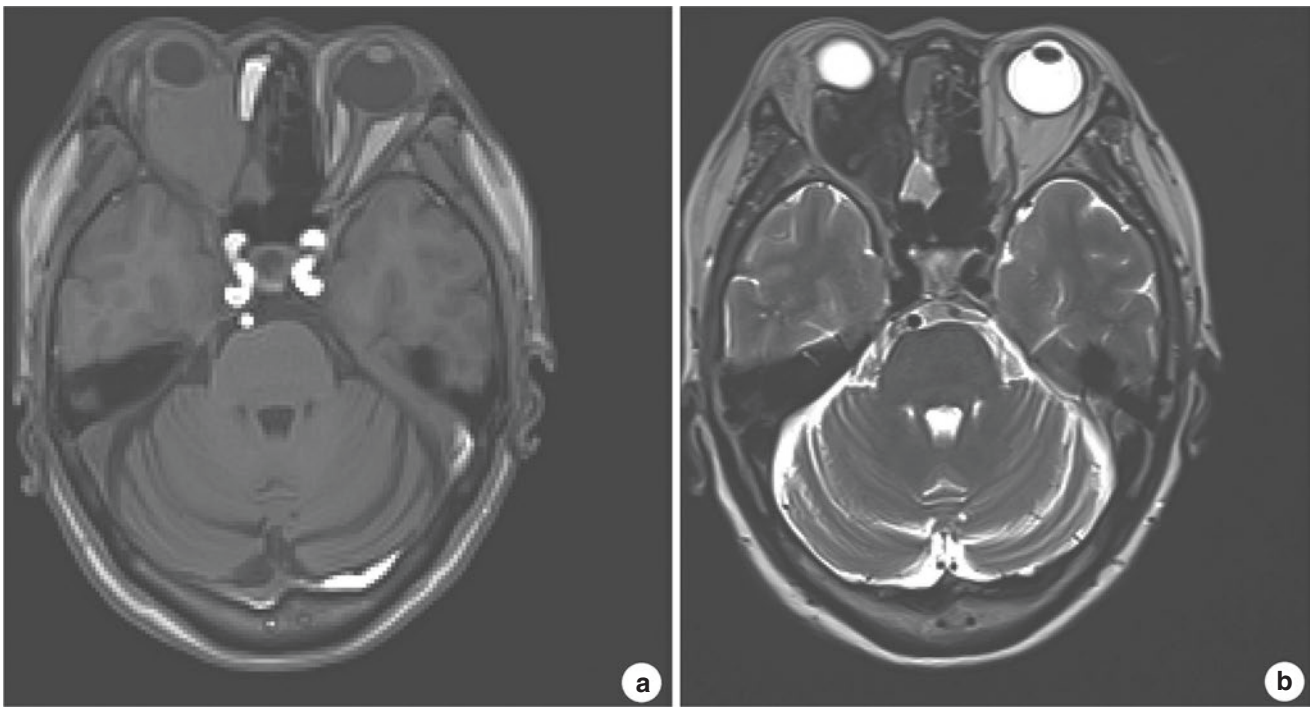

Fig. 15.7 Inflammatory pseudotumor at right orbit. A 50-year-old female patient. The right orbit is painful and swollen for half a year and worsened for 2 weeks. (**a**–**c**) According to MRI, there is a diffuse lesion at right orbit, which shows isointense on T_1WI and hypointense on T_2WI. Lesion boundary is not clear, and the right eyeball is compressed and deformed. (**d**) The lesion shows isointense on DWI. (**e** and **f**) Enhanced scan shows marked enhancement of the lesion

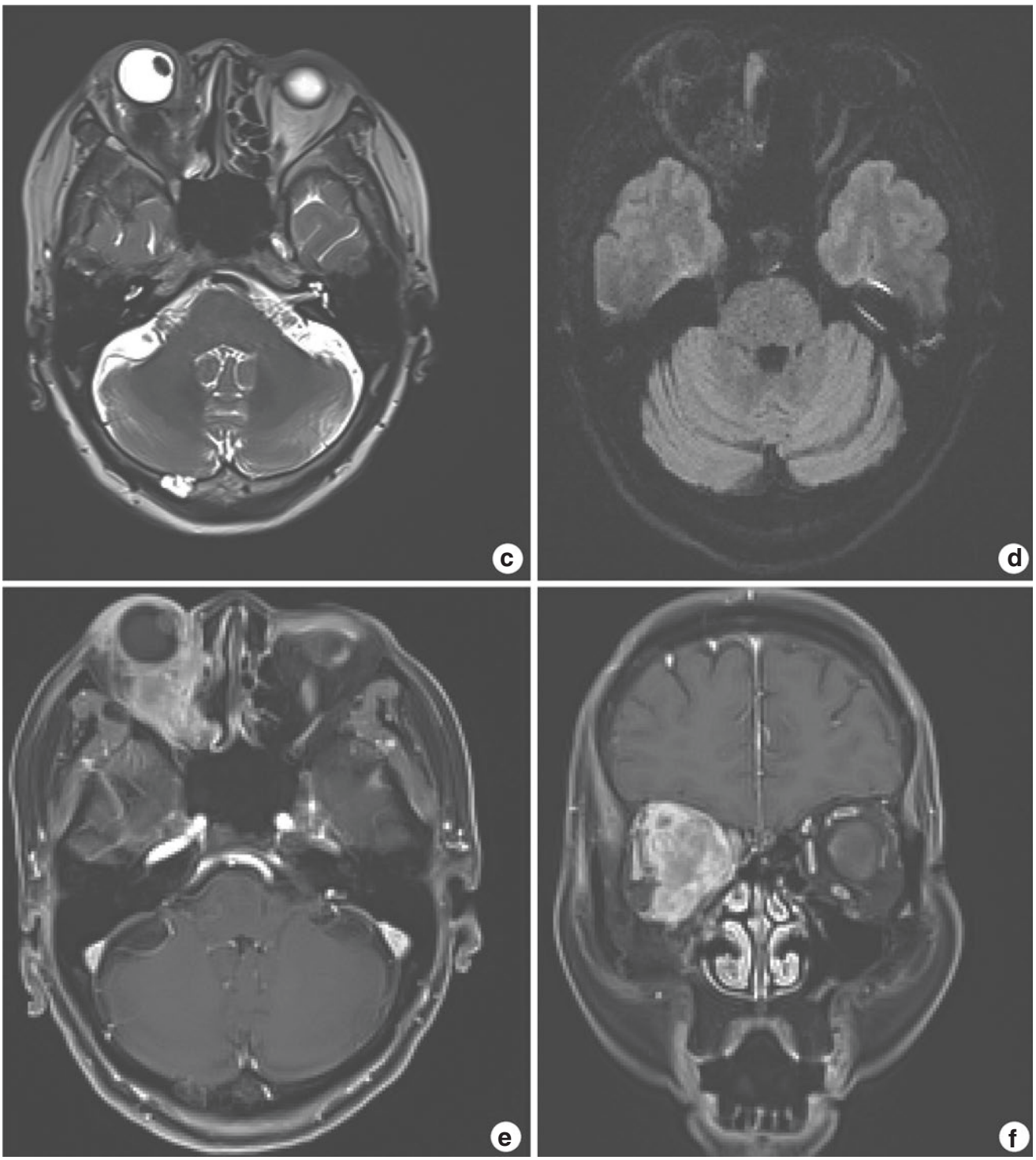

Fig. 15.7 (continued)

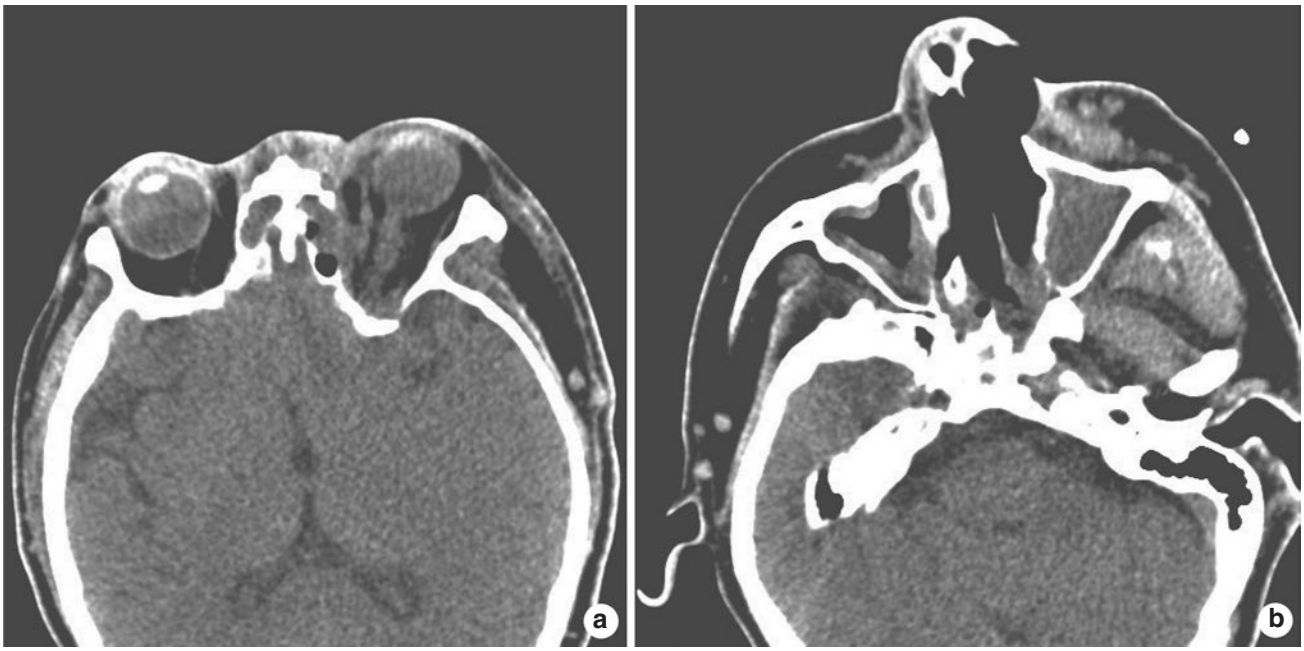

Fig. 15.8 Mucor infection at left orbit. A 45-year-old male patient. His nose and face are swollen and painful for 3 days and worsened for 1 day. The patient suffered from mucor infection in orbit and paranasal sinus. (**a**) CT shows marked swelling of soft tissue in left orbit, thickening of optic nerve, and left proptosis. (**b**) CT shows absence of bone structure destruction at left nasal cavity and swelling of subcutaneous soft tissue at left face. Soft tissue shadow can be seen in bilateral maxillary sinuses

which has density of soft tissue, can compress optic nerves with blurred border. Besides, proptosis can occur as well as atrophy of eyeball in an advanced stage. MRI examination can show involvement of dura mater and intracranial region, cavernous sinus thrombosis and embolus at cavernous segment of internal carotid artery. Granuloma shows isointense on T_1WI, hypointense on T_2WI, and no enhancement or mild enhancement after enhanced scan. Lesion involving intracranial area can cause abscesses in adjacent brain lobes, which often involves ipsilateral and sometimes bilateral frontal lobes (Fig. 15.9).

15.1.3.5 [Key Points of Diagnosis]

1. Most cases are rhinogenic infection complicated by paranasal sinus and intracranial changes. Immunocompromised people are vulnerable to the disease. Thrombosis occurs in blood vessels of eyelid and periorbital skin. The affected skin shows black, resulting in ischemic necrosis, accompanied by black pus and hemorrhagic effusion.
2. The lesion has coarse border and communicates with ipsilateral paranasal sinus. According to CT findings, the lesion results in wide involvement, fast progression and bone destruction. The lesion shows isointense on MRI T_1WI and hypointense on T_2WI. When intracranial area is involved, adjacent brain parenchyma shows hyperintense on T_2WI.

15.1.3.6 [Differential Diagnosis]

Early diagnosis of mucor infection is difficult. Differential diagnosis mainly includes differentiation from other intraorbital cellulitis and malignant tumor. Intraorbital cellulitis usually shows hyperintense on T_2WI, and results in no necrotic tissue or bacterial embolus in retinal artery. Malignant tumors in eyelid and orbital show slow onset and mild symptoms, and signs of tumor can be found in imaging findings.

15.1.3.7 [Status Quo and Progress of Research]

Rhino-orbito cerebral mucor infection is common in diabetic patients. Diabetes and combined diabetic ketoacidosis are the most common risk factors for mucormycosis. Patients with diabetic ketoacidosis are manifested as hyperglycemia, elevated serum ketone body, and metabolic acidosis, all of which underlie the in vivo growth and reproduction of mucor. Imaging examinations help understand the location and damage of the lesion. Any intracranial infection suggests a poor prognosis with a high risk of mortality. The lesion is characterized by rapid progression, swift expansion of inflammation and bone destruction. Therefore, diabetic patients who have lesion in the eye, paranasal sinus or brain shall be suspected of mucormycosis. CT examination is the first choice for mucor infection, which can evaluate whether there is bone destruction that progresses rapidly. MRI mainly

aims to evaluate whether the lesion involves other adjacent sites, such paranasal sinus and intracranial area [6].

15.2 Thyroid-Associated Ophthalmopathy

15.2.1 [Overview]

Thyroid-associated ophthalmopathy (TAO) is the most common orbit disease among adults. This is an autoimmune disease with unknown pathogenesis. Its annual incidence is between 0.2‰ and 0.5‰, among which the ratio of male to female is around 1:5 [6]. Patients may show normal thyroid gland function, hyperthyroidism and hypothyroidism. In the past, the disease was named endocrine exophthalmia, malignant proptosis or infiltrating proptosis. Cases with proptosis accompanied by hyperthyroidism (hyperthyroidism) were also called Graves' ophthalmopathy, and those without hyperthyroidism were called ocular Graves' disease. Now They are collectively called thyroid-associated ophthalmop-

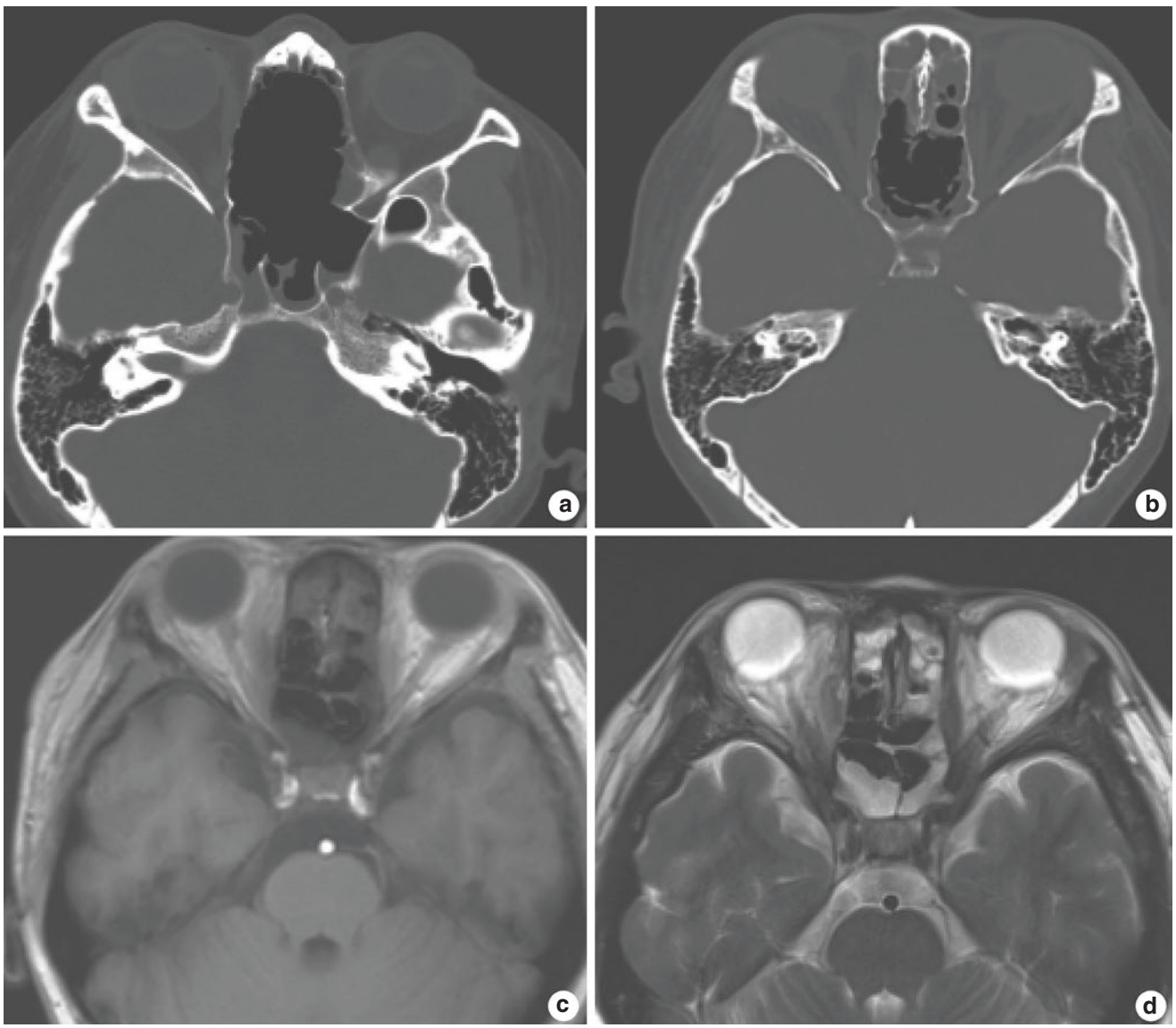

Fig. 15.9 Mucor infection in right orbit, bilateral ethmoidal sinus and frontal sinus, accompanied by intracranial abscess of mucor. A 23-year-old female patient. With 3-week history of acute leukemia, the patient suffered from swollen and painful nose and face for 3 days and worsened for 1 day. Mucor infection occurred in orbit and paranasal sinus, accompanied by intracranial abscess. (**a** and **b**) CT bone window shows soft tissue shadow in bilateral ethmoidal sinus and sphenoid sinus and thickening of medial rectus at right orbit. Bone structure destruction at bilateral cribriform plates disappeared. (**c** and **d**) According to MRI, fats medial and lateral to muscle cone of right orbit are blurred, T_1WI and T_2WI fat signals are reduced, bilateral ethmoidal sinus and sphenoid sinus show hypointense on T_1WI and hyperintense on T_2WI. (**e**) Coronal FLAIR with fat suppression shows that intraorbital signal of right eye increases, bilateral ethmoidal sinus and left maxillary sinus show hyperintense, and bilateral frontal lobes show patchy hyperintense shadows (arrow); (**f**) After enhanced scan, bilateral ethmoid sinus mucus as show enhancement and bilateral frontal lobes show ring enhancement

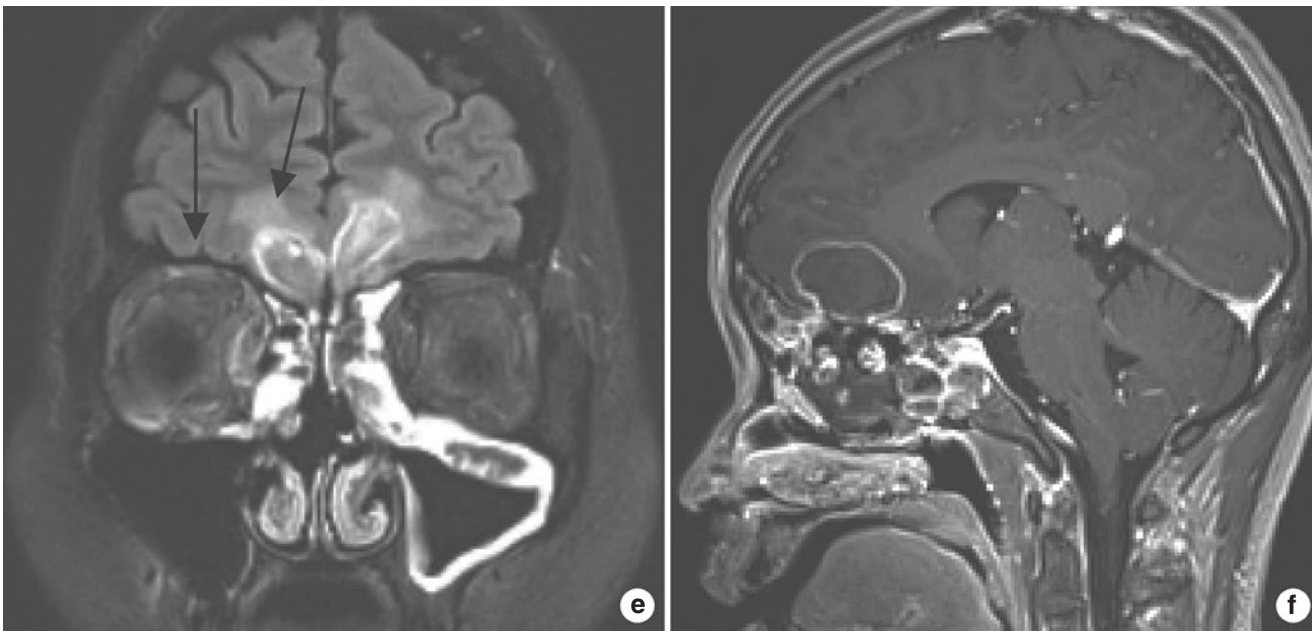

Fig. 15.9 (continued)

athy. Over 80% of TAO patients suffer from bilateral onset, mainly manifested as proptosis, diplopia, and congestion and edema at the ocular surface and periorbital area. Some patients may show severe symptoms, including exposure, ulcer and infection of the cornea, optic nerve compression and visual impairment. Physical examination can reveal proptosis, ocular muscle dysfunction, eyelid edema, eyelid contracture, incomplete eyelid closure, and increased intraocular pressure.

15.2.2 [Pathology Findings]

Tissues affected by TAO include muscles, connective tissues, fats, and lacrimal glands. Under light microscope, it can be seen that in active stage, extraocular muscle is enlarged, intercellular space is widened, and infiltration to varying degree occurs in immune cells and inflammatory cells, accompanied by fibroblast proliferation. Infiltrates are typically T lymphocyte, accompanied by plasma cell and monocyte and macrophage. Interstitial tissue is prevailed by lymphocytes infiltration, accompanied by a large number of glycosaminoglycans accumulated. Immune cells are arranged in clusters around blood vessels, and there are mastocytes and macrophages sometimes. Besides, adipocyte may exist between myocytes. In a resting stage, extraocular muscle fibers degenerate, some of which are subject to severe fibrosis, and most of muscle fibers show granular degeneration to varying degrees, with vacuoles and even obvious fibrosis. Blood vessels are dilated and congestive. Electron microscope findings show that muscle cell membrane is intact and thickened, while myofilaments and z-lines are arranged in an out-of-order way. Mitochondria are heavily hyperplastic and concentrated, with loose and swollen cristae. Stroma particles disappear, glycogen particles accumulate, the sarcoplasmic reticulum expands, and more lipid droplets can be seen in the cytoplasm. Interstitial capillaries increase, subject to dilation and congestion. Collagen fibers increase [7].

15.2.3 [Imaging Findings]

1. CT Examination. Transverse CT shows that proptosis can be confirmed when distance between eyeball anterior border and zygomatic arch anterior border is greater than 20 mm. CT at transverse plane combined with reconstructed image at coronal plane can clearly display each extraocular muscle. The order in which ocular muscles are involved is respectively medial rectus, inferior rectus, superior rectus and lateral rectus. The thickened eye muscles show fusiform swelling. The thickening mainly occurs in muscle belly, yet tendon is normal (Fig. 15.10).

Extraocular muscle shows decreased density with spot or patchy low-density shadows in TAO active stage and increased density with local or diffuse shadows in stable stage. Enhanced scan indicates mild to moderate enhancement of thickened ocular muscles in active stage, and no enhancement in advanced stage in case of fibrosis formed. Retrobulbar fats increase, pulling eyeball and orbital septum forward, wherein the density of the increased fat is normal. In case of severe proptosis, optical nerves subject to the pulling may lose physiological bending and become straight. Some severe cases show thickening of optical nerves. In a

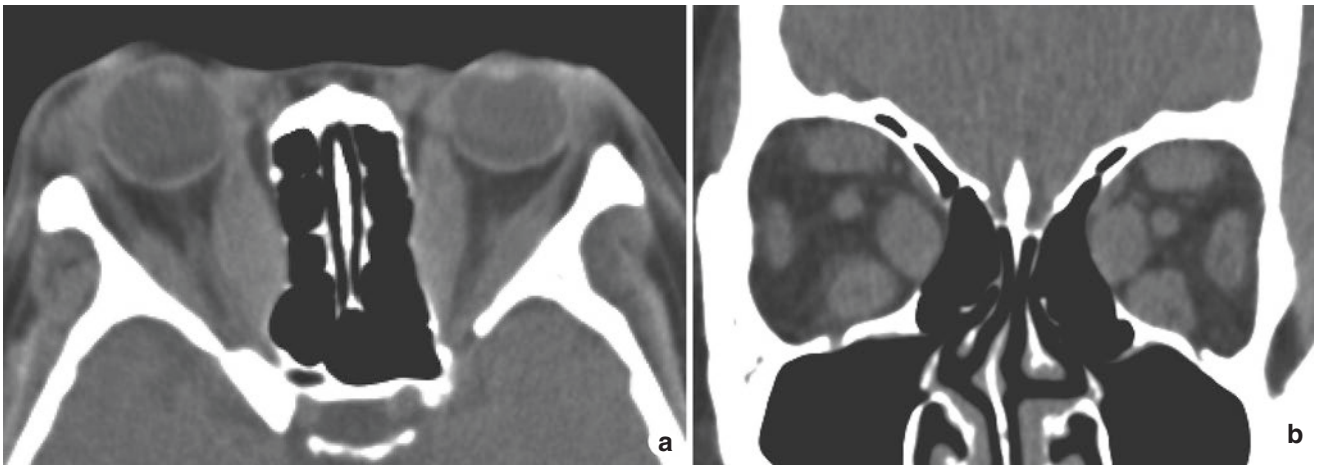

Fig. 15.10 Thyroid-associated ophthalmopathy (1). (**a**) CT of orbit at transverse plane shows bilateral proptosis, with obvious fusiform thickening of binocular medial rectus and mild thickening of binocular lateral rectus, wherein the thickening only occurs in muscle belly, not tendon. (**b**) CT of orbit at coronal plane shows marked thickening of binocular medial rectus and lateralis and ocular superior muscles and slight thickening of binocular lateral rectus, without thickening of bilateral optic nerves

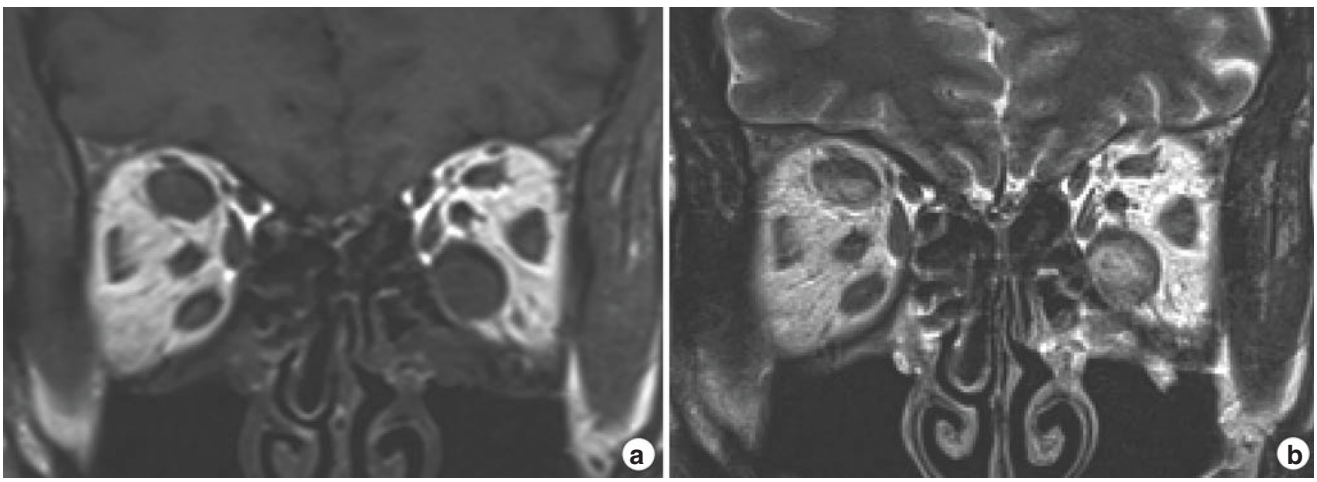

Fig. 15.11 Thyroid-associated ophthalmopathy (2). (**a**) According to orbital MR T_1WI sequence at coronal plane, superior rectus of right eye are remarkably thickened, while inferior rectus and lateral rectus of left eye are thickened, basically showing isointense, with distinct peripheral fat space; (**b**) Orbital MR at coronal plane shows patchy hyperintense shadow at the center of thickened muscle on T_2WI, while optic nerve shows no abnormal signal changes

small number of cases, hypertrophied bilateral medial rectus belly compresses bilateral medial walls, which are very thin and fragile, thus making the central part of the walls protrude inward.

2. MRI Examination. Axial MRI images on T_1WI can precisely measure the proptosis degree of TAO patients. Extraocular muscle shows slightly hypointense on T_1WI and slightly hyperintense, moderately or slightly hypointense on T2WI weighted image. Dynamic contrast-enhanced MRI (DCE-MRI) can evaluate microcirculation of rectus muscle, while differentiate active stage and stable stage of TAO. Upper eyelid levator hypertrophy can be best shown at sagittal plane and coronal plane. T_1WI without fat suppression can help diagnose degenerative changes in fat and muscle. Fatty degeneration and fibrosis of muscle show no enhancement on enhanced T_1WI with fat suppression. T_2WI signals can detect the presence of fibrosis and the degree thereof in extraocular muscle of TAO patients. Extraocular muscle showing isointense or hypointense on T_2WI suggests severe muscle fibrosis. Extraocular muscle showing hyperintense on T_2WI suggests that the muscle is in a stage of inflammatory edema (Figs. 15.11 and 15.12). Cases with lacrimal gland show hypointense on T1WI and hyperintense on T2WI, with cystic slight dilation and blurred border. Some cases may show tortuous phlebectasia of superior ophthalmic vein and thickening of optic nerve on MRI, wherein the thickened optic nerve has normal signals with smooth border. medial rectus shows the most obvious thickening when complicated by optic neuropathy.

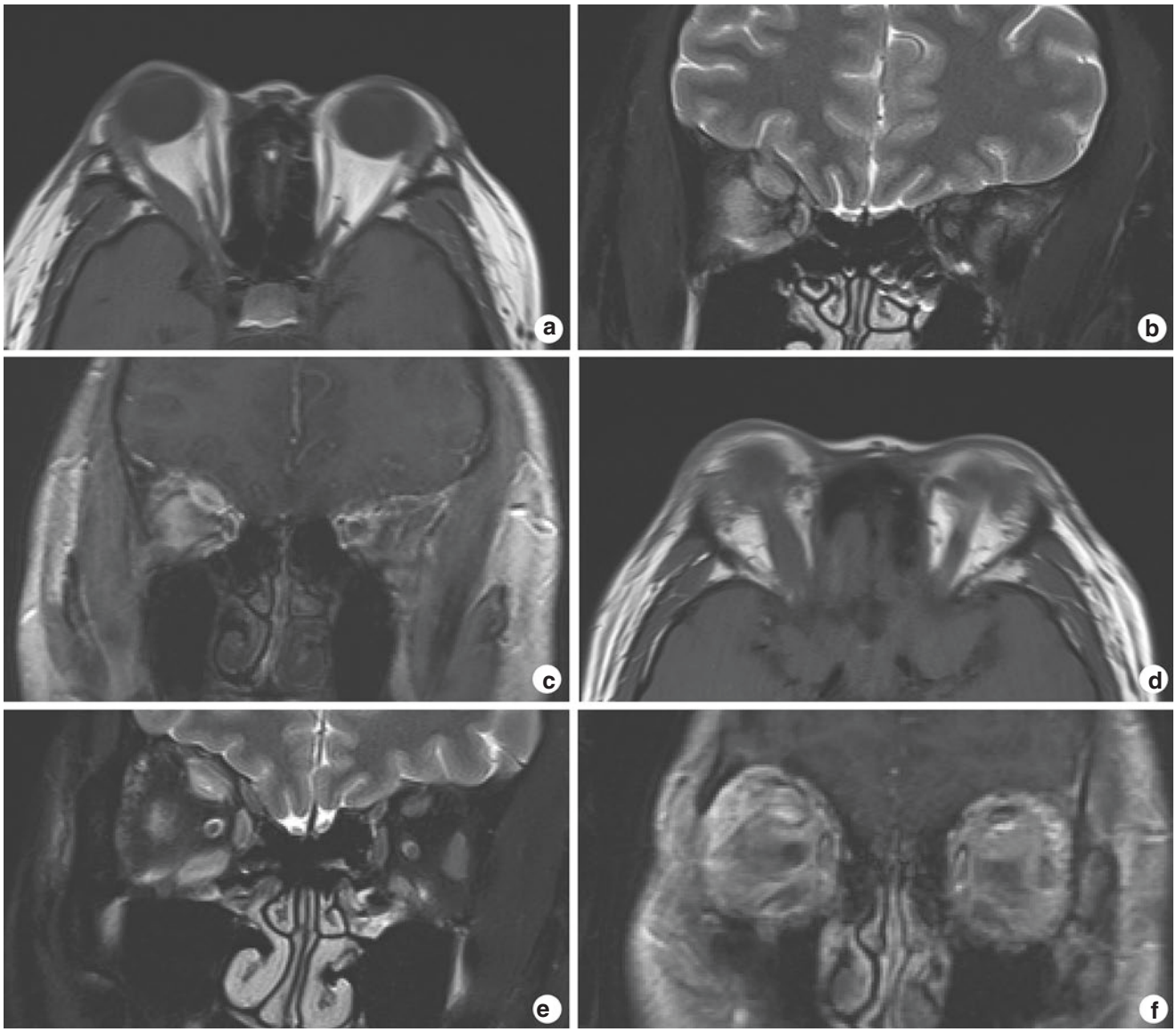

Fig. 15.12 Thyroid-associated ophthalmopathy (3). (**a** and **d**) According to orbital image at transverse plane, right ocular superior muscles and lateral rectus are significantly thickened on T_1WI, showing isointense, with clear peripheral fat space; (**b** and **e**) Orbital image at coronal plane shows obvious thickening of right ocular superior muscles, lateral rectus and inferior rectus muscle on T_2WI fat suppression sequence, with hyperintense banding signal shadows. Optic nerve shows no abnormal signal changes. (**c** and **f**) Orbital enhancement at coronal plane shows heterogeneous enhancement of thickened muscle on T_1WI

15.2.4 [Key Points of Diagnosis]

1. CT findings include thickening of extraocular muscle belly, normal tendon, and proptosis. Fatty degeneration and fibrosis of muscle can be shown on T_1W1, and the extent of extraocular muscle fibrosis of TAO patients can be shown on T_2WI. MRI enhanced scan can identify the progression of the lesion. Enhanced scan shows mild to moderate enhancement of thickened ocular muscle in active stage and no enhancement in advanced stage in case of fibrosis formed.
2. It is one of the most common orbital diseases among adults. Patients can be complicated by thyroid dysfunction, such as hyperthyroidism or hypothyroidism, or just show normal thyroid gland function.
3. The lesion is mostly bilateral, manifested as proptosis, diplopia, and congestion and edema at ocular surface and periorbital area.

15.2.5 [Differential Diagnosis]

1. Inflammatory Pseudotumor. The most common disease that needs to be differentiated is extraocular myositis (ocular inflammatory pseudotumor), whose lesions are typically unilateral, with thickening of both tendon and muscle belly,

accompanied by pain and rarely-occurring eyelid contraction. Glucocorticoid (GC) is effective for inflammatory pseudotumor.

2. IgG4 Related Disease. It is a chronic systemic disease closely related to IgG4, characterized by increased serum IgG4 levels and diffuse infiltration of IgG4-positive plasma cells in lacrimal glands, extraocular muscles, supraorbital nerves and other ocular appendages. CT shows diffuse thickening of the lacrimal gland and extraocular muscles, as well as thickening of supraorbital nerves. Glucocorticoid is effective.

15.2.6 [Status Quo and Progress of Research]

Currently, Studies on TAO imaging techniques mostly focus on activity staging and prediction of clinical efficacy, wherein MRI is the most widely used, owing to its multidirectional imaging, high resolution to soft tissue and being free from ionizing radiation.

Orbital MRI for TAO patients can identify position and nature of the lesion, with STIR serving as the main sequence for imaging and regular scan when evaluating the activity of TAO lesions. Studies by many scholars [8, 9] found that signal intensity ratio (SIR) of the extraocular muscle signal intensity to that of brain white matter or ipsilateral temporal muscle is positively correlated with the TAO clinical activity score. The SIR semi-quantitative analysis method is mature and widely applied in the evaluation of TAO active staging. At present, some studies [10] have obtained specific segmentation thresholds. In addition, DCE-MRI relevant parameters, such as enhancement coefficient in early stage and peak enhancement coefficient [11], DWI sequence ADC value, extraocular muscle T_2 relaxation time and sectional area [12] measured with T2 mapping imaging techniques, can reflect TAO activity, thereby providing new research directions.

Study on the application of MRI in TAO activity staging further involves prediction on TAO curative effect, which can provide important references for clinical decision. Studies [10] show that prognosis of TAO glucocorticoid therapy can be evaluated by SIR value of TAO patients to certain extent; T_2 mapping imaging techniques [13], can be used for evaluating immunosuppressive effect. ADC value from non-echo-planar DWI can supplement the prediction on curative effect [14].

At this moment, TAO imaging studies still lack consistent and comprehensive data standards, while the efficacy evaluation data has small sample size and requires further prospective studies. The application of MRI in TAO active staging and efficacy evaluation remains to be further studied in the future.

References

1. Mouriaux F, Coffin-Pichonnet S, Robert PY, et al. Orbital inflammation. J Fr Ophtalmol. 2014;37(10):818–24.
2. Tianqi L, Li Z, Weina C, et al. Application of 16-slice spiral CT reorganization technology in eye socket cellular tissue inflammation and abscess. J Med Imaging. 2011;21(1):12–5.
3. Tsirouki T, Dastiridou AI, Ibánez Flores N, et al. Orbital cellulitis. Surv Ophthalmol. 2017;63(4):534–53.
4. Patnana M, Sevrukov AB, Elsayes KM, et al. Inflammatory pseudotumor: the great mimicker. AJR Am J Roentgenol. 2012;198(3):217–27.
5. Yan J. Idiopathic orbital inflammatory pseudotumor with bone erosion. J Craniofac Surg. 2016;27(7):607–8.
6. Junfang X, Dapeng S, Xiaofeng T. Imaging of the head and neck·ophthalmology. Beijing: People's Medical Publishing House; 2014.
7. Smith TJ, Hegedüs L. Graves' disease. N Engl J Med. 2016;375(16):1552–65.
8. Qiuyue C, Zhiyi C, Chenzhong L, et al. Study on value of MRI SIR of extraocular muscle to ipsilateral brain white matter in evaluation of TAO activity. Chinese J Endocrinol Metabolism. 2018;34(2):106–11.
9. Higashiyama T, Iwasa M, Ohji M. Quantitative analysis of inflammation in orbital fat of thyroid-associated ophthalmopathy using MRI signal intensity. Sci Rep. 2017;7(1):16874.
10. Ortiz-Basso T, Vigo RL, Mariano S, et al. Triamcinolone for the treatment of graves ophthalmopathy tested with short tau inversion recovery magnetic resonance. Ophthal Plast Recons Sur. 2019;35(1):22–4.
11. Tong W, Dongrun T, Feng W, et al. The value of DCE-MRI in assessing the course of TAO. Chinese J Ophthalmol. 2017;53(6):430–5.
12. Wen C, Hao H, Xiaoquan X, et al. Application value of T2 mapping quantitative measurement for extraocular muscle in diagnosis and staging of thyroid-associated ophthalmopathy. Acta Universitatis Medicinalis Nanjing (Nat Sci). 2019;39(1):147–50.
13. Hong J, Fei Y, Junfang X, et al. T2 Mapping MRI study on immunosuppression therapy of TAO. Ophthalmology. 2018;27(5):339–43.
14. Lingam RK, Mundada P, Lee V. Novel use of non-echo-planar diffusion weighted MRI in monitoring disease activity and treatment response in active Grave's orbitopathy: an initial observational cohort study. Orbit. 2018;37(5):325–30.

Optic Neuritis

16

Shaowei Zheng and Lijun Wang

16.1 [Overview]

In general, optic neuritis refers to all inflammatory lesions that occur in the optic nerve. Currently, there are many classification methods. The disease can be divided into papillitis, neuroretinitis, retrobulbar neuritis and optic perineuritis by invasion site. Papillitis refers to the optic neuritis manifested as optic disc edema. Optic neuroretinitis refers to the inflammation that occurs retinal stellate exudation and optic disc edema simultaneously. Retrobulbar neuritis refers to cases who have normal optic disk morphology with typical clinical manifestations of optic neuritis. Optic perineuritis refers to inflammation involving optic nerve sheath, rather than optic nerve parenchyma, according to imaging findings. According to etiology, the disease can be divided into idiopathic optic neuritis, systemic autoimmune disease associated optic neuritis, infectious optic neuritis and postinfectious optic neuritis. Among them, idiopathic optic neuritis is the most common; thus it is also called typical optic neuritis. The rest of optic neuritis are collectively known as atypical optic neuritis, including idiopathic demyelinating optic neuritis (also known as classic multiple sclerosis-related optic neuritis), neuromyelitis optica related optic neuritis and other optic neuritis related to central nervous system demyelinating diseases). In general, infectious and autoimmune optic neuritis can be relieved along with the treatment of primary illness. They can rarely be relieved without interference or subject to relapse. Optic neuritis in children is often accompanied by optic disc edema and bilateral involvement, characterized by acute onset and good prognosis.

16.2 [Pathology Findings]

Main pathological changes caused by optic neuritis are demyelination, gelatinous fiber proliferation and sclerosis plaque formation. The extent to which demyelination, axon changes, perivascular cell infiltration, gliosis, and thickening of arachnoid are formed varies by different pathogenesis. Some suppurative inflammatory infiltrates such as orbital infection, rhinosinusitis caused by acute optic neuritis often form neutrophilic segmented granulocyte infiltration in optic nerve sheath and mononuclear infiltration in chronic stage. Degeneration of optic nerve fibers, proliferation of neuroglia cells, and optic atrophy can occur in advanced stage of various inflammations.

16.3 [Clinical Manifestation]

Idiopathic optic neuritis is usually unilateral, frequently occurring among people between 20 to 50 years old, with an average age of 30–35 years old, wherein the ratio of male to female is 1:3. It has become one of the major blind-causing optic nerve diseases among young and middle-aged population. Main clinical manifestations include vision loss, dyschromasia, pain in affected eyes, and changes in visual field and in pupil. The absence of direct light pupillary reflex can also occur. Visual loss is mostly monocular, yet can also be binocular. Visual acuity is severely damaged at 1 to 2 weeks after onset and then gradually recovered on its own. Within 12 months, 95% of patients' visual acuity can return to the normal level. Two out of three patients can suffer from retrobulbar neuritis, which shows normal fundus in the early stage of onset. One out of three patients can experience optic disk edema, and peripapillary hemorrhage occurs rarely. Atypical optic neuritis is relatively rare. It typically occurs among people below 15 or above 50 years old, characterized by occult onset, involving both eyes synchronously or one by one within a short time. Besides, it can result in severe vision loss, accompanied by persistent optic disc edema, severe disc hemorrhage, retina exudation, macular stellate exudation or folding, vitreoretinal inflammation and uveitis.

S. Zheng · L. Wang (✉)
The First Hospital of Dalian Medical University, Dalian, China

H. Li et al. (eds.), *Radiology of Infectious and Inflammatory Diseases - Volume 2*,
https://doi.org/10.1007/978-981-16-8841-6_16

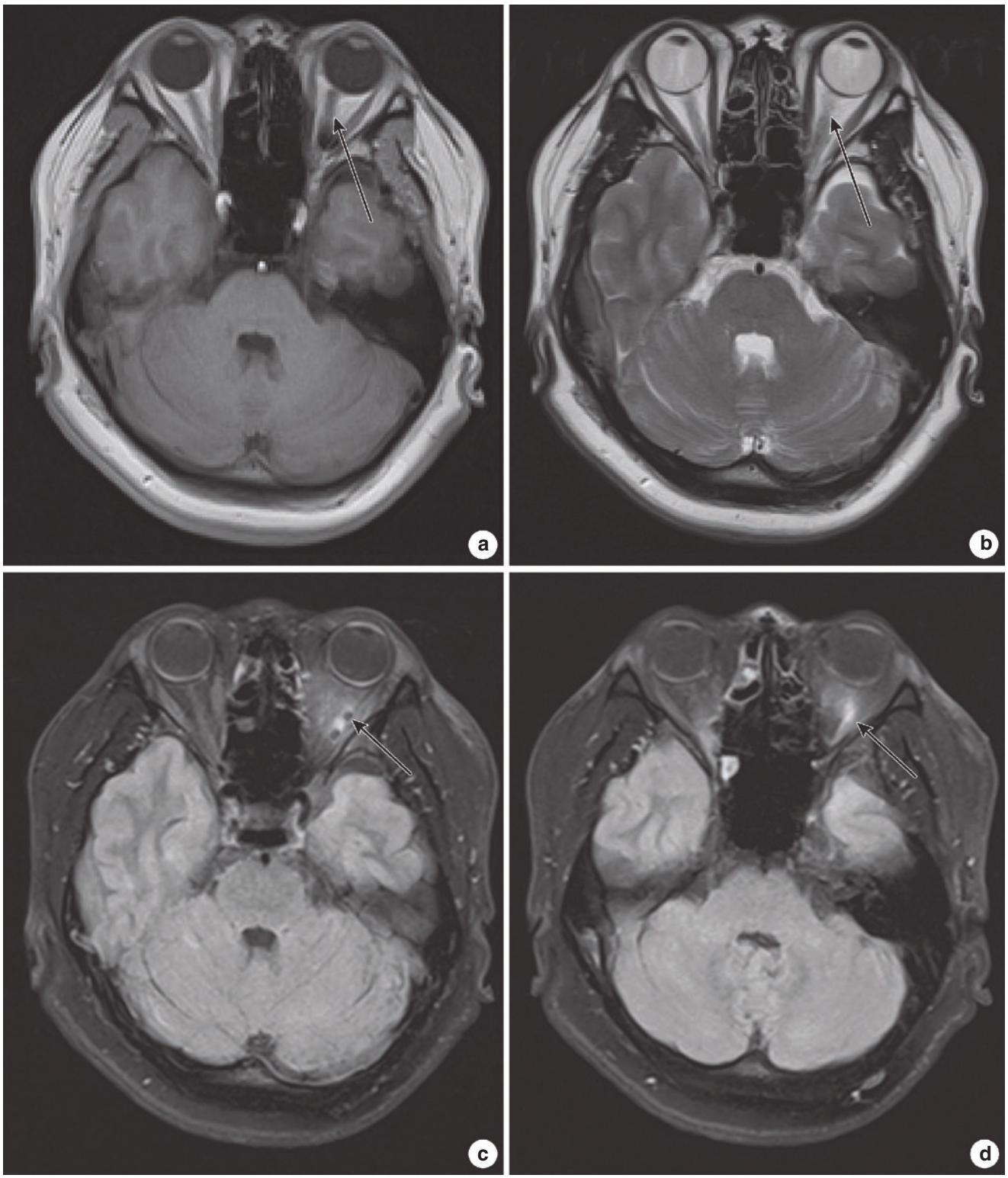

Fig. 16.1 Left optic neuritis. A 34-year-old male patient. The patient experienced vision loss of left eye for more than 1 year. (**a** and **b**) T_1WI and T_2WI show thickening of left optic nerve (arrow); (**c** and **d**) Lesion shows hyperintense on FLAIR (arrow)

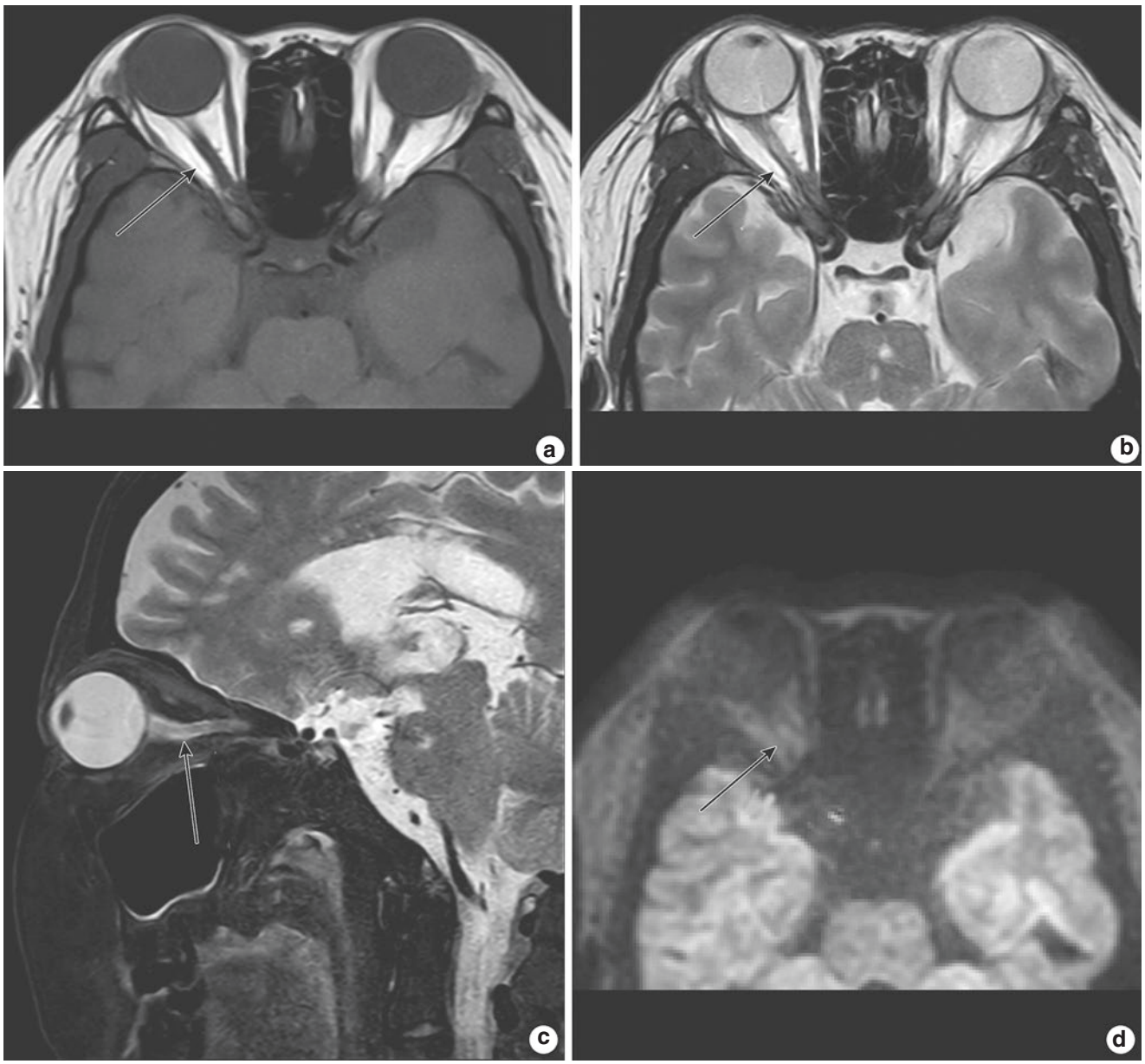

Fig. 16.2 Right optic neuritis. A 34-year-old male patient. The patient experiences vision loss of right eye for more than three years and the condition is worsened for more than 1 month. The patient has a history of systemic lupus erythematosus. (**a** and **b**) Non-enhanced MRI scan T_1WI and T_2WI show thickening of left optic nerve (arrow); (**c**) T_2WI fat-suppressed sequence shows increased optic nerve signal (arrow); (**d**) The lesion shows hyperintense on DWI (arrow)

16.4 [Imaging Findings]

1. CT Examination. Optic nerve is thickened without obvious mass, showing isointense in non-enhanced scan, and is enhanced to varying degrees with double-track sign after enhanced scan. Optic nerve sheath is enhanced, while optic nerve is not; Generally, CT cannot show optic neuritis without obvious enlargement of optic nerve.

2. MRI Examination. Intraorbital fat peripheral to optic nerve shows hyperintense and chemical shift artifacts on T_2WI sequence. For this reason, T_2WI fat suppression sequence can better show the contrast between the lesion and peripheral tissues. Images show local or diffuse thickening of optic nerve, wherein the thickness may be heterogeneous and involve the entire length. When T_2WI signal increases, STIR can better show the lesion. When the lesion shows isointense on T_1WI, DWI is the most sensitive, wherein the thickened optic nerve shows hyperintense. Enhanced scan with fat suppression shows marked enhancement in lesion area (Figs. 16.1, 16.2 and 16.3). In a small

number of cases, optic nerve sheath can be enhanced with double-track sign. Sometimes, relapsing optic neuritis shows no marked enhancement on enhanced T1WI. In such case, enhanced T2WI FLAIR can be used to identify any enhancement. Optic neuritis is typically an early manifestation of multiple sclerosis and neuromyelitis optica. Therefore, patients with optic neuritis must routinely receive brain and spinal cord MRI examination (including FLAIR sequence and enhanced scan) to diagnose multiple sclerosis as early as possible.

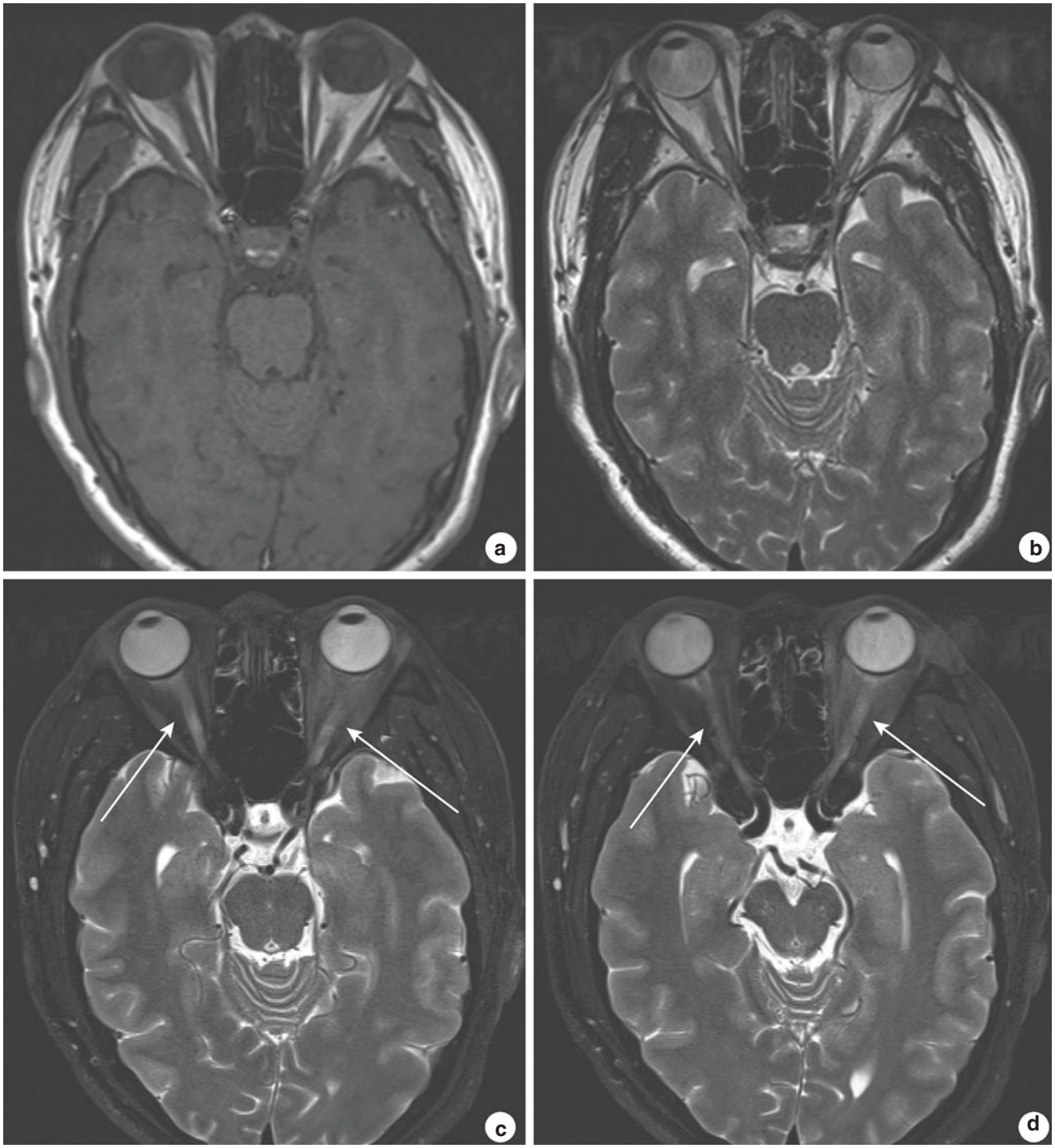

Fig. 16.3 Bilateral optic neuritis. A 43-year-old male patient. Binocular vision decreased for 1 week. (**a** and **b**) T_1WI and T_2WI show thickening of bilateral optic nerves; (**c** and **d**) Bilateral optic nerves show hyperintense on FLAIR (arrow); (**e**) The lesion shows limited diffusion on DWI; (**f**) ADC shows decreased signal

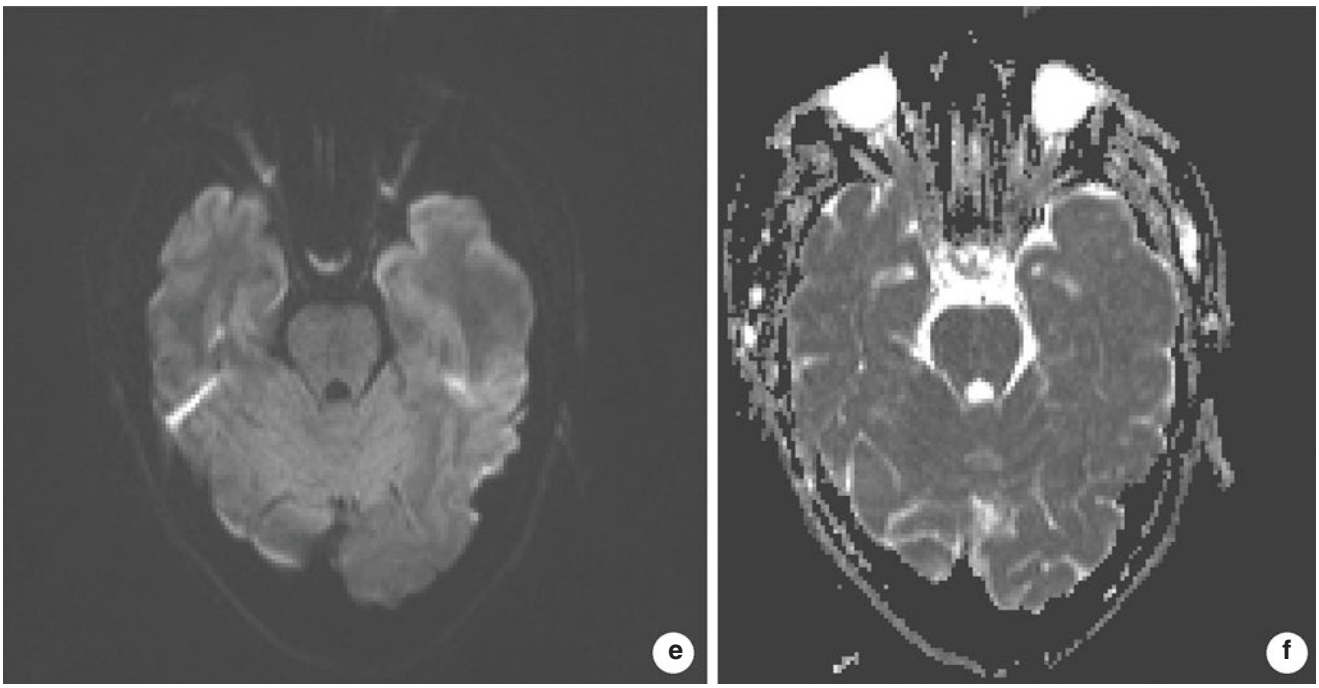

Fig. 16.3 (continued)

16.5 [Key Points of Diagnosis]

1. Visual acuity decreased rapidly in a short time and improved after hormone therapy.
2. Imaging findings show thickening of optic nerve on the affected side, with increased T_2WI signal. DWI shows limited diffusion. The lesion is enhanced after enhanced scan.

16.6 [Differential Diagnosis]

1. Meningioma of Optic Nerve. It is more common in adults. CT shows high density, and calcification can be observed sometimes. The lesion shows isointense on T_1WI and isointense or slightly hyperintense on T_2WI. After enhanced scan, the tumor is remarkably homogeneously enhanced, while optic nerve shows double-track sign, without marked enhancement.

2. Optic Nerve Glioma. It is common in children below 10 years old. The optic nerve is thickened in a shape of fusiform, manifested as a mass. The lesion can enter the intracranial area along the optic canal. After enhanced scan, optic nerve shows moderate to marked enhancement.

3. Ischemic Optic Neuropathy. The patient suffers from sudden loss of vision, without obvious pain during eye movement. Swelling of optic disc is prone to be grey white. Visual field defect of inferior area is the most common. After enhanced scan, the lesion shows no marked enhancement.

4. Toxic or Metabolic Optic Neuropathy. Medical history and related examination can help diagnose.

16.7 [Status Quo and Progress of Research]

As intraorbital fat peripheral to optic nerve produces hyperintense and chemical shift artifacts, fat-suppressed sequence is crucial to T_2WI. In case of acute optic neuritis, optic nerve sheath dilates, thus worsening the partial volume effect of cerebrospinal fluid. For this reason, the optimal T_2WI sequence shall suppress both water and fat signals.

If enhanced T_1WI shows that the lesion exceeds 50% of optic nerve in length or involves optic chiasma, neuromyelitis optica related optic neuritis is very likely to occur. The extent of abnormal enhancement of optic neuritis in the acute stage is significantly correlated with the severity of visual impairment in the early stage.

A variety of MRI functional imaging techniques provide a wide array of quantitative criteria for monitoring, outcome prediction and visual prognosis of optic neuritis. With zonal oblique multislice echo-planar imaging (ZOOM-EPI) sequence, optic nerves can be clearly shown in 1.5T MRI. ADC value of optic nerve is remarkably higher than that of brain white matter, which may be due to the different axonal structure and density. When compared with the normal brain parenchyma, acute optic neuritis shows isointense or hypointense in ADC map, while ADC value of chronic optic neuritis often increases. DWI can also be used for dif-

ferentiating optic neuritis from ischemic optic neuropathy. Hemorrhagic transformation of ischemic lesion or simple ischemic lesion can be manifested as limited diffusion, similar to the characteristics of brain ischemia on DWI. Radial diffusivity (RD), the most sensitive DTI parameter for identifying whether the optic nerve is involved, is closely related to vision recovery, electro-neurophysiological indicators, and optic nerve fiber layer thickness [1–3].

References

1. Toosy AT, Mason DF, Miller DH. Optic neuritis. Lancet Neurol. 2014;13(1):83–99.
2. Wilhelm H, Heine C, Tonagel F. Optic neuritis. Klin Monbl Augenheilkd. 2014;231(11):1073–83.
3. Lu P, Sha Y, Wan H, et al. Role of coronal high-resolution diffusion-weighted imaging in acute optic neuritis: a comparison with axial orientation. Neuroradiology. 2017;59(8):737–45.

Eyelid Lesions

17

Shaowei Zheng and Lijun Wang

17.1 Eyelid Inflammation and Abscess

17.1.1 [Overview]

Eyelid inflammation and abscess are typically caused by direct invasion of bacteria in the wake of adjacent tissue inflammation or eyelid trauma. Besides, it is also common in hematogenous dissemination of systemic lesion. Adjacent tissue inflammation is often evolved from hordeolum. It can also be involved by traumatic infection, orbital cellulitis, orbital pseudomonas aeruginosa periostitis, dacryoadenitis, or penetrating paranasal sinus empyema. The disease is more common in children, attributed to their low immunocompetence, poor barrier function and vulnerability to infection.

17.1.2 [Pathology Findings]

Pathologically, eyelid inflammation is mainly manifested as a large number of inflammatory cell infiltration, necrotic tissues seen in necrotic cavity of abscess, and granulation tissue in abscess wall peripheral to the lesion.

17.1.3 [Clinical Manifestation]

The disease may first manifests as blepharitis and gradually worsen, or cause sharp reaction in eye from the very beginning, accompanied by severe congestion and edema of eyelid, chemosis, and sense of fluctuation in case of any abscess formed (Fig. 17.1). The patient may suffer from severe local pain, typically accompanied by fever and other general reactions.

17.1.4 [Imaging Findings]

Patients are manifested as thickened eyelid, in which vomica that is typically irregularly shaped with blurred border can be observed. When compared with extraocular muscle, thickened eyelid shows isodense on CT, isointense on T_1WI, slightly hyperintense on T_2WI, and marked enhancement on enhanced scan, with blurred border. Vomica is manifested as a restricted low-density area on CT. It shows hypointense on MRI T_1WI, hyperintense on T_2WI, wherein linear septa can be seen, showing hyperintense on DWI. After enhanced scan, the septa and borders show ring enhancement. CT and MRI can show any lesion involved by inflammation of adjacent structures (Figs. 17.2, 17.3 and 17.4).

17.1.5 [Key Points of Diagnosis]

1. Common in children.
2. It has acute onset and severe local symptom.
3. Vomica is formed in swollen eyelid, manifested as low-density area on CT, showing hypointense on T_1WI and hyperintense on T_2WI and DWI. Besides, the vomica shows ring enhancement after enhanced scan.

17.1.6 [Differential Diagnosis]

Differential diagnosis mainly includes eyelid and intraorbital tumors, which have a relatively slow onset with mild symptoms. Imaging findings can show signs of mass, so the differentiation is not very difficult.

S. Zheng · L. Wang (✉)
The First Hospital of Dalian Medical University, Dalian, China

H. Li et al. (eds.), *Radiology of Infectious and Inflammatory Diseases - Volume 2*,
https://doi.org/10.1007/978-981-16-8841-6_17

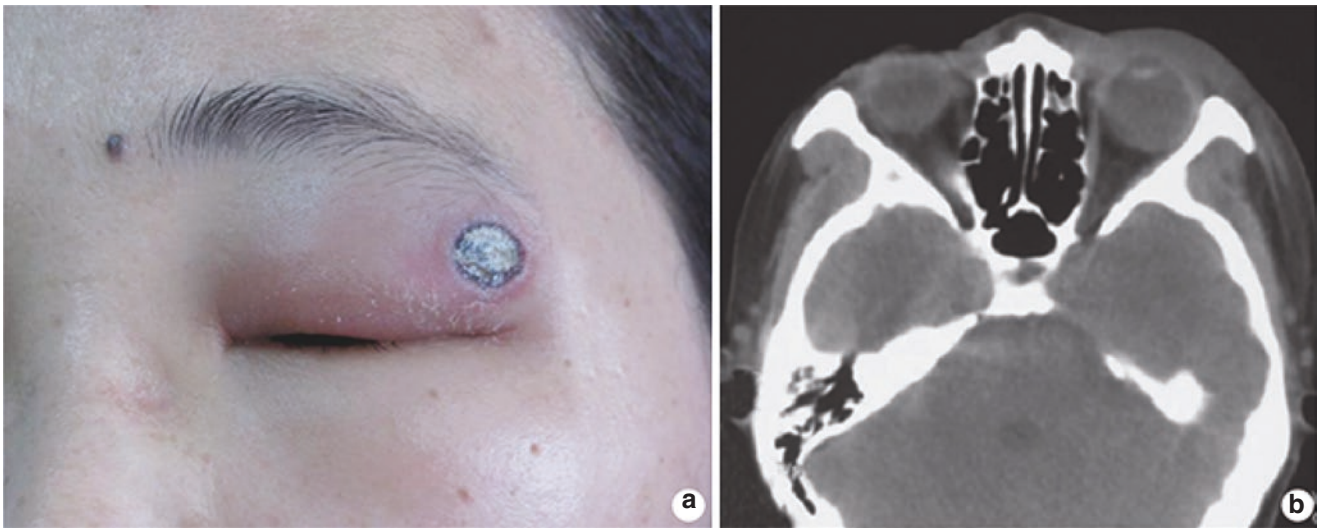

Fig. 17.1 Left eyelid inflammation (1). A 42-year-old female patient. Her left eyelid is swollen for 3 days. (**a**) The patient's left eyelid is red and swollen, with visible local necrosis; (**b**) CT shows soft tissue of left eyelid is obviously swollen, with blurred border

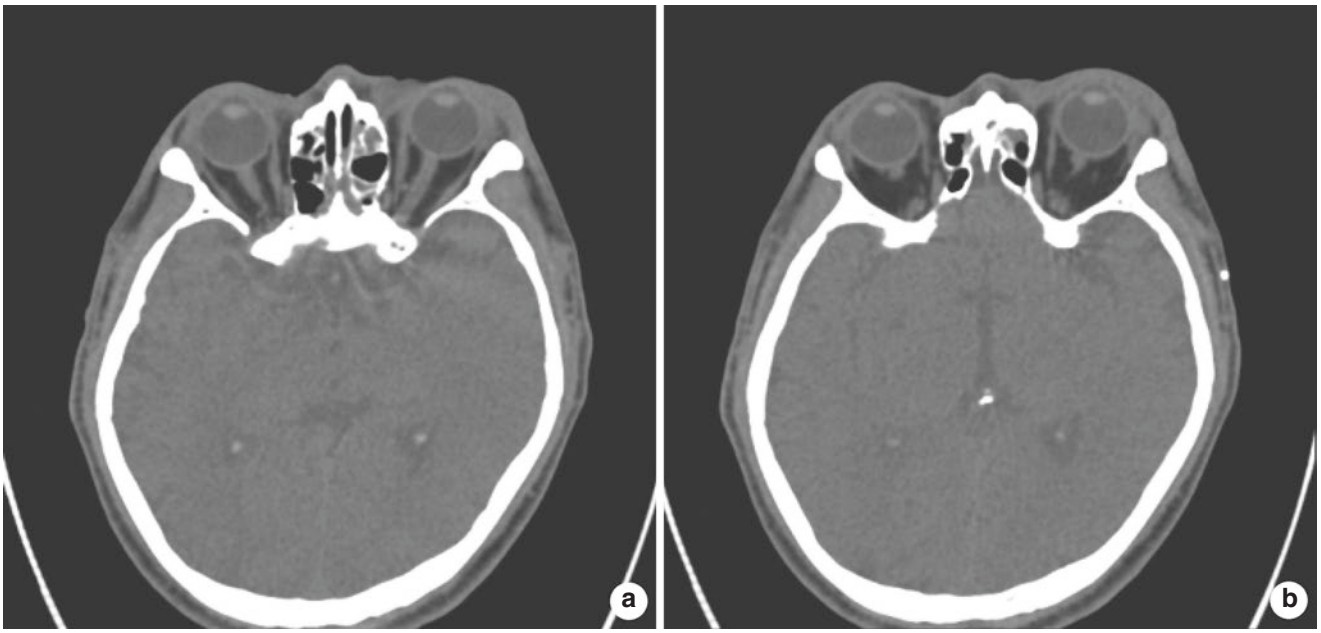

Fig. 17.2 Left eyelid inflammation (2). A 30-year-old male patient. Her left eyelid is swollen for 3 days. (**a** and **b**) CT shows soft tissue of left eyelid i obviously swollen, with blurred border

17.1.7 [Status Quo and Progress of Research]

Generally, it is not necessary to perform imaging examination for eyelid inflammatory lesions, as clinical anti-inflammatory therapy can deliver a desirable effect. Having said that, when anti-inflammatory therapy is ineffectual, CT and MR can provide guidance for clinical treatment by showing the involvement range of lesion. CT clearly shows lesion broadly involving adjacent soft tissues, wherein irregularity can be seen in bone substance of adjacent orbital wall [1].

17.2 Eyelid Xanthogranuloma

17.2.1 [Overview]

Eyelid xanthogranuloma is a chronic inflammatory change accompanied by histiocyte infiltration, involving skin and subcutaneous tissue of eyelid. It occurs rarely and is a type of non-Langerhans cell histiocytosis. The disease, with unknown cause, can invade both children and adults. Eyelid xanthogranuloma can form local lesion or part of general lesion. The prognosis, which is not consistent, can be good for occult onset and poor for invasive lesion. Among juve-

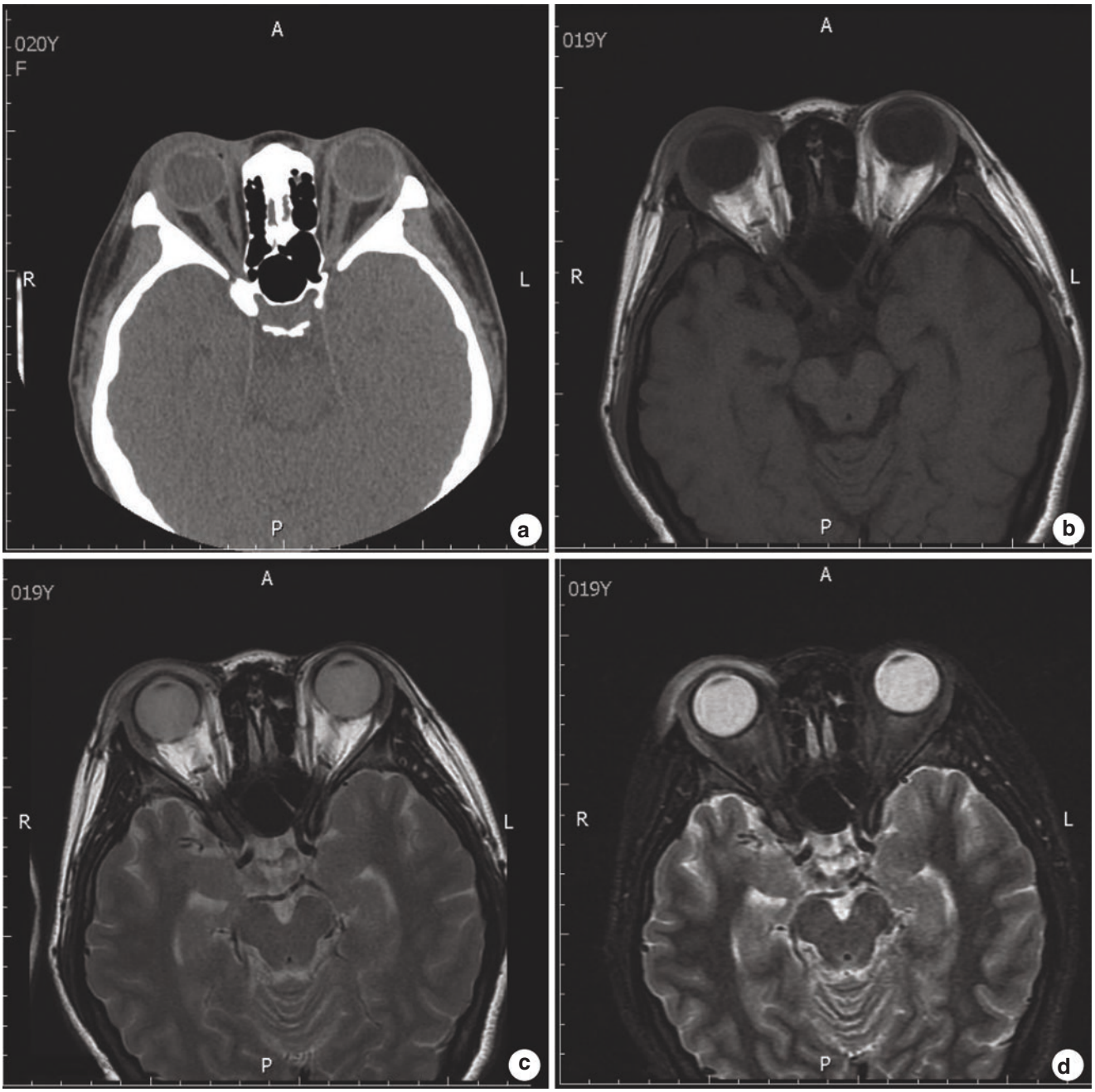

Fig. 17.3 Right eyelid inflammation. A 19-year-old male patient. His right eyelid is swollen for 3 days. (**a**) CT shows soft tissue of right eyelid is obviously swollen, with blurred border. (**b**) The thickened right eyelid shows isointense on T_1WI. (**c**) The lesion shows hyperintense on T_2WI. (**d**) The lesion shows hyperintense on T_2WI fat-suppressed sequence

niles, the disease is typically self-limited with rare systemic symptoms [2–4].

17.2.2 [Pathology Findings]

Its histocyte has rich lipid content, with small and round nucleus. Besides, there are a large number of vacuoles in the cytoplasm. It is hallmarked by the presence of scattered multi-nucleated Touton giant cells.

17.2.3 [Clinical Manifestation]

Typical manifestations of this disease include an orange-yellow bulge on eyelid, usually higher than the skin surface, accompanied by painless edema located at the upper and/or lower eyelids of both eyes. Beyond that, swelling and dislocation of lacrimal gland, as well as dry eyes, can occur [2]. The lesion can occur alone or complicated with other lesions.

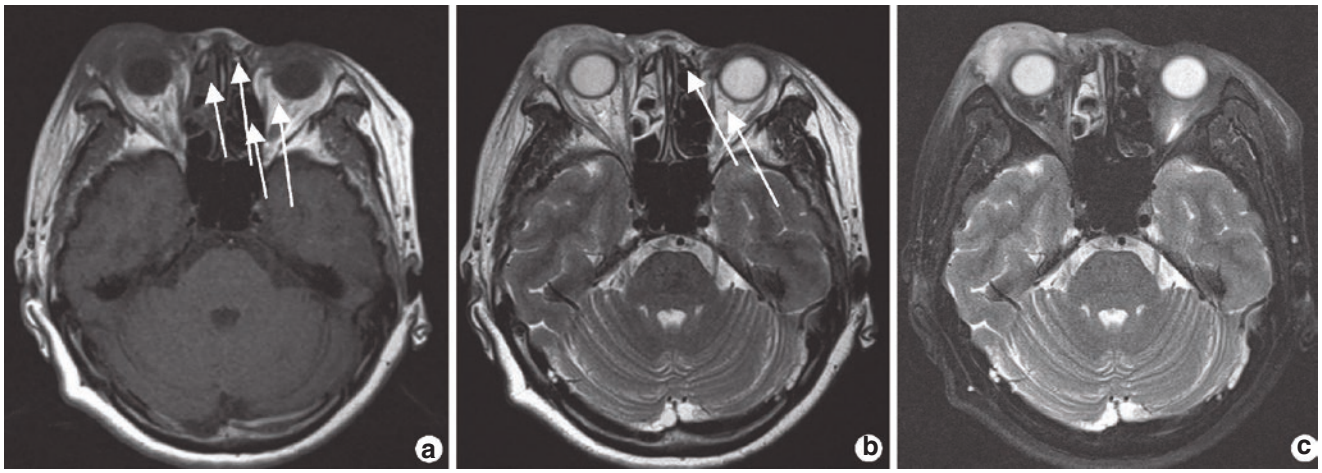

Fig. 17.4 Right eyelid inflammation and abscess. A 60-year-old female patient. Her right eyelid is swollen for 6 days. (**a**) The thickened right eyelid shows isointense on T_1WI (arrow). (**b**) The lesion shows hyperintense on T_2WI, wherein hyperintense shadow can be seen locally, suggesting abscess formation (arrow). (**c**) The lesion shows hyperintense on T_2WI fat-suppressed sequence

17.2.4 [Imaging Findings]

This disease can be manifested as diffuse thickening of unilateral or bilateral eyelid, with blurred boundary. Pre-orbital structure posterior to the lesion can be involved. Sometimes, thickening of extraocular muscle and enlargement of lacrimal gland can be observed. Bone destruction, enveloped optic nerve, and intracranial invasion are rare. Lesion area shows isointense on CT, with heterogeneous or homogeneous density, and slightly hypointense on T_1WI and T_2WI. Besides, the lesion area shows mild to moderate enhancement after enhanced scan.

17.2.5 [Key Points of Diagnosis]

1. Eyelid shows orange lump.
2. May be accompanied by other systemic lesions.
3. Eyelid is diffusely thickened with moderate enhancement, involving backwards preorbital structures.
4. Bone destruction is rare.

17.3 [Differential Diagnosis]

1. Inflammatory Pseudotumor. Most patients suffer from acute onset, accompanied by orbital pain. Affected eyelid shows no orange manifestation or other lesion manifestations. Cases with long course of disease may show hypointense area on T_2WI without enhancement.

2. Eyelid Inflammation. It is more common in children, with acute onset and severe local symptoms. Vomica is formed in swollen eyelid, manifested as low-density area on CT, and showing hypointense on T_1WI and hyperintense on T_2WI and DWI. Besides, the vomica shows ring enhancement after enhanced scan.

3. Graves' Ophthalmopathy. The lesion is mostly bilateral. Thickening of extraocular muscles, proptosis, eyelid retraction, and diffuse swelling of eyelids are rare.

4. Lymphoma. It can be manifested as thickening of eyelids and lacrimal gland enlargement, yet thickening of extraocular muscle is rare. It shows isointense on T1WI and T2WI and hyperintense on DWI.

17.3.1 [Status Quo and Progress of Research]

Adult xanthogranuloma is mainly manifested as swollen eyelid, periorbital lump and changes in skin color, typically without systemic involvement. CT and MRI mainly show involvement of soft tissues peripheral to eyelid, lacrimal gland and muscles. Diagnosis relies on pathological examination [5].

References

1. Junfang X, Dapeng S, Xiaofeng T. Imaging of the head and neck·ophthalmology. Beijing: People's Medical Publishing House; 2014.
2. Tingting W, Tingting L, Xun L, et al. Clinical analysis of adult orbital xanthogranuloma. Chinese J Ophthalmol. 2019;55(5): 381–6.
3. Jiaying Z, Jin L. Clinical advances in adult orbital xanthogranulomatous disease. Int Eye Sci. 2017;17(12):96–9.
4. Mori H, Nakamichi Y, Takahashi K. Multiple juvenile xanthogranuloma of the eyelids. Ocul Oncol Pathol. 2018;4(2):73–8.
5. Chiang E, Lissner G, Bryar PJ. Unusual presentation of xanthogranuloma on the eyelid of an adult. Ophthalmic Plast Reconstr Surg. 2014;30(6):155–6.

Lacrimal Apparatus Lesions

18

Shaowei Zheng and Lijun Wang

18.1 Dacryocystitis

18.1.1 [Overview]

Dacryocystitis can be divided into acute and chronic types. Acute dacryocystitis is caused by virulent bacteria such as *Staphylococcus aureus*, beta-hemolytic streptococcus or rare *Candida albicans*. In most cases, acute dacryocystitis is acute onset of chronic dacryocystitis, which can suddenly occur without a history of lacrimal passage. The pathogen of neonatal dacryocystitis are mostly *Haemophilus influenzae*. Chronic dacryocystitis is caused by obstruction of nasolacrimal duct and retention of dacryocyst secretions. Common pathogens are pneumococcus, streptococcus, and staphylococcus. The incidence is higher in female than in male. The cause of dacryocyst blockage in adults is unknown, which may be related to trachoma, lacrimal duct trauma, rhinitis, nasal septum deviation, and hypertrophic inferior turbinate.

18.1.2 [Clinical Manifestation]

Acute dacryocystitis features with a rapid onset, with affected eye showing congestion, lacrimation, and purulent secretions. dacryocyst is red, swollen, hot, and painful, typically involving eyelids and face. Swollen eyelid, conjunctiva hyperemia and edema, and submandibular and preauricular lymphadenectasis can occur. There may be systemic fever and discomfort. Patient with hypoimmunity or uncontrollable infection can evolve into eyelid preseptal cellulitis or abscess.

The main symptoms of chronic dacryocystitis include epiphora, and flushing and erosion of dacryocyst skin, with chronic eczema. Mucus or mucous secretions overflow from dacryon of extruded dacryocyst. If secretions in dacryocyst cannot be discharged smoothly for a long time, the dacryocyst may gradually grow bigger to form a dacryocyst bursa mucosa.

18.1.3 [Pathology Findings]

Acute dacryocystitis is mainly manifested as a large number of inflammatory cell infiltration. By naked eyes, dacryocyst with chronic dacryocystitis shows grey or grey red, mostly cystic and occasionally solid tissue mass. dacryocyst with chronic dacryocystitis shows enlargement mostly yet also atrophy occasionally. According to microscope findings, dacryocyst wall with chronic dacryocystitis is mostly thickened and rarely thinned. In some case, dacryocyst wall can be subject to degeneration, necrosis, shedding, or absence of epithelial covering. These areas are mostly characterized by diffuse infiltration of a large number of chronic inflammatory cells or polymorphonuclear leukocyte scattered infiltration. Subepithelial tissue of dacryocyst is manifested as varying degrees of thickening with chronic proliferative inflammatory cell infiltration, mainly lymphocytes, plasma cells, polymorphonuclear leukocytes, epithelioid cells and fibroblasts.

18.1.4 [Imaging Findings]

Contrast examination is not allowed to be used for acute dacryocystitis. According to CT and MRI findings, soft tissue shadow can be seen in dacryocyst area with blurred borders. The shadow shows isodense on CT, isointense on T_1WI, slightly hyperintense on T_2WI, and enhancement after enhanced scan. As the lesion evolves, abscess formation can be seen in the lesion. The lesion shows low-density on CT, hypointense on T_1WI and hyperintense on T_2WI and DWI. Patchy enhancement is shown in enhanced scan. CT and MRI can show the involvement of adjacent bone and nasolacrimal drainage channels.

S. Zheng · L. Wang (✉)
The First Hospital of Dalian Medical University, Dalian, China

H. Li et al. (eds.), *Radiology of Infectious and Inflammatory Diseases - Volume 2*,
https://doi.org/10.1007/978-981-16-8841-6_18

Chronic dacryocystitis is manifested as monosaccate or multisaccate dacryocyst enlargement on angiogram and MRI hydrography. It can atrophy and shrink after fibrous tissue proliferation and cicatrization. Lacrimal ductule is often dilated. Nasolacrimal duct is narrowed or has irregular borders. Contrast agent stagnates or suspends, and emptying is delayed, manifested as stenosis or blockage of lacrimal passage. When complicated by dacryolith, filling-defect shadows of dacryocyst and nasolacrimal duct can be observed. CT shows that soft tissue in dacryocyst area is thickened, with rough borders and showing isodense. Besides, CT also shows the sclerosis and thickening of adjacent bones and high-density dacryolith shadow in case of dacryolith formation. It shows hypointense on MRI T_1WI and hyperintense on T_2WI and DWI (Figs. 18.1, 18.2 and 18.3).

18.1.5 [Key Points of Diagnosis]

1. Acute dacryocystitis has marked inflammatory signs, while chronic dacryocystitis can relapse, with epiphora as clinical manifestation.
2. CT and MRI show soft tissue shadows in dacryocyst area, with coarse borders. Enhanced scan shows irregular patchy enhancement. Chronic patients may show sclerosis and thickening of adjacent bones.
3. Dacryocyst enlargement and lacrimal duct obstruction are quite common among chronic patients based on contrast examination.

18.1.6 [Differential Diagnosis]

The disease needs to be distinguished from tumor in dacryocyst area, of which the most common one is dacryocyst cancer, manifested in early stage as nodular, hard lump that grows bigger over time. With long course of disease, destruction can be seen in adjacent bones. Enhanced scan shows marked enhancement. Radiography of lacrimal duct shows filling-defect.

18.1.7 [Status Quo and Progress of Research]

Dacryocystitis is lacrima retention and infection caused by nasolacrimal duct blockage. Currently, low-dose spiral computed tomography-dacryocystography (CT-DCG) with reconstruction at coronal plane, and sagittal plane is an

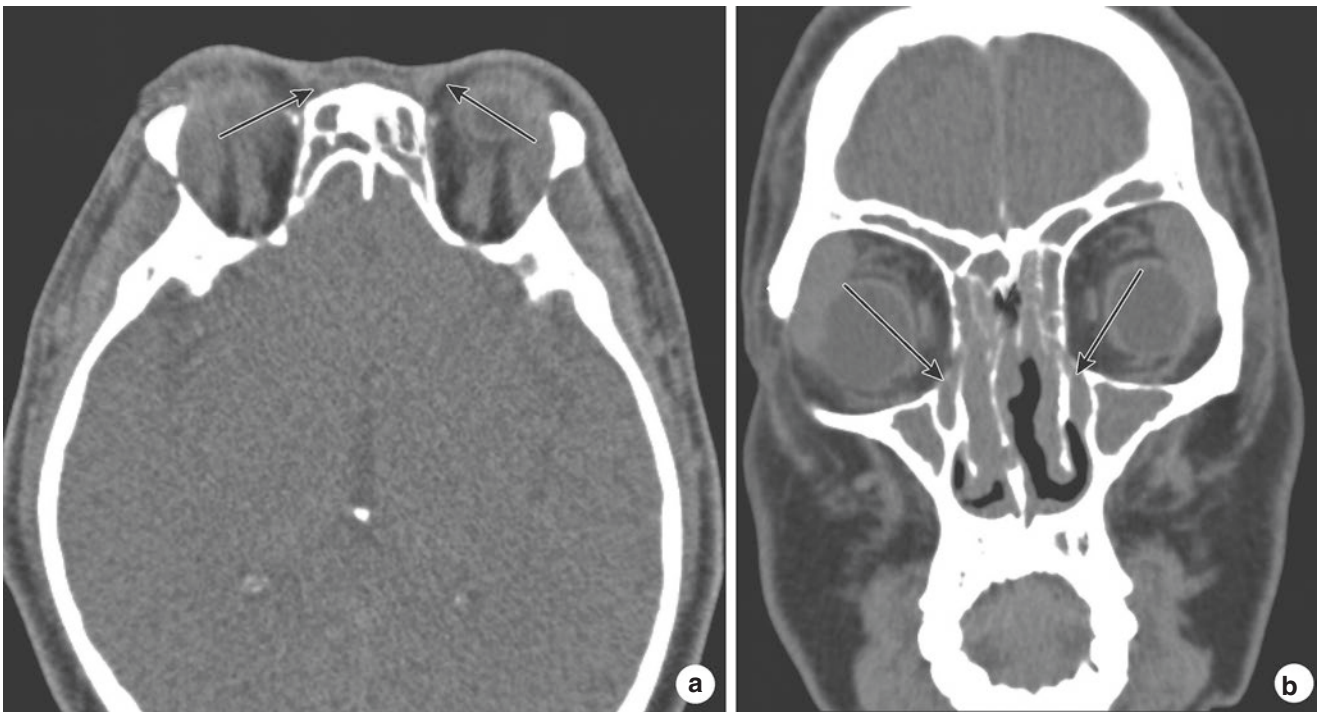

Fig. 18.1 Chronic inflammation of nasolacrimal duct and dacryocyst. A 43-year-old female patient. Bilateral epiphora relapsed for years. (**a** and **b**) CT soft tissue windows at coronal plane and transverse plane show thickening of bilateral dacryocysts (arrow **a**) and soft tissue shadow of nasolacrimal duct (arrow **a**). Contrast agent remains in dacryocyst area (**a** is soft tissue window and **b** is bone window), suggesting obstructed nasolacrimal duct, chronic nasolacrimal duct inflammation, and dacryocystitis

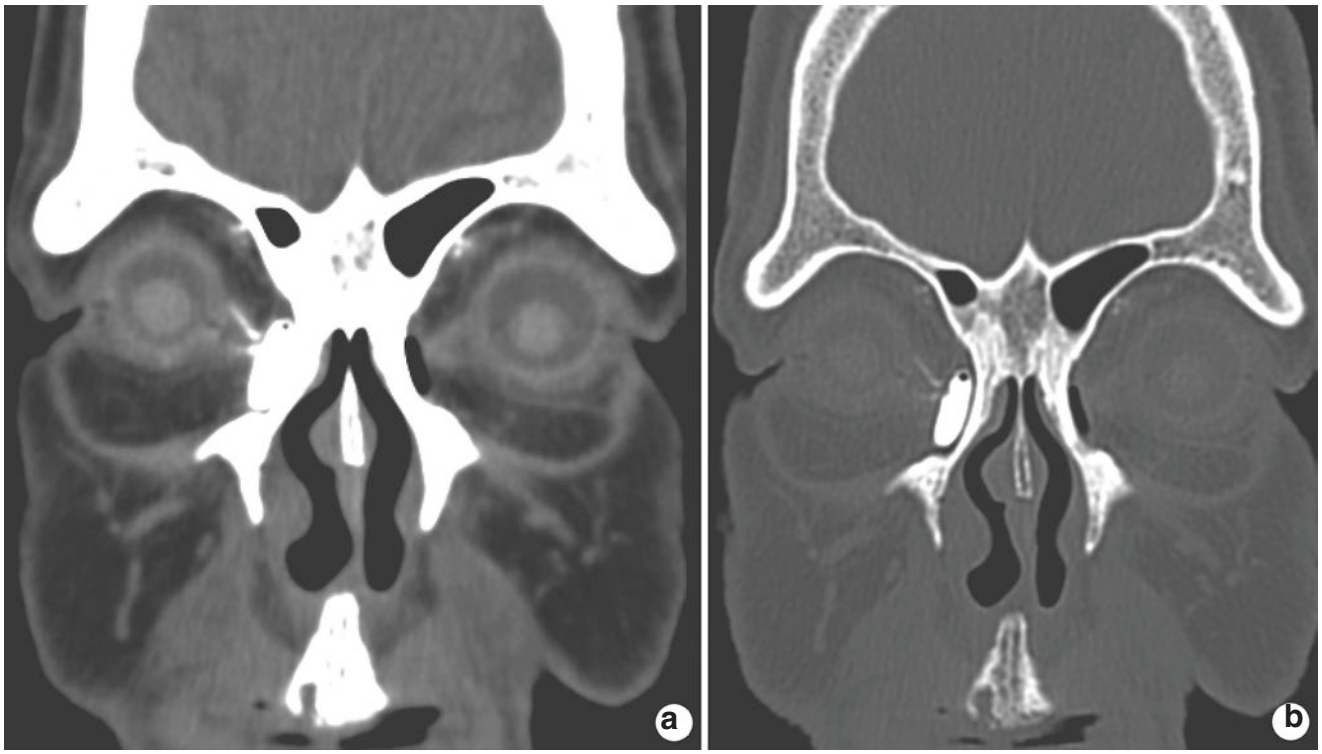

Fig. 18.2 Chronic inflammation of right nasolacrimal duct and dacryocyst. A 35-year-old male patient. Right epiphora relapsed for years. (**a** and **b**) According to radiography of nasolacrimal duct, contrast agent remains in dacryocyst area, suggesting obstructed nasolacrimal duct, chronic nasolacrimal duct inflammation, and dacryocystitis

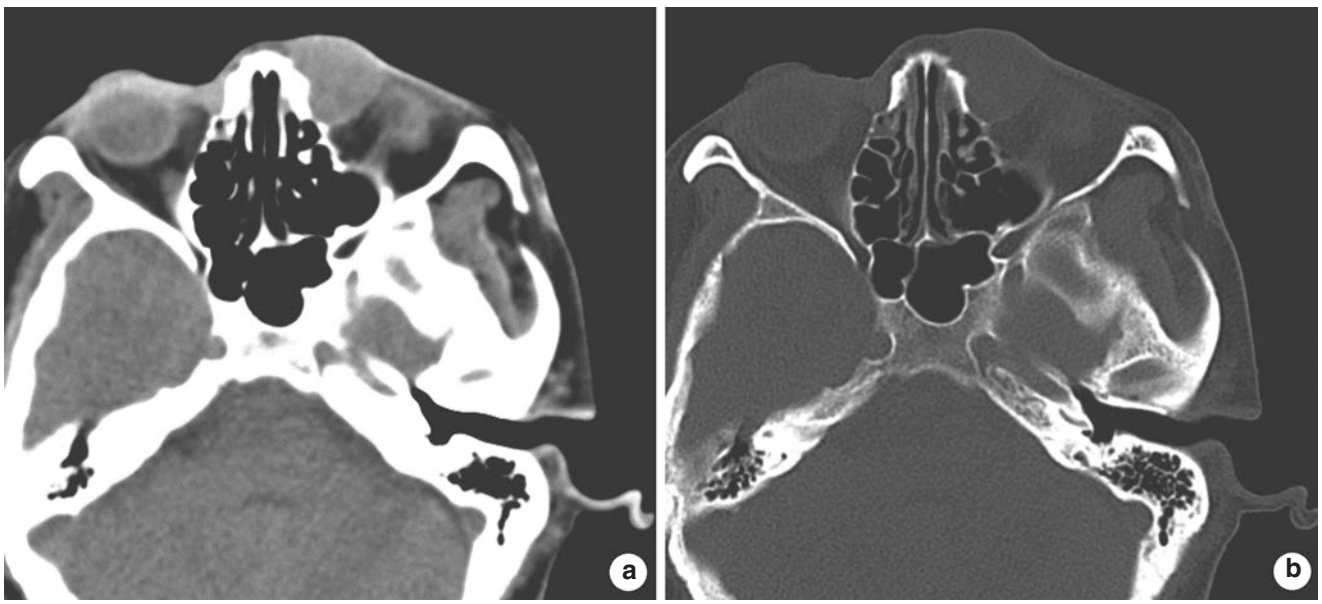

Fig. 18.3 Chronic inflammation of left dacryocyst. A 27-year-old male patient. Left epiphora relapsed for years. (**a**) CT soft tissue window at transverse plane shows soft tissue shadows of left dacryocyst area, with blurred border, and thickened left nasolacrimal duct. (**b**) CT bone window at transverse plane shows no abnormity in adjacent bones

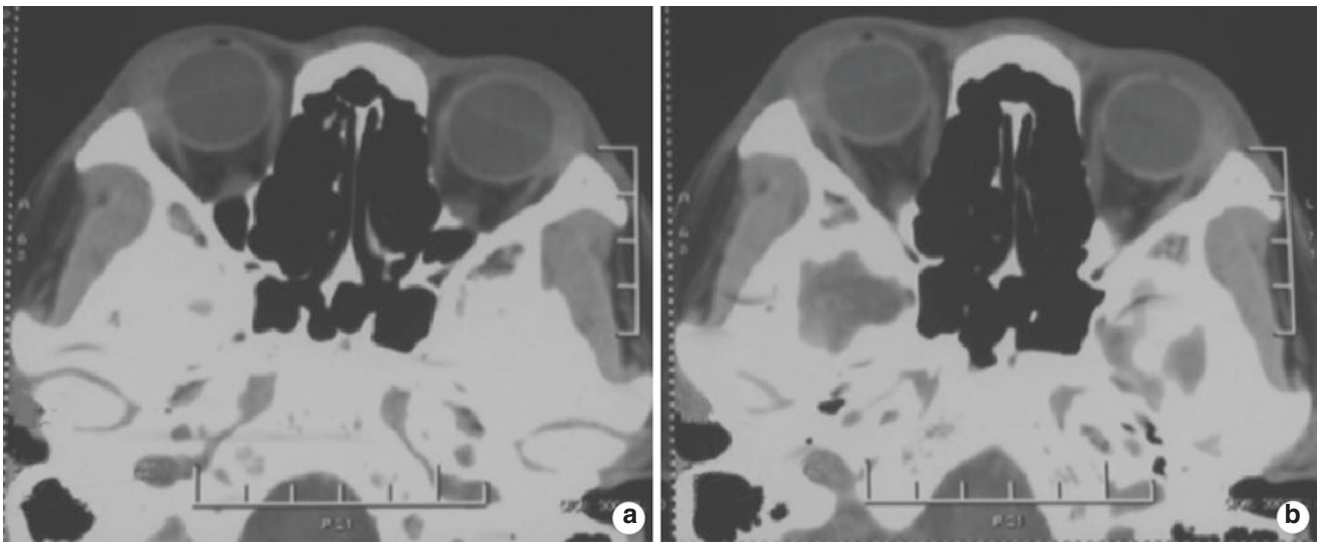

Fig. 18.4 Bilateral dacryoadenitis. A 35-year-old female patient. (**a** and **b**) CT shows enlargement of bilateral lacrimal glands, with blurred borders and swollen bilateral eyelids

ideal low-radiation imaging technique for nasolacrimal duct obstruction. By displaying all the relevant anatomical signs of dacryocystorhinostomy, spiral CT-DCG enables surgeons of head and neck to better plan the procedure. CT imaging after radiography of nasolacrimal duct is mainly used for displaying the involvement range of the inflammation [1].

18.2 Dacryoadenitis

18.2.1 Acute Dacryoadenitis

18.2.1.1 [Overview]

Acute dacryoadenitis is mostly caused by pathogen infection, wherein the pathogen is typically *Staphylococcus aureus* or pneumococcus, occasionally certain viruses, and rarely fungi. Acute dacryoadenitis is a simple inflammation, more common in children and young adults. Unilateral lesion is common and bilateral rare.

Acute dacryoadenitis is typically characterized by unilateral acute onset, red and swollen upper eyelid, conjunctival congestion, and shifting of eyeball inwards and downwards. Patients often suffer from discomfort and fever. Persistent inflammation can evolve into subacute or chronic dacryoadenitis and even intraorbital cellulitis or sepsis in severe cases. For this reason, early diagnosis is very important.

18.2.1.2 [Pathology Findings]

Acute dacryoadenitis is mainly manifested as a large number of inflammatory cell infiltration, with enlarged lacrimal gland.

18.2.1.3 [Imaging Findings]

Clinical diagnosis of acute dacryoadenitis is easy and does not rely on imaging examinations, which is attributed to the typical symptoms of the disease. Imaging examination mainly aims to judge the range of lesion and make differential diagnosis. CT is the preferred, showing swollen and enlarged lacrimal gland and isodense, with blurred border and reduced density of adjacent soft tissue (Fig. 18.4). It shows hypointense on MRI T_1WI, diffusely hyperintense on T_2WI, and hyperintense on DWI, with blurred border. Fat-suppressed sequence shows clearly (Fig. 18.5).

18.2.1.4 [Key Points of Diagnosis]

1. Children and young adults.
2. Acute onset and inflammatory signs.
3. Image findings show that the lacrimal gland is enlarged, border is coarse, and orbital wall bone is not involved.

18.2.1.5 [Differential Diagnosis]

1. Eyelid Abscess. Imaging examination shows eyelid thickening, unclear borders, vomica formation, swollen adjacent soft tissues, and increased density of subcutaneous fat. Besides, the lacrimal gland is normal in most cases.

2. Lacrimal Gland Tumor. Onset is relatively slow, and borders of benign tumors are clear. CT and MRI show soft tissue mass, and enhanced scan shows marked homogeneous enhancement. Borders of malignant tumor are indefinite, with irregular morphology. Adjacent bone structures are destroyed.

3. IgG4-Related Disease. It mainly involves multiple parts, including lacrimal gland, extraocular muscle and infraorbital nerve, in a symmetrically bilateral manner. Hormone therapy is effective.

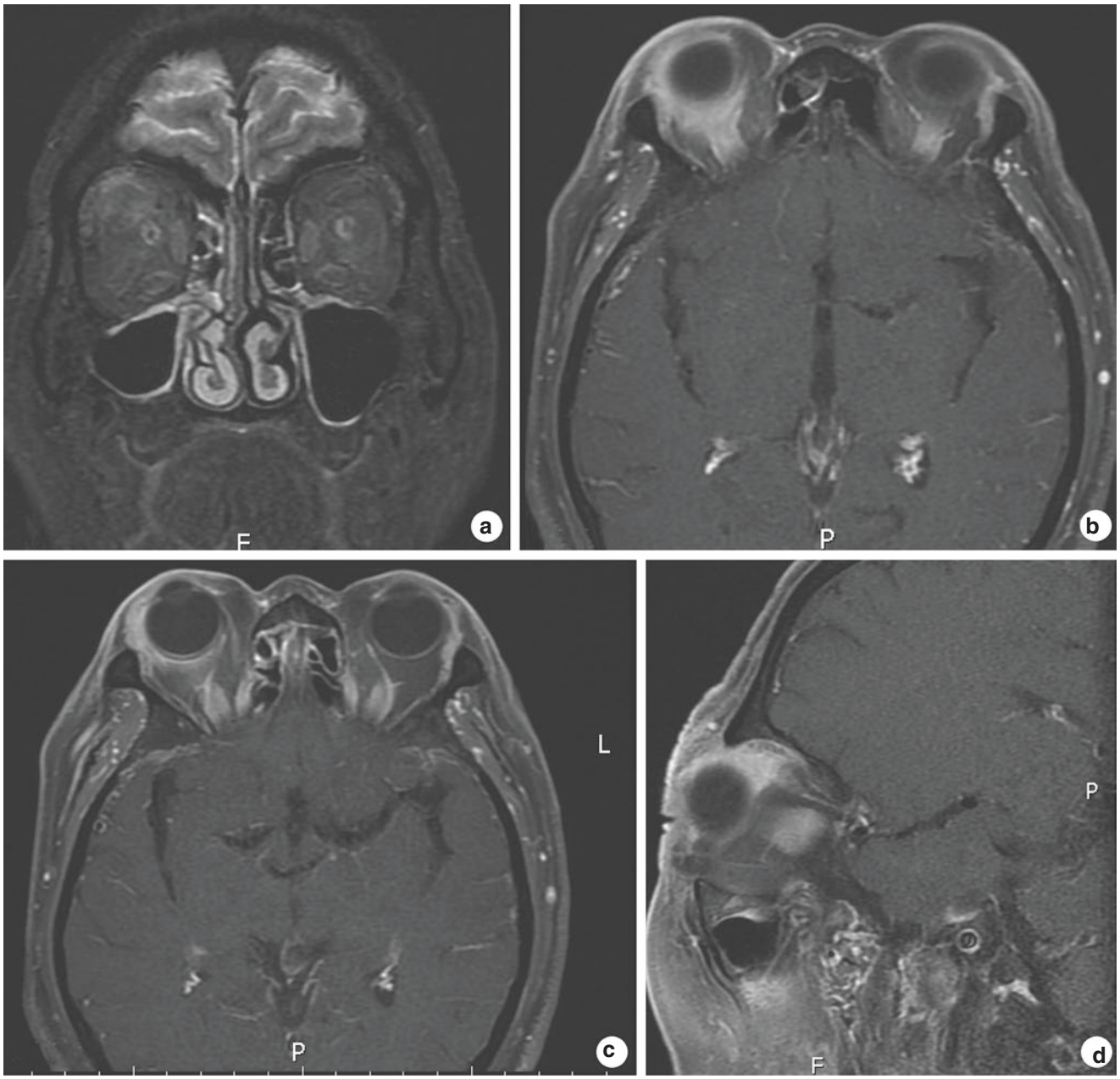

Fig. 18.5 Acute right dacryoadenitis. (**a**) MRI T_2WI coronal fat-suppressed sequence shows increased right lacrimal gland signal. (**b–d**) MRI enhanced scan shows marked enhancement of right lacrimal gland

18.2.2 Chronic Dacryoadenitis

18.2.2.1 [Overview]

Chronic dacryoadenitis is a proliferative inflammation with slow disease course. It typically involves bilaterally, yet unilateral involvement can also occur. Acute dacryoadenitis can evolve into chronic dacryoadenitis. But in most cases, chronic dacryoadenitis is primary, common in benign lymphocyte infiltration and tuberculosis. The disease can also involve lacrimal gland.

18.2.2.2 [Clinical Manifestation]

Chronic dacryoadenitis typically involves bilaterally, with slow progression. It can occur repeatedly. A lobulated painless mass is formed on the superolateral part of the eyelid, which is soft with good mobility. Proptosis and lacrimation are rare. Hormone therapy is effective for dacryoadenitis inflammatory pseudotumor. Histopathological examination for dacryoadenectomy can help diagnose.

18.2.2.3 [Pathology Findings]

Both enlargement or atrophy of lacrimal gland can occur. According to microscope findings, lacrimal gland shows degeneration and necrosis. These areas are mostly characterized by diffuse infiltration of a large number of chronic inflammatory cells or polymorphonuclear leukocyte scattered infiltration.

18.2.2.4 [Imaging Findings]

Lacrimal gland is increased diffusely. It may extend forwards and beyond orbital margin, or course backwards along orbital lateral wall or lateral rectus. Swollen lacrimal gland envelops eyeball, uniform with the contour of peripheral structures, and may be accompanied by peripheral structure inflammation. The lesion has blurred border, without compression on orbital wall bone or invasive changes. The lesion in lacrimal gland shows isodense on CT, isointense on MRI T1WI, slightly hypointense on T_2WI sometimes, isointense or slightly hyperintense on DWI, and marked enhancement after enhanced scan.

18.2.2.5 [Key Points of Diagnosis]

1. A painless mass is formed on the superior lateral part of the eyelid, which develops slowly and can occur repeatedly.
2. Image findings show that the bilateral lacrimal glands are enlarged, typically free from bone changes in orbital wall.
3. Hormone therapy is effective.

18.2.2.6 [Differential Diagnosis]

1. Lacrimal Gland Tumor. It usually grows unilaterally, manifested as a lump, which can press eyeball sometimes and contort muscle cone structures, resulting in sunk orbital wall or bone destruction. Besides, it has round contour and typically does not envelop eyeball.

2. Lymphoproliferative Lesion. It can be unilateral or bilateral, with similar findings as inflammatory pseudotumor on CT or MRI, which makes differentiation difficult. Due to the lack of specific imaging findings, differentiation can only rely on biopsy or follow-up observations.

3. Mikulicz's Disease. Currently, Mikulicz's disease cannot be differentiated from dacryoadenitis inflammatory pseudotumor based on imaging findings alone, so any suspected lacrimal gland lesion shall be subject to biopsy.

4. IgG4-Related Disease. It mainly involves multiple parts, including lacrimal gland, extraocular muscle and infraorbital nerve, in a symmetrically bilateral manner. Hormone therapy is effective.

18.2.2.7 [Status Quo and Progress of Research]

Definitive diagnosis for acute and chronic dacryoadenitis can be made according to typical clinical manifestations, thus do not require imaging examinations. CT and MRI mainly aim to evaluate the nature of lesion with poor therapeutic effect or make differential diagnosis. Dacryoadenitis can be bilateral or unilateral, mainly manifested as diffuse swelling of bilateral lacrimal glands with unclear borders. The main difference from inflammatory pseudotumor or IgG4-related diseases lies in that dacryoadenitis shows hyperintense on MRI T2WI, whereas the latter two diseases show isointense on MRI T2WI and remarkably limited diffusion on ADC [2].

References

1. Heichel J, Struck HG, Hammer T, et al. Pediatric acute dacryocystitis due to frontoethmoidal mucocele. HNO. 2019;67(6):458–62.
2. Tomita M, Shimmura S, Tsubota K, et al. Dacryoadenitis associated with Acanthamoeba keratitis. Arch Ophthalmol. 2006;124(9):1239–42.

Post-Traumatic Infection

19

Shaowei Zheng and Lijun Wang

19.1 [Overview]

Ocular trauma, an ophthalmic emergency, often leads to visual impairment and is a main culprit of blindness. It is more common in male. Ocular trauma infection can be very tricky. The condition develops rapidly, causing great damage to ocular tissues and visual function, even threatening life without timely treatment. Normally, eyelid skin and ocular surface structures are anatomical barriers against microorganisms. Lymphocytes and Langerhans cells in cornea and conjunctiva tissues, and lysozyme, gamma globulin and other antibacterial components in tears collectively form the first defensive barrier for ocular surface. Ocular trauma destroys such defensive function, resulting in infections under the action of pathogenic microorganisms. The main pathogenic bacteria include staphylococcus, streptococcus, and fungi. Eye infections caused by trauma include dacryocystitis, dacryoadenitis, keratitis, endophthalmitis, intraorbital cellulitis [1–3].

19.2 [Clinical Manifestation]

1. General Reactions. General reactions after infection include fever or hypothermia, increased heart rate, and polypnea. Generally, fever can occur in the wake of inflammatory reaction caused by trauma. Infection may happen, however, if the high body temperature does not subside for more than 3 days, or continues to rise, or hypothermia occurs accompanied by increased heart rate and respiratory rate with no specific cause and peripheral hemangiectasis. Drop of blood pressure in patients with infection suggests severe sepsis and septic shock, a warning of critical condition.

2. Local Symptoms. Common features of local infections are local redness, swelling, heat, pain, and dysfunction, which can be expressed as cellulitis or pyogenic infection, or both of them.

Local clinical manifestations caused by ocular trauma vary by injured parts. Infectious keratitis is manifested as impaired vision, photophobia, lacrimation, and other symptoms of eye irritation, as well as corneal infiltrate and ulceration. Traumatic endophthalmitis is mainly manifested as ocular pain and impaired vision. Physical examination can show eyelid and conjunctival congestion and edema, cotton-wool exudate and empyema in anterior chamber, ring ulcer or purulency in cornea, fibrin exudate in crystalline lens, flocculent turbidity or empyema in vitreous body, retinal hemorrhage, formation of infiltrating plaque and other signs. Panophthalmitis can be manifested as ocular muscle dyskinesia, proptosis, decreased vision, and increased intraocular pressure. The incubation period of bacterial infection is short, while that of fungal infection is long. The incidence of endophthalmitis after ocular rupture is 3% to 7% and is significantly higher among cases with intraocular foreign body. Foreign bodies, including wood, organic matter, and steel, have been reported to cause endophthalmitis. Lens rupture is the highest infection risk factor in the evaluation of clinical risk factors.

19.3 [Imaging Findings]

1. CT Examination. Tomography combined with 3D reconstruction can clearly show whether there is a fracture, the extent of the fracture, and the presence of a foreign body. It is especially helpful for detecting positive foreign bodies and showing the infiltration range of local infection. The combined infection of eyelid, eyeball, retrobulbar area, and lacrimal gland after trauma is manifested as diffuse soft tissue swelling with unclear borders. Enhanced scan shows marked enhancement with blurred border (Fig. 19.1).

Orbital abscess is manifested as clear borders, low-density lesion in central necrosis, no enhancement in enhanced scan,

S. Zheng · L. Wang (✉)
The First Hospital of Dalian Medical University, Dalian, China

H. Li et al. (eds.), *Radiology of Infectious and Inflammatory Diseases - Volume 2*,
https://doi.org/10.1007/978-981-16-8841-6_19

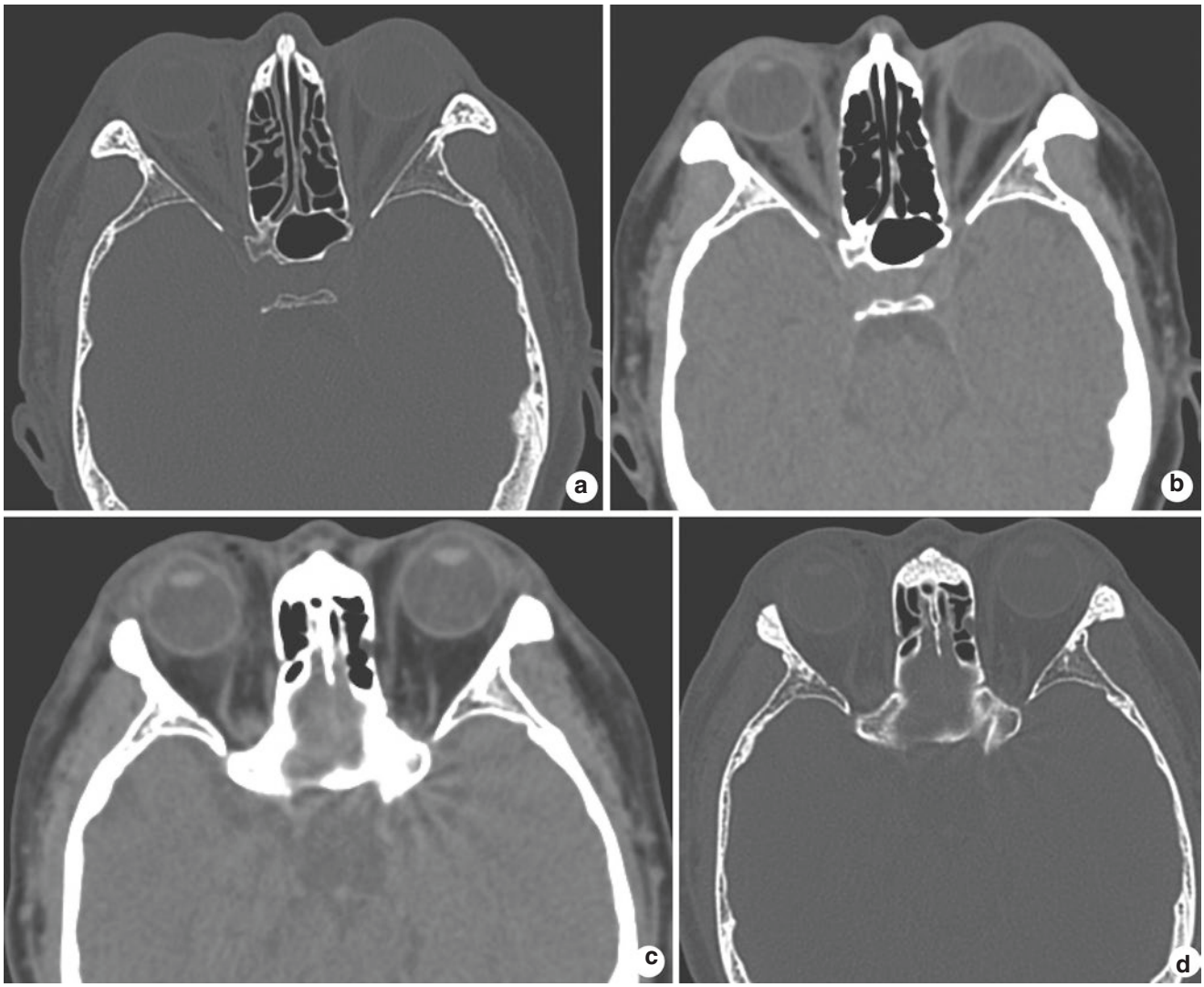

Fig. 19.1 Post-traumatic right periorbital and retrobulbar cellulitis. A 43-year-old male patient. Eyes were injured by hydraulic oil 27 days ago, accompanied by obvious redness and swelling of right eyelid for 8 days. (**a**–**d**) CT shows that right eyelid soft tissue is swollen, multiple gas density shadows are visible in retrobulbar and intraorbital areas, and retrobulbar fat spaces are blurred. Optic nerve is thickened and swollen

and band-like enhancement in peripheral area, which may be accompanied by fat linear shadows and thickened extraocular muscles.

2. MRI Examination. Do not apply MRI for cases with intraocular foreign body to prevent the foreign body from moving. Ultrasound can also be used for evaluation. MRI is mainly used to evaluate the presence of infection after trauma. If infection occurs, eyelids, eyeballs, and lacrimal glands show diffusely hyperintense on T2WI and hyperintense on DWI. Enhancement examination is mainly used to evaluate the presence of abscess, wherein any abscess formed can result in ring enhancement (Fig. 19.2).

19.4 [Key Points of Diagnosis]

1. In case of any specific trauma history, clinical symptoms include local or systemic infection such as fever, local redness, pain, and discharge from the wound.
2. CT and MRI show swelling of local soft tissue, while enhanced scan shows abscess formation. But in an early stage of inflammation, the manifestations have no specificity.

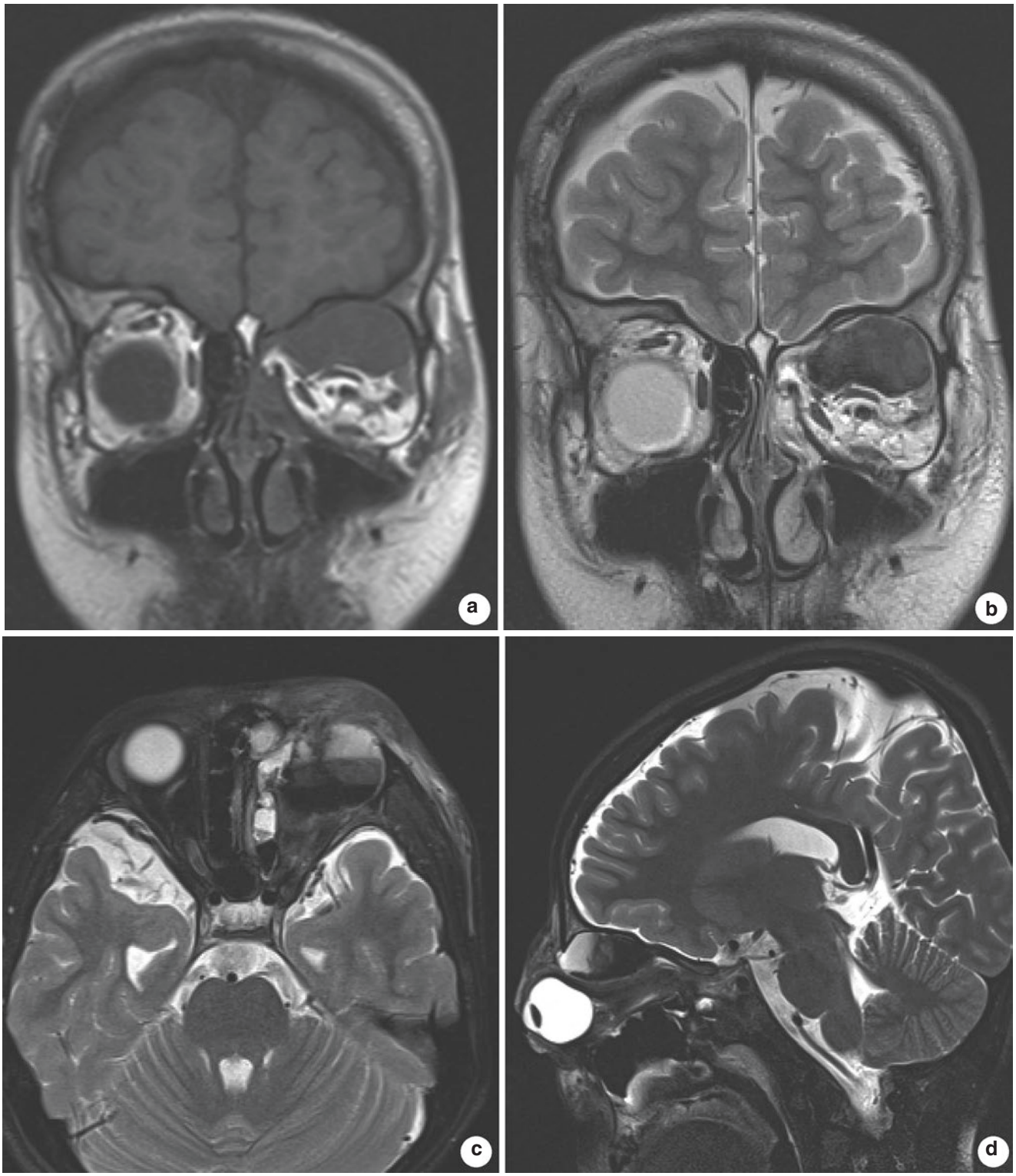

Fig. 19.2 Post-traumatic left superior wall subperiosteal abscess and periorbital cellulitis. A 12-year-old male patient. The patient went through acute onset, with red, swollen eyes for 5 days and proptosis for 4 days. He also has history of trauma. (**a**–**d**) MRI shows that irregular, abnormal signal shadow can be seen at inferior border of left superior wall, showing hypointense on T_1WI. The lesion is stratified as upper, middle, and lower layers on T_2WI, respectively showing hyperintense, isointense, and hypointense. Left eye proptosis, with slightly sunken eyeball moving along lateral inferior direction under the action of compression. Left periorbital subcutaneous soft tissue shows irregular hyperintense on T2WI. Frontal sinus and left ethmoidal sinus shows hyperintense on T2WI

19.5 [Differential Diagnosis]

This disease shall be differentiated from benign & malignant tumors and proliferative lesions of all kinds, based on medical history and relevant clinical examinations combined. Benign & malignant tumors and proliferative lesions are mainly manifested as lumps, with non-swollen adjacent soft tissues. Enhanced scan shows mild to moderate enhancement without vomica. The patient has no history of trauma, or symptoms of redness, swelling, heat, and pain.

19.6 [Status Quo and Progress of Research]

The disease mainly employs MR for functional imaging. DWI is sensitive to abscess formation, showing remarkably hyperintense. ADC value is decreased. MRS shows that characteristic amino acid peak is formed in abscess, wherein acetate peak, succinate peak and alanine peak are common [1–5].

References

1. Maonian Z. Traumatology of eye. Beijing: Military Medical Science Press; 2006.
2. Lianyang Z. Attach importance to imaging diagnosis of infection source after severe trauma. Chinese J Clin. 2011;5(8):2167–70.
3. Yin B, Jun W, Jin L, et al. Clinical analysis for otorhinolaryngology head and neck trauma. Inner Mongolia Med J. 2006;38(2):166–8.
4. Zubing L. Surgery of oral and maxillofacial trauma. Beijing: People's Medical Publishing House; 2011.
5. Yongquan T, Dongyi H, Fanglu C, et al. Otorhinolaryngology head and neck surgery. 8th ed. Beijing: People's Medical Publishing House; 2013.

Part IV

Infectious and Inflammatory Diseases of Ear

Otitis Media

20

Meizhu Zheng, Ya'nan Lyu, Jingshi Wang, and Shuang Xia

20.1 Secretory Otitis Media

20.1.1 [Overview]

Secretory otitis media is a non-purulent acute or chronic inflammation characterized by effusion in the tympanic cavity and hearing loss. It frequently occurs in winter and spring, in the wake of cold imperceptibly [1]. Pathogenesis: When adenoid hypertrophy, nasopharynx lymphoid tissue hyperplasia and nasopharynx tumors occur, auditory tube is blocked, and air in tympanic cavity and mastoid air cell is gradually absorbed, forming negative pressure and leading to expansion, swelling and infiltration of mucosal capillaries. Besides, effusion in tympanic cavity can occur due to a higher level of mucosal gland secretion.

Both children and adults can suffer from the disease. Common clinical symptoms include ear distention and congestion, hearing loss and tinnitus. Children may also become slow to react or absent-minded. Otoscope examination shows concave and congestive tympanic membrane and reticular expansion in peripheral blood vessels, wherein air bubbles may appear sometimes. As effusion accumulates, tympanic membrane gradually bulges outwards, wherein fluid can be extracted by puncture. At advanced stage, tympanic membrane is thickened, characterized by dark, turbid color, atrophy, thinning, extreme invagination and adhesion. Tuning fork and pure tone test show conductive deafness. In an early stage, acoustic immittance measurement shows C-shaped curve when tympanic cavity is under negative pressure and B-shaped curve when effusion occurs in tympanic cavity.

20.1.2 [Pathology Findings]

Middle ear mucosal epithelium is thickened and goblet cells increase, with a high level of secretion. Pathological gland-like tissues form inferior to epithelium. Infiltration dominated by lymphocytes and plasma cells appears peripheral to lamina propria blood vessels. The lesion may persist without timely treatment. In chronic stage, ossicular chain adhesion and fixation can occur due to fibrous tissue proliferation, resulting in persistent hearing loss, adhesive otitis media, or cholesteatoma caused by secondary infection [1].

20.1.3 [Imaging Findings]

1. X-ray. In case of poor pneumatization of mastoid process, the patient's plain film for temporal bone only shows decreased permeability of mastoid antrum and tympanic cavity. In case of good pneumatization of mastoid process, X-ray plain film shows dense tympanic cavity and mastoid antrum, thickened mastoid atrial septum and blurred contour, free of bone destruction [2].

2. CT Examination. The above changes are shown more clearly. Tympanic cavity is normal in size, morphology, and development, with complete ossicular chain and regular position. Air in tympanic cavity, mastoid antrum and mastoid air cell may fully or partially disappear, while atrial septum exists, air-fluid level is visible and tympanic membrane is intact. There is no bone destruction [3] (Fig. 20.1).

3. MRI Examination. MRI mainly displays changes in effusion in tympanic cavity, mastoid antrum and mastoid air cell, showing isointense or hypointense on T_1WI, hyperintense on T_2WI with no restricted diffusion on DWI. After enhanced scan, mucous membranes of tympanic cavity,

M. Zheng
Tianjin Third Central Hospital, Tianjin, China

Y. Lyu
Dalian Municipal Central Hospital, Dalian, China

J. Wang (✉)
Dalian Women and Children Medical Center, Dalian, China

S. Xia
Tianjin First Central Hospital, Tianjin, China

H. Li et al. (eds.), *Radiology of Infectious and Inflammatory Diseases - Volume 2*,
https://doi.org/10.1007/978-981-16-8841-6_20

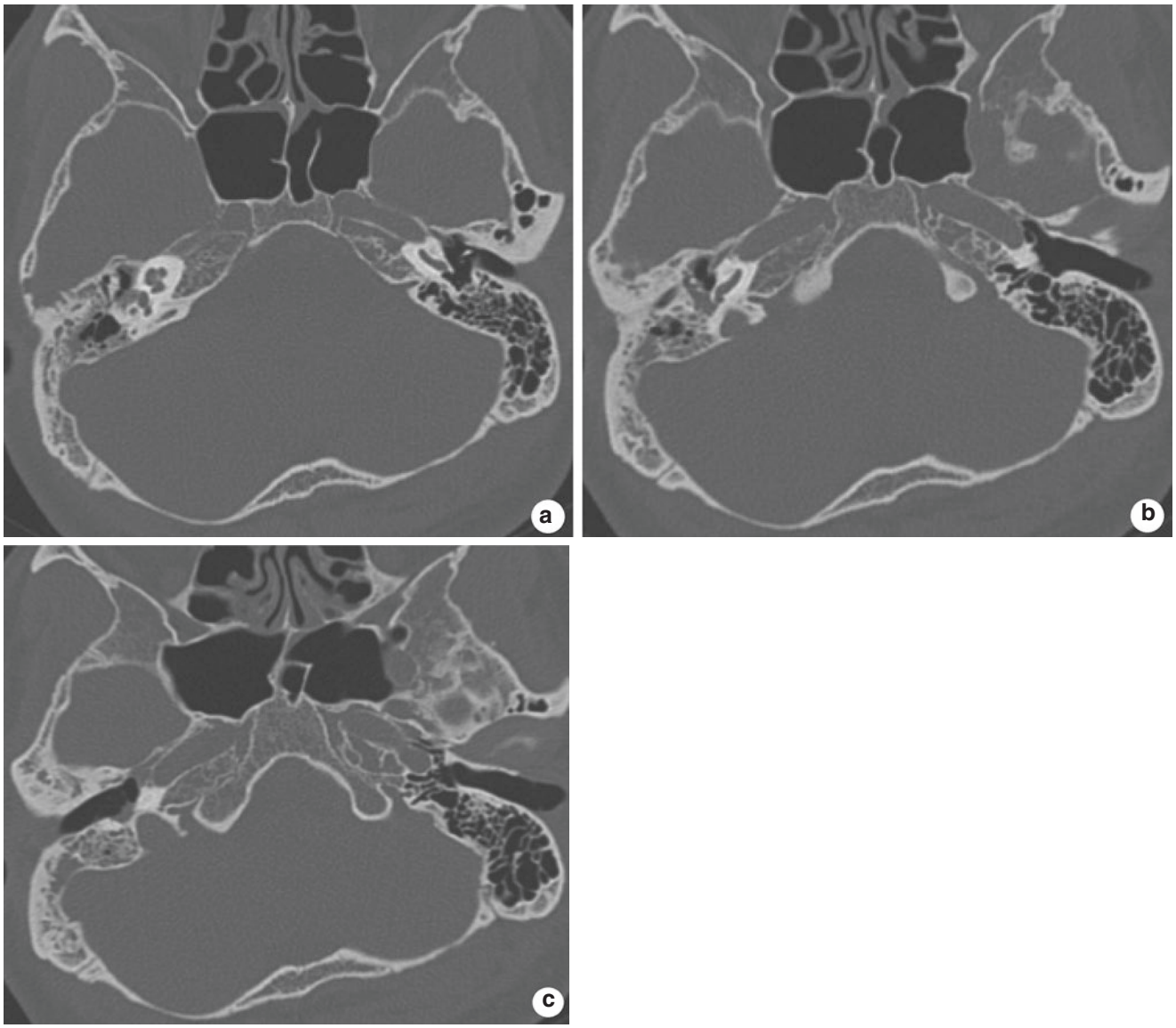

Fig. 20.1 Secretory otitis media. A 35-year-old male patient. He suffered from repeated distention at right ear for 15 years. History: The patient received grommet insertion at right ear. Repeated tympanocentesis at right ear shows no obvious effect. Clinical diagnosis: Right secretory otitis media (**a**). The tympanic cavity of right middle ear records that density is partially increased, shadow of air density is reduced, and right ossicular chain is partially enveloped, with intact bone structure. (**b** and **c**) CT of temporal bone shows poor pneumatization of right mastoid, some soft tissue density shadow can be seen in mastoid air cell, and bone septum is intact; The right inferior tympanic membrane is thickened and right facial nerve canal is intact

mastoid antrum and mastoid air cell show no thickening or enhancement.

20.1.4 [Key Points of Diagnosis]

1. Clinical manifestations include ear distention, ear swelling and hearing loss. It is typically accompanied by infection in other parts.
2. CT shows absence of air in the middle ear cavity and visible soft tissue density, without bone destruction.

20.1.5 [Differential Diagnosis]

Acute suppurative otitis media: Common in children; With acute onset, the patient normally has otalgia, with history of pus discharge. Physical examination shows punctured tympanic membrane. CT findings show diffuse slightly hyperintense in mastoid cavity of the middle ear. In the early stage, air cell septa are typically intact, while in advanced stage, air cell may be shrunk or damaged, forming big low-density cavity. Sometimes osteomyelitis or abscess may appear as the disease progresses [4].

20.1.6 [Status Quo and Progress of Research]

Temporal bone CT scan shows shadows with homogeneous density in tympanic cavity, which is not enlarged. However, this is not a routine examination [5]. Despite evaluating otitis media mastoiditis, imaging examination of secretory otitis media also aims to observe any lesions in nasopharynx, such as nasopharyngeal lymphadenia and nasopharyngeal cancer. Nasopharyngeal endoscopy and MRI examination should be performed in case of any suspected lesion in nasopharynx.

20.2 Suppurative Otitis Media

20.2.1 Acute Suppurative Otitis Media

20.2.1.1 [Overview]

As a common inflammation of middle ear mucosa in clinic, acute suppurative otitis media can occur in healthy ear or cause acute onset in ear with chronic otitis media. Main pathogens include pneumococcus, *Haemophilus influenzae*, and hemolytic streptococcus. Both children and adults may suffer from this disease, but it is more common in children. Infants' auditory tube is broad, short, straight and flat, while the position is low. Besides, milk or vomitus may enter the middle ear via auditory tube. For this reason, infants are more vulnerable to the disease than adults [3].

Clinical manifestations are sudden otalgia and ear distention, accompanied by obvious hearing loss. In addition to above symptoms, patients may also cry, scream, become restless, scratch ear or shake head. Physical examination shows congestive, thickened or punctured tympanic membrane and pulsatile pyorrhea spilling outward from tympanic membrane puncture and empyema in external auditory canal. When the disease is combined with acute mastoiditis, skin posterior to ear can be red and swollen, with tenderness in mastoid region. Hearing test indicates conductive hearing loss, and tympanogram usually shows type B.

20.2.1.2 [Pathology Findings]

Congestion and edema occur in middle ear mucosa, with increased secretion. There is serous exudate in the tympanic cavity. The exudate can become mucinous or even suppurative as the inflammation further evolves. Local necrosis and ulceration of tympanic membrane form tympanic membrane perforation, with pus discharged. Inflammation can further involve other adjacent structures, especially tympanic membrane, wherein obvious hyperemia and edema can be observed in tympanic membrane connective tissue layer. If the treatment is not timely and effective, as lesion further develops, the inflammation can reach peripheral bones, thus causing acute osteomyelitis.

20.2.1.3 [Imaging Findings]

1. X-ray Examination. Plain film shows that mastoid is typically well pneumatized bilaterally. In case of inflammation limited to tympanic cavity and mastoid antrum, images at skull base plane show absence of air in tympanic cavity and mastoid antrum at the affected side, with lowered permeability. When the inflammation spreads to the pneumatized mastoid, mastoid air cell will be thickened homogeneously, while interatrial septum typically remains intact and can be dimly seen.

2. CT Examination. Compared with plain film, CT can better show the extent and severity of lesion. Findings vary by the stage of disease and the extent to which temporal bone is involved. In early stage, the middle ear tympanic cavity and mastoid air cell record lower transmittance. As the disease progresses, diffuse changes in the middle ear mastoid cavity can be observed [6].

(1) Middle Ear Intramastoiditis: Mastoid is sclerotic, only manifested as visible soft tissue density in tympanic cavity and mastoid antrum. There is no tympanic cavity enlargement or bone destruction, and ossicular chain is complete.
(2) Otitis Media Mastoiditis: Mastoid process is well developed, while the density of mastoid air cell is increased or air-fluid level is formed. Interatrial septum is intact or slightly absorbed, and bone density is reduced (Fig. 20.2).
(3) Intracranial Complications: Refer to Chapter V Section III for meningitis and brain abscess.

3. MRI Examination. MRI examination is generally not required. When there is severe inflammation with postauricular abscesses or an intracranial infection is suspected, MRI is superior to CT in showing the extent of inflammation spread and intracranial involved structures.

20.2.1.4 [Key Points of Diagnosis]

1. With acute attack, the disease presents with otalgia, fever and pus discharge from the ear, accompanied by periauricular and postauricular soft tissue swelling.
2. Acute pyogenic infection in the middle ear mucosa.
3. CT shows tympanic cavity or tympanic antrum of the middle ear with or without disappeared gas and increased density in the mastoid process.

20.2.1.5 [Differential Diagnosis]

1. **Secretory Otitis Media.** Its clinical manifestations are ear fullness and distension and hearing loss, without abnormal ear secretions and vertigo. CT shows the absence of gas in the middle ear cavity, high-density soft tissue shadows, and no bone destruction.

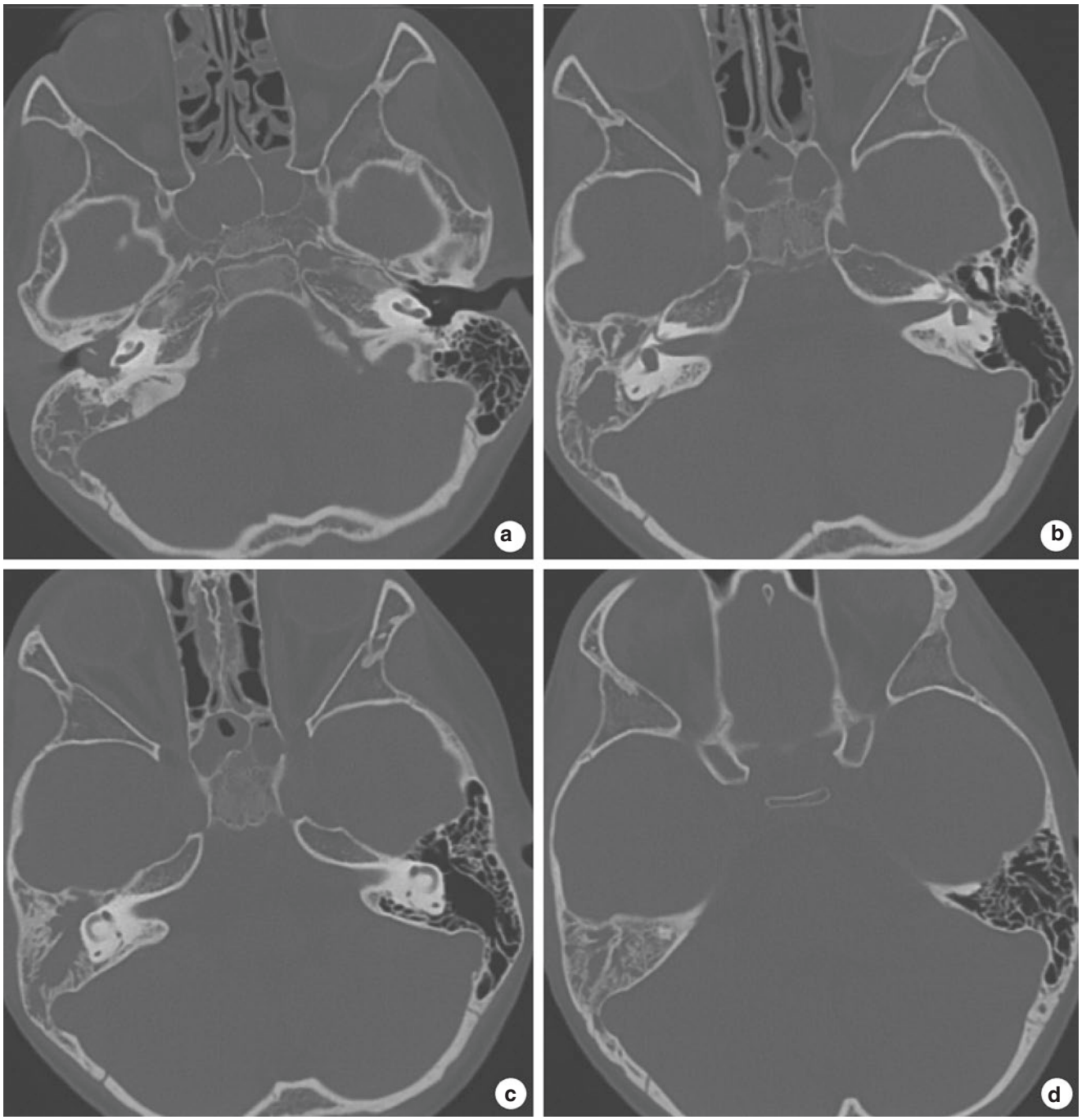

Fig. 20.2 Acute suppurative otitis media. A 6-year-old male patient. He was admitted to the hospital mainly because of upper respiratory tract infection, and suffered from right side otalgia five days later. CT examination showed slightly hyperintense in bilateral ethmoidal sinus and sphenoid sinus, promoting inflammation of bilateral ethmoidal sinus and sphenoid sinus. (**a**–**d**) CT bone window at transverse plane shows that right tympanic antrum wall and right air cell septum are partially damaged. (**a**) CT bone window at transverse plane shows incomplete tympanic membrane. (**b** and **c**) CT bone window at transverse plane shows that right middle ear tympanic cavity, tympanic antrum, right mastoid air cell and right ossicular chain peripheral regions are filled with soft tissue shadows

2. **Chronic Suppurative Otitis Media.** The patients have a history of long-term pus discharge from the ear and develop hearing loss. Imaging examination shows poor pneumatization of mastoid process on the affected side, and empyema, mucosal hypertrophy, patchy granulation tissue and spherical masses in the middle ear cavity, which are mostly associated with enlarged tympanic cavity and tympanic antrum and auditory ossicular chain destruction, and can involve the brain plate, horizontal semicircular canal and other structures [7].

20.2.1.6 [Status Quo and Progress of Research]

HRCT can clearly show the site and extent of the disease and bone destruction in the air cell septum, which is the preferred examination method for acute suppurative otitis media. When the disease involves surrounding structures, causing postauricular abscesses, thrombosis of sigmoid sinus and (or) intracranial infection, Enhanced CT and MRI examinations are required [1, 5].

20.2.2 Chronic Suppurative Otitis Media

20.2.2.1 [Overview]

Chronic suppurative otitis media is a chronic pyogenic inflammation, which occurs in the mucosa or periosteum of middle ear, or deep to the bone, mostly accompanied by mastoid inflammation. Severe patients have inflammation deep to the mastoid bone. The common clinical symptoms are long-term intermittent or persistent pus discharge, perforation of tympanic membrane and hearing loss. If the disease is protracted, intracranial or extracranial complications will be caused.

The etiology includes acute suppurative otitis media not treated thoroughly, decreased systemic or local immunity, and chronic lesions in the nose and pharynx. It has not been determined whether tympanic cavity catheterization can be complicated with this disease. Poor pneumatization of mastoid process may be associated with the disease. The most common pathogen is staphylococcus aureus.

Chronic suppurative otitis media can be traditionally divided into simple type, bone ulcer type (granuloma type) and cholesteatoma type. Currently, cholesteatoma of the middle ear tends to be considered as an independent disease. As the infection with pyogenic bacteria may be combined in the occurrence and development process of cholesteatoma, and important characteristics of chronic suppurative otitis media are maintained, the disease can be classified into two types: chronic suppurative otitis media with cholesteatoma or without cholesteatoma [8]. This section mainly describes the chronic suppurative otitis media without cholesteatoma. See Section 3 of this chapter "Cholesteatoma" for the chronic suppurative otitis media with cholesteatoma.

20.2.2.2 [Pathology Findings]

Patients with chronic otitis media have many proliferative granulation tissues in the ear mastoid cavity and most patients have bleeding. The proliferation of fibrous granulation tissue can be seen microscopically with the infiltration of monocytes/macrophages. Columnar epithelial metaplasia is found in the middle ear cavity. Most of patients have recurrent bleeding and unsmooth long-term drainage, which can lead to cholesterol granuloma. Calcification in the tympanic cavity can be observed in patients with long course.

20.2.2.3 [Imaging Findings]

1. X-ray Examination

(1) Simple Type: The tympanic cavity and mastoid antrum cavity of temporal bone show an increase in density, or with decreased transmittance of mastoid process. Most cases are diploetic type or sclerosis type, showing blurred mastoid air cell septum. The ossicles are normal.
(2) Bone Ulcer Type: There are soft tissue shadows in the tympanic cavity and tympanic antrum cavity, absorption and destruction of the ossicles, and limited mastoid bone destruction, which mostly occur in the tympanic cavity and tympanic antrum areas. Sclerosis and increased density are often seen at the bone margin, without significantly enlarged sinus cavity.
(3) Cholesteatoma Type: See Section 3 of this chapter "Cholesteatoma."

2. CT Examination. On HRCT, the perforation of tympanic membrane is often noted in patients with chronic suppurative otitis media, and residual tympanic membrane is usually thickened, which are clearly seen on the images. When a patient is at different phases, the transmittance of the middle ear cavity and mastoid process will be decreased partially or completely. Chronic suppurative otitis media usually results in the disruption of ossicular chain in the middle ear. The most common site of absorption and destruction is long crus of incus, followed by manubrium mallei. In severe cases, the absorption and destruction of anterior and posterior stapes arches may occur. For these cases, the use of MPR can more visually and clearly show the destruction of ossicular chains (Fig. 20.3). Some cases still may have absorption and destruction in the facial nerve canal, lateral semicircular canal and brain plate, and its incidence is lower compared with cholesteatoma.

(1) Simple type: The lesion is mainly limited to the mesotympanum in patients with poor pneumatization of mastoid process presenting sclerosis type, diploetic type or mixed type mastoid process. The lesions in the tympanic cavity of the middle ear present with cord-like soft tissue density shadows or only are thickened tympanic membrane and thickened and blurred bony walls of air cells. There is no enlarged tympanic cavity or tympanic antrum, no bone or ossicular destruction, and intact ossicular chain (Fig. 20.4).
(2) Bone Ulcer Type: There are soft tissue shadows in the tympanic cavity (or with mastoid process), moth-eaten destruction in septa, and bone erosion around the sigmoid sinus. The ossicles may be normal or destroyed. On enhanced scan, the granulation tissue can show enhancement [9] (Figs. 20.5 and 20.6).

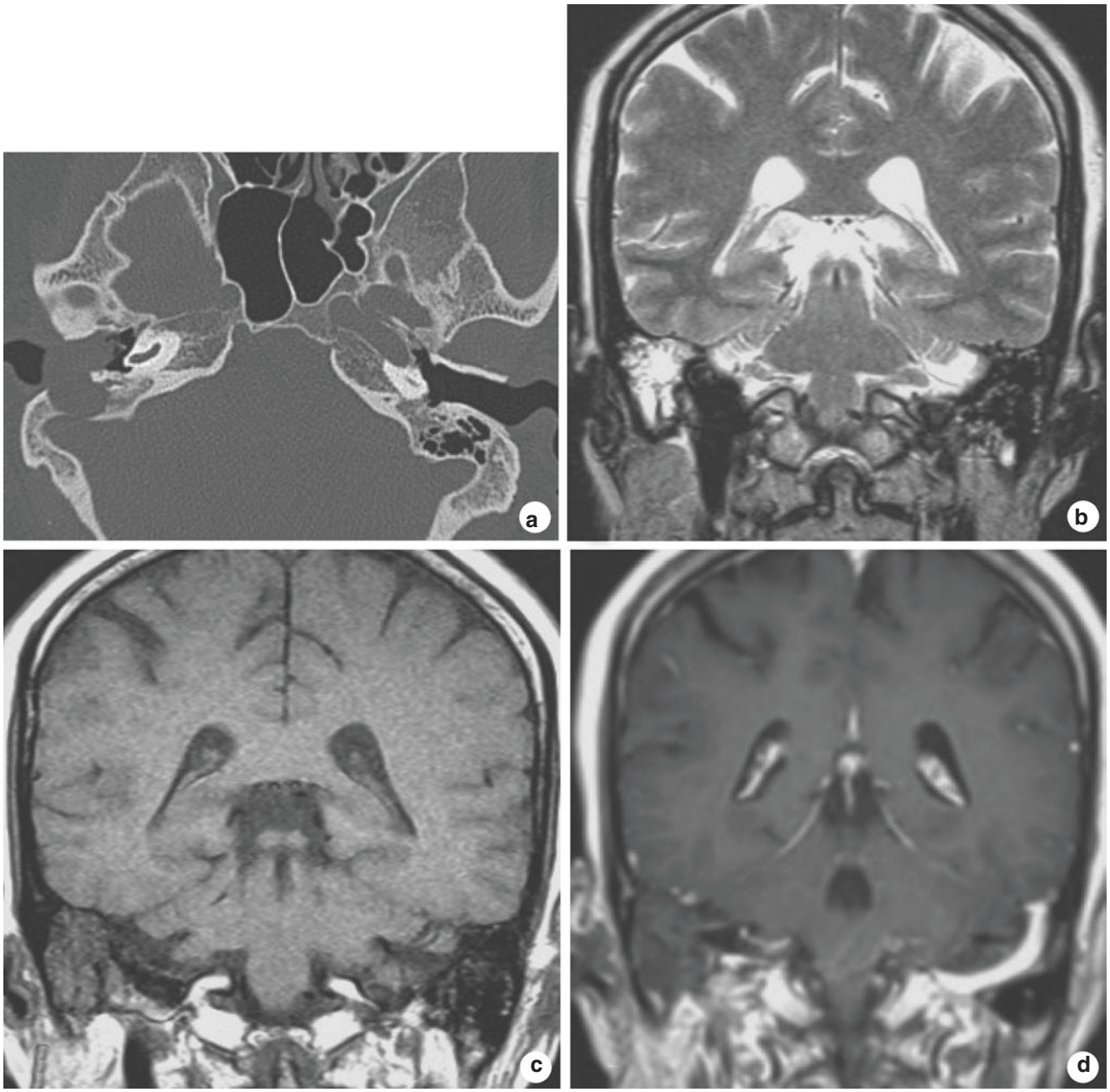

Fig. 20.3 Simple-type otitis media. A 59-year-old female patient with a sense of right ear fullness for the past 2 years. (**a**) CT of temporal bone shows soft tissue density shadows in the tympanic cavity of right middle ear and right mastoid process, and tympanic cavity and tympanic antrum not enlarged, good bone structures, poor pneumatization of bilateral mastoid processes and thickening of septum. (**b**–**d**) After 5 years, on MR, the patient shows hypointense on T1WI and hyperintense on T2WI in the right mastoid process and no enhancement on enhanced scan. The meninges show linear enhancement

(3) Cholesteatoma type: See Section 3 of this chapter "Cholesteatoma."

3. MRI Examination. It has some value in the diagnosis of patients with chronic suppurative otitis media. In addition to the differentiation of granulation tissue from pus and cholesteatoma by using previously noted T_1WI enhanced scan, MRI is valuable in the diagnosis of the complications of otitis media, which can detect labyrinthitis in the early stage and accurately determine intracranial infection and its extent.

(1) Simple Type: This type is mainly simple inflammatory lesion. The mastoid processes of pneumatic type and sclerotic type shows no-signal area. In no-signal area, soft tissue signal shadows are seen in the tympanic cavity or tympanic antrum, showing isointense or slightly

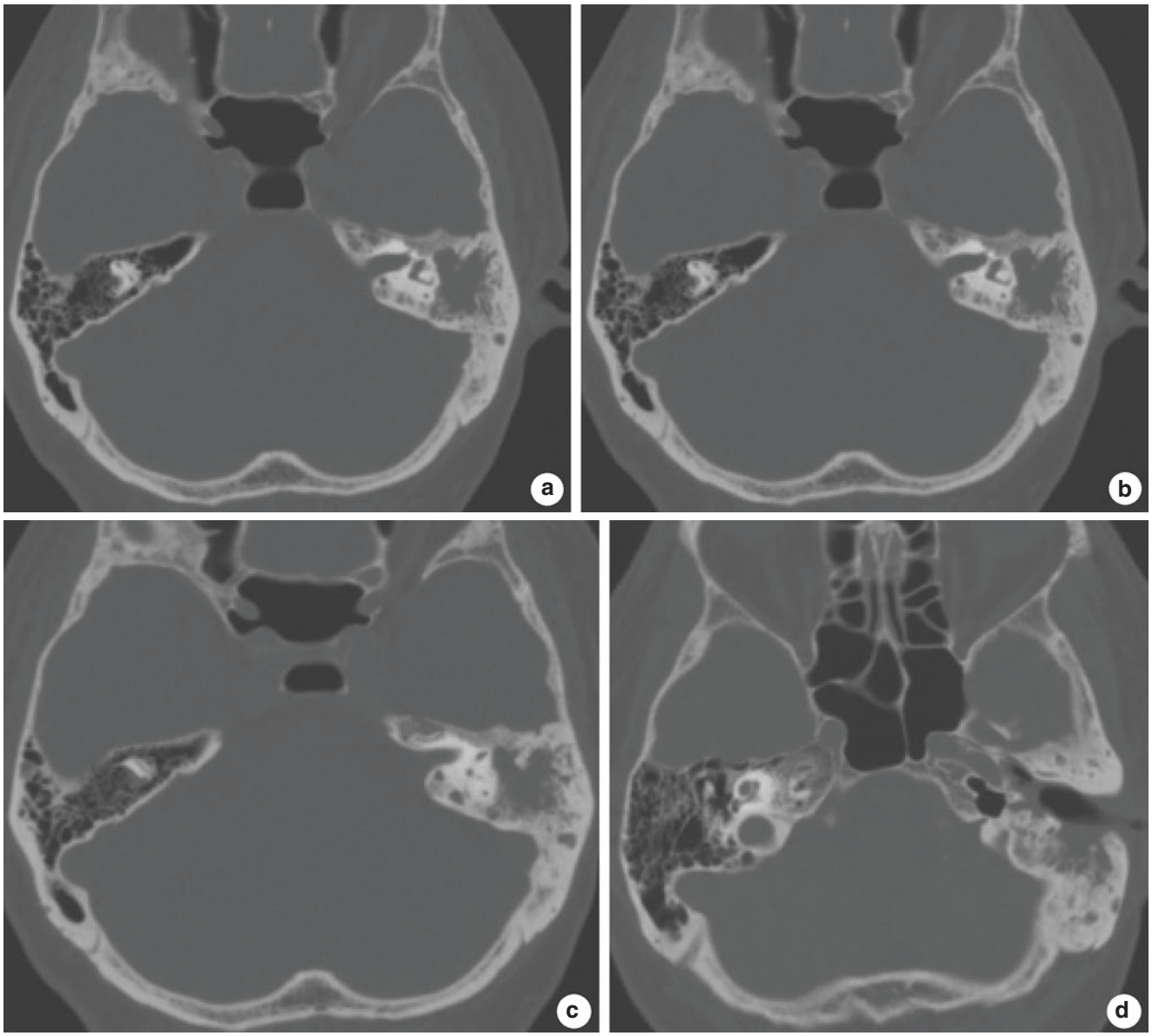

Fig. 20.4 Granulation-type suppurative otitis media. A 68-year-old male patient with chief complaint of "left otalgia and fluid discharge for the past 2 years and headache for the past 1 month". (**a**–**d**) CT of temporal bone in the transverse plane shows poor pneumatization of the left mastoid process with incomplete bone structure and crumby soft tissue density shadows inside. Soft density shadows are noted in the tympanic cavity and tympanic antrum of left middle ear and the left ossicular chain is not showed. There are complete bone structures in the left cochlea and lateral semicircular canal

hypointense on T_1WI and slightly hyperintense or hyperintense on T_2WI (Fig. 20.3b, c). Viscous pus may also show hyperintense on T_1WI and hyperintense on T_2WI. The ossicles in the middle ear are surrounded.

(2) Bone Ulcer Type: The main manifestations include the proliferation of inflammatory granulation and bone destruction. Soft tissue shadows in the tympanic cavity, mastoid air cells and mastoid antrum show heterogeneous signals on T_1WI and hyperintense on T_2WI (Fig. 20.7). On enhanced scan, the granulation tissue lesion shows marked enhancement (Fig. 20.5g). The adjacent basal temporal lobe, anterior cerebellum and cerebellopontine angle may be involved, manifested as thickening and enhancement of meninges (Fig. 20.8), and "otogenic" meningitis or "otogenic" encephalitis is caused [10].

(3) Cholesteatoma Type: See Section 3 of this chapter "Cholesteatoma." Comparison of MRI signals of cholesteatoma, granulation and pus: The signals on T1WI are isointense or hypointense, and the signal intensity is in descending order as follows: granulation, cholesteatoma, pus; the signals on T_2WI are hyperintense, and the

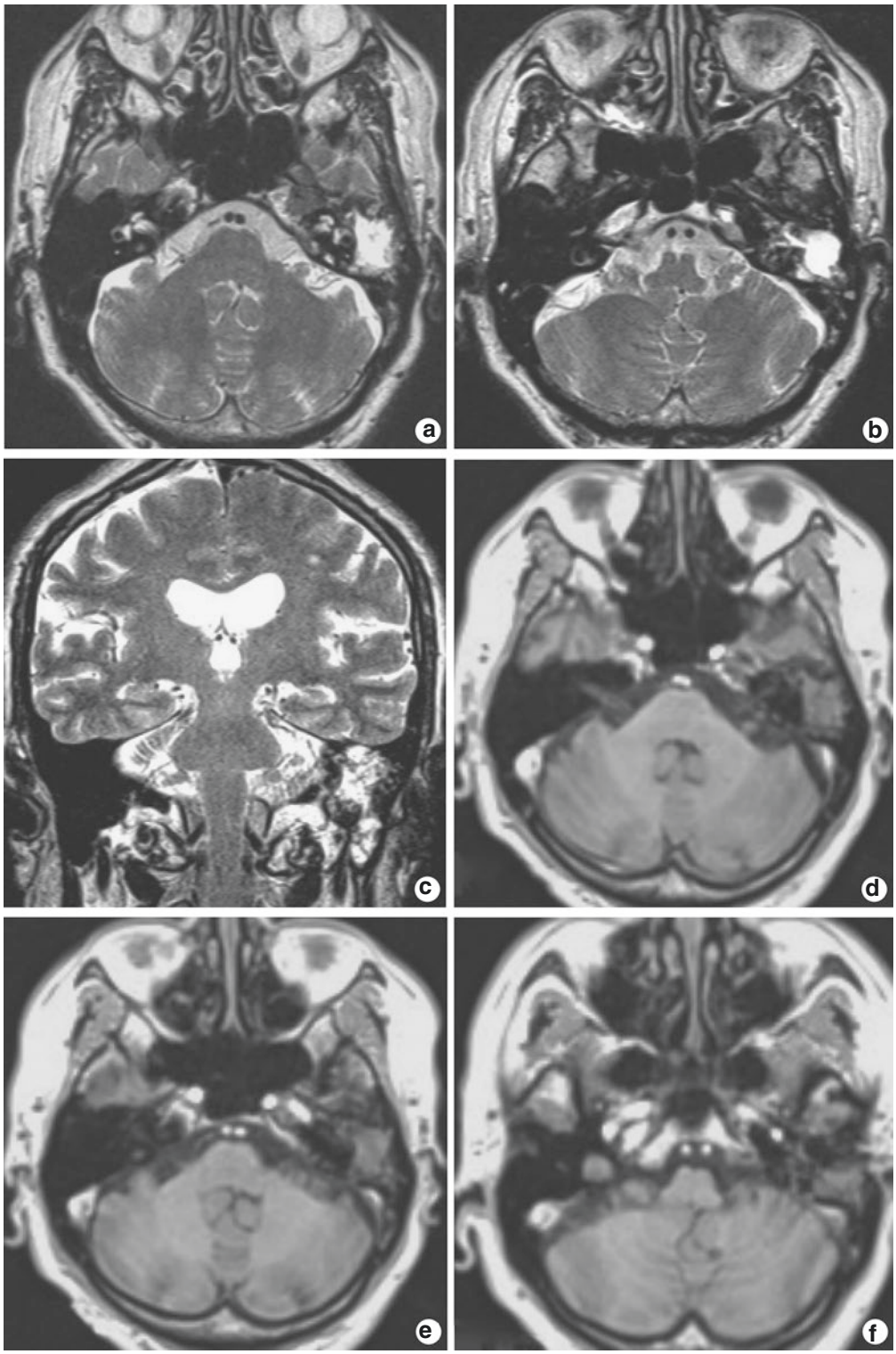

Fig. 20.5 Bone ulcer type suppurative otitis media (1). A 35-year-old female patient. with pus and fluid discharge from the left ear with headache for the past 1 week. (**a**–**f**) The lesion in the tympanic cavity and mastoid process of left middle ear shows isointense on T1WI and hyperintense on T2WI, with clear margin. (**g**–**i**) On enhanced scan, the lesion shows marginal linear enhancement; the lesion shows no enhancement, the adjacent meninges of left tempus reveals linear enhancement

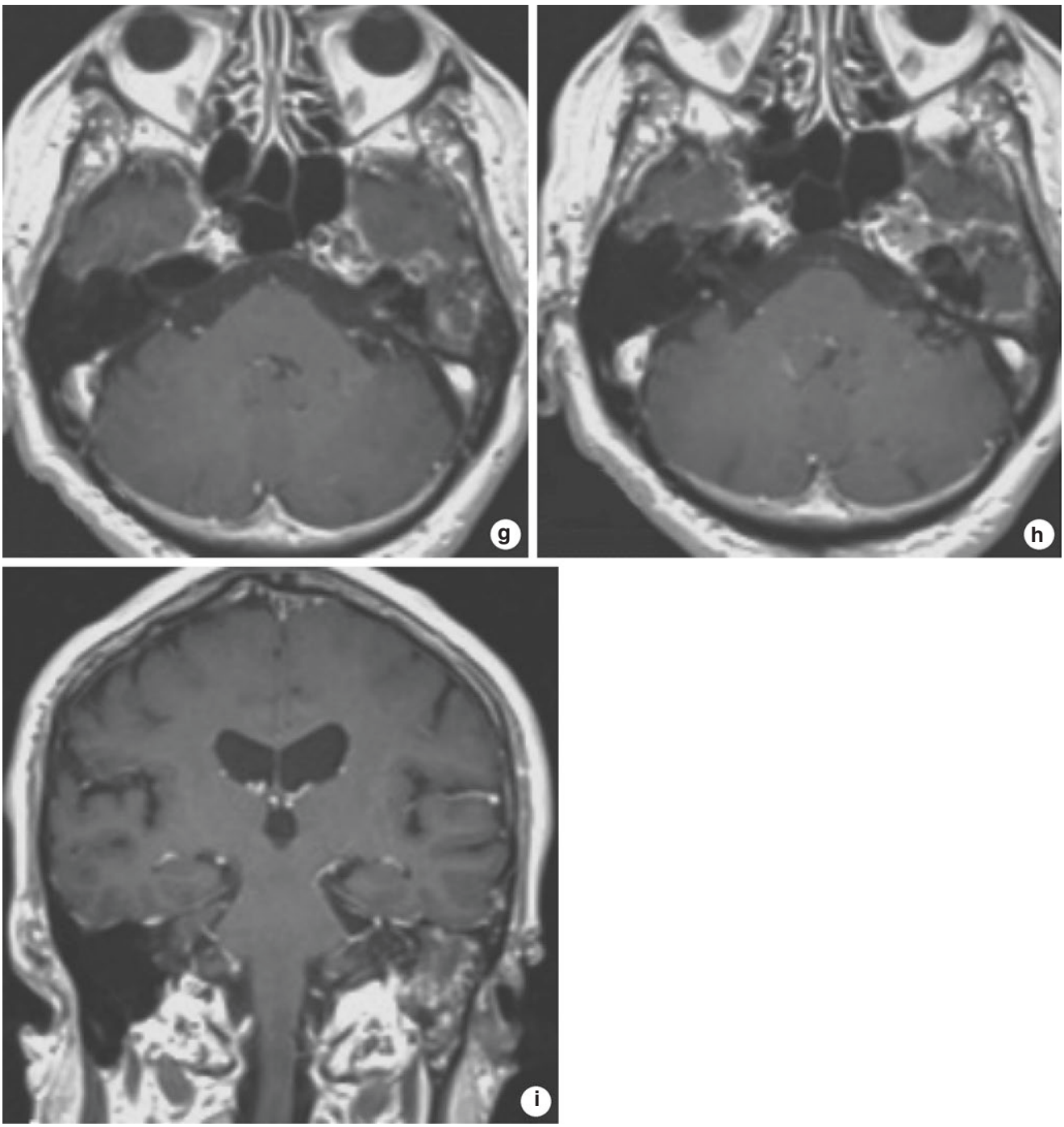

Fig. 20.5 (continued)

signal intensity is in ascending order as follows: granulation, cholesteatoma, pus.

20.2.2.4 [Key Points of Diagnosis]

1. The disease has a long course and recurrent attacks. The patients develop hearing loss, partly accompanied by tinnitus and vertigo; The hearing examination usually shows conductive deafness.
2. CT shows diffuse hypointensity in the mastoid cavity of middle ear, usually accompanied by absorption and destruction of the ossicular chain and tympanosclerosis in some cases.
3. The disease may be associated with intracranial meningitis, thrombus of sigmoid sinus, and aural subcutaneous and subperiosteal abscesses.

20.2.2.5 [Differential Diagnosis]

1. **Acute Otomastoiditis.** The disease is common in children with sudden onset, and significant otalgia, ear fullness and distension, which is mostly secondary to infections in the upper respiratory tract and nasopharynx. Acute patients only have liquid density shadows in the mastoid cavity of middle ear without bone absorption and destruction.

2. **Cholesteatoma Otomastoiditis.** The structure around the focus changes due to compression, mostly accompanied by bone absorption and destruction. The disease most typically occurs in the lateral attic space, presenting with blunted periosteum ridge and increased lateral attic space.

20.2.2.6 [Status Quo and Progress of Research]

HRCT can clearly show the site, extent and air cell septum of the disease, as well as bone destruction of ossicular chains, facial nerve canals and bony labyrinths, which is the preferred examination method for otomastoiditis. When the disease is complicated with labyrinthitis, facioplegia, intracranial infection and other diseases, MRI and enhanced examination are required [11].

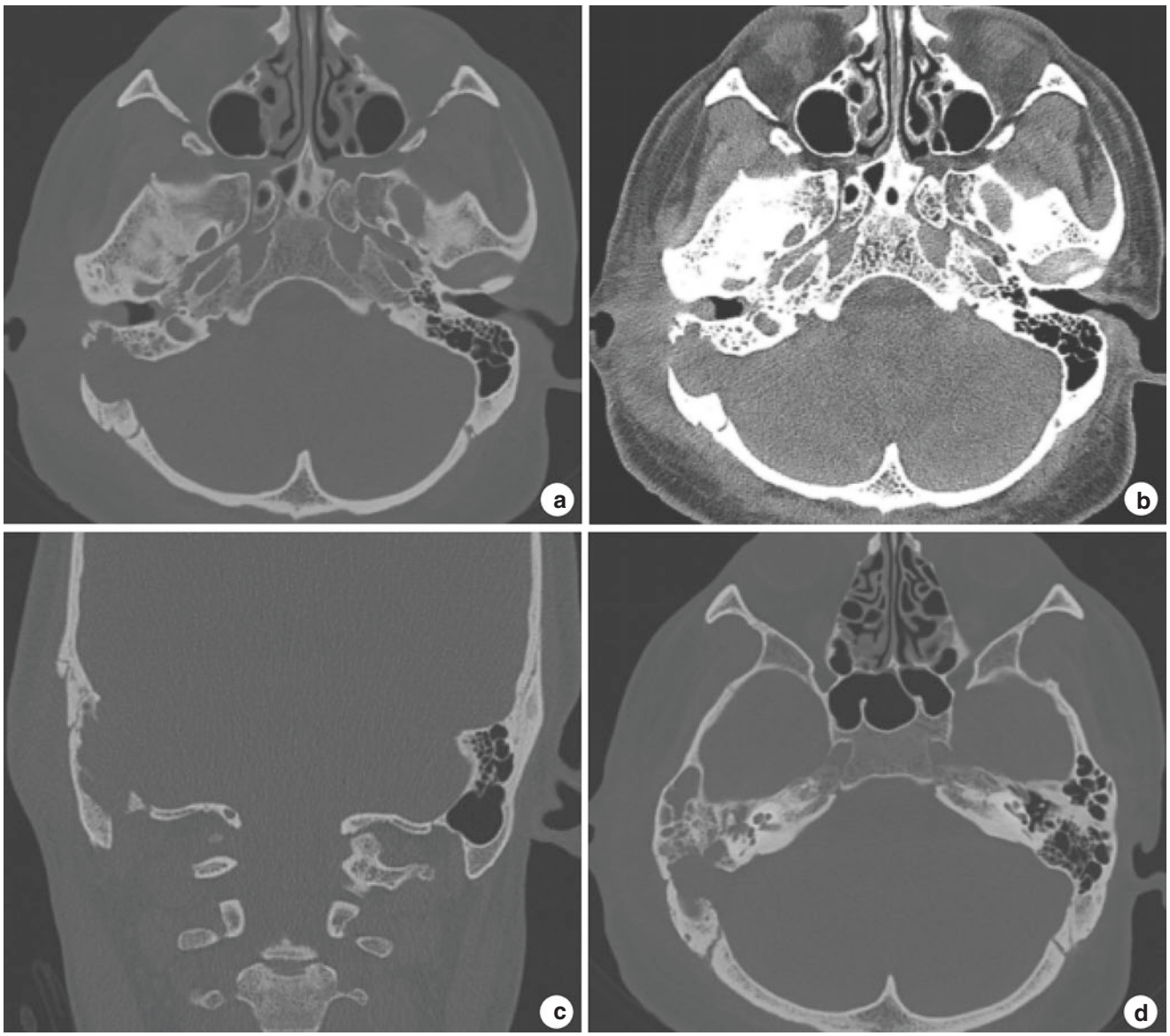

Fig. 20.6 Bone ulcer type suppurative otitis media (2). A 38-year-old male patient with bone ulcer type suppurative otitis media, accompanied by left postotic subcutaneous and temporal subperiosteal abscesses and abscesses adjacent to sigmoid sinus. (**a**–**f**) HRCT shows soft tissue density shadows in the tympanic cavity and mastoid process of right middle ear, surrounding the right ossicle, and destruction of mastoid bone structure, as well as destruction of lateral wall of right squamous part of temporal bone and right sigmoid sinus plate. On HRCT, bone surrounding the lesion shows moth-eaten destruction without expansive changes

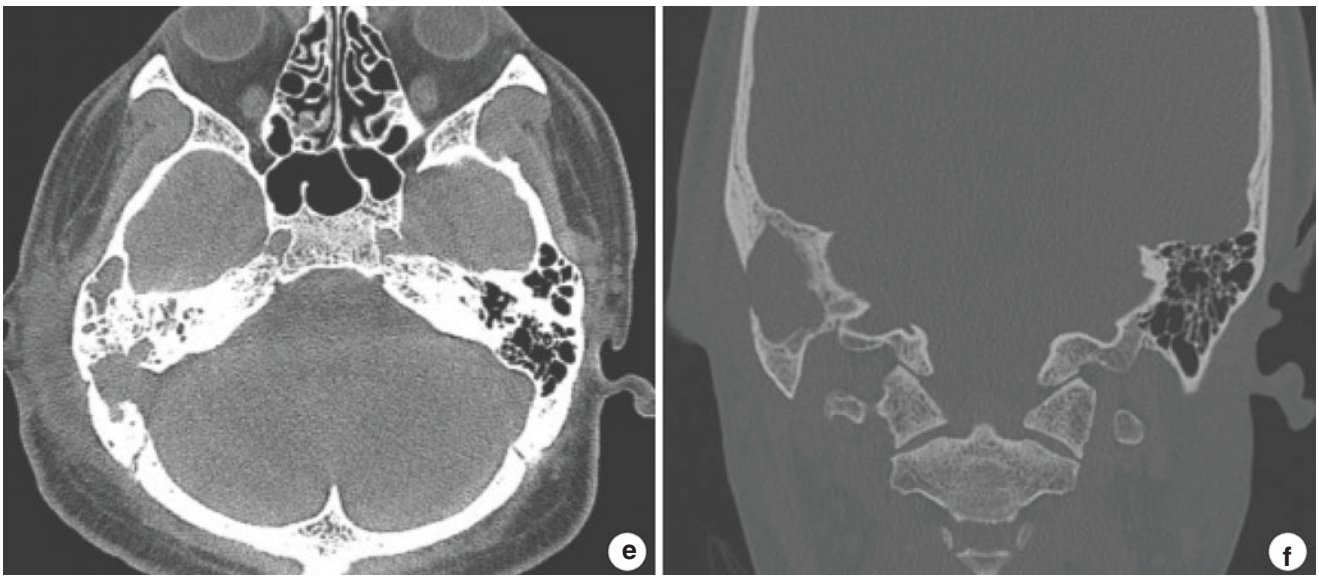

Fig. 20.6 (continued)

20.3 Cholesteatoma

20.3.1 [Overview]

Cholesteatoma is a cystic structure that is closely attached to the adjacent bony wall or tissue with a layer of fibrous tissue in different thickness, instead of a true tumor. The inner wall of the cyst is stratified squamous epithelium, and in addition to exfoliated epithelium and keratotic substances, the cyst may contain cholesterol crystals (uncommon). Hence, it is called cholesteatoma. Cholesteatoma is characterized by the destruction of peripheral bone, causing severe intracranial and extracranial complications, which is worthy of attention. Cholesteatoma within the temporal bone is most common in the middle ear [12], followed by petrous apex and external auditory canal. The disease can be divided into congenital and acquired cholesteatoma by origin [8].

Congenital cholesteatoma can be classified according to its location: (1) congenital cholesteatoma of temporal bone. It is mainly located at the petrous apex of the temporal bone and progresses to the mastoid process of the middle ear. (2) congenital ear deformity with middle ear cholesteatoma. Patients with congenital aural atresia and middle ear deformity are often accompanied by cholesteatoma, which is mainly confined to the middle ear cavity. It can progress in the temporal bone in a long term due to its sterility. The initial symptoms of the disease are mainly facioplegia, often followed by damaged cochlear and vestibular function, and nystagmus may occur when the lesion invades the labyrinth. Hearing loss, tinnitus and vertigo also occur, and the disease in the advanced stage may present headache, injury of cranial nerves and other symptoms.

Acquired cholesteatoma can be classified into two types: (1) acquired primary cholesteatoma. Patients with the disease have no history of suppurative otitis media and may have a past medical history of secretory otitis media. The lesion is insidious in onset, and the perforation is located at the posterosuperior pars flaccida or partes tensa of tympanic membrane. Later, suppurative inflammation may occur due to secondary infections. (2) acquired secondary cholesteatoma. The disease is secondary to chronic suppurative otitis media, and big or marginal perforation in the tympanic membrane and stratified squamous epithelium grows from the perforated edge to posterior tympanic cavity or attic, and tympanic antrum, forming cholesteatoma. Cholesteatoma in the external auditory canal also may be deemed as acquired secondary cholesteatoma after the invasion into the middle ear.

Cholesteatoma in the external auditory canal is not rare, of which causes include inflammation, trauma and surgery, and the pathogenesis is unclear [13].

20.3.2 [Pathology Findings]

Acquired cholesteatomas are usually "open," not "closed" or cystic, and located in the middle ear cavity, which are often accompanied by severe chronic otitis media. An acquired cholesteatoma is roughly a pearl-like gray structure that consists of dead, fully differentiated, nuclear-free keratinized squamous epitheliums, which is deemed as the keratinized layer of squamous epitheliums. As with any normal stratified squamous epithelium, there are 1–3 basal cell layers above which the prickle cell layer is located, consisting of 5–6 layers of cells with intercellular bridges. The deep layer of the

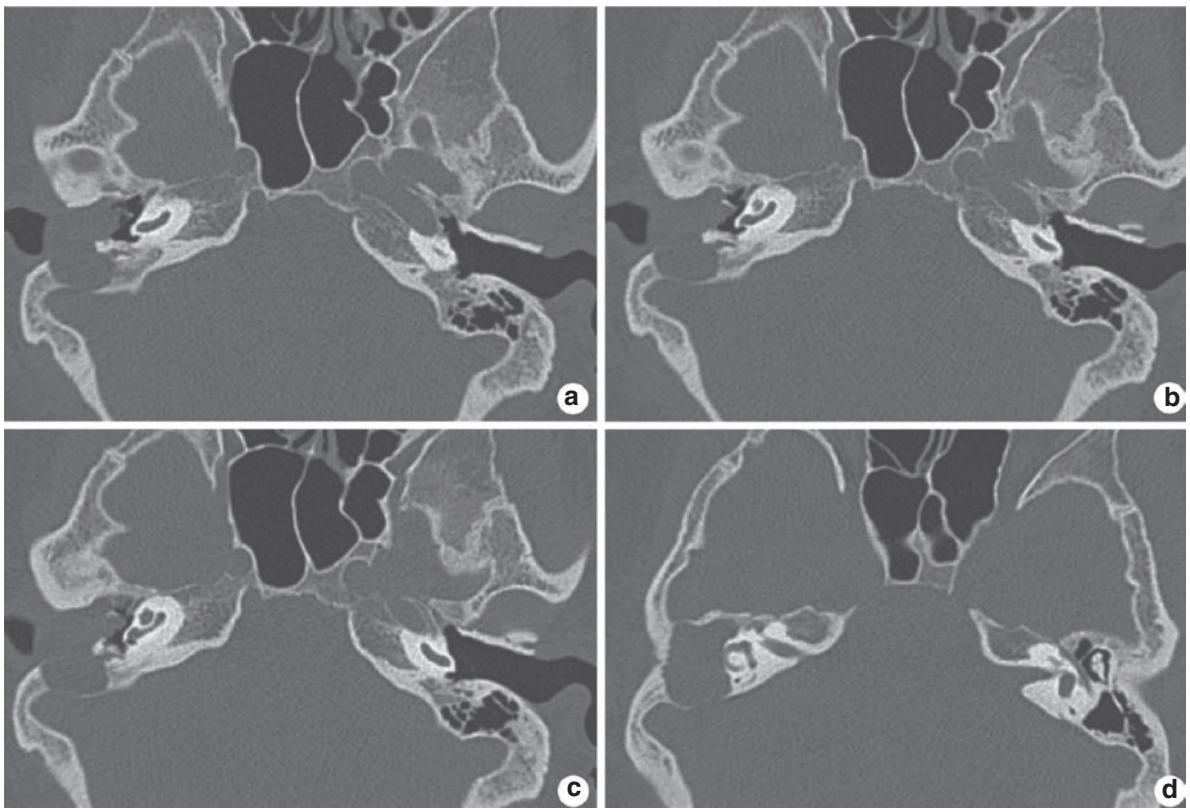

Fig. 20.7 Bone ulcer type suppurative otitis media (3). A 45-year-old male patient. with pus and fluid discharge from the right ear for the past 2 years and swelling and pain in the right ear for the past half a month. (**a**, **b**, **d** and **e**) MR non-enhanced scan shows crumby isointense on T1WI and heterogeneous signals on T2WI in the right external auditory canal, and the tympanic cavity, tympanic antrum and mastoid air cells of right middle ear, which protrude subcutaneously behind the right external auditory canal and spread along the subcutaneous soft tissue space. (**c** and **f**) On DWI, the lesion shows heterogeneous signal shadows. (**g**, **h** and **i**) There is a subperiosteal abscess in the right mastoid portion with the formation of postauricular subcutaneous abscess. The wall with hyperintense on T_2WI and pus with hyperintense on T_2WI are formed around the abscess. Bone absorption and destruction occurs in some right mastoid air cells and anterior outer wall of sigmoid sinus, which suggests bone ulcer type suppurative otitis media

epithelium within the stroma of cholesteatoma often actively grows and extends downwards into the connective tissue under epidermis.

Pathogenesis of congenital cholesteatoma: A small cluster of cells can be seen near the tympanic membrane in the anterior superior lateral middle ear within the temporal bone after 15 weeks of pregnancy, which is proved to be epidermoid cells in nature by immunohistochemistry. These "epidermoid structures" are derived from the active epidermis of the tympanic membrane. With age, the cholesteatoma has significantly increased volume while presenting increasing epidermal differentiation. In the normal development, the epidermoid cluster will disappear in the first year of life. If it does not regress and continue to grow, the cluster will become a congenital cholesteatoma. Among 10% congenital cholesteatoma, the lesion is "open" and exfoliated squamous epitheliums extend into the tympanic cavity. The stroma of congenital cholesteatoma is epidermis which is composed of monolayer basal cells, several layers of germinal cells, and a thin layer of granular cells. In open cases, the surface of dead and keratinized stratified squamous epithelium fuses with keratinized substance or keratinized layer in the cystic cavity, of which immunostaining presentations are similar to acquired cholesteatoma.

20.3.3 [Imaging Findings]

1. **X-ray Examination.** Schiller's view and Mayer's view are used for the diagnosis of temporal bone lesions. There is increased density of mastoid process in sclerosis type, enlarged attic and tympanic antrum, clear and sharp sclerotic bone margin. The large cholesteatoma in the mastoid antrum region can be seen in the open dural triangle of the sinus. The white bony line at the margin of sigmoid sinus dura is blurred or interrupted, suggesting destruction of sigmoid sinus. Occasionally, the ossicular chain is missing or incom-

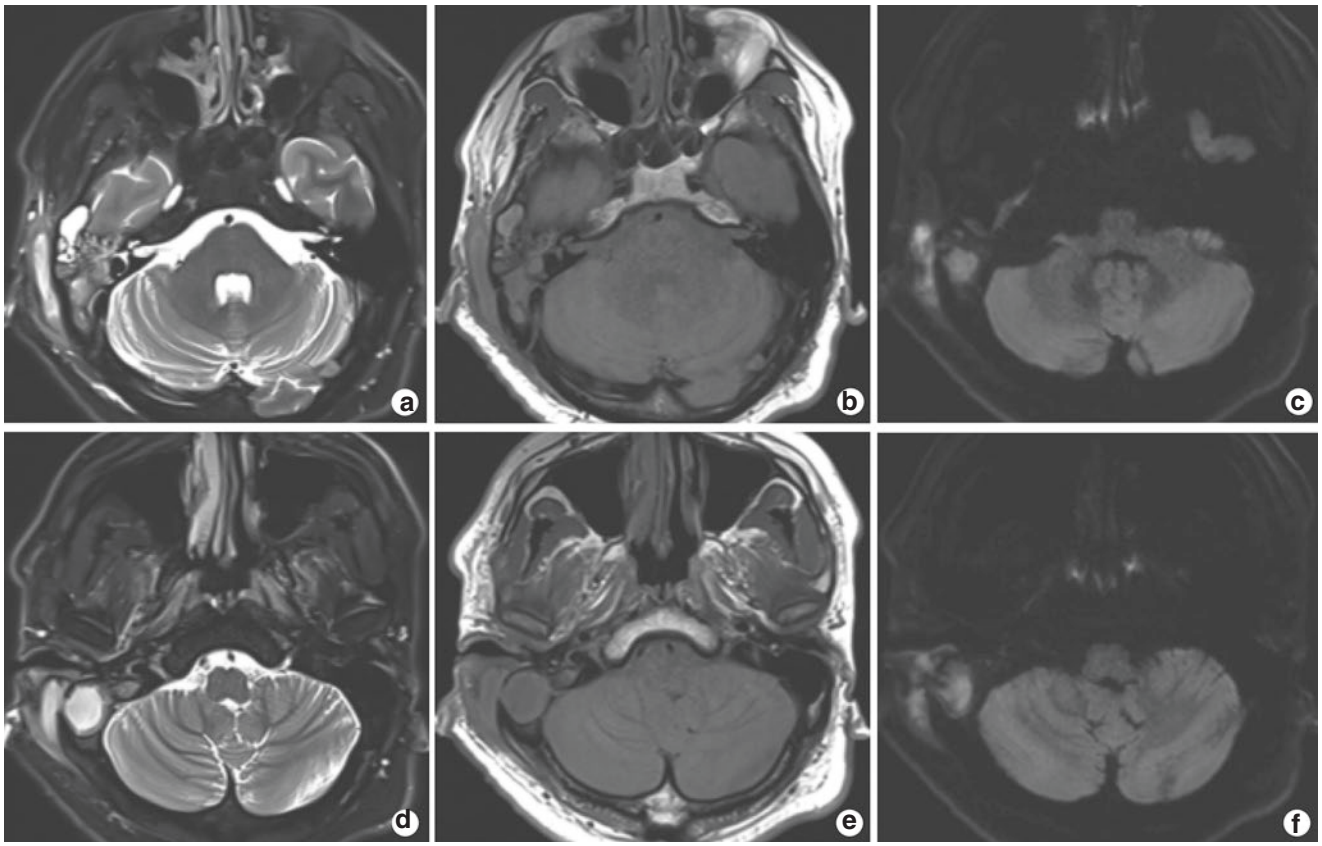

Fig. 20.8 Bone ulcer type suppurative otitis media (4). A 65-year-old male patient with pus and fluid discharge from the right ear for the past 2 years and headache on the right side for the past half a month. (**a–c**) MRI enhanced scan shows marked ring enhancement with homogeneous thickness in lesions in the tympanic cavity, tympanic antrum, mastoid air cells of right middle ear, and subcutaneous part behind right ear, which suggests marked enhancement of granulation component of abscess wall and no enhancement of central pus. (**d**) Crumby ring enhancement shadow is seen in the junction of right sigmoid sinus and transverse sinus, sigmoid sinus is compressed and flattened, and the strip-shaped no-enhancement area is noted inside, so thrombosis is considered

plete (radiolucent area where the external auditory canal overlaps).

2. **HRCT Examination**

(1) Congenital Cholesteatoma: The lesion may occur in any part of temporal bone and be most common in the petrous apex. It presents with the cavity of bone destruction at the petrous apex, accompanied by soft tissue masses in the cavity and smooth margin. The typical congenital cholesteatoma of the middle ear is mostly located at the anterior part of mesotympanum and can involve the petrous apex and ossicular chain. The tympanic membrane is usually intact, and the lateral attic wall is not damaged. The disease can be differentiated from the acquired cholesteatoma based on the above characteristics. A large cholesteatoma may also result in the destruction of ossicular chains, with the destruction of lateral attic wall starting from the internal surface. Patients with congenital aural atresia and middle ear deformity are often accompanied by cholesteatoma, which is mainly confined to the middle ear cavity.

(2) Acquired Cholesteatoma: Primary cholesteatoma with the perforation of tympanic membrane is difficultly differentiated from secondary cholesteatoma based on images. The acquired cholesteatoma has one or more of the following manifestations: (1) erosion of anterior part (tympanic scutum) and/or anterior tympanic crest of lateral attic wall. (2) Soft tissue nodules or masses lateral to the ossicle of attic. (3) increased space (Prussak's space) between the lateral attic wall and the ossicle which is caused by the medial movement of the ossicle due to compression and the erosion and destruction of the lateral attic wall. (4) tegmen tympani showing an arc-shaped contour with smooth margin when cholesteatomas fill the attic and progress to the tectum. (5) primary cholesteatoma is considered when the tympanic membrane is intact, and the head of malleus and body of incus in the ossicular chain are the most vulnerable to erosion. Secondary cholesteatoma is more common, and the head of malleus is usually in good shape while the long crus of incus is often eroded. (6) cholesteatoma may progress

backwards into the tympanic antrum. On CT, the expansion of aditus of tympanic antrum and the extent of the posterosuperior part of cholesteatoma are clearly observed. The short crus of incus in the incudal fossa is often eroded. The focus may gradually progress and partially and completely fill the tympanic antrum cavity, causing enlarged antrum cavity and further progress to the mastoid process, leading to progressive destruction and formation of large cavities with smooth and blurred contour (Figs. 20.9, 20.10 and 20.11).

(3) Cholesteatoma of the external auditory canal: The typical imaging findings are soft tissue masses in the external auditory canal accompanied by enlarged external auditory canal, compressive absorption of osseous segment, main involvement of inferior wall, and relatively smooth margin. When the focus is small, the tympanic membrane is usually not involved. A large cholesteatoma in the external auditory canal may extend inward to the middle ear, epitympanum and mastoid process.

3. **MRI Examination.** Compared with the grey matter, the focus shows isointense or slightly hypointense on T_1WI and slightly hyperintense or isointense to hyperintense on T_2WI, as well as bright hyperintense on T2-FLAIR sequence and DWI, which can be deemed as characteristic imaging manifestations of cholesteatoma. On enhanced scan the focus shows no enhancement and has enhancement in the surrounding area if inflammation occurs around it.

When the focus is small or there is a residual or recurrent focus after operation, it is often difficult to differentiate the focus from the peripheral inflammatory tissue and inflamma-

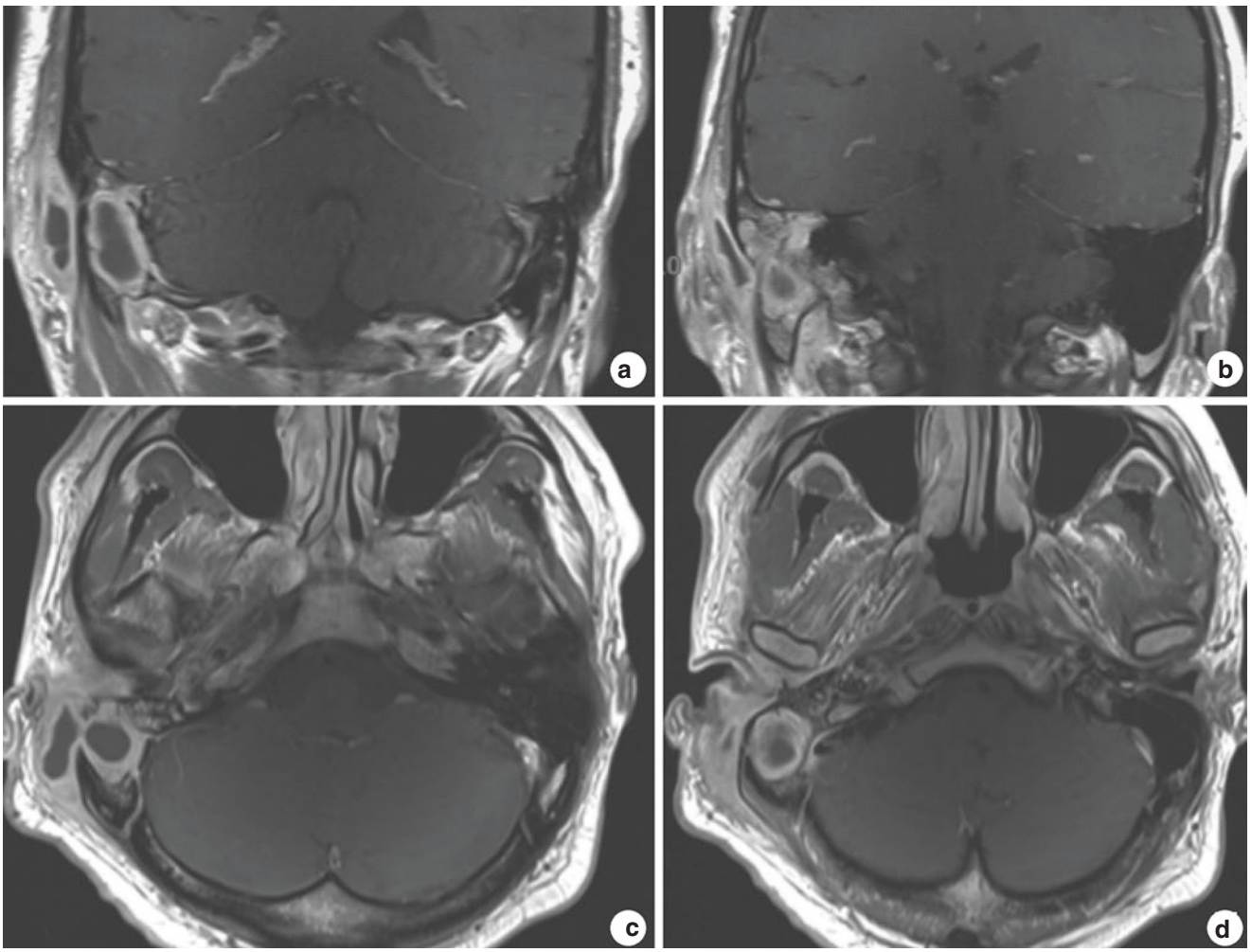

Fig. 20.9 Cholesteatoma in the left tympanic cavity. A 53-year-old female patient with fluid discharge from the left ear since over 10 years and aggravated condition since 2 months. (**a**–**d**) CT non-enhanced scan shows soft tissue density shadows in the tympanic cavity, tympanic antrum and mastoid air cells of left middle ear, irregular tegmen, and intact ossicular chain and facial nerve canal. Intraoperative: The tympanic membrane shows a big perforation with granulation. Granulation is observed in the tympanic antrum and attic. Complete ossicular chain, middle cranial fossa plate and sigmoid sinus plate, facial nerve bone canal and bone lamella of lateral semicircular canal are seen. The images are consistent with intraoperative findings

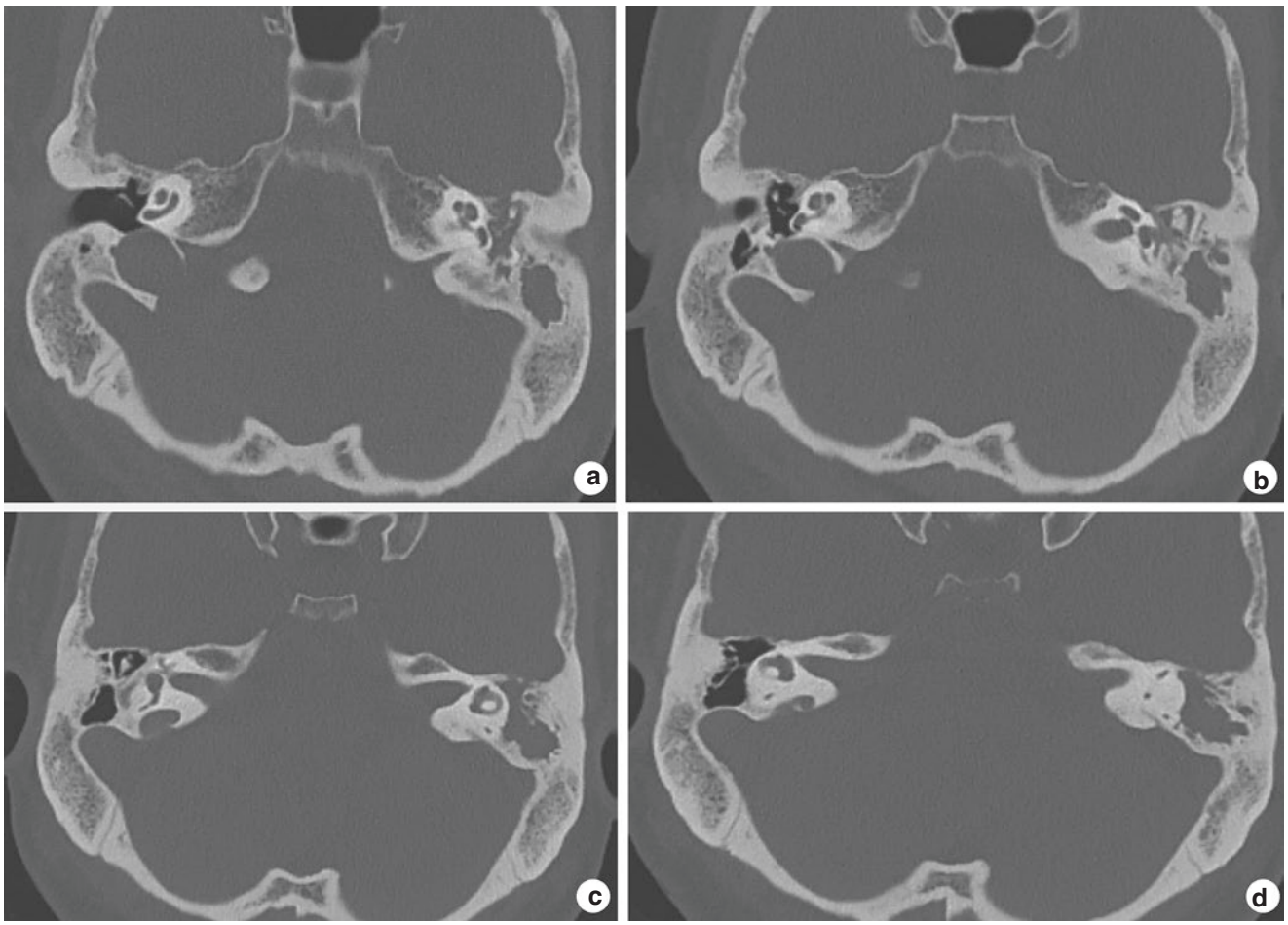

Fig. 20.10 Right chronic otitis media (pars flaccida cholesteatoma). A 44-year-old female patient with recurrent fluid discharge from the right ear with hearing loss since half a year. Physical examination: The upper wall of right external auditory canal collapses with plentiful purulent secretion. (**a**–**d**) CT non-enhanced scan shows crumby soft tissue density shadows in the right external auditory canal, and the tympanic cavity, tympanic antrum and mastoid air cells of right middle ear; the bone shape of right ossicular chain, right tegmen tympani, right anterior sigmoid sinus, right facial nerve cannal and right horizontal semicircular canal (lateral semicircular canal) is irregular (consistent with intraoperative findings)

tory swelling of the middle ear mucosa by enhanced images. In this case, the specific hyperintense on DWI is of value in the diagnosis of cholesteatoma. The enhancement of corresponding segments can be observed in a patient with the invaded facial nerve with inflammation [13] (Figs. 20.11 and 20.12).

20.3.4 [Key Points of Diagnosis]

1. The main clinical symptoms are long-term pus discharge from the external auditory canal, increased secretions, hearing loss and even conductive deafness; The lesion is the same as otomastoiditis after secondary infection.
2. Endoscopy shows the perforated tympanic membrane; at the perforation area, red fragmental or bean dregs-like substances can be seen in the tympanic cavity, with odor.
3. Through the HRCT and MR examinations, the soft tissue mass without enhancement can be seen in the Prussak's space, with the destruction of tympanic scutum and ingression of ossicles, which can suggest the diagnosis of cholesteatoma in the pars flaccida of tympanic membrane. The soft tissue mass without enhancement is found in the posterior tympanic cavity, with the destruction of tympanic antrum and facial nerve recess, and outward movement of ossicles due to compression, suggesting the diagnosis of cholesteatoma in the partes tensa of tympanic membrane. The soft tissue mass without enhancement is observed in the external auditory canal, with local enlargement of the external auditory canal and destruction of bony wall, suggesting the diagnosis of cholesteatoma in the external auditory canal [14]. DWI shows hyperintense in the mastoid process of middle ear, suggesting cholesteatoma.

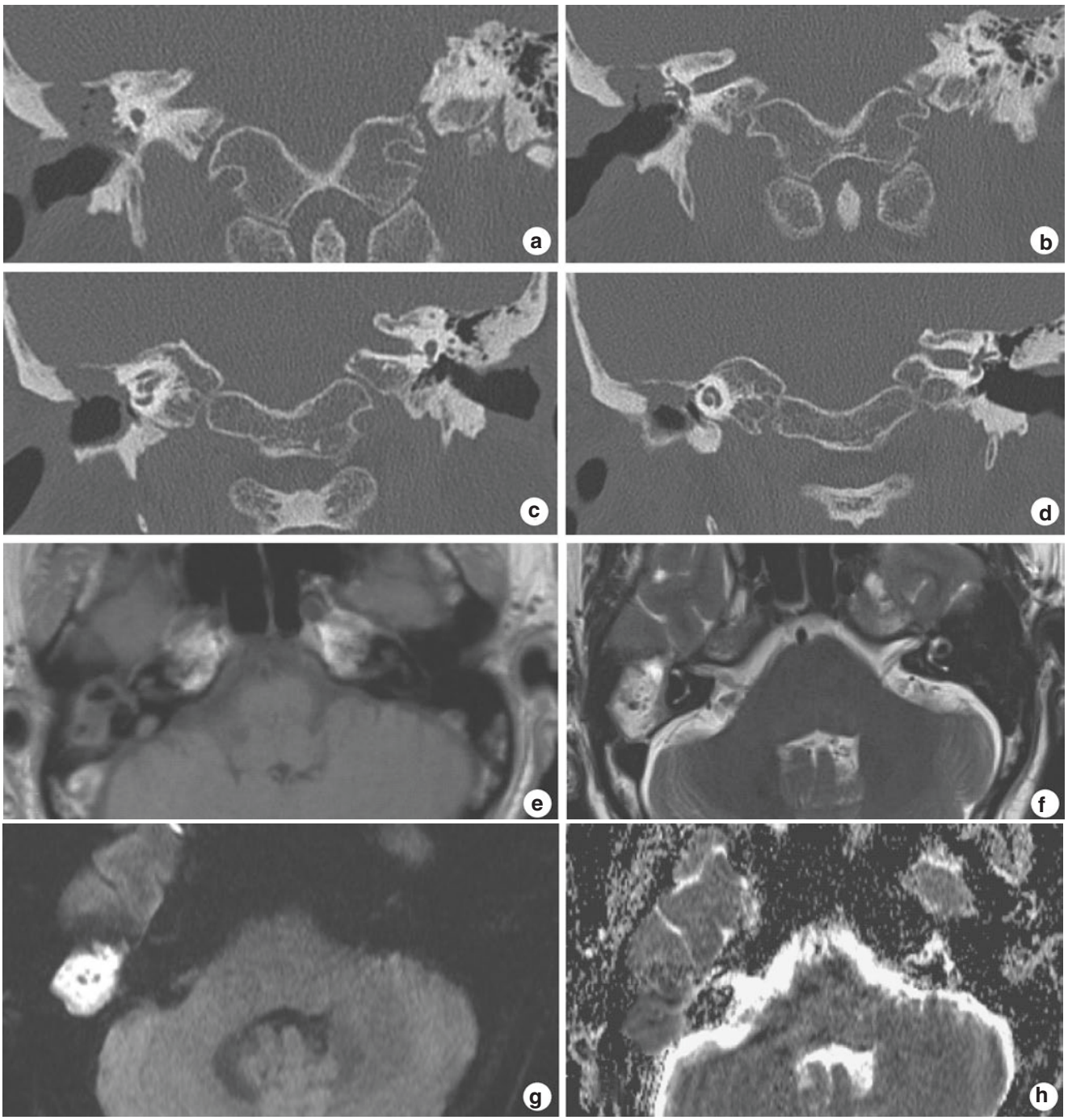

Fig. 20.11 Cholesteatoma in the right tympanic cavity (1). A 49-year-old male patient with pus discharge from the right ear with hearing loss for the past 20 years, aggravated condition since 1 month, and facioplegia since 10 days. Pathological diagnosis: cholesteatoma in the pars flaccida of tympanic membrane of right middle ear with formation of granulation tissue. (**a**–**d**) CT non-enhanced scan shows soft tissue density shadows in the tympanic cavity, tympanic antrum and mastoid air cell of right middle ear, and partially absent bony structure of right mastoid air cell. Incomplete right ossicular chain with partial agenesis and structural destruction of facial nerve canal are noted. (**e**–**h**) The MRI non-enhanced scan for the patient reveals masses in the tympanic cavity, tympanic antrum and mastoid air cells of right middle ear, showing heterogeneous isointense on T_1WI and hyperintense on T_2WI, marked hyperintense on DWI, and isointense on ADC

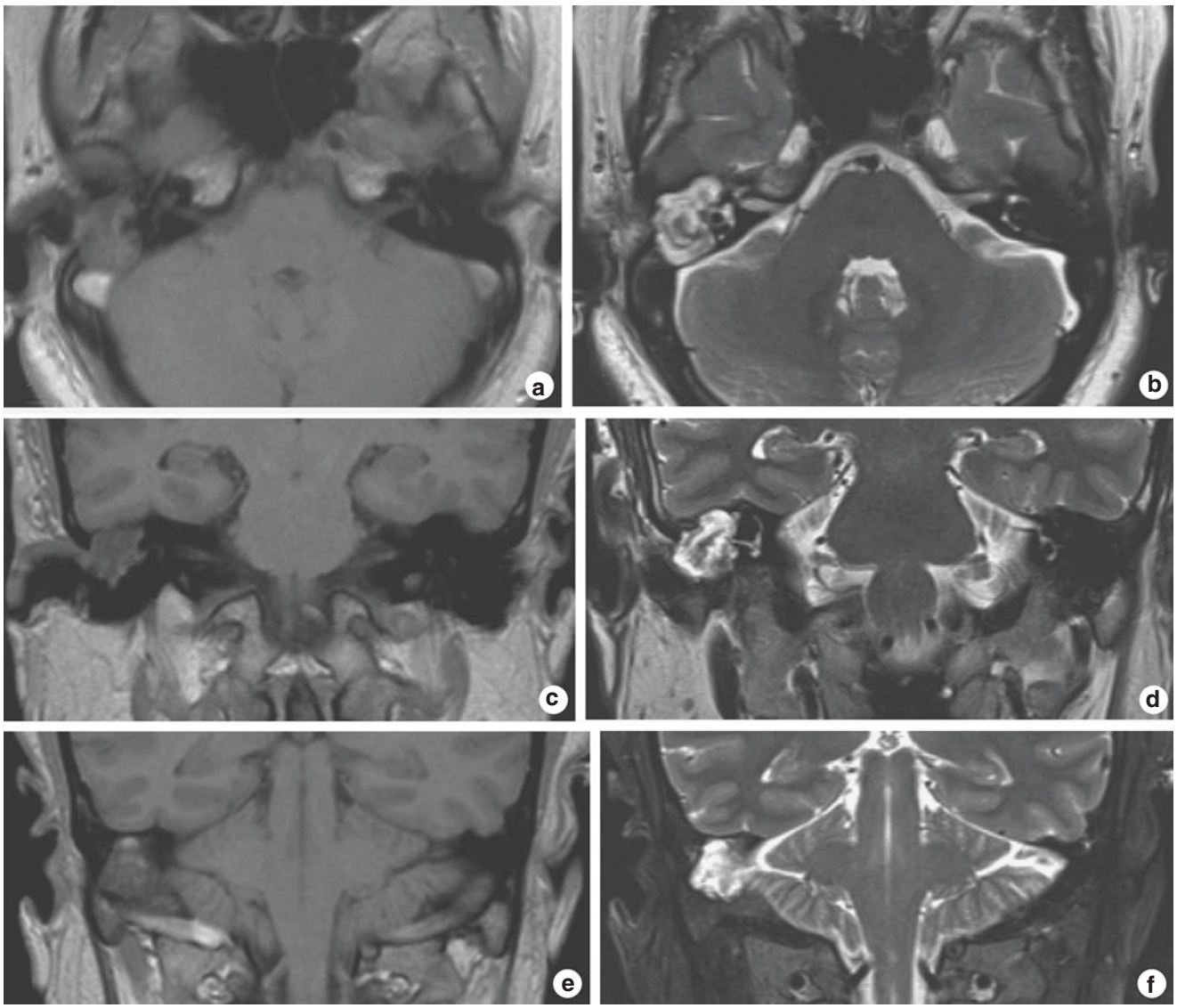

Fig. 20.12 Cholesteatoma in the right tympanic cavity (2). The same patient as that of Fig. 20.10 receives a MRI examination. (**a**–**f**) MRI shows isointense on T1WI and hyperintense on T2WI in the right external auditory canal, and the tympanic cavity, tympanic antrum and mastoid air cells of right middle ear, with heterogeneous signals inside, and the right horizontal semicircular canal (lateral semicircular canal) with ill-defined border from the mass; The mass invades to the right through the right tegmen tympani, and is closely associated with the anterior wall of right sigmoid sinus

4. Cholesteatoma may have many complications, including intracranial meningitis, brain abscess, venous sinus thrombosis, subcutaneous and subperiosteal abscesses. Care should be taken to identify complications on CT and MRI.

20.3.5 [Differential Diagnosis]

1. **Differentiation from Cholesteatoma of Petrous Apex**

(1) Cholesterol Granuloma: T_1WI and T_2WI show hyperintense for the two lesions.

(2) Petrous Apicitis: It is often secondary to otitis media and it shows enhancement on enhanced scan, commonly accompanied by enhancement of adjacent meninges and Meckel's cavity.

(3) Fat Marrow Space of Petrous Apex: It occurs in 5% of the population. It is easily mistaken for a soft tissue mass with osteolytic destruction on CT, and MRI fat saturation sequence may be applied for their differentiation.

(4) Cyst of Petrous Apex: It shows hypointense on T_1WI and hyperintense on T_2WI, which easily makes it mistaken for cholesteatoma. However, it shows hypointense on T_2-FLAIR and DWI, helping the differentiation from cholesteatoma.

2. **Differentiation from Cholesteatoma of Middle Ear**

(1) Chronic Suppurative Otitis Media: On CT, there is osteosclerosis in the mastoid air cells of the middle ear, but the lesion does not show expansionary changes. The destruction and absorption in ossicles may occur, but it is not usually accompanied by the destruction of tympanic scutum and expansion of Prussak's space. The lesion reveals typically inflammatory hyperintense on T_2WI and may show enhancement on enhanced scan.

(2) Other Space-Occupying Lesions of Middle Ear: Such lesions as cancer of middle ear and glomus tympanicum tumor may be manifested as soft tissue shadow in the tympanic cavity; CT shows obvious moth-eaten bone destruction, and enhanced MRI scan shows solid enhancement of the lesion.

3. **Differentiation from Cholesteatoma of External Auditory Canal**

(1) Ketatosis Obturans of External Auditory Canal: The differentiation of the two lesions mainly depends on clinical symptoms. The lesion often occurs simultaneously in two ears and has severe skin inflammation in the external auditory canal, presenting acute pain and keratinized epithelial thrombus occluding the whole bony external auditory canal.

(2) Malignant External Otitis: The disease is common in elderly patients with diabetes or immunodeficiency. It has a wide range of erosion and often involves space between peripheral tissues with serious bone destruction.

(3) External Auditory Canal Cancer: The disease is common in middle-aged and elderly patients who have a history of long-term chronic suppurative otitis media and develop otalgia and bleeding. The focus has a wide range of attack and causes severe peripheral bone destruction with moth-eaten changes. Enhanced MRI scan shows focal enhancement.

20.3.6 [Status Quo and Progress of Research]

HRCT is the first choice for imaging examination of cholesteatoma. In recent years, studies have found that hyperintense on DWI is of highly diagnostic value for cholesteatoma. Enhanced MRI scan is helpful to differentiate cholesteatoma from granulation tissue, tumors and other lesions. The combination use of HRCT and MRI plays a complementary role in imaging diagnosis of cholesteatoma. Currently, CT and MRI can be combined in the diagnosis of cholesteatoma of external auditory canal, and MSCT and CPR techniques can clearly show the enlargement of external auditory canal and bone condition. MRI can clearly display lesions of soft tissue [15].

References

1. Yanling H, Zhenhua W, Qiyong G. Guide series of differential diagnosis for medical imaging - guide for imaging differential diagnosis of five sense organs and neck. Beijing: People's Military Medical Press; 2005.
2. Mafee MF, Valvassori G, Becker M. Valvassori's imaging of the head and neck Edition 2. Translation: Liu Huaijun, et al. Beijing: China Medical Science Press; 2011.
3. Yan S, Dehong L, Hengguo L. Imaging of the head and neck: otolaryngology, head and neck surgery. Beijing: People's Medical Publishing House; 2014.
4. Körner H. Inflammatory diseases of the petrous portion of the temporal bone. Radiologe. 2014;54(4):336–9.
5. Pont E, Mazón M. Indications and radiological findings of acute otitis media and its complications. Acta Otorrinolaringol Esp. 2017;68(1):29–37.
6. Bogomil'sky MR, Polunin MM, Soldatsky YL, et al. Acute otitis media in a 5 year-old child complicated by mastoiditis and abscess of the temporomandibular joint. Vestn Otorinolaringol, 2017;82(2):74–6.
7. Er A, Erdağ TK, Çağlar A, et al. Luc abscess: an extraordinary complication of acute otitis media. Am J Emerg Med. 2016;34(1):117.e1–3.
8. Suisheng Z, Bin L. MRI Diagnosis and clinic - central nervous system, head & neck and skeletal muscles. Hefei: Anhui Science & Technology Publishing House; 2014.
9. Nanda A, Zeki D, Parperis K. Chronic suppurative otitis media complicated with mastoiditis: an unusual presentation of tuberculosis. Am J Med Sci. 2016;352(5):544.
10. Zhang LC, Tong B, Wang ZM, et al. A comparison of three MDCT post-processing protocols: preoperative assessment of the ossicular chain in otitis media. Eur Arch Otorhinolaryngol. 2014;271(3):445–54.
11. Gül A, Akdağ M, Kiniş V, et al. Radiologic and surgical findings in chronic suppurative otitis media. J Craniofac Surg. 2014;25(6):2027–9.
12. Jimei J, Hao Z, Luo Y, et al. Imaging diagnosis of middle ear cholesteatoma: comparative study on high resolution computed tomography and magnetic resonance imaging. Progr Mod Biomed. 2015;15(9):1700–4.
13. Sanjay V, Yogesh K, Neelam V, et al. Role of magnetic resonance imaging in cholesteatoma: the Indian experience. Indian J Otolaryngol Head Neck Surg. 2013;65(3):485–92.
14. Meeta B, Hiren D, Atul K, et al. Is routine use of high resolution computerized tomography of temporal bone in patients of atticoantral chronic suppurative otitis media without intracranial complications justified? Indian J Otolaryngol Head Neck Surg. 2018;70(1):79–86.
15. Wu YZ, Tang XL, Shao WF, et al. Effect of CT manifestations of cholesteatoma on MMP-2, MMP-9 and IL-6 in the serum of patients. Exp Ther Med. 2019;17(6):4441–6.

Special and Rare Ear Inflammation

21

Meizhu Zheng, Jingshi Wang, and Shuang Xia

21.1 Necrotizing External Otitis and Otitis Media

21.1.1 [Overview]

Necrotizing external otitis, also known as malignant external otitis, is an uncommon severe infectious lesion. It mostly presents in immunocompromised elderly patients with diabetes. The main pathogen is *Pseudomonas aeruginosa*. Aspergillus and other organisms may be pathogenic factors in patients with immunodeficiency or AIDS. Its clinical manifestations are persistent pain of external auditory canal, increased secretions and conductive deafness; At the advanced stage, the disease may cause facial nerve palsy and paralysis in cranial nerves IX–XII. Intracranial dissemination can lead to sigmoid sinus thrombosis, meningitis, and intracranial empyema [1].

Necrotizing external otitis, osteomyelitis of mastoid process and middle ear, osteitis of skull base, skull base osteomyelitis are used to describe osteomyelitis in the temporal bone. There is still a great confusion in its definition [2]. Necrotizing external otitis is an infection involving the external auditory canal and surrounding bones [3]. Considering that it is not a tumor, the name "malignant external otitis" is being replaced. In the osteomyelitis, infection involves blood vessels of bones, impairs blood flow, and causes new bone formation around the necrotic or infected bones and necrotic area, resulting in sequelae. The sudden occurrence of symptoms and signs at the initial infection period is suggestive for acute osteomyelitis. If the infection is not completely resolved at this stage, subacute or chronic osteomyelitis will become apparent.

21.1.2 [Pathology Findings]

The pathological findings are inflammatory granulation tissue and necrotic tissue. Autopsy studies have demonstrated that in addition to granulation and fibrous tissue, fibroblasts and papillary proliferation occur in cases with the diseases of outer ear [2]. Inflammation extends into the middle ear through the tympanic membrane, resulting in complete destruction of the tympanic membrane. A mass of osteoblast and osteoclast are produced in the bony wall of external auditory canal, and the ossicular chain is obviously destroyed. The auditory tube is full of granulation tissue. The dehiscence of horizontal part of facial nerve canal causes inflammatory cells to invade the bone canal and surrounding area of the nerve [4].

21.1.3 [Imaging Findings]

1. **X-ray Examination**. X-ray examination is not very helpful for early diagnosis. In some cases, the projection of the external auditory canal on the affected side is not complete on radiographs of Schiller' view or Mayer's view, with blurred bony high-density line shadow. For advanced cases, there is serious bone destruction of external auditory canal and mastoid process and petrous pyramid of temporal bone. The radiograph of skull base shows the external auditory canal with no air and increased density, blurred bony wall, bone destruction of petrous pyramid, and disappeared contour. The radiographs of Schiller' view and Mayer's view show bone destruction of petrous pyramid and mastoid process on the affected side, structure disorder, and lack of specificity.

M. Zheng
Tianjin Third Central Hospital, Tianjin, China

J. Wang
Dalian Women and Children Medical Center, Dalian, China

S. Xia (✉)
Tianjin First Central Hospital, Tianjin, China

H. Li et al. (eds.), *Radiology of Infectious and Inflammatory Diseases - Volume 2*,
https://doi.org/10.1007/978-981-16-8841-6_21

2. CT Examination

(1) Early stage: The examination shows no significant abnormality, or presents thickening and swelling of soft tissue of external auditory canal, narrow external auditory canal cavity, and mild erosion of bony wall. Subsequently, the lesion is gradually expanded so that the external auditory canal is filled with irregular moth-eaten bone destruction in bony wall of external auditory canal and coarse edge. Bone destruction of the corresponding bone canal can be observed if the facial nerve canal and other bony nerve canals be involved [4].

(2) Advanced Stage: The lesion has a very wide range of involvement. Soft tissue swelling of external auditory canal and cellulitis or abscess adjacent to deep space and bone destruction can be noted. The inflammation usually spreads downwards to soft tissue beneath the temporal bone through small cracks in the temporal segment of external auditory canal, and involves stylomastoid foramen and infratemporal fossa. The inflammation may also invade backwards mastoid air cells and inwards the tympanic cavity, internal ear region, parapharyngeal space, and soft tissue of nasopharynx. The focus may surround carotid artery, internal jugular vein and other blood vessels and may involve the carotid sheath region. Infection may rapidly involve forwards temporal-mandibular joints and parotid gland region through the infratemporal fossa region. The pain of temporal-mandibular joints may be the first symptom of necrotizing external otitis. Facioplegia is often the initial nerval symptom, suggesting the involvement of the course area of facial nerve canal. In severe cases, severe osteomyelitis may occur throughout the petrous pyramid and invade backwards the clivus of occipital bone and further the skull, causing secondary meningitis, brain abscesses, venous sinus thrombosis and other intracranial complications, and may even spread down through the vertebral canal. The involvement of jugular fossa in patients may also lead to sigmoid sinus and jugular embolism (Fig. 21.1a–d).

3. MRI Examination. The external auditory canal and surrounding soft tissue shadows show hypointense on T_1WI and heterogeneous signal on T_2WI. T_1WI shows the hyperintense shadow in bone marrow cavity fat of involved mandible and skull base replaced by the hypointense shadow (Fig. 21.1e–j). On enhanced scan, T_1WI reveals heterogeneous enhancement of diffuse soft tissue shadow and hypointense shadow of bone marrow cavity and no enhancement of abscesses. The dynamic curve of the solid part of the lesion is a plateau pattern, suggesting the inflammatory lesion. When the lesion involves the skull, enhanced MRI scan can clearly show the enhanced inflammatory focus. When the facial nerve is involved, the facial nerve shows segmental enhancement, and the involvement of adjacent meninges presents as thickening and enhancement (Fig. 21.2).

The four modes of peripheral extension in necrotizing external otitis are medial, anterior, crossed, and intracranial extension. Anterior extension: extension and involvement of masticatory space and/or condylar bone marrow infiltration; medial extension: thickening of side wall of ipsilateral nasopharynx and/or ipsilateral soft tissue infiltration; crossed extension: the side wall of contralateral nasopharynx thickened due to contralateral soft tissue infiltration; intracranial extension: enhanced cerebral dura mater. In addition to the above modes, lesions may also occur in blood vessels. Fungi normally spread in vessels, keeping the temporal bone relatively intact [2].

21.1.4 [Key Points of Diagnosis]

1. Patients are the elderly with diabetes or immunodeficiency. Severe otalgia, purulent bloody otorrhea, and granulation tissue at the junction of bone and cartilage of the basal wall of the external auditory canal, unlike signs, are non-specific initial manifestations.
2. *Pseudomonas aeruginosa* is found in a pathological biopsy of granulation tissue of external auditory canal.
3. CT and MRI show soft tissue foci in the external auditory canal with different degrees of tamponade inside and irregular moth-eaten bone destruction of adjacent bony wall. The enhancement of invaded nerve segments can be observed on enhanced MRI. The lesion easily spreads to peripheral tissues and space, and at the advanced stage, it has a wide range and invades the skull, causing severe intracranial infection.

21.1.5 [Differential Diagnosis]

1. **External Auditory Canal Cancer.** The disease has similar clinical symptoms and imaging findings to necrotizing external otitis. The main identification method relies on pathological biopsy. It is necessary to perform a timely and early biopsy of granulation tissue of basal wall of external auditory canal. Latent tumors that do not respond to routine anti-inflammation therapy may be excluded [4].

2. **Severe Non-Specific External Otitis.** The lesion generally do not invade the bony wall of external auditory canal and peripheral tissue space, and the bone plate does not have vascular necrosis and can be re-calcified.

3. **Nasopharyngeal Tumor.** In a few cases, necrotizing external otitis may occur bilaterally and infiltrate centrally. It needs to be differentiated from primary nasopharyngeal tumors. The key of identification is the center of nasopharyn-

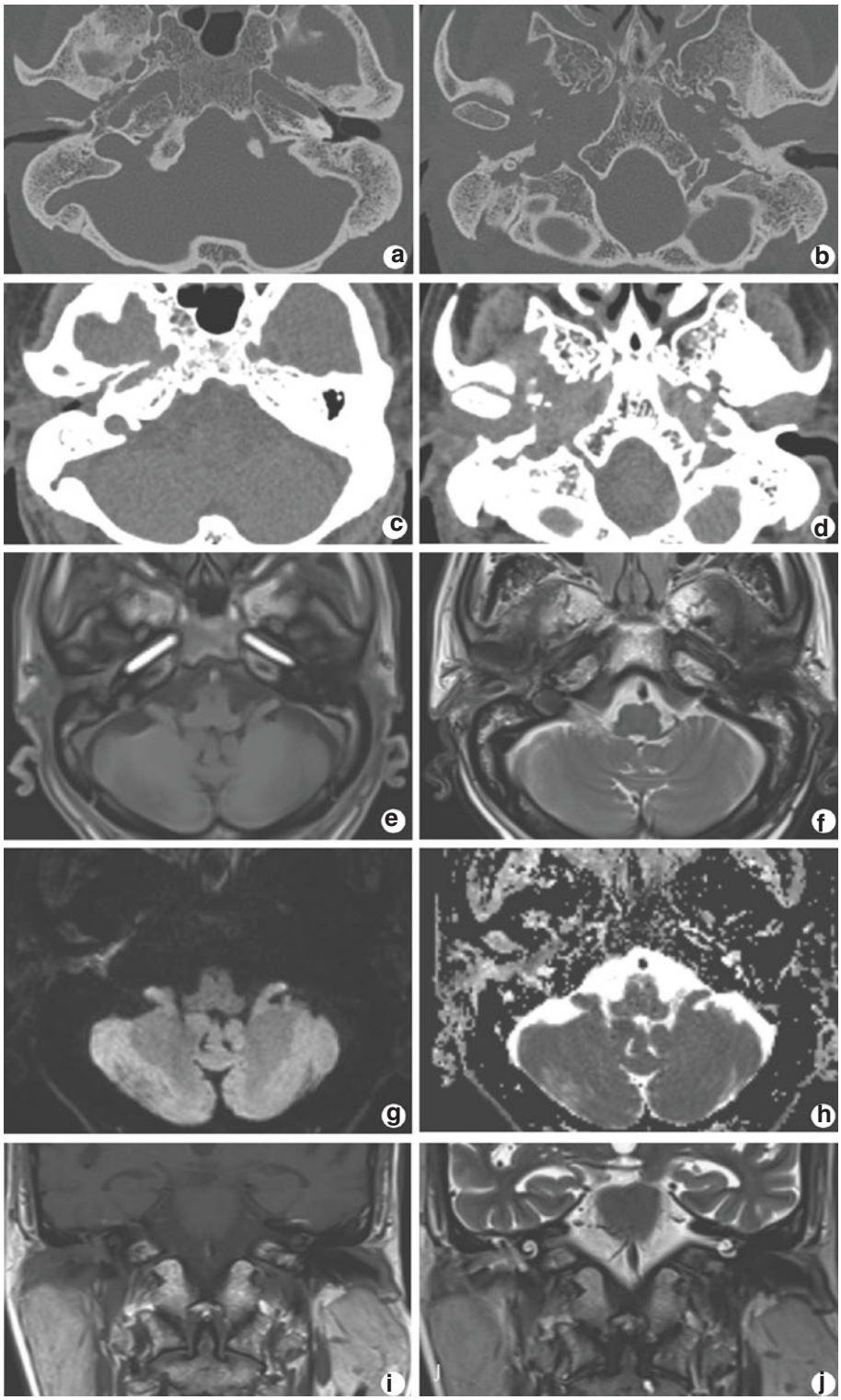

Fig. 21.1 Necrotizing external otitis (1). A 83-year-old male patient. with biopsy of nasopharyngeal mass. Pathological findings: chronic inflammation of mucosa with proliferation of lymphoid tissue, and some tissues deformed by compression. IHC: no obviously preponderant proliferation for CD3 and CD20, epithelial positive for CK, negative for CD56, negative for Syn, sparsely positive for Ki-67. Clinical diagnosis: Right necrotizing external otitis; endocarditis; right infection of parapharyngeal space; skull base osteomyelitis. (**a**–**d**) High-resolution CT of temporal bone shows soft tissue density shadow in the right external auditory canal, growing towards the petrous apex, incomplete bone structure of anterior wall of right external auditory canal with unsmooth surface, incomplete bone structure of right foramen lacerum, bone erosion of petrous apex, and bilateral mastoid process in diploetic type. (**e** and **f**). MRI shows strip-like isointense on T_1WI and slightly hyperintense on T_2WI in the right external auditory canal. (**g**) DWI shows isointense or slightly hyperintense. (**h**) ADC shows isointense. (**i**, **j**) Coronal MRI reveals soft tissue shadow, involving the posterior wall of tympanic cavity of middle ear, and connected with the skull

geal tumors located in the nasopharynx, usually not accompanied by soft tissue shadow in the external auditory canal and bone destruction of adjacent bony wall.

4. **Malignant Tumor of Temporal Bone.** Malignant tumors of temporal bone, including temporal osteosarcoma and metastatic tumor, cause bone destruction centered on the temporal bone, with slight changes in the outer ear in most cases, degree of destruction not directly proportional to mass size, and limited swelling of peripheral soft tissue.

5. **Cancer of Middle Ear.** The imaging examination shows bone destruction of middle ear cavity with irregular margin in silkworm-eaten appearance and local soft tissue

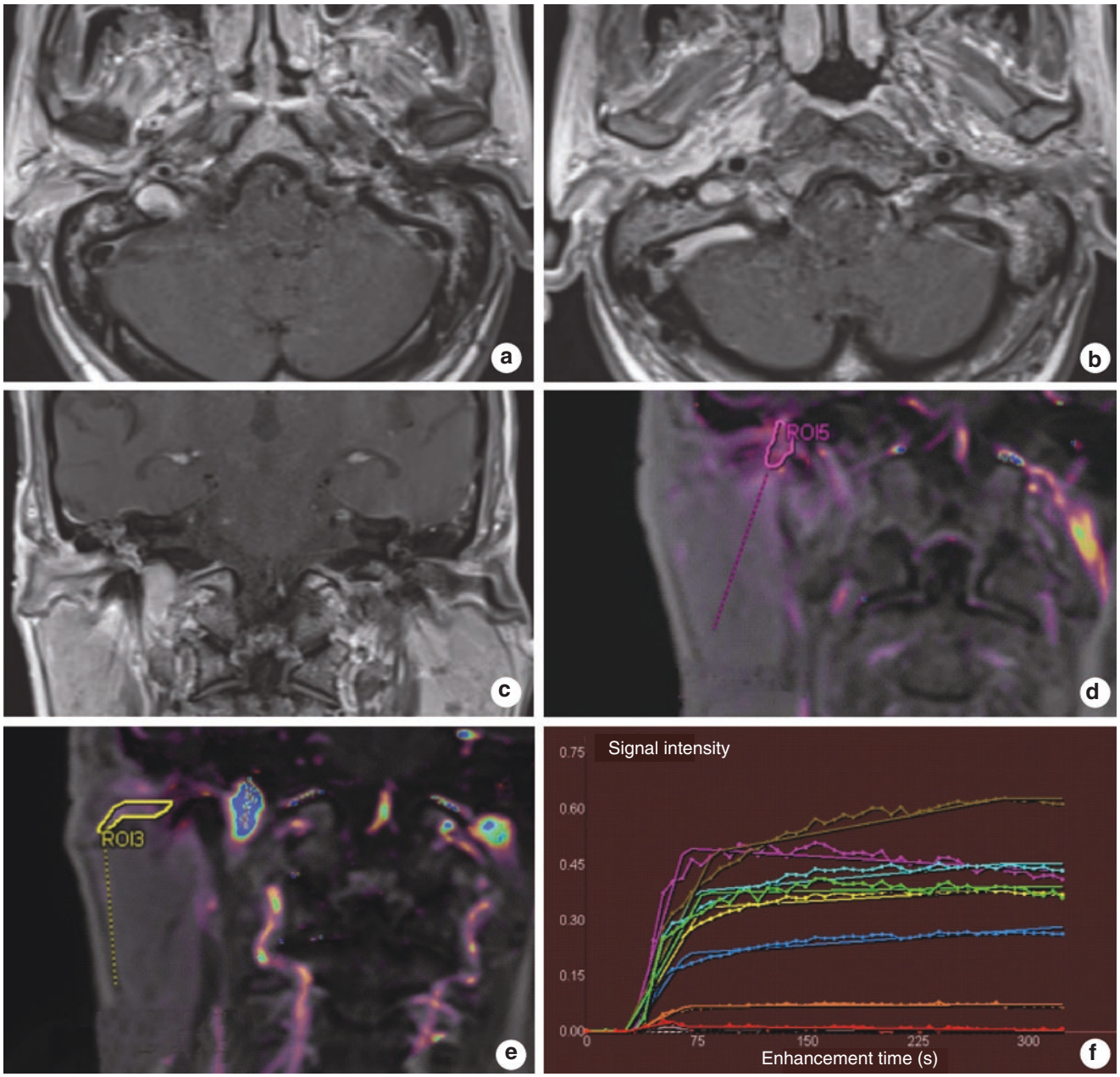

Fig. 21.2 Necrotizing external otitis (2). The same patient as that of Fig. 21.1 receives the dynamic contrast-enhanced MRI examination in order to determine the presence of intracranial invasion and bone marrow involvement. (**a** and **c**) Enhanced T_1WI in the coronal plane and transverse plane shows marked enhancement of soft tissue in the external auditory canal and the tympanic cavity of middle ear. (**c**) Enhanced T_1WI in the coronal plane shows the lesion surrounding the right temporal-mandibular joint and invading the right auditory tube and right parapharyngeal space, and thickened meninges of adjacent right temporal pole with linear marked enhancement (arrow). (**b**) Enhanced T_1WI in the transverse plane shows marked enhancement of bone marrow at the squamous part and the petrous apex of the right temporal bone. (**d**–**f**) The enhancement curve of soft tissue in the right external auditory canal and tympanic cavity of middle ear is a rapid plateau pattern. The enhancement curve of the meninges of right temporal pole is a rapid plateau pattern, suggesting the inflammatory lesion

mass. The lesion shows enhancement after enhanced scan. At the late stage, the external auditory canal may be involved.

21.1.6 [Status Quo and Progress of Research]

Imaging examination is very important for definitive diagnosis of malignant external otitis. CT can show bone destruction and soft tissue mass formation in the external auditory canal region in a convenient, fast, and clear manner, so it is recommended as the preferred examination for suspected patients. Patients who are suspected of intracranial infection or difficult to diagnose can further receive enhanced MRI examination. CT can definitely display the extent of infection and bone destruction occurring in late necrotizing external otitis and detect the abscess formation and the infection

involvement of middle ear, mastoid process, facial nerve canal, temporal-mandibular joint, infratemporal fossa, nasopharynx, petrous apex or carotid canal. However, at the early stage of osteomyelitis, prior to the occurrence of bone destruction, there may be no any positive finding on CT Moreover, decreased bone density of the skull base and other manifestations at the late stage may still persist after infection control, so CT is not suitable to judge therapeutic effect. In addition, it is not ideal for CT to observe the extent of intracranial infection and involvement of bone marrow. MRI can clearly show the involvement of intracranial soft tissue, skull base and bone marrow cavity, and enhancement of dura mater, but it is also unsuitable to monitor therapeutic effect as these imaging changes persist. MRI is not recommended as the imaging examination method for early diagnosis because it is unable to observe bone invasion in time. The technetium-99 bone scan can detect bone changes when CT cannot show sufficiently the extent of bone destruction. As destroyed bone cannot be re-calcified, CT is not suitable to observe the effect of antibiotic treatment, but gallium-67 bone scan is very applicable [5]. Patients who receive antibiotic treatment must undergo surgical drainage if sequestrum is found on CT. MRI can reveal the extent of soft tissue invasion.

21.2 Tuberculous Otitis Media

21.2.1 [Overview]

Tuberculous otitis media (TOM) is a rare cause of chronic pyogenic infection of the middle ear and mastoid process. It accounts for only 0.04% of all cases of chronic suppurative otitis media. The disease is common in young people or infants, mostly under the age of 15 and in male. The prevalence of AIDS contributes to continuously increased incidence of the disease. When a patient has a history of tuberculosis and develops chronic otitis media, the possibility of tuberculous otitis media should be considered in the patient. Tuberculous otitis media has three different routes of transmission: inhalation of mucus through the auditory tube; blood dissemination from other tuberculosis foci; direct implantation through the external auditory canal or tympanic membrane perforation. Tuberculous otitis media is more common in children than in adults as secretions can flow into the middle ear cavity through the auditory tube in children [6].

21.2.2 [Pathology Findings]

Histological examination is of great significance in the diagnosis of the disease. Three types of changes are frequently seen: miliary, granulomatous and caseous. The miliary type is associated with superficial infection, the granulomatous type with superficial bony involvement, and the caseous type with massive necrosis and sequestration.

Histological examination can show granuloma formation with caseous necrosis, epithelioid cells and Langhans multinucleated giant cells. The middle ear may be filled with ectopic bone in which the characteristic Langhans multinucleated giant cells, epithelioid cells and round cells are found. The ossicles, except for the stapes footplate, may be destroyed. Tubercles often occupy the facial nerve canal, in place of the nerve, just posterior to the geniculate ganglion.

21.2.3 [Imaging Findings]

1. **CT Examination.** The typical findings are the mastoid cavity of middle ear fully filled with soft tissue foci, with no or little residual air space. (1) In the early stage, no peripheral bone destruction is found on CT, so it is often difficult to be differentiated from the chronic suppurative otitis media. Honeycomb morphology of the bony wall of mastoid air cells of tuberculosis-caused otomastoiditis may persist, in which soft tissue shadows are filled. The bony wall usually has no sclerotic margin; soft tissue foci in the tympanic cavity may extend into the external auditory canal and may be accompanied by thickening of external auditory canal mucosa. (2) In the advanced stage, different degrees of moth-eaten bone destruction can be observed in the peripheral wall of external auditory canal, surrounding area of tympanic cavity, bony wall of mastoid air cells, ossicular chain (the destruction of the long crus of incus is the most frequently seen), and labyrinthine bony wall of internal ear, with irregular and coarse margin. Fragmental sequestrum can be found in soft tissue foci within the tympanic cavity, with abscesses around the auricle and mastoid fistula, etc. Foci in severe cases may invade the bone of skull base, causing tuberculous osteomyelitis (Fig. 21.3).

2. **MRI Examination**. Soft tissue signal shadows can be seen in the tympanic cavity and mastoid cavity of middle ear. Compared with the gray matter, the focus shows hypointense on T_1WI and isointense, slightly hypointense or slightly hyperintense on T_2WI, and the signals are heterogeneous.

(1) In the early stage, the internal ear is commonly not involved.
(2) In the advanced stage, severe cases have a wide range of foci and the labyrinth, external auditory canal and auricle may be involved. The invasion of skull base bone may cause changes of the signal in bone marrow cavity and presents as signs of highly sensitive and non-specific osteomyelitis: hypointense on T_1WI and hyperintense on T_2WI in the bone marrow cavity. On enhanced scan, the

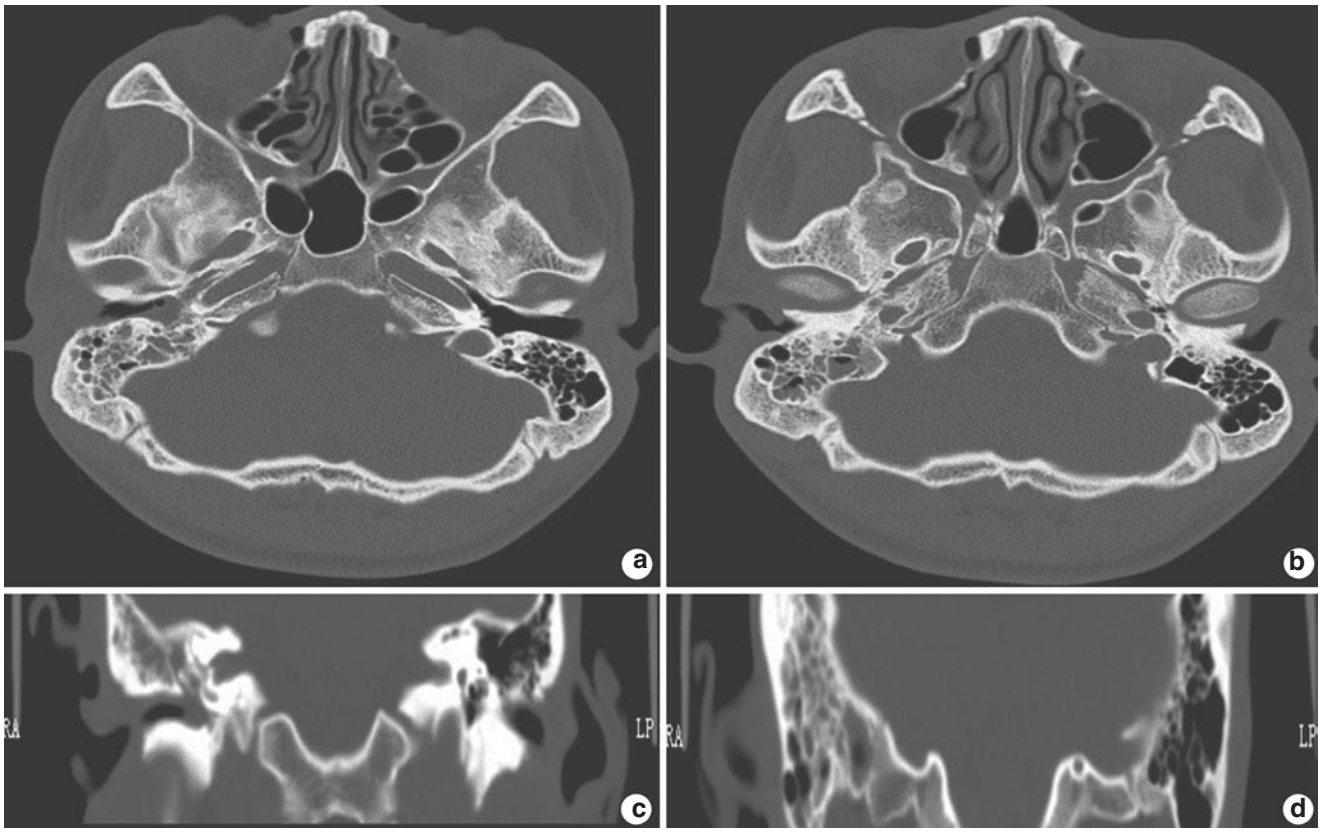

Fig. 21.3 Tuberculous otitis media. A 21-year-old male patient. Pleural effusion is tuberculous exudate on thoracentesis; acid-fast bacilli is found on the smear of right ear secretions. (**a**–**d**) CT non-enhanced scan shows soft tissue density shadows in the right external auditory canal and right mastoid air cell

foci show marked enhancement, with a more clear extent. If a patient's facial nerve is invaded, the facial nerve enhancement is caused, but it is often difficult to distinguish the enhancement from the focus.

21.2.4 [Key Points of Diagnosis]

1. The disease is common in teenagers or infants, mostly in males. Most patients have a history of pulmonary tuberculosis or tuberculosis in other parts of the body. Otoscopy shows multiple perforation of tympanic membrane and pale or pink granulation tissue in the tympanic cavity [7].
2. The typical findings of CT are the mastoid cavity of middle ear filled with soft tissue foci, with no or little residual air space, mastoid bony wall persisting in honeycomb morphology, without sclerotic margin. The lesion may have no peripheral bone destruction in the early stage and may widely involve adjacent structures in the advanced stage, and even invade the bone of skull base in severe cases.
3. On MR, the lesion presents isointense or hypointense on T_1WI, and isointense, slightly hypointense or slightly hyperintense on T_2WI, which are heterogeneous. The enhanced scan shows marked enhancement.

21.2.5 [Differential Diagnosis]

1. **Cholesteatoma Otitis Media.** It mostly occurs in Prussak's space, and the tympanic scutum is the first bone to be damaged, while the tympanic scutum in tuberculous otitis media is generally intact. The possibility of labyrinthine fistula and facioplegia in cases of cholesteatoma otitis media is significantly lower than that in cases of tuberculous otitis media. Cholesteatoma mostly presents with thickened mucosa of external auditory canal after treatment, while thickened mucosa of external auditory canal in tuberculous otitis media is usually not responsive to antimicrobial therapy [4].

2. **Chronic Suppurative Otitis Media.** Long-term chronic pyogenic inflammation in the tympanic cavity is often accompanied by osteosclerosis of tympanic cavity wall and mastoid air cells. MRI examination shows hyperintense typical of inflammation on T_2WI. In the early tuberculous otitis media, there is no sclerotic margin in adjacent bony wall; a wide range of bone destruction may occur in the advanced stage. The lesion shows slightly hyperintense on T_2WI [8].

3. **Secretory Otitis Media.** It is common in children with hypertrophy of nasopharyngeal vegetation. The obstruction of the auditory tube causes effusion in the tympanic cavity,

so the peripheral wall of tympanic cavity and the ossicular chain generally have no bone destruction. In MRI examination, the disease shows bright hyperintense on T_2WI.

21.2.6 [Status Quo and Progress of Research]

CT examination is first performed to observe the filling of soft tissue lesion in the mastoid process of middle ear and bone destruction. When intracranial infection is suspected, further enhanced MRI examination should be performed in time to determine. In patient with intracranial complications, MRI can monitor the therapeutic effect, helping clinical development of further treatment regimen [6, 7].

21.3 Other Rare and Special Otitis Media

21.3.1 [Overview]

The acquired immunodeficiency syndrome (AIDS) otitis media (Fig. 21.4), syphilitic otitis media (Fig. 21.5) and fungal otitis media among rare and special titis media refer to the culture of specific pathogens in the mastoid cavity of middle ear [9]. Untreated human immunodeficiency virus (HIV) infection and HIV-related immunosuppression can significantly increase the risk of opportunistic infections caused by bacteria, viruses, fungi and protozoa. Radioactive otitis media (Fig. 21.6) is necrosis of sterile radioactive tissue occurring after radiographic exposure of mastoid cavity of middle ear. It is usually manifested as chronic inflammation of the middle ear and mastoid cavity, presenting with repeated discharge of secretions through the perforation of the tympanic membrane or otorrhea.

21.3.2 [Pathology Findings]

The common pathological features of rare otitis media are mucosal swelling, effusion and secondary infection in the early stage and fibrotic changes in the advanced stage.

21.3.3 [Imaging Findings]

1. CT Examination

(1) Early Stage: No peripheral bone destruction is found on CT, so these types of otitis media are difficult to be differentiated from the chronic suppurative otitis media.

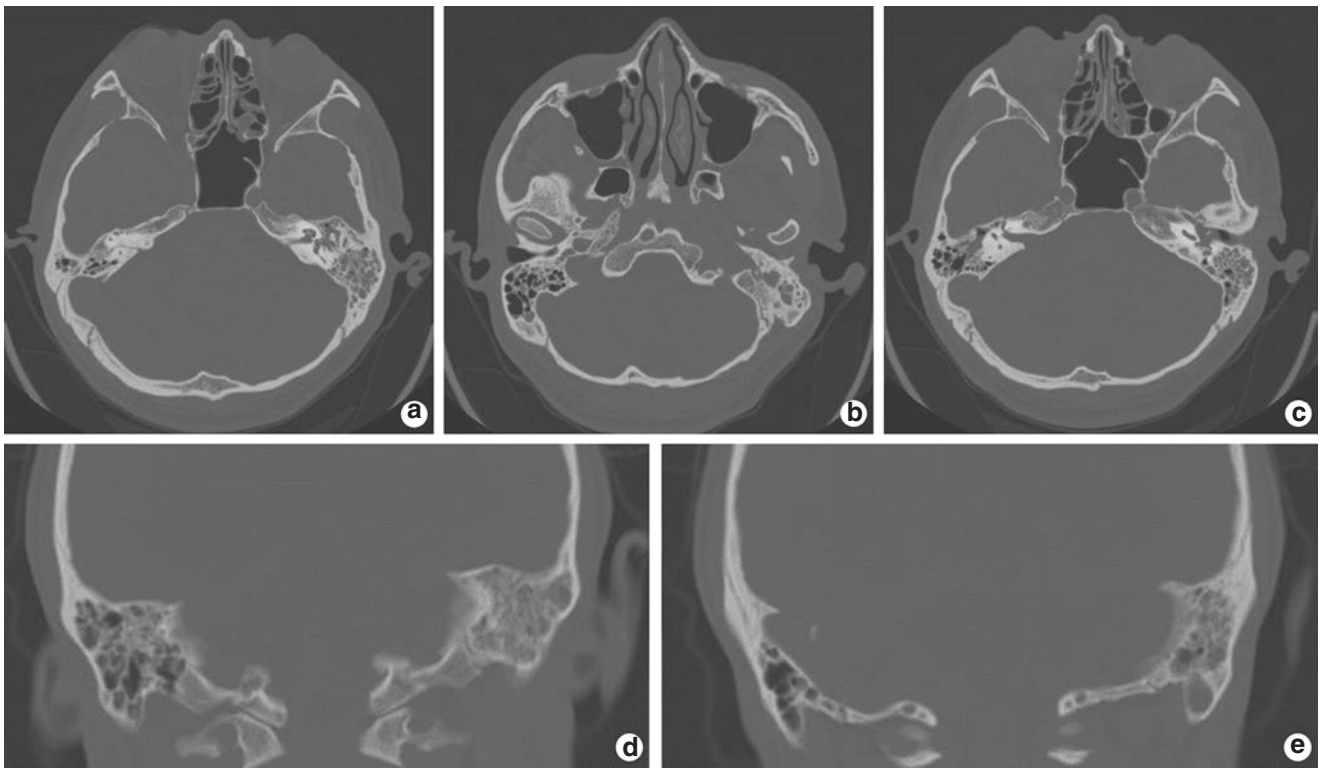

Fig. 21.4 AIDS otitis media. A 28-year-old male patient was found to have positive HIV antibody 10 months ago, blurry vision in the right eye more than 2 months ago, and hearing loss in the left ear 1 week ago, accompanied by tinnitus and pus discharge. CT non-enhanced scans in the transverse plane (**a**–**c**) and coronal plane (**d**–**e**) show soft tissue density shadows in the left tympanic cavity and mastoid process of middle ear, soft tissue density shadow in the left external auditory canal, and no obvious bone destruction in bilateral ossicles

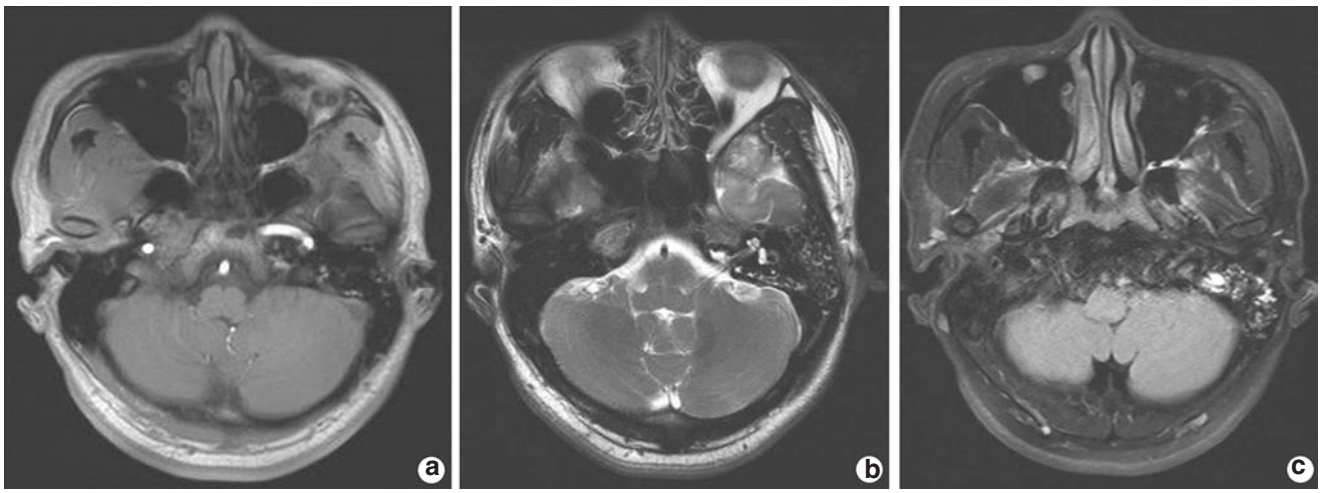

Fig. 21.5 Syphilitic otitis media. A 28-year-old male patient was found to be HIV antibody-positive 5 days ago and blood syphilis antibody positive. Symptoms, such as disturbance of consciousness, slow reaction, projectile vomiting, occur without any causes. (**a**–**c**) MRI non-enhanced scan shows spotted and patchy hyperintense on T_1WI and hyperintense on T_2WI in the mastoid process of left middle ear, and hyperintense on FLAIR

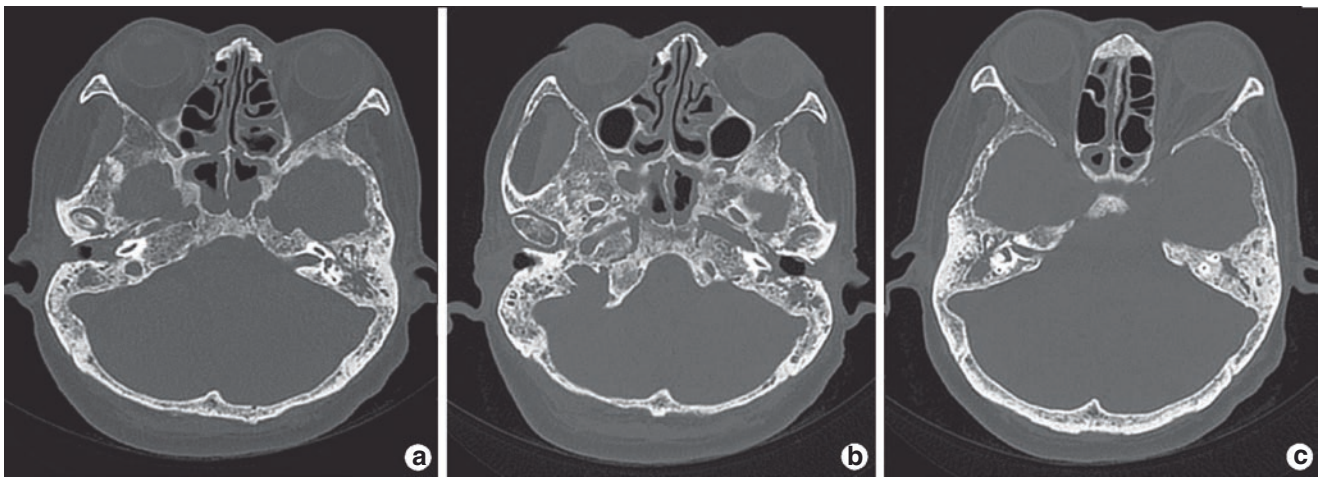

Fig. 21.6 Radioactive otitis media. A 65-year-old female patient with post-radiotherapy of nasopharyngeal carcinoma. (**a**–**c**) Non-enhanced CT scan shows diffuse bone cortex discontinuity in the sphenoid bone, occipital bone, mastoid process of bilateral temporal bones, and bilateral mandible, and bone trabecula in disorderly arrangement and with honeycomb-like change. Soft tissue density shadows can be seen in the mastoid air cells of bilateral middle ears and bilateral external auditory canals, with irregular local bone of bilateral ossicular chains

Honeycomb morphology may persist, and liquid tissue shadows are filled inside. The bony wall usually has no sclerotic margin; after the periosteum perforation, liquid density foci in the tympanic cavity may extend into the external auditory canal and may be accompanied by thickening of external auditory canal mucosa.

(2) Advanced Stage: Different degrees of bone destruction can be observed in the peripheral wall of the external auditory canal, around the tympanic cavity, bony wall of mastoid air cells, ossicular chain, and labyrinthine bony wall of internal ear, with coarse and irregular margin. Fragmental sequestrum can be found in soft tissue foci within the tympanic cavity, with abscesses around the auricle and mastoid fistula, etc. Foci in severe cases may invade the bone of skull base, causing osteomyelitis.

2. **MRI Examination.** Liquid signal shadows can be seen in the tympanic cavity and mastoid cavity of middle ear. Compared with the gray matter, the focus shows hypointense on T_1WI and isointense, slightly hypointense or slightly hyperintense on T_2WI, and the signals are heterogeneous.

(1) Early Stage: The internal ear is commonly not involved.
(2) Advanced Stage: Severe cases have a wide range of foci and the labyrinth, external auditory canal and auricle may be involved. The invasion of skull base bone may

cause changes of the signal in bone marrow cavity and presents as signs of highly sensitive and non-specific osteomyelitis: hypointense on T_1WI and hyperintense on T_2WI in the bone marrow cavity. On enhanced scan, the foci show marked enhancement, with a more clear extent. If a patient's facial nerve is invaded, the facial nerve enhancement is caused, but it is often difficult to distinguish the enhancement from the focus.

21.3.4 [Key Points of Diagnosis]

1. Untreated HIV infection and HIV-related immunosuppression can significantly increase the risk of opportunistic infections caused by bacteria, viruses, fungi, and protozoa.
2. The chronic inflammation of the middle ear and mastoid cavity presents with repeated discharge of secretions through the perforation of the tympanic membrane or otorrhea.
3. Otoscopy shows multiple perforation of tympanic membrane, pus or granulation tissue in the tympanic cavity, and pathogens that can be directly isolated.
4. The typical findings of CT are the mastoid cavity of middle ear filled with liquid or soft tissue foci, with no or little residual air space, mastoid bony wall persisting in honeycomb morphology, without sclerotic margin. The lesion may have no peripheral bone destruction in the early stage and may widely involve adjacent structures in the advanced stage, and even invade the bone of skull base in severe cases.
5. On MRI, the lesion presents isointense to hypointense on T_1WI and isointense, slightly hypointense or slightly hyperintense on T_2WI, which are heterogeneous. The enhanced scan shows marked enhancement.
6. The radiotherapy-induced otitis media are manifested as mucosal swelling, effusion and secondary infection in the early stage, and fibrotic changes in the advanced stage.

21.3.5 [Differential Diagnosis]

1. **Cholesteatoma Otitis Media.** It mostly occurs in Prussak's space and the tympanic scutum is the first bone to be damaged, while the tympanic scutum in most of special otitis media is generally intact. Cholesteatoma otitis media has a low possibility of labyrinthine fistula and facioplegia. Cholesteatoma mostly presents with thickened mucosa of external auditory canal only after treatment, while thickened mucosa of external auditory canal in special otitis media is usually not responsive to broad-spectrum antimicrobial therapy.

2. Chronic Suppurative Otitis Media. Long-term chronic pyogenic inflammation in the tympanic cavity is often accompanied by osteosclerosis of tympanic cavity wall and mastoid air cells. MRI examination shows hyperintense typical of inflammation on T_2WI. In the early stage of several special types of otitis media, there is no sclerotic margin in adjacent bony wall; a wide range of bone destruction may occur in the advanced stage. The lesion shows slightly hyperintense on T_2WI.

3. Secretory Otitis Media. It is common in children with hypertrophy of nasopharyngeal vegetation. The obstruction of the auditory tube causes effusion in the tympanic cavity, so the peripheral wall of tympanic cavity and the ossicular chain generally have no bone destruction. In MRI examination, the disease shows bright hyperintense on T_2WI.

21.3.6 [Status Quo and Progress of Research]

Special otitis media, including AIDS otitis media, syphilitic otitis media and fungal otitis media, are clinically rare. However, with the increasing AIDS infection rate, the incidence also rises. Diagnosis and treatment require specific pathogens cultured in the mastoid cavity of middle ear. In recent years, radiotherapy has been recognized in the efficacy in the treatment of nasopharyngeal carcinoma. However, secretory otitis media caused by radiotherapy easily lead to intractable otorrhea. Hence, radioactive otitis media caused by radiotherapy has also caused clinical attention. The pathogenesis and manifestations of radioactive otitis media should be understood and positive prevention measures should be taken [10].

References

1. Takahashi K, Morita Y, Ohshima S, et al. Bone density development of the temporal bone assessed by computed tomography. Otol Neurotol. 2017;38(10):1445–9.
2. Prasad SC, Prasad KC, Kumar A, et al. Osteomyelitis of the temporal bone: terminology, diagnosis, and management. J Neurol Surg B Skull Base. 2014;75(5):324–31.
3. van Kroonenburgh AMJL, van der Meer WL, Bothof RJP, et al. Advanced imaging techniques in skull base osteomyelitis due to malignant otitis externa. Curr Radiol Rep. 2018;6(1):3.
4. Yan S, Dehong L, Hengguo L. Imaging of the head and neck·- otolaryngology, head and neck surgery. Beijing: People's Medical Publishing House; 2014.
5. Balakrishnan R, Dalakoti P, Nayak DR, et al. Efficacy of HRCT imaging vs SPECT/CT scans in the staging of malignant external otitis. Otolaryngol Head Neck Surg. 2019;161(2):336–42.
6. Kryukov AI, Garov EV, Ivoilov AY, et al. The clinical manifestations and diagnostics of otitis media caused by tuberculosis. Vestn Otorinolaringol. 2015;80(3):28–34.

7. Manigandan G, Venkatesh C, Gunasekaran D, et al. Tuberculous otitis media and staphylococcus aureus coinfection in a five-year-old boy with miliary tuberculosis. J Glob Infect Dis. 2013;5(1):26–8.
8. Nanda A, Zeki D, Parperis K. Chronic suppurative otitis media complicated with mastoiditis: an unusual presentation of tuberculosis. Am J Med Sci. 2016;352(5):544.
9. Otology Group of Chinese Society of Otorhinolaryngology (ENT) of Chinese Medical Association, Otology Group of Editorial Board of Chinese Journal of Otorhinolaryngology Head and Neck Surgery. Guidelines for Clinical Classification and Surgery Typing of Otitis Media (2012). Chinese J Otorhinolaryngol Head Neck Surg 2013;48(2): 5.
10. Qiaxin C, Zhigang Z, Yiqing Z. Radioactive secretory Otitis media. J Otolaryngol Ophthalmol Shandong Univ. 2009;23(4):35–7.

Complications and Sequelae of Otitis Media

22

Meizhu Zheng, Jingshi Wang, and Shuang Xia

22.1 Extracranial Complications of Otitis Media

22.1.1 Subperiosteal Temporal Abscess

22.1.1.1 [Overview]

In the acute chronic suppurative otitis media and cholesteatoma, pus accumulated in the mastoid cavity can flow and accumulate beneath the periosteum of temporal bone through the rupture region of lateral bone lamella of mastoid process, forming the subperiosteal temporal abscess. The common causes include acute suppurative otitis media not treated thoroughly, decreased systemic or local immunity, and chronic lesions in the nose and pharynx. It has not been determined whether tympanic cavity catheterization can be complicated with this disease. Poor pneumatization of mastoid process may be associated with the disease. The most common pathogen is staphylococcus aureus.

22.1.1.2 [Pathology Findings]

Vomica formation can be generally seen under the periosteum of ear temporal bone. There is pus in the vomica, and surrounding fibrous granulation tissue forms the abscess wall. Microscopically, a large number of necrotic neutrophils are seen in the vomica; the abscess wall is fibrous granulation tissue, and the neutrophils and lymphocytes are infiltrated inside the wall. When combined with chronic otomastoiditis, it is often accompanied by the infiltration of monocytes and macrophages. Columnar epithelial metaplasia is found in the middle ear sinus cavity. If recurrent bleeding occurs, causing long-term inadequate drainage, cholesterol granuloma may be formed.

22.1.1.3 [Imaging Findings]

1. **CT Examination.** The findings are hypodense liquid or soft tissue density shadow filling the mastoid cavity of middle ear, quasi-circular or oval isodense or hypodense under the periosteum adjacent to the mastoid process, and extensive bone absorption and destruction at the apex of mastoid process. The enhanced scan shows ring enhancement. The non-enhancement hypodense region in the central part is vomica.

2. **MRI Examination.** The mastoid antrum cavity of middle ear shows isointense or hypointense on T1WI and hyperintense on T2WI. When the subperiosteal temporal abscess forms, pus mostly presents isointense or hypointense on T1WI and hyperintense on T2WI, and diffusion-limited hyperintense on DWI sequences. The surrounding abscess wall shows isointense or hypointense on this imaging. On enhanced scan, the abscess wall shows ring enhancement [1]. In the comparison of MRI signals of cholesteatoma, granulation tissue and pus, the signals on T1WI are isointense or hypointense, and the signal intensity is in descending order as follows: granulation, cholesteatoma, pus; the signals on T2WI are hyperintense, and the signal intensity is in ascending order as follows: granulation, cholesteatoma, pus (See Figs. 20.5 and 20.6).

22.1.1.4 [Key Points of Diagnosis]

1. It is secondary to otitis media, belonging to an extracranial complication of otitis media.
2. The mastoid region at the affected area behind the ear has redness, swelling, heat and pain and may develop systemic symptoms, such as chill and fever.
3. The mastoid bone destruction and periosteum destruction of adjacent temporal bone with periosteal proliferation and sclerosis can be seen in the CT bone window.
4. MRI shows ring enhancement and DWI sequences show diffusion-limited hyperintense in the vomica.

M. Zheng · S. Xia
Tianjin Third Central Hospital, Tianjin, China

J. Wang (✉)
Dalian Women and Children Medical Center, Dalian, China

H. Li et al. (eds.), *Radiology of Infectious and Inflammatory Diseases - Volume 2*,
https://doi.org/10.1007/978-981-16-8841-6_22

22.1.1.5 [Differential Diagnosis]

1. Acute Otomastoiditis. The disease is common in children with sudden onset, and significant sense of otalgia, ear fullness and distension, which is mostly secondary to infections in the upper respiratory tract and nasopharynx. Acute patients only have liquid density shadows in the mastoid cavity of middle ear without bone absorption and destruction.
2. Cholesteatoma Otomastoiditis. The structure around the focus changes due to compression, mostly accompanied by bone absorption and destruction. The disease most typically occurs in the lateral attic space, presenting with blunted periosteum ridge and increased lateral attic space.
3. First Branchial Fistula with Abscess Formation. The disease is often accompanied by skin fistula, with shallow location, and presents with swelling of soft tissue around the mastoid process of middle ear with abscess formation and absence of bone destruction changes in the mastoid process of middle ear.

22.1.1.6 [Status Quo and Progress of Research]

For acute ear infectious diseases such as acute otitis media, the occurrence of their complications is associated with individual immune state, individual anatomy and other host factors, and incomplete treatment. Complications may occur by hematogenous dissemination and spreading along the formed pathways (such as vestibular window, cochlear window, internal auditory canal or endolymphatic duct), which are usually divided into extracranial and intracranial complications. Extracranial complications are classified into extratemporal and intratemporal complications. In this section, the subperiosteal temporal abscess belongs to an extratemporal complication. In addition, if the middle ear cholesteatoma destroys the bone at the apex of mastoid process, and inflammation spreads to submaxillary space and parapharyngeal space along the digastric muscle, and further to the mediastinum along the deep cervical fascia space, it is known as Moure's abscess, which is also an extratemporal complication [2].

22.1.2 Labyrinthitis

22.1.2.1 [Overview]

Labyrinthitis is an infectious disease of the internal ear labyrinth caused by bacteria, viruses or other pathogens. In severe cases, it may lead to irreversible damage to vestibular and auditory functions. It can be clinically divided into circumscribed labyrinthitis, serous labyrinthitis, suppurative labyrinthitis and labyrinthitis ossificans, according to the development course of labyrinthitis. The main causes include chronic suppurative otitis media, cholesteatoma secondary to otitis media, meningitis (bacterial, viral, fungal), trauma, viral infection, air pressure change, operation, congenital labyrinthine fistula and autoimmune factors, among which the more common causes are otogenic, meningiogenic, and traumatic. Labyrinthitis with the infection from the tympanic cavity is unilateral, while meningiogenic or hematogenous labyrinthitis is generally bilateral. The most common cause is the acute and chronic infectious lesion of the mastoid process of middle ear directly invading the labyrinth. The routes of infection include vestibular window, cochlear window, promontorium tympani, and lateral semicircular canal fistula. Labyrinthitis may also be caused by pyogenic meningitis infecting perilymph via the subarachnoid space, which is mostly suppurative labyrinthitis. In children with bacterial meningitis, 10%~13.9% develop permanent deafness, which is the most common cause of acquired sensorineural deafness [3].

22.1.2.2 [Pathology Findings]

1. **Circumscribed Labyrinthitis.** It is only limited to local bony labyrinth and its endosteum. The membranous labyrinth itself often has no inflammation. Dizziness and other symptoms may occur due to inflammatory stimulation.

2. **Serous Labyrinthitis.** It may be regarded as the further development of circumscribed labyrinthitis. Inflammation spreads into the perilymph cavity via endosteum, resulting in infiltration of plasma cells (PC) and lymphocytes. The vestibular and auditory functions can be restored to normal as the structure of the membranous labyrinth is not destroyed.

3. **Suppurative Labyrinthitis.** The first two types of labyrinthitis can be transformed into suppurative labyrinthitis after aggravation and deterioration, making the endolymph and perilymph cavities in the whole membranous labyrinth filled with pus, so that irreversible destruction occurs in the vestibule and auditory end organ of middle ear. Its histopathological process has three stages.

(1) Acute Stage: Bacteria or other toxic substances accumulate in the perilymph cavity, causing an acute inflammatory response, and pus enters the endolymph space after further progress, leading to necrosis of membranous labyrinth and then serous fibrin deposits.
(2) Fibrotic Stage: There is fibrous granulation tissue in the perilymph space.
(3) Ossification Stage: When new bones gradually form from the cochlear basal turn, the disease develops into labyrinthitis ossificans.

22.1.2.3 [Imaging Findings]

CT Examination

(1). Circumscribed labyrinthitis: It is caused by labyrinthine fistula and may be manifested as circumscribed bony labyrinth destruction. For the serous labyrinthitis, CT cannot

detect fibrosis or bleeding, and exudate deposition in the labyrinthine lumen, so there is no any abnormal finding on CT of serous labyrinthitis.

(2). Suppurative Labyrinthitis

(1) Acute and Subacute Stages: No abnormality may be found on CT.
(2) Chronic Stage: If the disease at the acute stage is not relieved, it gradually progresses to the chronic stage, resulting in labyrinthine fibrosis and ossification, and the whole course may span months to years. In 2 weeks after labyrinthine infection, fibrous substances may be deposited in the perilymph cavity, without positive findings on CT.
(3) Ossification Stage: At the early stage of ossification, CT shows thickening of osseous spiral lamina or ill-defined inner margin of bony labyrinth. With the progress of the disease, any region of the labyrinthine lumen may present as increased homogeneous or heterogeneous bony density and labyrinthine lumen stenosis and even disappearance due to bone deposition, which is easily observed in patients with chronic sensorineural deafness. Bone deposition may be either focal or diffuse distribution. Focal distribution is most common in the cochlear base. If the whole labyrinthine lumen is filled with deposited bone, CT shows homogeneous bony density at the petrous apex region, without hypodense region of endolymph and perilymph space [4] (Figs. 22.1 and 22.2).

MRI Examination

(1) For the circumscribed labyrinthitis and serous labyrinthitis, the disappearance of fluid signals resulting from intralabyrinthine hemorrhage or exudate deposition may be observed, presenting focal or diffuse isointense or hypointense region on T1WI and T2WI, and slight enhancement is shown in the labyrinth on enhanced scan. If infection involves the facial nerve or vestibulocochlear nerve, neuropathological enhancement can be observed on the enhanced image.

(2) Suppurative Labyrinthitis

(1) Acute and Subacute Stages: The only imaging finding on MRI may be enhancement of normal labyrinthine fluid region with no enhancement on enhanced scan, which may be caused by the destruction of labyrinth-blood barrier due to necrosis of capillary endothelial cells. Such enhancement is usually slight, which is obviously different from the focal and marked enhancement showed in the intralabyrinthine schwannoma. The enhancement of labyrinthitis may be for a long time, persisting until 6 months after symptom alleviation. If combined with facioplegia, the pathological enhancement of facial nerve may occur, and labyrinthine segmental enhancement is not uncommon. The nature of deafness can reflect the degree of cochlea involvement. High-frequency sensorineural deafness suggests the involvement of cochlear base; low-frequency hearing loss suggests lesion involvement in the apex.
(2) Chronic Stage: The finding is disappearance of fluid signals from endolymph and perilymph space in the normal labyrinth cavity, which is easiest to be observed at the cochlear apex. In this period, enhanced MRI scan shows persistent enhancement (Fig. 22.3 a and b).
(3) Ossification Stage: The typical finding on MRI is also disappearance of labyrinthine fluid signals. Based on the extent of labyrinthine ossification, the location of

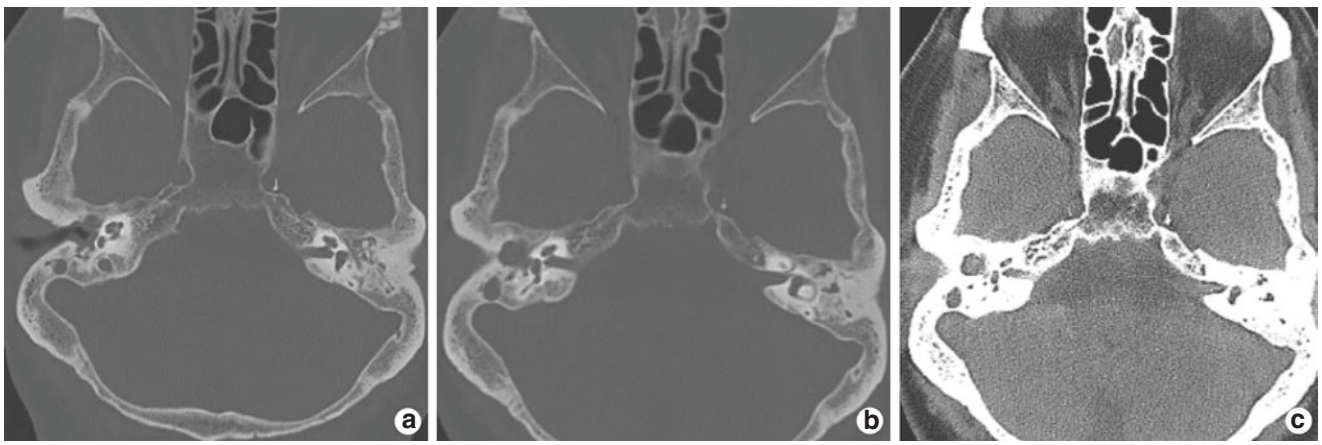

Fig. 22.1 Labyrinthitis. A 60-year-old female patient. with a sense of right ear blocking for the past 1 week with 4-day intermittent vertigo. (**a** and **b**) CT of temporal bone in the transverse plane shows right mastoid process in diploetic type, soft tissue density shadows in the tympanic cavity and tympanic antrum of right middle ear, peripheral bone destruction, and margin sclerosis. Right head of malleus and right incus are displayed unclearly, and the lateral semicircular canal is destroyed. These findings suggest cholesteatoma of right middle ear. (**c**) CT of temporal bone in the transverse plane shows strip-like dense bone deposition shadow at the right cochlear basal helix, suggesting labyrinthitis at the ossification stage

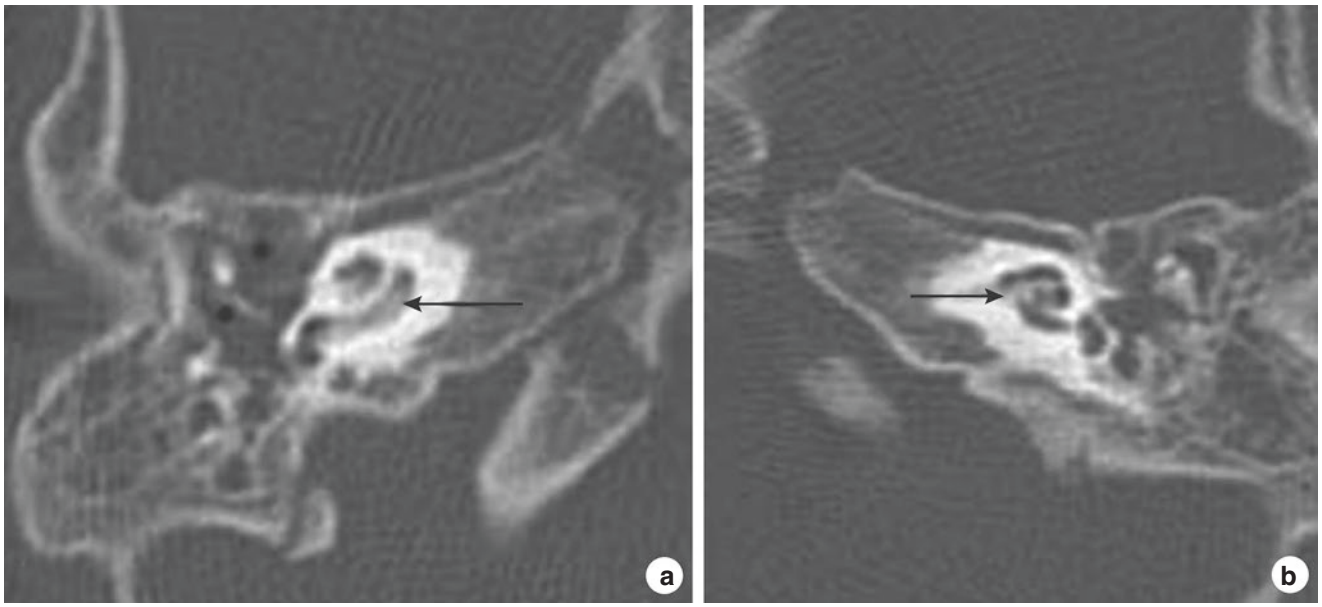

Fig. 22.2 Bilateral labyrinthitis at the ossification stage. A 4-year-old female patient with bilateral hearing loss for the past 2 years. (**a** and **b**) CT scan of temporal bone shows disappearance of gas density shadows in the tympanic cavity, tympanic antrum and mastoid air cells of bilateral middle ears, and slightly hyperdense. The right ossicular chain is not intact. The strip-like dense shadow can be seen in the bilateral cochlear basal helix, suggesting bone deposition

hypointense region on T2WI corresponds to bony composition in the labyrinth cavity on CT. If the labyrinth is fully ossified, the petrous apex region may present as homogeneous no-signal area, so that the labyrinth shape cannot be identified (Fig. 22.3c). On MRI enhanced images, the original bone deposition region in the bony labyrinth and labyrinthine lumen is non-enhancement hypointense region. If there is still pus accumulation or granuloma formation in the labyrinth, focal enhancement can be noted.

3. The imaging sequence of internal ear allows slice thickness to be thinner and provide more clear images. Its 3D-reconstructed labyrinth shape can be randomly rotated and viewed from multiple directions, providing more three-dimensional and visualized information (Fig. 22.3d).

22.1.2.4 [Key Points of Diagnosis]

1. There are often infection foci adjacent to the labyrinth, such as otitis media or meningitis.
2. There are typical auditory and vestibular function impairment symptoms corresponding to each stage of labyrinthitis.
3. Prior to the ossification stage in the labyrinth, CT may show no any abnormality. Labyrinthitis ossificans presents as different degrees of high-density bone deposition in the labyrinthine lumen.
4. The disappearance of fluid signals in the labyrinthine lumen can be observed on MRI. Fibrous matter deposition shows isointense or hypointense on T1WI and T2WI, while the bone deposition shows no-signal area.
5. Intralabyrinthine bone deposition is manifested as the hyperdense region on CT, of which the location corresponds to that of no-signal area in the labyrinth on MRI. The endolymph and perilymph space gradually narrows and disappears.
6. According to the differences in the distribution and extent of fibrosis and granulation tissue, enhanced MRI scan shows focal or diffuse mild to moderate enhancement, with fuzzy border, and the ossified areas are non-enhancement hypointense ones.
7. The affected sides in patients with the unilateral disease are compared with healthy sides for more easy diagnosis.

22.1.2.5 [Differential Diagnosis]

1. **Michel's Deformity.** The cochlea and vestibule are absent, and the outer wall of otocyst is flat. When labyrinthine ossification is serious and diffuse, labyrinthine "whitening" may be found on CT, presenting with increase in homogeneous bony density in the labyrinthine area. Labyrinthitis is difficult to be differentiated from Michel's deformity or cochlear aplasia. The key point of identification is the diameter of otocyst. Its size is normal in patients with acquired labyrinthine ossification, while it is short and small in patients with congenital deformities. In patients with Michel's deformity, the lateral margin of labyrinth is flat or dented inward, while the lateral semicircular canal in

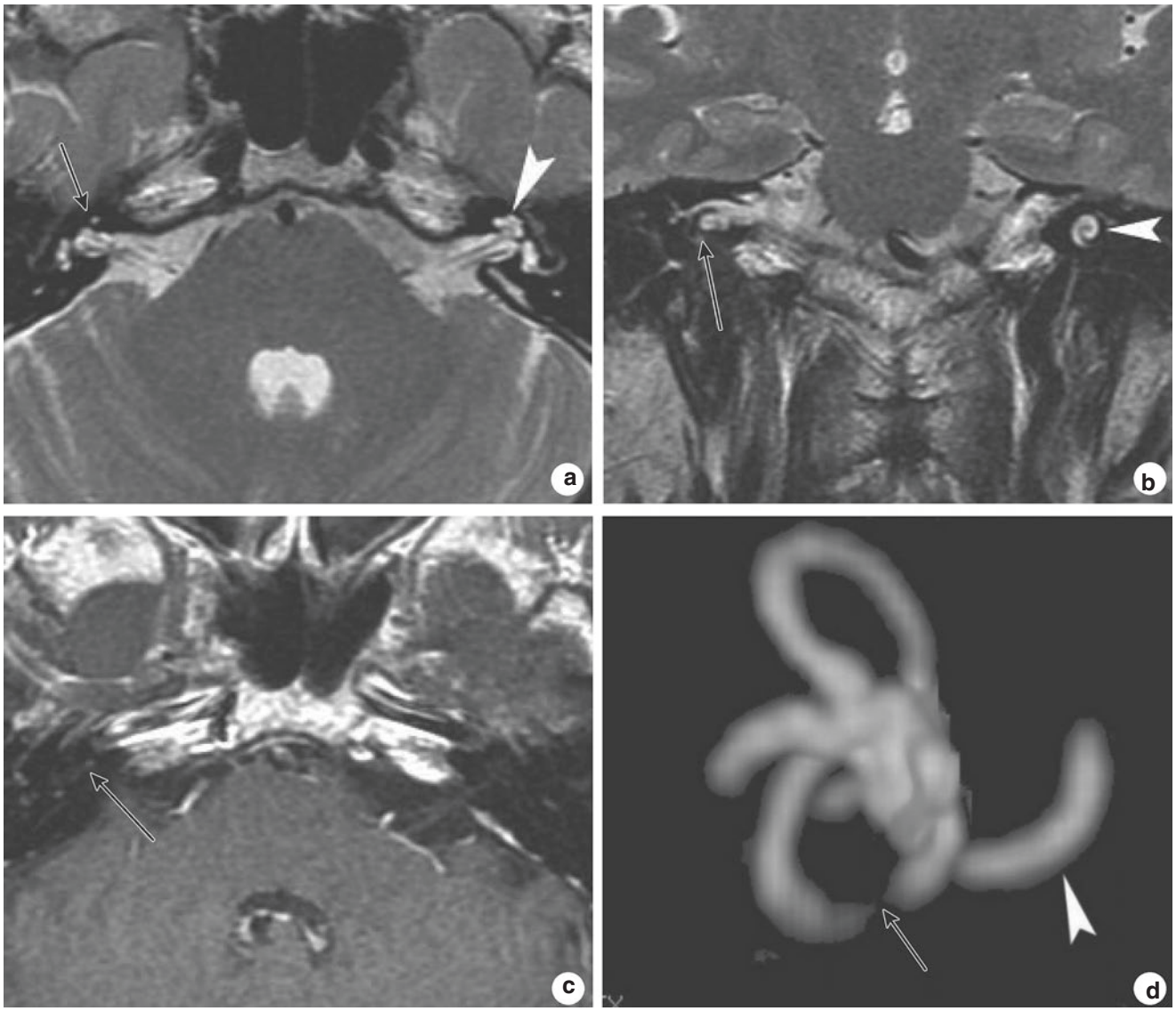

Fig. 22.3 Labyrinthitis at the chronic stage. A 36-year-old male patient with right hearing loss with unsteady walking after trauma for the past 1 year. (**a**–**d**) Non-enhanced MR scan reveals unclear right cochlear helix, disappearance of fluid signal of perilymph space at the cochlear apex, only faintly visible basal helix, discontinuous posterior and horizontal semicircular canals, and strip-like hypointense shadow. The horizontal image more clearly shows incomplete posterior and horizontal semicircular canals, with the base only visible. These findings suggest right labyrinthitis at the chronic stage or ossification stage

patients with labyrinthine ossification protrudes outward. Meanwhile, in combination with medical history, patients with labyrinthitis are manifested as progressive hearing loss and loss of vestibular function [5].

2. Cochlear Otosclerosis. An audiogram shows characteristic findings with perfect vestibular function. There are focal hypodense shadows in the bone around the cochlea, typically presenting as "double-ring sign."

3. **Intralabyrinthine Tumor.** It mainly includes intralabyrinthine schwannoma. The disease mostly occurs in the cochlear basal turn and middle turn. On T2WI, there are intralabyrinthine soft tissue mass shadows with clear and sharp border. On enhanced scan, T1WI shows marked and homogeneous focal enhancement [5].

22.1.2.6 [Status Quo and Progress of Research]

For circumscribed labyrinthitis, serous labyrinthitis and suppurative labyrinthitis at the acute stage, CT examination is of value in the exclusion of potential space-occupying lesions causing labyrinthine infections, and otomastoiditis and abnormal meninges enhancement related to labyrinthitis. In addition, CT examination allows to observe the lateral semicircular canal fistula or some congenital deformities that lead to abnormal communication of the middle ear with the laby-

rinth. The disappearance of local fluid signals in the labyrinthine lumen, with mild enhancement on enhanced scan, can be observed on MRI, which suggests the deposition of serous cellulose and other substances. However, most cases still have no positive finding. When the disease progresses to the late suppurative labyrinthitis, i.e., ossification stage, non-enhanced CT or MRI scan can be used to judge the extent of bone deposition of middle ear in patients with labyrinthitis ossificans. Their combined use is of more diagnostic value. Enhanced MRI scan can also reveal abnormal thickening or enhancement of invaded labyrinth or vestibulocochlear nerve and focal enhancement resulting from residual pus and granulation tissue in the labyrinth of serious fibrosis or ossification. In summary, MRI is more sensitive than CT in the diagnosis of labyrinthitis, which is taken as the preferred examination method. CT is superior to MRI in the display of labyrinthine bone changes, which can be used as an important supplementary examination means. Imaging evaluation is of particular importance for labyrinthitis patients who plan to receive artificial cochlear implantation. Intralabyrinthine bone deposition may affect the smooth placement of artificial cochlear electrodes into the cochlear window niche. Particularly, when the degree of bilateral lesions is different, surgeon may select the side with the milder lesion for artificial cochlear implantation [3, 6].

22.1.3 Petrous Apicitis

22.1.3.1 [Overview]

Anatomically, the petrous apex of the temporal bone is closely related to important neural and vascular structures. Hence, petrous apex infection may result in severe neurological damage. Due to the extensive pneumatolysis and the presence of rich bone marrow, the petrous apex is vulnerable to infection or inflammation, which is generally associated with mastoiditis. Inflammation can spread to the Dorello's Canal with the course of cranial nerves VI and Gasserian ganglion, causing triad of "petrous apex symdrome:" lateral rectus palsy, retro-orbital pain and otorrhea. Petrous apicitis should be suspected in the presence of both otorrhea and deep pain. Petrous apicitis has a low incidence because of the early application of antibiotic to early acute otitis media [7].

22.1.3.2 [Pathology Findings]

The most common pathogen of petrous apicitis is pseudomonas aeruginosa. Acute petrous apicitis often develops rapidly in a short time as the normally pneumatized air cell system at the petrous apex is suddenly blocked. Pus and granulation tissue can be found in the mastoid air cells to the petrous apex. The adjacent bone destruction affects the adjacent meninges, causing the change of meninges thickening. The pathogen, necrotic tissue, and pyocyte can be seen in pus, and there is bone destruction in the air cell septa of petrous apex. Thrombophlebitis or direct infection that spreads to the adjacent meninges, Meckel's cavity and cavernous sinus causes related cranial nerve palsy.

22.1.3.3 [Imaging findings]

1. **CT Examination.** The findings include disappeared air cells at the petrous apex or decreased air content, petrous apex air cells filled with soft tissue or fluid density lesions, destruction of air cell septa, and bone trabecula destruction at the petrous apex, which suggest the confluent petrous apicitis. The extent of involvement varies. The margin is unclear and may be in quasi-circular shape and flaky irregular shape. The adjacent bony labyrinth, jugular fossa, carotid canal or internal auditory canal may be involved (Fig. 22.4 a and b).

2. **MRI Examination.** The lesion at the petrous apex shows isointense or hypointense (often heterogeneous) on T1WI, and hyperintense on T2WI, with unclear edge. When an abscess forms, DWI shows diffusion-limited hyperintense. On enhanced scan, the scanned focus shows edge enhancement, with enhancement in the adjacent meninges. In severe cases, subdural abscesses and even intracranial abscesses may be combined. The Meckel's cavity and cavernous sinus at the same sideshow enhancement [8, 9] (Fig. 22.4 c–e).

22.1.3.4 [Key Points of Diagnosis]

1. Definition. The source of infection presents as petrous apex air cells with incomplete trabeculae and meninges involvement.

2. Image. CT shows confluent petrous apicitis, presenting with trabecular destruction in petrous apex air cells, and cellulitis and abscesses in confluent apex air cells.

3. Gradenigo's Syndrome. The clinical triad relating to petrous apicitis include otomastoiditis, cranial nerves VI palsy and deep facial pain.

22.1.3.5 [Differential Diagnosis]

1. Cholesterol Granuloma. It is manifested as well-defined expansive growth with trabecular destruction at the petrous apex. It shows hyperintense on T1WI and T2WI of MRI.

2. Congenital Cholesteatoma. It presents as well-defined expansive growth and shows hypointense on T1WI of MRI. There is peripheral bone destruction with osteosclerosis without enhancement and no meninges enhancement.

22.1.3.6 [Status Quo and Progress of Research]

The diagnosis can be confirmed by CT of the temporal bone. CT will show turbid and opaque mastoid air cell system and petrous apex, enhancement of cavernous sinus, and bone destruction inside the petrous apex. The gadolinium-enhanced high-resolution MRI of the temporal bone will show hypointense on T1WI and hyperintense on T2WI, as

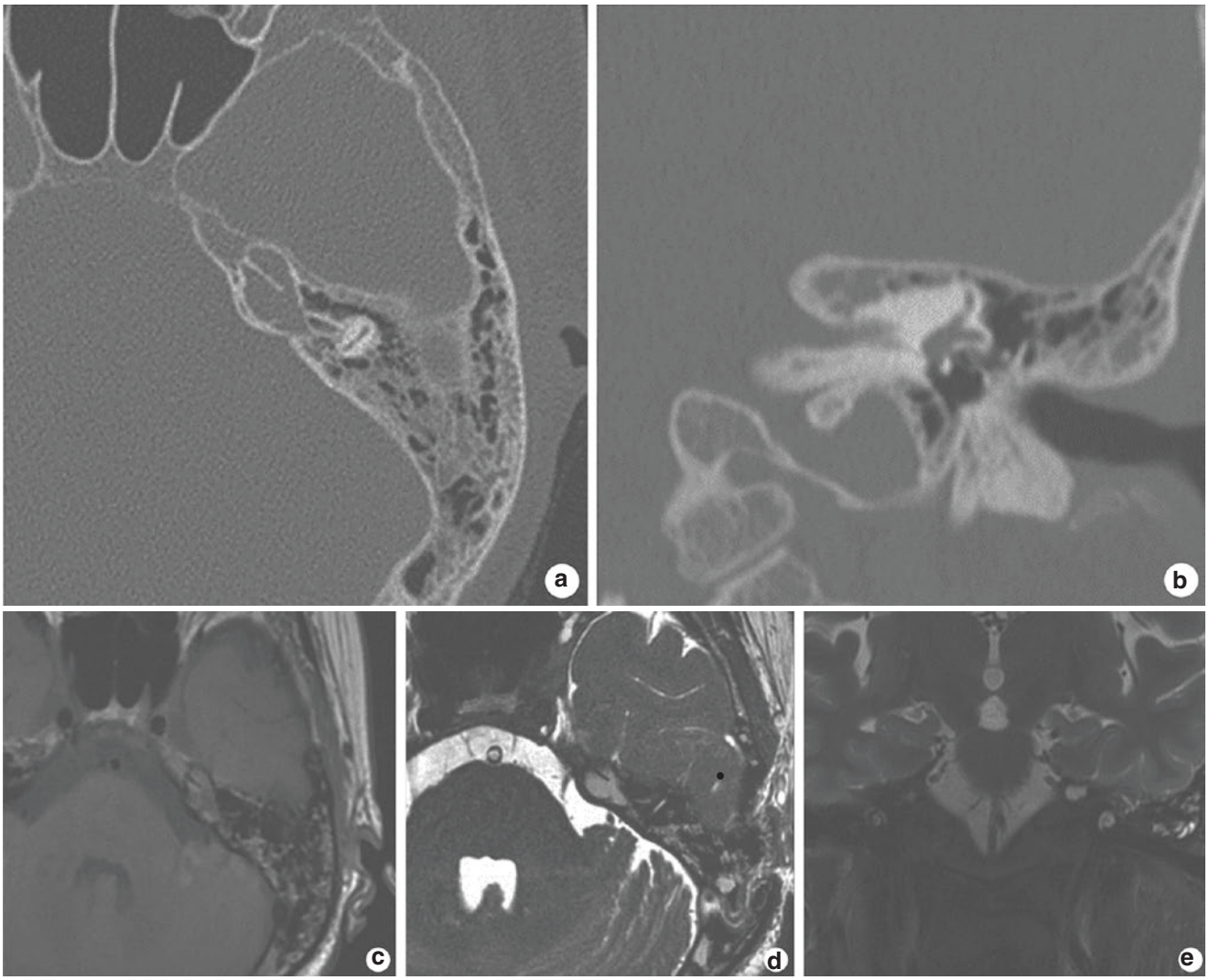

Fig. 22.4 Petrous apicitis. A 56-year-old female patient with left otalgia, trigeminal neuralgia, facial numbness and discomfort since over 1 year. (**a** and **b**) CT non-enhanced scan shows soft tissue density shadows in the mastoid air cells of left middle ear and left petrous apex air cell. (**c**–**e**) MRI non-enhanced scan shows isointense in the left petrous apex on T1WI, slightly hyperintense on T2WI, and isointense on T2 fat saturation sequence in the coronal plane

well as ring enhancement. MRI findings are very important in the differentiation of petrous apicitis from other petrous apex lesions. In the era of antibiotics, the incidence of acute petrous apicitis has markedly decreased due to routine application of antibiotics in the treatment of otitis media.

22.1.4 Facial Neuritis

22.1.4.1 [Overview]

Facial neuritis can be divided into two types: bacterial and viral facial neuritis. Bacterial facial neuritis is often accompanied by bacterial meningitis. Viral facial neuritis is common in Bell's palsy and Ramsay-Hunt syndrome, more common in Bell's palsy clinically, which is generally caused by herpes simplex virus [10]. Ramsay-Hunt syndrome is a rare and multiple cranial nerve inflammation caused by varicella-herpes zoster virus infection, which most commonly involves the facial nerve. Pathogenic factors include (1) facial nerve directly infected by viruses and bacteria; (2) adjacent tissue inflammation spreading to the facial nerve, including necrotizing external otitis, otomastoiditis, parotitis (Fig. 22.5), and embolic cavernous sinusitis; (3) head and face infected by herpes virus.

22.1.4.2 [Pathology Findings]

Pathological changes of facial neuritis include interstitial edema of facial nerve, inflammatory cell infiltration, neural degeneration (diffuse facial nerve demyelination), neurotropic virions, and bleeding. The internal auditory canal fun-

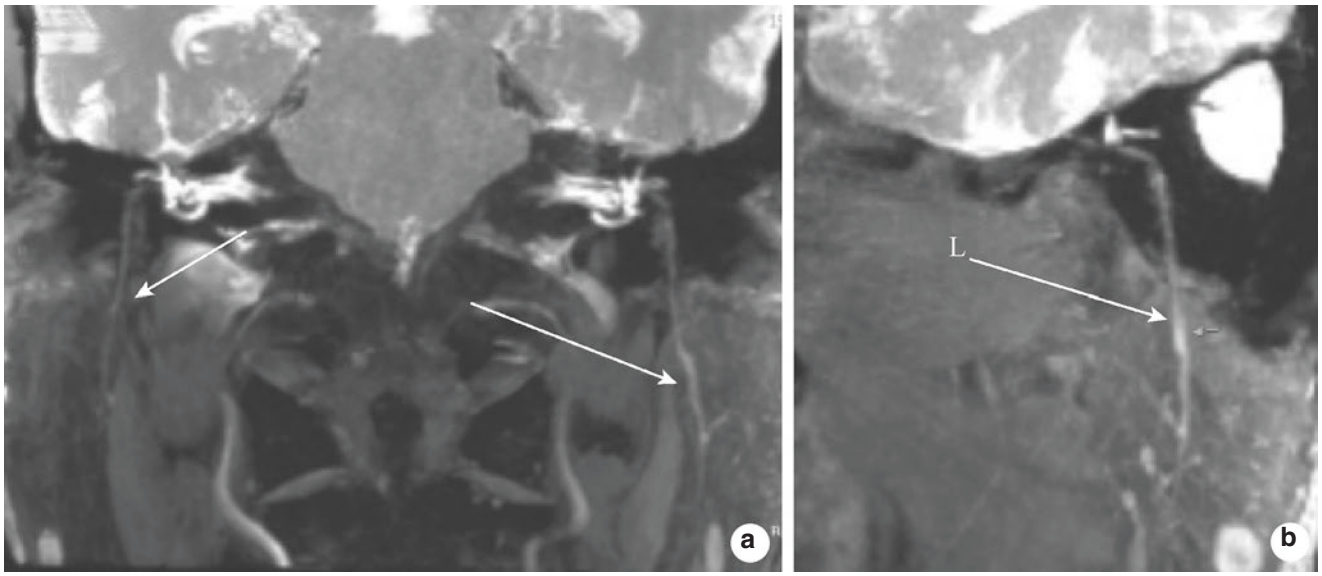

Fig. 22.5 Facial neuritis (1). An elderly male patient with left parotitis, (**a** and **b**) Non-enhanced MR scan shows heterogeneous thickening of parotid gland segment of left facial nerve and slightly increased signal, compared with the right side

dus and facial nerve canal of labyrinthine segment present stenosis and lack of vascular anastomosis, so they are the most vulnerable and most severely damaged parts [11].

22.1.4.3 [Imaging Findings]

Imaging examination is usually not performed for clinically typical Bell's palsy. However, imaging examination is very important for patients with facial palsy lasting more than 2 months, recurrent facial palsy, and slowly progressive facial palsy, so as to exclude other facial nerve diseases other than facial neuritis.

1. CT Examination. The findings are chronic otitis media with cholesteatoma or granulation and necrotizing external otitis. Abnormal changes in the bone wall of facial nerve canal can be found on CT examination. MPR images of the facial nerve canal are more intuitive.

2. MRI Examination. The typical manifestations of facial neuritis can be found in most patients when MRI examination is performed within 10 days after the onset of facioplegia. MRI non-enhanced scan images show diffuse thickening of facial nerve of the affected segment and increased signal on T2WI compared with the contralateral side, with enhancement on enhanced scan. Especially, the most vulnerable internal auditory canal fundus and facial nerve of labyrinthine segment should be carefully observed, and comparative observation is required for the two sides. There are abundant peripheral nervous vascular plexuses around the geniculate nerve fossa, tympanic cavity segment and mastoid segment of facial nerve. Normally, mild enhancement, and no thickening of facial nerve, but in bilateral symmetry can be found. When otitis media generally affects the facial nerve, MRI non-enhanced scan shows no abnormalities, and enhanced MRI can show thickening and enhancement of affected facial nerve, more marked than the contralateral side [12] (Figs. 22.6 and 22.7).

22.1.4.4 [Key Points of Diagnosis]

When facial neuritis is suspected clinically but difficult to be diagnosed, MRI enhanced scan is helpful for definitive diagnosis.

22.1.4.5 [Differential Diagnosis]

Facial Nerve Schwannoma: The peripheral facial paralysis may be the only symptom of facial nerve schwannoma, so it sometimes is misdiagnosed as Bell's palsy. When MRI shows circumscribed nodular thickening of the facial nerve, facial nerve schwannoma is highly suspected. The facioplegia caused by Bell's palsy is often acute in onset, presenting with abnormal segmental enhancement of facial nerve in the temporal bone, usually with no or mild thickening of facial nerve and no nodular changes.

22.1.4.6 [Status Quo and Progress of Research]

Multiple MR techniques can clearly display facial neuritis. In terms of consistency between observers, the contrast-enhanced three-dimensional T_1-weighted volumetric isotropic turbo spin echo acquisition (CE 3D T_1-VISTA) is superior to contrast-enhanced T_1WI turbo spin echo (TSE) in respect of imaging. CE 3D T1-VISTA imaging can improve the diagnostic performance of facial neuritis. CE 3D T1-VISTA has the advantage of free reconstruction without additional scanning. Therefore, for patients with unilateral facioplegia, CE 3D T1-VISTA is helpful and can routinely give images after intravenous injection of the contrast agent [12].

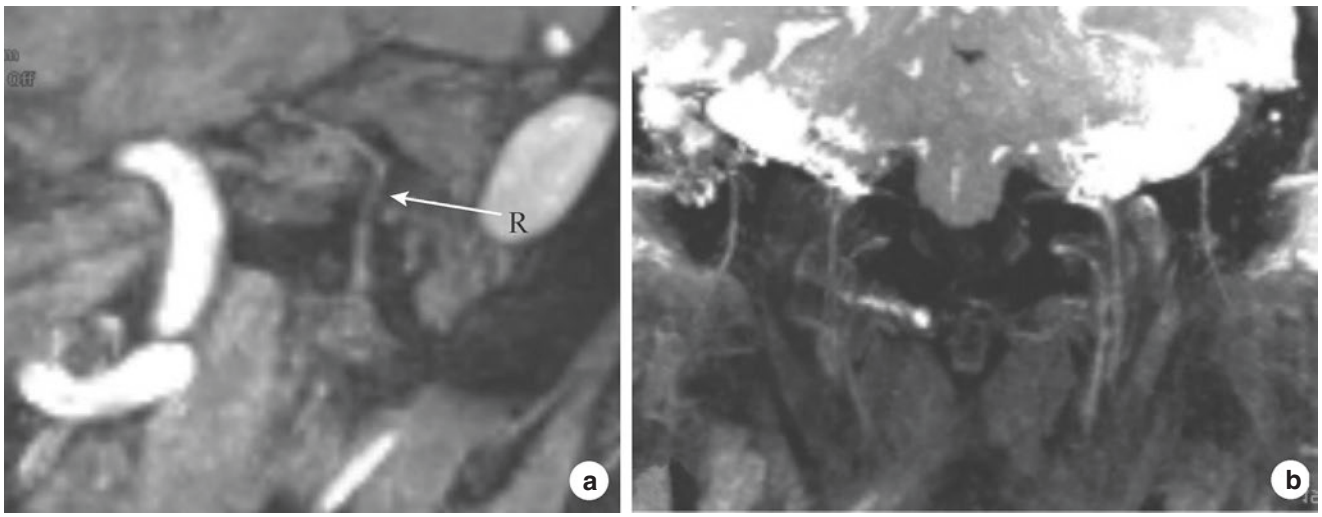

Fig. 22.6 Facial neuritis (2). A 30-year-old male patient. with sudden facioplegia since 1 day. (**a**) Enhanced MR scan shows thickening and mild enhancement of horizontal and vertical segments of right facial nerve. (**b**) Water imaging shows thicker medial course segment of temporal bone of right facial nerve compared with the left side. Crumby hyperintense can be noted in the right middle ear and right mastoid process, suggesting inflammation

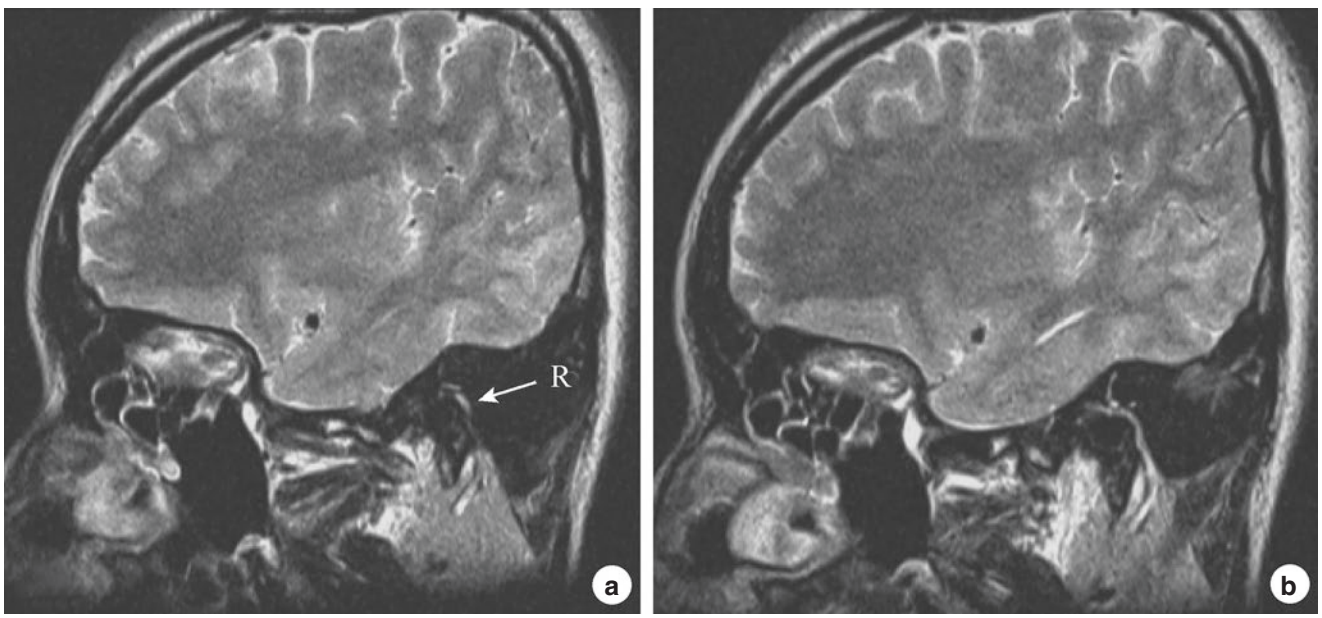

Fig. 22.7 Facial neuritis (3). An elderly female patient. (**a** and **b**) Reconstructed T2WI shows thickened right facial nerve compared with the left side, suggesting facial neuritis

22.2 Intracranial Complications of Otitis Media

22.2.1 [Overview]

The intracranial complications of otitis media are arranged in descending order of frequency: sigmoid sinus diseases (including peripheral abscess of sigmoid sinus and thrombophlebitis of sigmoid sinus), otogenic meningitis, brain abscess, extradural abscess (excluding peripheral abscess of sigmoid sinus), encephalitis, hydrocephalus and arachnoiditis. In addition, there is an intracranial complication associated with intractable otitis media, hypertrophic cranial pachymeningitis (HP), also known as hypertrophic cranial dural vasculitis. The small-vessel vasculitis of granulation or effusion in the middle ear can spread to the cerebral dura mater via several routes and leads to secondary HP. The routes of transmission are basically the same as those of other intracranial complications [13], specifically including

destroyed tympanic tegmentum; temporal suture or fissure; internal ear including labyrinth and vestibule; being associated with cerebral dura mater in the middle ear and (or) posterior cranial fossa through local circulation of venous return.

22.2.2 [Pathology Findings]

In prolonged infection, swollen inner mucosal layer and retained secretions will cause mechanical compression of the bone, and hyperemia and local acidosis. This results in active osteoclasts in the mastoid process, causing decalcification and bone resorption and progression to the stage of confluent mastoiditis. As inflammation progresses, osteoclasts resorb its peripheral bones and local complications. The bone trabecula of mastoid cells, middle ear and mastoid tectum, sigmoid sinus plate, and facial nerve canal are the sites of frequent bone loss. The reason for bone loss in these sites is that the bone in these sites is thin.

Infectious lesions basically have the following routes of transmission [10, 14].

1. Dissemination Via Eroded Bone Wall. This is the most common route of transmission (this is the route of transmission for most cases in this book). After spreading to the skull, infection mostly first form the extradural abscess, subdural abscess or peripheral abscess of sigmoid sinus, sigmoid sinus abscess and others, and then further invade brain tissues. When the tympanic cavity, tympanic antrum tegmen or tegmen mastoid, sigmoid sinus plate or Trautman's triangle are destroyed by cholesteatoma osteitis, the mastoid cavity of middle ear communicates with the middle cranial fossa or posterior cranial fossa. Sigmoid sinus infection combined with brain abscess of the temporal lobe in patients is not uncommon. In the petrous pyramid inflammation, the lesion may penetrate the bone wall at the petrous part and communicate with the middle cranial fossa or posterior cranial fossa, causing the extradural abscess. When the lateral bone wall or medial wall of the mastoid process is penetrated, a postauricular subperiosteal abscess may be formed. Some pus may spread to deep neck and parapharyngeal space along the sternocleidomastoid and digastric muscle, forming locally an abscess. Infection or bacterial toxin can invade the internal ear via damaged bony semicircular canal or promontorium tympani, resulting in labyrinthitis.

2. Hematogenous Route. The small vessels in the middle ear mucosa, emissarium mastoideum and venules in the bone canaliculi communicate with vessels on the surface of meninges and brain tissues; hence, infection can spread into the skull. Method: (1) direct delivery of infectious substances through blood flow, causing phlebitis and thrombosis. (2) infecting the skull after septicemia and septicopyemia occur. In the infection caused in this method, the bone wall of middle ear may be intact or very solid, and intracranial infection has been widely developed.

3. Normal Anatomical Approach. The inflammation of middle ear may invade the internal ear through the vestibular window and cochlear window, leading to labyrinthitis. Suppurative labyrinthitis spreads into the skull through the cochlear aqueduct and vestibular aqueduct, mostly causing cerebellar abscess.

22.2.3 [Imaging Findings]

22.2.3.1 CT Examination

(1) Thrombophlebitis of Sigmoid Sinus: Bone remodeling is found in the epitympanum and mastoid antrum. The sigmoid sinus plate at the affected side is not intact, with interrupted continuity (Fig. 22.8a). Enhanced CT scan shows the strip-like non-enhanced and slightly hypodense shadow in the sigmoid sinus.

(2) Pyogenic Meningitis: CT non-enhanced scan at the early stage shows no abnormality, and the enhanced scan shows abnormal meningeal enhancement. The different degrees of brain edema may be present. The scan at the advanced stage shows communicating hydrocephalus, encephalomalacia and brain atrophy.

(3) Brain Abscess: At the early stage, the flaky hypodense shadow with fuzzy margin is seen in the brain. The enhanced scan shows patchy or gyriform enhancement. After the formation of the abscess, a cystic hypodense focus is found. The abscess wall shows marked enhancement on enhanced scan. The abscess is characterized by homogeneous thickness in the abscess wall. Air bubbles or air-fluid levels can be noted in a small part of vomica.

(4) Subdural or Epidural Empyema: The crescent-shaped or fusiform hypodense shadow can be seen on the dorsolateral surface of the brain or alongside the cerebral falx. The enhanced scan shows homogeneous marked enhancement in meninges no enhancement in pus.

22.2.3.2 MRI Examination

(1) Thrombophlebitis of sigmoid sinus: The degree of enhancement at the junction of the transverse sinus and sigmoid sinus decreases, suggesting thrombosis (Fig. 22.8b and c, Fig. 22.9).

(2) Pyogenic Meningitis: (1) At the early stage, MRI non-enhanced scan shows no any abnormalities. With the progression of the disease, T2WI and FLAIR can show a higher signal in purulent secretion in the cerebral sulci, fissure and cistern compared with the signal of normal cerebrospinal fluid. Enhanced scan can show marked enhancement of the meninges. The enhanced meninges may present as localized thickening and extend into the

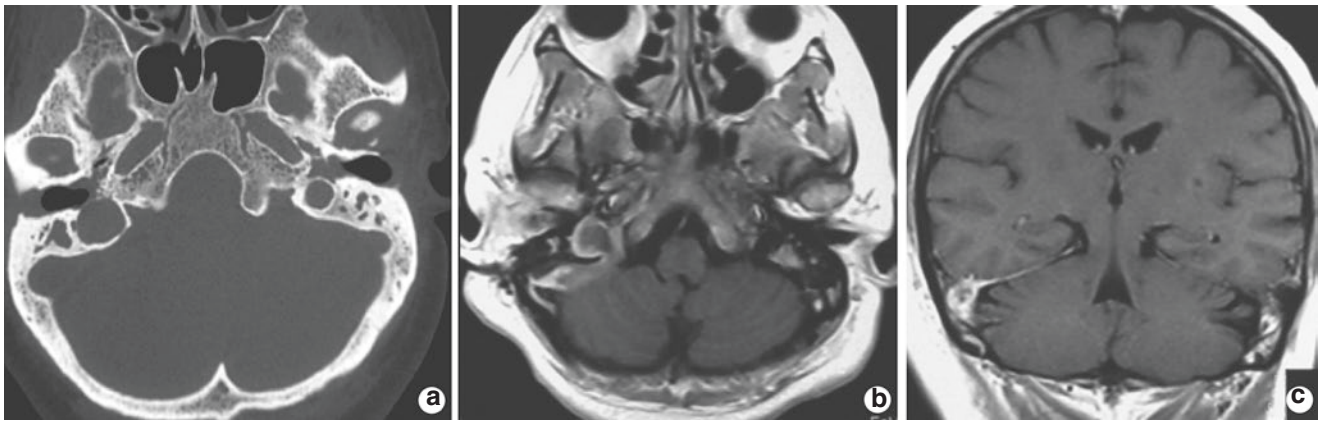

Fig. 22.8 Thrombophlebitis of sigmoid sinus. A 63-year-old female patient with bilateral otitis media for the past 5 years and dizziness since more than 1 month. (**a**) CT of temporal bone shows soft tissue density shadows in the tympanic cavity of bilateral middle ears and bilateral mastoid processes, enlarged right jugular foramen, and incomplete bone in the posterior wall. (**b** and **c**) MRI shows slightly hypointense in the intracranial right sigmoid sinus and right jugular vein, suggesting thrombosis

sulci. The enhancement of the meninges is the most important diagnostic basis for pyogenic meningitis (Fig. 22.9d). (2) At the advanced stage, communicating hydrocephalus or obstructive hydrocephalus may be caused due to arachnoid adhesion.

(3) Subdural or Epidural Empyema: MRI shows fusiform or crescent-shaped hypointense on T1WI and hyperintense on T2WI on the dorsolateral surface of the brain or alongside the cerebral falx. On T2WI, the signal of pus is slightly more intense than that of cerebrospinal fluid. The pus shows hyperintense on DWI. The abscess wall shows homogeneous ring enhancement on enhanced scan. There are different degrees of mass effect (Fig. 22.10).

(4) Brain Abscess: The abscess commonly occurs in the cerebellar hemispheres or temporal lobe.

(1) The early abscess presents as acute encephalitis and shows hypointense on T1WI and hyperintense on T2WI with irregular and fuzzy margin. There is often mild to moderate mass effect. The early lesion shows inapparent enhancement on enhanced scan. With the further progression of inflammation, patchy or gyriform enhancement.

(2) During abscess formation, there is ring-like isointense on T1WI and slightly hypointense on T2WI in the patchy hypointense on T1WI and hyperintense on T2WI, of which the center is hypointense on T1WI and hyperintense on T2WI. DWI shows hyperintense. Enhanced scan shows marked ring enhancement. It is characterized by homogeneous ring thickness (Fig. 22.10c).

(3) Brain edema around the abscess shows hypointense on T1WI and hyperintense on T2WI, with different degrees of mass effect.

(4) Small abscess often presents nodular or ring enhancement.

(5) Hypertrophic Cranial Pachymeningitis: Enhanced MRI scan can be used to diagnose the hypertrophic cranial pachymeningitis. The gadolinium-enhanced T_1-weighted MRI shows thickened cerebral dura mater with marked enhancement. Axial T2WI can be used to observe the inflammation of the middle ear and mastoid cavity [13] (Figs. 22.11 and 22.12).

22.2.4 [Key Points of Diagnosis]

1. The symptoms and signs of acute infectious systemic poisoning are fever, chills, fatigue, muscular soreness, loss of appetite, headache, and drowsiness etc. Meningeal irritation sign: positive for neck resistance, Kernig's sign, and Brudzinski's sign.
2. It is usually accompanied by aural pyogenic infectious lesions. Laboratory test shows an increase in white blood cell count, mainly neutrophils.
3. CT examination mostly shows bone destruction of skull base at the affected side. Enhanced MR examination can show abscess presentations and ring enhancement at relevant sites, with the abscess wall in homogeneous thickness.

22.2.5 [Differential Diagnosis]

1. Pyogenic meningitis primarily should be differentiated from meningeal metastasis, such as history of primary tumor at other sites; multiple, ring enhancement, and a large area of brain edema around the lesion.

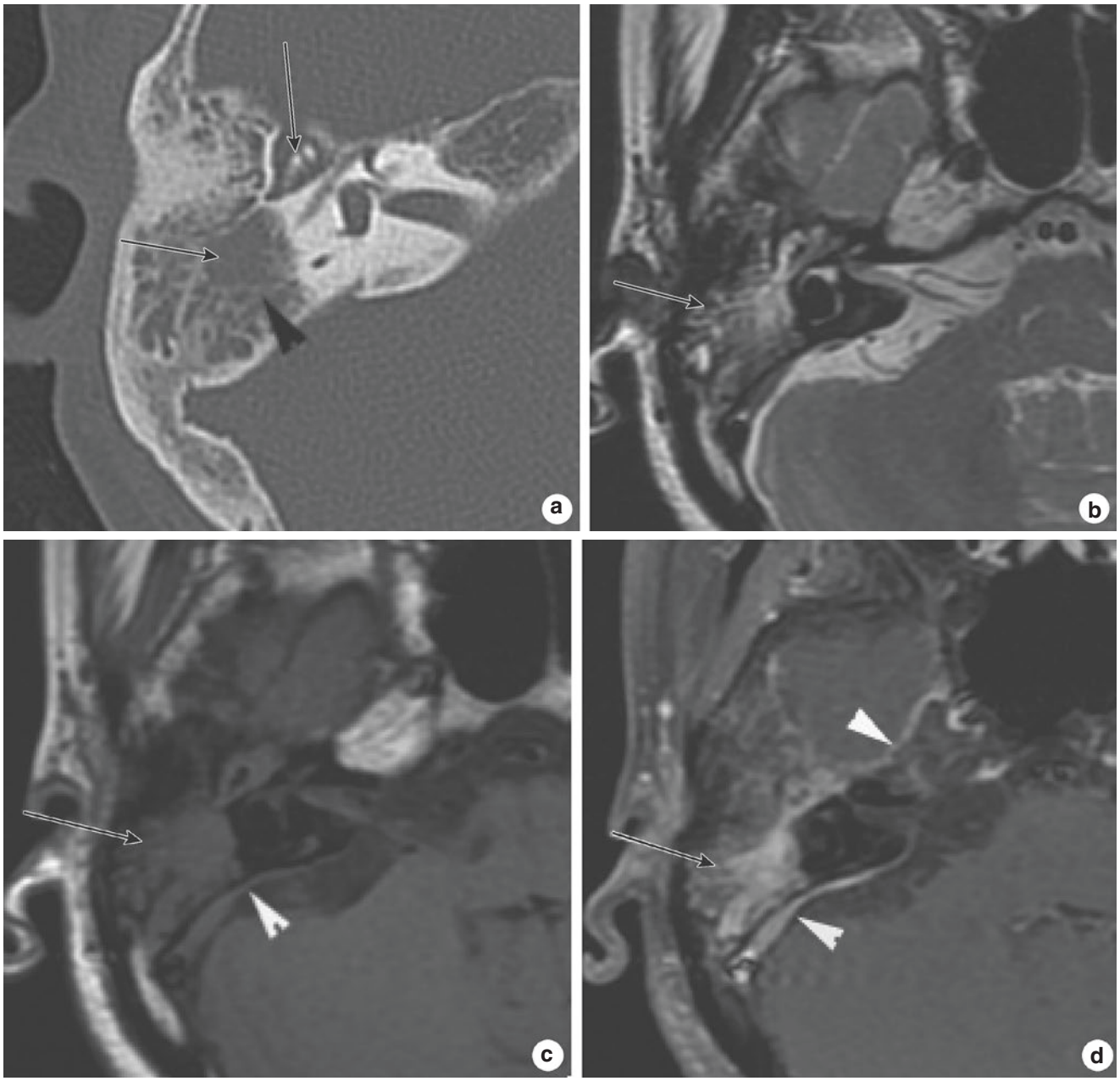

Fig. 22.9 Right chronic bone ulcer type otomastoiditis with meningitis and sigmoid sinus thrombosis. A 38-year-old male patient with pus discharge from the right ear since more than 7 years, hearing loss since 4 years, and recent vertigo. (**a**) CT of the temporal bone shows slightly hyperdense shadow in the tympanic cavity of right middle ear (black arrow) and right mastoid process, moth-eaten osteolysis in the right mastoid process, without expansion change, which suggest bone ulcer type otitis media. (**b** and **c**) MRI non-enhanced scan reveals slightly hypointense on T1WI and hyperintense on T2WI in the lesion within the right mastoid process, and shows marked enhancement on enhanced scan. (**d**) MRI enhanced scan shows linear marked enhancement in the meninges adjacent to the cerebellum and temporal fossa

2. Subdural or epidural empyema mainly should be differentiated from subdural or epidural effusion and hematoma.
3. Brain abscess primarily should be differentiated from tumor necrosis and cystic changes. The abscess wall is generally homogeneous in thickness. However, the wall is heterogeneous after cystic change of the tumor.

22.2.6 [Status Quo and Progress of Research]

The simple acute otitis media or otomastoiditis which is responsive to antibiotics requires imaging examination. When there is no perforation of tympanic membrane and tissue samples required for bacterial culture cannot be obtained, the original empirical antibiotic treatment may be ineffec-

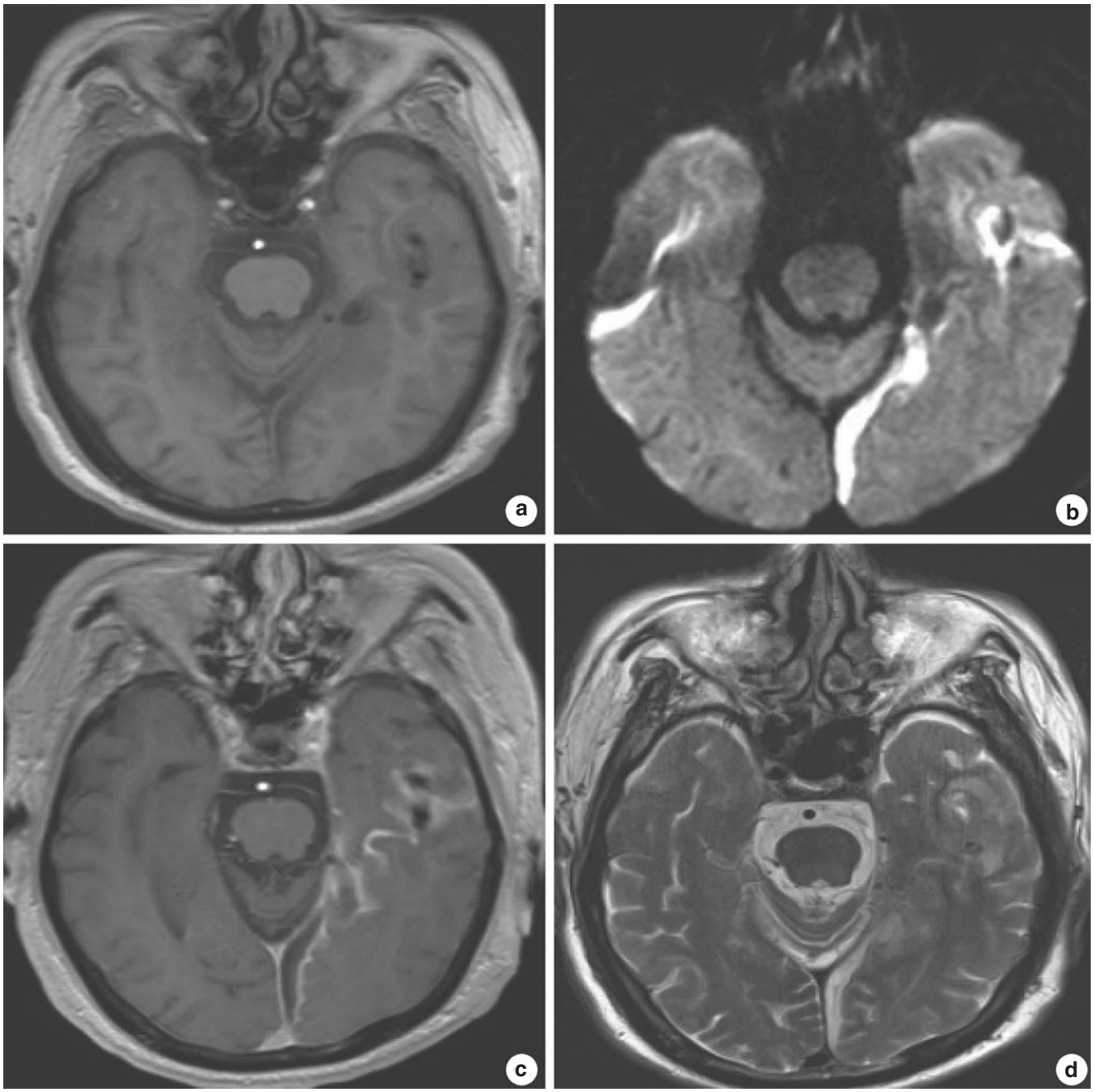

Fig. 22.10 Left otomastoiditis, brain abscess in the left temporal lobe, pyogenic meningitis, subdural empyema, and subdural effusion in the bilateral frontoparietal lobes. A 85-year-old male patient with headache for the past 2 months and aggravated condition for the past 1 week. (**a** and **b**) The partial gyral thickening of left temporal lobe shows slightly hypointense on T1WI and slightly hyperintense on T2WI, and multiple punctate hypointense shadows on T1WI, suggesting the presence of gas. (**c** and **d**) The thickening of the tentorial edge shows strip-like, slightly hypointense on T1WI and slightly hyperintense on T2WI, and hyperintense on DWI. With the decreased ADC value, DWI also shows hyperintense in the left tempus and cerebral falx. (**e** and **f**) The focus of the left temporal lobe presents ring enhancement, and the left tempus, left tentorium of cerebellum, and cerebral dura mater are thickened and show marked enhancement. The partial cerebral pia mater in the left parietal lobe, temporal lobe and occipital lobe shows marked enhancement

tive. CT non-enhanced scan can be performed for these cases and other low-risk patients in the emergency room so as to definitely exclude confluent mastoiditis. Even in low-risk patients, surgical treatment may also be performed for confluent mastoiditis, and enhanced CT examination should preferably performed. Enhanced CT examination can diagnose not only early bone loss but also other complications, such as intracranial spread, venous involvement, and soft tissue spread. The proper scanning time should be selected for enhanced CT scanning in order to detect venous and arterial

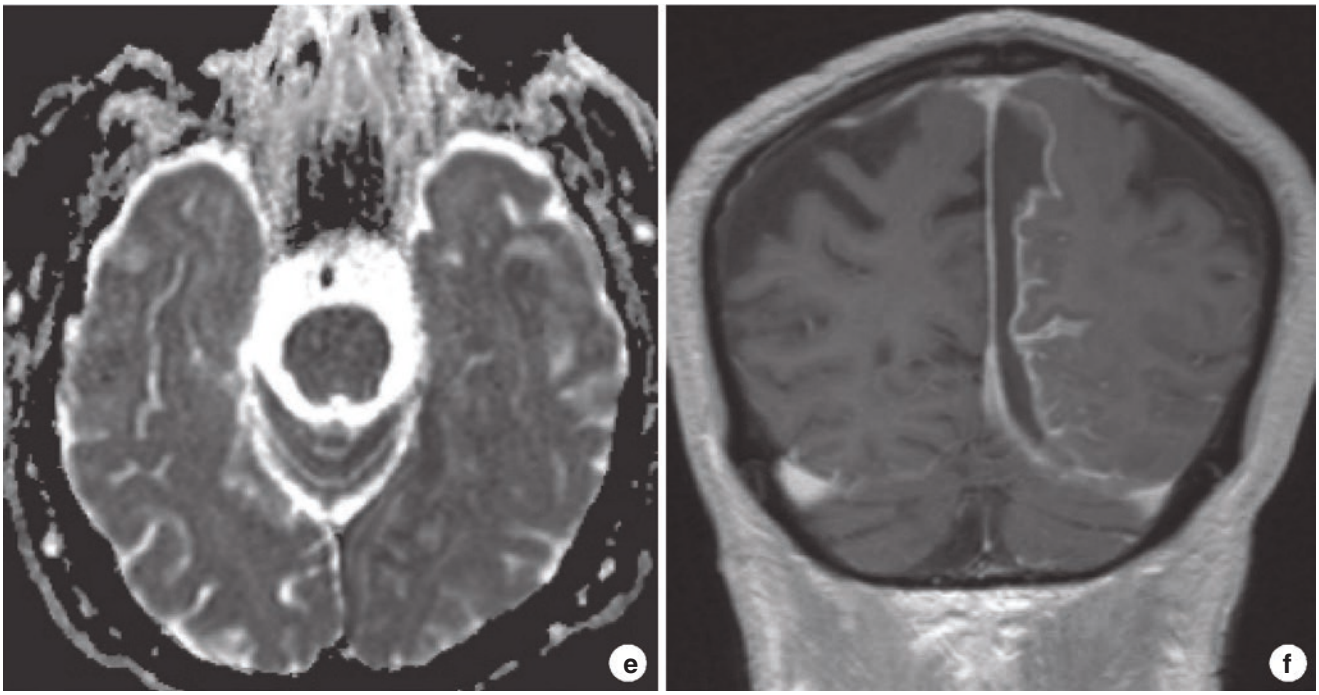

Fig. 22.10 (continued)

complications. Due to the low sensitivity of MRI to bone loss, MRI examination should not be applied in the initial classification of diseases. Other indications include etiological and pathological diagnosis (e.g., nasopharyngeal mass) and other complications (e.g., labyrinthitis and facial nerve involvement), as well as evaluation of antibiotic test responses. MR imaging should include MR venography and MR angiography. In addition, for potential intracranial and extracranial abscesses, the additional diffusion weighted imaging may be performed to diagnose. The fat-suppression enhanced T1WI imaging or non-enhanced/enhanced standard T1WI imaging scanning can also be used [13, 15].

22.3 Sequelae of Otitis Media

22.3.1 Atelectatic/Adhesive Otitis Media

22.3.1.1 [Overview]

Adhesive otitis media, also known as atelectatic otitis media, refers to fibrosis and adhesion between the acoustic structures of the middle ear and between the structures and the tympanic wall due to various reasons, which results in the systemic dyskinesia of acoustic structure system of middle ear, leading to conductive deafness. Adhesion is mostly located in the posterior mesotympanum, with thickened tympanic membrane and adhesion with promontorium tympani. The ossicles may form individual or complete adhesion around the vestibular window. The stapes and long crus of incus are embedded in the vestibular window by fibrous tissue. The vestibular window may be partially or completely closed. Histologically, the mucosal subepithelium is solid fibrous tissue that contains calcification or new bone formation, and the sclerosis is much less than tympanosclerosis. It is difficult to distinguish the two pathologies. The ossicles may also be partially resorbed, with interrupted ossicular chain. Adhesive otitis media is the proliferation of fibrous tissue or scar formation in the middle ear, as a result of past inflammation of the middle ear, which usually occurs in childhood. The main clinical symptoms are hearing loss, mostly conductive and rarely mixed, and total deafness. The main cause of internal ear damage is the inflammatory toxin of the middle ear entering the internal ear through the cochlear window. Patients often develop tinnitus and vertigo, and the latter symptom may be associated with auditory tube stenosis or obstruction [2].

22.3.1.2 [Pathology Findings]

The exudative phase is mainly characterized by the inflammatory cell infiltration and inflammatory exudates, mucosal epithelial hyperplasia, subepithelial interstitial congestion, edema, exudates accumulated in the tympanic cavity and mastoid air cells, cochlear window and vestibular window niche, ossicles surrounded by exudates, tensor tympani muscle hyperemia, inflammatory cell infiltration, and thickened and swollen tympanic membrane. The inflammatory granulation tissue phase is mainly characterized by inflammatory granulation tissue hyperplasia, abundant new blood vessels,

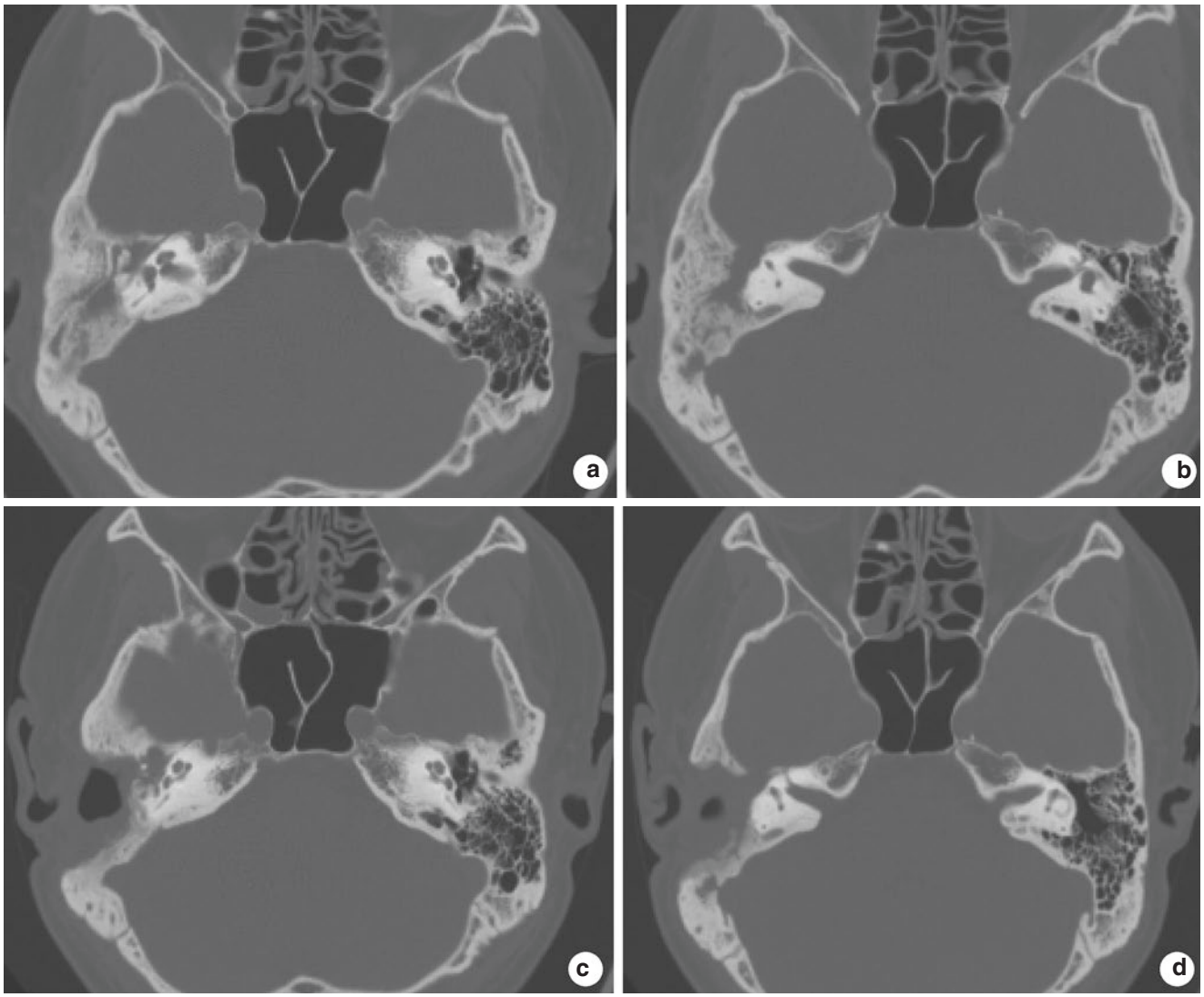

Fig. 22.11 Hypertrophic cranial pachymeningitis (1). A 40-year-old male patient with right temporal headache, low fever since 2 weeks, and otitis media surgery 3 months ago. (**a** and **b**). Preoperative TSCT of the temporal bone shows sclerosis in the mastoid process of the right temporal bone, soft tissue density shadows in the tympanic cavity and tympanic antrum of right middle ear, incomplete bone in the roof of right tympanic cavity, lateral semicircular canal invaded, and intact right ossicular chain. (**c** and **d**) Postoperative CT of the temporal bone shows incomplete bony structure in the mastoid portion of right temporal bone, and incomplete structure of the right ossicular chain. The roof of right tympanic cavity is more significantly destroyed

enormous inflammatory granulation tissue in the tympanic cavity and near the ossicles, and mastoid air cells filled with inflammatory granulation tissue. The histocytic response phase is mainly characterized by tissue effusion in the middle ear mucosa and under the mucosa, mainly containing abundant foam cell proliferation, and the foam cells may occur in the fibrous connective tissue around the ossicles and the mastoid air cells or tympanic cavity. The collagen fibroplasia phase is mainly characterized by tympanic fibrosis and adhesion, mastoid air cells filled with fibrous connective tissue, especially fibroblast proliferation, with inflammatory cell infiltration, the tympanic cavity separated by the fibrous connective tissue adhesion band to form cystic cavities in different sizes, otopiesis, adhesion with the promontorium tympani, cochlear window and vestibular window partially or completely filled with fibrous connective tissue [16].

22.3.1.3 [Imaging Findings]

CT of the temporal bone may show non-specific poor pneumatization of mastoid air cells, flaky increased density shadows in the mastoid air cells, mastoid antrum and tympanic cavity, ossicles surrounded by slightly hyperdense fibrous granulation tissue, and retraction or collapse of tympanic membrane, which is often caused by negative pressure in the

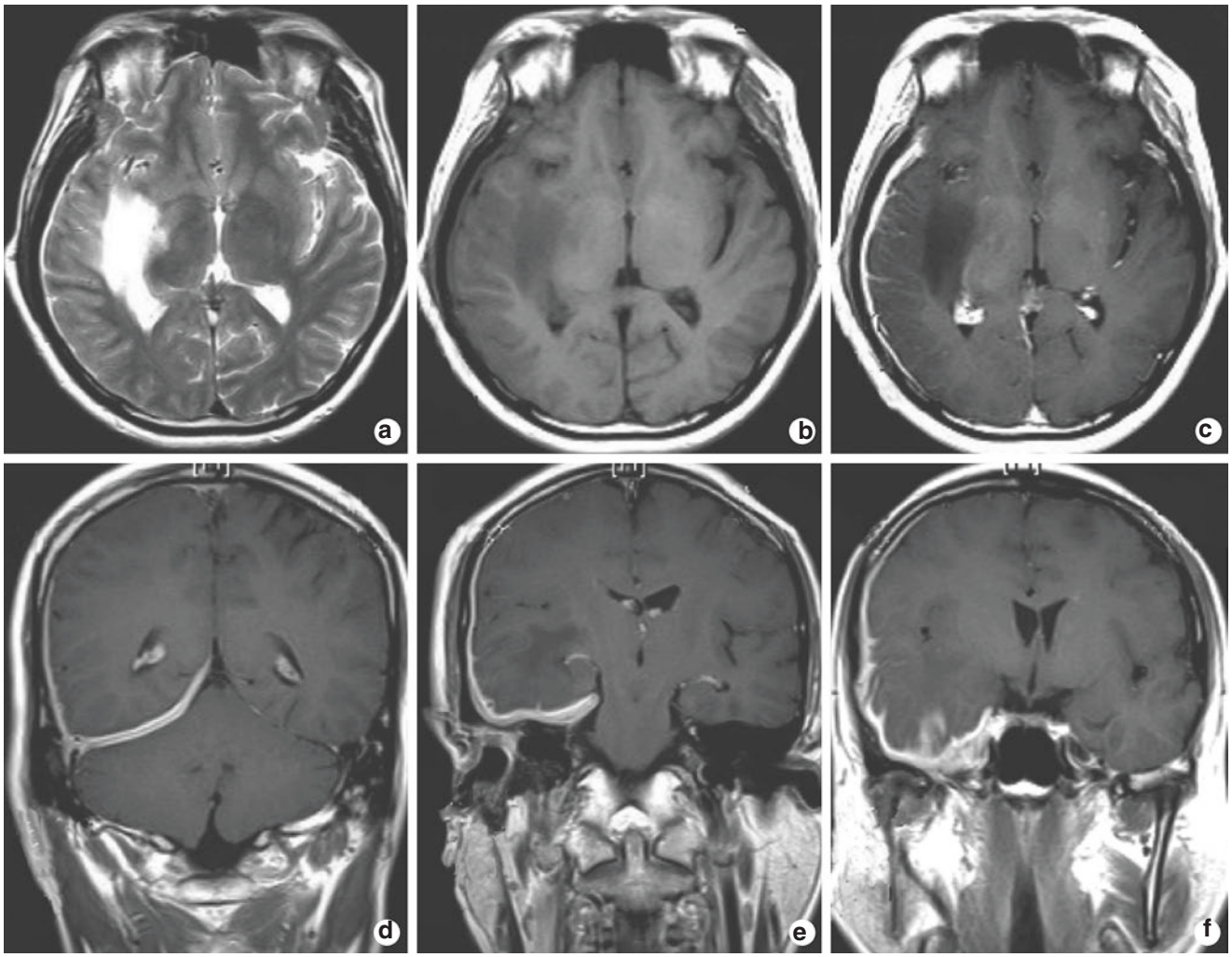

Fig. 22.12 Hypertrophic cranial pachymeningitis (2). (**a** and **b**) Non-enhanced scan on the above patient shows thickened cerebral dura mater in the right temporal part, presenting isointense on T1WI and hyperintense on T2WI. The right temporal lobe shows flaky hypointense on T1WI and hyperintense on T2WI, with unclear edge. These findings suggest brain edema. (**c**–**f**) Enhanced examination shows marked enhancement in the right temporal part and cerebral dura mater at right cerebellar tentorial edge

tympanic cavity due to auditory tube dysfunction. Atelectatic otitis media is usually accompanied by middle ear effusion. The atelectasis may be localized or extensive. Due to different degrees of atelectasis, localized atelectasis of the tympanic membrane may be associated with or without the formation of retraction pocket. CT findings are tympanic fibrosis and adhesion, mastoid air cells filled with slightly hyperdense fibrous connective tissue, the tympanic cavity separated by the fibrous connective tissue adhesion band to form cystic cavities in different sizes, and otopiesis. In the cases of severe atelectatic otitis media, there generally is a retraction pocket in the tympanic membrane; the retracted sites may be partes tensa, pars flaccida or both. If the retraction pocket persists, hearing loss and ossicular chain disruption will be caused. The otopiesis can be classified as mild retraction. The retraction has adhesion with the ossicles, tympanic cavity, and promontorium tympani. The cochlear window and vestibular window are partially or completely filled with soft tissue density and have adhesion with the tympanic antrum, finally accompanied by keratinized substance aggregation, causing cholesteatoma (Fig. 22.13).

22.3.1.4 [Key Points of Diagnosis]

1. The main clinical symptom is hearing loss, presenting as conductive deafness, mostly accompanied by tinnitus.
2. Endoscopy shows completeness, turbidity, retraction, calcific plaque, thickening or atrophy of the tympanic membrane. The tympanic membrane has irregular adhesion with the promontorium tympani, with poor mobility. When the tympanic membrane becomes thin due to atrophy, presenting pocket-shaped retraction, intratympanic structure can be clearly seen, which is easily misdiagnosed as perforation of tympanic membrane.

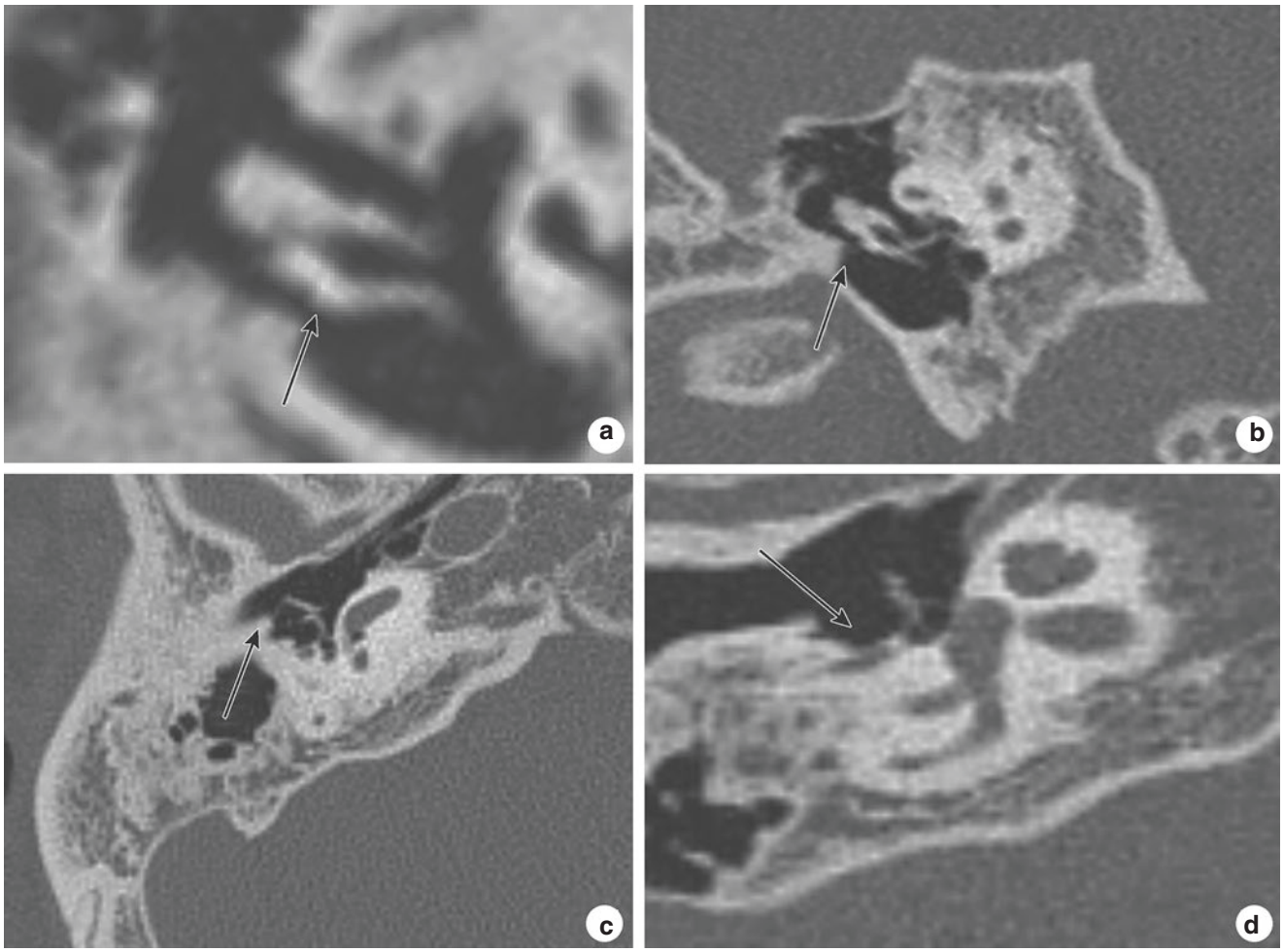

Fig. 22.13 Adhesive otitis media. (**a**) CT of the temporal bone shows a roughly parallel relationship between the normal manubrium mallei and long crus of incus (arrow). (**b** and **c**) CT of the temporal bone in a patient with adhesive otitis media shows manubrium mallei obviously close to the long crus of incus (arrow). (**d**) On CT of the temporal bone in another patient, a adhesion band is attached to the posterior crus of stapes (arrow), while the normal stapedial muscle is articulated with the neck of stapes, thus differentiating the two

3. The auditory tube dysfunction is common, and the acoustic impedance test showing type B pressure curve of the tympanic cavity, and the disappearance of stapedius reflex.
4. CT of the temporal bone shows poor pneumatization of the mastoid process.

22.3.1.5 [Differential Diagnosis]

1. Tympanosclerosis. The disease and adhesive otitis media are the inactive and inreversible lesions caused by protracted otitis media. Tympanosclerosis is mainly characterized by hyaline degeneration and calcification, and even ossification. After the calcification and ossification occur in tympanosclerotic plaques, HRCT can be used for definitive diagnosis. The substance deposits of hyaline degeneration in tympanosclerosis most commonly occur around the tympanic membrane, mucosa of promontorium tympani and attic, and often surround and fix the ossicular chain. CT shows punctate or linear hyperdense shadow in the tympanic membrane (Fig. 22.14).

2. Otosclerosis can be divided into cochlear and vestibular window types. Otosclerosis of vestibular window is typically manifested as abnormal bony density shadow circumscribed to the anterior side of vestibular window, accompanied by stapes footplate thickening and normal tympanic membrane. Sclerotic plaques generally do not occur within the tympanic membrane and (or) tympanic cavity. The mastoid process is mostly pneumatic. Cochlear otosclerosis is characterized by focal hypodense shadows in the bone around the cochlea, typically presenting as "double-ring sign."

22.3.1.6 [Status Quo and Progress of Research]

Adhesive otitis media usually develops from secretory otitis media, with long-term hearing loss as the main symptom. It is the structural adhesion of the tympanic membrane to tym-

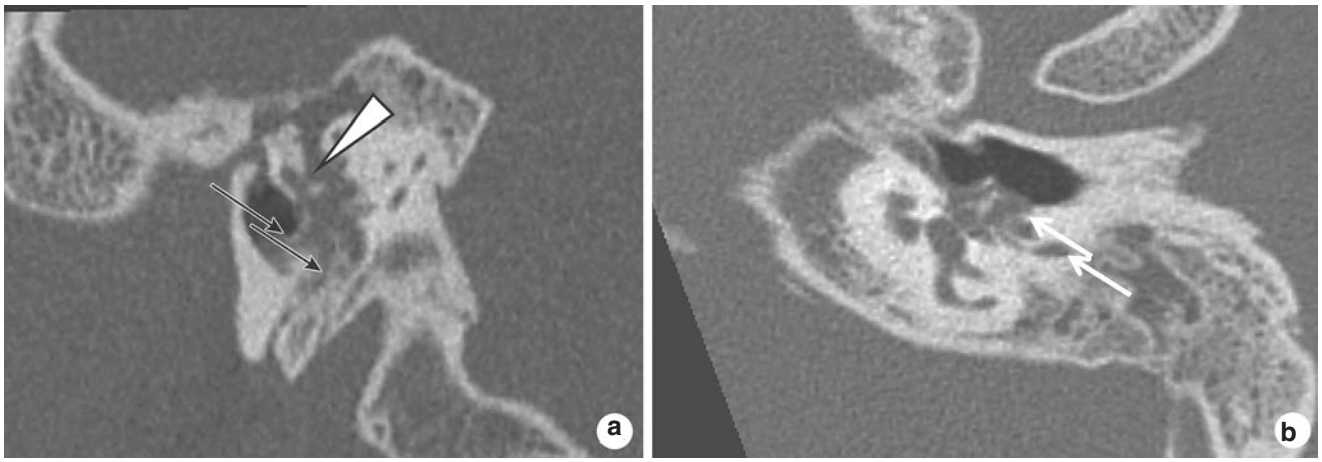

Fig. 22.14 Tympanosclerosis (1). A and B represent different patients respectively. (**a**) CT of the temporal bone in the patients with sclerotic otitis media shows calcification of the tympanic membrane (arrow), and partial bone erosion in the long crus of stapes (white triangle). (**b**) CT of the temporal bone in the patient with adhesive otitis media shows stapes embedded in the tissue adhesive mass

panic cavity caused by auditory tube dysfunction after long-term treatment or without systemic treatment. In severe cases, the tympanic membrane fuses with mucosa of promontorium tympani and epithelizes. Imaging examination, especially high-resolution CT can show reduce and disappearance of tympanic space and possible increased-density shadow in the tympanic cavity of mastoid process.

22.3.2 Tympanosclerosis

22.3.2.1 [Overview]

Tympanosclerosis is a pathophysiological change of the mucosa of tympanic cavity in the middle ear under the stimulation of inflammation and others. Its main causes are infection and mechanical injury. Tympanosclerosis is a degenerative change of connective tissue of mucosal lamina propria in the middle ear caused by long-term chronic inflammation. In this disease, massive calcium deposits in inflammatory repair tissue, forming visible hard plaques. In the stable period of inflammation, the process of calcification still remains progressive, often resulting in progressive and irreversible conductive hearing loss in patients, which is one of important causes of conductive deafness. *Guidelines for Clinical Classification and Surgery Typing of Otitis Media (2012)* definitively classifies tympanosclerosis as a sequela of otitis media [17].

22.3.2.2 [Pathology Findings]

Under light microscope, the disease is mainly manifested as hyalinization and calcium-phosphorus deposits. Under electron microscope, it is manifested as calcium phosphate compound and its surrounding collagenous fiber. The tympanic membrane and ossicular chain are the most main predilection sites of the disease. The promontorium tympani and attic are also possible primary sites. Most of tympanosclerosis cases result from recurrent attacks of long-term chronic nonspecific or specific inflammation (including suppurative and non-suppurative inflammation) or acute infection of mucosa Generally, in the acute inflammation phase, edema and inflammatory cell infiltration can be noted in the fibrous layer of tympanic membrane and the mucosal lamina propria of middle ear. After long-term or recurrent infections, fibroblast proliferation is found, with lamina propria of mucosa as collagen connective tissue Subsequently, cell components and capillaries gradually disappear, and these tissues produce hyaline degeneration, forming homogeneous white squamous substances, which are known as tympanosclerotic plaques. The tympanosclerosis lesion may cause sclerosis of vestibular window and annular ligament and ossification of ossicular ligaments and stapes tendon. Such plaques may spread to the promontorium tympani and tympanic antrum and surround the lenticular process of stapes and incus. In cases of extensive involvement, the cochlear window and auditory tube may be involved, so that the normal structure of middle ear disappears. In typical cases, the sclerosis focus surrounding the stapes is usually formed by layer-by-layer fusion of many squamous plaques. The lesion not only fixes the acoustic structure, but also interferes with the blood supply of the ossicles, resulting in the ossicular chain interruption and different degrees of conductive deafness.

22.3.2.3 [Imaging Findings]

The most specific CT finding of tympanosclerosis is hyperdense calcification or ossification in the tympanic cavity and tympanic antrum and/or calcific plaques in the tympanic membrane. Hyperdense shadows may be punctate, strip-like, patchy, and grid-like, which may exist alone or in combina-

tion with soft tissue shadows. Non-specific CT findings are soft tissue shadows in the tympanic cavity and tympanic antrum, rough and interrupted ossicular chain, hyperdense shadows in the mastoid air cells, mastoid antrum and tympanic cavity, and fuzzy ossicles due to the surrounding ossification lesion. HRCT can not only clearly show small structures and lesions in the ear, and shape and extent of sclerotic plaques, but well analyze different components in the tympanic sclerotic plaques based on different densities. HRCT can also show distinguishably soft tissue shadow and calcification and ossification shadows in the sclerotic plaques, and clearly display the relationship of sclerotic plaques and the ossicular chain, and anatomic landmarks and relatively hidden space in the tympanic cavity, such as the involvement of tympanic membrane, vestibular window, cochlear window, promontorium tympani, cochlear window niche, facial nerve recess, tympanic antrum and other sites [18, 19].

CT shows slightly hyperdense shadows in the middle ear, attic and tympanic membrane. Pathologically, the main findings include hyaline degeneration and calcified fibrous granulation tissue deposition (Fig. 22.15). The substance deposits of hyaline degeneration in tympanosclerosis most commonly occur around the tympanic membrane, mucosa of promontorium tympani and attic, and often surround and fix the ossicular chain (Fig. 22.16), which may appear as punctate or linear hyperdense shadow in the tympanic membrane, or flaky shadow corresponding to the shape of promontorium tympani (Fig. 22.17). The tympanosclerosis of attic presents as large block-shaped calcified shadow surrounding the ossicular chain, with the morphology of normal ossicular chain disappearing; a single plaque in the anterosuperior side of attic can fix the head of malleus in the tegmen tympani (Fig. 22.18).

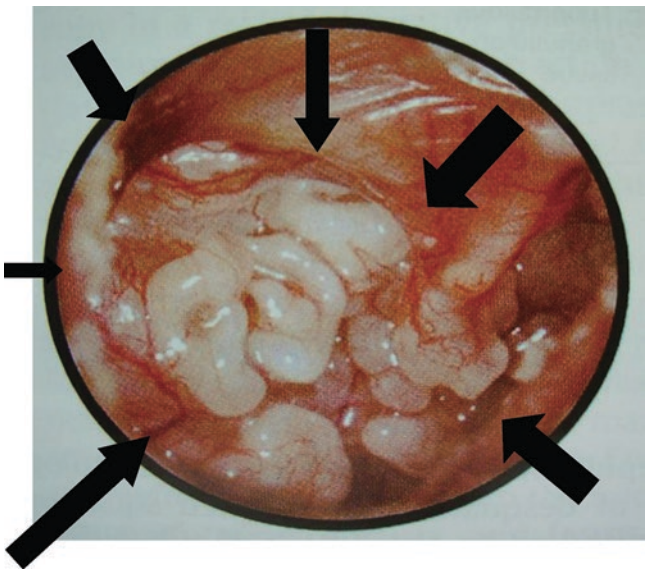

Fig. 22.15 Tympanosclerosis (2). Tympanosclerosis of right middle ear. Otoscopic findings: There is a large perforation in the tympanic membrane (arrow), with a direct view of white spherical deposits formed by tympanosclerosis

22.3.2.4 [Key Points of Diagnosis]

1. Clinical manifestations, history of long-term chronic otitis media and conductive deafness.
2. Otoscopy may show thickened tympanic membrane with or without tympanosclerotic plaques.
3. The degree of conductive deafness is not proportional to that of chronic inflammatory lesions.
4. Imaging findings. The most specific CT findings of tympanosclerosis are hyperdense calcification and ossification in the tympanic cavity and tympanic antrum, and/or calcific plaques in the tympanic membrane. Hyperdense shadows may be punctate, strip-like, patchy and grid-like, which may exist alone or in combination with soft tissue shadows.

22.3.2.5 [Differential Diagnosis]

1. **Otosclerosis** can be divided into cochlear and vestibular window types. HRCT findings of osclerosis of vestibular window are similar to the site and findings of tympanosclerosis. HRCT shows thickened stapes footplate, vestibular window filled with bone structure shadows, causing vestibular window stenosis or in closed form. The tympanic membrane is normal, and sclerotic plaques generally do not occur in the tympanic membrane and/or tympanic cavity. The mastoid process is mostly pneumatic. Otosclerosis of vestibular window is typically manifested as abnormal bony density shadow circumscribed to the anterior side of vestibular window, which usually occur bilaterally and is mostly found in females. Diffuse calcification of vestibular window more likely suggests tympanosclerosis.

2. Adhesive otitis media and tympanosclerosis are permanent, inactive and irreversible lesions caused by protracted otitis media. The lesion which mainly presents as organization and adhesion is called adhesive otitis media. The lesion which is mainly characterized by hyaline degeneration and calcification and even ossification is called tympanosclerosis. Their clinical symptoms and manifestations and medical history are very similar. After calcification or ossification occurs in sclerotic plaques, HRCT can be used for definitive diagnosis. Before the occurrence of calcification or ossification, it is difficult to distinguish the two diseases on HRCT as their findings are normal, thickened or retracted tympanic membrane. The soft tissue density shadow is found in the tympanic cavity and the bony wall and ossicular chain are connected (Figs. 22.13 and 22.14). The differential method is proved mainly by pathology or surgery.

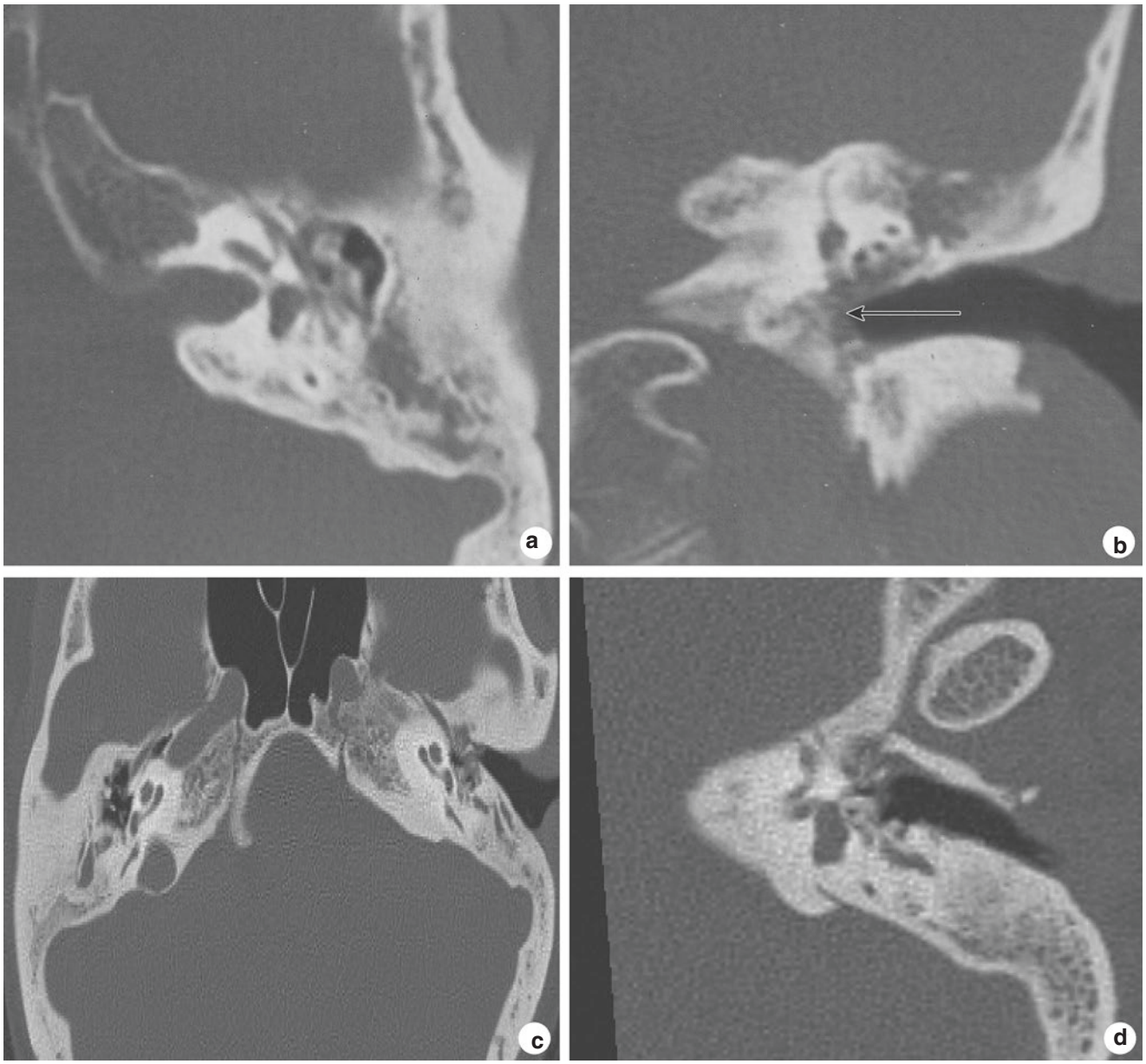

Fig. 22.16 Chronic tympanosclerotic otitis media. (**a** and **b**) CT of the temporal bone shows left middle ear cavity minified because of contraction of the tympanic membrane (arrow). Osteosclerosis is found around the attic and fixes the ossicular chain; the thickening of mastoid cell septa is seen. (**c** and **d**) CT of the temporal bone in another patient shows soft tissue shadow in the left middle ear surrounding the ossicles, causing malleus, incus and stapes out of normal arrangement

3. Chronic Otitis Media is the most common cause of tympanosclerosis. The tympanic cavity, mastoid antrum and mastoid air cells are filled with soft tissue density shadows, and air in the mastoid air cells decreases or disappears. Bone destruction may occur in the mastoid process and tympanic cavity wall, but there will be no calcification, which presents as thickened or retracted tympanic membrane. The tympanic cavity and/or mastoid antrum and mastoid air cells are filled with soft tissue density shadows, and air in the mastoid air cells decreases or disappears. Effusion sign may occur in the tympanic cavity and mastoid process, and the ossicles are destroyed and even disappeared. In a small number of patients, bone destruction may be found in the mastoid process and tympanic cavity, but there will be no calcification.

22.3.2.6 [Status Quo and Progress of Research]

The history of long-term chronic otitis media and CT findings (that are multiple hyperdense calcification focus in the mastoid cavity of middle ear (including tympanic membrane), with increased density shadows in the mastoid process of middle ear) may suggest the diagnosis of tympanosclerosis, but the sensitivity is very low. There are some limitations in simple temporal bone CT examination. Therefore, some scholars have proposed that CT of the temporal bone combined with pure tone audiometry can significantly improve accuracy in the diagnosis of tympanosclerosis [20, 21].

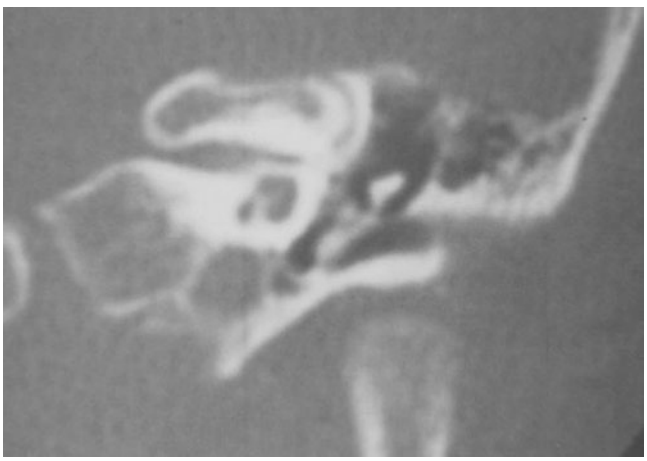

Fig. 22.17 Tympanosclerosis (3). CT in the left coronal plane shows thickened tympanic membrane, presenting plaque-shaped hyperdense shadow, and good pneumatization of middle ear and mastoid process

22.3.3 Cholesterol Granuloma of Middle Ear

22.3.3.1 [Overview]

Cholesterol granuloma is a granuloma containing cholesterol crystals and multinucleated giant cells. Cholesterol granuloma occurring in the tympanic antrum, mastoid process or tympanic cavity is called cholesterol granuloma of middle ear. Cholesterol granuloma is a non-specific lesion and a foreign body reaction of tissue to cholesterol crystals. If bleeding of middle ear, plasma exudation, tissue edema and tissue necrosis occur due to various causes, resulting in erythrocyte rupture and decomposition and fat degeneration, cholesterol may be released. As cholesterol continues to increase and reach saturation, cholesterol crystals are formed and deposited in tissue. With the long-term stimulation of cholesterol crystals, the peripheral tissues generate granulation tissue, which gradually enlarges and forms cholesterol granuloma. The etiology usually consists of three factors: obstruction of ventilation in the air space, drainage disorder and hemorrhage in the air space. Hemorrhage is considered as an important link in the formation process of cholesterol granuloma. Secretory otitis media and chronic otitis media are related to the formation of cholesterol granuloma. This disease is commonly found in the young and middle-aged population, and both male and female have an equal incidence. It is usually unilateral. The common clinical manifestations are a sense of ear fullness and distension or occlusion, ear bleeding due to unknown causes, or presentations of chronic suppurative otitis media. Except for cholesterol granuloma in chronic suppurative otitis media, this disease is generally a non-destructive lesion. However, some cases with the

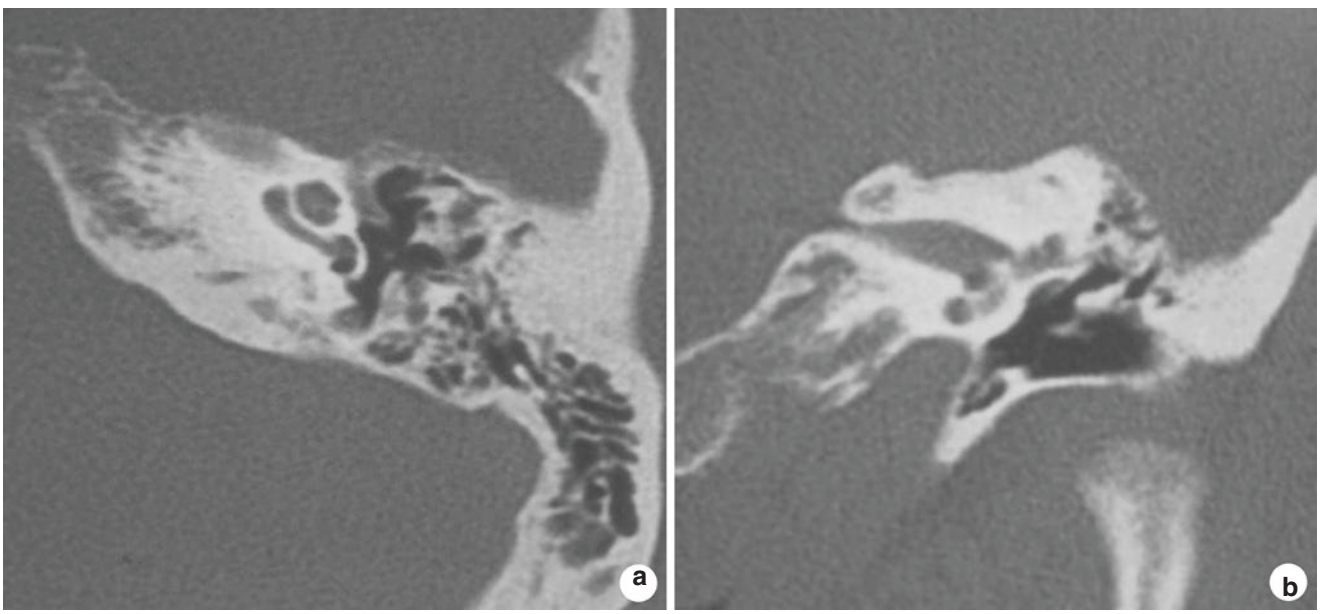

Fig. 22.18 Chronic otitis media caused tympanosclerosis. (**a** and **b**) CT non-enhanced scan shows sclerotic plaques in the anterosuperior side of tympanic cavity fixing the ossicular chain in the tegmen tympani wall, and the lateral wall blurred due to retractive sac shadow

complications of peripheral facioplegia, ossicular chain destruction, epidural cyst, sigmoid sinus plate destruction and cerebrospinal fluid otorrhea have been reported [11, 22].

22.3.3.2 [Pathology Findings]

Cholesterol granuloma is a type of granulation tissue containing abundant blood vessels. There are many clefts formed by the dissolution of cholesterol crystals, which are often rhomboid-shaped and arranged in concentricity. These clefts are surrounded by the infiltration multinucleated giant cells and macrophage, occasionally bleeding or hemosiderin deposition. In addition, a large number of lymphocytes, plasma cells and fibrin can be found in granuloma. Unlike cholesteatoma, in this disease, there is no stroma between granuloma and surrounding bones, and squamous metaplasia generally does not occur in the mucosa.

In gross findings, the granuloma is mostly dark red with varying shapes and soft texture, which is tougher than edematous granuloma. In addition to granulation tissue, coffee-colored fluid in different amounts is accumulated in the tympanic cavity and/or mastoid air cells, where tiny dotted cholesterol crystals can be noted.

22.3.3.3 [Imaging Findings]

1. CT Examination. On CT, the typical manifestations of cholesterol granuloma of the temporal bone appear as well-defined soft tissue density foci with smooth margin, mostly in round or quasi-circular shape, with peripheral expansile bone destruction; when bone destruction is mild, it may be accompanied by tympanic and mastoidal effusion.

(1) Cholesterol granuloma of middle ear appears as mass of expansile growth with smooth margin in the middle ear and/or mastoid cavity. CT findings of smaller cholesterol granuloma are an increased-density shadow in the tympanic cavity of middle ear, without bone remodeling or ossicle disappearance. CT findings of larger cholesterol granuloma are a lesion of expansile growth in the middle and/or mastoid cavity, with peripheral bone retraction and ossicle disappearance.
(2) Cholesterol granuloma of petrous apex appears as a well-circumscribed expansile lesion with smooth margin and the center located at the petrous apex, a soft tissue mass with smooth margin, with bone trabecula destruction and cortex thinning and defect. If the lesion is large, it may spread to the adjacent region, and involve inwards the clivus, backwards the meninges, prepontine cistern, and cerebellopontine angle cistern, and outwards the internal ear.

2. MRI Examination

(1) MRI signals of mature cholesterol granuloma are highly characteristic Compared with the gray matter, the lesion shows hyperintense on T1WI, with peripheral hypointense ring; it shows slightly hyperintense on T2WI. MRI shows no enhancement or slightly mild enhancement on enhanced scan.
(2) The characteristics of MRI signals of immature cholesterol granuloma depend on the proportion of chronic bleeding products, cholesterol crystals and protein component. The granuloma may present various signal characteristics on T1WI and T2WI. Therefore, it is difficult to differentiate the granuloma from cholesteatoma and bursa mucosa. The clinically definitive diagnosis should be made based on pathological diagnosis.
(3) Cholesterol granuloma in the petrous apex may invade the horizontal segment of internal carotid canal. MRI angiography is suggestive.

22.3.3.4 [Key Points of Diagnosis]

1. Clinical manifestations are related to the location of the lesion. Cholesterol granuloma in the middle ear, like chronic suppurative otitis media, is manifested as intermittent "soy sauce-colored" secretions from the ear, with a sense of ear fullness and distension, hearing loss and tinnitus.
2. The focus is mostly round or quasi-circular, with peripheral expansile bone destruction and tympanic and mastoidal effusion.
3. MRI signals of mature cholesterol granuloma are characteristic. The lesion shows hyperintense on T1WI and T2WI and no enhancement on enhanced scan.

22.3.3.5 [Differential Diagnosis]

1. **Differential Diagnosis of Cholesterol Granuloma of Middle Ear**

(1) Chronic Otitis Media with Hemorrhage: increased-density shadows fully filling the mastoid cavity of middle ear, without expansile bone change.
(2) Hemotympanum After Trauma: a definite history of trauma, with bone fracture.
(3) Glomus Tympanicum Tumor: The tumor is mostly located on the surface of promontorium tympani. It shows hypointense to isointense on T1WI and hyperintense on T2WI and marked enhancement on enhanced scan.

2. **Differential Diagnosis of Cholesterol Granuloma of Petrous Apex**

(1) Primary cholesteatoma of petrous apex: isointense of hypointense on T1WI; hyperintense on DWI (Fig. 22.19).
(2) Petrous apex retained fluid (effusion): non-expansile change, intact cortex and trabecula; hypointense to isointense on T1WI.
(3) Petrous apicitis: Diffuse destructive change of bone cortex and bone trabecula; hypointense on T1WI.

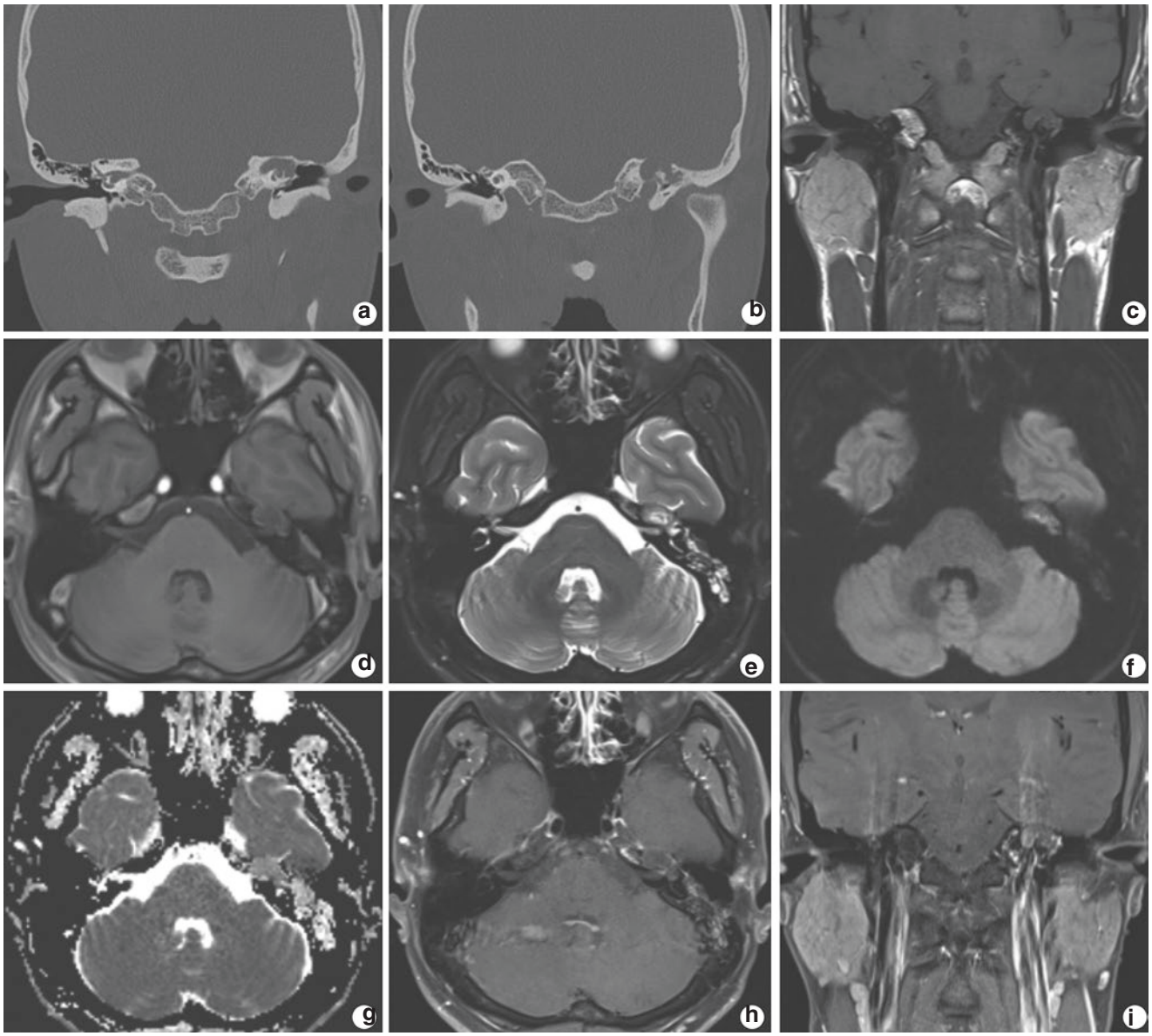

Fig. 22.19 Left petrous apex cholesteatoma. A 29-year-old male patient with acute onset and 1-week hospitalization mainly due to left facioplegia. Past medical history: Postoperative changes of left otitis media type C graph of left tympanic cavity. Postoperative pathology: left petrous apex cholesteatoma. (**a** and **b**) CT in the coronal plane shows soft tissue density shadows in the left mastoid process, residual cavity of left middle ear and petrous apex of temporal bone, and bone with irregular morphology in the left cochlea, vestibule, ossicular chain, facial nerve canal, carotid canal and petrous part of temporal bone. (**c**–**e**) MRI non-enhanced scan reveals the left petrous apex lesion, presenting slightly hypointense on T1WI and hyperintense on T2WI, with smooth margin. (**f**) DWI shows slightly hyperintense or isointense. (**g**) ADC value decreases. (**h** and **i**) Enhanced MRI scan shows mild enhancement in the margin of petrous apex lesion, and hyperintense on T2WI in the residual cavity and mastoid air cells of left middle ear, with no enhancement on enhanced scan. This case of congenital cholesteatoma of petrous apex is easily confused with the cholesterol granuloma of petrous apex

22.3.3.6 [Status Quo and Progress of Research]

The clinical manifestations of cholesterol granuloma are associated with the location of the lesion. CT can clearly show the soft tissue lesion with smooth margin, with peripheral expansile bone destruction space. On MRI, cholesterol granuloma shows hyperintense on T1WI and T2WI and no enhancement on enhanced scan. CT suggests the site, size and extent of the tumor, and corresponding peripheral bone changes. The characteristics of characteristic signals of MRI are of diagnostic value [22, 23].

References

1. Zhenchang W, Junfang X. Imaging of the head and neck·- otolaryngology, head and neck surgery. Beijing: People's Medical Publishing House; 2013.
2. Otology Group of Chinese Society of Otorhinolaryngology (ENT) of Chinese Medical Association, Otology Group of Editorial Board of Chinese Journal of Otorhinolaryngology Head and Neck Surgery. Guidelines for Clinical Classification and Surgery Typing of Otitis Media (2012). Chinese J Otorhinolaryngol Head Neck Surg. 2013;48(2): 5.
3. Lin HY, Fan YK, Wu KC, et al. The incidence of tympanogenic labyrinthitis ossificans. J Laryngol Otol. 2014;128(7):618–20.
4. Ruiz AP, Garcia GJM. Labyrinthitis ossificans in a cochlear implant patient with Usher syndrome. Otol Neurotol. 2013;34(3):10–1.
5. Körner H. Inflammatory diseases of the petrous portion of the temporal bone. Radiology. 2014;54(4):336–9.
6. Zhenchang W, Junfang X, Zhengyu Z. Tongren diagostic imaging manual of otorhinolaryngology head and neck surgery. Beijing: People's Military Medical Press; 2013.
7. Zhenchang W. Chinese clinical medical imaging·- head and neck. Beijing: Peking University Medical Press; 2016.
8. Wenhua L. Imaging differential diagnosis of head and neck diseases. Beijing: Chemical Industry Press; 2007.
9. Harnsberger HR. Head and neck top 100 diagnoses. Wang Zhenchang and Xian Junfang, trans. Beijing: Peking University Medical Press; 2006.
10. Mafee M, Valvassori G, Becker M. Valvassori's imaging of the head and neck. 2nd ed. Liu Huaijun, et al, trans. Beijing: China Medical Science Press; 2011.
11. Yan S, Dehong L, Hengguo L. Imaging of the head and neck·- otolaryngology, head and neck surgery. Beijing: People's Medical Publishing House; 2014.
12. Yun SJ, Ryu CW, Jahng GH, et al. Usefulness of contrast-enhanced 3-dimensional T_1-VISTA in the diagnosis of facial neuritis: comparison with contrast-enhanced T_1-TSE. J Neuroradiol. 2015;42(2):93–8.
13. Peng A, Yang X, Wu W, et al. Anti-neutrophil cytoplasmic antibody- associated hypertrophic cranial pachymeningitis and otitis media: a review of literature. Eur Arch Otorhinolaryngol. 2018;275(12):2915–23.
14. Xuanzhao H, Jibao W, Weijia K. Practice of otorhinolaryngology - head and neck surgery. 2nd ed. Beijing: People's Medical Publishing House; 2008.
15. Er A, Erdağ TK, Çağlar A, et al. Luc abscess: an extraordinary complication of acute otitis media. Am J Emerg Med. 2016;34(1):117.e1–3.
16. Deliang H, Sichang J, Weiyan Y, et al. Histopathology of the temporal bone in adhesive otitis media. Chinese J Otorhinolaryngol. 1996;31(5):287–90.
17. Otology Group of Chinese Society of Otorhinolaryngology (ENT) of Chinese Medical Association, Otology Group of Editorial Board of Chinese Journal of Otorhinolaryngology Head and Neck Surgery. Guidelines for Clinical Classification and Surgery Typing of Otitis Media (2012). Chinese Journal of Otorhinolaryngology Head and Neck Surgery, 2013, 48 (2): 5.
18. Zhaohui L, Zhenchang W, Jianhua T, et al. HRCT diagnosis of tympanosclerosis. Chinese J Med Imaging Technol. 2004;20(2):164–6.
19. Jing C, Yan Z. HRCT findings and surgical comparison of temporal bone in tympanosclerosis. Chinese J Otol. 2015;13(3):501–3.
20. Zhiyi D, Shifei W. Research progress of tympanosclerosis. J Youjiang Med Univ Nationalit. 2019;41(4):444–8.
21. Zhengpeng G, Huarong C, Houyu Z. Diagnostic significance of high-resolution CT combined with pure tone audiometry in tympanosclerosis. Chinese Arch Otolaryngol-Head Neck Surg. 2016;23(9):525–8.
22. Raghavan D, Lee TC, Curtin HD. Cholesterol granuloma of the petrous apex: a 5-year review of radiology reports with follow-up of progression and treatment. J Neurol Surg B Skull Base. 2015;76(4):266–71.
23. Radonjic A, Moldovan ID, Kilty SJ, et al. Complete recovery of sensorineural hearing loss following endoscopic transsphenoidal surgery for a petrous apex cholesterol granuloma: case report. Am J Case Rep. 2019;20:335–9.

Part V

Infectious and Inflammatory Diseases of Nose and Paranasal Sinus

Nose and Paranasal Sinus Diseases

23

Shuang Xia, Ting Liang, and Fuxing Li

23.1 Rhinosinusitis

23.1.1 Purulent Rhinosinusitis

23.1.1.1 Overview

Purulent rhinosinusitis is a frequently-occurring disease of the nose that often occurs bilaterally. It is common in paranasal sinuses. Most infections stem from the nasal cavity, while a few infections stem from the hypopharynx or tooth root. The infection may also be secondary to physicochemical stimuli, such as the traumatic fracture of paranasal sinus, infection of upper respiratory tract, allergic inflammation, and foreign matters or waste water into the paranasal sinus. Others (systemic chronic diseases, malnutrition, low immunity caused by old age and infirmity) can affect the occurrence and development of rhinosinusitis. More severe rhinosinusitis occurs in immunosuppression resulting from diabetes, medicine, drugs, and systemic diseases. The mucosae of the nasal cavity and paranasal sinuses are connected and close to the opening of each paranasal sinus cavity, so inflammation affects each other. The sinus ostia are narrow and swollen mucosa tends to block the openings, causing ventilatory and drainage disorders. The maxillary sinus and ethmoidal sinus develop early and the paranasal sinus mucosa easily develops edema, so infections mostly occur in childhood. The maxillary sinus has the maximum volume and the sinus ostium is higher than other openings, with unsmooth effusion drainage, so the incidence is highest. The air cells of ethmoidal sinus are small with poor drainage, so it is vulnerable to infection. The frontal sinus is close to the ethmoidal sinus which has a smaller infection chance. The sphenoid sinus is located deeply and has the smallest infection chance. The anatomic variations of nasal septum deviation, hypertrophy of nasal turbinates, and ostiomeatal complex form the basis of the regional anatomy of infections.

Rhinosinusitis is mostly a mixed infection, of which pathogens include staphylococcus, hemolytic streptococcus, streptococcus pneumoniae, and some anaerobes. The disease is clinically characterized by short course, acute onset, increased nasal secretions with nasal obstruction, and facial pain. Dysosmia may also occur. At the acute stage, it may be complicated with systemic infection symptoms. Pain or headache distribution helps to localize the lesion: The headache of frontal sinusitis radiates to the forehead part, with tenderness in the supraorbital margin. The pain of maxillary sinusitis is located in the cheeks and alveolar part. The pain of ethmoidal sinusitis occurs in the posterior part of nasion and inner canthus, with periodic attack. The anterior ethmoidal sinus usually has pain in nasion and forehead part, while the posterior ethmoidal sinus has pain in the posterior side of the eyeball, temporo-occipital part, and parietal part. Sphenoiditis is usually not characteristic, similar to the posterior ethmoidal sinus, and has occipital or retrobulbar pain. When the sinus ostium is completely blocked and the purulent secretions retain, pain is more severe. The progression leads to bone wall destruction and dissolution, causing intraorbital or intracranial complications. Chronic inflammation may be caused by allergic factors or may be due to prolonging of uncured acute inflammation, with recurrent attack. The clinical manifestations of the lesion may be acute or chronic.

23.1.1.2 Pathology Findings

In the acute stage, catarrhal inflammation occurs; there are mucosal vasodilatation, mucosal congestion and edema, and mucosal swelling which blocks the sinus ostium; there is the infiltration of lymphocytes and multinucleated giant cells

S. Xia (✉)
Tianjin First Central Hospital, Tianjin, China

T. Liang
First Affiliated Hospital of Xi'an Jiao Tong University, Xi'an, China

F. Li
Tianjin Baodi District People's Hospital (Baodi Clinical College of Tianjin Medical University), Tianjin, China

H. Li et al. (eds.), *Radiology of Infectious and Inflammatory Diseases - Volume 2*,
https://doi.org/10.1007/978-981-16-8841-6_23

inside, with enlarged gland and increased and retained serous secretions. Several days later, it develops into the purulent stage, in which there is neutrophil infiltration and ciliated epithelial necrosis and exfoliation, and secretions become mucous and purulent. The bone of the sinus cavity is usually normal, and a small part of periosteum has congestion and edema, with bone demineralization and resorption. Osteomyelitis is formed, causing bone destruction and even intraorbital and intracranial inflammation. In the chronic stage, there is mucosal fibrous hyperplasia and hypertrophy, granulation tissue proliferation, and interstitial edema, presenting polypoid hypertrophy. There are submucosal cysts and mucous glandular retention cysts. The inflammatory reaction of periosteum causes bone cortex rarefaction and resorption. In the long-term course of the disease, mucosal degenerative atrophy, squamous metaplasia of mucosal columnar epithelium, and submucosal fibrosis occur. Long-term chronic inflammation stimulation causes thickening and sclerosis of periosteum and bone in sinus wall.

23.1.1.3 Imaging Findings

X-Ray Examination

1. Acute purulent rhinosinusitis: It mostly occurs in bilateral maxillary sinuses or bilateral multiple sinus cavities. The turbinates are swollen; the paranasal sinus mucosa is thickened parallel to the sinus wall, presenting homogeneous annular or wavy soft tissue shadow. With acute progression, the sinus cavity has evenly reduced transmittance and becomes turbid, in which extensive cloudy density increases. Sitting projection shows air-fluid level. The lamina papyracea of ethmoid bone and the bony wall of maxillary sinus are generally continuous and intact, with clear bone white line. A small number of bones are resorbed and become thin, and the periosteum line is blurred [1].
2. Chronic purulent rhinosinusitis: The disease may be unilateral or bilateral, single or multiple, or mainly occur on one side. On the images of the chronic stage, there are various findings. The sinus cavity mucosa presents homogeneously annular or heterogeneously wavy polypoid hypertrophy, which may be circumscribed or diffused to the whole sinus cavity or the whole group of paranasal sinuses; the bone resorption and decreased density of sinus wall are found. In the advanced stage, granulation tissue proliferation is found; When it is associated with mucosal cysts or polypoid changes, a semicircular or irregular spherical mass protrudes into the sinus cavity. There are reactive proliferation and sclerosis in the bone of sinus wall, blurred white line in the sinus wall, hyperostosis and septal ridge formation in the cavity, and narrowed sinus cavity. The turbinate mucosa has an evolution process of swelling to atrophy.

CT Examination

1. Acute purulent rhinosinusitis: The swelling and thickening of the nasal cavity mucosa, turbinate enlargement, and nasal meatus stenosis are seen. In the early stage of the lesion, the swollen and thickened sinus cavity mucosa can be noted, which is mostly parallel with the sinus wall or presents polypoid changes [1, 2], showing medium- to low-density shadow; air in the sinus cavity decreases. When the sinus cavity is filled with retained exudates, the density is increased. The unobstructed sinus ostium presents as a characteristic air-fluid level [2] and may change with the body position. The non-enhanced scan shows hypodense or isodense in secretions. The enhanced scan shows no enhancement of secretions and marked enhancement of mucosa. There is stenosis in the infundibular part and semilunar hiatus of the ethmoidal sinus. In the acute stage, the bony wall of sinus cavity often shows no significant change; in combination with osteomyelitis, bone resorption and destruction and blurred surface are found. With acute attack, the disease may be complicated with cellulitis (Figs. 23.1 and 23.2a–c).
2. Chronic purulent rhinosinusitis: Acute purulent rhinosinusitis with incomplete treatment or recurrent attack may be prolonged and progress into chronic purulent rhinosinusitis, in which turbinate hypertrophy presents polypoid changes and the mucosa of sinus wall shows significantly homogeneous or irregular hypertrophy [3]. These appear as diffuse annular and circumscribed mound-like bulges, and lobulated medium to low heterogeneous density shadow. The wide base or narrow pedicle is close to the sinus wall and septa surface in smoothness. CT findings of obstructive rhinosinusitis include enlarged sinus cavity, heterogeneous increase in density of the sinus cavity with irregular shape, resorption and rarefaction of the sinus wall, and no bone destruction. In the advanced stage, the bony wall of sinus cavity has hypertrophy and sclerosis, with protrusion into septa or bone ridges in the cavity [1] and no bone destruction. Paranasal sinus hypoplasia and sinus cavity stenosis can be found in childhood. Odontogenic maxillary sinusitis should be considered in patients with unilaterally increased density in the maxillary sinus. The unilaterally high density in the frontal sinus, ethmoidal sinus, and maxillary sinus in patients are mostly caused by ostiomeatal complex syndrome. Chronic purulent rhinosinusitis may lead to intracranial complications (Figs. 23.3 and 23.4).

MRI Examination

1. Acute purulent rhinosinusitis: In the early stage of the lesion, there is turbinate hypertrophy; thickened paranasal sinus mucosa in parallel to the sinus wall or septa surface presents homogeneous lamellar or wavy isointense to slightly hypointense on T1WI and hyperintense on

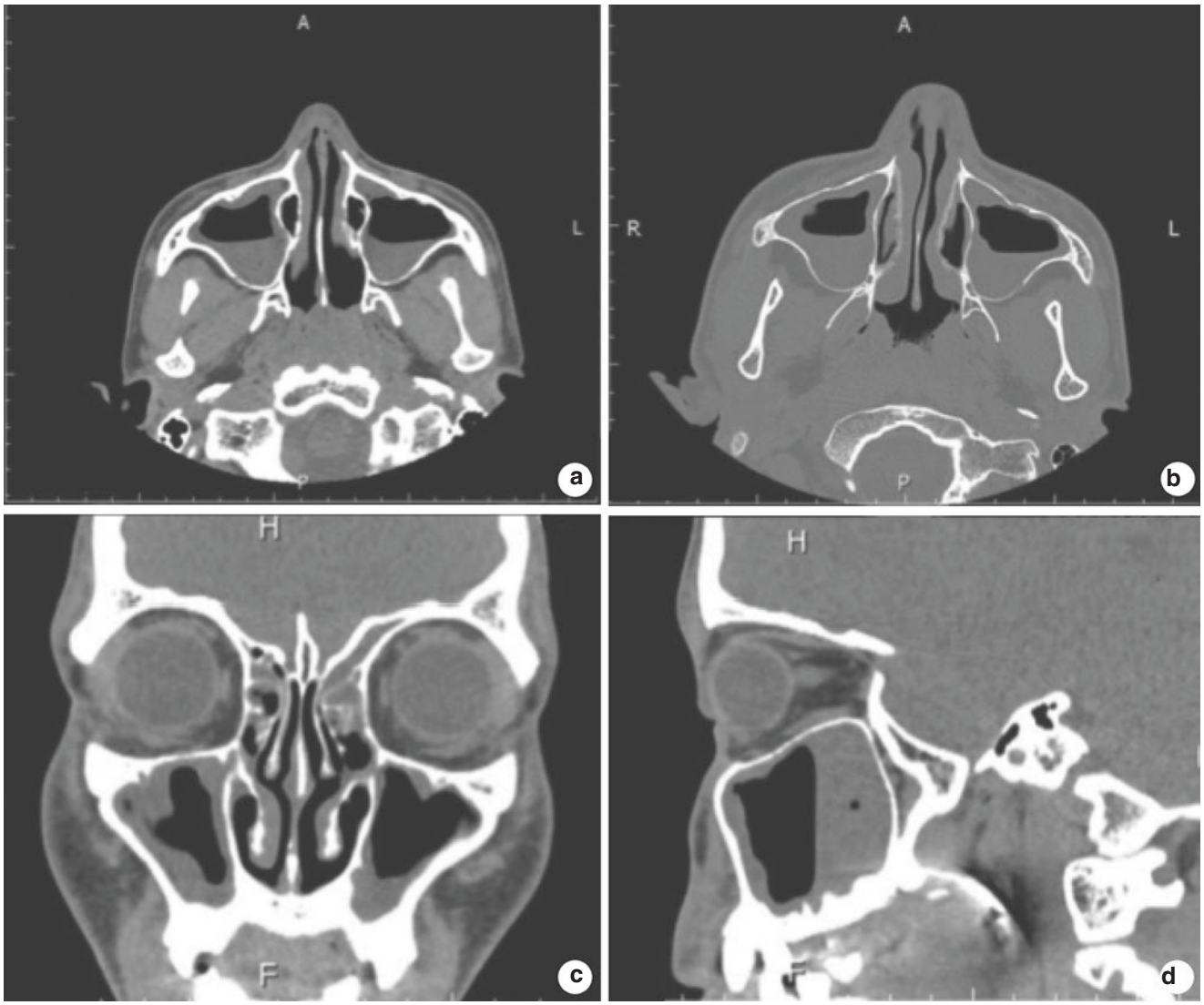

Fig. 23.1 Acute rhinosinusitis (1). A 14-year-old male patient. (**a**) CT non-enhanced scan shows annular lamellar thickening of sinus cavity mucosa of bilateral maxillary sinuses with homogeneous thickness, air-fluid level formed in the sinus cavity of bilateral maxillary sinuses, thickening of the posterior pharyngeal wall, and posterior nostril narrowing, which is the presentation of adenoidal hypertrophy. (**b**) Axial bone window shows no abnormal changes in the paranasal sinus wall. (**c**) Coronal recombination image shows thickening of mucosae of the whole group of paranasal sinuses. (**d**) Sagittal recombination image shows air-fluid level in the maxillary sinus

T2WI. When there are more secretions, the homogeneous turbid water sample from the sinus cavity shows hypointense on T1WI and hyperintense on T2WI; if there is fluid level, it is the characteristic finding. The retained fluid presents signal diversity with the effect of protein content. In empyema, viscous effusion shows isointense to slightly hyperintense, and effusion coagulation into the clot or increase in glycoprotein content may show double-hypointense [2]. On enhanced scan of veins, thickened mucosae show annular and homogeneous marked enhancement and secretions generally show no enhancement. When the opening is blocked, retention secretions may also show heterogeneous mild enhancement [3]. The polyp in the sinus cavity shows single or multiple round or obround soft tissue shadow, without enhancement, and it is complicated with acute osteomyelitis, and edema and destruction of the sinus wall. T1WI presents decreased signal of bone marrow and the fat-suppression image shows increased signal, with different degrees of enhancement (Figs. 23.2d–i, and 23.5a–f).

2. Chronic purulent rhinosinusitis: In the advanced stage, there is turbinate hypertrophy; thickened mucosa along the sinus wall or septa surface show parallel or lobulated soft tissue signals, which is polypoid granulation tissue, and shows hypointense on T1WI and hyperintense on T2WI [3]. Fibrotic tissue shows isointense to hypointense, and marked enhancement on enhanced scan [4]. Proliferative bone shows hypointense (Fig. 23.5g–i).

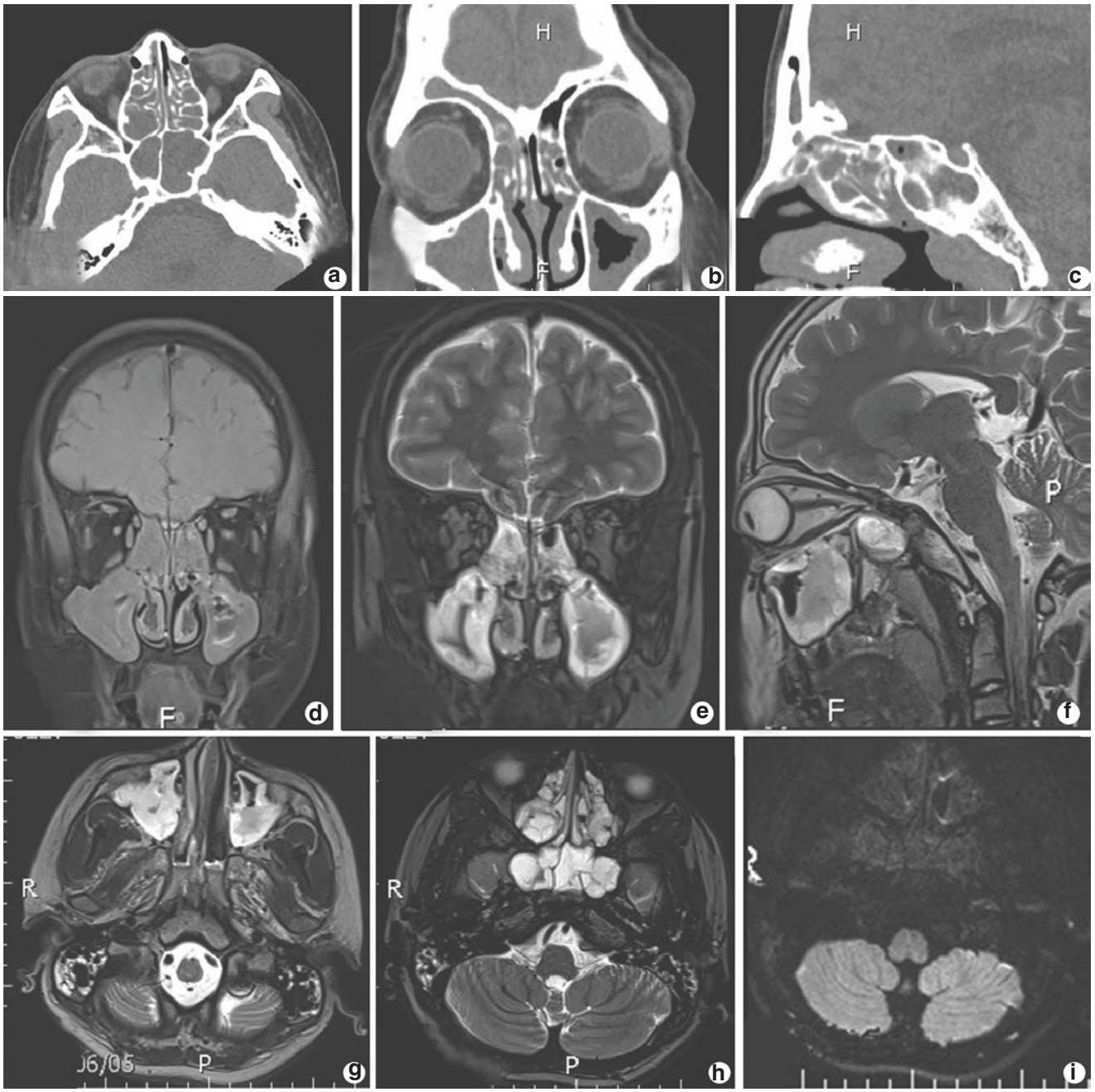

Fig. 23.2 Acute rhinosinusitis (2). A 12-year-old male patient. (**a**–**c**) CT non-enhanced scan in the axial, coronal and sagittal planes shows hypertrophy of bilateral inferior turbinates, annular thickening of mucosae of the paranasal sinus group, sinus cavity filled with soft tissue density shadow, and sinus wall without bone destruction. (**d**–**i**) MRI non-enhanced scan shows isointense on T1WI and hyperintense on T2WI in peripheral edema mucosa, and slightly hypointense on T2WI and slightly hypointense on DWI in the secretions of sinus cavity. The adenoidal hypertrophy, infiltration and involvement of soft tissue around the sinus cavity, and bilateral obstructive mastoiditis can be found. The mastoid cell shows sparsely hyperintense on T2WI

23.1.1.4 Key Points of Diagnosis

1. There is a history of acute rhinitis which mostly occurs after the infection of upper respiratory tract. The clinical manifestations are persistent nasal obstruction, purulent discharge, headache, brain distension.
2. CT non-enhanced scan: The sinus wall mucosa is thickened. The effusion in the sinus cavity and soft tissue density shadows in the paranasal sinus form a typical air-fluid level, with or without bony thickening of sinus wall. The sinus wall in the acute stage is not markedly expansile. In

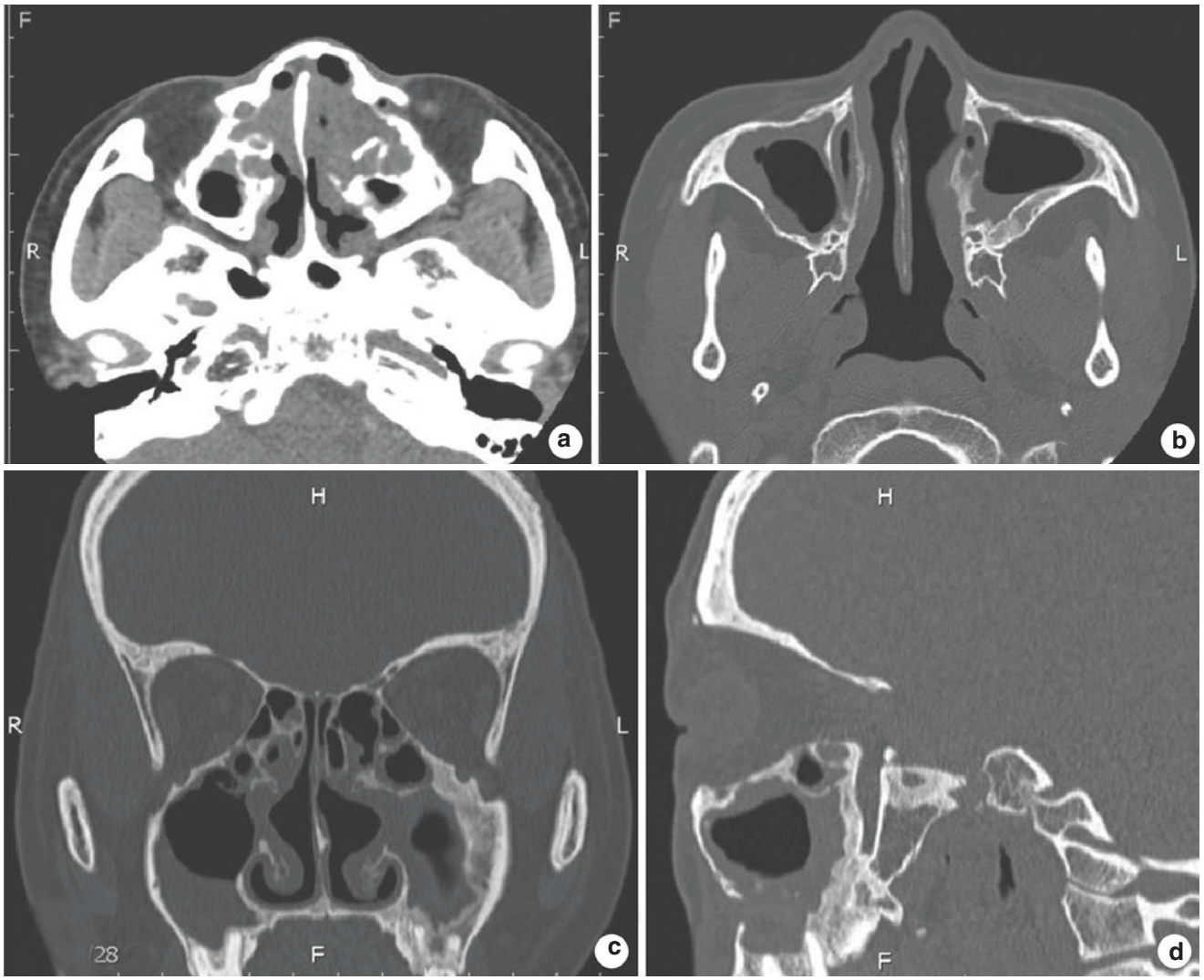

Fig. 23.3 Chronic rhinosinusitis (1). A 50-year-old female patient. With recurrent nasal discharge and hyposmia for the past 10 years, and status post nasal polypectomy, and absence of middle turbinate after turbinectomy. (**a**) CT non-enhanced scan shows nodular thickened soft tissue shadows in bilateral nasal meatus and left ethmoidal sinus, which is the presentation of chronic nasal polyp. (**b**–**d**) CT non-enhanced scan shows maxillary sinus mucosa with heterogeneous thickening and uneven surface, diffuse thickening of the sinus wall with sclerosis, thick bone trabecula, and circumscribed bone defect in the anterior wall

the chronic stage, the sinus wall is intact and continuous due to bony thickening, and the sinus cavity is narrowed.

3. Non-enhanced MR scan: Pus presents hypointense on T1WI and hyperintense on T2WI. When the protein content increases, T1WI shows increased signal intensity. The mucosa shows annular and wavy thickening. The enhanced scan shows marginal ring enhancement in the mucosa, and no enhancement in effusion.
4. Laboratory test: The leukocyte count increases significantly.

23.1.1.5 Differential Diagnosis

1. *Nasal polyp.* Soft tissue shadows are found in the nasal cavity and paranasal sinuses, and the turbinates are replaced by soft tissue shadows. The inflammatory polyp has a low density. MRI shows watery signals and usually no enhancement. The sinus cavity expands and deforms, and the piriform aperture is enlarged.
2. *Hemorrhagic necrotic nasal polyp.* Medium soft tissue shadows are found in the unilateral nasal cavity and maxillary sinus, with patchy high-density hemorrhage inside. The adjacent bones have compressive bone resorption, with an enlarged sinus cavity. MRI examination shows hemorrhagic characteristic hypointense iron ring, with progressive enhancement in the enhancement curve.
3. *Fungal rhinosinusitis.* The density in the sinus cavity is heterogeneous, and spherical and patchy calcification is shown in the fungal masses of paranasal sinus cavity,

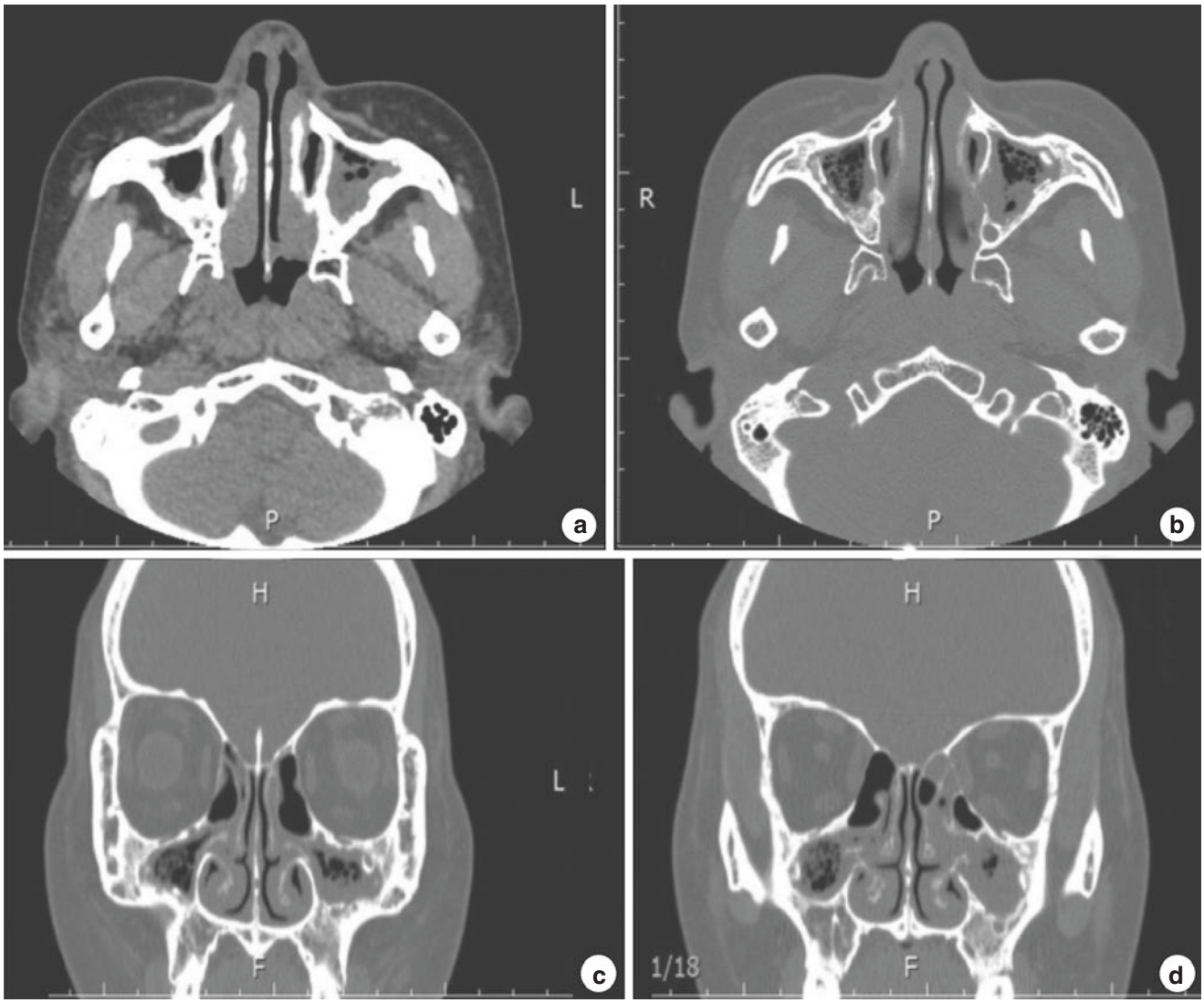

Fig. 23.4 Chronic rhinosinusitis (2). A 51-year-old female patient with a history of chronic rhinosinusitis in bilateral maxillary sinus. (**a**–**d**) Axial and coronal recombination images on CT non-enhanced scan show thickening and sclerosis of the bilateral maxillary sinus walls, unsmooth sinus walls, strip-like calcified plaques along the medial side of the sinus walls. Heterogeneous thickening is found in the mucosae of bilateral maxillary sinuses and left ethmoidal sinus. Linear hyperdense shadows are interwoven into the reticular structure in the sinus cavity. There are bilateral inferior turbinates in increased volume and thickened nasal cavity mucosa

which are characteristic changes. The compressive resorption or thickening and sclerosis occurs in the sinus wall.

4. *Papilloma.* It is a benign tumor of nasal cavity in elderly males and derives from the lateral wall of nasal cavity. There is an irregular soft tissue mass in the middle nasal meatus, with unsmooth surface and "bubble sign" inside. Some tumor may be calcified. The paranasal sinus cavity is enlarged. Obstructive inflammation occurs in the nasal meatus of nasal cavity on the affected side. The nasal septum shifts; the bone in the lateral wall is expanded and thinned or resorbed and destroyed. It is easy to differentiate it from inflammation on MRI. T1WI shows hypointense or isointense to slightly hypointense and T2WI shows hyperintense. The curly lobulated structure is seen inside and may extend to the maxillary sinus, ethmoidal sinus, and nasopharyngeal part. The enhanced scan shows heterogeneous gyriform enhancement.
5. *Wegener granulomatosis.* There is bone destruction in turbinate and nasal septum. The nodular soft tissue mass occurs in the midline of nasal cavity.
6. *Allergic rhinosinusitis.* Chronic purulent rhinosinusitis is often complicated with allergic rhinosinusitis. Allergic elements are the main causes of non-purulent rhinosinusitis. Imaging is difficult to differentiate the two diseases. Allergic rhinosinusitis is characterized by generally enlarged turbinates, nasal polyp in the nasal cavity, mostly

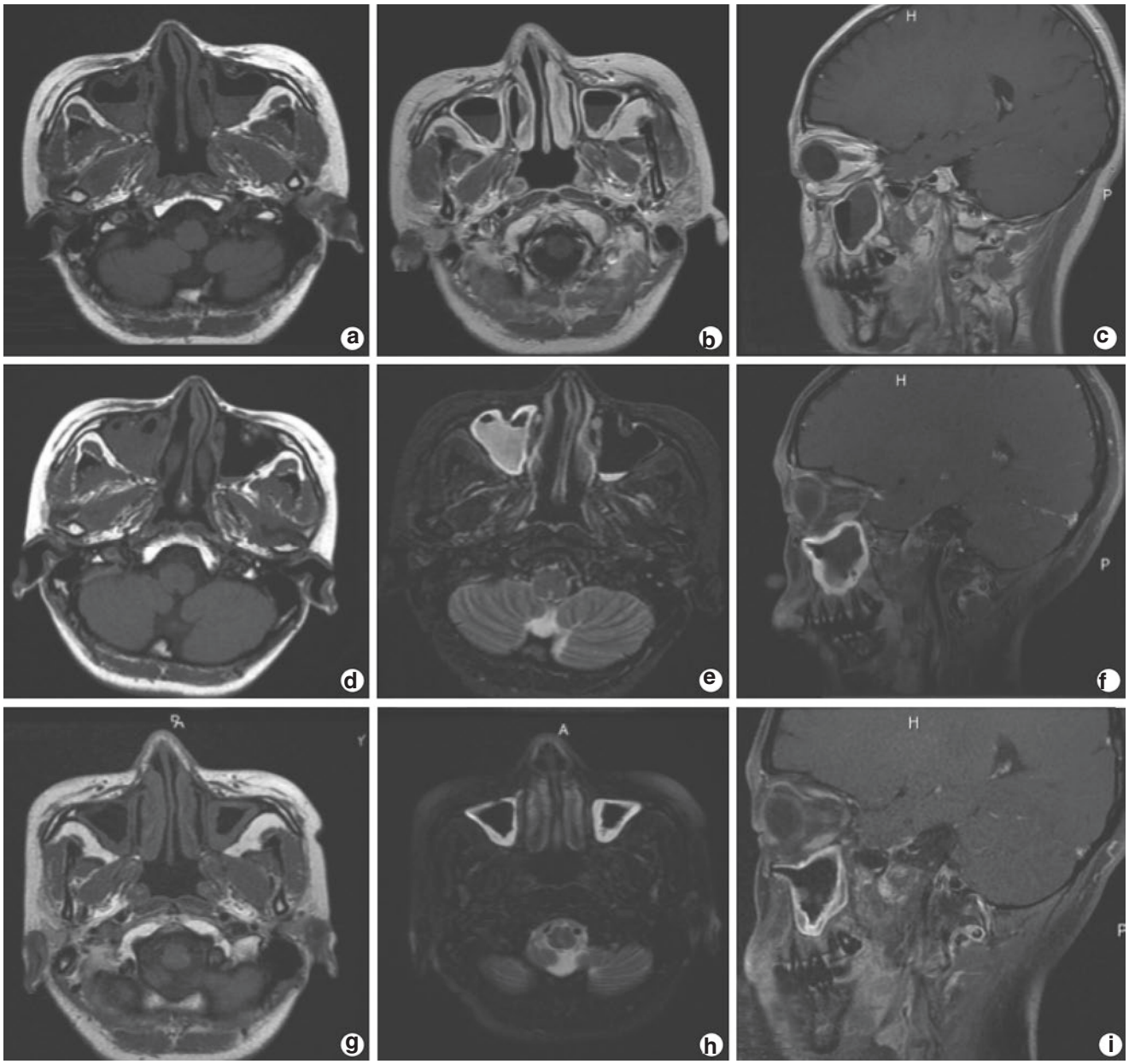

Fig. 23.5 Acute rhinosinusitis into chronic rhinosinusitis. A 27-year-old female patient. (**a–c**). In the first examination, MRI non-enhanced scan shows homogeneous mild thickening of bilateral maxillary sinus mucosae, intracavitary secretion retention, air-fluid level, and slightly hypointense of fluid on T1 WI. Enhanced MRI scan shows homogeneous enhancement in mild thickened mucosae and no enhancement in retained fluid. (**d–f**) In the reexamination after 15 months, rhinosinusitis is recurrent, and effusion in the right maxillary sinus increases; T1WI signal is intensified. Mucosae have lamellar hypertrophy, and still show homogeneous enhancement on enhanced scan. (**g–i**) In the reexamination after 8 months, the fluid disappears; bilateral maxillary sinus mucosae are thickened heterogeneously, which shows isointense of soft tissue on T1WI and heterogeneous signals on T2WI. T2WI shows a patchy slightly hypointense region inside. The enhanced scan shows heterogeneous enhancement and T2WI shows low enhancement in the corresponding hypointense region

bilateral involvement, mucosa with lobulated thickening, little fluid level, and intact and clear sinus wall, which are different from bone wall resorption and osteosclerosis of purulent rhinosinusitis.

7. *Paranasal sinus cyst.* The submucosal cyst is mostly manifested as the well-defined homogeneous low-density lesion, with no change in body position. The mucocele is a common lesion with an expanded sinus cavity and bone resorption of sinus wall. The enhanced scan shows no enhancement in the lesion in the sinus cavity.
8. *Surgical traumatic secondary changes.* The air-fluid level in the sinus cavity is a characteristic change of purulent rhinosinusitis. Definitive diagnosis can be generally made by combining the change with symptoms and signs of

infection. However, the sign is not unique. The air-fluid level may occur when past nasal drainage, trauma, surgery, barotrauma, and disturbance of blood coagulation lead to hemorrhage. Thus, the medical history should be closely combined to prevent misdiagnosis due to preconceptions.

23.1.1.6 Status Quo and Progress of Research

Combined with the clinical course and typical manifestations of thickened mucosa and air-fluid level in the paranasal sinus, CT is adequate to make an accurate diagnosis. In respect of infiltration of peripheral tissues and formation of bone destruction, if the involvement extent and the identification of tumorous lesions need to be understood, an additional MRI examination can be performed. The change of magnetic resonance signals can help to understand tissue components, distinguish other lesions to make an accurate diagnosis, and evaluate the stage characteristics and involvement extent of the lesion.

23.1.2 Fungal Rhinosinusitis

23.1.2.1 Overview

Fungus infection of paranasal sinuses is also known as fungal rhinosinusitis. The pathogen of fungal rhinosinusitis is mostly aspergillus, followed by mucor. Other rare pathogens include Candida albicans, Rhinosporidium, cryptococcus, and actinomycetes. The fungal infection of paranasal sinuses is relatively rare. The infection mostly occurs in the paranasal sinus with poor drainage, and most of the infections are found in the maxillary sinus, followed by the sphenoid sinus and ethmoidal sinus. The disease occurs unilaterally in most cases and may occur bilaterally. It is clinically common in adult females. It often occurs on the basis of chronic purulent rhinosinusitis and nasal polyps. The incidence in old and infirm patients with systemic diseases significantly increases.

The aspergillus infection lesion is relatively mild and localized, while the mucor infection is mostly severe. According to the fungal invasiveness and host immune status, the disease is divided into four types: fungal ball, allergic fungal rhinosinusitis, chronic invasive fungal rhinosinusitis, acute fulminant fungal rhinosinusitis.

1. *Fungal ball.* It is the most common type. It is chronic noninvasive fungal infection that usually occurs in healthy people. Thick cheese-like semisolids can be seen in the paranasal sinus cavity. The typical symptom is the discharge of brown hypha masses from the nasal cavity.
2. *Allergic fungal rhinosinusitis* mostly occurs in young and middle-aged patients with allergic constitution, among who 40% have a history of asthma. Brown or greenish-black mucus or white cheese-like matters can be noted in the sinus cavity.
3. *Chronic invasive fungal rhinosinusitis* progresses slowly and is easily misdiagnosed as malignant tumor, which is classified into chronic painless type and granuloma.
4. *Acute fulminant fungal rhinosinusitis* mainly occurs in patients with immunodeficiency who are often accompanied by underlying diseases, such as diabetes, long-term use of antibiotics or abuse of hormones, severe malnutrition or diseases after malignant tumor chemotherapy. The pathogen is mostly mucor. The mucor first invades the nasal part, causing rapid progression of the lesion, enlarged sinus cavity and destroyed sinus wall, spreads to the lateral region of nasal cavity and paranasal sinuses after a few days, and extends to the pterygopalatine fossa, infratemporal fossa, orbit and intracranial area, causing serious complications and threat to life. The mortality reaches 60% ~ 100%. Hence, the disease is also known as rhinocerebral mucormycosis.

23.1.2.2 Pathology Findings

1. *Fungal ball.* Thick cheese-like semisolids can be seen in the sinus cavity. Microscopically, it is characterized by nodular hypertrophy and hyperplasia of paranasal sinus mucosa, many inflammatory exudates and necrotic tissues, lymphocyte and multinucleated giant cell infiltration, and affected tissue densely populated with fungal spores and hyphae, with nonallergic mucin. After the necrotic fungal ball forms, metabolites including calcium phosphate, calcium sulfate, iron, manganese, and other heavy metal salts inside deposit.
2. *Allergic fungal rhinosinusitis.* Allergic mucin aggregation is found, and there are a large number of eosinophils, Charcot-Leydon crystals, and fungal hyphae. Fungal hypha does not invade the paranasal sinus mucosa and blood vessels.
3. *Chronic invasive fungal rhinosinusitis.* Invasive aspergillus can invade mucosal tunica intima and cause thromboarteritis; invade the paranasal sinus mucosa and submucosal bone and cause bone wall necrosis, and sinus wall osteosclerosis and destruction coexist. Inflammatory granulation tissue in paranasal sinus grows slowly and continuously, destroying the bone of sinus wall and perisinusoidal tissues. Bloody pus, granulation tissue, necrotic tissue, and caseous tissue are present in the lesion, which are similar to those of malignant tumors.
4. *Acute fulminant fungal rhinosinusitis.* As mucor infection is strongly aggressive, the lesion progresses rapidly and the mucor invades the mucosal arteries and submucosal bone of paranasal sinuses, and proliferates massively under the endarterium, causing arteritis and vascular

necrosis; leading to osteonecrosis in a short period and invading surrounding structures.

23.1.2.3 Imaging Findings

1. *X-ray examination.* Aspergillus is often confined to a single sinus cavity. Mucor is mostly invasive and involves multiple sinus cavities. The findings of plain films are similar to those of general chronic rhinosinusitis. Generally, the findings are soft tissue swelling in the nasal cavity, turbinate enlargement, floccus turbidness in single or multiple sinus cavities, heterogeneous annular thickening of mucosa, no air-fluid level, no enlargement of sinus cavity, and no change or thickening and sclerosis of sinus wall. The fungal ball appears as the soft tissue mass in the sinus cavity with patchy calcification area, which is a characteristic finding [5]. In allergic rhinosinusitis, ground-glass opacity is present in the sinus cavity, with enlarged sinus cavity, thinned sinus wall, and absorption of lamina papyracea of ethmoid bone. The extensive bone destruction occurs in the sinus wall and nasal septum, suggesting invasive rhinosinusitis. At this point, it should be differentiated from malignant tumor of paranasal sinuses.
2. *CT examination.*
   (a) Fungal ball: It mostly occurs in adult women, circumscribed to single paranasal sinus. It is the most common in the maxillary sinus and rare in the frontal sinus. The sinus cavity is filled with irregular polypoid granulation tissue. Residual air shadows may be seen, and there is generally no effusion or air-fluid level, presenting medium to slightly high density which is often heterogeneous. The inside is clustered with patchy and sand-like calcification (CT value of 160 ~ 350HU) or linear increased-density shadow [6], which represents the calcium, iron, manganese, and other heavy metals deposit in the necrotic area. The calcification is a typical presentation of the fungal ball, with an occurrence rate of 70% [7], which is often located near the sinus ostium of maxillary sinus. The enlarged sinus ostium, compressive bone resorption in uncinate process, and reactive proliferation and sclerosis in the sinus wall are found; bone destruction is relatively rare. The enhanced scan shows no enhancement in the fungal ball. With complications with pyogenic infection, the enhanced scan shows heterogeneous mild enhancement, with fluid level, multiple sinus cavities are involved (Figs. 23.6, 23.7, and 23.8a–b).
   (b) Allergic fungal rhinosinusitis: It is common, accounting for 7% of chronic rhinosinusitis. The sinusitis occurs in the half group or whole group of paranasal sinuses. The involvement of ethmoidal sinuses is common, with nasal polyps. The sinus cavity is enlarged and remodeled, which is filled with solid soft tissue density shadow, with flaky ground-glass opacity (mucin) in different shapes scattered in the center [3, 7] and surrounding low-density mucosa. Bone is resorbed and thinned due to compression. The orbit and anterior cranial fossa may be invaded (Fig. 23.9).
   (c) Chronic invasive fungal rhinosinusitis: Aspergillus is the most common pathogen. The disease is most common in the maxillary sinus, followed by the ethmoidal sinus and sphenoid sinus [3]. In the early stage, only non-specific mucosal thickening is found. In the progressive stage, a soft tissue mass with heterogeneous density is found in the sinus cavity, with calcification rare inside. The mass bulges into the adjacent paranasal sinus and nasal cavity. Bone destruction and proliferation and sclerosis are present in the sinus wall, usually causing large bone defects. The fat space around the sinus cavity is invaded with increased density, and the pterygopalatine fossa, infratemporal fossa, orbital and intracranial structures are affected, with erosion and destruction of orbital wall and skull, increased soft tissue in the orbit, extraocular muscle, and optic nerve involved, and eyeball protruding outward due to pushing pressure (Figs. 23.10a–c and 23.11a).
   (d) Acute fulminant fungal rhinosinusitis: It is mostly found in maxillary sinus, followed by the ethmoidal sinus and sphenoid sinus. In the early stage, the paranasal sinus mucosa is thickened and there is generally no air-fluid level. The rapid progression of the condition causes the infiltration of soft tissue around the maxillary sinus, diffuse swelling in the sinus cavity and perisinusoidal soft tissue, serious bone destruction of the sinus wall forming large defects, no deformation of the sinus cavity, and extensive invasion of adjacent structures [3] (Fig. 23.12a).
3. *MRI examination.*
   (a) Fungal ball: It often involves a single sinus cavity. The mucosal hypertrophy shows nodular changes. Due to calcium phosphate deposits, the intracavitary granuloma presents hypointense or isointense on T1WI, and calcification shows extremely hypointense on T2WI [7]. The enhanced scan shows no enhancement in the main body and mild ring enhancement in marginal mucosa (Fig. 23.8c–i).
   (b) Allergic fungal rhinosinusitis: Multiple sinus cavities are usually involved, with sinus cavity expansion, and the paramagnets including iron and manganese and secretion mucin in fungal hypha have different contents [3, 7]. T1WI signals vary from hypointense

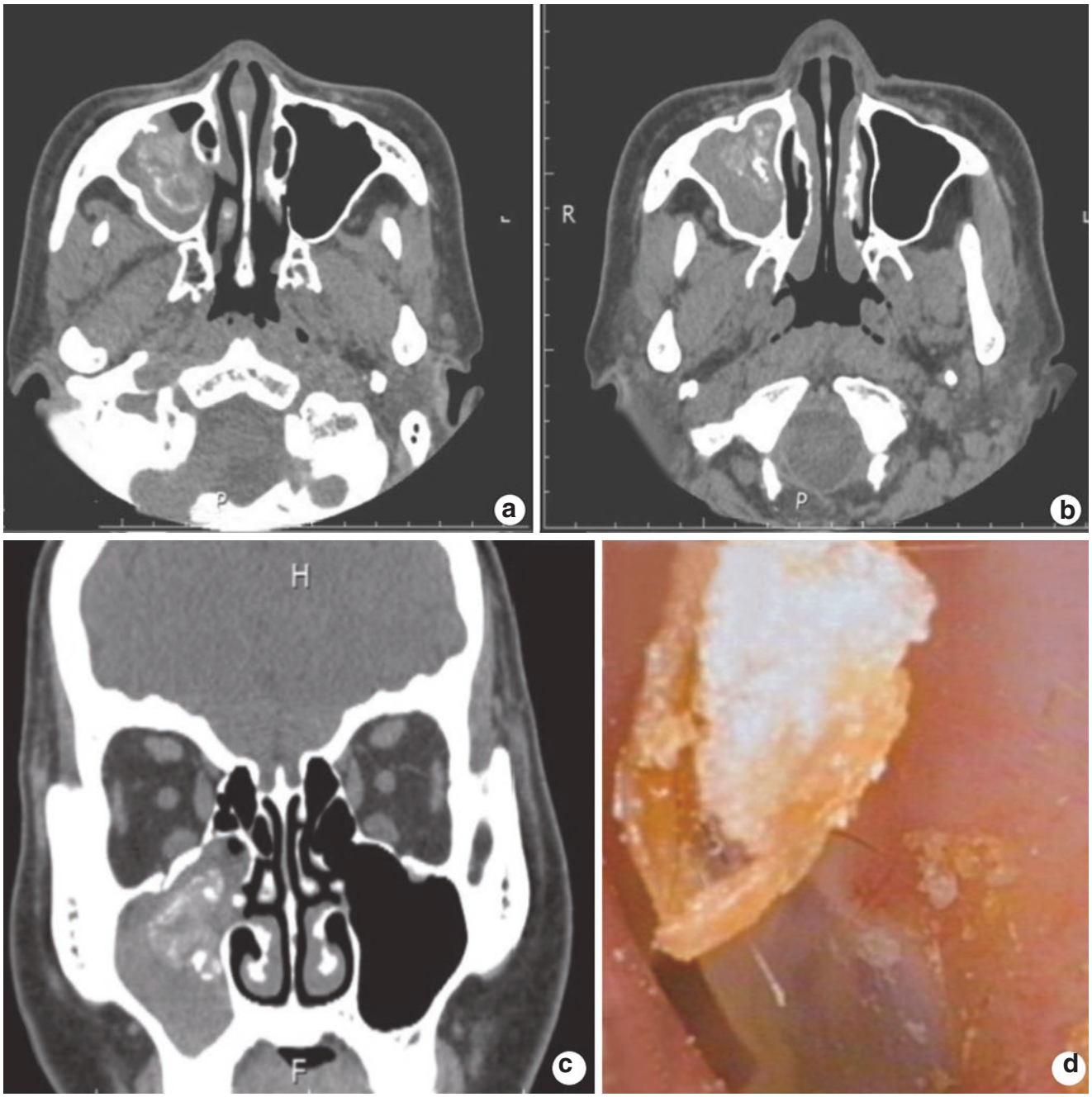

Fig. 23.6 Fungal ball of right maxillary sinus. A 47-year-old female patient. (**a–c**) CT in the transverse plane and coronal plane shows increased density in the right maxillary sinus cavity, filled with soft tissue density, patchy and annular calcification area inside with different degrees of calcification, and enlarged sinus ostium of maxillary sinus. (**d**) Nasal endoscopy shows calcified fungal ball presenting pale crumby structure

to hyperintense. T2WI shows heterogeneous hypointense. The enhanced scan shows no enhancement inside and linear enhancement in peripheral mucosa, with hyperintense in nasal polyps on T2WI.

(c) Chronic invasive fungal rhinosinusitis: As the paramagnet and mucin content affects magnetic resonance signals, it mostly shows isointense on T1WI, heterogeneous and large patchy hypointense on T2WI, with good performance in showing nerve invasion. Chronic invasive fungal rhinosinusitis often causes orbital apex cavernous sinus syndrome [8], in which the optic canal is invaded, the cavernous sinus

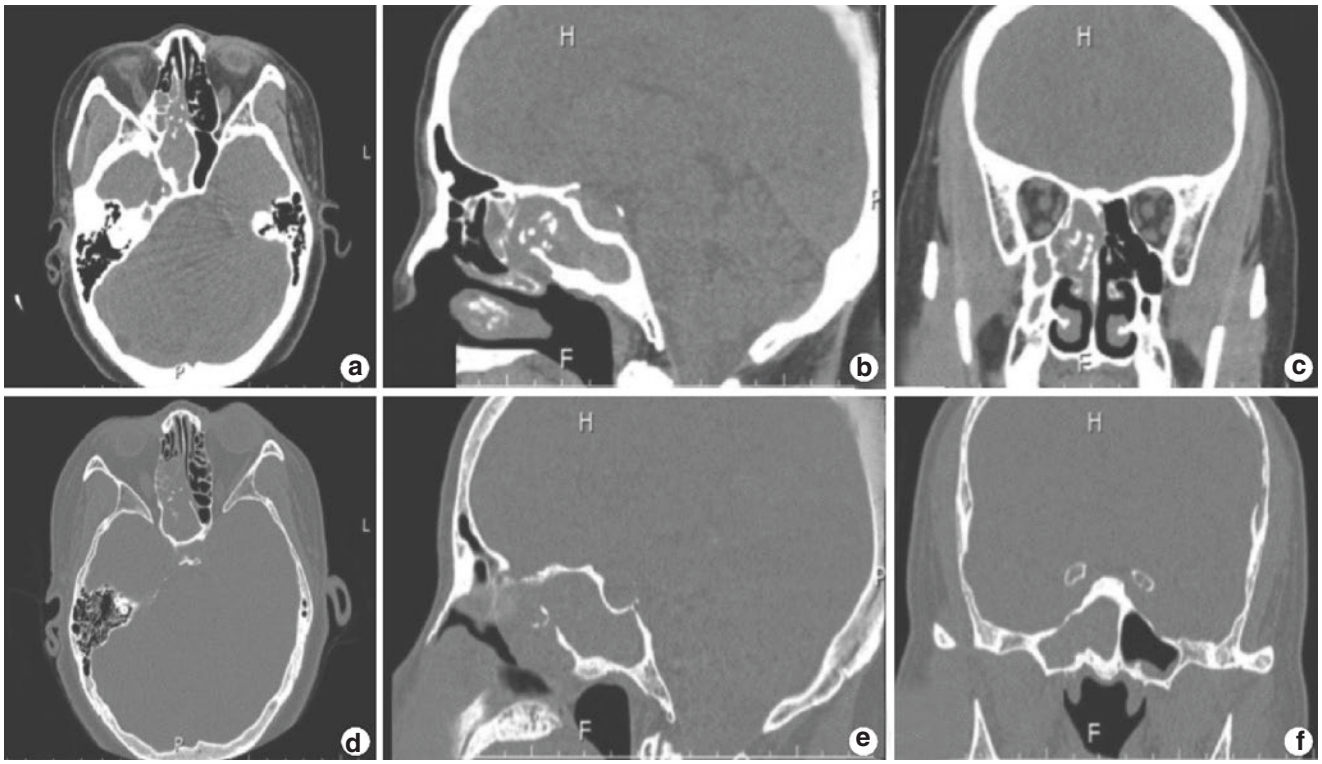

Fig. 23.7 Fungal ball of right posterior ethmoidal sinus and sphenoid sinus. A 63-year-old female patient (**a**–**f**) CT shows mild enlargement of right sphenoid sinus cavity, hypertrophy of sinus wall, and osteosclerosis. The sphenoid sinus is connected to the posterior ethmoidal sinus. The right posterior ethmoidal sinus and sphenoid sinus cavities are filled with soft tissue density, with lumpy calcification density area in the center

is widened, the soft tissue mass shows heterogeneous enhancement by enhanced scan, the involved meninges are thickened with linear enhancement, the cavernous sinus segment of the internal carotid artery is subject to compressive deviation, and the blood vessels become thinner (see Figs. 23.10d–i and 23.11b–i).

(d) Acute fulminant fungal rhinosinusitis: The fungi in the mucosa and blood vessels invade, with diffuse infiltration of soft tissue in the nasal cavity and paranasal sinus. The adjacent structures are extensively invaded, such as nasal cavity, sinus cavity, orbit, pterygopalatine fossa, infratemporal fossa, and cavernous sinus, which have serious bone destruction [9]. The extraocular muscle and optic nerve are swollen, and soft tissue in the orbital apex and cavernous sinus area is thickened and enhanced. Saltatory invasion is made to the skull, with meninges thickening and enhancement. Fungal brain abscess may be caused in the brain parenchyma, with obvious edema in peripheral brain tissues (Fig. 23.12b–i).

4. *Essentials for diagnosis.*

(a) Allergic fungal rhinosinusitis usually occurs in young people with allergies. Diabetics, tumor patients, and other immunocompromised patients are at high risk of invasive fungal rhinosinusitis.

(b) CT non-enhanced scan: Allergic fungal rhinosinusitis is usually symmetrical bilaterally. There is a lesion with flocculent and heterogeneous density in the nasal cavity and groups of paranasal sinuses, with increased density in the center. The lesion is accompanied by characteristic imaging findings of polymorphic calcification or ground-glass opacity. Fungal balls generally appear as an irregular hyperdense shadow in the sinus ostium of maxillary sinus, with soft tissue shadow in the maxillary sinus, ethmoidal sinus, and frontal sinus.

(c) MR non-enhanced scan: The scan shows hypointense or isointense on T1WI, extremely hypointense on T2WI, without solid enhancement, and can show marginal mucosa enhancement.

(d) Noninvasive fungal rhinosinusitis is characterized by hyperostosis and hypertrophy of sinus wall or compressive resorption, which generally does not invade surrounding structures.

(e) Chronic invasive fulminant fungal rhinosinusitis and acute fulminant fungal rhinosinusitis have rapidly progressive bone erosion and destruction, and they

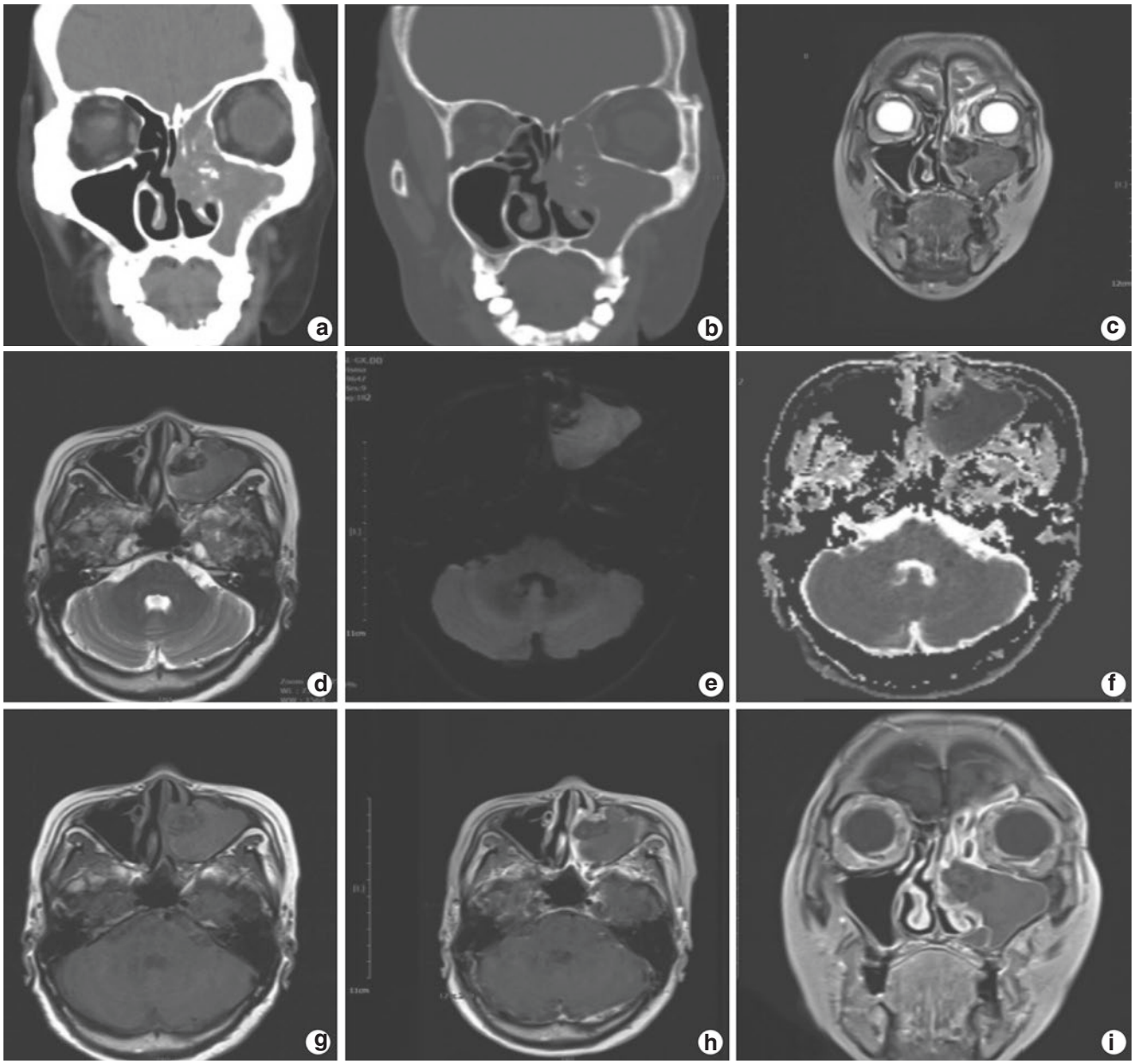

Fig. 23.8 Secondary mold ball of nasal polyps in the left maxillary sinus. A 78-year-old female patient. (**a** and **b**) Coronal CT shows the sinus cavities of left paranasal sinuses filled with high-density shadow, enlarged maxillary sinus, and lumpy calcified tissue around the ostiomeatal complex. (**c**, **d** and **g**) MRI non-enhanced scan shows contents in the maxillary sinus cavity presenting slightly hyperintense on T1WI and slightly hypointense on T2WI. (**e**) DWI shows the diffusion-limited lesion, with intensified DWI signal. (**f**) ADC image shows decreased ADC value, and irregularly extremely hypointense in sequences of sinus ostium area and calcification area. (**h** and **i**) Enhanced MRI scan shows no enhancement in the lesion in the left maxillary sinus cavity, and linear enhancement in peripheral mucosa. The obstructive rhinosinusitis in the left ethmoidal sinus and frontal sinus present marked enhancement

extensively invade the orbit, intracranial, pterygopalatine fossa and other adjacent structures.

23.1.2.4 Differential Diagnosis

1. *Chronic rhinosinusitis.* It has a high incidence and a long duration. It commonly shows mucosal thickening and dense concentrated secretion of multiple sinus cavities. Calcification is rare, and less than 3% of all cases have calcification or ossification. Calcification is often located around the lesion and punctate and linear calcification is found along the sinus wall, and the sinus wall has osteosclerosis.
2. *Inverting papilloma.* It is a benign nasal tumor common in elderly men, which originates from the lateral wall of nasal cavity. Irregular lobulated medium or slightly high-

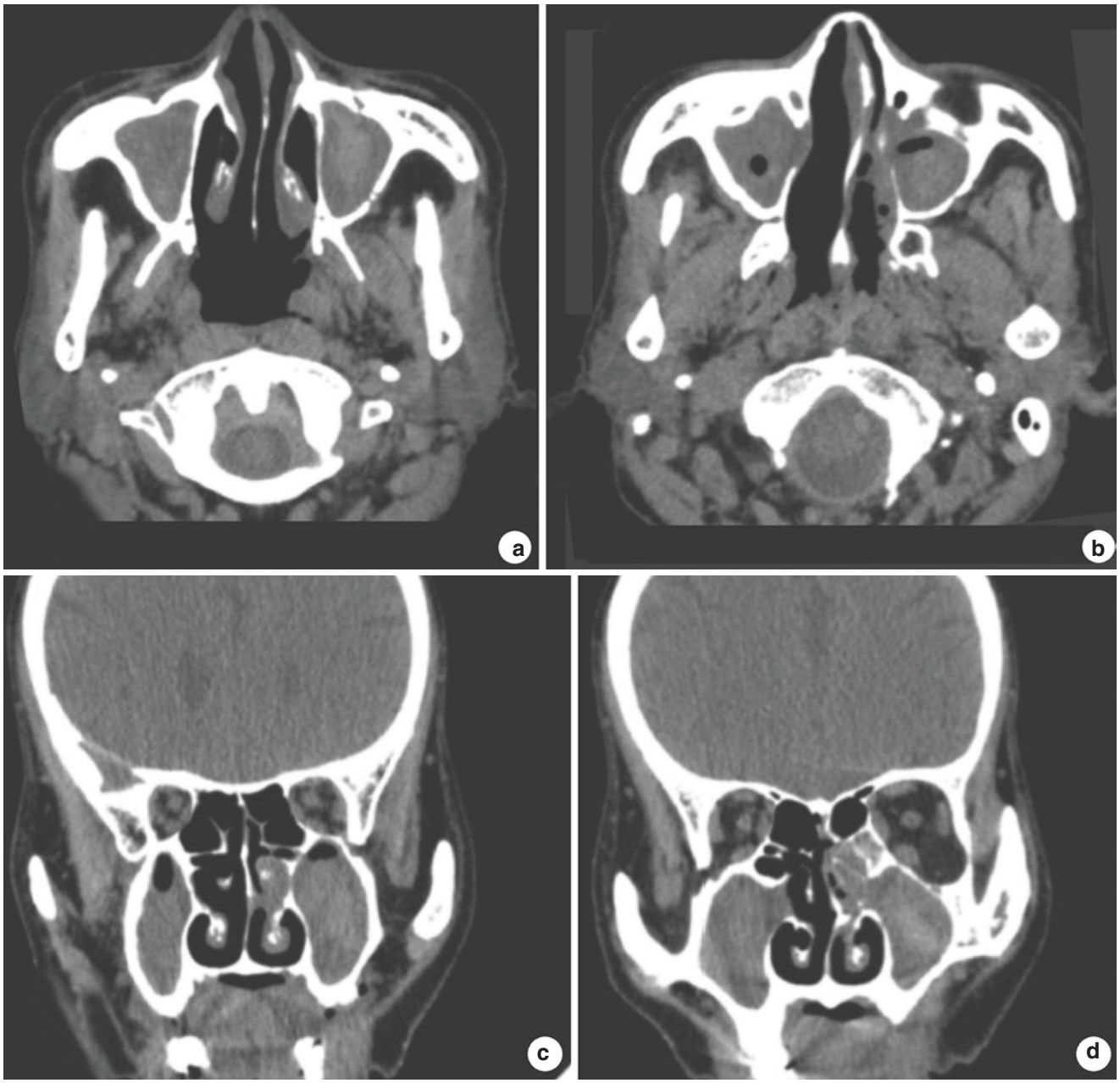

Fig. 23.9 Allergic fungal rhinosinusitis of bilateral maxillary sinuses. A 72-year-old male patient with nasal obstruction since over 10 days, intermittent nasal discharge and sneezing. The laboratory test shows a significant increase in eosinophils and fungal mixed infection. (**a**–**d**) Axial and coronal recombination images on CT non-enhanced scan show expansive deformation of bilateral maxillary sinus cavity, mildly dilated sinus ostium, inside mostly filled with solid soft tissue density shadow with flaky ground-glass opacity (mucin) in the center and surrounding low-density mucosa, and inapparent bone erosion of sinus wall (Images courtesy of Hao Zhiyong, Dongguan Shatian People's Hospital)

density masses are found in the middle nasal meatus of nasal cavity, with unsmooth surface and "bubble sign" inside. Calcification is found in about 10% of cases and invaginated bone fragments are found in 40%. The maxillary sinus shows isointense on T1WI and hyperintense on T2WI by MR. T2WI and enhanced T1WI show convoluted gyriform structures, which can extend to maxillary sinus, ethmoidal sinus, and nasopharyngeal part, causing local bone deformation, nasal septum deviation, bone resorption and destruction, and obstructive inflammation of unilateral nasal meatus of nasal cavity.

3. *Hemorrhagic necrotic nasal polyp.* The sinus cavity has heterogeneous density, with low-density inflammatory necrosis and high-density hemorrhage [3]. The enhanced

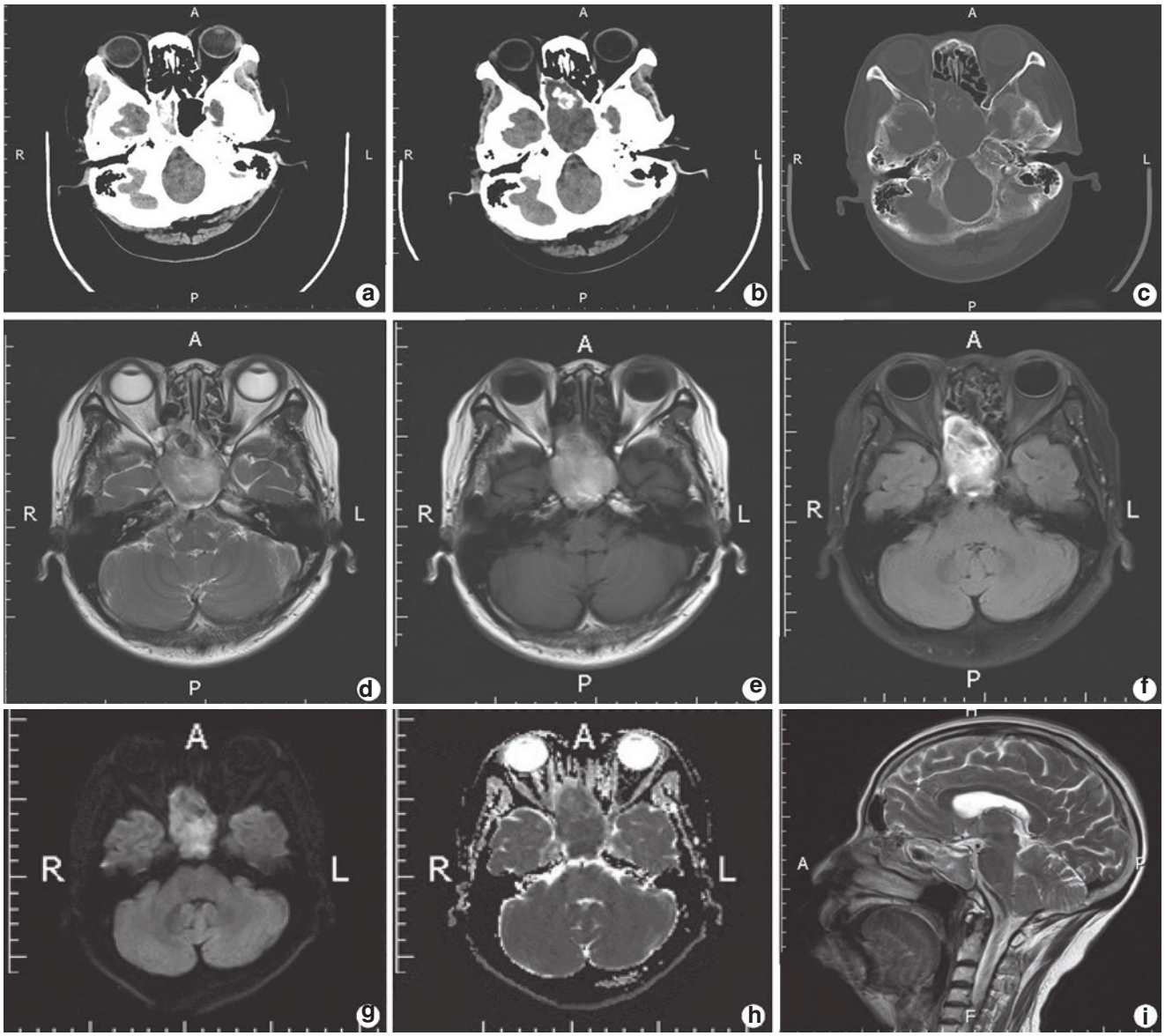

Fig. 23.10 Chronic invasive fungal rhinosinusitis of sphenoid sinus. A 70-year-old male patient. (**a**) The first CT non-enhanced scan of head and neck shows right sphenoiditis, with patchy calcification in the center. (**b** and **c**) In the CT reexamination after 5 years, the lesion progresses, and thick and big calcified plaques, dilated sphenoid sinus, and sinus wall thinned because of compressive resorption. (**d–i**) MRI non-enhanced scan shows heterogeneous signal mass in the sphenoid sinus cavity, increased T1WI signal, decreased and diffusion-limited T2WI signal, increased DWI signal, reduced ADC value, which suggests elevated protein content in the lesion. The hypointense calcification area in each sequence can be observed in the anterior center of the lesion

scan shows mild enhancement. The sinus cavity is enlarged and deformed, with local thinning due to bone resorption. It is difficult to differentiate hemorrhage from calcification using CT, while MRI has a high differentiation value. Calcification shows hypointense in each sequence, and hypointense of fungal rhinosinusitis is mostly located in the lesion center. Hemorrhage may show increased signal on T1WI, and most hemorrhagic necrotic nasal polyps show marginal hypointense ring on T2WI.

4. *Mucocele.* It is common in single nasal cavity, especially in the frontal sinus and sphenoid sinus. The sinus cavity expands and is filled with a large amount of mucus. Mucin content affects CT density and MRI signal of cyst [8]. The imaging findings are variable. Most lesions show hypodense or isodense shadow, with hypointense on T1WI and hyperintense on T2WI. When mucin content is high, the density increases, T2WI signal intensity decreases, and T1WI signal goes through a process from

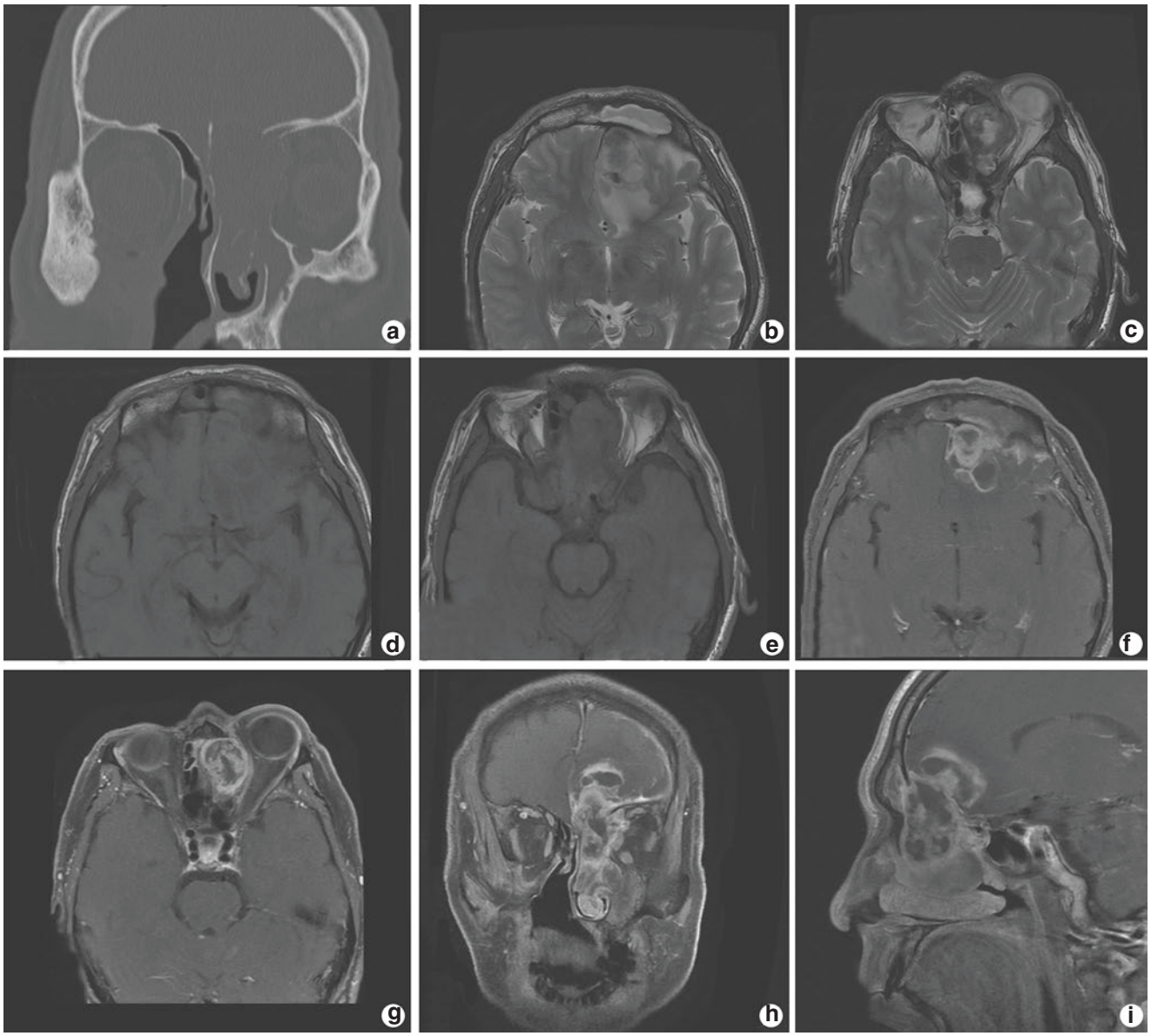

Fig. 23.11 Invasive aspergillus rhinosinusitis with encephalitis and brain abscess. A 37-year-old male patient. With fungal rhinosinusitis surgery over 10 years ago, nasal obstruction for the past 2 weeks, and convulsion after admission. (**a**) CT non-enhanced scan shows multiple postoperative bone defects in the right maxilla, right upper palatine bone, and partial turbinate of right nasal cavity. A soft tissue mass is noted in the left nasal cavity, which invades upwards the anterior cranial fossa and left orbital medial wall. The corresponding bone wall erosion and destruction form bone defects, without sclerotic margin. (**b**–**f**) MRI non-enhanced scan shows heterogeneous signals in soft tissue mass, with hypointense on T1WI and hyperintense T2WI in the center, and isointense on T1WI and hypointense on T2WI in the surrounding area. (**f**–**i**) MRI enhanced scan shows irregular lacery enhancement, intracranial abscess wall in heterogeneous thickness, local incompleteness, unremarkable enhancement of necrotic vomica in the center. The adjacent thickened meninges show linear enhancement. The left medial rectus is subject to compressive tortuous course

low to high and then to low. The sinus wall is thinned and displaced under compression.

5. *Nasal cavity melanoma.* The lesion is common in the elderly and presents multiple infiltrative growth. On CT, it appears as an irregular soft tissue mass, with deformation and destruction of peripheral bone. Melanin, hemorrhage, and free radicals can shorten the time of T1WI and T2WI [9], showing isointense or slightly hyperintense on T1WI, isointense or slightly hypointense to isointense on T2WI, and mild enhancement on enhanced scan.
6. *Epithelial malignant tumor.* Malignant tumor of nasal cavity or paranasal sinus is circumscribed and mostly

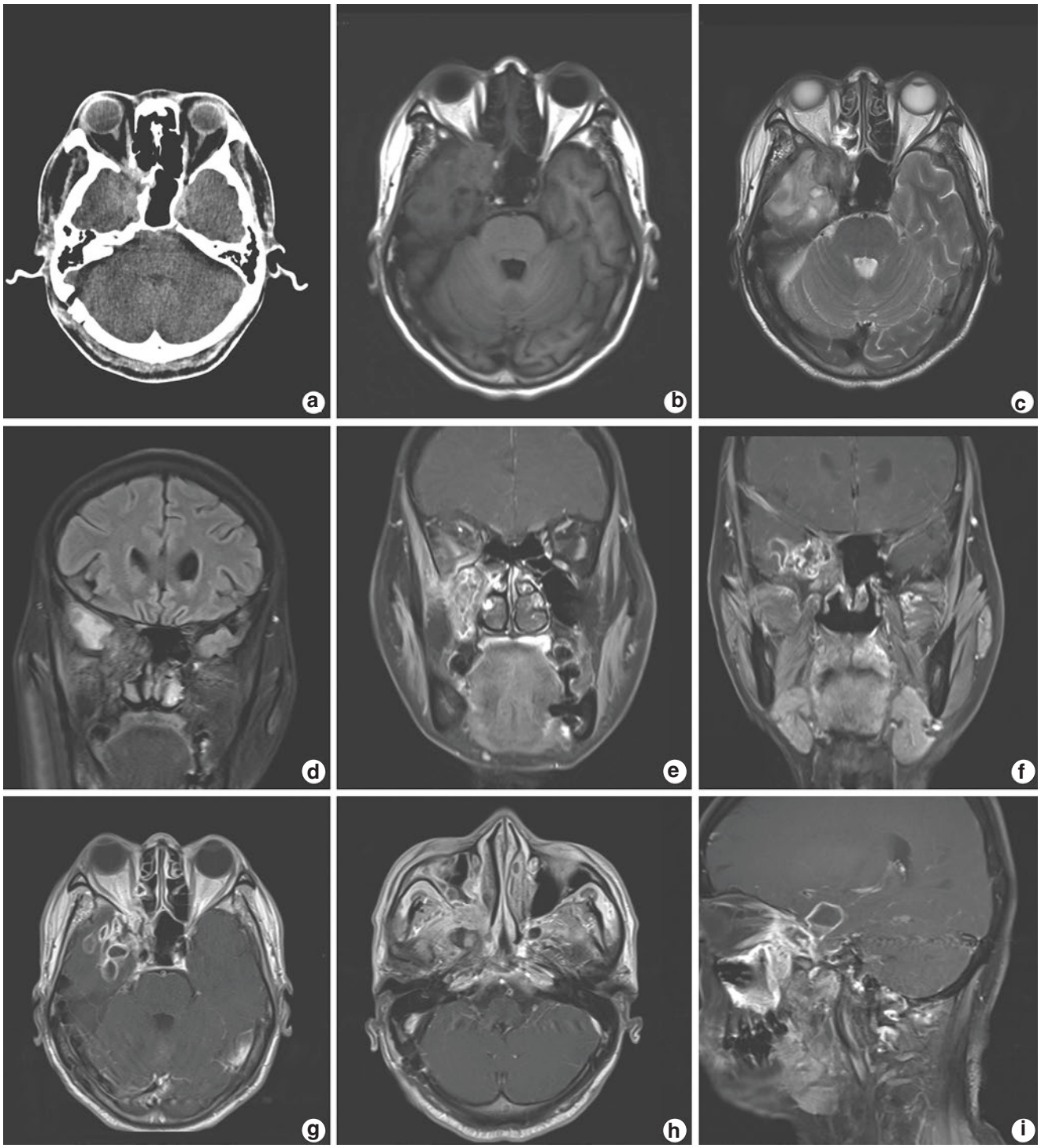

Fig. 23.12 Acute fulminant fungal rhinosinusitis - mucor encephalitis and brain abscess. A 52-year-old male patient with a history of type II diabetes, headache since over 5 months, blindness in right eye for the past 10 days, and recurrent fever. (**a**) CT non-enhanced scan shows widened cavernous sinus that is ill-defined, with increased density. (**b**–**d**) MRI non-enhanced scan shows heterogeneous signals in the lesion of skull base, with slightly hypointense on T1WI, and mainly hypointense in irregular shape on T2WI. The lesion invades the right cavernous sinus and orbital apex part, and extends along the pterygopalatine fossa space. The right maxillary sinus mucosa is heterogeneously thickened. Multiple thin-wall cystiform shadows can be noted in the right temporal lobe, surrounded by irregular edema region. (**e**–**i**) Enhanced MRI scan shows ring enhancement in the cyst wall of polycystic lesion of right temporal lobe, with homogeneous thickness of enhancement ring, and thickening and enhancement of adjacent meninges. The lesion in the right cavernous sinus, orbital apex, and pterygopalatine fossa shows cellular heterogeneous enhancement, with soft-tissue infiltration and rough and unclear contour. The right maxillary sinus and turbinate mucosae are thickened and enhanced (Images courtesy of Yu Shuilian, the People's Hospital of Guangxi Zhuang Autonomous Region)

occurs in the maxillary sinus and ethmoidal sinus. It is characterized by a short duration, rapid progression, strong invasion, irregular moth-eaten osteolytic destruction of sinus wall bone, mostly without sclerosis, soft tissue mass with heterogeneous medium- to high-density and irregular shape. It mostly shows isointense on MRI T1WI and T2WI, with obvious mass effect and significant invasion of peripheral tissues and structures. The enhanced scan shows heterogeneous marked enhancement in tumor. Compared with fulminant fungal rhinosinusitis, the lesion of maxillary sinus carcinoma is unilaterally located in a single sinus, which is limited in location with long course. With respect to the length of clinical duration of disease and the extent of bone destruction, the diseases are in descending order: chronic invasive fungal rhinosinusitis, sinus carcinoma, and acute fulminant fungal rhinosinusitis.

7. *Olfactory neuroblastoma.* It is manifested as a dumbbell-shaped soft tissue mass of which the center is located in the ethmoid bone. Calcification and hemorrhagic focus may be present in the center, with marked enhancement.
8. *Caseous rhinosinusitis.* It is obstructive chronic inflammation in unilateral nasal cavity and paranasal sinus. It is manifested as hypertrophy of nasal mucosa, thickening and sclerosis of paranasal sinus, and necrotic substances in the sinus cavity presenting heterogeneous consolidation tissue and with no enhancement on enhanced scan, compressive bone erosion in the sinus wall and nasal septum, with a clear margin.
9. *Rhinolith.* It is calcification in the nasal cavity caused by long-term calcium salt deposition centered on foreign matters, hemorrhage, and ectopic teeth.

23.1.2.5 Status Quo and Progress of Research

Routine CT non-enhanced scan shows pleomorphic calcification in the center of paranasal sinus and nasal cavity, definite diagnosis of a fungal ball can be made. For young people with allergic constitution, strip-like ground-glass opacity in the paranasal sinus cavity is combined with serological allergic reaction and increased eosinophil, with a high diagnostic accordance rate. If there is invasion outside the nose, MRI can be used as a supplementary examination method. Chronic invasive fungal rhinosinusitis tends to be misdiagnosed as malignant tumor. Acute progressive rhinosinusitis is characterized by rapid progression, extensive involvement, and high mortality, so the combination of CT and MRI examination is necessary, so that direct imaging diagnosis is provided for direct infiltration and destruction and saltatory intracranial invasion.

23.1.3 Pediatric Rhinosinusitis

23.1.3.1 Overview

Pediatric rhinosinusitis has a high clinical incidence, which is closely related to the physiological and developmental characteristics of children. Due to poor immunity and incomplete respiratory and immune function in children, respiratory infections and systemic diseases tend to cause nasal infections. As the mucosae of nasal cavity and paranasal sinuses are tender and blood vessels and lymph vessels are adequate, inflammatory stimulation easily contributes to congestion and edema. Local factors of rhinosinusitis include paranasal sinuses with hypoplasia or anatomical variations, sinus ostium of maxillary sinus in high location, and honeycomb structure of ethmoidal sinus. Nasal mucus inadequately drains and drips through the posterior nostril to the pharynx, which may lead to cough, nausea, and tinnitus in addition to general rhinosinusitis symptoms, such as nasal obstruction and nasal discharge.

Rhinosinusitis is divided into purulent, allergic, and specific types according to etiology. Allergic and specific rhinosinusitis rarely occurs. Purulent infection is more common, with clinically acute attack, and presents with fever, purulent mucus, poor nasal respiration, and cheek pain. The sources of infection may be seen in primary paranasal sinus infection, nasal cavity infection spreading, cross spread of paranasal sinuses, adjacent tissue involving in sinus cavity, hematogenous infection and sinus ostium blocked [10]. Bacteria tends to invade the maxillary sinus and periosteum and bone marrow of orbital bone, resulting in osteomyelitis, periostitis, subperiosteal abscess, and further spreads and causes intraorbital cellulitis, optic neuritis, otitis media, and meningoencephalitis. Pediatric rhinosinusitis is different from adult rhinosinusitis in respect of etiology and clinical features, so are its imaging characteristics.

23.1.3.2 Pathology Findings

Acute rhinosinusitis is characterized by nasal mucosal vasodilation, increased permeability, mucosal congestion and edema, epithelial swelling forming polypoid changes, slow ciliary movement, inflammatory cell infiltration in lamina propria, glandular hyperplasia causing increased serous or mucous secretions, ciliary columnar epithelia necrosis and exfoliation due to edema compression, exudate and bacteria mixed to form purulent secretions, stimulating periosteum and bone wall proliferation. In the chronic stage, epithelial cilia shed from mucosa of nasal cavity, lamina propria is thickened to cause localized bulge and polypoid hyperplasia, and the blocked glandular duct lead to cysts in the mucous gland.

23.1.3.3 Imaging Findings

1. *X-ray examination.* The application value of plain films of paranasal sinuses in children is limited due to incomplete development of their paranasal sinuses and poor pneumatization, poor display of site overlap and deep tissue, and poor cooperation of children. Mild cases only present with non-specific mucosal thickening, which may be homogeneous annular or heterogeneous wavy. With the aggravation of the disease, the permeability of the sinus cavity decreases gradually. In severe cases, the sinus cavity becomes turbid and the fluid level and other acute rhinosinusitis signs can be observed. Purulent infection may cause moth-eaten bone destruction of the sinus wall and present high-density osteonecrosis. If the sinus fistula is present, lipiodol radiography should be used.
2. *CT examination.*
   (a) Acute rhinosinusitis: The swelling and thickening of the nasal mucosa and hypertrophy of turbinates are seen. The consistent thickening of the sinus cavity mucosa along the sinus wall presents ring soft tissue density shadow [10, 11]. The effusion in the sinus cavity shows a consistent increase in density, and the air-fluid level can be seen in the sinus cavity, with a change in body position. The bone absorption and blurred contour of sinus wall are identified in rare cases. For patients with purulent rhinosinusitis, their sinus walls present irregular low-density osteoclasia, high-density sequestrum is formed in case of osteonecrosis, and subperiosteal abscess manifests as low-density stripy shadows adjacent to the bone wall, with possibly coarse margins. The cellulitis of peripheral soft tissue manifests as swelling of muscle and subcutaneous soft tissue with blurred spaces. The drainage fistula manifests as high-density shadow in soft tissue. The congested and thickened mucosa would show homogenous enhancement while the cellulitis of soft tissue shows heterogeneous reticular enhancement (see Figs. 23.13 and 23.14).
   (b) Chronic rhinosinusitis: In most cases, it manifests as annular isointense in a stripe pattern along the sinus wall [10], which would be homogeneous and smooth, heterogeneous or has nodular process, with possibly reactive bone thickening of the sinus wall.
   (c) Complications of rhinosinusitis: Nasal polyps manifest as multiple pedicled soft tissue shadows (in a quasi-circular or stripe pattern) along the sinus and nasal meatus, and enlargement of nasal cavity or paranasal sinus. Submucosal cyst manifests as broad-based, flat, moundy, or nodule-like prominence with smooth margins and surfaces, and has homogeneous density. Mucous cyst manifests as low-density shadows similar to that of water for casting in the sinus, and enlargement of the sinus with absorption and

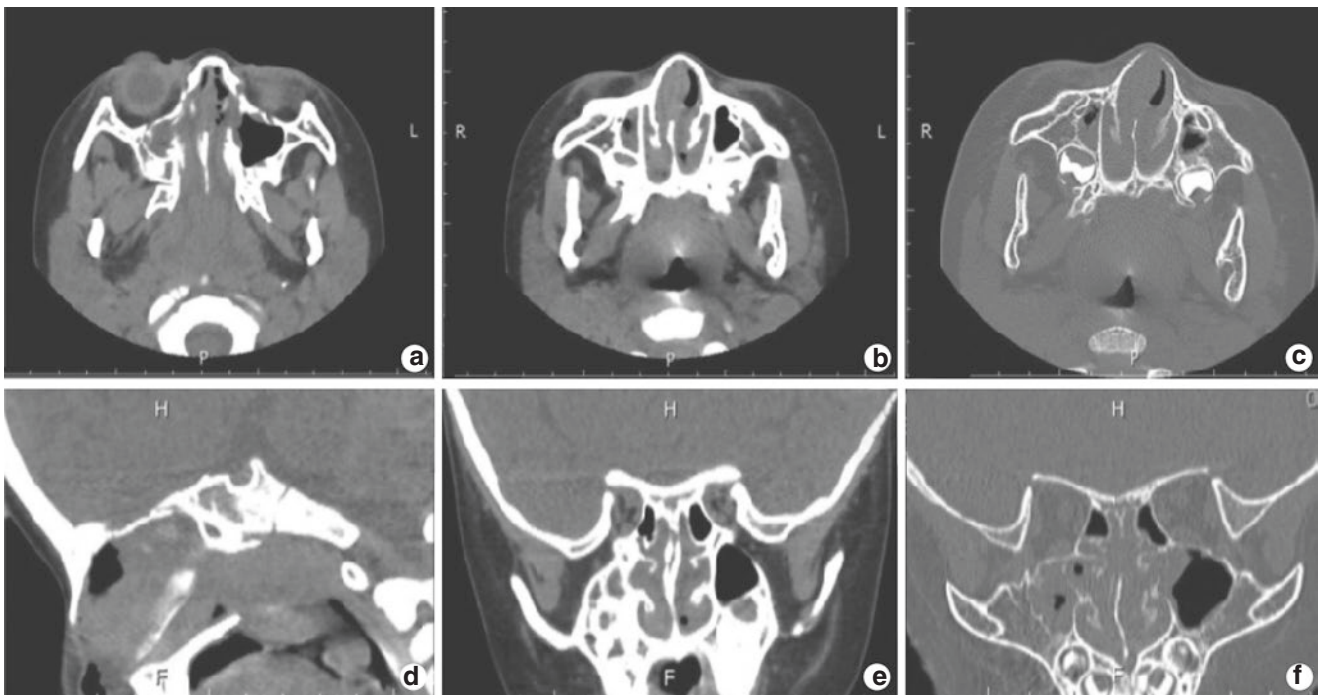

Fig. 23.13 Pediatric rhinosinusitis (1). A 2-year-old female patient. (**a**–**f**) CT shows that the frontal sinus is not pneumatized, and the air cavity of the remaining sinus is constricted, and the sinus wall shows annular mucosal thickening. The diffuse and significant thickening and edema of nasal mucosa are noticed from nasal vestibule to choana, and adenoid hypertrophy and airway stenosis are observed

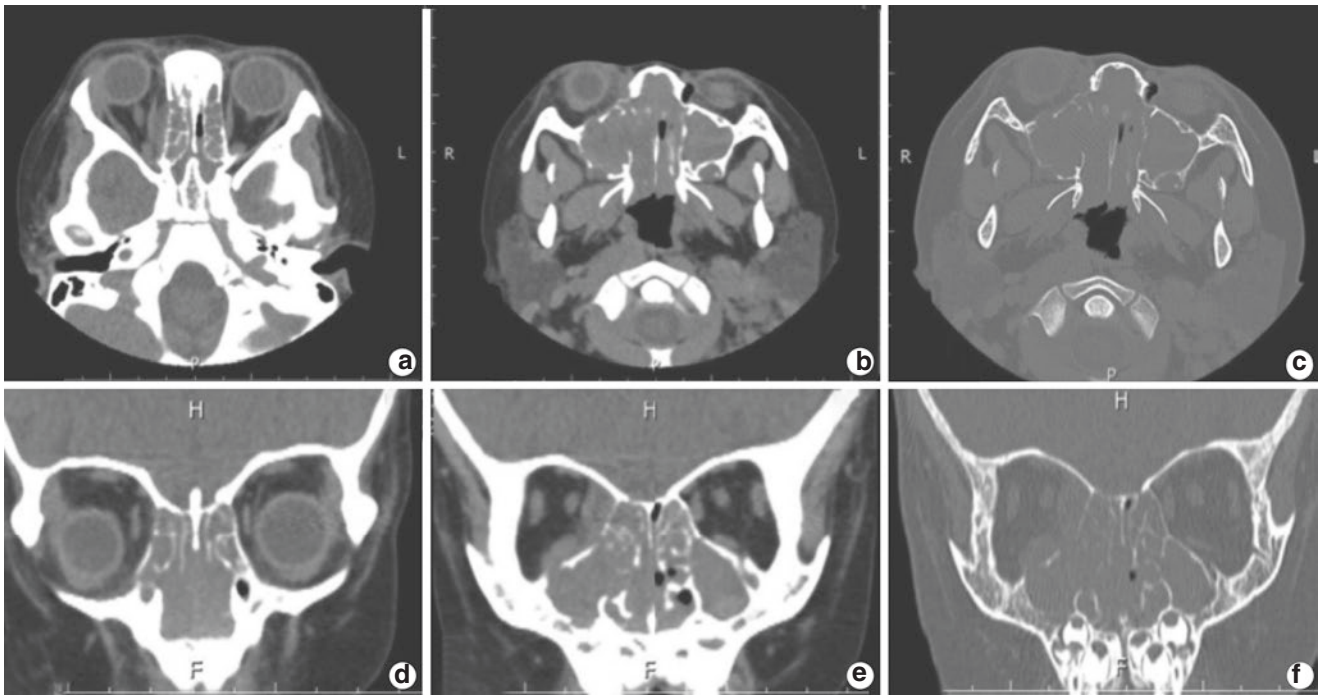

Fig. 23.14 Pediatric rhinosinusitis (2). A 3-year-old female patient. (**a**–**f**) CT shows diffuse swelling of bilateral ethmoidal sinus mucosa, bilateral maxillary sinus mucosa and nasal mucosa, the nasal cavity and paranasal sinus filled with soft tissue density shadows, and nasal meatus occlusion. Inflammatory lesions locally invade into the right orbit and form stripy subperiosteal abscess, and the corresponding medial and inferior walls are discontinuous in local areas

thinning of sinus wall. Adenoid hypertrophy: The transient physiological hypertrophy may occur in growing children, and repetitive inflammatory stimulation may cause pathological hyperplasia of adenoids, which manifests as thickening of soft tissue (exceeding 18 mm thick) of the posterior wall of nasopharynx, with nodule-like apophysis into the nasopharyngeal cavity and constricted choana (Figs. 23.13 and 23.14).

3. *MRI examination.* Magnetic resonance imaging (MRI) provides relatively high accuracy rates in differentiating and characterizing inflammatory tissues, such as mucosa with edema, polyp, retention fluid, and pus. Mucosal edema shows hypointense on T_1WI and hyperintense on T_2WI, and enhanced scan shows mucosal enhancement. Sinus effusion manifests as hypointense on T_1WI and hyperintense on T_2WI, and pus shows increased signal intensity on DWI. The signals of nasal polyp and submucosal cyst are similar to thickened mucosa; The mucous cyst signal intensity depends on viscosity, water content of tissue, and protein content [11]. Osteomyelitis manifests as increased signal intensity on T_2WI fat suppression for bone marrow of superior sinus wall, accompanied by lamellar periosteal reaction [1]. Pyogenic infection involves adjacent tissues, resulting in intraorbital cellulitis, meningitis, and otitis media. MRI shows hyperintense on T_2WI at lesions of corresponding tissues, and enhanced scan shows significant cellular enhancement (Fig. 23.15).

23.1.3.4 Key Points of Diagnosis

1. Patients suffer from nasal obstruction, nasal discharge and cough, and pyogenic infection with symptoms of acute infection, such as diffuse redness, swelling, fever, and pain in maxillofacial region.
2. CT shows sinus mucosal wall thickening with effusion in sinus and relatively low density of sinus contents. According to CT findings, chronic rhinosinusitis mainly manifests as mucosal thickening with relatively high content density, which is normally complicated with polypoid hyperplasia, submucosal cyst, and other signs.
3. Severe rhinosinusitis can cause bone absorption and blurring of sinus wall, moth-eaten bone destruction would be found in patients with pyogenic infection, and sequestrum would be formed in progressive stage, accompanied by laminated periostitis and subperiosteal abscess.
4. Laboratory test shows significantly increased leukocytes and erythrocyte sedimentation rate, and pathogens can be detected in spilled pus.

23.1.3.5 Differential Diagnosis

1. *Allergic rhinosinusitis.* Undulant mucosal thickening is common in polypoid hypertrophy, and can also be noticed

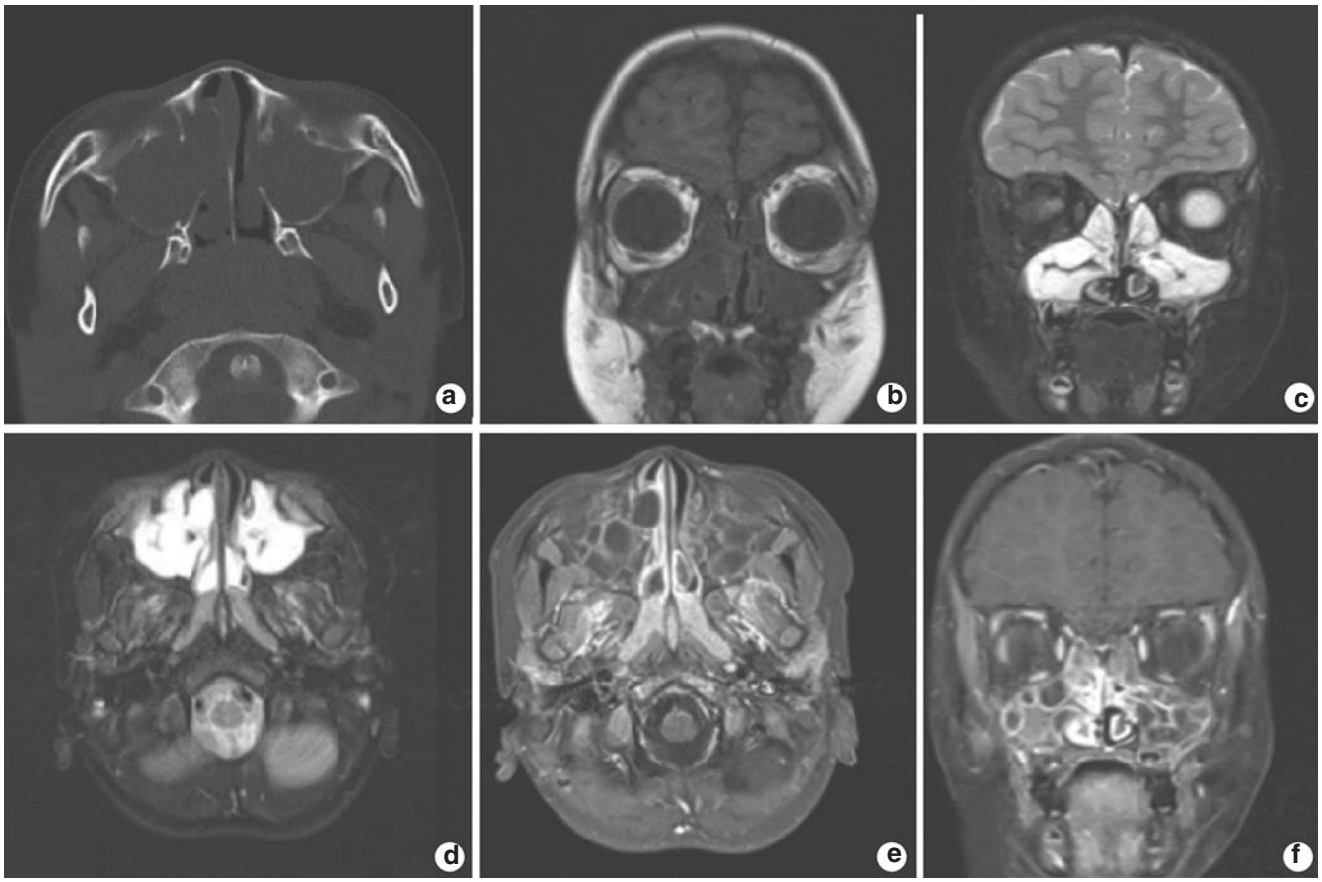

Fig. 23.15 Pediatric rhinosinusitis (3). A 5-year-old patient. (**a**) CT shows mucosal thickening of maxillary sinus and ethmoidal sinus filled with soft tissue density shadows, enlargement of sinus and thinning of sinus wall; (**b**–**d**) MRI re-examination shows annular significantly hyperintense on T_2WI at the thickened mucosa and hypointense on T_1WI at main body, with the strip-like slightly hyperintense signals noticed therein, which are considered to be protein component. (**e** and **f**) Enhanced MRI shows that the lesions manifest as multiple annular or septal enhancement, presenting cellular changes. In addition, the enlargement of inferior nasal concha and hypertrophy of posterior wall of nasopharynx are observed

in allergic rhinosinusitis [12]. It is difficult to differentiate between them if the undulant mucosal thickening occurs in both cases.

2. *Tonsillitis.* The pharyngeal lymphatic ring is enlarged, and the oropharyngeal cavity is constricted during acute stage.

23.1.3.6 Status Quo and Progress of Research

CT scan of the paranasal sinus is the most valuable and widely used method for diagnosing rhinosinusitis and identifying anatomical variations. The anatomical structures of nasal cavity and paranasal sinus are visually and clearly presented by multiplanar reformation imaging, thus indicating the location, shape, density, size, and scope of lesions, and accurately showing the erosion to surrounding bone substance and diffusion to adjacent structures, such as orbit and skull base. The determination of nature and degree of lesions according to imaging findings provides a reliable basis for diagnosis and is of great value for the selection of therapeutic approaches and prognosis evaluation. The prolonged and noisy scanning due to poor cooperation by children affects the implementation of MRI examination for paranasal sinus. For children with acute rhinosinusitis and diffusion in paranasal organs, MRI enhanced scan is capable of defining the infiltration scope and providing images to support the formulation of clinical therapy and evaluation of treatment effect.

23.2 Nasal Polyposis

23.2.1 Polyps in Nasal Cavity and Paranasal Sinus

23.2.1.1 Overview

Nasal polyposis is the most common chronic inflammatory edema disease of the nasal mucosa, which manifests as inflammatory edema and tissue proliferation of nasal mucosa caused by allergic reaction or chronic inflammation, resulting

in increased small mucosal vascular permeability and plasmexhidrosis. Under the chronical stimulation of purulent secretion, the thrombophlebitis and obstruction of lymphatic return occur in mucosa and result in extreme mucosal edema with submucosal liquid accumulation and formation of pedicled inflammatory mass [13]. There are multiple causes for the disease, which involve allergy theory, bacterial superantigen theory, middle nasal meatus microenvironment theory, eosinophilic inflammation, vasomotor rhinitis, and cystic fibrosis, and are also related to systemic diseases (e.g., aspirin intolerance) [14]. Nasal polyposis shows a significant tendency of postoperative recurrence.

Nasal polyps normally grow on the lateral wall of nasal cavity, especially the area posterior to the middle nasal meatus and adjacent to the sinus ostium. The nasal polyps may grow at maxillary sinus ostium, free margin of middle nasal concha, posterior end of inferior nasal concha, semilunar hiatus, olfactory cleft, uncinate process, and ethmoidal bulla. The nasal polyps may occur in nasal cavity or paranasal sinus or both, and bilateral nasal cavities are involved symmetrically in most cases. Polyps in paranasal sinus are less than those in nasal cavity and are relatively common in the ethmoidal sinus. Nasal polyps vary in size and form and deform with positions. The severely edematous nasal mucosa droops from the middle nasal meatus and paranasal sinus ostium to the nasal cavity, thus forming a pedicled long-stem polyp or broad-based polypoid lesion. When the paranasal sinus ostium is obstructed, the mucus retention in the sinus leads to expansion of the sinus, which belongs to a series of biochemical and immunological reactions caused by excessive protein content of the mucosal secretion.

Nasal polyps can be divided into three categories according to the etiology and pathogenic site.

1. *Allergic polyp.* It is noticed mainly in the inferior nasal concha and olfactory region in bilateral multiple manners.
2. *Inflammatory polyp*. It is formed unilaterally or singly. It is normally caused by local infection and is difficult to recur after resection.
3. *Choanal polyp*. It is common in young people. It is a solitary nasal polyp growing near the maxillary sinus ostium, extending backward from the anterior end of the middle nasal meatus into the choana and nasopharynx, and may protrude into the maxillary sinus in a dumbbell shape [15]. Similarly, choanal polyps in the sphenoid sinus can also protrude into the sphenoid sinus ostium.

23.2.1.2 Clinical Manifestation

It is related to the size and position of the polyp, and common symptoms include progressive nasal obstruction, headache, purulent nasal discharge caused by increased secretion, and dysosmia. Nasal polyps located in the nasal cavity cause persistent nasal obstruction. Huge nasal polyps can completely obstruct the nasal cavity and lead to complete obstruction, which results in closed rhinolalia. The external nose is subject to wide deformity and forms a "frog-shaped nose" [15]; The choanal obstruction caused by choanal polyps or huge nasal polyps results in snoring, and these polyps may protrude into the nasopharynx and obstruct the auditory tube, thus leading to tinnitus, hearing loss, and otitis media; The clinical symptoms caused by polyps localized in the sinus are mild ones.

23.2.1.3 Pathology Findings

These polyps can be histologically divided into edematous type, alveolar type, and fibrous type, wherein the edematous type is dominant.

1. *Visual findings.* The polyps are soft and edema-like loose tissues varied in size. They are sleek and shiny, gray or reddish (lychee-like) translucent substances, which are soft and not tender. They can move back and forth. They are not bleeding in most cases, but the hemorrhagically necrotic nasal polyps can bleed.
2. *Microscopical findings.* The degenerated pseudostratified ciliated epithelium adheres to the thickened mucosa surface, which is superior to the severely edematous and thickened stroma. The connective tissue space is obviously loose and enlarged [13]. Plenty of inflammatory tissue infiltration is observed, involving eosinophils, mastocytes, macrophages, plasma cells, and lymphocytes. The denervated glands decrease, and the secretion decreases due to the lack of effective mucosal glands. The vascular permeability increases, the blood supply is scarce, and some necrotic polyps are noticed.

23.2.1.4 Imaging Findings

1. *X-ray examination*. It shows no characteristic. There may be decreased transmittance of nasal cavity and paranasal sinus, enlarged middle nasal concha with blurred contour, the nasal cavity filled with soft tissue shadow protruding outward from middle nasal concha, constricted or disappeared nasal meatus, enlarged piriform aperture by compression, contralateral deviation of nasal septum, and osteoporosis of nasal cavity wall without destruction. Multiple spherically mural nodules are identified in the paranasal sinus, and the ipsilateral sinus manifests as obstructive inflammatory changes, such as turbidity and increased density. In the lateral view of paranasal sinus, the choanal polyp manifests as soft tissue masses with smooth and clear margins in the choana and nasopharynx.
2. *CT examination.* Solitary or multiple non-neoplastic hyperplasias of nasal mucosa with inflammatory swelling, manifesting as homogeneous low-density mass

shadows of unilateral or bilateral nasal cavities, ostiomeatal complex, ethmoidal sinus, and olfactory cleft. The typical manifestation is that the maxillary sinus mass connects with the masses in ipsilateral nasal meatus and nasal cavity with a narrow handle through the enlarged sinus ostium, and these masses are in irregular dumbbell shape [16]. If the lesion further extends backward to the choana and nasopharynx, and drops downward in a teardrop shape, the choanal polyps with pedicled and smooth margins will be formed. Most of them manifest as myxoid low-density shadows [15]; CT value is higher than that of water, but lower than that of muscle, which the disease may be complicated with hemorrhage. Simple edematous nasal polyp shows no enhancement or linear mild enhancement of mucosa; The inflammatory stimulation can lead to relatively significant enhancement of increased vascular permeability; Chronic hyperplastic polyps are inflammatory and show vascular proliferation, increased heterogeneity of density, and mild enhancement by enhanced scan. Simple nasal polyps can occur in any part of the sinus wall and are common in the inferior wall. When the sinus is filled with large polyps, the expansion of the sinus changes. The sinus ostium expands, the uncinate process becomes smaller due to absorption, the nasal concha and sinus wall are subject to compressive bone absorption, even localized bony defect, and polyp tissue can expand outward through the defect. Obstructive rhinosinusitis often occurs on the affected side. The maxillary sinus and ethmoidal sinus are subject to mucosal thickening accompanied by effusion, and mucous cyst is secondary to secretion accumulation. Soft tissue density shadows are observed around the sinus ostium (Figs. 23.16a, b, 23.17, 23.18, 23.19a and 23.20).

3. *MRI examination*. The simple nasal polyps manifest as mucosal edema, hypointense on T_1WI and hyperintense on T_2WI, which are similar to the signal intensity of water [16]. The signals of polyps in different periods (edema, adenoid, cystic degeneration, and fibrosis) mixed with inflammatory secretions can vary from hypointense to hyperintense. The T_1WI signal intensity increases with the mucinous protein, and the T_2WI signal intensity decreases in case of concentrated mucus macromolecules or chronic rhinosinusitis with fibrous tissue proliferation [3]. The enhanced scan indicates the polyps without enhancement and mucosa with annular and liner enhancement. Hemorrhagic necrotic nasal polyp is a special type of nasal polyp. Repeated bleeding causes heterogeneous signal, and hypointense rings formed by hemosiderosis are found around the polyp. Hypointense septa is found within the polyp, and patchy and nodular progressive and heterogeneous enhancement is found by enhanced scan (Figs. 23.16c to f, and 23.19b to i).

23.2.1.5 Key Points of Diagnosis

1. Repeated nasal obstruction, nasal discharge, and hyposmia for a long time.
2. CT indicates multiple mural soft tissue shadows in nasal cavities and paranasal sinuses, which are frequently noticed near the ostiomeatal complex, and subject to dumbbell-shaped connection through the enlarged ostium or nasal meatus, or protrude into the choana as a teardrop process, with an anterior part larger than the posterior part. Thinning of nasal sinus wall of nasal cavity due to compressive bone absorption.
3. Non-enhanced CT scan shows a density similar to that of water and smooth margins, no enhancement in most cases or marginal enhancement; compressive deviation and absorption of adjacent bone, with obstructive rhinosinusitis.
4. Non-enhanced MR scan indicates homogeneous intense in most cases, hypointense on T_1WI and hyperintense on T_2WI. The increased protein content can lead to hyperintense on T_1WI and decreased signal intensity on T_2WI. The increased fibrous hyperplasia can lead to decreased signal intensity on T_2WI. Hypointense on DWI.

23.2.1.6 Differential Diagnosis

1. *Hemorrhagic nasal polyposisosis.* It is mostly found in young people, and these patients often have a history of nosebleeds. Hemorrhagic nasal polyposis is a special type of nasal polyposis. The bleeding and necrotic polyps are intermixed. In case of bleeding polyps, it shows hyperintense on T_1WI, extremely hypointense on T_2WI in marginal zone, and progressive enhancement by the enhanced scan.
2. *Inverting papilloma.* It occurs mostly in middle-aged and elderly men, originates from the lateral wall of unilateral middle nasal meatus, and protrudes into nasal cavity. The papilloma with irregular surface is hard in texture and develops expansively. The surrounding bone substance is subject to compressive bone absorption. The papilloma easily spreads to the maxillary sinus and ethmoidal sinus and can invade adjacent bones. The papilloma rarely develops into the anterior nasal cavity and nasal vestibule, and its density indicated by CT scan is higher than that of nasal polyps. Punctate calcification is found in rare cases. MRI examination, T_2WI, and enhanced T_1WI show convoluted gyri form appearance.
3. *Fibroangioma*. It is common in male adolescents and originates from sphenopalatine foramen. The lesion center is often located in the choana area and pterygopalatine fossa of the nasopharynx, and rarely occurs in nasal cavity and paranasal sinus. The fibroangioma is large in size, expansively develops to the natural orifices and

fissures, and easily affects the orbit, paranasal sinus, and nasal cavity. Fibroangioma may compress and erode the surrounding bone substance to make it thinner or even lead to bone destruction, resulting in compressive deformation and antedisplacement of the posterior wall of maxillary sinus. Most fibroangiomas manifest as shadows with hyperintense and homogeneous density by CT scan, and the density extremely decreases in case of many fibrous components or necrotic tissues, which is easily confused with nasal polyps. However, high-density shadows with marked enhancement can also be noticed. MRI scan indicates hyperintense on T_2WI, and T_2WI and enhanced T_1WI show salt and pepper sign and thick vascular shadows. Nasal polyps show unremarkable enhancement or mild enhancement. It would be differentiated according to features of pathogenic site, marked enhancement, and easy bleeding.

4. *Allergic fungal rhinosinusitis.* It involves multiple nasal cavities and manifests as diffuse high-density shadows in the sinus, which is surrounded by mucosa with low-density shadows. The difference in protein content leads to varied signal intensities on T_1WI and hypointense on T_2WI. Most of the patients with the disease are young people with allergic histories.
5. *Wegener granulomatosis*. The nodular soft tissue mass is located on the midline of nasal cavity, complicated with destruction of nasal concha and nasal septum that forms a hollow.
6. *Nasal lymphoma*. The lesion with heterogeneous density often occurs in the anterior nasal cavity, and low-density

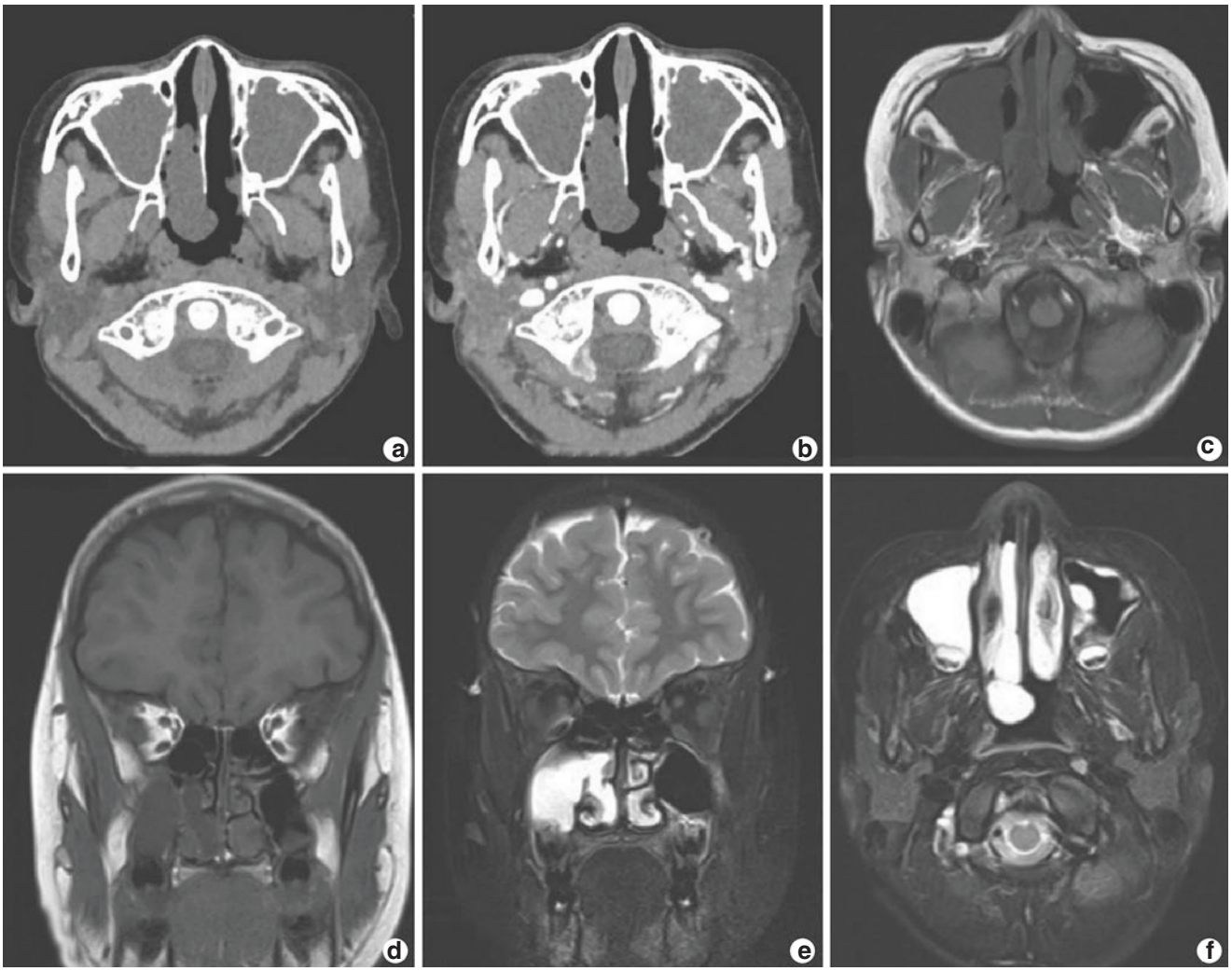

Fig. 23.16 Nasal polyps in bilateral maxillary sinuses and right nasal cavity. An 11-year-old male patient. (**a**) Non-enhanced CT scan indicates inflammatory polyps with homogeneous density shadows in bilateral maxillary sinuses, and the lesion in right maxillary sinus prolapses into the left nasal cavity and migrates to the choana; (**b**) The lesion has a smooth surface and homogeneous density, and unremarkable enhancement is presented by CT enhanced scan; (**c**–**f**) After 10 days of treatment, non-enhanced MRI scan indicates that the inflammatory lesion in the left maxillary sinus subsides and becomes smaller. The lesions in the right maxillary sinus and nasal cavity show significantly hypointense on T_1WI and hyperintense on T_2WI, indicating high water content that is consistent with the changes of edematous nasal polyp

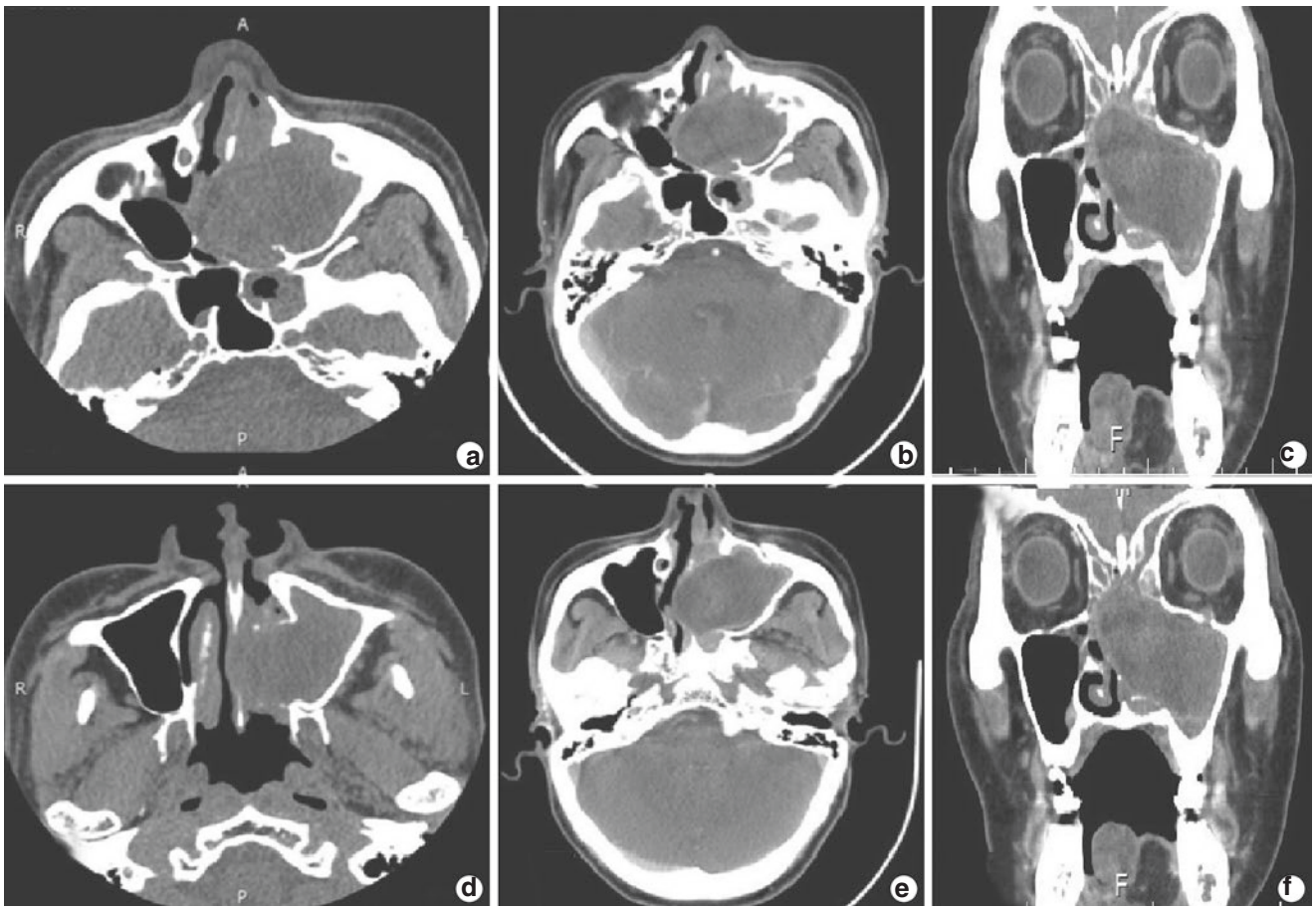

Fig. 23.17 Nasal polyp in left maxillary sinus with obstructive rhinosinusitis of ethmoidal sinus, sphenoid sinus and frontal sinus. A 70-year-old male patient. Pale pink neoplasm was found in the left nasal cavity, the surface of the neoplasm was smooth and tough, avoiding bleeding. (**a** and **d**) Non-enhanced CT scan indicates mucosal swelling of left maxillary sinus, ethmoidal sinus, frontal sinus, and sphenoid sinus. The sinus is filled with soft tissue density shadows, and spherical soft tissue mass with relatively high tension is found in the left maxillary sinus. The soft tissue mass protrudes into the left nasal cavity through the expanded maxillary sinus ostium, thus packing the left nasal cavity. The left maxillary sinus is enlarged, and the medial wall is subject to compressive bone absorption. (**b**, **c**, **e** and **f**) CT enhanced scan in arterial phase and venous phase shows progressive mild enhancement of the lesion center and annular moderate enhancement of the peripheral mucosa, especially in venous phase

shadows are often found due to necrotic tissues. There is no significant bone destruction in most cases. Large lesion usually involves bilateral ala nasi and soft tissue around the lymphoma. The lymphoma manifests as relatively homogeneous density and moderate enhancement.

7. *Nasopharyngeal carcinoma*. Its predilection site is pharyngeal recess, which manifests as thickened roof of lateral nasopharynx, occlusion of pharyngeal recess and narrow parapharyngeal space. The cervical lymph node of nasopharyngeal carcinoma has a high metastasis rate and moderate enhancement by enhanced scan.
8. *Maxillary sinus carcinoma*. Most patients are above middle age, and the disease has short duration and rapid progression. CT indicates infiltration growth of soft tissue masses in the nasal cavity and maxillary sinus, these masses manifest heterogeneous density, irregular shape, relatively marked enhancement, erosive bone destruction, and insignificant expansion of sinus. Isointense is dominant on MRI for the lesions, which are heterogeneous.
9. *Nasal meningoencephalocele*. It is mostly found in children and adolescents, with long duration and slow progression. There is a bony defect between the midline area of anterior cranial fossa, the nasal cavity, and the paranasal sinus. Some brain tissues protrude into the roof of nasal cavity or ethmoidal sinus through soft tissue fissures with the meninges or cerebrospinal fluid, and the density or signal of the herniated soft tissue mass equals that of the brain tissues, and the mass is surrounded by cerebrospinal fluid.
10. *Others*. Rare intracranial masses protruding into nasal cavity, such as chordoma, neuroblastoma, and pituitary adenoma.

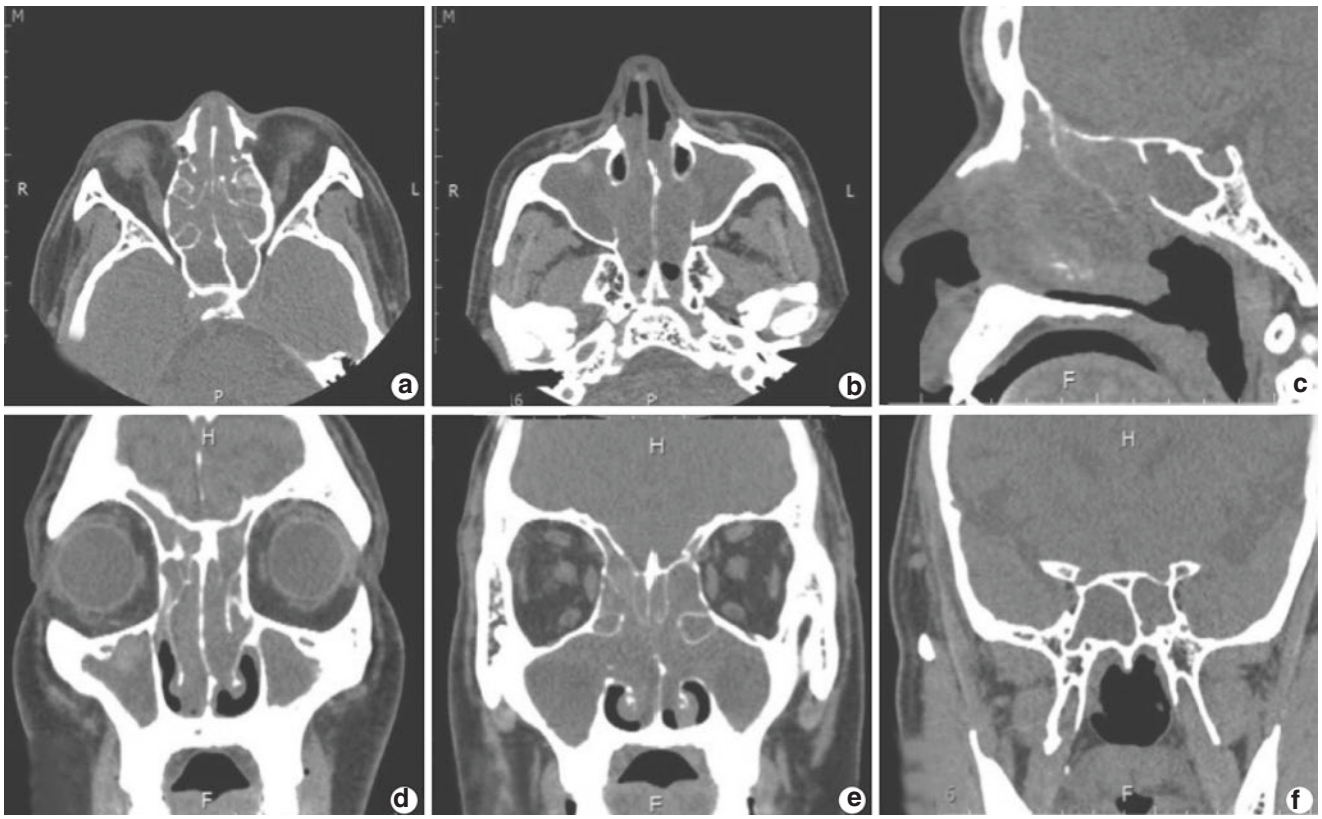

Fig. 23.18 Diffuse nasal polyps in nasal cavity and paranasal sinus. A 54-year-old male patient. (**a**–**f**) Axial, sagittal, and coronal non-enhanced CT scans show diffuse packing soft-tissue density of full set of paranasal sinuses, and local density of right maxillary sinus is slightly high. The middle and superior meatuses of the nasal cavity are occluded, only a few passages remained in the inferior meatus

23.2.1.7 Status Quo and Progress of Research

1. Edematous nasal polyps can be definitively diagnosed by conventional non-enhanced CT and MRI scans.
2. For nasal polyps with long duration, osteosclerosis is often found at the base of polyp due to inflammatory stimulation and vascular proliferation, and its pathogenesis is a research hotspot in recent years.
3. For polyposis involving compression and erosion of sinus wall, it manifests as invasive soft tissue masses by imaging and needs to differentiate neoplastic lesions. No increased intensity on DWI is noticed, and MRI enhanced scan shows complete and continuous mucosal linear enhancement.

23.2.2 Hemorrhagic Nasal Polyp

23.2.2.1 Overview

Hemorrhagic necrotic nasal polyp/angiomatous polyp/vasodilatory polyp is a special type of inflammatory nasal polyp, which features with hemorrhagic and necrotic lesions, and accounts for only 4% ~ 5% of all nasal polyps. It shows multiple unilateral lesions in maxillary sinus (87.1%) or nasal cavity (12.9%). The disease can occur at any age, but is most common in young people, showing no significant gender difference. There is no agreement on its name, but it is often named as hemorrhagic necrotic nasal polyp in China and angiomatous polyp or vasodilatory polyp at abroad.

The etiology is unknown, and it is generally believed that it may be associated with infection, allergic reaction, intramucosal hemorrhage, trauma, etc. (1) Allergic reaction: Due to the multiple reactions of nasal allergic reaction, in the presence of histamine, leukotriene and other chemical media, the small vascular permeability of nasal mucosa increases, and the plasmexhidrosis increases, resulting in extreme increase of nasal mucosa edema, which gradually droops by gravity and leads to the formation of hemorrhagic nasal polyp. (2) Chronic inflammation: Chronical stimulation by chronic rhinitis, rhinosinusitis, and suppurative secretion causes thrombophlebitis of nasal mucosa and lymphatic return disorder, leading to nasal mucosa edema and gradually forming hemorrhagic nasal polyp. In recent years, nasal polyp is found to be closely associated with aspirin intolerance. Aspirin-intolerant patients are predisposed to nasal polyp and bronchial asthma and are generally considered to be the result of using non-steroidal anti-inflammatory drugs (e.g., aspirin), which interfere with arachidonic acid metabolism. (3) Hemangioma: Blood supply disorder of hemangioma causes hemorrhage, necrosis, organization, and

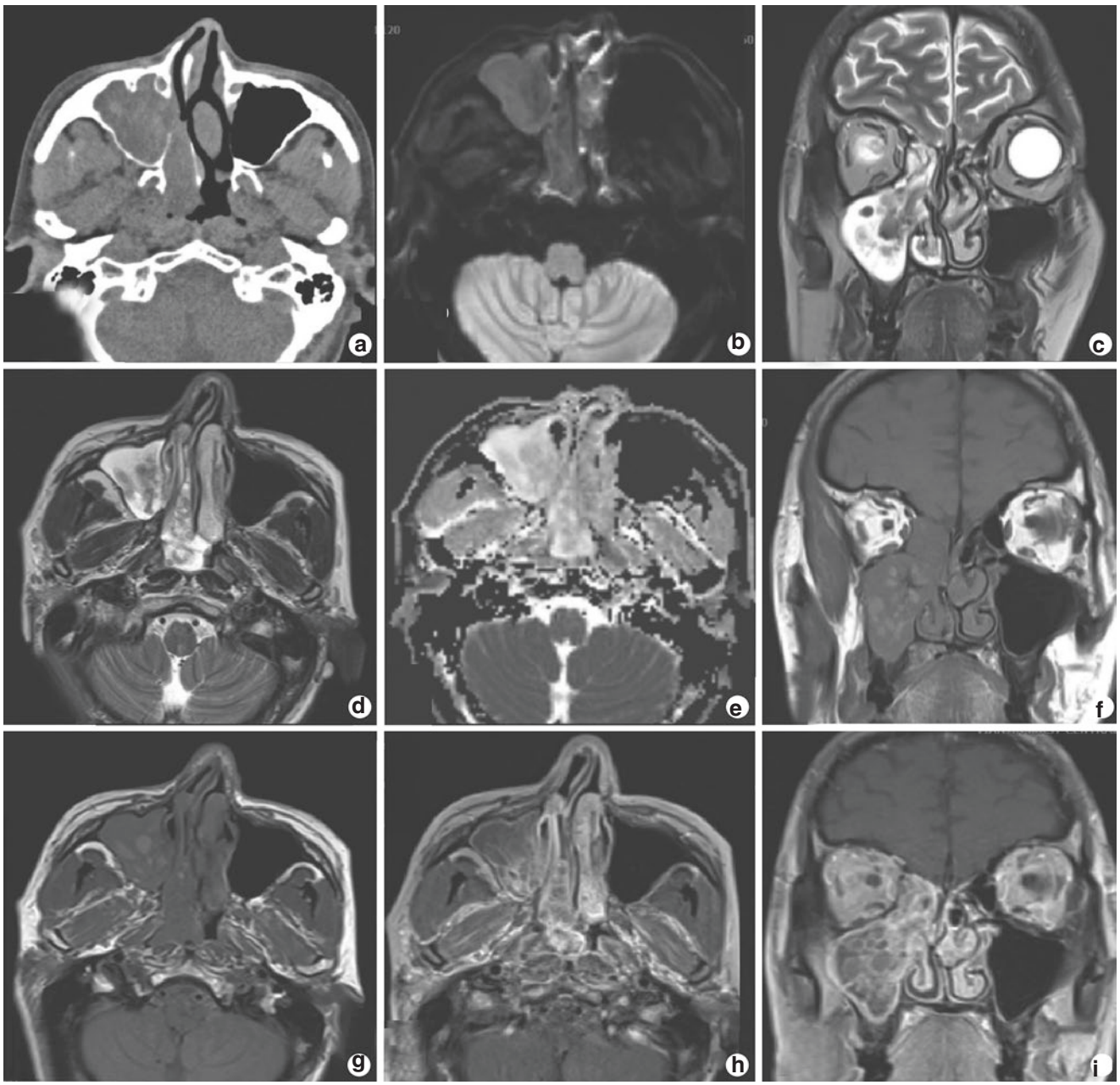

Fig. 23.19 Secondary infection of polyps in nasal cavity and paranasal sinus. A 61-year-old male patient. The patient suffered from intermittent nasal obstruction and nasal discharge for half a year, which aggravated in the last month. (**a**) Non-enhanced CT scan indicates dumbbell-shaped soft tissue mass in the right maxillary sinus and nasal cavity, and scattered, mottled and slightly high-density areas in the center; (**b**–**g**) Non-enhanced MRI scan shows heterogeneous signal (hyperintense and hypointense), multiple patchy hyperintense areas on T_1WI and hypointense areas on T_2WI, hypointense on DWI, and slightly decreased ADC value in central area. (**h**–**i**) MRI enhanced scan indicates lace-like and cellular enhancement of the lesion. Polypoid mass with translucent and lychee-like surface is found in the right maxillary sinus during the operation

obstruction of the sinus ostium, causing inflammation or edema and secondary polyps [17].

Pathogenesis: The hemangioma derives from nasal polyp in maxillary sinus and grows to nasal cavity and choana through the narrow maxillary ostium. The compression and occlusion of nourishing vessels are easily caused by obstruction of sinus ostium, pedicle torsion or external compression, thus leading to vascular stasis and angiectasis, and further leading to edema, infarction, hemorrhage, neovascularization, and other changes. This process is repeated, and the final result depends on the pathological period of patients undergoing the operation.

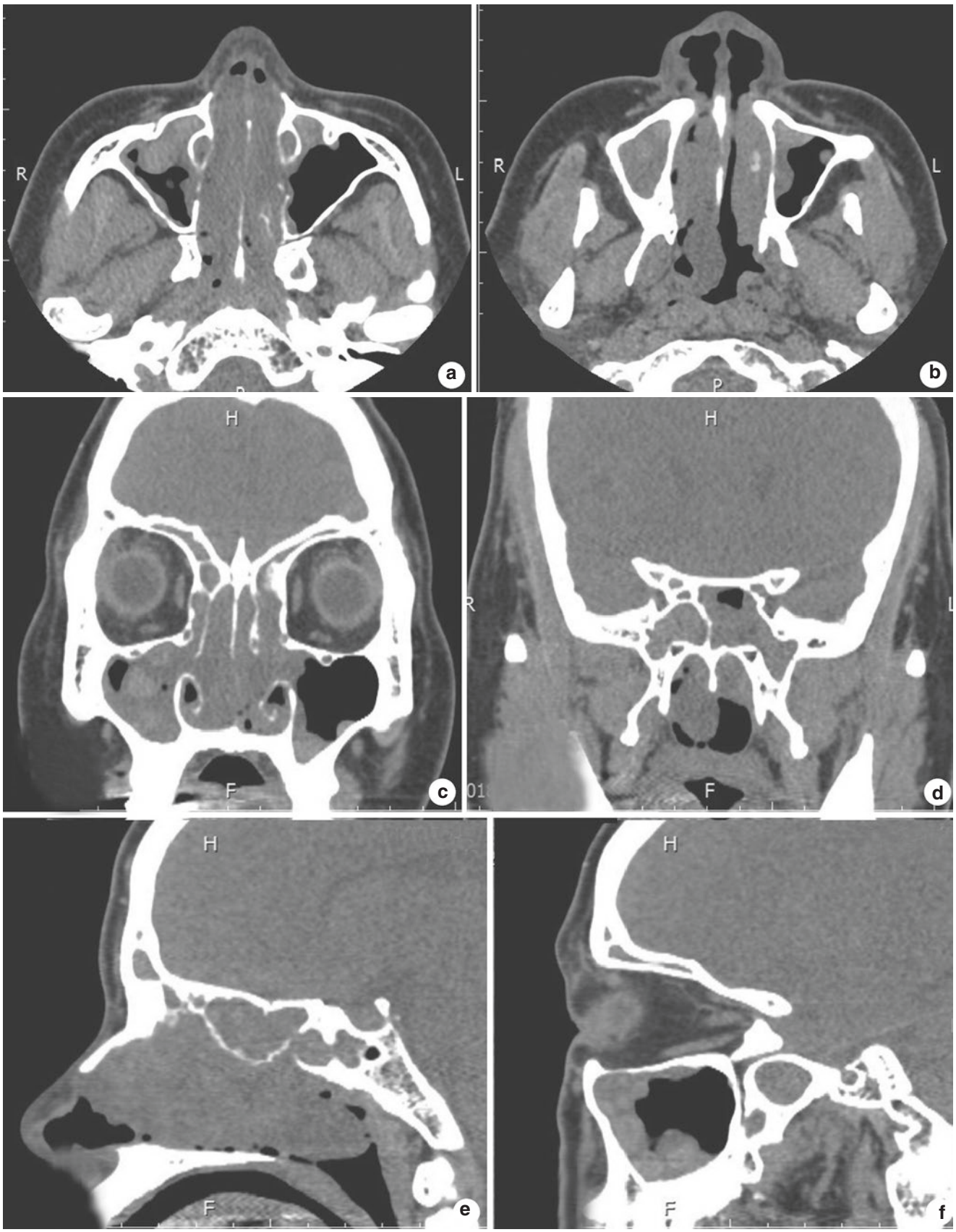

Fig. 23.20 Polyps in nasal cavity and paranasal sinus. A 49-year-old female patient. (**a**–**f**) The multiplanar reformation by axial, coronal and sagittal non-enhanced CT scans shows hypertrophy and edema of bilateral nasal concha, poor nasal cavity ventilation, and prolapsed polyp in the right choana area. The mucosa of full-set paranasal sinus is heterogeneously thickened, with irregular and corrugated surface, and nodular and spherical soft tissue protrusions and relatively high density in local areas. Enlargement and remodeling of nasal cavity

23.2.2.2 Pathology Findings

Polyps have abundant blood vessels, complicated with necrosis and hemorrhage. Plenty of irregular dark red, bright yellowish-brown blood clots are observed. Some sections are firm and others are brittle. There is more chronic inflammatory cell infiltration found in stroma. Fibrin thrombus is scattered in blood vessels, and most lesions are covered by patchy metaplastic squamous epithelium. Most lesions show irregular thin-walled vessels with scattered fibrin thrombosis. Cavernous vascular aggregation area intersects with the non-vascular area. Plenty of hemosiderin-containing macrophages are scattered in the lesions, complicated with recent hemorrhage in a patchy pattern. The lesion shows fibrinoid necrosis and a few typical inflammatory polyps. The histological performance determines the imaging diversity of the lesion in density or signal.

23.2.2.3 Imaging Findings

1. *CT examination.* It indicates enlargement of the maxillary sinus and/or nasal cavity, which are filled with soft tissue masses having heterogeneous density. High-density shadows are found at the margin and inside of the lesions at an average of 54 (±8) HU, indicating macrophages, fibrous components, and proteins that swallow plenty of hemosiderin, and the characteristics of hemorrhagic necrotic nasal polyps include some lesions with recent hemorrhage [3]. The low-density areas indicate polyps, hemorrhage, necrosis, and infection. Organization of calcified hematoma is found in some masses (calcium deposition often manifests as calcification after necrosis of pathological tissues). The enhanced scan shows nodular enhancement or patchy (cotton-wool) enhancement [3]. The maxillary sinus wall is subject to compressive bone absorption, and some areas occur moth-eaten bone destruction (inflammation stimulates activity of osteoclasts), especially the medial wall of maxillary sinus, which may be associated with the thin medial wall of maxillary sinus and the maxillary sinus ostium prone to the disease. Generally, it will not invade the peripheral soft tissues and pterygopalatine fossa. The disease is often complicated with edematous nasal polyps (Figs. 23.21a, 23.22 and 23.23a).
2. *MRI examination*. Heterogeneous signal of overall lesions is noticed, with a certain specificity. However, most of the lesions are made of vascular proliferation and angiectasis, thus indicating dominant hypointense on T_1WI and dominant hyperintense on T_2WI. Small patchy hyperintense on T_1WI (suggesting subacute/chronic hemorrhage or cystic cavity full of protein) is found in the lesion, with hyperintense on T_2WI in the center (polyp, hemorrhage, necrosis, and cystic degeneration). Irregular hypointense ring around the lesion and internal linear hypointense septa are found, which correspond to repeated hemorrhage, fibrosis, and hemosiderosis at different stages of the lesion (Figs. 23.21b–g, 23.23b–d and 23.24a–c).

By enhanced scan, the vascular proliferation and angiectasis areas are enhanced heterogeneously in varied forms, mainly manifesting as multiple patchy and nodular filling enhancement. The enhancement is heterogeneous. The TIC curve by dynamically enhanced scan shows a continuous upward trend, indicating progressive enhancement characteristics [17]. The progressive enhancement of heterogeneous filling indicates that the lesion is mainly made of vascular proliferation and angiectasis and fibrous components. The vascular components are enhanced and partially confluent,

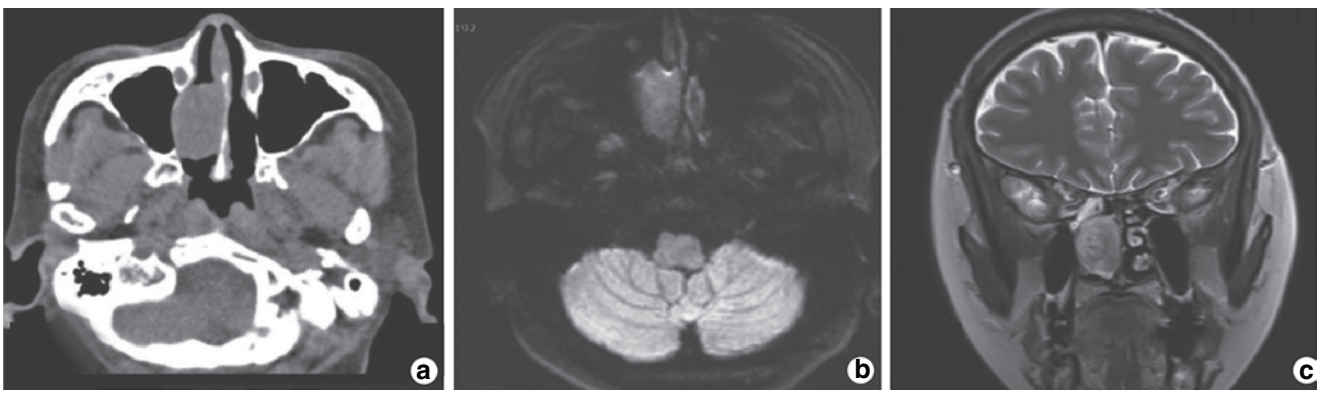

Fig. 23.21 Hemorrhagic necrotic nasal polyps in the right middle nasal meatus. A 56-year-old female patient Intermittent nasal obstruction of the right nasal cavity, with minor hemorrhage. (**a**) Non-enhanced CT scan indicates density shadows of oval-shaped nodular soft tissue in the middle nasal meatus of the right nasal cavity, and the medial wall of the right maxillary sinus is slightly compressed; (**b**–**g**) By non-enhanced CT scan, the nodules show isointense on T_1WI, with small punctate and patchy slightly hyperintense at the margin. The heterogeneous signal (hyperintense and hypointense) on T_2WI is indicated, with multiple stripy hypointense shadows within nodules and curved hypointense ring at the margin. Diffusion is not clearly limited, with isointenses on DWI and ADC. (**h** and **i**) MRI enhanced scan shows progressively marked enhancement of lesion, with curved low enhancement area at the margin

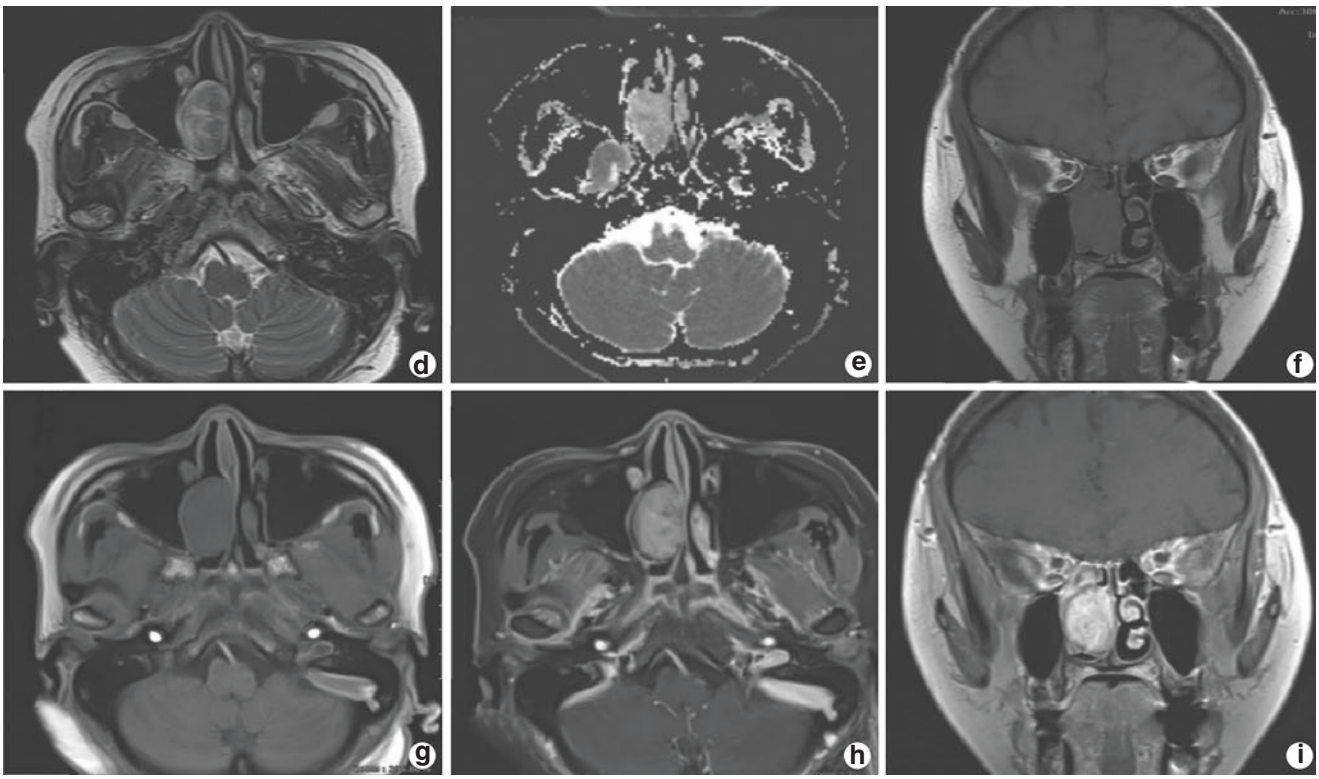

Fig. 23.21 (continued)

and the fibrous components are not enhanced, thus showing a "cauliflower-like" appearance [17]; By enhanced scan, the lesion shows unremarkable enhancement in central area and irregular enhancement on the periphery as the central area of the lesion is prone to hemodynamic disturbance, causing thrombosis in blood vessels and leading to hemorrhage and necrosis; however, cavernous vascular proliferation and angiectasis are significant due to inflammatory cell infiltration of peripheral tissues, which can manifest as marked enhancement; The annular remote hemorrhage area with hypointense on T_2WI is not enhanced (Figs. 23.21h, i, 23.23e, f, and 23.24d–f).

23.2.2.4 Key Points of Diagnosis

1. The disease is common in young adults. The soft tissue masses in maxillary sinus ostium- nasal cavity expansively grow, and the bone is absorbed by compression, resulting in localized bone discontinuity. The medial wall of maxillary sinus is the most vulnerable area.
2. CT indicates soft tissue mass of heterogeneous density, and intervally distributed high-density hemorrhage and low-density necrosis.
3. MRI indicates heterogeneous signal on T_2WI, heterogeneous hyperintense in lesion, which is surrounded by linear hypointense and internal hypointense septa.
4. Dynamical enhanced scan shows nodular and patchy "progressive filling enhancement," which is a critical characteristic that definitely suggests the hemorrhagic necrotic polyp, and no enhancement is in the hypointense area on T_2WI.
5. The disease can be complicated with edematous nasal polyp.

23.2.2.5 Differential Diagnosis

1. *Edematous nasal polyps*. These polyps are developed bilaterally in most cases, especially in ethmoidal sinus and maxillary sinus ostium. They grow from the nasal cavity or paranasal sinus to the choana, and most of them are pedicled with smooth margins and homogeneous texture. CT indicates low-density shadow similar to that of water (CT value is about 40HU), MRI shows isointense or hypointense on T_1WI and hyperintense on T_2WI, enhanced scan shows no enhancement or annular mild linear enhancement, and the surrounding bone substance has no significant expansive change.
2. *Inverting papilloma*. It is common in middle-aged and elderly men (40–50 years old). It is a unilateral disease originating from the free margin of middle nasal concha, occurring mostly in the lateral wall of nasal cavity and growing to the nasal cavity, with cauliflower-like or lobulated surface. Soft tissue mass is isointense or hypointense by CT, with homogeneous density and calcification. The mass manifests as slightly hypointense on T_1WI and heterogeneous signal (hyperintense and hypointense) on

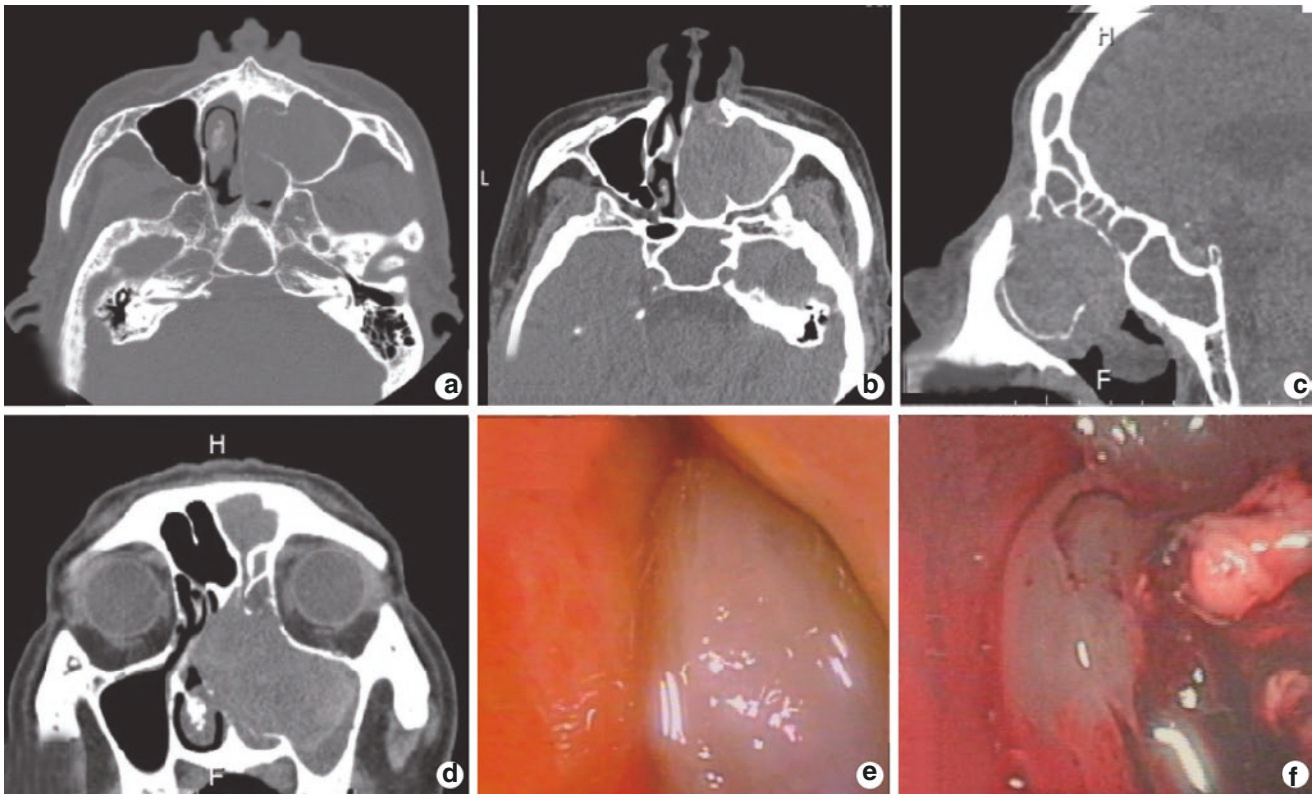

Fig. 23.22 Hemorrhagic necrotic nasal polyps in left maxillary sinus and left nasal cavity. A 64-year-old male patient. The patient suffered repeated nasal obstruction for more than half a year, which developed to intermittent hemorrhage of nasal cavity recently. (**a**–**d**) Axial, sagittal, and coronal non-enhanced CT scan shows that the left maxillary sinus is enlarged and full of soft tissue density shadows, with high-density in the central area. The lesion protrudes to the left nasal cavity through the enlarged maxillary sinus ostium, the left nasal meatus is packed, and the lesion reaches the nasal vestibule. Long pedicle-like low-density shadows drooped into the choana are noticed in the posterior inferior position. The lesion involves the left paranasal sinus, and obstructive inflammatory tissues of slightly low density are noticed in the peripheral area. Axial bone window shows compressive bone absorption of maxillary sinus wall, deviation of medial wall to nasal cavity and local discontinuity. (**e** and **f**) Endoscopy shows smooth and lychee-like surface of the mass, necrotic tissue in some areas of the mass, with bloody secretions in mucus

T_2WI. The enhanced scan indicates heterogeneous enhancement in the form of convoluted gyriform or palisade. There is no significant osteosclerosis and deviation of sinus wall or expansive change, sinus is not significantly enlarged, surrounding bone substance is compressed, absorbed and thinned and easily complicated with enlargement of paranasal sinus ostium. Irregular medium density mass is found on the lateral wall of nasal cavity and nasal concha, the nasal septum is subject to compressive deviation, and the lateral wall of nasal cavity is subject to bone absorption and destruction.

3. *Fungal rhinosinusitis-associated calcium pyrophosphate dehydrate deposition disease.* It is common in diabetic and tumor patients and mostly found in unilateral maxillary sinus and sphenoid sinus. Irregular mass soft tissue shadows are found in nasal cavity or paranasal sinus. CT shows heterogeneous (isointense or slightly hyperintense) density, with spot-like and patchy calcification or high-density shadows of linear septa. Hyperostosis and osteosclerosis of sinus wall are obvious. MRI shows isodense or slightly hyperintense on T_1WI and punctate and patchy hypointense on T_2WI. By enhanced scan, the lesion is not enhanced, and the peripheral mucosa is thickened and enhanced. The surrounding bone substance is absorbed by compression, but bone destruction is rare, while the hyperostosis and osteosclerosis of sinus wall are obvious. The expansion of sinus and bone destruction are rare. Invasive rhinosinusitis is often complicated with bone destruction and easily misdiagnosed as a malignant tumor.
4. *Nasopharyngeal angiofibroma*. It occurs frequently in male adolescents aged between 10 and 25 years, and repeated massive bleeding is the first clinical symptom. The disease originates from periphery of the sphenopalatine foramen, the posterior wall of the nasopharyngeal roof is a soft tissue mass with clear margin as well as smooth and sharp outer border. As the mass has invasive growth characteristics, the surrounding bone substance is

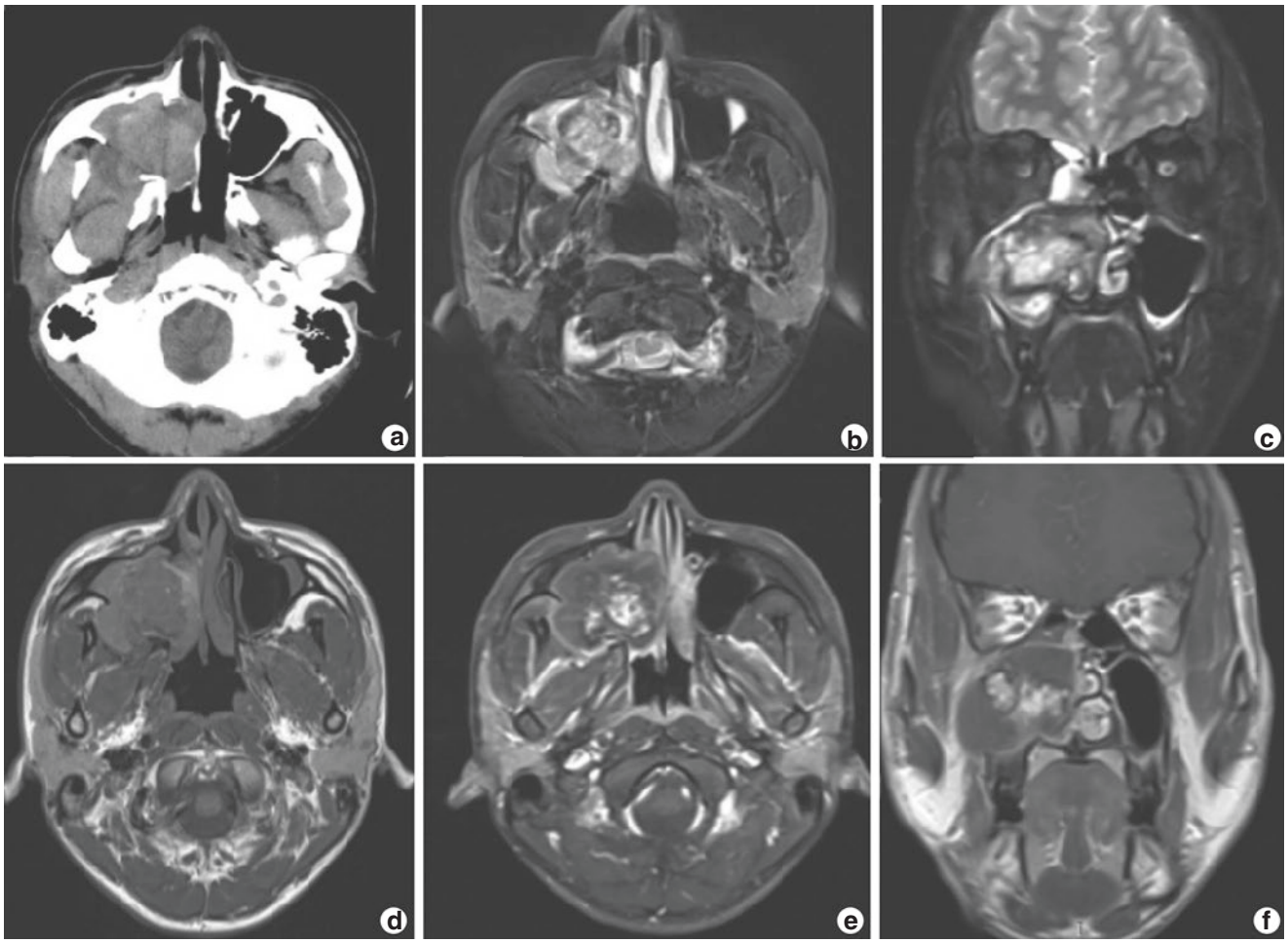

Fig. 23.23 Hemorrhagic necrotic nasal polyp in right maxillary sinus. A 20-year-old male patient. (**a**) Non-enhanced CT scan indicates the right maxillary sinus filled with patchy heterogeneous soft tissue density shadows, and patchy areas of higher density in the center, the lesion expands into the right nasal meatus with clear boundary, the bone absorption and destruction to different extents on the maxillary sinus annular wall, and localized bone discontinuity; (**b**–**d**) Non-enhanced MR scan indicates that space-occupying lesion of the right maxillary sinus breaks through the maxillary sinus wall and invades the pterygopalatine fossa in lateral posterior direction; slightly hypointense on T_1WI at main body of the lesion; and small patchy hyperintense on T_1WI at the margin; and heterogeneous signal (hyperintense and hypointense) on T_2WI, with hyperintense in the center, irregular hypointense ring around the lesion and internal linear hypointense septa, suggesting hemosiderin deposition. (**e**–**f**) Enhanced scan shows irregular patchy and nodular filling enhancement (Images courtesy of Hu Junhua, Jingdezhen Maternal and Child Health Hospital)

subject to compressive bone absorption and destruction. The mass grows forward and forms nasal cavity mass, which can invade paranasal sinus; the mass grows upward, destroying the bone of skull base and invading the sphenoid sinus and intracranial space; it invades pterygopalatine fossa outwards and develops to infratemporal fossa; it invades to the orbit along the orbital wall bone or the inferior orbital fissure, and mainly manifests as homogeneous and slightly high-density shadows with marked heterogeneous enhancement by CT scan; and MRI indicates the lesion showing isointense and hypointense on T_1WI and isointense and hyperintense on T_2WI. There is no significant intense of hemorrhage in periphery. That is, there is no significantly hypointense ring on T_2WI. The lesions often originate from basilar part of occipital bone, corpus sphenoidale, and medial periosteum of pterygoid process, and invade pterygopalatine fossa through sphenopalatine foramen; 80% of the lesions lead to widened pterygopalatine fossa, they can invade infratemporal fossa, invade orbit through inferior orbital fissure, and enter intracranial space through foramen rotundum, superior orbital fissure, and pterygoid canal. Lesions of invasive growth manifest as marked enhancement.

5. *Hemangioma*. It is common in the elderly, easily occurring in mucosa anterior to the nasal cavity and maxillary sinus, developing slowly, and prone to bleeding, infection, and necrosis. Hemangiomas are classified into capillary hemangioma, cavernous hemangioma and

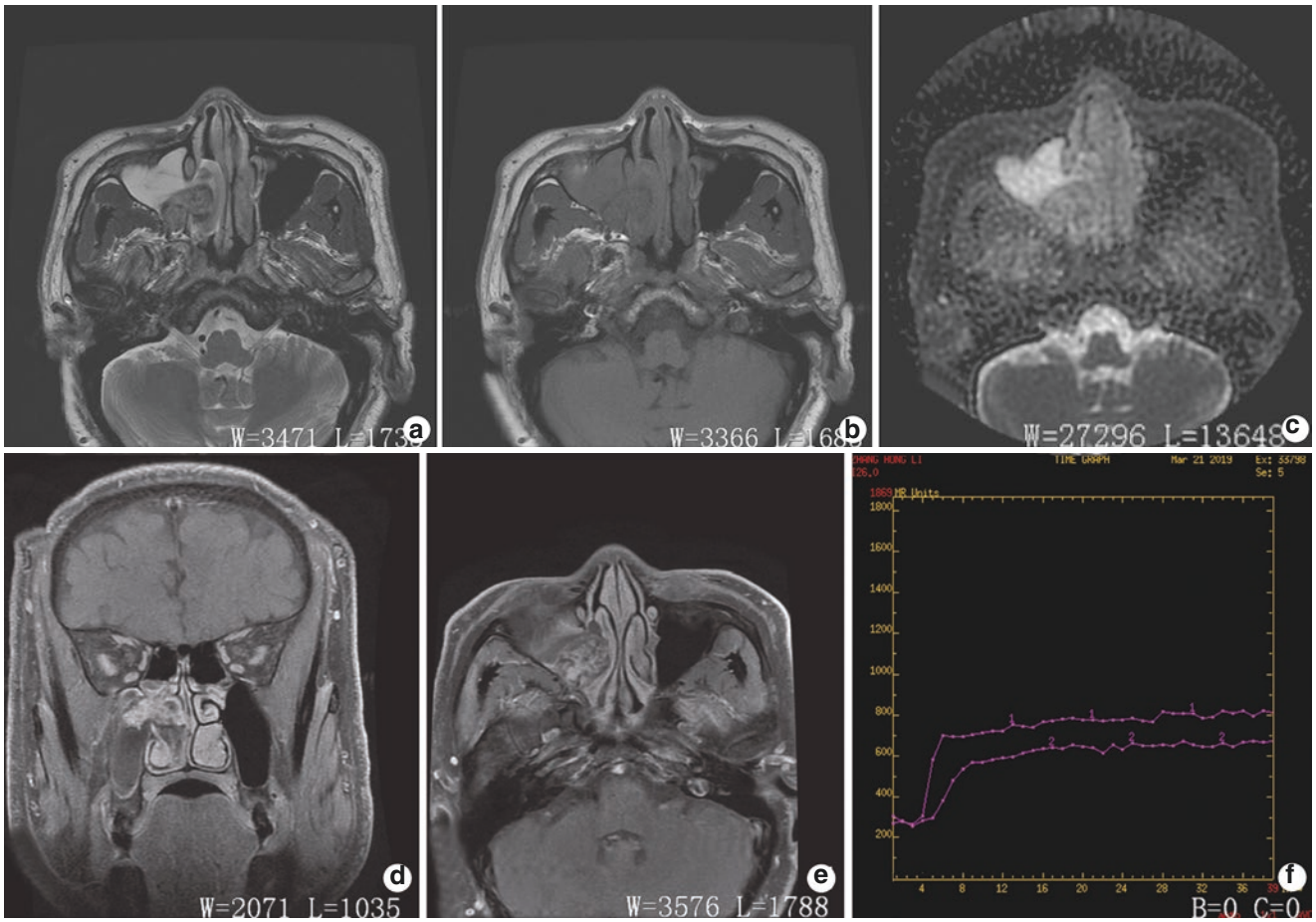

Fig. 23.24 Hemorrhagic necrotic nasal polyp in right maxillary sinus. A 47-year-old male patient. (**a**–**c**) Heterogeneous signal mass is found at the ostium of right maxillary sinus-nasal meatus sinus ostium, with patchy and annular hypointense on T_2WI. Isointense is dominant on T_1WI, with hypointense ring and decreased ADC value; (**d**–**f**) Enhanced MRI shows punctate and patchy heterogeneous enhancement. Dynamic enhanced scan shows progressive enhancement, and all multidraw enhancement curves are ascending

hemangioma racemosum. Soft tissue density masses expensively grow and have clear margins (large masses show heterogeneous density shadows), phlebolith or calcification are common in these masses. These masses directly invade orbit, pterygopalatine fossa, infratemporal fossa, and other structures. The compressive deviation, absorption and thinning or diffuse, osteolytic and moth-eaten destruction of bone of sinus wall are important diagnostic signs. The cervical lymphatic metastasis occurs. MRI indicates that the hemangioma is isointense on T_1WI and heterogeneous and slightly hyperintense on T_2WI. The signal is heterogeneous and free of attenuation. Enhanced scan indicates mild-marked heterogeneous enhancement, complicated with heterogeneous enhancement for infection and necrosis, unremarkable enhancement in case of thrombus and flowing void shadow.

6. *Malignant melanoma of nasal cavity.* It is common in the elderly, mostly located in nasal septum and middle and inferior nasal concha, but rarely found in maxillary sinus and nasal periphery. Most of the lesions show infiltrative growth. CT shows irregular high-density soft tissue masses without significant necrosis or cystic degeneration, significant absorption, and destruction of surrounding bone, showing knife-cut sign with clear and clear margin. Lesions can invade peripheral tissues and grow to the orbit, pterygopalatine fossa, face, and contralateral nasal cavity. MRI indicates heterogeneous signals, and the characteristic signals increase with melanin pigments, typically manifesting as hyperintense on T_1WI and hypointense on T_2WI. Most cases show slightly hyperintense on T_1WI and slightly hypointense on T_2WI. Diffusion is limited on DWI, and ADC indicates hypointense. Enhanced scan shows mild enhancement, and the TIC curve rapidly rises and slowly declines, indicating malignant melanoma of nasal cavity.
7. *Epitheliogenic malignant tumor of paranasal sinus.* It is common in the elderly with short duration and rapid progress. Soft tissue masses grow along the sinus wall or nerves in different directions throughout the sinus, and

the diffuse, osteolytic, and moth-eaten destruction of bone along the sinus wall is remarkable and considered to be an important diagnostic sign. Calcification is found on the surface or inside of some masses, which directly involves peripheral structures, such as orbit, pterygopalatine fossa, and infratemporal fossa, complicated with cervical lymphatic metastasis. CT shows soft tissue mass with heterogeneous density; isointense or slightly hypointense on T_1WI, heterogeneous and slightly hyperintense on T_2WI, and mild-marked heterogeneous enhancement by enhanced scan.

8. *Lymphoma.* It progresses slowly, easily occurs in the anterior nasal cavity or midline structure, and is common in nasal cavity and maxillary sinus. The change of bone swelling is unremarkable, and the degree of bone destruction is not proportional to the mass size. That is, the large mass does not indicate remarkable bone destruction, and is easy to invade the facial soft tissue. CT shows homogeneous soft tissue mass in sinus. MRI indicates slightly hypointense on T_1WI and isointense and slightly hyperintense on T_2WI. Enhanced scan shows mild to moderate homogeneous enhancement, which lacks characteristic manifestation.

23.2.2.6 Status Quo and Progress of Research

1. MRI is the first choice for diagnosing the disease. The lesion caused by hemorrhage shows hyperintense on T_1WI and specific hypointense ring in the marginal zone of T_2WI. By enhanced scan, the lesion shows nodular and cauliflower-like enhancement as the characteristic manifestation. Dynamic enhanced scan is the key to examination, and "progressive enhancement" provides diagnostic features.
2. Different from neoplastic lesions, the hemorrhage can result in hypointense on DWI and SWI.

23.3 Wegener Granulomatosis in Nasal Cavity and Paranasal Sinus

23.3.1 Overview

Wegener granulomatosis (WG) is a systemic, multiple organ, chronic, progressive, destructive, and giant cell ulcerative granulomatous lesion, which is renamed as granulomatosis with polyangiitis. Its basic pathological features are aseptic necrotizing vasculitis and granuloma formation in arterioles and venules. It is an autoimmune disease involving multiple immunopathological processes. Cytoplasmic antineutrophil cytoplasmic antibody (C-ANCA) is a very sensitive index for the diagnosis of multiple granulomas. The disease can be divided into systemic type (Wegener granuloma) and localized type (Wegener granulomatosis), which are in different progression stages of the disease. The focus often originates from the upper respiratory tract and starts from the nasal septum, then involves the nasal cavity, paranasal sinus, oral cavity, larynx, and trachea in turn. Lung and kidney are also commonly involved. The disease can further involve eyes, salivary gland, joints, skin, muscles, ears, pericardium and nervous system. In addition, it can involve the liver, lymph nodes, large and small intestines, tongue, esophagus, bone marrow, and adrenal gland.

The disease is common in young and middle-aged men aged 30–50 years. It has a slow onset in most cases and acute onset occasionally. Of all the cases, recurrent nasal obstruction and purulent nasal discharge with persistent aggravation account for 85% [9], which is easily misdiagnosed as rhinosinusitis, rhinitis, and nasopharyngeal carcinoma. Nasal endoscopy shows irregular masses and plenty of secretions, with occasional proptosis. Nasal obstruction and purulent nasal discharge are common symptoms in early stage, complicated with escharosis, blood-streaked nasal discharge, and otitis media caused by obstruction of the auditory tube. Bronchial granuloma can cause atelectasis, complicated with common symptoms (cough, bloody sputum, chest pain, and short breath) of lung involvement, and fever as a systemic symptom. When invading the kidney, the disease shows occult manifestations at first, followed by proteinuria, hematuria, and uremia at the later stage, with renal failure to the end. Skin lesion often occurs in limbs and can manifest as purpura blisters, nodules, ulcers, and masses.

23.3.2 Pathology Findings

Inflammatory necrotic granuloma of the upper and lower respiratory tract, focal or diffuse necrotic glomerulonephritis, and extensive necrotizing vasculitis are the pathological triad of the disease [9]. Multiple necrotizing vasculitis manifests as inflammation in the walls of arterioles, venules and capillaries, fibrinoid degeneration and necrosis of vascular walls, and destruction of muscularis and elastic fibers. The infiltration of epitheloid cells, neutrophils, monocytes, multinucleated giant cells, plasma cells, lymphocytes, fibroblasts, and a few eosinophils is found in the necrotic granuloma. Multiple nodules are formed in the lungs, and the central hollows are often formed due to necrosis. Anti-antineutrophilic cytoplasmic antibody (ANCA) plays an important role in the pathogenesis of vasculitis [18].

23.3.3 Imaging Findings

1. *X-ray examination.* It shows no characteristic manifestation in early stage and is similar to common rhinosinusitis, mainly manifests as mucosal thickening of nasal

cavity and paranasal sinus, increased density, decreased nasal cavity transmittance, paranasal sinus stenosis, or occlusion. In the progressive stage, the disease shows atrophy and defect of nasal concha, osteoporosis, and destruction of nasal septum, bone absorption and destruction of medial wall of maxilla and ethmoidal sinus are [3]. Perisinusoidal osteosclerosis causes sinus occlusion and involves orbit.

2. *CT examination.* With nasal cavity as the center, the lesion gradually and symmetrically involves maxillary sinus from nasal septum and nasal concha, and further spreads to other paranasal sinuses and orbits. Hard palate involvement is rare [3, 18].
   (a) In the early stage, it shows nonspecific chronic inflammatory manifestation. Only nodular mucosal thickening and irregular surface of nasal concha, nasal septum, and paranasal sinus are found, and the sinus may have liquid plane.
   (b) In the progressive stage, irregular stripy soft tissue masses are found in nasal septum, nasal concha, and maxillary sinus, and mucosa is ambiguous due to ulceration, complicated with obstructive rhinitis. Bone destruction centered on nasal cavity gradually expands to the medial wall of maxillary sinus, and the sinus wall may have proliferation and sclerosis, showing double-line sign [18].
   (c) In the advanced stage, the nasal concha and nasal septum are destroyed remarkably, and the nasal septum is necrotic and perforated [3]. The maxilla, ethmoidal septum, papyraceous lamina, and skull base can also be involved, and the remaining sinus wall bone is thickened and shows a double-line sign. The maxillary sinus is narrow or even occluded. The nasal dorsum collapses, and the nasal cavity expands to form a hollow, accompanied by multiple cord-like shadows, similar to postoperative changes [16, 18] (Fig. 23.25a–c). Soft tissue mass extends to orbit, nasopharynx, oropharynx, and glottic portion, showing soft tissue mass with bone destruction. Characteristic soft tissue nodules with hollow formation are found in the lung (Fig. 23.25d–f). The disease causes renal enlargement, poor blood supply, and glomerulonephritis.
3. *MRI examination*. It shows swelling and thickening of nasal mucosa, manifesting as isointense or hyperintense on T_1WI and hyperintense on T_2WI. Granulomatosis mostly shows hypointense on T_1WI and T_2WI, heterogeneous signal, and mild enhancement by enhanced scan.

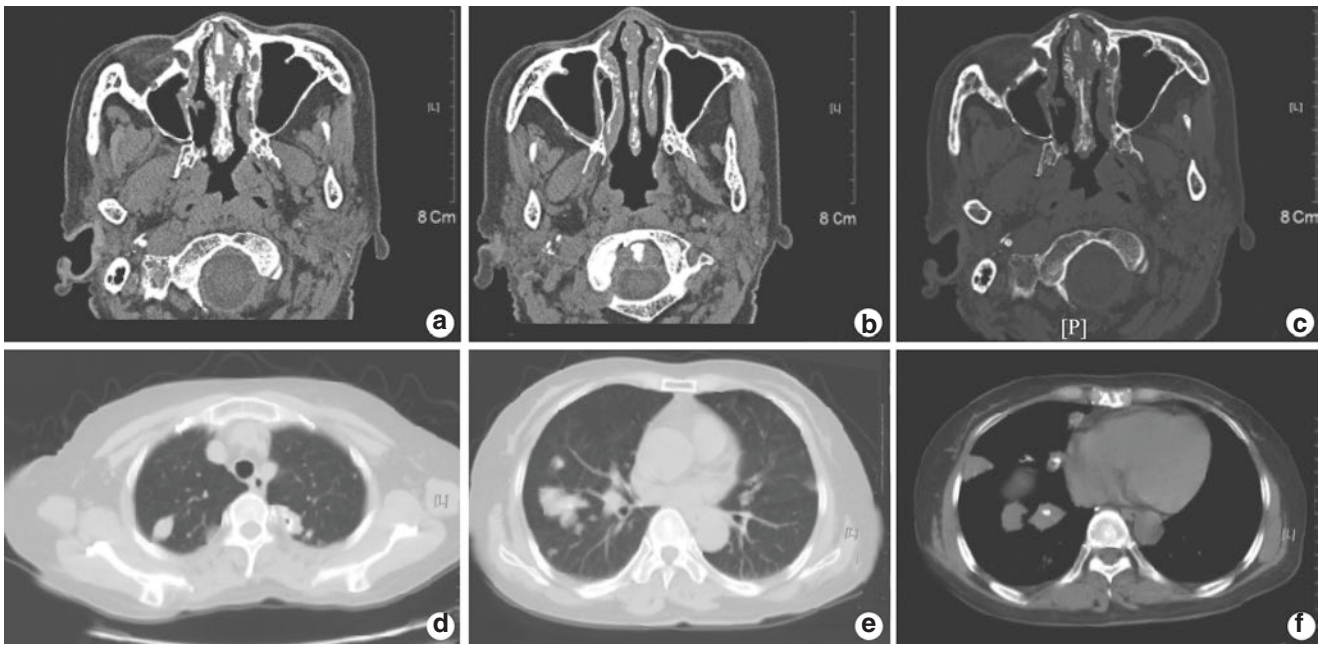

Fig. 23.25 Wegener granulomatosis in nasal cavity and lung. A 58-year-old female patient. The left nasal obstruction lasted for more than 1 week, with bloody nasal discharge for 6 days. Neoplasm was found in the middle-superior nasal concha and anterior border of middle nasal septum, with irregular surface, brittle texture, and easy to cause hemorrhage by touch. (**a–c**) Nasal CT shows local defect of nasal septum, hypertrophy of nasal septum and bilateral nasal conchas, forming irregular stripy soft tissue mass with multiple nodular calcification, irregular surface and mucosal thickening of bilateral maxillary sinuses; (**d–f**) Chest CT shows multiple masses and nodules in both lungs, which are located in the vascular center and subpleural area and mainly distributed in upper lungs, with patchy calcification in the center of lesion and small hollows in the posterior segment of the superior lobe tip of left lung (Images courtesy of Chen Wangqiang, The Second Affiliated Hospital of WMU)

The sinus wall is thickened, which is similar to the intense of spongy bone. Qualitative diagnosis is of little significance, but can clearly show the extent of involved peripheral tissues.

23.3.4 Clinical Diagnosis Criteria

Wegener granulomatosis is diagnosed according to the classification criteria developed by the American College of Rheumatology (ACR) in 1990 [18].

1. *Nasal or oral inflammation.* Painful or painless oral ulcer, purulent or bloody nasal secretion.
2. *Abnormal chest X-ray findings.* Nodules, fixed infiltrative lesions or hollows.
3. *Abnormal urinary sediment* Microscopic hematuria (RBC > 5/HPF) or red cell cast.
4. *Pathological granulomatous inflammatory changes*. Neutrophil infiltration on the arterial wall or around the artery, or outside the blood vessels (arteries or arterioles).

Wegener granulomatosis can be diagnosed if 2 or more criteria are met, and the sensitivity and specificity of diagnosis are 88.2% and 92.0%, respectively.

23.3.5 Key Points of Diagnosis

1. Progressive bone destruction in midline area of nasal cavity and paranasal sinus, nasal concha destruction, nasal septum perforation, a large hollow formed in the nasal cavity, saddle nose formed due to collapse of nasal dorsum, and double-line sign formed by neoplastic bone of the sinus wall.
2. The nasal cavity and paranasal sinus present diffuse irregular soft tissue granuloma, which extends symmetrically and involves the orbit, nasopharynx, glottic portion, oral cavity, and other parts, with the center located in the nasal cavity.
3. MR is a non-neoplastic lesion, showing hypointense or isointense on T_1WI, hypointense on T_2WI and heterogeneous signal. Enhanced scan indicates heterogeneous enhancement of lesions, and meninges thickening and enhancement when skull base is involved.
4. It is a systemic multisystem disease and multiple organs (e.g., lung and kidney) are involved, thus sarcoidosis needs to be differentiated [18].
5. Cerebrospinal fluid examination indicates that erythrocyte sedimentation rate increases rapidly, leukocytes increase significantly, and related pathogens can be detected from cerebrospinal fluid. C-ANCA is positive.

23.3.6 Differential Diagnosis

1. *Rhinoscleroma.* The bone is significantly destroyed, but the residual bone often has significant proliferation and sclerosis; The perinasal soft tissue is significantly thickened, the external nose is deformed, and the thoracic lymph nodes are enlarged.
2. *Paranasal sinus sarcoidosis.* It usually manifests as a systemic disease involving centrum and multiple organs (e.g., lung and kidney), rare involvement of nose, nodular mucosal thickening of nasal septum and nasal concha, and rare lump-like lesions. When the paranasal sinus is involved, it may manifest as soft tissue shadows and bone destruction of nasal cavity and paranasal sinus, and the nasal bone trabecula has wide reticular changes [18]. The enlargement of thoracic lymph nodes is common in relevant patients.
3. *Lethal midline granuloma.* The lethal midline granuloma, also known as Stewart granuloma and necrotic (gangrenous) granuloma, is considered to be NK/T-cell lymphoma of nasal cavity and paranasal sinus. The disease progresses rapidly and is extremely destructive. Plenty of tissues of organs in midfacial region are destroyed, thus forming severe defects, and structures near the midline of nasal cavity and paranasal sinus are extensively destroyed, such as defects of nasal septum, nasal concha and medial wall mucosa of maxillary sinus, irregular surface and bone destruction, which may be involved bilaterally. Necrosis lesion and sequestrum formation can occur in nasal bone, maxilla, and hard palate. Abscess formation can be found in soft tissue, resulting in "facial empty sign" [18], which involves large scope and severe destruction, destroys the patient's face in a short time, and results in death due to massive hemorrhage, organ failure, and complications. Lung and kidney are not involved.
4. *Non-Hodgkin lymphoma.* Mostly occurs unilaterally. In most cases, it can occur in nasal vestibule or inferior nasal concha, and the soft tissue swelling of nasal dorsum, ala nasi, and cheek is obvious; The bone destruction of nasal septum, nasal concha, hard palate and alveolar bone may be infiltrative, the contour of cortex remained without bone double-line sign. CT shows homogeneous isointense or slightly high density, MRI shows slightly hypointense on T_2WI, DWI shows hyperintense, and enhanced scan shows mild homogeneous enhancement.
5. *Fulminant fungal rhinosinusitis.* It has strong invasion, rapid destruction, and severe systemic and local symptoms. It is found that the density of the involved sinus increases, and the soft tissues within and surrounding the sinus are destroyed by diffuse infiltration. Orbital infiltration causes orbital apex cavernous sinus syndrome, and intracranial invasion causes meningitis and fungal granuloma [3].

6. *Nasal carcinoma.* It often occurs in the elderly, with nasal obstruction and nasal discharge as common symptoms, and masses with irregular surfaces are found in nasal cavity. X-ray and CT examination shows infiltrative soft tissue masses on nasal mucosa, which grow rapidly and invade paranasal sinus, orbit, and intracranial space, and lead to local bone destruction.

23.3.7 Status Quo and Progress of Research

CT is the first choice for imaging examination as it can indicate bone destruction of nasal cavity and paranasal sinus. If it is necessary to assess the involvement extent of soft tissues or differentiate neoplastic lesions, further MRI examination is required, which usually indicates double hypointenses.

For clinically suspected cases, imaging examination is an important method for finding the involvement of multiple organs. The paranasal sinus, lung, kidney, liver, heart, and vascular system should be comprehensively and systematically examined in combination with ultrasonography, CT, and MRI to detect any involvement of multiple organs, and the final diagnosis should be made according to clinical diagnosis criteria in combination with laboratory test results [19].

23.4 Rhinoscleroma

23.4.1 Overview

Rhinoscleroma is a rare chronic progressive granulomatous disease of nasal-paranasal sinus. Its pathogen, Klebsiella rhinoscleromatis (Frisch bacillus) is a Gram-negative low-toxicity bacterium with low infectivity, but its mode and route of infection are unknown. The disease occurs sporadically in region and is associated with multiple factors, such as climate, environmental sanitation, nutritional status, and individual immunity. It mostly occurs in poverty-stricken areas with poor sanitation and has been reported around the world, especially in Africa, Central and South America, Eastern Europe, and Sumatra Island. In China, relevant cases are mainly reported in Shandong Province. The onset age mainly ranges from 20 to 40 years old, and the disease is common in men. The disease has a long duration and lasts for months or years.

Ninety-eight percent of patients with rhinoscleroma manifest nasal involvement, which usually occurs bilaterally and symmetrically. The lesions of some cases are limited or distributed asymmetrically. Lesions are limited to the nasal cavity in early stage, and the nasal septum, inferior nasal concha, and nasal base are thickened, thus forming lumps. In the progressive stage, the nasal septum, nasal cavity wall, hard palate, and medial wall of maxillary sinus are destroyed by bone compression or erosion, and scar stenosis can be formed in the advanced stage [1]. Rhinoscleroma mostly occurs in maxillary sinus (ethmoidal sinus, sphenoid sinus, and frontal sinus in order), and easily spreads to adjacent structures, and gradually spreads to the inferior and posterior structures, including choana, soft palate, hard palate, tonsil, oropharynx, hypopharynx and trachea, and can be scattered throughout the respiratory tract with concurrent or recurrent occurrence. Thus, it is also called respiratory scleroma. There are a few cases with primary rhinoscleroma of lower respiratory tract. Its infiltration to anterior structures causes irregular thickening of ala nasi. It can spread to the superior orbit and lacrimal sac. It can enter the posterior nasopharynx and involve the auditory tube, causing otitis media.

23.4.2 Pathology Findings

Rhinoscleroma easily occurs in respiratory mucosa and usually originates from the junction of nasal vestibular squamous epithelium and fibrous columnar epithelium, and extends to paranasal sinus, larynx, and trachea along the proper membrane. The pathological changes can be divided into three stages: catarrhal stage, granulomatous stage, and cicatricial stage [1]. Each stage has different pathological features that can also overlap at the same time or appear as transition.

1. *Catarrhal stage.* Nasal mucosa is subject to edema, atrophy, dryness, and escharosis, followed by squamous metaplasia and formation of granulation tissue. Infiltration of neutrophils, lymphocytes, and plasma cells can be found on mucosa and submucosa. The inferior nasal concha becomes smaller, and the nasal cavity is enlarged, similar to atrophic rhinitis. Inflammatory manifestations and pathological sections are not specific. Detection of Klebsiella rhinoscleromatis in the tissue space and bacterial culture are helpful for diagnosis.
2. *Granulomatous stage.* Granulation tissues are found in nasal vestibule, inferior nasal concha and nasal septum, which form hard nodules and are merged into hyperplastic masses, resulting in nasal obstruction and external nose deformity. Giant foam-like cells (Mikulicz cells), fuchsin corpuscles (Unna or Russell corpuscles), plenty of plasma cells, and a few lymphocytes can be observed microscopically. Mikulicz cells, Russell corpuscles, and anti-Klebsiella rhinoscleromatis are the main pathological features of rhinoscleroma and the main bases for pathological diagnosis [1].
3. *Cicatricial stage.* There are many kinds of deformities in contracted fibrotic scar tissue, such as medial deviation of ala nasi, constriction and atresia of nasal vestibule, constriction of nasopharynx and laryngostenosis. Plenty of fibrous tissues are proliferated within the lesion, Mikulicz cells and Russell corpuscles decrease or disappear, and a few granulomatous lesions are scattered in fibrous tissues as isolated islands.

The disease is diagnosed mainly based on pathological examination, bacterial culture, and serum complement fixation test (CFT), and the characteristic that the phase III clinical lesions often exist simultaneously and the regional characteristic [3, 20].

23.4.3 Imaging Findings

1. *X-ray examination.* It shows that the lesions are confined to the nasal cavity in early stage, with thickening of nasal septum and nasal concha. In the advanced stage, the destruction by bone compression or erosion is found in nasal septum, nasal cavity wall, hard palate, and medial wall of maxillary sinus. Scar stenosis can be formed in the advanced stage.
2. *CT examination.*
   (a) Nonspecific mucosal thickening in early stage.
   (b) Localized or large soft tissue masses with clear contour are formed in granulomatous stage, with homogeneous density and unremarkable enhancement [1, 3]. The middle and inferior nasal conchas are deformed, atrophied and destroyed, the nasal septum is easy to be destroyed, and the stump shows osteosclerosis. When the paranasal sinus mucosa is invaded, the sinus is filled with irregular granulation tissue shadows and consolidation, the distal obstructive rhinosinusitis, the bone of the sinus wall deviates and atrophies, and extensive bone destruction and stump sclerosis coexist. When the orbit is invaded, the extraocular muscle displaces, the masses wrap around the extraocular muscle or optic nerves, invade the skull and cause thickened meninges, and form granuloma (Fig. 23.26).
   (c) In cicatricial stage, bone in nasal concha, nasal septum and medial wall of maxillary sinus have bone

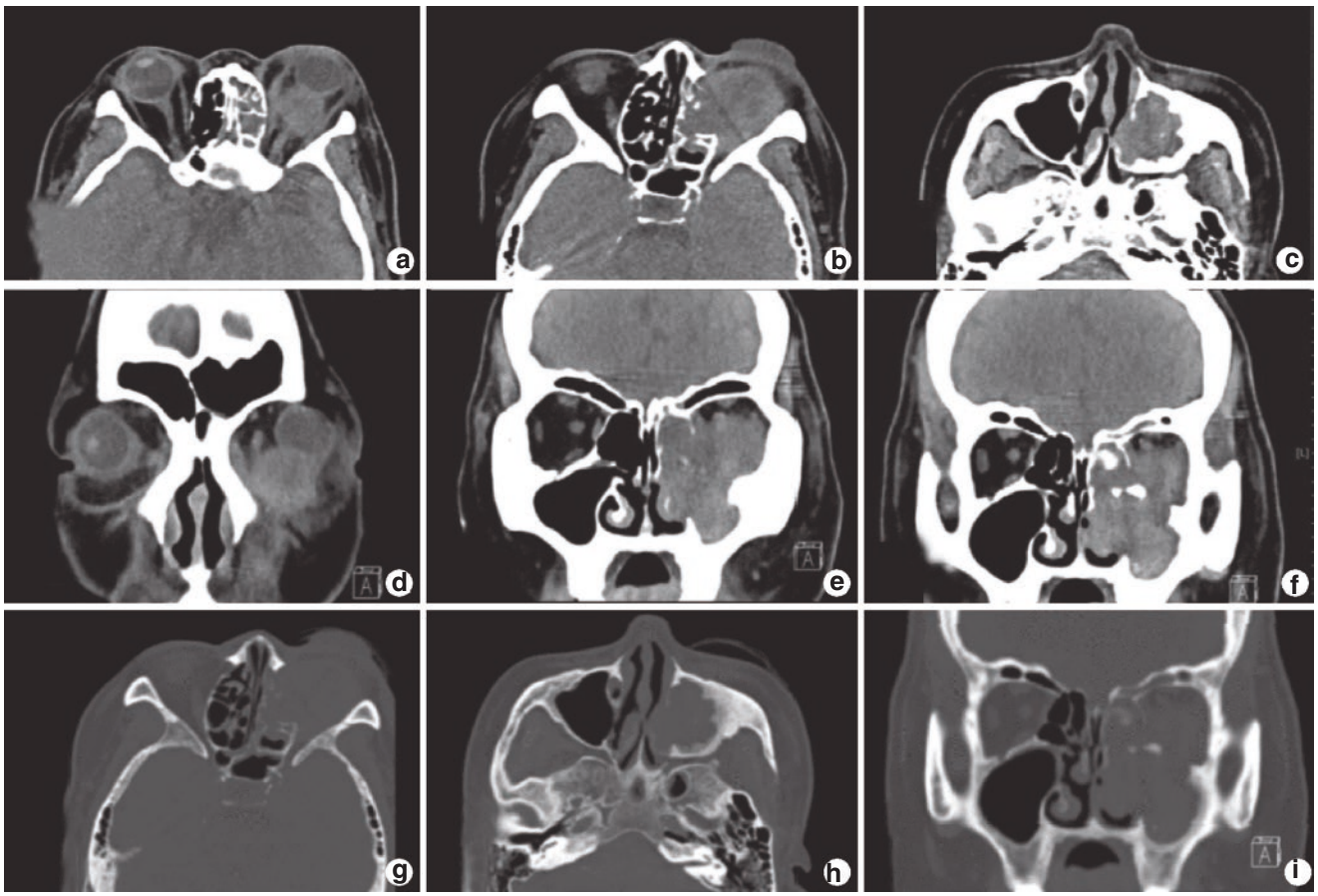

Fig. 23.26 Nasoantorbital Scleroma with Fungal Infection. A 59-year-old female patient. The patient suffers from toothache complicated with swelling pain on the left cheek for more than 2 years. Pathology shows acute and chronic inflammatory tissues of the left maxillary sinus and orbit, complicated with granulation tissue proliferation and fibrosis, and plenty of Aspergillus hyphae and spores can be seen. (**a**–**f**) Non-enhanced CT scan on soft tissue window indicates that the irregular soft tissue masses of left nasal cavity, left maxillary sinus and left orbit grew invasively, with heterogeneous density as well as patchy low-density necrotic area and high-density calcification area, and the left extraocular muscle is displaced by compression and partially infiltrated. (**g**–**i**) The scan on bone window shows extensive and erosive bone destruction in the medial wall of maxillary sinus, inferior wall, and medial wall of orbit, with neat stump edge complicated with sclerosis, and bone destruction and stump sclerosis coexisted

destruction and disappearance, and nasal cavity is enlarged, with scattered cord-like shadows [3]; The maxillary sinus is filled with irregular soft tissue masses, the bone of the remaining sinus wall is subject to hyperostosis and sclerosis, the sinus is deformed and constricted, the nose is collapsed and deformed [1], and the soft tissue of ala nasi is thickened significantly.

3. *MRI examination.* It shows nonspecific mucosal thickening in early stage, which is difficult to differentiate. In the granulomatous stage, the signal intensity of lesion is higher than that of muscle, with heterogeneous hyperintense on T_2WI and isointense and slightly hyperintense on T_1WI, which are characteristic manifestations [16]. The signal intensity decreases in cicatricial stage, especially on T_2WI. Mild heterogeneous enhancement is indicated by enhanced scan. The lesions do not develop synchronously, and the imaging manifestations in different periods can overlap. It can invade orbital and intracranial structures.

23.4.4 Key Points of Diagnosis

1. Nodular thickening and sclerosis of perirhinal soft tissue and deformation of external nose.
2. Multiple diffuse and solid soft tissue masses in paranasal sinus and nasal cavities, which are symmetrically and bilaterally distributed and involve adjacent paranasal sinus, larynx, pterygopalatine fossa, orbit, and intracranial space.
3. Deformity, atrophy, and destruction of nasal septum, middle and inferior nasal concha and sinus wall, osteosclerosis of stump and enlargement of nasal cavity.
4. The tumors of nasal cavity and paranasal sinus are excluded.
5. Serum C-ANCA is negative.

23.4.5 Differential Diagnosis

1. *Atrophic rhinitis.* It is caused by multiple reasons, with clinical manifestations of nasal cavity dryness, narium, and free of epistaxis. Imaging features include widened nasal cavity, atrophy of mucosa, mainly including atrophy of inferior nasal concha, no solid soft tissue mass in most cases, no invasion to paranasal sinus and less involvement outside the respiratory tract.
2. *Wegener granulomatosis.* It involves multiple systems, and the serum C-ANCA is positive. Ulcer and destruction progress slowly in the midline area of nasal cavity, extensive soft tissue masses complicated with bone destruction, bone destruction and disappearance of nasal septum, nasal concha, hard palate and medial wall of maxillary sinus, nasal cavity expanded to form a larger hollow, similar to postoperative changes of nasal cavity and paranasal sinus, and nasal dorsum collapses. It can involve larynx, orbit and intracranial space, and form soft tissue masses. All sequences of MRI show hypointense, and slightly hyperintense on T_1WI for scleroma.
3. *Nasal lymphoma.* The midline structures such as nasal septum and nasal concha are progressively destroyed in a short time, and soft tissue masses are formed in nasal cavity, invading nasal vestibule and ala nasi. Diffuse lesions can cause swelling of maxillofacial soft tissue, which invades hard palate, alveolar bone, infratemporal fossa, pterygopalatine fossa and orbit, and often infiltrates the tissue space around maxillary sinus. Bone destruction is rare, and infiltrative destruction is found without osteosclerosis. Clinical findings indicate that the disease is often complicated with systemic symptoms, such as hepatosplenomegaly and mild fever.
4. *Chronic invasive fungal rhinosinusitis.* It easily involves orbital apex and cavernous sinus, with bone erosion, destruction and mild hyperostosis and osteosclerosis, with hyperintense on T_1WI and hypointense on T_2WI.
5. *Malignant tumor of paranasal sinus.* It develops rapidly, forming irregular soft tissue masses and having infiltrative growth, showing heterogeneous enhancement and severe bone destruction without osteosclerosis and remodeling.

23.4.6 Status Quo and Progress of Research

1. The clinical manifestations in early stage are atypical and easy to be misdiagnosed. Patients often visit the doctor in nodular formation stage or cicatricial stage. The suspected patients should be examined by biopsy, bacterial culture, and serum-specific antibody test in time.
2. Pathology provides main bases of diagnosis, Mikulicz cells, and Russell corpuscles are the characteristic manifestations, and it is necessary to take multiple samples to avoid missed diagnosis or misdiagnosis.
3. Laboratory test of serum anti-Klebsiella rhinoscleromatis antibody can assist diagnosis, and immunoperoxidase has high sensitivity and specificity in identifying Klebsiella rhinoscleromatis isolated and cultured from pathological tissues or nasal secretions.
4. Imaging examination is of great value in diagnosis, differential diagnosis, and guiding clinical treatment of rhinoscleroma. CT is easy to indicate bone involvement, and it is the main imaging examination method for diagnosing scleroma. MRI is easy to indicate the soft tissue invasion scope of scleroma, and clearly shows imaging of changes in invasion to orbit and intracranial space. The

hyperintense on T_1WI is a characteristic to some extent. The combination of CT and MRI can improve the diagnosis confidence of rhinoscleroma.
5. With rare rhinoscleroma cases, there is a lack of relevant understanding from clinical findings to imaging, and lack of research and analysis of multimodal imaging examinations, such as energy spectrum CT and perfusion imaging.

23.5 Rhinogenic Orbital Inflammation

23.5.1 Overview

Rhinosinusitis is the most common cause of orbital infection, accounting for 60–84% of all cases, which is mostly caused by ethmoiditis, followed by frontal sinus, maxillary sinus, and sphenoid sinus. Among children and adolescents, orbital infection is the most common complication of rhinosinusitis, and even the primary manifestation of pediatric rhinosinusitis. Pathogens include staphylococcus, streptococcus, pneumococcus, pseudomonas, neisseria, haemophilus, and mycobacteria. The physiological bases of infection include the following aspects:

1. The orbit is anatomically close to paranasal sinus, thus the sinus ostium obstructed is difficult to drain, and nerves vessels passing through some natural orifices are easy to cause cross-infection.
2. The orbital papyraceous lamina is thin, the tension of paranasal sinus increases due to infection, and it is easy to penetrate and erode the orbital wall and cause orbital infection; The orbital periosteum is easy to form subperiosteal pus at the attachment of the sutura.
3. There is communication between anterior ethmoidal artery and posterior ethmoidal artery. Valveless veins in paranasal sinus and pterygopalatine fossa converge into superior and inferior ophthalmic vein and then converge into cavernous sinus. There are many communicating anastomosis branches between blood supply arteries and drainage veins. Acute infection can spread and cause intraorbital cellulitis and cavernous sinus thrombophlebitis.
4. Congenital dysplasia, surgery, and trauma also promote rhinogenic orbital infection to some extent.
5. Orbital septum is the only soft tissue barrier between orbit and paranasal sinus, which is a barrier to prevent cellulitis anterior to the orbital septum from invasion to soft tissues posterior to the orbital septum.

The main clinical manifestations of orbital infection are local symptoms such as red, swelling, fever and pain of orbits and systemic inflammatory toxic symptoms. Chandler divided the orbital complications into five categories according to their severity [21], which have a certain significance for the involvement scope and pathological process of the lesions. They are shown as below:

1. Orbital inflammatory edema: The infection is confined to the area anterior to the orbital septum, showing red, swelling, fever and pain of eyelids, and congestion of bulbar conjunctiva.
2. Cellulitis: Diffuse infection posterior to the orbital septum, proptosis, disorder of ocular movement, and diminution of vision.
3. Subperiosteal abscess: rhinosinusitis involves the orbit through the orbital wall, and purulent substances accumulate in the subperiosteal space, complicated with osteomyelitis and periostitis. It is mostly found in children, and there are clinical symptoms of puffy, diplopia, proptosis, and even visual defects.
4. Orbital abscess: it mostly manifests as the abscess of muscle cone, caused by extending subperiosteal abscess or localized cellulitis, resulting in proptosis and reduced movement.
5. Ophthalmic venous thrombosis: acute cavernous sinus thrombophlebitis, paralysis of cranial nerves III-VI, retinal venous congestion, and blindness caused by optic neuritis.

23.5.2 Pathology Findings

Acute suppurative inflammation of orbital soft tissue or inferior to periosteum is caused by such pathogens as hemolytic streptococcus or staphylococcus aureus. When osteomyelitis occurs, orbital bone destruction and periosteal reaction can be found. In severe cases, it is complicated with cavernous sinus thrombophlebitis, meningitis, and subdural abscess.

23.5.3 Imaging Findings

1. *X-ray examination.* Generally, X-ray plain film cannot show orbital lesions, it can occasionally show calcification of abscess capsule or pneumatosis or liquid plane in abscess [3]. The primary inflammatory changes of frontal sinus, ethmoidal sinus, or maxillary sinus can be found, the air content of sinus decreases with the permeability. When osteomyelitis is formed in orbital wall and sinus wall, bone is subject to erosion and destruction, the density decreases, and contour is blurred. Obvious swelling of orbital soft tissue can be observed.
2. *CT examination.* It indicates overlapping lesions in different stages, and it is difficult to differentiate them strictly. Intraorbital cellulitis and retrobulbar abscess con-

tinue with each other, while subperiosteal abscess and retrobulbar cellulitis usually coexist [3].

(a) Cellulitis anterior to orbital septum: increased diffuse density of soft tissue anterior to orbital septum, thickening of conjunctiva, eyelid swelling, lacrimal gland enlargement, and mild or moderate enhancement. The primary inflammation of paranasal sinus shows sinus mucosal thickening with effusion, decreased air in sinus, and blurred sinus wall and septum (Figs. 23.27, 23.28, 23.29, 23.30 and 23.31).

(b) Subperiosteal cellulitis and subperiosteal abscess: Periostitis manifests as layered high-density shadows parallel to the orbital wall, the subperiosteal space expands, inflammatory exudation increases and accumulates, and further forms abscess, which manifests as wide basal hillock-shaped soft tissue eminence between orbital wall and extraocular muscles [21, 22]. Extraocular muscles are subject to compressive deviation, with clear or rough margins, homogeneous internal density, or heterogeneous density caused by liquefactive necrosis. Enhanced scan shows marginal enhancement. Axial scan shows clear subperiosteal abscess of medial wall caused by ethmoidal rhinosinusitis, and coronal scan clearly shows subperiosteal abscess of upper wall caused by frontal sinusitis. The complicated osteomyelitis manifests as heterogeneous decrease of bone density of orbital wall, local erosion and destruction forming defects and blurred cortex. In the chronic stage, the bone is subject to hyperostosis

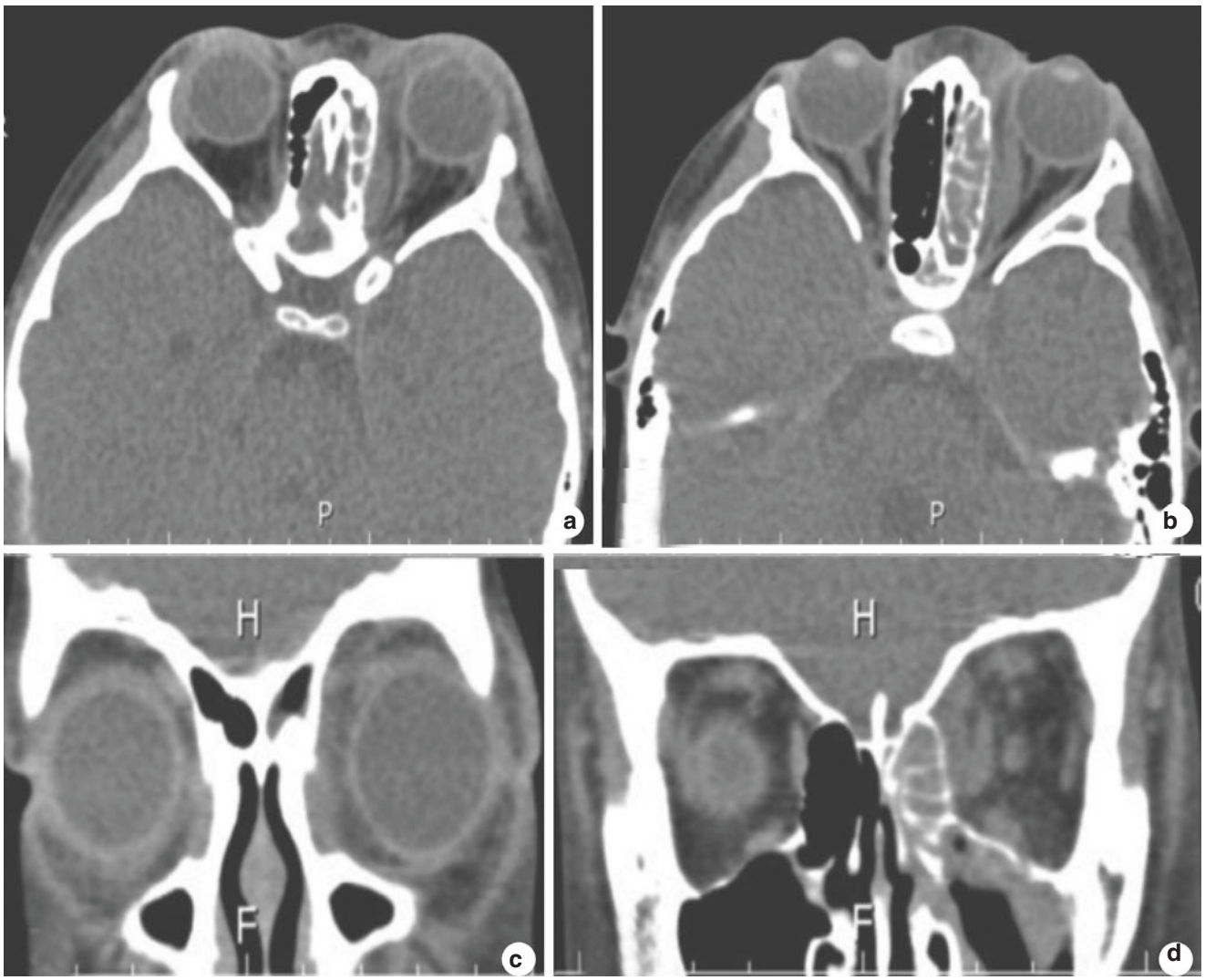

Fig. 23.27 Rhinogenic cellulitis anterior to orbital septum and subperiosteal abscess. A 4-year-old male patient. (**a**–**d**) Axial and coronal non-enhanced CT scan indicates heterogeneous mucosal thickening of the left maxillary sinus, and high-density shadows filled in the left ethmoid cell. The left orbit is infiltrated and involved, and the fusiform high-density shadows are formed inferior to the periosteum of the medial wall, with clear contour. The left medial rectus is subject to compressive deviation and tortuous course. The left eyeball has slight proptosis, the left eyelid is thickened, and the density of shadows anterior to orbital septum increases

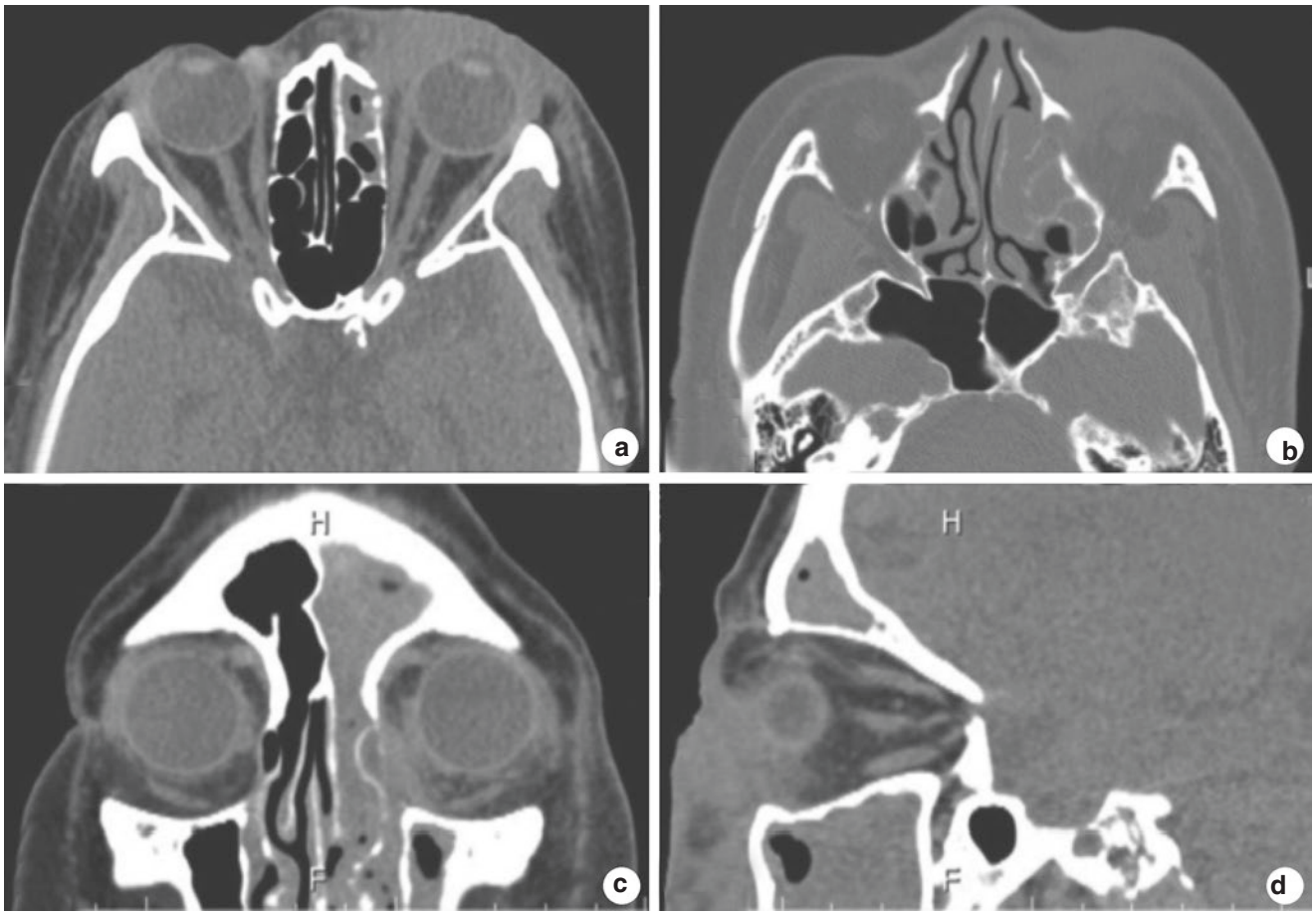

Fig. 23.28 Rhinogenic abscess anterior to orbital septum. A 48-year-old female patient. Lacrimation of left eye for 7 days, and redness and pus discharge for 5 days, and yellow-white purulent secretion is discharged from the left nasal cavity. (**a**–**d**) Axial, coronal, and sagittal non-enhanced CT scan shows that the left nasal cavity and half set of paranasal sinuses are filled with high-density shadows, the fat space anterior to the left orbital septum has diffuse swelling, with unclear margin, irregular lumpy abscess areas are formed in the medial and inferior parts, the center is not liquefied definitely, and the left lacrimal sac is involved

and sclerosis, and the periosteum is thickened and ossified (Figs. 23.27a–d, and 23.30d, e).

(c) Intraorbital cellulitis and retrobulbar abscess: Bacteria invade periorbital and retrobulbar fat and cause orbital cellulitis and retrobulbar abscess, which often coexist. The margin of normal structures in orbit is unclear or disappeared, the density of adipose body of orbit increases, and floccus and patchy high-density shadows are found, with lightly low density, and the surrounding blood vessels are congested and dilated, forming cord-like high-density shadows. Inflammation further develops to form a slightly low-density inflammatory mass, the central pus is necrotic area with lower density, the space inside and outside the muscle cone is diffusely involved, and the extraocular muscles is thickened and coarse. Neovascularization and granulation tissue around the lesion formed abscess wall, and enhanced examination shows irregular ring enhancement [22]. Air shadow can be formed by infection of aerobacter aerogenes (Fig. 23.31a and b).

(d) Retrobulbar optic neuritis: The optic nerves have diffuse thickening, blurred edge, mild enhancement by enhanced scan. It may lead to nerve atrophy in case of long duration of the disease [3].

(e) Intracranial spread: cavernous sinus thrombosis manifests as dilatation of cavernous sinus, thickening of superior ophthalmic vein, high-density of thrombus relative to cavernous sinus, filling defect shadows by enhanced scan [22], congestion and edema of extraocular muscles. Meningeal thickening shows cerebral gyriform or linear enhancement, and brain parenchyma abscess has ring enhancement, peripheral brain tissue has obvious edema, and subdural abscess or epidural abscess also can be found. Fungal Infection can lead to fungal aneurysm and internal carotid artery ectasia (Fig. 23.32a–c).

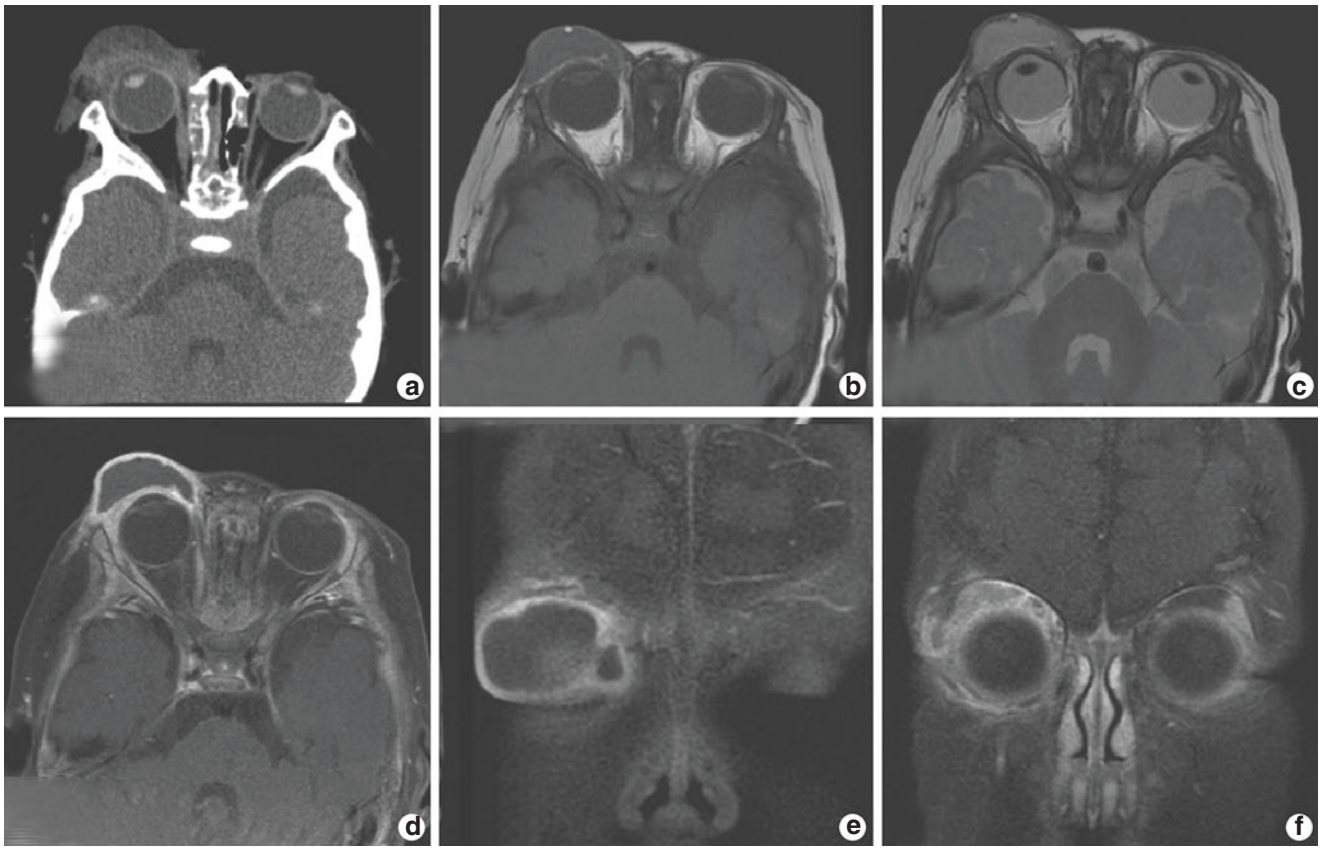

Fig. 23.29 Rhinogenic abscess anterior to orbital septum. A 10-month-old patient. (**a**) Non-enhanced CT scan indicates that the density of the right ethmoidal sinus increases, the medial rectus of the right orbit thickens, and the low-density abscess is formed in the space anterior to the orbital septum of the right orbit, without involving the ocular wall; (**b** and **c**) Non-enhanced MRI scan shows hypointense on T_1WI and hyperintense on T_2WI. (**d**–**f**) MRI enhanced scan indicates that the abscess wall has ring enhancement, the abscess wall is homogeneous, with unremarkable enhancement of central pus, and the periorbital cellulitis also has heterogeneous enhancement

3. *MRI examination.* It shows that the cellulitis anterior to orbital septum manifests as eyelid swelling and thickening of eye ring, and heterogeneous and hyperintense on T_2WI. Subperiosteal abscess shows fusiform hypointense on T_1WI and hyperintense on T_2WI with unclear margin. Intraorbital cellulitis manifests as unclear orbital structure, blurred orbital fat space, hypointense on T_1WI and hyperintense on T_2WI, while abscess manifests as a soft tissue mass with unclear margin, abscess wall is mainly composed of fibrous components, showing slightly hypointense on T_1WI and hypointense on T_2WI, central pus shows significantly hypointense on T_1WI and hyperintense on T_2WI, increased DWI signal, and extraocular muscle swelling shows hyperintense on T_2WI. Retrobulbar optic neuritis shows thickening of optic nerve, heterogeneous increase of fat suppression imaging signal, widening of optic nerve sheath with effusion; Osteomyelitis shows that fat shadow in bone marrow cavity is replaced by hypointense inflammatory tissue. Enhanced examination: peripheral enhancement of subperiosteal abscess; Cellulitis shows extensive and irregular enhancement in orbit. Abscess shows heterogeneous ring enhancement, and the enhancement of central liquefactive necrosis area is unremarkable; The fat-suppressibly enhanced scan shows optic neuritis with mild to moderate enhancement. MRI should pay attention to secondary complications, such as thrombosed cavernous rhinosinusitis and meningitis [22]. When venous thrombosis occurs, the signal intensities of the sequence increase and the cavernous sinus segment of internal carotid artery deforms. Fungal aneurysm is a severe complication of cavernous sinus thrombosis. In case of meningitis, both cerebral dura mater and cerebral pia mater can be enhanced (see Figs. 23.29b–f, 23.30a–c, 23.31d–f, and 23.34m).

23.5.4 Key Points of Diagnosis

1. *A clear history of paranasal sinus infection.* It is common in children and has acute onset.

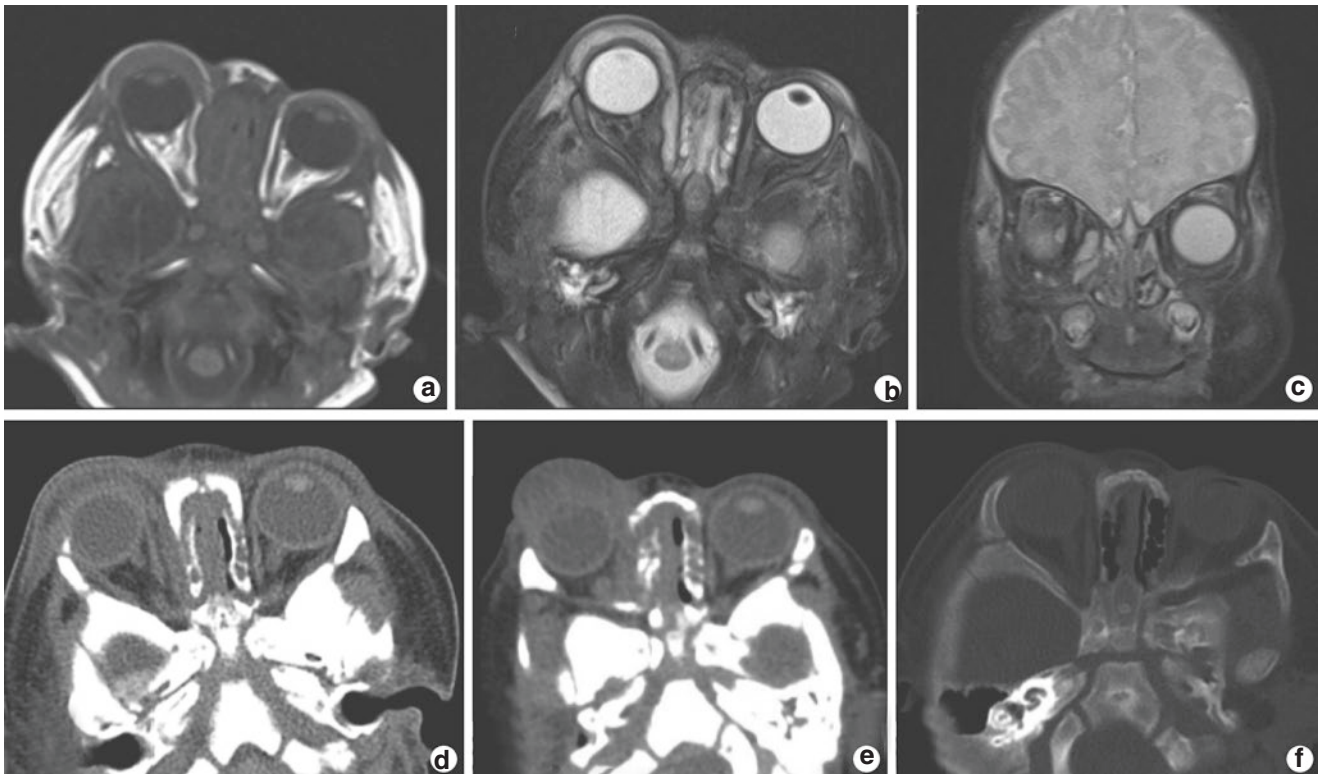

Fig. 23.30 Rhinogenic abscess anterior to orbital septum and subperiosteal abscess. A 1-month-old patient. (**a**–**c**) Non-enhanced MRI scan indicates mucosal thickening of bilateral ethmoidal sinuses and bilateral maxillary sinuses, stripy slightly hypointense on T_1WI, and hyperintense on T_2WI in right orbital subperiosteal abscess and abscess anterior to orbital septum. These shadows are connected, and T_2WI shows signal intensity slightly lower than that of vitreous body. (**d**) On the same day, non-enhanced CT scan indicates incomplete pneumatization of maxillary sinus, increased density of bilateral maxillary sinuses and bilateral ethmoidal sinuses, infiltration of papyraceous lamina by inflammatory lesions of right ethmoidal sinus and formation of slightly high-density stripy shadows inferior to the medial wall of right orbit, increased density anterior to right orbital septum, slightly low density in central area and blurred subcutaneous fat. (**e**) On the sixth day, CT shows the disease progression, the formation of abscess anterior to orbital septum, and the development of subperiosteal abscess to diffuse cellulitis posterior to the orbit; (**f**) After 2 months of treatment, CT shows that rhinosinusitis has healed and rhinogenic intraorbital cellulitis subsides

2. *Local intraorbital inflammatory symptoms.* Eyelid swelling, proptosis with pain, and diminution of vision. It may be complicated with systemic infection and toxic symptoms.
3. *CT scan.* It indicates that cellulitis shows diffuse inflammatory lesions, and the fat space in orbit is blurred, which can further develop to abscess, with soft tissue shadows of paranasal sinus. Subperiosteal abscess shows stripy or fusiform high-density shadows close to orbital wall, with relatively clear contour. Diffuse heterogeneous enhancement of inflammatory tissue is shown by enhanced scan.
4. *MR scan.* The pus shows hypointense on T_1WI and significantly hyperintense on T_2WI, the abscess wall shows isointense or slightly hypointense on T_2WI, and marked enhancement of the abscess wall ring by enhanced scan. The pus shows significantly hyperintense on DWI sequence.
5. *Laboratory test.* The leukocytes increased significantly.

23.5.5 Differential Diagnosis

1. Inflammatory pseudotumor. The CT manifestations are various, the diffuse inflammatory pseudotumor needs to be differentiated from intraorbital cellulitis. It can occur unilaterally, bilaterally, simultaneously or sequentially. Multiple structures in the orbit are involved, the structures in the orbit are replaced by desmoid tissues, the retrobulbar fat disappears, the diffuse irregular soft tissue density lesions are distributed from eyeball to orbital apex, the normal structures are covered and their borders are unclear, forming a "frozen orbit" [22], the optic nerves and extraocular muscles are thickened and enlarged without deviation (muscle tendon and muscle belly are generally thickened, medial rectus and superior rectus are mostly vulnerable), the ocular wall is diffusely thickened, eyelid is swollen, and lacrimal gland is enlarged with blurred margin. There is no distinctive lump and free of

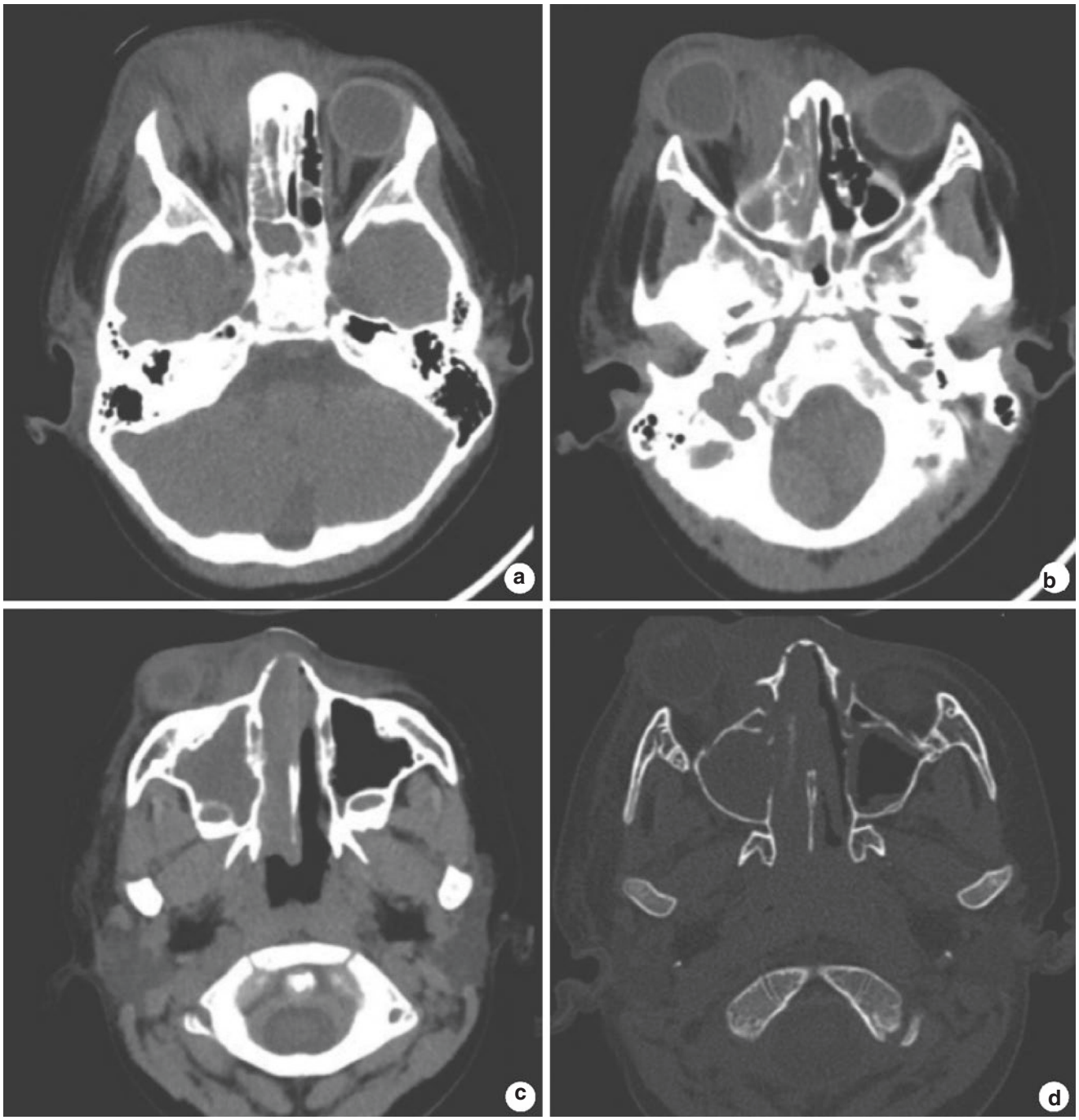

Fig. 23.31 Rhinogenic diffuse orbital abscess. A 5-year-old patient. (**a**–**c**) Non-enhanced CT scan on soft tissue window shows homogeneously increased density of right nasal cavity and half set of paranasal sinus, and inflammatory lesions infiltration involving the right orbit, high-density stripy shadows in the right orbital medial peripheral space, which is connected with inflammatory abscess in the space anterior to right orbital septum, and slightly low density in the central area. The right lacrimal gland is swollen and enlarged. The right eyeball is deformed and protruded by compression, and the extraocular muscles are thickened, displaced, and tortuous. The left maxillary sinus mucosa has slight and homogeneous thickening. (**d**), Scan on bone window indicates no distinctive bone destruction of sinus wall

bone destruction. Reticular enhancement can be shown by enhanced scan.

MRI mainly shows extensive irregular lesions, retrobulbar fat replacement, and unremarkable deviation of optic nerves and ocular muscles. Because of the large amount of fibrous tissues, MRI examination shows isointense or hypointense on T_1WI, hypointense on T_2WI and proton density weighted, and the signal is heterogeneous. Inflammatory reaction area with hypointense on T_1WI and hyperintense on T_2WI can be seen posterior to the eyeball, which shows mild to marked enhancement by enhanced scan.

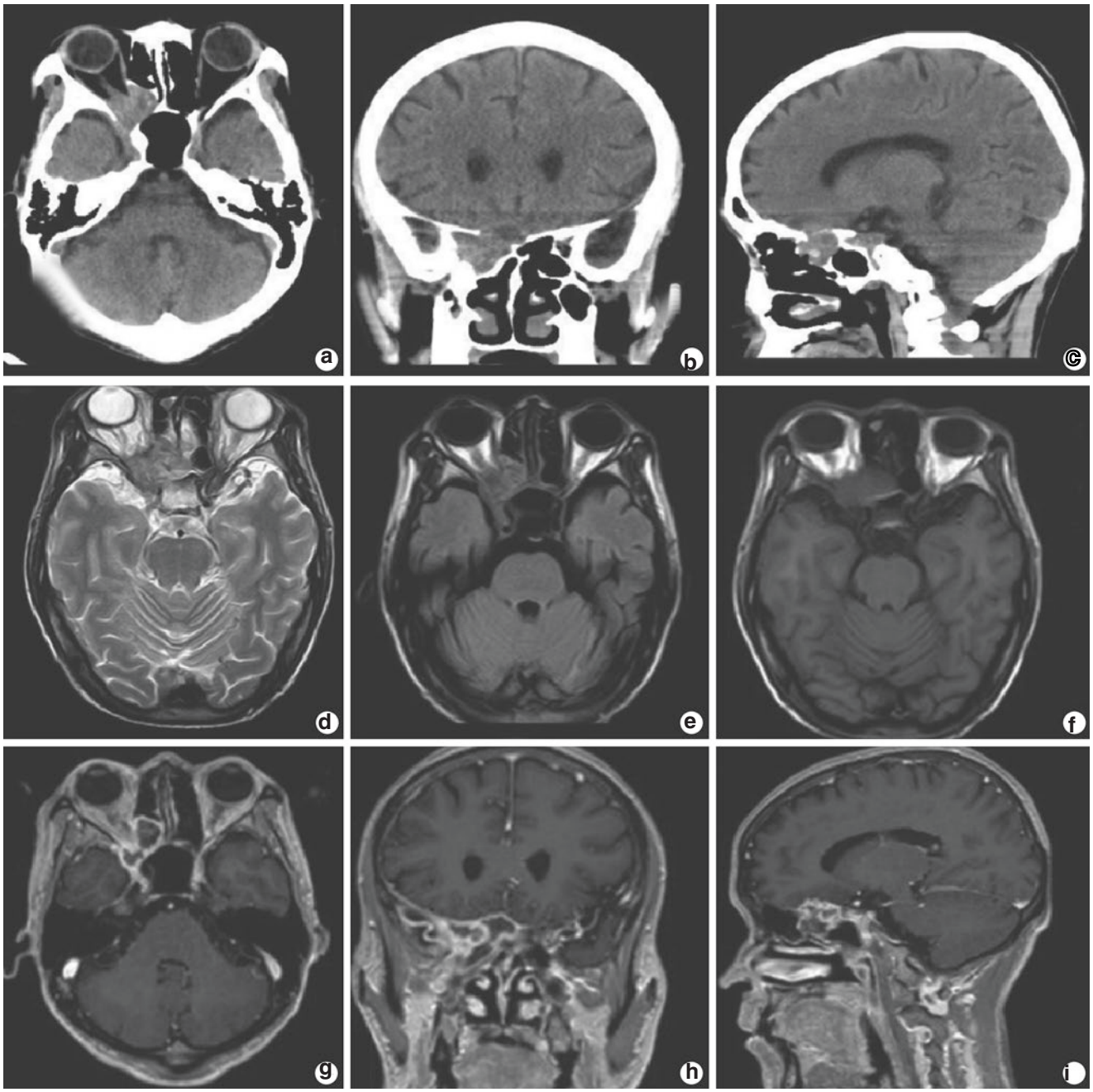

Fig. 23.32 Meningitis secondary to aspergillus ethmoiditis, subperiosteal abscess with cavernous sinus syndrome at orbital apex. A 41-year-old male patient. The patient had episodic headache for 3 months, the right eyelid could not be lifted up for 1 month, and aspergillus infection occurred in the posterior area of the right optic nerve. (**a**–**c**) Tri-planar reformation non-enhanced CT scan indicates mixed-density soft tissue mass of ethmoidal sinus in the right posterior group, which shows punctate calcification, eroding adjacent eroded medial optic canal, and breaking through anterior cranial fossa to form a slightly low-density fusiform eminence; (**d**–**f**) Non-enhanced MRI scan indicates the lesion showing isointense on T_1WI, heterogeneous signal (isointense and hypointense) on T_2WI, and slightly hypointense on T_2 FlAIR sequence. (**g**–**i**) Multiplanar MRI enhanced scan shows irregular lace-like enhancement around the lesion, and unremarkable enhancement in the central area, and fusiform annular wall enhanced abscess formed outside the dura mater of the anterior cranial fossa, involving the right orbital apex and cavernous sinus, and thickening and enhancement of the adjacent meninges (Images courtesy of Wang Wensheng, Guangdong 999 Brain Hospital)

2. *Rhabdomyosarcoma*. It is a common primary tumor in children, which manifests as soft tissue mass superior to the orbit posterior to the eyeball, with density similar to that of muscle and relatively homogeneous texture, and the necrosis density decreases heterogeneously in a few cases [3]. Infiltrative growth can invade optic nerve,

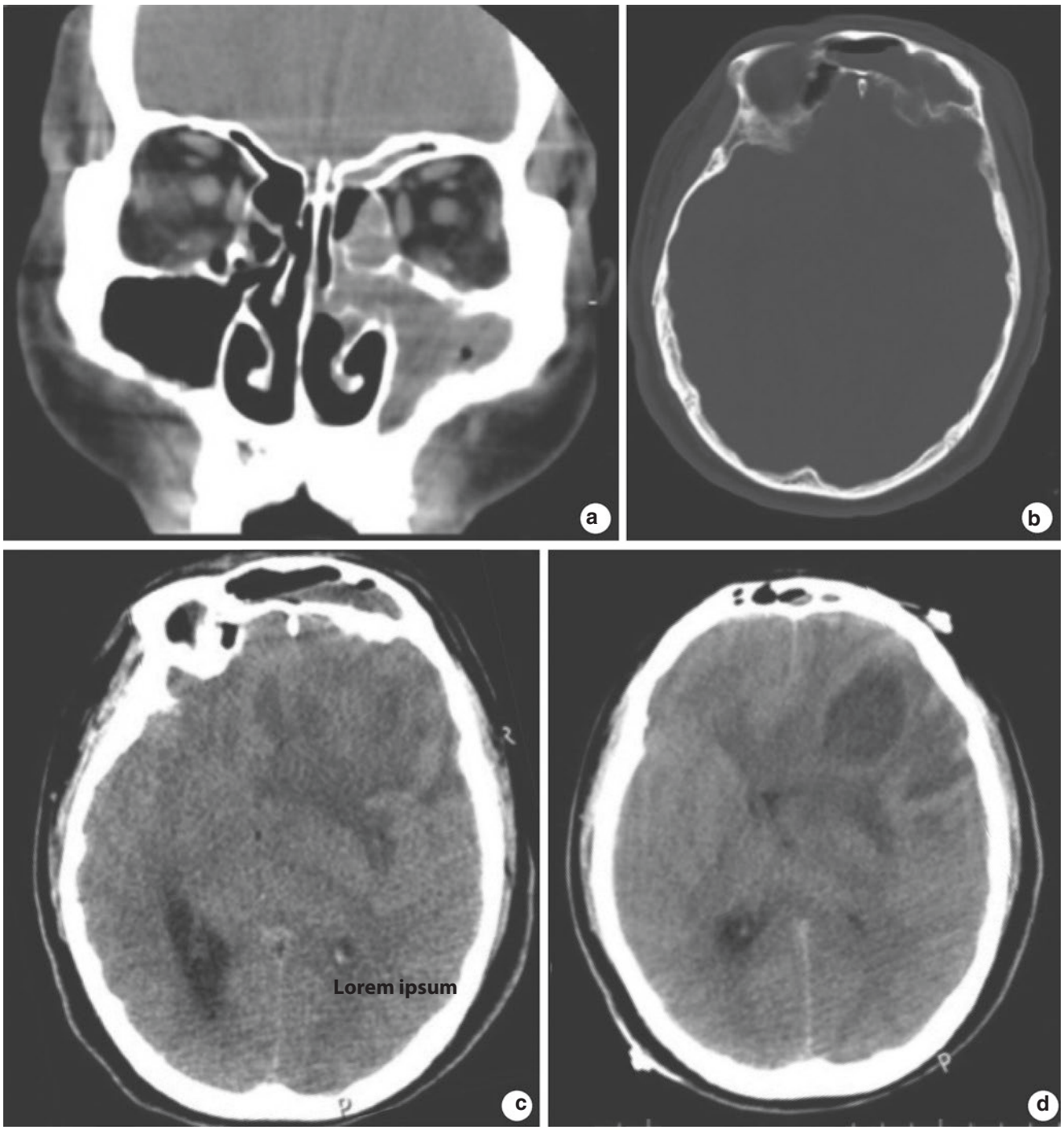

Fig. 23.33 Rhinogenic brain abscess. A 47-year-old male patient. (**a**) The non-enhanced coronal scan of paranasal sinus shows that the left half set of paranasal sinuses are filled with high-density shadows, and the sinus wall is not damaged, indicating that there is no abnormal density area in the brain parenchyma; (**b**–**d**) After 20 days, the non-enhanced cranial CT scan on bone window indicates that fissure shadow is faintly visible in the posterior wall of frontal sinus. The brain window shows that the left frontal lobe and left basal ganglia are covered with large patchy low-density shadows, and the right frontal lobe is involved along the corpus callosum, with liquefactive necrosis area in the center. Considering the formation of abscess, the abscess wall shows annular slightly high-density shadows, with visible large patchy low-density edema belt around it, showing significant occupying effect. The left frontal gyrus is swollen, the corticomedullary differentiation is unclear, the sulcus becomes shallow and disappears, and the supratentorial ventricle is deformed by compression

extraocular muscles, skull and paranasal sinus, and some bone erosion and destruction are observed at orbital wall, without inflammatory symptoms, so anti-infection is ineffective.

3. *Leukemia*. Childhood leukemia often invades the orbit and has rapid clinical progression. Extraocular muscles and optic nerves are thickened and kept in good shape. Granulocytic leukemia manifests as irregular soft tissue

masses posterior to the eyeball with homogeneous and isointense density, extensive moth-eaten bone destruction of skull base and orbital bone [22]. Radial spicules are found, and the signal intensity of marrow cavity decreases, which is mostly located in the orbital peripheral space in upper quadrant or subperiosteal space.

4. *Lymphoma*. It has slow onset, shows infiltration and spreading from soft tissue anterior to orbital septum to retrobulbar structure, with clear margin and high and homogeneous density. MRI shows isointense on T_1WI and slightly hyperintense on T_2WI, and enhanced scan indicates homogeneous and moderate enhancement. Bone density and signal are normal, enlarged lymph nodes are found in the neck, which are sensitive to radiotherapy [21].
5. *Wegener granulomatosis*. It is a multi-system disease with multiple organs involved, including nasal cavity, orbit and lung. Multiple orbital structures can be involved, and both the inner and outer space of muscle cone are involved, diffuse thickening of eye ring forms soft tissue mass with solid texture, homogeneous density, blurred edge, blurred fat space in orbit, enlarged lacrimal gland, thickened extraocular muscles and thickened optic nerve sheath, the mass can extend to orbital apex and involve cavernous sinus and pterygopalatine fossa. Meanwhile, the central structure of paranasal sinus is destroyed, and bilateral signs can be seen in the neoplastic bone formation.
6. *Non-infectious inflammatory lesions* Non-specific pathogen can cause iriditis of ocular cornea, resulting in thickening of eyeball wall, which can be complicated with

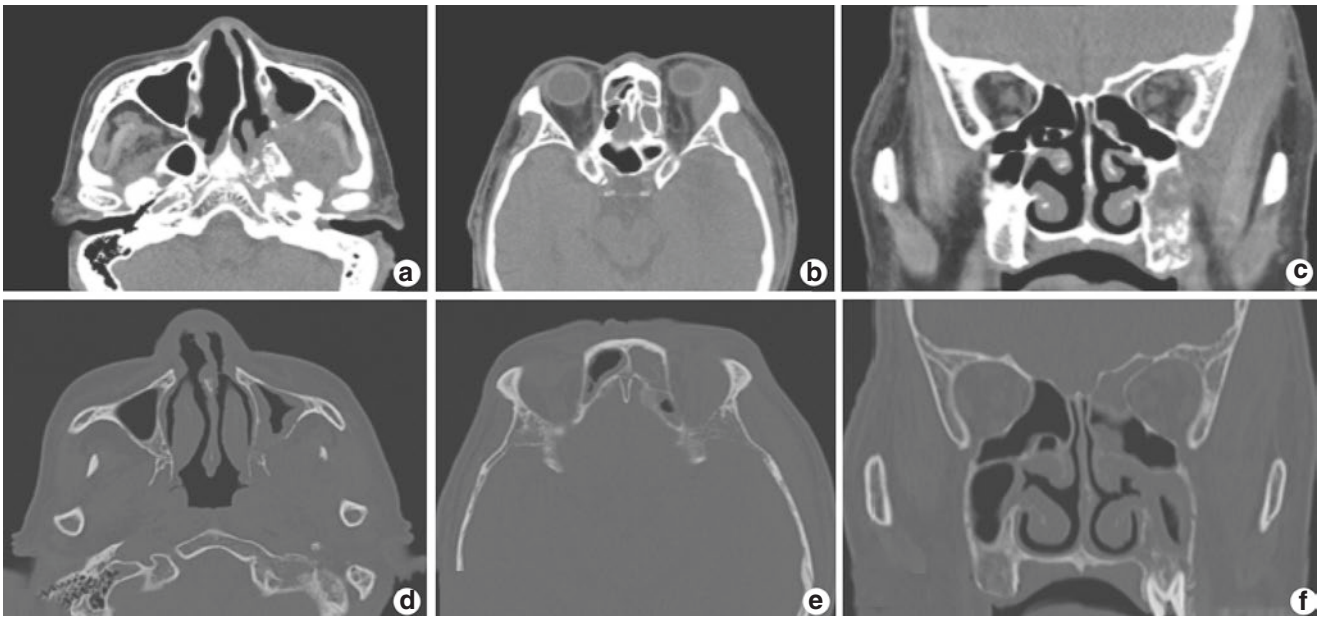

Fig. 23.34 Odontogenic paranasal sinus infection and secondary osteomyelitis of the jaws and skull, meningitis and brain abscess, and multiple abscesses in orbital and maxillofacial spaces. A 68-year-old male patient History of diabetes. (**a–c**). Non-enhanced CT scan indicates mucosal thickening of left frontal sinus, maxillary sinus, and bilateral ethmoidal sinuses. The fusiform vomica with slightly low density is formed inferior to the lateral periosteum of the left orbit. The soft tissues of the left pterygopalatine fossa and infratemporal fossa have swelling and the space is blurred. (**d–f**) CT on bone window shows that the left maxillary dental caries have residual roots, the space around the tooth roots widens, the density of alveolar process marrow cavity decreases heterogeneously, the bone in the posterolateral wall of the left maxillary sinus and the left pterygoid process of sphenoid bone is damaged and partially incomplete, and the density of bone marrow cavity of the left great wing of sphenoid bone decreases with blurred edges, showing manifestations as multiple osteomyelitis. (**g–l**) Non-enhanced MRI scan shows decreased signal intensity on T_2WI and T_1WI for alveolar process of left maxilla, thickening of peripheral soft tissue, and marginal bone erosion in left ascending ramus of mandible. The hyperintense of the left great wing of sphenoid bone and the lateral wall diploe of the left orbit disappear, and the bone cortex is blurred. Liquid hypointense on T_1WI and hyperintense on T_2WI are found in the left orbital peripheral space in upper quadrant and space anterior to orbital septum, and the wall is thickened homogeneously. There are multiple quasi-circular hypointense on T_1WI and hyperintense on T_2WI in the left temporal lobe, and a slightly hypointense ring on T_2WI is found around the lesion. The left sigmoid sinus is widened and irregular in shape. The sinus of left temporal mastoid bone is turbid, and the mastoid cell is filled with liquid signal shadows. The muscles of the left maxillofacial region are diffusely swollen, and the level of intermuscular space is unclear. (**m–r**) Enhanced MRI shows that the alveolar process of the left maxilla, the left great wing of sphenoid bone, and the lateral wall of the left orbit are enhanced heterogeneously, and the abscess of the left orbit has thin-walled ring enhancement. The abscess wall of the left temporal lobe formed, showing homogeneous thin-walled ring enhancement. The left temporal meninges were thickened and enhanced in a curved shape. By enhanced scan of the left sigmoid sinus, the contrast agent is not filled completely, showing hypointense filling defect shadows. The mucosal thickening of paranasal sinus shows irregular lace-like enhancement, but the enhancement of pus in the center of left frontal sinus is unremarkable. The left head and neck space show diffuse and heterogeneous enhancement, and the formation of irregular low-enhanced necrotic abscess is found locally

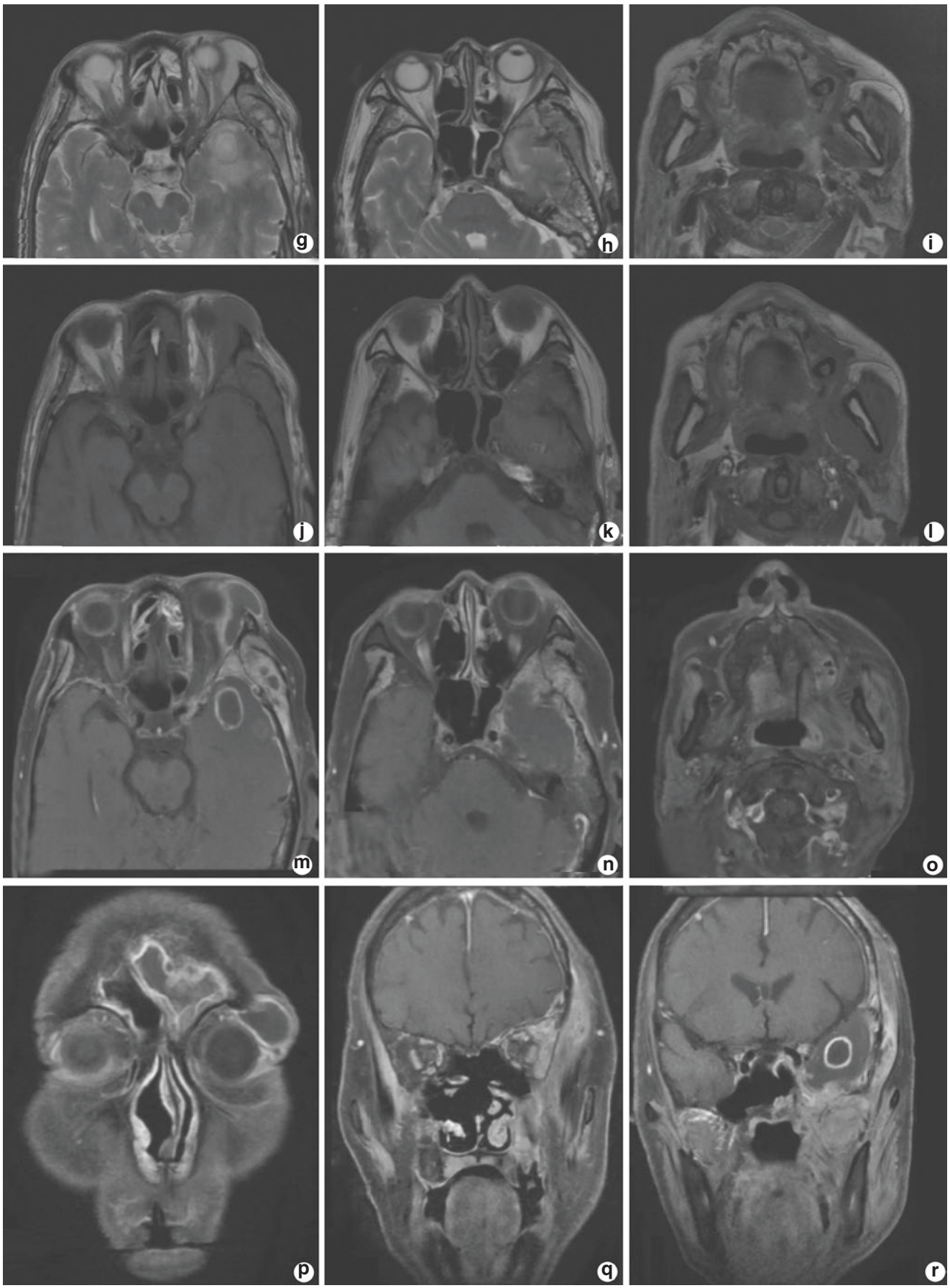

Fig. 23.34 (continued)

choroidal detachment, and ring enhancement is found by enhanced scan. Hormone therapy is effective, and imaging shows no characteristic manifestation.

23.5.6 Status Quo and Progress of Research

1. For orbital infectious lesion, the conventional CT examination can solve most clinical problems, and can directly show orbital wall destruction caused by the spread of rhinosinusitis.
2. Non-enhanced MRI scan and enhanced scan are the best imaging examination methods for diagnosing orbital infection, with high resolution of soft tissues, showing clear involvement of orbital structures, and the enhanced MRI directly shows the intracranial spread involving orbital apex, cavernous sinus, and meninges. MRI scan provides multi-directional and multi-sequence examination.
3. Orbital abscess has diffusion limitation and enhanced DWI signal, which can differentiate neoplastic lesions and judge the location and scope of lesions.

23.6 Rhinogenic Brain Abscess

23.6.1 Overview

Rhinogenic brain abscess is the most severe manifestation of rhinogenic intracranial complications, which can be found at any age, mostly in young and middle-aged people. Generally, it is caused by purulent bacterial infection of paranasal sinus and directly expands through valveless emissary vein at the skull base. Common pathogens of suppurative encephalitis include meningococcus, staphylococcus, bacillus influenzae, streptococcus pneumoniae, Escherichia coli, proteus, pseudomonas aeruginosa [23], and patients are subject to mixed infections in most cases. One or more complications may occur. Thrombophlebitis spreads to the skull and causes cavernous sinus thrombosis, and spreads to brain parenchyma to form purulent encephalitis and brain abscess, and meningeal involvement causes meningitis, subdural abscess and epidural abscess [24]. Fungal brain abscess is mostly found in patients with low immunity. Chronic invasive fungal infection and acute fulminant infection are easy to cause intracranial involvement. Most of the pathogens are Aspergillus and Mucor. Besides fungal granuloma in brain parenchyma, fungal aneurysm of internal carotid artery can also be formed.

The location of rhinogenic brain abscess is closely associated with the infection route, which is mostly secondary to frontal sinusitis, and it also can be secondary to maxillary sinusitis, sphenoid sinusitis, and ethmoidal sinusitis in rare cases, accounting for 10–20% of all patients with brain abscess. Rhinogenic brain abscesses mainly manifest as abscesses caused by frontal sinusitis in prefrontal part and orbital surface, followed by temporal lobe [23]. Biological behavior determines the spread and severity of infection. Abscess can be solitary or multiple. Abscesses are varied in shape and size, they can appear as round, oval, botryoidal, irregular and multilocular masses.

According to its development stages, brain abscess shows three clinical symptoms: in the stage of acute encephalitis, there are basic symptoms of rhinosinusitis, such as nasal obstruction, purulent nasal discharge and hyposmia, or acute systemic infection, such as fever; The main clinical manifestations in brain abscess formation stage are headache, vomiting, neck rigidity, optic disc edema, and other intracranial hypertension symptoms; Focal symptoms of brain are related to the location of abscess, which may show hemiplegia, hemianopia, aphasia, epilepsy and so on. Laboratory test shows that count of leukocytes increases and erythrocyte sedimentation rate increases rapidly.

23.6.2 Pathology Findings

The occurrence and development of suppurative encephalitis and brain abscess are combined as a continuous process, which cannot be definitely staged, but it can be divided into four stages according to different pathological manifestations [24].

1. *The stage of localized encephalitis and meningitis.* It lasts for 3–5 days, with congestion and edema of brain tissue, inflammatory cell infiltration, infiltration of multinucleated giant cells around blood vessels, gradual malacia and necrosis of the central lesion of encephalitis, and many small liquefaction areas. Inflammatory embolism of venules may show focal hemorrhage. Pathogenic microorganisms can be detected. Meningitis inflammatory reaction can be detected from superficial focus.
2. *Purulent necrosis stage.* It lasts for 4–10 days, and multiple necrotic and liquefied areas of encephalitis integrate into a large localized abscess, which may form multilocular brain abscesses by septa, with plenty of neutrophils, macrophages, and fibroblasts infiltration, with surrounding neovascularization and plenty of connective tissues proliferation, forming irregular inflammatory granulation tissues and adjacent gliosis.
3. *Capsule formation.* It often lasts for 1–2 weeks, the center of abscess has liquefactive necrosis, and granulation tissue, fibrillar connective tissue and neuroglia cells around the abscess proliferate to form abscess capsule.
4. *Advanced stage of capsule.* The abscess capsule is formed completely after 3–4 weeks or several months, and the

speed of capsule formation depends on the type and toxicity of pathogens, the immunity and the response to antibiotic treatment. The central vomica is reduced, the outer layer is thick wall formed by the proliferation of collagen and fibroblasts, and the innermost layer is suppurative effusion, granulation tissue and glial cells, plenty of new vessels, and neutrophil infiltration. The middle layer is composed of plenty of collagen fibers; The outer layer shows gliosis, brain edema, increased blood vessels and leukocyte infiltration. Meningitis manifests as congestion and edema of meninges, increased exudation of polymorphonuclear leukocytes and fibrin, inflammatory fragments in purulent cerebrospinal fluid sediments, congestion of ependyma, and choroid plexus. If the duration of disease is prolonged, it may cause collagenous fibrosis of meninges, adhesion of leptomeninges, and hydrocephalus due to ventricular obstruction. Cerebrospinal fluid shows increased protein and decreased glucose.

23.6.3 Imaging Findings

Intracranial infection can manifest as encephalitis, brain abscess, meningitis, ventriculitis, subdural empyema, vasculitis, arterial and venous cerebral infarction. Different infection routes and occurrence stages correspond to different imaging manifestations.

1. *X-ray examination.* X-ray plain films are insufficient for diagnosis of the disease in most cases. It shows inflammatory changes of frontal sinus, ethmoidal sinus or maxillary sinus are, occasional pneumatosis or liquid plane in abscess, and capsule calcification of chronic brain abscess.
2. *CT examination.*
   (a) Encephalitis and brain abscess, which is essentially intracranial focal pyogenic infection, show different CT manifestations due to different durations of disease.
      - Early stage of encephalitis: focal low-density focus with irregular shape and unclear margin at the subcortical/corticobulbar junction, which shows no enhancement or patchy and gyrus mild enhancement by enhanced scan.
      - Encephalitis in advanced stage: Encephalitis continues developing, the lesion center has necrosis and malacia, and gradually merges into a localized low-density area, and irregular and incomplete ring enhancement is shown around the area by enhanced scan [25]. The edema of peripheral brain tissue is obvious, the occupying effect is obvious, the gyrus is swollen, and the adjacent sulcus, fissure, cistern and ventricle are constricted, displaced or even disappeared by compression.
      - Early stage of capsule: necrotic tissue and inflammatory debris form a liquid density vomica, and the air-fluid level is found in rare cases with air abscess; surrounding complete or incomplete, regular or irregular slightly high-density fibrous capsule layer (Fig. 23.33). Enhanced scan indicates unremarkable enhancement of pus, complete but irregular mild ring enhancement of abscess wall, thick or thin annular wall, with blurred lateral wall border. After the abscess wall matures, a complete and homogeneous thin-walled enhancement ring is formed [25]. Compared with encephalitis, peripheral vasogenic brain edema is relieved, thus the occupying effect is relieved.
      - Capsule in advanced stage: After medical treatment or surgical aspiration treatment, the cavity of brain abscess collapses and contracts, the abscess decreases gradually, with density slightly higher than that of cerebrospinal fluid, the fibrous capsule is thickened, and the capsule wall is complete and smooth in ring shape or oval shape, with slightly high density, or is irregular. Enhanced scan shows marked enhancement, and ring enhancement can last for weeks to months and is gradually weakened or disappeared with time. Brain edema relieves and subsides.

   (b) Meningitis: the meninges are asymmetrically thickened with smooth appearance, the fissures and sulcus are shallow and fuzzy, the remodeling in high-density is found, the margin of gray matter is unclear, and enhancement is found by enhanced scan.

   (c) Ventriculitis: The pressure in the abscess is too high, resulting in local rupture of weak area of the abscess wall. If the abscess breaks into the ventricle, it will form a ventricular abscess, and high-density fragments will appear in the ventricle to form a liquid-liquid plane, and the ependyma will be thickened and enhanced. About half of the cases have cerebral hemispheric abscess complicated with dilatation to contralateral ventricle, while cerebellar abscess is often complicated with dilatation of contralateral ventricle and third ventricle.

   (d) Intracranial empyema: Epidural empyema and subdural empyema are located supratentorially, between the inner plate of calvaria and the brain parenchyma adjacent to the paranasal sinus with lesion, and a small part of subdural empyema is located beside the cerebral falx, with fusiform, stripy or crescent-shaped low-density liquid collection and marginal enhancement [24, 26].

(e) Primary lesion of paranasal sinus: the cavities of frontal sinus, ethmoidal sinus, and sphenoid sinus are full of inflammatory exudative lesions, and the posterior wall of frontal sinus, ethmoid plate and sphenoid sinus wall are partially ruptured or local osteomyelitis is caused (Fig. 23.34a–f).

3. *MRI examination.*
   (a) Encephalitis and brain abscess.
      • Early stage of encephalitis: It shows irregular isointense or slightly hypointense on T_1WI at the corticomedullary differentiation, while central inflammation, peripheral vasogenic edema, and accompanying infarction show hyperintense on T_2WI, with significant occupying effect. After Gd-DTPA enhanced scan, most of them show no enhancement, and a few of them show patchy or heterogeneous enhancement.
      • Encephalitis in advanced stage: Inflammatory necrotic areas integrate together and form localized abscesses, with center showing hypointense on T_1WI, hyperintense on T_2WI, and its periphery can show thin and irregular annular focus, showing isointense to slightly hyperintense on T_1WI, and isointense or slightly hypointense on T_2WI. Encephalitis and brain abscess have diffusion limitation, DWI signal intensity increases and ADC value decreases. Irregular and discontinuous ring enhancement is found by enhanced scan. In this stage, the peripheral vasculitis edema is the most significant, with a wide range of hypointense on T_1WI and finger-sheath edema belts with hyperintense on T_2WI. The normal contrast between gray matter and white matter disappears, the gyrus swells, the sulcus and fissure shallow and disappear, the ventricles are deformed by compression, and the midline structure displaces to the contralateral side.
      • Capsule formation stage: The sign of brain abscess formation is the appearance of abscess wall. The paramagnetic substances of collagen and reticular protein, focal hemorrhage, macrophage phagocytosis of free radicals in abscess wall shorten the relaxation time of local T_1WI and T_2WI. White matter shows annular isointense on T_1WI and slightly hypointense dark belt on T_2WI. The wall thickness of abscess is homogeneous, and the medial wall is smooth without nodules. Thin and homogeneous enhancement ring is found by enhanced scan, with clear and complete border. The pus in the vomica shows hyperintense on T_2WI and hypointense on T_1WI that is slightly higher than that of cerebrospinal fluid. There is a lot of protein and cellular components in pus, and the increase of viscosity results in diffusion limitation of water molecules. DWI sequence shows significantly hyperintense and ADC value decreases. SWI shows double-ring sign [26], with hypointense of outer ring and hyperintense of inner ring. Perifocal edema is relieved. The abscess wall rupture can form "sub-abscess" in the surrounding parenchyma, showing small nodular enhancement on the adjacent level. The multilocular abscess manifests as multiple connected enhancement rings (Fig. 23.34g, j, m and r).
      • Capsule in advanced stage: peripheral abscess wall is thickened, deep brain abscess wall is thinner than abscess wall proximal to cortex, T_2 hypointense gradually fades, enhancement decreases, central vomica contracts, ADC value increases. The pus shows hyperintense on DWI and relatively low MD value. MRS imaging: Creatine, N-acetyl aspartate and choline in abscess area decrease, and anaerobic glycolysis increases around the abscess area, showing peaks of acetate, lactate, alanine, succinic acid, pyruvic acid, and amino acids [26]. PWI or 3D-ASL perfusion imaging: During abscess wall formation, rCBV has little change, and rCBV in cyst decreases [24].
   (b) Meningitis: Inflammatory exudation causes hyperintense of T_2 FLAIR sequence in sulcus, fissure and cerebral cistern, especially in frontotemporal sulcus and basal cistern. By enhanced scan, the pia mater shows linear or gyriform enhancement, the thickened cerebral dura mater shows stripy enhancement, and the effusion has irregular enhancement. The T_2 FLAIR sequence with delayed enhancement is most sensitive to meningitis [26] (Figs. 23.32g–i, and 23.34m, n, q, r).
   (c) Ventriculitis: hydrocephalus dilation, with stratification in the ventricle, hyperintense of FLAIR sequence, with diffusion limitation, decreased ADC, ependymal thickening, and linear enhancement along the wall of ventricle. In the chronic stage, ventricular abscess formed inflammatory septa and small hollows.
   (d) Intracranial effusion and empyema: fusiform, stripy shadows or crescent-shaped pus accumulation in the epidural or subdural spaces [24], showing slightly hypointense on T_1WI, hyperintense on T_2WI, hyperintense on FLAIR relative to that of cerebrospinal fluid, hyperintense on DWI during empyema, linear hypointense of cerebral dura mater and deviation by compression. Peripheral inflammation and granulation tissue show marked enhancement (Fig. 23.32g–i).

(e) Other secondary changes: Fungal encephalitis can cause vasculitis, which manifests as abnormal T_2WI hyperintense shadow coursing along the blood vessels, and linear enhancement by enhanced scan. In the hyperintense area of DWI distributed along the blood vessels of secondary arterial cerebral infarction, artery stenosis or fungal aneurysm can be found by MRA. Secondary venous cerebral infarction is mostly located in the cerebral surface cortex. The hemorrhagic infarction shows hyperintense on T_1WI and hypointense on SWI, which is a "blooming effect." Magnetic resonance venography (MRV) can show venous sinus or cortical venous thrombosis, and enhanced scan shows the "empty triangle sign" (Fig. 23.34k and n).

4. *PET.* The uptake of ^{18}F-FDG and ^{11}C- methionine increased by brain abscess.

23.6.4 Key Points of Diagnosis

1. Nasal cavity and rhinosinusitis, exudate or soft tissue shadows. Headache, fever, and other systemic symptoms and meningeal irritation sign. Leukocytes increase significantly, and related pathogens can be detected from cerebrospinal fluid.
2. Different infection forms of encephalitis, brain abscess, meningitis, ventriculitis, and intracranial empyema can exist independently or simultaneously. Brain abscess has different imaging manifestations in different development periods. Encephalitis can cause secondary vasculitis, arterial cerebral infarction, venous cerebral infarction, hydrocephalus, and other complications.
3. CT scan shows the vomica of brain parenchyma has low density, the abscess wall shows isointense or slightly hyperintense density, the typical abscess wall shows homogeneously thin-walled marked ring enhancement, and the peripheral edema is obvious.
4. On MR scanning, the pus shows hypointense on T_1WI and hyperintense on T_2WI, and the abscess wall shows annular hypointense on T_2WI, surrounded by hyperintense edema belt. Encephalitis shows patchy enhancement in the early stage, irregular enhancement in abscess formation stage, smooth and complete thin-walled ring enhancement in capsule formation stage, and weakened enhancement in advanced stage of capsule. Meningeal thickening and linear enhancement. Marked ring enhancement with diffusion limitation is a typical manifestation of brain abscess.
5. Meningeal and ependymal thickening, linear enhancement, with hydrocephalus.
6. Intracranial empyema is located in the epidural or subdural space, showing fusiform or crescent-shaped changes, complicated with peripheral enhancement, limited DWI, and deviation of cerebral dura mater.

23.6.5 Differential Diagnosis

1. *Cerebral cysticercosis.* It often shows multiple cystic lesions. The scolex of eccentric growth can be found in the cystic cavity. Calcification often occurs in the scolex. The edema around the lesions is relatively mild. Cysticercosis necrosis shows enhancement of the scolex or mild ring enhancement.
2. *High-grade astrocytomas.* They are usually located in deep white matter, and often complicated with cystic degeneration, necrosis, and hemorrhage. Tumors show heterogeneous ring enhancement in thickness, irregular shape (lobulated or nodular shape), tumor with liquefactive necrosis, DWI generally shows hypointense, and relatively high-grade tumors show hyperintense in solid area. Choline peak on MRS spectrum increases.
3. *Brain metastatic tumor.* The metastatic tumor often occurs in middle-aged and elderly patients, and most of them have a history of primary malignant tumors. Generally, it shows multiple nodules complicated with significant brain edema, which is prone to necrosis and cystic degeneration. There are various ways of enhancement. The thickness of the cystic wall of some lesions with ring enhancement is heterogeneous, the medial wall is not complete and smooth, and mural nodules can be found. Most of the brain metastatic tumors show hypointense on DWI, the metastatic tumor showing hyperintense is rare.
4. *Intracerebral hematoma in evolution stage.* The absorption period of intracerebral hematoma covers history of trauma and cerebrovascular disease. In hematoma absorption, it is bean-shaped or kidney-shaped. CT scan shows high-density center of hematoma, the low-density periphery, and the peripheral thin layer with homogeneous capsule enhancement. MRI follows the signal evolution law of blood products in different periods.
5. *Demyelinating pseudotumor.* It may show ring enhancement in case of multiple sclerosis and during active stage of ADEM. The enhancement ring is usually incomplete and the occupying effect is mild.
6. *Subacute cerebral infarction.* The history of stroke, combined with the distribution of cerebral vessels, showing as gyriform enhancement by enhanced scan.
7. *Meningeal tumor.* Meningitis needs to be differentiated from metastatic tumor, cerebrospinal fluid implantation,

and metastasis of malignant central nervous system tumor, sarcoidosis, meningioma, RDD, and other tumorous diseases. Most meningeal neoplastic diseases show diffuse nodular enhancement, and most of them have a clear history of primary tumors.

8. *Tubercular meningitis.* The basal cistern and lateral fissure cistern are occluded, with increased density, the meninges of basal cistern are calcified in advanced stage, showing high-density tuberculoma, and obstructive hydrocephalus is common.
9. *Subdural hematoma.* Intracranial empyema needs to be differentiated from chronic subdural hematoma. MRI can show blood products. It is helpful to ask about medical history, auxiliary signs of fracture or rhinosinusitis for differential diagnosis.

23.6.6 Status Quo and Progress of Research

1. In clinical practice, non-enhanced MRI scan and enhanced scan are still the most routine imaging examination methods. Delayed T_2 FLAIR enhancement is more sensitive to meningitis and ependymatis than conventional T_1WI enhancement [26], and it is easier to highlight inflammatory lesions of meninges and brain tissues.
2. DWI is of great value in judging intracranial inflammatory lesions. DWI signal intensity increases and ADC value decreases, which is helpful to differentiate brain abscess from other neoplastic lesions. DWI is suitable for judging the location, nature, and scope of lesions, and it is easier to find complications such as disseminated sublesions. Moreover, DWI signal changes can also provide important information for the diagnosis of abscess staging.
3. Brain perfusion imaging (e.g., PWI and ASL) are often used to differentiate abscess from cystic tumor. Malignant brain tumors are rich in blood vessels, and break the blood–brain barrier, and have blood volume significantly higher than that of the abscess wall composed of collagen fibers.
4. SWI double-ring sign (hypointense of outer ring and hyperintense of inner ring) is helpful to differentiate it from other lesions with ring enhancement [26].
5. MRS can be used as an important supplementary imaging examination method to differentiate different metabolites. The anaerobic glycolysis of inflammatory lesions increases, the peak of lactate increases, and the peaks of acetic acid and succinic acid can appear. There are characteristic amino acid peaks in proteolysis of pus[25]. The liquefactive necrosis area lacks normal brain tissue metabolites, and NAA, Cho, and Cr peaks decrease or disappear.

23.7 Invasive Fungal Rhinosinusitis

23.7.1 Overview

Invasive fungal rhinosinusitis (IFRS) means the fungal hyphae invade the mucosa, submucosal blood vessels and bone of paranasal sinus, which often destroys the adjacent tissues and structures, involving multiple organs such as nose, orbit, and brain, with poor treatment effect and unfavorable prognosis. Most of the pathogens causing invasive fungal rhinosinusitis are aspergillus, followed by mucor, the disease mostly occurs in the paranasal sinus with poor drainage, and most of them are found in the maxillary sinus, followed by the sphenoid sinus and ethmoidal sinus. The disease occurs unilaterally in most cases, and can occur bilaterally [5]. Clinical findings indicate that it mostly occurs on the basis of chronic purulent rhinosinusitis and nasal polyps. Patients with low immunity (with diabetes and tumor) and treated with broad-spectrum antibiotics, chemotherapy, radiotherapy, adrenocortical corticoid, immunosuppressive agent, and patients undergoing intravenous intubation are at high risk of invasive aspergillosis. The aspergillosis lesions are relatively mild and limited, and most of them have chronic onset and are easily misdiagnosed as malignant tumors. They can be divided into chronic painless type and granuloma. Aspergillus infection is uncommon in patients with acquired immunodeficiency syndrome (AIDS), but the total mortality rate is 79%, which is worth heeding [6].

23.7.2 Pathology Findings

Invasive fungi can invade mucosal tunica intima and cause thromboarteritis; invade paranasal sinus mucosa and submucosal bone and cause bone wall necrosis, and sinus wall osteosclerosis and destruction coexist. Inflammatory granulation tissue in paranasal sinus grows slowly and continuously, destroying the bone of sinus wall and perisinusoidal tissues. Bloody pus, granulation tissue, necrotic tissue, and caseous tissue coexist in the lesion, which are similar to malignant tumor.

23.7.3 Imaging Findings

1. *X-ray examination.* The chronic invasive fungal rhinosinusitis is often limited to a single sinus. Plain film usually shows nasal soft tissue shadows, calcification, enlargement of nasal concha, floccus turbidity of one or more sinus cavities, heterogeneous annular mucosal thickening, no air-fluid level, destruction of sinus wall in the progressive stage, and involvement of nasal septum. Thus, it

is necessary to differentiate malignant tumors of paranasal sinus.

2. *CT examination.* It is common in maxillary sinus, followed by ethmoidal sinus and sphenoid sinus [3]. In the early stage, only non-specific mucosal thickening is found. In the progressive stage, soft tissue mass with heterogeneous density is found in the sinus, rare internal calcification, the mass expanding to the adjacent paranasal sinus and nasal cavity, coexisting bone destruction, proliferation and sclerosis of the sinus wall, forming a large bony defect, invasion to fat space around the sinus, resulting in increased density and further affecting pterygopalatine fossa, infratemporal fossa, orbit and intracranial structures, orbital wall, and skull subject to erosion and destruction, thickening of orbital soft tissues, involving extraocular muscles and optic nerve, and proptosis by compression (Figs. 23.35, 23.36a, 23.10a–c, and 23.11a).
3. *MRI examination.* As paramagnetic substances and mucin content affect magnetic resonance signals, it mostly shows isointense on T_1WI, heterogeneous and large patchy hypointense on T_2WI, with good performance in showing nerve invasion. Chronic invasive fungal rhinosinusitis often causes orbital apex cavernous sinus syndrome [27], in which the optic canal is invaded, the cavernous sinus is widened, the soft tissue mass shows heterogeneous enhancement by enhanced scan, the involved meninges are thickened with linear enhancement, the cavernous sinus segment of the internal carotid artery is subject to compressive deviation, and the blood vessels become thinner (see Figs. 23.36b–d, 23.10d–i, and 23.11b–i).

23.7.4 Key Points of Diagnosis

1. With the increasing incidence of diabetes and malignant tumor, the wide application of broad-spectrum antibiotics, chemotherapy, radiotherapy, adrenocortical corticoid and immunosuppressive agent in clinical practice, and the development of intravenous intubation technology, the incidence rate of invasive fungal rhinosinusitis increases, but it is easily ignored clinically because of its occult onset.
2. On a non-enhanced CT scan, the nasal cavity and paranasal sinus show multiple cotton-wool, filled solid lesions with increased central density, complicated with characteristic imaging manifestations of multiform calcification or ground-glass density shadows.

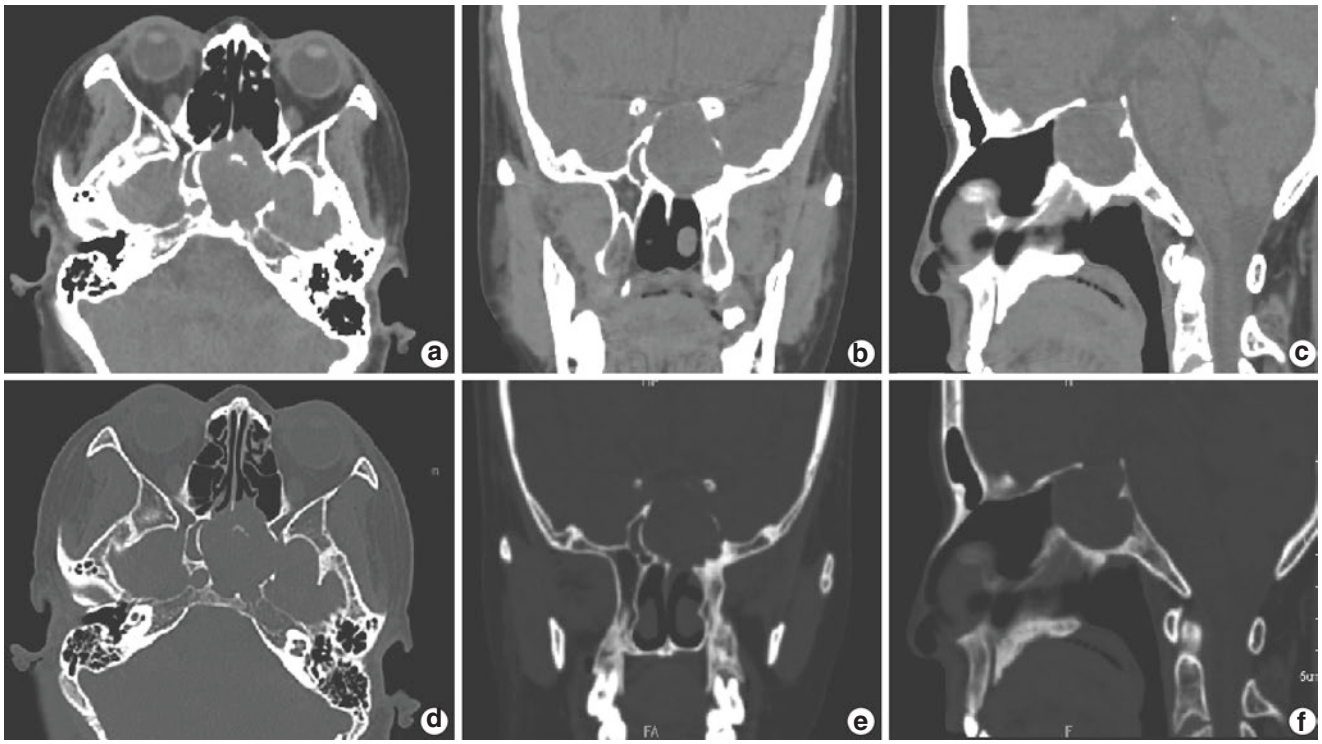

Fig. 23.35 Chronic invasive aspergillus rhinosinusitis of sphenoid sinus (1). A 57-year-old male patient. He was admitted to hospital due to headache for 1 year. (**a**–**f**) Non-enhanced CT scan indicates expansive dilatation of sphenoid sinus, soft tissue mass with stripy calcification in the mass, which invades the sella turcica upwards, local bone defect at the bottom of the sella turcica, protruding forward into the posterior ethmoidal sinus, and pressing the left bulbus caroticus backward, the corresponding eroded and destroyed bone wall forming a bony defect, without sclerotic margin

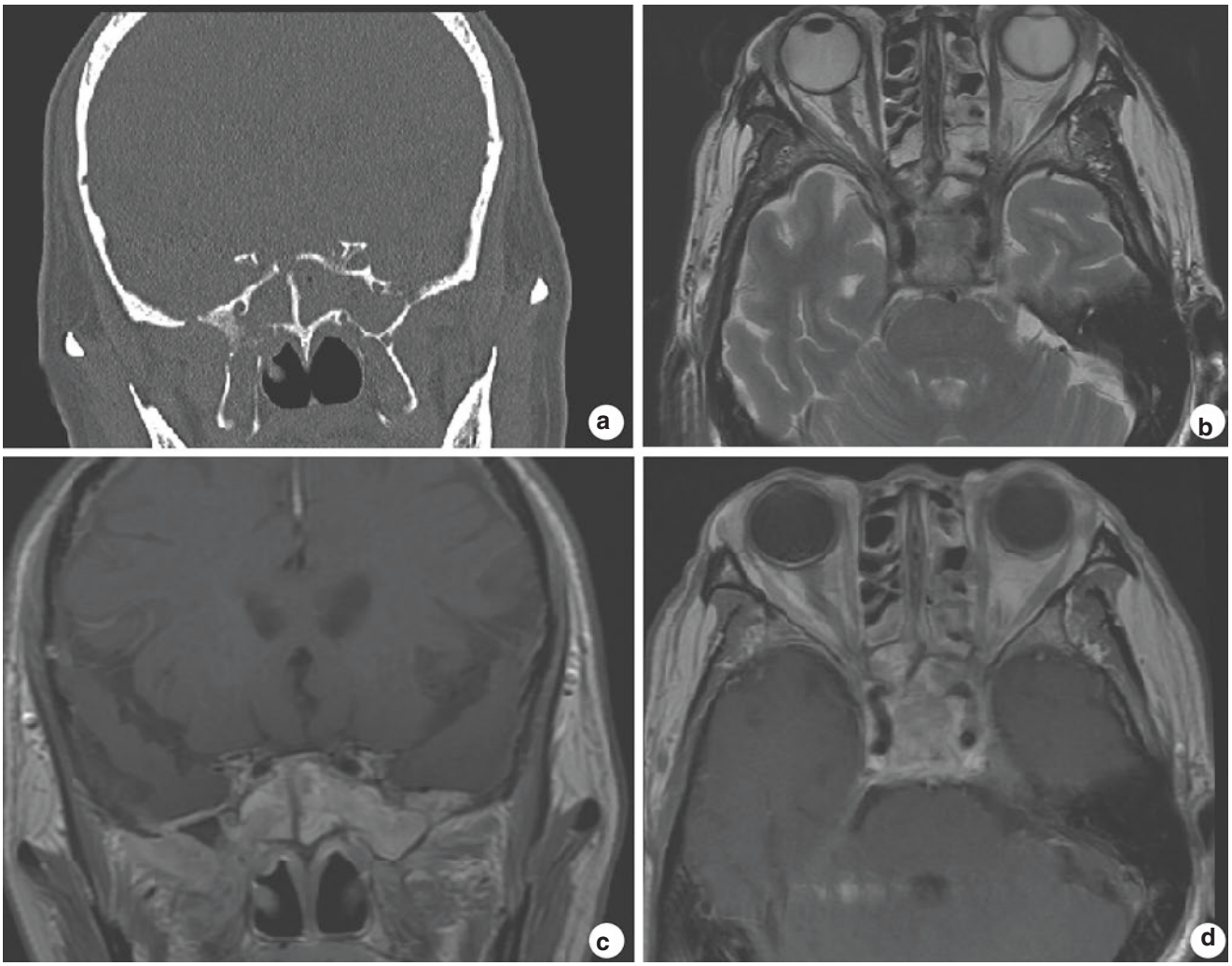

Fig. 23.36 Chronic invasive aspergillus rhinosinusitis of sphenoid sinus (2). A 46-year-old male patient. He was admitted to hospital due to headache for half a year. (**a**) Non-enhanced CT scan indicates that the sphenoid sinus is full of soft tissue shadows, which invades the sella turcica upwards, with local bone defect at the bottom of the sella turcica; (**b**) MRI shows that the soft tissue signal shadow in sphenoid sinus protrudes upward into sella turcica, and the margin with bilateral internal carotid arteries is unclear; (**c** and **d**) MRI enhanced scan indicates that the soft tissue signal shadow in sphenoid sinus shows marked and heterogeneous enhancement by enhanced scan

3. Non-enhanced MR scan shows hypointense or isointense on T_1WI, extremely hypointense on T_2WI, without solid enhancement, and can show marginal mucosa enhancement.
4. Chronic invasive aspergillosis manifests as rapid progressive erosion and destruction of bone, and extensive invasion to adjacent structures such as orbit, skull, and pterygopalatine fossa.

23.7.5 Differential Diagnosis

1. *Chronic rhinosinusitis.* It has a high incidence and a long duration. It commonly shows mucosal thickening and dense secretion of multiple sinus cavities. Calcification is rare, and calcification or ossification is less than 3% of all cases. Calcification is often located around the lesion and punctate and linear calcification is found along the sinus wall, and the sinus wall has osteosclerosis.
2. *Inverting papilloma.* It is a benign nasal tumor common in elderly men, which originates from the lateral wall of nasal cavity. Irregular lobulated high-density masses are found in the middle nasal meatus of nasal cavity, the surface is not smooth, and "bubble sign" is found in the masses, calcification is found in about 10%, and invaginated bone fragments are found in 40% of cases. The maxillary sinus shows isointense on T_1WI and hyperintense on T_2WI by MR. By T_2WI and enhanced T1WI, convoluted gyrus structures can extend to maxillary sinus, ethmoidal sinus, and nasopharynx, which can cause local

bone deformation, nasal septum deviation, bone absorption and destruction, and obstruction inflammation of unilateral nasal meatus of nasal cavity.

3. *Hemorrhagic necrotic nasal polyp.* Heterogeneous density of sinus, low-density inflammatory necrosis, and high-density hemorrhage appearing in a mixed way, [3] with mild enhancement by enhanced scan, enlargement and deformation of sinus, thinning of local bone due to absorption, difficulty in differentiating hemorrhage from calcification by CT, significant value of differentiating by MRI, hypointense of each sequence of calcification, and hypointense of fungal rhinosinusitis mostly located in the lesion center. Hemorrhage may show increased signal on T1WI, and most of hemorrhagic necrotic nasal polyps show marginal hypointense ring on T2WI.
4. *Mucous cyst.* It is common in single nasal cavity, especially in frontal sinus and sphenoid sinus. The sinus expands and is filled with a large amount of mucus. Mucin content affects CT density and MRI signal of cyst [27]. The imaging features are variable. Most lesions show low- or iso-density shadow, with hypointense on T_1WI and hyperintense on T_2WI. When mucin content is high, the density increases and T_2WI signal intensity decreases. T_1WI signal goes through a process from low to high and then to low. The sinus wall becomes thinner and is subject to compressive deviation.
5. *Nasal cavity melanoma.* The lesion is common in the elderly and presents multiple infiltrative growth. On CT, it appears as an irregular soft tissue mass, with deformation and destruction of peripheral bone. Melanin, hemorrhage and free radicals can shorten the time of T_1WI and T_2WI [9], showing isointense or slightly hyperintense on $_{T1}$WI, isointense or slightly low isointense on T_2WI, and mild enhancement by enhanced scan.
6. *Epithelial malignant tumor.* Malignant tumor of paranasal cavity or paranasal sinus shows limited scope, and mostly occurs in maxillary sinus and ethmoidal sinus. It has short duration, rapid progress, strong invasion, irregular moth-eaten osteolytic destruction of sinus wall bone, mostly without sclerosis, soft tissue mass with heterogeneous medium- to high-density and irregular shape, and MRI normally shows isointense. The occupying effect is obvious, the invasion to peripheral tissue structure is obvious, and the tumor has marked and heterogeneous enhancement by enhanced scan. Compared with fulminant fungal rhinosinusitis, the lesion of maxillary sinus carcinoma is unilaterally located in a single sinus, which is limited in location with long duration. With respect to the length of clinical duration of disease and the scope of bone destruction, chronic invasive fungal rhinosinusitis > sinus carcinoma > acute fulminant fungal rhinosinusitis.
7. *Olfactory neuroblastoma.* It manifests as a dumbbell-shaped soft tissue mass located at the center of ethmoid bont, showing calcification at the center and possible hemorrhage focus, with marked enhancement.
8. *Caseous rhinosinusitis.* It is obstructive chronic inflammation occurs to unilateral nasal cavity and paranasal sinus, showing hypertrophy of nasal mucosa, the hyperostosis and sclerosis of paranasal sinus, heterogeneous consolidation of tissues as necrotic substance in the sinus, no enhancement by enhanced scan, and possible compressive bone erosion with clear margin on the sinus wall and nasal septum.
9. *Rhinolith.* It is calcification in the nasal cavity caused by long-term calcium deposition centered on foreign matters, hemorrhage site, and ectopic teeth.

23.7.6 Status Quo and Progress of Research

Bone destruction found by CT is the main basis of invasive fungal rhinosinusitis. Strip-like ground-glass density lesions in paranasal sinus can also appear. Combined with serological allergic reaction and eosinophil granulocytosis, it reaches relatively high diagnostic coincidence rate. If there is invasion outside paranasal sinus and bone destruction, MRI can be used as a supplementary examination method. Chronic invasive fungal rhino-sinusitis is easily misdiagnosed as malignant tumor, which needs to be confirmed by pathology. In case of suspected fungal encephalopathy, the galactomannan (GM) test and β-D-glucan test on cerebrospinal fluid sampled by lumbar vertebra aspiration can improve the diagnostic method [7].

23.8 Maxillary Osteomyelitis in Infants and Young Children

23.8.1 Overview

Maxillary osteomyelitis has low clinical incidence and is mostly found in infants and young children. This section mainly introduces maxillary osteomyelitis in infant. Most of the related infections are caused by pathogen, such as staphylococcus aureus, followed by hemolytic streptococcus, diplococcus pneumoniae, staphylococcus albus, Escherichia coli, proteus and anaerobic aerobacteria, or it shows mixed infections. The etiology mainly includes the diffusion of local infection in maxillofacial region, or trauma or hematogenous infection.

1. *Odontogenic infection.* It is mostly found in clinical practice. Newborn maxilla is immature and is flat and wide in shape, with two rows of dental germs in it. Infections can diffuse to the maxilla through damaged oral mucosa or skin to form osteomyelitis in the following cases: bacteria

in the birth canal entering the maxilla through damaged alveolar mucosa during childbirth and cause infection; oral mucosa or dental germ damaged by improper feeding; and breastfeeding by mothers with mastitis.
2. *Rhinogenic infection.* Children have poor immunity and immature paranasal sinus with incomplete pneumatization, narrow paranasal sinus ostium. Therefore, if acute rhinitis or rhinosinusitis caused by upper respiratory tract infection or other infectious diseases prolongs, the inflammation will diffuse around and eventually lead to maxillary osteomyelitis.
3. *Hematogenous infection.* Newborns have thin maxillary cortex, abundant bone marrow, and good blood circulation. Therefore, bacteria can cause maxillary infection from any part of the body with infectious lesions by blood circulation, such as umbilical cord or skin infection, maternal birth canal infection, and iatrogenic infection.

In acute stage, its symptoms include congestion and edema of soft tissue on one cheek, hard palate or alveolus, swelling of nasal mucosa on the affected side, complicated with eyelid swelling and conjunctival edema, or proptosis, deviation, and ophthalmoplegia. It shows mucous purulent or bloody secretions are found in gums, hard palate, lower eyelid, medial and lateral canthus, and further develops to cheek abscess, intraorbital cellulitis, orbital abscess, or zygomatic abscess, which shows a sense of touchable fluctuation. The abscess will rupture naturally and form sinus or fistula in nasal cavity, palate, and cheek, with prolonged pyorrhea. After drainage and pus discharge, fistula can be healed or exist continuously. Sequestrum is found in maxilla, and dental germ is lost due to necrosis.

Maxillary osteomyelitis in infants and young children involves critical conditions and develops rapidly. Acute toxic symptoms such as chills and high fever exist in its acute stage, and convulsions and shock can occur in severe cases. In case of delayed diagnosis and treatment, it will lead multiple complications, even death. Common complications include orbital infection, sepsis, bronchopneumonia, lung abscess, nasal infection, pericarditis and pleuritis, and may be complicated with meningitis, brain abscess, cavernous sinus pyogenic thrombosis and blind, asymmetrical facial development, anodontia, or irregular dentition. Individual children may die of septicemia, bronchopneumonia, meningitis, or brain abscess.

23.8.2 Pathology Findings

Central osteomyelitis of the jaws mostly involves odontogenic infection. The central marrow cavity has congestion and edema in early stage, inflammatory cells have exudation and infiltration, and then spread along jaws to form focal or diffuse endosseous abscess, and cortex ulceration forms subperiosteal abscess and perimaxillary cellulitis, and the effusion contains necrotic fragments, neutrophils and pathogenic microorganisms. Chronic thromboangiitis causes osteonecrosis, sequestrum appears in the vomica, bony involucrum is eroded and destroyed by pus, thus forming fistula, with peripheral periosteal reaction, and hyperostosis and periosteal proliferation are formed by repair. Peripheral osteomyelitis of the jaws originates from cellulitis or subperiosteal infection in maxillofacial region, and diffuses from bone cortex to central marrow cavity. The pathological changes can refer to the central osteomyelitis of the jaws.

23.8.3 Imaging Findings

1. *X-ray examination.* It is limited in early diagnosis of the disease, and bone abnormality can only be found after 2 weeks.
   (a) Diffusive bone destruction stage: the alveolar process of maxilla is osteoporotic, the contour of bone trabecula is blurred and scattered punctate and patchy bone destruction or periosteal reaction is found.
   (b) Localized abscess stage: A large area of irregular radiolucent area due to bone destruction, with or without the formation of sequestrum, the contour tending to be clear, and sinus or fistula shown by lipiodol angiography.
   (c) Neoplastic bone formation stage: The lesion is limited with clear edge, the bone density is different, osmotic necrosis and repair sclerosis coexist, with low-density necrotic hollows and free sequestrum are in the center, and neoplastic bone formation can cause osteosclerosis and densification, increased and thickened bone trabecula, with peripheral layered thickened periosteum.
   (d) Healing stage: The local bone of the lesion shows eburnation and sclerosis, and incomplete repair causes structural deformation.
2. *CT examination.* It shows suppurative localized osteolytic bone destruction, marginal sclerosis strap, sequestrum formation, and granulation tissue enhancement.
   (a) Diffusive bone destruction stage: The bone marrow density in the lesion area decreases, and the punctate and patchy low-density bone destruction area is found. Some children show rhinosinusitis, dental caries, apical abscess, and other imaging manifestations. The cervical lymph nodes are enlarged (Figs. 23.37 and 23.38).
   (b) Localized abscess stage: large pieces of osteolytic bone destruction, showing liquid low density, air in

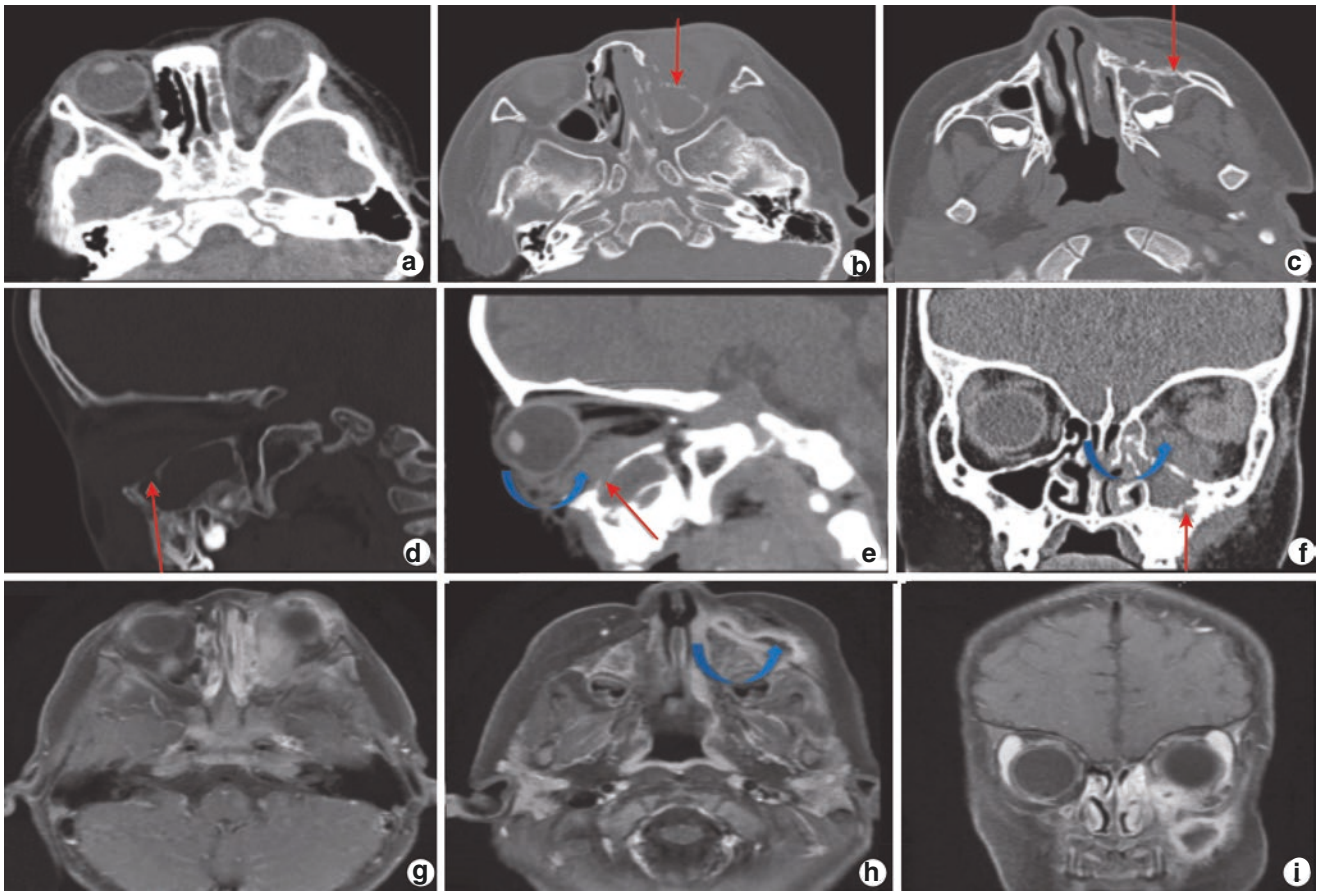

Fig. 23.37 Orbital surface cellulitis of paranasal sinus with maxillary osteomyelitis. A 2-year-old female patient. (**a**–**f**) Non-enhanced CT scan and MPR multiplanar reformation show less-developed paranasal sinus, increased density in left maxillary sinus and left ethmoidal sinus, the adjacent maxilla involved by inflammatory tissue destruction, the bone destruction of superior and anterior wall of maxillary sinus, heterogeneously decreased density of bone marrow cavity, discontinuous bone cortex, and periosteum lifted off. The increased density of the left orbit in the lower inner quadrant indicates cellulitis and subperiosteal abscess. (**g**–**i**) MRI enhanced scan indicates heterogeneous enhancement of the inflammatory tissue of orbital and facial regions, with cellular changes, and unremarkable enhancement of central pus. The deep multiple abscess along subperiosteal space of the anterior wall of maxillary sinus forms a stripy structure (red straight arrow: bone destruction; blue curved arrow: abscess)

some cases, the lesion localized with clear contour, and locally rupture of bone cortex. The subperiosteal abscess shows layered high-density shadows on the bone surface (Fig. 23.38e and f). Swelling of the surrounding maxillofacial soft tissues, disappeared fat space, blurred muscle contour, and reticular high-density shadows of the subcutaneous soft tissues. After liquefactive necrosis of soft tissues, central vomica is formed, with secondary intraorbital cellulitis (Fig. 23.38c, e and f). Enhanced scan shows heterogeneous enhancement of soft tissues, and cellular and lace-like enhancement can be seen if multilocular abscess is formed [3].

(c) Neoplastic bone formation stage: Necrotic hollows with clear contour formed in the center of vomica, with high-density sequestrum in it, and the cortex is destroyed to form drainage sinus [3], with heterogeneous sclerosis strap at the edge, and slightly enlarged jaw bone (Fig. 23.39).

(d) Healing stage: the sinus tract is closed, with stripy high-density shadows. Thickened periosteum forms lamellar ossification, bone hypertrophy and sclerosis, and incomplete repair causes jaw deformation [3].

(e) Marginal osteomyelitis of the jaws: initial thickening by periosteal reaction, inflammation spreading along subperiosteum, with linear low-density effusion and empyema, cortical destruction and absorption of alveolar bone with blurred margin, and swelling of peripheral soft tissue (Fig. 23.37c).

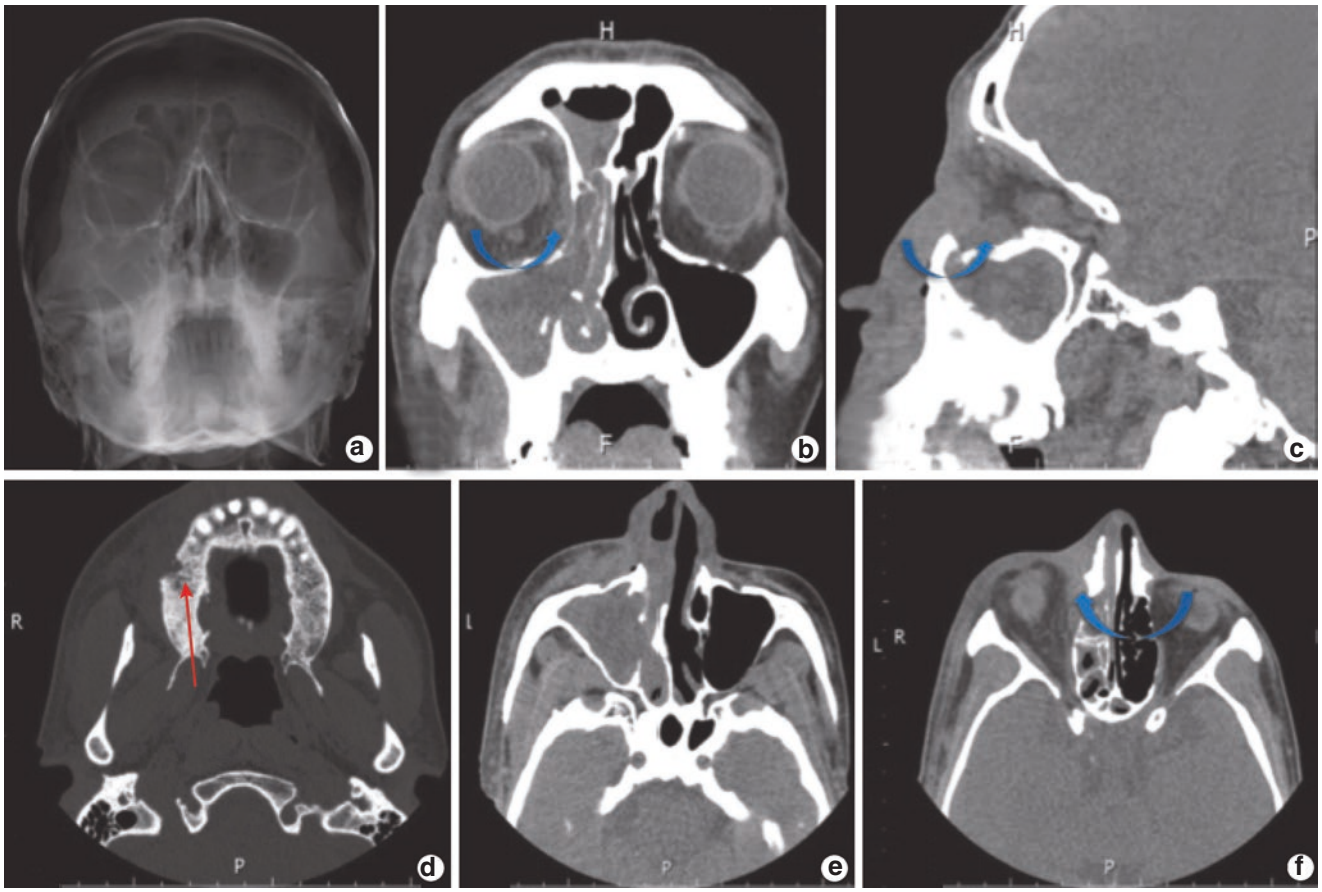

Fig. 23.38 Rhinogenic intraorbital cellulitis with maxillary osteomyelitis. A 59-year-old male patient. (**a**) The Water's plain film shows the paranasal sinus of right maxillary sinus, right ethmoidal sinus, and frontal sinus that are turbid with reduced transmittance and consistent ground-glass density shadows; (**b–f**) Non-enhanced CT scan indicates paranasal sinus of right half set filled with soft tissue density shadows and liquid plane is not found. Inflammatory tissue infiltrates the orbital wall, causing subperiosteal abscess in the right orbit and cellulitis anterior to orbital septum. The soft tissue in the right maxillofacial region and around the orbit is diffusely swollen, and punctate air density shadows are found locally. The fat space around the maxillary sinus wall is blurred, bone destruction is found in the maxillary alveolar process, the density is decreased heterogeneously, the edge is blurred, and the marginal bone cortex is incomplete

3. *MRI examination*

1. Diffusive bone destruction stage: MRI is sensitive to bone marrow edema in early stage, and the fat signal in marrow cavity is replaced, showing decreased signal intensity on T_1WI, heterogeneous hyperintense on fat suppression T_2WI, and blurred surrounding space.
2. Localized abscess stage: After abscess formation, the pus shows significantly hypointense on T_1WI and significantly hyperintense on T_2WI, the contour is clearer than that in acute stage, with hyperintense on DWI. Bone cortical involvement manifests as localized hyperintense areas in hypointense cortex showing hypointense. Periosteal thickening and subperiosteal abscess show layered hyperintense around cortex. Peripheral soft tissue has marked swelling, showing hyperintense on fat suppression imaging. The enhanced scan shows heterogeneous patchy and lace-like enhancement, indicating new granulation tissue, and hyperintense on DWI (Fig. 23.37g–i).
3. Neoplastic bone formation stage: the bone enlargement and deformation, the decreased signal of thickened bone cortex, and heterogeneously geographic changes of marrow cavity signal due to different degrees of fibrosis and sclerosis. All sequences of sequestrum and hyperplastic bone show hypointense, while the hollow and granulation tissue show slightly hyperintense on T_2WI. Soft tissue swelling is relieved.
4. Healing stage: The lesion area shows osteosclerosis, and the signal of marrow cavity of each sequence decreased.

23.8.4 Key Points of Diagnosis

1. The soft tissue of maxillofacial region is red, swelling, fever, and pain, and some lesions rupture with pus

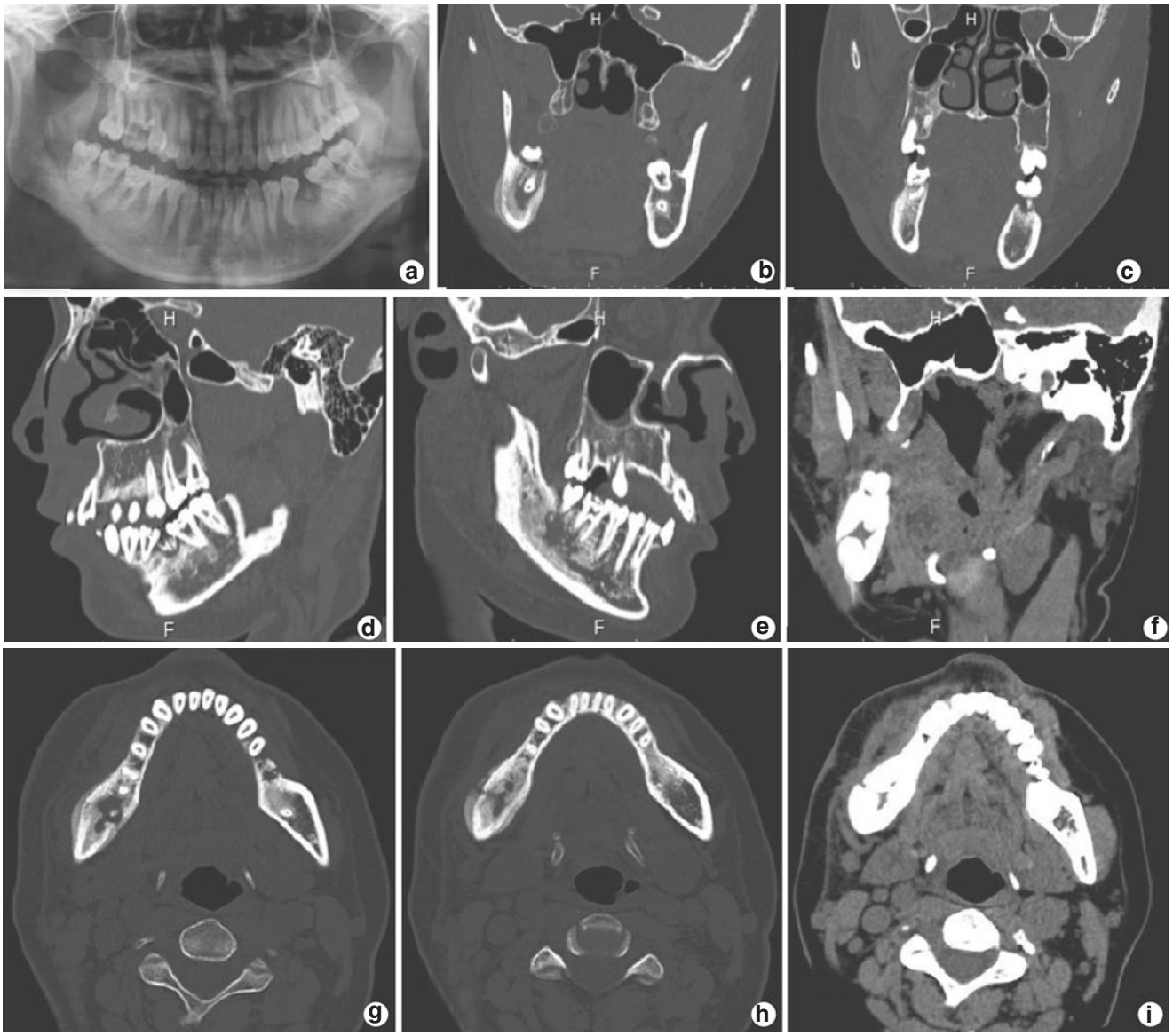

Fig. 23.39 Odontogenic osteomyelitis of mandible. A 24-year-old female patient. (**a**) X-ray oral panorama shows the residual root of the left lower first molar and the surrounding density is heterogeneous; The density around the apex of the right lower second molar decreased with unclear margin. (**b–i**) Non-enhanced CT scan indicates low-density bone destruction of left residual root, with surrounding sclerotic area; decreased density of marrow cavity around the right root tip, with irregular vomica; punctate and patchy high-density sequestrum in the center, incomplete local bone cortex with low-density tunnel, layered high-density shadows of peripheral periosteal reaction, and thickening of the skin and subcutaneous soft tissue around the sinus, with increased density

discharge. It is mostly caused by rhinosinusitis, dental caries or other causes, and maybe complicated with systemic infection symptoms.

2. CT scan indicates decreased density of jaw in acute stage, with patchy and moth-eaten bone destruction, central sequestrum formation, and peripheral periosteal reaction; soft tissue fistula formed in chronic stage, and gradual sclerosis and repair of jawbones.
3. MRI scan indicates bone marrow edema with hypointense on T_1WI and hyperintense on T_2WI, peripheral soft-tissue edema complicated with vomica formation. The pus shows significantly hyperintense on DWI sequence and heterogeneous patchy enhancement by the enhanced scan. Enlargement of cervical lymph nodes.
4. Laboratory test shows significantly increased leukocytes and increased neutrophils, and pathogen can be obtained by pus culture.

23.8.5 Differential Diagnosis

1. *Simple infection in maxillofacial region.* In early stage, it should be differentiated from acute dacryocystitis, erysipelas, simple facial cellulitis, and intraorbital cel-

lulitis. These diseases rarely occur in infants under 3 months old, with limited swelling of soft tissue and free of swelling of gums and hard palate. It shows clear anatomical contour and no bone destruction is found in jaw [28, 29].

2. *Tuberculosis of jawbone.* In adolescents, it shows painless swelling of maxillofacial region, most of the jaw bone destructions occur inferior to teeth, resulting in localized bone destructions with clear and irregular margins, most of which have no sequestrum or periosteal proliferation, and local cold abscess or sinus can be formed. The lamina dura line around dental germ of children disappears, and the teeth are completely normal.
3. *Periapical periodontitis and periapical abscess.* They are mostly confined to a single tooth, and the bone density of periapical alveolar process decreases.
4. *Abnormal fibrous proliferation of the jaws.* The jaw is enlarged, mostly manifesting as large-scale ground-glass homogeneous high-density shadows, unclear bone trabecular structure, and complete bone cortex. A few cases manifest as sclerosis of jaw or loofah sponge-like bright area, without thickening of soft tissue.
5. *Osteosarcoma of the jaws.* It has no symptoms of systemic infection and shows extensive osteolytic bone destruction with high-density osteosarcoma formation and solar radial periosteal reaction. Soft tissue masses are found in periphery.

23.8.6 Status Quo and Progress of Research

1. For suspected patients with osteomyelitis of the jaws, CT is the first choice for clinical examination, which can find low-density bone destruction and periosteal reaction of the jaws in time. The best imaging method is the enhanced CT examination, and the soft tissue window and bone window are applied to show the infiltration and destruction scope of the lesion.
2. MRI examination can find the scope of bone marrow edema and peripheral inflammatory exudation in early-stage depending on its high resolution of soft tissues, thus realizing early diagnosis and treatment.
3. ^{99m}Tc-MDP three-phase bone scan has high sensitivity and specificity to the diagnosis of osteomyelitis [30], but its application in infants and young children is limited due to its radiation.
4. Malignant tumors should be considered for prolonged soft tissue lesions with bone destruction, which requires a comprehensive evaluation by multiple imaging examinations.

References

1. Mafee M, Valvassori G, Becker M. Valvassori's imaging of the head and neck, edition 2. Liu Huaijun, et al, trans. Beijing: China Medical Science Press; 2011.
2. Harnsberger HR. Differential diagnosis of imaging experts - head and neck. Wang Zhenchang and Xian Junfang, trans. Beijing: People's Military Medical Press; 2012.
3. Yan S, Dehong L, Hengguo L, et al. Imaging of the head and neck·otolaryngology - head and neck surgery. Beijing: People's Medical Publishing House; 2014.
4. Dennison SH, Ask LS, Eriksson M, et al. Serious complications due to acute rhinosinusitis in children up to five years old in Stockholm, Sweden - still a challenge in the pneumococcal conjugate vaccine era. Int J Pediatr Otorhinolaryngol. 2019;121:50–4.
5. Ho CF, Lee TJ, Wu PW, et al. Diagnosis of a maxillary sinus fungus ball without intralesional hyperdensity on computed tomography. Laryngoscope. 2019;129(5):1041–5.
6. Seo MY, Lee SH, Ryu G, et al. Clinical pattern of fungal balls in the paranasal sinuses: our experience with 70 patients. Eur Arch Otorhinolaryngol. 2019;276(4):1035–8.
7. Candoni A, Klimko N, Busca A, et al. Fungal infections of the central nervous system and paranasal sinuses in onco-hematologic patients. Epidemiological study reporting the diagnostic-therapeutic approach and outcome in 89 cases. Mycoses. 2019;62(3):252–60.
8. Zhenchang W. Tongren Diagostic imaging manual of otorhinolaryngology head and neck surgery. Beijing: People's Military Medical Press; 2013.
9. Zuojun G, Bentao Y. Medical imaging atlas for Reading and diagnosis - head and neck. Beijing: People's Medical Publishing House; 2013.
10. Shuquan W, Zhenlian L, Yumei H, et al. The MSCT manifestations and clinical application of paranasal pediatric rhinosinusitis. Modern Medical Imageology. 2015;24(2):177–80.
11. Binbin Y. Pediatric Imageology and clinical pediatrics – head and neck and nervous system. Beijing: People's Military Medical Press; 2009.
12. Romero C, Bardo DME. Patient-friendly summary of the ACR appropriateness criteria: sinusitis-child. J Am Coll Radiol. 2019;16(8):35.
13. Kim HJ, Ahn HS, Kang T, et al. Nasal polyps and future risk of head and neck cancer: a nationwide population-based cohort study. J Allergy Clin Immunol. 2019;144(4):1004–10.
14. Calus L, Van BN, Bosteels C, et al. Twelve-year follow-up study after endoscopic sinus surgery in patients with chronic rhinosinusitis with nasal polyposis. Clin Transl Allergy. 2019;9:30.
15. Harnsberger HR. Differential diagnosis of imaging experts – head and neck. Translated by Wang Zhenchang and Xian Junfang. Beijing: People's Military Medical Press; 2012.
16. Zhenchang W. Manual of imaging diagnosis for otolaryngology, head and neck surgery of Beijing Tongren hospital. Beijing: People's Military Medical Press; 2013.
17. Wang X, Liu Y, Chen Q. Evaluation of multiparametric MRI differentiating sinonasal angiomatous polyp from malignant tumors. Neuroradiology. 2019;61(8):891–6.
18. Lasso JM, La Cruz ED. Reconstruction of wegener granulomatosis nose deformity using fascia lata graft. J Craniofac Surg. 2018;29(8):2179–81.
19. Kuan EC, Peng KA, Gonzalez LO. A case of squamous cell carcinoma of the nasal cavity in a patient with granulomatosis with polyangiitis (Wegener granulomatosis). Ear Nose Throat J. 2018;97(1–2):37–41.

20. Qi Z, Wei G, Shengzhong Z. Clinical and pathological study of Rhinoscleroma. Chinese Otolaryngology, Head and Neck Surgery. 2016;23(7):374–6.
21. Chandler JR, Langenbrunner DJ, Steuens ER. The pathogenesis of orbital complications in acute sinusitis. Laryngoscope. 1970;80(9):1414–28.
22. Junfang X, Dapeng S, Xiaofeng T. Imaging of the head and neck·ophthalmology. Beijing: People's Medical Publishing House; 2014.
23. Morrison JF, Narotam PK, Nathoo N. Rhinogenic metastatic brain and spinal cord abscesses in Crohn's disease. Clin Neurol Neurosurg. 2014;121:35–8.
24. Osborn AG. Brain imaging diagnostics. 2nd edition. Transated by Wu Weiping, Huang Xusheng, Zhang Xingwen, et al. Beijing: People's Medical Publishing House; 2013.
25. Mukherji SK. Clinical imaging of infections of central nervous system. 2nd edition. Translated by Wu Yuankui, Liu Xian, Lyu Guoshi, et al. Beijing: People's Military Medical Press; 2015.
26. Osborn AG, Digre KB. Neuroimaging. Transated by Lou Xin, Jiang Guihua. Beijing: Peking University Press, 2019.
27. Zhenchang W, Junfang X, Zhengyu Z. Manual of imaging diagnosis for otolaryngology, head and neck surgery of Beijing Tongren hospital. Beijing: People's Military Medical Press; 2013.
28. Feng Z, Chen X, Cao F, et al. Osteomyelitis of maxilla in infantile with periorbital cellulitis: a case report. Medicine(Baltimore). 2015;94(40):1688.
29. Krishnan N, Ramamoorthy N, Panchanathan S. Infantile maxillary sinus osteomyelitis mimicking orbital cellulitis. J Glob Infect Dis. 2014;6(3):125–7.
30. Bernadette·L. Koch, Bronwyn·E Hamilton, Patricia·A. Hudgins, et al. Imaging Diagnostics of the Head and Neck. Translated by Wang Zhenchang, Xian Junfang, Yan Fei, et al. Nanjing: Jiangsu Phoenix Science and Technology Press, 2019.

Part VI

Infectious and Inflammatory Diseases of Pharynx and Pharyngeal Space

Infectious and Inflammatory Diseases of Pharynx

24

Yang Cao, Xianjun Ye, Shuang Xia, Guoquan Li, and Meizhu Zheng

24.1 Chronic Pharyngitis

Overview

Chronic pharyngitis is a chronic inflammation of pharyngeal mucosa, submucosa, and lymphoid tissues. Diffuse pharyngeal inflammation is often a part of chronic inflammation of upper respiratory tract. Localized pharyngeal inflammation is mostly inflammation of pharyngeal lymphoid tissue. The disease is common in clinical practice, with long duration and easy recurrence [1].

Pathology Findings

Pathologically, chronic pharyngitis can be divided into the following 5 classifications:

1. **Chronic simple pharyngitis.** It is relatively common and manifests as chronic congestion of pharyngeal mucosa. The lesions are mainly concentrated in the pharyngeal mucosa layer, with abundant lymphoid tissue infiltration around the blood vessels, and infiltrations of leukocytes and plasma cells are also found. It shows proliferation of mucosa and submucosal connective tissue, complicated with hypertrophy of mucosal glands, hypersecretion of glands, and increased and viscous mucus secretions in some cases.
2. **Chronic hypertrophic pharyngitis.** It is also called chronic granular pharyngitis and lateral pharyngitis. Prolonged chronic simple pharyngitis can form chronic hypertrophic pharyngitis, which is common in clinical practice. The mucosal layer of pharynx is congested and thickened, with an extensive proliferation of connective tissues and lymphoid tissues in mucosa and submucosa, lymphadenosis and eminence around the mucosal gland. Multiple granular lymphoid follicles are found in the posterior pharyngeal wall, which present as chronic congestion, or integration of multiple lymphoid follicles. Inflammatory effusions from mucosal glands can be enclosed, and cystic white spots are formed at the eminence top of lymphoid granules, with yellow-white effusions in case of rupture. The lymphatic tissues of the lateral pharyngeal bands are often involved, leading to cord-like hypertrophy and thickening.
3. **Atrophic and dry pharyngitis.** It is rare in clinical practice. In the early stage of the disease, the secretion of mucosal glands decreases, and the secretion is thick and dry. Because of the chronic inflammation of submucosa, it has gradual organization and contraction, which compress glands and blood vessels, reducing gland secretion and leading to dystrophia, thus the mucosa and submucosa are atrophied and thinned gradually. There may be dry scab or pus scab attached to the posterior pharyngeal wall, which often has a bad smell.
4. **Chronic allergic pharyngitis.** It is also known as chronic allergic pharyngitis, which is an IgE-mediated type I allergic reaction occurring in pharyngeal mucosa. Allergen stimulates pharyngeal mucosa and makes IgM-synthesized plasma cells transformed into IgE-synthesized plasma cells, and IgE adheres to the surface of mastocytes and basophilic granulocytes, making pharyngeal mucosa in a sensitized state. When the same allergen contacts with the body again, the allergen combines with the IgE on the surface of mediator cell, which leads to degranulation of mediator cells, releasing a variety of inflammatory mediators including histamine and

Y. Cao
Shiyan Renmin Hospital, Affiliated People's Hospital of Hubei University of Medicine, Shiyan, China

X. Ye
Anhui Provincial Hospital, Hefei, China

S. Xia (✉)
Tianjin First Central Hospital, Tianjin, China

G. Li
Chongqing Three Gorges Central Hospital, Chongqing, China

M. Zheng
Tianjin Third Central Hospital, Tianjin, China

H. Li et al. (eds.), *Radiology of Infectious and Inflammatory Diseases - Volume 2*,
https://doi.org/10.1007/978-981-16-8841-6_24

synthetic prostaglandins, which can cause telangiectasia, increased vascular permeability and increased gland secretion, thus causing allergic reactions.

5. **Chronic reflux pharyngitis.** Inflammatory cells infiltration in pharyngeal mucosa and submucosa, causing gradual contraction and thinning of mucosa and submucosa of gland.

Imaging Findings

In clinical practice, inflammation can be definitively diagnosed without imaging examination. In case of poor treatment effect, imaging examination is required to exclude other related diseases. CT and MRI show diffuse swelling and thickening of mucosa of posterior wall and lateral wall of nasopharynx roof and torus tubarius, with straight or curved concave anterior border, bilateral pharyngeal recess structure existing with clear parapharyngeal space, smooth mucosa surface, and narrow nasopharyngeal cavity. CT shows iso-density shadows (Fig. 24.1). Slightly hypointense on T_1WI and slightly hyperintense on T_2WI (Fig. 24.2). By enhanced scan, the mucosal surface shows homogeneous and marked enhancement, with complete mucosal line. The criteria for judging the thickening of the posterior wall of nasopharynx roof: the thickness of the posterior wall of nasopharynx roof measured on the median sagittal plane T_1WI is not less than 5 mm, indicating thickening of the posterior wall of nasopharynx roof [2, 3].

Key Points of Diagnosis

1. Continuous history of pharyngeal discomfort for more than 3 months, the patient's pharyngeal mucosa is chronically congested, with varicose and dark-red small blood vessel, with a small amount of sticky secretion on the surface or multiple eminences of granular follicles on the posterior pharyngeal wall, showing chronic congestion, and the lymphatic tissue of the lateral pharyngeal bands

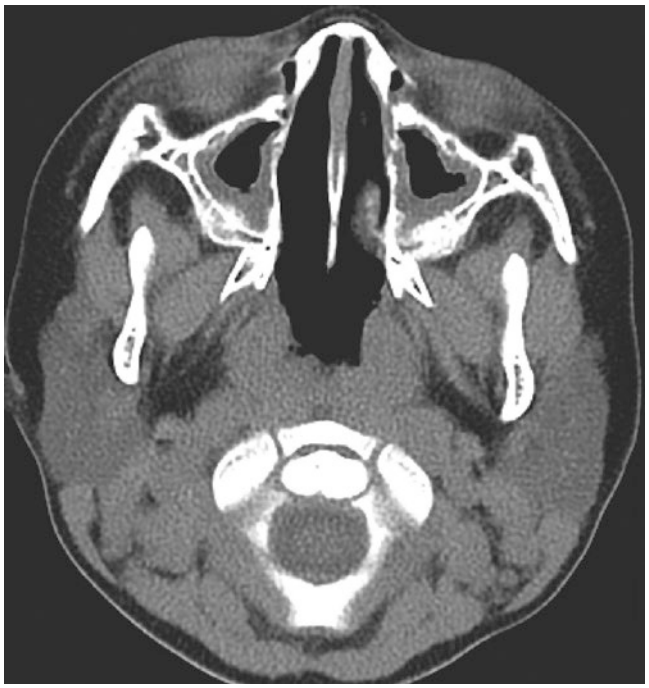

Fig. 24.1 Chronic pharyngitis (1). Axial CT images show that the soft tissues of the lateral wall and posterior wall of nasopharyngeal cavity are thickened with irregular shape. Bilateral pharyngeal recess structure existed

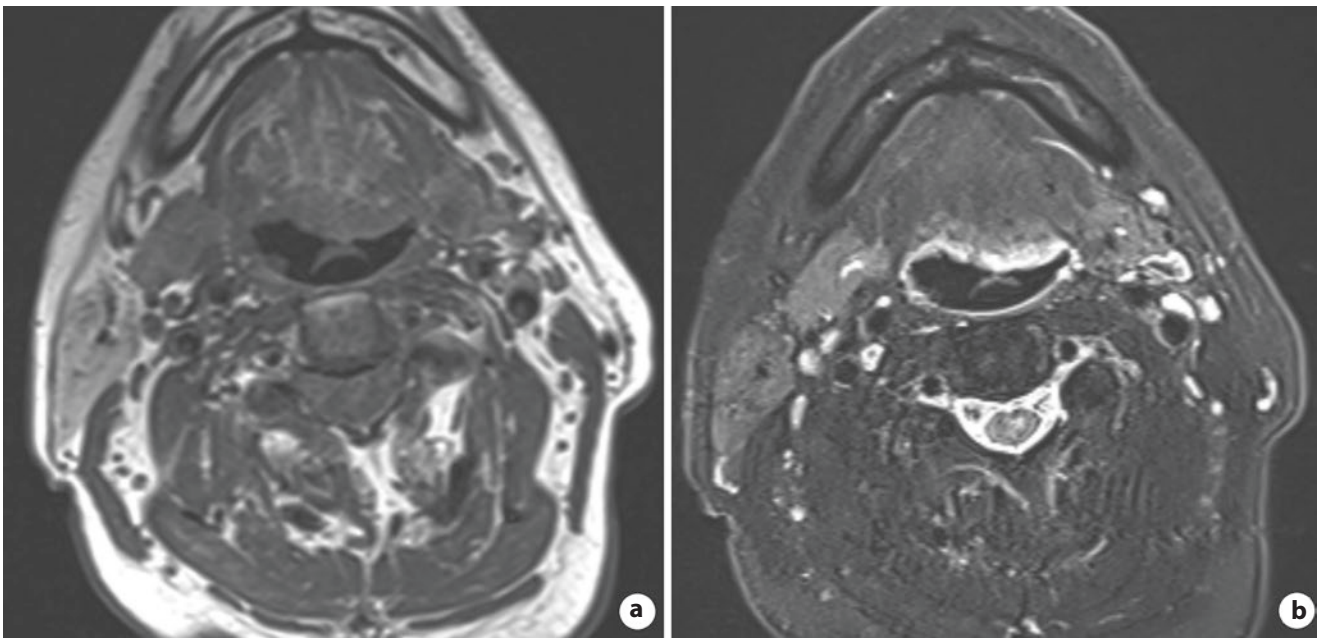

Fig. 24.2 Chronic pharyngitis (2). Axial MRI images show thickening of soft tissue of tongue root, isointense on T_1WI (**a**), hyperintense on fat-suppressed T_2WI (**b**) and hyperintense of surface mucosa

thickened in a strip pattern, or the pharyngeal mucosa is dry and thin, covered with purulent scab.
2. CT and MRI show that the soft tissues of the lateral and posterior walls of nasopharyngeal cavity were thickened in irregular shape. Bilateral pharyngeal recess structures exist, and there is no swelling of cervical lymph nodes and no infiltration of parapharyngeal structures.

Differential Diagnosis

1. **Adenoid hypertrophy.** Chronic pharyngitis and adenoid hypertrophy would manifest as thickening of the posterior wall of the nasopharyngeal roof, which makes it difficult to differentiate. However, the former has low thickening degree of the posterior wall of the roof, while the latter has significant thickening of the posterior wall of the roof, narrowing the airway. Adenoid hypertrophy mostly occurs in children and gradually atrophies after puberty. In addition, chronic pharyngitis can cause diffuse swelling and thickening of mucosa of posterior wall and lateral wall of nasopharyngeal roof and torus tubarius.
2. **Tornwaldt cyst.** It is found by accident and has unremarkable clinical symptoms. It is mostly located inferior to the mucosa of the midline of nasopharynx, and the soft tissue in the midline of the posterior wall of nasopharynx is slightly thickened and locally protruded, with 2–10 mm round or oval cystic lesions, which are easy to differentiate.
3. **Nasopharyngeal carcinoma.** It usually occurs in the pharyngeal recess, which manifests as asymmetric shallowing and disappearance of the pharyngeal recess and enlargement of levator veli palatini muscle in the early stage. Nasopharyngeal cavity masses can be formed with curved convex edges, irregular surface, asymmetric constriction of nasopharyngeal cavity and frequent invasion to parapharyngeal space and bone of skull base. Chronic pharyngitis usually manifests as diffuse swelling of nasopharyngeal soft tissue, smooth mucosal surface, clear margin with adjacent muscles, without bone destruction or infiltration.
4. **Nasopharyngeal lymphoma.** It can also cause diffuse thickening of the posterior wall and lateral wall of nasopharyngeal roof, which needs to be differentiated from chronic pharyngitis. The mucosal thickening caused by chronic pharyngitis is more homogeneous, and the degree of mucosal thickening is less than that of nasopharyngeal lymphoma. Nasopharyngeal lymphoma can cause swelling of cervical lymph nodes and infiltration of parapharyngeal structures. In addition, nasopharyngeal lymphoma is often associated with other systemic symptoms.

Status Quo and Progress of Research

The diagnosis of chronic allergic pharyngitis mainly depends on clinical manifestations. In addition to the corresponding allergen exposure history, symptoms and signs, allergen skin test, total IgE and serum-specific IgE should be used to determine the allergens. Chronic reflux pharyngitis can be tested by gastroesophageal reflux-related items.

It should be noted that many systemic diseases (especially tumors) only have symptoms similar to those of chronic pharyngitis in the early stage. Therefore, when the chief complaint does not coincide with the findings of physical examination or there are other doubts, we should not rashly diagnose it as chronic pharyngitis, but ask about the medical history in details, and thoroughly and carefully examine the occult lesions in nose, pharynx, larynx, trachea, esophagus, neck and even the whole body to avoid missed diagnosis. Imaging examinations of CT and MRI are used to exclude space-occupying lesions such as nasopharyngeal carcinoma. MRI can clearly show the soft tissue morphology of nasopharyngeal walls, mucosal or submucosal infiltration, muscle or intermuscular space involvement, shape and signal changes of parapharyngeal space, and the constricted nasopharyngeal cavity. CT can show the bone destruction of skull base, and can also be used to observe the shape of bilateral pharyngeal recesses and space-occupying lesion.

24.2 Adenoidal Hypertrophy

Overview

Adenoid, also known as pharyngeal tonsil or paraphyte, is located at the nasopharyngeal roof and the posterior pharyngeal wall, belonging to lymphoid tissue, with an orange slice-like surface. Under normal physiological conditions, pediatric tonsils develop to the maximum when children are 6–7 years old, and then gradually atrophy after puberty, and basically disappear when they are adults. Adenoid hypertrophy refers to pathological proliferation of adenoids due to repeated stimulation by inflammation, which causes nasal obstruction and mouth breathing, especially at night, with snoring and restless sleep. Children often turn over from time to time, especially when lying on their backs, and may have apnea in severe cases. The disease often occurs in children and is often complicated with chronic tonsillitis. The disease has a far-reaching impact on the normal development and health of children [4, 5].

Pathology Findings

Nasopharyngeal adenoid cells have proliferation and hypertrophy, which may be complicated with lymphocyte proliferation.

Imaging Findings

1. X-ray lateral view shows enlarged adenoids and narrow nasopharyngeal airway (Fig. 24.3). Lateral X-ray photography is an important method to diagnose adenoid hypertrophy. When taking lateral views of nasopharynx, it must be exposed when inhaling. When inhaling, the soft palate reaches the lowest position, and the anteroposterior diameter of nasopharyngeal cavity is the largest. At this time, the stenosis of nasopharyngeal cavity is reliable. Specific criteria: the ratio of the thickness of adenoid to the width of nasopharyngeal airway (A/N) is used to judge the hypertrophy degree of adenoid: result of less than 0.6 indicates normal condition; 0.61–0.70 indicates mild hypertrophy; more than 0.71 indicates pathological hypertrophy. The A/N ratio of plain film of nasopharynx can not only reflect the size of adenoids but also describe the nasopharyngeal airway volume, which provides reliable bases for clinical diagnosis and treatment [6].
2. CT and MRI can clearly show thickening of nasopharyngeal soft tissue, and compression of pharyngeal ostium of auditory tube and pharyngeal recess. The nasopharynx mucosa is intact (Figs. 24.4 and 24.5). It clearly shows that the nasopharyngeal cavity is deformed and constricted, the soft tissue of the posterior wall is thickened, protruding to the air cavity, the density or signal is homogeneous, the pharyngeal recess and pharyngeal ostium of the auditory tube are not clear, the parapharyngeal space is clear, without adjacent bone destruction. CT and MRI

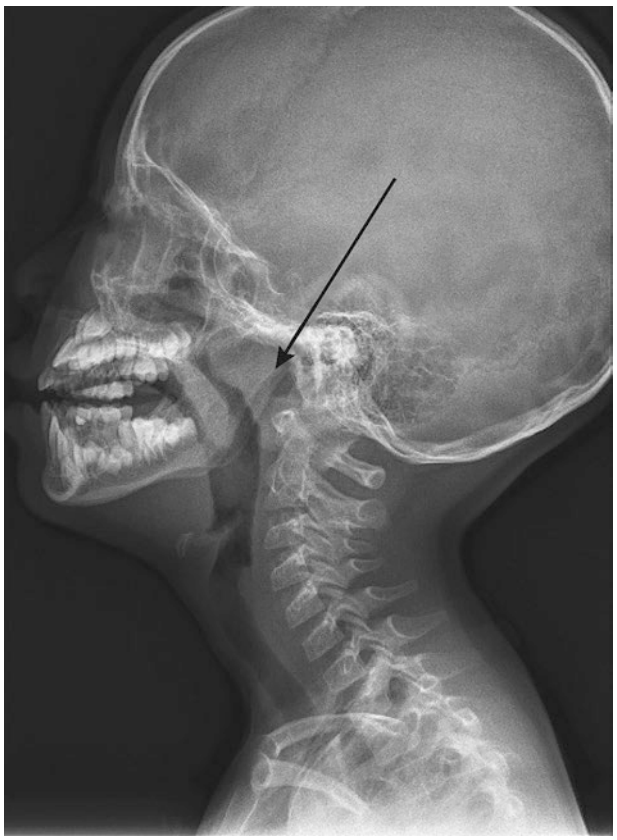

Fig. 24.3 Adenoid hypertrophy (1). A 5-year-old female patient, snoring while sleeping. Nasopharyngeal lateral view shows that the soft tissue of the posterior wall of nasopharyngeal cavity is significantly thickened and the airway is constricted (indicated by arrow)

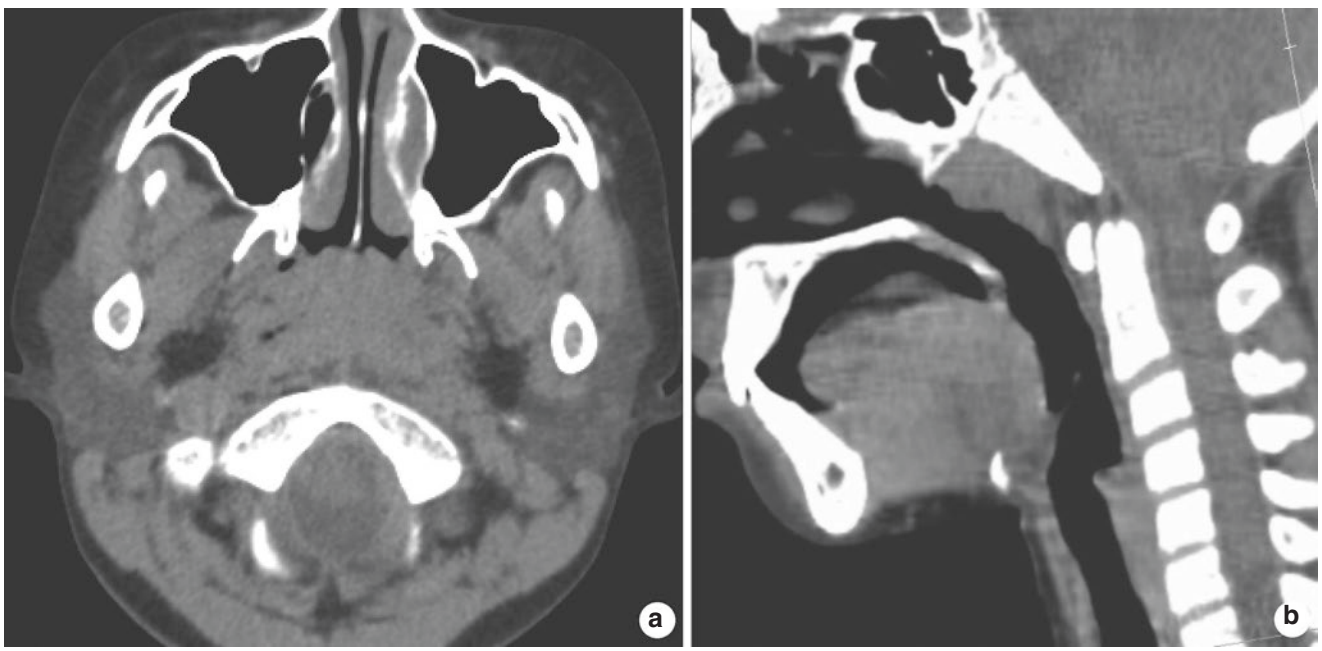

Fig. 24.4 Adenoid hypertrophy (2). A 9-year-old female patient. Snoring while sleeping. (**a**) Non-enhanced CT scan on transverse plane indicates thickening of the soft tissue of nasopharynx, with homogeneous density, smooth nasopharynx mucosa, and clear bilateral parapharyngeal spaces; (**b**) Non-enhanced CT scan on sagittal plane shows thickening of nasopharyngeal roof soft tissue and stenosis of nasopharyngeal cavity

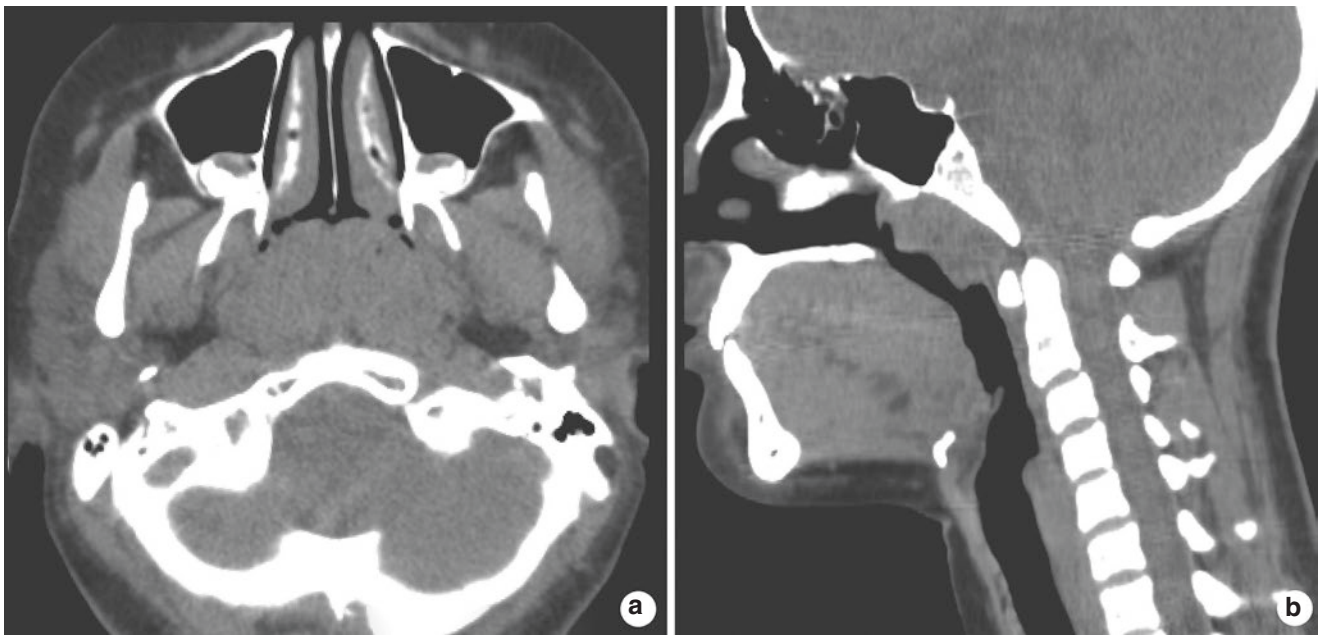

Fig. 24.5 Adenoid hypertrophy (3). A 10-year-old female patient. Snoring while sleeping. (**a**) Non-enhanced CT scan on transverse plane indicates thickening of the soft tissue of nasopharynx, with homogeneous density, smooth nasopharynx mucosa, and clear bilateral parapharyngeal spaces; (**b**) Non-enhanced CT scan on sagittal plane shows thickening of nasopharyngeal roof soft tissue and stenosis of nasopharyngeal cavity

examinations are important supplementary methods for diagnosing adenoid hypertrophy and complications in children [7].

Key Points of Diagnosis

1. The lateral X-ray photography of nasopharynx shows adenoid hypertrophy and narrow nasopharyngeal cavity.
2. CT and MRI clearly show thickening of nasopharyngeal soft tissue and compression of pharyngeal ostium of auditory tube and pharyngeal recess. Nasopharyngeal mucosa is intact.

Differential Diagnosis

1. **Nasopharyngeal carcinoma.** It is a common malignant tumor of nasopharynx in adults and mostly occurs in pharyngeal recess. In the early stage, the pharyngeal recess is asymmetrically shallowed and disappeared, and the levator veli palatini muscle is enlarged, which can form a nasopharyngeal cavity mass with curved convex edge and irregular surface, asymmetric constriction of nasopharyngeal cavity, with invasion to the parapharyngeal space and bone of skull base. By enhanced scan, the mass shows marked and heterogeneous enhancement. Adenoid hypertrophy mainly manifests as thickening of soft tissue in the posterior wall of the nasopharyngeal roof in childhood, which gradually atrophies after puberty, smooth mucosal surface, homogeneous enhancement of adenoids by enhanced scan, without bone destruction or infiltration.
2. **Retropharyngeal abscess.** It can occur with tonsil hypertrophy. There are significant infection-related symptoms of retropharyngeal abscess, and tonsil hypertrophy mainly manifests as airway obstruction symptoms, such as nasal obstruction and snoring. The retropharyngeal abscess is located in the prevertebral space, and the inflammation can also involve the peripheral structures such as tonsil and parapharyngeal space. The prevertebral space and parapharyngeal space are blurred and disappeared, and the abscess shows ring enhancement by enhanced scan. The margin between tonsil hypertrophy and surrounding muscles is clear, showing homogeneous enhancement by enhanced scan.
3. **Nasopharyngeal cyst.** It has no special clinical symptoms. It is located in the midline of the posterior wall of nasopharynx, the cyst can protrude out of the soft tissue of the posterior wall, which is in round or oval shape. The intracapsular signal intensity depends on the protein concentration of the contents and can show hypointense on T_1WI and hyperintense T_2WI, hyperintense on T_1WI, and hyperintense on T_2WI, or hypointense on T_1WI and hypointense on T_2WI. The hypointense on T_1WI and hyperintense T_2WI is common.

Status Quo and Progress of Research

At present, the quantitative diagnosis of adenoid hypertrophy can be made by CT MRP reconstruction technique and the scanning and measurement of A/N value on the median

sagittal plane by MRI SE T_1WI sequence. MRI examination is more suitable for children because it has no ionizing radiation. MRI films can be used to dynamically observe the movement of nasopharynx with breathing and clearly observe whether the nasopharyngeal cavity is narrow.

24.3 Tonsillitis and Intratonsillar Abscess

Overview

Tonsillitis and intratonsillar abscess (ITA) refer to inflammation and abscess formed by neutrophils and necrotic substances gathered in tonsil parenchyma. As main cause of these diseases, they are secondary to follicular tonsillitis, or suppurative inflammation caused by bacteria implanted into tonsils through blood and lymph. The clinical manifestations of tonsillitis and ITA are similar to those of peritonsillar abscess. They are usually unilateral tonsillar enlargement with fever, odynophagia, and dysphagia. However, physical examination shows that there is no significant fluctuation in the peripheral tissues. Some patients with ITA may have restrictions of mouth opening. Peritonsillar abscess (80%) may have murmur, but intratonsillar abscess has no such symptom [8–10].

The exact etiology of tonsillitis and ITA is unclear. It is reported that tonsil inflammation, especially acute follicular tonsillitis, leads to empyema in intratonsillar cleft, thus forming intratonsillar abscess. Intratonsillar abscess may also be caused by bacterial tonsil inoculation from blood or lymphatic vessels. Factors affecting lymphatic vessels and lymphokines may be important inducing factors of intratonsillar abscess: dehydration, inflammatory swelling of tonsillar follicles, and previous history of peritonsillar abscess.

Intratonsillar abscess is rare. Clinical symptoms may include pharyngalgia, dysphagia, and referred otalgia. Examination can show difficulty in opening mouth, asymmetry of tonsils, deviation of uvula, enlargement of cervical lymph nodes, and voice change. Phonological change is not a common symptom of intratonsillar abscess.

Pathology Findings

Plenty of leukocytes infiltration can be found in the lesions, and neutrophils are the most common, complicated with necrotic tissues and pus formation to different extents. If an abscess is formed, granulation tissues can be found on the abscess wall.

Imaging Findings

1. Conventional tonsillitis can be definitively diagnosed in clinical practice without imaging examination.
2. The clinical anti-inflammatory effect of tonsillitis is poor, thus CT and MRI examinations are needed to find any abscess or other diseases with inflammation.
3. Non-enhanced CT scan indicates significant swelling and hypertrophy of bilateral tonsils, unclear margin, heterogeneous density, blurred fat septa around tonsils, and parapharyngeal space (Figs. 24.6 and 24.8a).
4. By CT enhanced scan, intratonsillar abscess shows low-density focus gathered in the tonsil parenchyma with ring enhancement, and peritonsillar abscess is mostly located in the supratonsillar space, and the parapharyngeal space is often involved (Figs. 24.7 and 24.8b and c). MRI shows an unclear lesion border, and hyperintense on T_2WI and DWI (Fig. 24.9).
5. CT and MRI enhanced scan and DWI sequence have diagnostic advantages for tonsillitis, they are mainly used to detect the abscess, thus providing bases for the choice of clinical treatment scheme and avoiding injury to internal carotid artery when pus is discharged by incision or aspiration.

Key Points of Diagnosis

1. The tonsil is swollen, and the abscess shows low-density focus by non-enhanced CT scan, with marginal ring enhancement.
2. Non-enhanced MRI scan shows slightly hypointense on T_1WI, heterogeneous hyperintense on T_2WI, hyperintense on DWI, and ring enhancement.

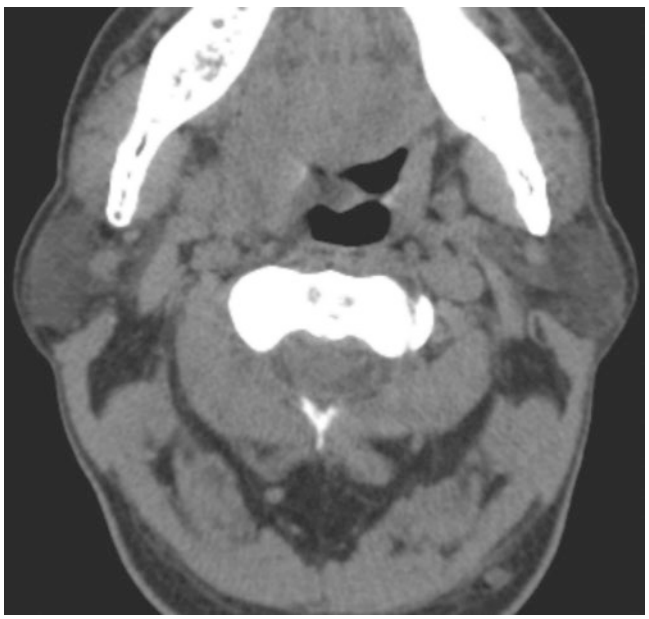

Fig. 24.6 Right tonsillitis. Enhanced CT examination shows that the right tonsil is significantly swollen, the oropharyngeal cavity is compressed and constricted, and the margin of the right parapharyngeal space is unclear

Differential Diagnosis

1. **Peritonsillar abscess.** It is often secondary to acute and chronic tonsillitis and mostly occurs unilaterally. It is common in adults. Severe unilateral pharyngalgia, which is aggravated during swallowing, and radiated to the ipsilateral aural region. CT shows diffuse swelling of soft tissue around tonsils with unclear margin and lower density shadows inside, indicating the formation of vomica. Enhanced examination shows marked enhancement of the abscess wall.
2. **Parapharyngeal abscess.** The lateral pharyngeal wall and tonsil on the affected side are pushed inward and may lead to restriction of mouth opening, but the inflammation of pharynx is mild, and the tonsil has no significant pathological changes. The lateral neck has severe radiation pain, with inflammatory abscess and significant tenderness. CT shows diffuse swelling of soft tissue around the parapharyngeal space, with unclear margin and lower density shadows inside, indicating the formation of vomica. Enhanced examination shows marked enhancement of the abscess wall.

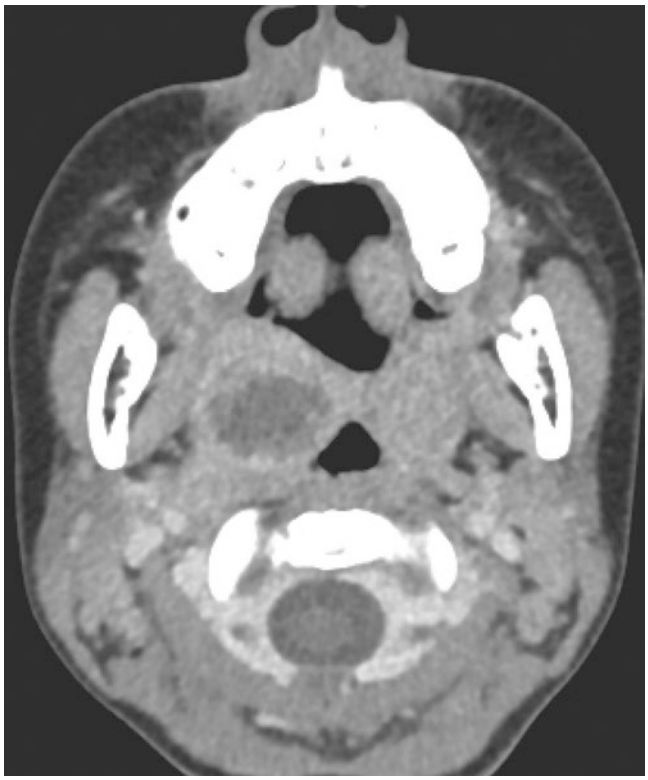

Fig. 24.7 Right palatine intratonsillar abscess (1). CT enhanced examination shows significant swelling of the right tonsil and ring enhancement. Oropharyngeal cavity narrowed by compression

Status Quo and Progress of Research

At present, CT or MRI examination is often used as the necessary means of preoperative examination, which can indicate the location and scope of abscess, and enhanced scan can show the complete abscess wall as well as compression on airway and great vessels, which is beneficial to the formulation of operative plan. With the gradual development of the treatment of pediatric peritonsillar abscess, the treatment of pediatric peritonsillar abscess develops to the field of surgical treatment (i.e., drainage or needle aspiration) [8]. Enhanced CT examination and DWI sequence mainly evaluate the formation of abscess, which plays a key role in the localization and clinical treatment of abscess.

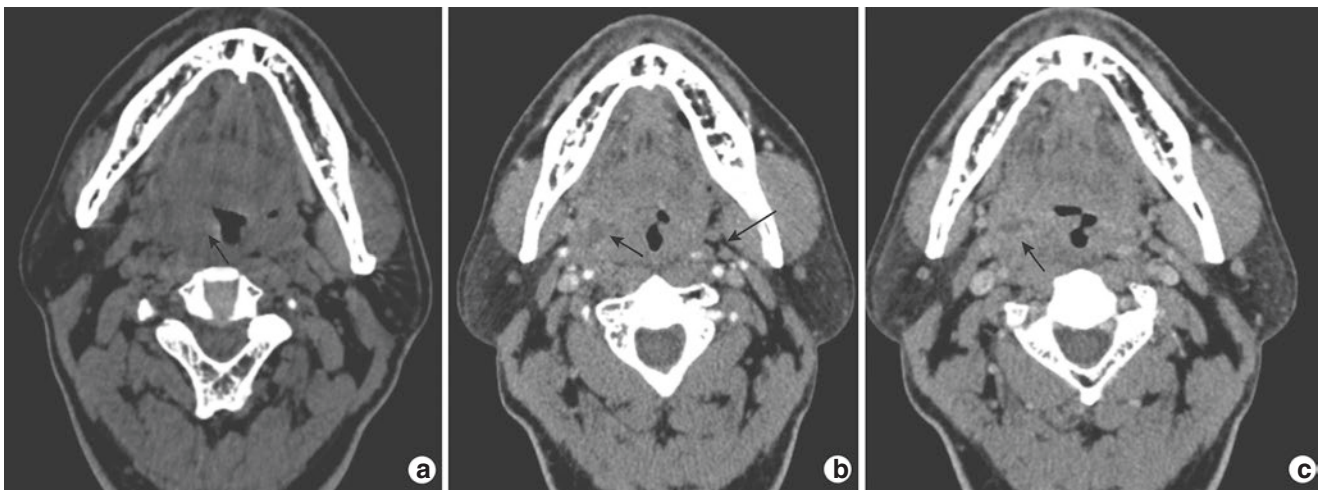

Fig. 24.8 Right palatine intratonsillar abscess (2). A 46-year-old male patient. The patient was admitted due to main cause of "right pharyngalgia for 1 week". Physical examination: Grade II enlargement of right tonsil. The operation confirmed that the right peritonsillar abscess was complicated with right parapharyngeal space infection. (**a–c**) Non-enhanced and enhanced scans show crumby slightly low-density shadows beside the right tonsil, which show heterogeneous and moderate enhancement in arterial phase and still show enhancement in venous phase. The center of the lesion shows a hat-shaped area without enhancement. The left parapharyngeal space is clear (indicated by arrow)

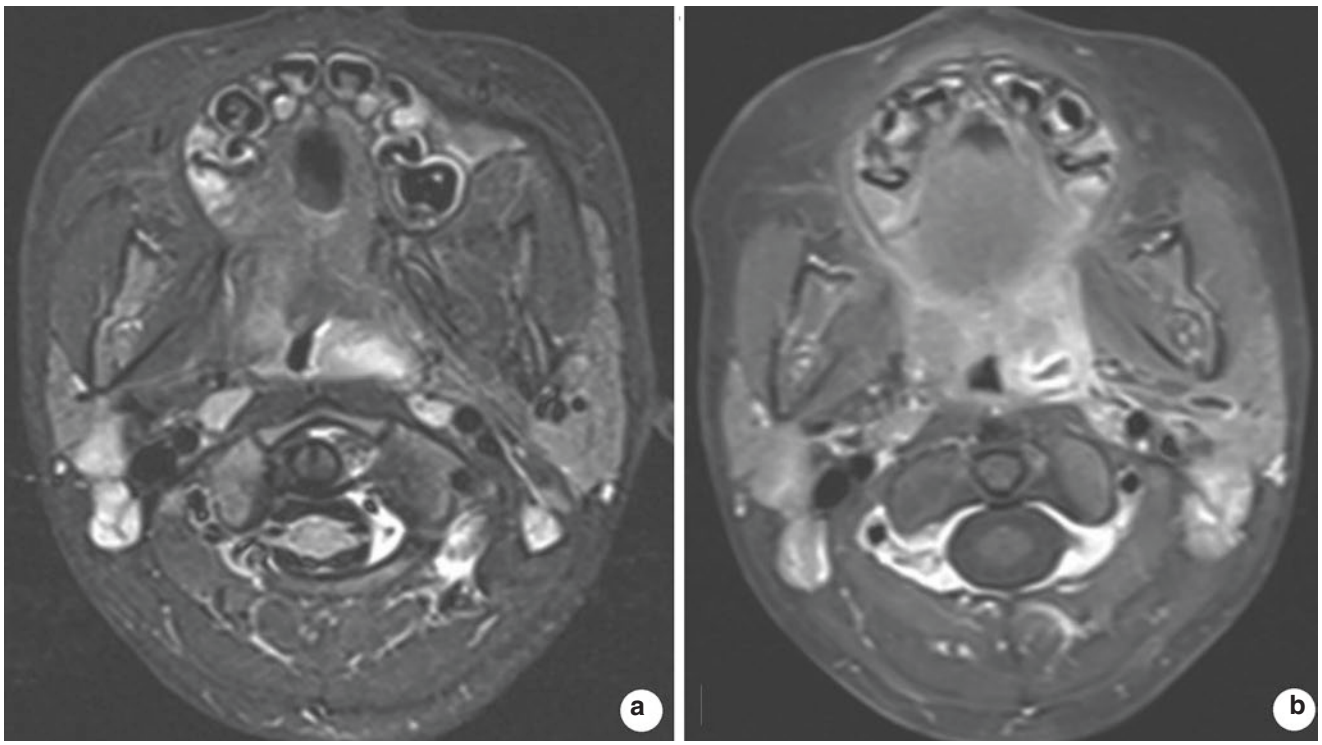

Fig. 24.9 Left palatine intratonsillar abscess. The left palatine tonsil is enlarged. (**a**) Axial T_2WI fat suppression imaging shows hyperintense of left palatine tonsil; (**b**) Axial T_1WI enhanced scan shows ring enhancement in the left palatine tonsil

24.4 Infection or Abscess of Retropharyngeal Space

Overview

The retropharyngeal space is a potential space inferior to the occipital bone of skull base, superior to the posterior mediastinum, posterior to the fascia buccopharyngea, and anterior to the prevertebral fascia. Infection of retropharyngeal space is a pyogenic infection occurring between the posterior wall of pharynx and esophagus and prevertebral fascia. The lower part of the retropharyngeal space is at the level of third–fourth cervical vertebrae plane with its walls adhere to each other, thus the abscess rarely descends into the posterior mediastinum of the chest cavity; Both sides and the parapharyngeal space are separated by incomplete fascia, thus the infection may spread between the two spaces. The etiology of retropharyngeal space abscess can be divided into traumatic cause and non-traumatic cause. Non-traumatic retropharyngeal abscess is a disease of children to a great extent, which is caused by abundant lymphoid tissues in retropharyngeal space of children. The disease mainly affects boys. It usually occurs in children under 7 years old after upper respiratory tract infection in winter. The common symptoms and signs are fever, cervical pain, torticollis, and neck swelling. Abscess in the space can be caused by multiple organisms, such as aerobic microorganisms (β hemolytic streptococcus and staphylococcus aureus), anaerobic microorganisms (bacteroides and veil bacteria) or Gram-negative bacteria (haemophilus influenzae). In recent 10 years, the recurrence of retropharyngeal space abscess in children is related to the increased incidence of β hemolytic streptococcus [11]. Although CT technology and diagnostic criteria have been improved, it is difficult to differentiate suppurative lymphadenitis from retropharyngeal space abscess. For pediatricians, radiologists, and otolaryngologists, it is still difficult to diagnose and control the retropharyngeal space abscess, as it may be mistaken for epiglottitis [11–13].

Retropharyngeal abscess is suppurative inflammation in retropharyngeal space, which can be divided into acute and chronic types due to different pathogenesis. Acute disease is common, which is caused by suppuration of retropharyngeal lymph nodes and is mostly found in children under 3 years old, and more than half of the patients are under 1 year old. In addition, after injury of posterior pharyngeal wall (foreign matters or other trauma), if infection or inflammation of adjacent tissues spreads into retropharyngeal space, the retropharyngeal abscess may also occur. Chronic cases are rare, and the abscess is mostly formed by cervical tuberculosis, also known as cold abscess. Because of oppression by abscess, the patients have laryngeal edema and difficulty in breathing and swallowing. Children speak or cry with quack voice because of the constriction of pharyngeal resonant cav-

ity. Physical examination revealed neck rigidity. Early incision and drainage of pus and systemic anti-infection treatment are recommended clinically [14, 15].

Pathology Findings

Infiltration of plenty of leukocytes is found in the soft tissue of retropharyngeal space, and neutrophils are the most common, complicated with necrotic tissues and pus formation to different extents. If an abscess is formed, granulation tissues can be found on the abscess wall. It can also be combined with inflammation of lymph nodes in retropharyngeal space. Plenty of inflammatory cells infiltrated can be found in enlarged lymph nodes

Imaging Findings

1. **X-ray examination.** It shows that cold abscess caused by cervical tuberculosis can locate in the central part, and local mucosa has unremarkable congestion. X-ray film of cervical vertebra can show the shadows of soft tissue eminence in prevertebral space, sometimes showing signs of liquid plane and bone destruction of cervical vertebra. The "air sign" in the lateral view of neck is very important for the diagnosis of abscess [15].
2. **CT or MRI examination.** The shadows of soft tissue eminence in prevertebral space are found by CT or MRI scan, and sometimes the liquid plane is found. For patients with acute type, vomica or foreign matters retention can be found; The signs of bone destruction of cervical vertebra can be found in patients with cervical tuberculosis, which is often complicated with pulmonary tuberculosis. Typical MRI imaging features include: (1) bow-tie expansion of retropharyngeal space, leading to the antedisplacement of the posterior pharyngeal wall; (2) hyperintense on T_1WI and hypointense on T_2WI, suggesting retropharyngeal edema and cellulitis. (3) enhanced scan showing localized liquid accumulation and marginal enhancement, indicating abscess; (4) hyperintense on DWI for central empyema area, and diffusion limitation in effusion area. By enhanced scan, the lesion shows marginal enhancement (Figs. 24.10, 24.11 and 24.12).

Key Points of Diagnosis

1. According to the history, symptoms, signs, and aspiration of pus, the diagnosis of retropharyngeal abscess is not difficult.
2. Cervical lateral X-ray photography shows antedisplacement of the posterior pharyngeal wall and widening of prevertebral soft tissue shadows, or shows effusion, which is helpful for diagnosis. Air sign is very important for the diagnosis of abscess.
3. CT or MRI shows eminence of soft tissue shadows of the posterior pharyngeal wall with the widening of the retropharyngeal space, and sometimes shows the liquid plane.

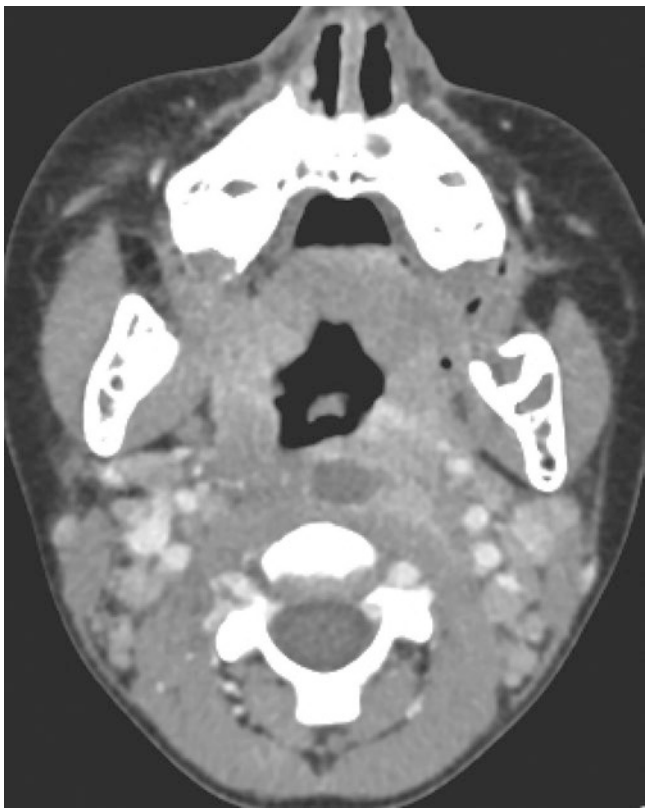

Fig. 24.10 Retropharyngeal abscess (1). A 35-year-old female patient. Neck discomfort for 1 week. CT shows that the soft tissue of the posterior pharyngeal wall is thickened, and enhanced examination shows the lesion with ring enhancement of the posterior pharyngeal wall, and multiple enlarged lymph nodes are found in bilateral II areas

The lesions spread along the retropharyngeal space and even reach the chest, with marginal enhancement by enhanced scan.

Differential Diagnosis

1. **Retropharyngeal lymphadenitis.** Neck lymphadenitis is an acute symptomatic cervical lymph node enlargement, which is a common problem for children of all ages. Pediatric retropharyngeal infection is most commonly caused by incomplete treatment of nasopharyngeal or oropharyngeal infection, which spreads to retropharyngeal lymph nodes by capillary lymphatic drainage. Infection leads to reactive lymph node enlargement, which manifests as homogeneous and low-density shadows on CT (compared with peripheral soft tissue). Then the infection may develop into suppurative adenitis, and the enlarged lymph nodes have liquefactive necrosis and are surrounded by edema during the period. Suppurative lymph nodes rarely break into the retropharyngeal space and lead to retropharyngeal abscess. Suppurative retropharyngeal lymph nodes are contained in lymph node cyst.

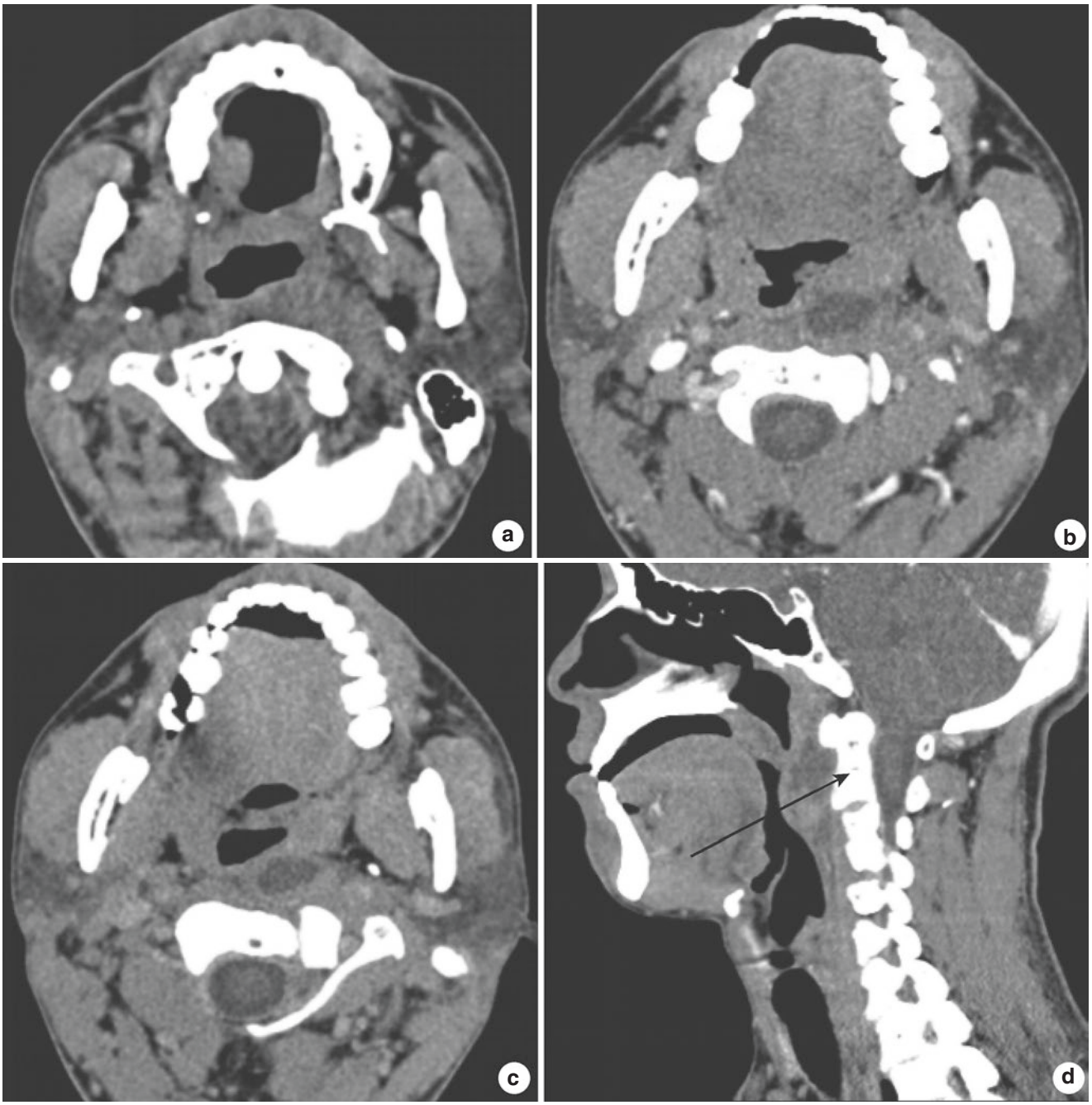

Fig. 24.11 Left retropharyngeal abscess. 36-year-old male patient The operation confirmed that tuberculous abscess occurred in the left retropharyngeal space. (**a**) Non-enhanced CT scan indicates that the density shadows of soft tissue in the posterior wall of left nasopharynx and oropharynx are thickened heterogeneous density; (**b** and **c**) In arterial phase and venous phase, crumby soft tissue density shadows are found in the left side of retropharyngeal space, showing ring enhancement; (**d**). The lesion spreads downward along the retropharyngeal space (indicated by arrow)

2. **Cellulitis in retropharyngeal space.** The CT manifestations are diffuse hypointensity shadows in retropharyngeal space, which has a wide scope of lesions and unclear margins, and can involve multiple spaces; Radionuclide imaging shows radioactive concentration [14].
3. **Edema in retropharyngeal space.** It is non-infectious, usually complicated with swelling of other spaces in the neck, and the lesion has no enhancement, thus it is necessary to clarify the medical history, such as heart failure. It can disappear after the cause of disease is eliminated.

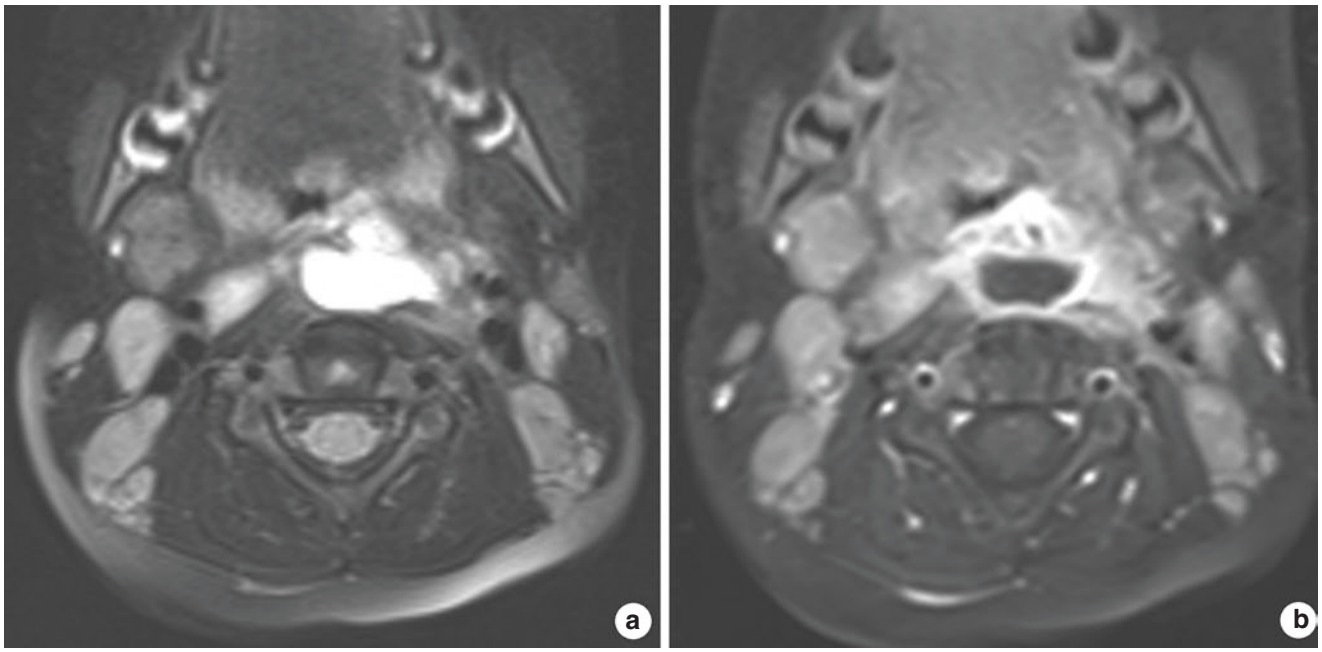

Fig. 24.12 Retropharyngeal abscess (2). A 56-year-old female patient Cervical pain with fever for 2 weeks. (**a**) Axial T_2WI fat suppression imaging shows hyperintense of prevertebral space; (**b**) Axial T_1WI enhanced scan shows lesion with ring enhancement in the prevertebral space

4. **Metastatic lymph nodes in retropharyngeal space.** Neck metastatic lymph nodes with central necrosis manifest as low-density shadows of soft tissue and its center on CT, and enlargement of multiple lymph nodes can be found in II-VI regions of neck.

Status Quo and Progress of Research

CT and MRI can distinctively differentiate retropharyngeal abscess from other diseases, such as retropharyngeal edema or suppurative retropharyngeal lymph nodes. Within 48 h of infection, CT scan has a certain influence on the diagnosis of lesions. However, after abscess formation, the low-density shadows inside the lesion are helpful to locate the lesion. CT and MRI can accurately show the involvement extent of retropharyngeal abscess, CT is more helpful to show the destruction extent of tuberculous abscess on vertebral body, and enhanced examination can completely show the abscess wall and the suppression on adjacent airway and great vessels. MRI can show different signal characteristics of abscesses depending on the phases and components, and diffusion limitation of DWI sequence has certain implications.

CT enhanced scan of neck is of great significance in diagnosis of retropharyngeal abscess and indication of surgical drainage. The imaging sign of abscess is the soft tissue density shadows in the central low-density area, which shows ring enhancement by enchanced scan, but sometimes it is difficult to differentiate abscess from cystic degeneration or cellulitis of malignant deep neck metastatic tumor. Enhanced CT has significant false-positive rate. MRI DWI can be used for differential diagnosis. The abscess shows hyperintense on DWI, while the metastatic lymph nodes show hypointense. By combining the two imaging techniques, it is possible to avoid unnecessary surgery for patients with cellulitis.

24.5 Infection or Abscess of Parapharyngeal Space

Overview

The parapharyngeal space is an anatomical space located on the lateral wall of the epipharynx, which is inverted pyramid-shaped and extends from the skull base to the level of hyoid bone. It can be divided into prestyloid space and poststyloid space. Differentiating infection between prestyloid process and poststyloid process is very important for guiding differential diagnosis and potential surgical methods of otolaryngologists. However, the importance of the parapharyngeal space also lies in its relationship with other spaces in the neck, especially the infection of the retropharyngeal (or prepharyngeal) space may lead to severe life-threatening complications, such as mediastinitis [16, 17]. The infection of parapharyngeal space is mainly caused by suppurative inflammation spreading from adjacent tissues or organs, such as acute adenoiditis, acute suppurative tonsillitis, mastoiditis; It is caused by rupture of or spread from adjacent abscesses, such as peritonsillar abscess, retropharyngeal abscess, molar area abscess, parotid gland abscess, otogenic deep cervical abscess. It may be caused by stab wounds and trauma by foreign matters in lateral pharyngeal wall;

Iatrogenic infection, such as tonsillectomy or tooth extraction and improper oral surgery. Infection of adjacent organs or tissues can involve parapharyngeal space through blood circulation and lymphatic system.

Infection of parapharyngeal space is a dangerous disease. The possible severe complications of the disease include mediastinitis, pericarditis, pleural abscess, meningitis, internal jugular vein thrombosis, septic shock, internal carotid artery rupture or aneurysm, airway obstruction, and death. An active therapeutic approach is required, i.e., emergency surgical drainage.

Parapharyngeal abscesses are another common deep cervical infection and the common deep cervical abscess second to the peritonsillar abscess. It can lead to severe and potentially fatal complications, such as airway damage, jugular vein thrombosis, Lemierre syndrome, Horner syndrome, mediastinitis, and carotid artery hemorrhage through retropharyngeal space.

Most oropharyngeal abscesses are caused by multiple bacterial infections. The main anaerobic bacteria isolated from parapharyngeal abscess are prevotella, porphyromonas, fusiform bacillus, and peptostreptococcus. Aerobic bacteria are streptococcus-a (pyogenic streptococcus), staphylococcus aureus and Haemophilus influenzae. Fusiformis necrophorus can easily cause septic thrombophlebitis and metastatic abscess of great vessels, especially related to deep cervical infection of lung abscess (Lemierre syndrome).

Parapharyngeal abscess can occur at any age, rarely before 8 years old, usually under 30 years old. The main symptoms are fever, sore throat, dysphagia, swelling, and myasthenia. Physical examination can show the asymmetry of oropharynx and tender neck mass, which may be associated with lymphadenopathy. The patients commonly have history of upper respiratory tract infection, pharyngitis, or tonsillitis. However, some of these infections are fulminant, and patients will seek treatment several hours after onset. Especially, the sore throat, oropharyngeal asymmetry, and lateral painful cervical lump can be considered as the pathological manifestations of parapharyngeal abscess, especially in case of "upper nasopharyngeal infection," such as pharyngitis or tonsillitis. Fever is not a constant sign but often occurs (50% of cases), such as head and neck infection, peritonsillar abscess, or odontogenic cellulitis [18].

Pathology Findings

Parapharyngeal abscess is a typical suppurative inflammation of parapharyngeal space, which is cellulitis in the early stage, and then the inflammatory tissue is necrotic and dissolved, forming a cavity filled with pus, i.e., abscess.

Imaging Findings

1. **CT examination.** With clinical diagnosis or suspicion of parapharyngeal abscess, non-enhanced CT scan and enhanced scan of neck are feasible, which are the best imaging methods for diagnosis and follow-up visit of parapharyngeal abscess. On CT, the abscess shows single or multi-cell low-density shadows, and its density is between soft tissue and water, with air and liquid density in the center (Fig. 24.13a). By enhanced scan, the abscess wall has enhancement and peripheral tissues of abscess wall have edema (Fig. 24.13b). Enhanced scan can also show the thrombosis and dilatation of internal jugular vein, and a clear wall around the low-density lumen. CT scan is sufficient to meet the clinical requirements, because it can confirm the clinical diagnosis of parapharyngeal abscess, show that parapharyngeal abscess spreads along the anatomical structure to the periphery of tonsils or retropharyngeal space, and show complications such as internal jugular vein thrombosis, lung abscess or mediastinitis on CT of neck and chest.
2. **MRI.** Compared with CT, MRI shows different signal intensities for different soft tissues, so it has absolute advantages in diagnosing diseases of vessels, nerves, and muscle. It can also diagnose thrombosis of internal jugular vein and erosion or rupture of carotid artery with images more accurately than that of CT. MRI can clearly show each fascial space, so the detection rate of infection of cervical spaces is higher than that of CT. The pus shows hypointense on T_1WI and hyperintense on T_2WI, and the peripheral soft tissue swelling shows hyperintense on T_2WI (Fig. 24.13c–e). DWI shows the abscess spread limited and showing hyperintense (Fig. 24.13f). By enhanced scan, the lesions show heterogeneous enhancement on T_1WI, with no enhancement inside and marked marginal garland-like enhancement. Therefore, MRI can more accurately locate the nature and scope of abscess and separate it from the surrounding normal tissues (Fig. 24.14).

Key Points of Diagnosis

1. Children or adolescents have fever, sore throat, and other symptoms, and may have a history of pharyngitis or tonsillitis
2. CT shows swelling and thickening of parapharyngeal soft tissues. After abscess formation, cloud-like low-density shadows can be found, with air and liquid shadows in these tissues, and a ring enhancement by enhanced scan.
3. MRI shows hypointense on T_1WI, hyperintense on T_2WI and hyperintense on DWI. By enhanced scan, it shows garland-like enhancement on T_1WI.

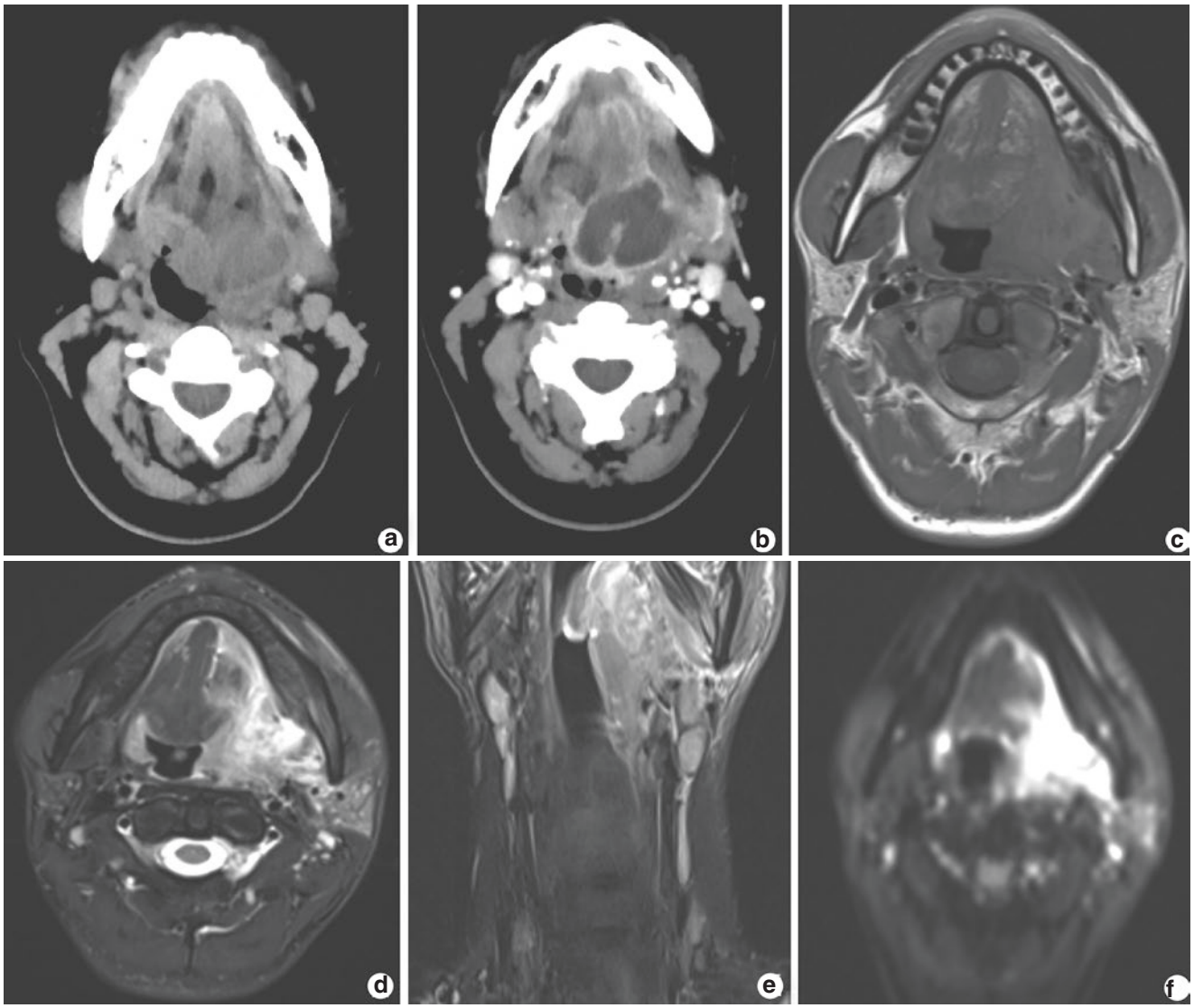

Fig. 24.13 Left parapharyngeal abscess (1). (**a** and **b**) A 24-year-old male patient. Pain in the left pharynx for 1 week. (**c–f**) A 47-year-old female patient. Pain in the left face for 2 weeks. Left parapharyngeal abscesses. (**a**) Non-enhanced CT scan indicates soft tissue swelling in the left parapharyngeal space, with low-density shadows; (**b**) CT enhanced scan shows lesions as marked ring enhancement; (**c**) Axial T_1WI shows isointenses in enlarged soft tissues; (**d**) Axial T_2WI shows heterogeneous hyperintense. (**e**) Coronal T_2WI clearly shows the extent of lesion involvement; (**f**) DWI shows diffusion limitation and hyperintense of abscess

Differential Diagnosis

1. **Oropharyngeal cancer.** It usually occurs in people aged 40–60 years old, manifesting as density mass of soft tissue in oropharynx, with unclear margin, cystic degeneration and necrosis, heterogeneous enhancement by enhanced scan, and cervical lymphatic metastasis in early stage.
2. **Neurilemmoma.** It manifests as quasi-circular soft tissue density mass with clear edges. The fat connective tissue in the parapharyngeal space is displaced anterolaterally, and the larger tumor is of mixed densities, which shows enhancement to different extents by enhanced scan.
3. **Lymphoma.** It is common in middle-aged men. It manifests as a soft tissue mass that develops in or around the pharyngeal cavity, with homogeneous density or signal intensity, and shows mild to moderate enhancement by enhanced scan. Most of them have no infiltration of parapharyngeal space or bone destruction of skull base.

Status Quo and Progress of Research

Because the position of parapharyngeal space is deep and the surface is covered with thick muscles, it is difficult to find abscess formation in early stage. CT scan can differentiate septa and fluid accumulation at different levels, and show the

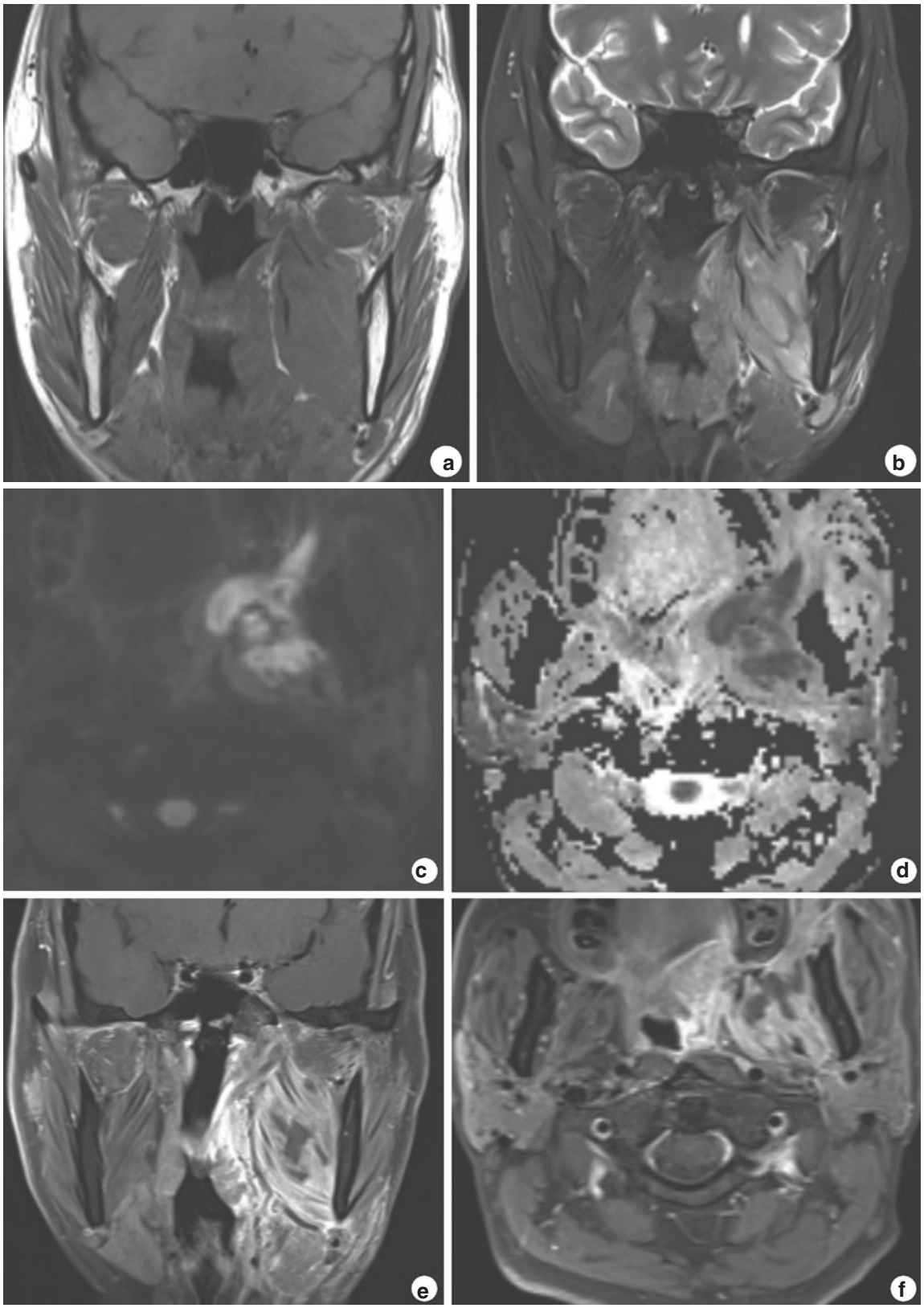

Fig. 24.14 Left parapharyngeal abscess (2). A 45-year-old male patient. Pain in the left pharynx, with swelling of left face and dysphagia for 1 week. (**a** and **b**) MRI T_1WI and T_2WI fat-suppressed sequence shows soft tissue swelling in the left parapharyngeal space, and increased signal intensity of the left medial pterygoid and lateral pterygoid on T_2WI fat-suppressed sequence, with a ring hyperintense shadow in the lesion and isointense on the wall. The left tongue root and lateral pharyngeal wall were compressed, and the oropharyngeal cavity became narrow. (**c**) DWI shows limited spread of lesions with hyperintense. (**d**) ADC shows hypointense of lesions. (**e** and **f**) Enhanced examination shows lesions having marked enhancement and irregular ring enhancement on the wall

great vessels in the neck, which can be differentiated from cellulitis. MRI can clearly show the location, scope, and surrounding relationship of lesions. MRI DWI sequence plays a very important role in evaluating the scope of lesions, abscess formation, and treatment response of abscess, and has become a routine sequence of parapharyngeal space infection at present.

24.6 Inflammatory and Hyperplastic Diseases of Pharyngeal Lymph Nodes

Overview

Pharyngeal reactive lymph node proliferation, also known as reactive adenopathy (RPS), is a common benign hyperplastic disease of lymph nodes or soft tissues. There are multiple reasons leading to lymph node enlargement and lymphadenosis in pharynx and other parts of the body, such as inflammation, virus infection, vaccination, some drug reactions, immune diseases, and other factors. Viral infection is the most common cause, which usually leads to slight enlargement of bilateral lymph nodes without peripheral inflammation. Cytomegalovirus infection, herpes simplex virus infection, chickenpox and rubella are common viral causes, but they usually need to be associated with clinical or laboratory data before making a definite diagnosis. Most of the patients with the disease are teenagers, and the common sources of infection are limited head and neck infections, such as pharyngitis and systemic virus infection.

Pathology Findings

Pathological lymph nodes vary in size, ranging from 1 cm to 3 cm in diameter, sometimes up to 10 cm. Microscopically, due to different pathogenic reasons, reactive proliferation of lymph nodes often has different histological structures. Histological manifestations are lymphoid follicular proliferation, paracortical proliferation, sinus histiocytosis, and mixed proliferation.

Imaging Findings

1. **CT manifestations.** CT can clearly show the location, scope, and number of enlarged lymph nodes, and also show the relationship between lymph nodes and peripheral tissues to guide clinical biopsy. The characteristic manifestation is the enlargement of lymph nodes in the parapharyngeal or retropharyngeal space, the short diameter of node is often ≤1.5 cm, and isolated enlarged lymph nodes are the most common. The density of non-enhanced scan is homogeneous, equal to or slightly lower than that of adjacent muscles, and it has marked enhancement by enhanced scan, and the enhancement is homogeneous [19, 20].
2. **MRI findings.** Homogeneous hypointense or isointense on T_1WI; homogeneous isointense on T_2WI; diffusion limitation and hyperintense on DWI. T_1WI enhanced scan shows various enhancement forms, most of which are marked enhancement (Figs. 24.15 and 24.16).

Key Points of Diagnosis

1. Young patients with pharyngitis or systemic virus infection.
2. CT shows homogeneous shadows of slightly enlarged retropharyngeal space nodules, with or without other related reactive nodules in the neck.
3. MRI shows round nodules with clear margin, homogeneous signal, and marked enhancement.

Differential Diagnosis

1. **Lymph node tuberculosis.** It is mostly found in young adults, and the enlarged lymph nodes have heterogeneous density and ring enhancement. When multiple lymph nodes are fused, a garland-like enhancement can be found.
2. **Lymphatic metastasis.** These patients mostly have history of primary tumors. The density of enlarged lymph nodes is heterogeneous, with cystic degeneration and calcification. No enhancement is found by enhanced scan, and the margin is unclear.
3. **Malignant lymphoma.** Often involves mediastinal lymph nodes, and enlarged lymph nodes are easy to integrate into a mass, which often manifests as mild or moderate enhancement.

Status Quo and Progress of Research

Cervical lymph nodes are regional lymph nodes for tumor metastasis and inflammation drainage in head and neck, and they are also important barriers for preventing inflammation invasion and preventing tumor cells from spreading. Therefore, it is very important to differentiate the benign and malignant cervical lymph nodes.

CT perfusion imaging is a non-invasive functional imaging method to evaluate the perfusion state of tissue blood flow, which can quantitatively analyze different pathological lymph node lesions in the neck, and has certain clinical value in differentiating cervical lymphatic metastasis and inflammatory reactive proliferation of lymph nodes.

Dual-energy spectrum analysis can provide some valuable information for differentiating benign and malignant lymph node lesions. CT value measurement corresponding to different single energy diagrams has a certain potential value for differentiating lymph node lesions of different pathological types.

Many studies on interstitial magnetic resonance lymphography have been carried out in recent years. By using

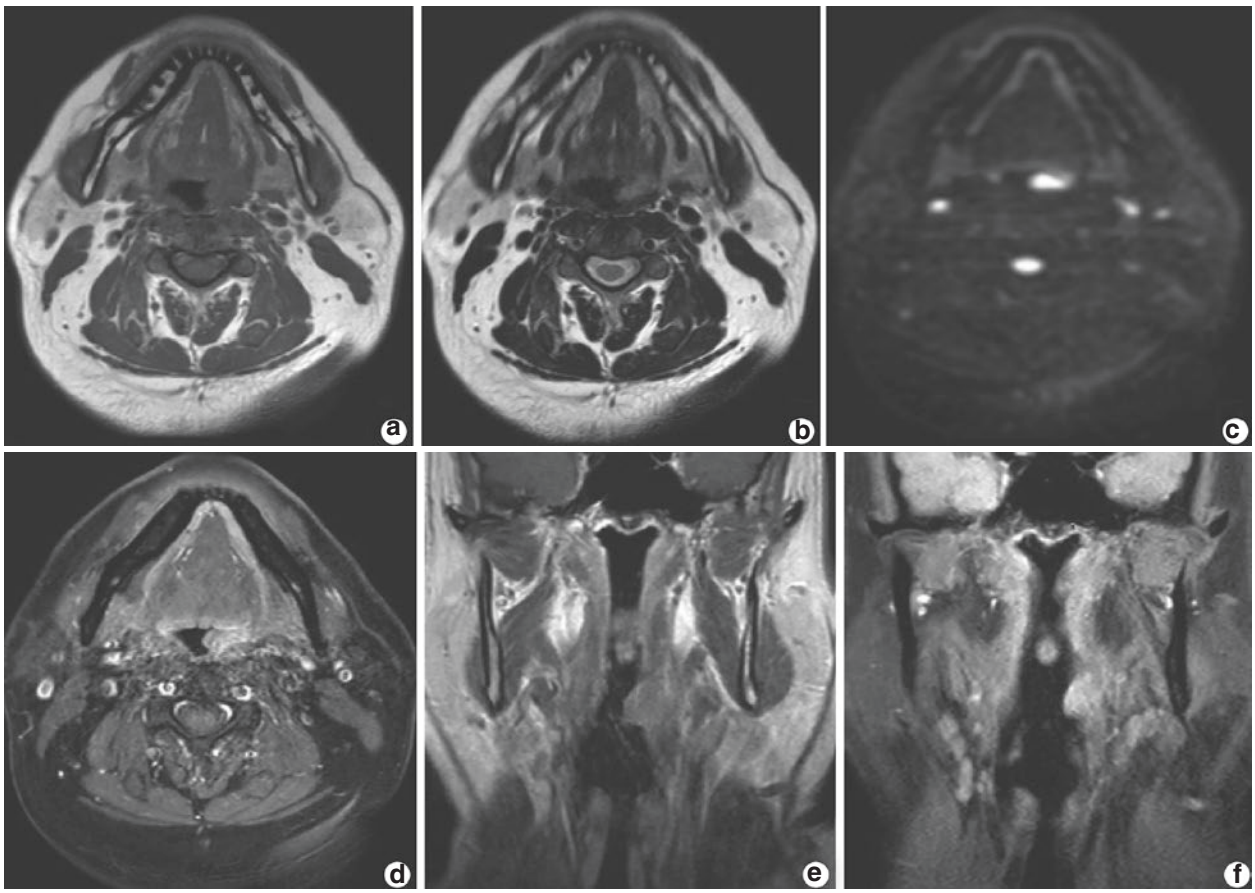

Fig. 24.15 Reactive adenopathy of left pharynx. A 47-year-old male patient. The pharyngeal mass of 6 months is found by physical examination. (**a**) Axial T_1WI non-enhanced scan indicates isointense nodules in the left pharynx; (**b**) Axial T_2WI shows hyperintense of nodules. (**c**) diffusion limition and hyperintense of nodule on DWI; (**d**) Axial T_1WI enhanced scan shows nodule with marked enhancement and continuous with the lymphatic tissue posterior to the tongue root. (**e**) Coronal T_1WI non-enhanced scan indicates that the left pharyngeal nodule protrudes to the pharyngeal cavity; (**f**) Enhanced T_1WI on coronal plane shows marked enhancement of nodules

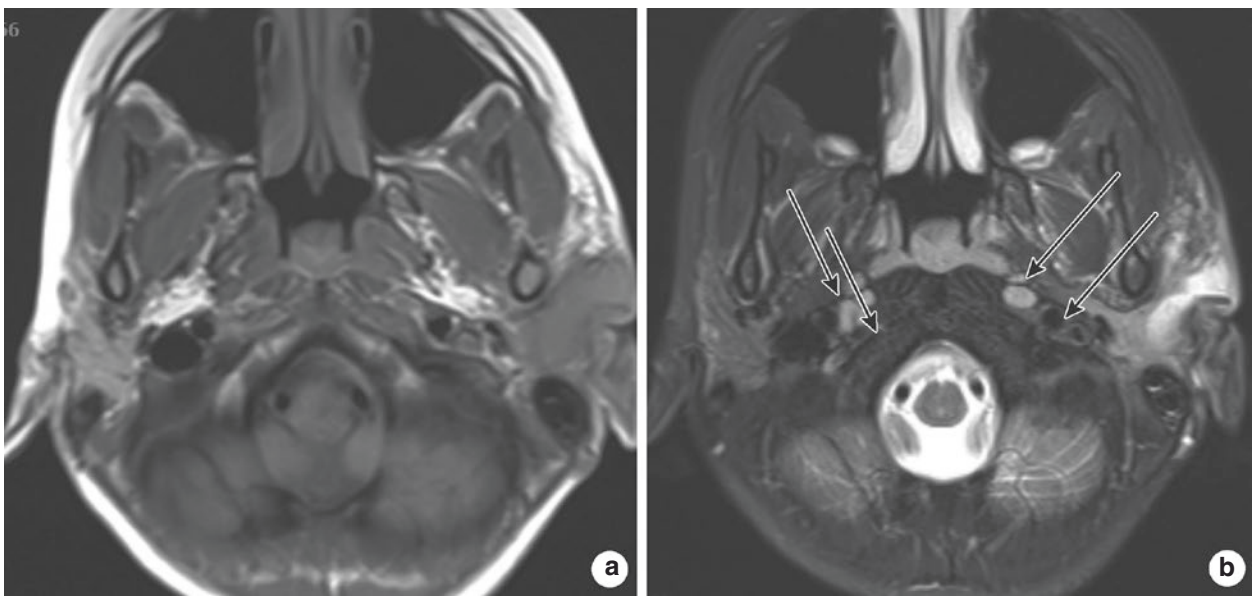

Fig. 24.16 Inflammatory and hyperplastic at the nasopharyngeal roof and acute inflammation of left parotid gland. An 11-year-old male patient. The left face is swollen and painful for 1 week. (**a**) Axial T_1WI non-enhanced scan indicates isointense of nodules at the nasopharyngeal roof. (**b**) Axial T_2WI shows hyperintense of nodules and enlarged lymph nodes (indicated by arrow) in bilateral retropharyngeal spaces. Diffuse enlargement of left parotid gland

magnetic resonance contrast agents combined with macromolecules, which has a large molecular weight and molecular volume, the technique can make target lymph node maintain at a higher enhanced level within an extended period, thus effectively developing the morphology of lymph vessels and lymph nodes in drainage area for reactive hyperplasia of lymph node and lymph node tumor metastasis. In this sense, it is of value for differentiating cervical lymph node metastasis and reactive hyperplasia [21, 22].

24.7 Granulomatous Lesions

24.7.1 Pharyngeal Tuberculosis

Overview

Tuberculosis is a common infectious disease. It mainly occurs in the respiratory system, and also involves the pharynx. Pharynx is a rare part affected by tuberculosis of head and neck besides lymph nodes. Pharyngeal tuberculosis is rare and can be primary or secondary to lung or systemic infection. Tuberculosis is a chronic caseous granuloma. The disease occurs in adults and is most common in the age group of 20–30 years. Head and neck involvement accounts for 12% of patients with extra-pulmonary tuberculosis. It is common in cervical lymph nodes, and also occurs in oral cavity, tongue, pharynx, larynx and parotid gland, but rarely occurs in paranasal sinus and petrosal bone. If the head and neck mucosal tuberculosis cannot be treated promptly and effectively, the patient may have calcification, liquefaction, abscess, sinus, and other symptoms in advanced stage. Pharyngeal tuberculosis clinically manifests as sore dry throat and hoarse cough, complicated with scorching effect and increased secretion. In severe cases, patients may have difficulty in eating. Fiberoptic nasopharynx laryngoscopy shows multiple superficial ulcers and erosions of soft palate, palatal arch, posterior pharyngeal wall, tonsil, etc., with irregular borders and gray-white or gray-yellow dirty secretion attached on the surface.

Pathology Findings

Pathological manifestations include granuloma, central necrotic granuloma, and fibrous calcification. The main pathological features are caseous necrosis, epitheloid cell granuloma formation, and lymphocytes surrounding Langhans giant cells

Imaging Findings

1. **CT examination.** It shows unilateral or bilateral lesions in pharyngeal tuberculosis, involving the tongue or palatine tonsil (Fig. 24.17), with parapharyngeal or retropharyngeal abscess and cervical lymphadenitis developed, and typical marginal ring enhancement sign by enhanced CT. CT scan of nasopharyngeal tuberculosis often shows diffuse mucosal thickening and polypoid mass at the nasopharyngeal roof, which has unremarkable invasion to peripheral structures. The adjacent structures are faintly visible on non-enhanced scan, and muscles in pharynx show clear margin by enhanced scan. The lesions are different in density, showing hyperintense, isointense and hypointense homogeneous density; heterogeneous density, with intetrnal low density shadows; the lesions of granulation tissue formation show isointense or hyperintense density, with caseous necrosis and heterogeneous hypointense density. On non-enhanced CT scan, the margin between the lesion with large scope and adjacent structures is unclear (Fig. 24.17). The central necrosis of the enlarged lymph nodes in the neck, and the marginal ring enhancement in early stage by enhanced scan has characteristic ignificance [23–25]
2. **MRI examination.** It usually shows mass or diffuse mucosal thickening, with isointense on T_1WI and T_2WI sequences, moderate enhancement by T_1WI enhanced scan, hypointense on T_1WI and hyperintense on T_2WI in the center of the lesion, indicating necrosis in the lesion.

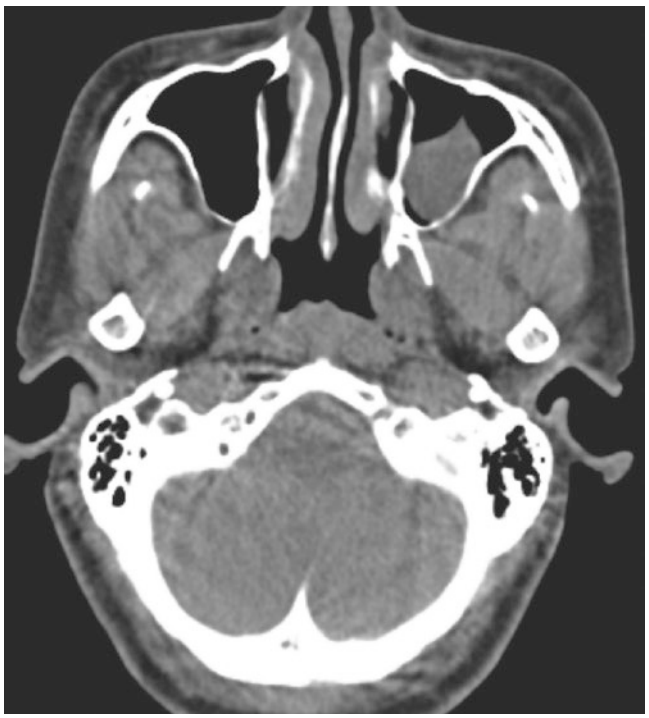

Fig. 24.17 Nasopharyngeal tuberculosis. A 55-year-old female patient. CT on soft tissue window shows swelling of soft tissue at the nasopharyngeal roof, irregular surface and bilateral pharyngeal recess

Key Points of Diagnosis

1. Patients mostly have clear symptoms of pharyngeal infection and a history of pulmonary tuberculosis
2. Lesions often involve palatine tonsils, epiglottis, parapharyngeal or retropharyngeal spaces, and nasopharyngeal roof, and local mucosal thickening or lumps.
3. On non-enhanced CT scan, it shows iso- and low-density mass shadows with unclear margin, and ring enhancement by enhanced scan.
4. MRI shows isointense on T_1WI and isointense on T_2WI, hypointense on T_1WI, and hyperintense on T_2WI in central necrotic area, with ring enhancement by enhanced scan.
5. The diagnosis must be confirmed by pathological biopsy.

Differential Diagnosis

1. **Nasopharyngeal carcinoma.** It mostly starts from the pharyngeal recess, develops unilaterally, easily invades the deep part, often has unclear margin with the peripheral structures, complicated with bone destruction of skull base. Cervical lymphatic metastasis mainly manifests as solid mass, with mild to moderate homogeneous enhancement, and rare necrosis
2. **Nasopharyngitis.** The mucosa at the nasopharyngeal roof is thickened, showing "small bubble sign," often complicated with nasal conchahypertrophy and rhinosinusitis, and rarely showing cervical lymph node enlargement.

Status Quo and Progress of Research

It has been reported [26] that the most common site of tuberculosis of head and neck is cervical lymph nodes; In addition, unlike tuberculosis, patients with pharyngeal tuberculosis may not have typical symptoms of tuberculosis infection, which makes the diagnosis very difficult. Traditional ultrasonography, CT and MRI are difficult to diagnose pharyngeal tuberculosis directly, which can only be diagnosed by referring to the clinical history.

24.7.2 Granulomatosis with Polyangiitis

Overview

In January 2011, the American College of Rheumatology (ACR), American Society of Nephrology (ASN), and European League Against Rheumatism (EULAR) Council recommended to rename the Wegener granulomatosis as granulomatosis with polyangiitis (GPA) [27]. Granulomatosis with polyangiitis is a kind of necrotic granulomatosis with polyangiitis, which is an autoimmune disease that can involve any organ or structure of the body. In most cases, granulomatosis with polyangiitis involves the nose, mouth, ears, lungs, and kidneys. Typical triad of granulomatosis with polyangiitis includes upper respiratory tract (paranasal sinus, middle ear, nasopharynx, and oropharynx), lower respiratory tract (trachea, bronchus, and lung parenchyma) and nephropathy. ENT manifestations are bloody nasal secretion and scab lasting for more than 1 month, or nasal ulcer; chronic rhinosinusitis, otitis media or mastoiditis lasting for more than 3 months; posterior orbital mass or inflammation; subglottic stenosis; Saddle nose deformity/nasal-paranasal sinus destructive disease.

Pathology Findings

The lesions involve small arteries, veins and capillaries, and occasionally large arteries. The typical pathological manifestation is inflammation of vascular walls, and it mainly invades upper and lower respiratory tract and kidney. It usually starts with focal granulomatous inflammation of nasal mucosa and lung tissue and then progresses to diffuse necrotic granulomatous inflammation of blood vessels. Otolaryngology is an early and easily involved part of the disease, which is mostly caused by local tissue inflammation, proliferation, and granuloma. There are multiple clinical manifestations of lesions in ear, nose and larynx, among which nasal obstruction, epistaxis, nasal cavity, and paranasal sinus tumors are the most common. Pathologically, various nonspecific inflammations by inflammatory cell infiltration are found, and granuloma, multinucleated giant cells, parenchymal necrosis, microabscess, and vasculitis can also be found [28].

Imaging Findings

When granulomatosis with polyangiitis involves nasopharynx and larynx, nasal septum and nasal concha can be involved, it spreads to other paranasal sinuses and eventually leads to the destruction and disappearance of maxillary sinus wall, ethmoidal sinus septum, papyraceous lamina and cribriform plate to form hollows (Fig. 24.18), which generally does not invade the hard palate. When the nasopharynx is involved, it shows irregular soft tissue shadows with bone destruction. Local lymph nodes are generally not swollen. GPA will affect many organ systems mainly lung and kidney. When the lung is involved, nodules or hollows may appear on CT, and some cases show multiple nodules distributed bilaterally. There are annular ground-glass shadows around the nodules, and the pleural effusion indicates pleural involvement [29]. MRI shows a wide scope of lesions, with irregular isointense T_1WI and isointense T_2WI, and mild to moderate enhancement by MRI enhanced examination.

Key Points of Diagnosis

1. The disease mainly occurs in older adults with inflammation in nose or mouth (painful or painless oral ulcer, or purulent or bloody nasal secretion)

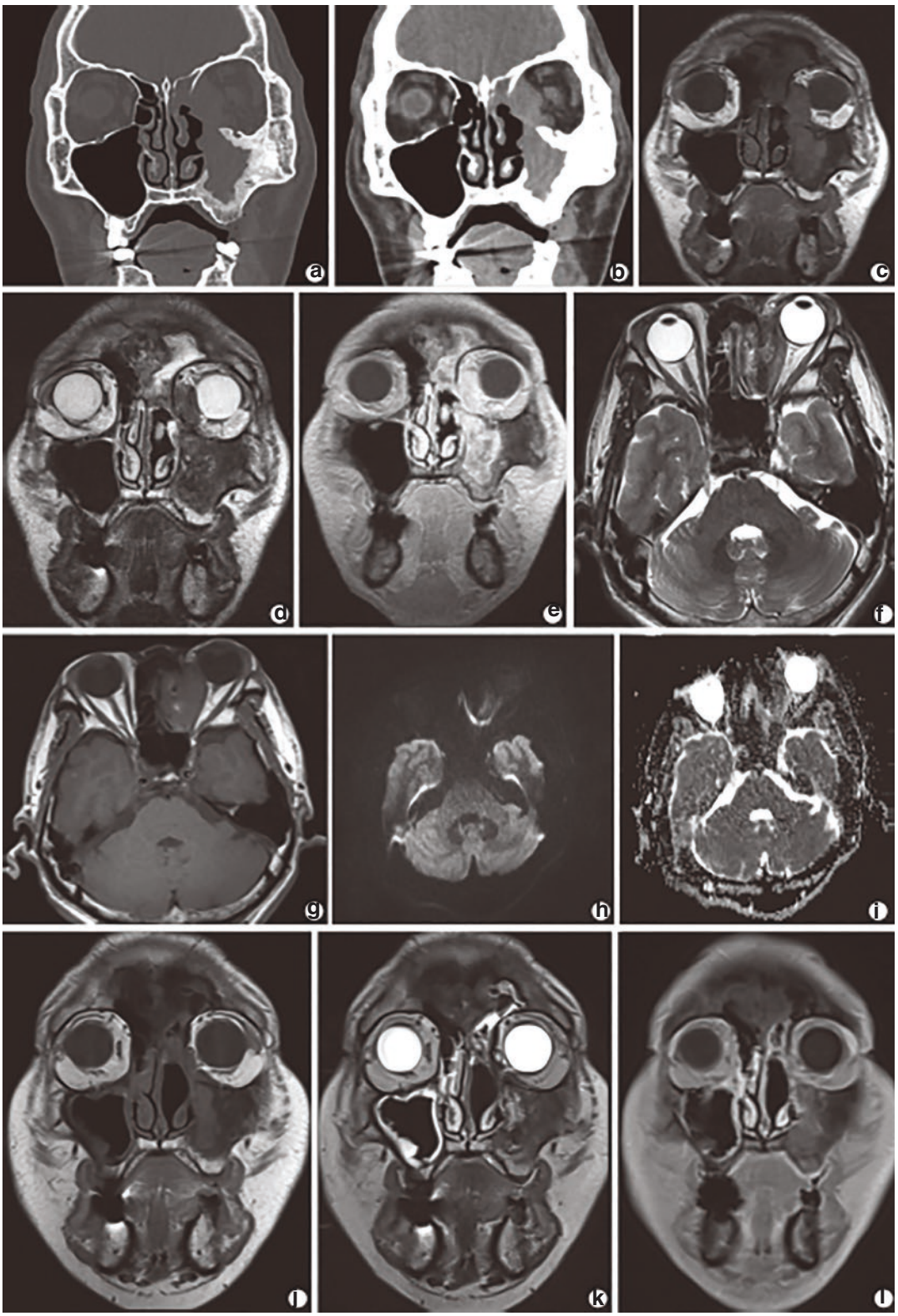

Fig. 24.18 Granulomatosis with polyangiitis of orbit and paranasal sinus. A 51-year-old male patient. Exophthalmos of left eye with lacrimation, swelling of the inner canthus in the left eye, conjunctival congestion, headache, and frequent sneezing; (**a** and **b**) CT coronal view shows soft tissue density shadows in left orbit, ethmoidal sinus, and maxillary sinus, with unclear margin with left medial rectus and inferior rectus, and bone destruction of partial cribriform plate, uncinate process, and maxillary sinus wall; (**c**, **d**, **f** and **g**) Non-enhanced scan indicates isointense on T_1WI, and slightly hypointense on T_2WI. (**e**) Enhancement shows marked and homogeneous enhancement; (**h**) Slightly hyperintense on DWI, and slight diffusion limitation of lesions; (**i**) ADC value of lesions in ADC diagram decreased slightly; (**j–l**) After nasal-orbital combined approach with resection of left orbital mass and paranasal sinus mass, non-enhanced MRI scan indicates that the lesions are significantly smaller than before, with isointense on T_1WI, isointense and hypointense on T_2WI, and unremarkable enhancement by enhanced scan

2. The typical manifestations are bone and cartilage destruction leading to saddle nose deformity and upper airway mass.
3. Chest X-ray examination is often conducted, and chest X-ray examination shows nodules, fixed infiltrative lesions or hollows; Abnormal urinary sediment, microscopic hematuria, or red cell cast.
4. Clinical triad includes upper respiratory tract symptoms (including rhinosinusitis, nasal mucosa ulcer, otitis media, subglottic stenosis), lower respiratory tract symptoms (cough, chest pain, hemoptysis), and glomerulonephritis.
5. CT shows that nasal septum, nasal concha, maxillary sinus wall, ethmoidal sinus septum, papyraceous lamina, and cribriform plate are destroyed and disappear to form hollows, which generally do not invade the hard palate. When the nasopharynx is involved, it shows irregular soft tissue shadows with bone destruction. MRI shows a wide scope of lesions, with irregular isointense T_1WI and isointense T_2WI, and mild to moderate enhancement by MRI enhanced examination.

Differential Diagnosis

1. **Lymphoma.** Most patients with Hodgkin's lymphoma have significant onset, most common in asymptomatic lymphadenopathy or mass found by chest X-ray examination, and a few patients may have nonspecific symptoms and signs that comply with infection rather than malignant tumor, and Hodgkin's lymphoma rarely conceals its onset. Lymphoma can damage the midline structures such as nasal septum and nasal concha in a short time when it involves otolaryngology, which involves more extensive scope, easy to invade the bone of maxillofacial skull base and resulting in soft tissue swelling.
2. Sarcoidosis. It can involve pharynx, larynx, nostril, and/or paranasal sinuses. All patients with systemic sarcoidosis and upper respiratory tract symptoms should be suspected of upper respiratory sarcoidosis. Laryngeal involvement of sarcoidosis usually involves supraglottic region, and subglottic region involvement is rare. Nasal obstruction, nasal scab formation, and anosmia are the most common symptoms in patients with rhinosinusitis caused by sarcoidosis. CT can show nonspecific mucosal thickening of nasal cavity and paranasal sinus, paranasal sinus with soft tissue shadows, and nasal sarcoidosis can cause bone destruction.

Status Quo and Progress of Research

When granulomatosis with polyangiitis involves nasal cavity and paranasal sinus, the imaging manifestations are mucosal thickening of paranasal sinus, bone destruction of nasal cavity and paranasal sinus, sclerosing osteitis and hyperostosis, etc. However, these signs are nonspecific and need to be confirmed by pathology and laboratory test. Granulomatosis with polyangiitis is a rare disease poorly understood, and we are unfamiliar with the clinical manifestations of GPA. If the clinical symptoms cannot be combined with imaging data, it is easy to cause misdiagnosis. Imaging findings of granulomatosis with polyangiitis are diverse, sometimes they are similar to other diseases, and it is difficult to make differential diagnoses. Therefore, the imaging diagnosis of GPA should be combined with clinical symptoms and other examinations, and referring to chest images to dynamically observe its changes to reduce the misdiagnosis rate [4].

24.7.3 Sarcoidosis

Overview

Sarcoidosis is a cryptogenic, immune-mediated multisystem disease pathologically featured by non-caseous epithelioid cell granuloma, which is most common in the lung and lymphatic system and can also involve the head and neck. It is common in nasopharynx, paranasal sinus, larynx, pharynx, salivary gland, and cervical lymph nodes. Sarcoidosis is distributed all over the world, regardless of age, sex, and region, people of any ethnic group can have sarcoidosis, but they are different in incidence rate. It is relatively common in female, non-smokers, and the onset age is usually under 50 years old, with peak period ranging from 20 to 29 years old. Sarcoidosis mostly occurs in people over 40 years old in China [30].

The severity of clinical manifestations of sarcoidosis is related to sarcoidosis classification, involved organs, and their functions. Patients with oropharynx involvement may have symptoms such as dyspnea, cough, stridor, dysphagia, obstructive sleep apnea. Patients with nasopharynx involvement may have symptoms such as progressive nasal obstruction, stuffy, tinnitus, and hearing loss; Painless enlarged lymph nodes in the neck are tender, and nasal mucosa is congested. Indirect nasopharyngoscopy shows nasopharyngeal mass, significant eminence in pharyngeal recess, smooth surface, and difficult hemorrhage by touch. The diagnosis of sarcoidosis needs to combine clinical symptoms, imaging findings, and pathological evidence, and exclude other granulomatous inflammatory diseases.

Pathology Findings

The general pathology is mostly isolated, well-defined, with red-yellow adenoid lobulated nodules that are mostly located in the midline of nasopharynx. The characteristic pathological change of sarcoidosis is isolated, dense, and non-caseous epithelioid cell granuloma. Epithelial granuloma consists of highly differentiated monocytes/macrophages (epithelioid cells and giant cells) and lymphocytes. The inclusions in the

cytoplasm of giant cells include astroid corpuscles and Schaumann corpuscles. The central part of granuloma is mainly composed of CD4+ lymphocytes, while CD8+ lymphocytes are in the periphery of granuloma. The diagnosis of sarcoidosis depends on pathological biopsy, which aims to find non-caseous epithelioid cell granuloma and exclude tuberculosis, metastatic tumor, lymphatic system tumor, or other granulomatous diseases.

Imaging Findings

1. **CT examination.** Swelling and thickening of the posterior wall of nasopharyngeal roof, iso-density shadows mass, which is not distinctively separated from the peripheral soft tissue, and marked enhancement by enhanced scan. No bone destruction of skull base. Enlarged lymph nodes in the neck [31].
2. **MRI examination.** MRI shows significantly thickened soft tissue shadows on the nasopharyngeal roof with unclear margin, homogeneous signal intensity, with isointense on T_1WI, hyperintense on T_2WI and slightly hyperintense on ADC, and homogeneous mild to moderate enhancement by enhanced examination. MRI can also show multiple enlarged lymph nodes in retropharyngeal space and neck.
3. **PET/CT examination.** ^{18}F-FDG PET/CT can obtain complete morphological and functional images of inflammatory activity localization of sarcoidosis, and visit the therapeutic effect of patients with sarcoidosis, and show specifically clinical application value, especially for atypical, complex and multi-system involvement cases. Imaging shows that the local metabolism of the lesion increased, and the sensitivity to larynx sarcoidosis can reach 80%.

Key Points of Diagnosis

1. Pharyngeal discomfort is a common clinical symptom, and the morphological manifestations detected by nasopharyngoscope show systemic sarcoidosis involving multiple systems
2. According to imaging, the lesions often involve the posterior wall of the nasopharyngeal roof, with local mucosal thickening or formation of lumps.
3. CT shows iso-density mass in nasopharynx with unclear margin, homogeneous signal on MRI, isointense on T_1WI, hyperintense on T_2WI, and slightly hyperintense on ADC, and homogeneous mild to moderate enhancement by enhanced examination. MRI can also show multiple enlarged lymph nodes in retropharyngeal space and neck.
4. ^{18}F-FDG PET/CT shows that the local metabolism of the lesion is increased, and similar lesions in multiple systems of the whole body can be found.
5. The diagnosis must be confirmed by pathological biopsy.

Differential Diagnosis

1. **Pharyngeal infection or abscess.** It has significant symptoms, such as sore throat and fever. Pharyngeal soft tissue is significantly swollen without clear margin. The enhanced scan shows mild enhancement, and it shows marked ring enhancement when abscess is formed.
2. **Pharyngeal tuberculosis.** Patients often have systemic tuberculosis poisoning symptoms, which are difficult to differentiate from sarcoidosis due to similar imaging findings, and biopsy is required for diagnosis.
3. **Pharyngeal tumor.** It usually manifests as iso-density masses by CT. MRI shows the masses more clearly, with mild and moderate enhancement by enhanced scan and clear margin from peripheral tissues. The malignant tumor shows heterogeneous density or signal intensity and necrosis, often complicated with regional lymph node enlargement.

Status Quo and Progress of Research

In recent years, ^{18}F-FDG PET/CT has been widely used in the diagnosis and follow-up of sarcoidosis. As a metabolic imaging technique, ^{18}F-FDG PET/CT imaging is sensitive to the evaluation of sarcoidosis and can find occult lesions that cannot be found by conventional imaging technologies, such as CT and MRI [32]. PET/CT examination shows that metabolic activity of part involved by sarcoidosis is enhanced, which is more sensitive than other imaging examinations, and it is directional for judging the other parts of the whole body involved by sarcoidosis, which is of great significance for judging parts requiring biopsy. Meanwhile, PET/CT can also be used to judge whether other important organs are involved, such as heart and nervous system, which also provides bases for evaluating prognosis.

24.7.4 Fungal Infectious Granuloma

Overview

Pharyngeal fungal infections include coccidiosis, histoplasmosis, spores, cryptococcus, candida, sporotrichosis, and many other fungi. It is mostly found in patients with cachexia, diabetes, hypoparathyroid glandism, AIDS, and receiving radiotherapy. Due to the wide application of corticosteroids and antibiotics, the incidence increases. The decrease of human immunity, especially the decrease of cellular immunity, is an important cause of the disease. In recent years, literature statistics at home and abroad show that the number of patients with unknown etiology increases, and 50% of the cases are hosts with normal immunity. Transmission routes may include respiratory tract, digestive tract and skin. Clinical manifestations include pharyngeal discomfort, gradually increased painless parapharyngeal lump, and no symp-

toms such as chills, fever, redness, and heat pain. Physical examination: Parapharyngeal mass, covered with mucosa.

Pathology Findings

For fungal granuloma, the pathogen can be identified according to clinical manifestations and fungal culture, but sometimes the positive results may be caused by pollution, and histopathology is the gold standard for diagnosis of fungal granuloma. Different from non-infectious granuloma, the main characteristic of tissue reaction of deep fungal Infection is the mixed inflammatory cell infiltration involving tissue cells. Histopathological biopsy by aspiration biopsy of lesion shows that inflammation significantly affects whole layers of tissue, and granuloma is infiltrated by histiocytes, multinucleated giant cells interspersed with lymphocytes, plasma cells, and neutrophils

Imaging Findings

1. **CT examination.** The soft tissue mass of pharynx shows unclear margin, infiltrative growth, and relatively low density in the center. Adjacent soft tissues, including muscles, may be invaded. Multiple cervical spaces can be involved across fascia. By enhanced scan, it shows moderate and relatively homogeneous enhancement. If there is central purulent necrosis, granulation tissue, and strong fibrosis around it, a marked ring enhancement can be found. Some cases may have mild regional reactive lymph node proliferation. CT scan is very helpful for early diagnosis, estimating the extent of lesions and patient response to treatment [33, 34].
2. **MRI examination.** Pharyngeal mass shows isointense on T_1WI and T_2WI with moderate enhancement by contrast-enhanced scan [33, 34].

Key Points of Diagnosis

1. It often occurs in patients with low immunity, manifesting as discomfort in pharynx and gradually increased painless parapharyngeal lump. No such symptoms as chills, fever, redness, and heat pain.
2. Imaging findings show pharyngeal soft tissue mass with iso-density shadows and indistinct border, isointense on T_1WI and T_2WI, moderate homogeneous enhancement by enhanced scan, and ring enhancement indicating the central tissue necrosis.
3. Biopsy is necessary to understand the histological features of lesions and determine the types of pathogens.

Differential Diagnosis

1. **Parapharyngeal abscess.** It shows severe infection symptoms, blurred edge of abscess, low density in center, typical ring enhancement by enhanced scan, and multilocular changes found occasionally.
2. **Pharyngeal tuberculosis.** Patients often have systemic tuberculosis poisoning symptoms, which are difficult to differentiate from fungal infection due to similar imaging findings, and biopsy is required for diagnosis.
3. **Pharyngeal malignant tumor.** It is a solid lump in pharynx, with relatively clear margin and heterogeneous enhancement by enhanced scan. Enlarged lymph nodes are found in corresponding areas, which is more common than fungal infectious granuloma.

Status Quo and Progress of Research

Fungal infection in larynx is relatively rare. Fungi can multiply in large numbers only under the conditions of decreased immunity, tumor radiotherapy, decreased resistance of local tissues, systemic wasting diseases, metabolic diseases, and inappropriate long-term application of antibiotics and steroid hormones. It is difficult to judge the histological characteristics and pathogen types of lesions by imaging examination, and biopsy is necessary for diagnosis. In some rare cases, fungal infectious granuloma may coexist with tumor. In that case, the common imaging methods are easy to lead to a missed diagnosis. Therefore, the histopathologic examination should be combined for improving detection rate [35].

References

1. Qibing C, Yan W, Fen L, et al. Research Progress on etiology and pathogenesis of chronic pharyngitis. J Audiol Speech Pathol. 2019;27(2):224–8.
2. Peng Z, Xinlian D, Yaohua Y, et al. MRI findings and clinical significance of thickening of Posterior Wall of nasopharyngeal roof. Chin Imaging J Integr Tradit Western Med. 2017;15(2):131–3. 136
3. Jidong P, Kanghua Z, Junyuan Z, et al. MRI diagnosis of chronic Nasopharyngitis. J Gannan Med Univ. 2013;33(1):20–2.
4. Abdel-Aziz M, El-Fouly M, Nassar A, et al. The effect of hypertrophied tonsils on the velopharyngeal function in children with normal palate. Int J Pediatr Otorhinolaryngol. 2019;119:59–62.
5. Dan W. Imaging diagnosis of adenoid hypertrophy in children. J Chin Health Nutr. 2017;27(13):316.
6. Surov A, Bartel-Friedrich S, Wienke A, et al. MRI of nasopharyngeal adenoid hypertrophy. Neuroradiol J. 2016;29(5):408–12.
7. Xiaoyun H, Zhenyan Z, Xiaomin L, et al. Comparison of CT and MRI examination in children with adenoid hypertrophy. Med J Nat Def For Southwest China. 2016;26(2):171–3.
8. Giurintano JP, Kortebein S, Sebelik M, et al. Intratonsillar abscess: a not-so-rare clinical entity. Int J Pediatr Otorhinolaryngol. 2019;119:38–40.
9. Shaojian W, Jiao C, Zhibang Z, et al. Value of CT enhanced scan in diagnosing tonsillar inflammatory lesions. J Practic Radiol. 2018;34(8):1176–8.
10. Bin Y, Qintai Y, Tao W, et al. Value of enhanced CT in differential diagnosis of Peritonsillar abscess from other diseases in tonsils. Chin J Otorhinolaryngol Head Neck Surg. 2014;49(2):131–5.
11. Klein MR. Infections of the oropharynx. Emerg Med Clin N Am. 2019;37(1):69–80.
12. Hong YY, Lin GB, Lin C, et al. Adult parapharyngeal and retropharyngeal abscesses: clinical features and their implications for

treatment strategy. Lin Chung Er Bi Yan Hou Tou Jing Wai Ke Za Zhi. 2018;32(17):1304–8.
13. Jain A, Singh I, Meher R, et al. Deep neck space abscesses in children below 5 years of age and their complications. Int J Pediatr Otorhinolaryngol. 2018;109:40–3.
14. Desai L, Shah I, Shaan M. Retropharyngeal abscess as a paradoxical reaction in a child with multi-drug-resistant tuberculosis. Paediatri Int Child Health. 2019;39(4):287–9.
15. Argintaru N, Carr D. Retropharyngeal abscess: a subtle presentation of a deep space neck infection. J Emerg Med. 2017;53(4):568–9.
16. Sudhanthar S, Garg A, Gold J, et al. Parapharyngeal abscess: a difficult diagnosis in younger children. Clin Case Rep. 2019;7(6):1218–21.
17. Kosko J, Casey J. Retropharyngeal and parapharyngeal abscesses: factors in medical management failure. Ear Nose Throat J. 2017;96(1):12–5.
18. Page C, Biet A, Zaatar R, et al. Parapharyngeal abscess: diagnosis and treatment. Eur Arch Otorhinolaryngol. 2008;265(6):681–6.
19. Ludwig BJ, Wang J, Nadgir RN, et al. Imaging of cervical lymphadeno-pathy in children and young adults. AJR. 2012;199(11):1105–13.
20. Yingying D, Kun L, Yongping W. CT diagnosis of reactive proliferation of lymph nodes. J Practic Radiol. 2006;22(5):584–6.
21. Shuixing Z, Ganjun J, Zhongping Z, et al. Differential diagnosis of nasopharyngeal carcinoma and inflammatory hyperplastic diseases by diffusion weighted imaging based on irrelevant motion in voxels. Chin J Radiol. 2013;47(7):617–21.
22. Tzankov A, Dirnhofer S. A pattern-based approach to reactive lymphadenopathies. Semin Diagn Pathol. 2018;35(1):4–19.
23. Sharma HS, Kurl DN, Kamal MZM. Tuberculoid granulomatous lesion of the pharynx-review of the literature. Auris Nasus Larynx. 1998;25:187–91.
24. Moon WK, Han MH, Chang KH, et al. CT and MR imaging of head and neck tuberculosis. Radiographics. 1997;17(2):391–402.
25. Hui D, Heng L, Gaofeng Z, et al. CT manifestations of nasopharyngeal tuberculosis. Sichuan Med J. 2017;38(2):229–31.
26. Pang P, Duan W, Liu S, et al. Clinical study of tuberculosis in the head and neck region-11 years' experience and a review of the literature. Emerg Microbes Infect. 2018;7(1):4.
27. Falk RJ, Gross WL, Guillevin L, et al. Granulomatosis with polyangiitis (Wegener's): an alternative name for Wegener's granulomatosis. Arthritis Rheum. 2011;63(4):587–8. 863–864
28. Dongfeng L, Xiaobing L, Feng H, et al. Clinical and pathological analysis of Wegener granulomatosis. Chin J Rheumatol. 2003;7(8):482–6.
29. Shuang W, Zhiyuan S, Wei H. Feature analysis of CT manifestations of granulomatosis with Polyangiitis. Jiangsu Med J. 2015;41(13):1570–1.
30. Morgenthau AS, Teirstein AS. Sarcoidosis of the upper and lower airways. Expert Rev Respir Med. 2011;5(6):823–33.
31. Braun JJ, Imperiale A, Riehm S, et al. Imaging in sinonasal sarcoidosis: CT, MRI, 67Gallium scintigraphy and 18F-FDG PET/CT features. J Neuroradiol. 2010;37(3):172–81.
32. Jingjing Z, Xinli X, Ke S, et al. Feature analysis of 18F-FDG PET/CT imaging of multisystem sarcoidosis. J Zhengzhou University (Medical Edition). 2017;52(06):779–82.
33. Razek AAKA, Castillo M. Imaging appearance of granulomatous lesions of head and neck. Eur J Radiol. 2010;76(1):52–60.
34. Park JK, Lee HK, Ha HK, et al. Cervicofacial actinomycosis: CT and MR imaging findings in seven patients. Am J Neuroradiol. 2003;24(3):331–5.
35. Shikino K, Ikusaka M, Takada T. Cervicofacial actinomycosis. J Gen Intern Med. 2015;30(2):263.

Part VII

Infectious and Inflammatory Diseases of Larynx

Larynx Lesions

25

Huazheng Dong and Yubo Lyu

25.1 Infantile Acute Laryngitis

Overview

Acute laryngitis in children is caused by viral infection of the upper respiratory tract, which mainly occurs in children from 6 months to 3 years old, with peak age at 2 years old, especially in male infants [1]. The most common pathogens are influenza virus, parainfluenza virus, adenovirus, interstitial lung virus, respiratory syncytial virus and coronavirus [1]. Most of the infections are secondary to upper respiratory tract infection, which is originated from nasopharynx and spreads along respiratory epithelium, then causing inflammation in larynx and glottic portion. Congestion and edema in the area are important causes of airway obstruction to different extents. When the originally unobstructed airway narrows due to mucosal swelling, the normal airflow is restricted, resulting in poor ventilation and dyspnea. The acute laryngitis deteriorates and progresses rapidly, thus the mild airway constriction develops to severe obstruction within 24–48 h. Children may have barking cough, dysphonia, aphonia, hoarse crying and inspiratory stridor. In some severe cases, in addition to severe dyspnea and dysphoria, pallor, cyanosis, numbness, epilepsy, apnea and even death may occur. Larynx cavity is narrow in children, which is about 1/5 of that of adults, and the laryngeal nervous system is underdeveloped, thus the secretion is difficult to be expectorated, and laryngospasm is more likely to occur.

Pathology Findings

Acute laryngitis in children mainly occurs in the laryngeal mucosa around the subglottic cavity, and inflammation developing downward may involve the trachea. Microscopically, congestion, edema, and neutrophil infiltration are found in mucosa and submucosa of subglottic cavity. In severe cases, cellulitis occurs inferior to the laryngeal mucosa, and abscess formation and even necrotizing inflammation are found in some cases.

Imaging Findings

1. **X-ray Examination.** PA view shows that partial arc-shaped eminence on the lateral wall of the normal subglottic trachea disappears, and the laryngeal mucosa shows "steeple sign" due to edema. In the lateral view, the hypopharyngeal cavity is over-expanded in inspiratory phase, and the subglottic trachea mucosa is blurred in expiratory phase.
2. **CT Examination.** Multiple parts of laryngeal mucosa have diffuse swelling and thickening, including aryepiglottic fold, vocal cords, ventricular fold and subglottic area, with smooth margins and bilateral symmetry, and the larynx cavity has constriction to different extents. However, the paralaryngeal space is clearly shown, without surrounding bone destruction (Fig. 25.1).
3. **MRI Examination.** Thickening and swelling of laryngeal mucosa, hypointense on T_1WI and hyperintense on T_2WI, and hyperintense on DWI. The paralaryngeal space is clear, without abnormal signal in the surrounding bone, and the larynx cavity has constriction to different extents.
4. **Ultrasonography.** The ultrasonography of adult larynx is seldom used in clinical practice. However, as thyroid cartilage in children has not been calcified, ultrasonography can clearly show the laryngeal structure. Ultrasonography of acute laryngitis in children can indicate swelling and thickening of laryngeal mucosa and stenosis of larynx cavity. When local abscess is formed by laryngeal inflammation, lumpy fluid sonolucent areas are found in the focus area, and the internal echo is heterogeneous (Fig. 25.2).

H. Dong
Tianjin Academy of Traditional Chinese Medicine Affiliated Hospital, Tianjin, China

Y. Lyu (✉)
Jiahui International Hospital, Shanghai, China

H. Li et al. (eds.), *Radiology of Infectious and Inflammatory Diseases - Volume 2*,
https://doi.org/10.1007/978-981-16-8841-6_25

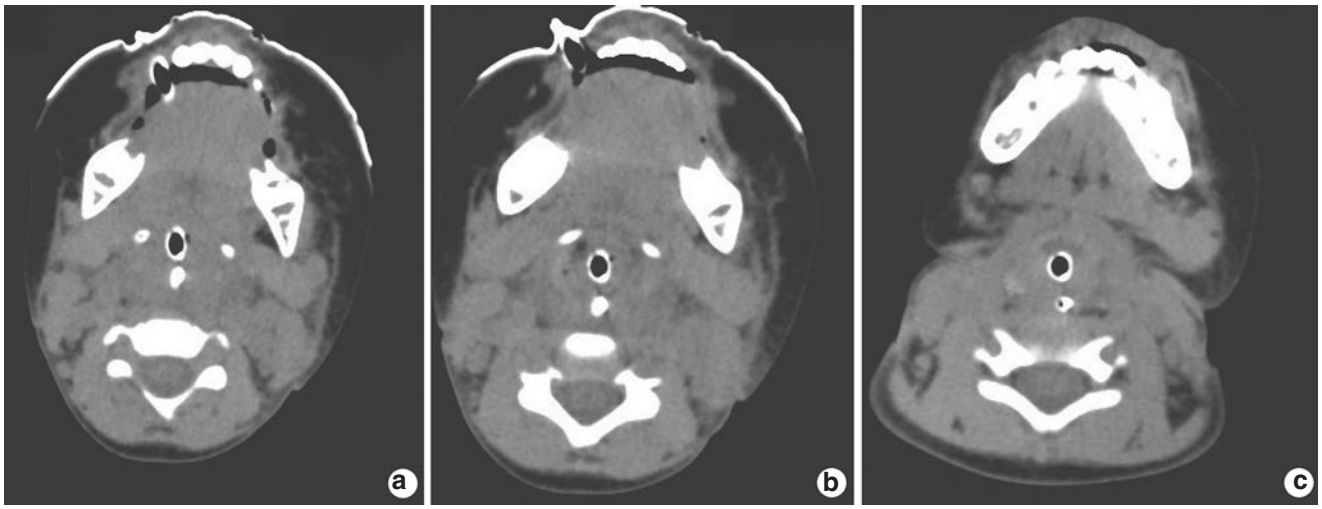

Fig. 25.1 Acute laryngitis in children. A 16-month-old female patient. Fever with acute dyspnea for several hours. (**a**–**c**) Non-enhanced scan of larynx shows significant thickening and swelling of mucosae of larynx in the scanning area, with smooth margins and bilateral symmetry, reduced larynx cavity, and cathetering shadows in the airway

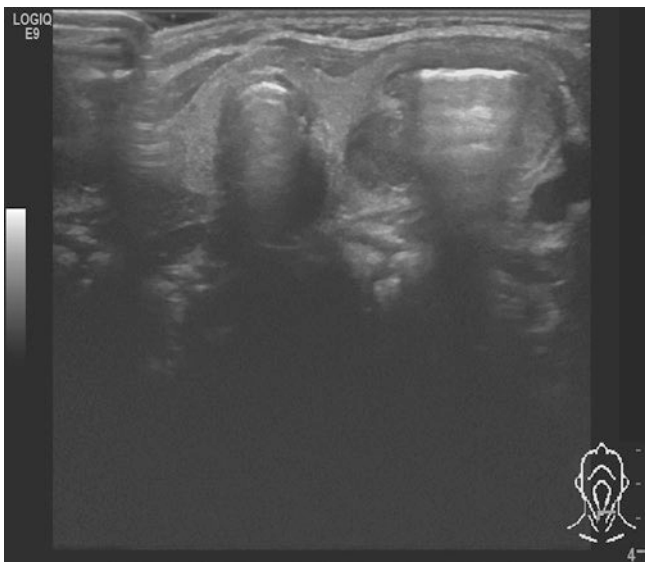

Fig. 25.2 Laryngitis with abscess formation. Laryngeal ultrasonography shows widened left piriform recess, with significant fluid sonolucent area and internal homogeneous echo, which is considered as piriform recess infectious inflammation with abscess and liquefaction

Key Points of Diagnosis

1. Clinical manifestations: Acute onset, barking cough and inspiratory dyspnea are the main clinical features of acute laryngitis in children.
2. X-ray shows disappearance of partial arc-shaped eminence on the lateral wall of the subglottic trachea and normal epiglottis, which are main imaging features.
3. CT shows multiple parts of laryngeal mucosa having diffuse swelling and thickening, including aryepiglottic fold, vocal cords, ventricular fold and subglottic area, with smooth margins and bilateral symmetry and the larynx cavity has constriction to different extents. However, the paralaryngeal space is clearly shown, without surrounding bone destruction.

Differential Diagnosis

1. **Foreign Matters in Respiratory Tract.** Patients mostly have history of inhalation of foreign matters, paroxysmal choking cough with inspiratory dyspnea, with slap sound by active foreign matters in trachea. X-ray photography can definitely diagnose radiopaque foreign matters. Ultrasound can detect foreign matters in larynx, including metallic and nonmetallic foreign matters. Foreign matters show strong echo with shadows in posterior. The shape of foreign matters and surrounding complications can be observed, and bedside dynamic observation is conducted to monitor and remove the foreign matters [2].
2. **Laryngospasm.** It is common in small infants. It has acute onset, shows no hoarseness and develops within a short period. Clinical symptoms are severe, and they can disappear immediately when the spasm is relieved.
3. **Throat Diphtheria.** It has slow onset and severe systemic toxic symptoms. Patchy gray-white albuginea is found in larynx examination. It is difficult to be wiped off and easy to bleed if it is peeled off forcedly. Sometimes, the cervical lymph nodes are enlarged, showing bovine neck shape. Diphtheria can be found by smear and culture.
4. **Acute Epiglottitis.** It is an acute inflammatory disease mainly involving the epiglottis and its peripheral tissues, characterized by severe edema of epiglottis. The lateral X-ray film of the neck shows that the epiglottis volume is

thickened, enlarged and swollen, and part of the anterior epiglottis space disappears. On non-enhanced CT scan, the epiglottis is thickened and swollen, showing soft tissue density shadows. In severe cases, the anterior epiglottis space disappears. If abscess is formed, irregular mass soft tissue density shadows are found. Ring enhancement is found by CT enhanced scan. On non-enhanced MRI scan, epiglottis thickening is found, showing hypointense on T_1WI and hyperintense on T_2WI.

Status Quo and Progress of Research

Acute laryngitis in children has a rapid onset and progress in clinical symptoms. Most patients can be diagnosed by physical examination and clinical symptoms. When complications such as laryngeal abscess occur, CT examination is often used to determine the scope of the lesion. Because of the sensitivity of minors to X-ray, especially the thyroid gland, which is a sensitive organ in the neck, CT examination should be avoided if possible, and should be replaced by laryngeal ultrasonography when necessary [2, 3].

25.2 Acute Epiglottitis

Overview

Acute epiglottitis, also known as supraglottitis, is a special acute inflammatory disease that mainly involves the epiglottis and its peripheral tissues (including vallecula epiglottic, aryepiglottic fold) in the supraglottic portion of larynx. It manifests as severe edema of epiglottis, rapid onset and critical condition, and is one of the acute and severe diseases in laryngology. If treatment is delayed, misdiagnosed or missed, resulting in untimely treatment or improper treatment, the patient will die within a few hours.

The causes of acute epiglottitis include infection, allergic reaction, trauma and acute inflammation of adjacently involved organs, among which infection is the most common cause. The most common pathogen is *Haemophilus influenzae* type B, which has been gradually eliminated by vaccination [4]. Trauma and systemic allergic reaction can cause inflammation and edema in epiglottal region. Acute inflammation of adjacent organs, such as acute tonsillitis and pharyngitis, can spread and invade epiglottis mucosa and cause edema; In addition, it can be secondary to acute infectious diseases.

Acute epiglottitis can occur in both adults and children all year round, mainly in winter and spring. The disease has rapid onset and progresses rapidly. The main symptoms are severe sore throat, slurred pronunciation, dysphagia and inspiratory dyspnea. Dyspnea appears early and progress rapidly in severe patients, and may have "three depressions signs", which lead to suffocation within a few hours. In addition, it can be complicated with systemic symptoms, and mild systemic symptoms are not obvious; Severe cases often have fever and chills, complicated with headache, fatigue, anorexia and other symptoms. Children and elderly patients have many significant systemic symptoms, and the disease progresses rapidly. Acute failure can occur in severe patients, which manifests as mental fatigue, physical weakness, cold moist limbs, pale face, fast and thin pulse, blood pressure drop, and even fainting and shock [4].

Pathology Findings

The mucosa of epiglottis lingual surface and its lateral aryepiglottic folds is relatively loose and has abundant vascular network [5], so its inflammation often starts from epiglottic lingual surface and causes epiglottic congestion and swelling, which can increase its thickness to six to seven times than normal case. Inflammation gradually extends to arytenoid cartilage or ventricular fold, and in severe cases, it involves adjacent pharyngeal tissue and anterior cervical soft tissue, but vocal cords and subglottic area are rarely involved. Pathological changes of acute epiglottitis can be divided into the following three types.

1. **Acute Catarrhal Type.** Diffuse mucosal congestion and edema, infiltration of monocytes and polymorphonuclear cells, epiglottitis swelling.
2. **Acute Edematous Type.** Epiglottis is enlarged spherically, interstitial tissue has significant edema, and inflammatory cell infiltration increases. Abscess may form locally in patients with severe inflammation.
3. **Acute Ulcer Type.** It is rare, and the disease develops rapidly and severely. Lesions usually invade submucosa and glandular tissues, with local suppuration and ulcer, erosion of vascular wall and hemorrhage.

Imaging Findings

1. **X-ray Examination.** It has certain value in the diagnosis of acute epiglottitis. The enlarged epiglottis is found on the lateral view of the neck, like a thumb, forming a "thumb sign". The shadow of hypopharynx cavity is reduced with clear margin. In severe cases, the trachea is constricted and obstructed.
2. **CT Examination.** The non-enhanced scan on transverse plane indicates diffuse edema, thickening and swelling of epiglottis, which may be complicated with involvement and thickening of aryepiglottic fold. The density of anterior epiglottis space increases and its margin is unclear. Adult vocal cords and subglottic portion are always normal, while laryngeal submucous tissue is loose in children, which can show expansive changes in subglottic area. When abscess is formed in epiglottis, a slightly high-density area appears in

edema area in the early stage, and the density is lowered when abscess is formed. CT examination has the risk of delaying diagnosis. It is mainly used to observe abscess formation, exclude other diseases such as deep cervical abscess and foreign matters in larynx. CT enhanced scan indicates thickening and swelling of epiglottis in arterial phase, showing marked and heterogeneous enhancement and the necrotic area shows liquid density shadows without marked enhancement. In venous phase, epiglottis shows mild enhancement. In case of abscess formation, the thin wall with ring enhancement and smooth capsule formation are found (Figs. 25.3 and 25.4).

3. **MRI Examination.** Epiglottis is enlarged, thickened, and swollen, with diffuse edema, unclear margin, hypointense on T_1WI and hyperintense on T_2WI, and airway obstruction in severe cases. DWI shows slightly hyperintense. However, MRI also has the risk of delaying diagnosis, it can be used to exclude other diseases and confirm related complications.
4. **Ultrasonography.** It shows swelling of epiglottis, blurred contour, increased antero-posterior diameter, and heterogeneous internal echo.

Key Points of Diagnosis

1. The patient has rapid onset, mostly with high fever and dysphagia, unremarkable hoarseness and cough, and dyspnea can occur quickly.
2. X-ray cervical lateral view in erect position is the first choice for imaging examination. It is found that the shadow of hypopharynx cavity is reduced and the swelling of epiglottis shows "thumb sign."
3. CT examination shows that the epiglottis is thickened and enlarged, with marked and heterogeneous enhancement, and the necrotic area shows liquid density shadows without marked enhancement. In venous phase, epiglottis shows mild enhancement. In case of abscess formation, thin wall with ring enhancement and smooth capsule formation are found.

Differential Diagnosis

1. **Acute Laryngotracheitis.** It has rapid onset in general, which takes 1–2 days. The clinical manifestations are high fever, with or without hoarseness, and most of them are paroxysmal cough. The laryngoscopy shows localized hemorrhage and swelling of subglottic cavity. It is often caused by *Staphylococcus aureus*.
2. **Laryngeal Foreign Matters.** Patients often have definite history of foreign matters inhalation, severe cough, dyspnea, and other symptoms. High-density foreign matter shadows are found by imaging examination.
3. **Laryngospasm.** Patients may have dyspnea to different extents, without hoarseness and barking cough. It has rapid onset and can disappear immediately when the spasm factor is eliminated. Imaging examination shows that the glottic space is significantly constricted, and there

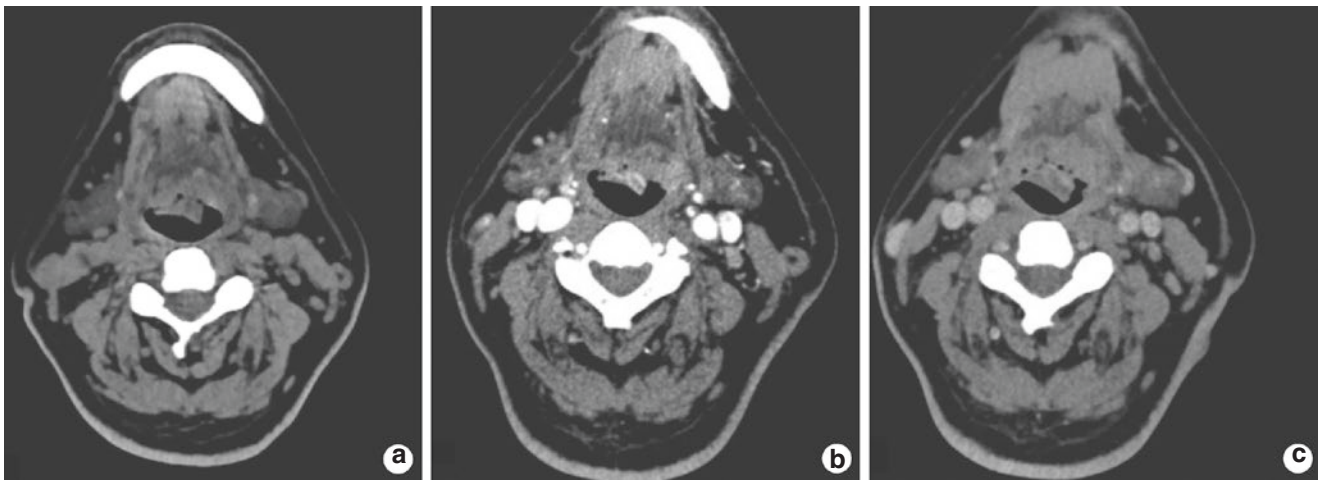

Fig. 25.3 Acute epiglottitis with abscess formation on the left side of anterior epiglottis space. A 60-year-old male patient. The patient was admitted mainly due to fever and upper respiratory tract infection for 1 week, with dyspnea for 1 h. (**a**) Non-enhanced CT scan of larynx shows that epiglottis is significantly thickened and swollen, and patchy soft tissue density shadows are found on the left side of the anterior epiglottis space. The CT value is about 35HU, the internal density is heterogeneous, involving the aryepiglottic fold, the left piriform recess is constricted, reaching the left paraglottic space, and the left anterior epiglottis space is significantly constricted or even partially disappears; (**b**) The swollen epiglottis mucosa with marked enhancement in the arterial phase by enhanced CT of larynx; (**c**) The thickened epiglottis shows homogeneous and mild enhancement during the venous phase by enhanced CT of larynx

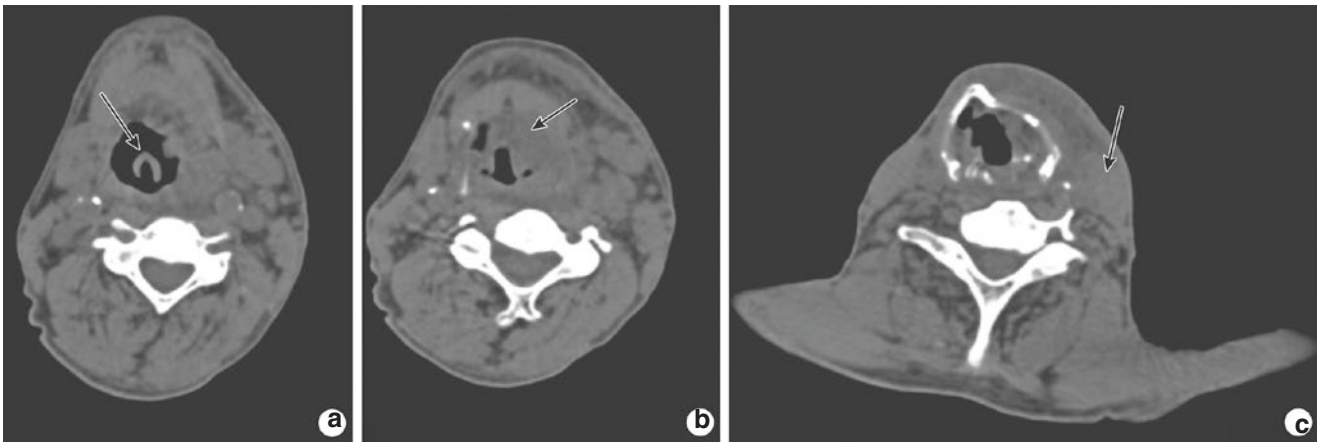

Fig. 25.4 Acute epiglottitis. A 63-year-old male patient. The patient was admitted mainly due to fever, severe sore throat and dyspnea, complicated with swelling and pain of soft tissue on the left side of neck for hours. (**a**) Non-enhanced CT scan of larynx shows that the mucosa of epiglottis free margin at the superior border of epiglottis on transverse plane is thickened; (**b**) The horizontal anterior epiglottic space of hyoid bone is blurred, soft tissue density shadows are found, and the parapharyngeal and prevertebral spaces are clear; (**c**) At thyroid cartilage level, the volume of left tonsil increases, soft tissue is thickened, and the shadow of subcutaneous soft tissue in neck is thickened. The above extensive lesions indicate inflammatory lesions: acute epiglottitis, inflammation of left tonsil and subcutaneous soft tissue of neck

is no significant abnormality in epiglottis and paraglottic space.

4. **Laryngeal Diphtheria.** It has a slow onset, which manifests as mild fever, complicated with hoarseness and severe cough. Endoscopy shows that local mucosa has gray-white pseudomembrane, which is difficult to be removed. Diphtheria is tested by bacterial culture of laryngeal secretion. Imaging examination shows that epiglottis enlargement is not obvious.

Status Quo and Progress of Research

X-ray cervical lateral view in erect position is the first imaging choice for diagnosis of acute epiglottitis. In 2018, Kim et al. [6] used objective radiographic parameters in X-ray plain film in cervical lateral view, including width of third cervical vertebra, width of epiglottis base, width of epiglottis roof, width of hypopharynx, retropharyngeal soft tissue, aryepiglottic fold and paratracheal soft tissue, to diagnose acute epiglottitis. The measured objective parameters of epiglottis base and bottom on X-ray plain film in cervical lateral view were very accurate, which could be used for screening and diagnosis of acute epiglottitis, but further research is needed to determine its applicability in clinical practice. CT examination mainly determines whether abscess is formed, thus prompting further clinical drainage treatment.

25.3 Chronic Hyperplastic Laryngitis

Overview

Chronic laryngitis is a nonspecific inflammation of the larynx, which lasts at least 3 weeks. Chronic hyperplastic laryngitis is a benign hyperplastic disease in larynx, which is evolved from chronic simple laryngitis, it involves a wide scope of lesions, mainly manifesting as thickening and proliferation of laryngeal mucosa. Its incidence rate is about 0.35% per year [7]. Clinical symptoms are usually nonspecific, including dysphonia, hoarseness, sore throat, chronic cough, and occasional dizziness and dysphagia. It is reported that [7] the etiology can be divided into three categories.

1. **Infection Factor.** It includes pathogens such as mycobacteria, blastomycete, parasporal bacteria, coccidiodes, histoplasma bacteria and cryptococcus, among which viral infection is rare [7].
2. **Inflammatory Factor.** It includes laryngopharyngeal reflux, idiopathic ulcerative laryngitis, allergic laryngitis and sarcoidosis.
3. **Autoimmune Disease.** Granuloma with multiple vasculitis, recurrent polychondritis, rheumatoid arthritis, Sjögren syndrome, systemic lupus erythematosus and mucosal pemphigoid.

Pathology Findings

The congestion and swelling of laryngeal mucosa is noted at the initial stage of the disease, which can infiltrate into deep tissues. The secretion of submucosal glands increases with lymphocytes infiltration. At this time, the above lesions are chronic simple laryngitis. The lesions continue and cause fibrosis and gland atrophy. The mucosa gradually thickens, changing from dark red to gray blue, the gland secretion decreases, the mucosa epithelium proliferates, showing squamous metaplasia and keratinization to different extents, and the submucosal lymphocytes and

plasma cells have infiltration, which is called chronic hyperplastic laryngitis.

Imaging Findings

1. **X-ray Examination.** It often shows unremarkable abnormity.
2. **CT Examination.** It shows that the laryngeal mucosa is generally thickened, with homogeneous density and wide scope of lesions. The ventricular fold, vocal cords and aryepiglottic folds are thickened, the vocal cords are uneven and asymmetric bilaterally, especially in the interarytenoid area, and the central part is raised or wrinkled. The paralaryngeal space is clear with no infiltration change and unremarkable change in laryngeal cartilage. The vocal cords show soft tissue proliferation, and enhanced scan shows that the lesions are thickened but the mucosa enhancement is unremarkable (Figs. 25.5 and 25.6).
3. **MRI Examination.** It can clearly show the larynx cavity structure, but it is easily affected by artifacts of respiratory motion. It is found that the laryngeal mucosa is generally thickened, showing isointense on T_1WI and slightly hyperintense on T_2WI, and the paralaryngeal space and laryngeal cartilage are usually normal.

Key Points of Diagnosis

1. According to the clinical characteristics of patients with slow onset, long duration and long-term hoarseness and results of laryngoscopy, a preliminary diagnosis can be made [8].
2. CT and MRI examinations are generally used to show thickening of vocal cords without significant infiltration and marked enhancement of peripheral structures.

Differential Diagnosis

1. **Laryngeal Tuberculosis.** It occurs mostly in young adults and is common in anterior larynx and mostly in the posterior vocal cords. The disease manifests as asymmetric and diffuse thickening of laryngeal structure, with heterogeneous density, no destruction to the surrounding laryngeal cartilage, and rare involvement in the subglottic region. The enhanced scan shows heterogeneous speckle enhancement. The diagnosis should be made in combination with chest-related imaging examination, sputum culture and body temperature monitoring, which are particularly important for the diagnosis of suspected cases.
2. **Amyloidosis Lrynx.** It mainly manifests as laryngeal masses by imaging examination, with a wide scope of lesions and calcification in some cases. The density of calcified foci is low, the CT value is 40–60 HU, scattered as sand. The deposited substance of amyloidosis is acellular and insoluble protein-like substance, which has characteristic features on MRI images, showing hypointense on T_1WI and hypointense on T_2WI.
3. **Laryngeal Cancer.** It mostly occurs in anterior larynx. In the early stage, it is mostly confined unilaterally, the lesion area develops rapidly, and the clinical symptoms

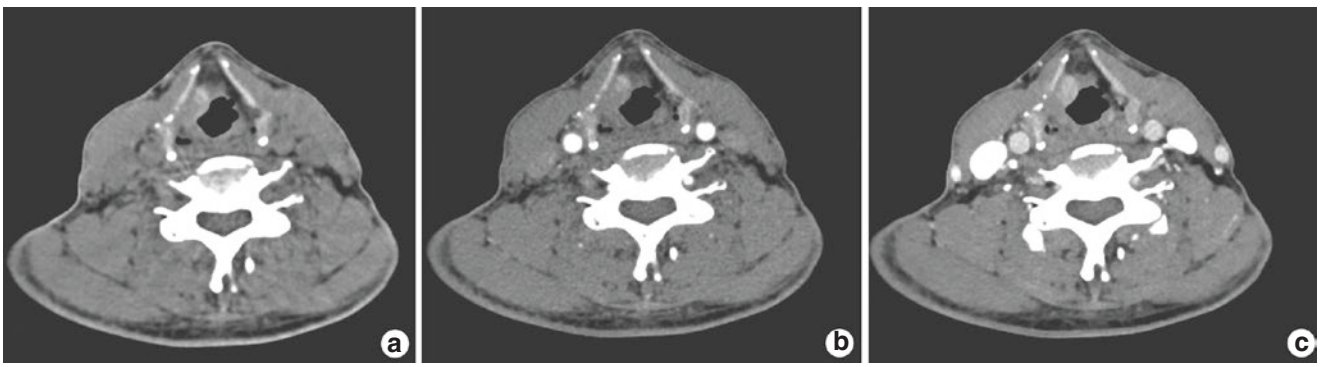

Fig. 25.5 Inflammatory granuloma of right ventricular fold and vocal cord. A 58-year-old male patient. The patient had slow onset, and was admitted to hospital mainly due to hoarseness for one and a half years. One and a half years ago, he went to see a doctor for the same symptoms, and underwent "Extended biopsy under self-retaining laryngoscopy + laryngectomy of lesion", and the postoperative pathological report showed it was inflammatory granuloma. In this admission, he received non-enhanced CT scan and enhanced CT examination of larynx. (**a**) Non-enhanced scan of larynx indicates that the right ventricular fold and vocal cords are swollen and the surface is not smooth; No abnormality is found in the left ventricular fold or vocal cords. (**b**, **c**) Enhanced CT of larynx shows that the tumors in arterial and venous phases have marked homogeneous enhancement with clear margin, and the peripheral structures including laryngeal cartilage and paraglottic space are not involved, and the lymph nodes are not enlarged or enhanced significantly. The postoperative pathological report was consistent with the proliferation of granulation tissue in the right vocal cord and ventricular fold

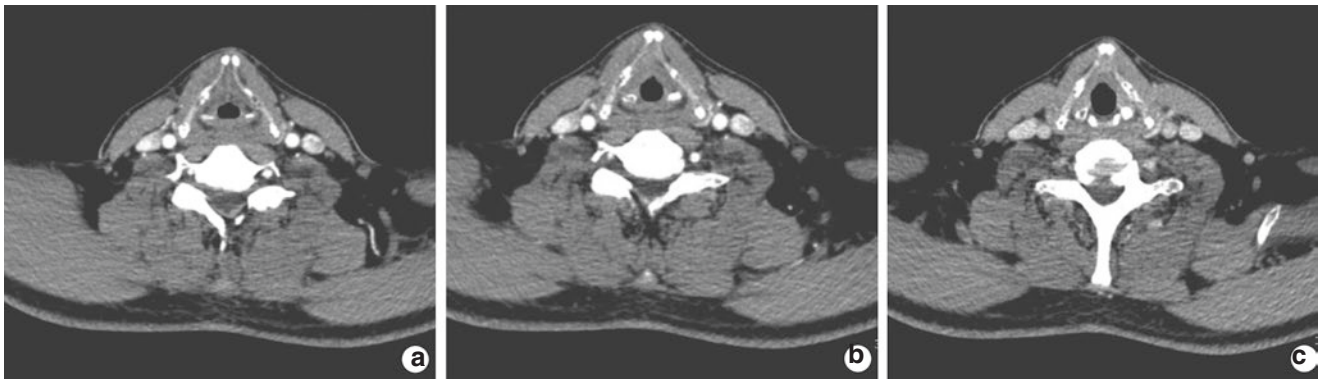

Fig. 25.6 Inflammatory granuloma of the anterior 1/3 of bilateral vocal cords. A 49-year-old male patient The patient had slow onset, and was admitted to hospital mainly due to hoarseness for 2 months. The laryngoscopy indicates tumor swelled in anterior commissure, the mucosa is pale, surface is not smooth, and bilateral ventricular hypertrophy obstructs the vocal cords. (**a**, **b**) Enhanced scan of larynx in the arterial phase shows that bilateral ventricular folds are thickened and have mild enhancement; (**c**) The enhanced scan of larynx shows unremarkable enhancement in venous phase. Pathological results were consistent with inflammatory granuloma

such as hoarseness develops rapidly. CT shows irregular thickening of vocal cords involving anterior commissure and paraglottic space. Enhanced examination shows marked enhancement. CT virtual endoscopy shows that the lesion is cauliflower-like. MRI mainly shows asymmetric thickening of unilateral vocal cords, slightly hyperintense on T_1WI than that on the normal side of thyroarytenoid muscle, significantly hyperintense on T_2WI, blurred mucosal line on free margin of vocal cords, and significantly hyperintense on DWI. By enhanced Gd-DTPA, the vocal cords on the affected side show marked enhancement. Chronic hyperplastic laryngitis usually manifests as thickening of vocal cords without significant infiltration of peripheral structures. Patients have a long duration of disease and slow progression [8].

Status Quo and Progress of Research

CT is the most common imaging method of larynx. Thin-layer CT, especially dual energy CT, can clearly show the normal anatomy and soft tissue lesions of larynx, and MPR can more intuitively show the involved scope of lesions. Many etiologies of chronic laryngitis may be associated with laryngeal cancer, so laryngeal cancer may be a complication [7]. Studies have shown that [9], the difference between laryngeal squamous cell carcinoma and chronic hyperplastic laryngitis lies in the expression of some special mRNA. When the cell activity increases and there are markers such as Ezrin, it is likely to indicate canceration. Virtual endoscopy can show diffuse thickening of vocal cords and ventricular folds with smooth surface and no cauliflower-like change.

25.4 Vocal Cord Polyp

Overview

Vocal cord polyp is a benign proliferative lesion occurring in the superficial layer of vocal cord lamina propria, which is a special type of chronic laryngitis. It is reported that [10] the lifetime prevalence of the disease is 1.31–16.9%. All kinds of causes for chronic laryngitis can cause vocal cord polyp, such as smoking, excessive or improper phonation, upper respiratory tract diseases, allergic reaction and hypopharynx reflux. The most common clinical manifestation is hoarseness of different degrees [11], and the hoarseness degree of patients is related to the size and location of polyps. Vocal cord polyp are mostly small lesions [11], and those with large polyps have severe hoarseness; Polyps growing on the upper surface of vocal cords have little influence on vocalization, while hoarseness is significant when they grow on the free margin of vocal cords. Large polyps with broad base can lead to complete aphonia. Polyps hanging in the subglottic cavity can cause cough. Huge polyps located between vocal cords may cause complete aphonia, even obstruct respiratory tract, lead to dyspnea and stridor, and even cause sudden death [11].

Pathology Findings

Vocal cord polyp is more common at the junction of the anterior and middle 1/3 of vocal cord edge. There are three explanations for this predilection site: (1) It is the middle point of the vocal cord mucosa, which has the largest amplitude and is vulnerable to damage when vibrating; (2) Vibration nodules exist here, which is easy to cause blood stasis and depo-

sition; (3) The vocal cord muscles are staggered and may cause twisting movement during vocalization. In addition, the distribution and structure of blood vessels are special, and the twisting movement makes extremely complicated change in the blood supply. Pathological changes of vocal cord polyp include edema of mucosa, hemorrhage, plasmexhidrosis, angiectasis, capillary proliferation, thrombosis, fibrin deposition, mucoid degeneration, hyalinosis and fibrosis. There may be a small amount of inflammatory cell infiltration and occasional calcification.

Imaging Findings

1. **X-ray Examination.** It shows unclear foci of vocal cord polyp. Soft tissue density shadows near the front 1/3 vocal cord are found in large lesions.
2. **CT Examination.** Non-enhanced CT scan shows slightly low density or soft tissue density nodule shadows on unilateral or bilateral vocal cords with pedicle, which locally protrudes into the larynx cavity, with clear and smooth margin, and the laryngeal ventricle exists. Large lesions can hang inferior to the glottic portion or even obstruct the glottic portion. There is no infiltration or involvement in the parapharyngeal space, and the parapharyngeal, retropharyngeal and prevertebral spaces are clear. There is no bone destruction in laryngeal cartilage around the lesion, with unremarkable enlargement of lymph nodes in most cases. Diffuse swelling and thickening of bilateral vocal cords are found when the lesion involves bilateral vocal cords. There is no marked enhancement by enhanced scan (Figs. 25.7 and 25.8).
3. **MRI Examination**
   (a) Conventional Non-enhanced Scan: vocal cord polyp is localized and prominent, showing broad-based or pedicled shape; Most of them are located at the junction of the anterior and middle 1/3 of vocal cords, which can protrude into the larynx cavity. They show isointense or hypointense on T_1WI and slightly hyperintense on T_2WI, the margin is clear and smooth, and there is no infiltration and involvement in the peripheral paralaryngeal space. There is no bone destruction, lymph node enlargement and abnormal signal in adjacent laryngeal cartilage.
   (b) Enhanced Scan: the lesions have no enhancement or mild enhancement.
   (c) Early small polyps are easy to be missed in diagnosis, so thin-layer scanning or reconstruction can be performed locally.
4. **Ultrasonography.** The vocal cord polyp usually shows hyperecho, lesions larger than 2 mm can be shown, and that smaller than 2 mm are difficult to differentiate. It is easy to show lesion accurately when it is located at the free margin of vocal cords and protrudes to glottic portion, and it is difficult to show it accurately when it is not located at the margin, and it should be dynamically observed [12].

Key Points of Diagnosis

1. **Clinical Manifestations.** They are mainly hoarseness to different extents. Polyps hanging in the subglottic cavity are often complicated with irritating dry cough. Huge

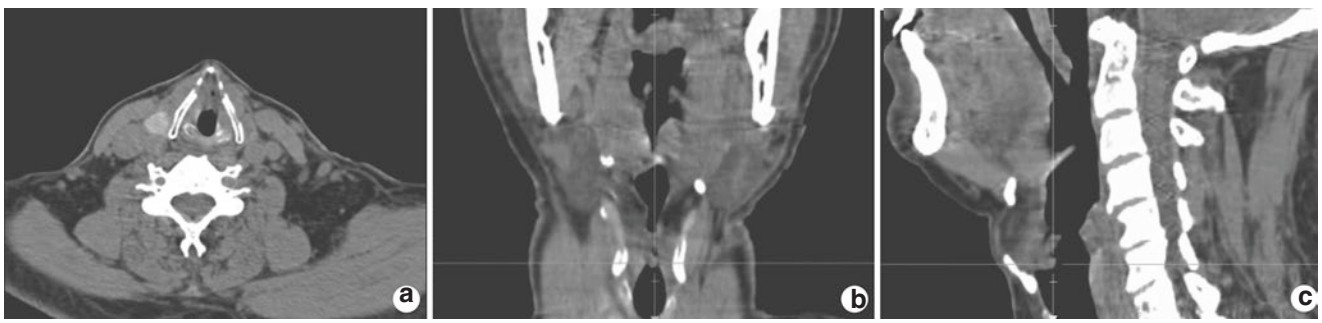

Fig. 25.7 Bilateral vocal cord polyp. A 58-year-old male patient. The patient was admitted mainly due to hoarseness and larynx discomfort for months. (**a**) Non-enhanced transverse CT scan shows that the nodular low-density shadows of anterior middle 1/3 of bilateral vocal cords protruding into the larynx cavity, and the nodule margin is smooth and clear, and the CT value is about 6HU. Laryngeal ventricle still exists, showing that there is no stenosis in pharyngeal cavity, and the retropharyngeal and prevertebral spaces are clear. (**b**) The reconstructed image on coronal plane shows nodular slightly low-density shadows of vocal cord area, with clear and smooth margin, and the larynx structures are bilaterally symmetric. (**c**) The reconstructed image on sagittal plane shows nodular slightly low-density shadows in vocal cord area, with clear and smooth margin and clear adjacent thyroid cartilage without involvement. The postoperative pathological results of the patient were: left vocal cord polyp with parakeratosis, right vocal cord polyp with parakeratosis and erosion, focal granulation tissue proliferation

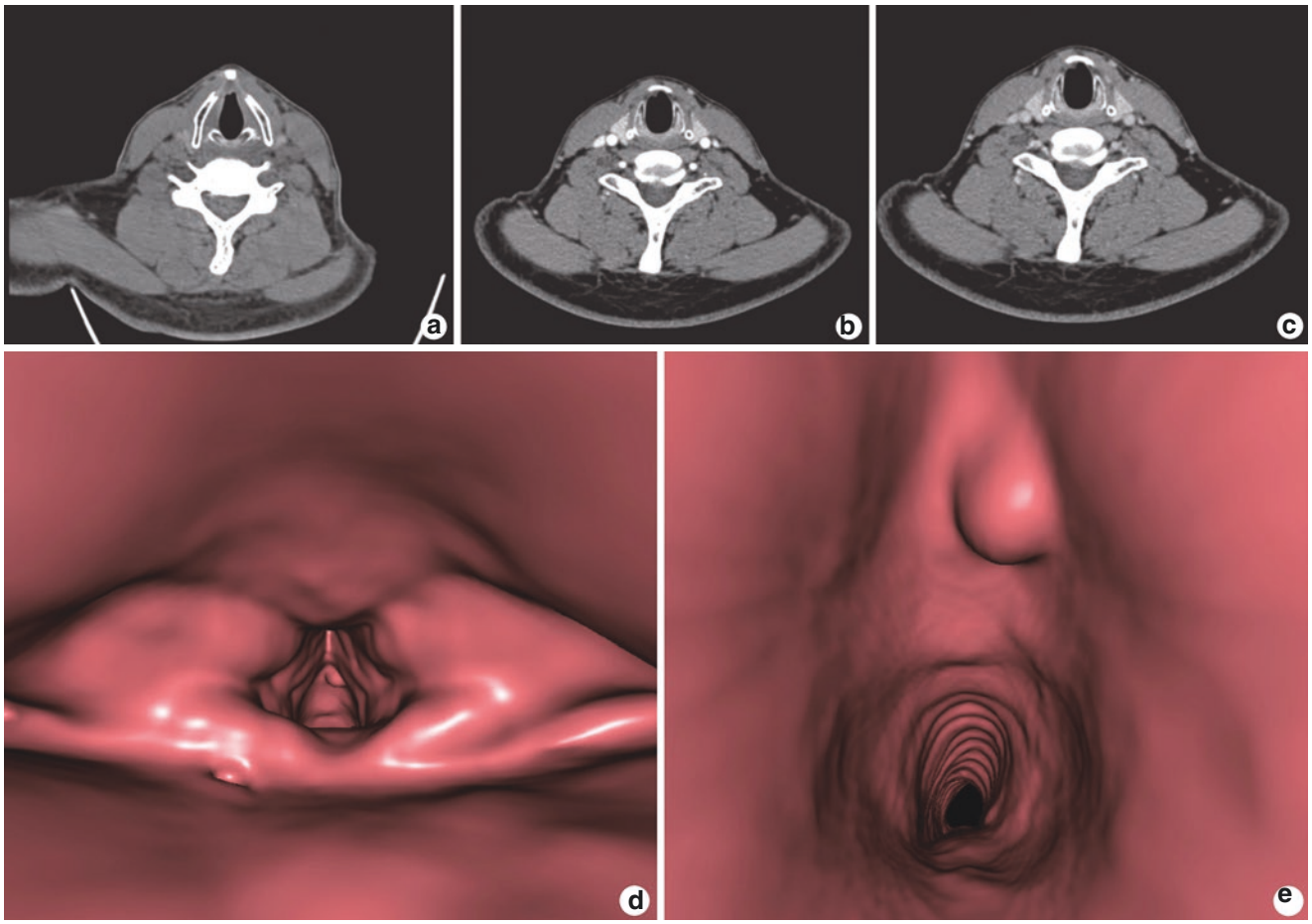

Fig. 25.8 Right laryngeal polyp of cricothyroid gland membrane in subglottic region. A 46-year-old male patient. The patient had chronic onset and previous operation of malignant laryngeal cancer, admitted mainly due to recurrence of laryngeal cancer after operation for 4 months. (**a**) Non-enhanced CT scan of larynx shows that the right small nodular limited protrusion of cricothyroid gland membrane midline protrudes into larynx cavity; Enhanced CT scan of larynx shows small nodular processes on the right side of cricothyroid gland membrane midline in arterial phase, with smooth margin. (**b**, **c**) Enhanced CT scan of larynx shows unremarkable enhancement in arterial and venous nodules. (**d**, **e**) Virtual endoscopy shows that the nodule is located in the laryngeal mucosa on the right side of cricothyroid gland membrane in subglottic region, and the nodule surface is smooth and clear, and the lesions are clearly shown. The postoperative pathology shows inflammatory granuloma

polyps can lead to complete aphonia and even cause dyspnea and stridor.

2. **CT Examination.** It shows soft tissue with pedicle or broad base or slightly low-density nodule shadows at the anterior middle 1/3 junction of unilateral vocal cord, with clear margin and local protrusion to larynx cavity. The structures, bones, and lymph nodes surrounding lesions are not involved. Enhanced scan indicates unremarkable enhancement. Virtual endoscopy shows that the lesion surface is smooth and the margin is clear.
3. **Laryngoscopy.** It indicates neoplasm with pedicle or broad base in the anterior middle 1/3 junction of vocal cords, with clear and smooth margins. Occasionally, diffuse growth is found throughout the vocal cords.

Differential Diagnosis

1. **Vocal Nodules.** Non-enhanced and enhanced CT scans show localized eminence at the junction of the anterior and middle 1/3 of bilateral vocal cords, local thickening of vocal cords, bilateral symmetry, and unremarkable enhancement.
2. **Vocal Cord Cyst.** Non-enhanced CT scan shows circular or quasi-circular water-like density nodule shadows in unilateral or bilateral vocal cords, with clear margin, clear paralaryngeal space without infiltration, and no enhancement by enhanced CT of lesions. MRI shows lesions with hypointense on T_1WI and significant hyperintense on T_2WI, with smooth margins and no involvement of adja-

cent tissues. Enhanced MRI shows no enhancement. In case of infection secondary to cyst, it is found that the cyst wall is thickened with ring enhancement. Ultrasonography shows hypoechoic shadows with smooth margins.

3. **Laryngeal Papilloma.** It is the most common laryngeal cancer. Lesions are mostly solitary and can be multiple, mainly located in vocal cords. Non-enhanced CT scan indicates papillary tumor on vocal cords or other laryngeal structures, with irregular shape and protruding into laryngeal ventricle. The lesions show iso-density shadow and may have mild enhancement by enhanced scan. On non-enhanced MRI, it shows slightly hypointense on T_1WI and slightly hyperintense on T2WI, and lesions mostly show mild and moderate enhancement by enhanced scan. There is no abnormal change in laryngeal cartilage and paralaryngeal space. When canceration occurs, it infiltrates and develops to the periphery and submucosa, and the paralaryngeal and parapharyngeal spaces disappear.
4. **Laryngeal Tuberculosis.** It can be divided into diffuse type and focal type. Focal type should be differentiated from polyp, but it lacks specific changes by imaging. Laryngoscopy shows pale and edema of laryngeal mucosa with multiple superficial ulcers, such as moth-eaten ulcers. Congestion and thickening of unilateral vocal cord may also occur.
5. **Laryngeal Carcinoma** (glottic type). It mostly occurs in the anterior middle 1/3 of vocal cords, and is easy to expand forward, manifesting as 1–2 mm small nodule shadows at the anterior commissure. Most supraglottic cancers can occur in epiglottis, manifesting as irregular masses in epiglottis. Advanced laryngeal cancer is often complicated with the invasion to surrounding cartilage, with enlarged and confluent lymph nodes around it. Enhanced scan shows the lesions with marked heterogeneous enhancement and the enlarged lymph nodes with marked heterogeneous enhancement. It is difficult to make differential diagnosis between laryngeal polyp and early laryngeal cancer, so it is necessary to make a definite diagnosis by biopsy.

Status Quo and Progress of Research

Vocal cord polyp can be diagnosed by clinical laryngoscopy. If CT examination reveals diffuse thickening of laryngeal soft tissue with deep invasion, the disease can be excluded. Early small polyps are easy to be missed in diagnosis. Virtual endoscopy shows that the lesion surface is smooth and the margin is clear. Virtual endoscopy can also be used as an imaging method to evaluate polyps.

25.5 Laryngeal Tuberculosis

Overview

Laryngeal tuberculosis (LTB) is a chronic infectious disease caused by mycobacterium tuberculosis. Laryngeal tuberculosis is rare in clinical practice [13], and its incidence rate is less than 1% of tuberculosis, but it is still one of the most common granulomatous diseases in larynx. The incidence of LTB in patients with pulmonary tuberculosis is 0.08–5.1% [14].

LTB is mostly found in male adolescents aged 20–30 years old, and the predilection sites are interarytenoid area, arytenoid cartilage, vocal cord, epiglottis and subglottic region in order. LTB perichondritis is common in epiglottis and arytenoid cartilage. The diffusion of blood and lymph is the cause of the occurrence and development of laryngeal tuberculosis. It is reported that [14], at least half of laryngeal tuberculosis is caused by blood transmission of mycobacteria tuberculosis. The early clinical manifestations of LTB are scorching effect and dryness in larynx, complicated with hoarseness, cough and sore throat. Sore throat is the most significant in clinical practice and can radiate to the aural region. The hoarseness is ingravescent and can lead to complete aphonia in advanced stage. Patients may be complicated with systemic tuberculosis, such as tuberculosis symptoms (cough, expectoration, hemoptysis) and systemic toxic symptoms (emaciation, mild fever, night sweat) [15].

Pathology Findings

The pathological types of LTB can be divided into three types: (1) Infiltration type: small round cells infiltration inferior to the laryngeal mucosa, forming tuberculous nodules. In that case, the surface of laryngeal mucosa is congested and edema and epiglottis is obvious. Tuberculous nodules can mostly evolve into ulcers, which can be absorbed and dissipated, leaving scars. (2) Ulcer type: mostly found in epiglottis, vocal cords and arytenoid cartilage. Confluent tuberculous nodules inferior to laryngeal mucosa, with caseous change, vascular thrombosis, necrosis of surface epithelioid cells, ulcer formation, and secondary infection. (3) Proliferative type: which is mostly found in the interarytenoid area or unilateral vocal cord. Tuberculosis infiltration can be healed by fibrosis, or new infiltration can occur, which can form tumor-like tuberculous nodules after repeated recurrences.

Imaging Findings

1. **X-ray Examination.** It shows laryngeal airway stenosis to different extents, and larynx mass formation in severe cases.

2. **CT Examination.** It lacks specificity and can be roughly divided into diffuse type and localized focus type. Diffuse type: Non-enhanced CT scan indicates diffuse thickening of laryngeal mucosa, involving epiglottis, vocal cords, ventricular fold, arytenoid cartilage area, posterior pharyngeal wall and other parts. Thickened mucosa shows decreased density, which is lower than that of adjacent muscles, CT value is 29–38 HU. The mucosa has marked enhancement in the advanced stage by enhanced scan. Bilateral anterior laryngeal spaces, paralaryngeal spaces and piriform recesses are constricted, and larynx cavity is constricted. The subglottic region may be involved in rare cases. The laryngeal tuberculosis generally does not invade the laryngeal cartilage framework, so the cartilage has no proliferation and sclerosis, which are the characteristics of the laryngeal tuberculosis. Localized focus type: Common swelling and thickening of the arytenoid area. Enhanced CT shows the lesions with heterogeneous enhancement, the mucosa with marked enhancement, and local nodular processes. Nodular enhancement and irregular low-density edema are seen in the submucosal area. Although the focal lesions manifest as local nodular asymmetric thickening, the lesions still manifest as bilateral occurrence. Laryngeal tuberculosis is often complicated with enlargement of cervical lymph nodes, with necrosis and calcification in the center. A few caseous necrosis substances are liquefied and have deep multiple abscess along the laryngeal space to form tuberculous abscess [16] (Figs. 25.9, 25.10, and 25.11).
3. **MRI Examination.** Compared with normal laryngeal mucosa, lesion area shows slightly hypointense on T_1WI and slightly hyperintense on T_2WI. The vocal cords, ventricular fold, and aryepiglottic fold show marked heterogeneous enhancement or ring enhancement of mucosa by enhanced scan. Enhanced scan shows that mucosal enhancement in advanced stage is more significant than enhancement in the early stage. In some cases, multiple enlarged lymph node shadows are found in the neck, necrotic liquefaction areas appear in some lymph nodes, showing hypointense on T_1WI and hyperintense on T_2WI shadows, and calcification lesions show hypointense on T_1WI and hypointense on T_2WI shadows.

Key Points of Diagnosis

1. **Clinical Symptoms.** The onset of the disease is slow and the disease has long duration. T-cell spots of tuberculosis infection are positive, and acid-fast bacilli could be found in larynx secretion smear.
2. **Imaging Manifestation.** It shows extensive bilateral asymmetric soft tissue thickening in larynx cavity, with or without mass. On enhanced examination, the laryngeal mucosa is enhanced to different extents, or there is unremarkable enhancement area. MRI shows bilateral diffuse asymmetric thickening of larynx, complete laryngeal cartilage framework, and unremarkable mass infiltration in paralarynx and anterior epiglottis space.
3. **Laryngoscopy.** It shows pale, edema, erosion, and exudation of laryngeal mucosa, and occasional irregular nodules or depressions.
4. **CT Examination.** When the Laryngeal tuberculosis is suspected or cannot be excluded, chest CT should be added to confirm whether there are suspicious tuberculosis lesions in the lungs. Laryngeal tuberculosis can be diagnosed if there are active tuberculosis or old tuberculosis lesions in the lungs or if the sputum contains eosinophilic bacilli.

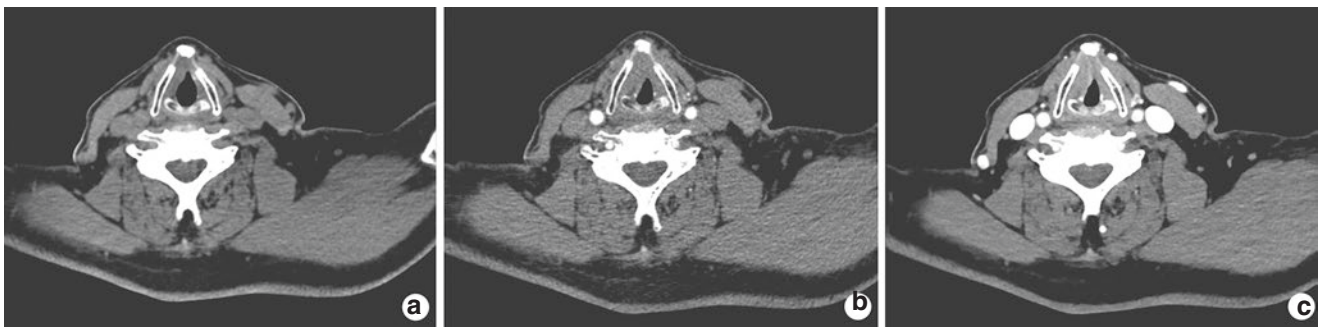

Fig. 25.9 Tuberculosis of right vocal cord. A 63-year-old male patient. The patient had chronic onset and was admitted mainly due to hoarseness for 2 months. (**a**) Non-enhanced scan of larynx indicates that the full length of the right vocal cord is thickened, involving the glottic anterior commissure, and the right paraglottic space disappears; (**b**, **c**) Enhanced scan shows the right vocal cords with heterogeneous enhancement, and no necrosis or calcification is found in the cervical lymph nodes. Chest CT of the patient shows mass and hollow in superior lobe of right lung, pulmonary tuberculosis is considered

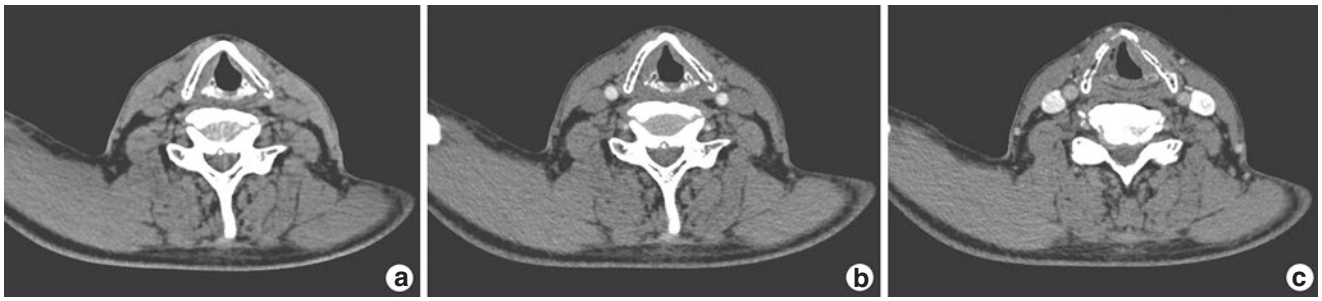

Fig. 25.10 Left vocal cord tuberculosis. A 53-year-old male patient. The patient had chronic onset and was admitted mainly due to hoarseness for more than 20 days. (**a**) Non-enhanced scan of larynx indicates eminence in the anterior 2/3 of the left vocal cord; (**b**, **c**) Enhanced scan shows no abnormal enhancement at the eminence. The chest X-ray of the patient shows old tuberculosis in the superior lobe of left lung

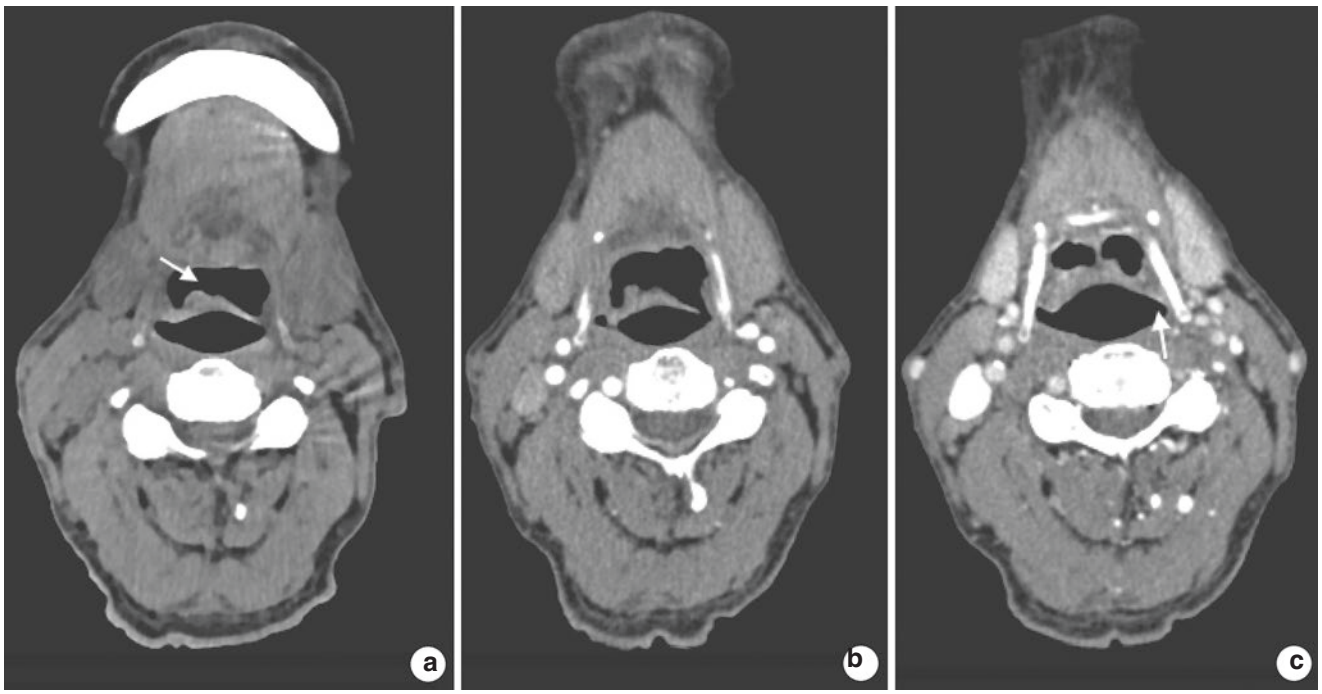

Fig. 25.11 Tuberculosis of epiglottis and left piriform recess. A 72-year-old male patient The patient had chronic onset and was admitted mainly due to hoarseness for 2 months, complicated with choking cough and pharyngeal obstruction. (**a**) Non-enhanced scan of larynx indicates that the root of epiglottis is thickened, the left piriform recess becomes shallow, with local eminence. There is no significant abnormality in the peripheral structure, and the paraglottic space exists. (**b**, **c**) Enhanced scan shows the mucosa of epiglottis root and left piriform recess with marked enhancement

Differential Diagnosis

1. **Chronic Laryngitis.** The laryngeal mucosa is generally thickened, with homogeneous lesion density and wide lesion scope. The ventricular fold, vocal cords and aryepiglottic folds are thickened, the vocal cords are uneven and asymmetrical, especially in the interarytenoid area. The paralaryngeal space is clear with no infiltration change and unremarkable change in laryngeal cartilage. The enhancement of mucosa is unremarkable in enhanced scan, and it is difficult to differentiate the imaging manifestations from tuberculosis.
2. **Vocal Cord Polyp.** Non-enhanced CT scan shows that one side of the vocal cord has a slightly low density or soft tissue density nodule with pedicle protruding into the larynx cavity locally, with clear margin, no infiltration or involvement in the paralaryngeal space, no bone destruction in the adjacent laryngeal cartilage, and unremarkable enlargement of lymph nodes. CT enhanced scan indicates that the lesions are not enhanced.
3. **Laryngeal Cancer.** Glottic carcinoma mostly occurs in the anterior middle 1/3 of vocal cords, and it is easy to expand forward, showing small 1–2 mm nodule shadows in the anterior commissure. Supraglottic cancer mostly

occurs in epiglottis, showing irregular masses in epiglottis. Subglottic cancer is usually from glottic cancer, showing thickening or asymmetry of soft tissue at the inferior border of glottic portion. Laryngeal cancer is often complicated with invasion and involvement of peripheral structures, bones, and lymph nodes.

4. **Amyloidosis Larynx.** It is a pathological change caused by the accumulation of amyloid in the larynx, which is not a true neoplasm. The main manifestations by imaging examination are laryngeal masses, which have wide scope of lesions and calcification in some cases. The density of calcified foci is low, the CT value is 40–60 HU, scattered as sand. The deposited substance of amyloidosis is acellular and insoluble protein-like substance, which shows manifestation on MRI images, with hypointense T_1WI and hypointense T_2WI.

Status Quo and Progress of Research

The clinical manifestations of LTB have undergone several changes in the past decades, which are summarized in Table 25.1. According to literature reports, as many as 40.6% of patients with normal lungs will be diagnosed with laryngeal tuberculosis [15, 17]. Imaging findings of some LTB patients are difficult to differentiate from chronic pharyngitis or laryngeal cancer, which increases the difficulty of clinical diagnosis. When LTB is suspected, and result by sputum microscopy is negative, biopsy is recommended, especially when tumor diagnosis cannot be excluded. Once tuberculosis is diagnosed, anti-tuberculosis treatment should be carried out in time to prevent chronic complications. In terms of treatment, the operation is limited to airway damage and chronic complications (posterior glottic portion stenosis, vocal cord paralysis when the cricoarytenoid joint or recurrent laryngeal nerves are involved).

Table 25.1 Clinical characteristics of laryngeal tuberculosis

Characteristics	Past	Now
Median age	20–30 years old	40–60 years old
Symptom	Dyspnea	Lung or systemic symptoms, hoarseness, and dysphagia
Involved parts of larynx	Posterior larynx (epiglottis, arytenoid process)	Vocal cord involvement is the most common
Type of lesion	Ulcerative or granulomatous hypertrophy	Exophytic type or polyp type
Pathogen transmission route	Bronchus	Blood or lymphatic transmission is becoming more common
Lung involvement	Advanced in most cases	The lungs are less involved, and the chest X-ray examination mostly shows negative result.

25.6 Laryngeal Perichondritis

Overview

Laryngeal perichondritis is an inflammatory disease occurring in the laryngeal cartilage membrane and its space. Patients with acute and primary laryngeal perichondritis are rare, while chronic and secondary ones are common, which often cause necrosis and suppuration of cartilage to form abscess, that is, larynx abscess, which is sometimes difficult to differentiate. Primary laryngeal perichondritis is rare, and mostly caused by other diseases, and is common in adults. Common causes of laryngeal perichondritis: (1) radiation injury; (2) laryngeal trauma; (3) systemic infectious diseases, such as tuberculosis, syphilis, diphtheria, etc., can damage perichondrium and cartilage or cause secondary infection; (4) malignant tumor of larynx directly invading the perichondrium and cartilage. Clinical manifestations often include general malaise, fever, sore throat, cough, hoarseness, dysphagia and dyspnea, and it may tender on the outside of larynx by neck palpation. Patients with chronic infection may have mild sore throat and chronic cough [18].

Pathology Findings

Laryngeal perichondritis mostly occurs in arytenoid cartilage membrane, followed by cricoid cartilage membrane and thyroid cartilage membrane, and most rare cases have epiglottitis infected. Traumatic laryngeal perichondritis often involves multiple laryngeal cartilages. In case of inflammation of the perichondrium, the exudate accumulates in the space inferior to perichondrium and gradually became pus, separating the perichondrium from the cartilage and the cartilage is ischemic and necrotic. At the beginning, edema or redness appears in the larynx, and sometimes swelling appears outside the larynx. Some cases with laryngeal perichondritis are non-suppurative, and mostly have scar formation and significantly thickened after healing. Laryngeal tuberculosis is most likely to invade arytenoid cartilage and often affects cricoid cartilage, making it stiff. Syphilis in larynx often invades thyroid cartilage [19].

Imaging Findings

CT shows thickening and swelling of soft tissue in neck and larynx and localized density reduction or homogeneous water-like density shadows in anterior cervical soft tissue, postcricoid region and paralaryngeal space. The larynx cavity is compressed and displaced. By enhanced scan, the liquefied part shows no enhancement, and the non-liquefied part and capsule show marked enhancement. When combined with aerogenic bacteria infection, shadows of scattered small bubbles may appear in the low-density area where the abscess is located. CT examination plays an important role in judging the location and extent of abscess and the occurrence

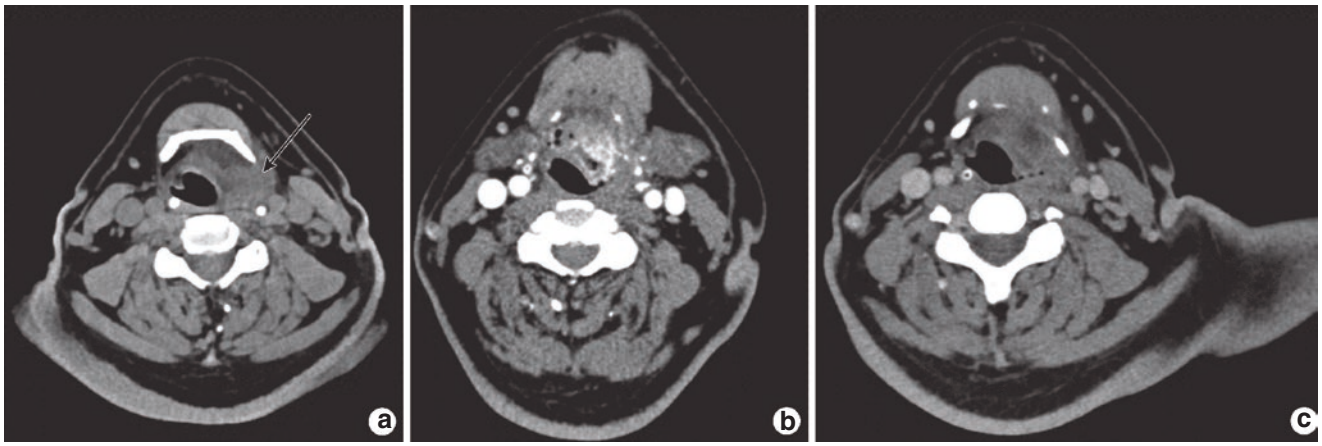

Fig. 25.12 Inflammatory lesions and local abscess formation in the left anterior epiglottis space. (**a**) Non-enhanced CT scan of larynx shows the density shadows of soft tissue on the left side of the anterior epiglottic space, which is heterogeneous in density and involves the left aryepiglottic fold, resulting in constriction of the left piriform recess; (**b**, **c**) Laryngeal CT enhanced scan shows the density shadows of soft tissue on the left side of the anterior epiglottis space with marked ring enhancement, and patchy areas without enhancement are noted in it

of complications (Fig. 25.12). MRI shows the soft tissue lesions with thickened larynx with hypointense on T_1WI, hyperintense on T_2WI and homogeneous signal intensity, and DWI shows hyperintense in case of abscess formation.

Key Points of Diagnosis

1. Physical examination: The neck is red, swelling, fever and pain, and the lymph nodes are significantly enlarged, which may be complicated with fever, sore throat, cough, hoarseness and other symptoms.
2. CT shows that the density shadows of laryngeal soft tissue with swelling and thickening, and homogeneous water-like density shadows.
3. Laryngeal perichondritis can easily evolve into laryngeal abscess, and CT examination can find and evaluate laryngeal abscess in time.

Differential Diagnosis

1. **Vocal Cord Polyp.** Non-enhanced CT scan shows mostly unilateral or bilateral pedicled vocal cord nodule shadows with slightly low density or soft tissue density, which locally protrude into the larynx cavity, with clear margin, no infiltration or involvement in the paralaryngeal space, no bone destruction in the adjacent laryngeal cartilage, and unremarkable enlargement of lymph nodes. CT enhanced scan indicates that the lesions are not enhanced.
2. **Laryngeal Cancer.** Glottic carcinoma mostly occurs in the anterior middle 1/3 of vocal cords, and it is easy to expand forward, showing small 1–2 mm nodule shadows in the anterior commissure. Supraglottic cancer mostly occurs in epiglottis, showing irregular masses in epiglottis. Laryngeal cancer is often complicated with the invasion to surrounding cartilage, and swelling and fusion of lymph nodes are found around it.
3. **Laryngeal Abscess.** It is mostly evolved from laryngeal perichondritis, and it is difficult to differentiate in the early stage.

Status Quo and Progress of Research

Patients with laryngeal perichondritis may have definite clinical symptoms in the early stage, but physical examination and even CT scan show negative results. Some studies indicated that [20] patients with active adult onset still's disease could have laryngeal pain, but unremarkable abnormality is found by physical examination and CT examination. The thickening of soft tissue shadows and abnormal intensity on the symptomatic side can be found by non-enhanced and enhanced MRI examination of larynx. After treatment, the abnormal soft tissue shadows and signal intensity disappear, indicating that MRI has significant value for lesions of laryngeal cartilage membrane in the early stage.

25.7 Cricoarytenoid Arthritis

Overview

Cricoarytenoid arthritis is mostly a local manifestation of systemic diseases such as rheumatism, rheumatoid diseases and gout, and can also be manifested as arthritis inflammatory changes caused by severe infection, trauma, intratra-

cheal intubation anesthesia injury or long-term vocal cord paralysis [21, 22]. The disease can occur in unilateral or bilateral cricoarytenoid joints.

The cricoarytenoid arthritis can be classified as acute and chronic types. The acute stage manifests as dyspnea, stridor, dysphonia, dysphagia, odynophagia, otalgia or larynx tenderness. Physical examination can reveal erythema, edema of aryepiglottic fold or impaired vocal cord activity. In chronic stage or stiffness stage, patients may have no symptoms, or only mild hoarseness, dyspnea or stridor [21, 22], depending on the position of vocal cords when the joint is stiff. Changes related to chronic cricoarytenoid arthritis include thickening of arytenoid mucosa, bending of vocal cords or fixation of arytenoid cartilage during inhalation. In addition, rheumatoid arthritis (RA) can also form rheumatoid nodules or bamboo-like nodules in the larynx [23].

Direct or indirect laryngoscopy can be used in combination with HRCT for definite diagnosis of cricoarytenoid arthritis. Studies have shown that [23], 80% of RA patients have cricoarytenoid arthritis, which can be detected by HRCT. Radiological abnormalities associated with cricoarytenoid joint involvement usually precede clinical symptoms. Laryngoscopy shows swelling of arytenoid cartilage in acute stage, edema of vocal cords in chronic stage and thickening of arytenoid mucosa [23].

Cricoarytenoid arthritis may lead to laryngeal edema, resulting in airway obstruction or vocal cord abduction damage. Acute and chronic diseases may lead to respiratory distress, which requires emergency tracheotomy. Therefore, the involvement of cricoarytenoid joint represents the life-threatening manifestation of rheumatoid arthritis.

Pathology Findings

1. **Rheumatic and Rheumatoid Cricoarytenoid Arthritis.** It shows inflammation of synovial layer and cartilage in the early stage, including synovial fluid exudation, synovial hyperplasia and cell infiltration. Subsequently, synovial membrane gradually thickens, articular cartilage is destroyed, fibrous tissue is proliferated and filled, pannus is formed, fibrous ankylosis occurs in articular cavity, and finally bony ankylosis and joint deformation occurs.
2. **Traumatic Cricoarytenoid Arthritis.** It occurs after a definite history of trauma. For example, after anesthesia intubation, the articular cartilage is destroyed, its integrity disappears, the normal articular cavity disappears with fibrosis, and the cricoarytenoid joint is fixed.
3. **Others.** Secondary cricoarytenoid joint lesions after long-term recurrent laryngeal nerves paralysis, such as fibrosis and bone ankylosis.

Imaging Findings

1. **CT Examination.** HRCT has high sensitivity for detecting cricoarytenoid arthritis. Even when the patients have unremarkable clinical symptoms or are asymptomatic, HRCT can still show positive signs, which precede clinical diagnosis. When clinical symptoms are unremarkable, cricoarytenoid articular cartilage thickening, synovial fluid increase, articular cavity widening and local erosion can be found. The cricoarytenoid articular process, erosion or subluxation to different extents can be found in the progressive stage, and the cricoarytenoid joint volume decreases the joint density increases, and even the joint ankylosis changes can be found in most patients. In some patients, soft tissue swelling or piriform sinus stenosis is found near the cricoarytenoid fossa.
2. **MRI Examination.** It can show the changes in shape and signal of laryngeal soft tissue and laryngeal cartilage framework in all directions, such as transverse, sagittal and coronal planes. A series of changes such as synovitis, tenosynovitis, bone marrow edema, tendonitis, articular cartilage involvement and bone erosion can appear on MRI images with the progression of the disease on the cricoarytenoid articular surface and articular cavity. The abnormal signal often precedes the change by CT examination, which can diagnose cricoarytenoid arthritis earlier and more sensitively [23].

Key Points of Diagnosis

1. **Clinical Symptoms.** Sore throat or dryness when swallowing or vocalizing and the pain spots are mostly located in the center of the posterior border of thyroid cartilage or at the thyrohyal space. The clinical symptoms in chronic stage depend on the fixed position of vocal cords when the joint has ankylosis, with occasional hoarseness or dyspnea.
2. **Laryngoscopy.** Congestion and swelling of mucosa at the notch between arytenoid cartilages and the vocal cords are mostly normal. It is necessary to clarify the medical history and improve the blood tests related to rheumatoid diseases.
3. **HRCT.** Thickening of cricoarytenoid articular cartilage, increase of synovial fluid, widening of articular cavity and local erosion in the early stage of disease. The cricoarytenoid articular process, erosion or subluxation can occur when clinical symptoms of different degrees appear in the progressive stage, and most patients show decreased cricoarytenoid joint volume, increased joint density, and even the joint ankylosis changes.

Differential Diagnosis

Unilateral Vocal Cord Paralysis. Common causes of vocal cord paralysis include aortic aneurysm, local inflammation or mass of vocal cords, mediastinal lesions, surgical sequelae and trauma. According to the patient's medical history, it can be differentiated from cricoarytenoid arthritis. Laryngoscopy can differentiate it effectively.

Status Quo and Progress of Research

Cricoarytenoid arthritis is often a local manifestation of systemic inflammatory diseases, which is common in RA. For RA patients, attention should be paid to the necessary physical examination and the cricoarytenoid joint. HRCT scan combined with clinical data is helpful for etiological diagnosis. Radiological abnormalities associated with cricoarytenoid joint involvement usually precede clinical symptoms. HRCT scan can diagnose laryngeal RA even if larynx symptoms are minimal or absent. Asymptomatic patients and patients with normal laryngoscopy results may have detectable abnormalities on HRCT. Studies show that [23, 24], laryngeal endoscopy can detect 13.3% of cases, while HRCT scan detect more than 80.0%. Therefore, HRCT should be the first choice in case of clinical suspicion of cricoarytenoid arthritis. MRI has higher soft tissue resolution than CT and can find the abnormality of cricoarytenoid joint signal earlier than CT. However, due to the limited imaging conditions, it is not the first choice for clinical examination.

References

1. Gelbart B, Parsons S, Sarpal A, et al. Intensive care management of children intubated for croup: a retrospective analysis. Anaesth Intensive Care. 2016;44(2):245–50.
2. Nadia MS, Alexis L, Poonam D. Ultrasound-guided removal of hypopharyngeal foreign body in the emergency department. Ultrasound. 2017;25(4):245–7.
3. Andrade JV, Vasconcelos P, Campos J, et al. Antibiotic prescribing in ambulatory care of pediatric patients with respiratory infections. Acta Medica Port. 2019;32(2):101–10.
4. Andrey M, Nissa JA, Nicole M, et al. Pasteurella multocida epiglottitis. Clin Pract Cases Emerg Med. 2017;1(1):22–4.
5. Shintaro S, Yuichiro K, Akira I. Pathological characteristics of the epiglottis relevant to acute epiglottitis. Auris Nasus Larynx. 2012;39(5):507–11.
6. Kim KH, Kim YH, Lee JH, et al. Accuracy of objective parameters in acute epiglottitis diagnosis. Medicine. 2018;97(37):12256.
7. Alisa Z, Verma SP. Identification and management of chronic laryngitis. Otolaryngol Clin N Am. 2019;52(4):607–16.
8. Yan S, Dehong L, Hengguo L. Imaging of the head and neck·otolaryngology, head and neck surgery. Beijing: People's Medical Publishing House; 2014.
9. Kakurina GV, Kondakova IV, Spirina LV, et al. Expression of genes encoding cell motility proteins during progression of head and neck squamous cell carcinoma. Bull Exp Biol Med. 2018;166(2):250–2.
10. Won SJ, Kim RB, Kim JP, et al. The prevalence and factors associate with vocal nodules in general population: cross-sectional epidemiological study. Medicine (Baltimore). 2016;95(39):4971.
11. Yasuyuki C, Ryota I, Yoshibumi K, et al. A giant vocal cord polyp mimics asthma attack. Clin Pract Cases Emerg Med. 2018;2(4):361–2.
12. Ongkasuwan J, Devore D, Hollas S, et al. Laryngeal ultrasound and pediatric vocal fold nodules. Laryngoscope. 2017;127(3):676–8.
13. Chen H, Thornley P. Laryngeal tuberculosis: a case of a non-healing laryngeal lesion. Australas Med J. 2012;5(3):175–7.
14. Reis JG, Reis CS, da Costa DCS. Factors associated with clinical and topographical features of laryngeal tuberculosis. PLoS One. 2016;11(4):0153450.
15. Iveta P, Vaiva M. Dysphonia—the single symptom of rifampicin resistant laryngeal tuberculosis. Open Med. 2016;11(1):63–7.
16. Li J, Yan L, Yong Z, et al. Comparative analysis of CT and MRI findings and laryngoscopy of laryngeal tuberculosis. Chin J Otolaryngol Head Neck. 2014;49(9):771–3.
17. World Health Organization. Global tuberculosis report 2012. Geneva, Switzerland: WHO Press; 2012.
18. Vanhille DL, Blumin JH. Laryngeal abscess formation in an immunosuppressed patient: a case report. Laryngoscope. 2017;127(12):2827–9.
19. Boyce BJ, de Silva BW. Spontaneous MRSA postcricoid abscess: a case report and literature review. Laryngoscope. 2014;124(11):2583–5.
20. Chen DY, Lan HHC, Hsieh TY, et al. Crico-thyroid perichondritis leading to sore throat in patients with active adult-onset Still's disease. Ann Rheum Dis. 2007;66(09):1264–6.
21. Iacovou E, Vlastarakos PV, Nikolopoulos TP. Laryngeal involvement in connective tissue disorders. Is it important for patient management? Indian J Otolaryngol Head Neck Surg. 2014;66(Suppl 1):22–9.
22. Greco A, Fusconi M, Macri GF, et al. Cricoarytenoid joint involvement in rheumatoid arthritis: radiologic evaluation. Am J Otolaryngol. 2012;33:753–5.
23. Østergaard M, Boesen M. Imaging in rheumatoid arthritis: the role of magnetic resonance imaging and computed tomography. Radiol Med. 2019;124(11):1128–41.
24. Ostrowska M, Maśliński W, Prochorec-Sobieszek M, et al. Cartilage and bone damage in rheumatoid arthritis. Reumatologia. 2018;56(2):111–20.

Part VIII

Infectious and Inflammatory Diseases of Maxillofacial Mouth Floor

Lesions of Maxillofacial Mouth Floor

26

Heng Liu, Mengmeng Yu, Xuedong Bai, Bangguo Li, Xinjiang Liu, Mingyu Li, and Shuang Xia

26.1 Pyogenic Osteomyelitis of the Jaws

Overview

The pyogenic osteomyelitis of the jaws is common in young people, which is mainly caused by odontogenic infection such as alveolar abscess, periodontitis, and pericoronitis of the third molar, accounting for about 90%. Secondly, it is caused by open injuries such as comminuted fractures or firearm injuries. Blood-borne infection is caused by septicemia or sepsis, mostly occurring in the maxilla of infants. A few cases have jaw involvement directly due to infection of maxillofacial skin or oral mucosa [1]. Pyogenic osteomyelitis of the jaws mostly occurs in mandible, where the most severe disease progression shows. It is mainly because of the mandible dense in bone, surrounded by dense fascia and rich muscle tissue, thus the pus of mandible is difficult to puncture and drain after infection. A few cases have jaw involvement directly due to infection of maxillofacial skin or oral mucosa. And the blood supply of mandible is poor, and it is easy to form sequestrum by vascular thrombosis. The main pathogen is Staphylococcus aureus, followed by Streptococcus and a few other pyogenic bacteria, and the disease mainly involves mixed infections.

According to the clinicopathological characteristics of odontogenic pyogenic osteomyelitis of the jaws, the disease that originated from spongy bone and bone marrow in the center of jaws is called central osteomyelitis. The lesion originated from periosteum and bone cortex around jaw bone is called marginal osteomyelitis. Central osteomyelitis is often secondary to acute suppurative periodontitis or apical abscess. The lesions first involve bone marrow, and then spread to the peripheral areas, involving bone cortex and periosteum. Marginal osteomyelitis mostly originates from pericoronitis of mandibular third molars and involves periosteum or bone cortex of adjacent mandible. Most of the lesions are limited, and can also go to deep layer, and involve bone marrow cavity. Both types are mostly found in mandible, central osteomyelitis is mostly found in mandible, and marginal osteomyelitis is mainly found in mandibular angle and mandibular branch.

Pathology Findings

Pathological changes of pyogenic osteomyelitis of the jaws mainly depend on clinical stages (acute, subacute, and chronic) and infection sites. Once the pathogens enter the bone, they can multiply in large numbers and cause acute inflammatory reaction, and plenty of neutrophil infiltration is found in the lesions. The increased pressure in bone marrow cavity, the compression of blood vessels and the release of acute inflammatory reaction factors lead to necrosis of osseous tissue with lesion. The foci involve periosteum through the haversian canal of bone cortex, forming subperiosteal abscess. When the inflammation expands further, it can penetrate the bone and involve the peripheral soft tissue. As the periosteum is lifted off, the blood supply of jaw bone is affected, that is, it causes suppuration with ischemic segmental osteonecrosis, with sequestrum in the lesion. If the inflammation can be treated in a timely and standardized way in acute stage, the inflammation can be relieved. If the treatment is delayed, the disease will enter chronic stage. Chronic inflammatory cells enter osteomyelitis focus and release cytokines, which leads to reparative reaction. Fibrillar connective tissue in bone marrow cavity proliferates under the

H. Liu (✉) · B. Li
Affiliated Hospital of Zunyi Medical University, Zunyi, China

M. Yu
Binzhou Medical University Hospital, Binzhou, China

X. Bai · M. Li
Affiliated Hospital of Chengde Medical University, Chengde, China

X. Liu
Shanghai Pudong Hospital, Fudan University Affiliated Pudong Medical Center, Shanghai, China

S. Xia
Tianjin First Central Hospital, Tianjin, China

H. Li et al. (eds.), *Radiology of Infectious and Inflammatory Diseases - Volume 2*,
https://doi.org/10.1007/978-981-16-8841-6_26

microscope. In severe cases, large sequestrums are formed or pathologic fractures can occur [2].

Imaging Findings

X-ray plain film can show the focus teeth and lesion scope of pyogenic osteomyelitis of the jaws, which can be used as the first choice for examination. However, X-ray photography has limitations in exploring lesions in early stage and tiny lesions, showing the details in the lesions, and finding the changes of peripheral soft tissues. Therefore, when the lesions are found, or lesions are not shown and the clinical manifestations support high suspicion of the infection, CT and MRI examinations should be further selected and applied.

1. Central Osteomyelitis of the Jaws
   (a) X-ray examination: The abnormal changes of bone usually can occur about 10 days after infection. In the beginning, it only shows blurred bone trabecula, and then there are multiple punctate and patchy low-density destruction areas, especially the area centered on causative tooth. The lesions gradually migrate to the surrounding normal osseous tissue, with unclear margins and spread scope. After the infection focus is limited, it shows a large low-density area, the margin between the lesion and normal bone is clear, high-density neoplastic bone formation is found around it, and sequestrums varied in size are found in the lesion, which may be complicated with pathologic fracture. In the neoplastic bone formation stage, the edge of the lesion is clear, and the bone trabecula near the bone increases and becomes thicker, and the density increases. In the healing stage, the bone is dense, the bone trabecula become thicker and disordered, and the jaw may have deformity.
   (b) CT examination: the tiny lesions in jaw can be found earlier than X-ray photography, which shows decreased local bone density in jaw and an unclear margin. With the further development of infection, the scope of lesions expanded, and irregular low-density areas appear on CT, surrounded by sclerosis straps with a clear margin [3]. Slight periosteal reaction can be found on CT, which is difficult to show on X-ray films. Sequestrums in lesions can show high-density shadows with different sizes and irregular shapes. When the soft tissue around the jaw is involved, it is found that the fat space disappears, the margin is blurred, the density of muscle tissue decreases, and sometimes with air shadows varied in sizes. When the abscess is formed, it shows that there is an abscess wall with band-shaped slightly high density around the localized low-density area. On CT enhanced scan, the lesions show marked ring enhancement. In the chronic stage, it shows hyperostosis and osteosclerosis, density increased, and bone cortex integrity in lesion area of jaws.
   (c) MRI examination: The destruction area in jaw shows hypointense on T_1WI and hyperintense on T_2WI during acute inflammation. MRI is more sensitive than X-ray photography and CT in finding lesions in early stage and showing the invasion scope of lesions. In addition, MRI is more sensitive to the detection of the involvement of soft tissue and fascia space around the jaws, and to the size and scope of the lesion. However, MRI is inferior to CT in finding small sequestrums in lesions and judging the hyperostosis and osteosclerosis around lesions.
2. **Marginal osteomyelitis of the jaws.** It originates from periosteum and bone cortex, which can be divided into hyperplastic type and dissolution-destruction type.
   (a) X-ray examination: the hyperplastic lesion shows less bone destruction, and the neoplastic bone proliferation is obvious. The neoplastic bone proliferation is found outside the bone cortex, and the lateral margin is neat and the bone is dense. Dissolution-destruction type is more common in subperiosteal abscess and infection of perimaxillary space. Dissolution-destruction type mostly occurs in bone cortex, and proliferation reaction is unremarkable. The X-ray photography shows a quasi-circular low-density area with a clear margin, with sclerosis strap around the area for patient having long duration.
   (b) CT examination: the main pathological features of the two types can be clearly shown, and the involvement extents of periosteum, bone cortex, and peripheral soft tissues can be found (Figs. 26.1, 26.2 and 26.3).
   (c) MRI examination: The neoplastic bone formed in the lesion shows hypointense on T_1WI and hypointense on T_2WI, and the dissolution-destruction area shows hypointense on T_1WI and hyperintense on T_2WI. When bone marrow of jaw bone is involved, hyperintense of normal fat disappears, and mainly replaced by hypointense on T_1WI and hyperintense on T_2WI.

Key Points of Diagnosis

1. Patient has a history of odontogenic infection and shows such clinical manifestations as toothache, percussion pain, loose teeth, local swelling, or systemic infection symptoms.
2. X-ray films, CT and MRI indicate diffuse or localized bone destruction, sequestrum, periosteal reaction, subperiosteum neoplastic bone formation, and other signs.

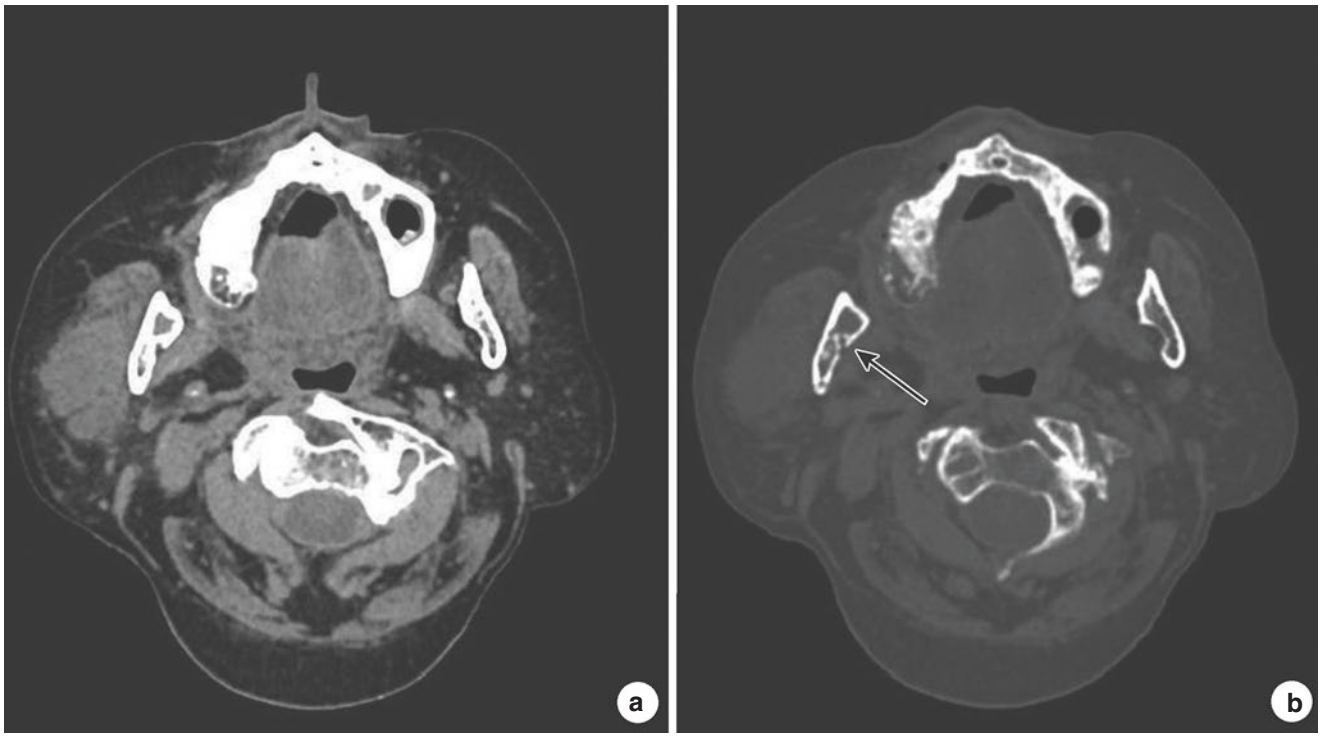

Fig. 26.1 Suppurative osteomyelitis of right mandible with swelling of peripheral soft tissue (1). (**a**) CT on soft tissue window shows swelling of masseter and adjacent soft tissue around the right ramus of mandible, and blurred fat space; (**b**) CT on bone window shows that the density of bone marrow cavity in the right ramus of mandible increases, with irregular bone fragments and discontinuous bone cortex (indicated by arrow)

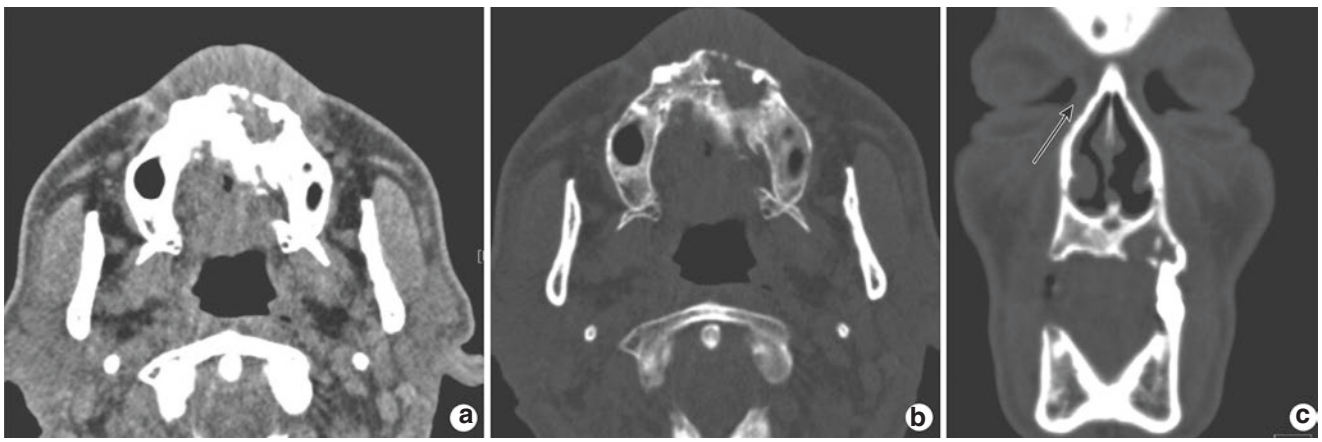

Fig. 26.2 Chronic suppurative osteomyelitis of maxilla with swelling of peripheral soft tissue. (**a**) CT on soft tissue window shows that the maxilla bone is irregular, the adjacent soft tissue is swollen, and the fat space is fuzzy; (**b** and **c**) Transverse and coronal CT on bone window show the discontinuity of maxillary bone cortex, with irregular sequestrum formation (indicated by arrow)

Differential Diagnosis

1. **Osteolytic osteosarcoma tumor.** It mainly shows dissolution and destruction in jaws, which should be differentiated from central osteomyelitis of the jaws. Central osteomyelitis of the jaws is bone destruction centered on the causative tooth, which gradually migrates to normal osseous tissue, but osteolytic osteosarcoma has no such characteristics.
2. **Osteogenic osteosarcoma.** It mainly manifests as the formation of multiple dense osteosarcomas in the jaws and peripheral soft tissues, which should be differentiated from marginal osteomyelitis of the jaws with significant

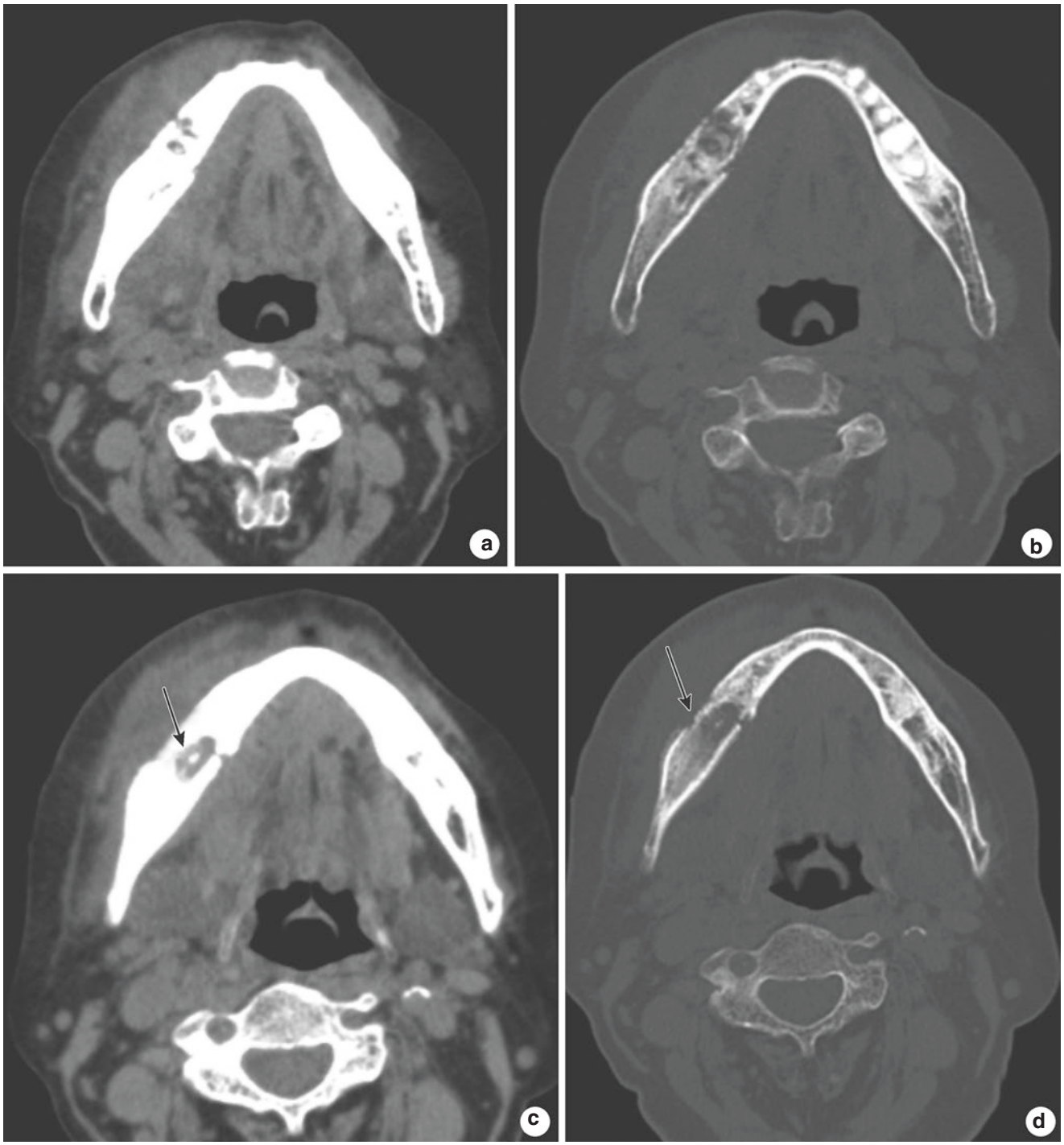

Fig. 26.3 Suppurative osteomyelitis of right mandible with swelling of peripheral soft tissue (2). (**a** and **c**) CT on soft tissue window shows swelling of masseter and adjacent soft tissue around the right mandible, and blurred fat space; (**b** and **d**) CT bone window shows discontinuous bone cortex of the right mandible, periosteal reaction (indicated by white arrow), increased bone marrow cavity density, and irregular sequestrum shadows (indicated by arrow)

neoplastic bone proliferation. The outer margin of subperiosteal neoplastic bone formed by marginal osteomyelitis of the jaws is more regular, while the bones and calcifications of osteogenic osteosarcoma are scattered in a shape similar to needle, which is different from each other.

Status Quo and Progress of Research

Imaging examinations, such as MSCT or MRI, can reflect the changes of bone marrow, bone cortex, periosteum and peripheral structures in pyogenic osteomyelitis of the jaws. Cone-beam computed tomography (CBCT) can perform multi-angle reconstruction depending on its high image resolution and low exposure dose, thus it shows bone destruction degree, bone marrow cavity density change and periosteal reaction superior to ordinary X-ray photography, and is widely used in clinical practice. However, at present, the pyogenic osteomyelitis of the jaws is mainly diagnosed according to results of laboratory test and pathological biopsy. Park et al. [4] thought that the quantitative analysis method with oral cavity radiography panorama could be used in early diagnosis of the osteomyelitis of the jaws, and 88.1% of patients could be diagnosed and classified accurately. Therefore, the imaging significance in early diagnosis of the disease needs further study.

26.2 Radiation Osteomyelitis of the Jaws

Overview

Radiation osteomyelitis of the jaws originates from radioactive therapy of nasopharyngeal carcinoma or oral and maxillofacial malignant tumor, which is related to many factors, such as individual sensitivity, radiation type, irradiation mode, irradiation field size, exposure dose, which causes aseptic endarteritis of jaws and swelling and thickening of tunica intima, then cause constriction and occlusion of lumen, finally resulting in osteoradionecrosis of the jaws. If the bone with lesion has odontogenic infection or local injury, the healing time of wound will prolong, and bacteria will invade and cause radiation osteomyelitis [5, 6].

The disease generally has long duration and develops slowly, with acute recurrence. Within six months to several years after radiotherapy, most patients have reduced saliva secretion, and their teeth are prone to rampant caries. With secondary odontogenic infection, or injuries such as tooth extraction, the wounds will not heal for a long time, and fistula will be formed with less purulent secretion, persistent pain, and halitosis. Sometimes the peripheral soft tissues may fester and necrose, but the sequestrums exposed is not loose, and relevant patients will have chronic inflammation for a long time. If secondary cellulitis occurs in adjacent tissues, it will show different degrees of restriction of mouth opening, which will cause large sequestrums in the jaws with long separation time, and the soft tissue in the lesion area will be hardening, resulting in scar formation. The patients with the disease generally have relatively poor general conditions, showing chronic wasting disease.

Pathology Findings

At present, the spontaneous necrosis of jaw is considered to be the result of a large dose of radioactive rays, and the irradiated osseous tissue has the characteristics of "three lows." That is, low cells, low blood supply, and hypoxia [5]. Pathologic tissue sections show bone cells shrinkage, empty bone lacunae, osteoblasts disappeared, fibrosis of periosteum and bone marrow cavity and nutrient vessels thrombosis. Due to the lack of blood supply in the pathological tissue, the osseous tissue lacks compensatory repair ability under the condition of hypoxia and low energy, which leads to the long healing period of wound, and the sequestrum in the lesion is difficult to be separated, finally presenting aseptic necrosis.

Imaging Findings

1. **X-ray examination.** It mainly shows patchy osteoporosis area surrounded by rough bone trabecula. When the lesion is extensive, there may be a large area of bone absorption, and the lesion may involve alveolar process. The patchy osteosclerosis complicated with osteoporosis area and sequestrums can be found in patients with long course of disease.
2. **CT examination.** It shows irregular low-density foci in bone absorption area, and there are common sclerosis straps around the lesions. If there is sequestrum, it shows as isolated high-density bone mass in low-density focus. Pathologic fractures and periosteal reactions are rare, and the peripheral soft tissues are often disorganized due to radiation therapy. If fistula is formed, the cord-like density shadows of soft tissues can be found to reach the skin surface directly from the necrotic area [6] (Fig. 26.4).
3. **MRI examination.** Hypointense on T_1WI, heterogeneous signal (hyperintense and hypointense) on T_2WI, and hyperintense on T_2WI in soft tissue around the lesion area.

Enhanced CT and MRI show enhancement of peripheral soft tissues, and the abscess in the soft tissues with ring enhancement.

Key Points of Diagnosis

1. Clinical history of radiotherapy for maxillofacial tumors.
2. X-ray films, CT and MRI show bone destruction areas varied in size in the jaws, and hyperostosis and osteosclerosis around the lesions, which may be complicated with sequestrum, and rare periosteal reaction. The peripheral soft tissue can be complicated with infection and internal fistula formation.

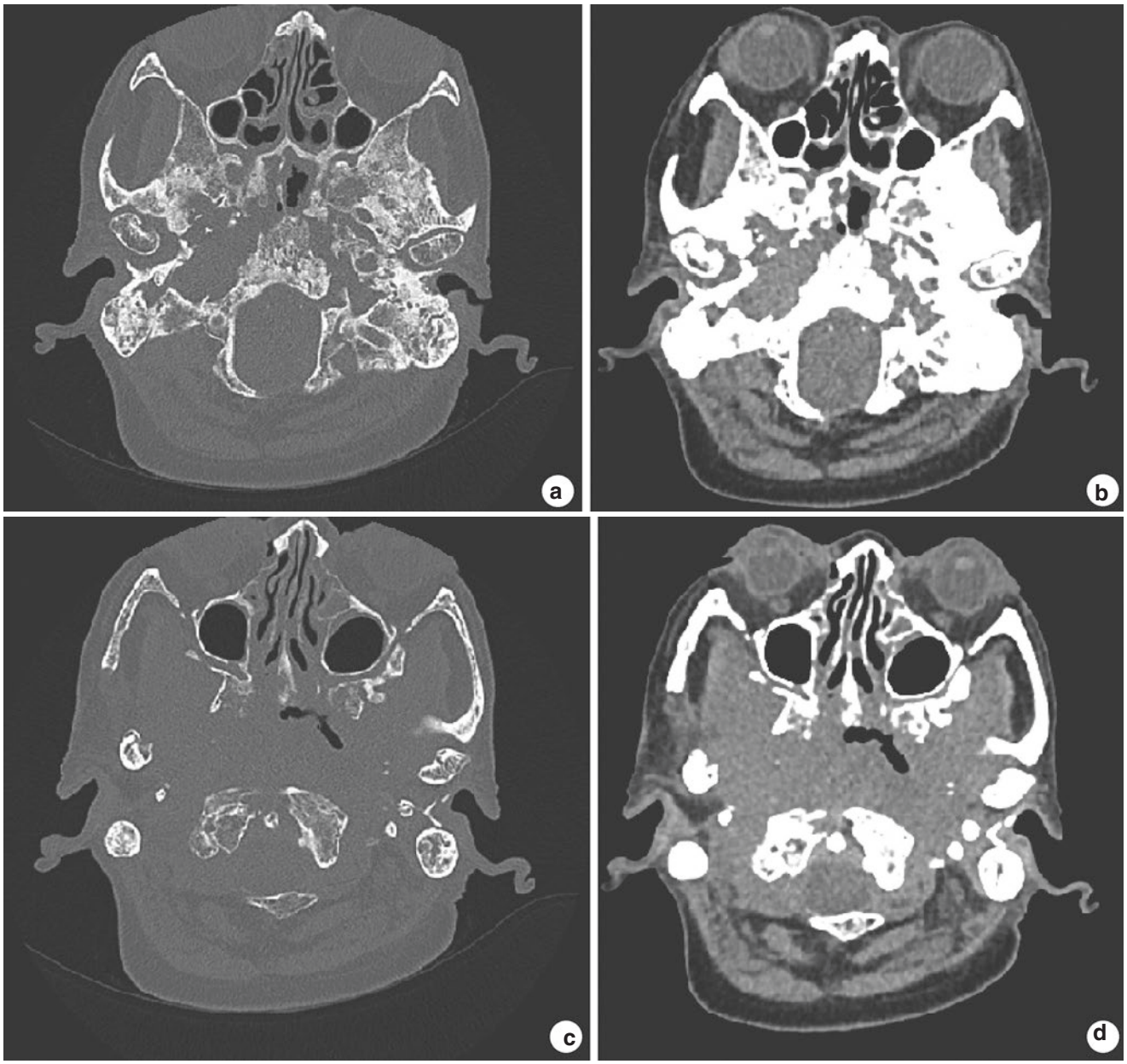

Fig. 26.4 Radiation osteonecrosis after radiotherapy for nasopharyngeal carcinoma. A 65-year-old female patient with post-radiotherapy of nasopharyngeal carcinoma. (**a–d**) Non-enhanced CT scan shows diffuse bone cortex discontinuity in the sphenoid bone, occipital bone, mastoid portion of bilateral temporal bones, and bilateral mandible, and bone trabecula in disorderly arrangement and with cellular change and local osteosclerosis. The nasopharyngeal roof is thickened with unclear margin, and irregular soft tissue density shadows in bilateral parapharyngeal space

Differential Diagnosis

1. **Suppurative osteomyelitis.** It has imaging manifestations similar to radiation osteomyelitis. The history of radiotherapy for maxillofacial tumors should be noted as it is of great significance to differentiate these diseases.
2. **Malignant tumor of the jaws.** Its recurrence often leads to rapid expansion of bone destruction area of the jaws and formation of peripheral soft tissue mass. Radioactive osteomyelitis has no localized mass in clinical practice and imaging, and there are a few sudden progression changes in the focus by radiographic follow-up, and the disease has long duration.

Status Quo and Progress of Research

In recent years, the incidence of radiation osteomyelitis of the jaws has decreased year by year and dropped to less than

5% [5] imaging examinations, such as X-ray, CT or CBCT, MRI are mostly used for clinical diagnosis and regular follow-up [5].

26.3 Drug-Related Osteomyelitis or Osteonecrosis

Overview

Drug-related osteomyelitis or osteonecrosis is the osteomyelitis or osteonecrosis of jaw bone caused by the treatment of systemic diseases with bisphosphonates or other targeted drugs. The disease is a new disease found in recent twenty or thirty years, and the occurrence of osteomyelitis and osteonecrosis is mainly associated with drugs. There are mainly two kinds of drugs that can cause osteomyelitis, one is anti-osteoclast drugs, and the other is anti-angiogenesis drugs. Zoledronic acid, for example, can combine with osteoclasts to arrest the metabolism of osseous tissue, thus causing inflammatory damage. These drugs are toxic to bones and to gums and mucosae, thus affecting the healing of osteomyelitis [7–10]. After tooth extraction, the gums, epithelium, and mucosa show very poor healing ability. The bone lacking self-repairing ability is easy to be infected when it is exposed for a long time and cannot be healed. Therefore, tooth extraction is the main local inducing factor. It mostly occurs in mandible, accounting for 73%; Occurrence in maxilla accounts for 22.5%; Simultaneous occurrence in maxilla and mandible accounts for 4.5%.

Pathology Findings

In the lesion area, it shows plenty of inflammatory cell infiltration, with vascular proliferation, granulation tissue formation, colonies and osteoid deposition, and sequestrum tissue.

Imaging findings

1. **X-ray examination.** It mainly shows patchy osteoporosis area surrounded by rough bone trabecula. During inflammation, a large scope of bone absorption area, periosteal reaction and swelling of soft tissue around the lesion are found. Patchy osteosclerosis is found in osteonecrosis stage, with bone decreased-density area and high-density sequestrum [11].
2. **CT examination.** The early pathological changes mainly show decreased density of ground-glass bone with unclear margin, periosteal reaction, and swelling of peripheral soft tissues. With the progress of the disease, the bone is destroyed irregularly, and large irregular low-density foci are found. Isolated high-density bone masses in the low-density foci indicate the existence of sequestrums, with common sclerosis straps in periphery. Pathologic fracture, periosteal reaction, and swelling of peripheral soft tissues are found, which can finally cause complete bone necrosis [11] (Fig. 26.5).
3. **MRI examination.** A definite diagnosis can be made by CT, and the value of MRI is to evaluate whether the jaw lesion is systemic metastasis or drug-related osteomyelitis. Osteomyelitis shows hypointense on T_1WI, heterogeneous signal (hyperintense and hypointense) on T_2WI, and hyperintense on T_2WI in soft tissue around the lesion. Mandibular metastasis shows soft tissue mass with infiltration growth, and the lesions show isointense on T_1WI and hyperintense on T_2WI. The soft tissue shadows show marked enhancement by enhanced examination.

Key Points of Diagnosis

1. Clinical history of using bisphosphonates and targeted drugs and having tooth extraction due to systemic diseases.
2. X-ray films, CT, and MRI show bone destruction areas in different sizes in the jaws, sequestrum formation, periosteal reaction, and peripheral soft tissue swelling.

Differential Diagnosis

1. **Suppurative osteomyelitis.** It has imaging manifestations similar to drug-related osteomyelitis. It should be noted that whether bisphosphonates and targeted drugs are used due to systemic diseases and the history of tooth extraction, as it is of great significance to differentiate these diseases.
2. **Radioactive osteomyelitis.** It has imaging manifestations similar to radiation osteomyelitis. It should be noted that whether patient has a history of radiotherapy for malignant tumors of the head and neck, as it is of great significance to differentiate these diseases. For radiation osteomyelitis, periosteal reaction and pathologic fracture are rare, while drug-related osteomyelitis and osteonecrosis are common.
3. **Malignant tumor of the jaws.** Its recurrence often leads to rapid expansion of bone destruction area of the jaws and formation of peripheral soft tissue mass. Radioactive osteomyelitis has no localized mass in clinical practice and imaging, and there are a few sudden progression changes in the focus by radiographic follow-up, and the disease has long duration.

Status Quo and Progress of Research

The disease was firstly reported by Marx in 2003. Since bisphosphonate-related osteonecrosis of the jaw (BRONJ) was reported, there were lots of patients with osteonecrosis of the jaw reported. Therefore, the AAOMS changed the BRONJ to medicine-related osteonecrosis of jaws (MRONJ). The incidence of MRONJ is 1.9% in cancer patients receiving drug therapy and 0.2% in patients receiving anti-angiogenic drugs. The incidence of MRONJ in patients

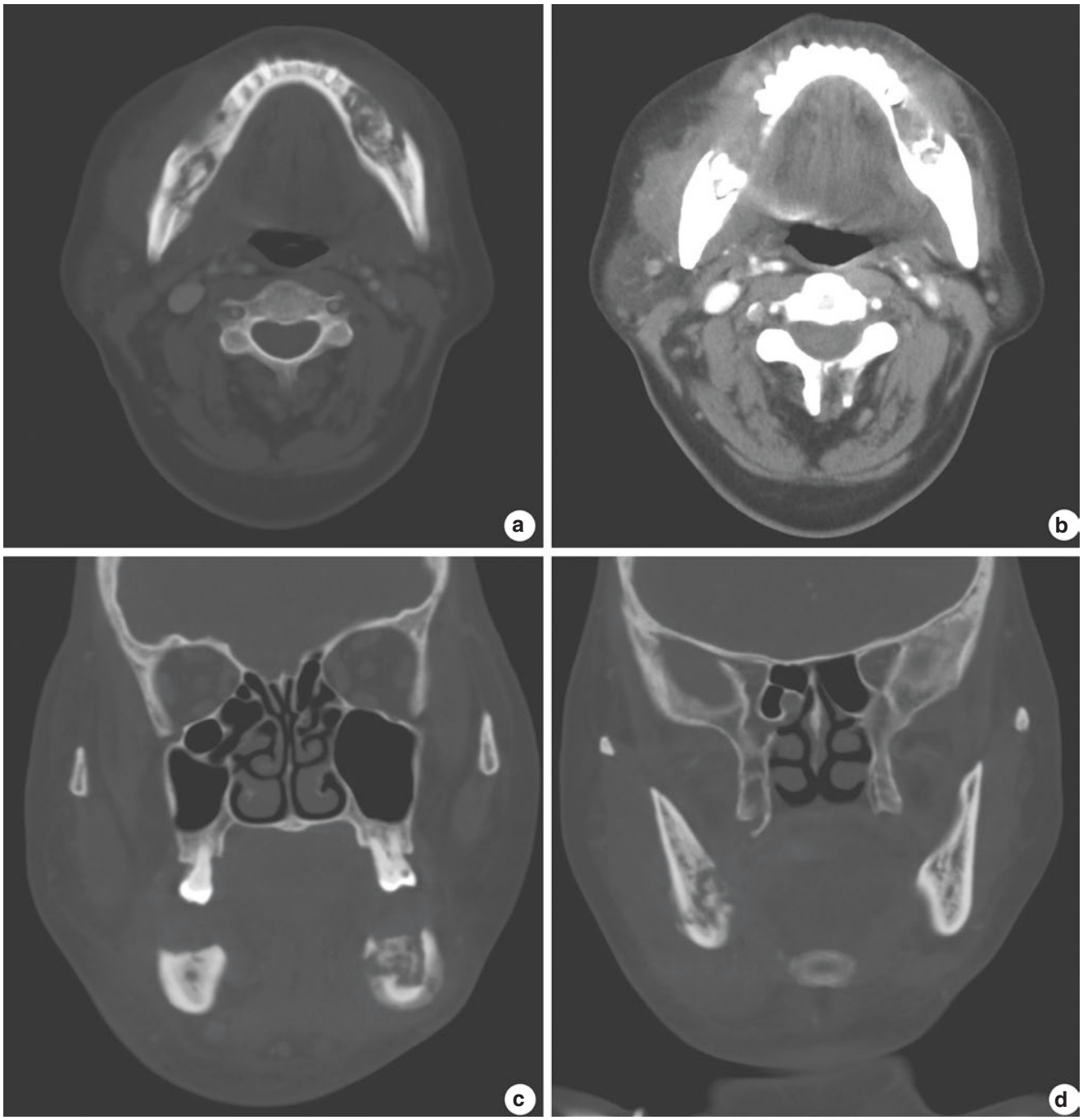

Fig. 26.5 Drug-related osteomyelitis. A 62-year-old female patient. After taking bisphosphate for 6 months, the swelling and pain of the left mandible gradually increased, and the anti-inflammatory treatment was ineffective. (**a–d**) Non-enhanced CT scan shows irregular bone decreased-density areas on the left and right sides of the mandible, and slightly high-density areas in the lesions, indicating the formation of sequestrums, discontinuity of bone cortex, indicating pathologic fractures and swelling of soft tissues adjacent to the lesions (Images courtesy of Zhu Ling and Tao Xiaofeng, the Shanghai Ninth People's Hospital, Shanghai JiaoTong University School of Medicine)

taking bisphosphonates orally after tooth extraction is 0.5%, and 1.6–14.8% in patients receiving bisphosphonates intravenously. The value of imaging is to evaluate the existence of lesions, the scope of lesions, and the existence of pathologic fracture. MRI is used to exclude the metastasis of systemic lesions and osteomyelitis caused by drugs.

26.4 Osteomyelitis with Tuberculosis of Jawbone

Overview

Tuberculosis of jawbone is often a secondary disease, which is mostly caused by blood-borne transmission. The primary tuberculosis lesions are mostly located in lung, digestive tract, pleura, and peritoneum. Mycobacteria tuberculosis firstly affects oral mucosa through saliva or sputum, or firstly infects gums and then invades jaws by mucosal ulcer or local trauma. Tuberculosis of jawbone commonly occurs in advanced stage of tuberculosis, mostly in mandible of adults, while maxillary tuberculosis mostly occurs in children. Tuberculosis of jawbone usually has unremarkable symptoms in early stage, with occasional spontaneous pain and systemic mild fever, and manifests as diffuse swelling of soft tissue in the lesion site, but there is often no congestion and redness of pyogenic infection on the skin surface or mucosa, and bone destruction is slow; If infection invades bone and peripheral soft tissue, cold abscess formation inferior to mucosa or skin can be found, and acid-fast bacilli can be found by pus smear examination [12, 13].

Tuberculosis of jawbone can be divided into alveolar process type and central type. Alveolar process lesion firstly appears in gingival mucosa, and then involves alveolar process. After the lesion deeply involves the alveolar process, the involved teeth become loose and fall off. When the diseased alveolar process swells or has fistula and does not heal for a long time, secondary pyogenic infection can occur. Central type is mostly caused by the spread of mycobacteria tuberculosis to jawbone, and is mostly found in areas with abundant spongy bone, such as mandibular angle.

Pathology Findings

Pathology shows that tuberculous granulation tissue is formed in the cavity of jaw bone marrow, which is composed of epithelioid cells, Langhans giant cells, and scattered inflammatory cells, forming epithelioid nodules.

Imaging Findings

1. **X-ray examination.** It shows bone destruction in the lesion area with blurred and irregular margin. When gingival tuberculosis spreads directly, it often involves alveolar bone, forming a cystic cavity at or below alveolar process, with small sequestrum pieces in it. People infected by hematogenous spread often invade the mandibular angle, frontal bone, and zygomatic suture. The bone cortex in the lesion area can show expansive changes, especially in children. Osteoporosis is often found around the destruction area. If it is complicated with infection, there may be hyperostosis and neoplastic bone formation similar to suppurative osteomyelitis.
2. CT examination. Alveolar process type shows incomplete cortical edge of alveolar bone, with irregular bone destruction area. Sequestrums varied in sizes can often be found in the destruction area, showing isolated high-density bone masses surrounded by low-density zones. The central destruction area is initially found in the spongy bone of the jaws. With expansion of the lesion, bone cortex can be involved. Both types of cold abscesses and caseous necrosis show low-density shadows, and the enhanced scan indicates ring enhancement. Most of the destruction areas are complicated with osteoporosis or hyperostosis and osteosclerosis, mostly occurring after secondary pyogenic infection. When fistulas are formed, cord-like slightly high-density shadows are found in the soft tissue between the bone destruction area and the skin.
3. MRI examination. It shows hypointense on T_1WI, hyperintense on T_2WI in the bone destruction area in the jaws and edema belt around the lesions. Sequestrum manifests as hypointense focus in hyperintense area on T2WI. The cold abscess adjacent to the bone destruction area shows significantly hypointense on T_1WI and hyperintense on T_2WI, with ring enhancement by enhanced scan. The soft tissue around the lesion is often complicated with swelling, especially around the fistula, and the signal intensity increases on T_2WI.

Key Points of Diagnosis

1. If patients are adolescents, they have a history of primary tuberculosis in the lung, digestive tract or other parts, or have gingival or oral mucosal tuberculosis lesions before jaw lesions.
2. On X-ray films, CT, and MRI images, the lesions can manifest as bone destruction in alveolar process, mandibular angle and infraorbital border, with irregular shape and small sequestrum mass, which mostly supports the diagnosis of tuberculosis of jawbone.

Differential Diagnosis

Tuberculosis of jawbone should be differentiated from suppurative osteomyelitis. In addition to the differences in clinical manifestations suppurative osteomyelitis is often complicated with subperiosteum neoplastic bone formation, while bone destruction is the main manifestation of tuberculosis of jawbone, and no neoplastic bone formation is found generally. When infection is secondary to tuberculosis of jawbone, hyperostosis and neoplastic bone formation are

found around the lesion, thus it is difficult to be differentiated from suppurative osteomyelitis, and should be comprehensively analyzed with other clinical information.

Status Quo and Progress of Research

MSCT can be used to detect benign tumors or tumor-like lesions of the jaw, and the accuracy rate of lesions is 100%, while the final diagnostic coincidence rate is 91.7% [14]. However, the clinical manifestations of patients with tuberculosis of jawbone are diverse and often atypical, and most of them are diagnosed according to the primary lesions, laboratory test, imaging findings, and pathological biopsy. At present, there are rare imaging researches on tuberculosis of jawbone.

26.5 Mouth Floor Cellulitis

Overview

Cellulitis of the floor of the mouth, also known as multi-space infection of the mouth floor, is one of the most severe and difficult infections in maxillofacial region, which involve a wide scope, including the mouth floor, retropharyngeal space, and even the superior mediastinum and chest wall. There are multiple groups of interlaced muscles between mandible and tongue and hyoid bone, which are filled with loose connective tissue and lymph nodes. Oral infections caused by various reasons are easy to extend and spread along spaces with weak resistance, thus forming multi-space infections in oral, maxillofacial, and cervical region.

According to the nature of infection, cellulitis at the mouth floor can be divided into suppurative and necrotic types. The former mostly manifests as bilateral submandibular, sublingual diffuse swelling and diffuse swelling at the mouth floor; the latter manifests as extensive paraedema of soft tissue, and involving the upper chest in severe cases [15].

Necrotizing cellulitis at the mouth floor, also known as Ludwig's angina, pyogenic submandibular inflammation, etc., refers to a wide scope of acute cellulitis occurring in multiple spaces at the mouth floor, such as inframandibular, sublingual, and submental spaces, and often involves the cervical fascia space and even the superior mediastinum. It is one of the most severe and dangerous infections in the head and neck, which threats to life if it is not treated properly. The pathogens of Ludwig's angina lead to mixed infection. In clinical practice, bacterial culture may show aseptic growth, which is mostly caused by lack of anaerobic culture. The infection is mostly caused by odontogenic disease, followed by submaxillaritis, lymphadenitis, acute tonsillitis, oral soft tissue and jaw injury, etc [15, 16].

The clinical manifestations of cellulitis at the mouth floor are swelling at the mouth floor, red and swollen mucosa, sharp pain, fever, difficulty in tongue movement, dysphagia and respiratory disturbance, soft tissue pneumatosis, systemic infection, and so on. Severe cases may have asphyxia and even mediastinal infection and bilateral pulmonary infection, which is life-threatening. Laboratory test shows an increase in leukocyte count.

Pathology Findings

Acute cellulitis refers to non-suppurative inflammation caused by acute bacterial infection in subcutaneous, subfascial, intermuscular space or deep fascial cellular tissue. The main pathogen is hemolytic streptococcus, followed by mixed infection of staphylococcus aureus and anaerobic bacteria. Hemolytic streptococcus can release hemolysin, streptokinase, hyaluronidase, etc. after infection, which makes inflammation to spread rapidly and fuse to normal tissues. It can cause extensive inflammation and edema of subcutaneous tissue in a short time and can lead to systemic inflammatory reaction syndrome and endotoxemia, but blood culture often shows negative results. If the pathogen is staphylococcus aureus, the lesion is limited due to the coagulase produced by staphylococcus aureus.

Pathological changes of necrotizing cellulitis are mainly acute necrotizing inflammation in dermis and subcutaneous tissues, including neutrophil and lymphocyte infiltration, dilation of blood vessels and lymphatic vessels, vascular thrombosis, necrosis of muscular tissue and fascia, and liquefaction of adipose tissue [17].

Imaging Findings

Oral, maxillofacial, and cervical multi-space infection can be diagnosed by general clinical examination due to significant symptoms. Local redness, swelling, heat, pain, fever, dysphagia, respiratory distress, restriction of mouth opening, mental fatigue, or irritability all suggest multi-space infection in oral, maxillofacial, and cervical regions. However, cellulitis or abscess in deep layer of soft tissue is difficult to be diagnosed only by symptoms and signs. At present the main imaging methods include CT and MRI.

1. **CT examination.** Cellulitis and abscess are the most common multi-space infections at the mouth floor. Among them, cellulitis shows thickening and edema of the skin in the involved part, flocculent and reticular high-density shadows in the subcutaneous fat layer, thickening and swelling of the involved muscles with blurred margins, disappearance or significant reduction of adipose tissue in the fascia space, and flocculent high-density image in the space. On CT, abscess shows low-density vomica, and air of different volumes is scattered in some vomica, and the abscess wall shows ring enhancement [15, 16] (Figs. 26.6, 26.7 and 26.8).
2. **MRI examination.** The cellulitis often shows swelling of soft tissue at the infected site and unclear margin with

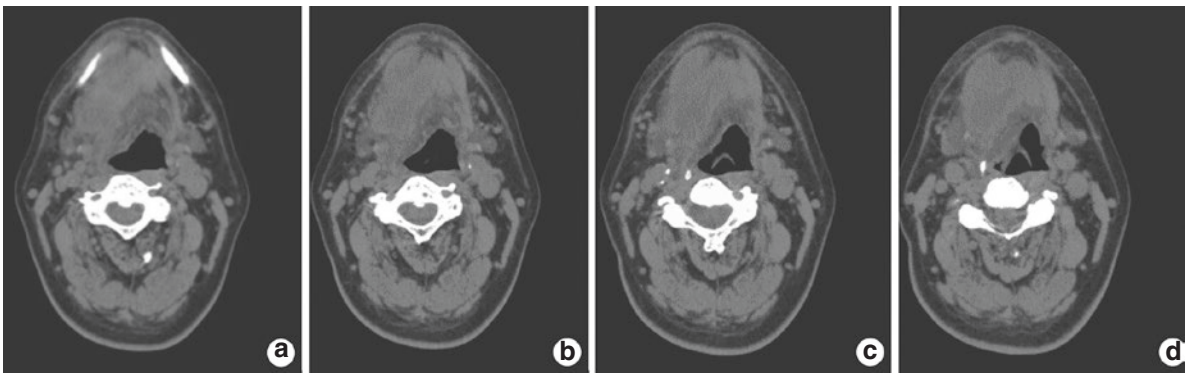

Fig. 26.6 Space infection of mouth floor (1). (**a–d**) Non-enhanced CT scan indicates soft tissue swelling in the right area of the mouth floor, with blurred fat space around it, patchy lower-density area and unclear margin in the right submandibular area, and multiple slightly large lymph nodes in I–II regions of bilateral neck. After anti-infection treatment in hospital, the condition improved significantly

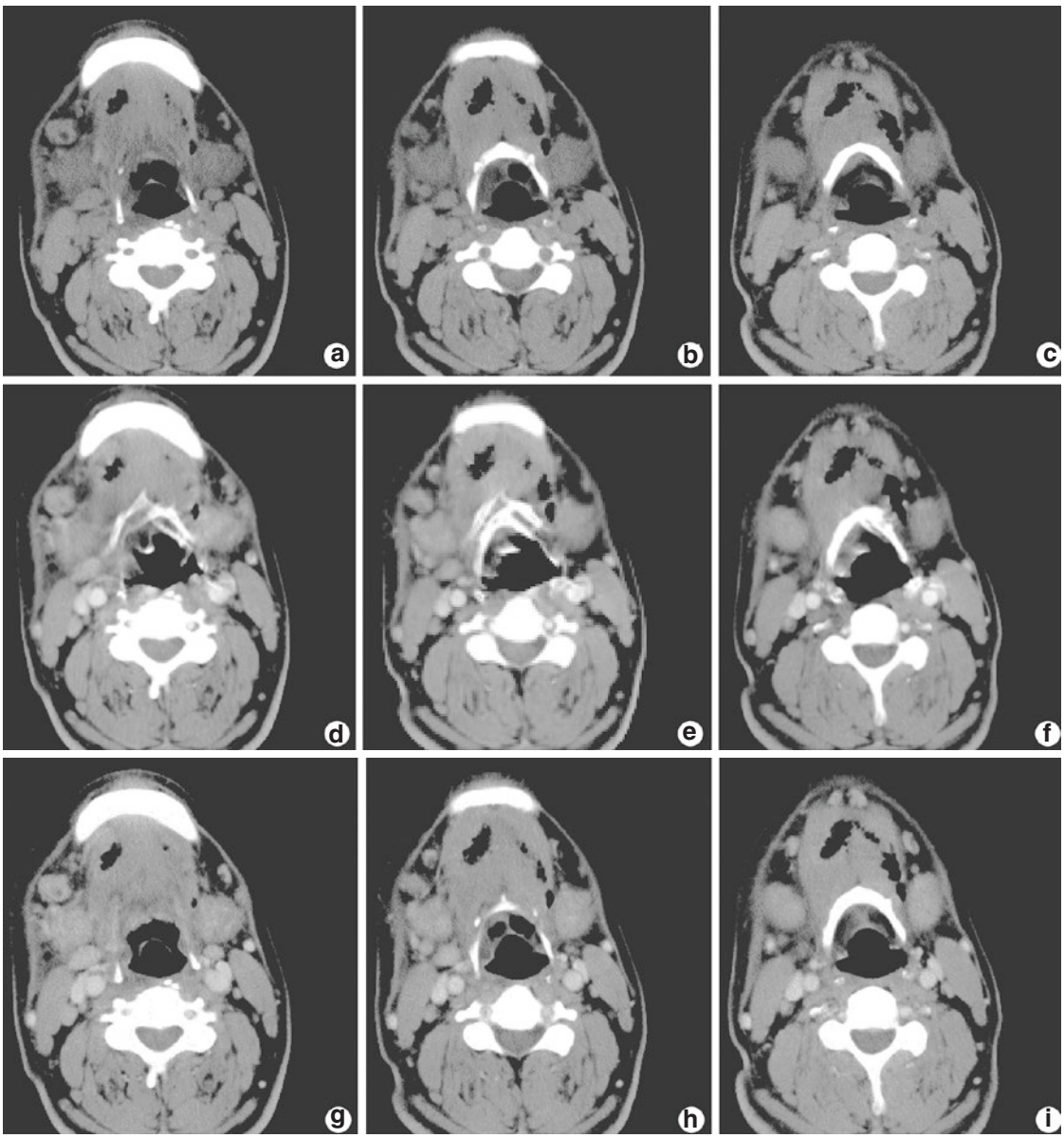

Fig. 26.7 Space infection of mouth floor (2). (**a–c**) Non-enhanced CT scan indicates bilateral submandibular glands swelling and density decreased, swelling and pneumatosis of bilateral submandibular space, sublingual space and soft tissue at the mouth floor, and blurred peripheral fat space; (**d–i**) Enhanced examination shows marked enhancement of the soft tissue in the lesion area in arterial and venous phases, blurred subcutaneous space in the neck, and enlarged lymph nodes in bilateral submental neck

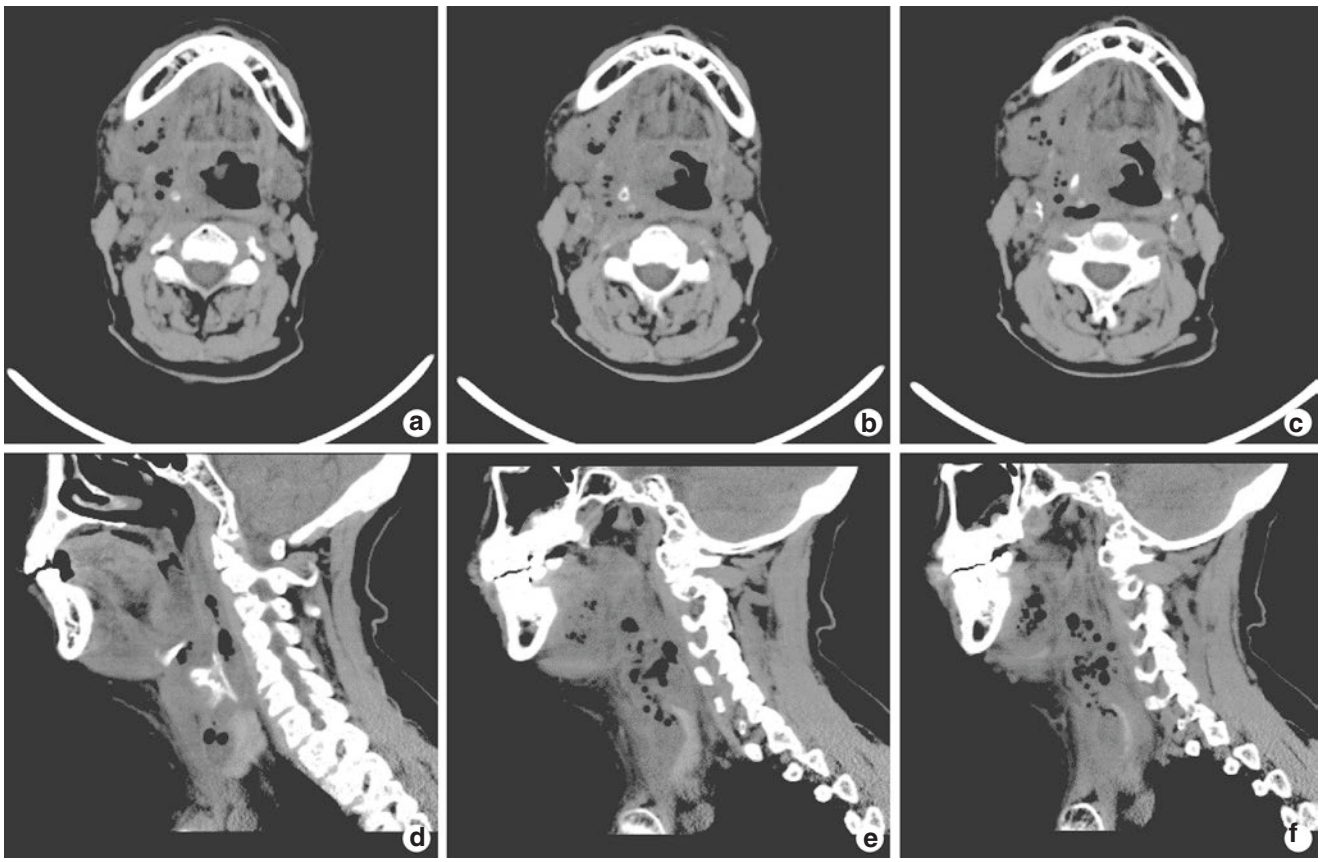

Fig. 26.8 Infection and pneumatosis of the space of mouth floor. (**a–c**) Non-enhanced CT scan indicates swelling of soft tissue in right submandibular area, right parapharyngeal space and right part of neck, local low-density area and pneumatosis shadows, unclear margin, and blurred surrounding fat space; (**d–f**) Sagittal reconstruction image shows a wide scope of lesions and multiple enlarged lymph nodes in bilateral necks

peripheral tissues, with isointense and hypointense on T_1WI and hyperintenses on T_2WI; significantly hyperintense on T_2WI of abscess and marginal enhancement on enhanced T_1WI; DWI and ADC are helpful to the diagnosis of abscess. MRI can clearly show the swelling of soft tissue and the deviation, reduction, or even disappearance of fat space.

Key Points of Diagnosis

1. On CT and MRI, it manifests as swelling of soft tissue, disappearance of fat space, ring enhancement of abscess wall, and hyperintense on DWI of vomica.
2. Combined with the clinical manifestations of swelling of the mouth floor, mucosa irritation, sharp pain, fever, etc.
3. Laboratory test shows leukocytes increased.

Differential Diagnosis

Combined with clinical manifestations and imaging findings, cellulitis at the mouth floor can be diagnosed definitely in most cases. Only some lesions need to be differentiated from tumors. Most of the tumors are invasive, and gradually increase so anti-inflammatory treatment is ineffective.

Status Quo and Progress of Research

Cellulitis at the mouth floor often causes multi-space infection in oral, maxillofacial, and cervical regions, which is difficult to be treated clinically due to large involvement scope. At present, the research on the disease mainly focuses on its infection spreading route, pathogen and drug resistance, clinical comprehensive treatment and prevention and treatment of severe complications. Imaging examination, such as multi-slice spiral CT or MRI, can show cellulitis or abscess, determine the location and number of involved spaces, early diagnosis of complications, such as mediastinitis and pneumonia, and assist clinicians in making operative plans [17].

References

1. Zhenchang W, Junfang X, Baosen L. Chinese imaging medicine - head and neck. 2nd ed. Beijing: People's Medical Publishing House; 2016.
2. Malina-Altzinger J, Klaeser B, Suter VGA, et al. Comparative evaluation of SPECT/CT and CBCT in patients with mandibular osteomyelitis and osteonecrosis. Clin Oral Investig. 2019;23(12):4213–22.

3. van de Meent MM, Pichardo SEC, Rodrigues MF, et al. Radiographic characteristics of chronic diffuse sclerosing osteomyelitis/tendoperiostitis of the mandible: a comparison with chronic suppurative osteomyelitis and osteoradionecrosis. J Cranio maxillo fac Surg. 2018;46(9):1631–6.
4. Park MS, Eo MY, Myoung H, et al. Early diagnosis of jaw osteomyelitis by easy digitalized panoramic analysis. Maxillofac Plast Reconstr Surg. 2019;41(1):6.
5. Yue H, Jinsong H, Xiaoguang L, et al. Expert consensus on clinical diagnosis and treatment of radiation osteonecrosis of mandible. Chin J Oral Maxillofac Surg. 2017;15(05):445–56.
6. Yuhan BT, Nguyen BK, Svider PF, et al. Osteoradionecrosis of the temporal bone. Otol Neurotol. 2018;39(9):1172–83.
7. Ohga N, Sato J, Asaka T, et al. Successful conservative treatment of jaw osteonecrosis caused by denosumab in patients with multiple bone metastasis. J Oral Sci. 2018;60(1):159–62.
8. Ghidini G, Manfredi M, Giovannacci I, et al. Medication-related osteonecrosis of the jaw: risk factors in patients under biphosphonate versus patients under antiresorptive-antiangiogenic drugs. Minerva Stomatol. 2017;66(4):135–40.
9. Suzuki N, Oguchi H, Yamauchi Y, et al. A case of tooth fracture occurred upon medicating bisphosphonate for an elderly person: preservation therapy and responses for stage 0 of bisphosphonate-related osteonecrosis of jaw. Eur J Denti. 2017;11(2):258–63.
10. Ribeiro NRB, Silva LDF, Santana DM, et al. Bisphosphonate-related osteonecrosis of the jaw after tooth extraction. J Craniofac Surg. 2015;26(7):606–8.
11. Guo Y, Wang D, Wang Y, et al. Imaging features of medicine-related osteonecrosis of the jaws: comparison between panoramic radiography and computed tomography. Oral Surg Oral Med Oral Pathol&Oral Radiol. 2016;122(2):69–76.
12. Tanwar R, Iyengar AR, Nagesh KS, et al. Primary tuberculosis: an unusual finding in the oral cavity. Oral Health Dent Manag. 2012;11(1):23–8.
13. Zhiping L, Jian M, Qianping G, et al. A case of bone tuberculosis in the ascending ramus of mandible. Chin J Dental Res (Electronic Edition). 2014;8(5):423–5.
14. Wen Xiaoling W, Dongsheng ZH, et al. Multi-slice spiral CT findings and pathological basis of benign tumors and tumor-like lesions of jaw. Chongqing Med. 2018;47(24):3223–6.
15. Maroldi R, Farina D, Ravanelli M, et al. Emergency imaging assessment of deep neck space infections. Semin Ultrasound CT MR. 2012;33(5):432–42.
16. La'porte SJ, Juttla JK, Lingam RK. Imaging the floor of the mouth and the sublingual space. Radiographics. 2011;31(5):1215–30.
17. Mingfeng T, Fujun Z, Rui C, et al. A case of severe multi-space infection at the mouth floor with cervical-mediastinal infection and literature review. J Modern Stomatol. 2018;32(5):313–5.

Temporal-Mandibular Joint Lesions

27

Mingyu Li, Li Yao, Heng Liu, Shuangyan Sun, and Shuang Xia

27.1 Pigmented Villonodular Synovitis

Overview

Pigmented villonodular synovitis (PVNS), also known as diffuse tenosynovial giant cell tumor, is a proliferative lesion of synovium or tendon sheath involving unilateral joint, ligament, and articular capsule. It often occurs in unilateral joint, mostly common in knee joint, followed by hip joint, ankle joint, shoulder joint, and elbow joint. It is rare in temporal-mandibular joint, which is usually related to trauma and hemorrhage [1]. According to the scope of joint involvement, the lesion can be divided into two types: localized type and diffuse type. The localized type is also called pigmented nodular synovitis); because the lesion develops locally in the joint. Diffuse type refers to the diffuse growth of lesions in joints, which is PVNS. Patients have repeated joint swelling for a long time, complicated with pain in some cases, limitation of motion due to swelling and pain, and temporal-mandibular joint lesions may be complicated with mass anterior to ears, ache, hearing loss, and so on. At present, the accepted therapeutic approach is resection, but due to its own characteristics, the lesions are widely distributed and deeply invaded in the articular cavity, especially diffuse PVNS, which often involves important structures in the joint, resulting in difficult resection and high recurrence rate.

M. Li
Affiliated Hospital of Chengde Medical University, Shanghai, China

L. Yao
Affiliated Stomatology Hospital of Zunyi Medical University, Zunyi, China

H. Liu (✉)
Affiliated Hospital of Zunyi Medical University, Zunyi, China

S. Sun
Jilin Cancer Hospital, Changchun, China

S. Xia
Tianjin First Central Hospital, Tianjin, China

Pathology Findings

General pathology shows thickened synovial tissue in the lesion area, which is brown or yellow, with villus structure on the surface; There may be hematocele in the articular cavity. Microscopically, synovial villi have hypertrophy, synovial cells proliferate significantly, the proliferated cells are in small round or oval shape, and the nuclei are similar to coffee beans. Benign giant cells are scattered in the lesions.

Imaging Findings

1. **X-ray and CT examination.** X-ray examination can show the change of joint space and the invasion to joint bone but is difficult to differentiate diseases with low specificity. CT examination has a high-density resolution and can clearly show soft tissue proliferation and bone destruction in joints, and can clearly show the sclerotic margin around the bone destruction area (Figs. 27.1, 27.2a–d and 27.3a–d). However, CT lacks specificity in judging the degree invasion to articular cartilage and peripheral soft tissue, and cannot observe hemosiderin deposition, and can only indicate lesion with definite hemorrhage.
2. **MRI examination.** Compared with X-ray plain film and CT, MRI is undoubtedly the best noninvasive examination with high accuracy and significant advantages. MRI examination has high resolution of soft tissue, and supports multi-parameter and multi-directional imaging, which can well show the lesion shape, tissue composition, and the involvement of peripheral soft tissue [2].
   (a) Diffuse PVNS shows synovial villi or nodular thickening, while localized PVNS shows local soft tissue masses.
   (b) On non-enhanced MRI scan images, PVNS pathologically shows plenty of capillaries in hyperplastic synovium, causing repeated hemorrhage. After cytophagy of hemosiderin by macrophages, the hemosiderin can cause heterogeneous magnetic field, showing characteristic T_1WI and hypointense on T_2WI (Figs. 27.2e–f and 27.3e–f).

H. Li et al. (eds.), *Radiology of Infectious and Inflammatory Diseases - Volume 2*,
https://doi.org/10.1007/978-981-16-8841-6_27

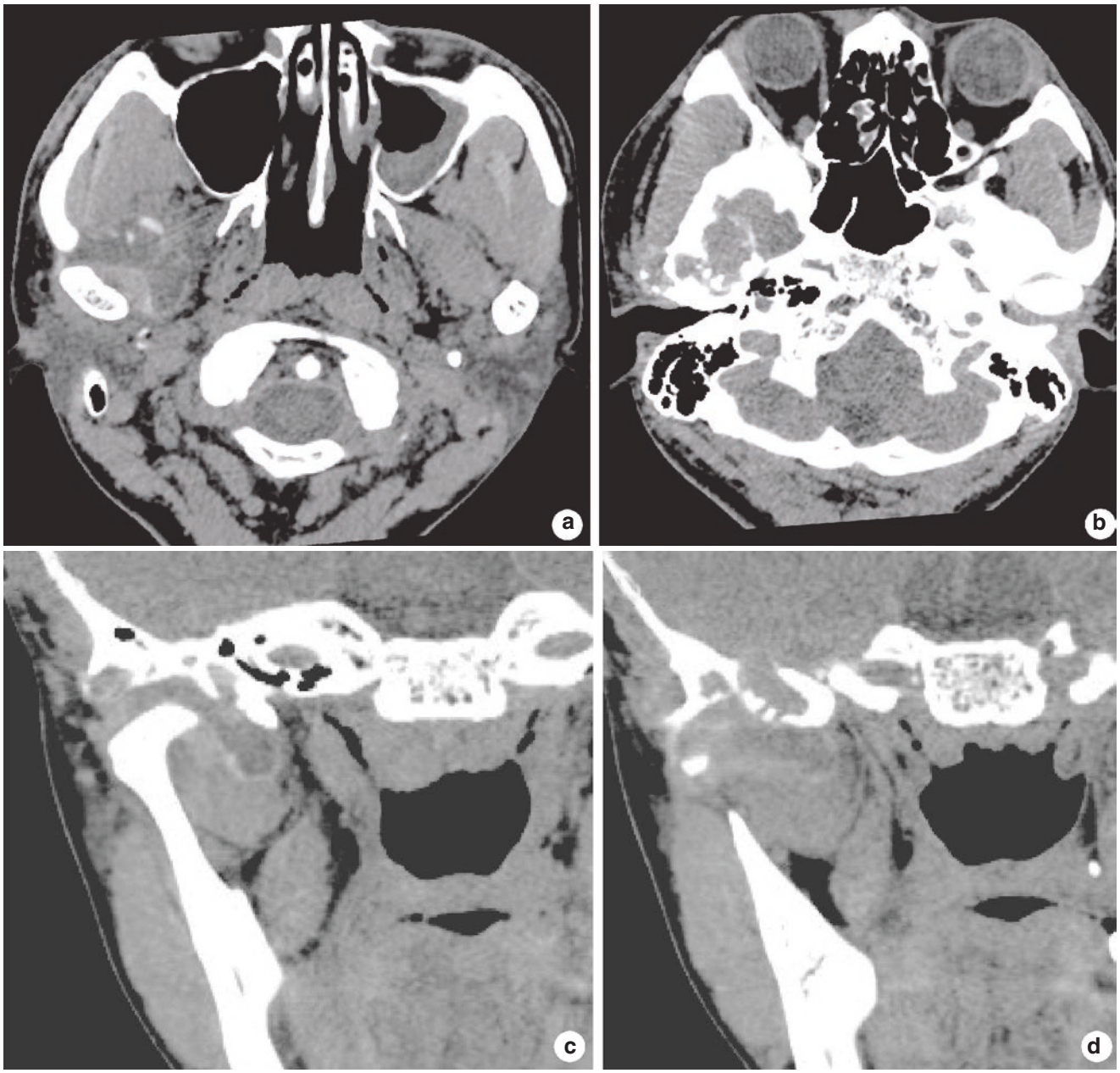

Fig. 27.1 Pigmented villonodular synovitis of the right temporal-mandibular joint. A 55-year-old male patient. Patient complained of discomfort of right temporal-mandibular joint and was difficult to open mouth for 1 month. (**a** and **b**) Transverse CT on soft tissue window shows nodular soft tissue shadow in the right temporal-mandibular joint, with swelling, heterogeneous density, calcification, and cystic degeneration area, and clear lesion margin; (**c** and **d**) Coronal CT on soft tissue window shows widened right temporal-mandibular joint, and expansive bone destruction in the temporal bone (Images courtesy of Zhang Jun and Hao Dapeng, Radiology Department of The Affiliated Hospital of Qingdao University)

(c) On T_2WI images, most of the lesions show multiple cystic hyperintense. This multi-cystic manifestation is either caused by cystic degeneration of focus, or by effusion accumulated in articular cavity separated by hyperplastic synovial tissues.
(d) Enhanced MRI examination shows enhanced findings in marginal area of the lesion (Fig. 27.2g–h). The articular surface of mandibular condyle and temporal bone can be eroded by pathological changes. Sometimes large-scale iron deposition can also produce magnetic-sensitive artifacts, especially on T_2WI.

Key Points of Diagnosis

1. Pain mass in temporal-mandibular joint area with disorganized occlusal relationship and restriction of mouth opening.

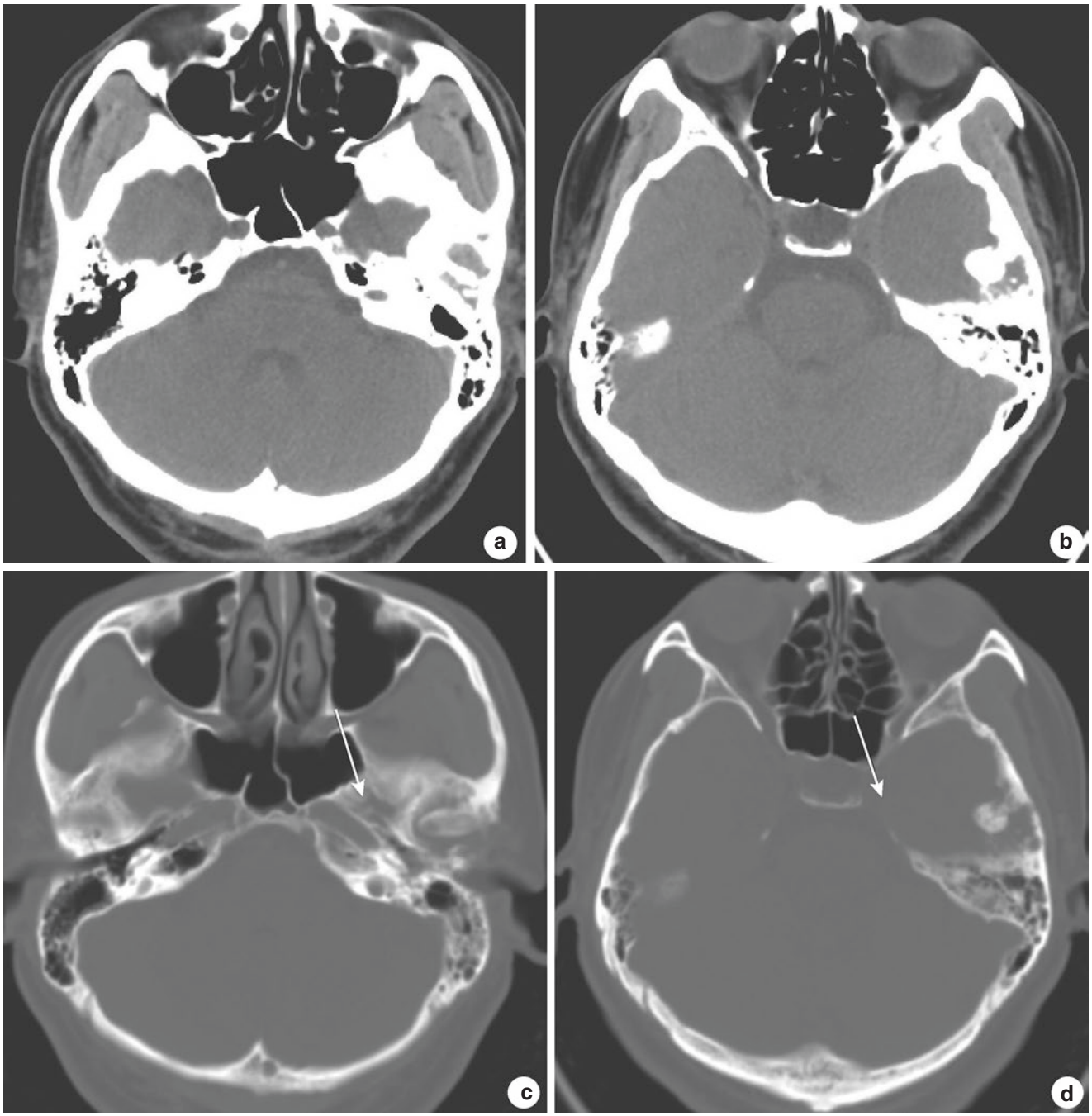

Fig. 27.2 Pigmented villonodular synovitis of the left temporal-mandibular joint (1). A 65-year-old female patient Long-term history of bruxism, discomfort of left temporal-mandibular joint, pain for 1 year. (**a** and **b**) Transverse CT on soft tissue window shows soft tissue shadows around the left temporal-mandibular joint, and unclear margin; (**c** and **d**) Transverse CT on bone window shows irregular bone destruction in adjacent bone, and moth-eaten bone destruction and hyperostosis in the left temporal bone. (**e** and **f**) Non-enhanced transverse MRI T_1WI and T_2WI scan shows isointense on T_1WI and hypointense on T_2WI in left temporal-mandibular joint. (**g** and **h**) Transverse and coronal MRI enhanced scan shows mild enhancement of lesions and marked enhancement of adjacent synovium (Images courtesy of Zhang Jun and Hao Dapeng, Radiology Department of the Affiliated Hospital of Qingdao University)

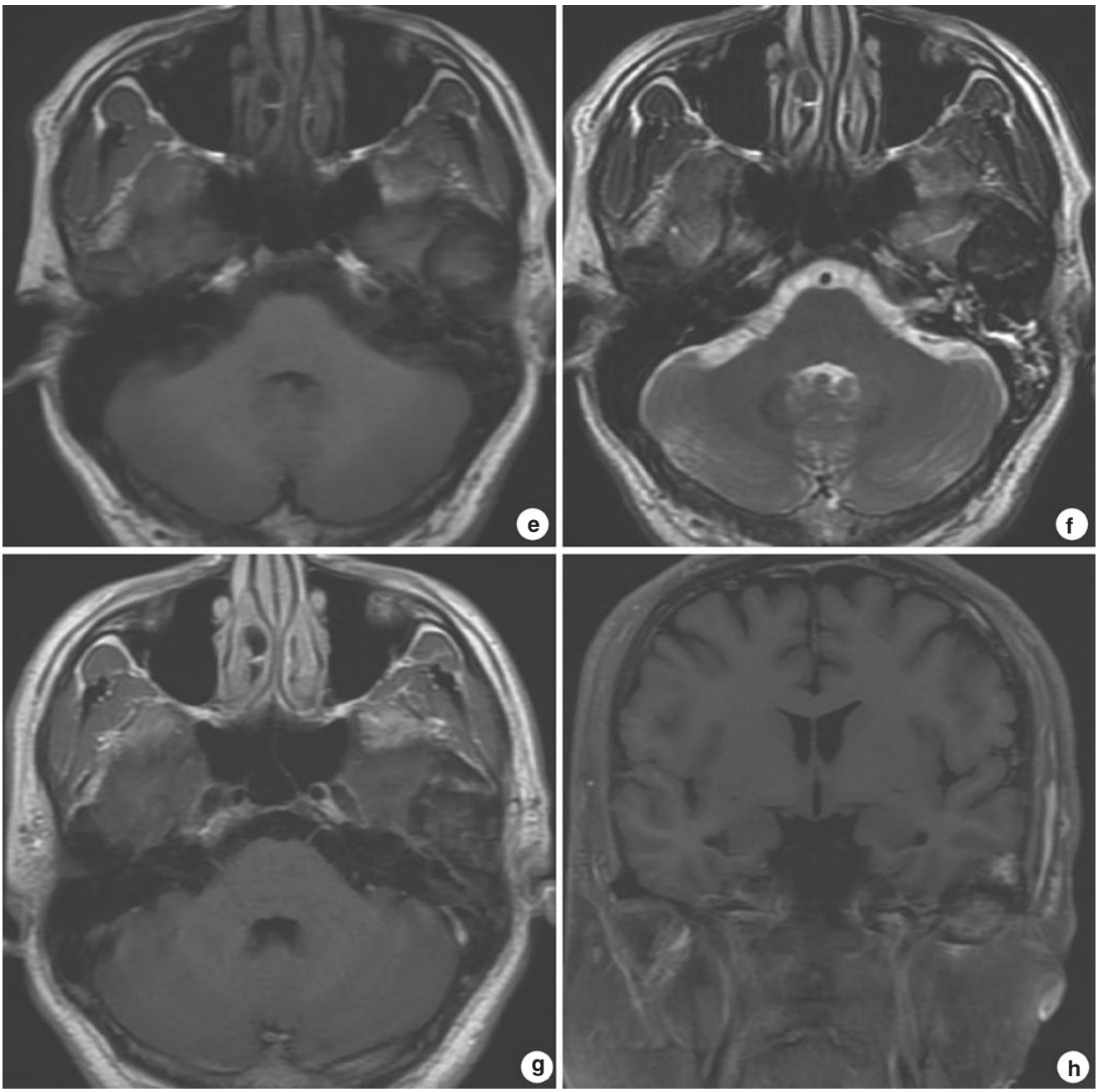

Fig. 27.2 (continued)

2. There is abundant hemosiderin deposition in the lesions, which manifest as characteristic hypointense on T_1WI and hypointense on T_2WI.
3. The lesions on T_2WI show multiple cystic hyperintense.
4. Enhanced scan shows marginal enhancement of lesion.

Differential Diagnosis

1. **Synovial chondromatosis.** Synovial chondromatosis in the temporal-mandibular joint mostly occurs in the superior articular cavity, characterized by multiple "pearl-like" free calcified corpuscles in the temporal-mandibular joint. On MRI images, the internal signals of Synovial chondromatosis mainly consist of three parts: abnormal effusion in articular cavity, thickened synovial metaplasia, and free chondroid corpuscles.
2. **Rheumatoid arthritis.** It is a systemic disease involving multiple joints. The synovium of the joint is firstly involved, and then there is exudate in the joint, and the synovial granulation tissue is formed and proliferated to form pannus covering the articular surface. On MRI, rheumatoid arthritis manifests as abnormal proliferation of synovial pannus and invasion to joint bone structure.

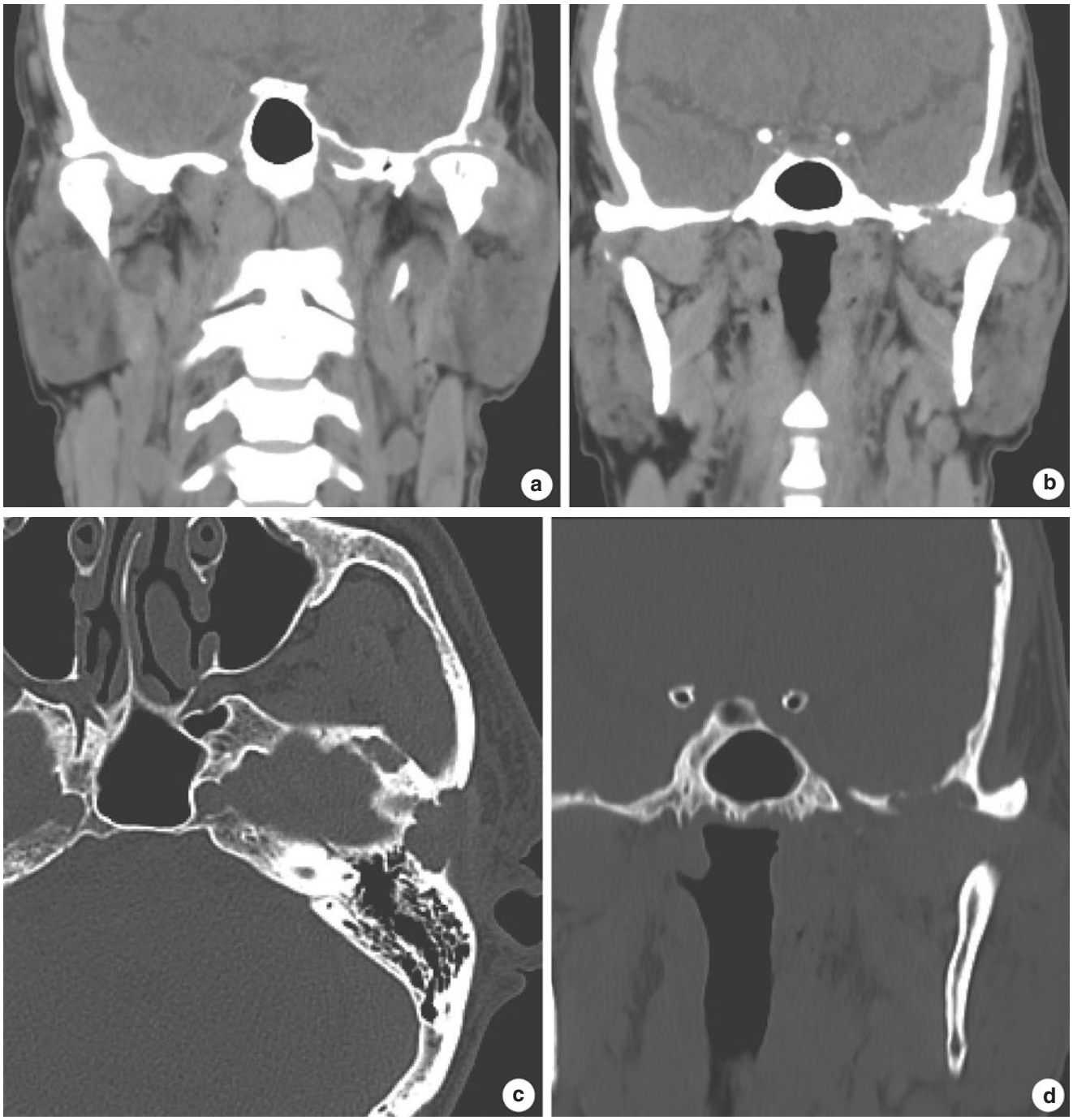

Fig. 27.3 Pigmented villonodular synovitis of the left temporal-mandibular joint (2). A 37-year-old male patient. The patient suffers from left temporal-mandibular joint pain for 1 year. (**a** and **b**) Coronal CT on soft tissue window shows multiple nodular shadows around the left temporal-mandibular joint, which are lobulated, with unclear margin and heterogeneous density; (**c** and **d**) Transverse and coronal CT on bone window shows irregular bone destruction in adjacent bone with clear margin; (**e** and **f**) Coronal MRI T_1WI and T_2WI shows the left temporal-mandibular joint with isointense on T_1WI and hypointense on T_2WI (Images courtesy of Li Fuxing, Radiology Department, Tianjin Baodi District People's Hospital)

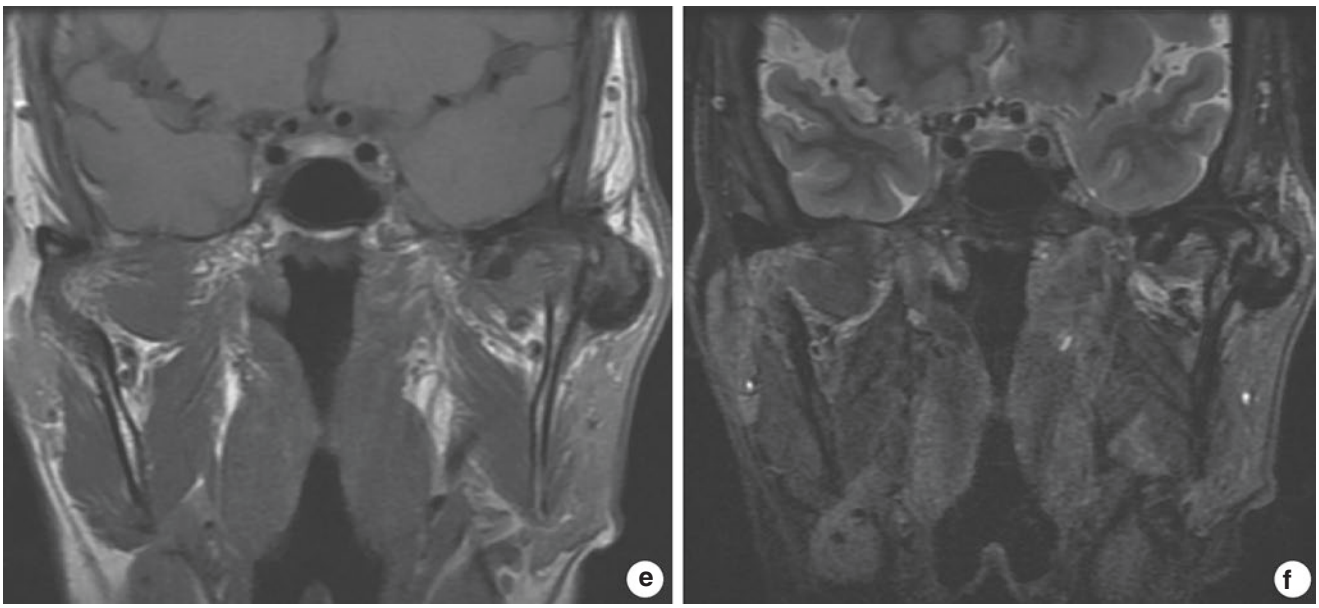

Fig. 27.3 (continued)

Usually, the proliferative synovial pannus shows isointense changes on T_2WI. Enhanced MRI shows marked enhancement of hyperplastic synovial tissue. Bone erosion in rheumatoid arthritis can be round or irregular. The lesion signal intensities on T_1WI and T_2WI are significantly lower than that of normal bone marrow, and the margin is blurred.

3. **Giant cell reparative granuloma.** It is a locally invasive non-neoplastic disease, which mainly occurs in the articular surface of temporal bone, and occurs mostly in young women. The recurrence rate is 5–15%. The pathogenesis is still unclear. Some scholars think that the disease is a reparative reaction of hemorrhage of bone and peripheral tissues due to inflammation or various stimulating factors, which is not necessarily related to trauma history. CT shows irregular bone destruction of temporal-mandibular joint and calcification in soft tissue. Enhanced CT shows moderate enhancement of expansive mass. Hemosiderin deposition, calcification, and fibrosis are common in lesions, and hypointense is found on T_1WI, T_2WI, and DWI.

Status Quo and Progress of Research

X-ray plain film and CT examination can show expansive destruction of bone, and residual bone changes are found at the margin of the lesion. MRI examination is the best imaging method to diagnose PVNS. However, some scholars believe that PVNS is over-diagnosed, synovial hyperplasia and/or hemosiderin deposition are not enough for diagnosis, and the disease must be differentiated by histopathologic examination. The clinical manifestations of pigmented villonodular synovitis lack specificity and it is easily misdiagnosed as parotid mass and temporal-mandibular joint disorder, and the disease is rare in temporal-mandibular joint. The main therapeutic approach of PVNS is to completely remove the pathological tissue by surgery, and bone involved should also be removed. If the removal is incomplete, there is a recurrence probability of 35–50% [3]. With the improvement of understanding of the disease, many doctors suggest postoperative radiotherapy. PVNS is generally not malignant, but there are multiple cases of recurrence and malignant after operation.

27.2 Pseudogout Arthritis

Overview

Pseudogout arthritis is a rare metabolic osteoarthropathy, also known as articular cartilage calcification, which is caused by calcium deposition in fibrocartilage, hyaline cartilage, synovium, joint capsule, tendon and intra-articular ligament of joint. The calcium salt is mainly composed of calcium pyrophosphate dehydrate, so it is also known as calcium pyrophosphate dehydrate deposition disease [4].

The average onset age of related patients is 74 years, with unremarkable gender difference. It can be divided into six clinical types: the first type shows periodic arthritis, and the symptoms disappear during the intermittent period; The second type shows persistent acute onset, which is rare; The third type shows acute onset of chronic persistent arthritis, which is the most common; The fourth type is chronic progressive arthritis without acute onset; The fifth type is only one arthritis; The sixth type is asymptomatic. The most common X-ray manifestation is stripy calcification 1–2 mm away

from the articular surface, which can be continuous or intermittent. Repeated onsets of the disease may lead to joint degeneration.

Pseudogout arthritis generally involves large joints, mostly in knee joint, followed by wrist joint, ankle joint, elbow joint, hip joint, and spine. It mostly involves unilateral joint, but also in bilateral joints. Acute symptoms are similar to gout, with acute onset and rapid progress, red, swelling and sharp pain in joints, patchy erythema on articular surface skin, and joint ankylosis in some patients. The duration of disease in acute stage is self-limited, with spontaneous remission within 1–3 weeks. Chronic cases show small nodules in the joint appendages, which gradually grow up with pain. The patients with long course of disease have joint damage, and some patients have no symptoms or only joint swelling. The disease is rare in temporal-mandibular joints.

Pathology Findings

The pathological changes mainly include punctate, patchy, or stripy calcification of fibrocartilage and hyaline cartilage of the joint, the hyperplastic and cystic degeneration of inferior bone trabecula, the hyperplastic synovial tissue as villous nodules, constriction of joint space, and osteophyte formation, and rare progressive bone destruction [5].

Imaging Examination

For the patients to be diagnosed clinically, the PA plain film should be taken on diseased joint, and the lateral view of the contralateral joint and the affected side should be taken when necessary. Temporal-mandibular joint needs lateral oblique film or panoramic radiography and CT of mandible. Imaging shows that the signs of calcium deposition mainly depend on the degree of deposition and the effective choice of detection means. Other joint tests can be selected at the same time. For example, the detection rate of articular cartilage calcification is about 90% in the PA view, the detection rate of knee joint and pubic symphysis is about 98% in the PA view, and the detection rate of knee joint, pubic symphysis, and wrist orthopedics is about 100% in the PA view.

Imaging Findings

Calcification of articular cartilage shows fine linear and arc-like calcification shadows, which is parallel to the bony articular surface, with a transparent space of 1–2 mm between them [6].

Fibrocartilage calcification manifests as irregular and heterogeneous high-density shadows.

Calcification of the articular capsule or soft tissue around the joint shows cloud-like dense shadows at the margin of the joint, while calcification of the peripheral soft tissue shows sheet-like or thin line shadows, which is separated from the attached bone (Fig. 27.4).

Pyrophosphate arthropathy manifests as heterogeneous constriction of joint space, hyperostosis at joint edge, irregular bone proliferation and sclerosis on articular surface and in subarticular space, cystic degeneration in sclerosis area inferior to the articular surface, enlargement of articular capsule, loose body in articular cavity, and disc-shaped erosive defect on articular bone surface.

Key Points of Diagnosis

1. Two or more joints show typical hyaline cartilage or fibrocartilage calcification excluding intervertebral disc calcification
2. Paracentesis of effusion from the joint with or without symptoms, monoclinic or polyclinic crystals are found by polarized light microscopy, lacking or showing weak positive birefringence.

Cartilage calcification is no longer the only characteristic sign in the diagnosis of pseudogout arthritis. Intra-articular calcification, juxta-articular calcification, and joint structure damage have the same diagnostic significance. The damage of joint structure can be used as an important sign to differentiate from degenerative osteoarthropathy [6].

Status Quo and Progress of Research

For pseudogout arthritis calcified lesions in joints and peripheral area cannot be observed on X-ray films or CT images occasionally and cystic degenerations of lesions can also appear in some patients on MRI images so the diagnostic criteria of the disease cannot only rely on imaging findings [8].

In addition, the morphology and location of pyrophosphate crystals can be observed by high-resolution ultrasound, which is helpful for the diagnosis of pseudogout arthritis [9].

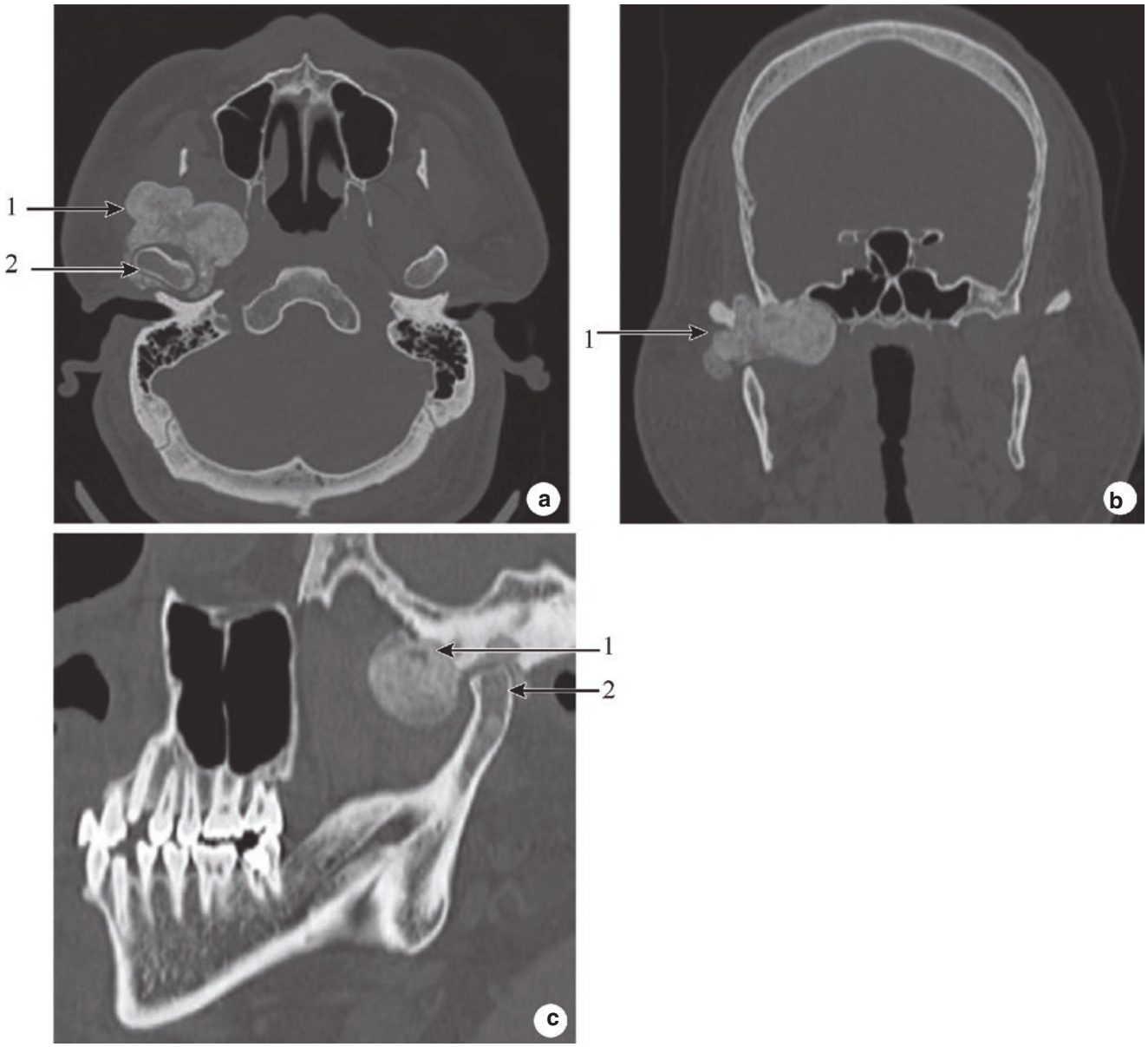

Fig. 27.4 CT scan of pseudogout arthritis of right temporal-mandibular joint [7]. (**a**) Transverse plane; (**b**) Coronal plane; (**c**) Sagittal plane. A 60-year-old male patient. Pain in the right temporal-mandibular joint for several years. CT shows a cloud-like dense shadow at the margin of the joint, and the peripheral soft tissue calcification, showing sheet-like or thin line shadows

References

1. Haihong B, Ying Z, Shuai W. A case of pigmented villonodular synovitis of temporal-mandibular joint. Chin J Pract Stomatol. 2011;4(2):126.
2. Ling S. Value analysis of susceptibility weighted imaging (SWI) in MRI diagnosis of pigmented Villonodular synovitis (PVNS). J Imaging Res Med Appl. 2018;2(19):76–7.
3. Verspoor FGM, Mastboom MJL, Weijs WLJ, et al. Treatments of tenosynovial giant cell tumours of the temperomandibular joint: a report of three cases and a review of literature. Int J Oral Maxillofac Surg. 2018;47(10):1288–94.
4. Filippou G, Adinolfi A, Cimmino MA, et al. Diagnostic accuracy of ultrasound, conventional radiography and synovial fluid analysis in the diagnosis of calcium pyrophosphate dihydrate crystal deposition disease. Clin Exp Rheumatol. 2016;34(2):254–60.
5. Patel T, Ryan L, Dubois M, et al. The prevalence of chondrocalcinosis of the symphysis pubis on CT scan and correlation with calcium pyrophosphate dihydrate crystal deposition disease. Clin Rheumatol. 2016;35(3):771–3.
6. Li Changqin F, Jianbin XY, et al. Imaging diagnosis of calcium pyrophosphate crystal deposition disease. Orthop J China. 2006;14(18):1404–6.
7. Kudoh K, Kudoh T, Tsuru K, et al. A case of tophaceouspseudogout of thetemporomandibular joint extending to the base of the skull. Int J Oral Maxillofac Surg. 2017;46(3):355–9.
8. Iwata M, Kasai H. A case of calcium pyrophosphate dihydrate crystal deposition disease suspected the tumor of temporomandibular joint. Int J Oral Maxillofac Surg. 2019;48(1):281.
9. Lin YY, Wang TG, Li KJ, et al. Imaging characteristics of calcium pyrophosphate dihydrate crystal deposition disease. Am J Phys Med Rehabil. 2014;93(3):272–3.

Part IX

Infectious and Inflammatory Diseases of Cervical Space

Inflammatory Lesions of Salivary Gland Space

28

Hui Dai, Haorong Zhang, Bangguo Li, and Heng Liu

28.1 Inflammatory Lesions of Salivary Gland

28.1.1 Epidemic Parotitis

28.1.1.1 Overview

Epidemic parotitis is a highly contagious disease, which is caused by the mumps virus, and its infection sources are mostly patients and carriers. Parotitis is mostly a childhood disease, which mainly occurs in children aged 5–9 years old, and is dominant in school-age children [1]. The disease occurs frequently in winter and spring, which are mainly transmitted through respiratory tract by droplets. The latent period of parotitis is 12–25 days after exposure. The main clinical feature is non-suppurative swelling of parotid gland, which can lead to meningitis, encephalitis, pancreatitis, and hearing loss. The disease may also develop into oophoritis in female patients and orchitis in male patients. Epidemic parotitis, like other childhood diseases, will increase in severity with age. The disease has an acute onset, with fever, headache, muscle soreness, anorexia, etc. The parotid gland swells after several hours to 1–2 days, lasting for about 10 days and then resolves spontaneously.

28.1.1.2 Pathology Findings

The main pathological change of epidemic parotitis is non-suppurative inflammation of parotid gland. Viral infection can cause swelling of parotid gland duct parietal cells, edema around duct and glandular stroma tissue, etc., which can cause obstruction of parotid gland duct, obstruction of saliva discharge, and amylase retention, thus increasing amylase in hematuria.

H. Dai · B. Li · H. Liu (✉)
Affiliated Hospital of Zunyi Medical University, Zunyi, China

H. Zhang
Children's Hospital of Shanghai, Shanghai, China

28.1.1.3 Imaging Findings

1. CT Examination It indicates diffuse swelling on unilateral or bilateral glands, and stripy and small nodular soft tissue density shadows in the low-density fat of normal parotid gland, without significant soft tissue mass. Enhanced scan mainly indicates homogeneous enhancement and thickening of interlobar septum and capsule. The peripheral soft tissues may have exudative changes and thickening of local superficial cervical fascia and platysma fascia.

2. MRI Examination The pathological features of epidemic parotitis are non-suppurative inflammation of parotid gland, inflammatory cell infiltration around parotid gland duct and glandular stroma, glandular stroma tissue edema, and fat signal of normal gland replaced by inflammatory exudation and proliferation nodules. Gland shows heterogeneous hypointense on T_1WI sequence and heterogeneous hyperintense on T_2WI and fat-suppressed sequence, with surrounding blurred fat space and exudation. Enhanced scan indicates that most lesions show homogeneous enhancement, while a few lesions with patchy and nodular heterogeneous enhancement.

28.1.1.4 Key Points of Diagnosis

1. Patients usually have a clear exposure history with patients with epidemic parotitis in 2–3 weeks.
2. Typical clinical symptoms are swelling of parotid gland centered on earlobe, which may be complicated with fever and headache.
3. Non-enhanced CT scan indicates diffusely increased volume of parotid gland, with density higher than the low-density fat in normal gland. On non-enhanced MRI scan, irregular isointense or slightly hypointenses on T_1WI for glands, while heterogeneous hyperintense on T_2WI and fat-suppressed sequence for inflammation of the gland and the surrounding edema area, with the surrounding blurred fat space, and most lesions with marked homogeneous enhancement.

H. Li et al. (eds.), *Radiology of Infectious and Inflammatory Diseases - Volume 2*,
https://doi.org/10.1007/978-981-16-8841-6_28

4. The diagnosis must be based on serological and etiological examination (RT-PCR experiment or virus culture).

28.1.1.5 Differential Diagnosis

Epidemic parotitis is one of the most common infectious diseases of parotid gland. According to the exposure history and parotid gland enlargement, it is not difficult to be diagnosed. At present, CT and MRI are the most important imaging techniques for diagnosing parotid gland diseases. In the early stage of infection, non-enhanced CT and MRI show no significant abnormity, and the imaging findings lack specificity. Its qualitative diagnosis mainly depends on specific medical history, signs, and laboratory test, and imaging findings can assist diagnosis and play a role in positioning.

1. Early Suppurative Parotitis The edema around the focus of suppurative parotitis is relatively mild in the early stage. With the progression of the disease, inflammation continues to spread, salivary gland tissue is necrotic, and multiple suppurative lesions are formed. By enhanced scan, they show ring enhancement and garland-like enhancement, generally without orchitis or oophoritis, and the leukocyte count of blood routine significantly increases. Generally, epidemic parotitis does not appear necrosis or vomica, and leukocyte counts are mostly normal or slightly increased.

2. Other Viral Parotitis Such as parainfluenza virus, influenza A virus, lymphocytic choroid plexus meningitis, and other viruses can cause parotitis, which need to be differentiated by serological examination and virus isolation, and it is difficult to differentiate them by imaging methods.

28.1.1.6 Status Quo and Progress of Research

Epidemic parotitis is mostly pediatric disease. Considering radiation and tolerance of children, ultrasound is still the first choice for imaging examination. High-frequency ultrasound can visually observe the thickness, contour, internal echo, blood flow distribution, and nodules in parotid gland, which can provide reliable information for clinical diagnosis of epidemic parotitis.

28.1.2 Acute Suppurative Sialadenitis

28.1.2.1 Overview

Based on etiology and pathophysiology, sialadenitis can be classified as bacterial, viral, immune, or granulomatous types, among which bacterial infection is the most common [2]. Other causes of acute sialadenitis include dehydration, immunosuppression, iatrogenic infection (drug-related), and rare blood-borne spread. Among them, acute parotitis is the most common disease, with common pathogen of staphylococcus aureus, a few infections by streptococcus and rare infections by pneumococcus. It mainly occurs in children. The pathogenesis of acute suppurative parotitis is divided into blood-borne infection and retrograde spread through parotid gland duct, the latter is more common, and the former is mostly found in newborns. It is reported [3] that the causes of acute suppurative parotitis in newborns include rupture of unclean oral cavity, traumatic rupture caused by forceps, infection of birth canal, infection by breastfeeding. Premature infants and small-for-date infants become high-risk groups because of imperfect parotid gland development. Most of the cases are involved unilaterally, with occasional reports of bilateral involvement. The clinical manifestation of sialadenitis is pain and swelling of salivary gland after eating, and purulent secretion may appear in case of bacterial sialadenitis. The common clinical manifestations of acute parotitis include fever, muscle pain, muscle discomfort, and other nonspecific symptoms. More specific features include 95% facial swelling (parotitis) and/or testicular pain (orchitis). If necessary, serum IgM antibody test can be used to diagnose parotitis. In early stage and 2–3 weeks of the disease, the titer of double serum increases more than four times, which is of diagnostic significance.

28.1.2.2 Pathology Findings

Pathogens of acute suppurative sialadenitis include Staphylococcus aureus, Streptococcus, Anaerobic bacteria, Gram-negative bacilli, among which Staphylococcus aureus is the most common one, with leukocyte infiltration and serous inflammatory exudation in the local lesions. The typical pathological feature of acute suppurative parotitis is suppurative inflammation of parotid gland in children, and the peripheral tissues of invaded glands often show punctate hemorrhage, acinus necrosis, lymphocyte infiltration, interstitial edema, and so on.

28.1.2.3 Imaging Findings

1. CT Examination

1. The glands are enlarged, the normal glands in the elderly become fat, and the density increases when inflammation occurs; the density decreases when inflammation occurs in the glands of young people, with blurred edge, and the enhanced scan shows marked enhancement, complicated with the density increase of adjacent fat and/or typical thickening of unilateral deep cervical fascia (Figs. 28.1, 28.2, and 28.3).
2. Segmental duct dilatation and stenosis caused by sialolithiasis or duct obstruction.
3. Intraglandular or extraglandular enlargement of lymph nodes, without specificity.
4. Abscess shows low-density shadows, which may be complicated with pneumatosis.

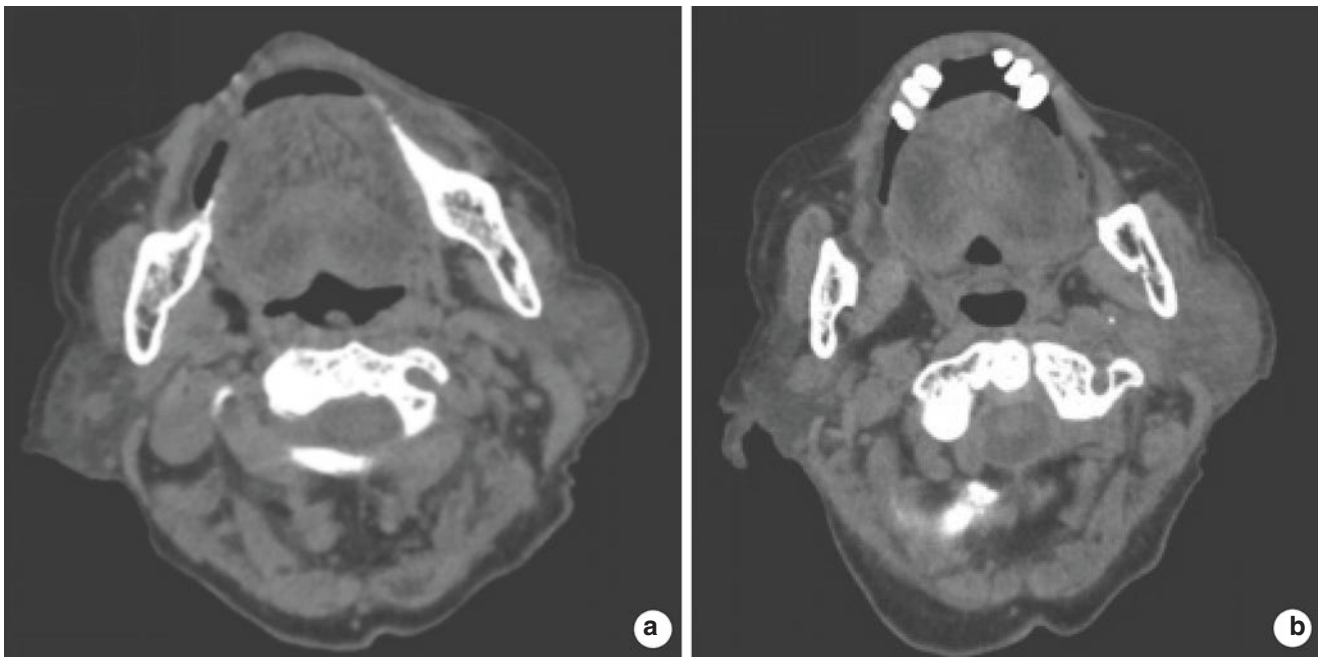

Fig. 28.1 Acute suppurative parotitis. A 45-year-old male patient. The left parotid gland swelled with pain for 1 week. (**a**, **b**) Non-enhanced CT scan indicates the left parotid gland increases in volume and density, with internal heterogeneous density and unclear margin

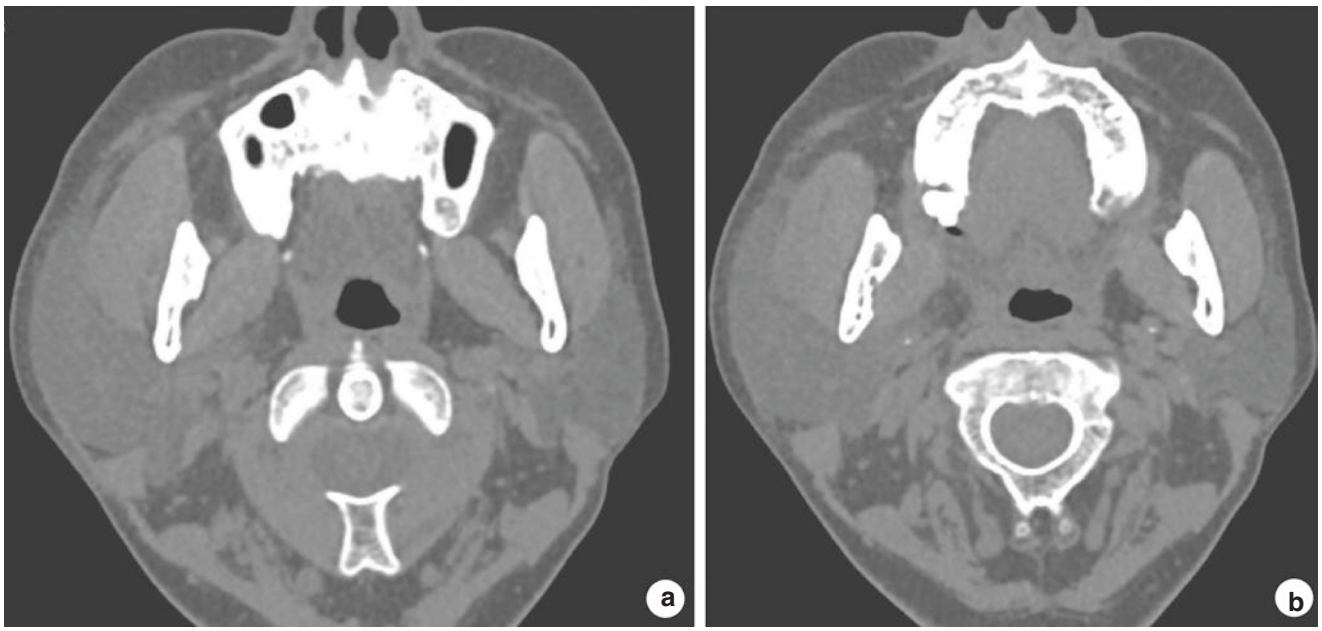

Fig. 28.2 Right acute suppurative parotitis. A 55-year-old male patient. Swelling of right parotid gland and face with pain for 2 weeks. (**a**, **b**) Non-enhanced CT scan indicates the right parotid gland increases in volume and density, with increased and heterogeneous density. Thickened right buccal fascia and increased subcutaneous fat density

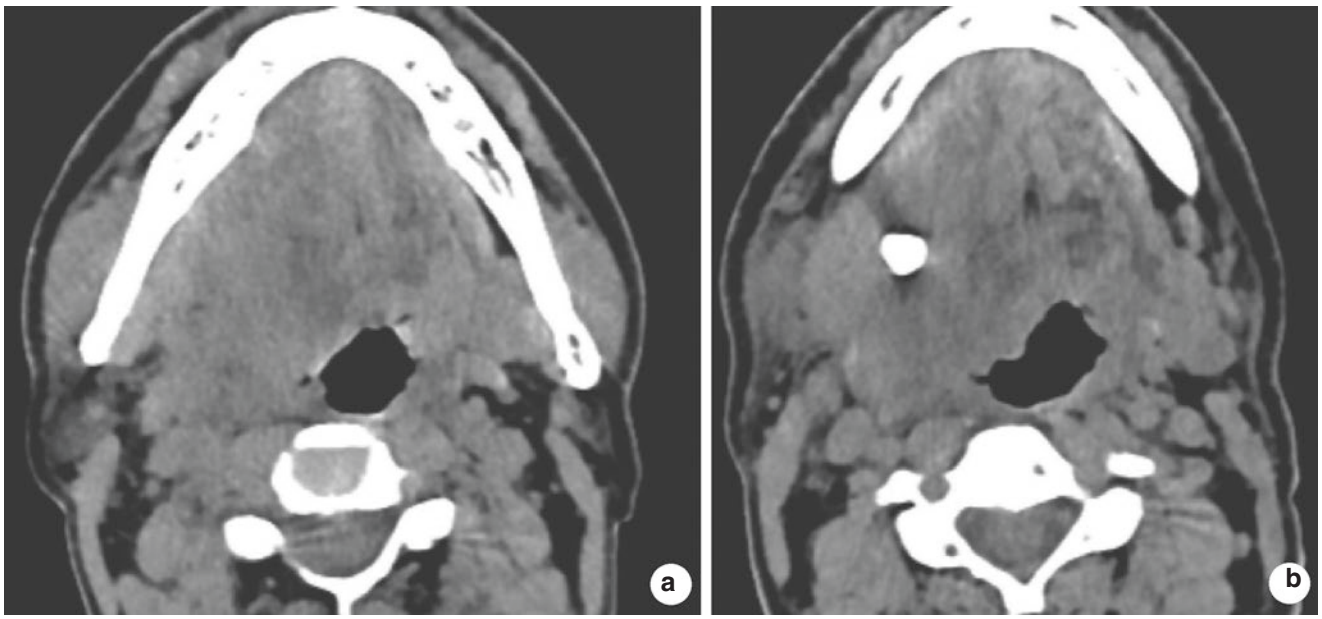

Fig. 28.3 Right acute suppurative submandibular gland calculi with submaxillaritis. A 45-year-old female patient. Swelling and pain in the right submandibular area, which were significant after eating. (**a**, **b**) Non-enhanced CT scan indicates the right submandibular gland increases in volume and density, with internal heterogeneous density. The margin between lesion and soft tissue at the mouth floor is unclear. Nodular high-density shadows found in the right submandibular gland, indicating calculi

2. MRI Examination It shows that glands are often enlarged with clear or fuzzy margins. The signal is often heterogeneous, mainly showing heterogeneous signal of hyperintense on T_1WI and hyperintense on T_2WI, and hyperintense on DWI (Fig. 28.4).

28.1.2.4 Key Points of Diagnosis

1. The gland is enlarged, with heterogeneous density/signal and marked enhancement, often complicated with intraglandular or ductal calculi. DWI shows a limited spread of lesions.
2. In early stage and 2–3 weeks of the disease, the titer of double serum increases more than four times, which is of diagnostic significance.
3. Facial swelling with fever and muscle pain.

28.1.2.5 Differential Diagnosis

1. Epidemic Parotitis It is one of the common acute respiratory infectious diseases in children, and patients have a typical history of epidemic exposure. The disease is caused by mumps virus. CT shows the increased density of enlarged parotid gland and mild enhancement by enhanced scan. MRI shows irregular isointense or slightly hypointense on T_1WI, diffuse hyperintense on T_2WI, often complicated with local hyperintense area, and enhanced scan indicates diffuse moderate enhancement. Most cases have bilateral involvement, enlarged glands, and mild pain. Laboratory test shows increased proportion of lymphocytes and amylase in serum and urine.

2. Cellulitis in Submasseteric Space It shows tenderness and swelling centered on mandibular angle, significant restriction of mouth opening, parotid gland duct without red swelling, and clear saliva secretion. Imaging shows that the masticatory muscles are enlarged, the space is dilated, with an unclear margin of the lesion and thickening of the adjacent fascia.

3. Lymphadenitis in Parotid Region It is also known as pseudoparotitis, manifests as swelling and pain in parotid region, no redness and swelling in parotid gland duct, and clear saliva secretion. Enhanced CT shows ring enhancement of lymph nodes with central low-density shadow, MRI shows isointense on T_1WI and diffuse or central hyperintense on T_2WI for lymph nodes, with peripheral marked enhancement and no central enhancement by enhanced scan.

28.1.2.6 Status Quo and Progress of Research

Acute suppurative sialadenitis mainly occurs in children, and salivary gland inflammation generally does not need imaging examination, but the tissue structures in parotid gland space are complex, so imaging methos are mainly to evaluate the

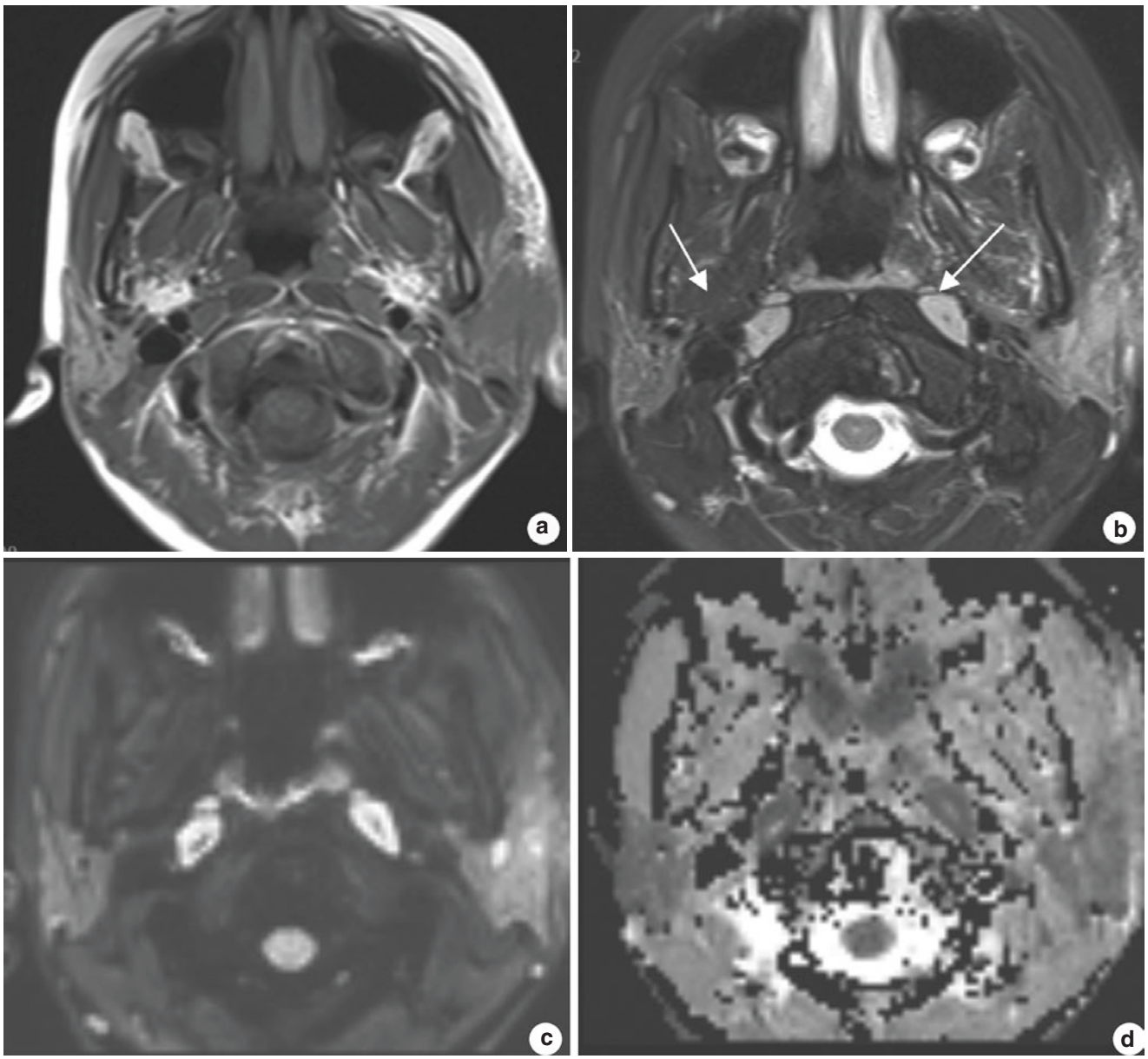

Fig. 28.4 Left acute suppurative parotitis. A 67-year-old male patient. Swelling of left parotid gland and face with pain for 2 weeks. (**a**, **b**) NOn-enhanced MRI scan shows the volume of left parotid gland increases, isointense on T_1WI, signal intensity increases on T_2WI, and unclear lesion margin. (**c**, **d**) DWI shows increased lesion signal intensity, indicating limited diffusion, and ADC shows decreased signal intensity of left parotid gland. Enlarged lymph nodes (indicated by arrow) in bilateral retropharyngeal spaces

formation of abscess. At present, CT is an important imaging technology for diagnosing parotid gland lesions. To find the parotid gland lesions, the lesions should be located firstly. The most widely used method is U-line location. That is, the line passes through the dorsal point of posterior mandibular vein and the dorsal point of ipsilateral cervical vertebrae. Without typical specific findings, the simple CT and MRI examination cannot be singly used to diagnose the disease at present and should be closely combined with clinical findings and related laboratory tests.

28.1.3 Chronic Sialadenitis with Calculi

28.1.3.1 Overview

Sialadenitis is an acute or chronic inflammation, which causes swelling and pain of salivary gland. Chronic sialadenitis with calculi is common in clinical practice, and most commonly in submandibular gland. There are two main causes: (1) hypoptyalism; (2) the obstruction of salivary duct by calculi causes saliva retrograding to the oral cavity. Oral bacteria exist in the form of free-swimming planktons or in

aggregated and sessile state, which is also called biofilm. Biofilm is becoming more and more important in chronic infection, and bacterial biofilm may be the pathogenic factor of salivary gland calculi. However, it is unclear whether biofilm participates in or exists in chronic suppurative sialadenitis of submandibular gland [1]. According to some studies, microorganisms contribute to the formation of salivary gland calculi. The main clinical manifestations of chronic recurrent sialadenitis include swelling and pain of glands, congestion and swelling of duct mouth and pus discharge.

It is reported that the annual incidence of salivary gland calculi is 1/10,000–1/3 [4]. It is generally believed that stagnation or reduction of salivary fluid can lead to the formation of salivary gland calculi. Salivary gland calculi mostly occur in young adults, especially aged 30–60 years old, affecting more men than women. Salivary gland calculi are the most common disease in salivary gland area, accounting for about 50%, especially the submandibular gland, accounting for 80–90%. The lesions are mostly single, or multiple. Swelling of salivary gland area on the affected side is significant, especially in eating, and it gradually relieves after eating. When calculi are large, intraglandular calculi with significant mobility can be touched. Acute inflammation of salivary gland can occur with bacterial infection, which may cause redness or pus overflow at the opening of the corresponding glandular duct.

28.1.3.2 Pathology Findings

Pathological manifestations of chronic recurrent sialadenitis include atrophy or destruction of acinus, proliferation of glandular duct epithelium, and proliferation of interstitial cells, producing plenty of collagen fibers. Salivary gland calculi are composed of highly calcified spherical nuclei varied in shape, surrounded by layered structures formed with inorganic substances and organic substances in alternating arrangement.

28.1.3.3 Imaging Findings

1. CT Examination

1. The fat in the glands of chronic sialadenitis is significantly atrophied, and the volume of parenchyma is reduced.
2. CT three-dimensional imaging: patients with salivary gland calculi show solitary or multiple dense shadows varied in size and shape of corresponding salivary gland or the duct course area, with different degrees of duct dilatation (Fig. 28.5).

2. MRI Examination

1. The gland becomes smaller, showing fat atrophy. Compared with the contralateral normal gland, the signal intensity on T_1WI increases, while the signal intensity of the gland parenchyma on T_2WI decreases. The lesions

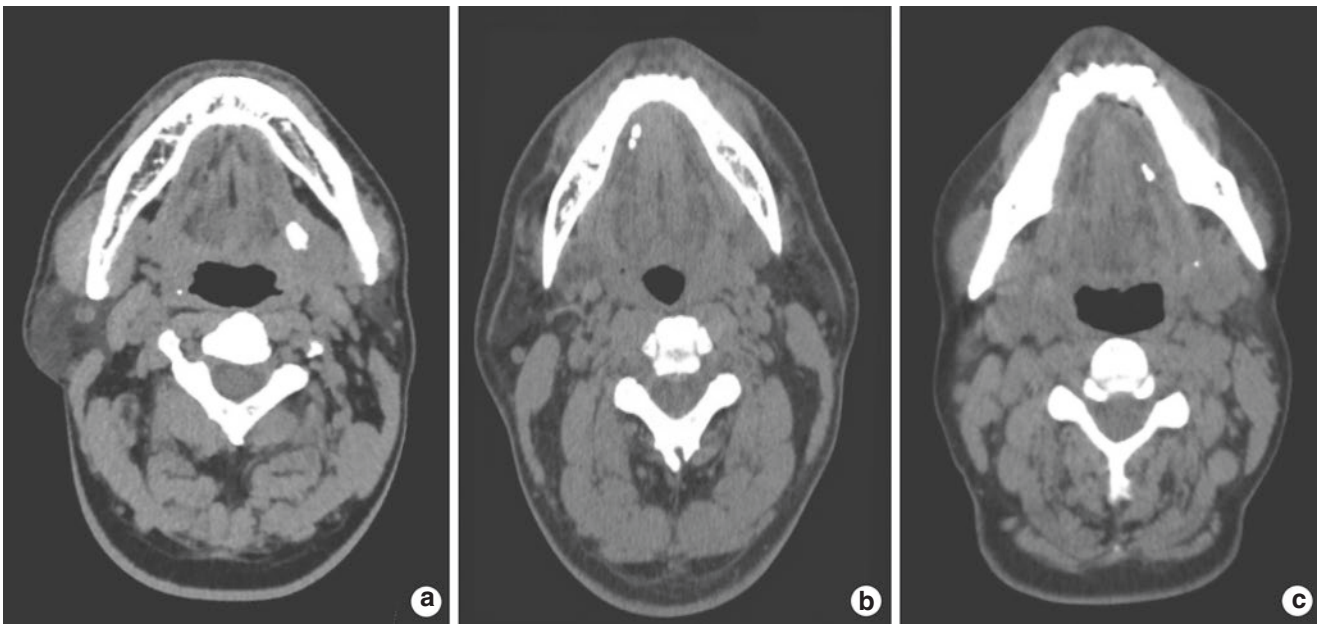

Fig. 28.5 Salivary gland calculi (different patients). (**a**) Non-enhanced CT scan indicates punctate and high-density shadows in the left submandibular gland area, with a size of about 11 mm × 7 mm and a CT value of about 617 HU; (**b**) Non-enhanced CT scan indicates multiple nodular high-density shadows in the distal opening of the right submandibular gland; (**c**) Non-enhanced CT scan indicates slightly increased volume of the left sublingual gland, slightly rough margin, and nodular high-density shadows at the anterior border. The left sublingual gland duct calculi are suspected

show heterogeneous hypointense on T_1WI, and the whole signal caused by fibrosis tended to be hypointense-isointense on T_2WI.
2. Calculi manifest as hypointense area in hyperintense salivary fluid on T_2WI.

3. Endoscopy of Salivary Gland It shows congestion, hemorrhage, and proliferation of mucosa on the medial wall of duct, and mucus embolus and calculi.

28.1.3.4 Key Points of Diagnosis

1. CT Examination It can clearly show the dense shadow of the corresponding salivary gland or the duct course area. In the early stage, the glands are diffusely enlarged after eating, the density of glands is heterogeneous, and gland atrophy can occur in advanced stage.

2. Typical Clinical Manifestations They include repeated swelling of salivary gland with local pain, which is aggravated during eating.

28.1.3.5 Differential Diagnosis

1. Calcification of Submandibular Lymph Nodes It is mostly distributed in the paravascular space in punctate or patchy pattern. Salivary gland calculi are mainly distributed along the course of duct.

2. Phlebolith or Angiolithic Degeneration It is closely associated with the corresponding blood vessels, and the enhancement of adjacent blood vessel shadows is found by enhanced scan.

28.1.3.6 Status Quo and Progress of Research

CT can clearly show high-density calculi and enlarged glands in the direction of salivary duct course. In addition, salivary gland ultrasonography is a convenient, simple, and effective method to diagnose calculi and inflammation, with sensitivity over 90%, especially in the treatment of various salivary gland calculi, it has been used as a routine auxiliary tool. Recently, some scholars [5] have proved that ultrasound can assist in the diagnosis of salivary gland calculi, and location of submandibular calculi in a non-invasive way by oral submandibular gland calculi resection, so ultrasound can be used as an alternative method of salivary gland endoscopy.

28.1.4 Parotid Gland Tuberculosis

28.1.4.1 Overview

Tuberculosis is a common chronic infectious disease, which is mainly caused by mycobacterium tuberculosis, common in the lungs, and can also occur in kidneys, bones, brains, spine and lymph nodes. Extra-pulmonary tuberculosis accounts for about 25% of all tuberculosis cases, among which tuberculous lymphadenitis is the most common extra-pulmonary tuberculosis, while tuberculosis of head and neck accounts for about 10% of extra-pulmonary tuberculosis [6].

Parotid gland tuberculosis is an extremely rare extra-pulmonary tuberculosis and is rarely reported even in countries where tuberculosis is prevalent. It has no specific manifestation, without tuberculosis lesions coexisting in other systems. Most of them are unilateral parotid gland progressive and painless swelling, a few have refractory irregular mild fever, and most of them have no typical tuberculosis poisoning symptoms, such as fatigue, night sweats, anorexia, and emaciation, which are easily misdiagnosed as parotid tumors in clinical practice. Parotid gland tuberculosis is prone to young women, mostly occurring in parotid lymph nodes, usually confined to the anterior auricular lymph nodes or inferior polar region of parotid gland. Parotid gland tuberculosis usually presents as a localized, slow-growing, and non-tender mass in parotid region. When the lesion is small, it has moderate hardness, smooth surface, and strong activity; with the enlargement of the lesions, they are hardened, and can adhere to the peripheral tissues with decreased mobility, and some of lesions merge with beading changes. Pain, abscess, fistula, and facial nerve palsy are the manifestations in advanced stage.

Patients often have no history of pulmonary tuberculosis and other extra-pulmonary tuberculosis. A few patients have refractory irregular mild fever, and most of them have no tuberculosis poisoning symptoms, such as night sweats, fatigue, emaciation and anorexia, which are easily misdiagnosed as parotid tumors. In the course of disease, history of exposure to tuberculosis patients, suspicious manifestations of pulmonary tuberculosis or extra-pulmonary tuberculosis, enlargement of ipsilateral cervical lymph nodes, HIV infection or carrying HIV, and previous hormone therapy history are all possible risk factors for parotid gland tuberculosis.

28.1.4.2 Pathology Findings

The pathogenesis of parotid gland tuberculosis is unknown. At present, there are two main pathogeneses to explain tuberculosis in parotid gland and lymph node: the one is associated with oral mycobacterial infection, which is released into salivary gland through its duct or transmitted to cervical lymph node through lymphatic drainage. The other is associated with hematogenous or lymphatic diffusion in the lung. During the development of salivary gland, the primordium of parotid gland develops firstly, and its capsule is formed until the end, thus the lymphatic system of parotid gland is wrapped by parotid capsule. Parotid gland tuberculosis rarely occurs in parotid parenchyma, but mostly in parotid lymph nodes. Tuberculous parotitis exists in two forms, the one is local nodule, which manifests as lesion involving internal or external glandular lymph nodes, similar to parotid tumors; The other is diffuse parenchyma, which is similar to

common parotid gland infection. Parotid gland lymph nodes and diffuse parenchyma can appear alone or in combination. Histopathologically, like tuberculosis in other parts, parotid gland tuberculosis basically manifests as exudation, proliferation, and caseous necrosis, which can transform and exist with each other. Pathological examination shows macrophages, lymphocytes, epithelioid cells, and Langans giant cells scattered in the lesions, partically complicated with fibrous tissue proliferation and focal necrosis.

28.1.4.3 Imaging Findings

CT or MRI manifestations of parotid gland tuberculosis are different in different pathological stages, and enhanced scan can further indicate its pathological features [7].

1. X-Ray Examination It provides limited diagnostic value for parotid gland tuberculosis. When the lesion is relatively large, X-ray can show the swelling and increased density of soft tissue in parotid region at affected side.

2. CT Examination It indicates that the parotid gland tuberculosis is similar to tuberculosis of other parts, and their CT manifestations are different in different pathological stages, as shown below:

1. When proliferation is the dominant change, tuberculosis nodules are the main manifestations. Non-enhanced scan can indicate soft tissue nodule shadows, with a clear margin and homogeneous density. The enhanced scan shows solid nodules with homogeneous enhancement.
2. With the progression of the disease, the focus mainly manifests as proliferation, with a small amount of caseous necrosis in the center, and there is basically no exudation change. At this time, enhanced CT shows lesions with thick-walled ring enhancement, and the medial and lateral walls of the enhancement ring are relatively smooth.
3. The lesion further progresses, with pathological manifestations of proliferation, necrosis, and exudation coexist. CT enhanced scan mainly shows thin-walled ring or garland-like enhancement, with blurred medial and lateral walls of the enhancement ring, and surrounding significantly blurred subcutaneous fat layer. Among them, the degree of necrosis and exudation of garland-like enhancement is more severe than that of thin-walled ring enhancement. It is generally believed that the former may be garland-like change caused by the fusion of multiple lesions with exudation.

3. MRI Examination

1. The pathological processes of parotid gland tuberculosis are proliferation, caseous necrosis, histolysis to form hollow or calcification in order. In the early stage, the acinus contains tuberculous nodules, the signal intensity of parotid gland parenchyma is heterogeneous, with irregular isointense or slightly hypointense on T_1WI, slightly hyperintense on T_2WI fat-suppressed sequence, and the peripheral structures are normal. When the lesion breaks through the acinus and invades the peripheral tissues, it forms nodules or granulomas, showing single or scattered soft tissue nodules with clear margin to the peripheral tissues, isointense on T_1WI and isointense on T_2WI, hyperintense on T_2WI fat-suppressed sequence, and mild homogeneous enhancement by enhanced scan.
2. The lesions further develop into caseous proliferation stage, with the pathological process of coexisting granulation tissue and caseous necrosis. Caseous substances have low water content and high protein content, and are difficult to be liquefied, thus showing no significantly different intense from the surrounding inflammatory granulation tissues. It shows isointense on T_1WI and isointense on T_2WI, and hyperintense on T_2WI fat-suppressed sequence. By enhanced scan, caseous substances show no enhancement due to lack of blood supply but can show heterogeneous enhancement due to the blood supply in inflammatory granulation tissues.
3. In the final stage of the lesion, caseous necrosis played a dominant role. The center of the lesion is a large fused caseous or liquefactive necrosis, and the peripheral areas are in granuloma structure. It shows isointense on T_1WI sequence and slightly hypointense on T_2WI sequence. The enhanced scan indicates that the granuloma structure has ring enhancement due to abundant blood supply. In the stage, the lesion is easy to invade periphery, resulting in adhesion and thickening of peripheral tissues, blurred fat space and heterogeneous signal.

28.1.4.4 Key Points of Diagnosis

1. With or without definite history of tuberculosis infection, common in young women.
2. The imaging findings of parotid gland tuberculosis are closely associated with its pathological process. The three pathological changes (exudation, proliferation, and caseous necrosis) often coexist, with one of them being dominant, and they can transform each other.
3. The diagnosis of parotid gland tuberculosis is based on clinical history, laboratory test, radiological examination, and histopathology.

28.1.4.5 Differential Diagnosis

1. Pleomorphic Adenoma It is the most common parotid tumor, which occurs in middle-aged women and is mostly located in the superficial lobe of parotid gland. On non-enhanced CT scan, the lesions are mostly circular, quasi-circular, or lobulated soft tissue masses with clear margins in parotid region, complete capsule, density significantly higher than normal parotid tissue, and occasional calcification, cystic degeneration, and necrosis. Small tumor often shows

homogeneous enhancement, and large one often shows heterogeneous enhancement.

2. Parotidean Lymphoma It is also known as Warthin tumor, is mostly found in males aged between 40 and 60 years old, mainly located in the superficial lobe and inferior polar of parotid gland, with clear lesion margin and easy cystic degeneration in the center. Small tumors also can have cystic degeneration. Because of its abundant blood supply, the enhanced scan shows a typical "fast-in and fast-out" enhancement mode.

3. Acute Suppurative Parotitis It can occur bilaterally or unilaterally, with significant clinical symptoms, such as redness, swelling, fever and pain, and a significant increase in leukocyte count; CT examination shows diffuse enlargement of parotid gland, increased density, and marked and heterogeneous enhancement; When abscess is formed, irregular cystic necrotic areas are found in parotid gland parenchyma, and abscess wall has marked enhancement.

28.1.4.6 Status Quo and Progress of Research

DWI technology is the only imaging method that can observe the microscopic movement of water molecules in viable tissue and can detect the physiological and functional changes related to water content of tissue in early stage. DWI can provide important information for the diagnosis and differential diagnosis of parotid gland abscess and tuberculosis [8]. The pus in parotid gland abscess contains a large amount of protein components, which can lead to viscosity of local tissue and limited diffusion of water molecules. DWI sequence shows significantly hyperintense. The vomica of parotid gland tuberculosis is formed by necrosis and liquefaction of caseous substances, it has little endocellular structures, so the diffusion of water molecules is accelerated, and the DWI image findings are supplemented, with increased ADC value. However, some studies have found that the ADC value of tuberculous brain abscess is relatively low, which is considered to be the result of inflammatory cells [9]. Imaging diagnosis plays an important role when the clinical manifestations and laboratory test of parotid gland tuberculosis are atypical.

28.1.5 Parotid Gland Cyst

28.1.5.1 Overview

Parotid gland cyst is relatively rare in salivary gland cysts (accounting for about 2.5% of parotid lesions), which can be divided into congenital cyst and retention cyst. Congenital cysts develop from epithelial components left in deep tissues during embryonic period and are divided into branchial cleft cysts and dermoid cysts. The saliva secreted by parotid gland is serous saliva, which is thin and contains a large amount of amylase. Moreover, the parotid gland duct is thick and straight, and it is difficult to retain liquid and form cyst, so parotid gland retention cyst is even rarer. The etiology of the disease is unknown, which may be associated with abnormal development of duct, acute and chronic inflammation of duct system, stenosis or occlusion of duct caused by salivary gland calculi, and cyst caused by saliva retention. Surgery or trauma is an inducement for formation of retention cyst [10], and postoperative or post-traumatic infection or trauma may also lead to the destruction of small ducts, the saliva extravasates to the tissue space, and is wrapped up by surrounding fibrillar connective tissue to form cysts, which occur at superficial sites [11]. The medical history ranges from 1 month to several years, with main manifestations being painless and cystic masses in parotid gland region, fluctuation during palpation, which can be complicated with infection and hemorrhage.

Parotid gland cyst is mostly found in elderly men and can occur in any part of the parotid gland. It is generally located between the superficial and superficial-deep lobes of the parotid gland [11]. It manifests as monosaccate or polycystic mass developing slowly and can be asymptomatic when it is small. When the cyst is enlarged to a certain extent, it can be found due to enlargement of parotid gland area, and when the cyst is complicated with hemorrhage or infection, it can be rapidly enlarged with pain. The aspiration biopsy can obtain a colorless and transparent liquid, and the capsule fluid contains amylase. Surgery is the main treatment method to prevent recurrence.

28.1.5.2 Pathology Findings

The disease is mostly caused by inflammation or obstruction of parotid gland duct by salivary gland calculi. The wall of the primary cyst is lined with pseudostratified or cuboidal epithelioid cells, while the secondary cyst is wrapped by fibrillar connective tissue or granulation tissue without complete epithelial cells lining.

28.1.5.3 Imaging Findings

1. Ultrasonography The parotid gland is round or quasi-circular, with a smooth margin and regular shape, no echo area in the capsule, and good sonolucency. CDFI: Blood flow signals are found at the margin of cyst, without blood flow signal in cyst. When combined with infection, it shows heterogeneous (isointense to hyperintense) echo and poor sonolucency, needing to be differentiated from hypoechoic solid masses.

2. CT Examination It shows homogeneous low-density cystic mass with thin wall and clear margin, no enhancement or enhancement of cystic wall by the enhanced scan. When the cyst is complicated with infection, the internal cystic density increases, the cystic wall thickens, and the enhancement of cystic wall is slightly delayed (Fig. 28.6).

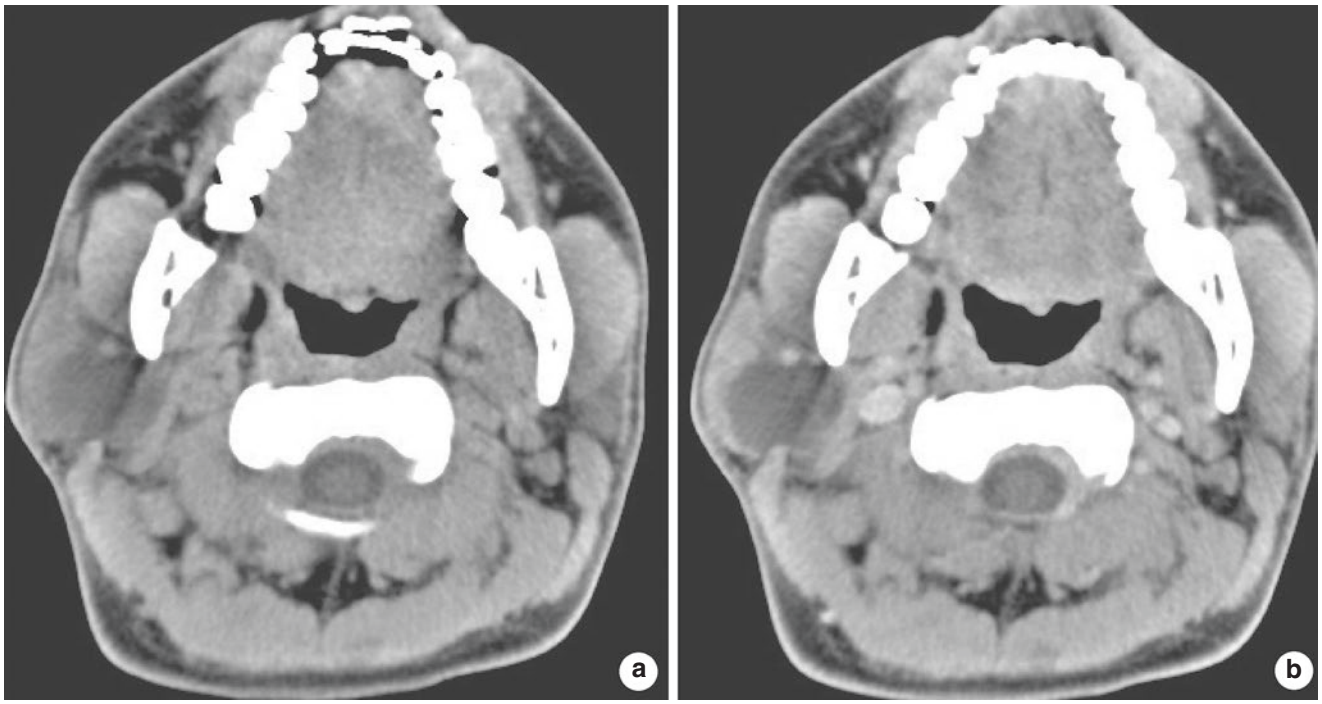

Fig. 28.6 Right parotid gland cyst (1). (**a**) Non-enhanced CT scan indicates quasi-circular low-density shadows on the right parotid gland; (**b**) CT enhanced scan shows ring enhancement of lesion edge

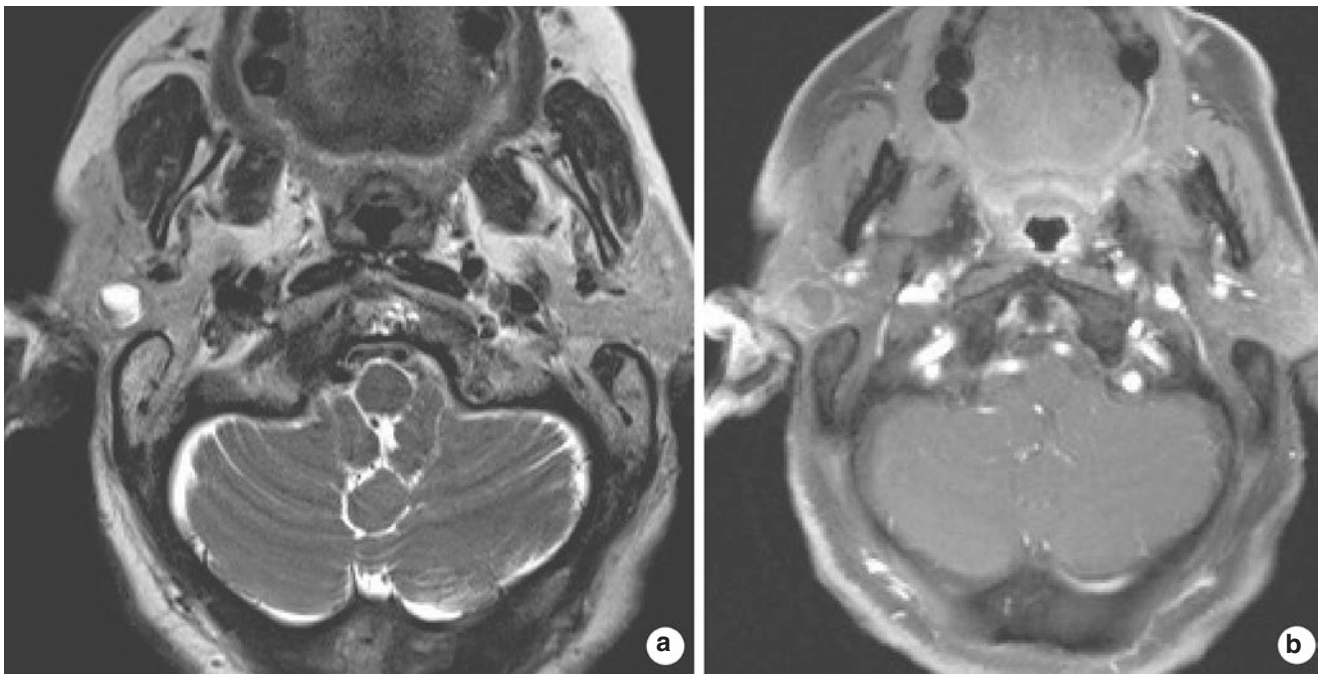

Fig. 28.7 Right parotid gland cyst (2). (**a**) The right parotid gland shows quasi-circular hyperintense on T_2WI, with patchy hypointense on T_2WI in it (indicating hemorrhage); (**b**) T_1WI enhanced scan indicates the lesion with ring enhancement

3. MRI Examination It shows hypointense on T_1WI and hyperintense on T_2WI in cystic cavity. When complicated with hemorrhage or infection, patchy hypointense on T_2WI can be found in the cystic cavity (Fig. 28.7), and the disease is easily misdiagnosed as mixed tumor and tuberculosis.

28.1.5.4 Key Points of Diagnosis

Circular or quasi-circular tumors in parotid gland region have smooth margin, regular shape, homogeneous density or signal intensity, and may have septa. When combined with infection, the density or signal intensity may be heterogeneous with unclear margin.

28.1.5.5 Differential Diagnosis

1. Mixed Tumors of Parotid Gland They are mostly located in the superficial lobe of parotid gland, which is quasi-circular, with heterogeneous low density by non-enhanced scan, including calcification or lower-density necrotic area in it, and delayed enhancement by enhanced scan, and no enhancement in necrotic area.

2. Lymphoma It is a malignant tumor originating from lymph nodes or other lymphoid tissues. Its clinical manifestation is multiple painless lymphadenopathies in the whole body, which may involve multiple systems and organs. It often manifests as swelling of multiple unilateral or bilateral lymph nodes, homogeneous density, mild to moderate enhancement, and the lesions can fuse into mass. Pathologically, lymphoma often shows corticospinal diffuse tumor cell infiltration in lymph node, with higher cell density, narrower intercellular space, significant diffusion limitation on DWI image and lower ADC value.

3. Epidermoid Cyst Parotid epidermoid cyst is rare and common in infants. It is located in parotid gland or subcutaneous area and can develop unilaterally or bilaterally. The clinical manifestation is a painless enlargement of tumor. The physical examination shows moderate hardness and smoothness. It can be complicated with infection and form fistula. It is difficult to differentiate the two diseases by imaging. The aspiration biopsy can obtain lacte liquid on epidermoid cyst, and transparent liquid on branchial cleft cyst.

28.2 Sjögren Syndrome of Salivary Gland

28.2.1 Overview

Sjögren syndrome (SS) is a chronic autoimmune inflammatory disease with unknown causes, which mainly involves lacrimal gland and salivary gland, and tends to gather in families. Primary Sjögren syndrome (pSS) is different from secondary Sjögren syndrome (sSS), which is a part of other autoimmune diseases. sSS is mainly secondary to systemic lupus erythematosus (15–36%), rheumatoid arthritis (20–32%), and limited and progressive systemic sclerosis (11–24%), and is rarely associated with multiple sclerosis, autoimmune hepatitis and thyroiditis. It is very important to differentiate primary Sjögren syndrome from secondary Sjögren syndrome with respect to the different disease progressions and therapeutic approaches. The global prevalence of primary Sjögren syndrome is 61 cases/100,000 persons, with the highest prevalence in Europe. The primary Sjögren syndrome is an autoimmune disease only inferior to rheumatoid arthritis with respect to incidence. In China, the incidence of Sjögren syndrome is on the rise in recent years, with the prevalence ranging from 0.3% to 0.7%. The number of female patients is significantly higher than that of male patients, and the gender difference is (9:1)–(19:1). The average age of firstly diagnosing pSS is 56 years old, and another peak appears in 20–40 years old. However, the initial symptoms may appear several years before diagnosis. Because of the diversity of clinical manifestations of Sjögren syndrome, patients may visit the department of ophthalmology, otolaryngology, or stomatology for the first time. Therefore, it is very important for doctors of different disciplines to understand the clinical manifestation, classification criteria, and treatment plan of the disease, which is helpful for early diagnosis of the disease. The main clinical manifestations of pSS are keratoconjunctivitis sicca (xerophthalmia), dry oral mucosa (xerostomia), and bilateral parotid gland enlargement.

28.2.2 Pathology Findings

The typical pathological manifestation of Sjögren syndrome is lymphocytes and plasma cells infiltration in salivary gland and lacrimal glands, resulting in dysfunction of target organs. Focal lymphocyte infiltration with complete acinar units is found in exocrine glands. The infiltration is mainly composed of $CD4^+$ T cells, $CD8^+$ T cells and $CD19^+$ B cells, plasma cells, and dendritic cells. When the respiratory mucosa is infiltrated by lymphocytes and the exocrine glands atrophy, the respiratory mucosa is damaged, which is often manifested as interstitial pneumonia, pulmonary interstitial fibrosis, and bronchiectasis.

28.2.3 Imaging Findings

1. X-Ray Radiography It shows dilation of distal duct in punctate or flocculent pattern, and the branch duct and primary duct have rough edges.

2. CT Examination It shows increased density of parotid gland parenchyma, with diffuse distribution of adipose tissue infiltration in parotid gland parenchyma (Figs. 28.8, 28.9, and 28.10).

3. MRI Examination Multiple punctate, utricular shadows in different sizes are found in the diffusely enlarged parotid gland, showing hypointense on T_1WI and hyperintense on T_2WI with clear margin and heterogeneous signal in glands. The parotid gland shows diffuse hyperintense on T_1WI and hyperintense on T_2WI, and hypointense on T_2WI fat suppression, the normal gland structure basically disappears, complicated with distal duct dilatation (Fig. 28.11).

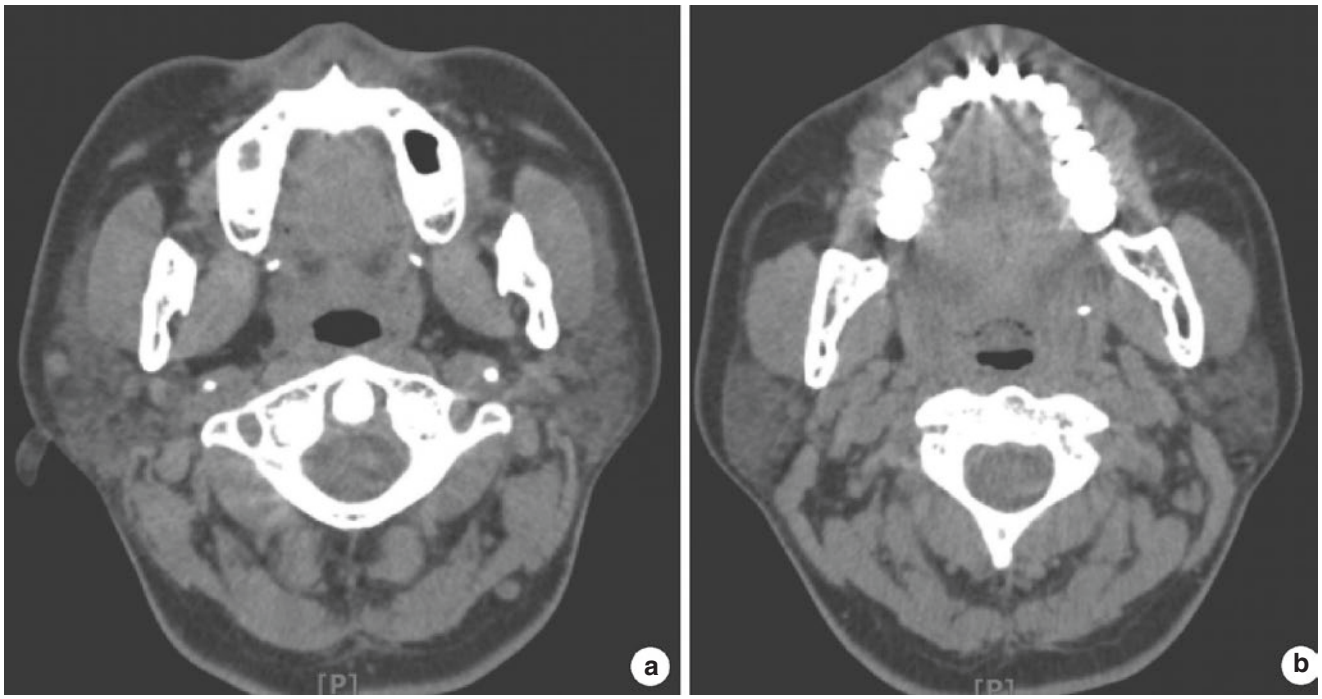

Fig. 28.8 Sjögren syndrome (1). (**a**, **b**) CT examination shows increased density of bilateral parotid gland parenchyma, and diffuse punctate and patchy adipose tissue infiltration

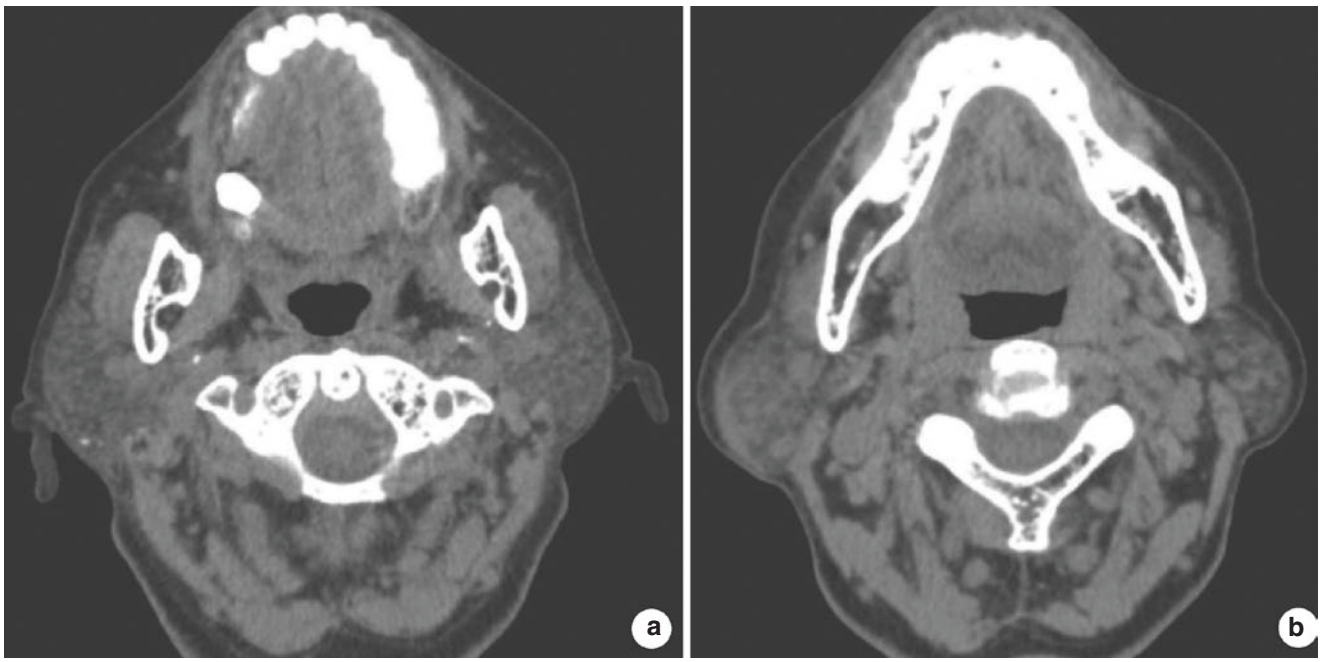

Fig. 28.9 Sjögren syndrome (2). (**a**, **b**) Non-enhanced CT scan indicates increased volume of right parotid gland, the heterogeneously increased density of bilateral parotid glands, patchy soft tissue density shadows in right parotid gland, and punctate calcification foci in bilateral parotid glands

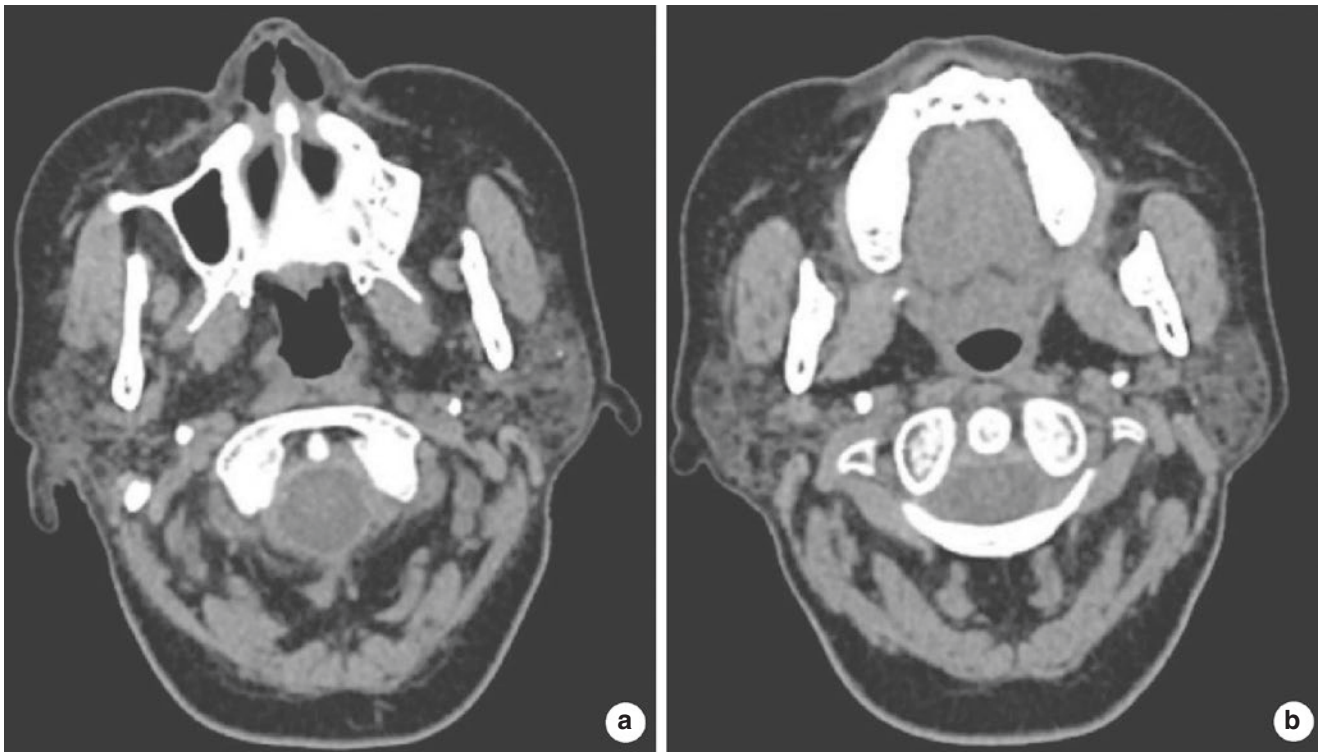

Fig. 28.10 Sjögren syndrome (3). (**a**, **b**) Non-enhanced CT scan indicates heterogeneous density of bilateral parotid glands and diffuse miliary nodules

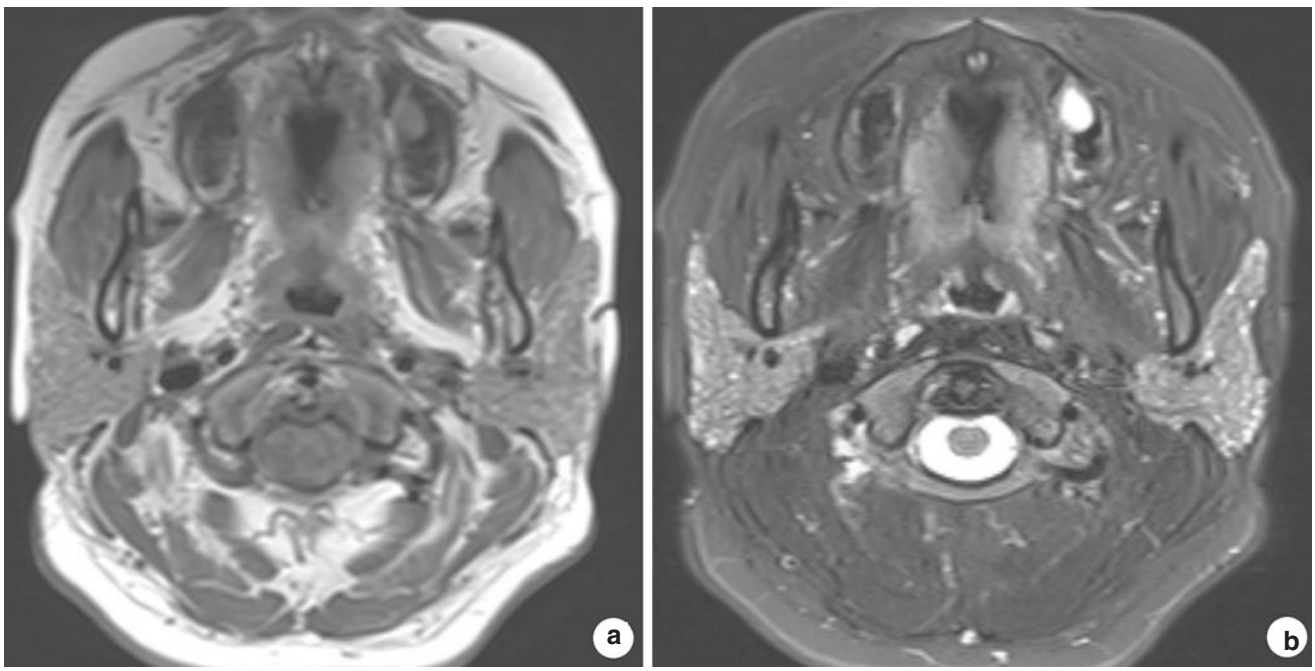

Fig. 28.11 Lymphoepithelial lesion of parotid gland caused by Sjögren syndrome. (**a**, **b**) Non-enhanced MRI scan shows increased volume of bilateral parotid glands. Parotid glands show heterogeneous isointense on T_1WI (**a**), heterogeneous hyperintense on T_2WI (**b**), and diffuse miliary nodule hyperintense shadows in it

4. MR Parotid Gland Duct Hydrography The lumen of the primary duct shows no dilation and smooth margin, while the parotid branches and distal ducts are dilated to different extents.

28.2.4 Key Points of Diagnosis

1. Ultrasonography It shows multicellular or reticular structures in atrophic glands, with heterogeneous or low/anechoic areas. CT examination shows multiple small nodules with high density in bilateral parotid glands, and the size of gland is related to the course of disease. MR T_1WI and T_2WI show parotid glands with pepper sign or cellular sign.

2. Main Clinical Manifestations Keratoconjunctivitis sicca (xerophthalmia), dry oral mucosa (xerostomia), and bilateral parotid gland enlargement.

28.2.5 Differential Diagnosis

Rheumatoid Arthritis It shows ankylosis in the morning, gradually progressing to joint deformity. Imaging examination shows moth-eaten destruction in joint; Sjögren syndrome generally shows no bone destruction and joint deformity.

28.2.6 Status Quo and Progress of Research

Magnetic resonance parotid gland duct hydrography is to realize imaging of water-bearing organs depending on the characteristics of long T_2WI relaxation time of liquid in human body. Therefore, the static liquid in parotid gland duct in parotid gland region shows hyperintense, while the fat-rich parotid gland shows hypointense, and the flowing blood shows extremely hypointense or no signal due to flowing void effect. The imaging feature makes a strong contrast between salivary parotid gland duct, acinus, and peripheral tissues. The accuracy of parotid gland duct hydrography in detecting Sjögren syndrome can be as high as 93%, which can provide auxiliary information for early diagnosis in clinical practice. It is the first choice for detecting Sjögren syndrome in the future and is worthy of wide clinical application [12].

At present, salivary gland ultrasonography is often used in clinical diagnosis of pSS. Zhang et al. [13] confirmed that the specificity and sensitivity of different scoring systems of salivary gland ultrasonography (SGUS) for pSS diagnosis can reach 93.0% and 88.6%, respectively, and the ultrasound score is positively correlated with clinical indicators such as serum rheumatoid factor and gamma globulin. This study suggests that salivary gland ultrasonography become a convenient means for clinical detection of pSS disease activity and evaluation of response evaluation.

28.3 Maxillofacial and Cervical Region Sarcoidosis

28.3.1 Overview

Sarcoidosis is a chronic systemic inflammatory disease with unknown causes, characterized by non-caseous granuloma, which is called Sarcoidosis abroad. Sarcoidosis can invade all organs or tissues of the whole system, and mostly involves lymph nodes, accounting for more than 90%, including intrathoracic (hilum of lung, mediastinal and intrapulmonary lymph nodes) and superficial lymph nodes. Maxillofacial region and neck region are areas with concentrated lymph nodes, which are superficial and easy to find. Jaw-cervical region sarcoidosis can be individual, i.e., jaw-neck type, or complicated with systemic sarcoidosis. Maxillofacial and cervical sarcoidosis usually involves lymph nodes in maxillofacial region, followed by parotid gland, submandibular gland, jaw bone, gums, and tongue. In the absence of typical systemic sarcoidosis, nodular granuloma in the jaw and neck is difficult to be diagnosed, with single occurrence mostly misdiagnosed as benign tumor and multiple occurrences mostly misdiagnosed as lymph node tuberculosis and lymphoma [14].

The etiology and pathogenesis of sarcoidosis are not clear, and most of the current studies tend to associate it with autoimmune diseases. The onset is related to a delayed allergic reaction, abnormal cellular immunity, environment, and genetic factors.

Maxillofacial and cervical region sarcoidosis usually have insidious onset, involve chronic process with unremarkable clinical symptoms, and are often found during physical examination. It is mostly found in young adults and middle-aged people over 50 years old and also occurs in children, and most of them have a benign course. The clinical commonalities of maxillofacial and cervical region sarcoidosis are as follows: painless chronic lymph node enlargement, which is easy to be ignored; the enlarged lymph nodes gather but do not adhere to each other, the capsule is complete, and the surface skin is normal; it is easily misdiagnosed as lymph node tuberculosis.

Maxillofacial and cervical region sarcoidosis are often complicated with intrathoracic lymph node sarcoidosis, so chest X-ray examination is necessary, showing bilateral hilar lymph node enlargement.

28.3.2 Pathology Findings

The diagnosis of sarcoidosis mainly depends on pathological examination. The pathological characteristics are as follows: (1) plenty of epithelioid cells gather into mass, a small number of lymphocytes and plasma cells form foci, and lymph node tissue is destroyed, but the capsule is complete; (2) sarcoidosis granuloma is usually non-necrotic and occasionally necrotic; (3) Langans giant cell or xenobiotic giant cell, asteroid inclusion body and calcified inclusion body are found. Histologically, sarcoidosis is similar to tuberculosis, but the difference is that there are no blood vessels in tuberculous nodules, and there is caseous necrosis in nodules. In addition to plenty of epitheloid cells, tuberculosis nodules also have significant lymphocyte infiltration.

28.3.3 Imaging Findings

Ultrasonography shows that the enlarged lymph nodes due to sarcoidosis are oval and irregular, and the ratio of long diameter to antero-posterior diameter (L/S) of the lymph nodes is higher than 1.8. The internal echo is heterogeneous, cloudy, and iso-echoic, without calcification. The echo of the medulla of the lymph nodes is enhanced, the cortex is homogeneously dilated, the echo is iso-echoic, and the echo of the capsule is heterogeneously enhanced, thickened, and completed. Over 90% of the patients have abnormal X-ray findings of lung, mainly manifested as symmetrical lymph node enlargement of hilum of lung and elevated serum angiotensin converting enzyme (SACE).

Sarcoidosis lymph nodes still maintain the normal basic structure of lymph nodes, complicated with local fibrous tissue, blood vessels and granulation tissue proliferation. Color Doppler shows regular and centered portal or rod-like blood flow signals with low blood flow velocity and low resistance index [15].

CT and MRI can show multiple lymphadenopathy, mostly involving cervical lymph nodes, followed by parotid gland, submandibular gland, jaw bone, gum, and tongue. The density or signal intensity of enlarged lymph nodes is homogeneous, internal necrosis is rare, and the lesions have no fusion tendency. It rarely invades adjacent structures.

28.3.4 Key Points of Diagnosis

1. Single and multiple cervical lymph node enlargement with clear margin, homogeneous density, and little necrosis.
2. Chest X-ray shows bilateral symmetrical lymph node enlargement of hilum of lung and sarcoidosis triad (left and right hila of lung and paratracheal lymph node enlargement).
3. Lymph node biopsy is the standard method for diagnosis, and SACE measurement is the auxiliary diagnosis and activity index of sarcoidosis.

28.3.5 Differential Diagnosis

1. Lymphoid Tuberculosis It is often beaded, with L/S > 2.0, in oval shape, with heterogeneous internal echo, concentrated or scattered liquefaction areas, and punctate and crumby strong echo with acoustic shadow. The patient is younger and has tuberculosis poisoning symptoms. The BCG protein derivative test shows positive results and tuberculosis treatment is effective. Caseous necrosis due to proliferative nodules is secondary to tuberculous enlarged lymph nodes, with later fibrosis and calcification. Color Doppler imaging shows deformed or varied portal scattered blood flow signals in dot or short-bar pattern, with low blood flow velocity and high resistance index.

2. Malignant Lymphoma Malignant tumor cells have infiltration growth, their structural levels are often destroyed, swelling is obvious, L/S < 1.5, marrow echo shows deformation and defect, mostly showing clinical manifestations and systemic manifestations of primary tumors, and the lesions progress rapidly. Because of tumor cell infiltration, structural destruction, blood flow disturbance, blood vessel compression and destruction of malignant tumor lymph nodes, the blood flow distribution is diversified, with abundant portal or reticular blood flow signals, high blood flow velocity, and high resistance index.

28.3.6 Status Quo and Progress of Research

The incidence of sarcoidosis is on the rise, and the sensitivity and specificity of single index in diagnosis of cervical lymph node sarcoidosis are not sufficient. It needs to be comprehensively evaluated by combining two-dimensional ultrasound, color Doppler flow imaging, chest X-ray, and clinical manifestations.

28.4 Eosinophilic Lymphoid Granuloma in Maxillofacial Region

28.4.1 Overview

Eosinophilic lymphogran-uloma (ELG) is a rare benign vascular hyperplastic disease with long course, and its etiology is still unknown, with subcutaneous mass and superficial

lymph node enlargement as typical manifestations. In 1937, Jin Xianzhai, a Chinese scholar reported seven cases of eosinophilic lymphoblastoma for the first time, which was considered as a new disease with unknown etiology. In 1969, Wells and Whster firstly proposed the name "eosinophilic lymphogran-uloma," also known as angiolymphoid proliferation with eosinophilia (ALHE). Its pathogenesis is unknown, and there are two hypotheses of its composition: proliferation from vascular tumor or lymphocyte [16]. The first hypothesis is related to arteriovenous shunt and previous trauma (friction, surgery, cold injury, laceration, etc.), similar to pyogenic granuloma. High estrogen status may be one of the pathogenesis of this situation. This phenomenon also exists in various vascular tumors during pregnancy. The second hypothesis holds that ALHE is a lymphoproliferative disease, which is supported by the progression and frequent recurrence of the disease. The rearrangement and monoclone of T-cell receptor gene have been observed in ALHE cases, which increases the possibility of considering the situation as low-grade T-cell lymphoma. It is worth noting that some ALHE cases are related to human herpesvirus and human T-cell lymphovirus. In a word, ALHE is a true vascular tumor, which is rich in inflammatory components and is also a lymphoproliferative process with reactive angiogenesis. The disease manifests as pruritus and pigmentation. Typical patients have touchable and painless soft tissue masses with blurred margins and local enlarged lymph nodes. It is prone to middle-aged men. Meanwhile, the eosinophil count in peripheral blood >0.05× 109/L can be used as an auxiliary diagnostic basis.

28.4.2 Pathology Findings

Tumors are mainly distributed in dermis, but rarely in subcutaneous tissue. The lesions can be combined with vasculitis components, capillary-sized vascular proliferation, lined with significant and enlarged endothelial cells, showing a typical cobblestone appearance. Most cells are cuboids, with vacuoles in cytoplasm and even ovoid nuclei. Lymphocyte and eosinophil infiltration is found in the lesion area. Mitosis is rarely observed. Vascular components are dominant in early stage or active ALHE, and lymphoid infiltration is more significant in advanced stage of disease. Histological evidence of arteriovenous shunt is found in 42% of cases.

28.4.3 Imaging Findings

1. Parotid Gland Duct Angiography The branch duct is displaced, and the glands are irregularly or regularly filling-defect.

2. CT Examination When the parotid gland is involved, the gland volume increases and many nodules with clear margins are found inside, and liquefactive and necrotic areas can be accompanied inside.

3. MRI Examination It shows that the lesion margin is unclear, and the lesion center is mostly liquefied and necrotic, with hypointense on T_1WI and hyperintense on T_2WI. In some cases, the necrotic area has septa, and the adjacent fat is atrophied and thinned. On T_1WI sequence, multiple thin line shadows are found to extend to the surrounding fat layer, and the thickness of the wall around the necrotic area is heterogeneous, showing isointense. Isointense is found around necrotic area on T_2WI sequence, and the lesion is surrounded by thin hyperintense edema belt. On T_2WI fat-suppressed sequence, the liquefactive necrosis area and edema belt are remarkable. The involved lymph nodes are enlarged with homogeneous signals. Enhanced scan shows peripheral wall and septa of the lesion with marked homogenous enhancement, but liquefactive necrosis is not enhanced. Enlarged lymph nodes have marked and homogeneous enhancement.

28.4.4 Key Points of Diagnosis

1. CT examination. It shows that the gland is enlarged in size, with multiple nodules with clear margins in it, and localized soft tissue masses. On MRI T_2WI sequence, isointense is found around the necrotic area, and the lesion is surrounded by thin hyperintense edema belt. The involved lymph nodes are enlarged with homogeneous signal. Enhanced scan shows peripheral wall and septa of the lesion with marked homogenous enhancement, but liquefactive necrosis is not enhanced.
2. The characteristic manifestation of the disease is pruritus and pigmentation in the lesion area.
3. The number of eosinophils in peripheral blood is >0.05× 109/L.

28.4.5 Differential Diagnosis

1. Kimura Disease ELG and Kimura disease are previously considered as manifestations of the same entity. Epidemiology, clinical and histopathological features then differentiate them from each other. Kimura disease is prone to young Asian men. The lesions mainly involve the auricle or parotid gland. It manifests as image triad: subcutaneous nodule, salivary gland mass, and lymph node enlargement; clinical triad: painless hard nodules, eosinophilia in blood or tissue and IgE elevation. Enhanced CT shows that subcutaneous mass with moderate enhancement, enlarged round

lymph nodes, and mild to marked enhancement. Enhanced MRI shows characteristic solid enhanced nodules.

2. Pyogenic Granuloma It is an explosive papule, sometimes complicated with erosion or ulcer of cuticle. Imaging findings are mass-like lesions with heterogeneous density or signal intensity, with heterogeneous enhancement and unremarkable occupying effect. Histologically, it is composed of capillary-sized blood vessels, which is in sharp contrast with immature vascularization.

28.4.6 Status Quo and Progress of Research

Eosinophilic lymphogran-uloma is a rare benign vascular hyperplastic disease, which can be preliminarily diagnosed according to bilateral parotid gland enlargement and multiple lymph node enlargements combined with clinical laboratory tests. Imaging mainly evaluates the scope of lesions, and the latest research [17] shows that contrast-enhanced ultrasound (CEUS) examination has high diagnostic efficiency for benign and malignant lesions of salivary gland. The main features of CEUS in malignant lesions of salivary gland are no complete enhancement ring by enhanced scan, unclear margin of the mass, and expanded scope of the mass by enhanced scan.

References

1. Gellrich D, Bichler M, Reichel CA, et al. Salivary gland disorders in children and adolescents: a 15-year experience. Int Arch Otorhinolaryngol. 2020;24(1):31–7.
2. Watanabe H, Odagiri T, Asai Y. Incidence of acute suppurative sialadenitis in end-stage cancer patients: a retrospective observational study. J Pain Symptom Manag. 2018;55(6):1546–9.
3. Velkoski A, Amoroso S, Brovedani P, et al. Presentation of acute suppurative parotitis in a newborn with incessant crying. Arch Dis Child Fetal Neonatal Ed. 2017;102(2):125.
4. Jiamei G, Qin C. Advances in imaging diagnosis of salivary gland diseases. Chin J Digestion Med Imageology. 2012;2(3):230–3.
5. Romero NJ, Fuson A, Kieliszak CR, et al. Sonolocation during submandibular sialolithotomy. Laryngoscope. 2019;129(12):2716–20.
6. Qian X, Albers AE, Nguyen DTM, et al. Head and neck tuberculosis: literature review and meta-analysis. Tuberculosis (Edinb). 2019;116:78–88.
7. Zhang D, Li X, Xiong H, et al. Tuberculosis of the parotid lymph nodes: clinical and imaging features. Infect Drug Resist. 2018;11:1795–805.
8. Munhoz L, Ramos E, Im DC, et al. Application of diffusion-weighted magnetic resonance imaging in the diagnosis of salivary gland diseases: a systematic review. Oral Surg Oral Med Oral Pathol Oral Radiol. 2019;128(3):280–310.
9. Zhu L, Wang J, Shi H, et al. Multimodality fMRI with perfusion, diffusion-weighted MRI and (1)H-MRS in the diagnosis of lympho- associated benign and malignant lesions of the parotid gland. J Magn Reson Imaging. 2019;49(2):423–32.
10. Jiayou Y, Fenghe Z, Zhenguang W. Clinical analysis of 8 cases of retention cyst of parotid gland. J Otolaryngol Ophthalmol Shandong Univ. 2002;16(6):359.
11. Jiangtai L. Retention cyst of parotid gland - analysis of 15 cases attached. Qinghai Med J. 1995;3:24–5.
12. Zhu L, Wang J, Shi H, et al. Multimodality fMRI with perfusion, diffusion-weighted MRI and 1H-MRS in the diagnosis of lympho-associated benign and malignant lesions of the parotid gland. J Magn Reson Imaging. 2019;49(2):423–32.
13. Zhang X, Zhang S, He J, et al. Ultrasonographic evaluation of major salivary glands in primary Sjögren's syndrome: comparison of two scoring systems. Rheumatology (Oxford). 2015;54(9):1680–7.
14. Shik KY, In JH, Jung KH, et al. Isolated cervical lymph node sarcoidosis presenting in an asymptomatic neck mass: a case report. Tuberc Respir Dis. 2013;75(3):116–9.
15. Baiyun YF, Junping L, et al. Diagnostic Singnificance of color doppler ultrasound in cervical sarcoidal lymphadenitis. Hebei Med J. 2008;9(30):1292–3.
16. Ciaramicolo N, Custodio M, De Sousa S, et al. Rare lesion, unusual location, uncommon presentation: a case of angiolymphoid hyperplasia with eosinophilia. Br J Oral Maxillofac Surg. 2019;57(5):479–80.
17. Wang XY, Yu J, Zhang FY, et al. Phenylephrine alleviates (131) I radiation damage in submandibular gland through maintaining mitochondrial homeostasis. Int J Radiat Oncol Biol Phys. 2019;104(3):644–55.

Lesions of Submasseteric Space and Parapharyngeal Space

29

Shuang Xia

29.1 Submasseteric Space Infection or Abscess

29.1.1 Overview

The submasseteric space is the potential space among fascia, muscle, and periosteum, which is filled with loose connective tissue and fat, and there is direct or indirect communication between them. In case of infection, it is easy to diffuse to adjacent spaces through fat and connective tissue with weak resistance, thus causing multi-space infection.

The submasseteric space is formed by superficial layer of the deep cervical fascia, that is, the cuff fascia, wrapping the masticatory muscles in layers. It includes fat space surrounded by temporal fossa, infratemporal fossa, masticatory muscles (temporal muscle, medial pterygoid muscle, lateral pterygoid muscle, masseter), ramus of mandible, ectopic salivary gland tissue, neurovascular, etc. Infection, tumor, and other diseases can occur in the space. The spreading route of infection: the submasseteric space communicates directly with the superior medial pterygopalatine fossa via pterygomaxillary fissure, directly communicates with the anterior medial buccal space via the sigmoid incision, connects with the medial parapharyngeal space via the medial pterygomandibular space, communicates with the posterior parotid space via the masseteric space, can break through the masseter fascia of parotid gland, and then enter the parotid gland, connecting with the inferior submandibular space and sublingual space, and invasion to the neck along the fascia and fascial space. The submasseteric space is mainly odontogenic infection, which is mainly caused by pericoronitis of mandibular third molars and periapical periodontitis of mandibular molars involving the space. It can also be caused by suppurative inflammation of temporal space, infratemporal space, pterygomandibular space, buccal space and parotid gland. The infection route can spread directly through the space, and can also cause infection in the space through vascular and lymphatic drainage. Osteomyelitis adjacent to mandible can also cause infection in submasseteric space. The masseteric and pterygomandibular spaces are involved firstly, and then involves parotid gland space and submandibular space.

The main characteristic of masticatory space infection is that the patient's jaws are closed, and the masseter area has palpable solid mass [1], often having clinical symptoms such as fever, maxillofacial pain, and swelling. Due to the strong obstruct of masticatory muscle fascia, inflammation can cause osteomyelitis adjacent to mandible, and involves buccal space, pterygomandibular space and parapharyngeal space, causing multi-space infection and breaking through parotid fascia and causing parotid gland abscess.

29.1.2 Pathology Findings

In the early stage of infection, neutrophil infiltration, edema, hemorrhage, necrosis of striated muscle and abscess formation occurs in the lesions. With the development of the disease, neutrophil infiltration and tissue necrosis become more severe, and then neutrophils disintegrate, cell fragments increase, fibroblasts proliferate, abscesses are wrapped to form abscess walls. In the chronic stage, the abscess wall is repaired by fibrous tissue and granulation tissue.

29.1.3 Imaging Findings

The submasseteric space infection can communicate directly through the space or connect indirectly through connective tissue and neurovascular bundle, and the infection often spreads to multiple spaces. MSCT can show the extent of infection [2]. Submasseteric space infection can spread and

S. Xia (✉)
Department of Radiology, Tianjin First Central Hospital, Tianjin, China

H. Li et al. (eds.), *Radiology of Infectious and Inflammatory Diseases - Volume 2*,
https://doi.org/10.1007/978-981-16-8841-6_29

involve buccal space, parotid gland space, submandibular space, subtemporal, and temporal space, parapharyngeal space, mandibular body space, pterygopalatine fossa and pterygoid intermuscular space. It can involve the neck, involves the level of thyroid gland isthmus and manubrium in the space between superficial cervical fascia and deep cervical fascia, and spread down to the level of the right extremitas sternalis claviculae along right sternocleidomastoid muscle [2].

Submasseteric space infection can manifest as cellulitis and/or abscess formation, which has the characteristics of spreading to peripheral tissues. CT shows soft tissue swelling with low density, unclear margin, intermuscular space effusion and muscle edema, and subcutaneous fat space shows flocculent and reticular changes. Abscess is formed in the focus area, which may have septa. CT shows a single-ring or multiple-quasi-circular lower density areas, and air shadow are found in some vomica (Fig. 29.1). MRI shows hypointense on T_1WI and hyperintense on T_2WI. When abscess forms, the content of vomica shows significant DWI restriction and edema around it, which can be differentiated from tumor necrosis. The enhancement is single-ring or multiple-ring enhancement, with smooth and homogeneous wall thickness. Osteomyelitis adjacent to mandible manifests as ramus of mandible with heterogeneous density, bone destruction and osteosclerosis, possible periosteal reaction, and increased fat density around the ramus of mandible.

29.1.4 Key Points of Diagnosis

1. CT shows soft tissue swelling with low density, unclear margin, effusion in intermuscular space and muscle edema, and subcutaneous fat space with flocculent and reticular changes. Abscess is formed in the focus area. CT shows single-ring or multiple-quasi-circular lower density areas, and air shadow is found in some vomica.
2. MRI lesions show hypointense on T_1WI and hyperintense on T_2WI. When abscess forms, DWI limitation of vomica contents is obvious, and peripheral edema is obvious. By enhanced scan, it shows single-ring or multiple-ring enhancement, with smooth and homogeneous wall thickness.
3. The disease can be complicated with osteomyelitis adjacent to mandible, which manifests as ramus of mandible with heterogeneous density, bone destruction and osteosclerosis, possible periosteal reaction, and increased fat density around ramus of mandible. Lesions may be complicated with multiple spaces.

29.1.5 Differential Diagnosis

Tumors in Submasseteric Space The tumors are regular or irregular masses, and the density by non-enhanced CT scan is similar to that of muscles, with isointense on T_1WI and hyperintense on T_2WI slightly higher than that of muscles.

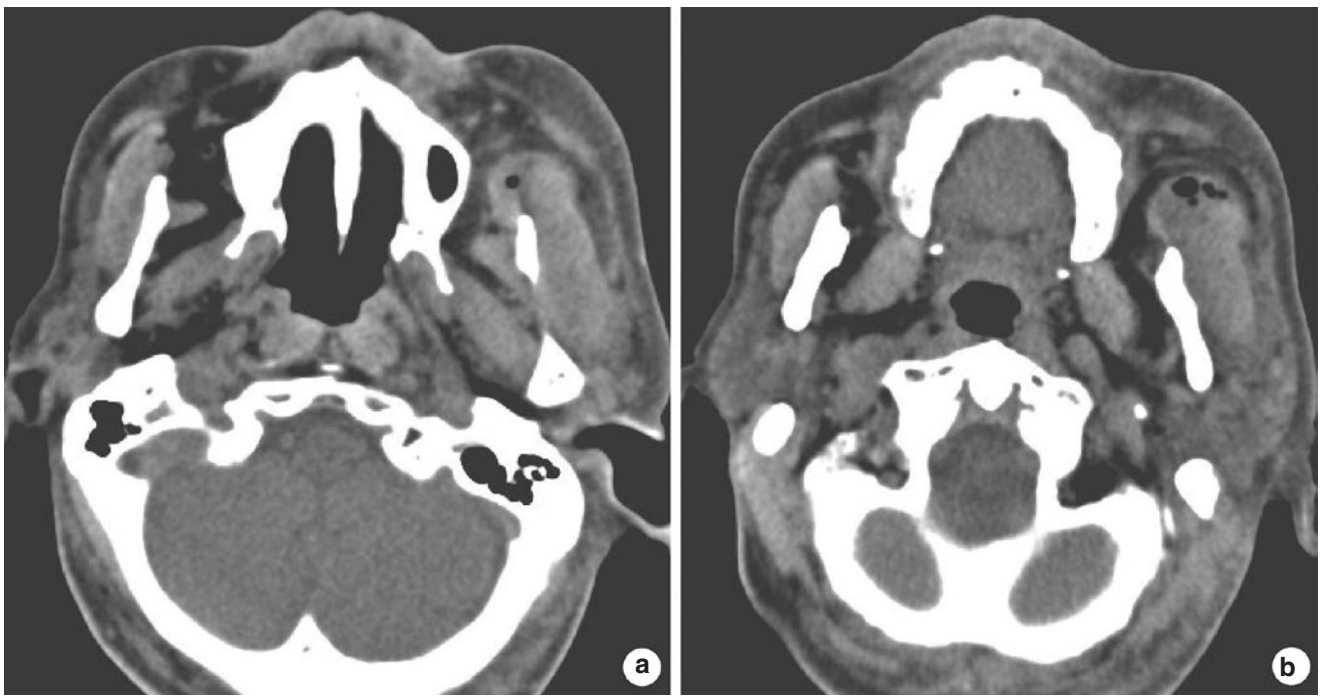

Fig. 29.1 Infection of the left submasseteric space. (**a**, **b**) Transverse non-enhanced CT scan indicates edema and blurring of subcutaneous fat layer in left maxillofacial region, enlargement of masseter, decreased density and bubble shadows in the area

Hypointense on DWI when tumor necrosis occurred, while DWI shows hyperintense in abscess. Occasionally, hemorrhage and calcification can occur in tumors, while infectious lesions rarely bleed. The enhanced scan indicates multiple masses with marked enhancement and margin, while the inflammation is heterogeneously enhanced, and the margin is unclear. The edema degree of muscle and subcutaneous fat layer adjacent to tumor is not as severe as that of infectious lesion [3].

29.1.6 Status Quo and Progress of Research

The two sides of the neck structure are basically symmetrical. CT and MRI examinations are easy to differentiate the unilateral primary lesions of the neck, and special attention should be paid to defining the scope of lesions involved in the diagnosis. Spiral CT can clearly show soft tissue shadow in submasseteric space, swelling of adjacent muscles, fascia and subcutaneous structure, and unclear margin. MRI is mainly used to differentiate inflammatory lesions from neoplastic lesions and to evaluate the extent of lesions. Meanwhile, MRI is more sensitive to bone marrow cavity edema than CT, and the combination of CT and MRI can accurately evaluate the nature of lesions.

References

1. Schwartz RH, Bahadori RS, Willis A. Submasseteric infection. Pediatr Emerg Care. 2015;31(11):787–8.
2. Shengsheng X, Tianyou L, Ming W, et al. Evaluation of infection and spreading route in maxillofacial and cervical fascia space by MSCT. J Third Military Med Univ. 2011;33(16):1751–4.
3. Yi W, Jiahe X, Ling Z. CT and MRI diagnosis of primary diseases in submasseteric space. J Clin Radiol. 2005;24(10):870–3.

Lesions of Sublingual Space

30

Mengmeng Yu, Xuedong Bai, Bangguo Li, and Heng Liu

30.1 Infection and Abscess in Sublingual Space

Overview

The floor of the mouth is divided into upper and inferior parts by the mylohyoid muscle, the superior part is sublingual space, and the inferior part is submandibular space and buccal space. The sublingual space can be divided into lingual septum space, sublingual caruncle space, and maxillofacial sulcus space, among which the latter can be further divided into maxillofacial sulcus medial space and maxillofacial sulcus lateral space.

The sublingual space is extremely complex in anatomy, and the generalized sublingual space is horseshoe-shaped, including all cellular spaces below the tongue and mouth bottom mucosa, above the hyoid muscle of the mandible and inside the mandible, that is, the sublingual space, the upper and lower spaces of the buchyoid muscle and the spaces between the buchyoid muscles. The sublingual space is divided into two symmetrical parts by buccolingual muscle and buccolingual skeletal muscle, which communicate in the deep surface of the frenum linguae. There are sublingual gland, deep submandibular gland and its ducts, lingual nerve, hypoglossal nerve, sublingual artery and vein, etc. in the sublingual space. The sublingual space communicates with the parapharyngeal space and the pterygomandibular space backward and upward, and communicates with the posterior inferior submandibular space [1].

Sublingual space infection refers to acute pyogenic infection of sublingual space. Its main clinical manifestations are inflammatory redness and tenderness in submandibular triangle, and inflammatory mass and tenderness in the early stage of onset. There is throbbing pain, fluctuation, and erubescence when entering the suppuration period. Pus is easy to be extracted by aspiration. Patients have different degrees of temperature rise, increased leukocyte count, and so on. The infection of sublingual space can be caused by odontogenic infection of mandibular teeth, injury of oral mucosa, ulcer wound, penetration of foreign matters, inflammation of sublingual gland and submandibular gland duct, and spread of infection of ipsilateral submandibular space [2].

Pathology Findings

There are a lot of inflammatory cell infiltration, angiectasis, and necrosis in the lesion area.

Imaging Findings

In the infection of floor of mouth and maxillofacial space, imaging examination has five main objectives: (1) assist clinical diagnosis; (2) define the scope of infection; (3) make sure whether there are complications; (4) determine whether there is abscess formation; (5) Dynamic monitoring of infection process in deep space [3, 4].

1. **X-ray examination.** It is difficult to make accurate qualitative and localized diagnosis for infection of the floor of the mouth and maxillofacial space. At present, CT and MRI examinations are widely used in the diagnosis of maxillofacial lesions, and can clearly diagnose the nature, location, and size of the lesions and the relationship between the surrounding great vessels and important structures such as trachea.
2. **CT examination.** Non-enhanced CT shows that the sublingual space is swollen, the density of fat space at the mouth floor increases or even disappears, and the margin is unclear, showing iso-density shadows or slightly low density. The low-density area in the lesion area indicates necrotic liquefied tissue. After abscess formation, the enhanced examination shows ring enhancement, the

M. Yu
Binzhou Medical University Hospital, Binzhou, China

X. Bai
Affiliated Hospital of Chengde Medical University, Chengde, China

B. Li · H. Liu (✉)
Affiliated Hospital of Zunyi Medical University, Zunyi, China

H. Li et al. (eds.), *Radiology of Infectious and Inflammatory Diseases - Volume 2*,
https://doi.org/10.1007/978-981-16-8841-6_30

abscess wall is thick, and the septa shadow can be found in some parts. The necrotic liquefied tissue has no enhancement, and the margin of abscess is blurred, which can extend along the adjacent space to the contralateral space (Figs. 30.1 and 30.2). CT examination can be used to reconstruct images on coronal, sagittal and any planes, show the anatomical relationship between fascia and interstitial fascia in detail, clearly determine the distribution location and spread way of infection, and help to differentiate the corresponding complications in early stage, such as perimaxillary and submandibular abscess. (1) Cellulitis: CT shows skin edema and thickening, adipose tissue density increased, muscular tissue density decreased and sublingual space disappeared; (2) Pus formation: the vomica has marginal enhancement, and the density of pus is between water and muscular tissue; (3) Pneumatosis: Dark shadows with sharp edges scattered in soft tissues.

3. **MRI examination.** It can differentiate the scope of infection, especially the show of congestion, edema and abscess in cellulitis is significantly superior to CT. The sublingual space is one of the three main spaces on the floor of the mouth. The imaging characteristics of its inflammatory changes are similar to those of cellulitis in

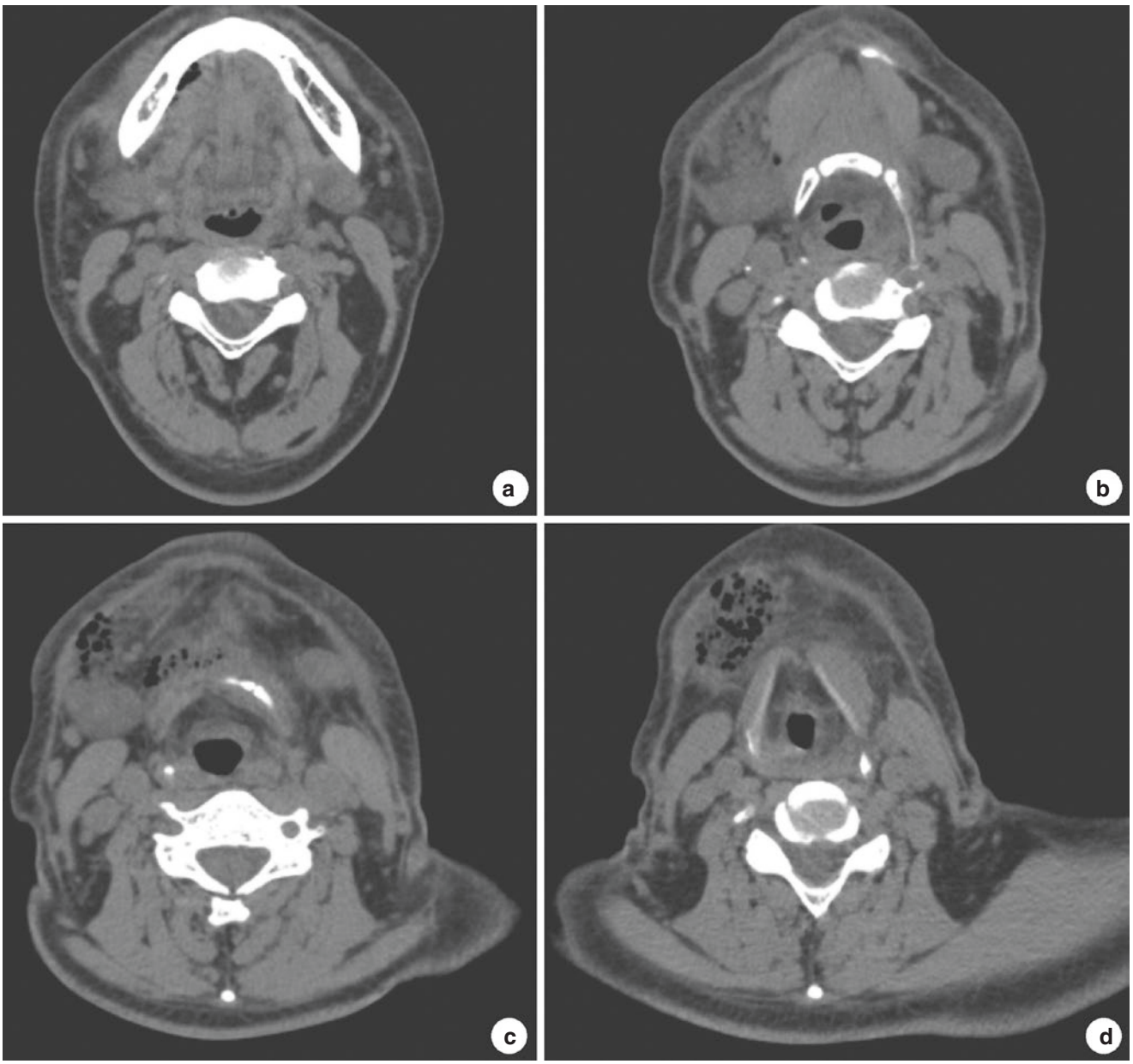

Fig. 30.1 Infection in sublingual space. (**a–d**) Non-enhanced CT scan indicates that the soft tissue of the right submandibular and mouth floor is swollen, the fat space is blurred, and the air density shadows can be found

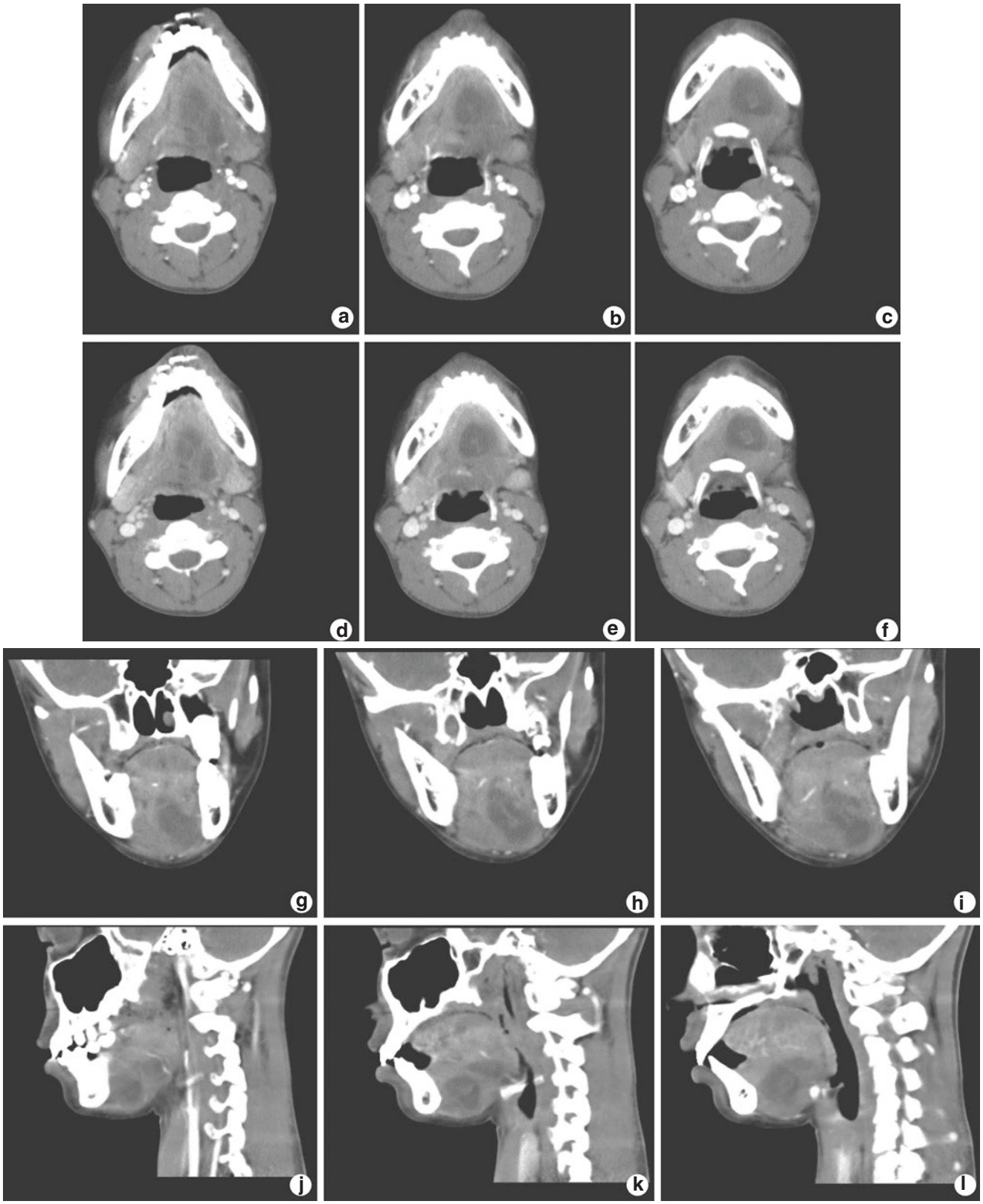

Fig. 30.2 Infection in sublingual space with abscess formation. (**a–f**) The arterial and venous scans of CT show that the left sublingual part is irregularly shaped and slightly low density. By enhanced scan, the lesion shows marked heterogeneous enhancement at the edge, with slightly low enhancement area in it, the inner edge is still smooth and the outer margin is blurred. (**g–l**) Coronal and sagittal reformation shows the overall shape and scope of the lesion

the floor of the mouth, including swelling of soft tissue in the floor of the mouth, reduced signal intensity of adipose tissue in the fascia space on T_1WI, unclear margin between swelling of the infected site and peripheral tissues, isointense and hypointense on T_1WI, and hyperintense on T_2WI. After abscess formation, it shows significantly hyperintense on T_2WI fat-suppressed sequence, and ring enhancement by enhanced T_1WI [2]. DWI and ADC are helpful for the diagnosis of abscess. The hyperintense on DWI is a characteristic [4].

Key Points of Diagnosis

1. Inflammatory redness and tenderness in the submandibular triangle are mostly found in children. Dental infection of mandibular teeth, oral mucosa injury, ulcer wound, inflammation of sublingual gland, submandibular gland duct and spread of infection of ipsilateral submandibular space can all cause the disease.
2. The characteristic manifestations of CT and MRI: (1) cellulitis, CT shows skin edema and thickening, adipose tissue density increased, muscular tissue density decreased and sublingual space disappeared; (2) Pus is formed, the vomica has marginal enhancement, and the density of pus is between water and muscular tissue; (3) Pneumatosis, and dark shadows with sharp edges scattered in soft tissues. If abscess is formed, it will be heterogeneous ring enhancement by enhanced scan, and pus will not be enhanced. DWI shows hyperintense when local pus is formed.

Differential Diagnosis

Sublingual space infection should be differentiated from diseases with similar symptoms at the mouth floor, and the diagnosis should be combined with clinical history and signs.

1. **Tongue cancer with infection.** It mainly shows lump, which usually involves tongue tissue. If the sublingual space is involved, the lesion margin is relatively clear, with isointense on T_1WI and hyperintense on T_2WI. If the lesion progresses rapidly, the imaging findings will overlap with benign infection lesions, and the diagnosis has some difficulties.
2. **Suppurative sublingual adenitis.** It shows diffuse swelling of gland with blurred contour. When abscess is formed, spot or hollow low-density necrotic area is formed, subcutaneous fat layer is blurred and density is increased. By enhanced scan, the abscess formed ring shape and garland-like shape enhancement.
3. **Infection of sublingual cyst.** Sublingual cyst has a clear margin. When it is complicated with infection, the cyst wall has marked enhancement, the shape is regular, the swelling degree of peripheral soft tissue space is low, and the focus often develops along the space.

Status Quo and Progress of Research

Sublingual space infection is secondary infection, and accurate diagnosis can be made according to clinical factors, clinical symptoms and signs. At present, the research on sublingual space infection mainly focuses on its infection spreading route, pathogen microbiology research, comprehensive treatment, maxillofacial trauma repair and prevention of corresponding space infection. Among them, imaging examinations, such as ultrasound, multi-slice spiral CT and MRI, are mostly used to observe cellulitis and abscess, so as to clarify the location, scope, and diffusion path of infection [5].

References

1. La'porte SJ, Juttla JK, Lingam RK. Imaging the floor of the mouth and the sublingual space. Radiographics. 2011;31(5):1215–30.
2. Tianqi L, Xinrong N, Xingquan Y, et al. Clinical characteristics and treatment of infection in Oral and maxillofacial region. Chin J Pract Stomatol. 2017;10(06):349–53.
3. Bingfeng C, Kai Z, Liqiang S, et al. Management of maxillofacial space infection (4) - diagnostic value and application of CT. J Pract Stomatol. 2018;171(04):142–5.
4. Lu Zhonghua G, Yihong ZZ, et al. Clinical analysis of 32 cases of deep cervical fascia space infection. Chin J Prim Med Pharm. 2018;25(16):2139–40.
5. Qijin W, Hongbo O. Research progress in diagnosis and treatment of maxillofacial space infection. Chin J Aesthet Med. 2017;26(12):143–5.

Lymphatic Gland Lesions in Neck

31

Min Tang, Hui Dai, Heng Liu, Yang Cao, Shuang Xia, and Ying Zou

31.1 Cervical Lymphnoditis

31.1.1 Overview

Cervical lymphadenitis is mostly secondary to odontogenic and oral infections and can also come from facial and neck skin injuries, furuncle, carbuncle, etc. Lymphadenitis in children is mostly caused by upper respiratory tract infection or inflammation of the pharyngeal tonsil. Because of the different pathogens, it can be divided into viral lymphadenitis, bacterial lymphadenitis and fungal lymphadenitis. In the early stage, the lymphadenitis manifests as enlarged local lymph nodes, palpable neck nodules, conscious pain or tenderness, and slight systemic reaction. If lymphadenitis is not controlled in time, abscesses may be formed, the pain will be aggravated, and the surrounding skin will show red swelling, and the skin temperature will rise. After a single lymph node capsule is festered, it can involve several adjacent lymph nodes and fuse with each other to form an inflammatory mass. After the abscess ruptures, a pale yellow sticky pus flows out. At this time, there are systemic toxemia symptoms such as high fever, chills, headache, and anorexia. Laboratory test shows that the leukocytes increase rapidly. In the chronic stage of lymphadenitis, hard nodules with slight pain are formed, with mild activity, tenderness, and unremarkable systemic symptoms. When the body's resistance decreases, lymphadenitis can have acute recurrence. After the proliferation and enlargement of inflammatory lymph nodes, even if the inflammation is controlled, it is difficult to completely subside [1].

M. Tang
Shanxi Provincial People's Hospital, Taiyuan, China

H. Dai · H. Liu
Affiliated Hospital of Zunyi Medical University, Zunyi, China

Y. Cao
Shiyan Renmin Hospital, Affiliated People's Hospital of Hubei University of Medicine, Shiyan, China

S. Xia (✉)
Department of Radiology, Tianjin First Central Hospital, Tianjin, China

Y. Zou
The First Affiliated Hospital of Tianjin University of TCM, Tianjin, China

31.1.2 Pathology Findings

Lymphadenitis mainly manifests as necrosis and plenty of inflammatory cell infiltration.

31.1.3 Imaging Findings

1. CT Examination One or more enlarged lymph nodes with different sizes appear unilaterally of the neck, which are round or oval with clear margin. Nodules can fuse with each other, but the margin is unclear. If the inflammation is not controlled, it can develop into suppurative lymphadenitis, with central necrosis of enlarged lymph nodes, reduced CT density and blurred edge (Fig. 31.1).

2. MRI Examination Lesion shows hypointense on T_1WI, hyperintense on T_2WI, hyperintense in the center of DWI sequence, and ring enhancement by enhanced scan on lesions, with smooth medial wall and homogeneous wall thickness.

31.1.4 Key Points of Diagnosis

1. Patient mostly have history of infection.
2. Enlarged lymph nodes with homogeneous density and marked homogeneous enhancement; DWI signal in the necrotic area of pyogenic lymphadenitis shows ring enhancement and smooth medial wall.

H. Li et al. (eds.), *Radiology of Infectious and Inflammatory Diseases - Volume 2*,
https://doi.org/10.1007/978-981-16-8841-6_31

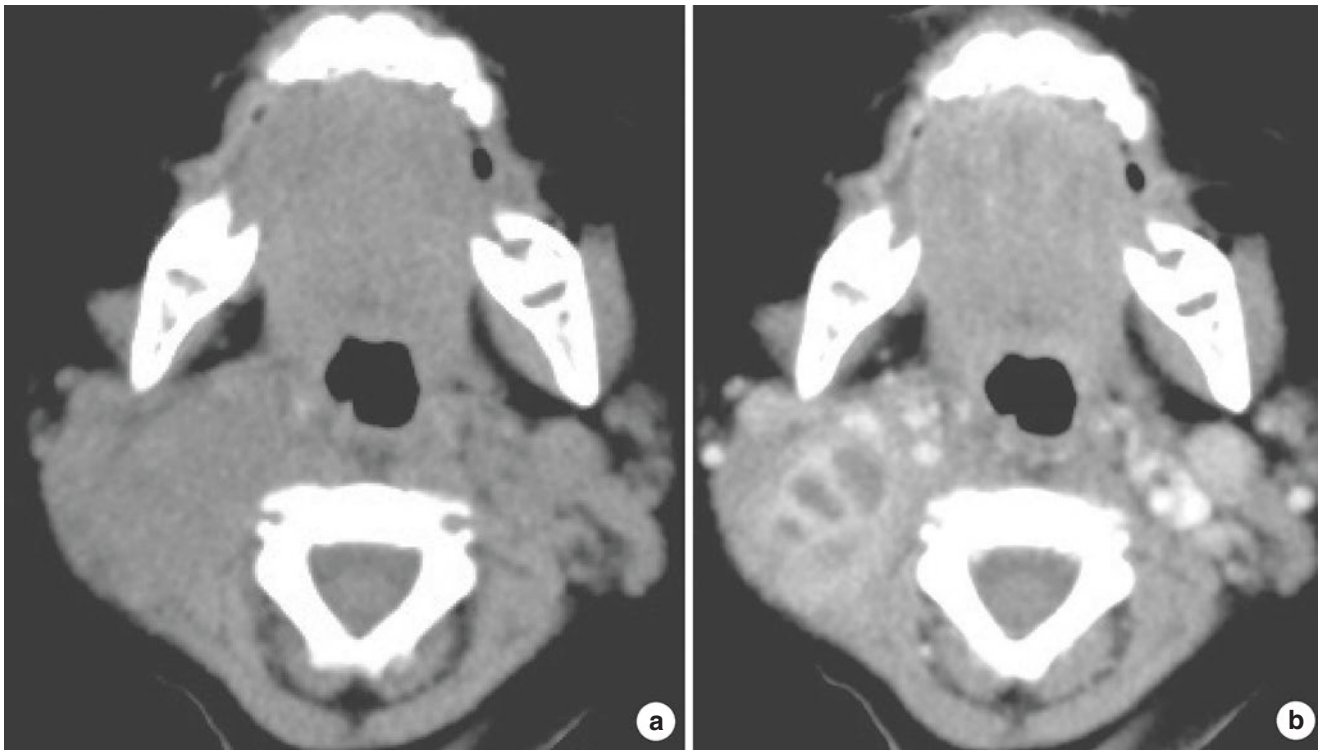

Fig. 31.1 Pyogenic lymphadenitis in left neck. (**a**) Transverse non-enhanced CT scan indicates multiple enlarged lymph nodes in the right neck, which are merged with each other, showing unclear margins; (**b**) Transverse CT enhanced scan shows multiple ring enhancement and homogeneous thick wall

31.1.5 Differential Diagnosis

1. Lymphoma Multiple enlarged lymph nodes occurring unilaterally or bilaterally, with homogeneous density, mild to moderate enhancement by enhanced scan, and the lesions could fuse into a mass shadow.

2. Metastatic Tumor Patients often have a history of primary tumors, and the density or signal intensity of enlarged lymph nodes is heterogeneous, and there may be cystic necrosis, which shows heterogeneous enhancement by enhanced scan.

31.1.6 Status Quo and Progress of Research

Dual-energy scanning realizes the separation of material components according to the different density characteristics of different materials under different energies. Dual-energy CT iodine map can show the distribution of iodine in images and can quantitatively evaluate the iodine concentration in lymph nodes, thus reflecting the distribution of lymph node blood perfusion. Inflammatory lymph node cortex contains plenty of secondary lymph nodules, with enlarged lymph follicles, abundant lymphocytes, thickened medullary cord and increased endothelial cells of medullary sinus. The significant thickening of small blood vessels may lead to increased iodine uptake and high perfusion. Metastatic lymph nodes and lymphomas manifest as imperfect development of lymph node basement membrane, loose connection of endothelial cells and heterogeneous distribution of angiogenesis in lymph nodes, resulting in lower iodine content than inflammatory enlarged lymph nodes and low perfusion [2].

31.2 Cervical Lymph Node Tuberculosis

31.2.1 Overview

Cervical lymph node tuberculosis is mostly found in children and young people. It usually occurs when the body's resistance is low. Mycobacterium tuberculosis mostly invades through tonsils and dental caries, and a few of them are secondary to pulmonary or bronchial tuberculosis. Cervical lymph node tuberculosis can occur unilaterally or bilaterally, with multiple enlarged lymph nodes varied in size. In the early stage, enlarged lymph nodes are hard and painless and can be pushed. With the development of pathological changes due to inflammation around lymph nodes, lymph nodes

adhere to skin and peripheral tissues, and various lymph nodes can also adhere to each other and fuse into mass. In the advanced stage, caseous necrosis and liquefaction occurred in lymph nodes, resulting in psychrapostema. After ulceration, bean dregs-like or rice soup-like pus can flow out, eventually forming prolonged sinus or chronic ulcer.

Cervical lymph node tuberculosis is a painless mass with slow growth, smooth surface, hard texture and no adhesion movement. It may have systemic symptoms such as afternoon low-grade fever and night sweat, and the erythrocyte sedimentation rate increases rapidly in laboratory test.

31.2.2 Pathology Findings

There are different pathological manifestations in different stages of lymph node tuberculosis, which can be divided into five stages, including inflammatory and hyperplastic stage (mainly mature small lymphocyte proliferation, complicated with primordial lymphocyte proliferation, no necrosis focus); Nodal stage of lymph nodes (mainly proliferation of lymph node cells and histiocytes, with lymph node nodes visible); Tuberculosis nodule stage (proliferation of epithelioid cells is dominant, and typical Langerhans giant cells are found in tuberculosis nodules); caseous necrosis stage (plenty of acid-fast mycobacteria); Cellulose proliferation period (mainly fibrillar connective tissue proliferation, complicated with a few fibers, fibrous cells and histiocytes).

31.2.3 Imaging Findings

Lymph node tuberculosis is hyperplastic granulation tissue, which shows homogeneous enhancement and no adhesion around it; In caseous necrosis of lymph nodes, the lymph nodes are ring enhancement, with smooth medial and lateral walls, and patchy areas without enhancement are found in them. The lesions invade the peripheral tissues and can form cold abscess and sinus tract (Fig. 31.2). When the lesion penetrates the lymph node capsule, the lymph nodes fuse and adhere to each other. On non-enhanced scan, low-density foci are found in the center of the lymph node, and it is usually ring enhancement when enhanced and typical petal-shaped enhancement when fused. Punctate calcification is found in some lesions, and calcification in the lesions has suggestive significance for tuberculosis (Fig. 31.3). MRI shows that enlarged lymph nodes show isointense on T_1WI and isointense on T_2WI, DWI shows no diffusion limitation, and enhanced examination shows homogeneous or ring enhancement. Lesion show no significant fusion tendency.

31.2.4 Key Points of Diagnosis

1. Lymph node tuberculosis is common in young people. Imaging examination shows multiple lymph node enlargements in the neck. CT shows iso-density shadows. MRI T_1WI and T_2WI show isointense, showing homogeneous or ring enhancement. Calcification is found in some lesions.
2. There are systemic symptoms such as afternoon low-grade fever and night sweat, and the erythrocyte sedimentation rate by laboratory test increases rapidly.

31.2.5 Differential Diagnosis

1. Lymphoma It manifests as multiple painless lymphadenopathy, which can involve multiple systems and organs. It often manifests as swelling of multiple unilateral or bilateral lymph nodes, homogeneous density, mild to moderate enhancement, and the lesions can fuse into mass. MRI examination shows that DWI image diffusion limitation is obvious, and ADC value is lower, often less than 0.996×10^{-3} mm^2/s [3].

2. Metastatic Tumor Attention should be paid on the detailed examination of the history of primary tumors, and the location of lymphatic metastasis is related to its drainage area. The primary tumors have different histopathology and different imaging findings. The enlarged lymph nodes often have irregular shape, heterogeneous density or signal, cystic degeneration and necrosis, heterogeneous enhancement by enhanced scan, heterogeneous thickness of the cystic wall and unclear margin.

31.2.6 Status Quo and Progress of Research

From the pathological point of view, both benign and malignant lymph nodes can have increased cell density, changed ratio of nucleus and cytoplasm, and different blood perfusion. Morphologically, it can manifest as enlarged lymph nodes, constriction and disappearance of lymph node portal structure, heterogeneity of lymph nodes and abnormality around lymph nodes. Therefore, there is a certain overlap between benign and malignant lymph node lesions observed from imaging, so in order to clearly diagnose the nature of lymph node lesions, DWI, perfusion imaging, elasticity imaging, dual-energy imaging, radiomics, and other advanced technologies have been extended to the application of lymph node diseases.

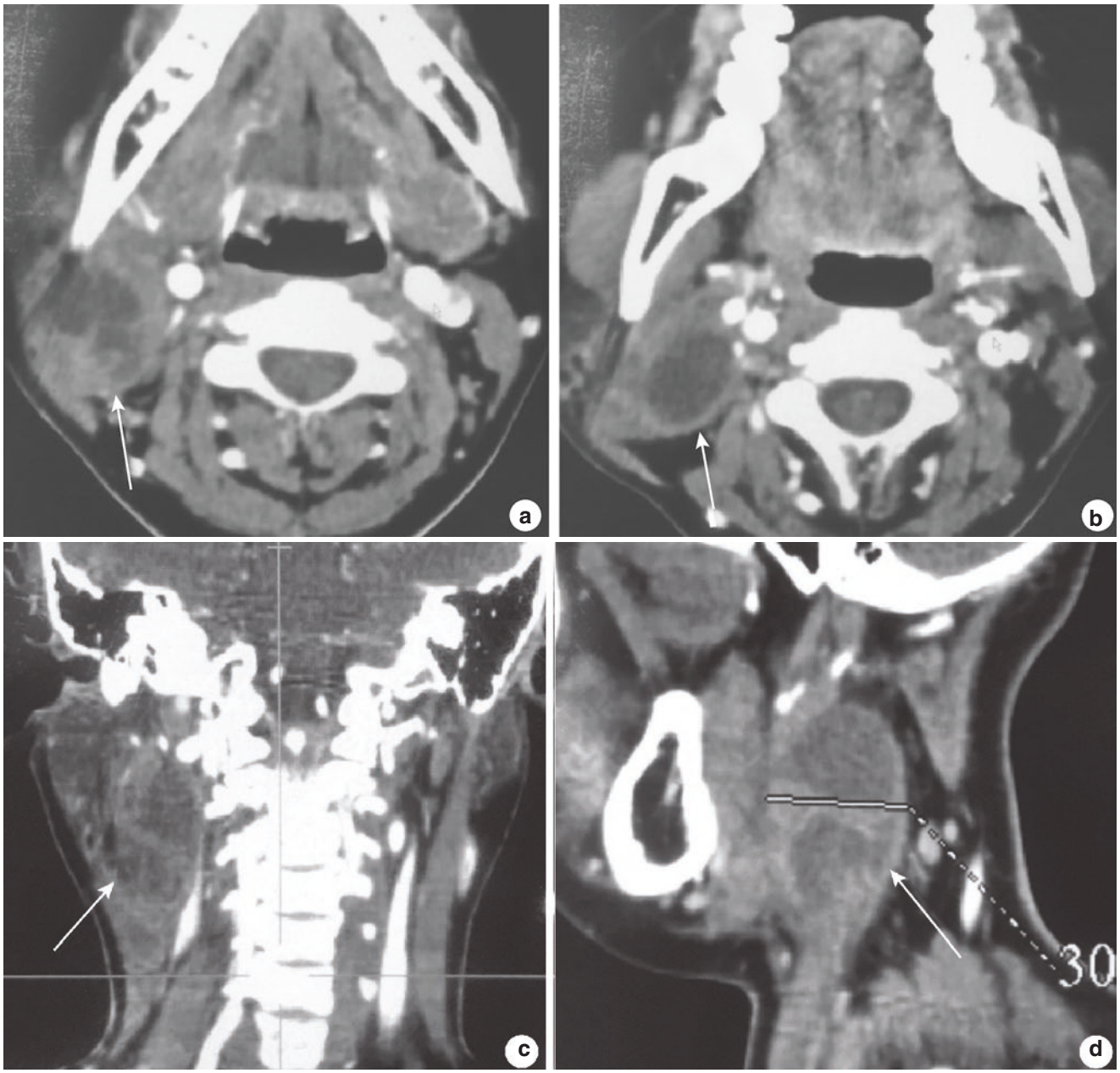

Fig. 31.2 Lymph node tuberculosis in right neck II region. A 25-year-old female patient. Mild fever for 1 month, with touchable enlarged lymph nodes in right neck. (**a**–**d**) Enhanced CT shows petal-shaped enhancement of lymph nodes in II region of the right neck, in which patchy area without enhancement (indicated by arrow) could be found

1. DWI Examination It is based on the pathological differences between inflammatory and malignant enlarged lymph nodes. Through DWI technology, the change of freedom of movement of water molecules diffusion in the extracellular space between them is studied. It is concluded that the diffusion of water molecules in malignant enlarged lymph nodes is significantly limited, while the diffusion of water molecules in inflammatory enlarged lymph nodes is relatively unrestricted. The diagnostic threshold of ADC is about 0.996×10^{-3} mm^2/s [3].

2. Energy Spectrum CT According to the different characteristics of energy density of different substances, it can realize the separation of substance components and can quantitatively evaluate the iodine concentration of lymph nodes under different pathological conditions, thus reflecting the distribution of lymph node blood perfusion. Inflammatory lymphadenopathy contains plenty of secondary lymph nodules, enlarged lymph follicles, increased number, abundant lymphocytes, thickened medullary cord, increased endothelial cells of medullary sinus and dilated small blood vessels, which may lead to increased

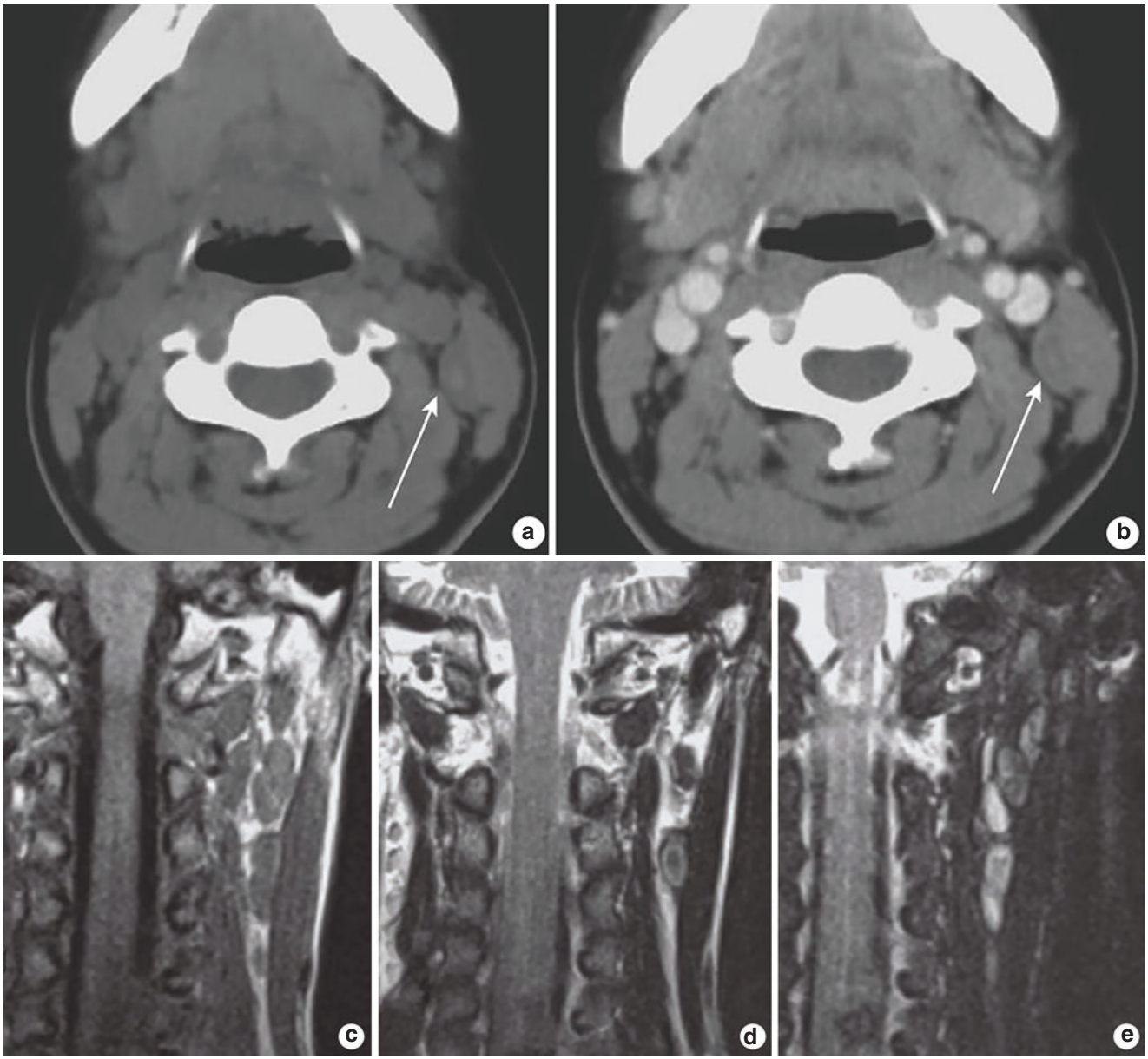

Fig. 31.3 Lymph node tuberculosis in II and III regions of left neck. A 40-year-old male patient. Mild fever, night sweat for 2 months, swelling of left neck. (**a**) Non-enhanced CT scan indicates that lymph node shadow are found in II region of left neck, with heterogeneous density, clear margin and slightly high-density shadows (indicated by arrow) inside; (**b**) CT enhanced examination shows ring enhancement of the wall of the lesion (indicated by arrow); (**c**–**e**) Coronal MRI T_1WI, T_2WI, and T_2WI fat-suppressed sequence indicates shadows of multiple enlarged lymph nodes in left II and III regions, and the lesions show isointense on T_1WI and hypointense on T_2W. Lesions show slightly hyperintense on T2WI fat suppression

iodine uptake, which is significantly higher than that of metastatic lymph nodes and lymphoma [4].

3. Elasticity Imaging Pathologically, there are differences in elastic coefficients between lymph node enlargement caused by different diseases and surrounding normal tissues. Elastic ultrasound has high sensitivity and specificity in differentiating benign and malignant lymph nodes [5].

4. CT Perfusion Imaging It leads to high perfusion in hemodynamics, short mean transient time (MTT), high permeability surface (PS), which is contrary to inflammatory enlarged lymph nodes, due to disorganized and immature new blood vessels in malignant lymph node lesions, incomplete vascular basement membrane, rapid blood flow velocity in new blood vessels, increased intravascular pressure and shortened blood circulation time [4].

5. Research on Radiomics Radiomics is to extract a large amount of image information from images with high throughput on the basis of conventional imaging, realize tumor segmentation, feature extraction and model building, and find out the connotation characteristics of diseases through deep data mining, thus reflecting the changes of human tissues, cells, and genes. By analyzing the features extracted from imaging histology, the benign and malignant lymph nodes can be judged.

31.3 Reactive Hyperplasia of Cervical Lymph Node

31.3.1 Overview

The reactive proliferation of cervical lymph nodes, also known as reactive adenopathy (RPS), is a common benign hyperplastic disease of lymph nodes or soft tissues, which is caused by various factors, such as inflammation, viral infection, vaccination, some drug reactions, immune diseases and so on, which may lead to lymph node enlargement and lymphadenosis in the pharynx and other parts of the body. Viral infection is the most common cause, which usually leads to slight enlargement of bilateral lymph nodes without peripheral inflammation. Cytomegaloviral infection, herpes simplex viral infection, chickenpox and rubella are common viral causes, but they usually need to be combined with clinical or laboratory test to make a definite diagnosis. It is prone to teenagers, and the common sources of infection are limited head and neck infections such as pharyngitis and systemic viral infection.

31.3.2 Pathology Findings

The pathological lymph nodes vary in size, generally ranging from 1 cm to 3 cm in diameter, sometimes up to 10 cm in diameter. Microscopically, reactive proliferation of lymph nodes often has different histological structures due to different pathogenic reasons. Histological manifestations were lymphoid follicular proliferation, paracortical proliferation, sinus histiocytosis and mixed proliferation.

31.3.3 Imaging Findings

1. CT Manifestations CT can clearly show the location, scope and number of enlarged lymph nodes, and also show the relationship between lymph nodes and peripheral tissues, so as to guide clinical biopsy. The characteristic manifestation is the enlargement of lymph nodes in the parapharyngeal or retropharyngeal space, the short diameter of node is often ≤1.5 cm, and isolated enlarged lymph nodes are the most common. The density of non-enhanced scan is homogeneous, equal to or slightly lower than that of adjacent muscles, and it has marked enhancement by enhanced scan, and the enhancement is homogeneous [6, 7].

2. MRI Findings Homogeneous hypointense or isointense on T_1WI; homogeneous isointense on T_2WI; diffusion limitation and hyperintense on DWI. T_1WI enhanced scan shows various enhancement forms, most of which are marked enhancement (Figs. 31.4 and 31.5).

31.3.4 Key Points of Diagnosis

1. Young patients with pharyngitis or systemic virus infection.
2. CT shows homogeneous shadows of enlarged retropharyngeal space nodules, with or without other related reactive nodules in the neck.
3. MRI shows round nodules with clear margin, homogeneous signal and marked enhancement.

31.3.5 Differential Diagnosis

1. Lymph Node Tuberculosis It is mostly found in young adults, and the enlarged lymph nodes have heterogeneous density and ring enhancement. When multiple lymph nodes are fused, a garland-like enhancement can be found.

2. Lymphatic Metastasis These patients mostly have history of primary tumors. The density of enlarged lymph nodes is heterogeneous, with cystic degeneration and calcification. The enhancement is found by enhanced scan.

3. Malignant Lymphoma often involves mediastinal lymph nodes, and enlarged lymph nodes are easy to integrate into a mass, which often manifests as mild or moderate enhancement.

31.3.6 Status Quo and Progress of Research

Cervical lymph nodes are regional lymph nodes for tumor metastasis and inflammation drainage in head and neck, and they are also important barriers for preventing inflammation invasion and preventing tumor cells from spreading.

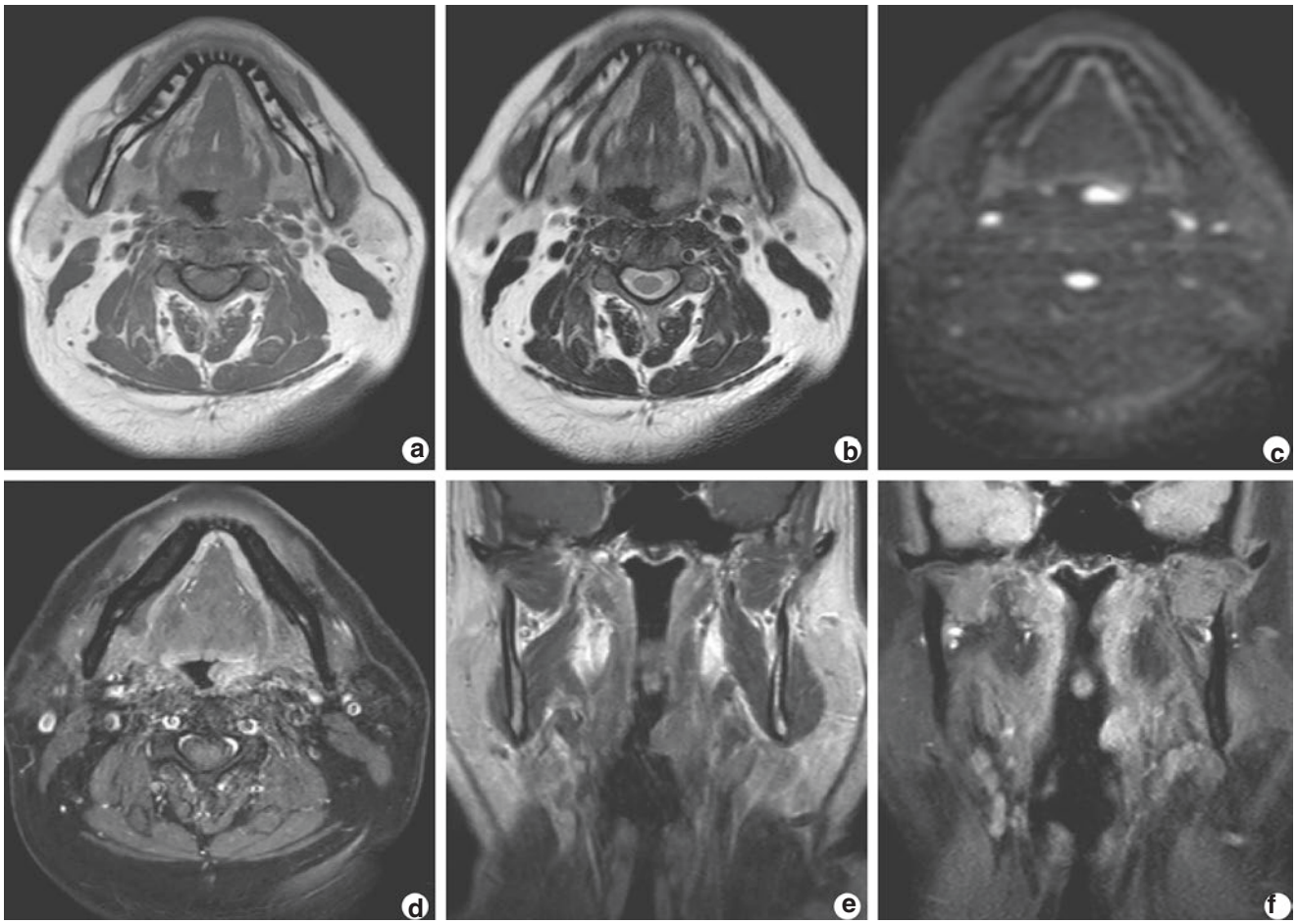

Fig. 31.4 Reactive adenopathy of left pharynx. A 47-year-old male patient. The pharyngeal mass of 6 months is found by physical examination. (**a**) Axial T_1WI non-enhanced scan indicates isointense nodules in the left pharynx; (**b**) Axial T_2WI shows hyperintense of nodules. (**c**) Diffusion limitation and hyperintense of nodule on DWI; (**d**) Axial T_1WI enhanced scan shows nodule with marked enhancement and continuous with the lymphatic tissue posterior to the tongue root. (**e**) Coronal T_1WI non-enhanced scan indicates that the left pharyngeal nodule protrudes to the pharyngeal cavity; (**f**) Enhanced T_1WI on coronal plane shows marked enhancement of nodules

Therefore, the differentiation between benign and malignant cervical lymph nodes is important for the selection of treatment method.

CT perfusion imaging is a non-invasive functional imaging method to evaluate the perfusion state of tissue blood flow, which can quantitatively analyze different pathological lymph node lesions in the neck, and has certain clinical value in differentiating cervical lymphatic metastasis and inflammatory reactive proliferation of lymph nodes.

Dual-energy spectrum analysis can provide some valuable information for differentiating benign and malignant lymph node lesions. CT value measurement corresponding to different single energy diagrams has certain potential value for differentiating lymph node lesions of different pathological types.

Many studies on interstitial magnetic resonance lymphography have been carried out in recent years. By using magnetic resonance contrast agents combined with macromolecules, which has a large molecular weight and molecular volume, the technique can make target lymph node maintain at a higher enhanced level within an extended period, thus effectively developing the morphology of lymph vessels and lymph nodes in drainage area for reactive hyperplasia of lymph node and lymph node tumor metastasis. In this sense, it is of value for differentiating cervical lymph node metastasis and reactive hyperplasia [8, 9].

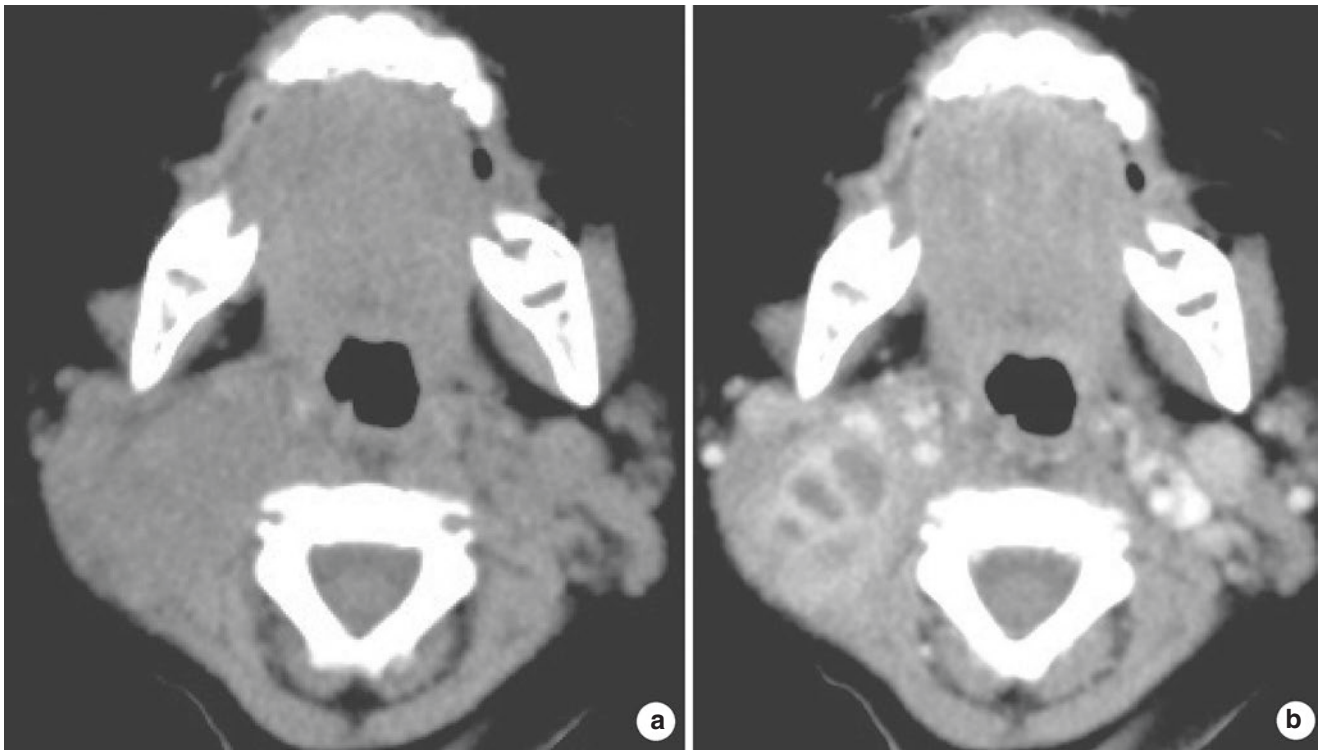

Fig. 31.5 Inflammatory and hyperplastic at the nasopharyngeal roof and acute inflammation of left parotid gland. An 11-year-old male patient. The left face is swollen and painful for 1 week. (**a**) Axial T_1WI non-enhanced scan indicates isointense nodules at the nasopharyngeal roof; (**b**) Axial T_2WI shows hyperintense of nodules. Enlarged lymph nodes (indicated by arrow) were found in bilateral retropharyngeal spaces. Diffuse enlargement of left parotid gland

31.4 Cat Scratch Disease

31.4.1 Overview

With the increase of pet owners, the incidence of cat scratch disease (CSD) rises accordingly. Cat scratch disease, also known as cat scratch fever, is a zoonotic disease caused by Rickettsia, which is a self-limiting infectious disease caused by infection of *Bartonella henselae* pathogen. The disease can manifest as abnormal changes in lymph nodes and/or skin of head and face when the immunity of human body is normal, but severe systemic diseases can occur when the immunity decreases. Bartonella is distributed all over the body. Animal hosts include cats, dogs and rodents, and vector insects include sandflies, mites, fleas and lice. Humans may be infected by close contact with cats, dogs and other animals carrying Bartonella or being bitten by fleas and lice. Fleas are the vectors of pathogen transmission between cats, and killing fleas plays an important role in preventing cats from infecting with Bartonella. More than 90% of CSD patients have a history of cat contact, and 75% of them have been caught or bitten by cats, especially kittens.

Because it lacks specificity of clinical symptoms and signs and is mainly characterized by local lymph node enlargement and pain, the disease occurs sporadically. Cat scratch disease is easily misdiagnosed as lymphoma, metastatic tumor or other inflammatory diseases.

31.4.2 Pathology Findings

Pathological manifestations mainly include lymph node necrosis and asteroid abscess formation, with neutrophil infiltration and granuloma. The discovery of black pathogens in perivascular, interstitial and macrophage cytoplasm by Warthin-Starry argentation is helpful to the diagnosis of cat scratch disease.

31.4.3 Imaging Findings

1. X-Ray Examination It shows abnormal soft tissue mass inferior to the lesion, often complicated with soft tissue edema in some areas.

2. CT Examination It can involve parotid gland, manifested as parotid gland enlargement, and can also involve multiple cervical lymph nodes. The enlarged lymph nodes

can be lumpy, lobulated, with unclear margin and subcutaneous soft tissue edema around the mass. Enhanced scan shows that the margin of the mass can be enhanced, and low-density shadows are found in the center of the mass, indicating that the lesion has abscess formation.

3. MRI Examination Abnormal subcutaneous mass with signal intensity similar to muscle, with significant subcutaneous edema in soft tissue around the mass, homogeneous or heterogeneous isointense or slightly hyperintense on T_1WI, and hyperintense on T_2WI for mass and peripheral area with edema. The enhanced scan indicates the lesion with ring enhancement, and the central non-enhanced area is abscess liquefactive necrosis area.

31.4.4 Key Points of Diagnosis

1. Patient has a contact history of cats, dogs and other animals or a history of being scratched and bitten with skin damage.
2. Aseptic pus can be extracted by aspiration of enlarged lymph nodes, and other diseases have been excluded.
3. CT and MRI examination shows that there were soft tissue masses in the output lymphatic vessels with edema of peripheral soft tissues.
4. Lymph node biopsy is consistent with pathological changes of cat scratch disease.

31.4.5 Differential Diagnosis

1. Lymph Node Tuberculosis The CT manifestations are mainly related to pathological stages. When lymph node tuberculosis is mainly proliferation or granulation tissue, the density of lymph nodes is homogeneous; If caseous necrosis occurs or the capsule is involved, the enhanced scan shows ring enhancement, lymph node tuberculosis can fuse and adhere to each other, and the space around the lesion is blurred.

2. Metastatic Lymph Nodes They mainly manifest as enlarged lymph nodes, which are quasi-circular, with a maximum transverse diameter of more than 1 cm. Necrotic areas can be found in the center of the lesions, and the enhanced scan shows ring enhancement. If the lesions break through the capsule, the edges of lymph nodes are blurred and adhere to the peripheral tissues.

3. Lymphoma The disease can be primary and limited, or it can be a part of systemic lymphoma. Lymphoma is widely distributed, mainly manifest as multiple occurrences, clear margin of lesions, less mutual fusion, homogeneous enhancement by enhanced scan, and no necrotic area in general lymph nodes.

31.4.6 Status Quo and Progress of Research

Recently, it is reported that [10] a 29-year-old female patient with Hodgkin's lymphoma showed complete metabolic response in mid-term FDG PET/CT. Fever and lymphadenopathy occurred after three cycles of chemotherapy. PET/CT showed several FDG concentrations in inguinal and iliac lymph nodes. Cat scratch disease was diagnosed after pathological analysis, biopsy and serological examination. Therefore, PET/CT examination is necessary for patients with cat scratch disease, and lymphoma and other diseases should be excluded.

References

1. Jidong L, Jianfu S, Bing L. Faciocervical lymphadenitis. Chin Pract J Rural Doct. 2017;24(2):13–4.
2. Liang Y, Dehong L, Yanfeng Z, et al. Diagnostic value of energy spectrum parameters in different lymphatic gland lesions in neck. J Med Imaging. 2015;25(12):2095–9.
3. Alamolhoda F, Faeghi F, Bakhshandeh M, et al. Diagnostic value of diffusion weighted magnetic resonance imaging in evaluation of metastatic neck lymph nodes in head and neck cancer: a sample of iranian patient. Asian Pac J Cancer Prev. 2019;20(6):1789–95.
4. Bo W, Hongna T, Pange W, et al. Prediction of rabbit axillary lymph node properties by one-stop CT perfusion imaging. Chin J Med Imag Technol. 2019;35(02):20–5.
5. Juan W, Chunhong W, Yibing L, et al. Value of elasticity imaging combined with cervical lymph node ultrasonography in differential diagnosis of benign and malignant thyroid gland nodules. J Clin Ultrasound Med. 2016;18(10):670–2.
6. Ludwig BJ, Wang J, Nadgir RN, et al. Imaging of cervical lymphadeno-pathy in children and young adults. AJR Am J Roentgenol. 2012;199(11):1105–13.
7. Yingying D, Kun L, Yongping W. CT diagnosis of reactive proliferation of lymph nodes. J Pract Radiol. 2006;22(5):584–6.
8. Shuixing Z, Ganjun J, Zhongping Z, et al. Differential diagnosis of nasopharyngeal carcinoma and inflammatory hyperplastic diseases by diffusion weighted imaging based on irrelevant motion in voxels. Chin J Radiol. 2013;47(7):617–21.
9. Tzankov A, Dirnhofer S. A pattern-based approach to reactive lympha-denopathies. Semin Diagn Pathol. 2018;35(1):4–19.
10. Zhou W, Gong L, Zuo C, et al. Typical and atypical 18FDG PET/CT findings in two cases of cat scratch disease. Clin Nucl Med. 2019;44(6):388–91.

Other Common Lesions

32

Zujiang Xiong, Heng Liu, Tao Wang, Jing Zhang, Min Tang, Hui Dai, Mengmeng Yu, Xuedong Bai, Haorong Zhang, and Bangguo Li

32.1 Branchial Cleft Cyst with Infection

32.1.1 Overview

Branchial cleft cyst (BCC) is a congenital disease, which is caused by the failure of normal fusion or atresia of the branchial arch and branchial cleft during embryonic development. In the third week of embryo development, there are five pairs of lateral arches, and the depression between the branchial arches is called branchial cleft. When the branchial arch is not fully developed, it may have various deformities. Branchial cleft cyst will occur if branchial cleft ostiole heals and branchial cleft does not heal, and branchial fistula will form if branchial cleft ostiole and branchial cleft do not disappear.

The abnormal development of branchial apparatus structure includes three forms: branchial fistula, branchial sinus, and branchial cleft cyst, among which the opening at both ends of the pharynx and lateral neck is called branchial fistula; the opening only at one end of the pharynx or lateral neck skin is called branchial sinus; in case no opening at both ends, the epithelial cavity remaining in the tissue with secretion retention will form branchial cleft cyst. Because the formation of branchial cleft cyst takes a relatively long time and process, it is often found in young and middle-aged people, while branchial fistula and branchial sinus are mostly found in infancy. The main symptom of branchial cleft cyst is painless masses in the neck or parotid gland region, which are variable in size and can grow slowly. When the mass suddenly increases with redness and pain, the infection should be considered.

The branchial cleft cysts are divided into the first, second, third, and fourth branchial cleft cysts according to their sources and locations. The second branchial cleft cyst is mostly found in clinical practice, followed by the first branchial cleft cyst, and the third and fourth branchial cleft cysts are rare. The first branchial cleft cyst originates from the superficial pharyngeal bursa of the first branchial groove, manifesting as cystic mass posterior to the auricle or around the parotid gland, with a clear margin, accounting for 5–7% of all branchial cleft cysts [1]. The second branchial cleft cyst is formed by the abnormal evolution of the second branchial groove and pharyngeal bursa, which can be divided into four types according to their anatomical positions: type I is located in the anterior border of sternocleidomastoid and deep surface of platysma; type II is the most common, located on the superficial surface of sternocleidomastoid, lateral carotid space and posterior to submandibular gland; type III is located between carotid bifurcation, external carotid artery and lateral pharyngeal wall; and type IV is located in the pharyngeal mucosa space. The third and fourth branchial cleft cysts are mostly located in the inferior neck, and the cyst wall can contain residual thyroid gland and thymus tissues. When it is found that the external fistula orifice is located on the anterior inferior border of sternocleidomastoid and the internal fistula orifice is located in piriform recess or upper esophagus, it indicates congenital dysplasia or fistula formation. Because of its course adjacent to thyroid gland, it is the most common infection route leading to acute thyroiditis.

Z. Xiong
Chongqing Fifth People's Hospital, Chongqing, China

H. Liu (✉) · H. Dai · B. Li
Affiliated Hospital of Zunyi Medical University, Zunyi, China

T. Wang · J. Zhang
The First Affiliated Hospital of USTC (Anhui Provincial Cancer Hospital), Hefei, China

M. Tang
Shanxi Provincial People's Hospital, Taiyuan, China

M. Yu
Binzhou Medical University Hospital, Binzhou, China

X. Bai
Affiliated Hospital of Chengde Medical University, Chengde, China

H. Zhang
Children's Hospital of Shanghai, Shanghai, China

H. Li et al. (eds.), *Radiology of Infectious and Inflammatory Diseases - Volume 2*,
https://doi.org/10.1007/978-981-16-8841-6_32

32.1.2 Pathology Findings

The first branchial cleft cyst shows cystic mass posterior to auricle or around parotid gland with clear margin. The second branchial cleft cyst shows a cyst on lateral carotid sheath and branchial cleft with clear margin. Microscopically, it is mainly composed of vascular sinuses varied in sizes and shapes, which are lined with thin and flat endothelial cells, and the stroma is fibrous tissue, often with hyaline degeneration. In some cases, the above epitheliums exist simultaneously, and squamous epithelium may be complicated with keratinization. Except for the first branchial cleft cyst, all the cysts are rich in diffuse lymphoid tissues, even complicated with the formation of lymphoid follicles and germinal centers.

32.1.3 Imaging Findings

1. CT Examination It shows that branchial cleft cyst occurs in special locations, mostly manifesting as quasi-circular or oval cystic masses on the course along the sternocleidomastoid, especially the second branchial cleft cyst on the superficial surface of sternocleidomastoid and the lateral area of carotid space. The density in the cyst is generally homogeneous. However, due to the different contents in the cystic cavity (mucus, cholesterol crystals, cell debris, lymphocytes and epithelioid cells), the CT value is different, and the cyst wall is generally thin or even cannot be shown, so no enhancement is found in the cyst by enhanced scan, and the cyst wall may have mild enhancement (Fig. 32.1). Branchial cleft cyst with infection manifests as increased density of cyst contents, thickened cyst wall marked enhancement (Fig. 32.2), and blurred fat space around the cyst; The liquid plane is found when the infection causes intracapsular hemorrhage. The first branchial cleft cyst usually appears in the scope from the external auditory canal to the hyoid bone plane, which can manifest as a solid cystic mass, and the surrounding margin is unclear when infection occurs (Fig. 32.3). Third, branchial cleft cyst is rare, fistula usually communicates with piriform recess, which can be combined with piriform recess to be constricted or even disappeared. Gas density shadows are found in the low-density focus adjacent to thyroid gland or on medial sternocleidomastoid, and the margin with peripheral tissues is

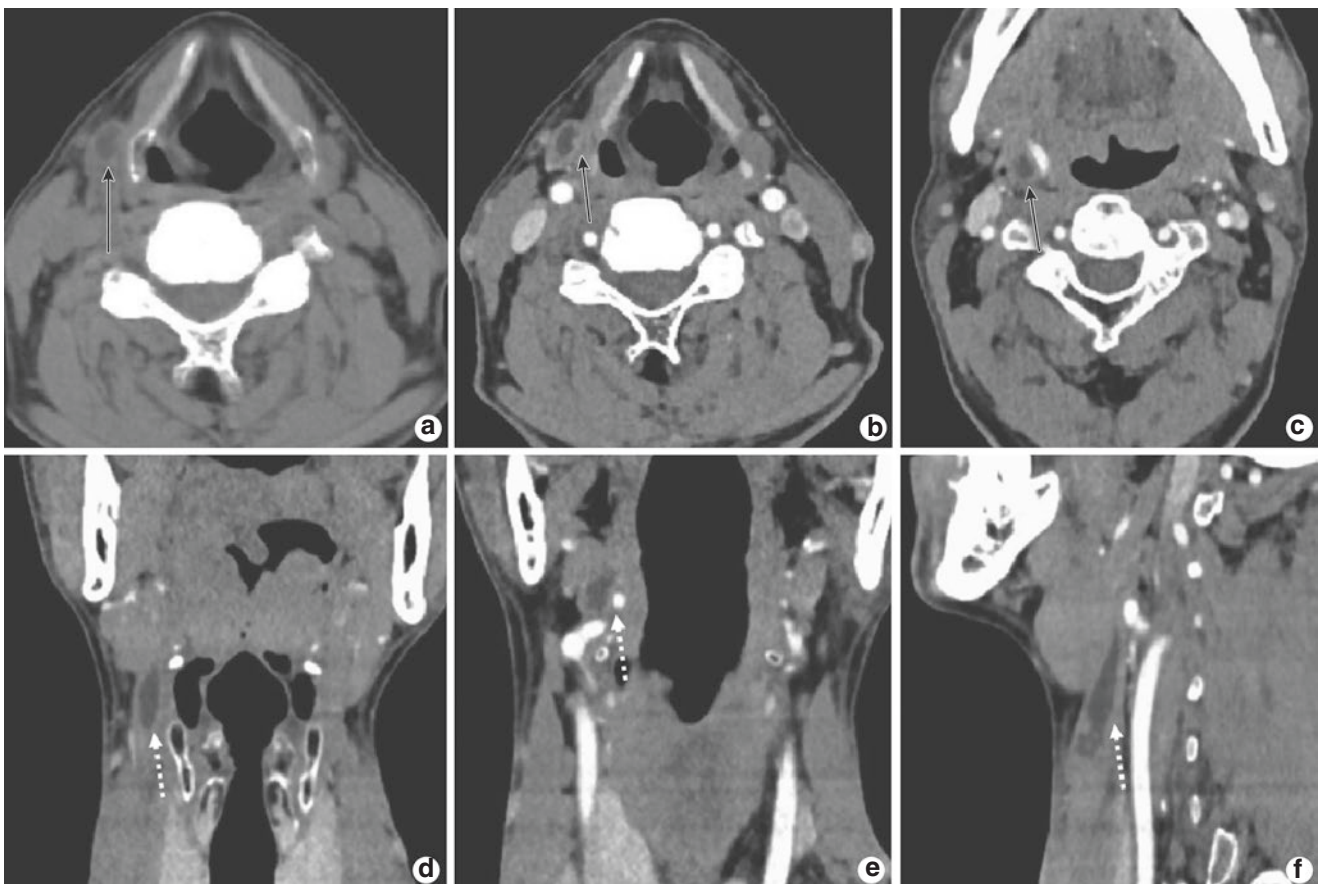

Fig. 32.1 Second branchial cleft cyst. (**a**) Non-enhanced CT scan indicates the right sternocleidomastoid and the strip cystic solid tumor anterior to the carotid sheath, with low-density shadows in the capsule (solid arrow); (**b**–**f**) CT enhanced scan indicates that the cystic wall of the lesion is partially enhanced (solid arrow and punctate arrow)

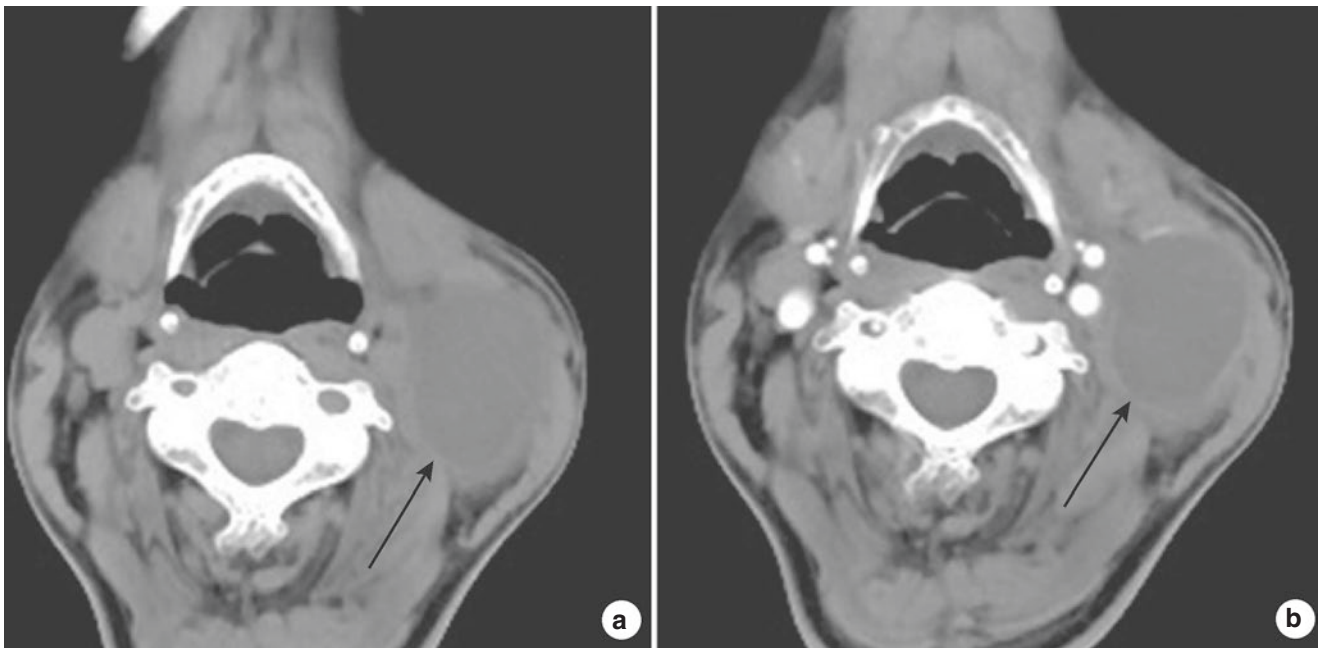

Fig. 32.2 Second branchial cleft cyst with infection. (**a**) Non-enhanced CT scan indicates a cystic mass on the medial left sternocleidomastoid, with thick cystic wall, blurred peripheral shadows, and homogeneous density (indicated by arrow); (**b**) CT enhanced scan shows partial enhancement of the cystic wall of the lesion; The left extracranial internal carotid artery moved to medial area (indicated by arrow)

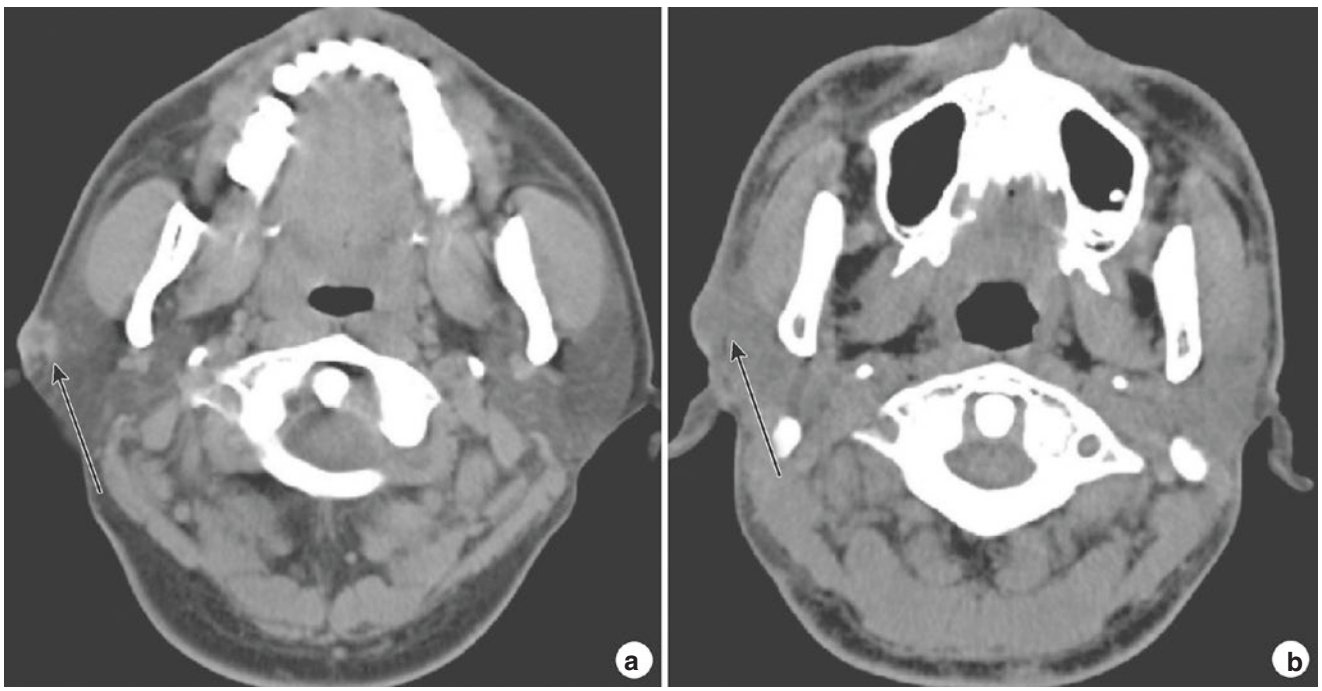

Fig. 32.3 First branchial cleft cyst with infection. (**a**, **b**) Non-enhanced CT scan indicates cystic and solid nodules posterior to the right external auditory canal with slightly low-density shadows (indicated by arrow)

unclear. Ring enhancement is found by enhanced scan, without enhancement in the middle low-density foci (Figs. 32.4 and 32.5). When complicated with thyroid gland inflammation, it may show heterogeneous density, and by enhanced scan, there is a region of decreased enhancement (Fig. 32.6).

2. MRI Examination It has high resolution in soft tissue examination, has the ability of imaging in any plane, and can clearly show the location, scope, size, and margin of branchial cleft cyst. When the cyst is complicated with infection, it is more accurate to show the inflammatory lesions around the cyst wall. Simple branchial cleft cyst usually shows

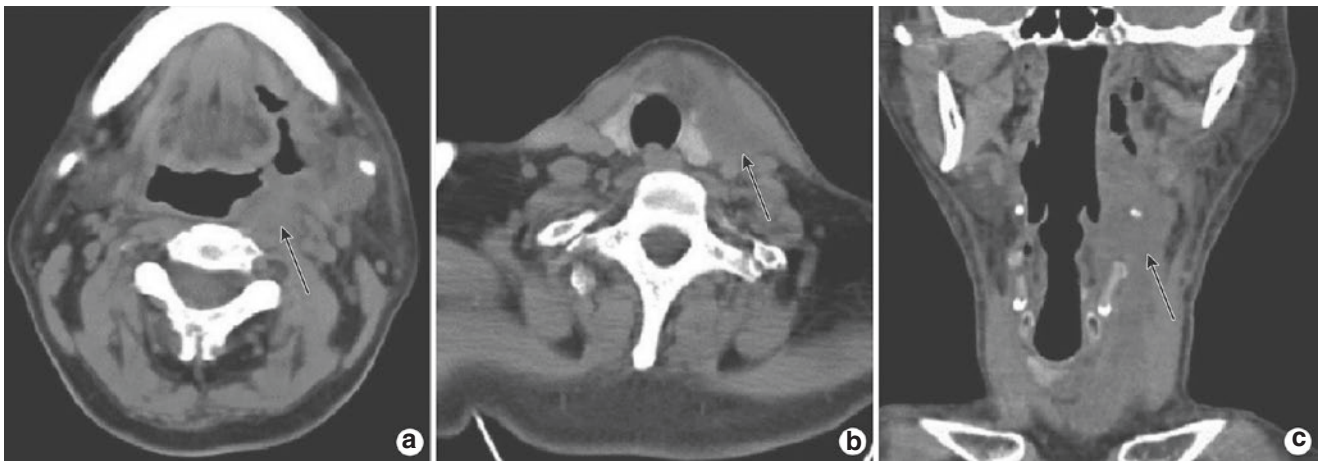

Fig. 32.4 Third branchial cleft cyst with infection and fistula formation. (**a**) Non-enhanced CT scan indicates swelling of the left parapharyngeal space (indicated by arrow); (**b**) Non-enhanced CT scan indicates cystic lesions in the left lobe of thyroid gland and beside isthmus, with high-density and blurred margin (indicated by arrow); (**c**) Coronal CT reformation shows the whole course of fistula, the internal fistula orifice is located in piriform recess, and the inferior border of cyst is located in the supraclavicular area of the lower neck

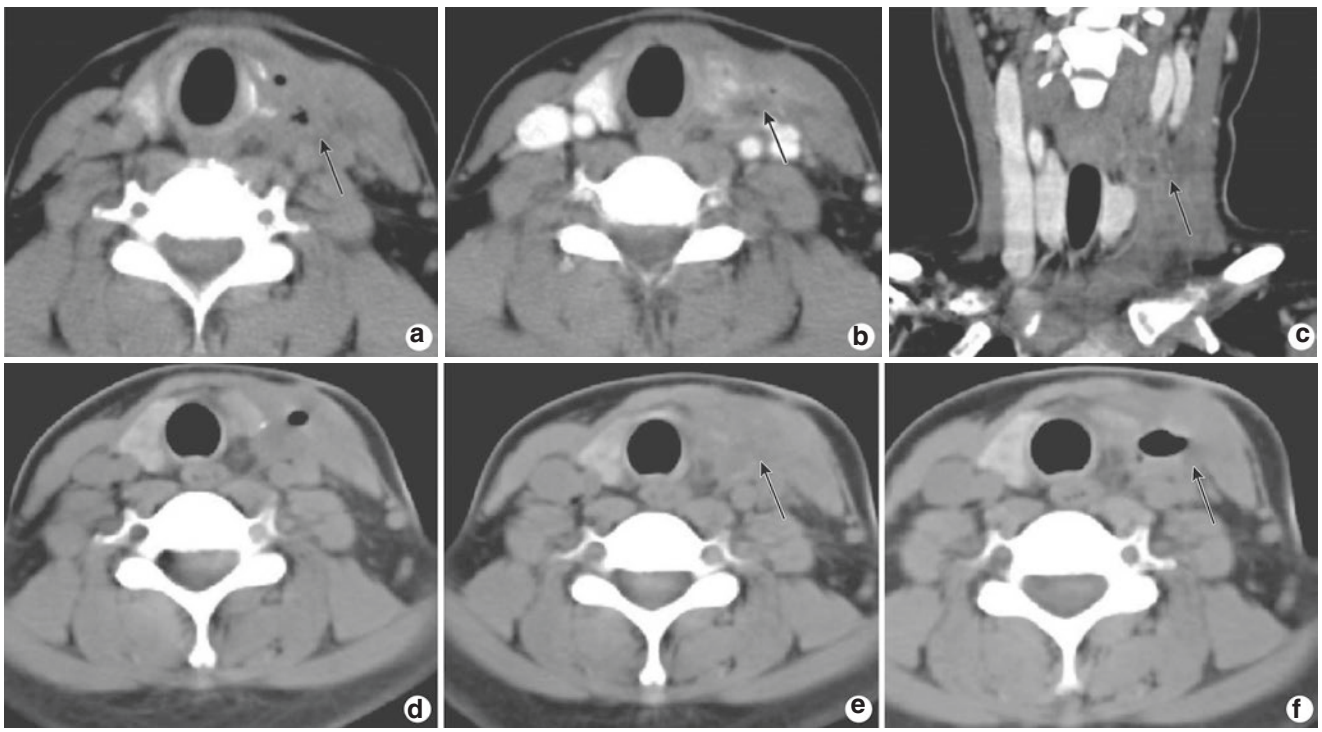

Fig. 32.5 Fourth branchial cleft cyst with infection. (**a**–**c**) Non-enhanced CT scan indicates lateral cystic mass of the medial thyroid cartilage plate of the left thoracic mastoid process muscle, with irregular shape and blurred border. Gas density shadows and low-density shadows are found in it, with partial enhancement by enhanced scan, but the low-density shadows in it are not enhanced (indicated by arrow) (**d**) Branchial fistula resection is performed, and the pathology is branchial fistula infection; (**e, f**) Reoccurred after 1 year (indicated by arrow)

hypointense on T_1WI and hyperintense on T_2WI changes, and the thickness of cyst wall is homogeneous. With the different components in the cystic cavity, the signal performance is different; When secondary infection occurs, the capsule wall is thickened with marked enhancement, with edema and inflammatory exudation around it (Fig. 32.7).

32.1.4 Key Points of Diagnosis

1. In the young and middle-aged period, soft mass of neck appears, which increases after upper respiratory tract infection. Fever with local pain can contract after antibiotic treatment.

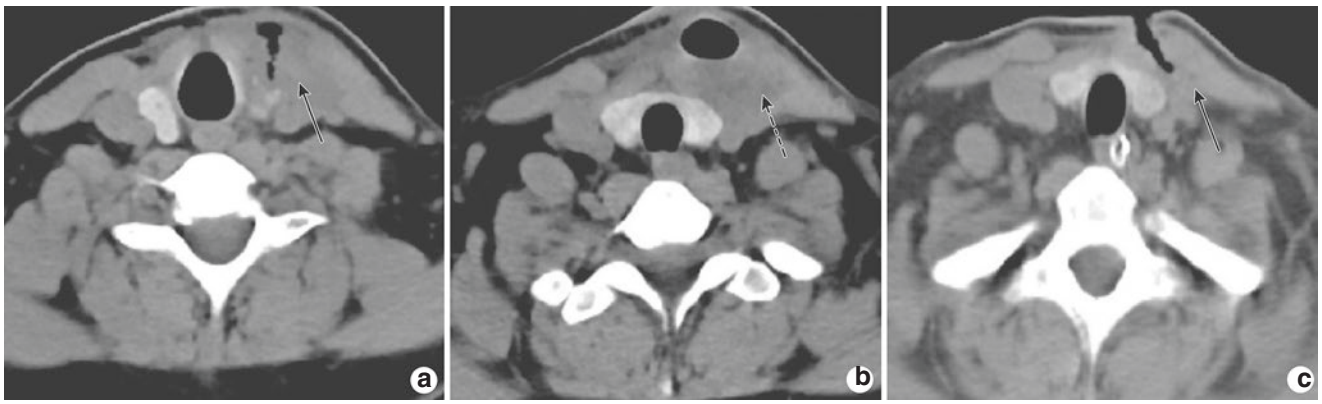

Fig. 32.6 Fourth branchial cleft cyst with pneumatosis. (**a**, **b**) Non-enhanced CT scan indicates cystic mass anterior to thyroid gland in the medial side of left thoracic mastoid process muscle with irregular shape and heterogeneous thyroid gland density (solid arrow and punctate arrow); (**c**) Incision and drainage of anterior cervical abscess (indicated by arrow) is performed, and the bacteria cultured are Streptococcus A

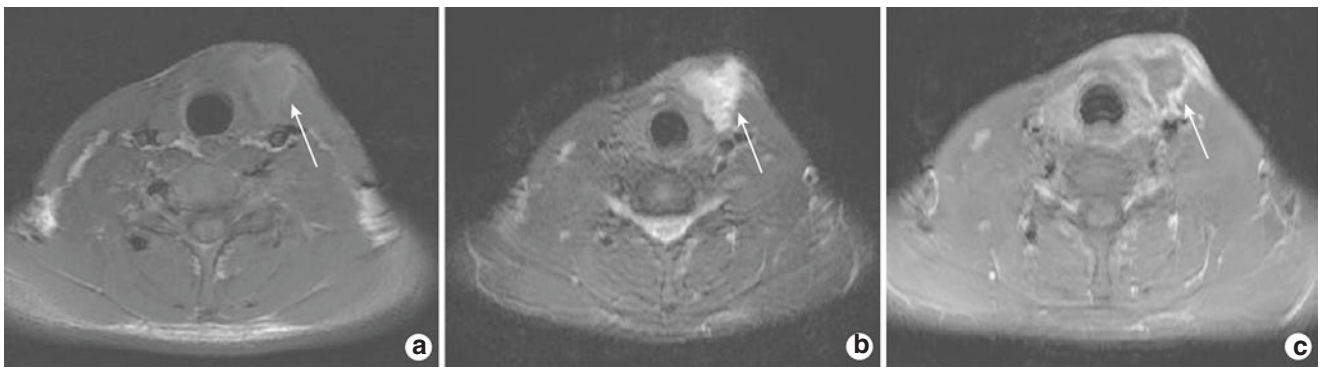

Fig. 32.7 Third branchial cleft cyst with infection. (**a**) Non-enhanced MRI scan shows left second branchial cleft cyst with isointense on T_1WI sequence, irregular shape, hyperintense of the cyst wall with unclear margin (indicated by arrow); (**b**) Non-enhanced MRI scan shows hyperintense on T_2WI fat-suppressed sequence for capsule wall and capsule contents (indicated by arrow). (**c**) Non-enhanced MRI scan and T_1WI enhanced scan indicate the capsule wall thickened with marked enhancement, with surrounding edema and inflammatory exudation, and the capsule contents are not enhanced (indicated by arrow)

2. Specific predilection site, the cystic mass is located in parotid gland with course along sternocleidomastoid, and extracranial internal carotid artery moves to the medial area.
3. Non-infectious lesions are thin-walled smooth cysts, but after secondary infection, the cystic wall is irregularly thickened and marked enhancement, and the peripheral fat space is blurred.

32.1.5 Differential Diagnosis

1. Thyroglossal Duct Cyst It is common in the midline of neck at hyoid bone level, and it is found in clinical examination that the lesion moves up and down with swallowing and tongue extension.

2. Cervical Lymphangioma It usually occurs in children under 2 years old. Because of the cystic mass formed by lymphatic dilatation, the disease is usually located in the posterior triangle of the neck. The mass is large, irregular in shape, with multiple septa, which manifests as creeping development toward the surrounding structural space.

3. Cervical Lymph Node Tuberculosis It generally has a history of tuberculosis and is frequent, and the enlarged lymph nodes grow slowly, and tuberculin test can be positive. When psychrapostema is formed, caseous necrotic pus can be extracted by aspiration, and the experimental treatment with antituberculosis drugs is effective.

4. Schwannoma It is mostly located in carotid sheath, and the larger ones may be complicated with cystic degeneration, but there are still solid components, which are marked enhancement after injection of contrast agent.

32.1.6 Status Quo and Progress of Research

Ultrasonography is a routine and convenient examination method with relatively high accuracy. The echographic features also reflect the characteristics of fibrous capsule wall coating epithelium to a certain extent, and the echographic features are related to its intracapsular components. When the cyst is lined with pseudo-stratified ciliated columnar epithelium and the contents are transparent mucus or serous fluid, the sonogram usually shows clear fluid sonolucent area, and occasionally fine septa light band; When squamous epithelium is lined, keratinized and infected exfoliated epithelium increases, and its contents are opaque turbid liquid or emulsion. At this time, the sonogram mostly shows unclear fluid sonolucent area, complicated with dim and thick spots with different numbers [2]. When chronic infection occurs for a long time, and the cystic fluid is concentrated and thickened, relying solely on ultrasonography may lead to higher misdiagnosis and missed diagnosis rate.

The accuracy of CT and MRI examination is higher than that of conventional ultrasonography. Especially, magnetic resonance parotid gland duct imaging and other technologies have become a research hotspot in the imaging diagnosis of head and neck in recent years. The application of new technologies can help us to obtain information on the hemodynamic state of tissues and organs and lesions and the internal fine structure of lesions. CT and MRI examinations mainly confirm whether branchial cleft cyst is complicated with infection, the location and depth of infection, which provide information for clinical operation. In particular, magnetic resonance duct imaging technology can accurately show the structure of branchial cleft cyst and fistula, and make clear the course and opening position of fistula, so as to help surgeons make a reasonable operative plan [3].

32.2 Postoperative and Post-Radiotherapy Cervical Infections

32.2.1 Overview

Postoperative infection refers to the infection occurring at or near the surgical incision within 1 month after operation. According to different infection sites, it can be divided into deep incision infection, superficial incision infection, and organ cavity infection. Due to the surgical treatment, repeated radiotherapy, chemotherapy, and immunotherapy, the physique and immunity of tumor patients are decreased, and various nosocomial infections are prone to occur. Infection after operation and radiotherapy may also be associated with factors such as nonstandard aseptic operation, long-term placement of intravenous indwelling needle, repeated aspiration causing damage to the medial wall of blood vessel and subcutaneous tissue of patients, and poor permeability of the exposed duct and dressing at the place where the duct is placed, which weakens the sterile protective barrier of the body and creates conditions for bacteria to invade the body [4].

Diagnostic criteria for postoperative infection in different sites are as follows:

1. Superficial surgical incision infection: it only involves skin and subcutaneous, and superficial incision has red, swelling, hot, painful, or purulent secretion, and bacterial culture is positive.
2. Deep surgical incision infection: pus is extracted or drained from the deep incision. Abscess or other evidence of infection involving the deep incision is found, and bacterial culture is positive.
3. Organ and lacuna infection: It can be diagnosed according to one of the following: (1) Pathology or imaging examination found evidence of organ/lacuna infection; (2) Pus obtained by drainage or aspiration; (3) Pathogenic bacterioscopy result is positive [5].

32.2.2 Pathology Findings

In early stage of infection, neutrophil infiltration, edema, hemorrhage, necrosis of striated muscle and abscess formation occurs in the lesions. With the development of the disease, neutrophil infiltration and tissue necrosis become more severe, and then neutrophils disintegrate, cell fragments increase, fibroblasts proliferate, abscesses are wrapped to form abscess walls. In chronic stage, the abscess wall is repaired by fibrous tissue and granulation tissue.

32.2.3 Imaging Findings

In the operation area or radiotherapy area, soft tissue swelling, intermuscular space effusion and muscle edema, subcutaneous fat space changes in a grid shape, soft tissue swells in CT with low density, MRI with hypointense on T_1WI and hyperintense on T_2WI, interstitial effusion with water-like density or signal, abscess formation in focus area, DWI of vomica content with hyperintense, enhanced scan with ring enhancement, smooth wall and homogeneous wall thickness (Fig. 32.8).

32.2.4 Key Points of Diagnosis

1. Within 1 month after surgery and radiotherapy, pus secretion appears in the operation area, or pathogens are cultivated in the secretion, or symptoms and signs of redness, swelling, fever, and pain appear.

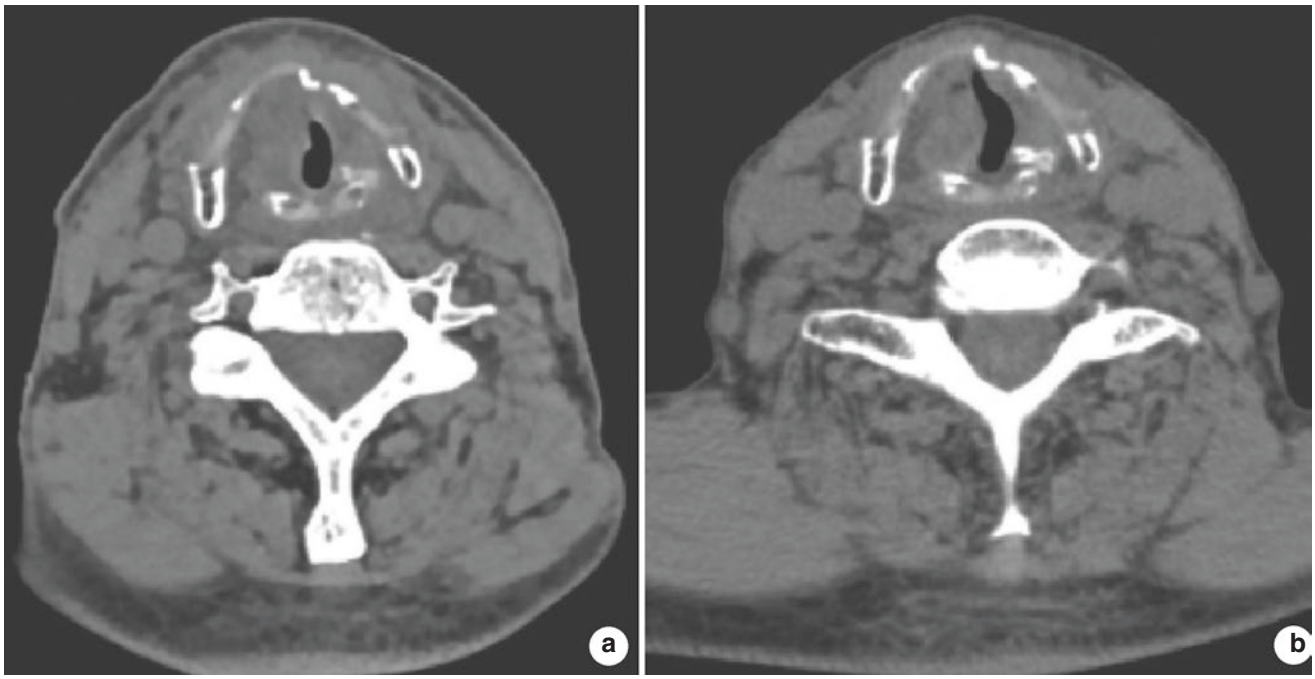

Fig. 32.8 Postoperative radiotherapy for laryngeal cancer. (**a**) Non-enhanced CT scan of right vocal cord tumor; (**b**) Swelling of vocal cords and peripheral soft tissues after radiotherapy

2. After operation and radiotherapy, the soft tissues swell extensively, the intermuscular space has effusion, the fat layer is blurred, the CT shows low density, MRI shows hypointense on T_1WI and hyperintense on T_2WI, and the abscess formation shows ring enhancement with homogeneous wall and thickness and air-fluid level by enhanced scan.

32.2.5 Differential Diagnosis

Soft tissue edema mainly manifests as subcutaneous and intermuscular space soft tissue swelling, without necrosis and hemorrhage, enhancement without enhancement, and clinical symptoms without redness, swelling, fever, and pain.

32.2.6 Status Quo and Progress of Research

With the progress and perfection of surgical aseptic technique, the overall incidence of postoperative infection is gradually reduced under control, but it cannot be completely avoided. The main reasons for the significant increase of mortality and disability rate of patients include the difficulty in obtaining etiological evidence after surgery and radiotherapy in early stage, dependence on empirical drugs, and increased permeability of blood–brain barrier. Once infection occurs, how to effectively control infection and reduce complications has always been highly valued. Ultrasonography, CT, and MRI can evaluate the infection after operation and radiotherapy, and MRI can sensitively show the focus scope. However, infection after operation and radiotherapy often overlaps with simple soft-tissue edema after operation and radiotherapy, which needs to be judged by combining clinical manifestations and related laboratory test results.

32.3 Cervical Necrotizing Fasciitis

32.3.1 Overview

Necrotizing fasciitis is a rare fulminant mixed infectious disease, which only damages subcutaneous tissue and superficial fascia, but does not cause necrosis of infected tissues and muscles [6]. The course of disease progresses rapidly and is in critical condition, often complicated with systemic toxic shock. According to the species of pathogens, the infection can be divided into four types: multi-microorganism synergistic infection, single-strain infection, Gram-negative single strain infection, and Fungal Infection [7]. Its pathogens include Bacteroides, Clostridium, Streptococcus, Proteus, Pseudomonas, Klebsiella pneumoniae, and Staphylococcus aureus. Necrotizing fasciitis is a rare clinical critical illness with rapid progression and high mortality. Accurate diagnosis according to clinical manifestations, laboratory and imaging examination, and timely treatment are the primary factors affecting the prognosis of patients.

32.3.2 Pathology Findings

Necrotizing fasciitis is a soft tissue infection characterized by edema, necrosis, and air generation in subcutaneous soft tissue and fascia. Inflammatory cell infiltration in the focus area and fibrin-like thrombosis of subcutaneous arterioles and venules are pathological signs of necrotizing fasciitis [8].

32.3.3 Imaging Findings

1. Ultrasonography It is an important tool to evaluate the location of soft tissue swelling, tenderness, and abscess in necrotizing fasciitis, which is often used for early diagnosis of necrotizing fasciitis. Ultrasonography often shows edema of skin, diffuse thickening of fascia, irregular shape, and effusion and pneumatosis in the space between fascia surfaces.

2. X-Ray Examination It has a limited diagnostic effect on necrotizing fasciitis, only showing soft tissue thickening, swelling, and pneumatosis.

3. CT Examination It is used to locate infection and define the scope of lesion, and the imaging finding is diffuse edema of skin and subcutaneous tissue; Subcutaneous fat shows cord-like and reticular enhancement. Thickening and enhancement of fascia; Pneumatosis in soft tissue; Multiple effusion in different anatomical spaces; Asymmetric muscle enhancement. With the progression of the disease, the muscles show thickening and destruction to different extents, and the contrast agent is rapidly extravasated. Image shows leakage of contrast agent entering the intermuscular space. Internal carotid artery and/or deep venous thrombosis; Reactive enlargement of lymph nodes (Fig. 32.9).

4. MRI Examination It has high soft-tissue contrast, which can show subtle signal changes of soft tissue including skin, subcutaneous fat, deep and superficial fascia and muscle, and can determine the location and scope of lesions, and determine the best biopsy location and detection effect. Imaging findings are subcutaneous tissue and deep and superficial fascia thickened, showing hypointense on T_1WI and hyperintense on T_2WI. An enhanced scan can differentiate necrotic tissue from inflammatory tissue, and necrotic tissue is not enhanced, but inflammatory tissue has marked enhancement; extravasation of the contrast agent is an important sign to clarify the invasion of the lesion; the extent and degree of muscle enhancement are related to the severity of lesion involvement.

32.3.4 Key Points of Diagnosis

1. Clinical Manifestation Rapid onset, complicated with redness, swelling, fever, and pain, and the infection index in laboratory test is increased.

2. Imaging Examination It shows large edema of skin and subcutaneous tissue, thickening and enhancement of fascia, pneumatosis in soft tissue, intermuscular space effusion, and less muscle involvement than subcutaneous soft tissue.

3. Soft Tissue Biopsy It shows inflammatory cell infiltration in subcutaneous soft tissue and fibrin-like thrombosis in subcutaneous arterioles and venules.

32.3.5 Differential Diagnosis

1. Cellulitis It only involves subcutaneous tissue, but not fascia. Imaging findings include edema of subcutaneous tissue, increased density of adipose tissue, and irregular enhancement of stripes, with or without subcutaneous and superficial fascia effusion, and normal deep structure.

2. Myositis and Nongangrenous Myonecrosis They manifest as muscle thickening, with or without heterogeneous enhancement by enhanced scan. Myonecrosis manifests as low-density area or muscle rupture in muscle enhancement part.

3. Fasciitis-Panniculitis Syndrome It has chronic onset, with swelling and scleroma of skin and soft tissue fascia, and the forearm and leg are mostly involved [9].

4. Soft Tissue Edema It is often complicated with cardiac and renal insufficiency, with symmetrical distribution of edema and diffuse fat strip shadow.

32.3.6 Status Quo and Progress of Research

MRI has high soft-tissue resolution and can be used for multi-parameter and multi-sequence imaging, among which DWI sequence can sensitively differentiate soft tissue edema and abscess. Due to the diffusion limitation of water molecules caused by necrotic debris and pus cells in pus, DWI shows significantly hyperintense, while the diffusion of edema area is not limited, and DWI shows isointense. MRI examination can define the focus area, guide aspiration and monitoring treatment, and is of great value in improving the cure rate and survival rate of necrotizing fasciitis patients.

32.4 Thyroglossal Duct Cyst with Infection

32.4.1 Overview

Thyroglossal duct cyst, also known as lingual nail cyst, is a congenital cyst, which is related to the development of thyroid gland and tongue. The thyroglossal duct starts from the thyroid gland primordia, and the primordial tissue begins

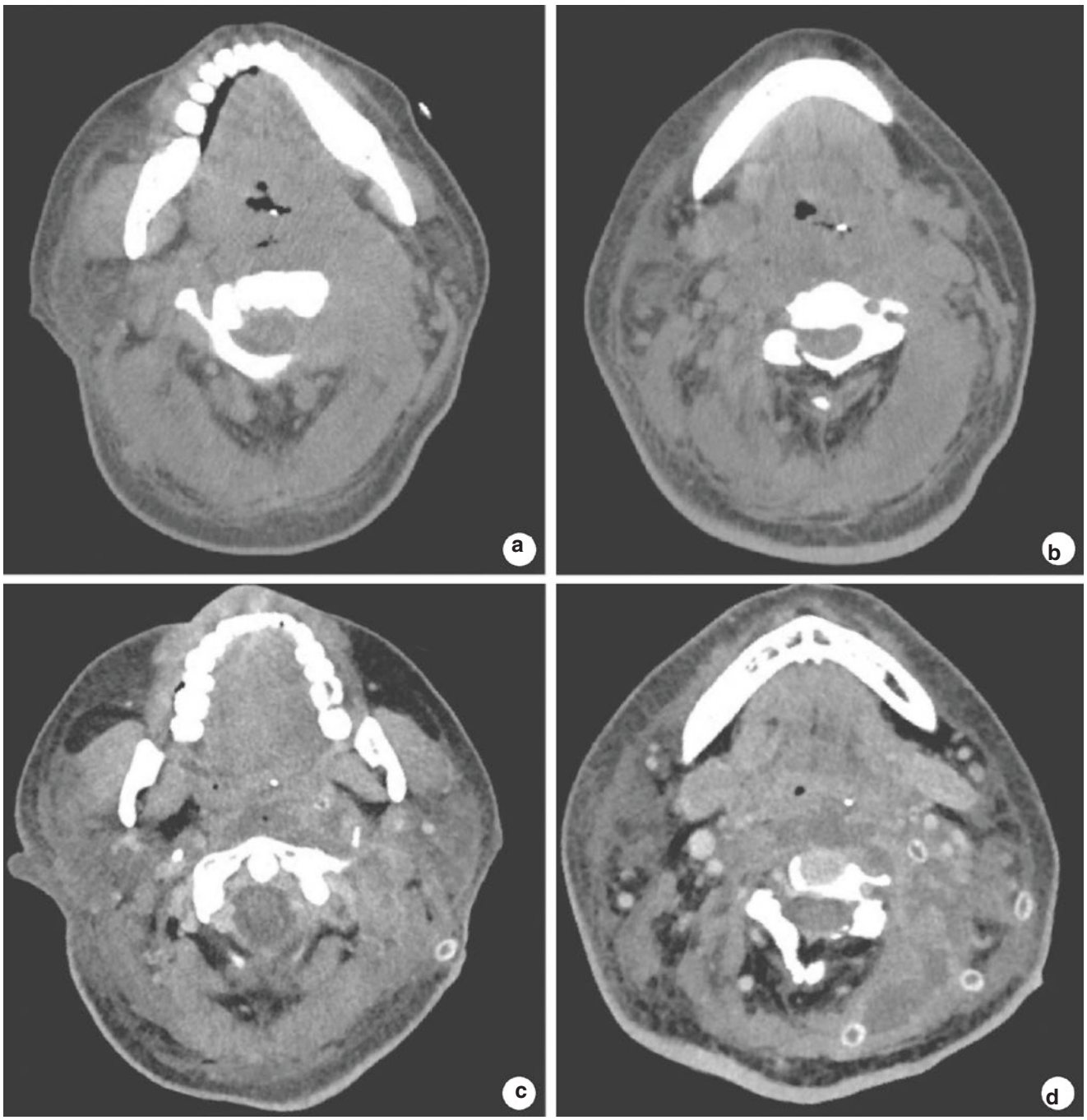

Fig. 32.9 Necrotizing fasciitis with retropharyngeal abscess. (**a, b**) Non-enhanced CT scan indicates diffuse edema of skin and subcutaneous tissue, thickening of fascia, pneumatosis in soft tissue, and reactive swelling of lymph nodes; (**c**, **d**) CT enhanced scan indicates that subcutaneous fat is enhanced in a cord-like and reticular pattern, and the lesions grow diffusely along the left posterior cervical space and retropharyngeal space

to descend at the fourth week of embryo and develops into the thyroglossal duct or thyroid gland capsule, which ends at the foramen cecum of tongue and develops into the thyroid gland at the inferior part. The thyroglossal duct should be closed after descending to the neck in the sixth week of pregnancy, and the tubular tissue between the thyroid gland and the foramen cecum of the tongue begins to atrophy and degenerate. If the thyroglossal duct does not disappear completely after 10 weeks, it will become residual tubular tissue with different lengths, and then it will develop into thyroglossal duct cyst.

Thyroglossal duct cyst is mostly found in children and adolescents under 15 years old, and one-third of the patients are born with the disease. Cysts are mostly located between the thyroid gland and hyoid bone in the anterior middle of the neck, and are most common up and down the hyoid bone,

with a diameter of 2–3 cm. The cysts are soft and have clear margin, and have no adhesion with the surface skin and peripheral tissues. During examination, the cysts are relatively fixed and cannot move upward and left and right, but the masses can move upward when swallowing or extending the tongue. If the cyst is located near the foramen cecum of the tongue, when it develops to a certain extent, it can raise the base of the tongue and cause swallowing and speech dysfunction. If secondary infection may be complicated with local epidermal redness and swelling, the lump will adhere to the skin; If the cyst is perforated, thyrohyoid fistula will be formed, and the fistula will not heal for a long time [10].

32.4.2 Pathology Findings

Most lesions of thyrohyoid cyst have a complete capsule, and the capsule wall is thin, which is surrounded by fibrous tissue. The medial wall of the capsule can be lined with pseudostratified ciliated columnar epithelium, squamous epithelium, stratified squamous epithelium, etc. There are abundant lymphoid tissues in the epithelium, thyroid gland tissues are found under the skin, and inflammatory cells can be found in the infected person. Most of the capsule contents are clear and thin liquid, and occasionally they may be mucus-like or jelly-like substances, which contain protein or cholesterol.

32.4.3 Imaging Findings

Thyroglossal duct cyst is the second most common benign lesion in the neck, which occurs in the specific area from the tongue root to the jugular vein notch in the anterior middle of the neck. Thyroglossal duct cyst is usually located in the midline, and a few of them can be deviated unilaterally. It can be divided into the central type and eccentric type according to the position of cyst, and 95% of eccentric lesions are located on the left side. In the relationship with hyoid bone, most lesions are located below hyoid bone, and a few lesions are located on hyoid bone or grow across tongue. Regardless of the lesion site, thyroglossal duct cysts are mostly round or oval lesions, and a few are irregular [11, 12].

1. CT Examination It is of significant value in the diagnosis of thyroglossal duct cyst. CT can determine the location, shape, margin of mass, and its relationship with hyoid bone, and measure the CT value of capsule contents and capsule wall after non-enhanced scan and enhancement. CT findings of thyroglossal duct cyst vary depending on the size, location, infection, and contents of the cyst. Its characteristic manifestations are: oval or round anterior to the neck, and a few are irregular cystic masses, with clear margin, thin capsule wall, and clear margin with the surrounding. The capsule is a homogeneous liquid, and its density can be changed according to the content of protein. If the capsule content contains less protein or cholesterol, the density is lower and the margin with the peripheral structure is clear. If the capsule content contains more protein or is complicated with infection, the density will increase. When infected, the capsule wall can be thickened, and an enhanced scan shows that the capsule wall is enhanced, but the capsule contents are not enhanced. When the mass is large, the adjacent organs may have signs of compression and deviation, and the bone structure is not absorbed or destroyed (Figs. 32.10 and 32.11).

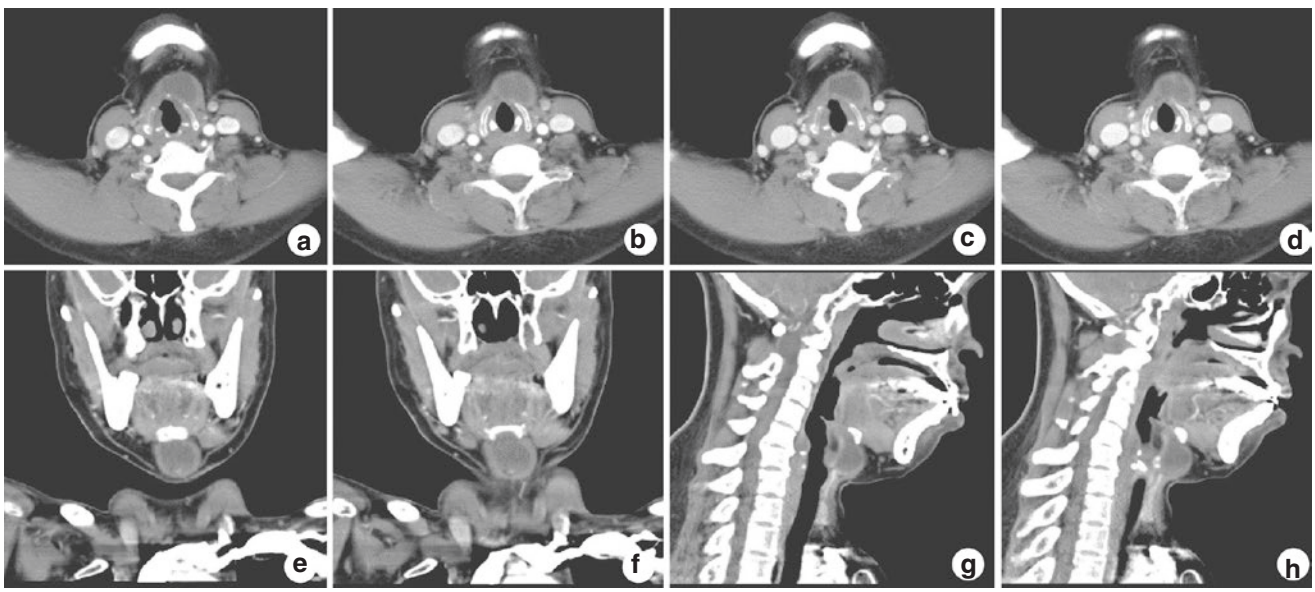

Fig. 32.10 Thyroglossal duct cyst with infection. (**a–h**) CT enhanced examination shows irregular cystic low-density shadows below hyoid bone and to the left of anterior part of thyroid cartilage in arterial and venous phases, and the edge of enhanced lesion has mild enhancement, but the inner low-density area shows no enhancement, the margin is clear, the adjacent structure is compressed, and the thyroid cartilage bone is not involved

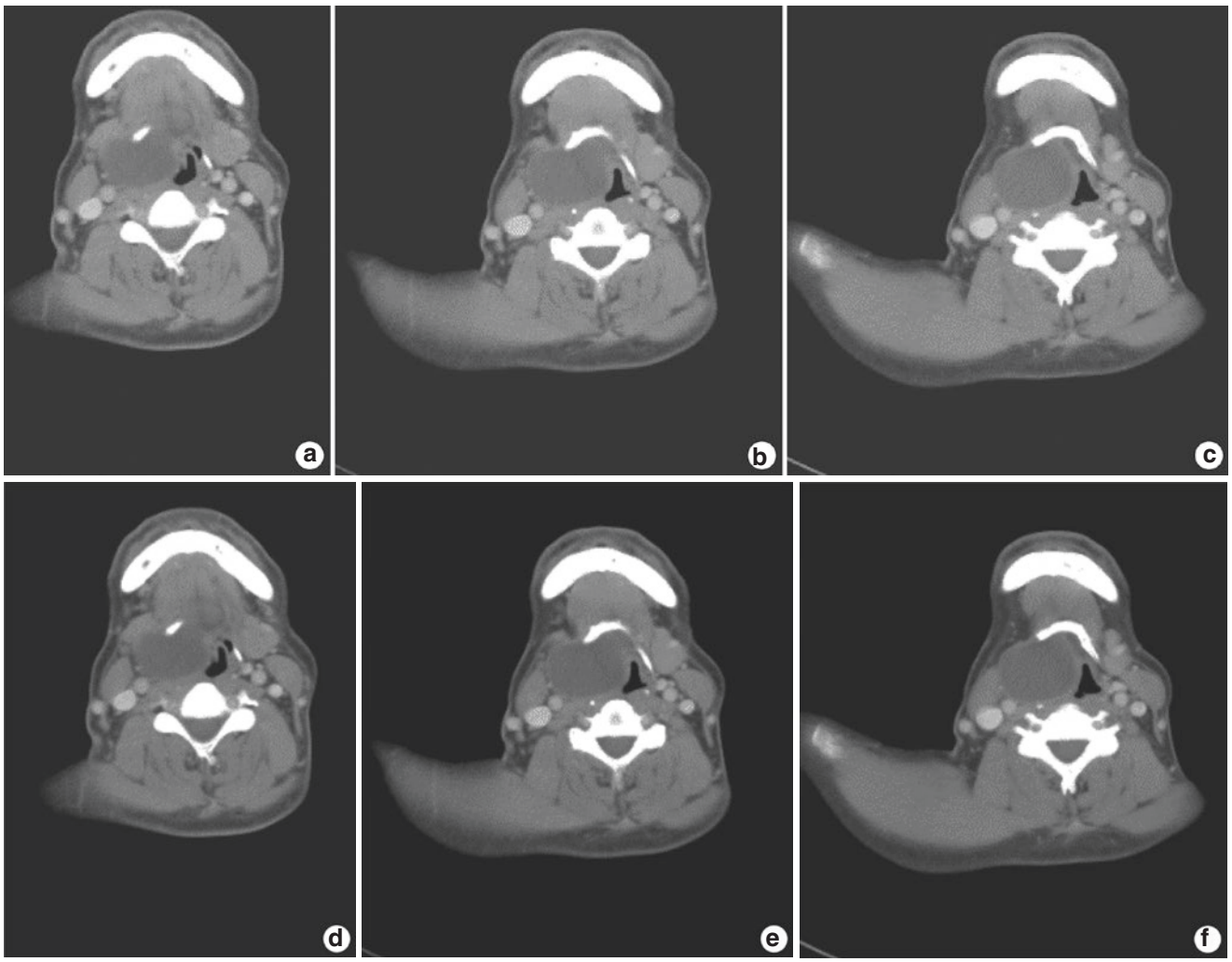

Fig. 32.11 Thyroglossal duct cyst (1). (**a–f**) CT enhanced examination shows irregular cystic low-density shadows on the right side of hyoid bone in arterial and venous phases. The edge of the enhanced lesion seems to have mild enhancement, but the low-density area in it shows no enhancement, and the margin is clear. The lesion grows up and down across hyoid bone, and the adjacent hypopharynx structure is compressed and constricted

2. MRI Examination It has good tissue resolution, can be multi-sequence and multi-directional, can reflect the shape, size, and location of lesions, and show the relationship between lesions and adjacent tissue structures. In addition, MRI can determine the pathological changes of the capsule wall and capsule contents of thyroglossal duct cyst according to the different signals in each sequence [12]. On MRI, thyroglossal duct cyst appears as a round or quasi-circular cystic mass with thin wall and clear margin with the peripheral area. The cyst is filled with homogeneous liquid, and the signal is related to the protein content of its contents. When the capsule is filled with clear, thin liquid and contains less protein substance, it usually shows hypointense on T_1WI and hyperintense on T_2WI, and its internal signal is often homogeneous with a clear margin. When there are more protein, mucus-like, or jelly-like substances in the capsule, it can show slightly hyperintense or hyperintense on T_1WI and isointense, slightly hyperintense or heterogeneous signal on T_2WI. When the capsule wall is thickened and rough as it is complicated with infection, the substance in the capsule often shows isointense or slightly hyperintense on T_1WI and slightly hyperintense or hyperintense on T_2WI. Enhanced scan often has no marked enhancement, in case of infection, irregular enhancement of capsule wall are found; if fistula is formed and fluid in the cyst flows out, the cyst is irregular in shape. With a high content of pus in cyst, DWI manifests as hyperintense (Fig. 32.12).

32.4.4 Key Points of Diagnosis

1. The characteristic features of CT and MRI: the fluid density/cystic signal lesions in the scope from the tongue root to the notch of jugular vein in the anterior middle of the neck, the cystic fluid showing different density/signal due

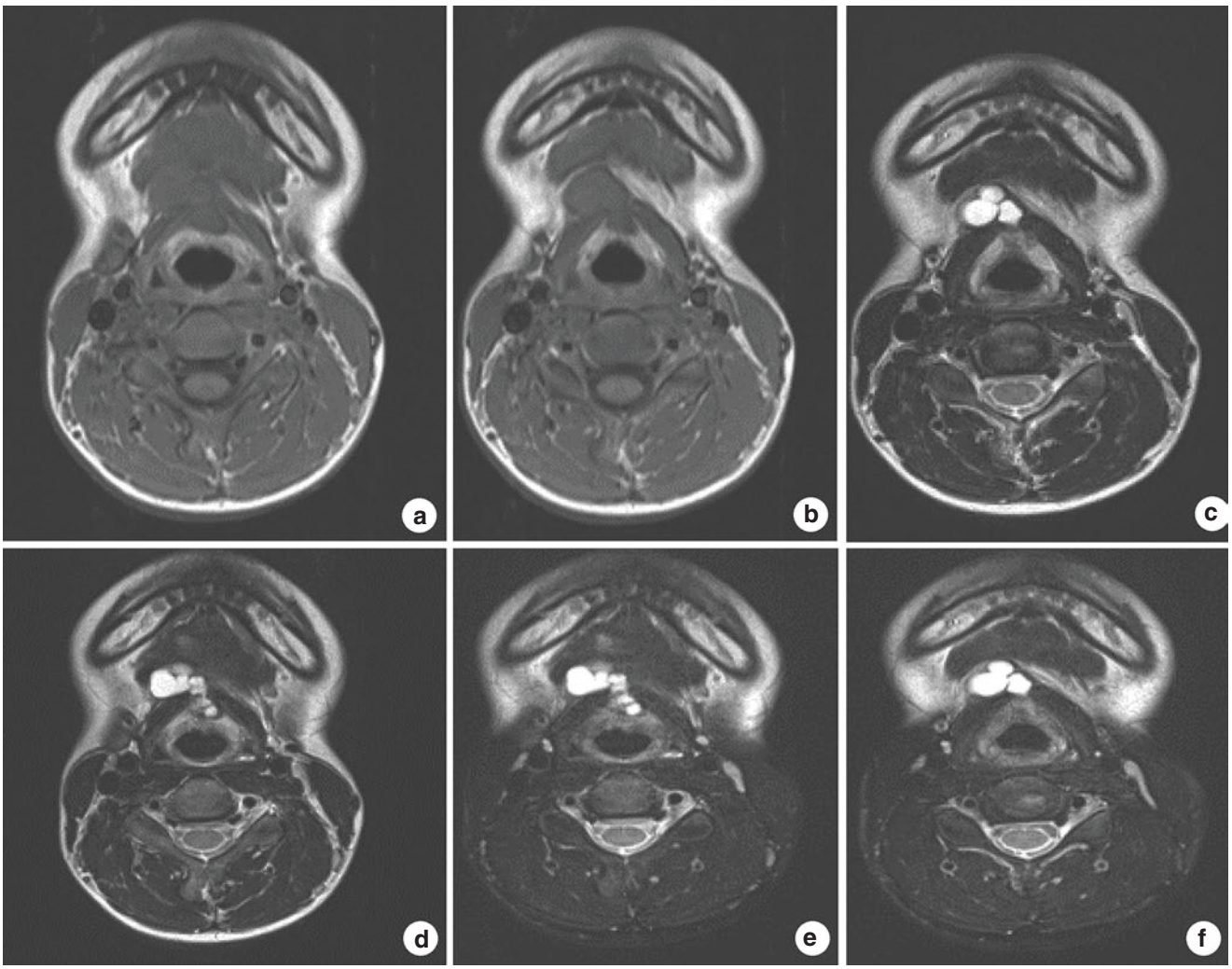

Fig. 32.12 Thyroglossal duct cyst (2). (**a, b**) T_1WI shows multiple utricular hypointense shadows on the right side of the anterior inferior hyoid bone at the root of the tongue. (**c**, **d**) Lesion shows hyperintense on T_2WI. (**e**, **f**) T_2WI fat-suppressed sequence shows the lesion with significantly hyperintense and growing across the hyoid bone, and no significant compression is found in the adjacent larynx cavity structure

to different contents, the cystic wall can be enhanced when it is complicated with infection, and the pus in the cystic fluid shows hyperintense on DWI.
2. It is found at any age, and prone to children under 15 years old.
3. Because it is connected with hyoid bone, the lump can move up and down with swallowing and tongue extension.

32.4.5 Differential Diagnosis

The typical location of thyroglossal duct cyst is an important basis for its diagnosis and differential diagnosis. Clinical diagnosis is not difficult, but it may be confused with other neck diseases and lead to misdiagnosis [13].

1. Anterior Cervical Ectopic Thyroid Gland It can occur anywhere from the foramen cecum of the tongue to the thyroid gland along sternal notch, and is mostly found in the root of the tongue. According to the existence of thyroid gland tissue in normal position of the neck, it can be divided into parathyroid gland and aberrant thyroid gland. If thyroid gland tissue is found in the normal position of the neck, the thyroid gland tissue in other parts is called parathyroid gland; If no thyroid gland tissue is in the normal position of the neck, it is called aberrant thyroid gland. Ectopic thyroid gland shows a soft tissue mass with slightly hard texture and high density, which can move with swallowing. Enhanced scan shows marked enhancement, which is different from thyroglossal duct cyst. If ectopic thyroid gland is suspected, further radionuclide examination is needed to differentiate it.

2. Branchial Cleft Cyst It can be divided into four types according to its development, and the second branchial cleft cyst is the most common. The lesion mainly occurs at the junction of the superior one-third and the inferior two-third of the

sternocleidomastoid, which is mainly differentiated from the thyroglossal duct cysts concentrated unilaterally. The branchial cleft cyst does not move with swallowing, and multiple lymphoid tissues are integrated in the cyst wall and periphery. The CT findings of the two cysts are similar. The MRI findings are liquid signal shadow between submandibular space and carotid space, with clear margin and homogeneous signal, and enhancement is found at the margin of enhanced scan, which can be basically identified according to its location.

3. Dermatoid or Epidermoid Cyst It can occur around hyoid bone, and it is mostly found in the floor of mouth and sublingual area. Because dermoid cyst is not connected with hyoid bone, it cannot move up and down during tongue extension and swallowing. As the lesion contains fat, fur or tooth-bone structure, the density or signal intensity on CT or MRI is variable; the contents of dermoid cyst contain lipids, CT value is often negative, and fat-suppressed sequence is hypointense, which is easy to diagnose; epidermoid cyst contains protein debris and other substances, and its density on CT is slightly higher than that of simple cyst. DWI sequence is sensitive to the diagnosis of epidermoid cyst, with hyperintense on DWI, and ADC indicates hypointense. When the cyst is located in the submaxillary area, it needs to be differentiated from the cyst of mouth floor.

4. Thyroid Gland Isthmus Tumor It mostly shows solid obstructy shadows with calcification, which are always connected with thyroid gland and can be differentiated by radionuclide examination.

5. Laryngeal Cyst It is the pathological expansion of the laryngeal ventricle. When the bursa exceeds the level of thyroid cartilage, it is called laryngeal cyst. Laryngeal cysts can be divided into three types: internal type, external type, and mixed type. The lesion is fixed in the larynx cavity and contained gas. Imaging characteristics are circular or oval masses adjacent to the larynx, containing air and/or liquid. The lesions are different in size, heterogeneous in density and signal, which are related to the endocrine substances in the capsule.

32.4.6 Status Quo and Progress of Research

Typical thyroglossal duct cyst can be diagnosed according to the onset age, symptoms, signs, specific disease location, and imaging findings of patients, and most patients are less than 15 years old. Ultrasound is often used for clinical diagnosis, and CT or MRI can be used for further examination when atypical diseases or complicated infections occur. CT mainly defines the scope of the disease and the relationship between the disease and hyoid bone, and can clearly show whether the disease is complicated with infection (whether the cyst wall is thickened or not). CT also needs to carefully observe whether there are wall nodules. When there are wall nodules in the lesion, it is necessary to be alert to the possibility of thyroglossal duct cancer. At this time, it is necessary to evaluate whether there is lymph node enlargement in the neck.

References

1. Haigang Z, Mingyue F, Xunwu D. Clinical analysis of 25 cases of branchial cleft cyst and fistula. Chin J Otolaryngol Skull Base Surg. 2015;21(6):493–5.
2. Jun G, Qingjiang M, Liqiang S, et al. Comparative analysis of ultrasound diagnosis and surgery pathology of branchial cleft cyst and branchial cleft fistula. Chin J Ultrasound Med. 2002;18(7):552–4.
3. Yun L, Yusheng Y, Jiang L. Clinicopathological analysis of 199 cases of branchial cleft cyst and fistula. China J Oral Maxillofac Surg. 2013;2(23):37–41.
4. Mangram AJ, Horan TC, Pearson ML, et al. Centers for Disease Control and Prevention (CDC) hospital infection control practices advisory committee. Am J Infect Control. 1999;27(2):97–132.
5. Ministry of Health of the People's Republic of China. Standard for Nosocomial Infection Diagnosis (Trial). Natl Med J China. 2001;81(5):314–20.
6. Ozalay M, Ozkoc G, Akpinar S, et al. Necrotizing soft-tissue infection of a limb: clinical presentation and factors related to mortality. Foot Ankle Int. 2006;27(8):598–605.
7. Morgan MS. Diagnosis and management of necrotising fasciitis: a multiparametric approach. J Hosp Infect. 2010;75(4):249–57.
8. Pan Xuekai S, Fei CX, et al. Diagnosis and treatment of necrotizing fasciitis. Chin J Clin. 2016;23:3608–11.
9. Lanzhu Z, Enhui Z, Suru L, et al. Clinical characteristics and treatment strategies of cervical necrotizing fasciitis. J Clin Otolaryngol Head Neck Surg. 2019;33(6):545–8.
10. Zander DA, Smoker WR. Imaging of ectopic thyroid tissue and thyroglossal duct cysts. Radiographics. 2014;34(1):37–50.
11. La'porte SJ, Juttla JK, Lingam RK. Imaging the floor of the mouth and the sublingual space. Radiographics. 2011;31(5):1215–30.
12. Ping Z, Wei Z. Analysis of thyroglossal duct cyst protruding into larynx cavity by CT. Jiangxi Med J. 2017;52(10):1085–6.
13. Jianshe Z. Analysis of the clinical diagnostic significance of CT examination in cervical cystic lesions. J Front Med. 2016;6(22):108–9.

Part X

Infectious and Inflammatory Diseases of Thyroid Gland

Thyroiditis

33

Zujiang Xiong, Hui Dai, Heng Liu, Jing Zhang, and Tao Wang

33.1 Acute Thyroiditis

33.1.1 Overview

Acute thyroiditis, also known as acute suppurative thyroiditis (AST), is a rare thyroid gland inflammation, which is often a complication of upper respiratory tract infection and can occur at any age. The disease is mostly caused by bacterial infection, which spreads to the thyroid gland through local diffusion or hematogenous dissemination, and the incidence rate accounts for 0.1–0.7% of thyroid gland diseases, and its infection scope can be limited or extensive. Infection caused by piriform recess fistula is often complicated with neck cellulitis or neck abscess, and pathogen can invade deep neck soft tissue or even mediastinum along the fistula. AST is usually acute and severe, with local cervical pain and lump, which may be complicated with general symptoms such as chills, fever, chills, and rapid heartbeat. Thyroid gland aspiration biopsy, such as aspiration of pus, is helpful for diagnosis. Pathogenic microorganisms cultured from the aspiration can be specifically diagnosed.

Causes and ways of acute thyroiditis infection: (1) Congenital piriform recess fistula is a common cause of AST in children. As the third or fourth branchial cleft tissue is not completely degraded during embryonic development, the fistula is formed. The fistula penetrates obliquely from the lateral wall or bottom wall of the piriform recess down through the lateral inferior border of thyroid cartilage and descends along the trachea, mostly ends at the superior polar of thyroid gland, and some of which can penetrate through thyroid gland and continue to descend. When abscess forms or even ruptures near thyroid gland, it can cause acute thyroid gland inflammation. Because the right side of branchial cleft tissue disappeared earlier, the infection caused in this way mostly occurs in the left side. (2) Blood-derived and lymphatic pathways are mostly secondary to septicemia, and patients with low or deficient immunity. (3) Inflammation near thyroid gland spread directly. (4) Medical operations such as iatrogenic injury, thyroid gland fine-needle aspiration and deep vein ductization are not strictly disinfected. (5) Eating hard food leads to injury and perforation of oropharynx and esophagus. (6) Neck trauma.

33.1.2 Pathology Findings

Because of the complete fibrous capsule, good blood supply and lymphatic drainage, and the high concentration of iodine ions in thyroid gland follicles, pathogens are usually difficult to invade. However, the persistent piriform recess fistula may be the most common route of infection, and the inflammation may diffuse to thyroid gland by local diffusion or hematogenous dissemination, and show acute inflammatory changes. Microscopically, it mainly manifests as neutrophil infiltration, which can form abscesses varied in size.

33.1.3 Imaging Findings

1. X-Ray Examination Although X-ray cannot reflect the direct signs of acute thyroiditis, barium swallow X-ray (BSX) can clearly show the existence and course of piriform recess fistula, which is more common on the left side, showing a caecum-like structure extending downward from the lower corner of piriform recess, filled with contrast agent. The examination method is simple, economical and intuitive, and can be used as an examination method for primary screening of diagnosis and reexamination after treatment.

Z. Xiong
Chongqing Fifth People's Hospital, Chongqing, China

H. Dai · H. Liu (✉)
Affiliated Hospital of Zunyi Medical University, Zunyi, China

J. Zhang · T. Wang
The First Affiliated Hospital of USTC (Anhui Provincial Cancer Hospital), Hefei, China

H. Li et al. (eds.), *Radiology of Infectious and Inflammatory Diseases - Volume 2*,
https://doi.org/10.1007/978-981-16-8841-6_33

2. CT Examination It is recommended to take oral water-soluble contrast agent for the CT examination. The contrast agent diffuses and remains in the soft tissue of neck through fistula with time. Meanwhile, CT can perform multiplanar and curved planar reformation, which can better show the characteristics of barium agent retention, deposition and the exact course of fistula, and provide an important basis for the choice of clinical treatment Scheme. CT findings of acute thyroiditis can be divided into simple inflammation stage and abscess formation stage. In the simple inflammatory stage, it is a stripy slow-density focus with blurred thyroid gland inner margin and blurred peripheral fat space. During the abscess formation stage, it shows a central low-density liquefactive necrosis area (Fig. 33.1), with pneumatosis and air-fluid level shadow in some lesions and soft tissues adjacent to the neck. The abscess is still low-density under enhanced scan, and the abscess wall shows ring or septa enhancement, with smooth and complete medial wall and blurred lateral wall border.

3. MRI Examination It has high resolution in soft tissue and can provide direct and indirect signs of inflammatory lesions in soft tissue of neck. In inflammatory stage, it shows irregular isointense or slightly hypointense on T_1WI sequence in thyroid gland with unclear margin, and hyperintense on T_2WI and fat-suppressed sequence for central inflammation and adjacent edema area. In the later stage of abscess formation, the lesions show hypointense on T_1WI sequence, hyperintense on T_2WI and fat-suppressed sequence in central area; isointense or slightly hyperintense on T_1WI, and slightly hypointense on T_2WI for peripheral abscess wall (Fig. 33.2). Enhanced scan shows marginal enhancement, but internal enhancement is unremarkable. When the pus contains a large amount of protein and leads to the diffusion limitation of water molecules, DWI sequence can show characteristic and significantly hyperintense.

33.1.4 Key Points of Diagnosis

1. Thyroid gland mass is complicated with pain, chills, high fever, and other symptoms. Laboratory test shows signs of acute inflammation such as increased leukocyte count and rapid erythrocyte sedimentation rate.
2. Oral barium for hypopharyngeal radiography (including CT scan after radiography) confirmed the existence of piriform recess fistula.
3. CT or MRI shows irregular stripy shadows abnormal density in thyroid gland or blurred signal area with surrounding fat space, and typical smooth and complete enhancement ring is formed in late abscess formation.
4. The pus shows hyperintense in DWI sequence.

33.1.5 Differential Diagnosis

1. Subacute Thyroiditis Patients have a history of upper respiratory tract infection or larynx inflammatory disease recently, and there is generally no acute inflammation such as local skin redness and skin temperature increase during physical examination; Subacute thyroiditis is not complicated with congenital piriform recess fistula, and the inflammatory exudation around the neck is generally mild, and no abscess will be formed in the later stage.

2. Thyroid Gland Tumor or Nodular Goiter The history is relatively long, and there are generally no acute infection symptoms such as cervical pain, chills, fever, and chills;

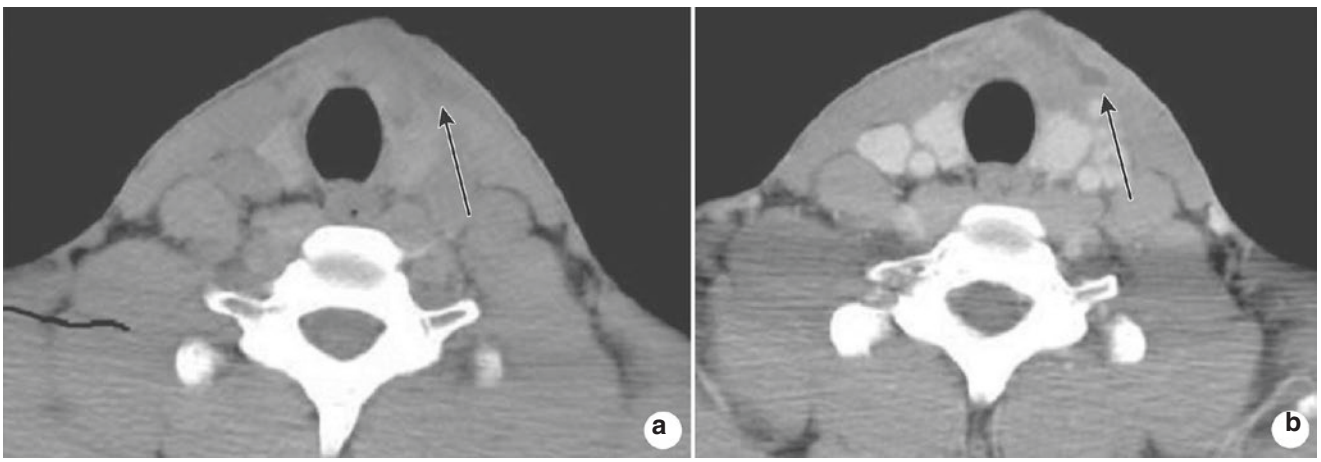

Fig. 33.1 Inflammation of left thyroid gland lobe with sinus formation. (**a**) Non-enhanced CT scan indicates that the shape of the left lobe and isthmus of thyroid gland increases, the density decreases, and the margin is unclear (indicated by arrow); (**b**) CT enhanced scan indicates heterogeneous flocculent enhancement of lesions, large-scale swelling of peripheral soft tissues with vomica and fistula shadow (indicated by arrow)

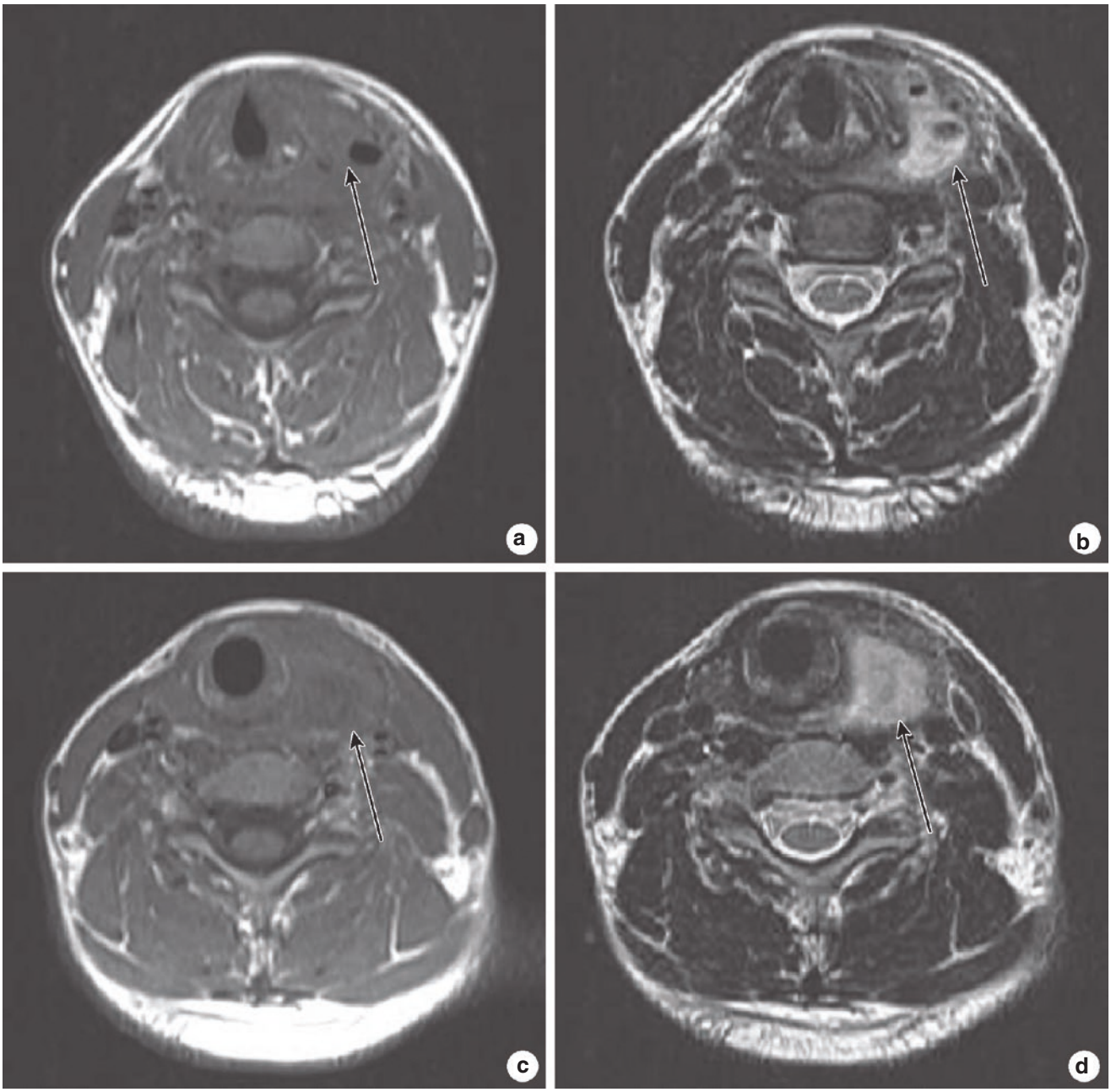

Fig. 33.2 Abscess formation in left thyroid gland lobe. (**a**, **b**) Non-enhanced MRI scan T_1WI shows that the left lobe of thyroid gland increases, the signal intensity heterogeneously decreases, and the margin is unclear (indicated by arrow). (**c**, **d**) Non-enhanced MRI scan T_2WI shows hyperintense in the left lobe of thyroid gland, with vomica and air signal shadow in it, and extensive edema (indicated by arrow) near scapulohyoid muscle and sternohyoid muscle (Images courtesy of Han Zhijiang, Hangzhou First People's Hospital)

Nodule or space-occupying effect is relatively strong, and fat space outside thyroid gland capsule is clearly shown.

33.1.6 Status Quo and Progress of Research

Oral administration of 50–60% (w/v) diluted barium or water-soluble contrast agent (such as meglumine diatrizoate solution) and reasonable combination of hypopharyngeal radiography, CT and MRI can improve the diagnostic accuracy of acute thyroiditis caused by congenital piriform recess fistula. However, some patients cannot have fistula development, especially in acute inflammation, the fistula orifice and fistula can be constricted or even obstructed due to mucosal reactive edema, granulation tissue proliferation of fistula orifice [1], swelling of peripheral soft tissue, etc., and

high-concentration barium agent is more likely to obstruct fistula orifice and cause missed diagnosis, so it is recommended to use 50–60% dilute barium or water-soluble contrast agent for hypopharyngeal radiography [2]. For some patients with negative results by contrast examination, it is necessary to receive multiple reexaminations after anti-inflammatory treatment.

After hypopharyngeal radiography, CT examination shows that contrast agent diffused and remained in the soft tissue of neck through fistula. Combined with CT multiplanar reformation technology, the course of piriform recess fistula can be shown more intuitively, especially for small fistula. In addition, CT can directly evaluate the characteristics of inflammation in thyroid gland and adjacent tissues, so CT examination has significant advantages in displaying fistula compared with ordinary radiography examination [3].

33.2 Subacute Thyroiditis

33.2.1 Overview

Subacute thyroiditis (SAT), also known as De Quervain thyroiditis, viral thyroiditis, or granulomatous thyroiditis, is mostly found in clinical practice. It is mostly found in middle-aged women aged 30–50 years old, and the incidence ratio of male to female is (1:3)–(1:6). The etiology is unknown, because it often occurs after viral upper respiratory tract infection, it is generally considered to be allergic reaction caused by viral infection. Virus antibody can be detected in patients' blood, which is a common cause of anterior cervical mass and thyroid gland pain. The disease is a self-limiting disease with a duration of several weeks to several months.

SAT has a seasonal onset trend, and its onset peak is in winter and spring, which generally goes through three typical stages: acute stage, remission stage, and recovery stage. In the acute stage, inflammation destroys thyroid gland follicles, which leads to the increase of serum thyroxine level and a series of hyperthyroidism symptoms. The patient's body temperature is slightly increased, which may be manifested as goiter and tenderness locally, and cervical lymph node enlargement, which lasts for 3–6 weeks. With the decrease of inflammation and depletion of thyroxine released by the destruction of thyroid gland follicular epithelioid cells, the hyperthyroidism symptoms disappear and improve significantly. Temporary hypothyroidism can occur in the stage, which lasts for several months, before the function of thyroxine synthesis is restored. Because SAT is a self-limiting disease, with the gradual decrease of inflammation and the return of thyroxine level to normal, patients will enter the recovery period of thyroid gland function, and only a few cases may have permanent hypothyroidism.

33.2.2 Pathology Findings

Pathological manifestations can be roughly divided into three stages: generally, the thyroid gland is usually enlarged bilaterally, often asymmetrical, and the lesion can also be limited to a part of the thyroid gland. There are scattered white-gray hard nodules in the section. Microscopically, some of the follicular destruction in early stage is replaced by neutrophils. As the disease develops, neuroglia overflows from the ruptured follicles, surrounded by histiocytes and multinucleated giant cells, forming granuloma, and eosinophils, lymphocytes, and plasma cells could be contained in the stroma. In the progressive stage of the disease, the involved glands are hard, and the glia overflows, forming unclear granulomatous nodules surrounded by histiocytes and multinucleated giant cells. In convalescence, multinucleated giant cells and histiocytes decrease or disappear, follicular epithelioid cells regenerate, which may be complicated with interstitial fibrosis and scar formation. The same gland often shows different stages of the lesion.

33.2.3 Imaging Findings

1. CT Examination It shows that the thyroid gland density decreased, and the lesion density is lower than that of normal thyroid gland by enhanced scan. The lymphocytes and plasma cells in the inflammatory area of arterial phase replace the normal thyroid gland tissue with abundant blood supply and high iodine content, so the enhancement is lower than that of normal thyroid gland. However, the enhancement amplitude increases but is always lower than that of normal thyroid gland due to the accumulation of contrast agent in the extracellular space of inflammatory area in venous phase. The typical manifestation is thyroid gland enlargement, one or more stripy slow-density shadows appear in the gland, and the occupying effect is relatively mild. Even if the lesion is large in shape, the compression of adjacent trachea and esophagus is still not obvious. On non-enhanced scan, the lesion density is lower than that of normal thyroid gland tissue, the margin between the margin and normal thyroid gland tissue is unclear, and the peripheral fat space is blurred. The enhancement degree of lesions varies with different stages of lesions during enhanced scan: in acute stage, the blood supply of lesions is less, which is lower than that of normal thyroid gland tissue, and the margin is still blurred (Fig. 33.3). In remission stage, the lesion is enhanced higher than the surrounding normal thyroid gland tissue due to increased blood supply.

2. MRI Examination The subacute thyroiditis shows isointense on T_1WI and slightly hyperintense on T_2WI on MRI, especially on fat-suppressed sequence, which is very

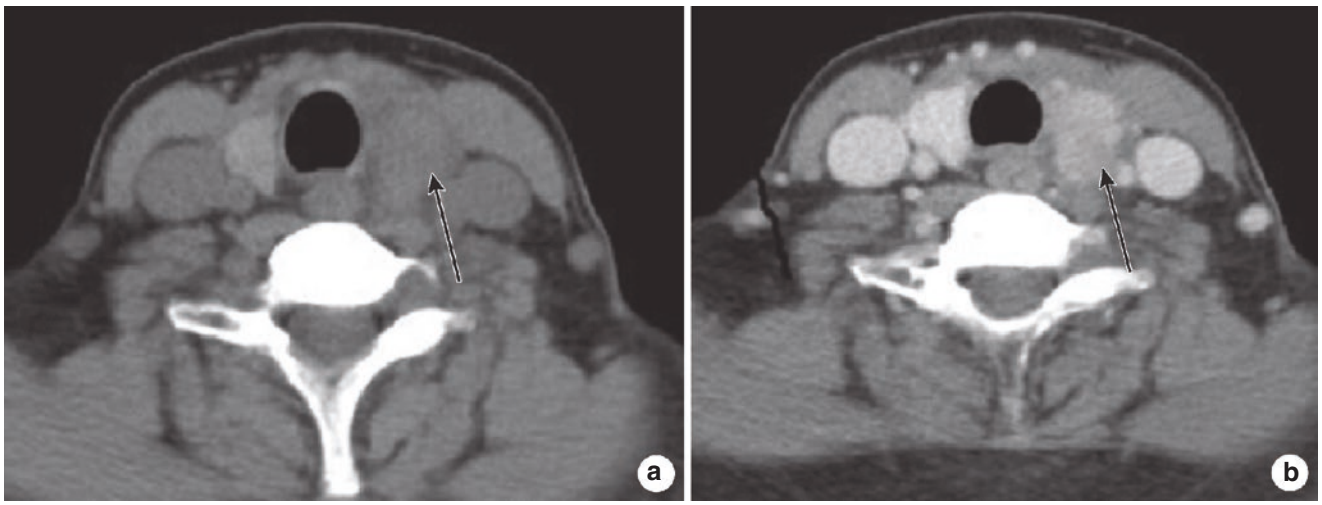

Fig. 33.3 Subacute thyroiditis in left thyroid gland lobe. (**a**) The shape of the left lobe of thyroid gland is enlarged, with density decreased and blurred peripheral fat space (indicated by arrow); (**b**) Enhanced scan shows mild and homogeneous enhancement of the left lobe, and no significant nodule or space-occupying effect is found (indicated by arrow)

sensitive to inflammatory exudation in gland and its periphery. Meanwhile, axial, coronal, and sagittal images can be used to evaluate the morphological characteristics of lesions.

33.2.4 Key Points of Diagnosis

Patients have a history of upper respiratory tract infection or larynx inflammatory disease recently, and have clinical manifestations such as acute goiter, paroxysmal pain with tenderness, and systemic symptoms like hyperthyroidism.

CT shows that there are solitary or multiple stripy slow-density lesions near the capsule in the ventral middle and superior thyroid gland, and the occupying effect is relatively mild, showing a "paint-splashing sign" change. The edge of lesions is still blurred by enhanced scan, and some lesions show high enhancement and benign lesions in remission stage.

Inflammatory exudation around the lesion resulted in blurred fat space display.

33.2.5 Differential Diagnosis

1. Acute Thyroiditis Thyroid gland mass has pain, high fever, chills, and other acute inflammatory symptoms. Oral administration of dilute barium or water-soluble contrast agent for hypopharyngeal radiography often leads to piriform recess fistula. CT or MRI shows the formation of inflammation or abscess in thyroid gland, and the peripheral inflammatory exudation is more significant and wider than SAT.

2. Hashimoto's Thyroiditis It shows enlarged thyroid gland, especially isthmus, diffuse or localized density of thyroid gland. Nodular Hashimoto's thyroiditis has a strong sense of nodules and can be complicated with massive calcification.

3. Nodular Goiter It has a regular shape. Non-enhanced CT scan often shows high or iso-density shadows follicular components and low density necrotic cystic areas of the nodules, and the density is heterogeneous. The margin of enhanced scan is clearer than that in non-enhanced scan, and the solid areas mostly have marked enhancement.

4. Papillary Thyroid Gland Carcinoma It mostly shows irregular nodules, with single occurrence and microcalcification. The contact surface between the tumor body and thyroid gland edge is straight and presents "cookie bite sign", some of which can invade the anterior cervical muscle structure. CT enhanced scan is mostly ground-glass enhancement with blurred and constricted border.

33.2.6 Status Quo and Progress of Research

At present, the pathogenesis of SAT is still unclear, and it is thought that it may be caused by viral infection and its autoimmunological reaction. Immunology can divide it into HLA-B35 positive type and HLA-B67 positive type according to the difference of human leukocyte antigen (HLA) it contained. The clinical manifestations of the two types are different: the former has hidden onset, hyperthyroidism and hypothyroidism are not obvious, and can occur in each

season; The latter generally experienced typical hyperthyroidism, hypothyroidism, and functional recovery, and most of them occurred in winter and spring.

The lesion area of subacute thyroiditis shows diffuse patchy or nodular low-density changes, and the margin between subacute thyroiditis and normal thyroid gland tissue is unclear. The diagnosis of lesions mainly depends on clinical laboratory test and ultrasound imaging, without CT or MRI examination. CT examination mainly evaluates the existence of malignant lesions. According to the statistics of receiver operating characteristic curve (ROC curve) of subacute thyroiditis group and normal thyroid gland group, the critical CT value between them is 45 HU, that is, taking CT value $\leq$ 45 HU as the sign of subacute thyroiditis has high sensitivity, positive predictive value and negative predictive value [4].

33.3 Hashimoto's Thyroiditis

33.3.1 Overview

Hashimoto's thyroiditis (HT), also known as chronic lymphocytic thyroiditis, is an autoimmune disease that can occur at any age, especially in women aged 40–60 years, and is the most common clinical thyroiditis. HT is also the most common cause of goiter and acquired hypothyroidism in children and adolescents. There may be no clinical symptoms in early stage. Most patients see a doctor with goiter or hypothyroidism for the first time, and in advanced stage, they have typical clinical symptoms of hypothyroidism such as apathy, chills, fatigue, dry skin, bradycardia, myxoedema, etc., which may be complicated with pharyngeal discomfort or mild dysphagia, with mild signs of goiter in diffuse lobulated or nodular form, mostly having hard texture and no adhesion with peripheral tissues.

At present, the pathogenesis of HT is not completely clear, which has genetic susceptibility and family aggregation and can coexist with other autoimmune diseases, so it is considered that HT is the result of the joint action of genetic factors and environmental factors [5]. Environmental factors mainly include infection, drugs, mental factors, and excessive iodine in diet, especially the increase of iodine intake can promote recessive thyroiditis to develop into clinical hypothyroidism. Meanwhile, genetic susceptibility genes also play a certain role in the occurrence and development of diseases.

33.3.2 Pathology Findings

Generally, the thyroid gland is diffusely and symmetrically enlarged, with complete, thickened, and smooth capsule, gray-white or gray-yellow section, tough as rubber, or gray nodules varied in size, without hemorrhagic degeneration or necrosis. Microscopically, the main pathological features are extensive lymphocyte infiltration in stroma, eosinophilia of thyroid gland follicular epithelium (Hurthle cells), infiltration of plasma cells and macrophages, and the formation of lymphatic follicles with significant germinal centers.

Pathological changes of Hashimoto's thyroiditis are also associated with the course of disease. In early stage, lymphocytes and plasma cells infiltrated widely, forming the germinal center of lymphatic follicles, and the thyroid gland follicles are atrophied and destroyed, and neuroglia decreases. With the progression of the disease, fibrillar connective tissue proliferated to different extents and surrounded follicular epithelium to form nodular or reticular structures. With the further progression of the disease course, the decrease of thyroxine leads to the increase of thyroid-stimulating hormone (TSH), which stimulates the regeneration of follicular epithelium of thyroid gland, and the compensatory proliferation of blood vessels between follicles. In advanced stage of the disease, thyroid gland follicles are severely atrophied, and fibrous tissue proliferation and hyaline degeneration can be observed, which may be complicated with malnutrition calcification and nodule formation with different sizes and components.

33.3.3 Imaging Findings

1. CT Examination The imaging findings of Hashimoto's thyroiditis are closely associated with pathology. HT can diffuse or locally destroy thyroid gland follicles, resulting in the decrease of iodine ion content, so CT can show diffuse, localized, or nodular low-density lesions.

Diffuse lesions show diffuse enlargement of thyroid gland to different extents, with isthmus thickening as the main part, with corrugated or lobulated edges (Fig. 33.4). With the progression of the disease, the thyroid gland can gradually return to normal size, and even become fibrotic and atrophy. Thyroid gland density decreased homogeneously or heterogeneously. Generally, CT value $\leq$ 75 HU is used as the sign of diagnosing diffuse Hashimoto's thyroiditis. However, other diseases that can reduce the iodine storage capacity of thyroid gland follicles, such as subacute thyroiditis, diffuse toxic and non-toxic goiter, can also lead to the decrease of thyroid gland density, and there may be low-density tumors in the low-density thyroid gland that cannot be recognized by naked eyes, which interferes with the accuracy of CT value measurement. Therefore, it is not appropriate to rely solely on the measurement of CT value as the basis for diagnosing HT, but need to make a comprehensive judgment in combination with clinical, laboratory test, and other imaging characteristics.

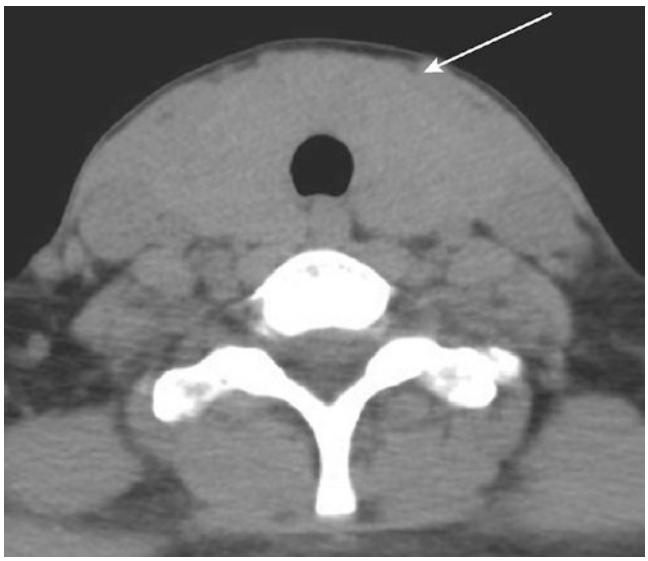

Fig. 33.4 Hashimoto's thyroiditis. Non-enhanced CT scan indicates that the shape of bilateral lobes and isthmus of thyroid gland increases, the edge changes in waves (indicated by arrow), the density homogeneousity decreases, and the isthmus thickness is 1.8 cm

Localized or nodular HT usually manifests as solitary or multiple low-density nodules with blurred edges. It is easily confused with subacute thyroiditis when the nodule feeling is not strong and the margin is unclear. Combining clinical features and laboratory test results is helpful to differentiate the two. CT images show nodules with coarse calcification, involving isthmus, and enhanced scan indicates a high enhancement in venous phase (Fig. 33.5), which is helpful to differentiate from other malignant nodules.

HT is a pathological process of lymphocyte infiltration with follicular destruction and fibrillar connective tissue proliferation, which has a long course of disease. In this course, reactive proliferation and enlargement often occur in the lymph nodes of bilateral IV and VI groups in the neck where thyroid gland lymph reflux is collected, which can provide a certain basis for the differential diagnosis of HT.

2. MRI Examination It shows diffuse thyroid gland with homogeneous signal intensity, hypointense on T_1WI and hyperintense on T_2WI.

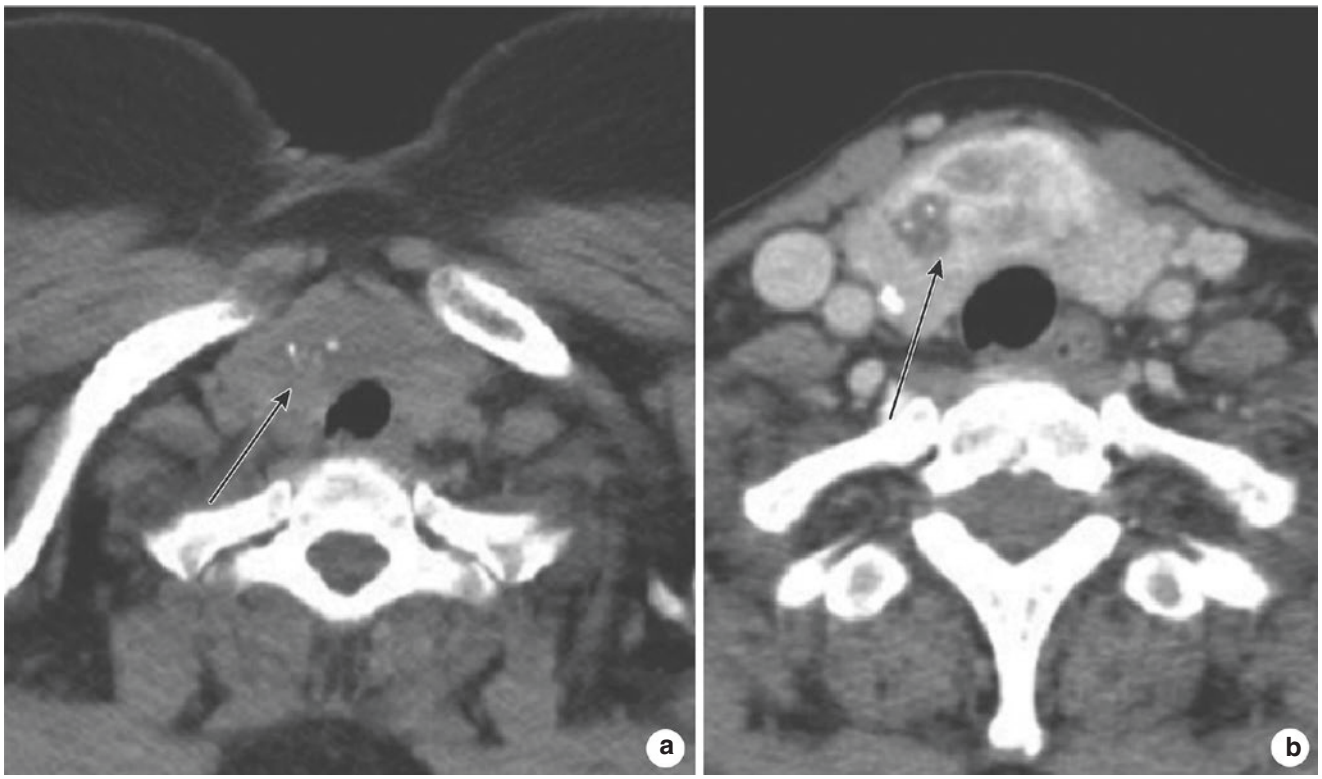

Fig. 33.5 Nodular Hashimoto's thyroiditis in thyroid gland isthmus. (**a**) Non-enhanced CT scan indicates a slight increase in thyroid gland morphology and a decrease in parenchymal density, with a lower density nodule in the isthmus of thyroid gland and a coarse calcification (indicated by arrow) inside; (**b**) CT enhanced scan shows some high enhancement areas and cystic degenerations in nodules during venous phase (indicated by arrow)

33.3.4 Key Points of Diagnosis

1. The disease occurs in young and middle-aged women aged 20–50 years, and has clinical symptoms related to hypothyroidism.
2. Diffuse enlargement of thyroid gland with isthmus thickening.
3. Thyroid gland density is even or heterogeneous, and CT value is mostly ≤ 75 HU.
4. Enhanced scan on nodular Hashimoto's thyroiditis shows marked enhancement in venous phase, complicated with massive calcification, isthmus involvement, and other benign nodules.
5. Reactive proliferation and enlargement of lymph nodes in bilateral IV and VI groups.

33.3.5 Differential Diagnosis

1. Hyperthyroidism The main clinical manifestation is hypermetabolism caused by excessive secretion of thyroxine. Imaging shows diffuse enlargement of thyroid gland with increased antero-posterior diameter, while HT shows isthmus thickening.

2. Subacute Thyroiditis It is often complicated with local pain. Most of the lesions are limited and located in the ventral side of thyroid gland, and the nodules are unconspicuous, showing "paint-splashing sign"; Lesions often lead to blurred show of peripheral fat space.

3. Papillary Thyroid Gland Carcinoma It mostly manifests as irregular nodules, single common, with microcalcification. The contact surface between the tumor and thyroid gland edge is straight and shows "cookie bite sign." The CT enhanced scan shows ground-glass enhancement with blurred and constricted border.

33.3.6 Status Quo and Progress of Research

HT leads to destruction of thyroid gland follicles and decrease of thyroxine secretion, which can lead to increase of TSH, atypical proliferation of thyroid gland follicular epithelioid cells, overlapping of transparent nucleus and nucleus, which is similar to thyroid gland papillary carcinoma. Moreover, Lee et al. [1] found that HT is at risk of developing differentiated papillary thyroid gland carcinoma by gene rearrangement testing and research. Therefore, for patients with diffuse HT, it is necessary to combine ultrasound or non-enhanced CT scan and enhanced scan to judge whether there are abnormal nodules in thyroid gland. Some nodules covered by non-enhanced CT scan can be shown by enhanced scan, while some nodules shown by non-enhanced CT scan may also be covered during enhanced scan. Therefore, non-enhanced CT scan and enhanced control can reduce the occurrence of missed diagnosis to a certain extent.

Very few patients with HT have no abnormality in thyroid gland shape, size, and gland density, and rely mainly on laboratory test for diagnosis. In laboratory indicators, only thyroid gland autoantibodies, including thyroglobulin antibody (TGAb) and thyroperoxidase antibody (TPOAb), are increased. The reason for this phenomenon may be that thyroid gland morphology and density have not changed in early stage of the disease. Although the proportion is small, for this kind of patients, thyroid gland antibodies should be combined and regular follow-up should be done.

33.4 Woody Thyroiditis

33.4.1 Overview

Riedel thyroiditis (RT), also known as chronic (invasive) fibrothyroiditis, is a rare disease characterized by thyroid gland fibrosclerosis, accounting for 0.04–0.30% of thyroid gland diseases, mainly occurring in middle-aged and elderly women, with a short medical history ranging from 2–3 weeks to decades. Patients' thyroid gland is as hard as stone or wood, with little or no activity, often involving blood vessels and recurrent laryngeal nerve, and appearing hoarseness, dyspnea or dysphagia. The compression symptoms are significant and not proportional to the degree of thyroid gland enlargement. Generally, cervical lymph node enlargement does not occur.

Woody thyroiditis is a self-limiting disease, and its exact pathogenesis is unclear, which may be associated with systemic diseases associated with immunoglobulin G4. In clinical cases, patients with hard and swollen thyroid gland complicated with hoarseness and inconsistent with the degree of goiter should consider the possibility of the disease.

33.4.2 Pathology Findings

RT manifests as fibrillar connective tissue replacing normal thyroid gland tissue, and normal glands can be totally or partially involved, and break through thyroid gland capsule and involves peripheral tissues. Macroscopically, the involved area shows tough fibrosis and "wood-like" changes, and inflammatory fibrous tissue invaded the peripheral tissues. Microscopically, the active proliferative inflammatory fibrosis leads to the destruction and disappearance of thyroid gland structure, and the degree of inflammatory cell infiltration varies, often lacking giant cell reaction, and skin and lymph nodes are generally not involved.

33.4.3 Imaging Findings

Woody thyroiditis was replaced by fibrillar connective tissue and destroyed normal thyroid gland follicles, resulting in loss of thyroid gland iodine storage function, so CT shows localized or diffuse hypointensity thyroid gland lesions. The margin between the lesion and the normal thyroid gland is unclear, no true or false capsule is formed, and it often breaks through the thyroid gland capsule and spreads to the peripheral tissues. CT shows diffuse peripheral structures such as trachea and blood vessels, while enhanced scan shows slight heterogeneous enhancement (Fig. 33.6).

33.4.4 Key Points of Diagnosis

1. The neck mass is tough, and palpation of thyroid gland hardens.
2. The lesions are low density, the margin is unclear, and they break through the thyroid gland capsule and involve the peripheral tissues, surrounding the trachea and blood vessels.
3. Enhanced scan shows slight heterogeneous enhancement.

33.4.5 Differential Diagnosis

1. Hashimoto's Thyroiditis It manifests as diffuse enlargement of thyroid gland with isthmus thickening, unsmooth surface, and clear peripheral fat space. Density is mostly less than 75 HU on non-enhanced CT scan; Reactive proliferation and swelling can occur in bilateral lymph nodes of groups IV and VI.

2. Subacute Thyroiditis It is often complicated with local pain. Most of the lesions are limited and located in the ventral side of thyroid gland, and the nodules are unconspicuous, showing "paint-splashing sign"; Lesions often lead to blurred show of peripheral fat space.

3. Primary Thyroid Gland Lymphoma It is mostly complicated with underlying Hashimoto's thyroiditis; CT shows homogeneous and low-density irregular tumor extending to tracheoesophageal groove; enhanced scan shows mild homogeneous enhancement; most of them were complicated with swelling of lymph nodes around thyroid gland, supraclavicular lymph nodes, and mediastinal lymph node.

33.4.6 Status Quo and Progress of Research

Woody thyroiditis has inflammatory fibrous tissue and vasculitis in fibrosclerotic tissue, and thyroid gland autoantibodies can be found in the serum of most patients, which indicates that autoimmune mechanism may play a role in the course of disease [6]. In addition, because histopathology found that there is eosinophilic follicular epithelium in the lesions, woodiness thyroiditis is considered to be the manifestation of Hashimoto's thyroiditis in advanced stage. However, in recent years, the analysis of histomorphological characteristics, clinical manifestations, thyroid gland function indicators, immune characteristics, prognosis, and so on did not find the inevitable connection between them, so they were considered to be independent diseases.

Because of its low incidence, the radiological manifestations of woody thyroiditis lack statistical analysis of large samples. However, combined with domestic and foreign case

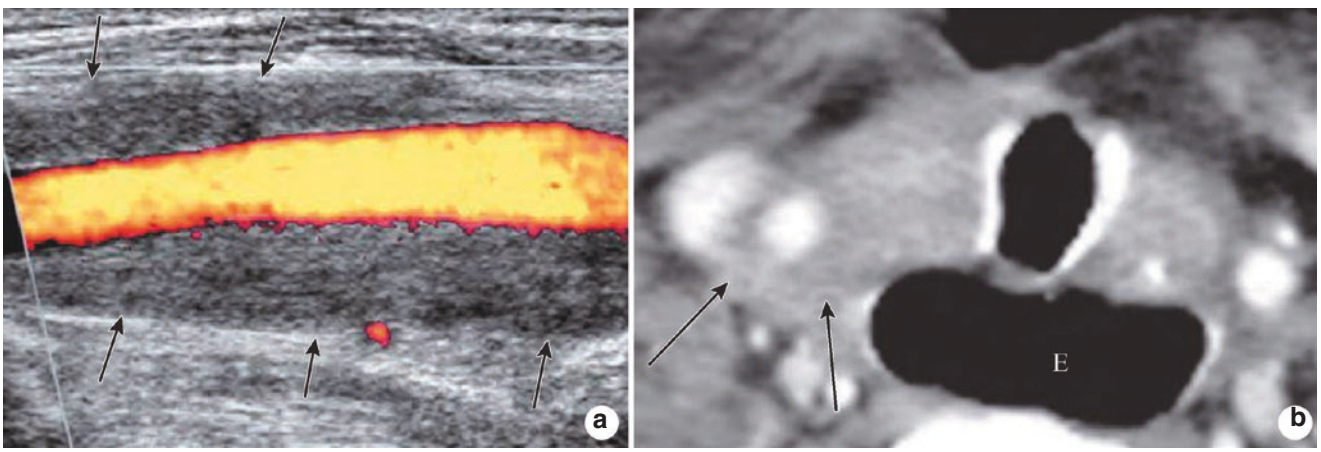

Fig. 33.6 Woody thyroiditis. (**a**) CDFI on long-axis section of the right common carotid artery shows low echo (indicated by arrow) surrounding the right common carotid artery, with sparse blood flow in it and unclear normal carotid tunica intima-media; (**b**) CT enhanced scan shows that the right lobe of thyroid gland enlarged and shows slight heterogeneous enhancement, and the lesion breaks through the thyroid gland capsule and diffuses around the right common carotid artery and jugular vein (indicated by arrow) (Images courtesy of Yuhang, Beijing Civil Aviation General Hospital)

reports, when the degree of goiter is not proportional to the compression symptoms caused by it, CT examination shows that the thyroid gland has low-density lesions and breaks through the capsule to involve peripheral tissues, and diffuses around the trachea and blood vessels, it is necessary to consider the possibility of woody thyroiditis.

References

1. Lee JH, Kim Y, Choi JW, et al. The association between papillary thyroid carcinoma and histologically proven Hashimoto's thyroiditis: a meta-analysis. Eur J Endocrinol. 2013;168(3):343–9.
2. Changmao D, Huiyu Z, Huifang S, et al. Application and clinical significance of esophageal barium meal in diagnosis of pyriform sinus fistula. Chin J Pract Med. 2013;40(15):16–7.
3. Dongqing W, Ling L, Limin Z, et al. Analysis of lymphatic metastasis of hypopharyngeal carcinoma based on CT. Chin J Rad Oncol. 2018;27(4):354–9.
4. Quan L, Weijun P, Feng T. CT diagnosis of subacute thyroiditis. Chin Comput Med Imaging. 2006;12(4):236–9.
5. Hanbo C, Dongyu Z, Wei S, et al. Research progress of Hashimoto's thyroiditis. Med Recapitulate. 2014;20(6):1074–6.
6. Lihong G, Xianghai Z. Research progress in diagnosis and treatment of Hashimoto's thyroiditis. Chin J Gen Pract. 2018;17(3):235–8.

Part XI

Infectious and Inflammatory Diseases of Skull Base

Skull Base Lesions

34

Ying Zou, Shuang Xia, Zujiang Xiong, Hui Dai, and Heng Liu

34.1 Skull Base Osteomyelitis

34.1.1 Overview

Skull osteomyelitis is a disease of skull infection and destruction caused by aerobic or anaerobic bacteria, mycobacteria or fungi, which is most common in frontal bone and parietal bone. Skull base osteomyelitis (SBO) is rare, and the etiology of SBO is not completely clear. SBO usually occurs in elderly diabetic patients or immunocompromised patients and often involves temporal bone, skull base, cranial nerves, and brain tissue. Its clinical manifestations are atypical, and its aggravation can threaten life. It generally develops rapidly and its prognosis is poor. SBO is often secondary to malignant external otitis (MEO) with invasive bone destruction. The lesions of MEO begin in the external auditory canal, and granulation tissue and cartilage necrosisare found at the bottom of the external auditory canal. The necrosis usually occurs at the junction of cartilage and soft tissue in the external auditory canal, and then spreads to the peripheral area. When the disease develops further, acute or chronic inflammation invades the stylomastoid foramen and jugular foramen through cartilage fissure of external auditory canal and milk fissure of middle eardrum, which leads to osteomyelitis of temporal bone or skull base osteomyelitis, leading to paralysis of cranial nerves function, meningitis or brain abscess, etc. Chronic mastoiditis and rhinosinusitis are also inducing factors of SBO. In addition, iatrogenic factors can also cause SBO, such as maxillectomy and mastoidectomy. Radiation osteomyelitis usually causes inflammation and necrosis of bone due to malignant tumors such as nasopharynx after high-dose radiotherapy.

34.1.2 Pathology Findings

The main pathogen of SBO is Pseudomonas aeruginosa, and its internal and external toxins can destroy the peripheral tissues. Because of its strong virulence, infesction is difficult to control, which can cause severe fatal infection. Other pathogens include Staphylococcus epidermidis, Streptococcus pneumoniae, Aspergillus, etc. Lee et al. [1] reported SBO caused by Enterobacter aerogenes infection in cases of sigmoid sinus thrombosis and necrotic pulmonary embolism.

1. Acute Suppurative Osteomyelitis It can be divided into the following three stages based on pathological changes.

1. Subperiosteal abscess stage: inflammatory cell infiltration in bone marrow cavity, mainly lymphocytes and plasma cells, which may contain a small amount of purulent blood.
2. Subperiosteal abscess stage: After 3–4 days of onset, pus in bone marrow cavity increased to subperiosteal, forming subperiosteal abscess.
3. Periosteum destruction stage: 7–8 days after onset, subperiosteal empyema penetrated into soft tissue, resulting in periosteum necrosis, destruction of bone blood supply, bone destruction in severe cases, blood vessel embolism, and formation of sequestrum.

2. Chronic Suppurative Osteomyelitis It is usually evolved from acute suppurative osteomyelitis. Plenty of lymphocytes, proliferating fibroblasts, and mesenchymal cells infiltrated into the bone marrow cavity, and bone reconstruction began with bone destruction, showing periosteum repair and hyperostosis.

Y. Zou
The First Affiliated Hospital of Tianjin University of TCM, Tianjin, China

S. Xia
Tianjin First Central Hospital, Tianjin, China

Z. Xiong
Chongqing Fifth People's Hospital, Chongqing, China

H. Dai · H. Liu (✉)
Affiliated Hospital of Zunyi Medical University, Zunyi, China

H. Li et al. (eds.), *Radiology of Infectious and Inflammatory Diseases - Volume 2*,
https://doi.org/10.1007/978-981-16-8841-6_34

34.1.3 Imaging Findings

The main manifestations of the disease are bone destruction, sequestrum formation, subperiosteal abscess, hyperostosis and osteosclerosis, periosteal reaction, and involvement of adjacent structures. Meanwhile, it is often complicated with the primary lesions of paranasal sinus, middle ear mastoid and orbit, such as rhinosinusitis, otomastoiditis, cholesteatoma, intraorbital cellulitis, and so on. Osteomyelitis located in the anterior skull base is mostly caused by ethmoidal sinusitis, frontal sinusitis and orbital inflammatory diseases.

1. CT Examination The manifestation of osteomyelitis in early stage is the decrease of local density of skull plate diploe. With the progression of pathological changes, bone destruction began to appear. Bone destruction manifests as skull plate diploe, irregular low-density area in internal and external plates, and clear or blurred border. Sequestrums are punctate or irregular high-density bone masses disconnected with the surrounding bone. Subperiosteal abscess is not common in osteomyelitis at the skull base. When inflammation involves the orbit, abscess formation inferior to the orbital periosteum, showing fusiform and stripy slow-density shadows inferior to the periosteum. By enhanced scan, the thickened periosteum can be enhanced, but the abscess is not enhanced. Hyperostosis and osteosclerosis show thickening of the internal and external plates of skull, increased density of diploe and unclear margin. Periosteal reaction is uncommon, showing thin-line, stripy, or layered high-density shadow. Extracranial soft tissue invaded shows swelling of soft tissue, thickening of muscles, unclear margin, and increased density of intermuscular fat space. Enhanced scan shows that the involved muscles and intermuscular space is heterogeneous enhancement, and the lesion scope is more clearly shown. If an abscess is formed in soft tissue, it shows a low-density area, and the abscess wall can be enhanced by enhanced scan (Figs. 34.1 and 34.2).

2. MRI Examination It shows bone marrow edema in early stage of osteomyelitis, with bone marrow manifesting as hypointense on T_1WI and slightly hyperintense on T_2WI, with irregular shape and unclear margin. Bone destruction shows hypointense on T_1WI and hyperintense on T_2WI, the signal is heterogeneous and enhancement of involved area can be found by enhanced scan. Sequestrum shows irregular hypointense area which is disconnected with surrounding bone. The subperiosteal abscess shows hypointense, isointense, or hyperintense on T_1WI and mostly hyperintense on T_2WI according to pus components. By enhanced scan, the thickened periosteum could be enhanced, but the abscess shows no enhancement. Hyperostosis and osteosclerosis show bone thickening, and bone marrow cavity shows hypointense on T_1WI and hypointense on T_2WI. Periosteal reaction shows hypointense on T_1WI and hypointense on T_2WI. Extracranial soft tissue invasion manifests as muscle swelling, with hypointense on T_1WI and hyperintense on T_2WI, and heterogeneous linear and stripy hypointense shadows in hyperintense area of intermuscular fat. By enhanced scan, the lesions are heterogeneous enhancement. If abscess is formed, the abscess wall is enhanced in a ring shape.

34.1.4 Key Points of Diagnosis

1. Often have a history of rhinosinusitis, otomastoiditis, orbital inflammatory diseases, etc.
2. With symptoms of bacterial poisoning, blood routine often shows abnormal results.
3. Acute osteomyelitis manifests as bone destruction, subperiosteal abscess, periosteal reaction, and inflammatory changes of adjacent soft tissues.
4. Chronic osteomyelitis manifests as hyperostosis, osteosclerosis, and deformity.

34.1.5 Differential Diagnosis

1. Eosinophilic Granuloma It is mostly found in children and adolescents, with long course of disease, mild clinical symptoms, eosinophilia in blood routine, clear margin of bone destruction, mostly solitary, complicated with soft tissue mass.

2. Metastatic Tumor It is mostly found in middle-aged and elderly people, usually with a history of primary tumors. Osteolytic bone destruction is more common, which can be solitary or multiple, with irregular shape and blurred margin, confluent foci, and can be complicated with soft tissue mass. Osteosclerosis and periosteal reaction are rare.

34.1.6 Status Quo and Progress of Research

CT is the preferred imaging method for skull base osteomyelitis, especially when the lesion is secondary to malignant external otitis, it can show moth-eaten bone destruction of bone of skull base [2]. The lateral soft tissue along petrosal bone and occipital bone can show "oval sign" on the bone window due to the remodeling and erosion of lateral bone edge caused by soft tissue inflammation. There is significant hole erosion in jugular foramen, carotid canal and stylomastoid foramen. Enhanced examination can be used to evaluate the patency of carotid artery and jugular vein to determine whether there are other malignant tumors.

MRI can be used as a supplement to CT examination, and MRI is more helpful to detect whether inflammation involves intracranial. Whether it is direct, peripheral, or vascular, MRI can better evaluate the involvement of occipital foramen [3–5].

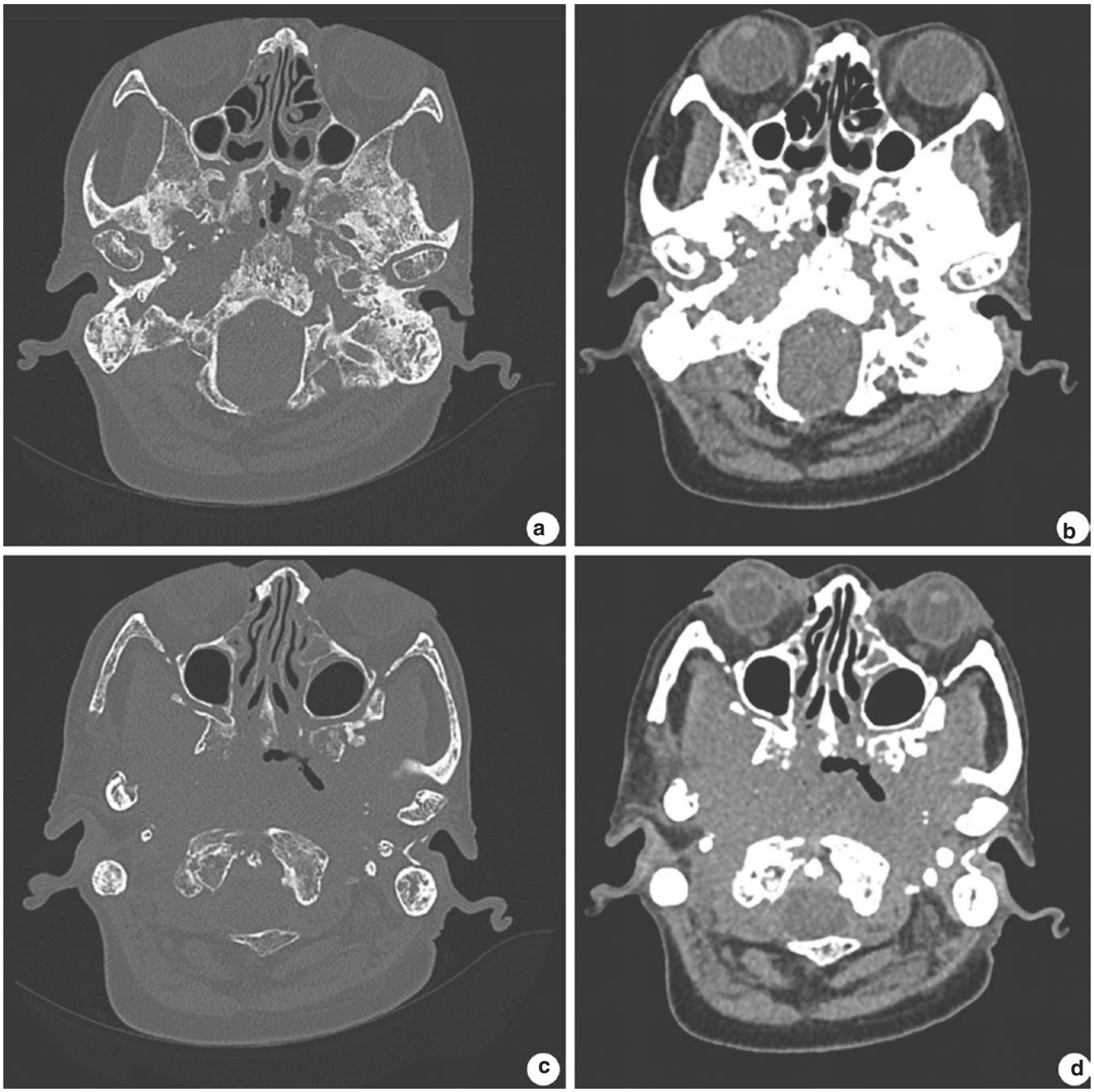

Fig. 34.1 Radiation osteomyelitis of bone of skull base. A 65-year-old female patient Postoperative radiotherapy for nasopharyngeal carcinoma. (**a**–**d**) Non-enhanced CT scan shows diffuse bone cortex discontinuity in the sphenoid bone, occipital bone, mastoid portion of bilateral temporal bones, and bilateral mandible, and bone trabecula in disorderly arrangement and with cellular change and local osteosclerosis. The nasopharyngeal roof is thickened with unclear margin, and irregular soft tissue density shadows in bilateral parapharyngeal space

34.2 Skull Base Bone Tuberculosis

34.2.1 Overview

Bone tuberculosis accounts for about 1% of systemic mycobacterium tuberculosis infection, skull tuberculosis accounts for only 0.20–1.37%, and bone of skull base tuberculosis is even rarer. Although the incidence of tuberculosis has greatly increased in the world, there are only a few reports of skull tuberculosis, especially skull base tuberculosis, only sporadic reports [6]. Bone tuberculosis of skull base is usually caused by the direct spread of tuberculosis in adjacent parts (such as orbit, paranasal sinus, nasopharynx, pituitary gland, meninges of skull base, etc.), or by the spread of blood and lymph circulation, and a few are caused by the hematogenous dissemination of tuberculosis of lung and kidney.

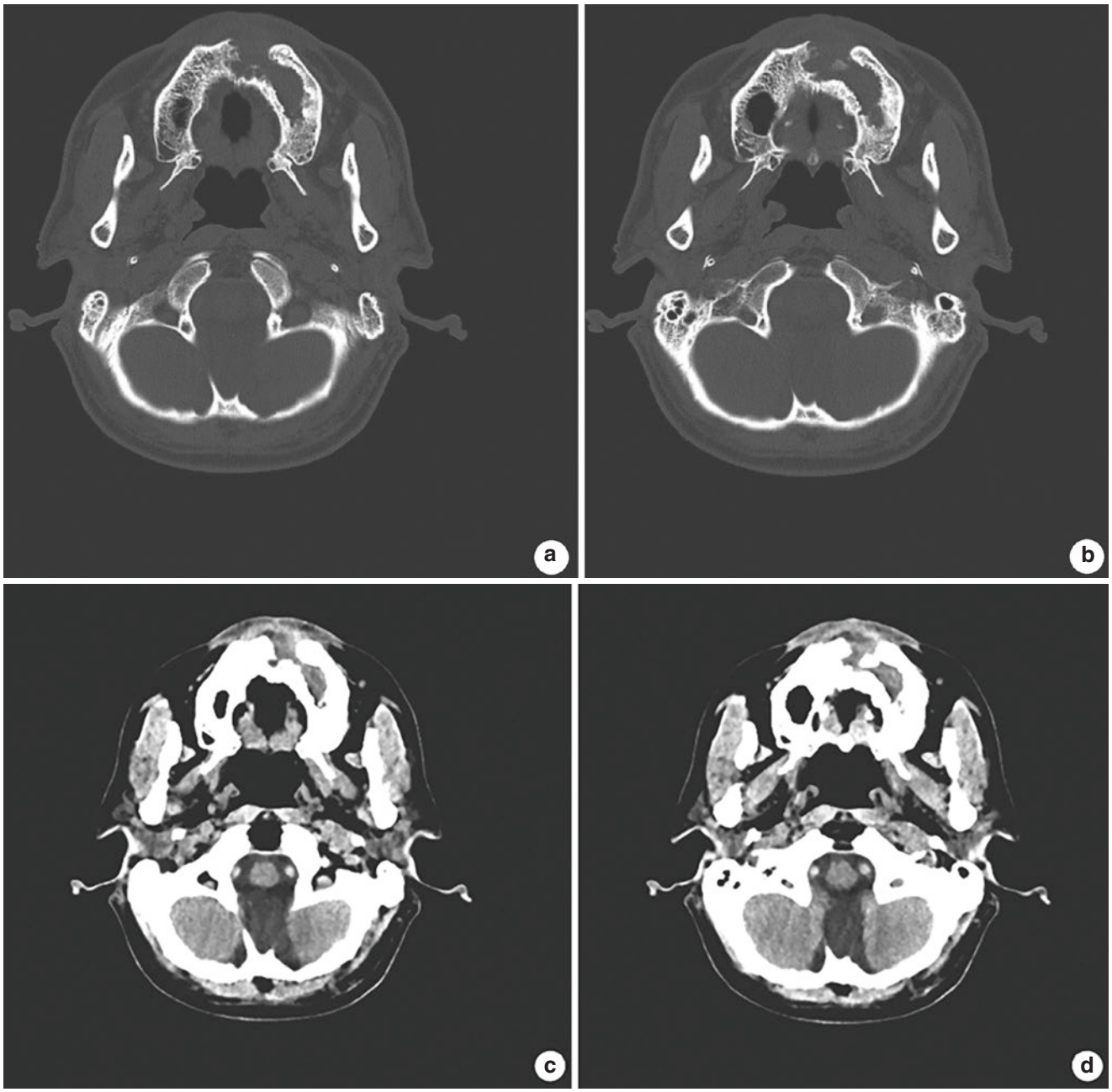

Fig. 34.2 Odontogenic maxillary osteomyelitis. A 60-year-old male patient. Pain in the left maxilla region with fever for more than half a month. (**a**, **b**) Non-enhanced CT scan on bone window shows bone destruction in the middle and left alveolar process of maxilla and edge sclerosis; (**c**, **d**) Non-enhanced soft tissue window CT scan shows axial soft tissue swelling

34.2.2 Pathology Findings

The pathological changes of skull tuberculosis are the same as those of bone tuberculosis in other parts, mainly showing three manifestations: exudation, degeneration, and proliferation. Macrophages and neutrophils are the main exudative lesions, complicated with cellulose exudation. Metamorphosis turned into caseous necrosis with calcification and sequestrum formation. Hyperplastic diseases become epitheloid cell proliferation, including Langerhans cells.

34.2.3 Imaging Findings

The main manifestations of the disease are bone destruction, sequestrum formation with hyperostosis and osteosclerosis, the adjacent structures are usually involved, and the periosteal reaction is mild or with unremarkable periosteal reaction. Meanwhile, there are multiple tuberculosis focus in adjacent structures such as paranasal sinus and orbit. Most of the lesions located in the anterior skull base were caused by the spread of tuberculosis in ethmoidal sinus and frontal sinus.

1. CT Examination The bone destruction usually shows that it penetrates the bony defect area of the inner and outer plates of skull, which is replaced by soft tissue density shadows, with irregular shape, clear or blurred margin, and unremarkable periosteal reaction. A few sequestrums and punctate calcifications can be found in the bony defect area. Sequestrums are small, showing irregular high-density bone masses which are disconnected with the surrounding bone. Hyperostosis and osteosclerosis is limited, which is manifested by thickening of skull around the destruction area and increasing density of diploe. Invasion to peripheral soft tissue shows soft tissue swelling, which could form irregular mass with unclear margin. In enhanced scan, the involved soft tissues show heterogeneous enhancement, and the lesion area is more clearly shown (Fig. 34.3).

2. MRI Examination As the pathological components of tuberculosis focus are complex, and exudative lesions, proliferative lesions, caseous necrosis, and calcification are mixed, so the MRI signals are very complex. Bone destruction shows hypointense on T_1WI and hyperintense on T_2WI. Sequestrums and calcification foci show punctate and small stripy hypointense on T_1WI and hypointense on T_2WI. The invasion to peripheral soft tissues often shows as mass shadow, isointense is dominant. Caseous necrosis shows hypointense on T_1WI and hyperintense on T_2WI. By enhanced scan, the components of proliferative granuloma in the lesion show marked enhancement, while the other components were not enhanced, but the adjacent meninges were enhanced.

34.2.4 Key Points of Diagnosis

1. Often have tuberculosis or other parts of the extrapulmonary tuberculosis history.
2. Tuberculosis infection often occurs in paranasal sinus area.
3. Bone destruction, formation of sequestrum with hyperostosis and osteosclerosis, involvement of adjacent structures, light periosteal reaction, or unremarkable periosteal reaction.

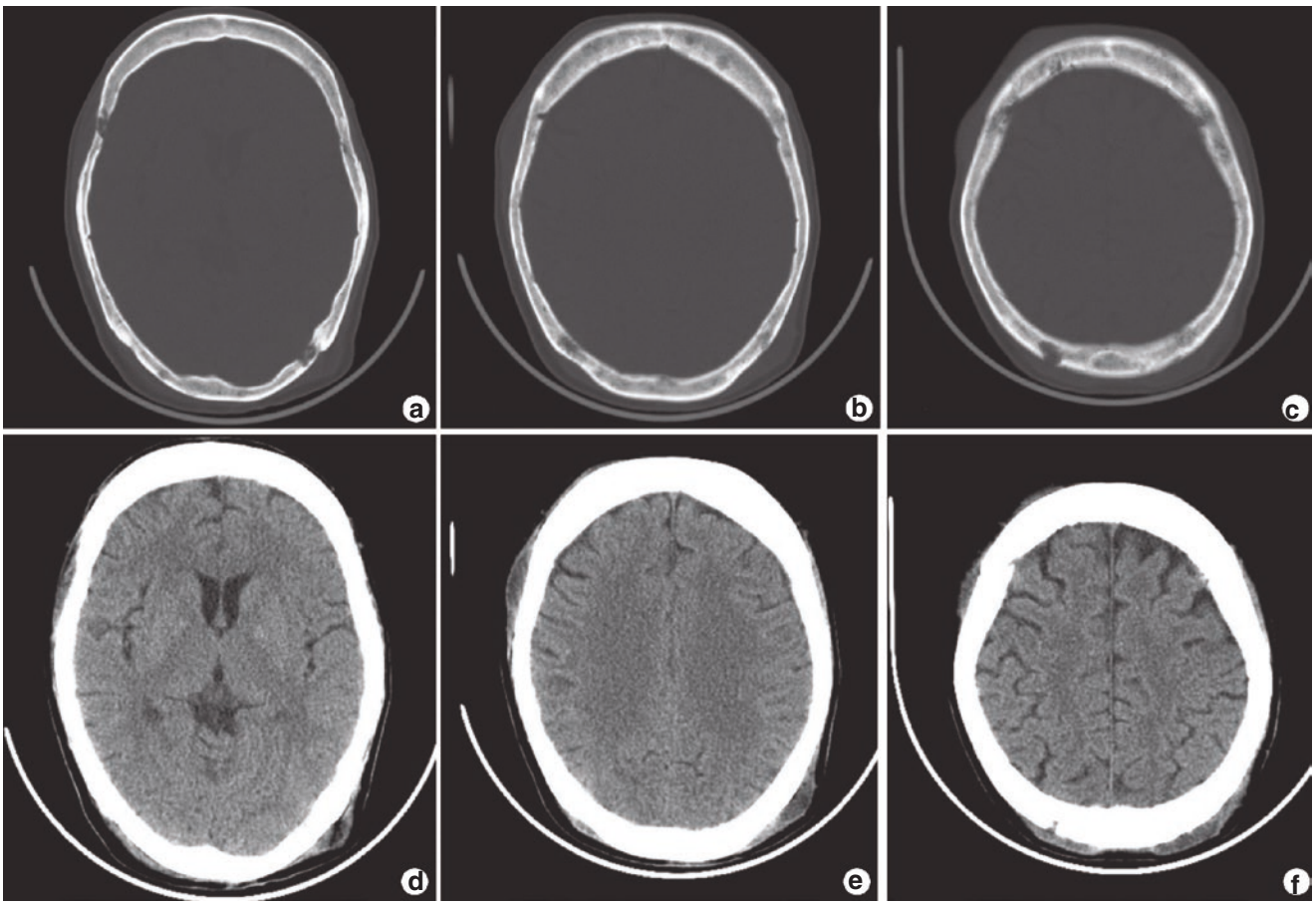

Fig. 34.3 Multiple bone tuberculosis in occipital bone. A 55-year-old female patient. Head lump was found with anorexia for more than half a month, and cough and expectoration increased for 1 week. According to diagnosis, the patient suffered from secondary pulmonary tuberculosis, bronchial tuberculosis, left ninth and tenth posterior rib tuberculosis and thoracic 12 cone tuberculosis. (**a**–**c**) Non-enhanced brain CT scan on bone window shows multiple bone destruction of skull; (**d**–**f**) Non-enhanced brain CT scan on soft tissue window shows that the bone destruction area is replaced by soft tissue density shadows, forming irregular mass with unclear margin

34.2.5 Differential Diagnosis

1. Myeloma It is mostly found in the elderly. Laboratory test shows that blood calcium is increased, serum-specific immunoglobulin is increased, with positive Bence Jones protein in urine. Bones of the whole body with abundant red bone marrow are usually involved. Skull is one of the common parts, which manifests as multiple, penetrating bone destruction, with quasi-circular shape, clear margin, and no sclerotic margin. May be complicated with soft tissue mass.

2. Eosinophilic Granuloma It is mostly found in children and adolescents, with long course of disease, mild clinical symptoms, eosinophilia in blood routine, clear margin of bone destruction, mostly solitary, complicated with soft tissue mass.

3. Metastatic Tumor It is mostly found in middle-aged and elderly people, usually with a history of primary tumors. Osteolytic bone destruction is more common, which can be solitary or multiple, with irregular shape and blurred margin, confluent foci, and can be complicated with soft tissue mass. Osteosclerosis and periosteal reaction are rare.

34.2.6 Status Quo and Progress of Research

For skull base bone tuberculosis, the diagnostic value of plain film is limited, and skull can show localized or diffuse solubility or localized periosteal lesions.

CT and MRI can clearly show osteolytic skull lesions, which destroy bone adjacent to epidural soft tissue mass, and show peripheral enhancement, low density, epidural mass, and peripheral enhancement performance is not clear, all of which indicate tuberculosis, and most patients have good clinical and laboratory performance.

34.3 Fungal Infection of Skull Base

34.3.1 Overview

Fungal Infection of skull base is not rare, and it usually occurs in patients with low immunity and long-term use of glucocorticoid or antibiotics. Fungal Infection of skull base is mostly rhinogenic, and often secondary to acute and chronic invasive fungal rhinosinusitis and allergic fungal rhinosinusitis.

34.3.2 Pathology Findings

The pathological basis of Fungal Infection of skull base caused by acute and chronic invasive fungal rhinosinusitis is that plenty of fungi in paranasal sinus invade adjacent skull base tissues or organs, mainly through blood vessels. The gross specimens of acute invasive fungal rhinosinusitis are black or dark brown, and most of them are shapeless broken tissues. Histologically, there is a large coagulation necrosis in the tissue, in which hyphae can be found. Visual observations of chronic invasive fungal rhinosinusitis are severe congestion and polypoid lesion of nasal mucosa, or surface covered with yellow or black massive soft tissue-like tumor. It can be seen through an electron microscope that submucosal issues have been invaded, including bones and blood vessels. Chronic suppurative granulomatous inflammation is the main form, which is usually accompanied by chronic nonspecific inflammation. In addition, coagulation necrosis and fungal vasculitis may also occur, with fungal hyphae observable in the necrotic tissues.

The pathological manifestations of allergic fungal rhinosinusitis are jam or putty-like yellow or yellow-brown secretions in the cavity of diseased paranasal sinus, with fungal hyphae or fungal spores observable on the secretion smear. Histopathologically, massive eosinophil infiltration can be observed.

34.3.3 Imaging Findings

1. CT Examination The CT findings of early lesions of acute and chronic invasive fungal rhinosinusitis are not specific, and only minor inflammatory changes such as thickening of the nasal cavity and/or paranasal sinus mucosa can be observed. The characteristic CT manifestations of acute invasive fungal rhinosinusitis at the progressive stage are progressive bone destruction, extensive lesions, easily spread to the orbit and skull, diffuse enhancement of the optic nerve and meninges, and intracranial abscess or infarction. The typical CT manifestations of chronic invasive fungal rhinosinusitis are bone expansion and destruction of involved sinus wall. In severe cases, defects may be formed, and adjacent bones may be subject to different degrees of proliferation and sclerosis. The sinus cavity is filled with irregular soft tissue shadow with uniform density and rare calcification. The characteristic CT manifestations of allergic fungal rhinosinusitis are unilateral or bilateral multi-sinus cavity enlargement and consolidation. Strip-like and cloud-like high-density shadows are visible in the consolidation tissue, with unilateral or bilateral nasal polyps. The lesions sometimes may destroy the bone at the skull base and involve the intracranial part, which is manifested as the soft tissue shadows in the paranasal sinuses protruding into the skull through the bony defect area at the skull base (Figs. 34.4 and 34.5).

2. MRI Examination The characteristic manifestations of acute invasive fungal rhinosinusitis include a wide range of involvement, mild disease of paranasal sinus or severely involved tissues and organs such as adjacent skull base,

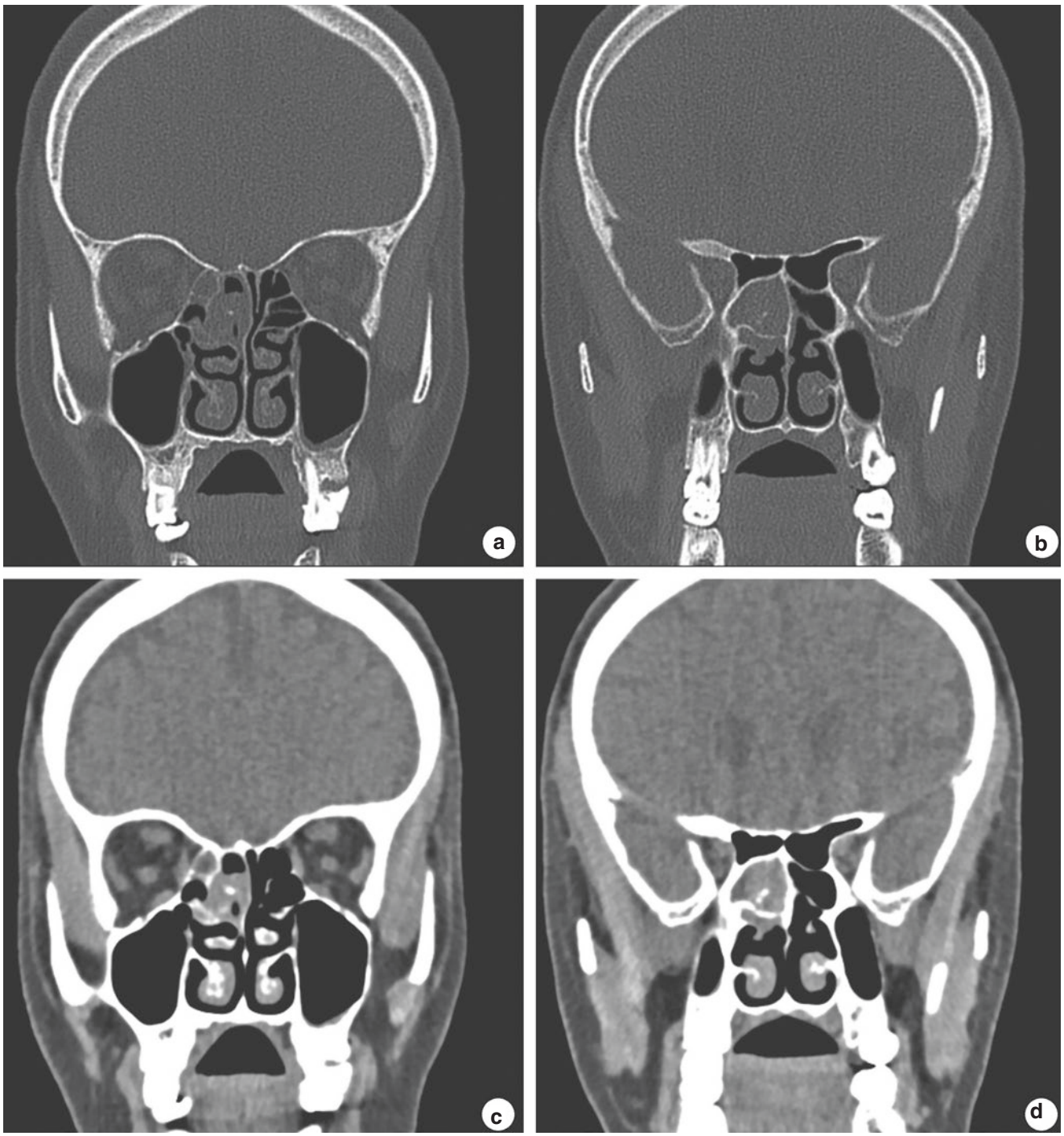

Fig. 34.4 Fungal sphenoiditis (1). A 60-year-old female patient. (**a**–**d**) The non-enhanced CT scan of paranasal sinus (coronal) shows soft tissue density shadows in the sphenoid sinus and right ethmoidal sinus, calcified shadow in them, unobstructed ostiomeatal complex, and unobstructed meatus nasi communis

orbits, and maxillofacial region. The fungal granuloma shows heterogeneous signal on T_1WI and significantly changing signals on T_2WI. The slight hypointense area in the lesion is the characteristic manifestation of fungal infection. The basicranial fungal meningitis shows isointense or hypointense on T_1WI, and mostly isointense or slightly hypointense on T2WI. Enhanced scan shows irregular enhancement of the meninges at the skull base or of the entire cerebral hemisphere, with possible local extradural abscess and cerebral dura mater or arachnoid enhancement. The chronic invasive fungal rhinosinusitis shows mostly isointense on T_1WI but uncertain signal on T_2WI, with mainly hyperintense at the early stage and hypointense at the advanced stage. The signal is often heterogeneous. The enhanced scan shows uneven enhancement of lesions. The allergic fungal rhinosinusitis shows

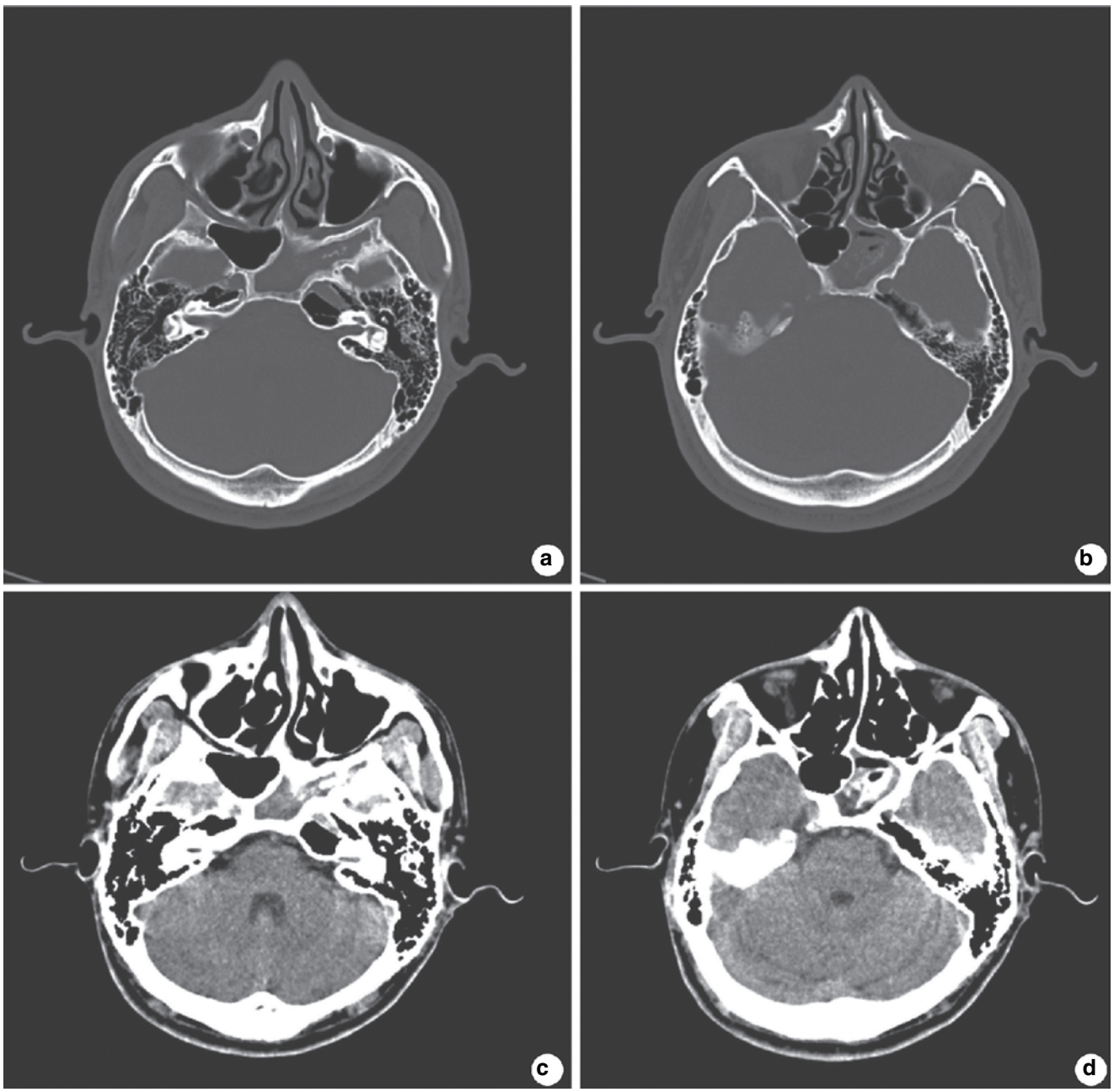

Fig. 34.5 Fungal sphenoiditis (2). A 28-year-old male patient. (**a**–**d**) The non-enhanced CT scan of the skull shows soft tissue density shadows in the sphenoid sinus, with visible calcified shadows and local sphenoid bone osteosclerosis

isointense or slightly hyperintense on T_1WI but extremely hypointense on T_2WI, and the enhanced scan shows its linear enhancement.

34.3.4 Key Points of Diagnosis

1. Acute Invasive Fungal Rhinosinusitis

1. The patient has a medical history of diabetes or is administered with a lot of hormones or antibiotics recently.
2. The patient has a persistent severe headache with or without symptoms of basicranial neurologic impairment.
3. The severity of rhinosinusitis is disproportionate to that of the invaded peripheral tissues.
4. The MRI examination shows a wide range of peripheral tissues and organs invaded by the lesion as well as thickening and enhancement of adjacent basicranial meninges.
5. The antifungal therapy is effective.

2. Chronic Invasive Fungal Rhinosinusitis

1. The disease is common in adults and sometimes in patients with immune deficiencies such as diabetes and leukemia.

2. The disease progresses slowly, and its early symptoms are similar to those of non-invasive fungal rhinosinusitis at early stage. Months or years later, symptoms such as headache, proptosis, impaired vision, and cranial nerve injury may occur.
3. Rhinosinusitis mostly involves single sinus involvement, with the maxillary sinus the most common. The sinus cavity expands, the bone of sinus wall is destroyed, and the bone adjacent to the bony defect area shows varying degrees of proliferation and sclerosis.
4. MRI examination can show the extent of involvement by lesions.

3. Allergic Fungal Rhinosinusitis

1. The disease is common in young patients with allergies but without immune deficiency.
2. The disease involves multiple paranasal sinuses on one or both sides, and the CT soft tissue window shows enlargement and consolidation of the sinus cavity involved by the lesions as well as multiple strip-like or cloud-like high-density shadows.
3. The CT bone window shows that the lesions erode the bone at the adjacent skull base and protrude the skull.
4. The disease is commonly accompanied by unilateral or bilateral nasal polyps.

34.3.5 Differential Diagnosis

1. Acute Invasive Fungal Rhinosinusitis When the lesion has no obvious bone changes, it is mainly distinguished from the non-fungal inflammation of skull base, including tuberculous meningitis and non-specific inflammation. Some cases are accompanied by bone erosion and destruction in the lesion area, requiring to distinguish it from the malignant tumor of skull base. Tuberculous meningitis usually occurs in young people, most of whom have a history of tuberculosis. It can be definitively diagnosed by biochemical analysis of the cerebrospinal fluid obtained by lumbar puncture as well as bacterioscopy. The lesion of basicranial non-specific inflammation usually shows more hyperintense on T_2WI, while that of the fungal inflammation shows a slightly hypointense on T_2WI, which is helpful for distinguishment. Malignant tumors of the skull base are mostly manifested as irregular-shaped soft tissue masses of skull base, which is accompanied by osteolytic destruction but without any history of diabetes or extensive use of hormones or antibiotics.

2. Chronic Invasive Fungal Rhinosinusitis The disease is mainly distinguished from paranasal sinus cancer invading the skull base. Sinus cancer has a short course and progresses quickly. Paranasal sinus cancer has a short course of disease and progress quickly in most cases. Common in the maxillary sinus, it is manifested as extensive bone destruction in the sinus wall, mostly without hyperostosis and osteosclerosis, as well as heterogeneous soft tissue density.

3. Allergic Fungal Rhinosinusitis It is necessary to distinguish it from the skull base abnormalities caused by other factors when the skull base is invaded. It is easy to distinguish it in combination with the characteristic CT manifestations of paranasal sinus and nasal cavity.

34.3.6 Status Quo and Progress of Research

CT examination is a primary examination approach when the fungal rhinosinusitis invades the skull base. It can clearly show the destruction and invasion of skull base bone by the lesions. Composed of a cone X-ray beam and a flat panel detector, cone-beam CT (CBCT) can move around the patient's head. It was originally used for dental imaging and has been widely used in ENT examinations. Compared with the traditional multidetector CT (MDCT), CBCT has higher resolution and less radiation exposure. Intrasinus calcification is a common manifestation of fungal rhinosinusitis, especially aspergillosis. CBCT can improve the detection rate of calcification to a certain extent [7].

Among all fungal rhinosinusitis, acute invasive fungal rhinosinusitis (AIFR) is dangerous and may endanger the patient's life. Some scholars [8] have established a simple and reliable CT-based diagnostic model through research, which can be used as a routine screening tool for high-risk patients. Ideally, this model will make the diagnosis or exclusion of AIFR more reliable than any previous one. Choi et al. [9] studied the relationship between the MRI imaging characteristics and AIFR and the prognosis and found that AIFR showed frequent invasion outside the paranasal sinus as well as variable MRI enhancement patterns. About half of the cases show the lack of contrast enhancement (LoCE) enhancement mode. Among various clinical radiological factors, LoCE enhancement mode is a unique prognostic factor.

34.4 Tolosa-Hunt Syndrome

34.4.1 Overview

Tolosa–Hunt syndrome (THS) is an idiopathic inflammation that often involves cavernous sinus and orbital apex. Its exact cause is not yet clear, and it may be an allergic disease Its typical clinical manifestation is the painful ophthalmoplegia caused by the inflammation of surrounding cavernous sinus. Tolosa-Hunt syndrome is essentially an exclusive clinical diagnosis. Because the diagnosis is mainly based on clinical features, the diagnosis of this

disease lacks objective evidence [10]. The disease usually occurs in 35- to 75-year-old persons, especially the about 50-year-old ones. No significant gender difference is observed, with slightly more male patients. It is generally unilateral, with no significant between left and rights sides. The first symptom is usually unilateral postorbital intractable pain, which usually occurs before ophthalmoplegia. The cause of such pain is mostly caused by the stimulated first branch of the trigeminal nerve. Most patients show the symptoms of cranial nerve paralysis after suffering ophthalmodynia for a period of time, which range from hours to 6 months. In this case, the cranial nerves III-VI are mainly involved. The clinical manifestations include ptosis of the affected side; paralysis of the extraocular muscles, which may be accompanied by strabismus, diplopia, corediastasis, and the pupil not reacting to the light; and eyeball fixation in a tiny minority of cases. Occasionally, it may affect optic nerves, facial nerves, and sympathetic nerves around the arteries, and the signs of obstructed orbital venous return may also occur. It is significantly effective to treat the disease with corticoid, and the pain disappears within days. It is relatively slow to recover from the symptoms of cranial nerve injury and they are easy to relapse, but the prognosis is good, and there are fewer patients remaining cranial nerve dysfunction.

34.4.2 Pathology Findings

The main pathological features of THS are the infiltration of lymphocytes and plasma cells, and the thickening of cerebral dura mater in the cavernous sinus. SIPHA periarteritis, or localized duritis pachymeningitis of the cavernous sinus.

34.4.3 Imaging Findings

1. CT Examination The extent of lesion mostly involves both the orbital apex and the adjacent cerebral dura mater. Enhanced scan shows marked enhancement of the lesions of cavernous sinus and orbital apex on the affected side as well as thickening and strip-like marked enhancement of the involved cerebral dura mater. The cavernous sinus area on the lesion side shows asymmetric enlargement, with or without enhancement. The internal carotid artery becomes narrower, and the superior orbital fissure and the orbital apex expand.

2. MRI Examination The disease is manifested as widening of the cavernous sinus on the affected side. Due to the large difference in size of the cavernous sinus between individuals, there is no recognized standard value. Therefore, whether the cavernous sinus is widened is mainly determined by comparing the cavernous sinuses on affected and unaffected sides. Re-examination after treatment can help confirm the diagnosis if the lesions are significantly reduced or disappeared. Thin-slice MRI enhanced examination is a main imaging method for diagnosing the disease. When the Tolosa-Hunt syndrome of cavernous sinus is suspected clinically, the acquisition slice is generally 2–3 mm thick, and there is no increment enhanced examination. Thin-slice MRI enhanced examination can show the inflammatory changes of frontal area of cavernous sinus, superior orbital fissure, and orbital apex. The signal characteristics are nonspecific and may be manifested as follows: Compared with muscle, the affected area shows isointense to hyperintense on T_1WI and hyperintense on T_2WI. The T1WI enhanced examination may show enhancement of the lesion at the active stage, and the resolution has improved after treatment (Figs. 34.6 and 34.7).

34.4.4 Key Points of Diagnosis

1. Tolosa–Hunt syndrome is mainly manifested as widening of the cavernous sinus. The thin-slice MRI enhanced examination can clearly show the marked enhancement of widened cavernous sinus, which may be accompanied by enhancement of the adjacent cerebral dura mater.
2. Symptoms are relieved after hormone treatment, and reduction or disappearance of the original lesions can be used as the diagnostic criteria for THS.

34.4.5 Differential Diagnosis

1. Painful Ophthalmoplegia Caused by Nasopharyngeal Carcinoma The onset is insidious and gradually worsens. Generally, it is first manifested as unilateral ophthalmoplegia, and then involves the opposite side and other cranial nerves. CT examination carried out at the advanced stage can show bone destruction, and the diagnosis can be confirmed by a biopsy of the nasopharyngeal cavity.

2. Sphenoid Sinus Cyst The onset is most subacute. The disease is manifested as obvious local tenderness and protruding eyeballs. In addition to cranial nerves III-VI, it may also involve the optic nerve. At the early stage of onset, the symptoms can be alleviated by treatment with dehydrators and steroid hormones. Its diagnosis can be confirmed by CT and MRI examinations.

3. Intracerebral Aneurysm (Posterior Communicating Artery Aneurysms) The disease only involves the second

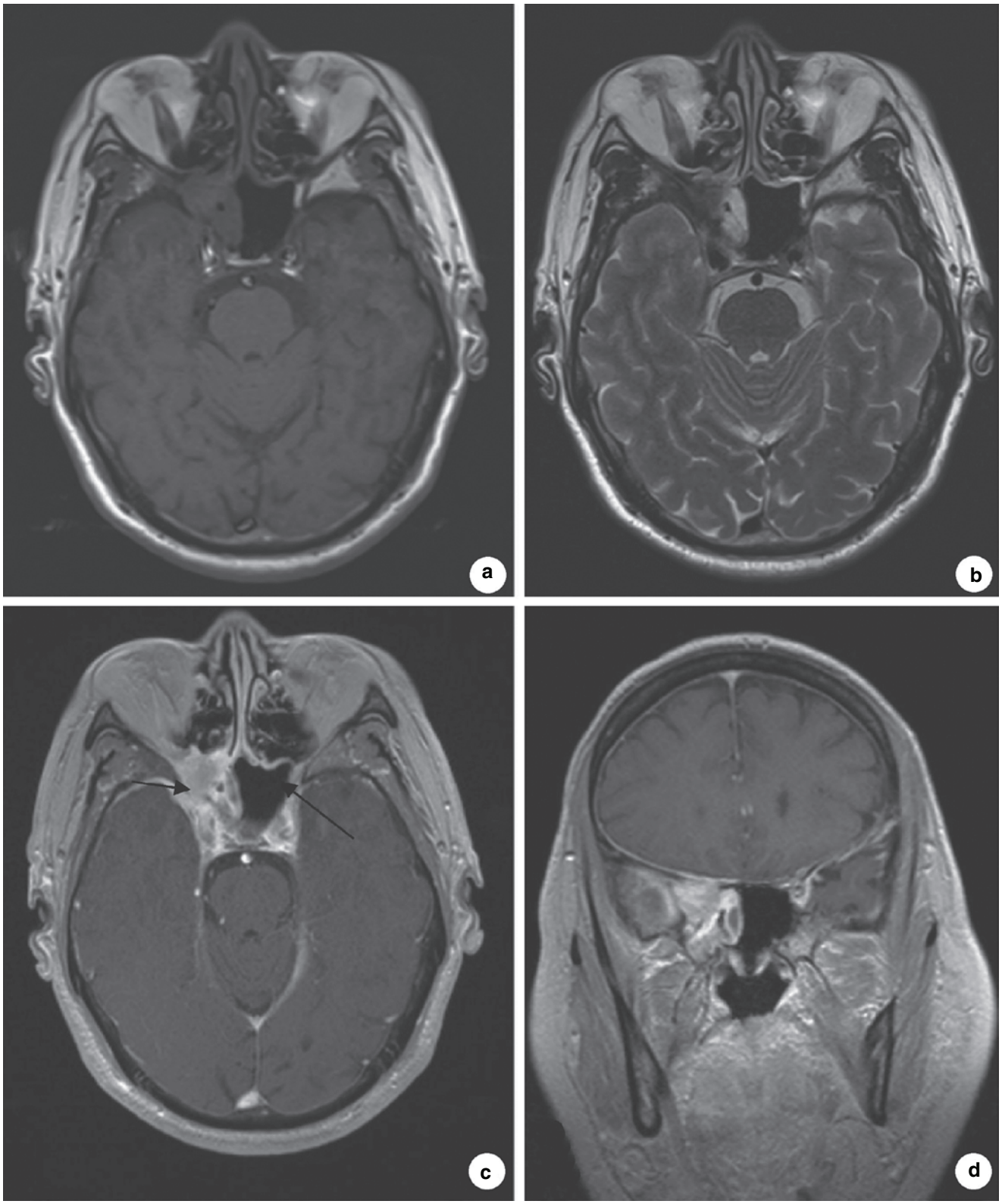

Fig. 34.6 Tolosa-Hunt syndrome (1). A 60-year-old female patient. Pain in both eyes for more than 1 month, and strabismus in the right eye for 1 week. (**a**, **b**) Non-enhanced MRI scan by T_1WI and T_2WI shows widening of the right cavernous sinus and heterogeneous signals. (**c**, **d**) Enhanced scan of T_1WI-CE transverse plane and coronal shows marked enhancement of the meninges adjacent to the right cavernous sinus, local thickening, and heterogeneous signals

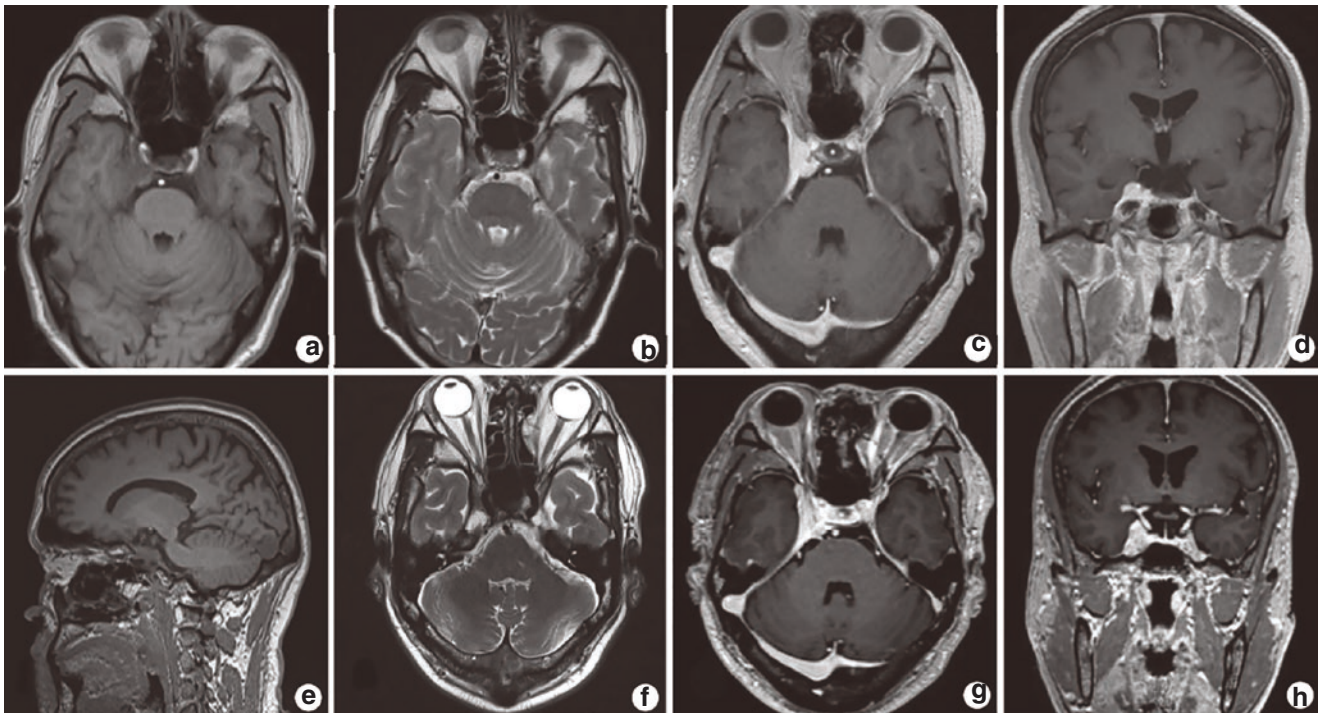

Fig. 34.7 Tolosa-Hunt syndrome (2). A 67-year-old female patient. Both eyes seeing an article as if it is two ones suddenly for 1 week. (**a**, **b**) Non-enhanced MRI scan by T_1WI and T_2WI shows local widening of the right cavernous sinus and visible abnormal shadow. (**c**, **d**) MRI enhanced examination shows abnormal reinforced nodule in the rear part of the right cavernous sinus. (**e**, **f**) After treatment with methylprednisolone, MRI re-examination shows that the abnormal enhanced nodule in the rear part of the right cavernous sinus has become smaller

cranial nerves, generally with light pain. It can be definitively diagnosed by angiography. The onset is slow, and it is accompanied by impaired vision and visual field defect. Its diagnosis can be confirmed by X-ray sella turcica plain film, CT examination, and MRI examination.

34.4.6 Status Quo and Progress of Research

THS is a rare neurological and ophthalmological disease, and MRI is the preferred imageological examination method. Compared with traditional brain MRI scan, thin-slice MRI scan and enhanced scan of cavernous sinus can better show the location, signal performance and scope of the lesion, which is helpful for diagnosis, differential diagnosis and follow-up observation of THS.

The advantages of 128-slice CT scan for TSH: After the CT scan is completed, any slice thickness and inter-slice increment can be reconstructed to avoid the shortcoming of conventional head MRI scan, i.e., some lesion details are missing due to big slice thickness and inter-slice increment. Even the thin-slice scan of cavernous sinus area has the disadvantages of small SFOV and inter-slice increment. After the 128-slice CT scan is completed, multi-plane recombination at any angle and slice thickness can be carried out, which can make the bilateral structure symmetrical and facilitate bilateral comparative observation. Once the MRI examination is completed, neither the angle nor the slice thickness can be adjusted. This is particularly important for the diagnosis and differential diagnosis of THS because the current THS imaging diagnosis mainly depends on bilateral contrast observation. After the 128-slice CT enhanced scan is completed, direct head angiography and blood vessel analysis can be performed, while MRI requires a separate blood vessel scan sequence. CT can easily show the calcification of blood vessel wall, skull base, and adjacent cerebral dura mater, helpful for the differential diagnosis of skull base tuberculosis, fungal infection of areas adjacent to the cavernous sinus, and so on. In addition, THS is often accompanied by severe pain, even nausea, vomiting, and other symptoms, making it difficult to check for immobilization for a long time. The quick speed of 128-slice CT examination is one of its advantages. Combined with CT post-processing VR imaging, it can show the tortuosity, dilation, and other changes of the drainage veins adjacent to the cavernous sinus. With quick scan speed and abundant image post-processing software, the 128-slice CT gradually shows its advantages in diagnosis and differential diagnosis of THS.

References

1. Lee SJ, Weon YC, Cha HJ, et al. Acase of atypical skull base osteomyelitis with septic pulmonary embolism. J Korean Med Sci. 2011;26(7):962–5.
2. Ahmed M, Syed R, More YI, et al. Stenotrophomonas skull base osteomyelitis presenting as necrotizing otitis externa: unmasking by CT and MRI-case report and review. Radiol Case Rep. 2019;14(10):1241–5.
3. Kilich E, Dwivedi R, Segal S, et al. Symptomatic stroke complicating central skull base osteomyelitis following otitis media in a 2-year old boy: case report and review of the literature. Int J Pediatr Otorhinolaryngol. 2016;89:140–4.
4. Khan MA, Quadri SAQ, Kazmi AS, et al. A comprehensive review of skull base osteomyelitis: diagnostic and therapeutic challenges among various presentations. Asian J Neurosurg. 2018;13(4):959–70.
5. Van Kroonenburgh A, Van Der Meer WL, Bothof RJP, et al. Advanced imaging techniques in skull base osteomyelitis due to malignant otitis externa. Curr Radiol Rep. 2018;6(1):3.
6. Zhiyun Y, Shurong L, Qiaolan X, et al. A case of multiple tuberculosis of bone and joint in sphenoid-saddle area of skull base and whole body. Chin J Radiol. 2007;41(12):1413–5.
7. Yamauchi T, Tani A, Yokoyama S, et al. Assessment of non-invasive chronic fungal rhinosinusitis by cone beam CT: comparison with multidetector CT findings. Fukushima J Med Sci. 2017;63(2):100–5.
8. Middlebrooks EH, Frost CJ, De Jesus RO, et al. Acute invasive fungal rhinosinusitis: a comprehensive update of CT findings and design of an effective diagnostic imaging model. Am J Neuroradiol. 2015;36(8):1529–35.
9. Choi YR, Kim JH, Min HS, et al. Acute invasive fungal rhinosinusitis: MR imaging features and their impact on prognosis. Neuroradiology. 2018;60(7):715–23.
10. Brandy-García A, Suárez-Cuervo C, Caminal-Montero L. Tolosa-Hunt syndrome as an initial presentation of sarcoidosis. Reumatol Clin. 2020;17(3) https://doi.org/10.1016/j.reumae.2019.07.001.